

AD _____

Award Number: DAMD17-99-2-9007

TITLE: Georgetown Institute for Cognitive and Computational
Sciences

PRINCIPAL INVESTIGATOR: Alan I. Faden, M.D.

CONTRACTING ORGANIZATION: Georgetown University Medical Center
Washington, DC 20007-2197

REPORT DATE: April 2004

TYPE OF REPORT: Final, Phase III

PREPARED FOR: U.S. Army Medical Research and Materiel Command
Fort Detrick, Maryland 21702-5012

DISTRIBUTION STATEMENT: Approved for Public Release;
Distribution Unlimited

The views, opinions and/or findings contained in this report are those of the author(s) and should not be construed as an official Department of the Army position, policy or decision unless so designated by other documentation.

REPORT DOCUMENTATION PAGEForm Approved
OMB No. 074-0188

Public reporting burden for this collection of information is estimated to average 1 hour per response, including the time for reviewing instructions, searching existing data sources, gathering and maintaining the data needed, and completing and reviewing this collection of information. Send comments regarding this burden estimate or any other aspect of this collection of information, including suggestions for reducing this burden to Washington Headquarters Services, Directorate for Information Operations and Reports, 1215 Jefferson Davis Highway, Suite 1204, Arlington, VA 22202-4302, and to the Office of Management and Budget, Paperwork Reduction Project (0704-0188), Washington, DC 20503

1. AGENCY USE ONLY (Leave blank)		2. REPORT DATE April 2004	3. REPORT TYPE AND DATES COVERED Final, Phase III (1 Apr 01 - 31 Mar 04)	
4. TITLE AND SUBTITLE Georgetown Institute for Cognitive and Computational Sciences			5. FUNDING NUMBERS DAMD17-99-2-9007	
6. AUTHOR(S) Alan I. Faden, M.D.				
7. PERFORMING ORGANIZATION NAME(S) AND ADDRESS(ES) Georgetown University Medical Center Washington, DC 20007-2197 E-Mail: fadena@giccs.georgetown.edu			8. PERFORMING ORGANIZATION REPORT NUMBER	
9. SPONSORING / MONITORING AGENCY NAME(S) AND ADDRESS(ES) U.S. Army Medical Research and Materiel Command Fort Detrick, Maryland 21702-5012			10. SPONSORING / MONITORING AGENCY REPORT NUMBER	
11. SUPPLEMENTARY NOTES Original contains color plates. All DTIC reproductions will be in black and white.				
12a. DISTRIBUTION / AVAILABILITY STATEMENT Approved for Public Release; Distribution Unlimited				12b. DISTRIBUTION CODE
13. ABSTRACT (Maximum 200 Words) Understanding and modifying plasticity/recovery within the central nervous system (CNS) represents the over-arching theme of this multidisciplinary research program. Participating investigators have used tools from cellular and molecular neurobiology, as well as systems neuroscience, to study mechanisms of neuronal cell death, as well as plasticity, after acute or chronic CNS injury. This included development/evaluation of pharmacological strategies to limit tissue damage and enhance recovery after acute or chronic neurodegeneration. Magnetic resonance imaging and spectroscopy were utilized as tools to evaluate changes in response to injury and/or treatment. Computational modeling was also used to predict both plasticity and for drug discovery. Together, these complementary research efforts were intended to elucidate mechanisms/processes relating to CNS injury and plasticity, with particular reference to language disorders, traumatic brain injury, spinal cord injury, and Alzheimer's disease.				
14. SUBJECT TERMS brain trauma, Alzheimer's disease, spinal cord injury, mechanisms of cell death, nervous system plasticity, drug discovery, cognition, computational neuroscience/structural biology				15. NUMBER OF PAGES 513
				16. PRICE CODE
17. SECURITY CLASSIFICATION OF REPORT Unclassified	18. SECURITY CLASSIFICATION OF THIS PAGE Unclassified	19. SECURITY CLASSIFICATION OF ABSTRACT Unclassified	20. LIMITATION OF ABSTRACT Unlimited	

NSN 7540-01-280-5500

Standard Form 298 (Rev. 2-89)
Prescribed by ANSI Std. Z39-18
298-102

I.	I. Cover	1
II.	SF 298	3
III.	Introduction	4
IV.	Body	5
IVa.	CNS Injury/Plasticity	5
IVb.	Computational Neuroscience/Structural Biology	119
IVc.	Cognitive Neuroscience	123
V.	Key Research Accomplishments	133
VI.	Reportable Outcomes	136
VII.	Conclusions	142
VIII.	References	144
IX.	Appendices	166

III. Introduction

Understanding and modifying plasticity/recovery within the central nervous system (CNS) represents the over-arching theme of this multidisciplinary research program. Participating investigators have used tools from cellular and molecular neurobiology, as well as systems neuroscience, to study mechanisms of neuronal cell death, as well as plasticity, after acute or chronic CNS injury. This included development/evaluation of pharmacological strategies to limit tissue damage and enhance recovery after acute or chronic neurodegeneration. Magnetic resonance imaging and spectroscopy were utilized as tools to evaluate changes in response to injury and/or treatment. Computational modeling was also used to predict both plasticity and for drug discovery. Together, these complementary research efforts were intended to elucidate mechanisms/processes relating to CNS injury and plasticity, with particular reference to language disorders, traumatic brain injury, spinal cord injury, and Alzheimer's disease.

IVA. CNS Injury/Plasticity

Hypothesis #1. Combined use of *in vitro* and *in vivo* models can be used to elucidate molecular mechanisms of neuronal apoptosis and traumatic/ischemic neuronal injury.

1. Model of Diffuse Traumatic Brain Injury in Rats

Few experimental models are available that mimic the biomechanics and pathobiology of human diffuse brain injury¹⁻⁵. We have developed a highly controlled rat model of moderate diffuse traumatic brain injury (DTBI), and characterized the major morphological, physiological, and biochemical changes induced by such injury.

The injury device consists of an air-driven high-velocity impactor that is targeted to contact a steel disc cemented onto the rodent skull. The animal's head is supported by a molded, gel-filled base (Handstands, Taiwan), which also acts to decelerate the head after impact. Impact is then initiated wherein the velocity of the impactor is constant (3.25 m/sec), however the distance the impactor travels after contacting the steel disc is under user control. This distance thus determines the injury severity. Force of impact is controlled and recorded on a personal computer connected to the device through a PowerLab (Stoelting, Wood Dakem IL, USA). In this study, the total impact energy at the end of the impactor was 512.717 N, meaning that 6.528 N/mm² of impact energy was delivered to the disc (Fig. 1).

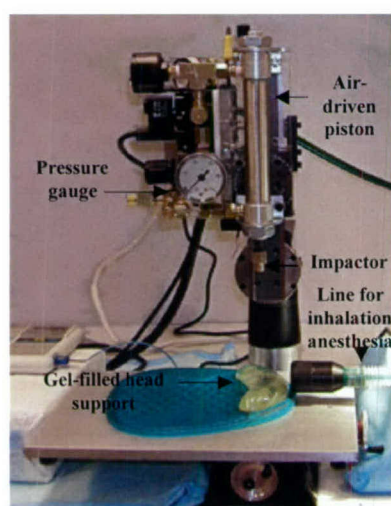


Figure 1. Device for inducing diffuse traumatic brain injury.

Male Sprague-Dawley rats (380 ± 30 g; $n=360$) had access to food and water *ad libitum*. Animals were initially anesthetized with 4% isoflurane and 1-1.5% for maintenance; the anesthetic was evaporated in a gas mixture containing 30% oxygen/70% nitrous oxide and applied through a nose-mask. The animals were allowed to breathe spontaneously without tracheal intubation. A midline incision exposed the dorsal surface of the skull upon which a 10 mm x 3 mm diameter steel disc was cemented centrally between lambda and bregma using a polyacrylamide adhesive. Rectal temperature was maintained at 37°C using a thermostatically controlled heating blanket.

The 16 mm vertical displacement of the head caused no mortality, whereas the 17 mm head depression produced a mortality rate of 12%. Moderate severity of head injury (26% mortality) was caused by 18 mm head depression. Severe TBI was produced by 19 mm (56% mortality) and 20 mm (90% mortality) of head depression. Death occurred within 5 minutes of injury and resulted from cardiorespiratory depression. The moderate injury level (18 mm) was subsequently used in all further experiments (Fig. 2).

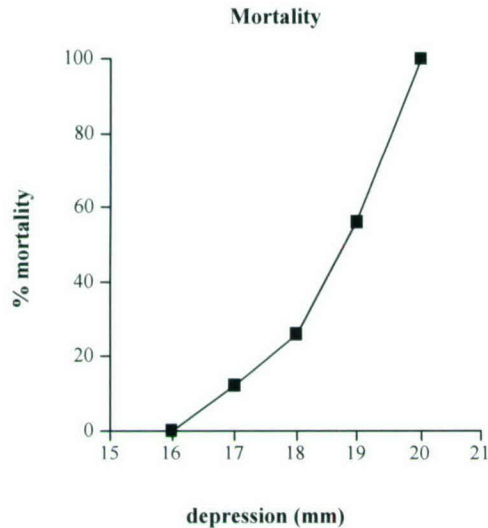


Figure 2. Mortality rates depending on the vertical displacement of the head (depression) measured 24 h after injury.

The percentage water content in cortex of sham control animals was $78.45 \pm 0.24\%$, whereas in hippocampus it was $77.94 \pm 0.18\%$. At 20 min after injury, the water content in cortex of injured animals was $79.20 \pm 0.17\%$ ($p < 0.05$) and in hippocampus $79.77 \pm 0.26\%$ ($p < 0.001$) indicating acute edema development after moderate diffuse traumatic brain injury (Figure 3a). Increased cortical water content was also seen at 4 h ($79.40 \pm 0.10\%$, $p < 0.05$) and 24 h (80.25 ± 0.22) post-trauma. In hippocampus, the water content was also increased at 4 h (80.52 ± 0.22 , $p < 0.001$) and 24 h (82.38 ± 0.64 , $p < 0.001$) after injury (Fig. 3a). The changes in edema measured by wet/dry weight method were confirmed using diffusion-weighted MRI. Additionally, this method is accepted as a sensitive tool for distinguishing between vasogenic and cytotoxic edema following traumatic brain injury⁶. Increased apparent diffusion coefficient (ADC) in the brain indicates vasogenic edema whereas reduced ADC suggests cytotoxic edema⁶. Significant changes in ADC were found in both cortex and hippocampus at 20 min, 4 h and 24 h following injury, compared to control values (Fig. 3b). ADC maps derived from the DWI are shown in Figure 3c. ADC was significantly increased in cortex and hippocampus of injured animals at 20 min and 4 h following injury, which reflects vasogenic edema. This is manifested as areas of hyperintensity on the ADC maps. At 24 h post-trauma, decreased ADC suggested development of cytotoxic edema. Indeed, the ADC map showed regions of hypointensity diffusely scattered throughout the brain, reflecting a decrease in the molecular motion of water, consistent with accumulation of water within the intracellular space. Such a biphasic development of edema has been previously reported in other diffuse models of brain trauma.

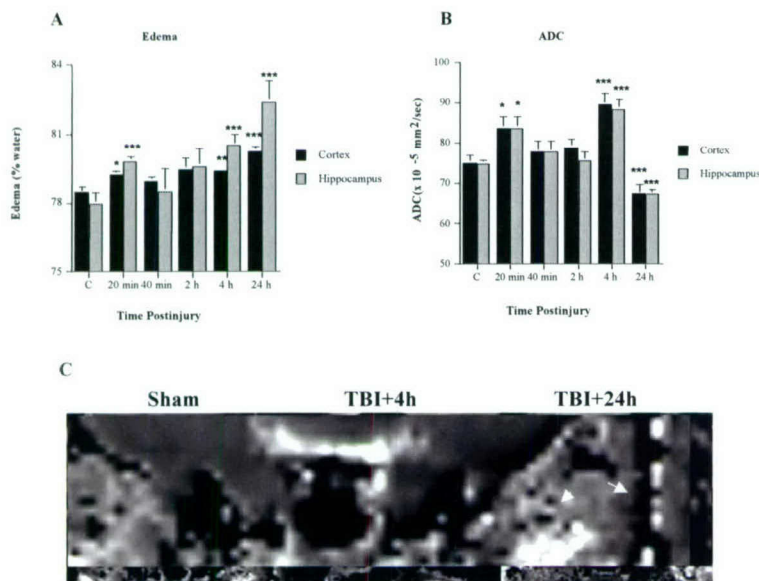


Figure 3. A. Changes in water content measured in cortex in hippocampus by wet weight/dry weight method following moderate traumatic brain injury; B. Apparent diffusion coefficients (ADC) obtained in cortex and hippocampus following traumatic brain injury in rats; * $p < 0.005$, ** $p < 0.01$, and *** $p < 0.001$ compared to sham control values; C. Apparent diffusion coefficient maps derived from the diffusion-weighted magnetic resonance images obtained in sham control animals and in animals with moderate traumatic brain injury at 4 h and 24 h postinjury. Areas of subcortical hyperintensity in injured animals at 4 h postinjury indicates vasogenic edema, while scattered regions of hypointensity at 24 h postinjury suggests development of cytotoxic edema.

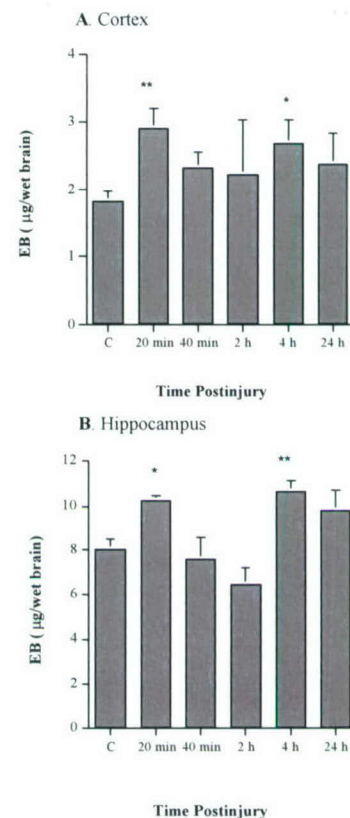


Figure 4. Changes in blood-brain barrier permeability to Evans blue dye in cortex and hippocampus of rats subjected to moderate traumatic brain injury. * $p < 0.05$ and ** $p < 0.001$ compared to sham control (C).

Increase in ADC was associated with a significant increase in the permeability of the blood-brain barrier (BBB) at 20 min and 4 h after injury as assessed by penetration of Evans blue dye (Fig. 4). Since increased BBB permeability associated with edema at early time points following TBI has been seen to correspond to vasogenic edema⁷, these results support our DWI findings suggesting a vasogenic origin of acute edema. Moreover, significantly reduced ADC and the lack of a significant increase in Evans blue dye concentration in brain structures at 24 h post-trauma confirm cytotoxic edema formation at this time point.

Motor and cognitive outcomes are summarized in Figure 5. All animals demonstrated a significant decline ($p < 0.05$) in motor function after moderate (18 mm) trauma (Fig. 5a). Although the deficits are moderate, they are consistent with those previously described in other rodent models of diffuse trauma as determined by the composite motor tests used in the present study⁸. The Morris Water Maze was performed over four consecutive days starting at 14 days after sham surgery or TBI (Fig. 5b). The mean latency to locate the platform immersed below the surface of the water was significantly increased in injured animals at 15 ($p < 0.001$), 16 ($p < 0.05$) and 17 ($p < 0.001$) days postinjury, compared to sham control animals.

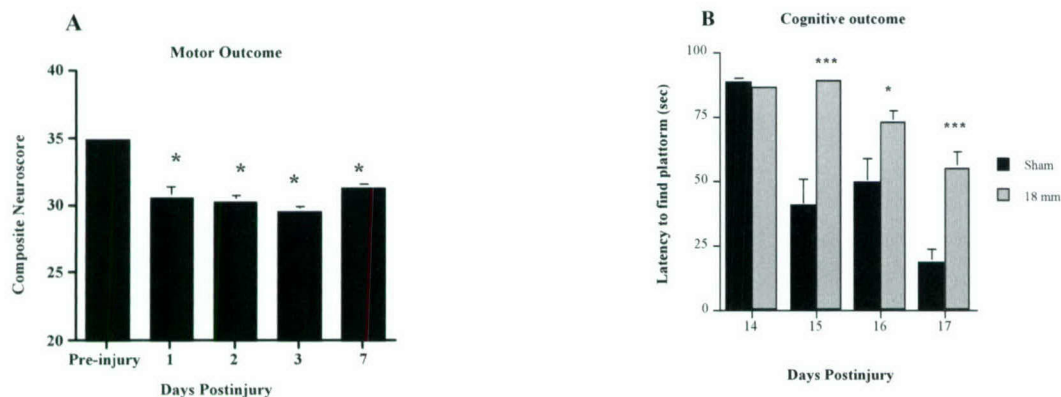
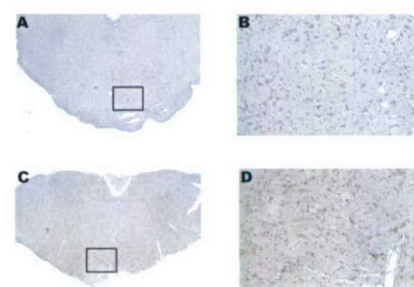
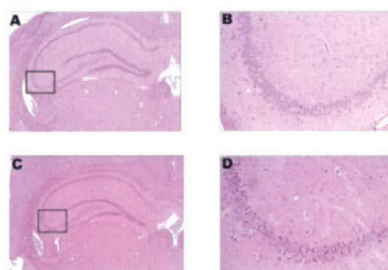
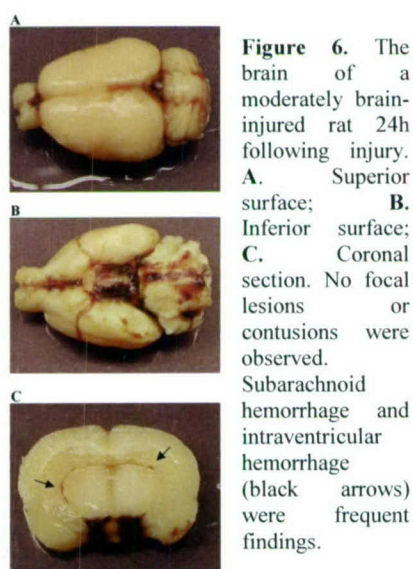


Figure 5. **A.** Changes in composite neuroscore 1, 2, 3, and 7 days after moderate traumatic brain injury in rats; **B.** Water maze cognitive score after moderate traumatic brain injury in rats measured at 14, 15, 16, and 17 days postinjury. * $p < 0.05$ and *** $p < 0.0001$ compared to sham control animals.

Gross pathological observation of the brains following moderate (18 mm) brain injury show an absence of focal lesions or contusion. Subarachnoid hemorrhage was usually observed in the basal cisterns, cisterna magna and over the cerebral hemispheres (Fig. 6). Histological examination of hematoxylin and eosin (H&E) stained tissue sections demonstrated profound dark cell change and reduced neuronal density in the CA3 pyramidal layer of the hippocampus (Fig. 7). There were also shrunken neurons associated with perineuronal vacuolation in supraventricular cortical areas and the dentate gyrus after injury, together with pericapillary edema in supraventricular regions of the cerebral cortex, brainstem and thalamus; in these areas several congested capillaries also were seen (results not shown). A profound increase in APP immunoreactivity in neuronal cell bodies was also present at 24 h, particularly in the brainstem (Fig. 8). This increase in APP has been noted in other models of diffuse traumatic brain injury and is thought to represent an acute phase post-traumatic stress response⁹.



Induction of moderate (18 mm) TBI resulted in internucleosomal DNA fragmentation as assessed by the positive Terminal Deoxynucleotidyl Transferase Biotin-dUTP Nick End Labeling (TUNEL) histochemistry. TUNEL stained cells were clearly apparent throughout the brain at 1, 2, and 3 days post-trauma. These TUNEL positive cells were found mainly in cortex, thalamus and brainstem. The largest number of TUNEL positive cells was seen 24 h following injury (Figure 9b), whereas no TUNEL positive cells were detected after 7 d post-trauma. Sham control (non-injured) tissue did not demonstrate any TUNEL positive cells at any time point. The TUNEL findings were confirmed by the Fluoro-Ruby technique, which showed cells with condensed nuclei and margined chromatin in cortex and thalamus (Figure 9d). To elucidate whether caspase-3-mediated apoptosis was associated with the TBI-induced cell death, the distribution of a cleaved (active) caspase-3 in the brain of injured animals was measured by qualitative immunocytochemistry (Fig. 10). The antibody used {cleaved caspase-3 (Asp175) (5A1) monoclonal antibody; Cell Signaling Technology} does not detect the pro-caspase-3 form; it identifies endogenous levels of the large fragment (17/19 kDa) of activated caspase-3 resulting from cleavage adjacent to Asp175. As such, this antibody can be used as a cellular marker of caspase activation. The cleaved form of caspase-3 was expressed in cortex, hippocampus (not shown), and widely distributed throughout the entire region of brainstem by 24 h after injury (Fig. 10).

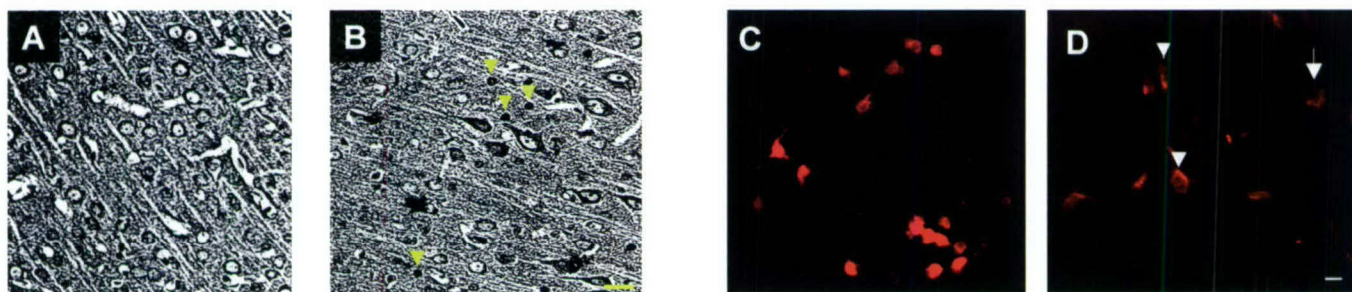


Figure 9. **A** and **B**: TUNEL immunocytochemistry in rat brain cortex at 24 h after moderate traumatic brain injury. Darkly stained TUNEL positive nuclei (arrows) are clearly observed distributed throughout the cortex (**B**). Such dark staining nuclei are absent in sham control (**A**). Scale bare = 100 μ m. **C** and **D**: Representative photomicrograph of Fluoro-Ruby labeled cells in thalamus. Cells with condense nuclei and margined chromatin (arrows) are clearly observed at 24 h postinjury (**D**) compared to a sham control (**C**). Scale bar = 50 μ m.

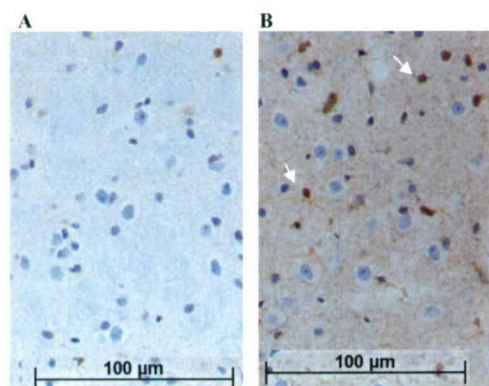


Figure 10. Immunocytochemical staining of paraffin-embedded rat brain shows darkly stained apoptotic cells (white arrows) in the brainstem 24 h following injury using cleaved Caspase-3 (Asp175) (5A1) Rabbit Monoclonal Antibody, which detects endogenous llevels of the large fragment (17/19 kDa) of activated caspase-3. Scale bar = 100 μ m.

Analysis of morphological characteristics and distribution of Fluoro-Ruby labeled cells showed microglia and cell debris in supraventricular cortical areas (Fig. 11c and d) and in brainstem (not shown) at 24 h after injury. At 7 d post-trauma, a significant reduction of neurons and further increase in microglia were observed (Fig. 11 g and h). Similarly, Fluoro-Ruby labeled axons in the caudate putamen showed mild axonal pathology 24 h after injury (Fig. 12b), whereas retraction balls, broken fibers and disrupted axons were observed at 7 d post-injury (Figure 12d).

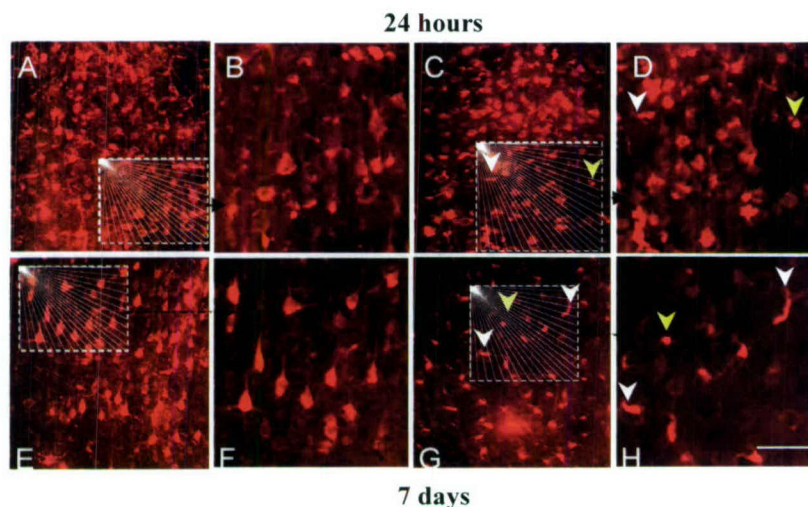


Figure 11. Representative photomicrographs of Fluoro-Ruby labeled cells in cortex. **A, B, E, and F** show cortex in a sham control animal, while **C, D, G, and H** show cortex in an injured animal. **A, C, E** and **G** are with a lower magnification (the scale bar represents 50 μ m), whereas **B, D, and H** demonstrate a region (white box) with a higher magnification (the scale bar represents 200 μ m). At 24 hours postinjury (**C**), there are few microglia (white arrows) and cell debris (yellow arrows); at 7-day postinjury (**F**) decrease in neuronal cell number, increased number of microglia (white arrows), and presence of debris (yellow arrows) are observed.

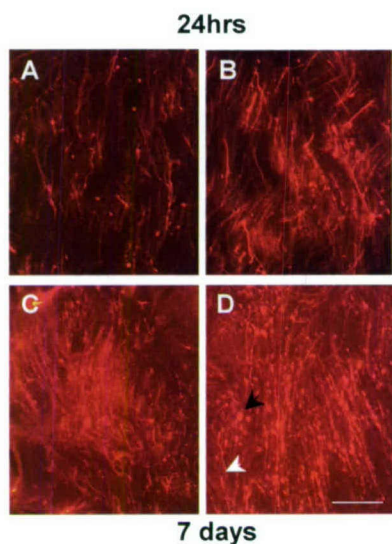


Figure 12. Representative photomicrographs of Fluoro-Ruby labeled axons in the caudate putamen. **A** and **C** show caudate putamen in a sham control animal, while **B** and **D** represent caudate putamen in a moderately injured rat. At 24 h postinjury (**B**) there is no noticeable change compared to sham control (**A**); at 7 d (**D**) postinjury retraction balls (black arrow) and broken fibers (white arrow) are visible. Scale bar = 50 μ m.

In conclusion, we have developed a new model for diffuse traumatic brain injury, which induces biochemical and neurological changes consistent with the diffuse axonal injury produced in other models and comparable to alterations found after clinical TBI. This model offers a high level of control of mechanical force inflicting the injury, thereby reducing the intersubject and outcome variability. Moreover, by reproducing both features of necrosis and apoptosis, this model is suitable for studying complex mechanisms of post-traumatic cell death, and testing novel therapeutic approaches targeting diffuse axonal damage.

2. Developmental model of traumatic brain injury

It has long been known that young animals may have differing sensitivities to the consequences of brain insult as compared to adults¹⁰. For example, young animals show considerably more resistance to the effects of hypoxia than do adults and experimental studies demonstrate that the duration of hypoxia leading to a given percentage of tissue loss is inversely proportional to developmental age^{11, 12}. Since this form of hypoxic injury generally causes necrosis, these findings suggest that young animals may be more resistant to necrotic cell death than adults. In contrast, there is increasing evidence that molecular pathways associated with apoptotic cell death are markedly upregulated at birth and shortly thereafter, and decline with increasing developmental age¹³. Together, such observations suggest that traumatic brain injury in perinatal animals may be fundamentally different from those in adults, showing preferentially larger amounts of apoptosis and probably greater resistance to necrosis.

Using our newly development model of diffuse TBI, we utilized different depression levels in four age groups of animals (7 d, 14 d, and 21 d post-natal, as well as young adults; n=50/age group) in order to achieve the same injury severity. We chose mortality as the first major criteria in comparing injury severity. Figure 13 demonstrates the mortality rate in 7 d, 14 d, and 21 d old rats 24 hour after diffuse traumatic brain injury (DTBI), comparing with the mortality in injured young adults. Our results showed that moderate injury severity (mortality between 20-25%) was achieved by applying 6.4 mm of depression in 7 d old, 8.6 mm in 14 d old, and 10.6 mm in 21 d old animals. Comparable injury severity was induced by 18 mm vertical displacement in adult animals.

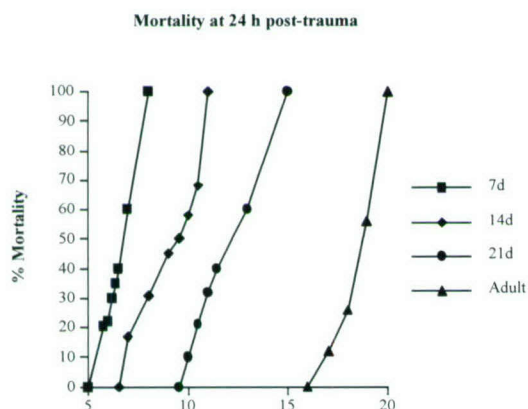


Figure 13. Mortality rates in 7d, 14 d, and 21 d old rats, as well as young adult animals after DTBI.

Additionally, we compared brain water content in different age groups of naïve animals, as well as edema formation following moderate DTBI using diffusion-weighted MRI. This method is accepted as a sensitive tool for distinguishing between vasogenic and cytotoxic edema following traumatic brain injury⁶. The apparent diffusion coefficient (ADC), calculated on the basis of diffusion-weighted image (DWI), significantly correlates with the changes of extracellular water¹⁴. Increased ADC in the brain indicates vasogenic edema whereas reduced ADC suggests cytotoxic edema⁶. Since significant increase in ADC was confirmed in adult rats at 4 h following moderate DTBI, which suggested development of vasogenic edema, the same time point was chosen to measure ADC values in immature rats. Although there was statistically significant difference between the ADC values measured in the brain of 7 d old naïve rats and values measured in the

brains of older naïve animals (Fig. 14), the intensity of post-traumatic brain edema development was similar in all age groups (Fig. 15).

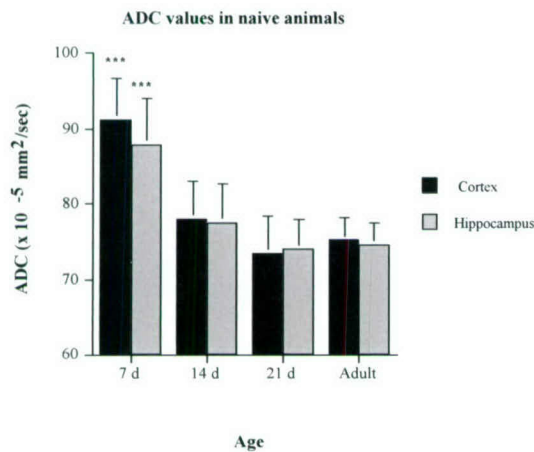


Fig. 14. ADC values in cortex and hippocampus of naïve 7 d, 14 d, and 21 d old animals, as well as young adults.

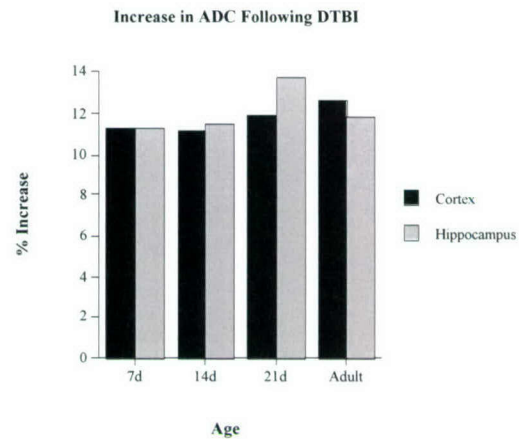


Fig. 15. Percentage of ADC increase in cortex and hippocampus of 7 d, 14 d, and 21 d old rats, as well as young adults at 4 h post-trauma. The increase in ADC values was comparable in all age groups.

After establishing injury severity levels analogous in four age groups, we compared the age-dependent pathomorphology induced by DTBI. Functional integrity of neuronal cell body and visualization of axons were analyzed using a vital fluorescent dye Fluoro-Ruby (Molecular Probes Inc., Eugene, OR, USA). Analysis of morphological characteristics of Fluoro-Ruby labeled cells showed reduction of neurons, increase in microglia and accumulation of cell debris in supraventricular regions and brainstem at 7 d post-trauma (Fig. 16).

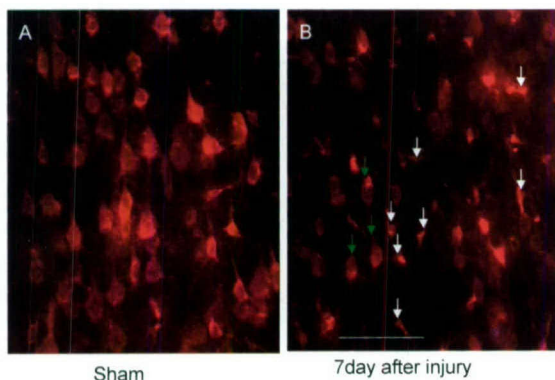


Fig 16. Representative photomicrographs of Fluoro-Ruby labeled cells in the cortex of 21 d old rat, which was injured at day 15 postnatal, and sacrificed at 7 post-injury (i.e. 21 d postnatal). **A:** age matched sham control; **B:** cortex at 7 d post-injury. In sham cortex there is no noticeable change. At 7 day post-injury only few healthy cells (green arrow) remained, while the number of microglia (white arrow) is increased. Scale bar = 10 μ m.

In conclusion, our preliminary results demonstrate that the newly developed diffuse traumatic brain injury model could be useful to clarify age-dependent differences in complex molecular mechanisms underlying post-traumatic deficits.

3. Anandamide-induced neurotoxicity

It is now known that much of the brain damage produced by head impact results not only from primary mechanisms of tissue destruction occurring at the time of the insult, but also depends on complex secondary injury mechanisms initiated by trauma. One of the secondary processes that may play a role in delayed neuronal death is sustained activation of phospholipase-mediated signaling pathways that leads to membrane phospholipid degradation¹⁵. For example, release of polyunsaturated fatty acids such as arachidonic acid and activation of downstream signaling pathways have been implicated in brain edema and tissue damage after various central nervous system (CNS) insults¹⁶.

Endocannabinoids are endogenous ligands that are capable of binding to the same cannabinoid receptors (CB1, CB2), which mediate the effects of Δ^9 -tetrahydrocannabinol, the active compound of Cannabis¹⁷. There are three members of the endocannabinoid family discovered to date: N-arachidonylethanolamine (anandamide; AEA), 2-arachidonoylglycerol (2-AG), and 2-arachidonoyl glyceryl ether (2-AGE; noladin) with different affinities for CB1 and CB2 receptors and distinct biological effects¹⁸. Recent studies indicate that there is endocannabinoid signaling in both neurons and astrocytes, and that astrocytes can use this system to communicate with surrounding neurons, or other astrocytes¹⁹. Over the last decade, a considerable amount of work has demonstrated protective biological effects of endocannabinoids after brain damage²⁰. However, activation of CB1 receptors can induce cytotoxic effects in a number of cultured cell systems²¹ including cultured hippocampal²² and cortical neurons²³. It is highly possible that CB1 activation may lead to both neurotoxicity and neuroprotection depending on a variety of influences such as nature and intensity of the toxic insult, as well as the cell type under the study^{21,24}.

Anandamide was the first identified endocannabinoid²⁵. A member of the N-acylethanolamines (NAE), AEA can be synthesized as a hydrolytic product of N-acylated species of phosphatidylethanolamine (NAPE) through a process catalyzed by phospholipase D²⁶. Although AEA originally has been identified as an endogenous cannabinoid receptor ligand²⁵, more recent data suggest that it may interact directly also with other molecular targets, including non-CB1, non-CB2 G-protein-coupled receptors (GPCRs)^{27,28}, gap junctions²⁹, various ion channels^{18,30-32}, and vanilloid (VR1) receptors³³. Although a substantial body of evidence demonstrates that activation of CB1 receptors by endocannabinoids^{34,35}, including AEA^{17,20,36}, has neuroprotective effects, stimulation of VR1 receptors has been found to increase intracellular Ca²⁺ and lead to subsequent cytotoxicity³⁷.

In our extensive preliminary studies, we have found that AEA shows neurotoxicity both in vivo and in vitro, and that such toxicity is mediated by both VR1 and calpains (*vide infra*). We suggest that the effects of AEA in cell death depend upon the relative balance between its actions at CB1 or VR1 receptors. Furthermore, we propose that AEA is an important secondary injury factor following traumatic brain injury, where AEA shifts the balance toward VR1-related effects and subsequently contributes to neurotoxicity, through both necrotic and apoptotic pathways.

3.1. Neurotoxic Effects of Anandamide *In Vitro*

3.1a Anandamide induces dose-dependent cell death in rat cortical and cerebellar granule cell cultures.

Administration of AEA both to rat cortical neuronal cultures (RCN) and cerebellar granule cell cultures caused cell death in a dose-dependent manner (Fig. 17a and b). The neurotoxic effects were measured by lactate-dehydrogenase (LDH) ³⁸ release and calcein AM cell viability assay ³⁹. The AEA-induced cell death was observed at a 25 μ M concentration in RCN, whereas it was evident in cerebellar granule cell cultures at doses of 10 μ M and higher. The metabolically stable AEA-analog meth-anandamide also caused cell death in neuronal cultures, albeit at somewhat higher concentrations than required from AEA (Fig 17c).

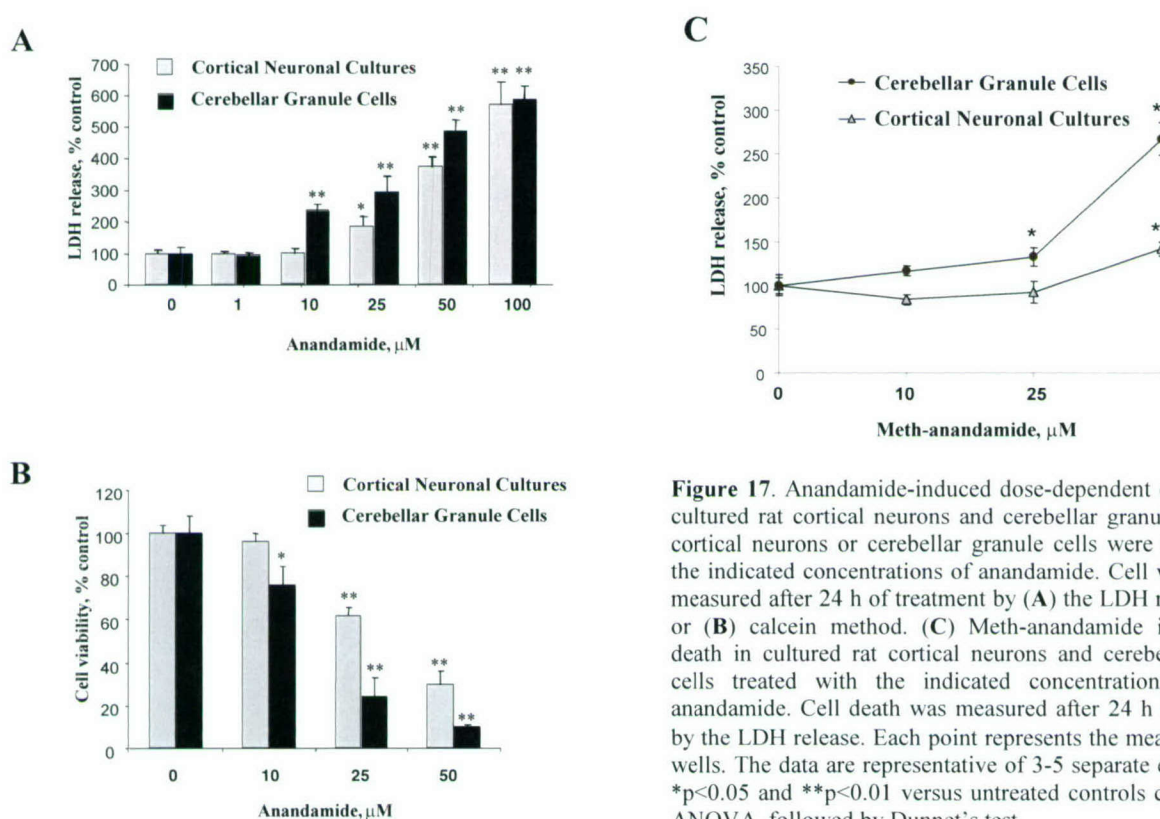


Figure 17. Anandamide-induced dose-dependent cell death in cultured rat cortical neurons and cerebellar granule cells. Rat cortical neurons or cerebellar granule cells were treated with the indicated concentrations of anandamide. Cell viability was measured after 24 h of treatment by (A) the LDH release assay or (B) calcein method. (C) Meth-anandamide induced cell death in cultured rat cortical neurons and cerebellar granule cells treated with the indicated concentrations of meth-anandamide. Cell death was measured after 24 h of treatment by the LDH release. Each point represents the mean \pm SD of 8 wells. The data are representative of 3-5 separate experiments. * $p < 0.05$ and ** $p < 0.01$ versus untreated controls compared by ANOVA, followed by Dunnet's test.

3.1b Anandamide exacerbates stretch injury in rat cortical neuronal cell cultures.

We subsequently analyzed the input of AEA on rat cortical neurons exposed to a moderate stretch injury (Fig.18). This model ⁴⁰ has been proposed as a model for studying diffuse axonal injury-induced molecular and biochemical responses *in vitro* and induces both necrotic and apoptotic pathways of cell death ⁴¹. Addition of 25 μ M AEA into the cell culture media significantly increased the stretch trauma-induced LDH release (Fig. 18), indicating exacerbation of the neuronal injury by AEA.

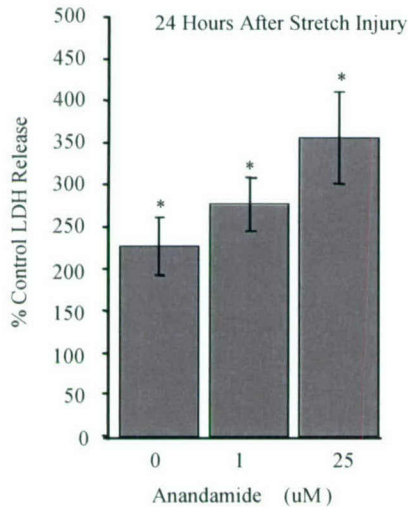


Figure 18. Moderate stretch injury (7.5 mm) increases LDH release in mixed glial-neuronal culture. Twenty-five μ M anandamide added to the growth media immediately before injury significantly increased the injury-induced LDH release. An analysis of variance (ANOVA) with Dunnett's *post hoc* test was performed: * denotes $p<0.05$ difference from control, † denotes $p<0.05$ from stretch-injured cells.

3.1c Anandamide causes early upregulation of calpain and calpain inhibition provides protection against anandamide-induced cell death.

Since calpain has long been implicated in many models of cell death, both *in vivo* and *in vitro*^{42, 43}, we utilized immunoblot analysis of cleaved α II-spectrin protein breakdown, a well-recognized marker for the calpain generated protein breakdown⁴², to examine AEA-induced alterations in calpain activity. As shown in Figure 19a, treatment with AEA caused significant increase in 145 kDa fragment of cleaved α II-spectrin in cortical neuronal cells, as compared to intact cultures. Moreover, AEA-induced α II-spectrin cleavage was almost entirely blocked by co-administration of 25 μ M calpastatin, a calpain inhibitor (Fig. 19b). It should be noted that levels of 120 kDa α II-spectrin fragment, known to be generated by caspase-3-induced cleavage⁴⁴, remained unchanged until 24 h of treatment with AEA (Fig. 19a).

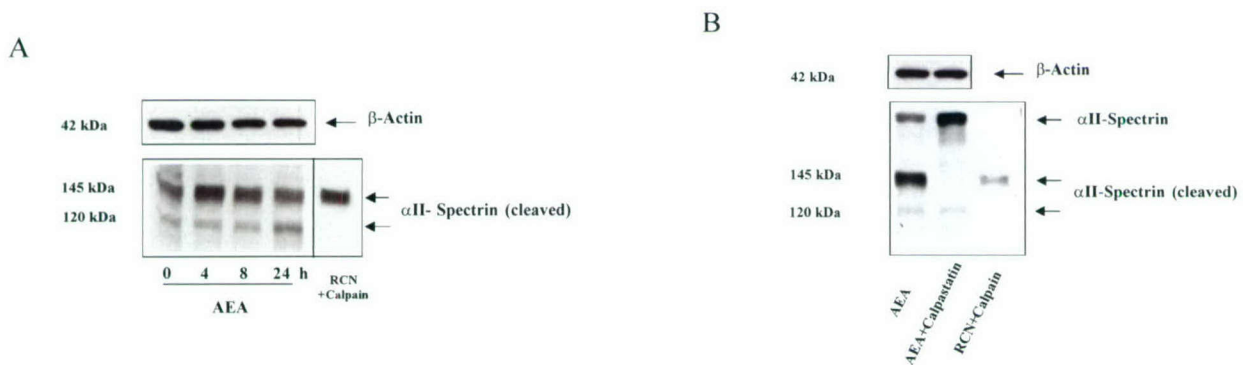


Figure 19. Anandamide induced significant upregulation of cleaved α II-spectrin in rat cortical neuronal cultures (RCN). Treatment with calpastatin reduces anandamide-induced α II-spectrin cleavage. Cultures were treated with 30 μ M anandamide after indicated period of time, harvested, fractionated by 5% SDS-PAGE and subjected to immunoblot analysis (**A**). Cell were pretreated for 30 min with 25 μ M calpastatin, followed by the addition of 30 μ M anandamide, and after 4 h of incubation harvested, prepared and subjected to immunoblot analysis (**B**). To ensure equal protein loading aliquots from the same samples were subjected to 12% SDS-PAGE following by immunoblot analysis using β -actin antibody. Twenty-five μ g of protein from RCN lysates incubated with m-calpain were used as a positive control for cleaved α II-spectrin (RCN+calpain).

Pretreatment with cell-permeable calpain inhibitor calpastatin significantly increased viability of cortical neurons exposed to AEA, as demonstrated by calcein AM assay (Fig. 20a). Moreover, application of the same dose (25 μ M) of calpastatin blocked α II-spectrin cleavage in AEA-treated cortical neuronal cultures (Fig. 20b). Administration of another cell-permeable calpain inhibitor, calpeptin, also significantly protected against AEA-induced cell death in neuronal cultures (Fig. 20b).

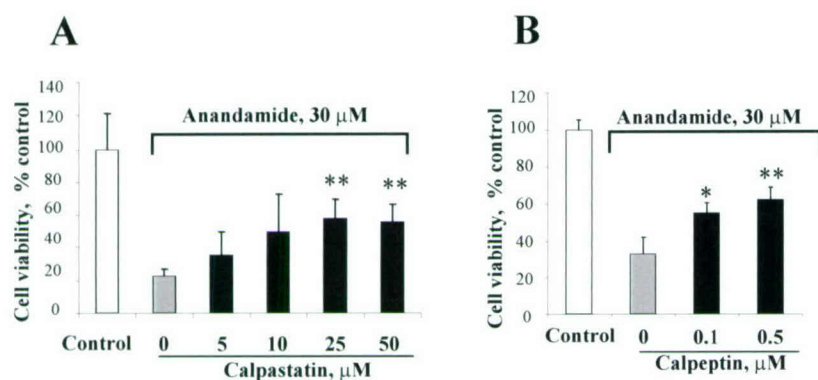


Figure 20. Pretreatment with the calpain inhibitor calpastatin (A) or calpeptin (B) reduced anandamide-induced cell death in rat cortical neuronal cultures. Cell viability was measured by calcein AM assay 24 h after incubation with 30 μ M anandamide with or without 45 min pretreatment with the indicated concentrations of calpain inhibitor calpastatin. The data are representative of 3-5 separate experiments. Histograms indicate cell viability (calcein AM fluorescence) as percentage of controls \pm SD; n=8 cultures per condition; **p<0.01 versus cells treated with anandamide alone compared by ANOVA, followed by the Dunnett's test.

3.1d. Anandamide causes late caspase-3 activation in cortical neuronal cultures

Immunoblot analysis of cytosolic protein extracts from cortical neuronal cells, incubated for different time periods with 25 μ M of AEA showed a significant increase in active caspase-3 protein levels after 16 and 24 h of treatment (Fig. 21a). Caspase-3-like activity was also examined in cytosolic protein extracts from cortical neuronal cells treated with 25 μ M AEA for 24 h, and compared to that in sister control cultures. The fluorometric assay, using DEVD-AMC as a substrate, showed an approximate 4-fold increase in the caspase-3-like activity in AEA-treated cells (Fig. 21b).

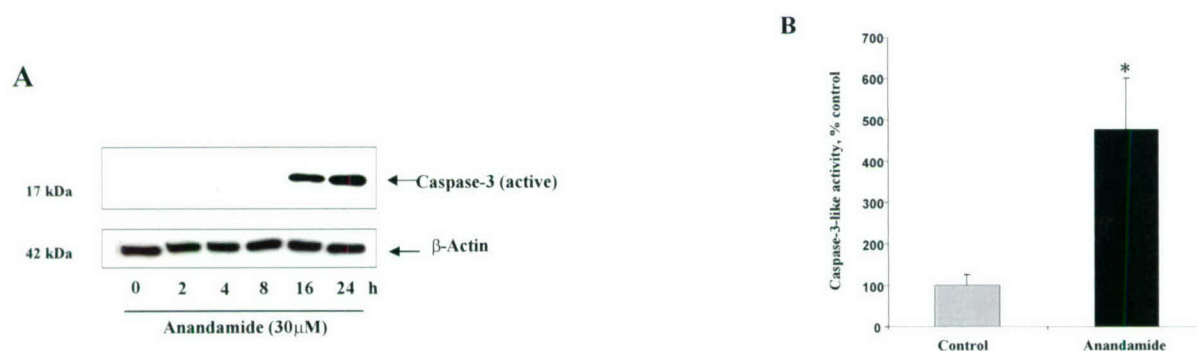


Figure 21. (A) Treatment with anandamide significantly increased active caspase-3 protein levels in rat cortical neuronal cells. Cultures were treated with 30 μ M anandamide; after indicated time periods, cells were harvested and subjected to immunoblot analysis. β -Actin was used as an internal control. (B) After 24 h of treatment with anandamide, caspase-3-like activity was measured fluorometrically, and upregulates caspase-3-like activity in rat cortical neuronal cells. Histograms represent caspase-3-like activity as a percentage of the activity in control cells. *p<0.01 versus untreated controls compared by Student's two-tailed *t*-test.

3.1e. Anandamide induces cell death in caspase-9 and caspase-8 dominant-negative SH-SY5Y cells and caspase-3-deficient MCF-7 cells.

We also utilized the effects of AEA on dominant-negative caspase-9 and caspase-8 SH-SY5Y neuroblastoma cells stably transfected with mutant caspase-9 and caspase-8 constructs. Moreover, we analyzed the effect of AEA on cell viability in caspase-9 and caspase-8 dominant-negative SH-SY5Y cells in comparison to that for cells transfected with the empty vector (pcDNA3). Anandamide caused cell death in SH-SY5Y cells in dose-dependent manner, as estimated by LDH assay after 24 h of treatment (Table 1). Furthermore, the AEA-induced cell death was not significantly reduced in caspase-8 or caspase-9 dominant-negative SH-SY5Y cells, compared to SH-SY5Y cells that were transfected with empty vector (Table 1). Using MCF-7 human breast carcinoma cells, which lack expression of caspase-3 due to a deletion in the caspase-3 gene^{45, 46}, we further analyzed the possibility of caspase-3 related mechanisms in AEA-induced cell death. In this system, AEA was able to induce significant cytotoxicity at 20 and 50 μ M concentrations (Table 1) suggesting that the caspase-dependent pathway is not crucial for AEA-induced cell death.

Anandamide (μ M)	LDH Release, % Control			
	SH-SY5Y (EV)	SH-SY5Y(C8 ^{-/-})	SH-SY5Y(C9 ^{-/-})	MCF-7
10	100 \pm 4.6	100.2 \pm 2.4	104.9 \pm 12.3	98.16 \pm 5.07
20	116.9 \pm 14.7	107.8 \pm 5.4	117.3 \pm 10.7	165.736 \pm 9.08*
50	282.6 \pm 36.4*	254.6 \pm 10.7*	354.2 \pm 42.2*	198.95 \pm 9.17*
100	313.2 \pm 21.7*	299.9 \pm 13.3*	382.4 \pm 19.5*	Not tested

Table 1. Anandamide induces cell death in caspase-8 dominant-negative (C8^{-/-}), caspase-9 dominant-negative (C9^{-/-}), and mock-transfected (EV) SH-SY5Y cells, as well as in caspase-3-deficient MCF-7 cells. Cultures were treated with indicated concentrations of anandamide and 24 h after cell death was measured by LDH release assay. Data are shown as a percentage of LDH release in untreated controls \pm SD; n=8 to 16 cultures per condition. *p<0.01 versus untreated control cells compared by ANOVA followed by Dunnett's test.

3.1f. Calpain inhibition provides significant protection against AEA-induced cell death in caspase-3-deficient MCF-7 cells.

Administration of calpastatin at 25 μ M significantly protected caspase-3-deficient MCF-7 cells (Fig. 22) against AEA-induced cell death as measured by calcein AM assay.

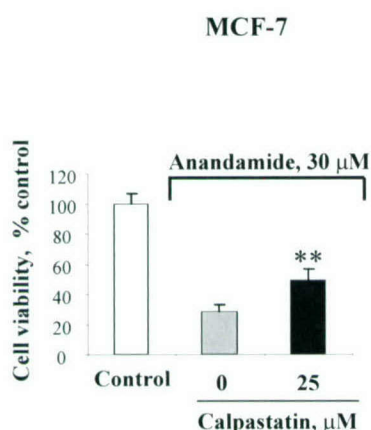


Figure 22. Pretreatment with the calpain inhibitor calpastatin reduced anandamide-induced cell death in caspase-3 deficient MCF-7 cells. Cell viability was measured by calcein AM assay 24 h after incubation with 30 μ M anandamide with or without 45 min pretreatment with indicated concentrations of calpain inhibitor calpastatin. The data are representative of 3-5 separate experiments. Histograms indicate cell viability (calcein AM fluorescence) as percentage of controls \pm SD; n=8 cultures per condition; **p<0.01 versus cells treated with anandamide alone compared by ANOVA, followed by the Dunnett's test.

3.1g. Anandamide increases intracellular Ca^{2+} levels in cortical neuronal cells.

Since the upregulation of intracellular Ca^{2+} is known to be essential for calpain activation⁴⁷ and is a known effect of AEA⁴⁸, we examine effects of AEA on Ca^{2+} levels in cortical neuronal cells (Fig. 23). We used imaging analysis utilizing the fluorescent indicator Fluo-3 for assessment of intracellular free calcium ion concentration. Figure 7 shows significantly increased Ca^{2+} levels in cortical neurons treated with anandamide in the presence of 1 mM extracellular Ca^{2+} , whereas in cells incubated in Ca^{2+} -free solution AEA did not alter intracellular Ca^{2+} concentration. Although baseline measurements appear to have slight fluctuations at approximately 10 sec prior to perfusion of AEA, recorded values were not significantly different from baseline values. Such fluctuation was periodically caused by the proximity of the Y-tubing perfusion system to the region of interest.

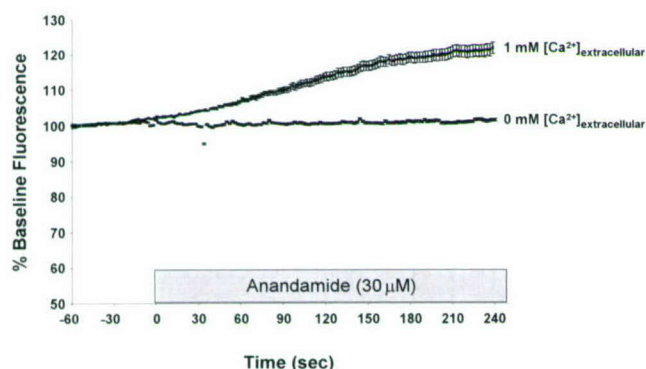


Figure 23. Anandamide increased intracellular Ca^{2+} levels in rat cortical neuronal cells. Cortical neuronal cells cultured on glass coverslips were loaded with 2 μM anandamide in the presence or absence of 1 mM CaCl_2 ; after indicated time periods, Fluo-3 fluorescence was measured using a Sensicam digital fluorescence imaging system. Anandamide significantly increased intracellular calcium from baseline levels in the presence, but not absence, of 1 mM extracellular Ca^{2+} , 30 seconds after initial perfusion; Ca^{2+} levels remained increased throughout the remainder of the experiment ($n=126$, $p<0.05$ compared by ANOVA followed by the Bonferroni/Dunn test. Data are expressed as a percentage of mean baseline control \pm SE.

3.1h. Anandamide reduces mitochondrial membrane potential and causes cytochrome c translocation, which can be attenuated by calpain inhibition.

Next we analyzed whether AEA-induced cell death in cortical neuronal cultures is related to changes in mitochondrial membrane potential and cytochrome c release. Significant decrease in mitochondrial membrane potential was found in anandamide-treated cells, measured by the emission shifts in JC-1 fluorescence (Fig. 24). Moreover, marked upregulation in cytochrome c protein levels was found in the cytosol of the cells incubated with anandamide, as assessed by immunoblot analysis of protein extracts (Fig. 25a). Application of caspase-3 inhibitor z-DEVD-fmk did not change AEA-stimulated cytochrome c translocation, whereas incubation with calpain inhibitor calpastatin significantly reduced upregulation of cytochrome c levels in cytosolic extracts from AEA-treated cortical neurons (Fig. 25b). Additionally, administration of calpastatin significantly decreased anandamide-induced increase in active caspase-3 levels, as revealed by immunoblot assay (Fig. 25c).

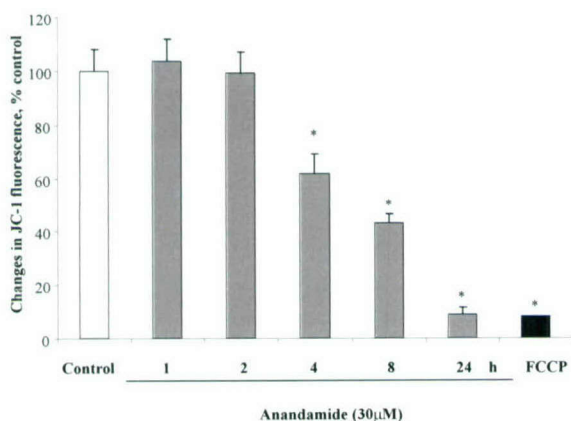


Figure 24. Anandamide-induced changes in mitochondrial potential. Cortical neurons cultured in 24-well plates were incubated for 30 min with JC-1 followed by the addition of 30 μM anandamide. After indicated periods of time, alterations in mitochondrial membrane potential ($\Delta\psi_m$) associated with changes in the red/green fluorescence intensity ratio of JC-1 were measured. Cells treated for 2 h with 10 μM carbonyl cyanide-4-trifluoromethoxyphenylhydrazone (FCCP) were used as positive control for ($\Delta\psi_m$) decrease. The data are representative of 3 separate experiments. Each individual treatment/time point reflects 4 replicates. * $p<0.01$ versus in treated controls compared by ANOVA, followed by the Dunnett's test.

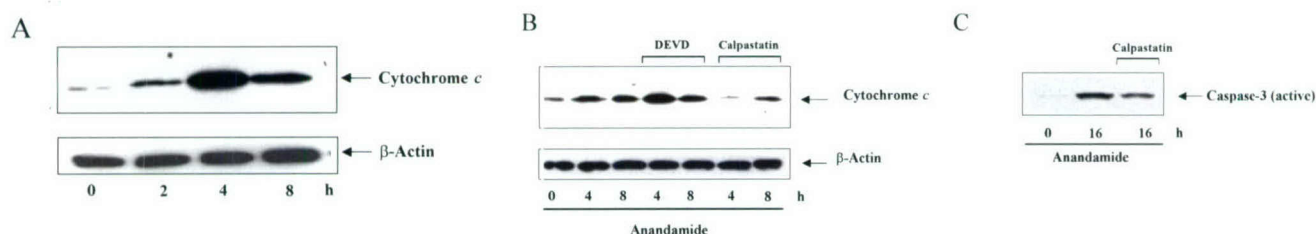


Figure 25. Immunoblot analysis of anandamide-treated rat cortical neuronal cultures showed significant upregulation of cytochrome c protein levels in the cytosol (A). Treatment with calpastatin reduced anandamide-induced cytochrome c release (B). Administration of calpastatin reduced levels of active caspase-3 in anandamide-treated cultures (C). Cultures were treated with 30 μ M anandamide with or without 45 min pretreatment with 150 μ M z-DEVD-fmk or 25 μ M calpastatin and after indicated time period harvested and subjected to immunoblot analysis. β -actin was used as an internal control.

The present findings suggest an important role for calpain in AEA-induced cell death. That AEA-induced calpain activation may contribute to caspase activation, which appeared at later time point in our model, is supported by our finding showing that levels of active caspase-3 can be significantly reduced by calpain inhibition in AEA-treated cortical neurons. This also suggests that anandamide-mediated calpain activation in cortical cultures is upstream of caspase stimulation.

3.2. Neurotoxic Effects of Anandamide *In Vivo*

3.2a. *Traumatic brain injury causes increase in N-acyl-ethanolamine phospholipid (NAPEs) and anandamide concentrations in rat brain.*

We examined whether synthesis or the release of AEA in the brain is altered as a function of brain injury. Concentrations of total N-acyl-ethanolamine phospholipids (NAPE), potential precursors for AEA synthesis, and AEA were measured by gas chromatography/mass spectrometry (See Material & Methods). Total NAPE concentration was 72.93 ± 5.366 pmol/ μ mol P in cortex and 133.32 ± 15.07 in hippocampus, whereas AEA levels were 0.17 ± 0.044 pmol/ μ mol P in cortex and 0.23 ± 0.08 pmol/ μ mol P (average \pm SD; n=7) in sham control animals. Lateral fluid percussion injury in rats caused a rapid and significant sustained increase in N-acyl-ethanolamine phospholipids (NAPE), potential precursors for AEA synthesis, in the traumatized hemisphere (Fig. 26a). This was accompanied by significantly increased levels of AEA in both ipsilateral cortex and hippocampus compared with those in controls, with highest values measured at 4 h post-injury (Fig. 26b).

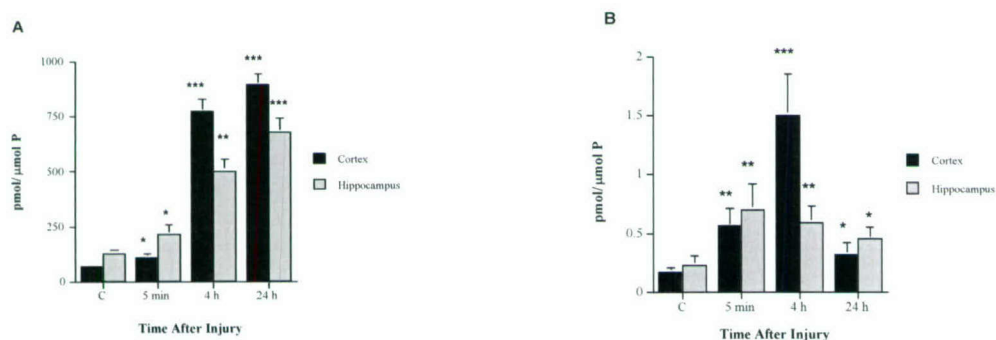


Figure 26. (A) Total N-acyl-ethanolamine phospholipid (NAPE) (B) and N-arachidonoyl-ethanolamine (anandamide, AEA) concentrations in ipsilateral cortex (gray bar) and hippocampus (black bar) 5 minutes, 4 hours and 24 hours after lateral fluid percussion injury in rats. Concentrations of NAPE and AEA were calculated as pmol/ μ mol P, and the statistical comparison was performed using Kruskal-Wallis test combined with Newman-Keul's *post hoc* test. The results are presented as mean \pm SD. At all time points, there was a significant increase in NAPE and AEA concentrations in both brain structures. * $p < 0.05$, ** $p < 0.01$ and *** $p < 0.001$ compared to values in sham-operated animals (C).

To address whether AEA is neurotoxic *in vivo* and the potential mechanisms involved, we administered 20 nM AEA into the right cerebral ventricle in uninjured rats, either alone or in combination with a CB1 receptor antagonist, VR1 receptor antagonist, caspase-3 inhibitor, or a calpain-inhibitor, and monitored edema formation using diffusion-weighted (DWI) magnetic resonance imaging (MRI), as well as working memory in the same animals using the Morris Water Maze and associated cell counts in the hippocampus.

3.2b. Anandamide causes brain edema, which is prevented/reduced by a VR1 antagonist or a calpain inhibitor but not by a caspase-3 inhibitor.

Intracerebral administration of AEA significantly increased apparent diffusion coefficient (ADC) in cortex and subcortex bilaterally. The elevation in ADC levels following AEA administration persisted up to 7 d post-injection, implying sustained vasogenic edema (Fig. 27). Hyperintense area shown on DWI also indicated edema development 24 hours following AEA injection (Fig. 28b). Administration of a VR1 antagonist capsazepine (35 nM/rat icv, 5 min after AEA injection; n=6) prevented AEA-induced ADC increase both in cortex and hippocampus. Injection of the specific CB1 receptor antagonist AM251 into the right cerebral ventricle (35 nM/rat, 5 min after AEA injection; n=6) reduced ADC values significantly below control levels (Fig. 27) in both cortex and hippocampus. Because reduced ADC is often considered as an indicator of cytotoxic edema, these findings may reflect enhanced cytotoxic edema, where block of the CB1 receptors by AM251 may have nullified the proposed neuroprotective action of CB1 receptors¹⁷. However, decreased ADC could also reflect reduced volume of the extracellular space, perhaps caused by astrocytic swelling. AEA-induced increase in ADC was prevented by administration of a calpain inhibitor SJA6017 (1 µg/rat icv, 5 min after AEA injection; n=6) (Fig. 27). Caspase-3 inhibitor z-DEVD-fmk (160 ng/rat icv, 5 min after AEA injection; n=6) prevented the AEA-induced increase in ADC in both cortex and hippocampus following AEA administration (Fig. 27).

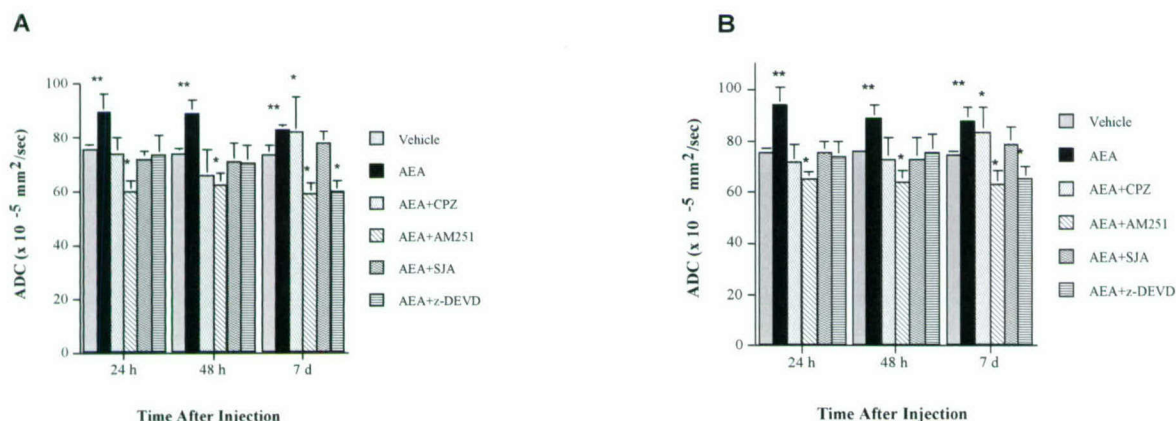


Figure 27. Apparent diffusion coefficient (ADC) measured by diffusion-weighted nuclear magnetic resonance imaging 24 h, 48 h, and 7 d following anandamide/AEA (20 nM) injections into right cerebroventricle (icv) in cortex (A) and hippocampus (B). Drugs were injected icv 5 minutes after AEA administration: vanilloid VR₁ receptor antagonist, capsazepine/CPZ (35 nM); cannabinoid CB₁ receptor antagonist, AM251 (35 nM); calpain inhibitor VI, SJA6017 (1 µg); caspase-3 inhibitor, z-DEVD-fmk (160 ng). Data are expressed as means ± SEM. Comparison between groups were made using ANOVA followed by Tukey's *post hoc* test. *p<0.05, **p<0.01 compared to vehicle treated animals.

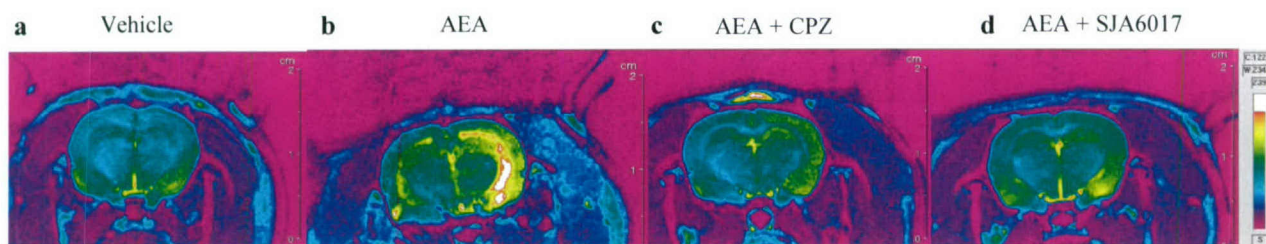


Figure 28. Representative diffusion-weighted images 24 h following intracerebral (icv) injections (right ventricle, 5 μ L final volume) of **a**, saline; **b**, anandamide (AEA; 20 nM); **c**, 5 min after AEA administration, a VR1 antagonist capsazepine (CPZ; 35 nM) was injected into the right ventricle; **d**, a calpain VI inhibitor SJA6017 (1 μ g) was administered icv into right ventricle 5 min after AEA injection. The clearly recognizable hyperintense area (**b**) suggests edema development induced by AEA injection, which was significantly reduced by CPZ (**c**) and SJA6017 (**d**).

Recent results demonstrate that there is a cross-talk between calpain and caspase proteolytic systems during neuronal cell death⁴⁹. Hence, we hypothesize that administration of z-DEVD-fmk early after AEA injection might reduce calpain-activation and the subsequent calpain-related brain edema.

3.2c. *Anandamide causes cognitive deficit, which is prevented by a VR1 antagonist or calpain inhibitor but not by a caspase-3 inhibitor.*

Cognitive performance was measured using the Morris Water Maze, which was performed starting at 17 days after AEA or vehicle administration during 4 consecutive days. The mean latency to locate the platform immersed below the surface of the water for the vehicle treated animals at the end of the 4th training day was 27 ± 1 seconds. In contrast, animals treated with AEA demonstrated a mean latency of 45 ± 5 sec at the same time-point, i.e., 20 days after injection, showing significant cognitive deficit, manifesting as increased latency necessary to find the platform as compared to vehicle controls ($p < 0.01$) (Fig. 29). The CB1 receptor antagonist, AM251, had no significant influence on the Morris Water Maze performance (Fig. 29a), indicating that the CB1 receptor had no significant effect on AEA-induced cognitive deficits. VR1 antagonist capsazepin (Fig. 29b) and calpain inhibitor SJA6017 (Fig. 29c) prevented, whereas specific caspase-3 inhibitor z-DEVD-fmk had not influence on AEA-induced cognitive deficits.

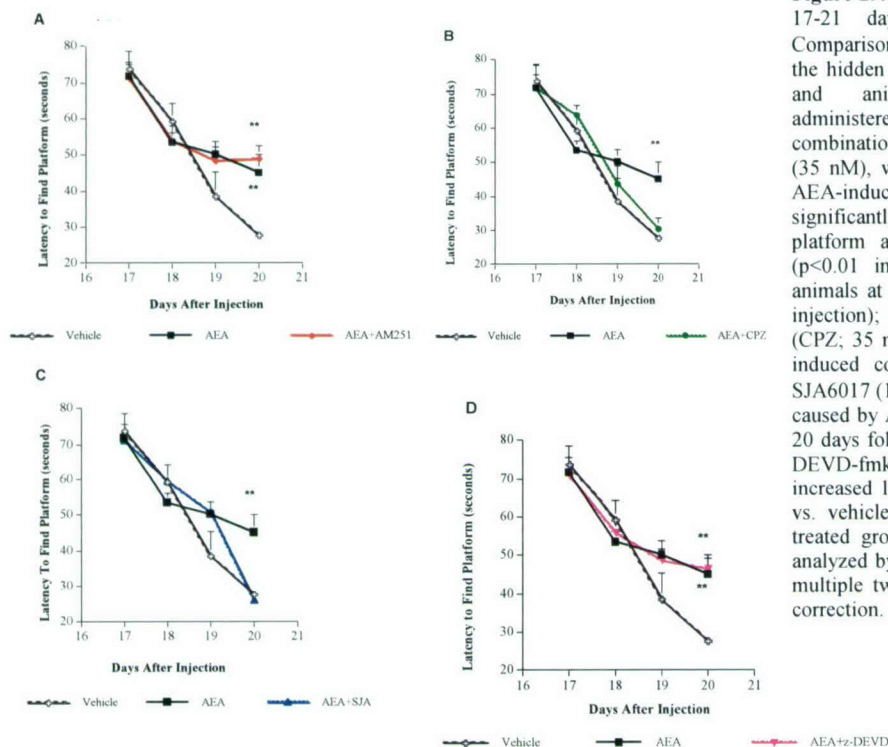


Figure 29. Morris Water Maze performance assessed 17-21 days following injection ($n=10/\text{group}$). Comparison of the mean latency (\pm SEM) to locate the hidden platform between vehicle treated animals and animals with intracerebroventricularly administered anandamide (AEA) alone or in combination with **a**, CB1 receptor antagonist AM251 (35 nM), which had no significant influence on the AEA-induced cognitive deficit, manifesting as significantly increased latency necessary to find the platform as compared to vehicle treated animals ($p<0.01$ in both AEA and AEA+AM251 treated animals at the 4th day of training, i.e., 20 days after injection); **b**, VR1 receptor antagonist capsazepine (CPZ; 35 nM) that successfully prevented the AEA-induced cognitive deficit; **c**, calpain inhibitor VI SJA6017 (1 μg), which prevented the cognitive deficit caused by AEA at the 4th day of the assessment, i.e., 20 days following injection; **d**, caspase-3 inhibitor z-DEVD-fmk (160 ng), which had no influence on the increased latency caused by AEA injection ($p<0.01$ vs. vehicle controls in both AEA- and AEA+CPZ treated groups, 20 days after injection). Data were analyzed by repeated measures ANOVA followed by multiple two-tailed t-tests with Bonferroni (Dunn's) correction.

We hypothesize that although the early given z-DEVD-fmk modified the calpain-induced brain edema, it was unsuccessful in preventing other non-caspase-3 mechanisms (for example, calpain-induced cathepsin release) involved AEA-induced cognitive deficit.

3.2d. Anandamide leads to neuronal cell loss and structural changes, which is prevented/reduced by a VR1 antagonist or calpain inhibitor but not by a caspase-3 inhibitor.

We next examined whether the observed functional deficits and their VR1- and calpain-dependence are related to structural alterations in the brain. T2-weighted MRI showed hyperintense area in right hemisphere, corresponding to the location of hippocampus, dentate gyrus, and cerebral ventricle, 24 h following AEA injection (Fig. 30). Results published by us¹⁴ and others⁵⁰ demonstrated that mechanical brain injury could cause early (<24 h postinjury) alterations in these regions, including ventricles and periventricular regions, although these changes were maximal after several days. Ventricular enlargement was also demonstrated early after intraventricular infusion of N-methyl-D-aspartate into lateral ventricle of adult rats⁵¹; these changes were confirmed by histology. Comparable regions of hyperintensity were not found in the animals treated with CPZ or SJA6017 following AEA administration (Fig. 30).

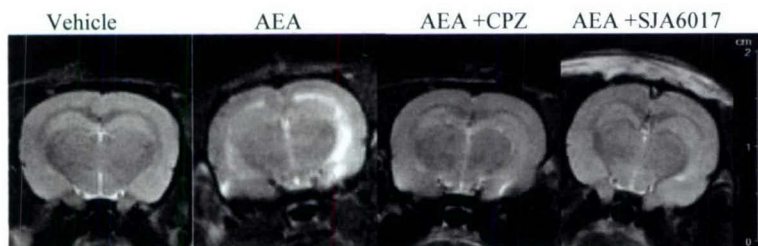


Figure 30. Representative T2-weighted images obtained 24 h after right icv injection of vehicle, AEA (20 nM), AEA with VR1 receptor antagonist CPZ (35 nM), or AEA with calpain VI inhibitor SJA6017 (1 μg). Increased signal intensity (white arrows) shows regions with increased ADC (hippocampus, dentate gyrus, cerebral ventricle) suggesting presence of edema.

To verify further if AEA administration causes hippocampal cell death, we counted the total number of neurons in CA3 region of the ipsilateral hippocampus 24 hours after AEA injection; this region shows preferential cell loss following traumatic brain injury in rats⁵². Significant cell loss was found in AEA-treated animals compared to vehicle controls (254 ± 4 neurons/mm³ vs. 195 ± 4 neurons/mm³; $n=6$ /group) (Fig. 31). The VR1 receptor antagonist CPZ, as well as the calpain inhibitor SJA6017, significantly reduced such neuronal loss. Interestingly, the caspase-3 inhibitor z-DEVD-fmk enhanced the AEA-induced neuronal cell loss in hippocampus, which supports the possibility that inhibition of caspase-dependent apoptosis facilitated the necrotic pathway leading to cell death.

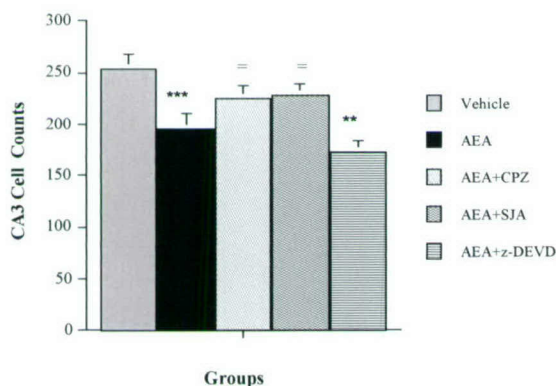


Figure 31. Cell loss 7 d after intracerebroventricular (icv) administration of AEA (20 nM). Cell counts in ipsilateral CA3 hippocampal sub-region are expressed as average \pm SD. Cell count data were analyzed statistically using the *t*-test for independent samples of groups. Icv administration of AEA (20 nM) significantly reduced the number of cells (***) $p < 0.001$ vs. vehicle control) measured 24 h following injection. Treatment with CPZ (35 nM) and SJA6017 (1 μ g) prevented the AEA-induced cell loss (in both group $\dagger p < 0.05$ vs. AEA-treated group). Administration of caspase-3 inhibitor z-DEVD-fmk (160 ng) did not prevent the AEA-induced cell loss (** $p < 0.01$ vs. vehicle control).

3.2e. Anandamide causes alterations of genes involved in inflammation and trophic support.

Since intensity and type of cell death, as well as processes involved in regeneration and plasticity, may be related to alterations in gene expression⁵³, we utilized oligonucleotide microarray hybridization to analyze 8,800 genes using probes prepared from the brain structures (cortex and hippocampus, ipsilateral to the injection) of rats at different time points (24 h, 48 h, 7 d) following AEA administration. Of the 8,800 probe sets represented on each microarray, approximately 50% were maintained in both the cortex and hippocampus following the normalization and scrubbing procedures. Of these 4,500 probe sets retained, 331 (7.4%) probe sets in the cortex and 89 (2.0%) in the hippocampus demonstrated significant changes in expression level (vehicle vs. AEA) at one or more time points, when using > 1.5 -fold change and $p < 0.05$ as criteria for significance. Genes within each region that met these criteria were subjected to hierarchical clustering, producing gene trees. This organizational strategy demonstrated regional differences in temporal mRNA expression following AEA injection, and although each region displayed a unique transcriptional response to AEA, genes involved in inflammation were rapidly upregulated in both regions (Fig. 32a and 32b). Genes in this functional group showing sustained increase in mRNA levels throughout a 7-day post-injection period included major histocompatibility complex (MHC) class II, fractalkine, granulins, and Fc gamma receptor in cortex, and galectin-3 and Ox-44 in hippocampus. Osteopontin and TIMP-1 were found to be upregulated at 24-h and 48-h time points in both brain structures.

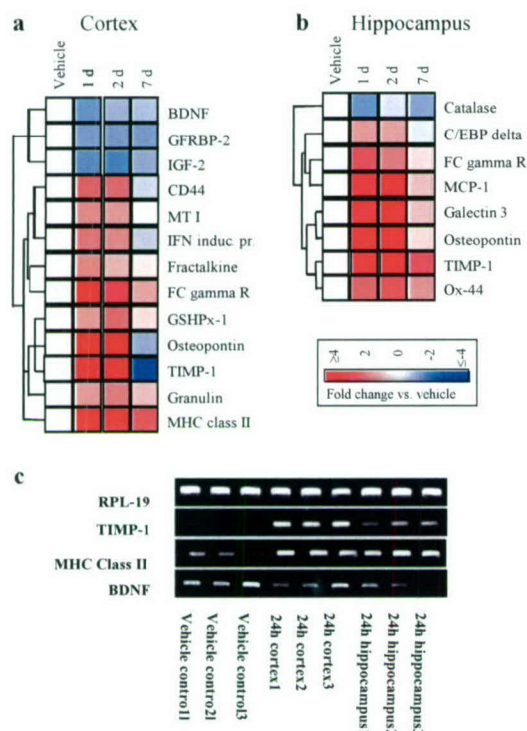


Figure 32. Temporal profile of gene alterations 24 h, 48 h and 7 d ($n=4/\text{time point}$) icv injection of AEA (20 nM) measured by oligonucleotide microarray technique. Signal intensity from each vehicle and AEA-injected microarray is normalized to the mean signal intensity from naïve cortex. Mean of the normalized signal intensity data is calculated for the vehicle microarrays, as well as for the AEA-injected microarrays at each time point. Genes showing at least a 1.5 fold change in one or more time points and a Welch t-test p value < 0.05 between vehicle and AEA-injected groups for at least one time point were considered significant. Genes with significant changes and involved in inflammation and trophic support are shown as a dendrogram. Red indicates upregulation; blue, downregulation of gene expression after AEA injection vs. vehicle injection (white). The color intensity indicates magnitude of induction or repression. **a**, Gene profile alterations in cortex and **b**, hippocampus show significant and sustained upregulation of inflammatory genes after AEA injection (BDNF: brain derived growth factor; GFRBP-2: growth factor receptor bound protein 2; IGF-2: insulin-like growth factor II; MT 1: metallothionein I; INF induc. pr.: interferon inducible protein; FC gamma R: FC gamma receptor; GSHPx-1: glutathione peroxidase; TIMP1: tissue inhibitor of metalloproteinase I; MCP-1: monocyte chemoattractant protein). **c**, Estimation of mRNA level for several genes in cortex and hippocampus 24 h after icv injection of vehicle or AEA (20 nM), using semi-quantitative RT-PCR as a confirmation of gene profile alterations measured by microarray technique.

3.2f. Anandamide upregulates VR1 receptors *in vivo*.

Having established detrimental *in vivo* effects of AEA, we next examined the involvement of VR1 receptors first. Increased expression of VR1 receptors, compared to vehicle controls, was demonstrated by immunocytochemistry 24 h following icv injection of AEA (Fig. 33). Although such an observation may appear contrary to the generally occurring phenomenon of an inverse relationship between receptor binding capacity for hormones/drugs and the concentrations of such ligands, it has not uncommonly been found that exposure of target tissue to increased ligand concentrations may lead to enhanced binding⁵⁴.

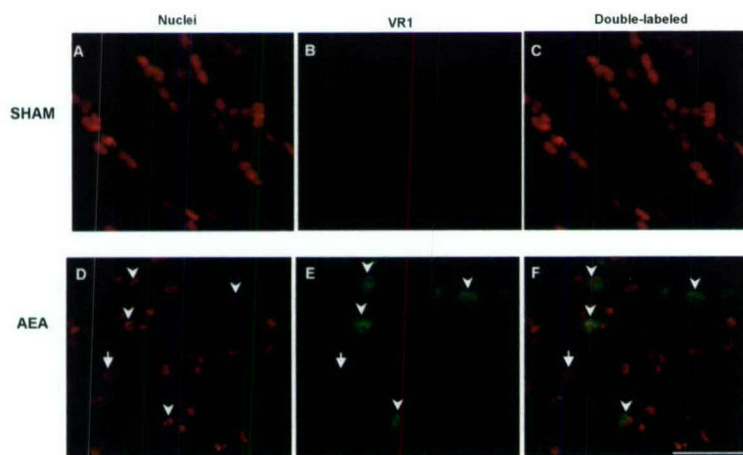


Figure 33. Representative photomicrographs showing expression of VR1 (**B**, **E**) or a DNA marker (**A**, **D**) in cortex of vehicle treated (**A**, **B**, **C**) or AEA-treated (20 nM icv, right ventricle) (**D**, **E**, **F**) rats 24 hours after injection. Green immunofluorescence shows VR1 expression (**B**, **E**), while red fluorescence shows expression of TO-PRO-3, a DNA marker (**A**, **D**). Panels **C** (vehicle) and **F** (AEA) show double-labeled neurons. Immunofluorescence was analyzed using confocal microscope Zeiss LSM 510 META. Expression of VR1 is significantly increased after AEA injection (**E**), especially in cells demonstrating condensed and fragmented chromatin (**F**), as indicated by arrow heads. Normal cells with homogenous chromatin have low expression of VR1 and are indicated by arrows. There are no VR1 positive cells in the cortex of a vehicle-treated animal. Scale bar 50 μm .

3.2g. *VR1 receptor antagonist prevent/reduces AEA-induced brain edema, cognitive deficit or neuronal cell loss in vivo.*

Furthermore, parameters of functional outcome such as changes in water diffusion and cognitive performance were measured after icv administration of capsazepine (CPZ), a VR1 receptor antagonist (35 nM/rat, right cerebral ventricle, 5 min after AEA injection). Blocking VR1 receptors completely normalized ADC values during the first 48 hours after AEA injection (Fig. 27 and 28). Nevertheless, the levels of ADC were again elevated in the CPZ-treated animals at 7-day post-injection, which may reflect the limited duration of the VR1 antagonism achieved by a single injection of CPZ (Fig. 27). Furthermore, the cognitive deficit caused by AEA injection was completely prevented by CPZ (Fig. 29).

3.2h. *Traumatic brain injury upregulates VR1 receptors.*

Bearing in mind that VR1 is activated not only by vanilloid ligands but also by low pH, and increased calcium concentration⁵⁵, it seemed feasible that such a system may be upregulated after TBI. To ascertain if this is the case, we used microchip gene expression analysis to screen for the vanilloid receptor subtype 1 (VR1) gene following traumatic brain injury. We demonstrated increased expression of VR1 gene in the cortex and hippocampus after traumatic brain injury (Fig 34). Expression was maximal in the cortex during the first few hours postinjury, coincident with the time point associated with maximum blood brain barrier permeability in this model of trauma (lateral fluid percussion injury), while sustained upregulation of VR1 was shown in hippocampus.

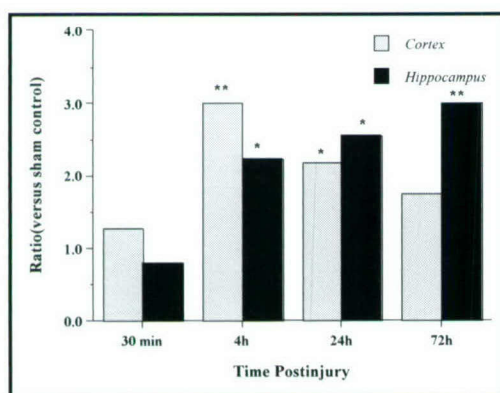


Figure 34. Ratio of VR1 gene expression versus sham control in cortex and hippocampus following lateral fluid percussion injury in rats (Injured : n = 4 / time point and Vehicle / Sham: n = 3 / time point. Gene profiling by oligonucleotide microarray was performed as previously described by us (Natale et al, 2003).

3.2i. *Inhibition of caspase-3 does not prevent/reduce AEA-induced brain edema, cognitive deficit or neuronal cell loss in vivo.*

Extensive studies have now shown that tissue damage after brain trauma results in both apoptotic and necrotic types of neuronal cell death. The cells that die within the first 24 h after the injury are thought to do so primarily by necrosis, while the cells that die at much later time points (24-72 h) are thought to undergo a process known as apoptosis⁵⁶. Both types of cell death are believed to proceed in parallel in the lesion tissue and, at times, cannot be differentiated as two separate entities⁵⁷. Indeed, there is now evidence to suggest that a switch between the two types of cell death can occur within a single cell depending on the cellular environment and energy supply⁵⁸. Neuronal apoptosis after TBI is often associated with activation of caspase-3, and is attenuated by treatment with the caspase antagonist z-DEVD-fmk⁵⁹. To elucidate whether caspase-3-mediated apoptosis is associated

with AEA-induced neurological dysfunction, we examined the ability of z-DEVD-fmk to alter the changes in ADC and cognitive function following AEA injection. z-DEVD-fmk, at a dose shown to provide neuroprotection after TBI in rats ⁵⁹ (160 ng icv), was administered 5 minutes after icv injection of AEA; such treatment normalized the ADC in the observed brain structures during the first 48 hours following AEA injection. However, there was a significant reduction in ADC below baseline levels in z-DEVD-fmk treated animals at 7-days post-injection suggesting cytotoxic edema (Fig. 27).

Treatment with z-DEVD-fmk also failed to prevent the AEA-induced cognitive deficit (Fig. 29d). Importantly, neither immunocytochemistry (data not shown) nor immunoblotting showed caspase-3 (Fig. 35) or caspase-9 activation (data not shown) following AEA-administration. Additionally, a caspase activity assay demonstrated no changes in caspase activity in ipsilateral hippocampus 24 h following AEA injection (Fig. 36). Consistent with the caspase inhibition studies, these findings indicate that the AEA-induced functional deficits are unlikely to be related to caspase-3-mediated apoptosis.

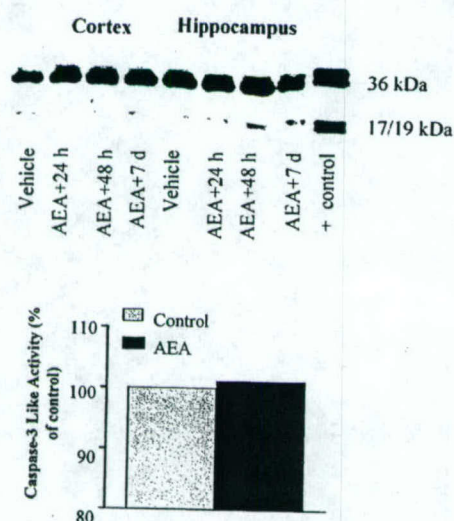


Figure 35. Temporal expression of pro-caspase and caspase-3 cleavage fragments in ipsilateral parietal cortex and hippocampus after icv administration of vehicle or anandamide (20 nM), measured by immunoblot at various times after injury (24 h-7 d). A blot shows results from one animal at each time point, which is representative of results obtained from all animals in each group (n=3 rats/group). Vehicle treated animals served as controls. The molecular weight of each cleavage fragment is shown on the right. Bands corresponding to a 35-kDa pro-form and a 17-kDa cleavage fragment are present in positive control but not in cortex and hippocampus of treated animals:

Figure 36. Caspase-3 activity

is shown in ipsilateral hippocampus 24 h after injection of 20 nM anandamide into right cerebral ventricle. Activity measured in AEA animals (n=7) is expressed as % of activity measured in naïve (n=7) and vehicle-injected controls (n=5) processed identically and in the same assay. Two-tailed Mann-Whitney U test was used to compare the AEA-treated group vs. control. Activity observed in naïve and vehicle injected controls was not statistically different.

3.2j. Calpain inhibition prevent/reduces AEA-induced brain edema, cognitive deficit or neuronal cell loss.

Intracellular accumulation of excessive levels of calcium has long been considered as an essential part of the final common pathway leading to neuronal cell death following CNS injury ⁶⁰. This has been mainly due to the recognition that calcium is a ubiquitous second messenger whose intracellular excess can initiate a series of destructive enzymatic processes ⁶¹. Our preliminary *in vitro* data show that AEA leads to a significant increase in intracellular calcium concentration (Fig. 23). Our *in vivo* results demonstrate that a calpain inhibitor SJA6017 prevents AEA-induced brain edema (Fig. 27 and 28), cell loss (Fig. 31) and cognitive deficit (Fig. 29). Furthermore, increased expression of spectrin, the calpain breakdown product (not shown), and increased calpain activity (Fig. 37) was shown in ipsilateral hippocampus 24 h after injection of 20 nM AEA into right cerebral ventricle.

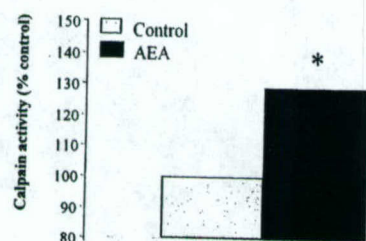


Figure 37. Calpain activity measured in anandamide (AEA, 20 nM icv)-treated animals (n=7) is expressed as % of activity measured in naïve (n=7) and vehicle injected controls (n=5) processed identically and in the same assay. *p=0.001 by two-tailed Mann-Whitney U comparison of AEA versus control. Activity observed in naïve and vehicle injected controls was not statistically different.

In conclusion, our results demonstrate neurotoxic effects of anandamide, which are at least in part mediated through VR1 receptors and most probably calpain activation. Furthermore, the increased vasogenic edema and the gene profiling changes induced by AEA suggest that AEA may initiate a neurogenic inflammation. Therefore, it is plausible to expect that in the situations of increased AEA synthesis and release, such as TBI, this particular mediator exhibit neurotoxic effects leading to neuronal cell death and subsequent neurological deficit.

4. Metabotropic Glutamate Receptors

Metabotropic glutamate receptors (mGluR) family includes eight G-protein coupled receptors subtypes that have been separated into three major groups on the basis of structural homology, mechanisms of signal transduction, and pharmacological properties^{62, 63}. Group I mGluR include type 1 and type 5 receptors. Stimulation of both mGluR1 and mGluR5 leads to activation of phospholipase C, with phosphoinositide {PI} hydrolysis and mobilization of intracellular calcium^{62, 63}. Despite similar signal transduction pathways, mGluR1 and mGluR5 show considerable differences with regard to modulation of neuronal injury. Using selective mGluR1 antagonists or antisense oligonucleotides directed at mGluR1 or mGluR5, it has been shown that mGluR1 inhibition is neuroprotective in both in vitro and in vivo injury models⁶⁴⁻⁶⁶ (Fig. 38). In contrast, inhibition of mGluR5 by selective antagonists does not provide neuroprotection except at high concentrations that block NMDA receptors⁶⁶⁻⁶⁸. However, activation of mGluR5 is neuroprotective in cell culture models of neuronal apoptosis induced by etoposide or staurosporine⁶⁹ (Fig. 39-40).

Apoptotic cell death has been implicated in the pathophysiology of both acute and chronic neurodegenerative disorders. Neuronal degeneration associated with Alzheimer's disease is believed to result, in part, from apoptotic cell death triggered by accumulation of β -amyloid peptide⁷⁰⁻⁷³. Recently we explore the effects of mGluR5 modulation on neuronal apoptosis induced by β -amyloid using in vitro model of β -amyloid neurotoxicity in rat cortical neuronal cultures. We found that selective activation of mGluR5 significantly reduced the number of cells with apoptotic morphology and attenuated cell death in cortical neuronal cultures subjected to β -amyloid toxicity (Fig. 41-42).

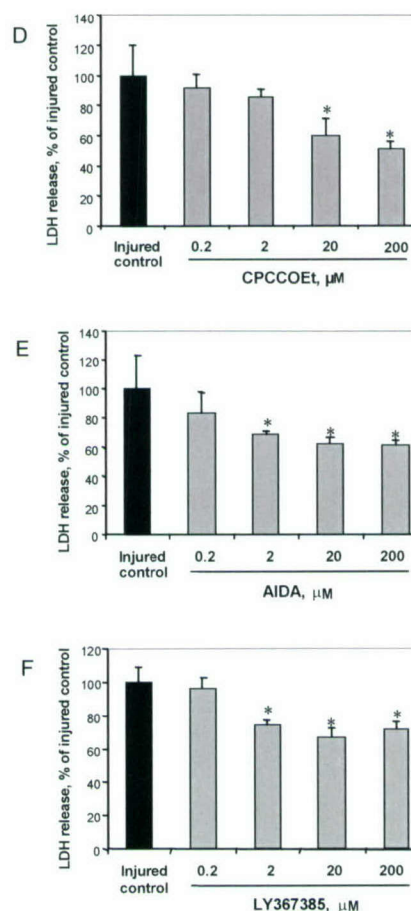


Fig. 38. A) Effect of selective mGluR1 antagonists on recovery of motor function in rats after TBI. AIDA-treated animals showed significantly higher composite neuroscores than controls at 2 wk. Histograms represent mean composite neurological scores at indicated times after TBI \pm SEM. ** $P < 0.01$ versus vehicle-treated controls. B) Representative MRI T2-weighted images of control and mGluR1 antagonist treated rat brains at day 21 after TBI. C) AIDA and MCPG treated animals showed significantly smaller lesion volumes after TBI. Histograms reflect average lesion volume (μ L) \pm SEM. * $p < 0.05$ versus vehicle-treated controls; Pretreatment with mGluR1 antagonists attenuated injury-induced LDH release in rat cortical neuronal cultures. At 7 DIV indicated concentrations of CPCOEt (D), AIDA (E) or LY367385 (F) were added to cultures 30 min prior to mechanical injury. LDH release was measured after 24 hours of treatment. Histograms represent LDH release as percentage of injured control \pm SD, $n = 8$ to 16 cultures per condition. *, $P < 0.05$ versus injured control compared by ANOVA, followed by the Student-Newman-Keuls test.

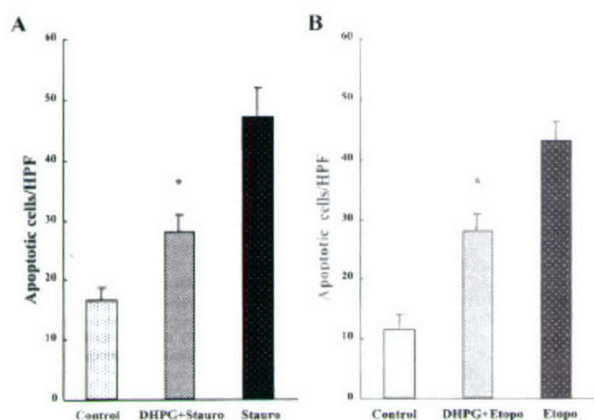


Fig. 39: Group I mGluR activation significantly reduces the number of apoptotic cells following staurosporine or etoposide treatment. (A) Staurosporine-induced increases in cells containing condensed or fragmented nuclei stained by Hoechst 33258 is significantly attenuated by application of DHPG (50 μ M). (B) DHPG (50 μ M) also reduces the number of apoptotic cells after etoposide treatment. Cell counts performed at 400 x by selecting a random field. Bars represent mean \pm SEM, $n=5-11$ cultures per condition. * $P<0.05$ vs. staurosporine (A) or etoposide (B) treatment. HPF = high power field.

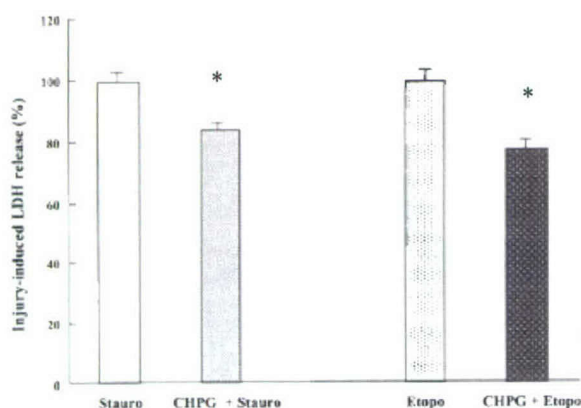


Fig. 40: Selective activation of mGluR5 protects against staurosporine- or etoposide-induced cell death. Application of CHPG (20 μ M) during treatment with staurosporine (Stauro) or etoposide (Etopo) significantly reduces LDH release at 24 h. Bars represent mean \pm S.E.M., $n=21-24$ cultures per condition. Data expressed as a percentage of staurosporine- or etoposide-induced LDH release. * $P<0.001$ vs staurosporine or etoposide treatment (Student's t-test).

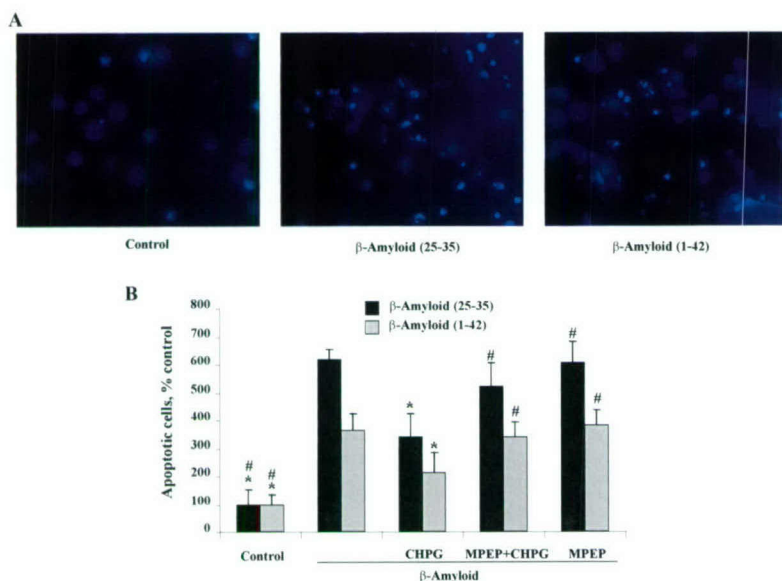


Fig. 41. (A) Representative images of control and β -amyloid-treated rat cortical neuronal cells stained by Hoechst 33258. At 7 DIV, cortical neuronal cultures were treated with 25 μ M A- β (25-35) or A- β (1-42) for 48 h; cells were fixed in 4% formaldehyde, stained with Hoechst 33258 and visualized by fluorescent microscopy. (B) Pretreatment with the mGluR5 agonist, CHPG, significantly decreased the number of cells with apoptotic morphology in β -amyloid-treated rat cortical neuronal cultures. The protective effect of CHPG was attenuated by the mGluR5 antagonist, MPEP. At 7 DIV, 1mM CHPG, with or without 15 min pretreatment with 2 μ M MPEP was added to cultures 15 min prior to addition of 25 μ M of A- β (25-35) or A- β (1-42). After 48 h of treatment cells were stained with Hoechst 33258, and the number of cells with apoptotic morphology for each treatment was counted in 5-7 randomly chosen fields using fluorescent microscopy. Histograms indicate number of apoptotic cells as a percentage of controls \pm SD; *, $P<0.01$ versus A- β -injured controls, #, $P<0.05$ versus A- β + CHPG compared by ANOVA, followed by the Dunnett's test.

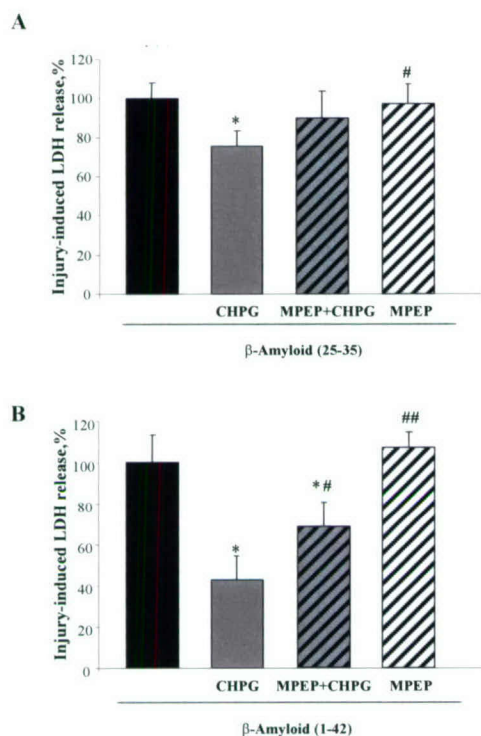


Fig 42. (A) Pretreatment with the mGluR5 agonist, CHPG, significantly decreased β -amyloid-induced LDH release in rat cortical neuronal cultures. The protective effect of CHPG was attenuated by the mGluR5 antagonist, MPEP. At 7 DIV, 1 mM CHPG, with or without 15 min pretreatment with 2 μ M MPEP, was added to cultures 15 min prior to addition of 25 μ M of β -amyloid peptide (25-35). (B) MGLuR5 agonist, CHPG, significantly attenuated β -amyloid (1-42)-induced LDH release in rat cortical neuronal cultures. The protective effect of CHPG was significantly reduced by the mGluR5 antagonist, MPEP. At 7 DIV, 1 mM CHPG, with or without 15 min pretreatment with 2 μ M MPEP, was added to cultures 15 min prior to addition of 25 μ M of β -amyloid peptide (1-42). LDH release was measured after 48 h of treatment. Histograms indicate LDH release as percentage of β -amyloid-injured controls \pm SD; $n = 8$ to 16 cultures per condition; *, $P < 0.05$, **, $P < 0.01$ versus A- β -injured controls, #, $P < 0.05$, ##, $P < 0.01$ versus A- β + CHPG compared by ANOVA, followed by the Dunnett's test.

This observation extends our previous finding showing that mGluR5 activation by its agonist CHPG significantly reduces cell death in neuronal/glial cultures subjected to apoptosis by treatment with staurosporine or etoposide⁶⁹. Staurosporine and etoposide induced apoptosis are highly caspase-3-dependent; β -amyloid toxicity is also associated with activation of multiple caspases and can be partially attenuated by a caspase-3 inhibitor⁷⁴. It is widely accepted that cytochrome *c* released from mitochondria is critical for the formation of the apoptosome, a complex of cytochrome *c* with Apaf-1 and dATP, which binds and activates procaspase-9, leading to subsequent activation of caspase-3 and associated apoptosis⁷⁵. We demonstrated that β -amyloid-induced cell death was associated with cytochrome *c* release and caspase-3 cleavage/activation. CHPG attenuated both cytochrome *c* release and caspase-3 activation (Fig. 43A,B, Fig. 43C). We have also found that β -amyloid-induced neuronal loss in cortical cultures is associated with significant increases in cytosolic levels of apoptosis – inducing factor (AIF) (Fig. 43A, Fig. 44). AIF is a mitochondrial protein, whose translocation to the nucleus appears to mediate caspase-independent apoptosis in a number of model systems⁷⁶⁻⁸¹. Release/translocation of AIF in cultured cortical neurons subjected to β -amyloid toxicity does not appear to be dependent on caspase activation, as it was not altered by either a pancaspase or caspase-3 inhibition. In contrast, treatment with the pancaspase inhibitor Boc-D-fmk markedly reduced cytochrome *c* release in the same system (Fig. 43C). This effect may be caused by inhibition of caspase-8 and/or caspase-2, which act upstream and can regulate cytochrome *c* release through interaction with Bid⁸²⁻⁸⁴. Our findings suggest that β -amyloid toxicity may result not only from caspase-mediated, but also from caspase-independent apoptosis. This conclusion is consistent with our results showing that caspase inhibition provides only partial protection against β -amyloid cytotoxicity. Our study also demonstrated that stimulation of mGluR5 caused a marked decrease in translocation of cytochrome *c* and reduction of active caspase-3 in β -amyloid-treated cells. Moreover, CHPG attenuated β -amyloid-induced increase in AIF release (Fig. 45). Thus, mGluR5 modulation may limit

not only caspase-mediated cell death, but may also modify caspase-independent pathway/s of cellular apoptosis.

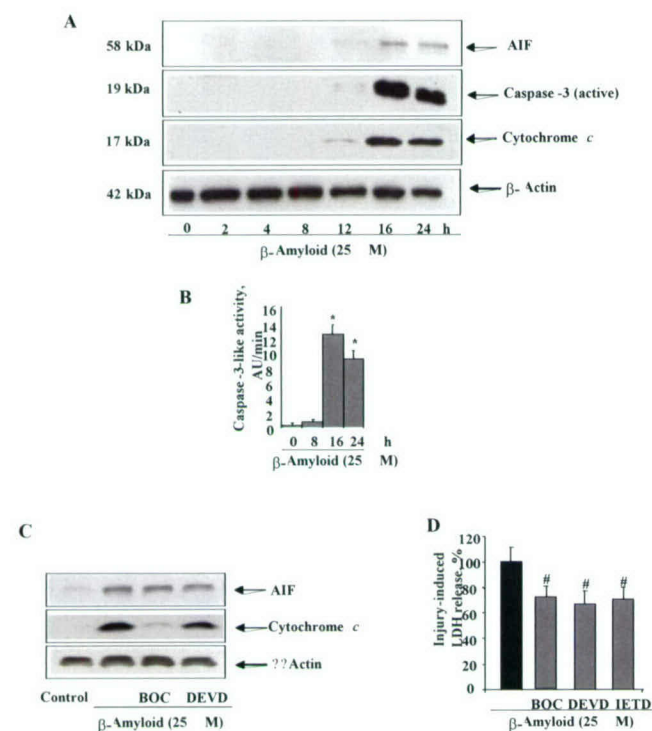


Figure 43. (A) Immunoblot analysis of β -amyloid-treated rat cortical neuronal cultures revealed upregulation of cytochrome c, AIF and active caspase-3 protein levels. At 7 DIV, cultures were treated with 25 μ M of β -amyloid peptide (25-35). Images are representative of immunoblot analysis of samples from three separate experiments. (B) β -amyloid significantly upregulated caspase-3-like activity in rat cortical neuronal cells. Cultures were treated with 25 μ M of β -amyloid peptide (25-35). Histograms represent caspase-3-like activity as a percentage of the activity in control cells; * $p < 0.01$ versus untreated controls, Student's two-tailed t -test. (C) Pretreatment with pan-caspase inhibitor, Boc-D-fmk or caspase-3 inhibitor, z-DEVD-fmk does not alter translocation of AIF but reduces cytochrome c release in cultures treated with β -amyloid. At 7 DIV, 25 μ M of β -amyloid peptide (25-35) with or without 1 h pretreatment with Boc-D-fmk or z-DEVD-fmk (each at 150 μ M) was added to rat cortical neuronal cultures. After 16 h of treatment cells were harvested and subjected to immunoblot analysis. Images are representative of immunoblot analysis of samples from three separate experiments. (D) Pretreatment with the pan-caspase inhibitor, Boc-D-fmk, caspase-3 inhibitor, z-DEVD-fmk, or the caspase-8 inhibitor, z-IETD-fmk attenuated β -amyloid-induced LDH release in rat cortical neuronal cultures. At 7 DIV, 25 μ M of β -amyloid peptide (25-35) with or without 1 h pretreatment with the caspase inhibitors (each at 150 μ M) was added to cultures. LDH release was measured after 32 h of treatment. Histograms indicate LDH release as percentage of β -amyloid-injured controls \pm SD; $n = 8$ to 16 cultures per condition; #, $P < 0.05$ versus β -amyloid-injured controls compared by ANOVA, followed by the Dunnett's test.

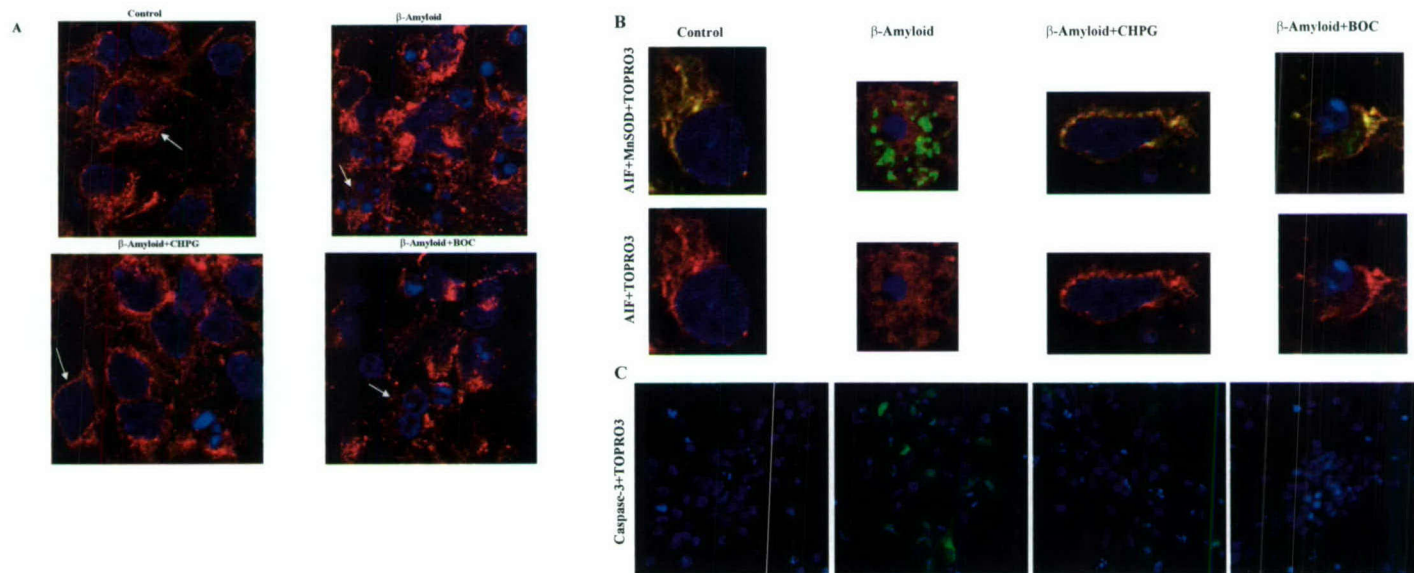


Figure 44. Treatment with β -amyloid caused translocation of AIF into the cytosol/ nucleus and activation of caspase-3. Co-administration of CHPG with β -amyloid attenuated AIF translocation and caspase-3 activation. Pretreatment with pancaspase inhibitor Boc-D-fmk prevented activation of caspase-3 but did not alter the release of AIF. At 7 DIV, 25 μ M of β -amyloid peptide (25-35), with or without 1 h pretreatment with Boc-D-fmk (150 μ M) or 15 min pretreatment with CHPG (1 mM), was added to rat cortical neuronal cultures. After 18 h of treatment cells were subjected to immunolabeling with various antibodies and chromatin staining with TO-PRO-3. Panel (A) illustrates staining with anti-AIF (red) and TO-PRO-3 (blue). Panel (B) represents staining with anti-AIF (red), anti-Mn SOD (green) and TO-PRO-3 (blue). Panel (C) represents staining with anti-cleaved-caspase-3 (green) and TO-PRO-3 (blue). Arrows indicate cells undergoing characteristic changes.

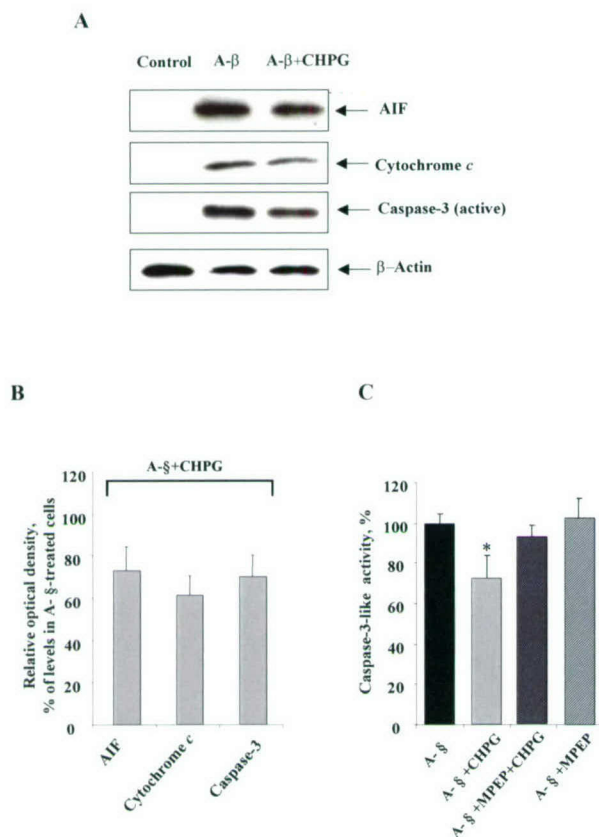


Figure 45. (A) CHPG attenuated release of AIF and cytochrome *c* and decreased active caspase-3 immunoreactivity in β -amyloid-treated rat cortical neurons. At 7 DIV, cultures were treated with 25 μ M β -amyloid peptide (25-35) (A- β) with or without 15 min pretreatment with 1 mM CHPG; after 16 h of incubation cells were harvested and subjected to immunoblot analysis as described in Materials and Methods. Images are representative of immunoblot analysis of samples from three separate experiments. (B) Relative optical density of bands revealed by immunoblot analysis have been analyzed using Scion Image software and presented as a percentage of the levels in A- β -treated cells. Histograms represent optical density analysis of samples from three separate experiments. (C) Treatment with CHPG decreased β -amyloid-induced caspase-3-like activity in rat cortical neuronal cells. At 7 DIV, 1mM CHPG, with or without 15 min pretreatment with 2 μ M MPEP, was added to cultures 15 min prior to addition of 25 μ M of β -amyloid peptide (25-35); after 16 h of incubation, caspase-3-like activity was measured fluorometrically as described in Materials and Methods. Histograms represent caspase-3-like activity as a percentage of the activity in β -amyloid-treated cells \pm SD; $n = 6-8$ cultures per condition; * $p < 0.05$ versus cells treated with β -amyloid only compared by Student's two-tailed *t*-test.

In conclusion, taken together, these data demonstrate that activation of mGluR5 may provide neuroprotection against A- β -induced neuronal cell death through multiple mechanisms and suggest a potential therapeutic role for mGluR5 agonists in the treatment of β -amyloid-induced neuronal degeneration.

5. In vitro Axonal Injury

Combined use of in vitro and in vivo trauma and ischemia models, along with other *in vitro* neuronal injury models, can be used to elucidate molecular mechanisms of apoptotic cell death—particularly to elucidate the role of regulatory and effector caspases, as well as their upstream and downstream signal transduction pathways.

It is well established that traumatic brain injury (TBI) and associated diffuse axonal injury (DAI) cause severe neurological disorders or death in both pediatric and adult human subjects with underlying age-dependent differences^{85, 86}. However, the intimate relationship between mediating biomechanical, and modulating biochemical events underlying DAI remain unclear. Since *in vivo* models of DAI inherently possess multiple confounding variables, which complicate mechanistic studies, *in vitro* traumatic neuronal injury (TNI) models that apply stretch (strain) to primary tissue cultures in an effort to study mechanisms underlying DAI have been developed^{40, 87-89}. Of these models, only the Ellis Model⁴⁰ has been extensively utilized by multiple laboratories. Following the successful integration of this *in vitro* traumatic neuronal injury (TNI) device (Fig. 46)⁴⁰ into our repertoire, we tested the hypothesis that PKC-associated-group I metabotropic glutamate receptors (mGluRs) are involved in this model of injury. This hypothesis was derived from an earlier study in which mild stretch-injury was shown to enhance NMDA receptor activity by reducing the voltage-dependent Mg^{2+} block⁹⁰. The effects of this stretch-induced enhancement of NMDA receptor activity were partially reversed by the PKC inhibitor calphostin C⁹⁰. Group I mGluR mediate their signaling, in part, through the activation of PKC.

Using cultures where neurons were plated in either the absence (PN) or presence (NG) of a glial monolayer, we 1) confirmed the stretch-induced change in the Mg^{2+} block⁹⁰, 2) discovered that glia are not essential for the stretch-induced enhancement of neuronal NMDA receptors to occur, 3) found a significant stretch-induced increase in maximal NMDA receptor current (current measured in the absence of extracellular Mg^{2+}) that was dependent upon group I mGluR activation and influenced by the presence or absence of a glial monolayer^{91, 92} (Figs. 47-49), and 4) found that stretch injury alters the kinetic behavior of NMDA receptors as demarcated by a change in peak/steady state current ratio⁹¹. Changes in NMDA current can occur through several potential mechanisms including: PKC-mediated enhancement of NMDA receptor activity, or changes in the polymerization state of the actin cytoskeleton mediated by either the calcium/calmodulin pathway or through alterations in $[Ca^{2+}]_i$ ⁹³⁻⁹⁹. Moreover, increases in maximal NMDA receptor current can occur

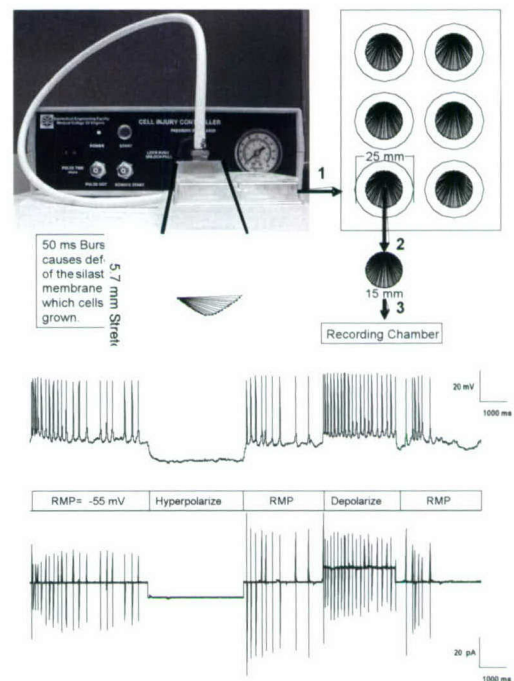


Fig. 46 The Ellis device and protocol. A) 1. Following 5.7 mm stretch of the silastic membrane to which the cultures adhered, cultures were returned to the incubator for at least one hour prior to recording. 2) After one hour post-injury incubation, a 15 mm portion of the silastic membrane was punched out of one 25 mm diameter well in the six well stretch plate. 3) The 15 mm membrane was transferred to a recording chamber undergoing continuous perfusion. B) A single control experiment demonstrating spontaneous synaptic activity, a normal resting membrane potential and the ability to induce action potentials in a cell from the 15 mm portion of silastic membrane. Cellular responses (upper panel) to current injection (lower panel) show that in the absence of current injection, cells exhibit normal resting membrane potentials (RMP), in addition to spontaneous synaptic activity. Hyperpolarization blocked spontaneous synaptic activity, and depolarization of the membrane induced a train of action potentials (depolarization, upper trace).

by modulatory changes in the expression of NMDA receptors, increases in peak open probability, or a change in receptor subtype expression with different open probabilities¹⁰⁰. These latter three possibilities reflect a change in NMDA current density.

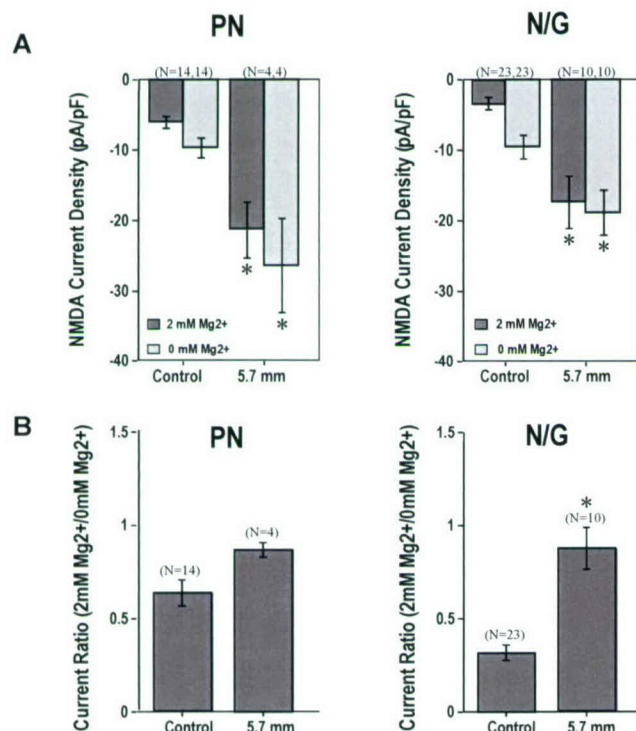


Fig. 47. Effects of stretch-injury on NMDA receptor activity. A) Mild stretch increased INMDA in both the presence ($p < 0.05$; ANOVA) and absence ($p < 0.05$; ANOVA) of 2 mM extracellular MgCl₂ and in both rat cortical neurons cultured in the presence (NG) and absence (PN) of a glial monolayer. B) In NG, mild stretch significantly increased the ratio of INMDA measured in the presence to that measured in the absence of 2 mM extracellular MgCl₂ ($p < 0.05$; ANOVA). The ratio in PN did not reach significance ($p > 0.05$; ANOVA). Ratios in control PN were significantly different from control NG ($p < 0.05$; ANOVA). Whole cell currents were recorded from 14-25 DIV cultured cortical neurons voltage clamped at -60 mV. *Significant differences from controls.

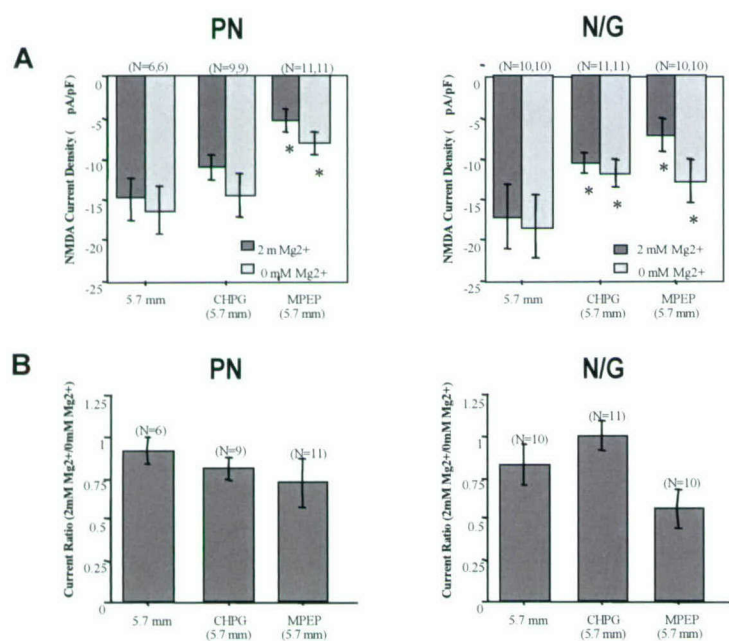


Fig. 48. Effects of mGluR1 modulation prior to mild stretch-injury. A) Pretreatment of NG cortical neurons with MPEP followed by DHPG caused a significant reduction in mild stretch-enhanced INMDA measured in the presence ($p < 0.05$; ANOVA), but not absence ($p > 0.05$; ANOVA) of 2 mM extracellular MgCl₂. Pretreatment of PN ($p < 0.05$; ANOVA), but not NG ($p > 0.05$; ANOVA) cortical neurons with CPCCOEt caused a significant reduction in mild stretch-enhanced INMDA measured in the presence and absence of 2 mM extracellular MgCl₂. B) Pretreatment with CPCCOEt alone caused a significant increase in the mild stretch-enhanced ratio of INMDA in NG cortical neurons ($p < 0.05$; ANOVA) and a significant decrease in PN cortical neurons ($p < 0.05$; ANOVA). PN ratios measured after pretreatment with CPCCOEt and post-stretch injury were similar to non-stretched control levels ($p > 0.05$; ANOVA). Whole cell currents were recorded from 14-25 DIV cultured cortical neurons voltage clamped at -60 mV. *Significant differences from mild (5.7 mm) stretched neurons.

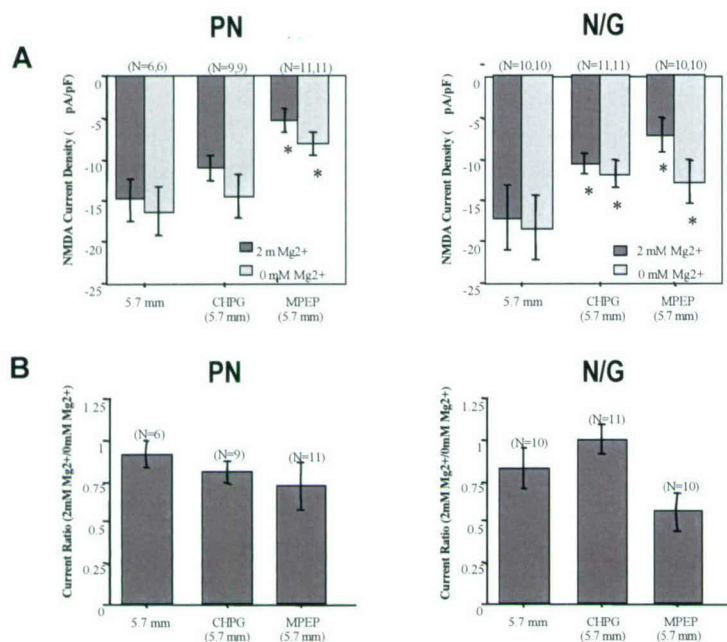


Fig. 49 Effects of mGluR5 modulation prior to 5.7 mm stretch-injury. A) Pretreatment of NG, but not PN, cortical neurons with the mGluR5 agonist CHPG (1 mM) caused a significant reduction in the enhanced NMDA inward current seen after 5.7 mm stretch ($p < 0.05$; ANOVA). Pretreatment of both NG and PN cortical neurons with the mGluR5 antagonist MPEP (2 μ M) caused a significant reduction in the enhanced NMDA inward current seen after 5.7 mm stretch ($p < 0.05$; ANOVA). B) Neither pretreatment with CHPG nor MPEP had any significant effect on the ratio of (INMDA) measured after 5.7 mm stretch ($p > 0.05$; ANOVA) although significant differences were found between CHPG and MPEP treated NG neurons (\dagger ; $p < 0.05$; ANOVA). Whole cell currents were recorded from 14-25 DIV cultured cortical neurons voltage clamped at -60 mV. *Significant differences from 5.7 mm stretched neurons.

Neuronal and Glial mGluR modulate NMDAR activity—Our findings support the prediction that group I mGluR1 and mGluR5 subtypes may differentially utilize multiple mechanisms to affect changes in NMDA receptor current¹⁰¹⁻¹⁰⁴. Furthermore, our findings suggest that both glial and neuronal mGluR participate in this process. We acquired strong evidence that group I mGluR modulate NMDA receptor activity through an unidentified glial/neuronal interaction. First, by inhibiting the mGluR5 subtype with the specific antagonist MPEP followed by activation of mGluR1 with the nonspecific group I mGluR agonist DHPG (currently no specific agonists for mGluR1 exist), we found that in PN cultures (no glial monolayer) activation of mGluR1 had no effect on stretch-induced enhancement of rat cortical neuronal NMDA receptor activity. In contrast, in NG culture neurons (glial monolayer present), mGluR1 activation prevented this enhancement. Second, inhibition of mGluR1 with the specific antagonist CPCCOEt had opposite effects. mGluR1 inhibition prevented the enhancement of NMDA receptor activity in PN, but not NG neurons⁹¹. Third, while activation of mGluR1 had no effect on the stretch-reduced Mg²⁺ block in either PN or NG neurons, mGluR1 inhibition prevented this reduction in PN neurons, and exacerbated the reduction in NG neurons⁹¹. Combined, our findings suggest that both neuronal and glial mGluR1 modulate neuronal NMDA receptor activity and that glial mGluR1 work through an as yet unidentified mechanism to regulate the neuronal NMDA receptor Mg²⁺ block (Fig. 48). In support of a role for glial mGluR1, we demonstrated that indeed mGluR1 are expressed in glia allowed to grow to a confluent monolayer (Fig. 50).

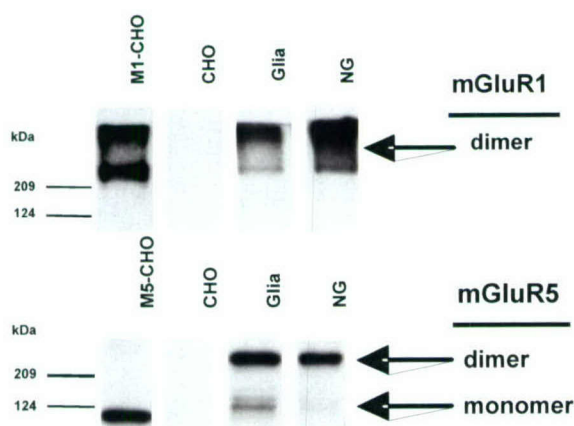


Fig. 50 Glial and NG cultures derived from rat cortices express both mGluR1 and mGluR5. A) Western blot analysis of Chinese Hamster Ovary (CHO) cells, CHO cells expressing mGluR1 or mGluR5, glia and neuronal/glial (NG) cells derived from rat cortices using antibodies selective for mGluR1a or mGluR5. The mGluR1 receptor migrated to a position consistent with approximately twice the predicted molecular mass in both CHO expressing mGluR1 cells, glia and NG. B) In CHO expressing mGluR5 cells, mGluR5 migrated to a position shifted from the predicted molecular mass of the monomeric form of the receptor (128 kDa), whereas, in glia and NG, the mGluR5 receptor migrated to both a position consistent with approximately twice the predicted molecular mass and a position similar to that found in the CHO-expressing mGluR5 cells.

Similar to mGluR1, our data strongly suggest that both glial and neuronal mGluR5 can modulate NMDA receptor activity as well. First, activation of mGluR5 with the specific agonist CHPG, had no effect on stretch-induced enhancement of rat cortical neuronal NMDA receptor activity in PN cultures, whereas activation of mGluR5 in NG culture prevented this enhancement. Second, inhibition of mGluR5 with the specific antagonist MPEP prevented the enhancement of NMDA receptor activity in both PN and NG neurons⁹². Third, while activation of mGluR5 had no effect on the stretch-reduced Mg^{2+} block in PN neurons, mGluR5 activation appears to exacerbate the stretch-reduced Mg^{2+} block in NG neurons. Moreover, inhibition of mGluR5 limits the stretch-reduced Mg^{2+} block in both PN and NG neurons as indicated by a decrease in the current ratio (ratios were not significantly different from controls)⁹². It is important to note that mGluR5 activation and inhibition have significantly different effects on the stretch-reduced Mg^{2+} block in NG neurons (exacerbate and limit, respectively). Combined, our findings suggest that both neuronal and glial mGluR5 modulate neuronal NMDA receptor activity and that glial mGluR5 also work through an as yet unidentified mechanism to regulate the neuronal NMDA receptor Mg^{2+} block (Fig. 49).

Our results suggest significant glial group I mGluR and neuronal NMDA receptor interactions. Although it is generally well-accepted that glial cells predominantly express the mGluR5 subtype¹⁰⁵⁻¹⁰⁸ and the effects of mGluR5 activation⁹² may be due to a glial component¹⁰⁹, our mGluR1 data suggests that glial cells also express the mGluR1 subtype. This finding is supported by a previous study showing mGluR1 expression in a small number of astrocytes¹¹⁰. To our knowledge, the neuromodulatory effects of activating glial mGluR1 receptors has not been reported. Using immunoblot analysis and antibodies directed against either mGluR1 or mGluR5 (Fig. 50), we confirmed that: 1) both mGluR1 and mGluR5 are expressed in our rat cortical-derived glial cells which are allowed to grow to confluency; and 2) that they both remain present following seeding of neurons upon this glial monolayer⁹¹. The predominant migration position of the mGluR1 and mGluR5 in glia and glial/neuronal cultures is greater than that expected for a calculated molecular mass of 128 kDa¹¹¹ and falls closer to that expected for the dimeric form of the receptors^{112, 113}. The migrating positions of both monomeric and dimeric forms of the receptors have been previously shown and are in support of our data¹¹⁴.

The concentrations of mGluR compounds used in these studies were based upon previous experience from this lab^{67, 68} and others¹⁰² as well as published EC_{50} and IC_{50} doses⁶³. Nevertheless, we also tested the ability of the various group I mGluR compounds to directly modulate NMDA-evoked peak current influx in control (non-stretched) cells at the concentrations selected for our studies and found no effects (Fig. 51)⁹². However, variability in NMDAR desensitization was observed. Ratios of peak to steady state current (P/SS) and time to peak current to time to steady state current (tP/tSS) data, when combined with our control and stretch alone data, suggest that the ability of the various mGluR compounds to modulate the stretch-induced enhancement of NMDA receptor activity, reflects, in part, their ability to modulate alterations in the desensitization of these receptors caused by stretch injury alone (Table 2)⁹¹.

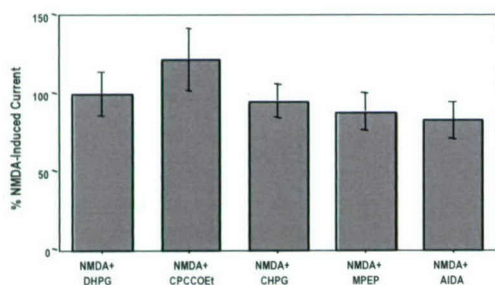


Fig. 51. Effects of various group I mGluR compounds on NMDA-induced inward current in unstretched NG cortical neurons. Normalized to NMDA-induced currents, inward currents evoked by NMDA (200 μ M) and either DHPG (200 μ M; N=7), CPCCOEt (100 μ M; N=7), CHPG (1 mM; N=7), MPEP (2 μ M; N=6), or AIDA (20 μ M; N=7), show no significant effects of these various group I mGluR compounds on NMDA-induced peak inward current ($p > 0.05$; ANOVA).

Table 2. Effects of group I mGluR compounds on stretch-induced NMDA receptor activity

PN					
	N	2mM Mg²⁺		0mM Mg²⁺	
		P/SS ± SE	tP/tSS ± SE	P/SS ± SE	tP/tSS ± SE
Control	18	2.8 ± 0.48	0.2 ± 0.02	2.1 ± 0.27	0.3 ± 0.03
5.7 mm	17	2.0 ± 0.20	0.2 ± 0.02	1.4 ± 0.07 *	0.3 ± 0.03
DHPG+5.7mm	5	1.7 ± 0.27	0.3 ± 0.08	1.6 ± 0.28	0.4 ± 0.08
MPEP/DHPG+5.7mm	6	1.7 ± 0.49	0.4 ± 0.10	1.1 ± 0.04	0.4 ± 0.08
CPCCOEt+5.7mm	7	2.3 ± 0.23	0.3 ± 0.05	1.4 ± 0.14	0.4 ± 0.05
MPEP+5.7mm	8	1.5 ± 0.11	0.4 ± 0.08	1.3 ± 0.07	0.5 ± 0.04

NG					
	N	2mM Mg²⁺		0mM Mg²⁺	
		P/SS ± SE	tP/tSS ± SE	P/SS ± SE	tP/tSS ± SE
Control	22	1.7 ± 0.18	0.4 ± 0.03	1.8 ± 0.14	0.3 ± 0.07
5.7 mm	17	1.6 ± 0.20	0.4 ± 0.08	1.3 ± 0.06 *	0.4 ± 0.04
DHPG+5.7mm	9	1.6 ± 0.14	0.3 ± 0.04	1.5 ± 0.12	0.4 ± 0.06
MPEP/DHPG+5.7mm	6	2.2 ± 0.43	0.3 ± 0.05	1.4 ± 0.07	0.3 ± 0.06
CPCCOEt+5.7mm	6	1.5 ± 0.09	0.2 ± 0.03	1.4 ± 0.12	0.3 ± 0.05
MPEP+5.7mm	6	1.4 ± 0.18	0.4 ± 0.06	1.6 ± 0.26	0.4 ± 0.07

Table 2. Peak to steady state current (P/SS) ratios and time to peak current to time to steady state current (tP/tSS) ratios measured in PN and NG in the presence and absence of magnesium. Top Panel) *PN*: In PN, stretch had no effect on peak to steady state current (P/SS) ratios, or time to peak current to time to steady state current (tP/tSS) ratios measured in the presence of magnesium ($p > 0.05$; unpaired t-test). In contrast, stretch significantly reduced the P/SS ratio measured in the absence of magnesium ($p < 0.05$; unpaired t-test), but had no effect on the tP/tSS ratios measured in the absence of magnesium. In the presence of magnesium, pretreatment with DHPG, MPEP and DHPG, CPCCOEt or MPEP had no effect on stretch-induced changes in PN cortical neuron P/SS ratios ($p > 0.05$; ANOVA), whereas pretreatment with MPEP and DHPG and MPEP alone significantly increased the tP/tSS ratio from levels measured following stretch injury alone ($p < 0.05$; ANOVA). In the absence of magnesium, pretreatment with DHPG, MPEP and DHPG, CPCCOEt or MPEP had no effect on stretch-induced changes in P/SS ratios ($p > 0.05$; ANOVA), whereas, pretreatment with MPEP and DHPG, CPCCOEt and MPEP alone significantly increased the tP/tSS ratio from levels measured following stretch injury alone ($p < 0.05$; ANOVA). Bottom Panel) *NG*: Stretch had no effect on P/SS or tP/tSS ratios measured in the presence of magnesium ($p > 0.05$; unpaired t-test), whereas stretch significantly reduced the P/SS ratio measured in the absence of magnesium ($p < 0.05$; unpaired t-test), but had no effect on the tP/tSS ratios. In the presence of magnesium, pretreatment with MPEP and DHPG significantly increased the P/SS ratios measured in NG ($p < 0.05$; ANOVA), whereas DHPG, CPCCOEt and MPEP alone had no effect ($p > 0.05$; ANOVA). Moreover, pretreatment with CPCCOEt alone significantly reduced the tP/tSS ratio ($p < 0.05$; ANOVA), whereas DHPG alone, MPEP and DHPG and MPEP alone had no effect ($p > 0.05$; ANOVA). In the absence of extracellular Mg²⁺, neither the P/SS, nor the tP/tSS ratio is altered following pretreatment with any of the mGluR compounds ($p > 0.05$; ANOVA). * Denotes significant differences from controls. † Denotes significant differences from mild (5.7 mm) stretched neurons.

The role of group I mGluR (mGluR1 and mGluR5) in neuronal injury and neurodegeneration has been controversial. In part this relates, until recently, to the lack of highly selective agonists/antagonists for these receptors. However, because previous in vitro studies have used either pure neuronal or mixed neuronal/glial cultures, some of this controversy may be explained by our observations of the presence of glial mGluR1, and their modulatory role on NMDAR in neurons.

We have begun to develop methods to better understand this neuronal/glial interaction during stretch-induced injury. These include the use of murine derived pure neuronal and mixed

neuronal/glial cultures from knockout and wild-type animals, and the use of a small removable insert capable of separating neuronal from glial populations. It has already been demonstrated that the latter paradigm allows the study of stretch-injured axons that extend through the area previously covered by the removable barrier. Moreover, because the generation of mixed neuronal/glial cultures requires the use of two animals, and because such requirements will greatly impact the success of our breeding colony, we have used a modification of Ellis and colleagues culture technique that allows the generation of mixed neuronal/glial cultures that can be grown from a single seeding and that do not show the characteristic 'islands' of glia and neurons. Thus, our modified technique provides a short time frame for the glia to become confluent before the neurons begin to extend their processes.

Because acute slices and three-dimensional rather than two dimensional cultures inherently possess 3-D cytoarchitecture, and because it is believed that the former preparations more closely resemble the *in vivo* situation, we are currently investigating methods for attaching slices and 3-D cultures to the deformable membrane. Currently we have been challenged with the discontinuation of the Flex I plate. This has led to our development of an adapter device to allow the use of the injury controller developed by Ellis and colleagues to stretch the membrane on the newer BioFlex series plate. Although we have been successful in producing strains as a function of pressure that work in a linear range (Fig. 52), and although the newer BioFlex plate allows for imaging via inverted scopes due to its new optically clear membrane, the size of this particular plate and individual wells (both 2x the size of the Flex I), the >5 mm displacement of the silastic membrane from the bottom of the BioFlex plate, and the inability of the injury controller to measure real time strain rates continues to preclude the use of this model for the study of biomechanical alterations. We plan to address these issues by producing a new *in vitro* trauma device capable of allowing: 1) real-time measurements of strain and strain rate; 2) live cell imaging, using culture preparations of primary cortical neurons; and 3) determination of the relative roles of mechanical damage to cells and axons. Because the principle of this model is to culture cells on a deformable material, this system permits the use of multiple cell types, including non-neuronal cells, and has the potential for adaptation to other fields, such as connective tissues. Moreover, because this model proposes to use an upward deflection of the silastic membrane, adaptation for multimodal injury studies (tension and compression, shear or transection) can be performed by the addition of an adjustable platen/stylet component. The goal of this study will be to develop a more reproducible, consistent and flexible *in vitro* injury system that can be widely used by neurotrauma investigators. A particularly unique aspect of this system will be the incorporation of computer controlled servo hydraulic speed control principles. These principles allow for precision controlled stress generation while maintaining cost effectiveness. This proposed model was recently submitted to NINDS as an R21 and promises to extend the initial studies obtained with the current DOD support.

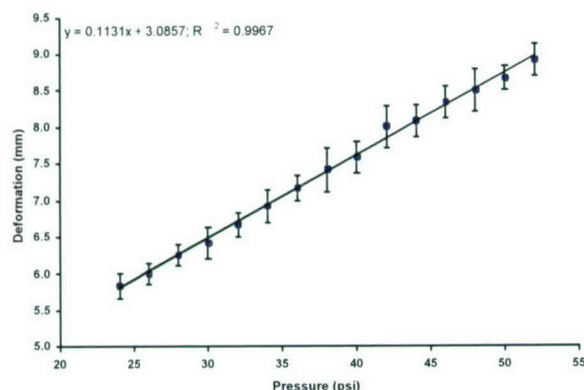


Fig. 52. Bioflex® membrane deformation. Preliminary characterization performed by the PI using an adapter to fit the larger well size of the Bioflex® plate demonstrates that the Bioflex® membrane (same as the StageFlexor®) can be easily manipulated to achieve similar displacements to the Flex I series membrane with less pressure, but at the same pressure pulse duration.

In addition to the reported findings above, it is important to note here that parallel findings between *in vivo* and *in vitro* systems underlie the strength of this hypothesis. Indeed, parallelism can be found between both *in vivo* and *in vitro* systems in our metabotropic glutamate receptor (mGluR), and small peptide (35b) studies (see these corresponding sections for details).

In conclusion, *in vivo* models have many advantages over *in vitro* models, including the ability to study trauma-induced changes in behavior, physiology, metabolism, the blood/tissue interface, the blood brain barrier, and/or inflammatory- and immune-mediated responses. However, *in vivo* models inherently possess multiple interacting variables and the complexity of these interactions hinders research efforts to distinguish key mechanisms associated with neuronal cell death and subsequent morphological, physiological and behavioral changes. Advantages of *in vitro* cell culture systems include: minimized numbers of experimental variables; the ability to study the role of specific receptors and intracellular events such as induction of second messenger systems; the ability to control the experimental environment; the potential to rapidly screen selective pharmacotherapies, and reduced cost. In contrast, a primary disadvantage is the inherent variability between models caused by the culture system (egs. acute slices, organotypic slice cultures, dissociated primary cultures or cell lines). Nevertheless, *in vitro* trauma models have proved useful for delineating discrete mechanisms of cell death at both the cellular and molecular level that are similar across models used. An understanding of these processes in both the developing and adult brain remains essential as key findings suggest significant differences between both the biochemical and biomechanical sequelae that can potentially impact the choice of therapy following traumatic brain injury.

Hypothesis #2: Novel neuroprotective drugs can be developed through rational drug discovery using molecular modeling, synthetic chemistry, and biological modeling.

We have carried out research with the goal to develop new computational methods to study protein structures and functions for the design and development of novel small-molecule ligands as potential therapeutic agents for the treatment of neurological disorders and conditions such traumatic brain injury and Alzheimer's disease. Some of the results have been published in four peer-reviewed publications. The major accomplishments are summarized below.

1. PTEN

We are interested in designing novel neuroprotective agents by targeting PTEN, a phosphatase, which regulates the activity of AKT/PKB. Our hypothesis is that inhibitors of PTEN will activate AKT in neuronal cells and have the therapeutic potential to be developed as novel neuroprotective agents. Starting from the X-ray structure of PTEN, we have performed computational structure-based database screening of more than 500,000 compounds to identify potential nonpeptidic small-molecule inhibitors of PTEN. Based upon predicted binding scores, we have selected 200 putative small-molecule inhibitors for evaluation of their inhibition of the enzymatic activity of PTEN. In collaboration with Dr. Zhong-Yin Zhang at the Albert Einstein College of Medicine, we have tested these 200 putative small-molecule inhibitors of PTEN and confirmed that 10 compounds have potent activity in inhibition of PTEN. See further details under PTEN section below, page 47.

2. Novel Small Peptides

The tripeptide thyrotropin-releasing hormone (TRH) and/or related analogues have shown neuroprotective activity across multiple animal models of CNS trauma and in a small clinical trial of spinal cord injury. The metabolic product of TRH (cyclo-his-pro) retains physiological activity, although not itself neuroprotective. We have rationally designed a series of novel cyclic dipeptides, somewhat structurally related to cyclo-his-pro, and have examined their neuroprotective activity across multiple *in vitro* models of neuronal injury and after traumatic brain injury (TBI) in mice. Four test compounds were compared to vehicle control and all reduced cell death after trophic withdrawal or traumatic injury in primary neuronal cultures; the two most potent agents also protected against glutamate or β -amyloid neurotoxicity. All four compounds showed highly significant improvement in motor and cognitive recovery, and markedly reduced lesion volumes as shown by high field magnetic resonance imaging. The ability of these small peptides to attenuate both necrotic and apoptotic cell death, and their effectiveness *in vivo*, suggests their potential utility in clinical head injury.

Traumatic brain injury (TBI) or traumatic spinal cord injury (SCI) cause not only direct mechanical damage to tissue, but induce biochemical changes that lead to delayed neural cell loss^{115, 116}. It has been increasingly recognized that such secondary injury may substantially contribute to chronic neurological disability, which has lead to the search for neuroprotective agents¹¹⁷. Based upon animal studies, several drugs have been evaluated and shown to improve outcome in human SCI^{118, 119}. Although no neuroprotective treatment strategy has proved unequivocally effective in human head injury, the SCI studies have provided "proof of principle" support for the concept of secondary injury in acute neurodegenerative conditions¹¹⁷.

Among the treatments that have shown promise in clinical SCI, thyrotropin-releasing hormone (TRH) has been found to be more effective than these agents, as well as many other major neuroprotective drug classes in experimental SCI^{115, 120-125}. TRH and structurally related TRH analogs also improve outcome in experimental TBI^{115, 126-128}. TRH appears to provide neuroprotection through multiple mechanisms. It can physiologically antagonize or modify the actions of a number of secondary injury factors including endogenous opioids, platelet activating factor, peptidyl-leukotrienes, and glutamate; TRH also improves cellular bioenergetic state and cerebral blood flow^{115, 129, 130}. However, TRH is a tripeptide that is rapidly metabolized, and it has a variety of physiological actions – endocrine, autonomic, and analeptic – that may limit its utility as a neuroprotective agent¹³¹. To address these problems, we have developed a series of modified TRH analogues, through substitutions at both the N-terminus and imidazole ring, which result in neuroprotective compounds with a relatively long duration of action and few of the other major physiological actions of TRH¹²⁷. In the process of developing such analogues, we serendipitously produced a novel cyclic dipeptide, structurally related to an active metabolic product of TRH (cyclo-his-pro)¹³²; this compound 1-ARA-35b (35b) proved to have strong neuroprotective activity in multiple rodent models of TBI and attenuates both necrotic and apoptotic neuronal cell death *in vitro*^{133, 134}.

We have produced a series of other cyclic dipeptides and tested their neuroprotective activity *in vitro* (Fig. 53). Among these, three compounds significantly reduced neuronal cell death in two or more *in vitro* models. These agents were directly compared to 35b in a well-characterized mouse model of controlled cortical impact (CCI)¹³⁵, as well as in a series of standardized *in vitro* models of neuronal cell death¹³³.

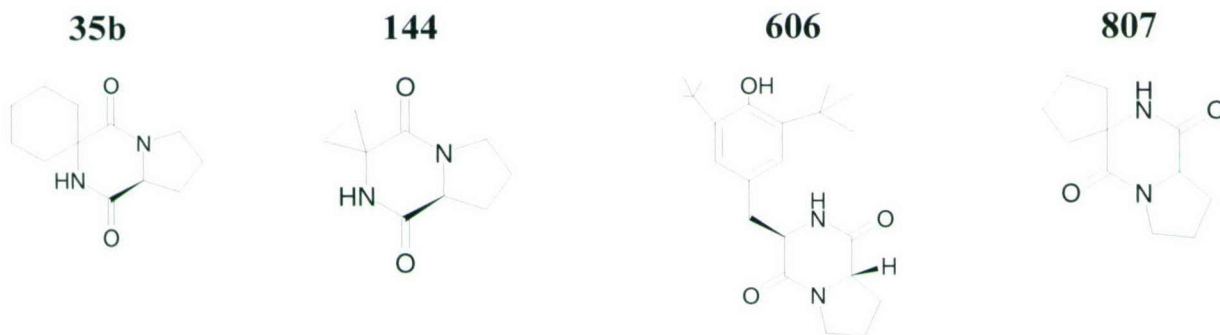


Fig. 53 Chemical structures of the evaluated cyclic dipeptides: 35b, 144, 606, and 807.

3. *In Vitro* Studies

All of the dipeptides showed neuroprotection in the punch injury and trophic withdrawal models (Fig. 54A,B). The former shows almost exclusively necrotic cell death, whereas the latter

reflect largely caspase-dependent apoptosis¹³³. Thus, these cyclic dipeptides are able to modulate the two major forms of cell death identified in *in vivo* models of TBI as well as in clinical head injury¹¹⁷.

Dose-response *in vitro* studies showed that 35b and 606 were more effective and provided neuroprotection at far lower concentrations than 144 or 807 in the punch (trauma) model (Fig. 54A), and the former group showed statistical significance (albeit similar percentages of cell death reduction) at lower concentrations than the latter group in the trophic withdrawal model as well (Fig. 54B). Also of possible importance for potential clinical application of the compounds is the fact that 35b and 606 showed significant neuroprotection in models of glutamate toxicity and β -amyloid toxicity, whereas 144 and 807 were ineffective at any concentration (Fig. 54C,D). The glutamate toxicity model, as used here, causes primarily necrotic cell death, whereas β -amyloid leads to caspase-dependent apoptosis as well as perhaps caspase-independent apoptosis⁷⁴. As there is strong evidence for the role of glutamate-mediated excitotoxicity in experimental TBI¹³⁶, and both β -amyloid and head injury have been implicated in the pathology of Alzheimer's disease¹³⁷, these *in vitro* studies when combined with *in vivo* data provide experimental support for the possible utility of 35b or 606 in clinical brain injury.

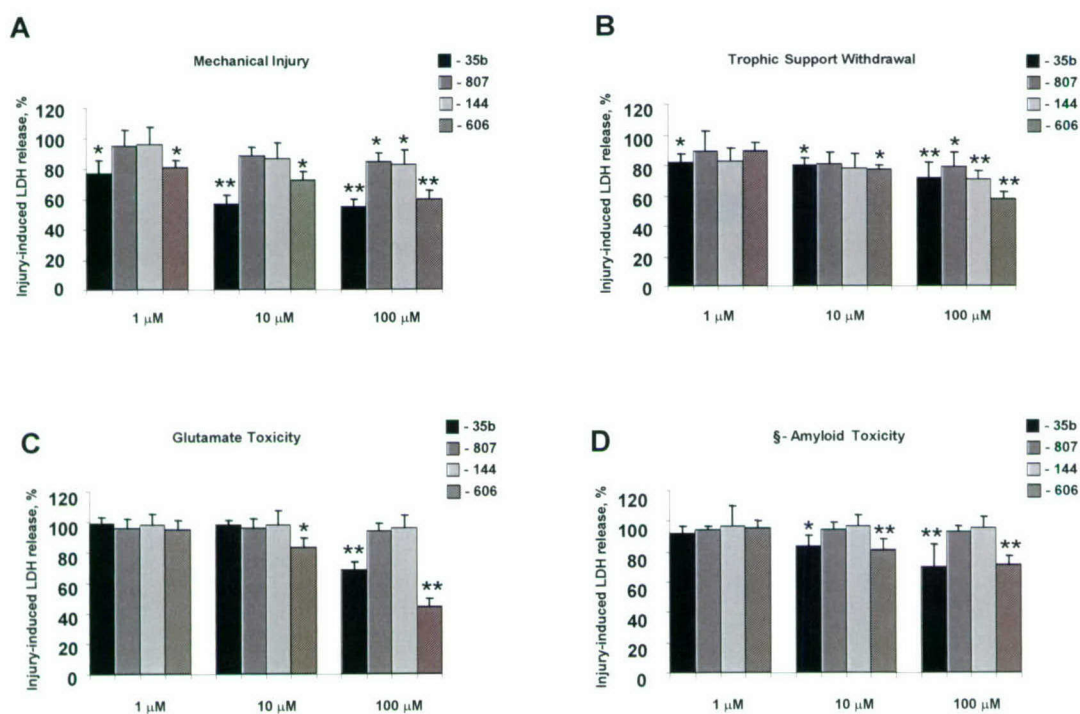


Fig. 54 A) Comparison of effects of various diketopiperazines on mechanical injury-induced cell death in rat cortical neuronal cultures. Indicated concentrations of 35b, 807, 144, or 606 were added to cultures subjected to mechanical injury. LDH release was measured after 24 hr of treatments. B) Comparison of effects of various diketopiperazines on trophic support withdraw-induced cell death in rat cortical neuronal cultures. Indicated concentrations 35b, 807, 144 or 606 were added to cultures subjected to trophic support withdrawal, as described in Methods. LDH release was measured after 48 hr of treatments. C) Comparison of effects of various diketopiperazines on glutamate-induced toxicity in rat cortical neuronal cultures. One hundred and fifty μM of Na-glutamate was administered to cell cultures immediately after the addition of 35b, 807, 144, or 606 at indicated concentrations. LDH release was measured after 48 hr of treatments. D) Comparison of effects of various diketopiperazines on β -amyloid-induced toxicity in rat cortical neuronal cultures. Twenty-five μM of β -amyloid peptide was administered to cell cultures immediately after the addition of 35b, 807, 144, or 606 at indicated concentrations. LDH release was measured after 48 hr of treatments. All histograms indicate LDH release as a percentage of injured controls \pm SD; $n = 8$ to 16 cultures per condition. *, $p < 0.05$, **, $p < 0.01$ versus vehicle-treated injured controls as shown by ANOVA, followed by the Dunnett's test.

4. In Vivo Studies

4.1. Motor Outcome: 35b, 144, 606, and 807 all showed a highly significant and virtually identical improvement in motor function as compared to vehicle treated controls at 2 and 3 wks after injury (each $p < 0.001$). However, the protective effects of 606 were only observed beginning at 2 wks, in contrast to other compounds that showed clear and significant protection by 3 days (Fig. 55).

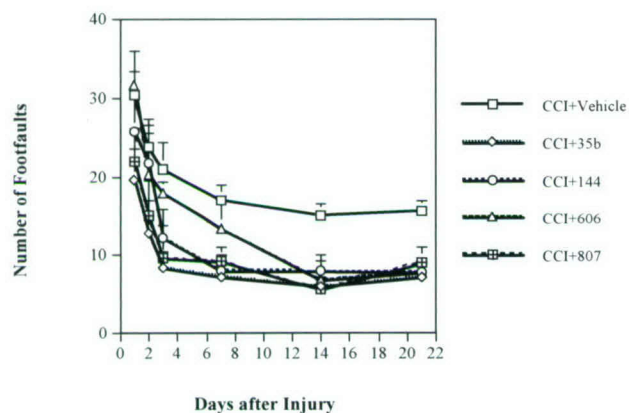


Fig. 55 Comparison of effects of diketopiperazines 35b, 144, 606 and 807 on motor function measured by beam walk test at 1, 2, 3, 7, 14 and 21 days post-trauma. All diketopiperazines significantly ($p < 0.001$) improved motor function at 14 and 21 days after injury, compared to vehicle-treated injured animals. 35b, 144, and 807 also showed significant protection at 3 and 7 days.

4.2. Cognitive Assessment: Morris Water Maze evaluation was conducted on days 14 through 17. 35b, 144, 606, and 807 all showed significantly reduced latencies ($p < 0.05$) to find the submerged on the final two testing days (Fig. 56). Although not statistically different, 606 animals showed the lowest latencies and 807 the highest latencies on days 16 and 17.

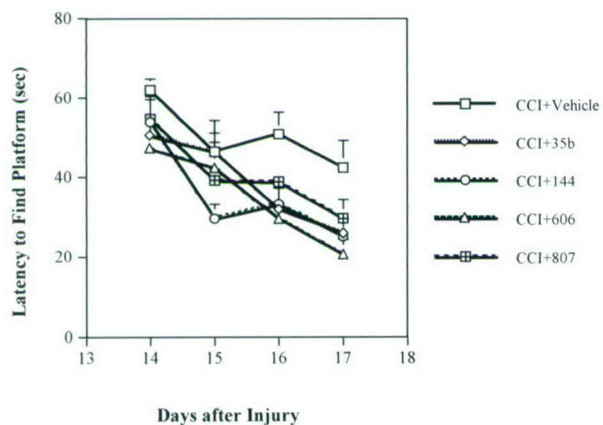


Fig. 56 Water maze cognitive score after controlled cortical injury (CCI) in mice measured at 14, 15, 16, and 17 days post-injury. Diketopiperazines 35b, 144, 606 and 807 significantly ($p < 0.05$) improved cognitive function at 16 and 17 days after injury, compared to vehicle-treated injured mice.

4.3. Lesion Volume Measurements: T-2 weighted lesion volume measurements showed highly significant reduction in lesion size in all dipeptide treatment groups as compared to vehicle treated controls (Fig. 57). The greatest reduction for lesion volumes was observed in the 35b-treated group (approximately 65%) and the smallest reduction (approximately 45%) in the 606-treated group.

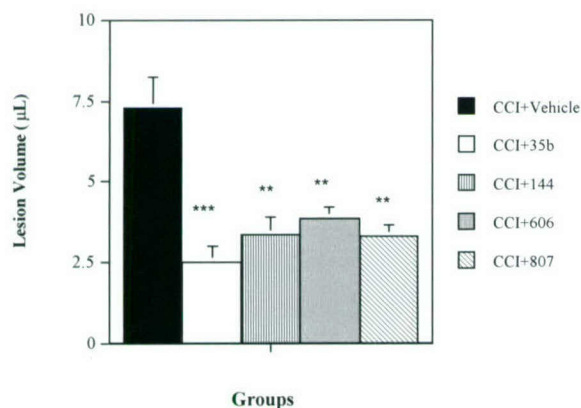


Fig. 57 Comparison of effects of diketopiperazines 35b, 144, 606 and 807 on lesion volume at 21 days post-injury. Diketopiperazines significantly reduced lesion volume caused by controlled cortical injury (CCI). ** $p < 0.01$ and *** $p < 0.001$ compared to vehicle-treated injured animals.

Although the various dipeptides showed considerably different *in vitro* neuroprotective properties, all compounds proved protective against punch-induced trauma. This *in vitro* trauma model has been used extensively by us for a number of years and has proved remarkably predictive of neuroprotection in rodent TBI models^{64, 133, 138}. Yet 35b and 606 showed superior effects in both the *in vitro* trauma model and across the spectrum of *in vitro* tests utilized. In the trauma model, 35b and 606 showed comparable effects; both were substantially more protective than either 807 or 144 at 100 µM and were effective at 1% the dose required for neuroprotection by 807 or 144.

Glutamate-induced neurotoxicity is a well-established in culture models and as given to these pure neuronal cultures produces largely necrotic cell death⁶⁷. Here 606 was clearly most effective, reducing cell death by more than 50% at a concentration of 100 µM, but showing significant activity at 10 µM. 35b treatment was also protective at 100 µM, reducing cell death by almost 25%, whereas neither 807 nor 144 was effective at any of the doses used. Two models of apoptosis were also studied—trophic withdrawal¹³³ and β-amyloid toxicity⁷⁴. Both cell death models involve caspase activation. Trophic withdrawal involves largely caspase-3, whereas β-amyloid toxicity appears to involve multiple caspases⁷⁴, and may also reflect translocation of AIF, a caspase-independent mitochondrial factor (Movsesyan et al., unpublished observations, 2003). All compounds showed neuroprotective activity in the trophic withdrawal model at 100 µM, with 606 showing the largest reduction in cell death (~30%). Only 35b and 606 were significantly effective at 10 µM, and only 35b at 1 µM, but reductions in cell death even at lower doses were relatively similar (~20%). In contrast, only 35b and 606 were protective in the β-amyloid model.

Separate from the present studies we have also examined the neuroprotective effects of 35b and 606 (but not the other dipeptides) in several other *in vitro* models - maitotoxin, FeSO₄, and/or oxygen/glucose deprivation (OGD); both were effective in the maitotoxin and OGD models (data not shown). Maitotoxin is a marine toxin that causes relatively pure necrosis secondary to opening of multiple calcium channels¹³⁹. OGD was developed as an *in vitro* model to simulate brain ischemia and also causes largely necrotic cell death⁶⁹. 606 was also very effective in blocking cell death caused by FeSO₄, a model of free radical-induced damage¹⁴⁰. Taken together, these observations suggest that 35b and 606 may have utility in a variety of other models of acute or chronic neurodegeneration, such as cerebral ischemia or Alzheimer's disease. Perhaps relevant to the latter application, 35b treatment

of chronic head injured mice markedly improved spatial learning/memory ¹³⁴, suggesting a nootropic action.

In conclusion, the present studies reinforce and extend our earlier work showing that diketopiperazines structurally related to the physiologically active metabolite of TRH (cyclo-his-pro) ^{132, 141} have considerable neuroprotective activity ^{133, 134, 140}. They also emphasize the value of rational drug design, as 606 was developed to enhance the antioxidant potential of this class of compounds by adding an antioxidant moiety (di-tert-butylphenol) ¹⁴⁰. Compound 35b is being actively developed by Research Corporation Technologies, Inc. for the possible clinical treatment of head injury. The current studies further support the potential utility of this compound but also demonstrate that another related cyclic dipeptide (606) may have substantial clinical potential for acute and possibly chronic neurodegeneration.

Hypothesis #3: The novel suppressor gene, PTEN, is an important upstream pro-apoptotic modulatory factor.

PTEN is a recently identified tumor suppressor factor. Accumulating evidence suggest its functions are linked to the lipid phosphatase activity of PTEN which allows PTEN to antagonize phosphatidylinositol 3-kinase (PI3K) pathways. Akt is one of the major downstream targets activated by PI3K. We have demonstrated that induction of neuronal apoptosis in culture, following trophic withdrawal, is associated with a significant upregulation of PTEN message and protein levels. Moreover, transfection of primary neuronal cultures with PTEN is associated with decreased levels of phosphorylated Akt. In addition, preliminary studies demonstrate that traumatic brain injury is associated with a significant upregulation of PTEN in the early period (15 min-4 h) following fluid percussion-induced TBI in rats. Taken together, these observations suggest that PTEN is upregulated after trauma and may contribute to posttraumatic apoptosis by modulating Akt, and thereby contributing to the activation of caspase-3, as well as possibly through non-caspase pathways.

1. Role of PTEN in Neuronal Apoptosis and Measurement of PTEN Changes after TBI

We have examined a potential role for PTEN in neuronal apoptosis, utilizing the classical model of neuronal apoptosis-induction of trophic withdrawal in cerebellar granule cell cultures. PTEN is a dual action phosphatase that is highly specific for acidic substrates such as phosphatidylinositol (3,4,5)-triphosphate, which mediates growth factor induced activation of intracellular signaling through the serine-threonine kinase Akt. High levels of phosphorylated Akt are found in PTEN-deficit immortalized mouse embryonic fibroblasts. Moreover, a number of tumor cell lines also show low or absent levels of PTEN protein, which are associated with high levels of activated Akt. Together these findings suggest that PTEN affects tumor cell growth through its modulation of Akt. Akt may also serve a critical modulator role in apoptosis, possibly through phosphorylation of the pro-apoptotic protein BAD or of caspase-9. Whether PTEN activity regulates Akt signaling in neuronal cells has not been previous addressed.

We examined the potential relationship between PTEN gene expression and Akt regulation in neuronal apoptosis, using primary cultured CGCs subjected to trophic withdrawal. Serum and potassium deprivation induced PTEN protein and mRNA. Immunofluorescent staining of CGC cultures with specific anti-PTEN antibodies demonstrated early changes in staining intensity following the apoptotic stimulus: a significant increase in PTEN immunolabeling was observed after 30 minutes of serum and potassium deprivation (Fig. 58). Quantitative analysis of PTEN immunostaining using confocal microscopy showed a more than two-fold increase at 30 min after serum/potassium withdrawal, as compared to untreated control cells (Fig. 58B). Specificity of PTEN immunostaining was examined by Western blot analysis of CGC protein extracts; this showed a band with apparent molecular weight of approximately 57kD, consistent with the results of confocal microscopy (Fig. 58C). Western blotting qualitatively demonstrated an increase in PTEN protein content in CGCs at 30 minutes after induction of apoptosis, returning to control levels within 2-4 hours. RT/PCR data demonstrated that PTEN mRNA was markedly elevated by 15 min and returned to control levels by 6 h following serum and potassium withdrawal (Fig. 58D). To examine a possible role of PTEN in neuronal apoptosis, CGCs were transiently transfected with PTEN cDNA fused in a frame with the green fluorescent protein (GFP) coding region or with GFP only. Levels of endogenous and recombinant PTEN after transfection were estimated by Western blot using anti-PTEN antibodies. Activity of recombinant PTEN was examined by the Western analysis of the Akt phosphorylation state (Fig. 59). The prostate cancer cell line PC3, which lacks a functional PTEN gene and expresses high levels of P-Akt, was used in these experiments as a control for specificity of PTEN and P-Akt

immunostaining. Overexpression of GFP-PTEN in CGCs resulted in marked decreases in Akt phosphorylation (Fig. 59).

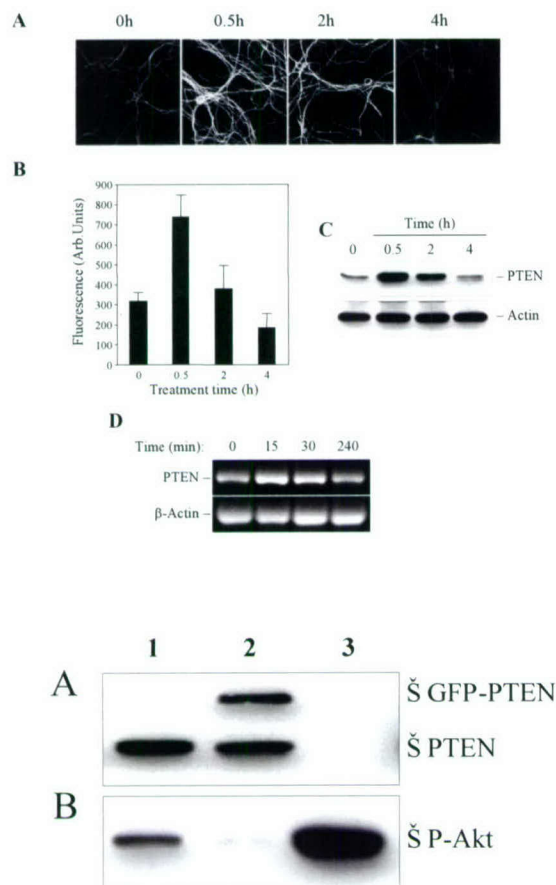


Fig. 58 Induction of PTEN protein content in CGCs following serum and K^+ withdrawal. A) Immunofluorescent staining of the cultured neurons. Cells were subjected to serum and K^+ deprivation and cultured for indicated periods of time. Immunostaining was performed using PTEN antibodies. B) The average fluorescence of PTEN staining was quantified using "Flouview" confocal software. Data are expressed as arbitrary fluorescent units and are means \pm SD of three independent experiments. C) PTEN Western blot analysis was performed using antibodies specific to PTEN or β -actin at the time points identical to those for (A). D) RT-PCR analysis of the abundance of transcripts encoding the rat PTEN in CGCs subjected to serum and K^+ deprivation. Total RNA from the primary neuronal cultures at the



Fig. 59 PTEN overexpression in CGCs results in Akt dephosphorylation. Western blot analysis of proteins extracted from CGC cultures transfected with the empty expression vector (1) or GFP-PTEN fusion construct (2). PC3 cells (3), shown to lack PTEN protein and to express high amounts of P-Akt, served as a control.

PTEN phosphatase activity can inhibit Akt through a PI3-kinase dependent pathway. Because Akt kinase activity appears to be a factor essential for self-survival, we therefore examined the effect of PTEN overexpression on cell viability during apoptosis of CGCs induced by trophic withdrawal. Neuronal cultures were transiently transfected with either GFP or GFP-PTEN expression constructs. At 24 hours after transfection, cultures were subjected to serum and potassium deprivation; the viability of green fluorescent cells at various times was estimated by morphological analysis and counting of appetite of nuclei after standing with Hoechst 33258 (Fig. 60). There was significant exacerbation of cell death at early time points in cultures transfected with GFP-PTEN as compared to GFP transfected control cultures.

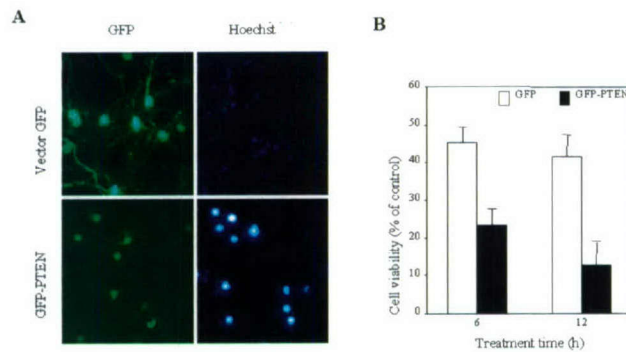


Fig. 60 PTEN overexpression in CGCs results in exacerbation of apoptosis induced by serum and K^+ withdrawal. The cultures were transiently transfected with either GFP or GFP-PTEN expression constructs. A) At 24 h after transfection, cultures were subjected to serum and K^+ deprivation; the viability of green fluorescent cells at various times was estimated by morphological analysis and counting of apoptotic cell nuclei after staining with Hoechst 33258. B) The average numbers of nuclei with apoptotic morphology \pm SD. Data in are expressed as percent of untreated controls and represent means of three independent experiments.

We also examined whether potentiation of CGC apoptosis by PTEN is associated with caspase-3 activation, presumably through an Akt-caspase-9 pathway. CGC cultures were transiently transfected with PTEN tagged with FLAG at its C terminus or with the expression vector only. Twenty-four hours after transfection, cells were subjected to serum and potassium withdrawal. Cleavage of pro-caspase 3 into fragments specific for the active form of the caspase was examined by staining with antibodies specific for the p17 subunit. Western blot analysis revealed notable activation (cleavage) of caspase-3 at 6 hours after treatment in PTEN transfected cultures, whereas in control cultures the p17 subunit was detected only at a later (12 h) time point (Fig. 61). To examine whether PTEN overexpression results in activation of caspase 3 within the same cells, we double labeled transfected apoptotic CGCs (at 6 h after treatment) with fluorescent antibodies recognizing FLAG apoptotic and p17 caspase-3 fragments (Fig. 61). The immunostaining experiments showed readable p17 staining and FLAG positive cells, but not in FLAG negative cells or in control mock transfected cultures.

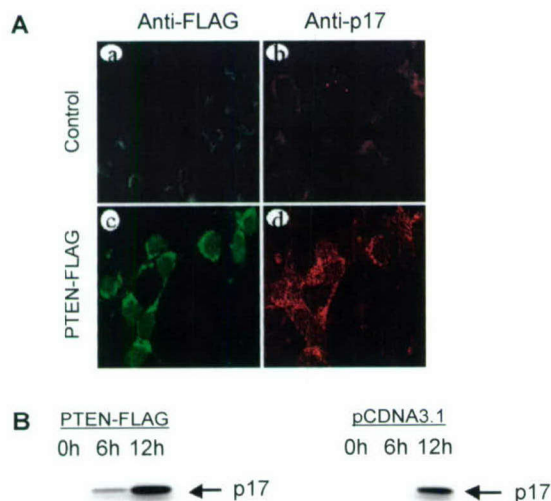


Fig. 61 Overexpression of PTEN potentiates Caspase-3 activation during CGC apoptosis. The cells were transiently transfected with the PTEN-FLAG expression construct; at 24 h after transfection, cultures were subjected to serum and K^+ deprivation. A) The same microscopic fields were stained with anti-FLAG (a, c), and anti-p17 (b, d). Double immunofluorescence for PTEN-FLAG and activated caspase-3 revealed a majority of PTEN-expressing cells also express increased amounts of cleaved caspase-3. B) Western blot analysis of caspase-3 activation in GCG cultures transfected with the empty expression vector or PTEN-FLAG construct at indicated times after serum and K^+ withdrawal.

In very preliminary studies, we have also examined the potential modulatory effect of treatment with antisense directed at PTEN. Transfection with PTEN antisense significantly reduced neuronal cell death in CGCs subjected to trophic withdrawal, as compared to the empty vector (Fig. 62). In preliminary studies, we have also examined whether PTEN is expressed in rat brain and whether it is modulated by traumatic brain injury. Rats were subjected to fluid percussion induced traumatic brain injury. Tissue taken from ipsilateral cortex following trauma showed increases in PTEN expression from 15 min to 4h after injury, using confocal microscopy (Fig. 63); at 4h upregulation of PTEN activity in neurons was co-localized with activated caspase-3 and caspase-9 (Fig. 64).

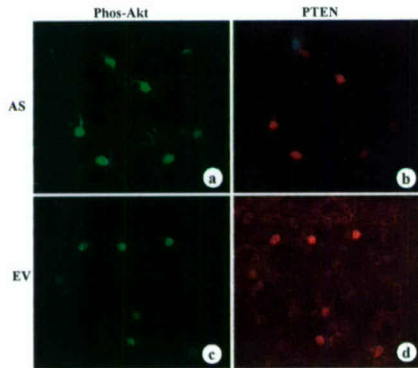


Fig. 62 A morphology pattern of CGCs transfected with PTEN antisense (AS) and empty vector (EV). Following serum/ K^+ deprivation at 6h, the cells were fixed by using immunofluorescent double staining. The panels show transfection with AS significantly increased phos-Akt protein expression (a) and down regulated PTEN protein expression (b); the surviving cells appear large, with intact processes compared to empty vector (c, d).

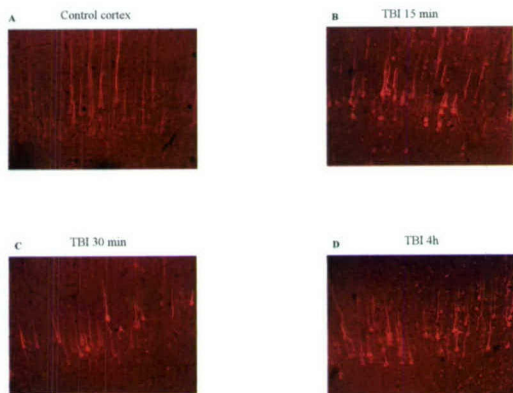


Fig. 63 The expression of the PTEN protein is significantly increased in neurons in the rat parietotemporal cortex between 15 min and 4h after fluid percussion induced TBI in rats. Photomicrographs represent staining with anti-PTEN antibodies of the corresponding cortical areas in sham-operated (A) and injured animals: (B) 15 min; (C) 30 min and (D) 4 h.

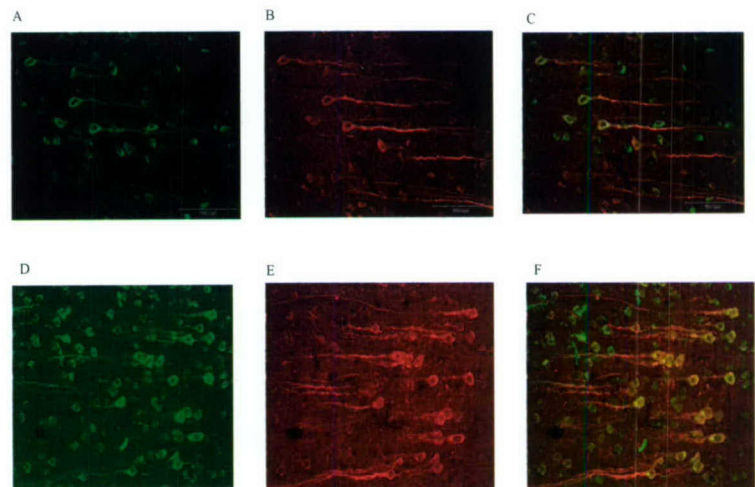


Fig. 64 The expression of the PTEN protein is significantly increased in neurons in the rat parietotemporal cortex between 15 min and 4h after fluid percussion induced TBI in rats. Photomicrographs represent staining with anti-PTEN antibodies of the corresponding cortical areas in sham-operated (A) and injured animals: (B) 15 min, (C) 30 min, and (D) 4 h.

2. Discovery of small molecule PTEN antagonists

Structure-based approach has become a powerful tool for drug discovery and design. To date, no PTEN small molecule inhibitor has been reported. Therefore, we sought to discover small molecule lead compounds as PTEN inhibitors using structure-based 3D-database searching. Based upon the 3D structure of PTEN, we can perform computational searching to identify small and drug-like organic compounds from large, three-dimensional, small molecule databases that complementarily bind to the active site of PTEN. These small molecules are ranked based upon their "scoring" function. Top ranked compounds are considered as potential PTEN inhibitors and tested in a biochemical assay for their ability to inhibit the phosphatase activity of PTEN.

Dr. Wang has developed a number of computational methods for structure-based drug design and successfully applied this approach for the discovery of novel lead compounds. Structure-based 3D-database searching requires an accurate 3D structure of PTEN and large 3D structural databases of small organic compounds. An accurate 3D structure of PTEN has recently been determined through X-ray crystallography. Dr. Wang's lab has utilized a number of large 3D-databases, with more than 700,000 small organic compounds, including the NCI 3D-database of 206,000 compounds and the Available Chemical Database of 275,000 compounds.

To date, we have searched both the NCI and the ACD 3D-databases, using the DOCK program developed by Dr. Kuntz of the UCSF, and identified approximately 1000 small organic compounds as potential PTEN inhibitors. In collaboration with Dr. Zhong-Yin Zhang in the Albert Einstein College of Medicine, a highly recognized expert in phosphatase field, we have examined 275 of these compounds using biochemical assays. Twenty-five compounds were confirmed to potently inhibit the phosphatase activity of PTEN, with an IC₅₀ value from 10 to 169 μ M (Table 3). To assess their specificity, we have begun to test these PTEN inhibitors against seven other phosphatases, including PTP1B: to date, three have been identified as specific phosphatase inhibitors against PTEN. Also in a preliminary study, we investigated the toxicity of various PTEN inhibitors and their ability to downregulate PTEN activity in cultured primary rat cortical neurons. Of these new PTEN antagonists identified, **PTI-9**, **PTI-10**, and **PTI-11** were found to be most cell-permeable and have low toxicity, although they are not the most potent PTEN antagonists in the biochemical assay. These three compounds were further evaluated for their ability to inhibit the PTEN activity in cultured primary rat cortical neurons. Treatment with the compounds at 1 h resulted in the dose-dependent decrease in PTEN activity, as measured by the PTEN lipid phosphatase activity assay (data not shown). It should be noted that these PTEN inhibitors represent the first generation of such compounds and promising lead compounds for further chemical modifications. We are currently carrying our structure-based design and extensive chemical modifications to further improve the potency and selectivity of these lead compounds.

To provide an understanding for the structural basis of the interaction between PTEN antagonists and PTEN, we have carried out extensive docking studies using the program AUTODOCK, as developed by Dr. Olson. In Figure 65, the interactions between **PTI-10** and PTEN are depicted. PTI-10 binds to PTEN in its active site and forms a number of optimal and specific hydrogen bonds with PTEN. It is of note that the hydrogen bond network mimics closely to the observed hydrogen bonds found between the pseudo-substrate and PTEN in the X-ray structure. This putative binding model provided us with a starting point for further structure-based design and chemical modifications to derive PTEN antagonists with improved potency and/or selectivity.

Table 3. Representative Small Molecule PTEN Inhibitors Discovered To Date

PTEN INHIBITORS	IC ₅₀ (μM)	MOLECULAR WEIGHT
PTI-1	51	290
PTI-2	32	353
PTI-3	33	379
PTI-4	45	277
PTI-5	50	336
PTI-6	10	477
PTI-7	12	326
PTI-8	10	302
PTI-9	47	302
PTI-10	26	370
PTI-11	169	342

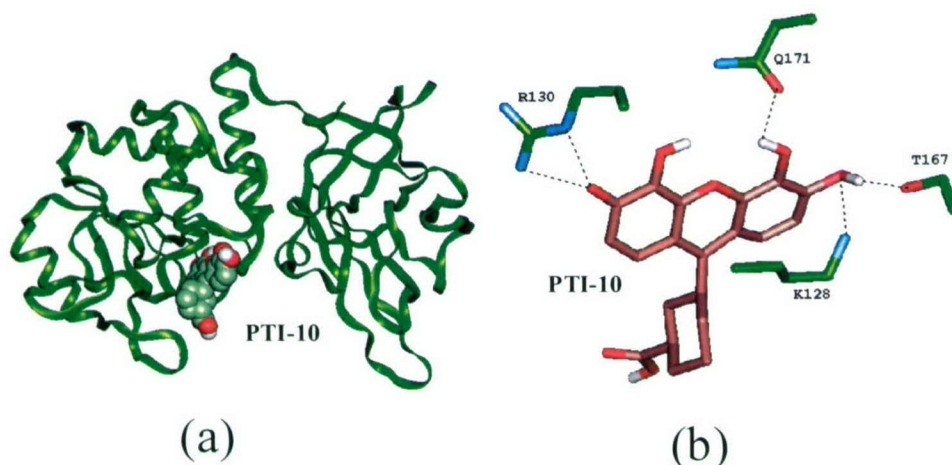


Fig. 65 Predicted binding model of PTI-10 with PTEN. A) PTI-10 binds to the active site of PTEN. B) Specific hydrogen bonding interactions between PTI-10 and PTEN. Specifically, PTI-10 forms hydrogen bonds with Lysine 128 (K128), Threonine 167 (T167), Glutamine 171, and Arginine 130 (R130).

In conclusion, studies demonstrate that PTEN may be elevated after traumatic brain injury in cells showing caspase-3/caspase-9 activation, and that *in vitro* it correlates to cell death through a caspase-mediated mechanism. Novel compounds have been identified that act as PTEN antagonists. Further development of such work through a combination of molecular modeling and synthetic chemistry may lead to identification of novel neuroprotective agents.

Hypothesis #4: β FGF binding protein enhances the activity of β FGF as a neuroprotective agent.

Basic fibroblast growth factor (bFGF or FGF-2) is a well-characterized member of FGF's family of proteins, which play important role in regulation of development and functioning of various cell types in both growing and adult organisms. bFGF was shown to act as neurotrophic factor, which not only promote cell survival but also positively regulates axonal sprouting and neurite outgrowth (for review see ¹⁴²). These findings suggest potential important role for bFGF as a neuroprotective agent in neuronal injury. FGF binding protein (FGF-BP) purified from human epidermoid carcinoma cells has been shown to bind FGF noncovalently, prevent bFGF immobilization and serve as a chaperone protein presenting bFGF to its high affinity receptor on target cells ¹⁴³⁻¹⁴⁵. As it was demonstrated by work of Dr. Wellstein group from the Lombardi Cancer Center at the Georgetown University, FGF-BP markedly upregulates mitogenic activity of bFGF and positively regulates its effects on signal transduction pathways in NIH-3T3 fibroblasts ¹⁴⁶. Based on the above-mentioned results we hypothesized that co-application of FGF-BP with bFGF will enhance neuroprotective activity of bFGF. To test this hypothesis we conducted series of experiments using well-established *in vitro* models of neuronal injury induced in rat cortical neuronal cultures by trophic support deprivation or by glutamate toxicity. In these experiments, bFGF was given to injured cells with or without co-treatment with FGF-BP. Outcome was measured by cell viability assays. Our results, however, indicate that FGF-BP did not enhance neuroprotection provided by bFGF alone in cortical neuronal cultures subjected to trophic support deprivation (Fig. 66); similar results were obtained in cultures subjected to glutamate toxicity (data not shown). The lack of effects of FGF-BP on neuronal cell survival may be explained, in part, by cell type specificity of its action.

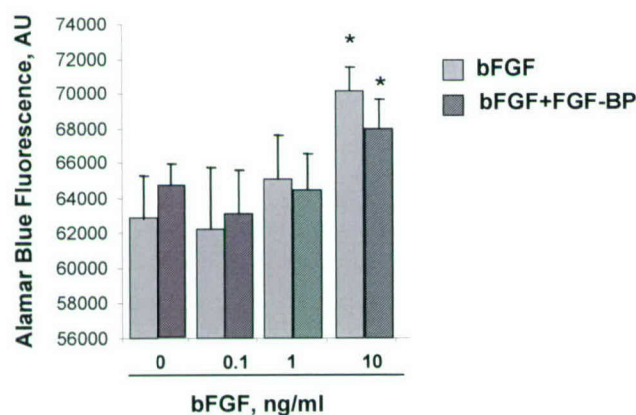


Figure 66. Co-treatment with the bFGF and FGF-BP did not enhance neuroprotection provided by bFGF in rat cortical neuronal cultures subjected to trophic deprivation. Cell viability was measured in trophic support deprived rat cortical neuronal cultures by Alamar Blue assay after 72 h of incubation with indicated concentrations of bFGF with or without co-application of FGF-BP (1ng/ml). Histograms represent Alamar Blue fluorescence \pm SD; $n = 8$ cultures per condition; * $p < 0.01$ versus injured cells compared by ANOVA, followed by the Dunnett's test.

Hypothesis #5: Induction of ceramide plays an important role in neuronal apoptosis and posttraumatic neuronal injury.

Using DOD support our group has performed a detailed investigation of molecular mechanisms involved in neuronal cell death. To address Hypothesis 5 we focused on ceramide-dependent neuronal cell death. Using in vitro models of neuronal apoptosis based on primary rat cortical neurons and cerebellar granule cells we demonstrated that exposure to soluble ceramide analogs (C_2 ceramide) (Fig. 67) or to treatments that induce accumulation of endogenous ceramide in cells¹⁴⁷ causes neuronal cell death. We also showed that endogenous ceramide accumulation occurs in neurons during cell death in vitro, in models that reflect conditions thought to be present in human neuropathology such as trophic factor deprivation (Fig. 68) or exposure to agents that induce DNA damage¹⁴⁷.

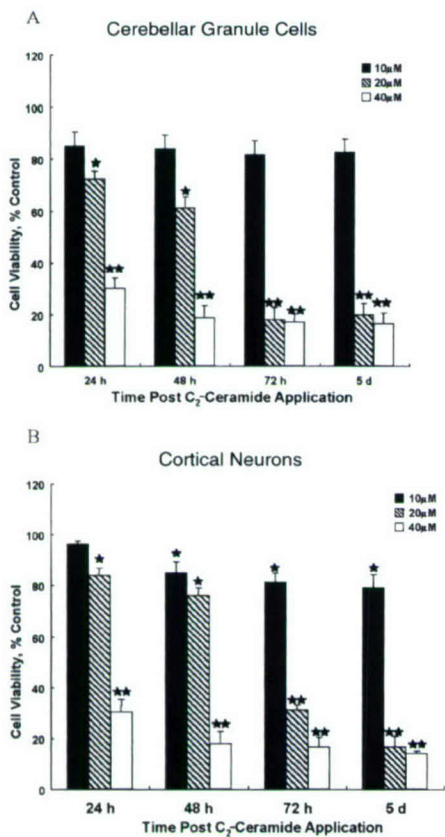


Fig. 67 C_2 -ceramide reduces viability of cerebellar granule cells (A) and cortical neurons (B). Seven DIV cultures were treated with the indicated concentrations of C_2 -ceramide and viability was measured after the indicated time periods by the calcein AM method. Each point is the mean \pm SE of eight wells. The data is representative of three to five separate experiments. $p < 0.05$; $p < 0.01$ vs. control (ANOVA, Kruskal-Wallis post-hoc).

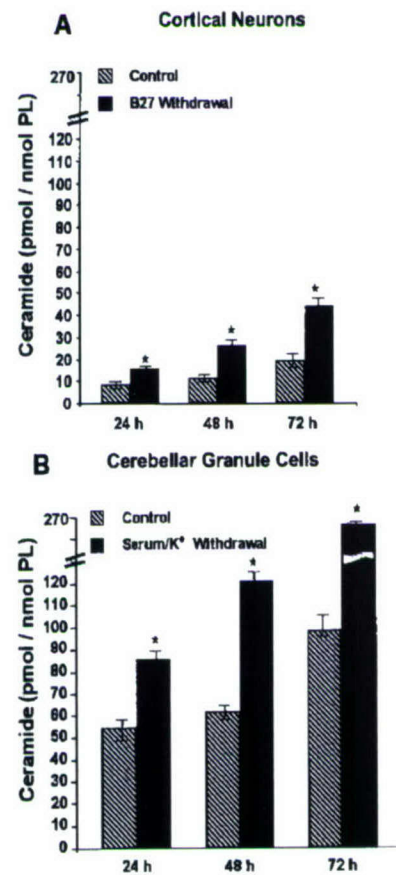


Fig. 68 Trophic withdrawal markedly enhances ceramide accumulation. Cortical neurons (A) and cerebellar granule cells (B) were cultured in serum free medium in the presence or absence of B27 or 25 mM KCl , respectively. Intracellular ceramide levels were measured at the indicated times. The data are expressed as pmol ceramide per nmol total phospholipids. Each point is the mean \pm SE of triplicate samples and similar results were obtained in two additional experiments. $p < 0.05$ vs. control, compared by two-tailed Student's t -test.

We determined that apoptosis and caspase-dependent mechanisms play an important part in ceramide-induced neuronal cell death¹⁴⁸. Ceramide-induced initiation of the intrinsic caspase activation pathway as demonstrated by the presence of active caspase-9 and caspase-3 (Fig. 69). Furthermore, using specific pharmacologic inhibitors (Fig. 70) and/or dominant negative constructs we demonstrated the importance of caspase-9 and caspase-3 activation for ceramide-induced neuronal cell death. A significant effort was dedicated to decipher signaling events induced by ceramide that are upstream of caspase-9 activation. It is known that initiation of the intrinsic caspase pathway and activation of caspase-9 requires cytochrome c release from the mitochondria. We demonstrated that mitochondria are a critical ceramide target, as release of multiple pro-apoptotic mitochondrial proteins occurs after ceramide administration (Fig. 71). The importance of the mitochondria for ceramide-induced cell death is also indicated using agents that prevent the opening of the mitochondrial pore transition complex (MPTC) such as Bongkrekic acid. Pretreatment with Bongkrekic acid attenuates cell death after ceramide administration as well as caspase-3 and caspase-9 activation (Fig. 72).

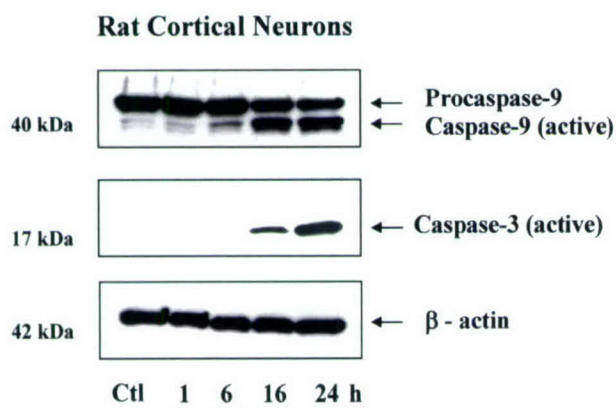


Fig. 69. Immunoblot analysis of C2-ceramide-treated rat cortical neuronal cultures revealed upregulation of active caspase-3 and caspase-9 protein levels. Active caspase-8 immunoreactivity was undetectable in this system (data not shown). At 7 DIV, cultures were treated with 40 M C2-ceramide; after indicated periods of time cells were harvested and subjected to immunoblot analysis as described in Materials and Methods. β-Actin was used as an internal control.

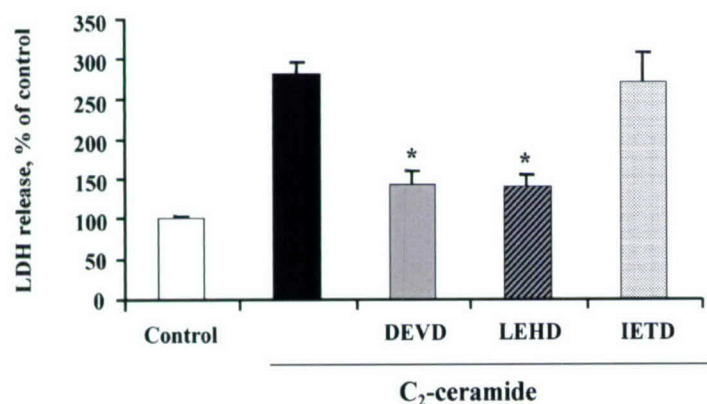


Fig. 70. Pretreatment with the caspase-3 inhibitor z-DEVD-fmk, or the caspase-9 inhibitor, z-LEHD-fmk, but not the caspase-8 inhibitor z-IETD-fmk, significantly reduced C2-ceramide induced cell death in rat cortical neuronal cultures. Cell death was measured by LDH release assay after 24 h of incubation with 40 M C2-ceramide with or without 1 h pretreatment with selective caspase inhibitors (each at 150 M). Histograms indicate LDH release as percentage of controls ±SD; n=8–16 cultures per condition; *P<0.01 versus C2-ceramide-injured cells compared by ANOVA, followed by Dunnett's test.

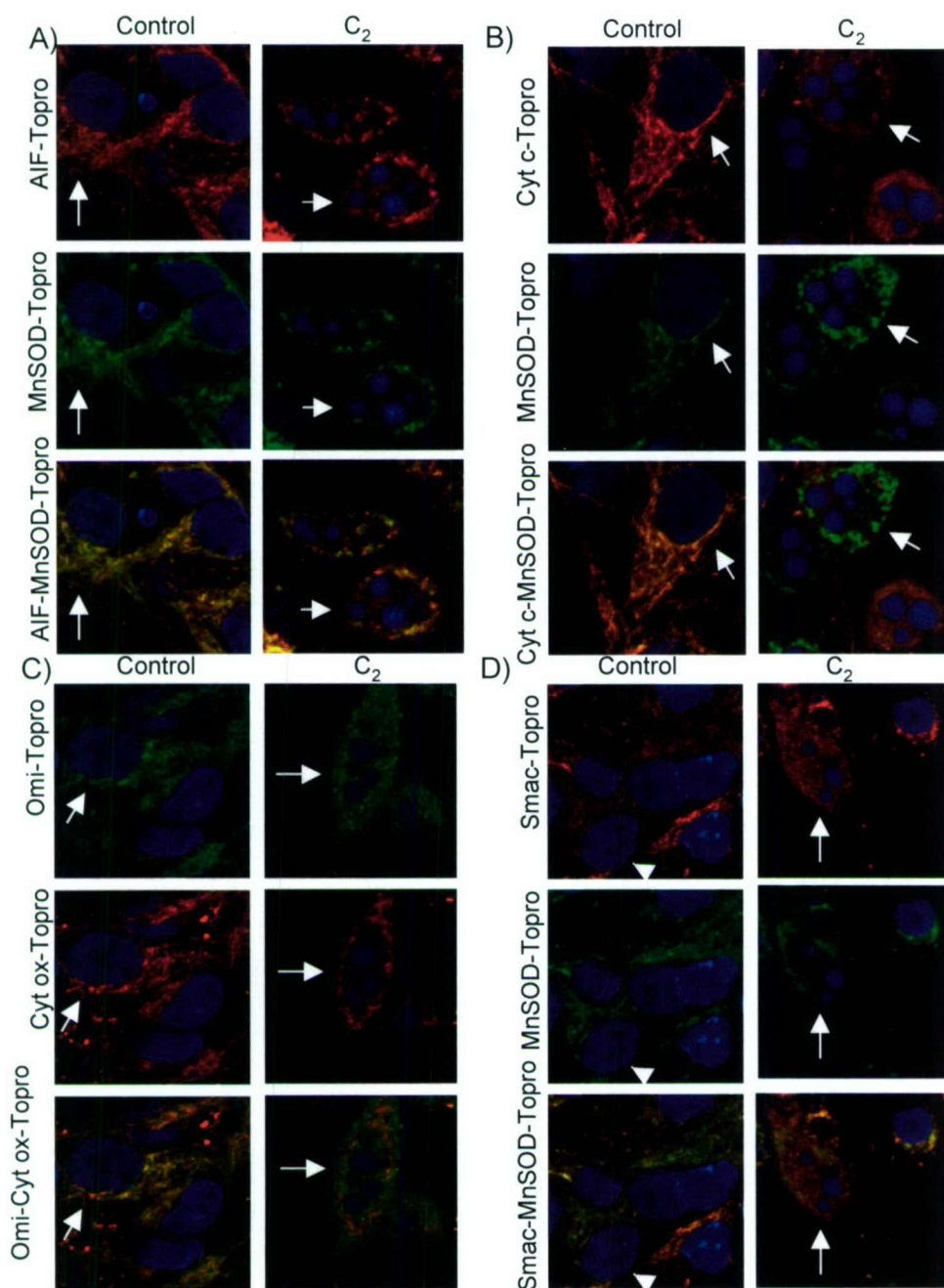


Fig. 71 C₂ ceramide administration causes release from the mitochondria of cytochrome c, AIF, SMAC and Omi in primary rat cortical neurons. Cortical neurons were exposed to 50 μ M C₂ ceramide for 24 h and localization of pro-apoptotic proteins, AIF (A, red), cytochrome c (B, red), Omi (C, green), SMAC (D, red) and in relation to mitochondrial markers MnSOD (A, B, D, green) and cytochrome oxidase (C, red) was evaluated by laser scanning confocal microscopy. Mitochondrial release was indicated by dissociation between the signal corresponding to the pro-apoptotic proteins and that of mitochondrial markers. The status of chromatin condensation was visualized by staining with TO-PRO-3 (blue). Images contain combinations of two or three optical channels as indicated. Representative cells are designated by arrows.

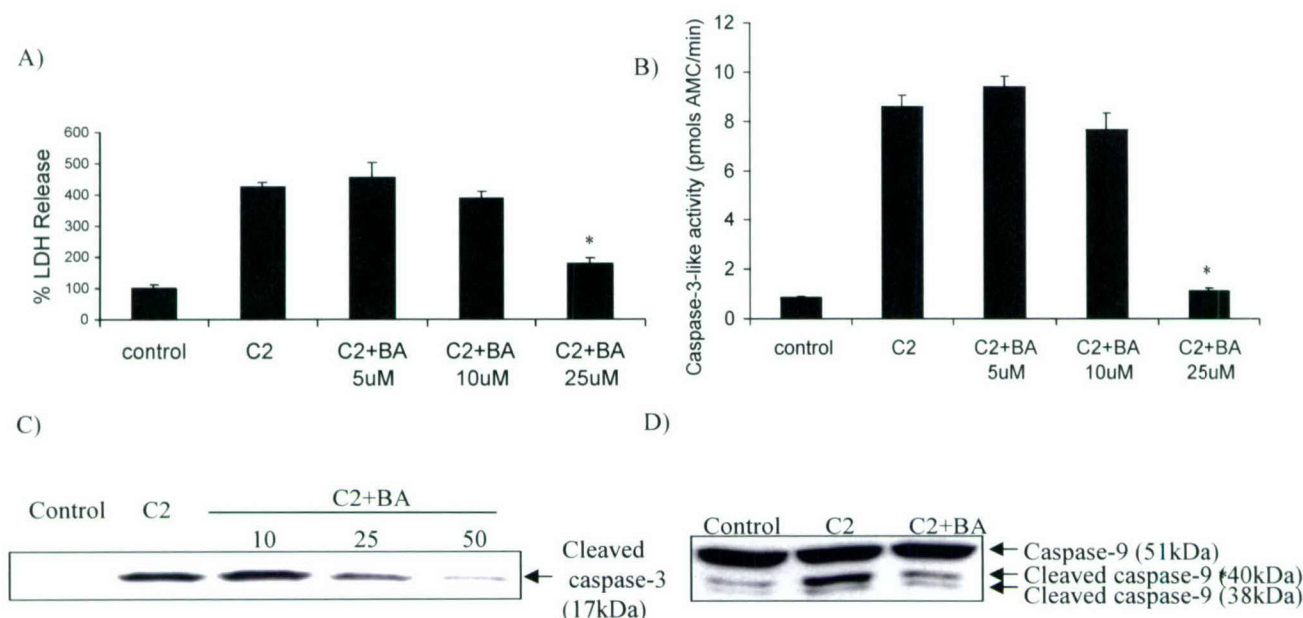


Fig. 72 Bongkreik acid prevents both the cell death and caspase-3 activation induced by C₂ ceramide. Rat primary cortical neurons were treated with 50 μ M of C₂ ceramide (C2) for 24 h in the presence of various concentrations of bongkreik acid (C2+BA). Cell death was evaluated by measuring LDH release in the culture media (A). The same neuronal plates were then assayed for caspase-3 activity with the Ac-DEVD-AM fluorogenic caspase-3 substrate (B). * represents significant difference from control (n=6 per treatment, p<0.05 Bonferroni/Dunn). Bongkreik acid prevents the cleavage of caspase-3 and caspase-9 induced by C₂ ceramide. Rat primary cortical cells were treated for 24 h with 50 μ M of C₂ ceramide with (C2+BA) or without (C2) various concentrations of bongkreik acid. 25 μ g of cell lysate was resolved on SDS gels, transferred on nitrocellulose membranes and probed with antibodies specific for the cleaved fragment of caspase-3 (C) and caspase-9 (D).

Various proteins kinase pathway such as AKT and MAPK are known to influence the mitochondria. Ceramide causes AKT dephosphorylation on critical Ser473 residues and inhibition of AKT kinase activity (Fig. 73) resulting in dephosphorylation and activation of pro-apoptotic molecules (Fig. 74) such as BAD (Bcl2 family member that translocates to the mitochondria), FKHR and GSK3b (activators of pro-apoptotic transcription factors)¹⁴⁹. Ceramide also causes increased phosphorylation of p38 MAPK. Furthermore, we demonstrated that activation of the p38 MAPK pathway is crucial for ceramide-induced neuronal cell death because pretreatment with p38 inhibitors attenuates cell death after ceramide administration (Fig. 75).

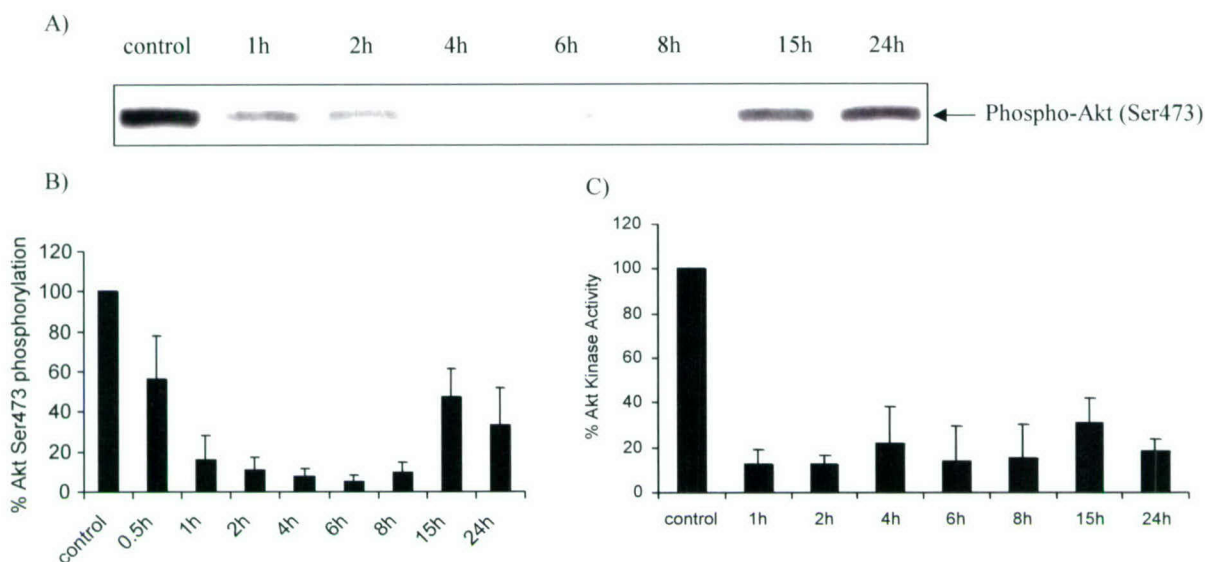


Fig. 73 C_2 ceramide induces rapid and extensive dephosphorylation of Ser 473 Rat primary cortical neurons were treated with 50 μ M of C_2 ceramide for different time intervals, as indicated. Protein concentration was measured and 25 μ g of protein was separated on SDS gels, transferred on nitrocellulose membranes and levels of Akt phosphorylated on Ser 473 (A) were probed with phosphorylation-specific antibodies. Quantitative analysis of the level of Ser 473 in cortical neurons treated with 50 μ M C_2 ceramide for various time intervals was performed using Western Immunoblot and densitometry (B). C_2 ceramide treatment results in decrease in Akt kinase activity (C). Rat primary cortical neurons were treated with 50 μ M of C_2 ceramide for the indicated time intervals. Akt kinase activity was measured from Akt immunoprecipitated from cell extracts.

Fig. 74 C_2 ceramide induces dephosphorylation of FKHR on Thr 24 (A), GSK-3 β on Ser 9 (B) and BAD on Thr 112 (C). Rat primary cortical neurons were treated with 50 μ M of C_2 ceramide for different time intervals, as indicated. Protein concentration was measured and 25 μ g of protein was separated on SDS gels, transferred on nitrocellulose (B) membranes and phosphorylation levels of FKHR Thr 24, GSK-3 β Ser 9 and BAD Thr 112 were probed with phosphorylation specific antibodies. (D) Quantitative analysis using Western Immunoblot and densitometry confirms the data presented in (A), (B) and (C). The totals levels of FKHR, GSK-3 and Bad do not decrease after C_2 ceramide treatment.

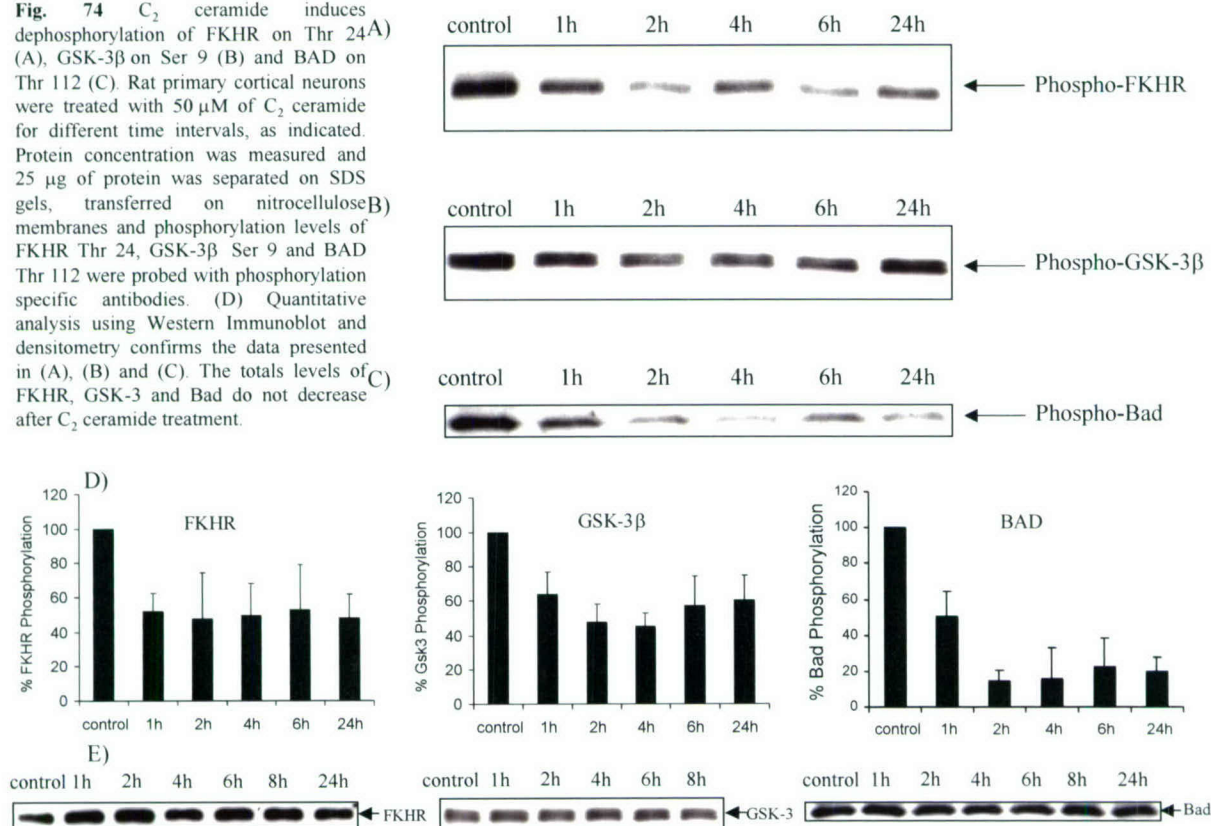
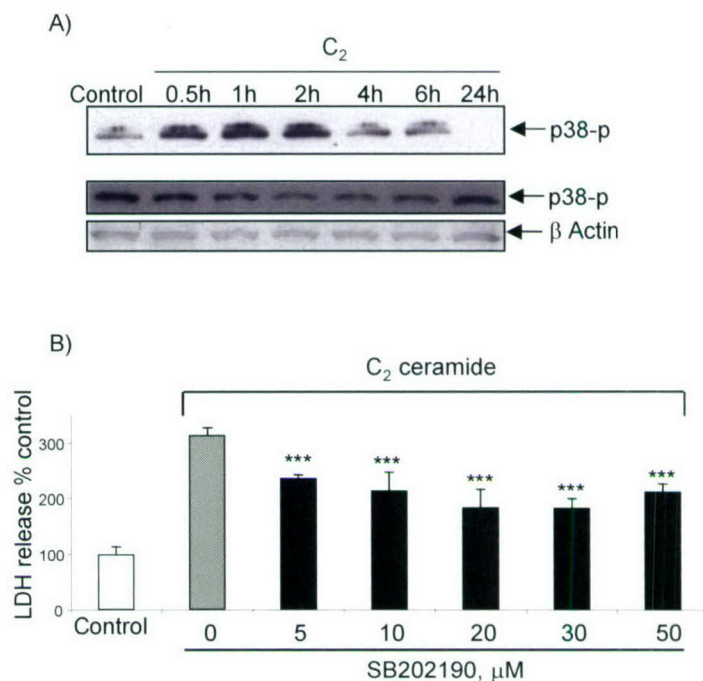


Fig. 75 C₂ ceramide increases the phosphorylation of p38 kinase (A). The total expression level of these kinases undergoes no significant changes. Rat primary cortical neurons were treated with 50 μ M C₂ ceramide for different time intervals, as indicated. 25 μ g of total cell extract were separated on SDS gels transferred to nitrocellulose membranes and the phosphorylation levels of p38 MAP Kinase on residues Thr180/Tyr182 were probed with phosphorylation specific antibodies. The same extracts were probed for total expression level of p38 followed by immunoblot with β -Actin to verify equal gel loading. Inhibitors of the p38 MAP kinase pathway attenuate specifically C₂ ceramide induced cell death in primary rat cortical neurons as evidenced by reduction in LDH release (B). Cortical neurons were pretreated with various concentrations of the p38 pathway inhibitors SB202190 exposed to 50 μ M C₂ ceramide for 24 h and then the extent of cell death was evaluated by detection of LDH release into the medium. LDH values were normalized to control and represented as mean \pm SD. The data were analyzed by one-way ANOVA followed by Tukey post test. *** $P < 0.001$ compared to C₂ treated, $n = 6$.



In conclusion, we believe ceramide causes important changes in upstream kinase cascades (Akt, MAPK) followed by mitochondrial depolarization and permeabilization, the release of pro-apoptotic factors such as cytochrome c, AIF, SMAC, Omi and ultimately activation of both caspase-dependent and caspase-independent apoptotic pathways. A better understanding of these mechanisms will help the development of new treatment strategies aimed at preventing neuronal cell death.

Hypothesis #6: DNA Chip technology can help define interactions among genes that play a role in secondary neuronal injury and endogenous neuroprotection.

Traumatic brain injury (TBI) induces a cascade of biochemical responses, both neurotoxic and neuroprotective that substantially determine subsequent tissue loss and associated functional deficits. However, molecular mechanisms underlying such delayed responses are not fully understood. Moreover, although it has long been recognized that TBI causes changes in gene expression patterns, until recently such studies have examined relatively small numbers of genes and/or their protein products. Microarray-based technologies can evaluate gene expression changes in a highly parallel manner, allowing the measurement of changes of thousands of genes and/or expressed sequence tags as a function of time after injury. The purpose of the present study was to identify common gene expression changes across different, albeit well-defined, injury models (fluid percussion vs. controlled cortical impact) and species (rat vs. mouse) in order to address the hypothesis that common changes across pathobiologically different models and species may help to identify the more important secondary injury responses. Importantly, we examined the same brain regions (parietal cortex directly underlying cortical impact site) in both models and compared injured to sham-injured tissue at all time points. We also studied multiple time points (4, 8, 24, 72 h), used replicate samples in order to conduct statistical analyses while holding constant the ratio of sham to experimental chips (2:3), conducted all expression profiling on the Affymetrix platform, and consistently applied normalization and filtering criteria prior to stringent statistical analyses.

1. RNA Extraction, Amplification, and Hybridization to Microarrays

To ensure adequate tissue for RNA extraction (~100 mg), three mouse cortex disks were pooled prior to RNA extraction. Pooling produced two naive (from six mice) samples, and for each experimental time point two sham (from six mice) and three injured samples (from nine mice) were obtained (n = 22 profiles). However, cortical tissue from one rat provided sufficient RNA without the need for pooling (n = 25 profiles). Total RNA was purified using an RNeasy kit (Qiagen Inc., Valencia, CA) prior to quantification. To detect extensive degradation, purified RNA was run on an agarose gel prior to cDNA synthesis. Degraded RNA was not used for hybridization¹⁵⁰. Each fragmented cRNA sample was hybridized to rat U34A or mouse Mu74Av2 oligonucleotide microarrays (Affymetrix Inc., Santa Clara, CA) for 16 h at 60 rpm at 45°C. The mouse Mu74Av2 microarray contains ~12,500 full-length sequences and expressed sequence tags (referred to as probe sets or genes throughout this text), while the rat U34A microarray contains ~8800 probe sets. Raw intensity data were captured, and the Affymetrix GeneChip® software MAS 5.0 was used to calculate signal intensity values for each oligonucleotide probe set in each genome (mouse or rat). A scaling factor, with a target intensity of microarray sector fluorescence to 800, was automatically applied to each microarray by the MAS 5.0 algorithm, permitting reproducible interarray comparisons. Probe sets hybridization performance (pairs of 20 perfect match and mismatch 25mer oligonucleotides per probe sets) identified signal intensities that were reliably detected as present, and eliminated most non-specific cross-hybridization signals, as previously described (Chen et al., 2000; Bakay et al., 2002).

2. Microarray Quality Control, Correction for Saturated Probe Sets, and Normalization

Within both species, each microarray underwent a stringent quality control evaluation as previously described¹⁵⁰. The following parameters were considered: cRNA fold changes (amount of cRNA obtained from starting total RNA); scaling factor; percentage of probe sets reliably detected (present); mean signal value indicating the relative abundance of a probe set; and correlation

coefficient of mean signal values for each transcript between microarrays at the same experimental time point. In addition, control charts were generated using scaling factor and percentage present probe sets to identify systematic errors in the expression profiling process. Identification of microarrays with scaling factor or percent present ≥ 2 standard deviations above or below the mean, as shown in Figure 76, alerted us to the possibility of significant errors in laboratory methods.

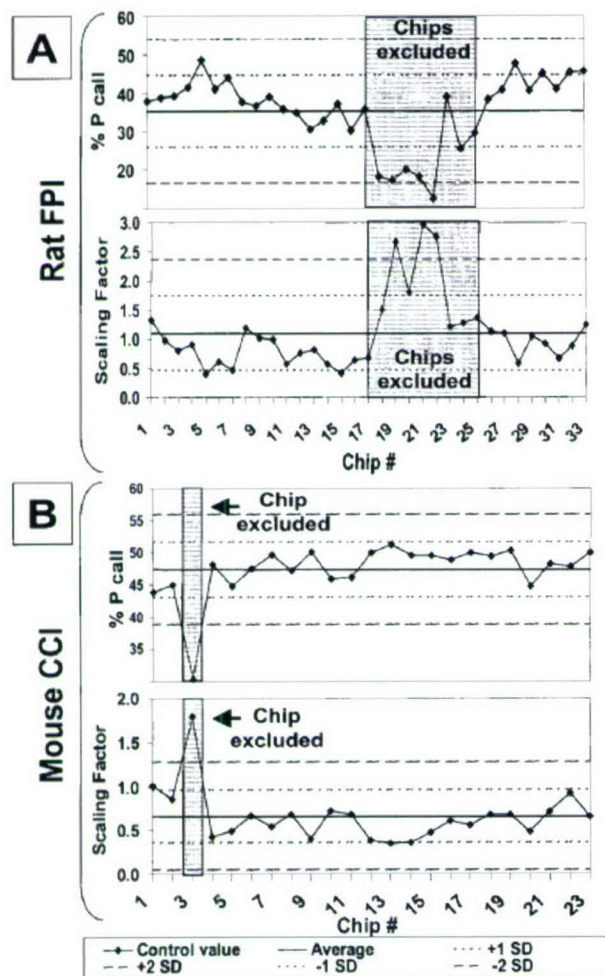


FIG. 76. Control charts showing variability in microarray processing across each experiment. (A) Rat fluid percussion injury experiment. Percentage present call (upper panel) and scaling factor (lower panel) are plotted for each chip in the order that chips were hybridized. Mean and standard deviation for percentage present call or scaling factor were calculated for all chips in the experiment. Horizontal lines indicated the mean (solid line), one standard deviation (dotted lines), and two standard deviations (dashed lines) above and below the mean. Chips with control values falling outside 2 standard deviations from the mean are flagged (chips 20, 22, 23). All chips processed under the same conditions as flagged chips are excluded (gray region) from further analysis. (B) Mouse controlled cortical impact. Same as A. One chip, 3, failed to meet control standards and was excluded.

3. Data Filtering and Statistical Analysis

We based all further analysis only on those probe sets that were detected in 40% or more of the microarrays comprising the complete microarray series for each experimental model. This data scrubbing retained the probe sets with the most reliable and consistent performance between multiple measurements among arrays of the same experimental group¹⁵⁰. Experiment normalization and statistical analysis were performed using GeneSpring software, version 5.0 (Silicon Genetics, Redwood, CA). For each probe set, signal intensity from injured and sham controls were normalized to the mean signal intensity generated from the same cortical region from three naive rats or mice. The combination of fold change threshold and p values serves to eliminate most false positives, producing a more stringent list. To accurately identify significantly regulated genes shared by both species, cross species probe set matches were identified using UniGene and the Program in Genomic Applications web site <http://pga.tigr.org/tigrscripts/xref/list.pl>. Furthermore, each match was verified by direct sequence matching of significantly regulated rat and mouse genes.

4. Microarray Validation: Semi-Quantitative Reverse Transcriptase–Polymerase Chain Reaction

One mg of total RNA was used for cDNA synthesis using SuperScript reverse transcriptase and oligo (dT)- primer (Invitrogen Corp., Carlsbad, CA). The amount of synthesized cDNA was evaluated by PCR using primers specific for ribosomal protein RPL19. Polymerase chain reactions (PCR) were performed in a PTC-225 Thermal Cycler (MJ Research, Waltham, MA) using AmpliTaq polymerase (Applied Biosystems, Foster City, CA).

5. Functional Classification of Genes

The 82 differentially expressed genes were assigned functional annotations based on information in publicly available sources including Gene Ontology and PubMed. It is recognized that a given gene may have multiple functions and that a variety of assignment systems can be constructed. For these analyses, each gene was assigned to only one functional class.

5.1. Comparison across the Two Models Identifies Commonly Expressed Genes

Our analyses focused on identification across species and models of “essential” genes consistently responding to the stress of traumatic injury. Overall, 82 genes identified were significantly regulated across both models and all subsequent analyses focus on this subset of genes. The 82 genes regulated in common across the two models were categorized with respect to known functions, as displayed in Figure 77. The highest proportion of genes commonly altered between the two models reflected inflammation (17%) or transcription regulation (16%). However, we identified numerous genes related to cell adhesion/extracellular matrix, cytoskeleton, and RBC-related, which have previously received little attention in TBI molecular pathobiology.

Gene functions were broadly grouped into those involved in biological processes or cellular functions. As shown in Figure 78, we examined the proportion of genes in each biological process class that was regulated at each time point and within each model. For example, of the genes regulated at 4 h after fluid percussion injury in the rat, 8% were in the apoptosis/cell cycle class. These data demonstrate expression of genes regulating cell adhesion, inflammation, and oxidative stress in both models by 4–8 h. By 8 h, genes associated with apoptosis/cell cycle are upregulated in the mouse injured cortex. Similarly, Figure 79 shows the relative contribution of the seven cellular functional classes that were regulated at each time point and within each model. Expression of RBC-related genes occurred rapidly, suggesting mRNA release from damaged RBC quickly after injury. Genes associated with the actin cytoskeleton and cellular motility were upregulated 8–72 h after cortical injury. Genes related to proteolysis were markedly upregulated at 72 h. Taken together, these results indicate that inflammation and oxidative stress, as well as changes in transcriptional regulation and calcium binding, participate in the brain’s response to injury. Furthermore, the induction of genes related to cell adhesion/ECM, cytoskeleton, and proteolysis appear to reflect more delayed components of the secondary injury response. Other novel genes, not previously associated with TBI, were identified across models (Fig. 80).

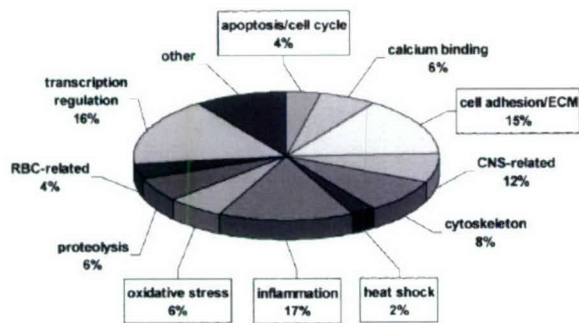


FIG. 77. Functional classes of the 82 genes regulated in both models and across both species. Genes were assigned to a functional class based on their reported function. Pie chart showing percentage of genes assigned to each functional category. Both up and downregulated genes are shown. Five functional classes (box surrounding name) are involved in biological processes while the remaining seven relate to cellular functions. CNS, central nervous system; ECM, extracellular matrix; RBC, red blood cell.

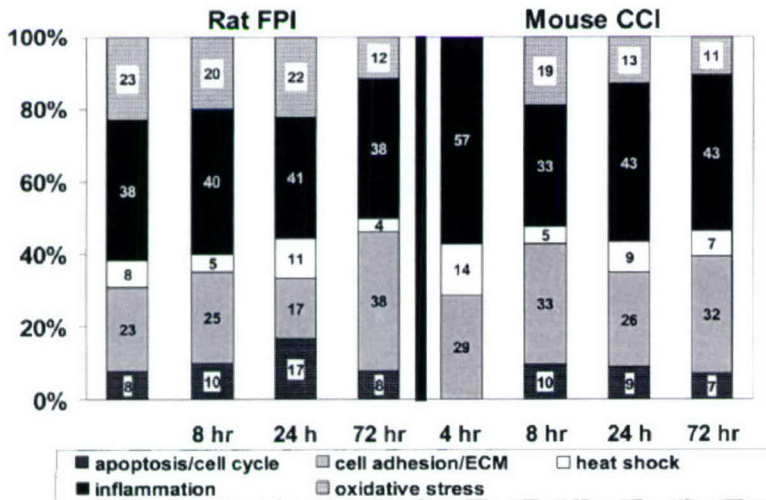


FIG. 78. Relative contribution of the five biological processes to overall gene expression at each time point. Numbers in each segment corresponds to the proportion of genes in each biological process class regulated at each time point. Left panel: Rat fluid percussion injury (FPI). Right panel: Mouse controlled cortical impact (CCI). ECM, extracellular matrix.

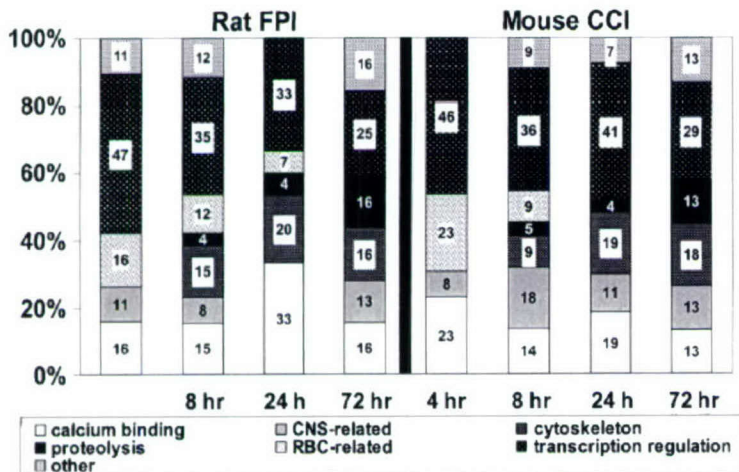


FIG. 79. Relative contribution of the seven cellular functional classes to overall gene expression at each time point. Numbers in each segment corresponds to the proportion of genes in each cellular functional class regulated at each time point. Left panel: Rat fluid percussion injury (FPI). Right panel: Mouse controlled cortical impact (CCI). CNS, central nervous system; RBC, red blood cell.

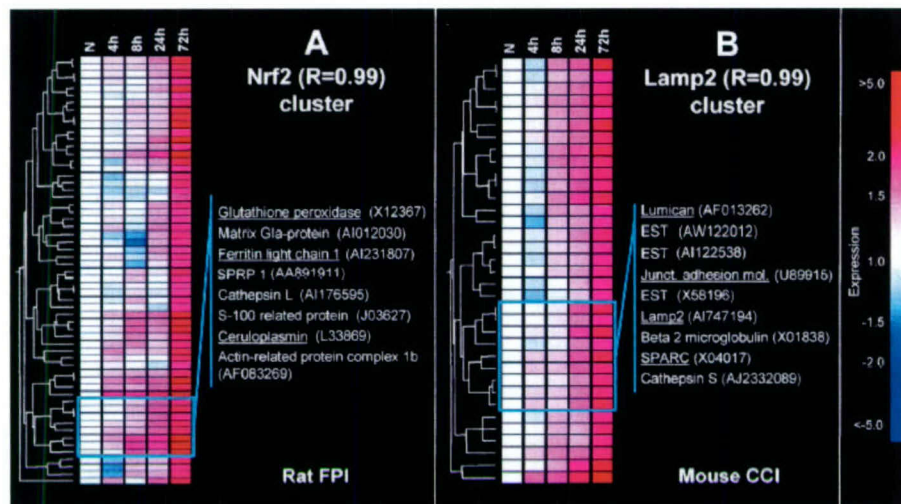


FIG. 80. Hierarchical cluster of genes coordinately regulated to two genes not previously implicated in traumatic brain injury pathophysiology. Upregulated genes (red) and downregulated genes (blue) in injured parietal cortex at 4, 8, 24, and 72 h after fluid percussion injury (FPI) in rat (A) or controlled cortical impact (CCI) in mouse (B). Expression level after injury normalized to expression level in parietal cortex at same time point after sham injury. Panel A: Genetree containing 59 genes with expression pattern highly correlated (Pearson correlation, $R = 0.99$) with NF-E2-related factor 2 (Nrf2) after FPI. White box encloses a tree sub-branch containing 3 oxidative stress response genes (names underlined) that share a similar expression pattern. Panel B: Gene tree containing 35 genes with expression pattern highly correlated (Pearson correlation, $R = 0.99$) with lysosomal membrane glycoprotein 2 (Lamp2). White box encloses a tree sub-branch containing three cell adhesion/extracellular matrix genes (names underlined) that share a similar expression pattern. EST, expressed sequence tag; Junct. Adhesion mol., junctional adhesion molecule; SPARC, secreted acidic cysteine rich glycoprotein; SPRP 1, small proline-rich protein 1.

5.2. Microarray Result Validation: RT-PCR

To validate our microarray results, we used semi quantitative RT-PCR with nine genes representing most functional categories. RT-PCR confirmed the direction and relative magnitude of change in gene expression between sham and injured samples (Fig. 81). Between comparison of the magnitude of the microarray and the RT-PCR expression results, these two independent methods show the same general pattern of expression for all genes studied.

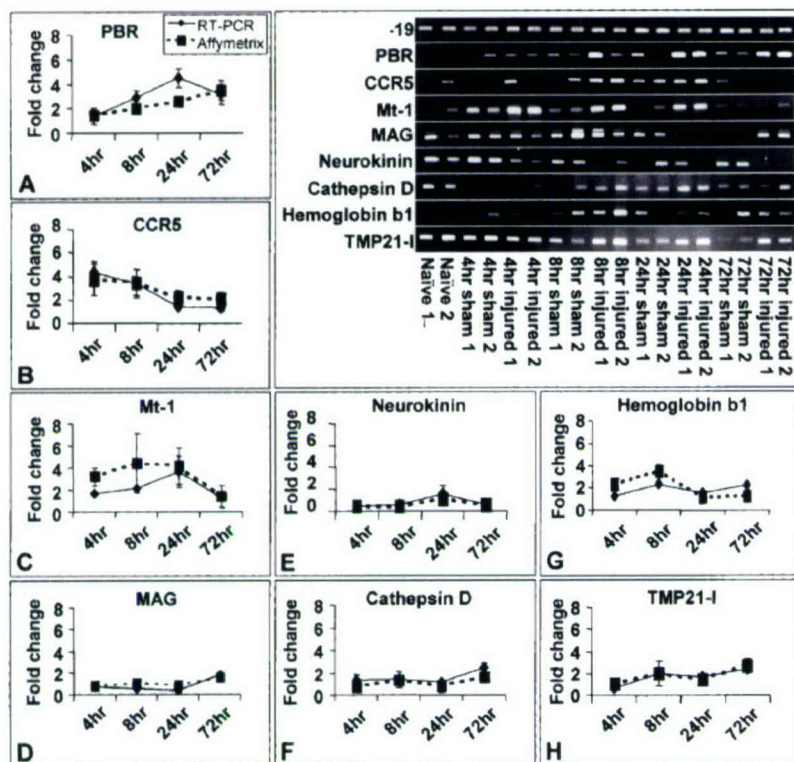


FIG. 81. Validation of expression changes observed by microarray with RT-PCR in nine genes across four time points after experimental TBI. Magnitude and pattern of gene expression of eight genes shows significant induction. (A) Peripheral benzodiazepine receptor (PBR), (B) C-C chemokine receptor 5 (CCR5), (C) metallothionein I (Mt-1), (D) myelin-associated glycoprotein (MAG), (E) neurokinin, (F) cathepsin D, (G) hemoglobin b1, (H) transmembrane protein (TMP21-I).

5.3. Secondary Brain Injury: Novel Gene Expression Patterns Suggestive of Degeneration or Regeneration

TBI expression profiling revealed altered regulation of processes linked both to neural degeneration and regeneration. In the injured cortex we observed altered regulation of numerous genes that have been associated with neurodegenerative or restorative processes in a variety of models of CNS disease or injury. Several genes identified in this study but not previously implicated in TBI that have been associated with tissue degeneration: the transcription factor ATF3 (member of ATF/CREB family of transcription factors induced by stress in neurons), myelin associated glycoprotein, and lysosomal membrane glycoprotein 2 (receptor for substrate proteins of chaperone mediated autophagy). Other previously unreported gene changes may reflect endogenous neuroprotective mechanisms such as lipocortin 1 (an antiinflammatory calcium binding protein); calponin 3 (an actin-binding protein enriched at neuronal growth cones); gelsolin (an actin severing protein that mediates calcium influx in neurons by altering mobility of NMDA receptor subunits); Id-1 (a helix-loop-helix transcription factor expressed during neuronal proliferation and differentiation); and p45 NF-E2 (Nrf2, a bZIP transcription factor that regulates phase 2 antioxidant genes by binding to the antioxidant response element in their promoters).

5.4. Analysis of Sequential Gene Expression

IRF1 was the first nuclear transacting factor demonstrated to contribute directly to cerebral ischemic damage and its binding to the interferon response factor element is known to be essential for interferon gamma-induced MHC class II expression. Furthermore, Matzilevich also found IRF1 to be

upregulated following traumatic brain injury. It is, therefore, not surprising that in our experiments MHC class II expression consistently followed the expression of IRF1. This was true even though the exact timing of these events was not the same in the mouse and rat models. Over half of genes upregulated at 72 hours were not expressed at earlier time points, suggesting that a new set of molecular and cellular responses are initiated relatively late after injury. These include factors related to inflammation, oxidative stress, cytoskeleton and proteolysis, among others. For example, the bZip transcription factor Nrf2, an essential activator of genes encoding antioxidant enzymes and phase II detoxifying enzymes through the antioxidant response element was among genes showing initial upregulation at 72 h. The Nrf2-regulated genes HO-1 and ferritin were also upregulated at 72 h. Furthermore, the expression patterns of an additional two oxidative stress response genes, glutathione peroxidase and ceruloplasmin, were highly correlated ($R = 0.99$) with the pattern of Nrf2. The coordinated regulation of Nrf2 with oxidative stress sensitive genes suggests a delayed oxidative stress to which a transcriptional response is mounted. Increased F2-isoprostane-containing lipids in cerebrospinal fluid 5–7 days after TBI in children support the presence of such a late oxidative stress.

6. Limitations and Strengths

It is important to recognize both the methodological limitations and strengths of this work. We performed RNA extraction from brain tissue at four-time points following traumatic brain injury. Therefore, we describe a heterogeneous cell population that is tissue-specific rather than cell-specific. Furthermore, the distribution of particular cell types is likely to differ at the four time points. Because the methods that we employ provide sensitivity that is affected by the relative distributions of various transcripts, rare transcripts were less likely to be detected. Subsequent work using cell-specific profiling would address some of these limitations.

Our experimental approach does, however, also contribute significant strengths. First, we examined expression of almost 9000 genes/ESTs at four time points over 72 h, thus improving our ability to understand the alterations induced by injury. Second, our sampling in both the experimental and sham animals was regionally specific and included extraction of the same tissue sample volume. This provided a consistent and directly comparable source of RNA for analysis. Third, we have reduced the rate of false positive results, a prevailing concern in microarray experiments, by eliminating microarray results that fail to meet high quality control standards and by imposing stringent statistical criteria for identification of differentially regulated genes. Moreover, we identified a group of consistently regulated genes from two species and two injury models that are dissimilar in a number of ways, suggesting that the molecular pathways reported here may be characteristic of the genomic response to CNS injury.

In conclusion, expression of 82 genes in 12 functional categories was significantly changed in both rat and mouse models of TBI. The largest number of gene expression changes were found in the functional groups related to inflammation (17%), transcription regulation (16%), and cell adhesion/extracellular matrix (15%). Fifty percent of genes similarly altered across models had not been previously implicated in traumatic brain injury. Of particular interest were expression changes in genes linked to neurodegeneration, such as ATF3 and lysosomal membrane glycoprotein 2, and to neuroprotection including lipocortin 1, calponin 3, gelsolin, Id-1, and p45 NF-E2. Gene expression profiling across species and models may help identify candidate molecular pathways induced by brain injury, some of which may provide novel targets for therapeutic intervention. Parallel microarray studies have been conducted in spinal cord injury; these are described in Hypothesis #8.

Hypothesis #7: High field magnetic resonance imaging and spectroscopy can be used to examine mechanisms of CNS injury and effects of treatment.

The development of irreversible tissue damage following brain injury is caused by both primary and secondary injury mechanisms. Primary injury is the mechanical events associated with the initial injury to the brain, whereas secondary injury is the chemical or metabolic changes initiated by the original insult. These secondary changes then develop over minutes to days after the primary event to cause further brain injury. This gradual development of secondary injury with time provides a window of opportunity to attenuate, or even prevent, the secondary injury process and subsequently improve the outcome. However, the factors that contribute to secondary injury first need to be identified before appropriate "anti-factors" can be developed. One of the major difficulties associated with the identification of secondary injury factors has been the use of invasive physiological and biochemical techniques that by their nature destroy tissue. Moreover, such techniques are limited to single time points and do not permit the correlation of measurements of physiological and metabolic changes with the ultimate survival and neurological outcome following brain injury. One class of techniques that has gained increasing acceptance as a valuable tool in the study of brain injury is magnetic resonance spectroscopy (MRS) and imaging (MRI). These magnetic resonance (MR) techniques are noninvasive and permit the repeated monitoring of various metabolic and physiologic changes over time. Moreover, at an experimental level, a brain-injured animal can be allowed to recover and evaluated with regard to long-term neurological outcome and histopathology. Thus, each animal serves as its own control, and correlations can be made between early metabolic and physiological changes and chronic behavioral recovery or tissue damage.

1. Magnetic resonance spectroscopy (MRS)

The application of MR techniques to the study of biological systems was first performed in the 1950s, but it was not until the advent of surface coil techniques in 1980 that the technology was successfully applied to the study of organ metabolism *in vivo*. Since then, the investigation of brain metabolism by MR techniques has resulted in literally thousands of medical and scientific research studies. Although a number of nuclei can be evaluated with MR, most MR studies in brain injury have concentrated on either phosphorus or proton resonances. Phosphorus MRS allows the monitoring of metabolic events involving phosphorus metabolites. Because many of the critical energetic processes occurring in the cell are essentially phosphate transfer reactions, phosphorus MRS has grown to be the most widely used MRS technique in the study of metabolism. Several metabolites can be identified including phosphomonoesters (PME), inorganic phosphate (Pi), phosphodiester (PDE), phosphocreatine (PCr), and the three phosphates of adenosine triphosphate (ATP). The integrated area under each peak is directly proportional to the concentration of that metabolite, whereas the chemical shift (i.e., position) of the peak provides information about the ionic environment of that metabolite. For example, the Pi peak is commonly used to determine the intracellular pH, the chemical shift of the Pi peak being dependent on the dissociation state of HPO_4^{2-} . Similarly, intracellular free magnesium concentration (Mg^{2+}) can be determined on the basis of the chemical shift of $\alpha\text{-ATP}$, which is dependent on the relative concentrations of Mg^{2+} -bound ATP and Mg^{2+} -free ATP (Fig. 82). Thus, change in the position of the peaks provides valuable information about the intracellular ionic environment, whereas change in the intensity of the peaks provides an indication of the relative concentrations of the metabolites. Application of proton MRS to the study of the brain has been somewhat slower than that of phosphorus MRS because of difficulties inherent in this method. The relative concentrations of the intracellular metabolites is in the millimolar range, whereas the concentration of water approaches 40 M, which is equivalent to 80 M in protons. Thus, to observe the

less concentrated metabolites, effective suppression of the dominant water peak is essential. Furthermore, the difference in chemical shifts between metabolites is far less than that observed in phosphorus MRS. For example, the normal phosphorus spectrum extends over approximately 40 parts per million (ppm), whereas most observable proton resonances occur within a 10-ppm range. Thus, there is significant overlap between metabolites in a proton spectrum that makes identification of individual resonances somewhat difficult. Nevertheless, proton MR techniques have been developed that allow for the monitoring of certain metabolites, including lactate, *N*-acetyl aspartate (NAA), total creatine (creatine plus phosphocreatine), total choline, lipids, and amino acids (Fig. 83). Furthermore, as higher field magnets are developed and applied to brain studies, the degree of overlap between individual resonances will be reduced providing greater chemical shift dispersion and improved detection sensitivity such that more metabolites will be visible. Numerous MRS studies have reported "normal" values for various parameters in brain. From phosphorus studies, intracellular pH is approximately 7.1, and intracellular free Mg^{2+} concentration ranges from 0.3 to 0.6 depending on age, gender, and species. Although absolute concentration values of metabolites in brain have been reported, these values vary depending on the methods used. Therefore, it is usual in phosphorus MRS to report ratios that avoid the pitfalls of absolute quantitation. The ratios so far reported are somewhat species dependent; PCr/Pi ranging from 2.0 in humans to 4.0 in rats; the PCr/ATP ratio ranges from 1.0 to 2.0, respectively. It should be noted that these are adult values, and results are lower for neonatal brain. ADP concentration has been calculated from the creatine kinase equilibrium reaction to be approximately 20 to 30 μ moles/g tissue wet weight. This calculation uses in vitro values for PCr and ATP, and the MRS measured values for pH and free Mg^{2+} . Because this value for ADP concentration is significantly less than previous values determined using in vitro techniques, it is thought to represent the free cytosolic pool and not the total ADP pool. In water-suppressed proton MR spectra of normal brain NAA is the dominant metabolite with a concentration of approximately 13 mM, although the exact value is dependent on age and to a small degree by location (gray matter versus white matter). Originally used as an internal standard, it is now known that the NAA concentration varies with pathophysiological state and cannot be used as a concentration standard. Indeed, it is widely accepted that NAA is a neuronal marker reflecting both neuronal integrity and neuronal metabolic activity. It is commonly expressed in terms of a ratio with other visible metabolites including total choline (NAA/Cho) or total creatine (NAA/Cr), with the latter being the more frequently used. The normal value for NAA/Cr is approximately 1.35 and varies according to brain location and age. The degree of water suppression affects peak intensities of those metabolites closest to the water frequency, and this should be borne in mind when examining relative metabolite concentrations. Although very important after brain injury, lactate is normally not visible in normal brain because it is present at submillimolar concentrations¹⁵¹.

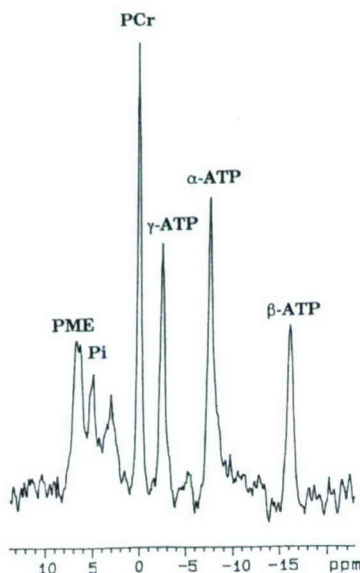


Figure 82. Phosphorus MRS spectrum obtained at 7.0 tesla from the left hemisphere of a rat immediately before induction of trauma. Peaks include phosphomonoesters (PME), inorganic phosphate (P_i), phosphocreatine (PCr), and the three phosphates of ATP.

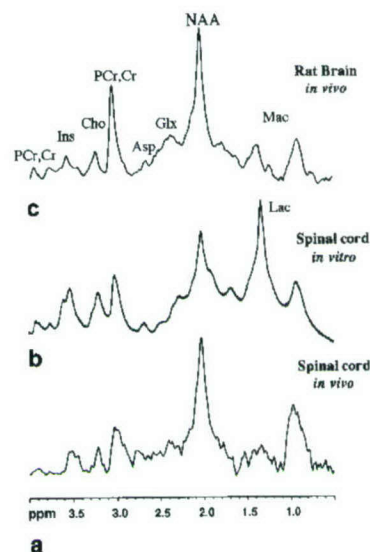


Figure 83. Proton MRS from the rat spinal cord *in vitro* (a) spinal cord *in vivo* (b), and rat brain (c). Peaks include phosphocreatine (PCr), creatine (Cr), inositol (Ins), choline (Cho), Asp (aspartate), N-acetyl-aspartic acid (NAA) and lactate (Lac).

Changes in MRS metabolites following experimental brain trauma are dependent on the injury severity. For example, trauma that results in mild to severe levels of motor dysfunction does not cause loss of ATP or sustained lactic acidosis. It is only when very severe levels of trauma are induced that there is a depletion of ATP reserves, most likely as a result of secondary ischemia caused by the extreme nature of the insult. Nonetheless, there are significant changes in the MRS spectra following less severe levels of traumatic brain injury. Brief acidosis is apparent in the immediate post-traumatic period, although the acidosis is slight (pH decreases to a minimum value of 6.8) and transient, recovering by 1.5 hours after the injury. The development of intracellular acidosis is correlated with accumulation of lactic acid, which, as shown in ischemia studies, is linearly related to intracellular acidosis. Cellular bioenergetic state also decreases following trauma as reflected in declines in PCr/ P_i ratio and calculated cytosolic phosphorylation potential. This decline in the bioenergetic state is thought to reflect an increased energy demand in response to attempts to maintain ionic gradients after trauma (Fig. 84). Significant correlation between decreased cytosolic phosphorylation potential and motor deficit has also been demonstrated following moderate traumatic brain injury in rats (Fig. 85)

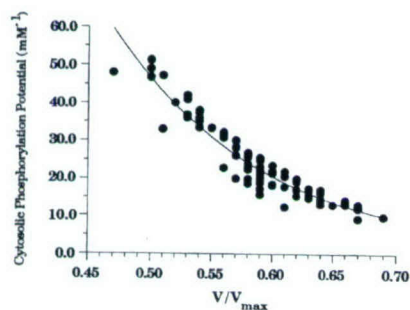


Figure 84. Relationship between mitochondrial oxidative capacity (V/V_{\max}) and cytosolic phosphorylation ratio following moderate traumatic brain injury in the rat. $R=0.95$; $p<0.001$.

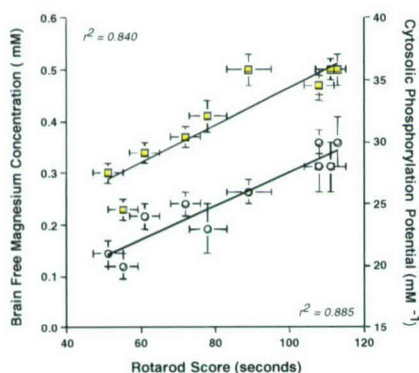


Figure 85. Relationships between cytosolic phosphorylation, brain free magnesium concentration and motor function measured by rotarod following moderate traumatic brain injury in rats.

Phosphorus MRS has also shown that the brain intracellular free Mg^{2+} concentration decreases by as much as 60% after brain injury. In addition to being mandatory for all energy producing and energy consuming reactions, the magnesium ion is essential for membrane stability, modulation of K^+ , Ca^{2+} , and *N*-methyl-D-aspartate channel activity, protein synthesis, RNA aggregation, DNA synthesis, and regulation of vascular tone. Thus, decline in the free and tissue concentration of this ion may be involved in many of the reported secondary events following trauma. The evidence demonstrating that intervention that restores Mg^{2+} levels following CNS trauma improves neuronal survival and improves functional outcome suggests that Mg^{2+} may be a critical early factor leading to irreversible tissue damage after CNS trauma. Although the importance of the magnesium ion has long been recognized, MRS studies have now provided evidence, at least in trauma, stroke, migraine, and substance abuse, that free Mg^{2+} may play a central role in metabolic regulation *in vivo*.

Proton MRS studies have demonstrated that NAA declines following trauma in a fashion similar to that observed in ischemia. Moreover, the decline in NAA, and particularly gray matter NAA, has been reported to predict outcome after trauma, and more specifically, overall neuropsychological performance. Because NAA is restricted to neurons, it has also been proposed that the loss of this metabolite is a marker for neuronal cell death. However, recent observations suggest that NAA decline may also occur through metabolic depression or in response to altered osmolar state. As such, the use of NAA as an assay of neuronal numbers should be discouraged, although its use as an indicator of neuronal status seems valid¹⁵¹.

2. Magnetic resonance imaging (MRI)

MRI differs from MRS in that total signal intensity is mapped against location giving an image of the signal distribution. Most studies have mapped the proton intensity of water, whose concentration varies by 14% between tissues, thus giving excellent soft tissue contrast, particularly in brain. In addition to anatomical images of brain structure, the technology can also be used to obtain information on vascular anatomy, blood flow, edema development, water diffusion and perfusion, glucose turnover, and more recently, metabolic information has been obtained by using an exciting MRI development termed functional imaging. Functional imaging provides information on the relationships between brain structures and their function. Numerous studies have used MRI in the study of brain injury, particularly with respect to characterizing lesion location and size after insult (Fig. 86). Studies in both traumatic and ischemic brain injury have demonstrated a correlation between lesion size and

histopathology (Fig. 87), with experimental and clinical studies showing that the MRI-detected lesion size is correlated to outcome¹³⁴. Indeed, a reduction in lesion size by pharmacological means has been noted to result in an improvement in outcome¹³⁴.

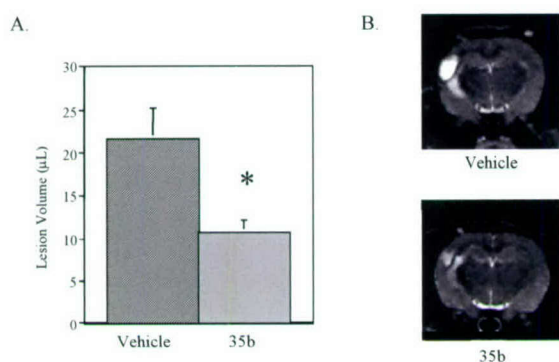


Figure 86. Effect of a small peptide 35b on lateral fluid percussion-induced lesion volume 21 days after injury in the rat. Data are from rats treated 1 hour after injury with 35b or saline vehicle. **(A)** Lesion volume (mean \pm SEM) and **(B)** representative T₂-weighted magnetic resonance imaging of vehicle- and 35b-treated rats. Regions of marked hyperintensity are evident in the hippocampus, cortex, and corpus callosum. * p < 0.05 versus vehicle.

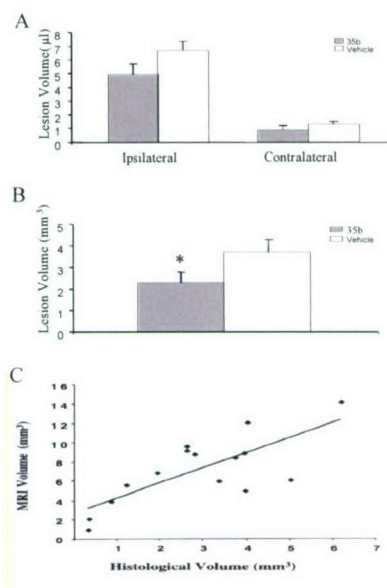


Figure 87. Effect of 35b on controlled cortical impact-induced lesion volume 21 days after injury in the mouse. Data are from the mice treated 1 hour after injury with 35b or saline vehicle. **(A)** Lesion volume in the injured ipsilateral or injured contralateral hemisphere (x-axis) as assessed by magnetic resonance imaging. **(B)** Lesion volume as detected by histologic assessment in the injured ipsilateral hemisphere from the same animals. * p < 0.05 versus vehicle. **(C)** A significant correlation was detected between lesion volume values obtained with the two methods (p < 0.05, regression ANOVA).

Trauma studies have further demonstrated that it is not only the size of the lesion but also the location of the lesion that is related to posttraumatic motor outcome, cognition, and memory performance, a promising application of MRI in the clinical management of head injury. More recently, diffusion-weighted imaging has been used to characterize the time course and early localization of lesion development after injury. This application of MRI can detect lesion development within minutes of the insult (Fig. 88).

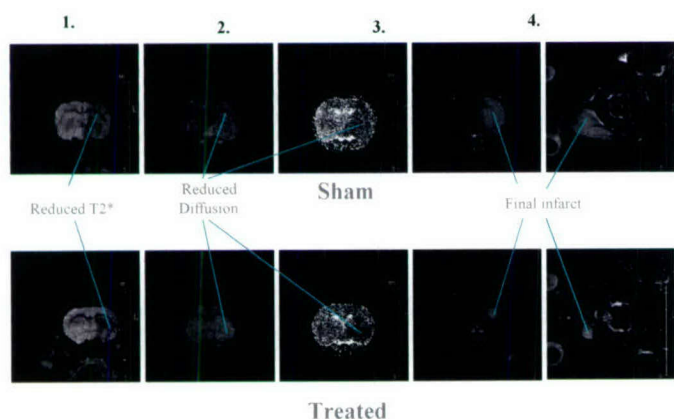
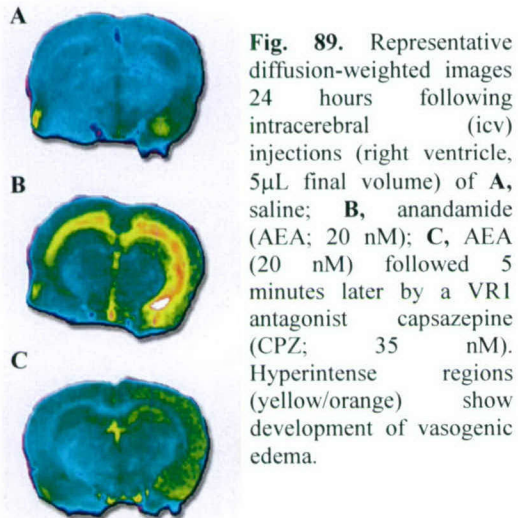
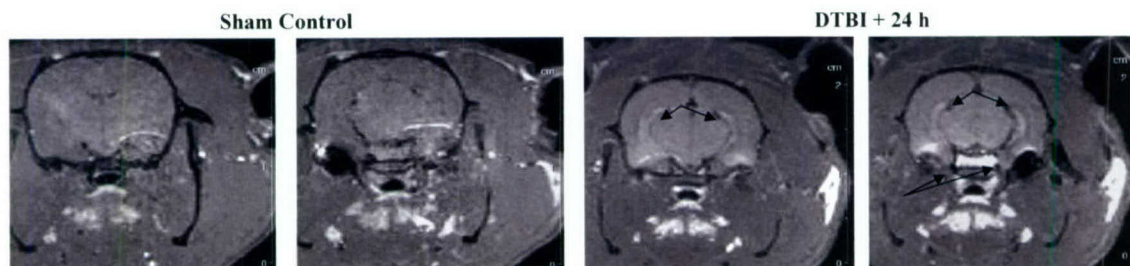


Figure 88. Localization of the infarct lesion developed in rat's brain after middle cerebral artery occlusion. **1.** T₂-weighted, **2.** diffusion-weighted, and **3.** perfusion-weighted MRI 24 hours after middle cerebral artery occlusion. **4.** Final localization of the infarct measured by T₂-weighted MRI 21 days after injury.

Moreover, the data provides information on edema formation, and can differentiate between cytotoxic and vasogenic edema. Findings to date have shown that the former is always present in ischemia or at later time points following traumatic brain injury, whereas the latter is present in the initial stages of mild to severe brain trauma (Fig. 89 and 90). Although the reasons for this difference are still unclear, it has been proposed that cellular energy status may be a contributing factor.



Recently, Lin and Koretsky¹⁵³ demonstrated that focal injections of manganese (Mn^{2+}) within the mouse central nervous system combined with *in vivo* high-resolution magnetic resonance imaging (MRI) demarcate neuronal tracts originating from the site of injection. Others, using alternative (intraarterial) route of injection coupled with artificial opening of the blood-brain barrier, confirmed the usefulness of Mn^{2+} contrasted magnetic resonance imaging in rats^{154, 155}. Manganese, similarly to Ca^{2+} in various biological systems¹⁵⁶, is known to enter glial cells and/or neurons *via* voltage-gated Ca^{2+} channels following the triggering of an action potential¹⁵⁷. Indeed, this new visualization method is described as a useful tool to detect manganese accumulation caused by permanent ischemia in rat brain, whereas manganese hyperintensity reflected the increased Ca^{2+} influx¹⁵⁵. Here we demonstrate for the first time the utilization of this method in experimental TBI (Fig. 91), and show its usefulness in differentiation of neuronal structures activated by trauma. Since traumatic brain injury induces blood-brain barrier breakdown, which is well-documented by literature data as well as our own results, in this study there was no need for artificial opening the blood-brain barrier by administration of a hyperosmolar agent, necessary for the entry of $MnCl_2$ into brain parenchyma. Although future experimental work is necessary to fully define the potential and limitations of this methodology in TBI, these findings indicate that Mn^{2+} contrasted MRI may be a useful technique for investigating the trauma-induced functional changes in the brain.



To better understand the mechanisms of CNS injury and effects of treatment many parameters are taken under consideration. Anatomical morphological changes, changes in tissue quality and changes in brain chemistry are the three parameters that may be probed with the MRI instrument.

One of the benefits of MRI is that it is a technique that can render this data *in-vivo* in a non-invasive fashion inasmuch longitudinal studies can be performed using MRI. The challenge in these studies is how to compare data from one time point to the next. In *ex vivo* studies the rodent brain is excised and sliced in slice sections generally not more than 10 microns thick. Since the MR microscope generally cannot supply in-vivo brain images thinner than 50 microns thick, regional specificity can be difficult to achieve. For this reason a stereotaxic device was designed and implemented (Fig. 92).

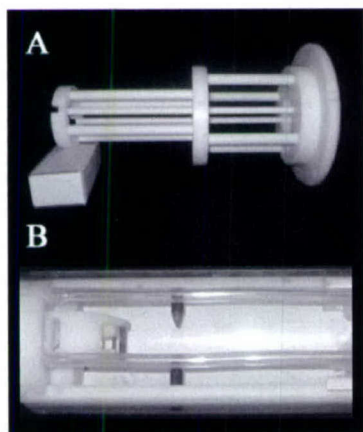


Figure 92. Mounting plane (A) custom designed for 20 cm bore MRI. Stereotaxic device (B) showing ear and teeth bars plus gas anesthetic supply and scavenging lines.

Typically small animal MR images are obtained after placing the animal in the center of the imaging device using beds or platforms, and then adjusting the position after obtaining a scout image. Such a process does not permit the reproducible visualization of the same anatomical plane with repeated examinations. We have developed a device that allows stereotaxic placement of an animal in precisely the same position for repeated examinations. The instrument incorporates a full range of physiological monitoring and life support systems including temperature control, anesthesia delivery and respiratory monitoring. Using magnetic resonance imaging, the accuracy and reliability of this device is demonstrated in a rat traumatic brain injury model (Fig. 93).



Figure 93. Coronal slice of rat brain obtained using diffusion-weighted imaging on (A) day 1 and (B) day3. Note the vasculature identifying the slices as being the same in both images.

In Hypothesis 7 it was stated that diffusion imaging would be performed. One of the inherent problems in diffusion imaging is involuntary movement of the animal due to respiratory motion. To alleviate this problem the animal was fixed in the stereotaxic holder so that the brain was fixed in space and respiratory motion no longer influenced the outcome. Figure 94 shows three pictures taken using diffusion weighted MRI. Normally these images suffer from blurring due to motion artifacts, these images are of excellent quality. Not only are the diffusion data from these images marvelously clean but direct anatomical comparisons can be ascertained by direct examination of these images. Note in Figure 94C the shift of the midline of the rodents brain and in Figure 94D the return to normal. Since the skeletal coordinates of the interaural line and the incisor are used to align the animal in the stereotaxic holder all of the changes in size and shape of the anatomical features in Figures 94 B-D. Likewise imaging stability is important in spectroscopy. Figure 95 shows the result of spectroscopy performed on a DTI rat brain model. Using the stereotaxic device, spectra can be compared across runs and time.

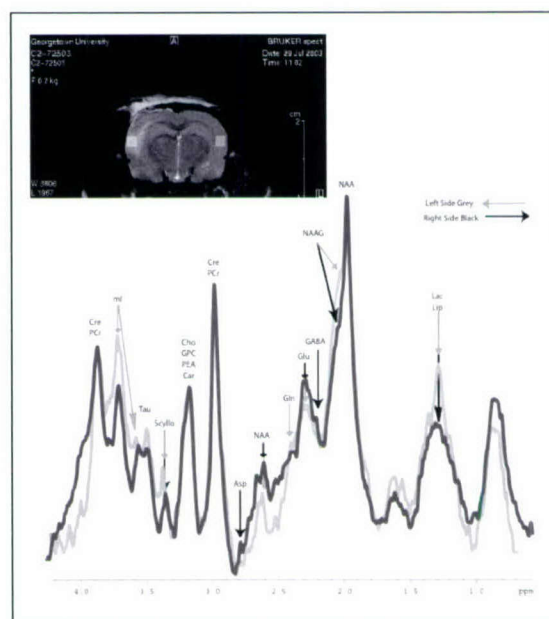
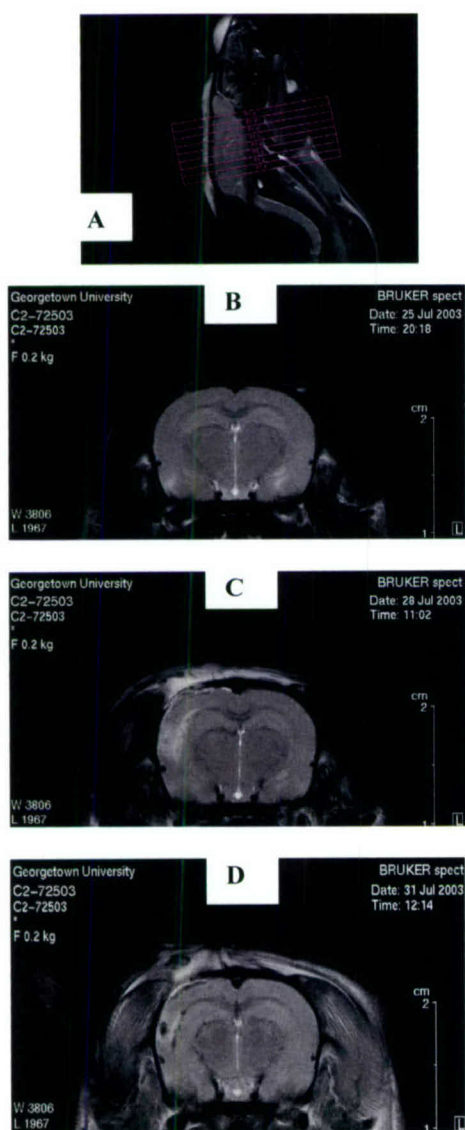


Figure 95. Spectra from left and right side of TBI rat brain (same brain as in Figure 78). One voxel 2 mm on edge (8 microliters) was positioned on lesion and another on the contralateral side. Differences in Lactate, Glutamate, NAAG, NAA and mio Inositol are evident.

Figure 94. Diffusion-weighted imaging time course study (longitudinal) of rat brain prior to and following traumatic brain injury. Sagittal slice (A) showing position of coronal slices. Coronal slice (B) prior to injury; (C) coronal slice 24 h after injury; (D) 96 hours after injury. Images C and D were obtained without the use of scout images and without the use of slice localization.

Quantitative diffusion and perfusion measurements suffer from motion. Motion artifacts are clearly visualized in images due to excessive blurring. Images such as those in Figures 96 and 97 are free from movement artifact and can therefore be used for quantitative measurements. Many investigators rely upon respiratory gating to reduce movement artifacts. However, the signal that is measured depends on the effective echo time, which in part reflects respiratory rate that can be variable. Spin labeled perfusion measurements also have been successfully performed. This technique was chosen above contrast injection methods because the timing of contrast bolus injection may affect the outcome of an experiment. In Figure 97a, blood in the extracranial circulation of the animal is tagged; this blood flows to the brain and can be subsequently interrogated for a signal. Figure 97a shows where the blood is labeled and where the imaging slice of interest is taken (chosen to be at the level of a TBI lesion). Again the quality of this image indicates that it is well suited for quantitative measurements.

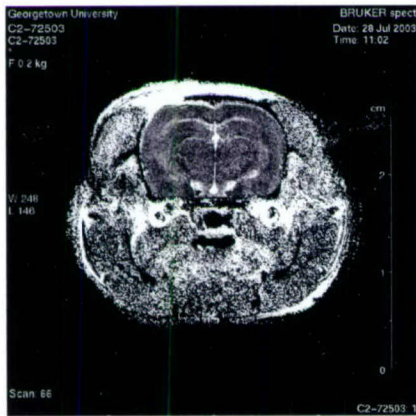


Figure 96: Diffusion map, diffusion coefficient is calculated from a series of images taken with increasing diffusion gradient strengths. Brighter areas indicate greater diffusion, black no diffusion.

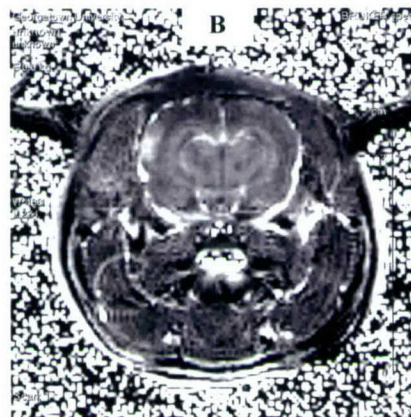


Figure 97: Perfusion image. A) Blood flowing into the brain is radiofrequency labeled. Those spins later give up their energy at a point rostral from the labeling point in the neck. B) Brighter areas indicate higher perfusion.

The combination of diffusion and perfusion imaging techniques can provide information that is complementary. High quality diffusion images (Figure 98a) and perfusion images (Figure 98b) were mapped to each other, and show a diffusion-perfusion mismatch image (Figure 98c). The mapping of diffusion images to perfusion images (Figure 98c) can show the overlap of the data. Diffusion and perfusion images both show lesions little chance of tissue recovery is predicted as increased diffusion and perfusion indicate irreversible cell damage. Areas where lesion is found in only either diffusion or in perfusion image with no overlap, tissue is still considered damaged but not irreversibly.

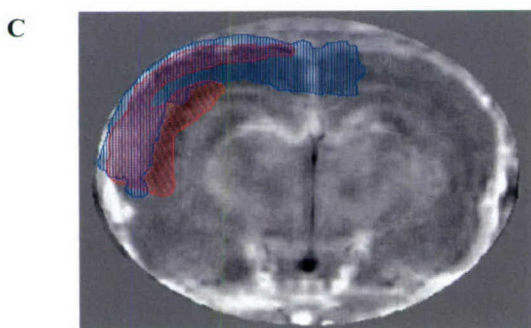
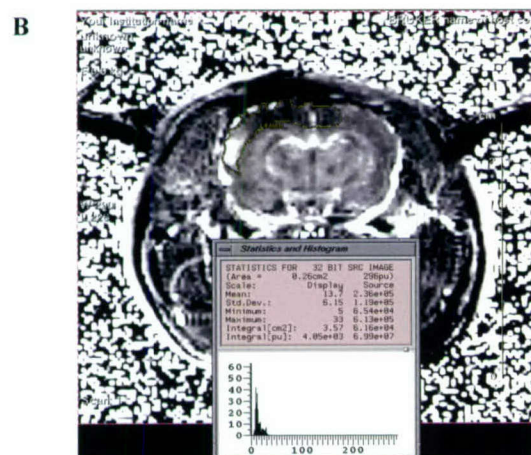
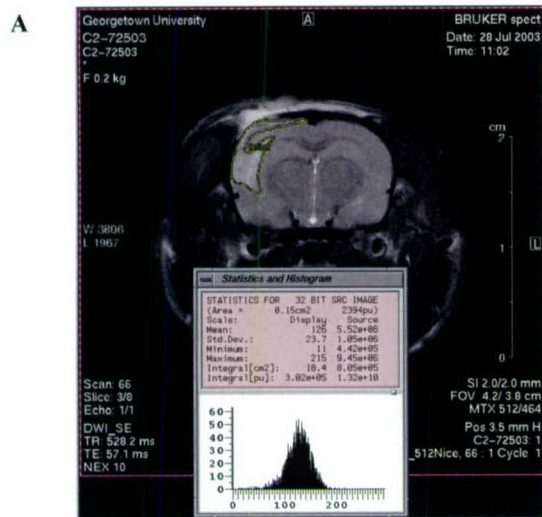


Figure 98. Images in A-C are of the same animal. Image A is raw data diffusion image. Visible lesion is outlined by hand. Statistics are performed on pixel intensities found in the lesion area. B) Perfusion image map which is an image that is derived from two images, the first being an image where the perfusing blood is not encoded and the second where the perfusing blood is labeled. Subtraction between the two and scaling that includes the distance between the labeling slice and the imaging slice, gradient strength and T2 decay are taken into account so that pixel intensities represent actual perfusion velocities. Lesion is outlined by hand, note that the visible lesion has different sizes and shapes in the “B” with respect to “A”. This difference is exploited in image “C” where the lesion sizes and shapes are overlapped to better point out the difference. Image “C” is the “diffusion – perfusion mismatch”. The area where the lesion found using the diffusion imaging technique and the area where the lesion found using the perfusion technique overlap is considered an area where of irreversible tissue damage.

3. Spinal Cord Imaging:

3-D sequences are currently available for the first time permit the 3-D rendering of the spinal cord of a living mouse (Figure 99). The quality of the *in vivo* image is sufficient to note roots at each spinal level. Rat spinal cord imaging has also been achieved in rat models and shows remarkable detail (Figure 100).

Work in the area of spinal cord injury continues. *In vivo* lesion measurements are being compared to histological results. Figure 101 shows a typical lesion imaged *in vivo*. Coronal slices can be analyzed at different points along the spinal cord. Lesion size can be tracked over time to better understand lesion development due to trauma or transection and the effectiveness of treatment.

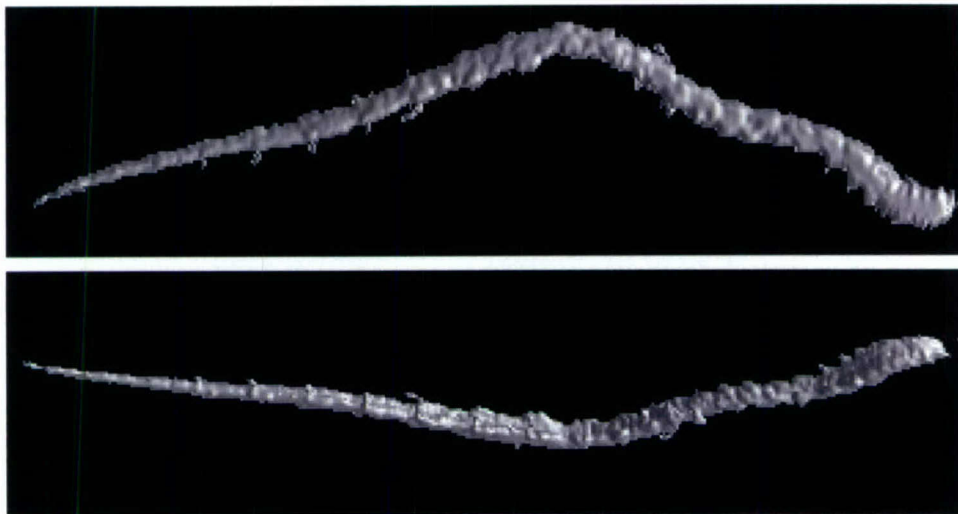


Figure 99: Ray tracing of the mouse spinal cord with two light sources pointing from the head towards the tail on either side. Specular reflection provides contrast via a shiny appearance to the areas directly illuminated by the light sources. The viewing angle was rotated to show the spine from different angles.

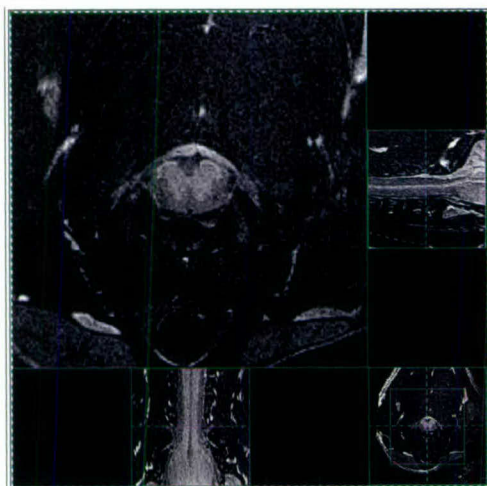


Figure 100: Rat spinal cord images. Note typical “butterfly” pattern in coronal slice shows good grey white tissue contrast.

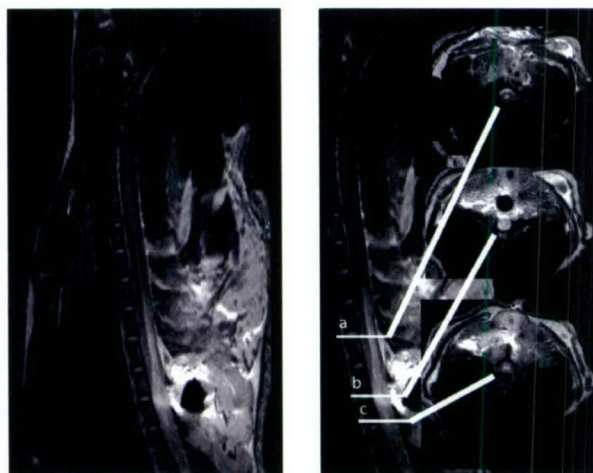


Figure 101: Lesion in spinal cord of rat. Coronal images taken rostral (a) central (b) and caudal (c) to the lesion.

In conclusion, a variety of MR techniques, including both imaging and spectroscopy, have been applied to models of acute neurodegeneration. Comparisons of perfusion/diffusion changes may identify penumbral regions. ^1H and ^{31}P MRS allows biochemical characterization of injury non-invasively in vivo; particularly useful are measurements of neurotransmitter changes, pH, and cellular bioenergetics. Other imaging techniques have included T2-weighted images for lesion volumes, Mn imaging to try to identify transsynaptic changes, and fMRI to identify plasticity. Development of a novel positioning apparatus allows faithful repeated measurements over time and may be widely applied to temporal biological studies.

Hypothesis #8: Anti-apoptotic factors are associated with neurite outgrowth and modulate regenerative responses after injury.

1. Spinal Cord Injury Related Work

Spinal cord injury (SCI) induces a sequence of endogenous autodestructive changes known as secondary injury, as well as reactive biochemical changes that are neuroprotective and/or promote recovery. The balance between these delayed neurodestructive and neuroprotective changes is believed to determine the extent of ultimate tissue damage and recovery potential^{115, 158-160}. Although some of these biochemical alterations reflect more passive events, such as reduction of cellular bioenergetic state with subsequent loss of ionic homeostasis, it is increasingly clear that changes in gene expression after SCI lead to alterations in protein expression that may affect both post-traumatic cell death and restorative responses^{150, 161-163}. Such gene expression changes were previously demonstrated for a relatively small number of genes using techniques such as RT-PCR^{158, 164}. However, recent application of oligonucleotide or cDNA based microarray approaches has allowed the concurrent measurement of many thousands of genes/expressed sequence tags (ESTs). Moreover, during the past several years improvements in bioinformatics applications has allowed more powerful and functionally relevant analyses of gene expression changes and potential gene-gene interactions¹⁵⁰.

Using high-density oligonucleotide-based arrays (Affymetrix), we have examined sequential changes in gene expression for more than 25,000 genes/ESTs after impact SCI in rats, from 30 min to 6 wk after injury¹⁵⁰. Analysis revealed sequentially induced inflammatory, degenerative and regenerative processes after trauma. Inflammation and neurodegeneration related gene/protein expression are upregulated primarily in the first hours after injury, although more delayed apoptosis of some cells may occur over longer periods¹⁵⁰. In contrast, genes/proteins associated with regeneration or plasticity are typically upregulated days to weeks after injury¹⁶³.

Applying both functional and temporal clustering bioinformatics approaches to our gene profiling experiments after rat SCI, we identified a cluster of genes involved in cell cycle activation that were associated with cell death in post-mitotic cells such as neurons¹⁵⁰. This cluster was up-regulated between 4 and 24 h after injury; these changes were confirmed by quantitative PCR and also at the protein level for a number of genes including c-myc, gadd45a, PCNA, cyclin D/Cdk4, Rb, and E2F5. Protein expression increases in neurons after SCI for most of these genes were associated with evidence of apoptosis and active caspase-3 expression. Preliminary studies have confirmed these observations in primary neuronal cell cultures, in which various injury stimuli were associated with increased expression of cell cycle proteins and apoptosis. Moreover, selected inhibition of the cell cycle using Flavopiridol was associated with reduced cell cycle protein expression and significantly decreased cell death. Together, these observations suggest that induction of cell cycle proteins after in vivo or in vitro neuronal injury is associated with cell death and that inhibition of this process may reduce apoptotic cell death. This pathway may offer the opportunity for uniquely targeted therapeutic strategies in SCI.

The delayed functional loss following SCI appears not only to reflect secondary cell degeneration but also the relatively poor capacity of surviving neurons within the adult CNS to show axonal plasticity and sprouting^{150, 158-160, 165, 166}. It has been well-documented that neurite outgrowth and axonal regeneration can be promoted or impaired through the modulation of a large number of pathways, including metabolic pathways related to lipid metabolism¹⁶⁷, cytoskeletal assembly machinery¹⁶⁸⁻¹⁷⁰, secreted tissue factors/growth factors^{171, 172}, extracellular matrix proteins and myelin associated glycoproteins¹⁷³⁻¹⁷⁸. Glycoproteins and membrane-bound proteins such as GAP-43 and cell

adhesion molecules (CAM) family, which are involved in cell contact and cell adhesion appear to be particularly important players in neurite outgrowth and plasticity after injury¹⁷⁹⁻¹⁸³.

Axonal plasticity and neurite outgrowth occur during development and certain of these developmental pathways are recapitulated after injury and may lead to either cell death (*vide supra*) or help to promote recovery¹⁸⁴⁻¹⁸⁸. Molecular regulation of neuronal apoptosis and differentiation/regeneration are developmentally regulated and may be inversely linked. For example, certain factors promoting cell death in adult neurons may inhibit neurite outgrowth/plasticity and certain cell death inhibitors may enhance neurite outgrowth. Thus, Bcl-2 promotes axonal outgrowth as well as cell survival^{189, 190}. It is strongly regulated during development and high levels are expressed during the period of axonal elongation. Cultured retinal neurons overexpressing Bcl-2 show increased axonal length and improved survival¹⁸⁹. In addition, Bcl-2 increases expression of the cell cycle inhibitor p27; in contrast, aberrant cell cycle re-entry in mature neurons results in cell death and arrest of neurite elongation¹⁹¹.

In our preliminary SCI experiments, we observed an inverse relationship between the expression of cell cycle genes on the one hand and those related to neuritogenesis/neuroplasticity on the other. This increased expression of cell cycle proteins at 24 h after mild injury was associated with reduced expression of a group of coordinately regulated genes that include neuritin, attractin, Mtap1a, and Mog (*vide infra*). Expression of these transcripts progressively recovered at later time points associated with functional recovery. Another group of co-regulated transcripts whose expression was induced only at 7 and 14 d after injury includes synaptogyrin, synaptotagmin 1 and 2, VAMP 5, filamin, tensin, annexin, coronin 1b, ninjurin 1, collagen XVIII, IGF, Rap1b, RAB13, and P2X. In pilot studies, we have tested the ability of members of these latter clusters to induce neurite outgrowth. Synaptogyrin, synaptotagmin 1, VAMP 5, coronin 1b, ninjurin 1, Rap1b, and RAB13, have been overexpressed in vitro using PC-12 cells, neuroblastoma cell lines, and DRG neurons. They promoted neurite outgrowth in each of these model systems (*vide infra*). Thus, we believe that expression changes relating to cell cycle genes after SCI not only cause apoptotic neuronal cell death, but also serve to suppress expression of genes related to neuritogenesis and plasticity. Indeed, inhibition of cell cycle proteins using Flavopiridol not only suppresses neuronal apoptosis in vitro, but also promotes neurite outgrowth.

1.1 Gene expression changes after SCI

We have recently shown that gene expression changes following SCI include a number of functional classes that are temporally regulated and participate in either neurodegenerative or neurorepairative processes¹⁵⁰. Strong induction of immediate early genes appears to drive expression of genes related to inflammation, oxidative stress, and cell cycle in the first 24 h after injury (Fig. 102). As these factors decline, there is activation of genes involved in cell adhesion, tissue remodeling, cytoskeleton dynamics - all of which potentially participate in the delayed reparative response after injury. These latter molecular changes are associated with functional improvement in animals subjected to mild injury.

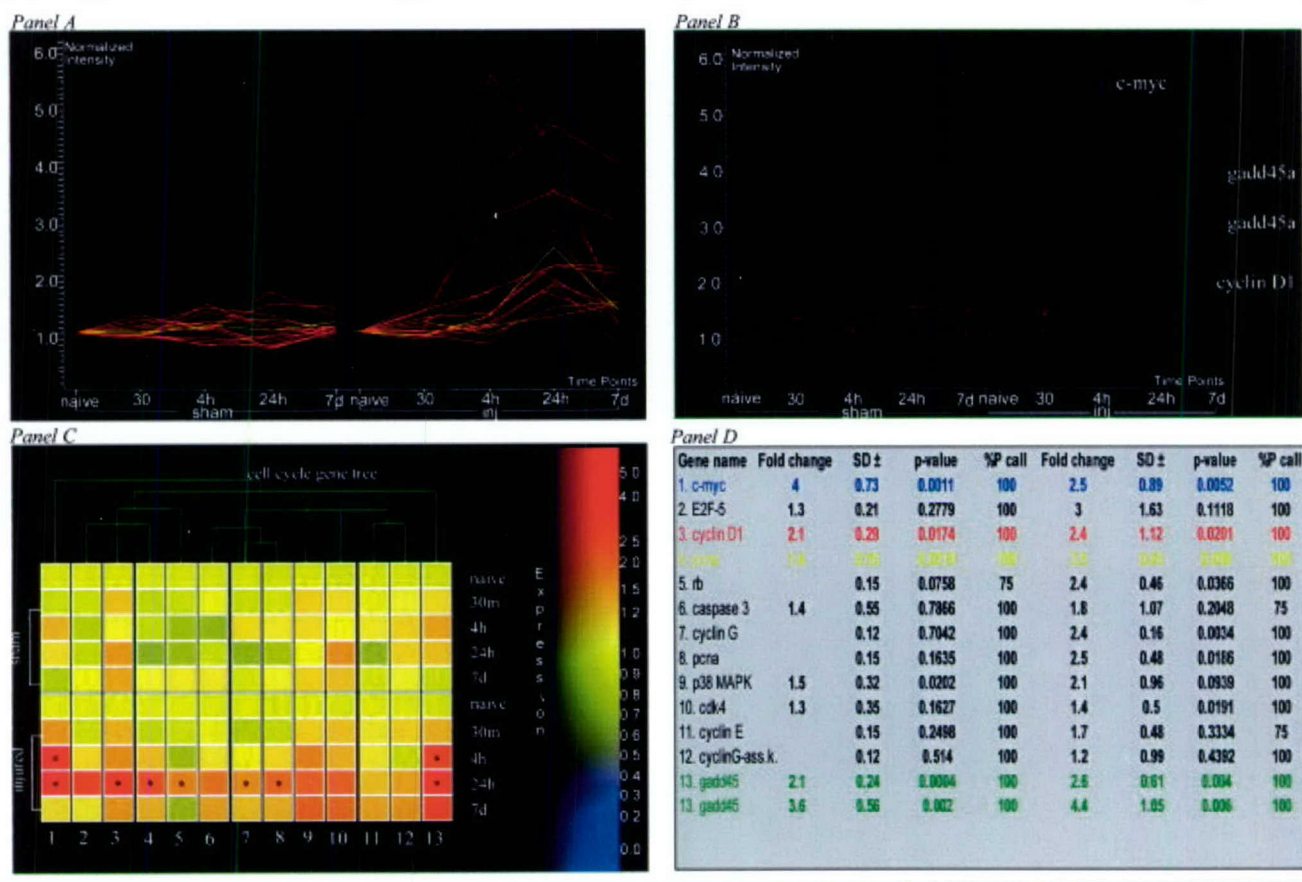


Fig. 102: Functional clustering of cell cycle genes shows high expression 4 to 24 h after injury. Genes of this functional cluster also belong to smaller temporal clusters (*gadd45a* showed temporal clustering with *c-myc*, $R^2 = 0.99$), whereas *pcna*, *cyclin D1*, *cyclin G*, *Rb*, and *E2F5* belonged to the same temporal cluster, $R^2 = 0.99$). Data for all cluster members are shown in panels A, C, and D, whereas data with standard deviations for multiple animals are shown in B. A self-organizing map graph subcluster applied to the cell cycle gene cluster (A) is shown in B. Those genes showing significant p values (<0.05) and fold changes (two-fold) between sham and injured time points are indicated with an asterisk in C.

1.1a. Cell Cycle Cluster

Due to the importance of DNA damage and aberrant cell cycle activation upon neuronal cell death, we examined genes involved in cell cycle regulation with particular reference to DNA damage response and transition from the G1 to S phase. Using functional and temporal clustering techniques, we identified a group of cell cycle related genes, and showed that they play a role in neuronal DNA damage and cell death. mRNAs from these were coordinated and upregulated at 4 and 24 h in the injured spinal cord. They include *c-myc*, *gadd45a*, *pcna*, *cyclin D1*, *cyclin G*, *Rb*, and *E2F5*. *C-myc* and *gadd45* showed a maximum expression increase at 4 hours, and *cyclin D1* at 24 h. *Pcna*, *cyclin G*, and *Rb* were upregulated at 24 h (Fig. 1). *Gadd45a* showed strong temporal clustering with *c-myc*, as did *pcna*, *cyclin D1*, *cyclin G*, *Rb*, and *E2F5* (each $R^2 = 0.99$). Additional genes showed temporal clustering to the 24-h peak but did not fulfill our stringent criteria of both a two-fold increase and significant p value relative to the corresponding sham profiles: *CDK4*, *E2F5*, and *caspase-3* ($R^2 = 0.95$). *Cyclin E* and *p38 mapk* profiles showed a peak expression level in the injured group at 24 h and were included in our further analysis based on their close functional relationship with other cluster members. The increased expression of some of these cluster members (*gadd45a*, *c-myc*, and *pcna*)

was validated by QMF-RT-PCR; nearly identical expression changes were shown by the two methods (Table 4). Increased protein expression was also found 24 hours after injury for members closely related to cell cycle progression (*c-myc*, *cyclin D1*, *cdk4*, *pRb*, *E2F5*, and *pcna*). Several of these cell cycle proteins were co-expressed in neurons and were found in neurons that were TUNEL-positive or expressed *caspase-3*, a protein associated with apoptosis. Certain of these neurons expressing cell cycle proteins also showed morphological features of apoptosis by Hoechst staining.

Table 4. Comparison between Affymetrix and QMF-RT-PCR Data

	Fold Change \pm SD	<i>p</i>	Fold Change \pm SD	<i>p</i>	Time Point (hr)
<i>c-myc</i>	4.0 \pm 0.73	0.001	3.8 \pm 2.3	0.035	4
<i>gadd45</i>	3.5 \pm 1.05	0.003	3.8 \pm 1.45	0.03	24
<i>pcna</i>	3.0 \pm 1.06	0.01	3.2 \pm 1.3	0.007	24

QMF-RT-PCR = quantitative multiple fluorescent reverse transcription polymerase chain reaction

Consistent with other studies, our data support the hypothesis that the genes belonging to the cell cycle progression pathway are involved in neuronal responses to DNA damage and/or cell stress after SCI. Emerging consensus is that progression through the cell cycle has different and sometimes opposite effects in mitotic versus postmitotic cells^{192, 193}. In postmitotic cells, such as neurons, cell cycle reentry may induce apoptotic cell death. Apoptotic neuronal cell death occurs after spinal cord injury and may contribute to the subsequent neurological dysfunction^{194, 195}. On the other hand, astrocytic proliferation is known to induce posttraumatic tissue scar formation that can impede functional regeneration (see Fawcett and Asher¹⁹⁶ and McDonald and Sadowsky¹⁹⁷ for review). Thus, genes favoring cell cycle progression may be involved in both neuronal apoptosis and astrocytic proliferation. Importantly, the cyclin-dependent kinase inhibitor *p21(waf1)*, present in our U34A genome, did not show mRNA expression changes between sham and injured animals at any time point. This suggests that the observed mRNA changes in cyclin members after injury were specific¹⁹⁸.

A body of evidence supports the concept that these cell cycle members participate in a common pathway involved in neuronal damage and cell death. Both *c-myc* and *gadd45a* can be activated by diverse conditions that serve to damage cells, and both act as DNA damage-responsive transcription factors¹⁹⁸⁻²⁰³. When induced, *c-myc* can serve as a proapoptotic factor through mechanisms related to activation of caspases or cell cycle progression to the G2 phase^{198, 199}. *c-Myc*-associated apoptosis can be induced by a variety of stimuli, including DNA damage, infection, serum or growth factor deprivation, and TNF α or Fas signaling^{204, 205}. *c-Myc*-dependent apoptosis also can be induced by downstream activation of *p38 MAPK* and caspases^{198, 206}. *p38 MAPK* may directly phosphorylate the Rb protein and release its inhibition of E2F family members²⁰⁷. *c-Myc* also can influence transcription of *cyclin D1-cdk4* and *cyclin D2*, and in quiescent cells can activate the expression of *cyclin E-cdk2*^{208, 209}. Both *c-myc* and *E2F* members have the ability to induce cell cycle reentry in quiescent cells and induce apoptosis²¹⁰⁻²¹⁵. Phosphorylation and consequent inactivation of *Rb* (mainly at serine residue 95) by cyclin/cdks results in release and activation of the transcription factor family *E2F*, which in turn promotes S-phase transition and cycle progression²¹⁶. Importantly, *Rb* null mice, mimicking phosphorylation of *Rb*, exhibit neurological deficits and neuronal apoptosis²¹⁷. *Gadd45a* plays a role at the G1-S and G2-M checkpoints, regulating cell cycle progression: it mediates DNA repair together

with PCNA²¹⁸, is a sensor of DNA damage, and also may be involved in apoptosis regulation and genomic stability.

In vitro experiments have shown that *c-fos*, *cyclin D/cdk4*, *cyclin G*, and *Rb/E2F* members play a role in apoptotic cell death of postmitotic neurons after trophic factor withdrawal, DNA damage, or KCL deprivation^{217, 219-222}. In vivo studies of both cortical and spinal cord neurons after ischemia or excitotoxic-mediated DNA damage have shown the occurrence of apoptotic cell death associated with *cyclin D-cdk4*, *cyclin G*, *pcna*, or *Rb/E2F* protein and mRNA overexpression²²³⁻²²⁶. In addition, the expression of *cyclin D1*, *cyclin A*, *cdk4*, and *pcna* have been documented in apoptotic cerebellar granule cells from Weaver mice²²⁵. This further suggests that re-expression of cell cycle proteins may be related to DNA damage, repair, and apoptosis in injured neurons.

Our temporal profiling data are consistent with the hypothesis that SCI causes early induction of *c-myc* and *gadd45a*, followed by downstream upregulation of *E2F-5* family members either directly or through the activation of *cyclinD/cdk4*; in turn, these may promote *Rb* phosphorylation and the release of active *E2F* transcription factor (see Bartek and Lukas²²⁷ for review). SCI caused increased ser795 phosphorylated RB, temporally associated with overexpression of *cyclinD1/cdk4*, *p38MAPK*, and *E2F-5* at the mRNA and protein levels. Increased protein expression in neurons at 24 h was found for many of the cell cycle proteins that showed increases by expression profiling. Subsets of these neurons also demonstrated apoptotic features, as shown by TUNEL, *caspase-3* and Hoescht staining (not shown).

1.1b. Neuritin Cluster

It is likely that plasticity of surviving cells contributes to functional recovery that is often observed after incomplete traumatic injuries of the spinal cord. Neurite outgrowth and axonal regeneration can be promoted or impaired through the modulation of several pathways, including metabolic pathways related to lipid metabolism¹⁶⁷, cytoskeletal assembly machinery¹⁶⁸⁻¹⁷⁰, secreted tissue factors/growth factors^{171, 172}, extracellular matrix proteins and myelin associated glycoproteins¹⁷³⁻¹⁷⁸. Importantly, axonal plasticity and regeneration are processes that occur during normal development, and some of the embryonic developmental pathways are recapitulated after injury and may promote recovery¹⁸⁴⁻¹⁸⁷.

As noted above, the expression of cell cycle genes appeared to be inversely correlated to changes in the expression of a cluster of genes potentially involved in axonal plasticity and outgrowth, including neuritin, Mtap1a, attractin and Mog. We first identified neuritin, a protein known to be important in neuritogenesis and plasticity, which showed significantly reduced expression at 24 h, and subsequent recovery between 7 d and 14 d (Fig. 103).

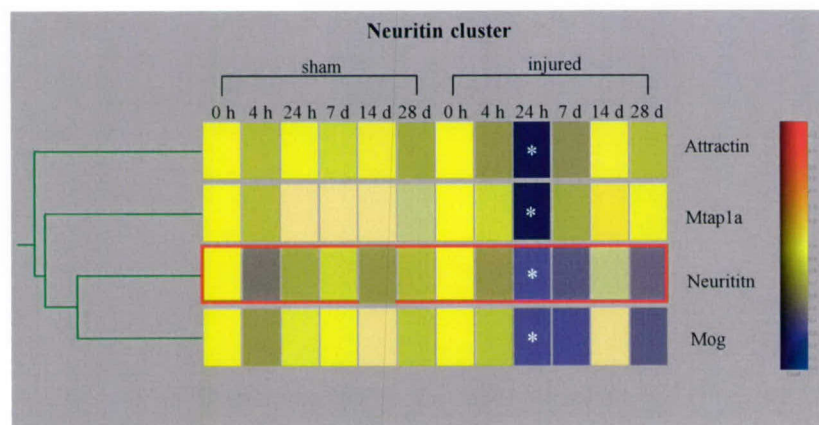


Fig. 103: Gene Tree reveals temporally coordinated gene profiles obtained by neuritin nucleated temporal cluster. Gene tree shows neuritin cluster obtained using neuritin as anchor gene (red box) to nucleate transcripts with a similar profile across time point (R^2 : 0.98). All genes show significant downregulation following injury compared to sham controls at the 24 h time point (asterisk indicates a Welch t test p value < 0.05). mRNA expression levels recover to normal levels by 14 d after injury. Gene expression levels in both sham and injured groups were normalized to time point 0 (naïve animals). Bar graph on the right shows the color code for gene expression level (red: high; blue: low).

The neuritin temporal profile was used to identify potentially related transcripts based upon a correlation coefficient of 0.98; these included Mtap1a, attractin and MOG. Regulation of this group of genes was also investigated in single neurons, and confirmed at the mRNA and protein levels. We also examined co-labeling of neuritin cluster proteins with the regeneration marker GAP-43, which showed co-localization in neurons and axons (Fig. 104). We have also evaluated expression levels of neuritin, Mtap1a, and attractin *in vitro* in DRG neurons at 1, 2, 3, and 5 wk after NGF induction and showed that increased expression was associated with enhanced axonal outgrowth.

Neuritin, which is highly conserved across species, is expressed at peak levels during development, at times of afferent axonal, dendritic growth, and synaptogenesis²²⁸⁻²³⁰. It is a GPI-linked membrane protein localizing to non-myelinated regions, with a major role in modulating plasticity and neurite outgrowth^{231, 232}.

Although its function in post-mitotic neurons of the DRG or spinal cord has not been a focus of study, neuritin also has a putative role in establishment of motor circuits, based upon the detection of its message and protein in the spinal cord by developmental stage 47²³³. Due to its clear association with neuritogenesis and its expression pattern following spinal cord trauma, we selected neuritin as the target gene member of a cluster for which we could then search for other gene products with similar expression profiles. This resulted in the identification of attractin, Mog and Mtap1a as other members of the group with the inference that they too may function in the regenerative phase following injury.

Attractin has been shown to be involved in the regulation of neurite extension, pigmentation, and immune cell interactions; its pleiotropic functions seems to reflect an ability to influence the activity of positively-charged peptides including agouti and chemokines. There exists the possibility that this regulation may extend to the positively-charged neurotrophin family including NGF, BDNF and GDNF. Attractin mRNA is expressed throughout the CNS in neurons, with high expression found in ventral horns, intermediolateral nuclei and dorsal horns in spinal cord²³⁴. Attractin knock-out mice develop tremor at three weeks of age and flaccid paresis of the hind limbs at 6 months²³⁵. The main pathological findings are progressive hypomyelination and vacuolation in CNS including spinal cord grey matter, pons and cerebellum. The phenotype appears to be the result of defects in axonal-glial interaction, thereby impairing myelin assembly and formation. Experimental evidence suggests that membrane attractin may play a role in neurite formation in human cortical cells *in vitro*, probably by interacting with microtubules, and promoting their stabilization²³⁶.

The putative interaction of attractin with the microtubular network leads to examination of the role of MAP1A/Mtap1a. This protein is not believed to function during patterning of the nervous system where Map1b appears to have the dominant role, although there is one report suggesting a role

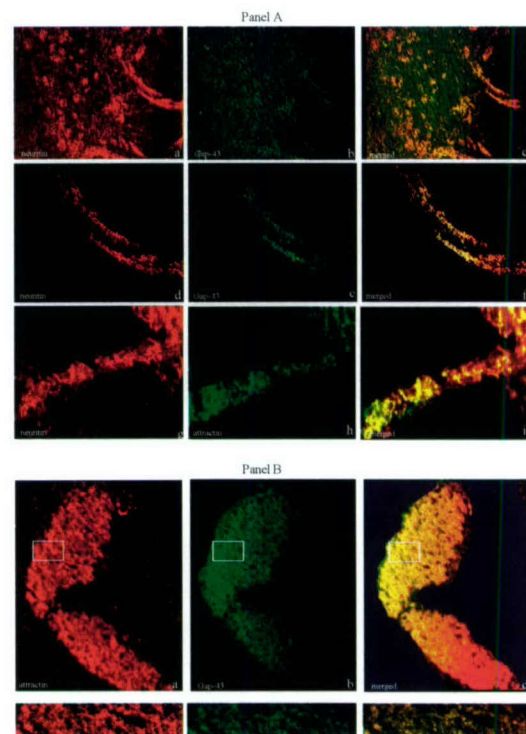


Fig. 104: Mtap1a, Mog, attractin, and GAP-43 are co-expressed in neurons and axons in injured spinal cord. **Panel A.** Double immunofluorescence for Mtap1a/Mog, and GAP-43/Mog demonstrates that myelinated fibers co-express markers of axonal plasticity. Immunostaining for Mtap1a (a, d) and GAP-43 (b, e, m, p) at 14 d post-injury co-localize with Mog (h, l, o and merged: c, f, i, n, q) shows myelinated axons undergoing plasticity responses. Orig. magnification: 125x (a-c); 250x (d-n); 400x (o-q). **Panel B.** Double immunofluorescence for attractin and GAP-43 in corticospinal tracts shows co-localization. Immunohistochemistry for attractin (a), GAP-43 (b), and merged (c) in corticospinal tracts in injured cords 14 d after injury. Attractin and GAP-43 are co-localized.

in late embryonic spinal cord fiber formation²³⁷⁻²³⁹. Rather, Mtap1a functionality is believed to be expressed in brain regions where neurite growth persists in the adult and is expressed robustly during CNS myelination²⁴⁰, precisely the same developmental period that leads to neuropathology in mutant attractin animals. Mtap1a plays a key role in microtubule stabilization and maintenance. It has been suggested that MAP1a renders neuronal microtubules stable enough to support process outgrowth, but still moderately dynamic so growing neurites remain plastic²³⁷. Taken together, these data support a role for Mtap1a in neuritogenesis and axonal plasticity.

Mog also enhances neurite outgrowth in embryonic spinal cord neurons co-cultured with CHO cells²⁴¹, and supports axonal myelination. Mog expression is associated with myelin deposition²⁴², and, unlike other myelin proteins, is specifically present in myelinated axons. This property enabled us to use Mog as a marker of new myelination following injury. More recently Mog immunoreactivity has been described in NG2 positive oligodendrocytes precursors, implying a role of Mog in oligodendrocyte differentiation from precursor cells²⁴³.

1.1c. *Ninjurin Cluster*

In addition to this neuritin cluster, we identified a cluster of genes, coordinately regulated (R: 0.98) to ninjurin 1, that showed high expression levels at 7 and 14 d after injury. These genes /ESTs include synaptogyrin, synaptotagmin 1 and 2, VAMP 5, filamin, tensin, annexin, coronin 1b, collagen XVIII, IGF, Rap1b, RAB13, and purinergic receptor P2X (Fig. 105). We have validated and quantified the mRNA levels for a subset of these genes by real time RT-PCR, by immunoblotting, and immunocytochemistry *in vivo* at 7 and 14 d after injury. These transcripts are directly involved or belong to families of genes involved in axon migration, polarity, growth, guidance, dendrite elongation, plasticity and synapse formation. Some of these genes (synaptotagmin, collagen XVIII, ninjurin, and IGF) have already been partially characterized *in vitro* and/or *in vivo*, and appear to play a role in axonal outgrowth, synaptic plasticity, and regeneration²⁴⁴. It should be noted that the molecular and biological features for several members have not yet been characterized with regard to a potential role in regeneration. These include Ras-related GTPases Rap 1b and Rab13, actin-binding protein coronin, and the cell adhesion protein ninjurin. However, several Ras superfamily members are involved specifically in growth cone elongation, are induced by NGF, and promote neurite outgrowth²⁴⁵. Rap1b seems to play a role in the activation of the NGF dependent ERK pathway leading to axonal elongation²⁴⁶. Rab13 regulates intracellular vesicle trafficking and exocytosis within the trans Golgi network (TGN)²³⁵. Actin binding proteins, including the coronin family of proteins, play a role in cytoskeletal organization and remodeling which is essential during sprouting and axonal elongation²⁴⁷. Cell adhesion molecules have also been related to axonal outgrowth²⁴⁸: ninjurin itself is induced by nerve injury and promotes axonal outgrowth in sciatic nerve and DRG neurons²⁴⁹. Nevertheless, no data are available about its role in CNS regeneration. Finally, of particular interest was the discovery of three ESTs associated with synaptotagmin (Syt1), synaptogyrin (SNG1), and myobrevin (VAMP5) members of the synaptobrevin family. These factors are particularly active throughout the entire synapse formation process and are involved with vesicle docking, exocytosis, and endocytosis of synaptic vesicles.

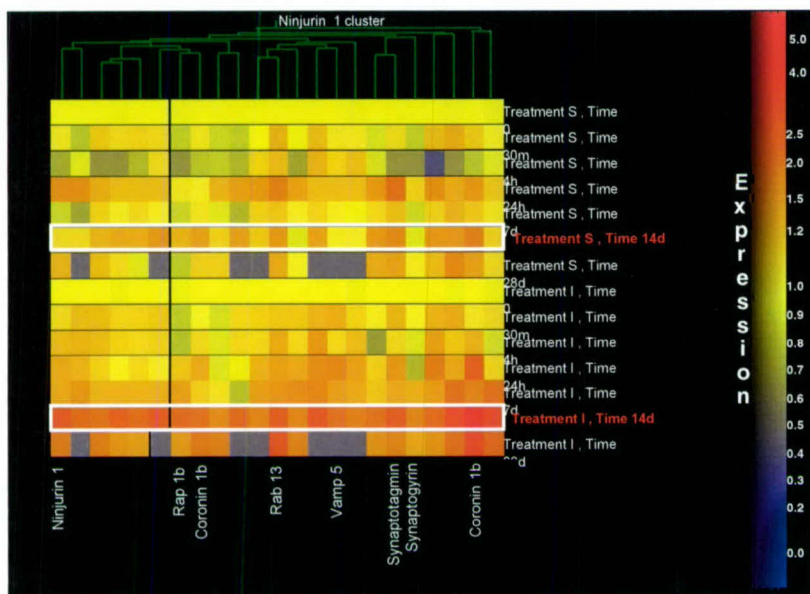


Fig. 105: Gene Tree shows temporally coordinated gene profiles obtained by ninjurin nucleated temporal cluster. Shown is a gene tree showing ninjurin cluster obtained using neuritin as anchor gene (red box) to nucleate transcripts with a similar profile across time point ($R^2: 0.98$). All genes show significant upregulation (Welch t test p value < 0.05) following injury compared to shams at the 7 d time point (see white box). Gene expression levels in both sham and injured groups were normalized to time point 0 (naïve animals). Bar graph on the right shows the color code for gene expression level (red: high; blue: low).

As noted above, the upregulation of cell cycle genes/proteins after SCI appears to be inversely correlated with the regulation of the neuritin and ninjurin clusters. Such a relationship is teleologically plausible, as it makes sense that neural plasticity is suppressed at a time when cell death processes are most active. In pilot studies, we have found that inhibition of cell cycle proteins causes enhanced neurite outgrowth. This observation is consistent with a small but persuasive body of literature suggesting that selected anti-apoptotic factors may enhance neurite outgrowth^{230, 231}. Together, these observations suggest that combined inhibition of cell cycle pathways and enhanced expression of ninjurin cluster members may provide additive or synergistic actions with regard to neural plasticity after SCI.

1.2. Drug mediated modulation of cell cycle in primary neurons

In order to demonstrate that DNA damage and trigger of cell cycle progression could be directly responsible for neuronal cell death, we induced DNA damage and aberrant cell cycle progression in cultured primary cortical neurons. We treated the cells with the DNA damaging agent Etoposide (E) and showed the occurrence of cell death 24 h after treatment, accompanied by induction of cyclin D1, PCNA, and reduction of p27. Co-treatment with cell cycle inhibitor Flavopiridol (E+F)I significantly reduced cell death, inhibited protein expression of cyclin D1, CDK4 and PCNA, and enhanced p27. Moreover, measurement of neurite length before and after DNA damaging treatment with and without Flavopiridol, showed that Flavopiridol had a positive effect upon restoring neurite extension close to physiological levels (Fig. 106).

Taken together these data suggest that cell cycle inhibition following DNA damage and aberrant cell cycle re-entry is able to both protect neurons from cell death, and to promote physiological neurite extension. This data provides first evidence that re-programming neurons to their differentiated state is helpful not only to protect them from death, but also to put them in the conditions to grow their processes. It will be important to further delineate the relationships between inhibition of aberrant cell cycle progression and the genes and proteins that promote survival and neurite outgrowth.

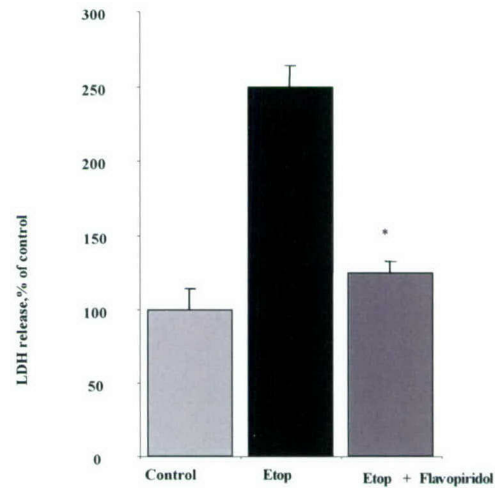
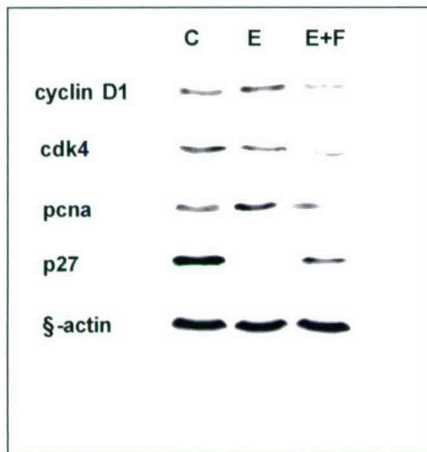
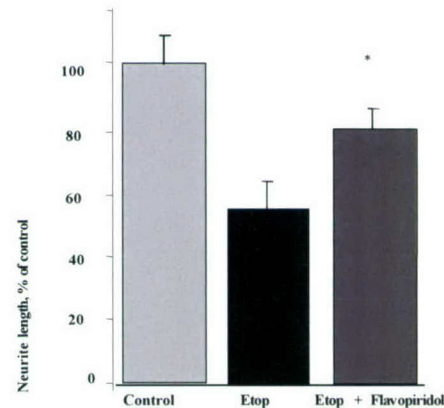


Fig. 106: Treatment with cell cycle inhibitor Flavopiridol protects cortical neurons from Etoposide-induced cell death and promotes neurite outgrowth in surviving cells. **Panel A.** Treatment with cell cycle inhibitor flavopiridol protects cells from death induced by DNA damaging agent Etoposide. Presented is a bar graph showing LDH release measurement in primary cortical neurons expressed as percentage of control after Etoposide and Etoposide+Flavopiridol treatments at the 24 h time point. Flavopiridol, when administered along with Etoposide protects cells from death compared to Etoposide alone. **Panel B.** Treatment with cell cycle inhibitor Flavopiridol promotes neurite length of surviving cortical neurons after DNA damage induction. Shown is a bar graph showing neurite length expressed as percentage of control in primary cortical neurons after treatment with Etoposide and Etoposide plus Flavopiridol. Flavopiridol treatment restores neurite length in damaged surviving cells close to control values. The length of the longest neurite per cell was measured.



2. In vitro gene mediated modulation of Neuritin cluster

Neuritin, membrane attractin, and MAP1A-LC2 were transfected into DRG neurons to evaluate their effect upon neurite outgrowth. Positive cells were detected by eGFP, and only cells immunostained with both beta III tubulin, a neuronal marker, and GAP-43 were analyzed 72 hours post-transfection. Over-expression of neuritin cDNA in DRG neurons resulted in 42% increase in neurite length, as compared to transfection of attractin or MAP1A-LC2 alone, which were similar to control (Fig. 107).

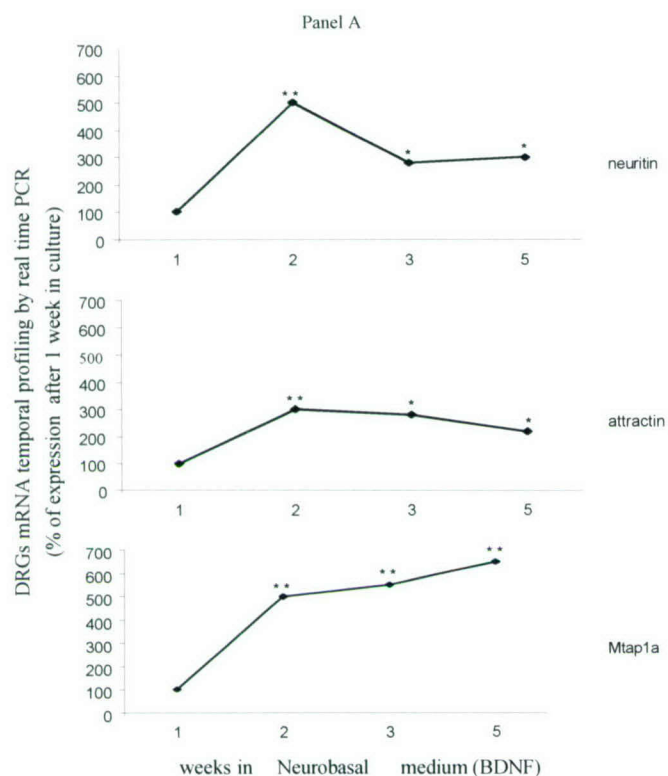
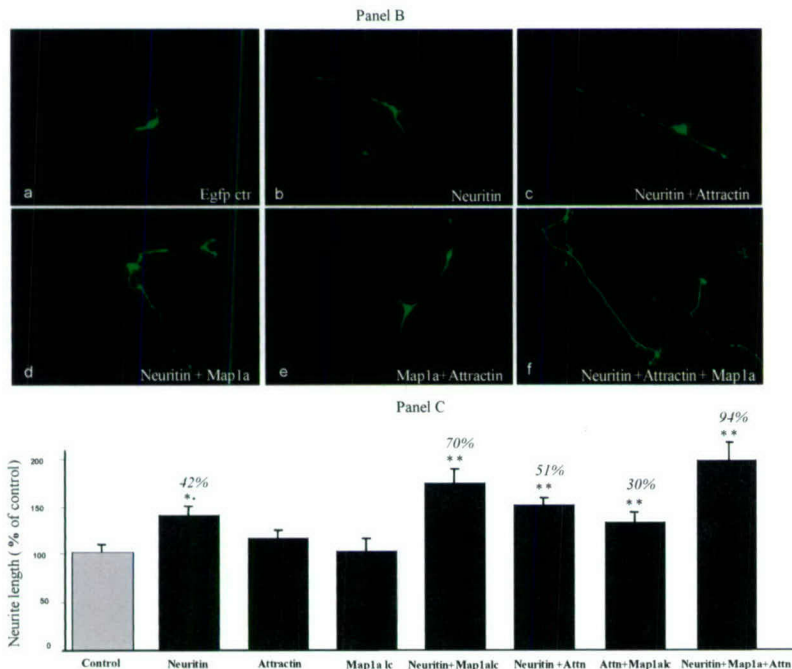


Fig. 107: Neuritin, attractin, and Mtap1a are expressed in DRG neurons, and over-expression drives synergistic neurite outgrowth in additive fashion. **Panel A.** Real time PCR temporal profiling shows induction of neuritin, attractin, and Mtap1a mRNAs in DRG cells in differentiation medium. Shown is induction of mRNA for neuritin, attractin, and Mtap1a at the 2, 3, and 5 wk time points in cultures with Neurobasal medium containing BDNF, considering 1 wk as baseline (100% expression). **Panel B.** Over-expression of neuritin, membrane attractin, and MAP1a LC2 in DRG neurons promotes neurite outgrowth. Shown is increased neurite length of eGFP positive DRG neurons after transfection. Co-transfection of eGFP with naked DNA (a); neuritin (b); neuritin and MAP1a LC2 (c); neuritin and attractin (d); attractin and MAP1a LC2 (e); neuritin, attractin, and MAP1a LC2 (f). **Panel C.** Bar graphs show neurite length expressed as percentage of control in DRG cells after transfection measuring the length of the longest neurite per cell (T test p values <0.01: **; <0.001: ***).



DRG neurons by over-expression of neuritin cDNA (42%) suggests that this factor may play an important role in neuritogenesis. Interestingly, no effect upon neurite outgrowth was seen when attractin or MAP1A-LC2 were over-expressed in DRGs, but combined over-expression of the two resulted in increased neurite elongation, suggesting potential synergy. Although the LC2 chain is free to associate with MAP1B/Map1b as well as MAP1A/Mtap1a, it is a post-translational cleavage product

Nevertheless, combined transfection of attractin and MAP1A-LC2 had a synergistic effect that resulted in significant neurite extension (30% increase). Co-transfection experiments including combination of neuritin with MAP1A-LC2 (70% increase), and of neuritin with attractin (51% increase), resulted in significant increased neurite elongation compared to neuritin alone. Finally, when all three genes were concurrently over-expressed neurite length was increased by 94%; this is consistent with an additive or synergistic interaction among these proteins in promoting neurite outgrowth. The positive effect upon neurite outgrowth in

from the MAP1A mRNA. Accordingly, any change in expression and translation of Mtap1a will result in a coordinated change in expression of the LC2, and physical proximity following cleavage will likely lead to preferential association with the main Mtap1a chain. Importantly, using the yeast two-hybrid technique and expressed recombinant protein association, we observed that the cytoplasmic tail of attractin (completely conserved across all mammalian species) interacts with the LC2 of human MAP1A (W Tang, JH Kim, JS Duke-Cohan, personal communication 2003). Therefore, we now show that this protein-protein interaction has a functional correlate in increased neurite outgrowth.

Enhanced effects on neurite outgrowth were observed by over-expressing neuritin with either attractin (51%) or MAP1A-LC2 (70%). A further effect on neurite elongation was achieved by over-expressing the three proteins together (94%), suggesting that temporal co-regulation and co-expression of these proteins results in a coordinated biological function; thus the coordinated expression of cluster members may reflect regulation of a regeneration-associated functional complex.

We speculate that these genes might behave at the single cell level in a coordinated and sequential manner: neuritin triggering initial neurite development as well as axonal, dendritic and synaptic plasticity; attractin helping to track developing processes and possibly to interact with Mtap1a, thus enhancing cytoskeleton re-arrangements appropriate for neurite extension; while Mog may provide support for neurite extension and subsequent myelination. Therefore, systematic and coordinated use of microarray analysis with subsequent confirmation of protein behaviour provides a useful methodology for identifying potential therapeutic interventions to enhance regeneration aimed at enhancing regeneration.

2.1. In vitro gene mediated modulation of Ninjurin cluster

Ninjurin cluster members including ninjurin, Rab13, coronin 1b, synaptogyrin, VAMP5, Rap1b, and synaptotagmin were cloned and transfected into PC-12, neuroblastoma, and DRG cells, to evaluate their effect upon neurite outgrowth (Fig. 108). Positive cells were detected by eGFP, and only cells immunostained with both beta III tubulin, a neuronal marker, and GAP-43 were analyzed 72 h post-transfection. These experiments showed a significant increased neurite length in PC-12 and neuroblastoma cell lines for all members. Co-transfection experiments demonstrated synergy for Rab13 and coronin 1b. Transfections in DRG neurons showed marked, and significant increase in neurite extension for ninjurin, Rab13, coronin 1b, and VAMP5. These data suggest the potential role of these factors in promoting re-connectivity after injury through stimulation of axonal elongation.

2.2. Promoter analyses

Identification of neuritin and ninjurin gene clusters led us to hypothesize that these genes were regulated by common transcription factors, which were themselves differentially activated during the course of recovery after injury. We tested this hypothesis using the ninjurin gene cluster. This pilot analysis included rat ninjurin, Rab13, Rap1b, and coronin 1b genes, as their complete sequences were available from the rat genome database. The genes were analyzed using the FrameWorker, a part of the complex Genomatix software tool that allows to extract a common *framework* of elements from a set of DNA sequences (Munich, Germany). In our case, these elements were transcription factor binding sites within predicted promoter regions of the genes, since this tool is designed for the comparative analysis of promoter sequences. This software returns the most complex models that are common to the input sequences (and satisfying the user parameters). All elements that occur in the same order and in a certain distance range in all (or a subset of) the input sequences, thus providing a model of transcriptional regulation of gene activity. In four predicted core promoters of ninjurin cluster we have identified five common elements. All five elements were located on plus-strands of the

promoters. These elements and their schematic relative positions within promoters are listed in Table 5 and Figure 109.

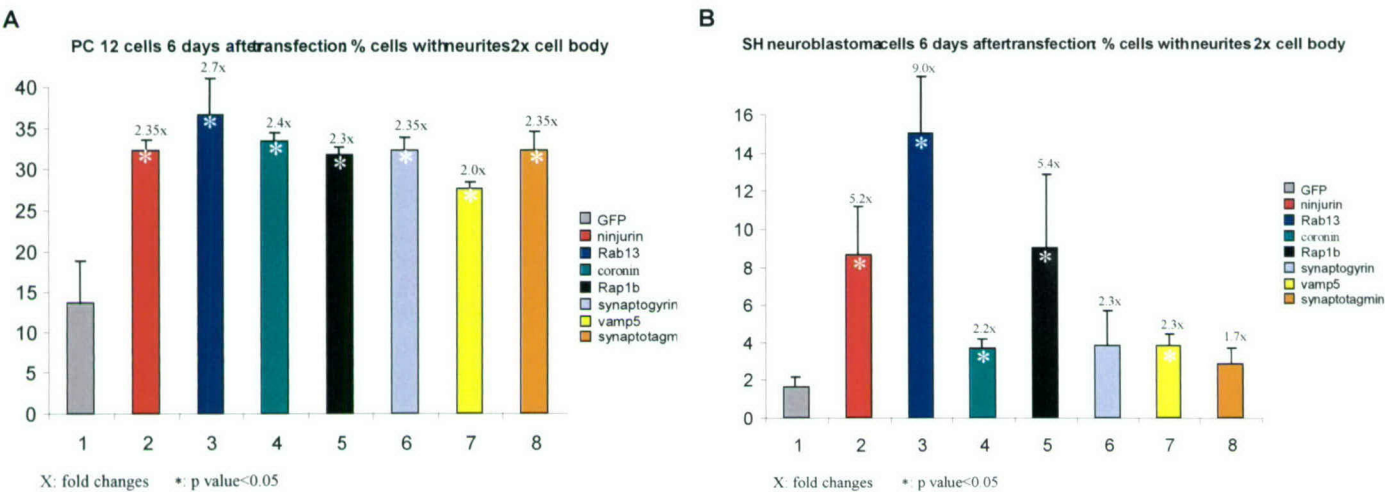


Fig. 108: Over-expression of ninjurin cluster members in both PC-12 and SH neuroblastoma cells neurons promotes neurite outgrowth. Bar graphs show increased neurite length for PC-12 (**Panel A**), and SH neuroblastoma cells (**Panel B**), after co-transfection with each of ninjurin cluster members with eGFP. Neurite length is expressed as percentage of control after transfection measuring the length of the longest neurite per cell. Fold changes are noted.

Table 5. Common Transcription Factors for the Promoters of the Ninjurin Gene Cluster				
Element	Strand	Matrix similarity	Common to	FW-Scores
V\$GATA	±	Optimized (min. 0.93)	100 %; 9 matches	0.44
V\$HOXF	±	Optimized (min. 0.79)	100 %; 6 matches	0.67
V\$MYT1	±	Optimized (min. 0.84)	100 %; 6 matches	0.67
V\$P53F	±	Optimized (min. 0.91)	100 %; 7 matches	0.57
V\$SP1F	±	Optimized (min. 0.91)	100 %; 9 matches	0.44

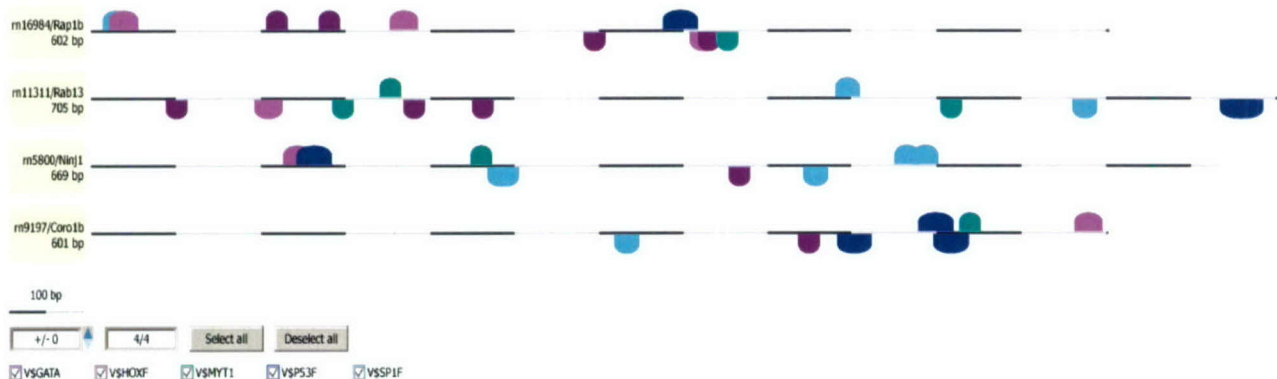


Fig. 109: Schematic presentation of results of the comparative *FrameWorker* analysis of the predicted promoter regions of the Ninjurin cluster. A subset of five common elements is present on the plus-strands of all four promoters in a certain order and a distance range from the transcription start site.

Of considerable potential importance is the observation that all four tested promoters that are activated in response to neuronal injury have common multiple p53- and MyT1-binding sites. Previous studies have demonstrated that p53 plays an essential role in DNA damage-induced cell growth arrest and apoptosis; however, it has also been shown that this transcription factor can influence expression of a number of other genes²⁵⁰. On the other hand, MyT1 zinc finger factor has been more specifically implicated in primary neurogenesis²⁵¹.

In conclusion, spinal cord injury studies showed that activation of pro-apoptotic cell cycle genes after injury was associated with suppression of multiple genes associated with regeneration in plasticity. These observations have major implications for therapy.

Hypothesis #9: Critical factors involved in neuronal apoptosis differ as a function of development

Neuronal apoptosis plays an essential role in early brain development and contributes to secondary neuronal loss following acute brain injury. Recent studies have provided evidence that neuronal susceptibility to apoptosis induced by ischemic or traumatic injury decreases during brain development; however, the molecular mechanisms responsible for this age-dependent phenomenon remain unclear. Our studies were intended to address the following hypotheses: 1) Neuronal susceptibility to apoptosis progressively declines during brain maturation; 2) Developmental decreases in apoptotic potential reflect, in part, reduced Apaf-1 and Caspase-3 gene expression, which contribute to the intrinsic pathway of neuronal apoptosis; and 3) Injury-induced neuronal apoptosis requires reactivation of these key apoptotic genes.

Clinical observations suggest that age influences outcomes and mortality after brain injury; however, why the same insult results in different response to injury in adults and in infants remained unclear. Using different models of experimental brain injury, recent reports suggest age-dependent differences in susceptibility to apoptosis. Initiation and progression of apoptosis are often stimulus-specific. Thus, in a variety of cell types, apoptosis can be regulated by extracellular death factors. These factors are members of the TNF family of cytokines and include Fas ligand (Apo-1/CD95 ligand), TNF- α , TRAIL/Apo-2 ligand, and TWEAK^{252, 253}. The pathway involves transduction mechanisms, where an important role has been attributed to a "death domain" sequence motif in the cytoplasmic segments of corresponding receptors²⁵⁴. In this pathway, caspase-8 appears to play the major role in the initiation of caspase cascade²⁵⁵⁻²⁵⁷. Stimulation of death receptors by their respective ligands induces oligomerization of the receptors and the formation of a death-inducing signaling complex (DISC)²⁵⁸. The intracellular domain of the death receptor binds to the adaptor molecule FADD, which in turn recruits procaspase-8 allowing its autocleavage and activation. The released active caspase-8 activates downstream executioner caspases-3 and -7²⁵⁴.

Active caspase-8 can initiate also downstream cleavage of executioner caspases by mitochondrial-dependent mechanisms. Thus, recent studies suggest that cell death receptors may amplify their suicide signal by activating the apoptosome. In this pathway, caspase-8 cleaves Bid, a BH3 domain-containing proapoptotic Bcl2 family member²⁵⁹. C-terminal cleavage product of Bid translocates from cell cytosol to mitochondria and interacts with Bax, thus triggering its translocation from cytosol to mitochondrial membranes followed by the release of cytochrome c, and activation of caspase-9 and downstream executioner caspases^{82, 260}. In addition, Bid fragments can act as a membrane destabilizing agent, increasing release of cytochrome c²⁶¹. The cytochrome c releasing activity of Bid is antagonized by Bcl2⁸² and effectively inhibited by the protein FLIP (for FLICE-inhibitory protein): two alternatively spliced forms of FLIP interact with the adaptor protein FADD and the caspase-8, thus potentially inhibiting apoptosis induced by death receptors²⁶².

While studying the biochemical mechanism of caspase activation, Xiaodong Wang's group had discovered that cell extracts contained three major protein factors that worked together to activate caspase-3 and induce apoptosis^{75, 263, 264}. Identification of those factors revealed an intrinsic cell death pathway that is initiated by release of cytochrome c from mitochondria to the cytosol⁷⁵.

In the presence of ATP (or dATP), cytochrome c binds to the cytosolic adaptor protein Apaf-1⁷⁵. The N-terminal 85 amino acids of Apaf-1 show 53% similarity to the N-terminal prodomain of the *C. elegans* Ced-3. This is followed by 320 amino acids that show 48% similarity to Ced-4. The C-terminal region of Apaf-1 comprises multiple WD repeats, which are proposed to mediate protein-protein interactions²⁶³. Binding of cytochrome c to Apaf-1 allows the recruitment and activation of caspase-9 within the apoptosome⁷⁵. Caspase-9 and Apaf-1 bind to each other via their respective N-terminal Ced-3 homologous domains. This event leads to caspase-9 activation⁷⁵. Active caspase-9, in

turn, activates executioner caspases-3 and -7. Activated caspase-3 is required for the activation of four other caspases (-2, -6, -8, and -10) in this pathway and also participates in a feedback amplification loop involving caspase-9^{75, 265}.

Similarly to null mutants of caspase-3, both Apaf-1 and caspase-9 knockout mice demonstrate a variety of hyperplasias and disorganized cell deployment in the brain leading to death during embryonic development²⁶⁶⁻²⁶⁹. This suggests that *activation of caspase-3 by apoptosome-mediated caspase-9 activation has a critical role in the developing central nervous system*^{266, 270, 271}.

1. Developmental changes in potential of the intrinsic apoptotic pathway in rat brain cortex

The following experiments provided essential data that determined the direction of our proposal. They were designed to assess effectiveness of the intrinsic pathway of caspase-3 activation in rat brain. We used a well-established cell-free assay of cytochrome c-dependent caspase-3 activation. Cytochrome c and dATP are necessary for the oligomerization and binding of Apaf-1 to procaspase-9 followed by autoactivation of this caspase. Active caspase-9, in turn, cleaves and activates downstream caspases including caspase-3.

Therefore, we incubated cytosolic extracts isolated from rat brain cortex on embryonic day 17 (E17) or postnatal days 2, 7, 14, and 60 (P2-60) in the absence or presence of cytochrome c, and dATP. As an outcome, we measured caspase-3-like (DEVDase) enzyme activity using a fluorometric assay.

High levels of cytochrome c-induced DEVDase activity were found in extracts from E17 and P2 rat cortex with no considerable difference between these two age groups. In contrast, activity of DEVDase in P7 protein extracts decreased to approximately 65% of embryonic and neonatal level. DEVDase activity in P14 extracts decreased further reaching nearly 10% of E17 and was not detected in extracts from mature (P60) brain. Low background DEVDase activity was detected in extracts preincubated in the absence of cytochrome c (Fig. 110A).

Because cytochrome c-dependent activation of caspase-3 requires activation of caspases-9, we next examined cleavage of these two caspases by Western blot analysis. Using a monoclonal 5B4 anti-caspase-9 antibody (MBL, Japan) that recognizes both rat procaspase-9 and its large subunit we observed nearly complete cleavage of procaspase-9 in E17, P2, and P7 extracts (Fig. 110). The degree of caspase-9 cleavage was markedly decreased in P14 extracts and was not detected in P60 extracts. Using a polyclonal anti-caspase-3 antibody (Cell Signaling Technology) that recognize only the p20 and p17 cleaved fragments we found that, consistent with results of DEVDase activity assay, caspase-3 was cleaved to its active form in E17, P2, and P7 but not in P14 or P60 extracts (Fig. 110B). We have also analyzed apoptotic potential in brains of 6- and 8-months-old animals and did not find significant differences compared to 60-days old (data not shown). Similar age-dependent changes in cytochrome c-dependent apoptotic susceptibility were found in developing mouse brain (data not shown).

This observation is consistent with recent reports on age-dependent differences in injury-induced caspase-3 activation and susceptibility to apoptosis in mammalian brain^{10, 272, 273}. Results of Western blot experiments showed that age-dependent decline in cytochrome c-dependent activation of caspase-3 in rat brain cortex was parallel to the extent of procaspase-9 processing in the *in vitro* assay. This suggested that repression of cytochrome c-dependent apoptotic potential might be regulated at the level of the apoptosome. Therefore, further experiments were aimed to analysis of Apaf-1, caspase-9, and caspase-3 gene expression.

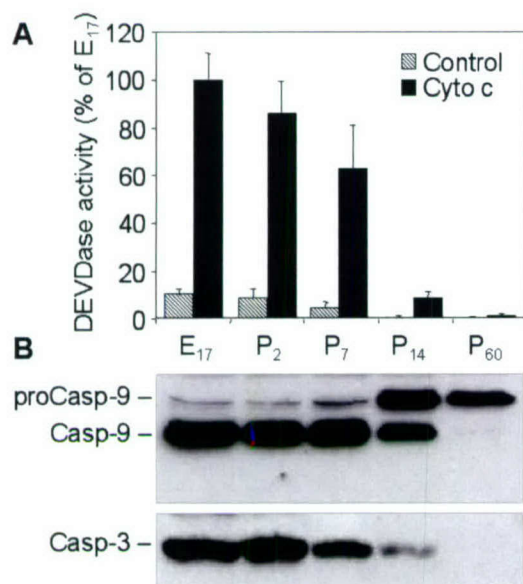


Figure 110. Age-dependent susceptibility of cytosolic protein extracts from rat cortex to cytochrome c/dATP-dependent activation of caspase-3. (A) Fifty μ g aliquots of cytosolic protein extracts isolated from cortex of embryonic (E, day 17) or postnatal (P, days 2, 7, 14, and 60 after birth) rat brains were incubated in the presence or absence of cytochrome c and dATP. Caspase-3-like activity in treated and control extracts was assayed fluorometrically by measuring the accumulation of free AMC resulted after cleavage of Ac-DEVD-AMC. Protease activity is expressed in arbitrary fluorescence units (increase of fluorescence per minute). (B) Fifty μ g aliquots of cytosolic extracts were treated as described in Figure 86A, subjected to 12% SDS-PAGE and transferred to a nitrocellulose filters. The filters were probed with a monoclonal anti-caspase-9 antibody (clone 5B4, MBL, Japan) or with a rabbit polyclonal antibody against p17 cleaved form of caspase-3 (Cell Signaling Technology). The antigen-antibody complexes were visualized by an ECL method. These experiments were repeated three times with similar results.

2. Age-dependent changes in expression of the apoptosome components in rat brain cortex

In order to identify a potential molecular basis for observed age-dependent change in cytochrome c-dependent apoptotic potential, we examined expression of each component of the apoptosome during rat brain development at mRNA and protein levels. mRNA levels were estimated by RT-PCR analysis. These experiments were based on the available rat Apaf-1, caspase-3, and caspase-9 mRNA sequences (GenBank accession numbers NM023979, U58656, and AF262319, correspondingly). RT-PCR technique that we used in this study is not strictly quantitative; however, it provides realistic estimate of relative gene expression, as determined in our several previous studies^{39, 59, 158, 164}. These experiments revealed that Apaf-1 and caspase-3 mRNA levels were notably decreased in the rat brain cortex between 1 week and 2 weeks after birth, and were maintained at this decreased level in the mature tissue (Fig. 111A).

To examine if the observed decrease of caspase-3 and Apaf-1 mRNA correlates with decreased expression of the corresponding proteins, we estimated Apaf-1, procaspase-3, and procaspase-9 protein expression in rat cortex at the same times in rat brain development. Protein expression was assayed by Western blot analysis. Identification of procaspase-3 and procaspase-9 was performed by staining with H-277 and 5B4 antibodies (Santa Cruz Biotechnology and MBL, correspondingly). Among a number of anti-Apaf-1 antibodies tested in this study only a polyclonal rabbit antibody (#AB16941, Chemicon International) recognized a band of ~140 kDa corresponding to predicted molecular weight of rat Apaf-1 (140 kDa), while the rest of tested antibodies stained a ~110 kDa-protein of unknown origin. Specificity of this antibody was confirmed in preliminary experiments where staining of Apaf-1 in rat brain samples was compared with staining of Apaf-1 preparations purified from bovine thymus and recombinant human Apaf-1 (these particular results were obtained in collaboration with Dr. K. Yoshihara, Japan; data not shown).

As shown in Fig. 111B, levels of both Apaf-1 and caspase-3 proteins in cortical extracts were markedly decreased after 1 week of age, and were minimal in the mature tissue. Age-dependent decrease in caspase-3 mRNA content in rat brain tissue was consistent with the recent report²⁷⁴. Developmental regulation of Apaf-1 gene expression in mammalian brain can be also suggested on the basis of previously published data²⁶³. Profiles of gene expression, examined in this work, were comparable with the developmental profile of cytochrome c-mediated caspase-3 activation in rat brain.

Interestingly, caspase-9 gene activity, at both mRNA and protein levels, did not change notably during brain development.

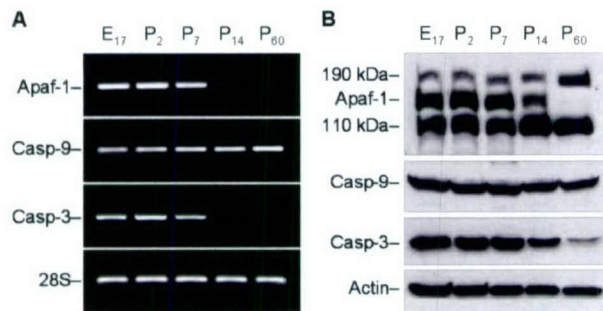


Figure 111. (A) RT-PCR analysis of the abundance of transcripts encoding rat Apaf-1, caspase-9, and caspase-3 in cortex of embryonic (E 17) or postnatal (P2-60) rat brain. Amplification of 28S rRNA was used as an internal control. (B) Western blot analysis of the abundance of Apaf-1, procaspases-9 and -3 in rat cortex during development. β -Actin protein abundance was used as an additional control for gel loading and transfer. These experiments were repeated four times with similar results.

3. Downregulation of apoptotic potential and Apaf-1 protein expression during neuronal maturation *in vitro*

Because of poor specificity of available anti-Apaf-1 antibodies *at the time then the experiments were initiated*, we were not able to examine directly cell type specificity of Apaf-1 expression in the brain. Therefore, we examined Apaf-1 protein expression, cytochrome c-dependent activation of caspase-3, and etoposide-induced apoptosis in primary rat cortical neurons cultured for 1 day or 14 days *in vitro* (DIV).

Western analysis showed that Apaf-1 expression was clearly decreased in 14 DIV primary neurons compared to 1 DIV cells, a result consistent with Apaf-1 protein expression in developing rat cortex (Fig. 112A). Incubation of cytosolic extracts from 1 DIV primary neurons in the presence of cytochrome c and dATP led to marked activation of caspase-3; in contrast, activation of caspase-3 in extracts from 14 DIV neurons was approximately 5 fold lower than that in 1 DIV extracts (Fig. 112B). Similar difference in levels of caspase-3 activity was observed in the cytosol from primary neurons treated with etoposide. Thus, 5 h treatment of 1 DIV cells resulted in activity of caspase-3 corresponding to 18.7 ± 0.4 AUF; in contrast activity in 14 DIV extracts was only 4.7 ± 0.1 AUF (Fig. 112C). Changes in caspase-3 activity in the etoposide-treated neurons correlated inversely with the degree of cell survival. Thus, after 24 h incubation of 1 DIV neurons with etoposide, $45 \pm 6\%$ of cells survive, whereas in 14 DIV cultures $69 \pm 5\%$ cells were viable (Fig. 112D).

In preliminary transfection studies using dominant negative mutant constructs of caspase-8 and caspase-9 (a gift from Dr. Dixit), we have demonstrated that etoposide-induced apoptosis in rat primary cortical neurons, as well as in the SH-SY5Y neuroblastoma cell line, proceeds through a caspase-9-dependent pathway (data not shown).

Collectively, these data demonstrate that neuronal maturation *in vitro* leads to repression of cytochrome c-dependent apoptotic susceptibility and that this process parallels to decrease in Apaf-1 protein expression in rat cortical neurons

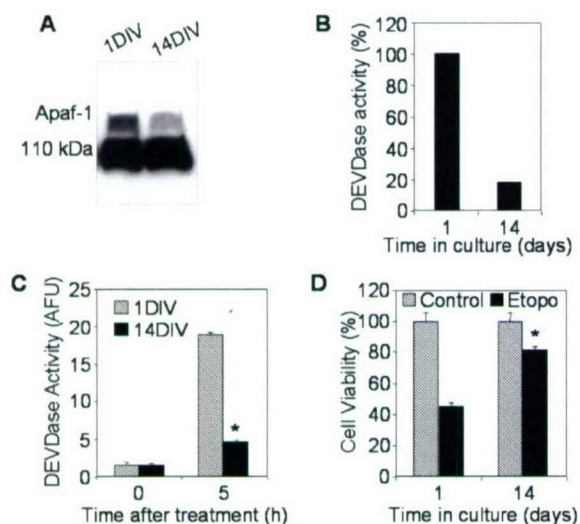


Figure 112 (A) One hundred μ g of cytosolic proteins from 1 DIV or 14 DIV primary rat cortical neurons were separated in 5% SDS-PAGE followed by staining with an Apaf-1 antibody (Chemicon International). (B) Protein extracts from 1 DIV or 14 DIV primary rat cortical neurons were incubated in the presence of cytochrome c and dATP. Caspase-3-like activity was assayed fluorometrically by measuring the accumulation of free AMC resulted after cleavage of Ac-DEVD-AMC. Data are expressed as percent of 1 DIV induced caspase activity. (C) 1 DIV or 14 DIV primary rat cortical neurons were treated with 50 μ M etoposide for 5 h. Control cultures (0 h) served as negative controls. Caspase-3-like activity in cytosolic extracts from treated or control cells was assayed fluorometrically. Protease activity is expressed in arbitrary fluorescence units \pm SD (n=6). * $p < 0.0001$, compared with caspase-3 activity in treated 1 DIV cells, by ANOVA and Dunnett's test. (D) 1 DIV or 14 DIV primary neurons were treated with 50 μ M etoposide for 24 h, and cell viability was analyzed by measurement of calcein fluorescence. Data are expressed as a percentage of the value for control cells not exposed to etoposide \pm SD (n=6), * $p < 0.0001$, compared with viability of 1 DIV cells after 24 h etoposide treatment, by ANOVA and Dunnett's test.

4. Activation of Caspases as a Function of Age after HI-induced brain Injury: In vivo Studies

Our preliminary *in vitro* studies demonstrated significant decrease in potential of the intrinsic pathway of apoptosis in rat brain tissue with drastic differences between ages of P7 and P14. This observation has inspired us to investigate whether similar age-dependent differences exist in respect to apoptotic response to brain injury. We have chosen a well-established and reliable model of HI brain injury that has been reported inducing neuronal apoptosis in experimental animals of various ages^{273, 275, 276}. Our choice in favor of HI rather than TBI was determined by selected early age of animals and by difference in their brain size — two factors that make available in our laboratory TBI models inadequate for such comparative studies. However, recent reports from Chrysanthi Ikonomidou's group^{10, 272} have motivated us developing a modified TBI model in rats where injury severity could be adjusted appropriately to the brain size, to use such a model in future developmental studies.

P7 and P14 pups underwent the right CCA ligation followed by exposure to 8% O₂ for 90 min. In case of sham-injured animals the ligature was passed around the artery and removed. Brains of sham-control and experimental animals were collected at 4, 24, and 48 h of recovery from HI. Activity-specific cleavage of caspases-9 and -3 was analyzed in cytosolic extracts from ipsilateral cortex using Western blot technique (Fig. 113). Results clearly demonstrated that HI induced early cleavage of both caspases in injured but not in control rat cortex with more severe effect in P7 compared to P14 brain.

Western blot results were consequently confirmed by immunohistochemistry approach demonstrating increased neuronal expression of active caspase-3 in brain regions of P7 compared to P14 rats (Fig. 114).

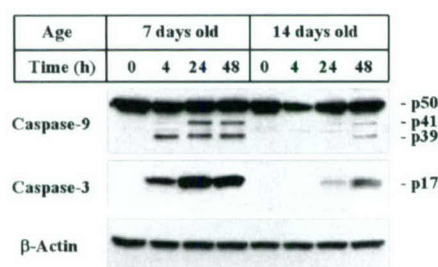


Figure 113. HI-induced cleavage of caspase-9 and caspase-3 in brain cortex of P7 and P14 rats. Eighty μ g aliquots of cytosolic protein extracts isolated from sham-control (0h) or injured cortex at indicated times after HI were subjected to SDS-PAGE and transferred to a nitrocellulose filter. The filter was probed with antibodies against caspase-9 or p17 cleaved form of procaspase-3. β -Actin protein abundance was used as an additional control for gel loading and transfer. Significant increase in cleavage of both caspases is observed in P7 animals.

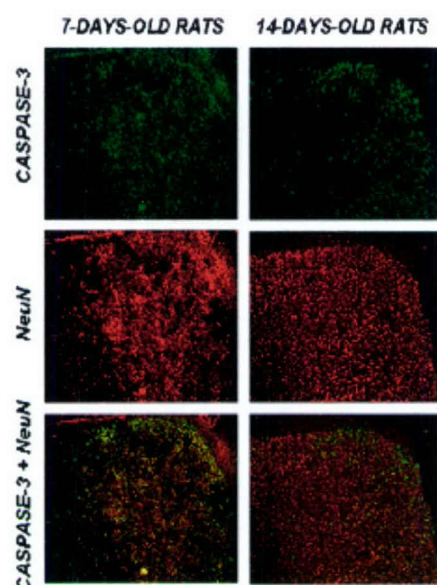


Figure 114. Identification of neurons expressing active caspase-3 in the 7 days old rat brain cortex 48 hr after HI. Photographs represent 100x magnification; the same microscopic fields were stained with anti-p17 (a fragment of active caspase-3) and anti-neuronal nuclear protein. Double immunofluorescence revealed higher neuronal expression of active caspase-3 in 7 days old compared to 14 day-old brain (see Figure 88 for comparison).

5. Activation of Caspases as a Function of Time after TBI: In Vivo Studies

Our early reports suggested that brain trauma in mature rats also results in activation of caspase-3⁵⁹. Because activation of caspase-3 results from specific cleavage of the precursor protein, we examined such cleavage of caspase-3 using Western analysis as a function of time after TBI. Consistently with previous findings, very low levels of the cleaved forms of caspase-3 were detected beginning 4h after trauma, but increased markedly at 48h after injury (Fig. 115).

Given the present and previous observations that apoptotic potential in mature brain tissue is normally repressed and that brain injury causes activation of caspase-3 and related neuronal apoptosis, we examined possibility whether TBI recapitulates apoptotic potential via reactivation of caspase-3 and Apaf-1 genes. In part, this hypothesis is supported by results of our previous studies where we found that TBI results in early increase in caspase-3 mRNA content in the injured brain regions⁵⁹. In this study, we examined protein expression of procaspase-3 in injured cortex as a function of time after brain trauma. Using Western blot analysis we found that procaspase-3 protein levels were elevated in injured cortex by 4-to-48 hr after TBI (Fig. 116A).

Because of the limitations of Western blot for quantitative analysis of protein expression, we developed a sensitive in vitro assay to assess relative levels of procaspase-3 protein expression. The assay is based on ability of active recombinant caspase-9 to cleave and activate procaspase-3 in cytosolic protein extracts. Thus, protein extracts from rat cortex isolated at different times after TBI were treated with active recombinant human caspase-9 and DEVDase activity was measured fluorometrically. As shown in Fig. 116B, TBI induced a significant elevation of caspase-9-mediated caspase-3 activity in extracts from injured cortex. Approximately 1.5 fold increase in caspase-9-dependent caspase-3 activation was observed in extracts isolated from injured cortex 4 h after TBI. This induced activity was further increased at later time points after TBI exceeding twice control levels by 2 days after injury. No such changes in caspase-3 activity were detected in contralateral brain regions (data not shown).

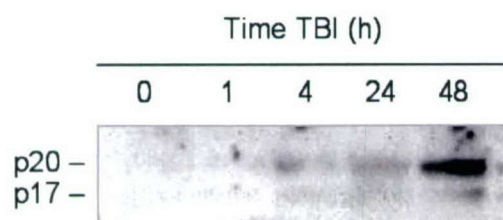


Figure 115. TBI-induced specific cleavage of procaspase-3 in rat brain cortex. Eighty μ g aliquots of cytosolic protein extracts isolated from sham-control or traumatized rat cortex at indicated times after TBI were subjected to 12% SDS-PAGE and transferred to a nitrocellulose filter. The filter was probed with a rabbit polyclonal antibody against p17 cleaved form of procaspase-3. Significant increase in caspase-3 cleavage is observed at 48 h after injury.

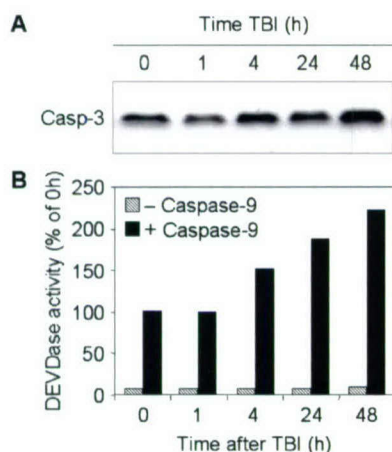


Figure 116. (A) Fifty μ g aliquots of cytosolic protein extracts isolated from sham-control or traumatized rat cortex at indicated times after TBI were subjected to 12% SDS-PAGE and transferred to a nitrocellulose filter. The filter was probed with the antibody against procaspase-3. (B) Fifty μ g aliquots of cytosolic protein extracts isolated from sham-control or traumatized rat cortex at indicated times after TBI were incubated with or without active recombinant human caspase-9 (20 U, Biomol) in 50 μ l of caspase activation buffer at 37° C for 1 h. Caspase-3-like activity was assayed fluorometrically.

Injury-induced increases in caspase-3 protein expression observed in this study are in accord with increased activity of this caspase after TBI. On the other hand, activation of caspase-3 requires prior activation of upstream initiator caspases. We found that in the mature brain the caspase-9-dependent apoptotic pathway is repressed, whereas it is highly potent in the immature brain (Fig. 110). Moreover, preliminary analysis of caspase-8 cleavage and activation in cortical protein extracts after brain injury did not suggest for a role of caspase-8 in TBI-induced cell death (data not shown). Therefore, we examined whether specific cleavage caspase-9 could be detected after TBI. This was assessed by Western analysis of cortical protein extracts in a time course after injury.

Amino acid sequence analysis of the rat procaspase-9 (50 kDa) revealed that, like human procaspase-9, it contains a SEPD potential autoactivation cleavage site and a DQLD caspase-3 recognition site. Correspondingly, cytochrome c-mediated autoactivation is expected to produce 39 kDa large subunit recognizable by the antibodies, whereas, a 41 kDa large fragment is expected after cleavage with caspase-3 (Fig. 116). Indeed, treatment of P17 cortical extracts with cytochrome c and dATP resulted in cleavage of caspase-9 corresponding to the 39 kDa subunit, whereas treatment of the extracts with recombinant active rat caspase-3 (Alexis) primarily resulted in appearance of 41 kDa fragment. Notably, processing of procaspase-9 by caspase-3 was less efficient compared to that by cytochrome c treatment (Fig. 116).

Western blot analysis of protein samples of injured cortex showed accumulation of the 39 kDa caspase-9 subunit after TBI. At 48 h after injury, the 41 kDa caspase-9 fragment also became apparent, reflecting increased caspase-3 activity in the samples at this time point (Fig. 117).

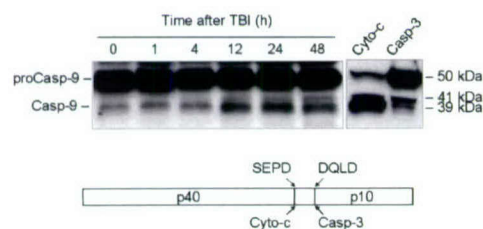


Figure 117. Eighty μ g of cytosolic protein extracts isolated from sham-control or traumatized rat cortex at indicated times after TBI were subjected to 10% SDS-PAGE and transferred to a nitrocellulose filter. As a positive control for cleavage specificity, 80 μ g aliquots of protein extracts from 2 days-old rat cortex were preincubated in presence of either caspase-3 or cytochrome c and dATP. The filter was probed with the antibody against caspase-9. A schematic diagram illustrates processing of procaspase-9. Procaspase-9 is processed preferentially at SEPD site within the apoptosome and at DQLD site by caspase-3 to generate the large subunit (p40) and small subunit (p10) of mature caspase-9.

Injury-induced cleavage of procaspase-9 at autoactivation specific site presumes that injury reactivates the apoptosome complex, which is normally repressed in the mature brain. Therefore, we next examined whether expression of Apaf-1 is affected by TBI.

6. Regulation of Apaf-1 Gene Expression as a function of time after TBI: In Vivo Studies

Results of semi-quantitative RT-PCR showed that Apaf-1 mRNA content increased in the injured cortex reaching $143\% \pm 10\%$ of control (sham) levels by 12h, $180\% \pm 5\%$ by 24 h, and $211\% \pm 9\%$ by 48h after TBI (Fig. 118 A,B). Furthermore, Western blot revealed increased intensity of Apaf-1 protein band in cortical extracts isolated 24h after injury with a peak expression at 48 h (Fig. 119).

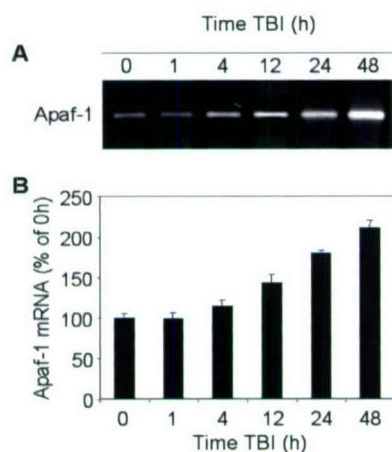


Figure 118. The time course of Apaf-1 mRNA expression in rat cortex at indicated times after TBI or in sham-operated controls (0 h). (A) Levels of mRNA were measured by using semiquanti-tative RT-PCR. (B) Levels of Apaf-1 mRNA are expressed as the proportion of individual RT-PCR product mean optical density to GAPDH RT-PCR product optical density of the same RNA sample.

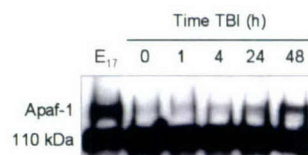


Figure 119. Eighty μ g aliquots of cytosolic protein extracts isolated from rat brain cortex at the embryonic day 17 (E17) or from sham-control (0 h) or traumatized rat cortex at indicated times after TBI were subjected to 5% SDS-PAGE and transferred to a nitrocellulose filter. The filter was probed with a rabbit polyclonal antibody against human Apaf-1. This experiment was repeated three times with similar results.

Consequent double immunostaining of control and injured rat cortex with the anti-Apaf-1 13F11 antibody (kindly provided by Dr. David Huang)²⁷⁷, and anti-NeuN antibodies demonstrated neuronal localization of Apaf-1 protein and its increased expression in traumatized rat cortex (Fig. 120). Specificity of 13F11 antibody has been confirmed using western immunostaining (Fig. 121).

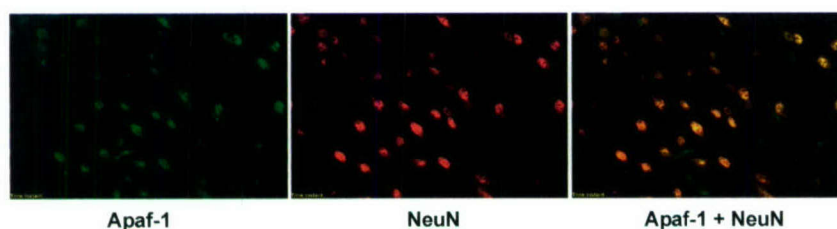


Figure 120. Identification of neurons expressing Apaf-1 in the rat parietotemporal cortex 48 hr after TBI. Photographs represent 400x magnification; the same microscopic fields were stained with anti-Apaf-1 and antineuronal nuclear protein (NeuN). Double immunofluorescence for Apaf-1 and antineuronal nuclear protein revealed a majority of these cells to be neurons.

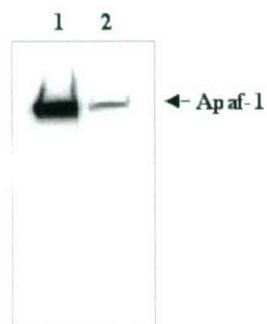


Figure 121. Thirty μ g aliquots of cytosolic extracts from P2 (1) and P60 (2) rat brain cortex were subjected to 7.5% SDS-PAGE and transferred to a nitrocellulose filters. The filters were probed with the rat monoclonal anti-Apaf-1 13F11 antibody. The antigen-antibody complexes were visualized by an ECL method. Staining revealed a single band of ~ 140 kDa differentially expressed during brain development.

In conclusion, our findings are consistent with previous observations on differential susceptibility to apoptosis and associated caspase-3 activity in developing and mature brain tissues^{10, 272, 273}. In addition, the results support our hypotheses and indicate that (1) Apaf-1 and caspase-3 genes expression is normally repressed in the adult brain and (2) acute brain injury recapitulates earlier expression patterns for these pro-apoptotic genes that may lead to increase in apoptotic potential of injured brain tissue.

Hypothesis #10: Multidisciplinary approaches can be used effectively to accelerate discoveries related to the mechanism and treatment of spinal cord injuries.

1. Development of a New Mouse Model of Spinal Cord Injury

A new mouse model of contusion injury was developed by Dr. Rosenberg for application in future studies utilizing transgenic and knockout animals. For this model, a laminectomy was performed, and a custom-designed device was used to deliver an impact injury to the exposed spinal cord. The device consisted of a pneumatic piston that was computer controlled, to allow precise quantitation of the velocity of impact and the amount of subsequent spinal cord deformation. Using this model, graded injury was induced and characterized behaviorally and histologically.

After several pilot studies to determine optimal dwell time and velocity for delivery of injury, the piston velocity was set at 4 m/sec with a dwell time of 20 msec. Cord displacements of 0.3 (mild), 0.5 (moderate) and 0.7 (severe) mm were examined (n = 17 mice/group). At 24 h after SCI, five mice from each group were anesthetized and the tissue processed for electron microscopy. The other 12 mice per group were behaviorally followed for 4 weeks then anesthetized and perfused with 4% paraformaldehyde. Mice subjected to severe injury exhibited profound neurological dysfunction and none survived for more than 11 days. Examination of the tissue from these animals showed that their cords were nearly transected (data not shown). It was concluded that this injury level was too severe to represent contusion injury, and data from this group were not developed further.

1.1. Behavioral Recovery

Although locomotive gait in the mouse is different from that of the rat, we and others have adapted the BBB behavioral test to evaluate hind function and locomotion following SCI. Mice in the mild and moderate injury groups showed similar hind limb function over the first week following injury (Fig. 122). Extensive movement in the hip, knee and ankle was typically seen by 7 d after SCI. By 14 d after SCI, recovery in the two injury groups was significantly different (two factor ANOVA repeated measures, $p = 0.001$; Tukey, $p < 0.05$). Mice in the mild group were capable of coordinated plantar stepping most of the time. Recovery in the mild group stabilized around the third week (21 d) with no further improvement seen in the fourth week of study. Moderately injured mice regained extensive hind limb movement. Their stepping, however, remained uncoordinated. Behaviorally, these animals demonstrated very little improvement from about day 14 out to day 28 when the study terminated.

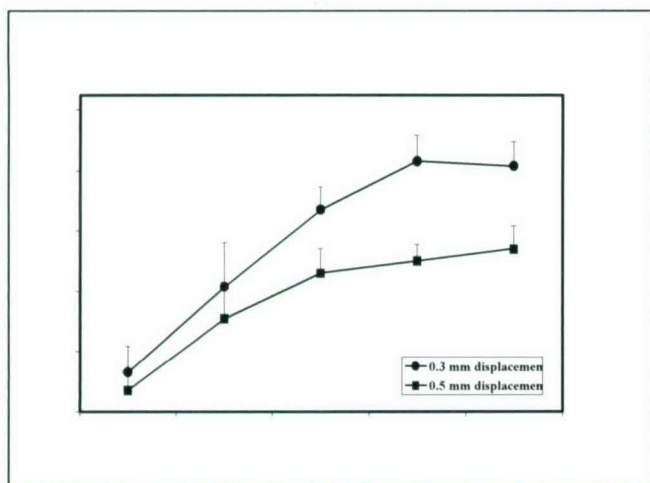


Figure 122. Functional recovery of hind limb locomotion over a four-week period in mice subjected to mild (0.3 mm) or moderate (0.5 mm) spinal cord injury (SCI). The BBB is an open field locomotor test with scores ranging from 0-21. Animals with complete hind limb paralysis receive a score of zero. At day 1 after SCI, animals in both the 0.3 mm and 0.5 mm spinal cord displacement groups demonstrate hind limb dysfunction and paralysis. By day 14, two weeks after the initial trauma, animals in the 0.3 mm group regained their ability to hind limb step. Animals in the 0.5 mm group were capable of weight bearing stance but still unable to step. One month after injury, animals in the 0.3 mm group were walking with mild deficits while the 0.5 mm injured animals were able to step occasionally. Asterisks indicate statistical differences between groups as determined with a two factor (time and displacement) ANOVA ($p < 0.001$) and post-hoc Tukey test ($p < 0.05$).

1.2. Histological Changes

Tissue collected 24 h after mild or moderate injury ($n = 5/\text{group}$) was processed for electron microscopy. After mild injury, a central, focal area of tissue destruction was localized to the dorsal white matter funiculus (Figure 123, upper panels). Separation of gray and white matter was evident and both areas exhibited damage. In lateral white matter, some of the axons appeared dilated with a few microcysts (axon profiles without axoplasm) scattered throughout. Ventral white matter showed slightly greater damage compared to the lateral areas, as microcysts were more prevalent in this region. Spacing between axons was increased, giving the appearance of lower axon density. After moderate injury, extensive damage was observed in the dorsal white matter region (Figure 123), lower panels). While a small amount of intact white matter was typically present along the pial rim, substantial cell loss was noted in the underlying grey and dorsolateral regions. Lateral white matter contained holes, likely indicative of axon loss, as well as microcysts. Axon loss was also suggested by increased intra-axonal glial spacing. Ventral white matter often retained a rim of intact axons along the pial edge, but otherwise the region contained numerous microcysts and moderately large holes suggestive of axon loss.

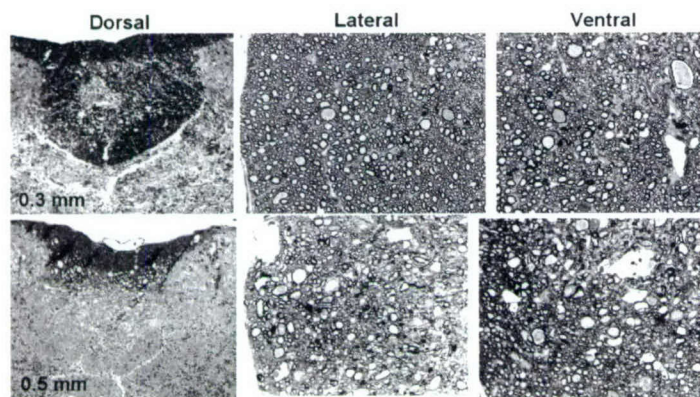


Figure 123. Effect of spinal cord injury on the number of oligodendrocytes and astrocytes in the ventral white matter 4 weeks later. Representative bright-field image of ventral white matter stained with CC1 (A) and GFAP (B) antibodies, which are markers for oligodendrocytes and astrocytes, respectively. Cellular density of oligodendrocytes and astrocytes was unchanged by injury in both the lateral and ventromedial white matter areas (Two-factor ANOVA, $p > 0.05$).

Chronic (one month) assessment of tissue damage following SCI was performed on erichrome stained sections. Damage was symmetrical around the impact epicenter. In the mild injury group, a fairly wide rim of white matter extended from the mid-lateral down through the ventral region (Figure 124A). Most of the dorsal and central gray cyto-architecture was dramatically altered and replaced with glial scarring at the lesion epicenter. One millimeter out from the epicenter, distinction between gray and white matter was apparent, and damage was restricted to dorsal and central gray areas with only moderate involvement of lateral regions. Two mm out from the epicenter, gray and white matter was relatively intact, with damage focused in the central gray and corticospinal tract, but also in mid-line lateral areas. Three millimeters out from the lesion epicenter, the tissue looked normal. After moderate injury extensive damage was noted at the lesion epicenter, and only a thin rim of white matter remained. The remainder of the tissue showed evidence of glial scarring and connective cell invasion/proliferation. No intact neurons or axons were visible with bright-field microscopy. At 1 mm from the epicenter, a moderate increase in white matter sparing was observed along the ventral edges. Occasionally, a cavity filled with connective tissue was also seen (Figure 124B). Two millimeters from the epicenter, damage was present in dorsal white matter and central gray areas. Holes were present throughout the white matter, suggesting axon loss. After moderate injury, dorsal white matter and central gray regions 3 mm out from the epicenter were clearly damaged.

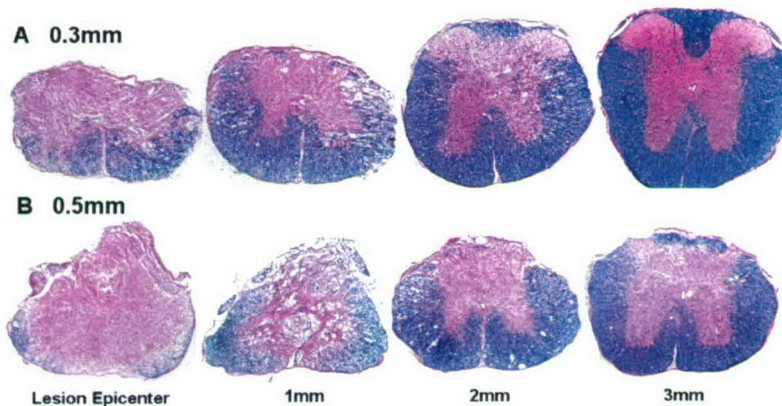


Figure 124. Representative images of erichrome and hematoxylin stained tissue sections collected 4 weeks after mild (0.3 mm) (A) or moderate (0.5 mm) (B) SCI. Images are representative of white and grey matter changes observed over increasing distance (1, 2 or 3 mm) away from the site of impact (lesion epicenter).

Residual white matter sparing was measured over a 0.5 mm length of cord, centered on the lesion epicenter. Every fifth or sixth erichrome stained section (a minimum of 50 μ m; maximum of 60 μ m) was viewed with 20X magnification bright-field microscopy. Residual white matter (blue stained tissue) was traced and the volume computed (data not shown). Compared to normal, mild and moderate injuries resulted in 25-30% or 40-45% decreases in white matter at the lesion epicenter at one month after SCI. Such changes were significantly different from normal, but not between injured groups (ANOVA $p < 0.005$; with post-hoc Tukey's tests ($p < 0.05$ for significance)). Linear regression analysis indicated that white matter sparing correlated with improved hind limb function (Regression, $r^2 = 0.611$, $p < 0.001$). The number of oligodendrocytes and astrocytes that were present in residual white matter one month after injury was assessed by counting peroxidase-labeled CC1+ (oligodendrocytes) and GFAP+ (astrocytes) (Figure 125 A,B). Neither mild nor moderate injury significantly altered the number of oligodendrocytes (Figure 125 C,D) or astrocytes (Figure 125 E,F) in this region 4 weeks later, in comparison to uninjured controls.

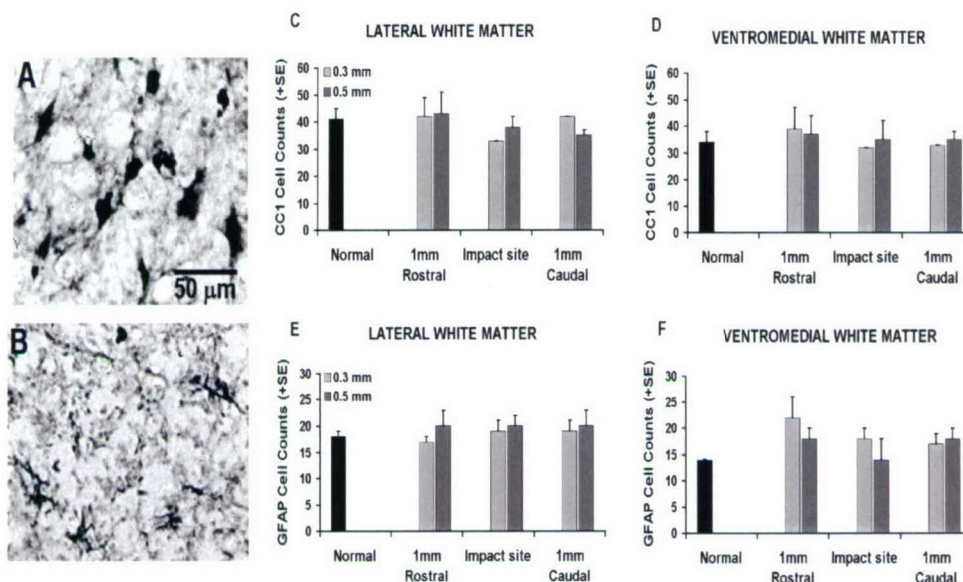


Figure 125. Effect of spinal cord injury on the number of oligodendrocytes and astrocytes in the ventral white matter 4 weeks later. Representative bright-field image of ventral white matter stained with CC1 (A) and GFAP (B) antibodies, which are markers for oligodendrocytes and astrocytes, respectively. Cellular density of oligodendrocytes and astrocytes was unchanged by injury in both the lateral and ventromedial white matter areas (Two-factor ANOVA, $p > 0.05$).

In conclusion, these data indicate that a custom-made pneumatic impounder device can be reproducibly used to produce a graded contusion injury response in the mouse. These data also provide a framework for further fine-tuning of the model to: a) show pharmacological effects of drugs known to improve recovery in other SCI models b) characterize the response to severe, but non-transecting, injury (between 0.5-0.7 mm deformation).

2. Neuroprotective dipeptide

Initial studies utilized *in vitro* preparations of spinal cord neurons to evaluate the effect of novel cyclic dipeptides developed by Drs. Faden and Kozikowski. Data from these studies suggested that cyclic dipeptides were neuroprotective in spinal (Figure 126), as well as cortical, neuronal cultures (see results presented under Hypothesis #2).

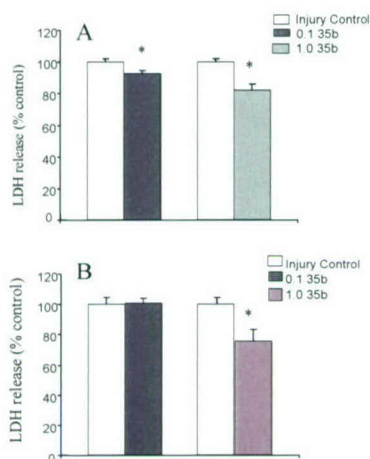


Fig. 126 Effect of 35b on cell death induced by 2 apoptotic agents: A) 0.3 μ m Staurosporine B) 10 μ m Thapsigargin. Staurosporine induces apoptosis by inhibition of protein kinases, whereas Thapsigargin induces apoptosis via cytochrome c release. Bars represent means and SEM for injured controls vs. micromolar concentrations of 35b as indicated. $*=p<0.05$ vs. control by t-test.

3. Caspases and Spinal Cord Injury

An *in vivo* weight-drop model of spinal cord contusion in the rat was re-established in the laboratory, based on Dr. Knoblach's prior expertise. The model was subsequently used to evaluate the role of caspase proteases in apoptosis and neurological dysfunction after spinal cord injury. For this, rats were subjected to severe injury and then euthanized from 1-168 hr later. Their spinal cords were removed and homogenates of tissue from the injury site were processed by specific caspase fluorometric activity assays and/or immunoblotting methods. Caspases 3, 8, and 9 were activated from 1 to 72 hr after injury, whereas caspases 1, 2 and 6 were not (Figures 127-129). Additional animals were also injured and their spinal cords removed and processed via immunohistochemistry for active caspase subunits and cell-type specific double-labeling, or TUNEL staining, to identify cells with condensed or fragmented DNA.

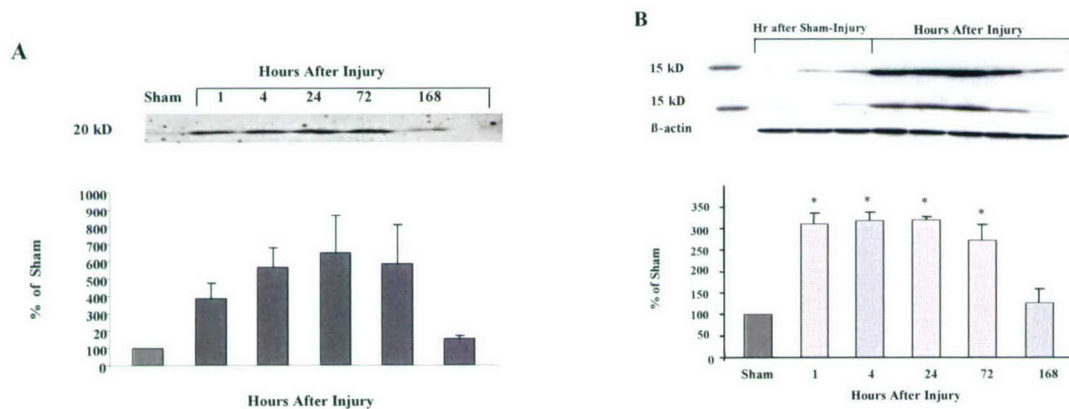


Figure 127. Caspases-8 and 9 were significantly increased from 1-72 hr after severe spinal cord injury. Results from semi-quantitative analysis are shown below representative immunoblots for caspase 8 in A, and for caspase 9 in B. Bars represent the % increase over sham for each time after injury ($n=4$ /group) as noted on the x-axis. The sham group consisted of samples taken at 4, 24 or 72 h ($n=2$ /group) after sham-injury. Rat spleen served as a positive control (+). In B, the 2 top blots were obtained using different caspase 9 antibodies and the β -actin procedural control from a representative blot is shown below. Results from antibody shown in the top blot were used for quantitation. $*=p<0.05$ by 1-way ANOVA and post-hoc Dunnett's test on square-root transformed data (to adjust for %).

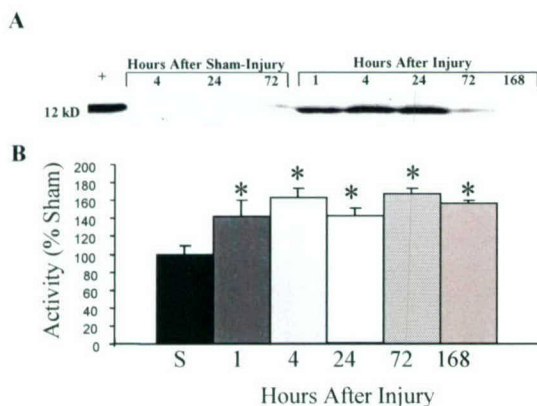


Figure 128. Caspase 3 was increased from 1-72 h after severe spinal cord injury. A representative immunoblot is shown in A, and results from an activity assay are shown as a bar graph in B, where bars represent means \pm SEM for activity in homogenates from the injury site at the times indicated on the x-axis (n=5/group). S=sham-injury samples (n=2) combined from each timepoint. * p <0.05 by 1-way ANOVA and post-hoc Dunnett's test on square-root transformed data (to adjust for %).

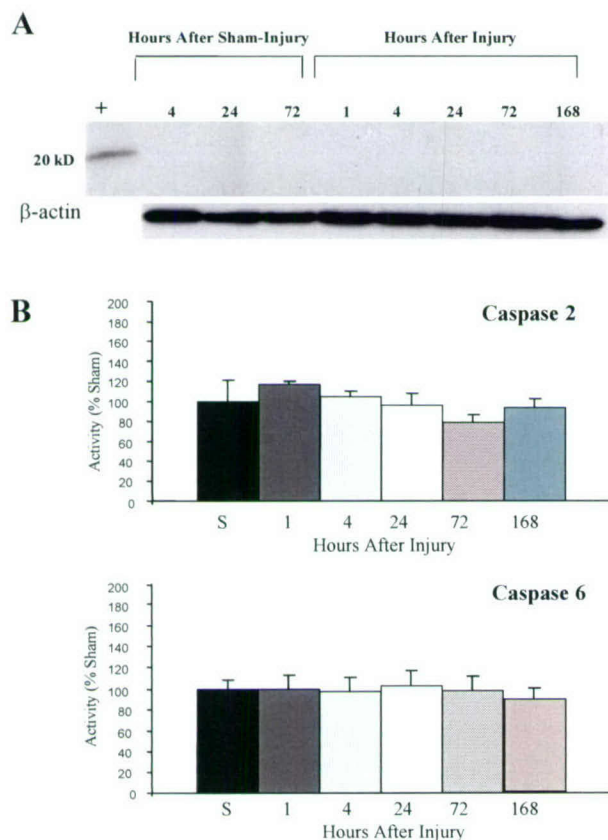


Figure 129. Caspases 1, 2 and 6 were not activated from 1-168 h after severe spinal cord injury in the rat. In A, bars represent means \pm SEM from activity assays for each caspase, performed using homogenates from the injury site at the times indicated on the x-axis (n=5/group). S=sham-injury samples from each timepoint (n=2) used for injured samples. A representative immunoblot for active caspase 1 is shown in B, with times after sham-injury (n=2/group) or injury (n=4/group) indicated above. Rat spleen served as a positive control (+).

Active caspase 8 was expressed in neurons at 4 and 72 hr after injury and white matter oligodendrocytes at 72 hr after injury. In contrast, active caspases 3 and 9 were expressed mainly in neurons at these times (Figure 130). Active caspases- 3, -8 and -9 were also expressed in astrocytes at 4 and 72 hr after injury, though only occasionally (data not shown). In addition, active caspases 3 and 9 were partially localized to grey matter motor neurons with apoptotic morphology as defined by condensed, fragmented DNA. Notably, upregulation of active forms of all 3 caspases were observed more than 2 segments rostral or caudal to the impact site. Intrathecal injection of the pan-caspase inhibitor z-Boc-d-fmk at 15 min after injury significantly improved locomotor function 21 and 28 days later, when compared to non-specific inhibitor peptide and vehicle controls (FM/DMSO) (Figure 131). Similar treatment with the selective caspase-3 inhibitor z-DEVD-fmk resulted in trends toward

improved function. These data support that caspases may be differentially activated in white and grey matter after spinal cord trauma and that such activation may contribute to subsequent neurological dysfunction.

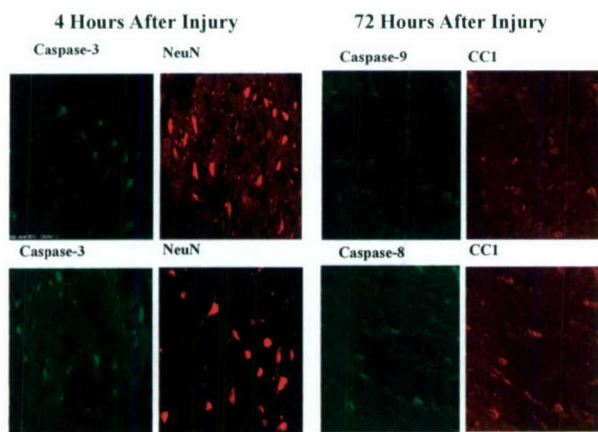


Figure 130. Representative images (100x) of cell-type (Neun=neurons; CC1=oligodendrocytes) specific staining for active caspase 3, 8, or 9 at 4 or 72 hr after severe injury in ventral grey (Neun) or ventrolateral white matter (CC1) 3 mm caudal to the site of injury impact.

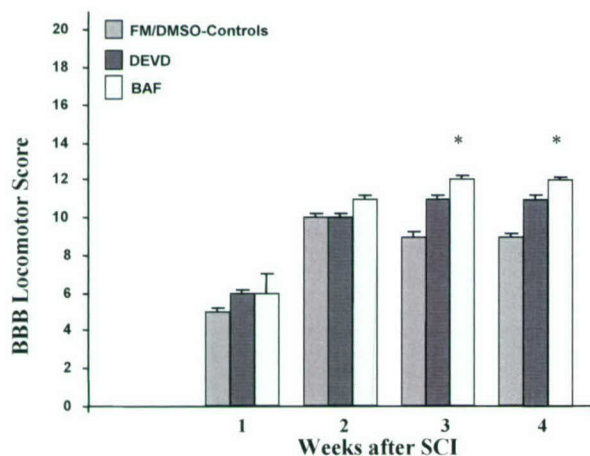


Figure 131. Basso-Beattie-Bresnahan (BBB) scores of locomotor recovery over time after spinal cord trauma followed by treatment with either a pan-caspase (BAF) or caspase-3-specific inhibitor (DEVD) or a non-specific peptide and/or vehicle control (DMSO) (both control groups combined) ($n=6-7$ /group).

A second project concerned a pilot study that employed Affymetrix DNA microarrays to evaluate the expression of >32,000 genes at 30 min, 4 h and 7 days after moderate spinal cord injury. Results from this study suggested that expression of many genes changes temporally after injury, and moreover, revealed many genes that were not previously associated with secondary injury mechanisms (Table 6). Drs. Knoblach and Faden combined these data with those from the caspase studies described above to support (in collaboration with Dr. Eric Hoffman at Children's National Research Institute) an application for an NIH-sponsored microarray contract aimed at elucidating gene expression changes after traumatic spinal cord injury. This contract was eventually awarded to Dr. Faden.

Table 6. Specific mRNA Increases in Rat Spinal Cord 4 hr after Moderate Contusion Injury
Data obtained from the site of impact + 1 spinal cord segment rostral and caudal

<4 Fold Increase	4-10 Fold Increase	>10 Fold Increase
2.2 tissue factor	4.1 serum and glucocorticoid-regulated kinase	10.4 epithelial membrane protein-1
2.2 DOC-2	4.1 leucine zipper protein	11.6 plasminogen activator inhibitor-1 (PAI-1)
2.2 Ssecks 322	4.1 phosphodiesterase (PDE4)	12.0 heme oxygenase
2.2 protein-tyrosine kinase (JAK2)	4.2 GTP cyclohydrolase I	12.9 pJunB
2.3 interleukin 4 receptor	4.3 MAP-kinase phosphatase (cpg21)	14.6 RL/IF-1 mRNA
2.3 inducible carbonyl reductase	4.4 intercellular adhesion molecule-1	17.6 heat shock protein 70
2.3 gene-inducible enhancer-binding protein 1	4.4 PKC binding protein	18.8 immediate-early serum-responsive JE
2.4 GADD45	4.6 endothelial receptor for oxidized low-density lipoprotein	19.7 MIP-1 beta
2.5 amidophosphoribosyltransferase	4.6 urokinase-type plasminogen activator	24.0 mob-1
2.6 antizyme inhibitor	4.6 thioredoxin reductase	32.3 immediate-early serum-responsive JE
2.7 manganese-containing superoxide dismutase	4.7 liver arginase	35.4 CELF
2.7 UDP-glucose dehydrogenase	4.7 intracellular calcium-binding protein (MRP14)	
2.7 Fc-gamma receptor	4.9 oxidative stress-inducible protein tyrosine phosphatase	
2.8 protein-tyrosine phosphatase	4.9 S-adenosylmethionine synthetase	
2.8 interleukin-1 receptor type 2	4.9 adrenomedullin precursor	
2.9 FBR-murine osteosarcoma	5.1 CD14	
2.9 Fc-gamma receptor	5.2 heat shock protein 70 (HSP70)	
3.1 TIS 11	5.2 Gal/GalNAc-specific lectin	
3.1 GTP cyclohydrolase I	5.5 activity & neurotransmitter-induced early gene 6	
3.1 progression elevated gene 3 protein	5.6 heparin-binding EGF-like growth factor	
3.2 interferon regulatory factor 1 (IRF-1)	5.8 nerve growth factor induced factor A	
3.3 activity & neurotransmitter-induced early gene 6	6.8 c-myc oncogene and flanking regions	
3.3 nuclear factor kappa B p105 subunit mRNA	6.9 type II hexokinase	
3.3 zinc finger protein AT-BP1	7.4 Krox-24	
3.4 PRG1	7.5 silencer factor B	
3.4 CC chemokine receptor	8.0 nerve growth factor-induced (NGFI-A)	
3.4 krox20	8.5 transcriptional repressor CREM	
3.4 GADD45	8.8 hexokinase II	
3.5 c-fos mRNA	9.5 interleukin 1-beta mRNA	
3.5 non-hepatic-type S-adenosylmethionine synthetase		
3.5 CREMdeltaC-G		
3.6 transcription factor NGFI-B		
3.7 lipocortin I		
3.7 protein tyrosine phosphatase (rVH6)		

Currently, the laboratory is continuing the initial studies of Dr. Rosenberg to establish and characterize a new mouse model of spinal cord impact injury. In collaboration with David Zapple, a mechanical engineer, a new device has been constructed which includes sensors that provide more detailed information about the position of the impactor tip relative to the spinal cord (Figure 132). In addition, the device has been modified to accommodate spinal cord motion that occurs due to respiration. Ongoing studies will evaluate whether these changes, and other modifications, will allow us to construct an injury severity curve which covers greater range of contusion levels, without increasing mortality or producing a transection lesion.

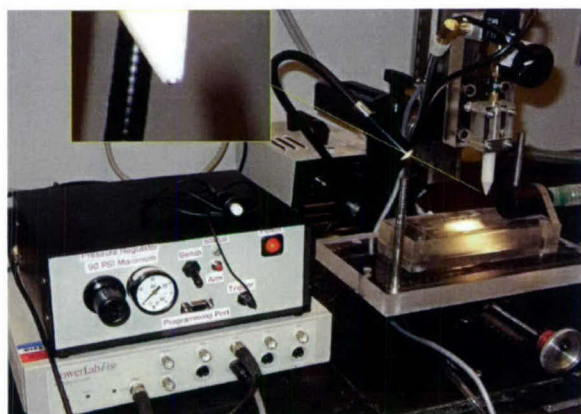


Figure 132. Photograph of the second generation mouse injury device being developed to refine a mouse model of controlled impact spinal cord injury. The inset shows the new tip of the impactor, which features an outer shell that senses contact with the cord, and an inner titanium piston that can be retracted and released with controlled velocity and dwell time.

4. STAT Transcription Factors

Dr. Linda MacArthur focuses on signaling pathways activated in neurons after injury and inflammation. The dorsal root ganglia (DRG), which contain the cell bodies of primary sensory neurons, are not protected by the blood-brain barrier and are thus exposed to the peripheral effects of inflammatory mediators, therapeutic drugs, or diseases that alter blood chemistry such as diabetes. The specific hypotheses being tested are that STAT transcription factors regulate the neuronal response to injury and inflammatory mediators in primary sensory neurons and in spinal cord microglia. Because STAT proteins are critical for immune cell function as well, these studies may lead to the identification of intracellular second messengers in neurons that effect neuronal damage caused by immune cell activation.

4.1. Neuronal Response to Noxious Inflammatory Input

The dorsal root ganglia (DRG) contain the cell bodies of primary afferent neurons, and represent the first level of processing of neuronal information from the periphery. In this study we focused on signaling pathways activated in drg by noxious stimulation from the periphery. Male Sprague-Dawley rats received either a unilateral subcutaneous injection of formalin into the hindpaw, a model for acute inflammatory pain, or ligation of the sciatic nerve at mid thigh (chronic constriction injury, cci), a model for neuropathic pain that results from nerve injury. L4-L5 (the site of sciatic nerve innervation) were removed, whole cells extracts were prepared, and gelshifts were performed with stat consensus sequences. Our results demonstrated that stat-like proteins are present in the rat drg and regulated by noxious input (Figure 133). There was an increase in the binding of stat-like protein(s) to the consensus sequence in extracts prepared from drg ipsilateral to the painful stimulus. This increase was detected 60 min after formalin injection and 6 days after cci, times consistent with behavioral measures of increased sensitivity to pain.

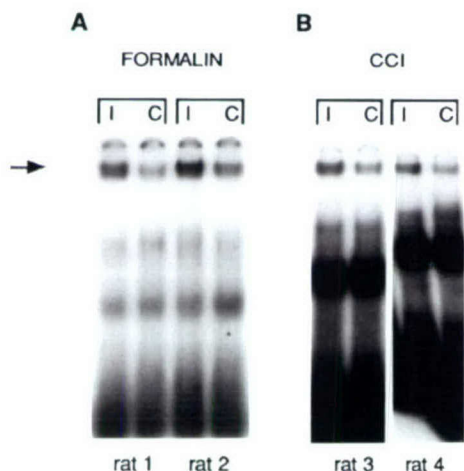


Figure 133. Gelshift analysis of STAT protein activity. Rats received a formalin injection into a single hindpaw (A) or ligation of the sciatic nerve (chronic constriction injury, CCI)(B). L4/L5 DRG were removed and examined for STAT activity. I=ipsilateral, C=contralateral side. Arrow indicates binding of STAT-like proteins to a STAT consensus sequence.

To confirm the presence of STAT proteins in rat DRG we used RT-PCR analysis to determine if STAT mRNA was detectable. Total RNA was derived from embryonic (E14), postnatal day 3, and adult rat DRG and used in RT-PCR reactions. Bands of the expected size were detected for STATs 1,3,5b and 6 at the three developmental time points (Figure 134). The identity of the PCR products was confirmed by subcloning into the PCR 2.1 vector using TA cloning and by DNA sequencing.

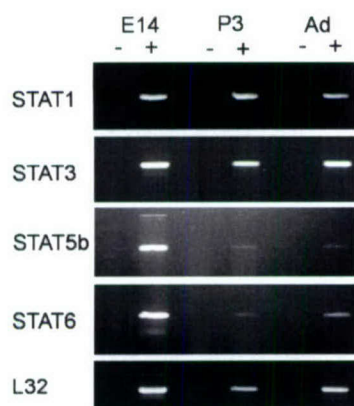


Figure 134. Total RNA was isolated from embryonic (E14), postnatal day 3 (P3) and adult rat DRG (Ad) and subjected to RT-PCR with STAT gene specific primers. Products were fractionated on a 4% NuSieve gel and photographed under UV illumination.

An immunohistochemical screen of DRG and spinal cord tissue with STAT antibodies led us to focus our efforts on STAT6. We used Western blot analysis to determine if STAT6 protein was detectable in rat DRG and to determine if it was the expected size. L4/L5 DRG were homogenized in sample buffer by standard methods. Proteins were resolved on a 6% SDS-polyacrylamide gel and transferred to PVDF membrane. Membranes were probed with an antibody to STAT6 and the immunoblots were developed using appropriate secondary antibodies and chemiluminescence. A single band of the expected molecular weight was observed in both DRG and control A431 extracts (Figure 135).



Figure 135. STAT6 protein in rat DRG. Rat DRG samples were resolved on 6% SDS-PAGE gels followed by Western blot analysis for STAT6 protein. Extracts from A431 cells were loaded in the left lane as a positive control.

STAT 6

Immunohistochemistry was used to determine if STAT6 protein is localized to neurons and/or satellite cells of the DRG. Normal animals were perfused with saline and paraformaldehyde and the L4/L5 DRG were removed and embedded in paraffin. Sections were stained with a STAT6 antibody that recognizes both basal and phosphorylated (activated) STAT6 (Figure 136). Both neurons and glia were positively stained. STAT6 was expressed in the majority of small-medium, and large diameter neurons in both the nucleus and the cytoplasm. Most satellite cells and some Schwann cells were also STAT6 positive.

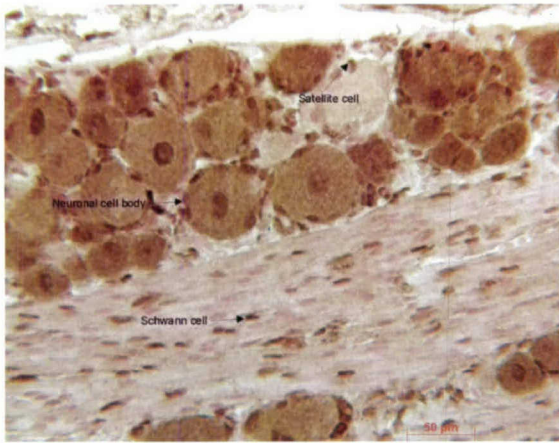


Figure 136. Immunohistochemistry of adult rat DRG cross sections stained with STAT6 antibody. Slides were developed with DAB and lightly counterstained with Nuclear Fast Red. Arrows show positive staining of a neuronal cell body, a satellite cell surrounding an unstained neuronal cell body and a positively stained Schwann cell.

STAT6 activation occurs by the addition of phosphates to tyrosine residues on the STAT6 protein (pYSTAT6). Upon activation in the immune system, STAT6 translocates from the cytoplasm and outer membrane to the nucleus. We used immunohistochemistry with an antibody directed against tyrosine phosphorylated STAT6 to determine if there was activated STAT6 in normal DRG and its location. Two distinct staining patterns were observed. In the small-medium diameter neurons, activated STAT6 (pYSTAT6) was observed in the cytoplasm and nucleus (Figure 137, arrow A). In the large diameter neurons, pYSTAT6 was detected as punctuate staining mostly in the nucleus (Figure 137, arrow B). A few large neuronal cell bodies had satellite glia surrounding them with weak staining (Figure 137, arrow C).

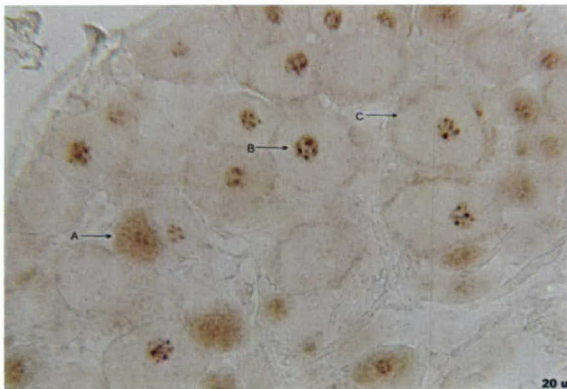


Figure 137. Immunohistochemistry of adult rat DRG cross sections stained with anti-phosphotyrosine STAT6 antibody. Sections were developed with DAB. Arrows show diffuse nuclear and cytoplasmic staining in small cells (A), punctuate nuclear staining in large cells (B) and weaker staining of satellite cells (C).

We next assessed the activation of STAT6 in DRG neurons in response to noxious input. We used the formalin test because we had previously seen activation of STAT-like proteins (using a gelshift assay) in the lumbar DRG after formalin injection into the hindpaw. Dilute formalin (1.8%) was injected into the rat hindpaw and DRG were harvested 30 minutes later. DRG were embedded in paraffin, sectioned and hybridized to the anti-pYSTAT6 antibody. Images were then captured and the cross sectional area of all of the cells in a section was measured. Cells were considered positive if they had distinct staining. The number of positive cells was graphed as a function of cell size. Since the majority of the small-medium and large cells were positively labeled, a typical distribution of cell size for rat DRG was observed, with the majority of the labeled cells in the small-medium size range (small is $<600 \mu\text{m}^2$, medium = $600\text{--}1200 \mu\text{m}^2$, and large is $>1200 \mu\text{m}^2$) (data not shown). There was no apparent difference in the number of positive pYSTAT6 cells after formalin injection into the hindpaw. However, visual inspection of the slides showed an increase in the intensity of pYSTAT6 staining in some small-medium size neurons in the DRG ipsilateral to formalin injection (Figure 138, Top).

To quantify the effect of formalin concentration on the level of pYSTAT6 staining, we measured pixel intensity as a function of cell size. This requires that all sections being compared to each other must be stained together and captured together under identical illumination conditions. (NOTE- In this pilot experiment, comparisons were made only within each group; eg. ipsilateral versus contralateral for 1%. Therefore, pixel intensity comparisons between groups, such as 1% versus 5% cannot be done. A lower pixel intensity for 5% formalin in this experiment does not mean less staining than for 1% or 1.8%. In future experiments, slides will be stained and captured together so that the intensity between groups is uniform).

Rats received formalin injections into the left hindpaw and DRG were harvested 40 minutes after injection and stained with pYSTAT6 antibody as before. A 1% formalin concentration elicited no measurable difference in pYSTAT6 staining (Figure 114, second panel) between the ipsi- and contralateral sides. Increasing the formalin concentration to 1.8% produced an increase in pYSTAT6 staining in the small-medium sized, nociceptive neurons. At the highest formalin concentration, 5%, there was a more pronounced increase in pYSTAT6 staining in the small-medium sized neurons and an increase in staining in large size neurons ipsilateral to formalin injection. Thus, STAT6 responded in DRG neurons to a noxious stimulus in a concentration dependent manner, with neurons in the small-medium size range showing greater sensitivity to the stimulus than large size neurons.

Studies in progress are focusing on the mechanism by which formalin activates STAT6, the effect of anti-inflammatory drugs on constitutive expression of neuronal STAT6, and the role STAT6 in inflammatory pain in STAT6 knockout mice.

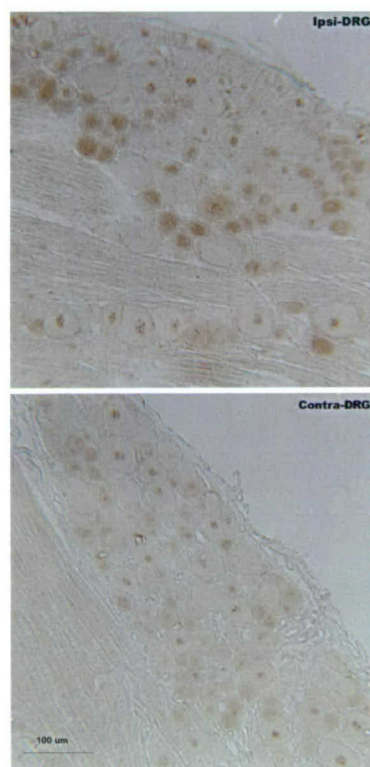


Figure 138. Cross-section of adult DRG stained with pYSTAT6 after formalin injection. Ipsi=ipsilateral to formalin, contra=the contralateral hind-paw. There was an increase in the intensity of staining on the ipsilateral side.

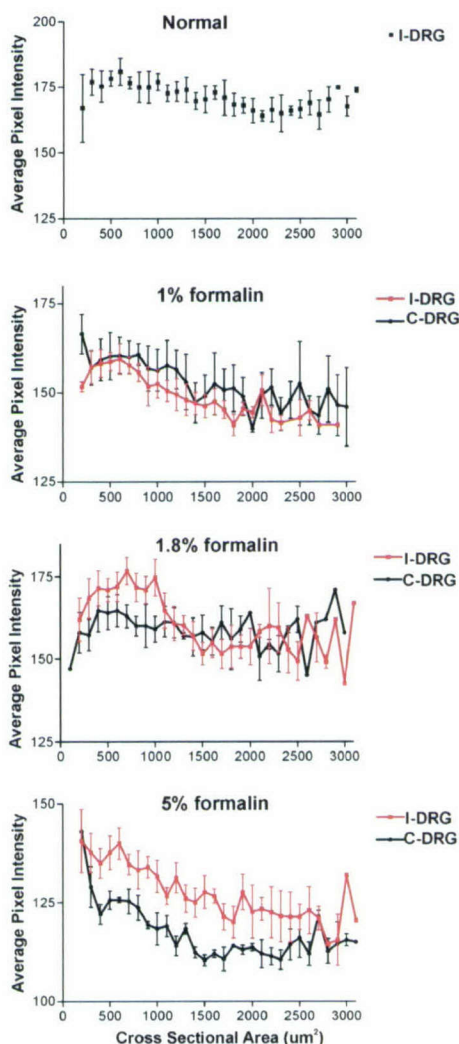


Figure 139. Effect of formalin concentration on the pixel intensity of pYSTAT6 stained DRG neurons. I=ipsilateral to formalin injection, C=contralateral to injection.

4.2. Spinal Cord Glial Response to Sciatic Nerve Injury

While examining STAT6 activation in drg neurons after noxious input, we looked at the response of the DRG and spinal cord to sciatic nerve injury. We observed a dramatic activation of STAT6 in glia of DRG (satellite cells) and in the spinal cord ipsilateral to a sciatic nerve crush. In DRG, satellite cells that had previously had weak or diffuse staining now showed dark punctuate staining (Figure 140, arrows) on the ipsilateral side to nerve crush. In the lumbar spinal cord, the site of sciatic innervation, there was a dramatic increase in the number of pYSTAT6 positive cells ipsilateral to nerve crush (Figure 141, left side). The glial morphology of the positive cells suggests that they are microglia. Studies are currently underway to confirm this.

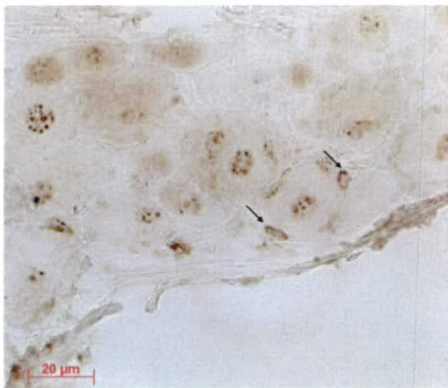


Figure 140. Cross-section of adult DRG stained with pYSTAT6 after crush of the sciatic nerve. Many satellite glia became pYSTAT6 positive (arrows).

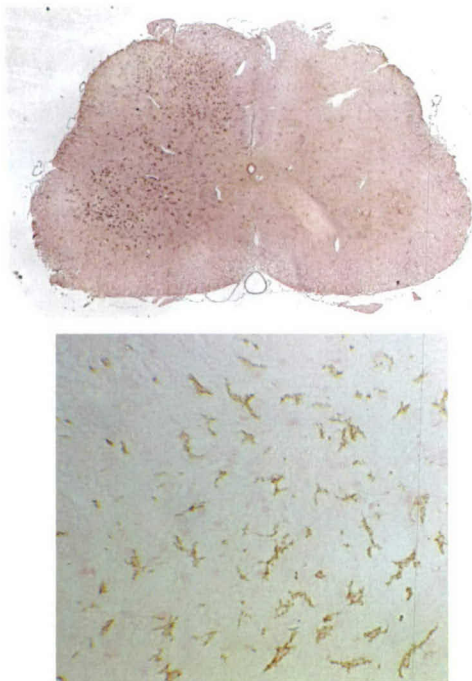


Figure 141. Cross-section of adult rat spinal cord stained with pYSTAT6 after crush of the sciatic nerve (top). There was an increase in glial staining ipsilateral to injury (left side). The bottom panel is a higher magnification of glia in the top panel.

The data from these two studies suggests that STAT proteins in neurons and glia are responsive to noxious input and nerve injury. We have observed two types of altered signaling through STAT6 in the nervous system: a neuronal response, in which DRG neurons respond to noxious input from formalin injection, and a glial response, in which DRG satellite cells and spinal cord glia respond to sciatic nerve crush.

We are currently testing the hypothesis that inflammatory activation of STAT6 in spinal cord microglia contributes to neuropathic pain. Studies in progress are examining the effect of STAT6 on neuropathic pain in STAT6 knockout mice.

Hypothesis #11: Transgenic approaches, including use of knockout animals and viral vectors, can be used effectively to elucidate mechanisms of neural injury and recovery.

1. Comparison of Knockouts and Pharmacological Antagonists

Metabotropic glutamate receptors (mGluRs) are known to modulate ionotropic glutamate receptors (iGluRs), various calcium and potassium channels, and neurotransmitter release (Fig. 142)⁹³. Because many of these systems are involved in the pathophysiology of acute CNS injury, drugs that activate or inhibit mGluR have been examined with regard to post-traumatic or post-ischemic cell death^{278, 279}. The mGluRs have been categorized into three groups, on the basis of structure, signal transduction mechanisms and pharmacological sensitivities^{63, 280}. Group I mGluR include mGluR1 and mGluR5. Activation of mGluR1 appears to exacerbate necrotic cell-death after trauma or ischemia, in part by activating NMDA receptors^{69, 281}. However, the role of mGluR5 has been more controversial because of the lack of truly selective antagonists. Several purportedly selective mGluR5 antagonists have been developed, such as MPEP²⁸² and SIB-1893²⁸³. Although both compounds show some neuroprotective activity, such actions occur only at concentrations that inhibit NMDA receptors and are substantially higher than that required to inhibit agonist induced PI hydrolysis^{67, 68}. These findings are consistent with a prior study using antisense oligonucleotides (ODN) directed against mGluR1 or mGluR5 receptors; at concentrations that equally reduced agonist-induced IP₃, only inhibition of mGluR1 was neuroprotective⁶⁴.

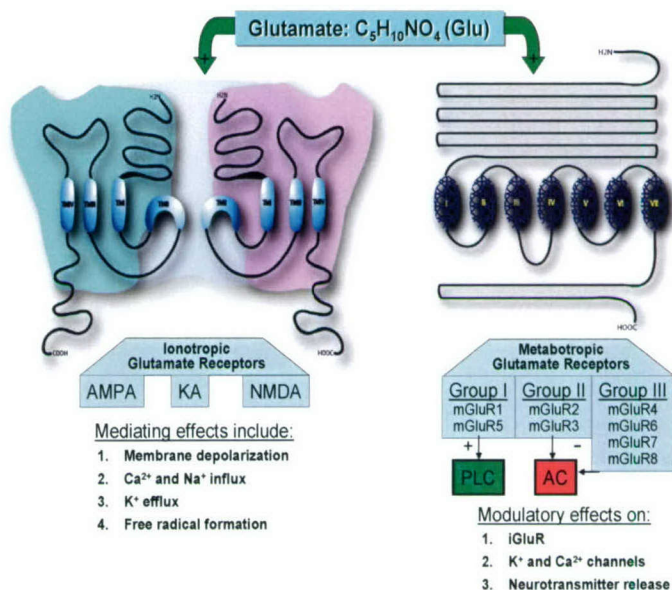


Figure 142. Glutamate signals through two distinct classes of receptors. (Left) The ionotropic class of glutamate receptors (iGluR), consisting of AMPA, KA and NMDA ion channel receptors, mediate membrane depolarization. When these receptor channels are open, such as when excessive glutamate is released during acute injury, potassium, sodium, and calcium (the latter ion through NMDA and some AMPA receptors), move through the membrane in a direction governed by the electrochemical equilibrium of the particular ion. Ion movement through the NMDA receptor is normally blocked by a Mg²⁺ ion located in its pore structure; however processes such as membrane depolarization and trauma can remove or reduce this blocking effect. (Right)-Glutamate also signals via slower G-protein coupled metabotropic receptors (mGluR). The mGluRs are categorized into three groups based upon sequence, pharmacology, and function. Group I mGluR (mGluR1 and 5) utilize the inositol triphosphate/diacylglycerol (IP₃/DAG) second messenger cascade following phospholipase C activation via Gq proteins. Group II (mGluR2 and 3) and III mGluR (mGluR4, 6, 7 and 8) reduce cAMP levels by inhibiting adenylylcyclase via Gi/o proteins. Through the mGluRs, glutamate can modulate the activity of iGluR, various potassium and calcium ion channels, and the presynaptic release of neurotransmitter. Both the iGluR and mGluR are intimately associated with mediating and modulating (respectively) acute and chronic neurodegeneration.

Recently, a non-competitive mGluR5 specific antagonist was developed. MTEP (3-[(2-methyl-1, 3-thiazol-4-yl)ethynyl]pyridine) appears to have greater selectivity at mGluR5 than other antagonists²⁸⁴. *In vivo* and *in vitro* characterization of MTEP²⁸⁴⁻²⁸⁶ indicates that it is highly selective for mGluR5 over mGluR1, has no effect on other mGluR subtypes, and has fewer off target effects than MPEP²⁸⁴. In the present studies we compared the selectivity and neuroprotective actions of MPEP and MTEP against glutamate or NMDA-induced toxicity in primary cortical neuronal cultures. We also compared the actions of these compounds in mGluR5 deficient neuronal cultures (Fig. 143).

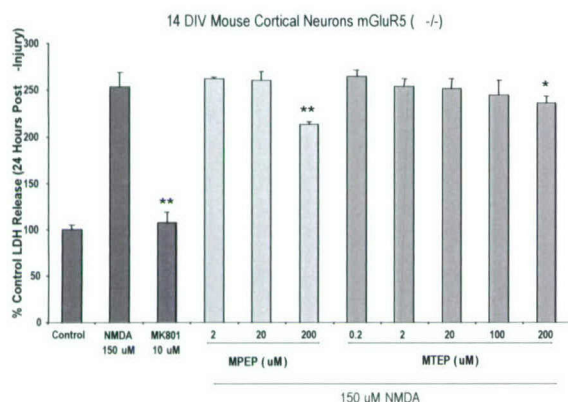
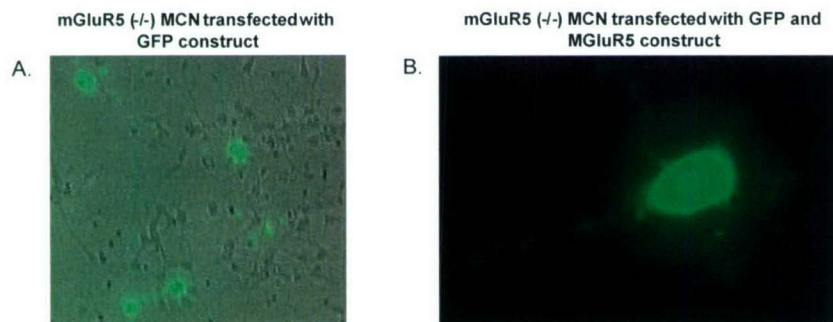


Fig. 143 Comparison of effects of MTEP, MPEP and MK801 on NMDA-induced cell death in mGluR5 deficient mouse cortical neuronal cultures. MPEP, MTEP or MK801 at indicated concentrations were added to cultures 20 min prior to administration of NMDA (150 μ M). Cell death was measured by LDH release after 24 hr of treatment. Histograms indicate LDH release as percentage of that in intact controls \pm SD; $n = 8$ to 16 cultures per condition. *, $P < 0.05$, **, $P < 0.01$ versus injured cultures as shown by ANOVA, followed by the Student-Newman-Keuls test.

We demonstrate that MTEP significantly inhibits CHPG mediated IP hydrolysis at concentrations as low as 0.02 μ M. In contrast to MPEP, which significantly reduces glutamate or NMDA mediated cell death in primary rat neuronal cultures at a concentration of 20 μ M, small neuroprotective effects were observed with MTEP only at a concentration of 200 μ M. These neuroprotective effects of MTEP at very high concentrations, like those of MPEP, reflect ability to inhibit NMDA receptor activity. We also compare the effects of MPEP and MTEP in primary cortical neuronal cultures from mGluR5 knockout mice. Both agents were neuroprotective, but only at very high concentrations (200 μ M) in the knockout cultures. These studies support the conclusion that MTEP has greater mGluR5 selectivity than MPEP, and that neuroprotection provided by either antagonist in neuronal cultures does not reflect inhibition of mGluR5 receptors. These findings are significant in that they put to rest the notion, spurred by the non-specific actions of MPEP, that blocking neuronal mGluR5 is protective.

The use of transgenic mGluR5 knock-out animals has proven invaluable. We have recently obtained mGluR5 constructs that have allowed us to transfect primary neurons derived from mGluR5 knock-outs with mGluR5 constructs (Fig. 144). These mGluR5 knock-in cultures will be beneficial in further elucidating mechanisms through which mGluR5 mediates its neuroprotective effects.

Figure 144



2. Viral vectors

To further ongoing studies aimed at themes of apoptosis and caspase activation (Hypothesis #1), we used a non-replicating type 5 adenoviral construct to deliver X-linked inhibitor of apoptosis (XIAP) to the mouse brain. XIAP is an endogenous direct inhibitor of caspases 3, 7 and 9. In addition, it inhibits other proteins with pro-apoptotic functions, such as Smac/DIABLO, Omi/HtrA2 and XAF1. The pAdex1CAwt construct is a E1a/E1b/E3 deletion mutant with a chicken β -actin promoter.

For this experiment, the left hippocampus and overlying cortex of mice were injected with either Adeno-LacZ, Adeno-XIAP, or an equal volume of saline. Seven days later, the mice were subjected to moderate controlled cortical impact injury of the left hemisphere. Motor function was assessed as the number of foot-faults made while traversing a balance beam on selected test days until 28 days after injury. Adeno-XIAP injected mice performed significantly better than Adeno-LacZ or saline controls on this test at 7, 14, 21 and 28 days after injury (Figure 145).

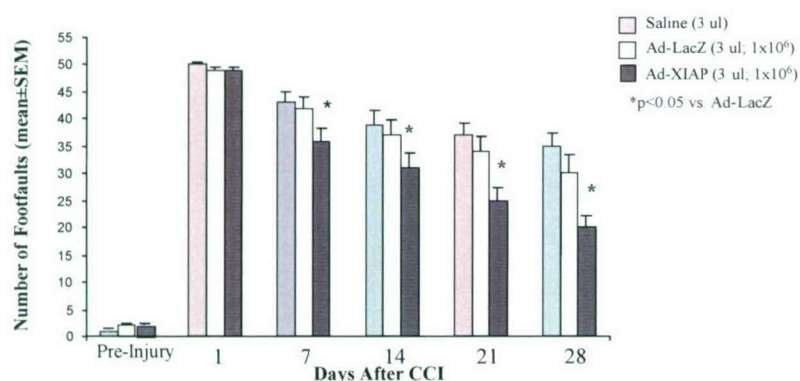


Figure 145. Adenoviral over-expression of XIAP improves motor performance after controlled cortical impact brain injury in the mouse. Three μ l of either AdenoXIAP (1×10^6 pfu/ μ l; $n=13$), AdenoLacZ (1×10^6 pfu/ μ l; $n=15$) or saline ($n=8$) was injected in the left hippocampus and cortex of mice 7 days before traumatic brain injury was induced. Motor function was assessed as the number of footfaults (missteps) made by mice as they traversed 50 steps on a 6 mm wide beam at different times after injury as indicated on the x-axis. Bars indicate means \pm SEM for each group as shown in the key. *= $p<0.05$ vs. AdenoLacZ or saline by repeated measures 2-way ANOVA, followed by post-hoc t -tests with Bonferroni correction.

Cognitive function was also evaluated using a Morris water maze. In this test, Adeno-XIAP injected mice showed trends toward improved function, compared to mice injected with Adeno-LacZ or saline (Figure 146). At 28 days after injury, mice were euthanized and their brains were perfused with fixative. Lesion volumes were quantified using a Cavalieri method, and were significantly smaller in the Adeno-XIAP group, compared to Adeno-LacZ controls (data not shown). Another group of mice were injected, injured and then euthanized 24 hr later, to obtain extracts of the injured cortex. Extracts were processed by immunoblotting analysis for α -spectrin breakdown products, to obtain an indirect measure of activation of caspase 3 and calpain. Data from this experiment indicated that XIAP showed trends toward a reduction of caspase 3 activation in sham-injured and injured animals, in comparison to Adeno-LacZ controls (Figure 147). Paradoxically, however, XIAP injected mice showed enhanced activation of calpain after injury, compared to Adeno-LacZ injected controls. Though unexpected, this finding is not inconsistent with reported interactions between these 2 classes of cysteine proteases. Considered together, these data suggest that XIAP significantly improves motor

outcome after TBI, though the precise mechanisms behind the beneficial effect are not entirely clear. Though the data lend some support to the hypothesis that intrinsic apoptotic cascades may play an important role in cell death and neurological impairment after TBI, they also suggest that XIAP potentially modulates other pathways, as well.

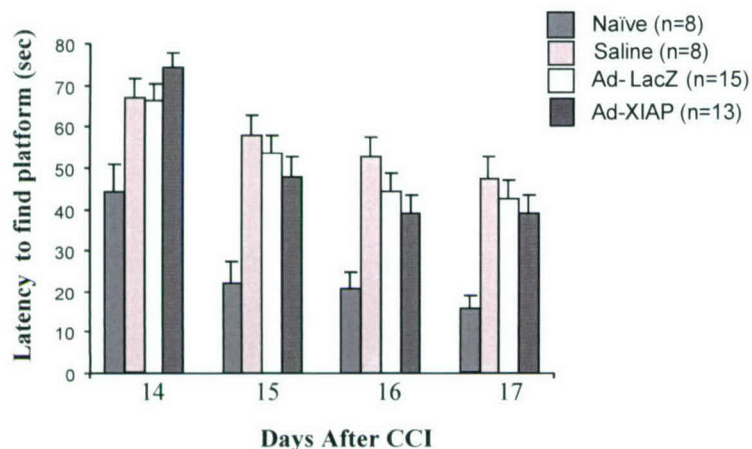


Figure 146. Adenoviral over-expression of XIAP results in trends toward improved performance after controlled cortical impact brain injury in the mouse. Data are from the same mice/experiment described in previous figure. Cognitive function was assessed as the amount of time (latency) required for mice to locate a fixed, hidden resting platform in a 4 foot diameter tank of water. Four 1.5 minute trials (30 min apart) were performed each day on days 14-17 after injury, as indicated on the x-axis. Bars indicate means ± SEM for each group as shown in the key.

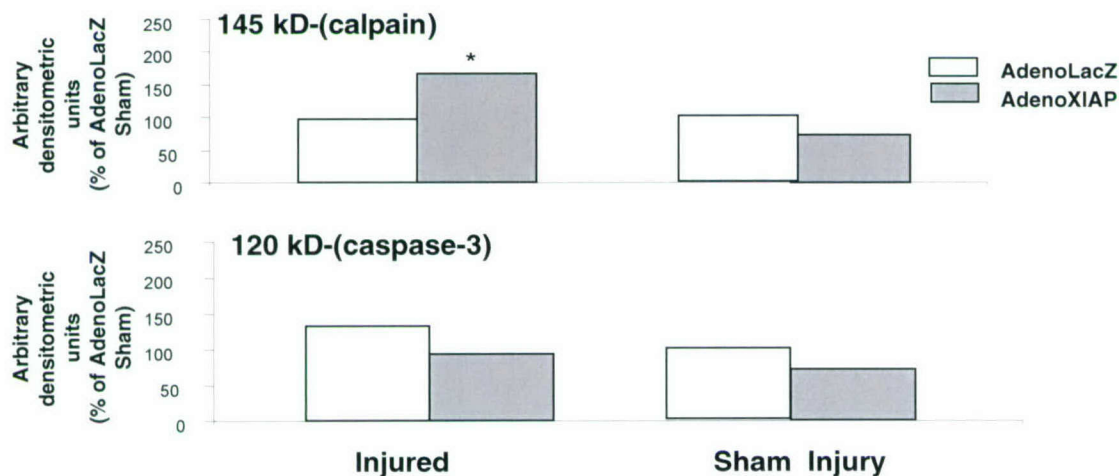


Figure 147. Effect of XIAP over-expression on the accumulation of 145 kD calpain- or 120 kD caspase-3- specific a-spectrin breakdown products at 24 h after controlled cortical impact injury or sham-injury. Injection of adenovirus and injury was performed as described in prior 2 figures and text. Specific a-spectrin breakdown products were assessed by semi-quantitative immunoblotting methods. *= $p < 0.05$ by Student's *t*-test comparison.

In conclusion, use of knockout mice and transfection of proteins using viral vectors provide important tools for elucidating molecular mechanisms in acute neurodegenerative disorders.

Hypotheses #12: Inflammatory activation of microglia may contribute to the neuropathology of Alzheimer's Disease, which can be modulated pharmacologically.

The Memory Disorders Program, in the Department of Neurology, has continued to enjoy steady growth since its inception in 1999. At present, the staff includes three physicians (one with a Ph.D. in Psychology), two nurse practitioners, a sociolinguist, a program coordinator and a research. Over four hundred patients with memory disorders, primarily Alzheimer's disease, are followed in the program.

As noted in our previous progress report, the Memory Disorders Program has been the central site for multiple therapeutic trials:

1. Multicenter Trial of Naproxen and Rofecoxib in AD (Aisen, Project Director)

This study has been completed, with the primary results reported last year in *JAMA* (see below).

2. Pilot Study of Nimesulide in AD (Aisen, P.I.)

This trial was completed, with the results reported in *Neurology* (see below).

3. Pilot Study of High-Dose Vitamins to Reduce Homocysteine in AD (Aisen, P.I.)

The results of this trial were reported last year in the *American Journal of Geriatric Psychiatry* (see below). The findings led to the initiation of a large multicenter trial of homocysteine reduction to slow cognitive decline in AD, being led by the Memory Disorders Program at Georgetown.

4. Multicenter Vitamin E Trial in Aging Persons with Down Syndrome (Dalton, Aisen, Sano, co-Directors)

This international study is still underway, with approximately 150 subjects enrolled to date.

5. Plasma neopterin may serve as a marker for microglial inflammation in Alzheimer's disease.

While the hypothesis was supported by our findings on plasma neopterin levels in AD (Hull M, Pasinetti GM, Aisen PS. Elevated Plasma Neopterin Levels in Alzheimer's Disease. *Alzheimer Disease and Associated Disorders*, 14: 228-230, 2000.), our major study ultimately revealed that microglial activation may not be a promising therapeutic target (Aisen PS, Schafer K, Grundman M, Pfeiffer E, Sano M, Davis KL, Farlow M, Jin S, Thomas R, Thal LJ for the Alzheimer's Disease Cooperative Study. Effects of Rofecoxib or Naproxen vs Placebo on Alzheimer Disease Progression. *Journal of the American Medical Association*. 289:2819-2826, 2003).

Hypothesis #13: Immunogenetics may influence inflammatory mechanisms that contribute to Alzheimer's Disease.

It has been proposed that HLA-DR alleles influence the disease incidence, progression and response to anti-inflammatory treatments for Alzheimer's disease.

Although initial studies provided support for the hypothesis (Aisen et al, 1998), but the definitive answer came from our clinical trial (reportable outcome). In this trial, HLA-DR genotype was not associated with progression rate or response to anti-inflammatory treatment.

IVB. Computational Neuroscience/ Structural Biology

Hypothesis #14: Mathematical modeling techniques can be developed to study axon guidance modulated by chemical gradients

It has been hypothesized for many decades that growth cones could guide axons to their targets in the developing and regenerating nervous system by sensing concentration gradients of molecules in their environment. In the past few years much progress has been made in identifying the gradient molecules involved. However, the understanding of how growth cones sense gradients at a mechanistic level has not kept pace. The goal of this project was to develop a new technology to allow the response of axons in precisely controlled gradients to be analyzed and quantified.

Objectives:

- 1. To establish concentration gradients of chemotropic molecules of precisely known steepness in a collagen gel.**
- 2. To grow axons in these gradients and measure how their response depends on the parameters of the gradient.**

We have now achieved both these objectives. In particular we have developed a new technology for establishing precisely controlled molecular gradients in collagen gels. We have also used this technology to examine how the response of dorsal root ganglion (DRG) axons to gradients of Nerve Growth Factor (NGF). By varying NGF gradient steepness while maintaining a fixed baseline NGF concentration we have shown that axons may be the most sensitive gradient detectors in nature. In addition, by varying the baseline NGF concentration while maintaining a constant gradient steepness we have shown that axons have only a limited ability to adapt to external ligand concentration.

Hypothesis #15: Molecular modeling can be utilized to elucidate ligand/receptor interactions, with particular reference to caspases and phosphatases, and pharmacophore modeling may help identify novel neuroprotective structures.

In collaboration with Dr. Shaomeng Wang, now at the University of Michigan, we have carried out research with the goal to develop new computational methods to study protein structures and functions for the design and development of novel small-molecule ligands as potential therapeutic agents for the treatment of neurological disorders and conditions such traumatic brain injury and Alzheimer's disease. Some of the results have been published in four peer-reviewed publications. The major accomplishments are summarized below.

1. Elucidation of the structural basis of ligand binding to protein kinase C (PKC) and RasGRP proteins through computational docking and experimental site-directed mutagenesis studies.

These studies provide a solid structural basis for the binding and selectivity of small-molecule modulators of PKC and RasGRP and greatly facilitate the design of selective ligands for PKC isozymes. Potent and selective PKC ligands have the therapeutic potential to be used as a novel therapy for the treatment of Alzheimer's disease, among other conditions (Rong et al. 2002; Pak et al, 2001; reportable outcome).

2. Development of new computational methods for structure-based design of new therapeutics for the treatment of traumatic brain injury and Alzheimer's disease.

Toward the design of novel therapeutics for the treatment of traumatic brain injury and Alzheimer's disease, it is crucial to be accurately predict how precisely a small-molecule ligand binds to its target protein and how strong they bind. We have developed several computational methods to enhance our ability to predict the interaction between proteins and ligands and their binding affinities. The methods and results have been published in three publications (Wang et al., 2002; Wang et al., 2001; Pak et al, 2001; reportable outcome).

Hypothesis #16: Molecular dynamics simulations can be used to elucidate the folding and misfolding mechanisms of amyloid (1-42) in Alzheimer's Disease and such information can be used to identify potential drug molecules that can prevent conversions of the amyloid from the α to the β form.

We are interested in understanding of the molecular basis of protein folding and misfolding, which could lead to a better understanding of Alzheimer's disease and to design of effective treatment for Alzheimer's disease. Using a new molecular dynamics method (the self-guided molecular dynamics method) we have developed, we have performed extensive molecular dynamics simulations of beta-Amyloid peptide in the explicit water molecules. Our results showed that beta-Amyloid peptide can adopt both helical conformation and beta-conformation, which provide a molecular basis for the folding and mis-folding of beta-Amyloid peptide. Our results can be used to directly design small-molecule inhibitors that can bind to alpha-helical conformation and prevent the formation of toxic beta-sheet conformation of beta-Amyloid. A new manuscript is being prepared.

Hypothesis #17: More powerful computational methods can be developed for the study of protein/drug docking.

We have performed extensive studies on protein-drug docking and also developed new computational docking methods to improve the accuracy in protein-drug docking.

In particular, we have elucidated the structural basis of ligand binding to protein kinase C (PKC) and RasGRP proteins through computational docking and experimental site-directed mutagenesis studies (Rong et al. 2002; Pak et al, 2001). These studies provide a solid structural basis for the binding and selectivity of small-molecule modulators of PKC and RasGRP and greatly facilitate the design of selective ligands for PKC isozymes. Potent and selective PKC ligands have the therapeutic potential to be used as a novel therapy for the treatment of Alzheimer's disease, among other conditions.

Toward the design of novel therapeutics for the treatment of traumatic brain injury and Alzheimer's disease, it is crucial to be accurately predict how precisely a small-molecule ligand binds to its target protein and how strong they bind. We have developed several computational methods to enhance our ability to predict the interaction between proteins and ligands and their binding affinities. The methods and results have been published in three publications (Wang et al., 2002; Wang et al., 2001; Pak et al., 2001).

IVC. Cognitive Neuroscience

Hypothesis #18: Different anatomical localizations subserve declarative and procedural memory; patients with specific classes of neurological disorders can be used to discriminate such differences.

The long-term objective of this project was to further elucidate the neurocognitive underpinnings of the distinction in language between idiosyncratic and rule-governed mappings. The project focused on four issues: separability, computation/representation, domain-specificity/domain-general, and neural correlates. "Dual-system" models claim that the distinction between the two types of mappings reflects the existence of two separable language components: the mental lexicon of stored information, and the mental grammar, whose rules underlie the composition of complex linguistic representations. However, different dual-system models make quite different claims regarding the computational, representational, and neural bases of these components, and whether they are dedicated to language or domain-general. On one view – the "declarative/procedural" (DP) model – the learning and use of lexical knowledge depends upon a well-studied "declarative memory" system, which is rooted largely in temporal-lobe structures and underlies the learning and use of conceptual/semantic knowledge; the acquisition and use of aspects of grammar relies on a "procedural memory" system, which is rooted largely in left frontal/basal-ganglia circuits, and supports the acquisition and expression of motor and cognitive skills (e.g., riding a bicycle). Most other dual-system views rather assume that one or both language components are domain-specific, and make at least somewhat different claims regarding their underlying neural substrates. "Single-mechanism" (SM) theories posit a single computational system for all linguistic forms, and deny any categorical distinction between stored forms and rule-governed complex representations. A recent influential model proposed by Joanisse and Seidenberg (JS) claims that in at least some domains of language, idiosyncratic and rule-like mappings differentially depend on semantic and phonological (rather than lexical and grammatical) processes. However, just as dual-system models vary in their specific claims, so do single-system models. For example, a model proposed by Dominey posits common neurocognitive substrates between syntax and procedural memory²⁸⁷. Thus this model and DP share certain claims, despite their computational differences. Importantly, the various competing dual- and single-system models make contrasting predictions that can be tested and falsified, allowing the models to be empirically distinguished. Previous psycholinguistic, developmental, neurological and neuroimaging studies, including those funded in this project, have tested many of the models' predictions. Although the data do not unambiguously falsify or support any one model at this point, they have begun to elucidate the general issues of interest, and have helped tease apart and constrain the competing models. Here we summarize our findings, in the context of other experiments addressing the same issues.

1. Evidence from Developmental Disorders: Specific Language Impairment (SLI)

SLI refers to developmental language disorders without any apparent social, psychological or neurological cause. Though it is a heterogeneous disorder, many individuals with SLI have similar patterns of impairment, including difficulty with rule-governed compositional aspects of grammar, across domains: syntax, morpho-syntax, including regular morpho-phonology, and phonology. In contrast, knowledge of simple lexical forms and irregulars remains largely spared. Certain complex forms (e.g., regulars) that are normally composed may be memorized in SLI, suggesting that lexical memory may compensate for impaired grammar. We found several of these patterns in studies of two language-impaired sub-groups^{288, 289}. SLI is also strongly associated with impairments of non-linguistic functions, including motor skills, especially those involving complex sequences. In contrast, declarative memory remains largely spared. A retrospective examination of the literature suggests that

frontal and basal ganglia structures, especially Broca's area and the caudate, are strongly implicated in SLI²⁹⁰. Together, the behavioral and brain data have led us to suggest that SLI may be viewed as a disorder of procedural memory²⁹⁰⁻²⁹². The data argue against the domain-specificity of grammar, and do not appear to be compatible with either the dual-system view that regulars are never stored (MWT), or with previously proposed single-mechanism models^{288, 289, 293}.

2. Aphasia

There are at least two fundamental categories of aphasia. *Anterior aphasia* is associated with damage to left frontal regions, in particular Broca's area and nearby cortex, the BG, and portions of inferior parietal cortex. Characteristic of anterior aphasia is "agrammatism": syntactic and morphological impairments in production and comprehension, and especially in the use of free and bound grammatical morphemes (e.g., auxiliaries, determiners, and affixes such as *-ed*). Damage limited to the BG can also produce agrammatic aphasia. In contrast, anterior aphasics are relatively spared in their use of non-compositional content words (e.g., nouns, adjectives), particularly in receptive tasks. As would be expected with a role for inferior frontal cortex in word retrieval or selection, word recall is typically problematic. Intriguingly, some evidence suggests that anterior aphasics can access knowledge about complements²⁹⁴. Anterior aphasia is also associated with impairments in the expression of motor skills (ideomotor apraxia). *Posterior aphasia* is linked to damage of left temporal and temporo-parietal regions, and impairments in the production, reading, and recognition of the sounds and meanings of content words. In contrast, posterior aphasics tend to produce syntactically well-structured sentences, and not to omit morphological affixes (e.g., the past tense *-ed* suffix)²⁹⁵. Intriguingly, damage in and around inferior parietal cortex can lead to certain types of grammatical impairments²⁹⁵, supporting a role for this region in aspects of grammar. Posterior aphasia is also linked with semantic impairments in non-language domains^{296, 297}.

WR/DP predicts that anterior aphasics should have more trouble with (non-rhyming) regulars than irregulars, whereas posterior aphasics should show the opposite pattern. MWT makes a similar prediction. DP additionally predicts that the double dissociation should be reliably found in men but not in women. The compositional nature of irregulars as well as regulars in DM leads to the expectation that anterior aphasics should be impaired at both, though it might be argued that the memorized link between irregular stem and affix may help these patients with irregulars²⁹⁸. Due to this memorized link, DM expects the same pattern in posterior aphasia as does WR/DP and MWT. JS predicts that anterior aphasics should *not* show worse performance at regulars than well-matched irregulars, and that posterior aphasics' deficit at irregulars *must* be accompanied by a semantic deficit.

Previous studies of regular/irregular morphology show the following pattern. A number of studies have found that *anterior aphasics* are worse at producing, reading out loud) writing from dictation²⁹⁹, repeating³⁰⁰, and judging regular and novel *-ed*-suffixed past-tenses as compared to irregular past tense forms, even when controlling for factors such as word frequency and length. Anterior aphasics also have greater difficulty reading and writing regular than irregular plurals, and show past-tense/stem priming for irregular but not regular past-tenses. These aphasics are also slower at detecting the difference between spoken regular past-tenses and their stems (*called/call*) relative to matched mono-morphemic words (*bald/ball*) and irregular pairs (*wrote/write*). Thus the regular deficit has been reported in at least nine studies (see refs^{293, 294, 301}), and has survived several attempts to eliminate it by controlling for phonological complexity, frequency, and other factors. Japanese patients also show a relative deficit with regulars in a judgment task of derivational morphology³⁰². Nevertheless, a relative impairment of regulars is *not* always found in anterior aphasia. A recent study of English past-tense found that most (though not all) of the regular disadvantage disappeared when phonological complexity was controlled for between regulars and irregulars. The regular deficit also has not been found in aspects of German³⁰³ and Greek³⁰⁴ inflection (perhaps due to DM-like

affixation of irregulars in these paradigms), and in a recent study of patients with focal lesions of the left basal ganglia³⁰⁵. *Posterior aphasics* reliably elicit worse performance at irregular than regular or –*ed*-suffixed novel past tenses in production^{305, 306}, reading³⁰⁶, judgment³⁰⁶ and priming³⁰⁷⁻³⁰⁹. Japanese posterior aphasics are worse at judging irregular than regular derivational forms³⁰². A recent study reports a patient with a relative deficit for irregular past-tenses, but *no* semantic deficits³¹⁰. In sum, the empirical picture is still somewhat mixed, though certain patterns are emerging: posterior aphasics perform worse at irregulars than regulars, and anterior aphasics generally show the opposite pattern, at least in English past-tense inflection, especially when phonological complexity is not controlled for.

On a DP view, verb-forms that depend on higher functional categories should rely more on the grammatical/procedural system than those that depend on lower functional categories, because of the increased amount of structure building involved in the former. Our preliminary studies confirm these morpho-syntactic predictions^{311, 312}. Anterior aphasics had more trouble with finite forms (*walks, breaks*) than participials (*walking, broken*) than stem forms (*walk, break*). This graded pattern was found, *within* and across subjects, in expressive (production, reading) and receptive (judgment) tasks. Similar patterns in other languages have been reported. Posterior aphasics did not show this pattern^{311, 312}. The data are compatible with the DP view, and, other than the graded pattern within subjects, with Grodzinsky and Friedmann's perspective as well.

3. Neurodegenerative Disease

3.1. Alzheimer's disease (AD) largely affects medial and neocortical temporal-lobe structures, leaving frontal cortex (particularly Broca's area and motor cortex) and the BG relatively spared^{313, 314}. The temporal lobe dysfunction may explain AD patients' impairments in learning new and using established lexical and conceptual knowledge. They are relatively spared at acquiring and expressing motor and cognitive skills, and at aspects of syntactic processing³¹⁵⁻³¹⁹. We found that AD patients with severe deficits at object naming or fact retrieval make more errors producing past tenses of irregulars than of non-rhyming regulars or –*ed*-suffixed novel verbs. Across AD patients, error rates at object naming and fact retrieval correlated with error rates at producing irregular but not non-rhyming regular or –*ed*-suffixed novel past tenses^{305, 320}. Italian AD patients also have more trouble producing irregular than regular Italian present tense and past participle forms^{321, 322}. These findings on regular/irregular morphology, while originally predicted by DP^{305, 323}, are also consistent with MWT, DM (because of the memorized irregular stem-affix link) and JS. One way to tease these models apart is by testing both male and female AD patients; only DP predicts distinct regular/irregular patterns for the two sexes.

3.2. Parkinson's disease (PD) is associated with the degeneration of dopaminergic neurons, especially in the BG. This causes high levels of inhibition in the motor and other frontal cortical areas to which the BG circuits project, and can explain why PD patients show the suppression of motor activity (hypokinesia) and have difficulty expressing motor sequences. It may also account for their impairments at acquiring motor and cognitive skills, and at grammatical processing. In contrast, temporal-lobe regions remain relatively undamaged and the recognition of words and facts remains relatively intact in low- or non-demented PD patients. In our studies of morphology^{305, 320}, severely hypokinetic PD patients showed a pattern opposite to that found among the AD patients, making more errors when producing non-rhyming regular and –*ed*-suffixed novel past-tenses than irregular past-tenses. This result held when the regular and irregular forms were matched on phonological complexity. The patients were not, however, impaired at producing rhyming or doublet regulars³²⁰. Across PD patients, the level of right-side hypokinesia, which reflects left BG degeneration, correlated with error rates at the production of non-rhyming regular and –*ed*-suffixed novel forms but not

irregular forms. Intriguingly, left-side hypokinesia did not show the analogous correlations with error rates in the production of any past tense type, underscoring the role of left frontal/BG structures in grammatical rule use^{305, 320, 323, 324}. Error rates in the production of novel and non-rhyming regular past-tenses correlated with error rates at naming manipulated but not non-manipulated objects (only the former is linked to motor skill procedural knowledge), whereas error rates at irregulars correlated with error rates in naming both object types (both are associated with conceptual knowledge)³²⁵. These correlations, which suggest a link between regulars (but not irregulars) and procedural knowledge, are not predicted by other models, and appear to be problematic for models which posit the domain-specificity of grammar. The pattern with rhyming regulars seems inconsistent with the view that no regulars are stored (MWT). The regular deficit is also not consistent with the predictions of JS. We recently examined sex differences in PD³²⁶ (Ullman and Estabrooke, in preparation). The men showed the correlation pattern similar to that found in our previous study³²⁷, in which 22 of 28 patients were male: production rates of non-rhyming regulars but not irregulars correlated with hypokinesia and naming manipulated objects, whereas production rates of irregulars but not regulars correlated with naming non-manipulated objects. The women displayed a different pattern. Their production rates of regular as well as irregular past-tenses correlated with naming non-manipulated objects, but not with manipulated objects or hypokinesia. (Future research should shed light as to why performance at irregulars correlated with performance at naming manipulated objects in the first but not the second study.) Moreover, the interaction between regular/irregular and male/female was significant, with a sex difference between regulars but not irregulars. These contrasting patterns between male and female PD patients further support the high rate of memorization of regulars by females only. They also link only regulars and only in males to procedural memory and frontal/BG structures. We are currently aware of one other study that has examined regular/irregular inflectional morphology in PD. This study did *not* find a regular disadvantage in the production of German regular/irregular past-participle morphology³²⁸. The reasons for this result are not clear, though low levels of hypokinesia among the patients (PD initially affects the putamen, only latter striking the caudate³⁰⁵, and DM-type affixation of German irregular participles, may both have contributed to the lack of a regular deficit. Future studies are clearly necessary, both in English and in other languages.

3.3. Although Huntington's disease (HD) is like PD in causing degeneration of the BG, it strikes different portions of these structures. Unlike in PD, this damage results in the disinhibition of frontal areas receiving BG projections³²⁹. This leads to the unsuppressible movements (chorea, a type of hyperkinesia) found in patients with HD. Patients with HD show the opposite pattern to those with PD not only in the type of movement impairment (suppressed vs. unsuppressed), but also in the type of errors on *-ed*-suffixed forms^{320, 327}. HD patients produced forms like *walkeded*, *plaggeded*, and *dugged* — but not analogous errors on irregulars like *dugug* or *keptet*, suggesting that the errors are not attributable to articulatory or motor deficits. Rather the data suggest unsuppressed *-ed*-suffixation. This conclusion is strengthened by the finding that the production rate of these over-suffixed forms correlated with the degree of chorea, across patients. The contrasting findings in PD and HD, linking movement and *-ed*-suffixation in two distinct types of impairments related to two types of BG damage, strongly implicate frontal/BG structures in *-ed*-suffixation. They also support the hypothesis that these structures underlie grammatical composition as well as movement, and suggest that they play a similar role in the two domains.

4. Amnesia

Bilateral damage to medial temporal lobe structures leads to anterograde amnesia — an inability to learn new information about facts, events, and words. Neither phonological nor semantic lexical knowledge is acquired, supporting the hypothesis that these structures underlie the learning of word

forms as well as word meanings. Knowledge acquired well before lesion-onset tends to be spared. Thus knowledge of words learned during childhood should be largely intact in adult-onset amnesia. A study of the amnesic patient H.M.³³⁰ revealed that he did not differ from normal age- and education-matched control subjects at syntactic processing tasks, or at his production of regular or irregular forms in past-tense, plural and derivational morphology. The data fit the DP model's specific predictions regarding the functional neuroanatomy of lexical memory – namely, that medial temporal lobe structures are important in the learning of new lexical knowledge, including phonological forms, but not in the use of this knowledge once it has become well established.

In conclusion, we have established that there are different and distinct anatomical sites that subserve declarative versus procedural memory. Moreover, patients with selected neurological disorders that show different localization of pathology can be used to discriminate such site specific substrates for different types of memory.

Hypothesis #19: Event-Related Potentials (ERPs) can be used to investigate the brain substrates for lexicon and grammar.

Event-Related Potentials (ERPs) reflect the real-time electrophysiological brain activity of cognitive processes that are time-locked to the presentation of target stimuli. Difficulties in conceptual-semantic processing, with either lexical³³¹⁻³³³ or non-linguistic^{334, 335} stimuli, elicit central/posterior bilateral negativities that peak about 400 milliseconds post-stimulus onset ("N400s"). These involve bilateral temporal lobe structures³³⁴⁻³⁴², and possibly ventro-lateral frontal cortex as well³⁴³⁻³⁴⁶. We have posited that N400s depend on lexical/declarative memory^{347, 348}. Disruptions of syntactic processing can yield (though do not always; see below) early (150-500 ms) left anterior negativities³⁴⁹⁻³⁵¹ – "LANs" – which have been linked to rule-based automatic computations^{331, 352, 353} and left frontal structures^{354, 355}. LANs have been elicited cross-linguistically by violations of syntactic word-order^{349, 351, 356, 357}, morpho-syntax³⁵⁸⁻³⁶⁴, and regular morpho-phonology (see below). (Left anterior negativities have also been reported for verbal working memory demands, but working memory effects are not expected to contribute to the effects predicted for the violations employed in the present proposal^{360, 365}.) However, not all studies examining these types of violations have reported LANs^{350, 363}. It is not clear at this point why LANs have been found by some studies and not by others, even for the same types of violation³⁶³. However, both task and subject variability may have contributed to the problem. The laterality of LANs also seems to vary^{355, 366-368}, at least in part as a function of subjects' language proficiency, with higher proficiency associated with greater left-lateralization and earlier onset of the effect^{369, 370}. Given this variability in lateralization, the more reliable topographic dimension to distinguish (L)ANs and N400s is along the anterior/posterior axis, with (L)AN components being anterior and N400 components being more posterior. Note that frontal N400s are rare and atypical; indeed, they have often been attributed to other overlapping components^{371, 372}, especially those reflecting phonological processing³⁷³. We have posited that anterior negativities (which we will continue to refer to here as "LANs", for the sake of simplicity) reflect grammatical/procedural processing³⁴⁷, and agree with the preponderance of studies that the distributional differences between N400 and LANs are real, and reflect functional differences^{351, 353, 356, 365, 374, 375}. Importantly, syntactic processing difficulties also tend to elicit late (600 ms) centro-parietal positivities ("P600s")^{363, 376}, which are associated with controlled processing^{352, 353, 377}. Although P600s do not appear to be linked to frontal brain structures^{354, 355}, recent evidence (from ERP studies of patients) suggests that they may involve the BG^{355, 378, 379}, implicating them in aspects of syntactic processing. However, this is a somewhat surprising result, given the controlled nature of the P600, and it warrants further investigation. Finally, difficulties in processing stored syntactic knowledge (about verb complements) generally elicit an N400 rather than a LAN: Violations of the semantics^{359, 364} or number^{359, 380} of complements have yielded N400 effects.

ERP studies have also examined regular and irregular inflectional morphology, in German^{381, 382}, Italian³⁸³, Spanish³⁸⁴, and English^{357, 385-388}. All of these have found distinct ERP patterns for regulars and irregulars. Although the specific results have varied somewhat, certain trends emerge from these studies. (Here we focus on the violation^{357, 382, 383, 385, 387} rather than the priming^{384, 386} studies, since our research employs the former approach.). (1) *Regular affixation and LANs*. First, inappropriate regular affixation (i.e., anomalous addition or omission of the affix) generally leads to a LAN. In English, violations of regular past tense (stem form in past tense context; e.g., *Yesterday I walk over there*) in male subjects (see below for females) have been found to elicit a LAN^{357, 387}. In German^{382, 389} and Italian³⁸³, incorrectly adding a regular affix to an irregular verb has also resulted in anterior negativities, as compared to the signal elicited by the correct irregular form. These anterior negativities were predominant in left fronto-temporal regions in the German studies^{382, 389}, but had a broader distribution in the Italian experiment³⁸³. Another study of English³⁸⁵ did *not* find a LAN in

response to violations of regular verbs (past tense form in a future tense sentence context). It is not yet clear why this experiment elicited a different pattern. (2) *Irregular inflection and N400s*. Inappropriate irregular inflection has led to a somewhat different pattern than inappropriate regular inflection, eliciting either N400s or no effect at all. In one German experiment, adding an irregular past-participle affix to a regular verb yielded an N400-like negativity³⁸². In English, violations of irregular inflection (stem form in a past tense context) elicited an N400 effect^{357, 387}. However, this enhancement of the N400 in the incorrect stem condition was revealed indirectly rather than in the direct comparison to the correct irregular past-tense form (i.e., *keep* as compared to *kept*), since the latter *also* showed enhanced N400s. This was demonstrated by the presence of an N400 in the comparison between the correct irregular and correct regular past-tense conditions (e.g., *kept* vs. *walked*). The enhancement of the N400 for *correct* irregular forms is likely due to the increased lexical processing difficulties for these forms as a consequence of their inherent irregularity (e.g., *sing-sang*, *bring-brought*, *fight-fought*), as demonstrated in previous behavioral studies³⁹⁰⁻³⁹⁴. N400s were not reported in three other studies of violations to irregular morphology^{381, 383, 385}. (3) *P600s*. P600 effects have been observed for both regular *and* irregular past-tense violations in studies of English^{357, 385, 387}, although these effects have differed somewhat in latency³⁸³ or distribution^{357, 387} between the two verb types. P600s were not reported in the ERP studies of inflection in German and Italian³⁸¹⁻³⁸³, likely because the stimuli contained violations only of morpho-phonology, not of morpho-syntax. (4) *Conclusion*. Thus previous experiments of regular/irregular morphology have been somewhat mixed, although certain trends seem to be emerging: if any N400 or LAN effects are found at all, violations of regular inflection elicit the former, while violations of irregular inflection elicit the latter; if violations of morpho-syntax are also present, P600s are found for both types of forms.

We recently examined sex differences in ERPs^{392, 393}. Men and women were visually presented with anomalous and control sentences probing four conditions: regular and irregular past-tense (in which the stem form or correct past-tense was presented in a past tense context; e.g., *Yesterday I dig a hole*), syntactic word-order, and lexical/semantic processing. Analyses performed for both the 300-400 and the 400-500 ms time windows revealed that the most reliable regular/irregular differences occurred between 300 and 400 ms. In both sexes, incorrect (stem) forms of irregular verbs yielded an early N400-like negativity

(see just above) rather than a LAN; past tense violations of regular verbs, in contrast, yielded a LAN in males that was absent in females (N400). Semantic incongruities elicited N400s in both sexes; however, the amplitude was significantly larger among the women than the men, underscoring neurocognitive sex differences in lexical/semantic memory. Consistent with previous studies of syntactic word-order violations^{351, 374}, men displayed a LAN. Surprisingly (see discussion below), women instead showed only a posterior negativity, which was larger in the left hemisphere (Fig. 148). A statistical analysis comprising both the word-order and the regular past-tense violations revealed a shared effect, across the two conditions, of a significantly more left and anterior distribution for men than women, which moreover did not differ between the two types of violations. Respective sex differences also resulted in corresponding significant interactions in the global (and intermediate) ANOVAs (thus justifying direct comparisons). These results support a common mechanism in men for processing regular-past tense and syntactic word-order violations (as predicted by DP), and suggest that the sexes differ in their reliance on the two hypothesized language systems not only in the processing of regular past-tense forms, but also, surprisingly, for certain syntactic representations (see just below for discussion). In the subsequent 400-500 ms time window, *both* past-tense types elicited a

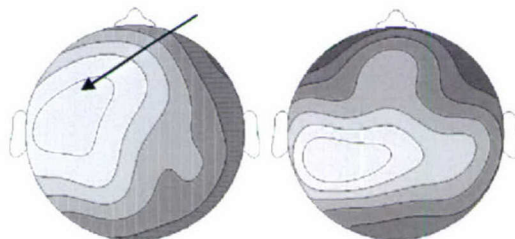


Fig. 148: ERP sex differences for word order violations. A left anterior negativity was found in men (left) but not women (right).

LAN in *both* sexes. This suggests that morpho-phonological processing (which yielded distinct patterns for regulars and irregulars from 300-400 ms) precedes morpho-syntactic processing, and that *morpho-syntactic* structures do *not* tend to depend on memory in the way that regular past-tense or syntactic word-order do in women (see just below for discussion). Finally, all three grammatical violations (syntactic word-order and both past-tense types), but not lexical/semantic incongruities, elicited the expected late posterior P600s. These did not differ in distribution or amplitude between the sexes.

In sum, previous ERP evidence, including studies carried out in our lab, paints a somewhat mixed picture. The data seem at least partially, though *not* completely, consistent with the claims of the DP model. Several issues in particular require further investigation, including the role of the BG in the P600 and/or the LAN, and the reliability of (L)AN effects across grammatical conditions. Additionally, the absence of a LAN among women for the word-order but not the morpho-syntactic violation is intriguing and potentially important. It suggests that women may tend to store some sort of representation in the first but not the second case. One possible interpretation is based on the hypothesis that transition probabilities between words should not be difficult to memorize, particularly when adjacent words co-occur frequently in the same syntactic frame. Indeed, transition probabilities form the basis of many computational models of grammar, including connectionist models of syntax^{395, 396}. In contrast, morpho-syntactic representations such as those involving tense and agreement typically depend on longer-distance dependencies, which should be difficult to memorize. This leads to predictions that can and will be tested in the proposed research. In particular, *no* sex differences are expected for morpho-syntactic violations, whereas sex differences *should* be observed for violations of regular morphology and syntactic word-order (both of which should elicit N400s in women, and LANs for men). Much of the evidence presented above also seems largely consistent with other dual-system models, in particular that of Friederici, although such models would have to accommodate the sex differences if they are shown to be reliable. It is not entirely clear how the full set of ERP results, including the sex differences, speak to Dominey's model. However, at least the LAN effects for syntactic and morpho-syntactic violations are compatible with his perspective³⁹⁷. Finally, the pattern of previously reported data, in particular the apparent equivalence of the anterior negativities for regular morpho-phonology and syntax, does not appear to be entirely consistent with JS.

Hypothesis #20: Functional magnetic resonance imaging (fMRI) can be used to evaluate anatomical sites for specific components of language and memory.

Activation in temporal/temporo-parietal regions is strongly linked with lexical and non-linguistic conceptual-semantic representation or processing³⁹⁸. Similarly, using lexically stored syntactic knowledge (i.e., of complements) has yielded left inferior temporal lobe activation. The selection or retrieval of lexical and semantic knowledge reliably leads to activation in ventro-lateral frontal cortex, especially in BA 45. A variety of tasks designed to probe syntactic processing have elicited preferential activation in Broca's area³⁹⁹ premotor cortex (in particular SMA³⁹⁸), the BG (especially but not only the caudate), and anterior superior temporal cortex. Within Broca's area, many of these studies have implicated BA 44 (pars opercularis) and the adjacent frontal operculum, suggesting that these regions play a particularly important role in grammatical processing. It is noteworthy that at least one of the studies that reported BG activation⁴⁰⁰ was carried out to disprove the involvement of BG in syntactic processing. However, it is important to note that the BG have not been as robustly activated across studies as has Broca's area. Indeed, in one study carried out in our own lab, semantic but not syntactic processing violations elicited BG (caudate) activation³⁹⁸. This result is unlikely to be explained by the task paradigm, since those studies which did obtain caudate activation also involved syntactic violations, and moreover of a similar sort as in our study. Further research, including the replication of our own study, is needed. Several neuroimaging studies of language have probed sex differences. In studies of sentence processing, women showed greater temporal-lobe activation than men^{401, 402}, supporting the DP hypothesis of greater female reliance on stored complex representations. In neuroimaging studies of tasks involving lexical but *not* grammatical processing⁴⁰³ (and thus in which a greater dependence on lexical memory by women is *not* expected by DP), *no* sex differences were found. A number of PET and fMRI studies have examined regular and irregular forms, in English past-tense production^{404, 405} and judgment⁴⁰⁶, and in German past-tense and past-participle production. These have found differential activation in frontal and temporal regions for the two types of forms. However, the data are difficult to interpret because the specific regions have varied to some extent across the studies. Importantly, violations of regular – but not irregular – past-tense (incorrect vs. correct; e.g., *Yesterday I walk over there* vs. *Yesterday I walked over there*)⁴⁰⁶ and violations of syntactic c word-order³⁹⁸, which were examined in the same event-related fMRI experimental paradigm, both showed activation in left premotor cortex and its vicinity. This suggests that the processing of regular past-tense morpho-phonology and syntactic word-order may depend on common neural correlates. Moreover, these data suggest that such judgment tasks are quite well-suited to examine the neural basis of regular morpho-phonology and syntactic word-order, with fMRI as well as ERP (for ERP, see just below). In sum, the hemodynamic data seem broadly compatible with both DP and Friederici's model. However, a number of findings appear to be problematic (e.g., the BG are inconsistently activated), indicating the need for further investigation. The dissociations in activation between grammatical and lexical processes do not appear to be consistent with SM views that assume a single system for lexicon and grammar. It has been argued that the regular/irregular activation patterns are consistent with previously proposed SM mechanism models (e.g., JS)^{407, 408}, although this claim remains controversial⁴⁰⁹. An fMRI investigation of carefully matched regular/irregular stimuli, which are not expected by JS to yield greater frontal activation for regulars, might help resolve the issue.

V. Key Research Accomplishments

Hypothesis #1

- A new and highly effective/consistent diffuse traumatic brain injury (DTBI) model was developed and characterized.
- This DTBI model was also shown to be useful for studying brain injury mechanisms at different developmental ages.
- The endogenous cannabinoid anandamide was shown to cause neuronal death *in vivo* and *in vitro*, necessitating modification of the concept that endocannabinoids are uniformly neuroprotective.
- mGluR activation was shown to be highly neuroprotective against apoptotic neuronal cell death, including after β -amyloid administration, which may have implications for the treatment of Alzheimer's disease.
- Neuronal/glia interactions were shown to determine the effects of group I metabotropic glutamate receptors.

Hypothesis #2

- We demonstrated that novel neuroprotective drugs can be developed through rational drug discovery using molecular modeling, synthetic chemistry, and biological modeling.
- Such modeling methods were used to develop novel PTEN modulators, which may have actions in either neurodegeneration or cancer, and novel diketopiperazines, which have both neuroprotective and nootropic properties.

Hypothesis #3

- We showed that the novel tumor suppressor gene PTEN is an important upstream pro-apoptotic modulating factor and may play a role in traumatic brain injury.

Hypothesis #4

- We found that fibroblast growth factor (FGF) binding factor protein did not modify neuroprotection provided by FGF alone.

Hypothesis #5

- We found that ceramide, a brain lipid, plays an important role in neuronal apoptosis after post-traumatic neuronal injury.
- Signal transduction cascades activated by ceramide were identified, including Akt-mediated and MAP kinase-mediated.

Hypothesis #6

- We showed that advanced DNA microarray technology can help to identify the role of genes, including novel genes, in cell death, inflammation and regeneration/plasticity.
- This technology identified a common group of genes whose message was similarly altered across multiple models of CNS injury and rodent species.

Hypothesis #7

- High-field magnetic resonance imaging and technology was shown to be useful for delineating mechanisms of CNS injury, as well as effects of treatment.
- A novel stereotaxic device was developed to allow reproducible, reported scanning over time in the same animals.

Hypothesis #8

- Pro-apoptotic factors relating to cell cycle were shown to be inversely correlated with neurite outgrowth.
- Inhibition of such factors both reduces cell death and enhances neurite outgrowth.
- Novel gene clusters associated with regeneration and plasticity were identified.
- Promoter analyses showed that the tumor suppressor gene p53 upregulates genes involved in regeneration.

Hypothesis #9

- A number of critical genes associated with apoptosis were shown to be developmentally regulated, suggesting different mechanisms may be involved in young animals versus adults, requiring different therapeutic approaches.
- Changes in such gene expression, suppressed in adulthood, is reactivated after brain injury.

Hypothesis #10

- Multidisciplinary approaches were effectively used to model and evaluate injury mechanisms after spinal cord trauma.
- A new mouse model of spinal cord injury (SCI) was developed.
- The role of distinct caspases in various cell types was characterized after SCI.
- STAT transcription factors were shown to play a role in the neuronal response to injury.
- These studies illustrate a novel role for STAT6, an immune system transcription factor essential for normal immune system function, in the function of the nervous system.
- STAT6 may coordinate activation of the immune system and nervous system.
- These studies illustrate a novel role for STAT6, an immune system transcription factor essential for normal immune system function, in the function of the nervous system.
- STAT6 in its activated and un-activated form is constitutively expressed in DRG neurons suggesting a role in neuronal homeostasis and response to peripheral input and injury.
- Signaling through STAT6 occurs in DRG neurons after noxious input.
- Signaling through STAT6 occurs in DRG glia (satellite cells) and spinal cord glia ipsilateral to a crush injury of the sciatic nerve.
- STAT6 may coordinate activation of the immune system and nervous system.

Hypothesis #11

- Transgenic approaches using mGluR5 knockouts were shown to be useful for elucidating mechanisms of neuronal injury and recovery.
- Viral vectors were effectively used to examine mechanisms of apoptotic cell death after brain injury.

Hypothesis #12

- Inflammatory activation of microglia does not appear to a primary target for the treatment of Alzheimer's disease.

Hypothesis #13

- HLA-DR alleles do not appear to influence the progression rate of AD or the response to anti-inflammatory treatment.

Hypothesis #14

- A new technology was developed for establishing precisely controlled molecular gradients in collagen gels.
- This technology has been used to examine the response of dorsal root ganglion axons to gradients of nerve growth factor (NGF), showing that axons have limited ability to adapt to external ligand concentrations.

Hypothesis #15

- Molecular modeling was used to elucidate the structural basis of ligand binding to protein kinase C (PKC) and Ras GRP proteins.
- New computational methods were developed for structure-based designs of new therapeutics for treatment of TBI and Alzheimer's disease.

Hypothesis #16

- A new molecular dynamics methods was used to study molecular dynamics simulation of β -amyloid peptide, providing a molecular basis for folding and misfolding of this protein associated with Alzheimer's disease.
- This approach may be effectively used to design novel small molecule inhibitors and potentially prevent β -amyloid toxicity.

Hypothesis #17

- New computational docking methods were developed to improve accuracy in protein-drug docking.

Hypothesis #18

- Different anatomical localizations were shown to subserve declaration and procedural memory, and related to specific classes of neurological disorders.

Hypothesis #19

- Event-related potentials can be effectively used to investigate brain substrates for lexicon and grammar.

Hypothesis #20

- Functional magnetic resonance imaging (fMRI) can be effectively used to evaluate anatomical sites for specific components of language and memory.

VI. Reportable Outcomes

1. Manuscripts

Faden AI. Exacerbation of neuronal cell death by activation of group I metabotropic glutamate receptors: role of NMDA receptors and arachidonic acid release. *Exp Neurol* 169:449-460, 2001.

Faden AI. Neuroprotection and traumatic brain injury: the search continues. *Arch Neurol* 58:1553-1555, 2001.

Lea PM IV and AI Faden. Traumatic brain injury: developmental differences in glutamate receptor response and the impact on treatment. Special Issue: The glutamate signalling in developmental and in neonatal brain injury. *Mental Retardation & Developmental Disabilities Research Reviews* 7:235-248, 2001.

Yakovlev AG and AI Faden. Caspase-dependent apoptotic pathways in CNS injury. *Mol Neurobiol* 24:131-144, 2001.

Bao WL, Williams AJ, Faden AI, and Tortella FC. Selective mGluR receptor antagonist or agonist provides neuroprotection in a rat model of focal cerebral ischemia. *Brain Res* 922:173-179, 2001.

Yakovlev AG, Ota K, Wang G, Movsesyan V, Bao WL, Yoshihara K, and Faden AI. Differential expression of apoptotic protease-activating factor-1 and caspase-3 genes and susceptibility to apoptosis during brain development and after traumatic brain injury. *J Neurosci* 21:7439-7446, 2001.

Vink R, Mullins PG, Temple MD, Bao W, and Faden AI. Small shifts in craniotomy position in the lateral fluid percussion injury model are associated with differential lesion development. *J Neurotrauma* 18:839-847, 2001.

Toman RE, Movsesyan V, Murthy SK, Milstien S, Spiegel S, and Faden AI. Ceramide-induced cell death in primary neuronal cultures: Upregulation of ceramide levels during neuronal apoptosis. *J Neurosci Res* 68:323-330, 2002.

Lea PM IV, Custer SJ, Vicini S, and Faden AI. Neuronal and glial mGluR5 modulation prevents stretch-induced enhancement of NMDA receptor current. *Pharmacol Biochem Behav* 73:287-298, 2002.

Ota K, Yakovlev AG, Itaya A, Kameoka M, Tanaka Y, Yoshihara, K. Alteration of Apoptotic Protease-Activating Factor-1 (APAF-1)-Dependent Apoptotic Pathway During Development of Rat Brain and Liver *J Biochem (Tokyo)* 2002; 131(1):131-135.

Prakash KR, Tang Y, Kozikowski AP, Flippen-Anderson JL, Knoblach SM and Faden AI. Synthesis and biological activity of novel neuroprotective diketopiperazines. *Bioorg Med Chem* 10:3043-3048, 2002.

Knoblach SM and Faden AI. Administration of either anti-intercellular adhesion molecule-1 or a nonspecific control antibody improves recovery after traumatic brain injury in the rat. *J Neurotrauma* 19:1039-1050, 2002.

Movsesyan VA, Yakovlev AG, Dabaghyan EA, Stoica BA and Faden AI. Ceramide induces neuronal apoptosis through the caspase-9/caspase-3 pathway. *Biochem Biophys Res Commun* 299:201-207, 2002.

Knoblach SM, Nikolaeva M, Huang X, Fan L, Krajewski S, Reed JC, and Faden AI. Multiple caspases are activated after traumatic brain injury: Evidence for involvement in functional outcome. *J Neurotrauma* 19:1155-1170, 2002.

Faden AI. Neuroprotection and traumatic brain injury: theoretical option or realistic proposition. *Curr Opin Neurol* 15:707-712, 2002.

Faden AI, Fox GB, Di X, Knoblach SM, Cernak I, Mullins P, Nikolaeva M, Kozikowski AP. Neuroprotective and nootropic actions of a novel cyclized dipeptide after controlled cortical impact injury in mice. *J Cereb Blood Flow Metab* 23(3): 355-363, 2003.

Faden AI, Knoblach SM, Cernak I, Fan L, Vink R, Araldi GL, Fricke ST, Roth BL, Kozikowski AP. Novel diketopiperazine enhances motor and cognitive recovery after traumatic brain injury in rats and shows neuroprotection *in vitro* and *in vivo*. *J Cereb Blood Flow Metab* 23(3):342-354, 2003.

Di Giovanni S, Knoblach SM, Brandoli C, Aden SA, Hoffman EP and Faden AI. Gene profiling in spinal cord injury shows role of cell cycle in neuronal death. *Annals of Neurol* 53:454-468, 2003.

Stoica BA, Movsesyan VA, Lea PM IV, and Faden AI. Ceramide-induced neuronal apoptosis is associated with dephosphorylation of Akt, BAD, FKHR, GSK-3 β , and induction of the mitochondrial-dependent intrinsic caspase pathway. *Mol Cell Neurosci* 22:365-382, 2003.

Lea PM IV, Faden AI. Modulation of metabotropic glutamate receptors as potential treatment for acute and chronic neurodegenerative disorders. *Drug News Perspect* 16 (8):513-22, 2003. (Cover Story)

Natale JE, Ahmed F, Cernak I, Stoica B, Faden AI. Gene expression profile changes are commonly modulated across models and species after traumatic brain injury. *J Neurotrauma* 20 (10):907-27, 2003.

Lea PM IV, Custer SJ, Stoica BA, Faden AI. Modulation of stretch-induced enhancement of neuronal NMDA receptor current by mGluR1 depends upon presence of glia. *J Neurotrauma* 20 (11):1233-49, 2003.

Yakovlev AG, Faden AI. Mechanisms of neural cell death: implications for development of neuroprotective treatment strategies. *NeuroRx* 1 (1):5-16, 2004.

Cernak I, Vink R, Natale J, Stoica, B, Lea PM, Movsesyan V, Ahmed F, Knoblach SM, Faden AI. The "dark" side of endocannabinoids: a neurotoxic role for anandamide. *JCBFM* 24:564-78, 2004.

Fricke, S.T., Vink, R., Chiodo, C., Cernak, I., Ileva, L. and Faden, A.I. Consistent and reproducible slice selection in rodent brain using a novel stereotaxic device for MRI.: *J Neurosci Methods* 136:99-102, 2004.

Movsesyan VA, BA Stoica, AG Yakovlev, SM Knoblach, PM Lea IV, and AI Faden. Anandamide-induced neuronal death in primary neuronal cultures: role of calpain and caspase pathways. *Cell Death and Differentiation*, in press.

Movsesyan VA, Stoica BA, Faden AI. MGluR5 activation reduces b-amyloid-induced cell death in primary neuronal cultures and attenuates translocation of cytochrome C and apoptosis-inducing factor. *J Neurochem*, In Press.

Aisen PS, Schmeidler J, Pasinetti GM. Randomized Pilot Study of Nimesulide Treatment in Alzheimer's Disease. *Neurology*, 58: 1050-54, 2002.

Aisen PS, Egelko S, Andrews H, Diaz-Arrastia R, Weiner M, DeCarli C, Jagust W, Miller JW, Green R, Bell K, Sano M. A Pilot Study of Vitamins to Lower Plasma Homocysteine in Alzheimer's Disease. *American Journal of Geriatric Psychiatry*, 11: 246-9, 2003.

Aisen PS, Schafer K, Grundman M, Pfeiffer E, Sano M, Davis KL, Farlow M, Jin S, Thomas R, Thal LJ for the Alzheimer's Disease Cooperative Study. Effects of Rofecoxib or Naproxen vs Placebo on Alzheimer Disease Progression. *Journal of the American Medical Association*. 289:2819-2826, 2003.

Aisen PS, Dalton A, Sano M. Design and Implementation of a Multicenter Trial of Vitamin E in Aging Individuals with Down Syndrome. Submitted.

Aisen PS, Luddy A, Durner M, Reinhard JF Jr. and Pasinetti GM. HLA-DR4 influences glial activity in hippocampus of patients with Alzheimer's disease. *Journal of the Neurological Sciences*, 161: 66-69, 1998

Hull M, Pasinetti GM, **Aisen PS**. Elevated Plasma Neopterin Levels in Alzheimer's Disease. *Alzheimer Disease and Associated Disorders*, 14: 228-230, 2000.

S-B Rong, IJ. Enyedy, L Qiao, L Zhao, D Ma, LL Pearce, PS Lorenzo, JC Stone, PM Blumberg, **S Wang**, and **AP Kozikowski**, Structural Basis of RasGRP Binding to High-Affinity PKC Ligands, *Journal of Medicinal Chemistry*, **2002**; 45, 853-860.

R Wang, L Lai and **S Wang**, Further development and validation of empirical scoring functions for structure-based binding affinity prediction, *J. Computer-Aided Molecular Design*, **2002**, 16, 11-26.

R Wang and **S Wang**, How Does Consensus Scoring Work for Virtual Library Screening? An Idealized Computer Experiment, *J Chem Info and Comp Sci*, **2001**, 41, 1422-1426.

Y Pak, IJ Enyedy, J Varady, J Kung, PS Lorenzo, PM Blumberg, and **S Wang**, Structural Basis of Binding of High-Affinity Ligands to Protein Kinase C: Prediction of the Binding Modes through a New Molecular Dynamics Method and Evaluation by Site-Directed Mutagenesis, *J Med Chem*, **2001**; 44, 1690-1701.

Kensinger, E. A., **Ullman, M. T.**, & Corkin, S. (2001). Bilateral medial temporal lobe damage does not affect lexical or grammatical processing: Evidence from the amnesic patient H.M. *Hippocampus*, 11(4), 347-360.

Newman, A. J., Pancheva, R., **Ozawa, K.**, Neville, H. J., & **Ullman, M. T.** (2001). An event-related fMRI study of syntactic and semantic violations. *Journal of Psycholinguistic Research*, 30(3), 339-364.

Steinhauer, K., Pancheva, R., Newman, A.J., Gennari, S., & **Ullman, M. T.** (2001) How the mass counts: An electrophysiological approach to the processing of lexical features. *Neuroreport*. 12(5). 999-1005.

Ullman, M. T. (2001a). The declarative/procedural model of lexicon and grammar. *Journal of Psycholinguistic Research*, 30(1), 37-69.

Ullman, M. T. (2001b). A Neurocognitive Perspective on Language: The Declarative/Procedural Model. *Nature Reviews Neuroscience*, 2, 717-726.

Ullman, M. T. (2001c) The neural basis of lexicon and grammar in first and second language: The declarative/procedural model. *Bilingualism: Language and Cognition*. 4(1). 105-122.

van der Lely, H. K. J., & **Ullman, M. T.** (2001). Past tense morphology in specifically language impaired and normally developing children. *Language and Cognitive Processes*, 16(2), 177-217.

Drury, J.E. and **Ullman, M. T.** (2002) The Memorization of Complex Forms in Aphasia: Implications for Recovery. *Brain and Language*. 83. 139-141.

Estabrooke, I. V., Mordecai, K., Maki, P. M., & **Ullman, M. T.** (2002). The effect of sex hormones on language processing. *Brain and Language*. 83. 143-146.

Pinker, S. and **Ullman, M. T.** (2002) The past and future of the past tense.. *Trends in Cognitive Sciences*. 6(11). 456-463.

Pinker, S. and **Ullman, M. T.** (2002) Combination and structure, not gradedness, is the issue. *Trends in Cognitive Sciences*. 6(11). 472-474.

Steinhauer, K., & Ullman, M. T. (2002). Consecutive ERP effects of morph-phonology and morpho-syntax. *Brain and Language*. 83. 62-65.

Ullman, M. T., Estabrooke, I.V., Steinhauer, K., Broveto, C., Pancheva, R., Ozawa, K., Mordecai, K., & Maki, P. M. (2002). Sex differences in the neurocognition of language. *Brain and Language*. 83. 141-143.

Pinker, S. and **Ullman, M. T.** (2003) Beyond one model per phenomenon. *Trends in Cognitive Sciences*. 7(3). 108-109

Rosoff, W.J., Urbach, J.S., Esrick, M., Richards, L.J. & **Goodhill, G.J.** (2004). A novel chemotaxis assay reveals the extreme sensitivity of axons to molecular gradients. *Nature Neuroscience* 7:678-682.

MacArthur, L., Iarakov, H., Ruda, M.A., and Bregman, B.S. Regulation of STAT6 in rat DRG after noxious stimulus and nerve crush. In preparation.

2. Book Chapters

Cernak, I., PM. Lea IV, and **AI. Faden**. Experimental Models of Brain Trauma. *Neuroprotection: Models, Mechanisms and Therapies*, Edited by Mathias Bahr, in press.

Knoblach, SM and **AI Faden**, Proteases in traumatic brain injury. *Proteases in Biology and Disease, Volume 3: Proteases in the Brain*, Edited by Nigel Hooper and Uwe Lendeckel, in submission.

3. Proceedings/Abstracts/Presentations

Lea, P.M. IV, S. Vicini and **A.I. Faden**. Group I mGluR modulation of NMDA receptor currents in stretch injured cortical neurons in culture. *Thirty-First Annual Meeting of the Society for Neuroscience*, San Diego, California, November 10-15, 2001. Abstracts 27: 262.15.

Yakovlev AG, Ota K, **Wang G**, **Movsesyan V**, **Bao WL**, Koichiro Yoshihara K, and **Faden AI**. Differential expression of Apaf-1 and caspase-3 genes and susceptibility to apoptosis during brain development and after traumatic brain injury. *Society for Neuroscience, 31 Annual Meeting*, San Diego, CA, November 10 - 15, 2001.

Yakovlev AG. Regulation of apoptotic susceptibility during brain development. *Spring Hippocampal Research Conference*, Grand Cayman, British West Indies, April 13 - 20, 2002.

Newman, A.J., Pancheva, R., Ozawa, K., Neville, H., & **Ullman, M. T.** (2001) Neural Localization of Syntactic and Semantic Anomaly Processing: An Event-Related fMRI Study. Journal of Cognitive Neuroscience, Supplement.

Rhee, J., Clark, D., Casasanto, D., **Ullman, M. T.**, Wagner, A., & Pinker, S. (2001). Neural Substrates of English Past Tense Generation. Journal of Cognitive Neuroscience, Supplement, 131.

Steinhauer, K., Pancheva, R., Newman, A.J., **Ullman, M. T.** (2001) ERP Correlates of Lexical Feature Processing Without Employing the 'Violation Paradigm'. Journal of Cognitive Neuroscience, Supplement.

Ullman, M. T., Newman, A. J., Pancheva, R., & Steinhauer, K. (2001). Male/female differences in lexical-conceptual and syntactic processing: Evidence from event-related potentials. Journal of Cognitive Neuroscience, Supplement.

Steinhauer, K., Pancheva, R., Newman, A.J., & **Ullman, M. T.** (2001) Monitoring the processing of lexical features: ERP evidence without employing violations. *The Neurological Basis of Language: An Interdisciplinary Conference on Aphasiological, Computational, and Neuroimaging Approaches*. Groningen, The Netherlands.

Steinhauer, K., Pancheva, R., Newman, A.J., & **Ullman, M. T.** (2001) Processing the lexical mass/count feature: ERP evidence without employing violations. Proceedings of the 14th Annual CUNY Conference on Human Sentence Processing.

Ullman, M. T., Estabrooke, I., Newman, A. J., Steinhauer, K., Pancheva, R., Broveto, C., & Ozawa, K. (2001). Sex differences in the computation of complex linguistic representations. Proceedings of the 14th Annual CUNY Conference on Human Sentence Processing, Philadelphia, PA.

Ullman, M. T., Walenski, M., Prado, E., Ozawa, K., & Steinhauer, K. (2001). A new method for investigating the real-time composition of complex linguistic forms. Proceedings of the Fourteenth Annual CUNY Conference on Human Sentence Processing (Vol. 14, pp. 64).

Lea, P.M. IV, S. Custer, S. Vicini and **A.I. Faden**. Modulation of neuronal and glial group I mGluRs prevents stretch-induced enhancement of NMDA receptor current. *The First Joint Symposium of the National and International Neurotrauma Societies*, Tampa, Florida. *J. Neurotrauma* 19(10): 1383, 2002.

Estabrooke, I. V., Mordecai, K., Maki, P., & **Ullman, M. T.** (2002) Sex hormone effects on language. Proceedings of the 15th Annual CUNY Conference on Human Sentence Processing. 2002.

Steinhauer, K., Portner, P., Walenski, M., & **Ullman, M. T.** (2002) Comparing unlicensed Negative Polarity Items and other linguistic violations: An ERP study. Proceedings of the 16th Annual CUNY Conference on Human Sentence Processing.

Ullman, M. T. (2002) The Declarative/Procedural Model: A Neurocognitive Perspective on First and Second Language Acquisition and Processing. Proceedings of the Fourth International Symposium on Bilingualism.

Drury, J. and **Ullman, M. T.** (2002) Neighborhood and frequency effects for regular past tense forms in anterior (but not posterior) aphasia: Implications for recovery. Journal of Cognitive Neuroscience, Supplement.

Estabrooke, I. V., Mordecai, K., Maki, P., **Ullman, M. T.** (2002) Sex hormones affect language. Journal of Cognitive Neuroscience, Supplement.

Newman, A. J., **Ullman, M. T.**, Pancheva, R., Waligura, D. L., & Neville, H. J. (2002). Regular and irregular English past tense verbs elicit distinct patterns of neural activity: an event-related fMRI study. Journal of Cognitive Neuroscience, Supplement.

Ullman, M. T., & Steinhauer, K. (2002). ERPs reveal consecutive effects of morpho-phonology and morpho-syntax. Journal of Cognitive Neuroscience, Supplement.

Hartshorne, J.K., Walenski, M., and **Ullman, M. T.** (2003) An investigation of the role of the declarative and procedural memory systems in language using a dual-task paradigm. Journal of Cognitive Neuroscience, Supplement.

Newman, A.J., Waligura, D.L., Neville, H.J., & **Ullman, M. T.** (2003) Effects of late second language acquisition on neural organization: Event-Related Potential and functional Magnetic Resonance Imaging evidence. Journal of Cognitive Neuroscience, Supplement.

Steinhauer, K., Portner, P., Walenski, M., Ortinski, P., Weisberg, J., Wood, R., & **Ullman, M. T.** (2003) Event-related potentials of negative polarity items and other linguistic violations. Journal of Cognitive Neuroscience, Supplement.

Ullman, M. T., Estabrooke, I. V., Steinhauer, K., Walenski, M., Broveto, C., Pancheva, R., Ozawa, K., Hartshorne, J.K., Mordecai, K., Maki, P. (2003) Sex differences and the role of estrogen in the neurocognition of language. Journal of Cognitive Neuroscience, Supplement.

Ullman, M. T. (2003) The Declarative/Procedural Model of Language. Workshop on Perception, action, syntax and the brain: Broca's area and ventral premotor cortex in sensorimotor mapping and language at the Max Planck Institute of Cognitive Neuroscience. Leipzig, Germany. 2003.

Estabrooke, I. V., Mordecai, K., Maki, P. M., & **Ullman, M. T.** (2003) Language processing is modulated by endogenous estrogen and oral contraceptives. Society for Neuroscience Abstracts.

MacArthur, L. "Stimulus-induced Stat6 Transcription Factor Activation in Rat Dorsal Root Ganglia." Interdisciplinary Program in Neuroscience, Georgetown University, Washington, D.C. May 2003 (Abstract).

4. Informatics databases:

<http://microarray.cnmcresearch.org>

5. Funding applied for based on work supported by this award

(PI Bregman) "Spinal Cord Injury: Plasticity and Recovery of Function" NIH-NINDS.

(PI Cernak) "Anandamide Induced Neurotoxicity in Brain Injury" NIH-NINDS

(PI Cernak) "Blast (Explosion)-Induced Brain Injury" NIH-NINDS

(PI Faden) "Novel Treatment Strategy for Spinal Cord Injury" NIH-NINDS

(PI Faden) "Characterization of a New Developmental Model of Diffuse Traumatic Brain Injury" NIH-NINDS

(PI Faden) "Multipotential Drug Treatment Strategies in Neurotrauma (TRH)" NIH-NINDS

(PI Fricke) "Small Animal Handling Devices for Multiplatform Injury" NIH-NINDS

(PI Goodhill) "Mechanisms of Axonal Gradient Detection" NIH

(PI Knoblach) "Cathepsins in Traumatic CNS Injury" NIH-NINDS.

(PI Lea) "The Role of Neuronal/Glial Interactions in Age-Dependent Changes in Group I mGluR-Mediated Modulation of N-methyl-D-Aspartate Receptors" NSF

(PI Lea) "The Development and Characterization of a New In Vitro Trauma Device" NIH_NINDS

(PI MacArthur) "Role of STAT Proteins in Dorsal Root Ganglia" NIH-NINDS

(PI Stoica) "Role of Ceramide in Traumatic Neuronal Injury and Neuronal Apoptosis" NIH-NINDS

Research Corporation Technologies, Inc. Funding was received for the study of the cyclic dipeptides.

6. Academic Promotions

Ibolja Cernak, M.D., Ph.D. – Research Fellow to Associate Professor

Susan Knoblach, Ph.D. – Post-doctoral Fellow to Assistant Professor

Paul Lea IV, Ph.D. – Post-doctoral Fellow to Instructor

Vilen Movsesyan, Ph.D. – Research Instructor to Assistant Professor

Bogdan Stoica, M.D. – Research Instructor to Assistant Professor

VII. Conclusions

The common theme underlying this multidisciplinary research program was to better understand and modify plasticity/recovery within the central nervous system. Four major sub-themes included: 1. elucidating mechanisms of neural cell death as well as recovery after acute or chronic neurodegeneration; 2. developing or evaluating pharmacological strategies to limit tissue damage and improve recovery in such conditions; 3. evaluating magnetic resonance imaging and spectroscopy as tools to examine changes in injury, plasticity or response to treatment; and 4. using computational models to predict plasticity modulation and for drug discovery.

A new, highly consistent rodent model of diffuse brain injury was developed and shown to be useful for examining clinically relevant brain injury in both adult and young animals. The model was used to demonstrate that both mechanisms of cell death and cell death phenotype differ as a function of developmental age. This observation has important implications for the treatment of pediatric versus adult head injury. Other *in vivo* and *in vitro* injury models were used to show important pathophysiological roles for the tumor suppressor PTEN and the lipid ceramide, both of which appeared to cause injury in large part by modulating the actions of the endogenous protective factor Akt (protein kinase B). In addition, the endogenous cannabinoid anandamide was shown to cause or contribute to cell death, revising the accepted notion that endogenous cannabinoids are uniformly neuroprotective. A new model of spinal cord injury in the mouse was also developed, and mechanism studies of spinal cord injury in rodents identified roles for caspases and STAT transcription factors. Moreover, knockout models and viral vectors were effectively used to examine mechanisms of cell death and modulation of cell death after injury.

Molecular mechanisms of cell death and recovery were examined using a number of complementary techniques. High density oligonucleotide based microarrays were used to examine gene expression changes after brain or spinal cord injury in rodents. Among the more than 25,000 genes and EST's studied, several hundred showed consistent, significant time related changes after injury. A number of complementary biochemical methods were used to validate these observations including PCR, *in situ* hybridization, immunoblots and immunocytochemistry. Approximately 80 genes showed consistent changes across different models and species, suggesting that these are of generic importance in the injury response. Noteworthy was the identification of a large cluster of genes related to cell cycle, which were shown to be consistently up-regulated after injury and associated with apoptotic cell death. In addition, two novel gene clusters were identified that play a role in plasticity and regeneration. Moreover, a new technology was developed to examine molecular gradients, such as for growth factors, on axonal growth.

Several clinical studies of Alzheimer's disease were conducted, in part supported by this co-operative agreement. Inflammatory activation of microglia do not appear to be as important a target for treatment of AD as previously believed; nor do HLA-DR alleles appear to influence the progression rate or response to anti-inflammatory treatment. Cognitive studies in patients showed that different anatomical localizations sub-serve declarative versus procedural memory. Moreover, functional MRI and evoked related potentials were effectively used to investigate brain substrates for language and memory.

A number of advanced modeling methods were used to develop novel drug treatment approaches for injury and to enhance cognition. These included new computational methods to develop structure-based designs for treatment of traumatic brain injury and Alzheimer's disease; new molecular methods to model protein-drug docking and protein folding/mis-folding. Among new drug classes identified or developed were PTEN antagonists, and cyclic di-peptides with neuroprotective and cognitive enhancing properties. In addition, drugs that activate a specific class of non-ionotropic glutamate receptors (metabotropic glutamate receptor 5 or mGluR5) were shown to be highly protective against apoptosis and to reduce the toxicity of beta-amyloid, a factor believed to contribute to Alzheimer's disease.

In addition to improving our understanding of central nervous system injury and plasticity, a number of scientific /medical “products” were developed under this contract. These include: development of new predictive experimental injury models for brain and spinal cord; identification of a number of injury/plasticity factors that can be used to develop novel drug approaches; development/application of new computational and molecular modeling approaches that can be used to evaluate plasticity factors, to understand protein folding disorders, and to improve drug discovery; identification/development of novel drug classes that have neuroprotective and/or cognitive enhancing properties; demonstrating the utility of DNA microarray approaches to identify novel injury and plasticity factors; and demonstrating the effectiveness of various MRI related techniques, in both animals and humans, for addressing issues related to cognition and response to injury.

VIII. References

1. Beckman, D. L. and Bean, J. W. Pulmonary pressure-volume changes attending head injury. *J Appl Physiol*, 29: 631-636, 1970.
2. Bakay, L., Lee, J. C., Lee, G. C., and Peng, J. R. Experimental cerebral concussion. Part 1: An electron microscopic study. *J Neurosurg*, 47: 525-531, 1977.
3. Nilsson, B., Ponten, U., and Voigt, G. Experimental head injury in the rat. Part 1: Mechanics, pathophysiology, and morphology in an impact acceleration trauma model. *J Neurosurg*, 47: 241-251, 1977.
4. Marmarou, A., Foda, M. A., van den Brink, W., Campbell, J., Kita, H., and Demetriadou, K. A new model of diffuse brain injury in rats. Part I: Pathophysiology and biomechanics. *J Neurosurg*, 80: 291-300, 1994.
5. Hall, E. D. The mouse head injury model: utility in the discovery of acute cerebroprotective agents. *In*: S. T. Ohnishi (ed.), *Central Nervous System Trauma Research Techniques*, pp. 213-233. Boca Raton, FL: CRC Press, 1995.
6. Li, F. H. and Fisher, M. Diffusion-weighted and perfusion magnetic resonance imaging and ischemic stroke. *Drugs of Today*, 32: 615-627, 1996.
7. Tanno, H., Nockels, R. P., Pitts, L. H., and Noble, L. J. Breakdown of the blood-brain barrier after fluid percussive brain injury in the rat. Part 1: Distribution and time course of protein extravasation. *J Neurotrauma*, 9: 21-32, 1992.
8. Heath, D. L. and Vink, R. Impact acceleration-induced severe diffuse axonal injury in rats: characterization of phosphate metabolism and neurologic outcome. *J Neurotrauma*, 12: 1027-1034, 1995.
9. Van den Heuvel, C., Blumbergs, P. C., Finnie, J. W., Manavis, J., Jones, N. R., Reilly, P. L., and Pereira, R. A. Upregulation of amyloid precursor protein messenger RNA in response to traumatic brain injury: an ovine head impact model. *Exp Neurol*, 159: 441-450., 1999.
10. Bittigau, P., Siffringer, M., Pohl, D., Stadthaus, D., Ishimaru, M., Shimizu, H., Ikeda, M., Lang, D., Speer, A., Olney, J. W., and Ikonomidou, C. Apoptotic neurodegeneration following trauma is markedly enhanced in the immature brain. *Ann Neurol*, 45: 724-735., 1999.
11. Towfighi, J., Mauger, D., Vannucci, R. C., and Vannucci, S. J. Influence of age on the cerebral lesions in an immature rat model of cerebral hypoxia-ischemia: a light microscopic study. *Brain Res Dev Brain Res*, 100: 149-160, 1997.
12. Towfighi, J. and Mauger, D. Temporal evolution of neuronal changes in cerebral hypoxia-ischemia in developing rats: a quantitative light microscopic study. *Brain Res Dev Brain Res*, 109: 169-177, 1998.
13. Yakovlev, A. G., Ota, K., Wang, G., Movsesyan, V., Bao, W. L., Yoshihara, K., and Faden, A. I. Differential expression of apoptotic protease-activating factor-1 and caspase-3 genes and susceptibility to apoptosis during brain development and after traumatic brain injury. *J Neurosci*, 21: 7439-7446, 2001.
14. Albensi, B. C., Knoblach, S. M., Chew, B. G., O'Reilly, M. P., Faden, A. I., and Pekar, J. J. Diffusion and high resolution MRI of traumatic brain injury in rats: time course and correlation with histology. *Exp Neurol*, 162: 61-72., 2000.
15. Homayoun, P., Parkins, N. E., Soblosky, J., Carey, M. E., Rodriguez de Turco, E. B., and Bazan, N. G. Cortical impact injury in rats promotes a rapid and sustained increase in polyunsaturated free fatty acids and diacylglycerols. *Neurochem Res*, 25: 269-276., 2000.
16. Chan, P. H., Longar, S., Chen, S., Yu, A. C., Hillered, L., Chu, L., Imaizumi, S., Pereira, B., Moore, K., Woolworth, V., and et al. The role of arachidonic acid and oxygen radical metabolites in the pathogenesis of vasogenic brain edema and astrocytic swelling. *Ann N Y Acad Sci*, 559: 237-247, 1989.

17. Mechoulam, R. Discovery of endocannabinoids and some random thoughts on their possible roles in neuroprotection and aggression. *Prostaglandins Leukot Essent Fatty Acids*, 66: 93-99., 2002.
18. Di Marzo, V., De Petrocellis, L., Fezza, F., Ligresti, A., and Bisogno, T. Anandamide receptors. *Prostaglandins Leukot Essent Fatty Acids*, 66: 377-391., 2002.
19. Walter, L., Franklin, A., Witting, A., Moller, T., and Stella, N. Astrocytes in culture produce anandamide and other acylethanolamides. *J Biol Chem*, 277: 20869-20876., 2002.
20. van der Stelt, M., Veldhuis, W. B., Maccarrone, M., Bar, P. R., Nicolay, K., Veldink, G. A., Di Marzo, V., and Vliegenthart, J. F. Acute neuronal injury, excitotoxicity, and the endocannabinoid system. *Mol Neurobiol*, 26: 317-346., 2002.
21. Downer, E. J., Fogarty, M. P., and Campbell, V. A. Tetrahydrocannabinol-induced neurotoxicity depends on CB1 receptor-mediated c-Jun N-terminal kinase activation in cultured cortical neurons. *Br J Pharmacol*, 140: 547-557., 2003.
22. Chan, G. C., Hinds, T. R., Impey, S., and Storm, D. R. Hippocampal neurotoxicity of Delta9-tetrahydrocannabinol. *J Neurosci*, 18: 5322-5332., 1998.
23. Downer, E., Boland, B., Fogarty, M., and Campbell, V. Delta 9-tetrahydrocannabinol induces the apoptotic pathway in cultured cortical neurones via activation of the CB1 receptor. *Neuroreport*, 12: 3973-3978., 2001.
24. Guzman, M. Neurons on cannabinoids: dead or alive? *Br J Pharmacol*, 140: 439-440, 2003.
25. Devane, W. A., Hanus, L., Breuer, A., Pertwee, R. G., Stevenson, L. A., Griffin, G., Gibson, D., Mandelbaum, A., Etinger, A., and Mechoulam, R. Isolation and structure of a brain constituent that binds to the cannabinoid receptor. *Science*, 258: 1946-1949., 1992.
26. Schmid, H. H. O. Pathways and mechanisms of N-acylethanolamine biosynthesis: can anandamide be generated selectively? *Chem Phys Lipids*, 108: 71-87, 2000.
27. Sagan, S., Venance, L., Torrens, Y., Cordier, J., Glowinski, J., and Giaume, C. Anandamide and WIN 55212-2 inhibit cyclic AMP formation through G-protein-coupled receptors distinct from CB1 cannabinoid receptors in cultured astrocytes. *Eur J Neurosci*, 11: 691-699, 1999.
28. Di Marzo, V., Breivogel, C. S., Tao, Q., Bridgen, D. T., Razdan, R. K., Zimmer, A. M., A., Z., and Martin, B. R. Levels, metabolism and pharmacological activity of anandamide in CB(1) cannabinoid receptor knockout mice: evidence for non-CB(1), non-CB(2) receptor-mediated actions of anandamide in mouse brain. *J Neurochem*, 75: 2434-2444, 2000.
29. Venance, L., Piomelli, D., Glowinski, J., and Giaume, C. Inhibition by anandamide of gap junctions and intercellular calcium signalling in striatal astrocytes. *Nature*, 372: 590-594, 1995.
30. Szoke, E., Balla, Z., Csernoch, L., Czeh, G., and Szolcsanyi, J. Interacting effects of capsaicin and anandamide on intracellular calcium in sensory neurones. *Neuroreport*, 11: 1949-1952., 2000.
31. Hampson, A. J., Bornheim, L. M., Scanziani, M., Yost, C. S., Gray, A. T., Hansen, B. M., Leonoudakis, D. J., and Bickler, P. E. Dual effects of anandamide on NMDA receptor-mediated responses and neurotransmission. *J Neurochem*, 70: 671-676., 1998.
32. Maingret, F., Patel, A. J., Lazdunski, M., and Honore, E. The endocannabinoid anandamide is a direct and selective blocker of the background K(+) channel TASK-1. *Embo J*, 20: 47-54., 2001.
33. Zygmunt, P. M., Petersson, J., Andersson, D. A., Chuang, H., Sorgard, M., Di Marzo, V., Julius, D., and Hogestatt, E. D. Vanilloid receptors on sensory nerves mediate the vasodilator action of anandamide. *Nature*, 400: 452-457., 1999.
34. Nagayama, T., Sinor, A. D., Simon, R. P., Chen, J., Graham, S. H., Jin, K., and Greenberg, D. A. Cannabinoids and neuroprotection in global and focal cerebral ischemia and in neuronal cultures. *J Neurosci*, 19: 2987-2995., 1999.

35. Panikashvili, D., Simeonidou, C., Ben-Shabat, S., Hanus, L., Breuer, A., Mechoulam, R., and Shohami, E. An endogenous cannabinoid (2-AG) is neuroprotective after brain injury. *Nature*, 413: 527-531., 2001.
36. Sinor, A. D., Irvin, S. M., and Greenberg, D. A. Endocannabinoids protect cerebral cortical neurons from in vitro ischemia in rats. *Neurosci Lett*, 278: 157-160., 2000.
37. Olah, Z., Karai, L., and Ladarola, M. J. Anandamide activates vanilloid receptor 1 at acidic pH in DRG neurons and cells ectopically expressing VR1. *J Biol Chem*, 1: 1, 2001.
38. Mukhin, A. G., Ivanova, S. A., Knoblach, S. M., and Faden, A. I. New in vitro model of traumatic neuronal injury: evaluation of secondary injury and glutamate receptor-mediated neurotoxicity. *J Neurotrauma*, 14: 651-663, 1997.
39. Eldadah, B. A., Yakovlev, A. G., and Faden, A. I. The role of CED-3-related cysteine proteases in apoptosis of cerebellar granule cells. *J Neurosci*, 17: 6105-6113, 1997.
40. Ellis, E. F., McKinney, J. S., Willoughby, K. A., Liang, S., and Povlishock, J. T. A new model for rapid stretch-induced injury of cells in culture: characterization of the model using astrocytes. *J Neurotrauma*, 12: 325-339, 1995.
41. Pike, B. R., Zhao, X., Newcomb, J. K., Glenn, C. C., Anderson, D. K., and Hayes, R. L. Stretch injury causes calpain and caspase-3 activation and necrotic and apoptotic cell death in septo-hippocampal cell cultures. *J Neurotrauma*, 17: 283-298, 2000.
42. Pike, B. R., Zhao, X., Newcomb, J. K., Posmantur, R. M., Wang, K. K., and Hayes, R. L. Regional calpain and caspase-3 proteolysis of alpha-spectrin after traumatic brain injury. *Neuroreport*, 9: 2437-2442., 1998.
43. Buki, A., Siman, R., Trojanowski, J. Q., and Povlishock, J. T. The role of calpain-mediated spectrin proteolysis in traumatically induced axonal injury. *J Neuropathol Exp Neurol*, 58: 365-375, 1999.
44. Wang, K. K., Posmantur, R., Nath, R., McGinnis, K., Whitton, M., Talanian, R. V., Glantz, S. B., and Morrow, J. S. Simultaneous degradation of alphaII- and betaII-spectrin by caspase 3 (CPP32) in apoptotic cells. *J Biol Chem*, 273: 22490-22497, 1998.
45. Janicke, R. U., Sprengart, M. L., Wati, M. R., and Porter, A. G. Caspase-3 is required for DNA fragmentation and morphological changes associated with apoptosis. *J Biol Chem*, 273: 9357-9360, 1998.
46. Yang, X. H., Sladek, T. L., Liu, X., Butler, B. R., Froelich, C. J., and Thor, A. D. Reconstitution of caspase 3 sensitizes MCF-7 breast cancer cells to doxorubicin- and etoposide-induced apoptosis. *Cancer Res*, 61: 348-354, 2001.
47. Sato, K., Saito, Y., and Kawashima, S. Identification and characterization of membrane-bound calpains in clathrin-coated vesicles from bovine brain. *Eur J Biochem*, 230: 25-31, 1995.
48. Mombouli, J. V., Schaeffer, G., Holzmann, S., Kostner, G. M., and Graier, W. F. Anandamide-induced mobilization of cytosolic Ca²⁺ in endothelial cells. *Br J Pharmacol*, 126: 1593-1600., 1999.
49. Neumar, R. W., Xu, Y. A., Gada, H., Guttman, R. P., and Siman, R. Cross-talk between calpain and caspase proteolytic systems during neuronal apoptosis. *J Biol Chem*, 278: 14162-14167, 2003.
50. Dijkhuizen, R. M., Muller, H. J., Josephy, M., Spruijt, B. M., and Nicolay, K. Mechanical lesions of the fimbria fornix in rat brain studied by 1H-magnetic resonance imaging. Evidence for long-lasting dynamic alterations in the ipsilateral ventricular system. *Eur Neuropsychopharmacol*, 6: 21-27, 1996.
51. Dietrich, W. D., Halley, M., Alonso, O., Globus, M. Y., and Busto, R. Intraventricular infusion of N-methyl-D-aspartate. 2. Acute neuronal consequences. *Acta Neuropathol (Berl)*, 84: 630-637, 1992.
52. Bramlett, H. M., Green, E. J., and Dietrich, W. D. Exacerbation of cortical and hippocampal CA1 damage due to posttraumatic hypoxia following moderate fluid-percussion brain injury in rats. *J Neurosurg*, 91: 653-659, 1999.

53. Hermann, D. M., Kilic, E., Hata, R., Hossmann, K. A., and Mies, G. Relationship between metabolic dysfunctions, gene responses and delayed cell death after mild focal cerebral ischemia in mice. *Neuroscience*, 104: 947-955., 2001.
54. Krumins, S. A. and Faden, A. I. Traumatic injury alters opiate receptor binding in rat spinal cord. *Ann Neurol*, 19: 498-501, 1986.
55. Szallasi, A. Vanilloid-sensitive neurons: a fundamental subdivision of the peripheral nervous system. *J Peripher Nerv Syst*, 1: 6-18., 1996.
56. Nicotera, P., Leist, M., and Manzo, L. Neuronal cell death: a demise with different shapes. *Trends Pharmacol Sci*, 20: 46-51, 1999.
57. Raghupathi, R., Graham, D. I., and McIntosh, T. K. Apoptosis after traumatic brain injury. *J Neurotrauma*, 17: 927-938, 2000.
58. MacManus, J. P. and Buchan, A. M. Apoptosis after experimental stroke: fact or fashion? *J Neurotrauma*, 17: 899-914, 2000.
59. Yakovlev, A. G., Knoblach, S. M., Fan, L., Fox, G. B., Goodnight, R., and Faden, A. I. Activation of CPP32-like caspases contributes to neuronal apoptosis and neurological dysfunction after traumatic brain injury. *J Neurosci*, 17: 7415-7424, 1997.
60. Young, W. Role of calcium in central nervous system injuries. *J Neurotrauma*, 9: S9-25., 1992.
61. Zipfel, G. J., Babcock, D. J., Lee, J. M., and Choi, D. W. Neuronal apoptosis after CNS injury: the roles of glutamate and calcium. *J Neurotrauma*, 17: 857-869., 2000.
62. Pin, J. P. and Duvoisin, R. The metabotropic glutamate receptors: structure and functions. *Neuropharmacology*, 34: 1-26, 1995.
63. Schoepp, D. D., Jane, D. E., and Monn, J. A. Pharmacological agents acting at subtypes of metabotropic glutamate receptors. *Neuropharmacology*, 38: 1431-1476, 1999.
64. Mukhin, A., Fan, L., and Faden, A. I. Activation of metabotropic glutamate receptor subtype mGluR1 contributes to post-traumatic neuronal injury. *J Neurosci*, 16: 6012-6020, 1996.
65. Faden, A. I., O'Leary, D. M., Fan, L., Bao, W., Mullins, P. G., and Movsesyan, V. A. Selective blockade of the mGluR1 receptor reduces traumatic neuronal injury in vitro and improves outcome after brain trauma. *Exp Neurol*, 167: 435-444., 2001.
66. Meli, E., Picca, R., Attucci, S., Cozzi, A., Peruginelli, F., Moroni, F., and Pellegrini-Giampietro, D. E. Activation of mGlu1 but not mGlu5 metabotropic glutamate receptors contributes to postischemic neuronal injury in vitro and in vivo. *Pharmacol Biochem Behav*, 73: 439-446, 2002.
67. O'Leary, D. M., Movsesyan, V., Vicini, S., and Faden, A. I. Selective mGluR5 antagonists MPEP and SIB-1893 decrease NMDA or glutamate-mediated neuronal toxicity through actions that reflect NMDA receptor antagonism. *Br J Pharmacol*, 131: 1429-1437, 2000.
68. Movsesyan, V. A., O'Leary, D. M., Fan, L., Bao, W., Mullins, P. G., Knoblach, S. M., and Faden, A. I. mGluR5 antagonists 2-methyl-6-(phenylethynyl)-pyridine and (E)-2-methyl- 6-(2-phenylethenyl)-pyridine reduce traumatic neuronal injury In vitro and In vivo by antagonizing N-methyl-D-aspartate receptors. *J Pharmacol Exp Ther*, 296: 41-47., 2001.
69. Allen, J. W., Knoblach, S. M., and Faden, A. I. Activation of group I metabotropic glutamate receptors reduces neuronal apoptosis but increases necrotic cell death in vitro. *Cell Death Differ*, 7: 470-476, 2000.
70. Mark, R. J., Blanc, E. M., and Mattson, M. P. Amyloid beta-peptide and oxidative cellular injury in Alzheimer's disease. *Mol Neurobiol*, 12: 211-224, 1996.
71. Vickers, J., Dickson, T., Adlard, P., Saunders, H., King, C., and McCormack, G. The cause of neuronal degeneration in Alzheimer's disease. *Prog Neurobiol*, 60: p139-165, 2000.

72. Yaar, M., Zhai, S., Pilch, P. F., Doyle, S. M., Eisenhauer, P. B., Fine, R. E., and Gilchrest, B. A. Binding of beta-amyloid to the p75 neurotrophin receptor induces apoptosis. A possible mechanism for Alzheimer's disease. *J. Clin. Invest.*, 100: 2333-2340, 1997.
73. Wellington, C. L. and Hayden, M. R. Caspases and neurodegeneration: on the cutting edge of new therapeutic approaches. *Clin Genet*, 57: 1-10, 2000.
74. Allen, J. W., Eldadah, B. A., Huang, X., Knoblach, S. M., and Faden, A. I. Multiple caspases are involved in beta-amyloid-induced neuronal apoptosis. *J Neurosci Res*, 65: 45-53., 2001.
75. Li, P., Nijhawan, D., Budihardjo, I., Srinivasula, S. M., Ahmad, M., Alnemri, E. S., and Wang, X. Cytochrome c and dATP-dependent formation of Apaf-1/caspase-9 complex initiates an apoptotic protease cascade. *Cell*, 91: 479-489., 1997.
76. Susin, S. A., Lorenzo, H. K., Zamzami, N., Marzo, I., Snow, B. E., Brothers, G. M., Mangion, J., Jacotot, E., Costantini, P., Loeffler, M., Larochette, N., Goodlett, D. R., Aebersold, R., Siderovski, D. P., Penninger, J. M., and Kroemer, G. Molecular characterization of mitochondrial apoptosis-inducing factor. *Nature*, 397: 441-446, 1999.
77. Daugas, E., Susin, S. A., Zamzami, N., Ferri, K. F., Irinopoulou, T., Larochette, N., Prevost, M. C., Leber, B., Andrews, D., Penninger, J., and Kroemer, G. Mitochondrio-nuclear translocation of AIF in apoptosis and necrosis. *Faseb J*, 14: 729-739, 2000.
78. Joza, N., Susin, S. A., Daugas, E., Stanford, W. L., Cho, S. K., Li, C. Y., Sasaki, T., Elia, A. J., Cheng, H. Y., Ravagnan, L., Ferri, K. F., Zamzami, N., Wakeham, A., Hakem, R., Yoshida, H., Kong, Y. Y., Mak, T. W., Zuniga-Pflucker, J. C., Kroemer, G., and Penninger, J. M. Essential role of the mitochondrial apoptosis-inducing factor in programmed cell death. *Nature*, 410: 549-554, 2001.
79. Zhang, X., Chen, J., Graham, S. H., Du, L., Kochanek, P. M., Draviam, R., Guo, F., Nathaniel, P. D., Szabo, C., Watkins, S. C., and Clark, R. S. Intranuclear localization of apoptosis-inducing factor (AIF) and large scale DNA fragmentation after traumatic brain injury in rats and in neuronal cultures exposed to peroxynitrite. *J Neurochem*, 82: 181-191, 2002.
80. Yu, S. W., Wang, H., Poitras, M. F., Coombs, C., Bowers, W. J., Federoff, H. J., Poirier, G. G., Dawson, T. M., and Dawson, V. L. Mediation of poly(ADP-ribose) polymerase-1-dependent cell death by apoptosis-inducing factor. *Science*, 297: 259-263, 2002.
81. Wang, H., Shimoji, M., Yu, S. W., Dawson, T. M., and Dawson, V. L. Apoptosis inducing factor and PARP-mediated injury in the MPTP mouse model of Parkinson's disease. *Ann N Y Acad Sci*, 991: 132-139, 2003.
82. Luo, X., Budihardjo, I., Zou, H., Slaughter, C., and Wang, X. Bid, a Bcl2 interacting protein, mediates cytochrome c release from mitochondria in response to activation of cell surface death receptors. *Cell*, 94: 481-490, 1998.
83. Guo, Y., Srinivasula, S. M., Druilhe, A., Fernandes-Alnemri, T., and Alnemri, E. S. Caspase-2 induces apoptosis by releasing proapoptotic proteins from mitochondria. *J Biol Chem*, 277: 13430-13437, 2002.
84. Ivins, K. J., Thornton, P. L., Rohn, T. T., and Cotman, C. W. Neuronal apoptosis induced by beta-amyloid is mediated by caspase-8. *Neurobiol Dis*, 6: 440-449, 1999.
85. Ommaya, A. K., Goldsmith, W., and Thibault, L. Biomechanics and neuropathology of adult and paediatric head injury. *Br J Neurosurg*, 16: 220-242, 2002.
86. Meythaler, J. M., Peduzzi, J. D., Eleftheriou, E., and Novack, T. A. Current concepts: diffuse axonal injury-associated traumatic brain injury. *Arch Phys Med Rehabil*, 82: 1461-1471., 2001.
87. Cargill, R. S., 2nd and Thibault, L. E. Acute alterations in [Ca²⁺]_i in NG108-15 cells subjected to high strain rate deformation and chemical hypoxia: an in vitro model for neural trauma. *J Neurotrauma*, 13: 395-407, 1996.
88. Morrison, B., 3rd, Meaney, D. F., and McIntosh, T. K. Mechanical characterization of an in vitro device designed to quantitatively injure living brain tissue. *Ann Biomed Eng*, 26: 381-390, 1998.

89. Smith, D., Wolf, J., Lusardi, T., Lee, V., and Meaney, D. High tolerance and delayed elastic response of cultured axons to dynamic stretch injury. *J Neurosci*, 19: p4263-4269, 1999.
90. Zhang, L., Rzigalinski, B. A., Ellis, E. F., and Satin, L. S. Reduction of voltage-dependent Mg^{2+} blockade of NMDA current in mechanically injured neurons. *Science*, 274: 1921-1923, 1996.
91. Lea IV, P. M., Custer, S. J., Stoica, B. A., and Faden, A. I. Modulation of Stretch-Induced Enhancement of Neuronal NMDA Receptor Current by mGluR1 Depends Upon Presence of Glia. *J. Neurotrauma*, *accepted*, 2003.
92. Lea, P. M., Custer, S. J., Vicini, S., and Faden, A. I. Neuronal and glial mGluR5 modulation prevents stretch-induced enhancement of NMDA receptor current. *Pharmacol Biochem Behav*, 73: 287-298, 2002.
93. Anwyl, R. Metabotropic glutamate receptors: electrophysiological properties and role in plasticity. *Brain Res Brain Res Rev*, 29: 83-120, 1999.
94. Rosenmund, C. and Westbrook, G. L. Calcium-induced actin depolymerization reduces NMDA channel activity. *Neuron*, 10: 805-814., 1993.
95. Holohean, A. M., Hackman, J. C., and Davidoff, R. A. Mechanisms involved in the metabotropic glutamate receptor-enhancement of NMDA-mediated motoneurone responses in frog spinal cord. *Br J Pharmacol*, 126: 333-341, 1999.
96. Krupp, J. J., Vissel, B., Thomas, C. G., Heinemann, S. F., and Westbrook, G. L. Interactions of calmodulin and alpha-actinin with the NR1 subunit modulate Ca^{2+} -dependent inactivation of NMDA receptors. *J Neurosci*, 19: 1165-1178., 1999.
97. Zhang, S., Ehlers, M. D., Bernhardt, J. P., Su, C. T., and Huganir, R. L. Calmodulin mediates calcium-dependent inactivation of N-methyl-D- aspartate receptors. *Neuron*, 21: 443-453., 1998.
98. Ehlers, M. D., Zhang, S., Bernhardt, J. P., and Huganir, R. L. Inactivation of NMDA receptors by direct interaction of calmodulin with the NR1 subunit. *Cell*, 84: 745-755, 1996.
99. Hisatsune, C., Umemori, H., Inoue, T., Michikawa, T., Kohda, K., Mikoshiba, K., and Yamamoto, T. Phosphorylation-dependent regulation of N-methyl-D-aspartate receptors by calmodulin. *J Biol Chem*, 272: 20805-20810., 1997.
100. Chen, N., Luo, T., and Raymond, L. A. Subtype-dependence of NMDA receptor channel open probability. *J Neurosci*, 19: 6844-6854., 1999.
101. Ugolini, A., Corsi, M., and Bordi, F. Potentiation of NMDA and AMPA responses by group I mGluR in spinal cord motoneurons. *Neuropharmacology*, 36: 1047-1055, 1997.
102. Ugolini, A., Corsi, M., and Bordi, F. Potentiation of NMDA and AMPA responses by the specific mGluR5 agonist CHPG in spinal cord motoneurons. *Neuropharmacology*, 38: 1569-1576., 1999.
103. Kawabata, S., Tsutsumi, R., Kohara, A., Yamaguchi, T., Nakanishi, S., and Okada, M. Control of calcium oscillations by phosphorylation of metabotropic glutamate receptors. *Nature*, 383: 89-92, 1996.
104. Kawabata, S., Kohara, A., Tsutsumi, R., Itahana, H., Hayashibe, S., Yamaguchi, T., and Okada, M. Diversity of calcium signaling by metabotropic glutamate receptors. *J Biol Chem*, 273: 17381-17385, 1998.
105. Condorelli, D. F., Dell'Albani, P., Corsaro, M., Giuffrida, R., Caruso, A., Trovato Salinaro, A., Spinella, F., Nicoletti, F., Albanese, V., and Giuffrida Stella, A. M. Metabotropic glutamate receptor expression in cultured rat astrocytes and human gliomas. *Neurochem Res*, 22: 1127-1133, 1997.
106. Miller, S., Romano, C., and Cotman, C. W. Growth factor upregulation of a phosphoinositide-coupled metabotropic glutamate receptor in cortical astrocytes. *J Neurosci*, 15: 6103-6109, 1995.
107. Schools, G. P. and Kimelberg, H. K. mGluR3 and mGluR5 are the predominant metabotropic glutamate receptor mRNAs expressed in hippocampal astrocytes acutely isolated from young rats. *J Neurosci Res*, 58: 533-543, 1999.

108. Ferraguti, F., Corti, C., Valerio, E., Mion, S., and Xuereb, J. Activated astrocytes in areas of kainate-induced neuronal injury upregulate the expression of the metabotropic glutamate receptors 2/3 and 5. *Exp Brain Res*, 137: 1-11., 2001.
109. Nicoletti, F., Bruno, V., Catania, M. V., Battaglia, G., Copani, A., Barbagallo, G., Cena, V., Sanchez-Prieto, J., Spano, P. F., and Pizzi, M. Group-I metabotropic glutamate receptors: hypotheses to explain their dual role in neurotoxicity and neuroprotection. *Neuropharmacology*, 38: 1477-1484, 1999.
110. Silva, G. A., Theriault, E., Mills, L. R., Pennefather, P. S., and Feeney, C. J. Group I and II metabotropic glutamate receptor expression in cultured rat spinal cord astrocytes. *Neurosci Lett*, 263: 117-120, 1999.
111. Romano, C., Yang, W. L., and O'Malley, K. L. Metabotropic glutamate receptor 5 is a disulfide-linked dimer. *J Biol Chem*, 271: 28612-28616, 1996.
112. Romano, C., Miller, J. K., Hyrc, K., Dikranian, S., Mennerick, S., Takeuchi, Y., Goldberg, M. P., and O'Malley, K. L. Covalent and noncovalent interactions mediate metabotropic glutamate receptor mGlu5 dimerization. *Mol Pharmacol*, 59: 46-53., 2001.
113. Robbins, M. J., Ciruela, F., Rhodes, A., and McIlhinney, R. A. Characterization of the dimerization of metabotropic glutamate receptors using an N-terminal truncation of mGluR1alpha. *J Neurochem*, 72: 2539-2547, 1999.
114. Romano, C., Saito, I., and O'Malley, K. L. Metabotropic glutamate receptor dimers. In: D. E. Pellegrini-Giampietro (ed.), *Metabotropic Glutamate Receptors and Brain Function*, pp. 1-7. London and Miami: Portland Press, 1998.
115. Faden, A. I. Pharmacological treatment approaches for brain and spinal cord trauma. In: J. T. Povlishock (ed.), *Neurotrauma*, pp. 1479-1490. New York: McGraw-Hill, 1996.
116. McIntosh, T. K. Neurochemical sequelae of traumatic brain injury: therapeutic implications. *Cerebrovasc Brain Metab Rev*, 6: 109-162., 1994.
117. Faden, A. I. Neuroprotection and traumatic brain injury: theoretical option or realistic proposition. *Curr Opin Neurol*, 15: 707-712., 2002.
118. Bracken, M. B. and Holford, T. R. Effects of timing of methylprednisolone or naloxone administration on recovery of segmental and long-tract neurological function in NASCIS 2. *J Neurosurg*, 79: 500-507., 1993.
119. Pitts, L. H., Ross, A., Chase, G. A., and Faden, A. I. Treatment with thyrotropin-releasing hormone (TRH) in patients with traumatic spinal cord injuries. *J Neurotrauma*, 12: 235-243., 1995.
120. Arias, M. J. Treatment of experimental spinal cord injury with TRH, naloxone, and dexamethasone. *Surg Neurol*, 28: 335-338., 1987.
121. Ceylan, S., Ilbay, K., Baykal, S., Sener, U., Ozmenoglu, M., Kalelioglu, M., Akturk, F., Komsuoglu, S. S., and Ozoran, A. Treatment of acute spinal cord injuries: comparison of thyrotropin-releasing hormone and nimodipine. *Res Exp Med*, 192: 23-33, 1992.
122. Akdemir, H., Pasaoglu, H., Arman, F., Coksevim, B., and Pasaoglu, A. Effects of TRH and high-dose corticosteroid therapy on evoked potentials, and tissue Na⁺, K⁺ and water content in experimental spinal injury. *Res Exp Med*, 193: 297-304, 1993.
123. Behrmann, D. L., Bresnahan, J. C., and Beattie, M. S. Modeling of acute spinal cord injury in the rat: neuroprotection and enhanced recovery with methylprednisolone, U-74006F and YM-14673. *Exp Neurol*, 126: 61-75., 1994.
124. Puniak, M. A., Freeman, G. M., Agresta, C. A., Van Newkirk, L., Barone, C. A., and Salzman, S. K. Comparison of a serotonin antagonist, opioid antagonist, and TRH analog for the acute treatment of experimental spinal trauma. *J Neurotrauma*, 8: 193-203., 1991.
125. Faden, A. I., Jacobs, T. P., Smith, M. T., and Holaday, J. W. Comparison of thyrotropin-releasing hormone (TRH), naloxone, and dexamethasone treatments in experimental spinal injury. *Neurology*, 33: 673-678, 1983.

126. Faden, A. I., Labroo, V. M., and Cohen, L. A. Imidazole-substituted analogues of TRH limit behavioral deficits after experimental brain trauma. *J Neurotrauma*, 10: 101-108., 1993.
127. Faden, A. I., Fox, G. B., Fan, L., Araldi, G. L., Qiao, L., Wang, S., and Kozikowski, A. P. Novel TRH analog improves motor and cognitive recovery after traumatic brain injury in rodents. *Am J Physiol*, 277: R1196-1204., 1999.
128. McIntosh, T. K., Vink, R., and Faden, A. I. An analogue of thyrotropin-releasing hormone improves outcome after brain injury: ³¹P-NMR studies. *Am J Physiol*, 254: R785-792., 1988.
129. Koskinen, L. O. Effect of low intravenous doses of TRH, acid-TRH and cyclo(His-Pro) on cerebral and peripheral blood flows. *Br J Pharmacol*, 87: 509-519., 1986.
130. Vink, R., McIntosh, T. K., and Faden, A. I. Treatment with the thyrotropin-releasing hormone analog CG3703 restores magnesium homeostasis following traumatic brain injury in rats. *Brain Res*, 460: 184-188., 1988.
131. Yarbrough, G. G. On the neuropharmacology of thyrotropin releasing hormone (TRH). *Prog Neurobiol*, 12: 291-312, 1979.
132. Prasad, C. Bioactive cyclic dipeptides. *Peptides*, 16: 151-164, 1995.
133. Faden, A. I., Knoblach, S. M., Cernak, I., Fan, L., Vink, R., Araldi, G. L., Fricke, S. T., Roth, B. L., and Kozikowski, A. P. Novel diketopiperazine enhances motor and cognitive recovery after traumatic brain injury in rats and shows neuroprotection in vitro and in vivo. *J Cereb Blood Flow Metab*, 23: 342-354., 2003.
134. Faden, A. I., Fox, G. B., Di, X., Knoblach, S. M., Cernak, I., Mullins, P., Nikolaeva, M., and Kozikowski, A. P. Neuroprotective and nootropic actions of a novel cyclized dipeptide after controlled cortical impact injury in mice. *J Cereb Blood Flow Metab*, 23: 355-363., 2003.
135. Fox, G. B., Fan, L., Levasseur, R. A., and Faden, A. I. Sustained sensory/motor and cognitive deficits with neuronal apoptosis following controlled cortical impact brain injury in the mouse. *J Neurotrauma*, 15: 599-614, 1998.
136. Faden, A. I., Demediuk, P., Panter, S. S., and Vink, R. The role of excitatory amino acids and NMDA receptors in traumatic brain injury. *Science*, 244: 798-800, 1989.
137. Graham, D. I., Gentleman, S. M., Nicoll, J. A., Royston, M. C., McKenzie, J. E., Roberts, G. W., Mrak, R. E., and Griffin, W. S. Is there a genetic basis for the deposition of beta-amyloid after fatal head injury? *Cell Mol Neurobiol*, 19: 19-30, 1999.
138. Allen, J. W., Ivanova, S. A., Fan, L., Espey, M. G., Basile, A. S., and Faden, A. I. Group II metabotropic glutamate receptor activation attenuates traumatic neuronal injury and improves neurological recovery after traumatic brain injury. *J Pharmacol Exp Ther*, 290: 112-120, 1999.
139. Zhao, X., Pike, B. R., Newcomb, J. K., Wang, K. K., Posmantur, R. M., and Hayes, R. L. Maitotoxin induces calpain but not caspase-3 activation and necrotic cell death in primary septo-hippocampal cultures. *Neurochem Res*, 24: 371-382., 1999.
140. Prakash, K. R., Tang, Y., Kozikowski, A. P., Flippen-Anderson, J. L., Knoblach, S. M., and Faden, A. I. Synthesis and biological activity of novel neuroprotective diketopiperazines. *Bioorg Med Chem*, 10: 3043-3048, 2002.
141. Metcalf, G. Regulatory peptides as a source of new drugs--the clinical prospects for analogues of TRH which are resistant to metabolic degradation. *Brain Res*, 257: 389-408., 1982.
142. Abe, K. and Saito, H. Effects of basic fibroblast growth factor on central nervous system functions. *Pharmacol Res*, 43: 307-312, 2001.
143. Czubayko, F., Liaudet-Coopman, E. D., Aigner, A., Tuveson, A. T., Berchem, G. J., and Wellstein, A. A secreted FGF-binding protein can serve as the angiogenic switch in human cancer. *Nat Med*, 3: 1137-1140, 1997.

144. Czubayko, F., Smith, R. V., Chung, H. C., and Wellstein, A. Tumor growth and angiogenesis induced by a secreted binding protein for fibroblast growth factors. *J Biol Chem*, 269: 28243-28248, 1994.
145. Kurtz, A., Wang, H. L., Darwiche, N., Harris, V., and Wellstein, A. Expression of a binding protein for FGF is associated with epithelial development and skin carcinogenesis. *Oncogene*, 14: 2671-2681, 1997.
146. Tassi, E., Al-Attar, A., Aigner, A., Swift, M. R., McDonnell, K., Karavanov, A., and Wellstein, A. Enhancement of fibroblast growth factor (FGF) activity by an FGF-binding protein. *J Biol Chem*, 276: 40247-40253, 2001.
147. Toman, R. E., Movsesyan, V., Murthy, S. K., Milstien, S., Spiegel, S., and Faden, A. I. Ceramide-induced cell death in primary neuronal cultures: upregulation of ceramide levels during neuronal apoptosis. *J Neurosci Res*, 68: 323-330, 2002.
148. Movsesyan, V. A., Yakovlev, A. G., Dabaghyan, E. A., Stoica, B. A., and Faden, A. I. Ceramide induces neuronal apoptosis through the caspase-9/caspase-3 pathway. *Biochem Biophys Res Commun*, 299: 201-207, 2002.
149. Stoica, B. A., Movsesyan, V. A., Lea, P. M. t., and Faden, A. I. Ceramide-induced neuronal apoptosis is associated with dephosphorylation of Akt, BAD, FKHR, GSK-3beta, and induction of the mitochondrial-dependent intrinsic caspase pathway. *Mol Cell Neurosci*, 22: 365-382, 2003.
150. Di Giovanni, S., Knoblach, S. M., Brandoli, C., Aden, S. A., Hoffman, E. P., and Faden, A. I. Gene profiling in spinal cord injury shows role of cell cycle in neuronal death. *Ann Neurol*, 53: 454-468, 2003.
151. Vink, R. and Cernak, I. Brain injury, investigating metabolic aspects using magnetic resonance. *In: B. Smith (ed.), Encyclopedia of Neuroscience*, 3rd Edition edition, Vol. CD-ROM. Amsterdam: Elsevier Science Publisher, 2003.
152. Vink, R. and Cernak, I. Regulation of intracellular free magnesium in central nervous system injury. *Front Biosci*, 5: D656-665, 2000.
153. Lin, Y. J. and Koretsky, A. P. Manganese ion enhances T1-weighted MRI during brain activation: an approach to direct imaging of brain function. *Magn Reson Med*, 38: 378-388, 1997.
154. Morita, H., Ogino, T., Seo, Y., Fujiki, N., Tanaka, K., Takamata, A., Nakamura, S., and Murakami, M. Detection of hypothalamic activation by manganese ion contrasted T(1)-weighted magnetic resonance imaging in rats. *Neurosci Lett*, 326: 101-104, 2002.
155. Aoki, I., Ebisu, T., Tanaka, C., Katsuta, K., Fujikawa, A., Umeda, M., Fukunaga, M., Takegami, T., Shapiro, E. M., and Naruse, S. Detection of the anoxic depolarization of focal ischemia using manganese-enhanced MRI. *Magn Reson Med*, 50: 7-12, 2003.
156. Shibuya, I. and Douglas, W. W. Indications from Mn-quenching of Fura-2 fluorescence in melanotrophs that dopamine and baclofen close Ca channels that are spontaneously open but not those opened by high [K⁺]_o; and that Cd preferentially blocks the latter. *Cell Calcium*, 14: 33-44, 1993.
157. Narita, K., Kawasaki, F., and Kita, H. Mn and Mg influxes through Ca channels of motor nerve terminals are prevented by verapamil in frogs. *Brain Res*, 510: 289-295, 1990.
158. Yakovlev, A. G. and Faden, A. I. Molecular biology of CNS injury. *J Neurotrauma*, 12: 767-777., 1995.
159. Kalb, R. K. and Strittmatter, S. M. *Neurobiology of Spinal Cord Injury*, p. 113-158. New Jersey: Humana Press, 2000.
160. Dumont, R. J., Okonkwo, D. O., Verma, S., Hurlbert, R. J., Boulos, P. T., Ellegala, D. B., and Dumont, A. S. Acute spinal cord injury, part I: pathophysiologic mechanisms. *Clin Neuropharmacol*, 24: 254-264., 2001.
161. Carmel, J. B., Galante, A., Soteropoulos, P., Tolias, P., Recce, M., Young, W., and Hart, R. P. Gene expression profiling of acute spinal cord injury reveals spreading inflammatory signals and neuron loss. *Physiol Genomics*, 7: 201-213., 2001.

162. Song, G., Cechvala, C., Resnick, D. K., Dempsey, R. J., and Rao, V. L. GeneChip analysis after acute spinal cord injury in rat. *J Neurochem*, 79: 804-815., 2001.
163. Bareyre, F. M. and Schwab, M. E. Inflammation, degeneration and regeneration in the injured spinal cord: insights from DNA microarrays. *Trends Neurosci*, 26: 555-563, 2003.
164. Yakovlev, A. G. and Faden, A. I. Sequential expression of c-fos protooncogene, TNF-alpha, and dynorphin genes in spinal cord following experimental traumatic injury. *Mol Chem Neuropathol*, 23: 179-190., 1994.
165. Hill, C. E., Beattie, M. S., and Bresnahan, J. C. Degeneration and sprouting of identified descending supraspinal axons after contusive spinal cord injury in the rat. *Exp Neurol*, 171: 153-169, 2001.
166. Beattie, M. S., Hermann, G. E., Rogers, R. C., and Bresnahan, J. C. Cell death in models of spinal cord injury. *Prog Brain Res*, 137: 37-47, 2002.
167. Marcus, J. and Popko, B. Galactolipids are molecular determinants of myelin development and axo-glial organization. *Biochim Biophys Acta*, 1573: 406-413, 2002.
168. Dewar, D. and Dawson, D. A. Changes of cytoskeletal protein immunostaining in myelinated fibre tracts after focal cerebral ischaemia in the rat. *Acta Neuropathol (Berl)*, 93: 71-77, 1997.
169. Nunez, J. and Fischer, I. Microtubule-associated proteins (MAPs) in the peripheral nervous system during development and regeneration. *J Mol Neurosci*, 8: 207-222, 1997.
170. Azmitia, E. C. Cajal's hypotheses on neurobionics and neurotropic factor match properties of microtubules and S-100 beta. *Prog Brain Res*, 136: 87-100, 2002.
171. Schwab, M. E. Repairing the injured spinal cord. *Science*, 295: 1029-1031, 2002.
172. Markus, A., Patel, T. D., and Snider, W. D. Neurotrophic factors and axonal growth. *Curr Opin Neurobiol*, 12: 523-531, 2002.
173. Solly, S. K., Thomas, J. L., Monge, M., Demerens, C., Lubetzki, C., Gardinier, M. V., Matthieu, J. M., and Zalc, B. Myelin/oligodendrocyte glycoprotein (MOG) expression is associated with myelin deposition. *Glia*, 18: 39-48, 1996.
174. Merkler, D., Metz, G. A., Raineteau, O., Dietz, V., Schwab, M. E., and Fouad, K. Locomotor recovery in spinal cord-injured rats treated with an antibody neutralizing the myelin-associated neurite growth inhibitor Nogo-A. *J Neurosci*, 21: 3665-3673, 2001.
175. Fouad, K., Dietz, V., and Schwab, M. E. Improving axonal growth and functional recovery after experimental spinal cord injury by neutralizing myelin associated inhibitors. *Brain Res Brain Res Rev*, 36: 204-212, 2001.
176. Condic, M. L. and Lemons, M. L. Extracellular matrix in spinal cord regeneration: getting beyond attraction and inhibition. *Neuroreport*, 13: A37-48, 2002.
177. Wang, K. C., Koprivica, V., Kim, J. A., Sivasankaran, R., Guo, Y., Neve, R. L., and He, Z. Oligodendrocyte-myelin glycoprotein is a Nogo receptor ligand that inhibits neurite outgrowth. *Nature*, 417: 941-944, 2002.
178. Menet, V., Prieto, M., Privat, A., and Gimenez y Ribotta, M. Axonal plasticity and functional recovery after spinal cord injury in mice deficient in both glial fibrillary acidic protein and vimentin genes. *Proc Natl Acad Sci U S A*, 100: 8999-9004, 2003.
179. Alonso, G., Ridet, J. L., Oestreicher, A. B., Gispén, W. H., and Privat, A. B-50 (GAP-43) immunoreactivity is rarely detected within intact catecholaminergic and serotonergic axons innervating the brain and spinal cord of the adult rat, but is associated with these axons following lesion. *Exp Neurol*, 134: 35-48, 1995.
180. Gavazzi, I. Semaphorin-neuropilin-1 interactions in plasticity and regeneration of adult neurons. *Cell Tissue Res*, 305: 275-284, 2001.
181. Raineteau, O. and Schwab, M. E. Plasticity of motor systems after incomplete spinal cord injury. *Nat Rev Neurosci*, 2: 263-273, 2001.

182. Bulsara, K. R., Iskandar, B. J., Villavicencio, A. T., and Skene, J. H. A new millenium for spinal cord regeneration: growth-associated genes. *Spine*, 27: 1946-1949, 2002.
183. Mori, N. and Morii, H. SCG10-related neuronal growth-associated proteins in neural development, plasticity, degeneration, and aging. *J Neurosci Res*, 70: 264-273, 2002.
184. Aubert, I., Ridet, J. L., and Gage, F. H. Regeneration in the adult mammalian CNS: guided by development. *Curr Opin Neurobiol*, 5: 625-635, 1995.
185. Nicholls, J. and Saunders, N. Regeneration of immature mammalian spinal cord after injury. *Trends Neurosci*, 19: 229-234, 1996.
186. Kikukawa, S., Kawaguchi, S., Mizoguchi, A., Ide, C., and Koshinaga, M. Regeneration of dorsal column axons after spinal cord injury in young rats. *Neurosci Lett*, 249: 135-138, 1998.
187. Kawasaki, T., Nishio, T., Kawaguchi, S., and Kurosawa, H. Spatiotemporal distribution of GAP-43 in the developing rat spinal cord: a histological and quantitative immunofluorescence study. *Neurosci Res*, 39: 347-358, 2001.
188. Pellier-Monnin, V., Astic, L., Bichet, S., Riederer, B. M., and Grenningloh, G. Expression of SCG10 and stathmin proteins in the rat olfactory system during development and axonal regeneration. *J Comp Neurol*, 433: 239-254, 2001.
189. Holm, K. and Isacson, O. Factors intrinsic to the neuron can induce and maintain its ability to promote axonal outgrowth: a role for BCL2? *Trends Neurosci*, 22: 269-273, 1999.
190. Holm, K. H., Cicchetti, F., Bjorklund, L., Boonman, Z., Tandon, P., Costantini, L. C., Deacon, T. W., Huang, X., Chen, D. F., and Isacson, O. Enhanced axonal growth from fetal human bcl-2 transgenic mouse dopamine neurons transplanted to the adult rat striatum. *Neuroscience*, 104: 397-405, 2001.
191. Vairo, G., Soos, T. J., Upton, T. M., Zalvide, J., DeCaprio, J. A., Ewen, M. E., Koff, A., and Adams, J. M. Bcl-2 retards cell cycle entry through p27(Kip1), pRB relative p130, and altered E2F regulation. *Mol Cell Biol*, 20: 4745-4753, 2000.
192. Copani, A., Uberti, D., Sortino, M. A., Bruno, V., Nicoletti, F., and Memo, M. Activation of cell-cycle-associated proteins in neuronal death: a mandatory or dispensable path? *Trends Neurosci*, 24: 25-31., 2001.
193. Liu, D. X. and Greene, L. A. Neuronal apoptosis at the G1/S cell cycle checkpoint. *Cell Tissue Res*, 305: 217-228., 2001.
194. Liu, X. Z., Xu, X. M., Hu, R., Du, C., Zhang, S. X., McDonald, J. W., Dong, H. X., Wu, Y. J., Fan, G. S., Jacquin, M. F., Hsu, C. Y., and Choi, D. W. Neuronal and glial apoptosis after traumatic spinal cord injury. *J Neurosci*, 17: 5395-5406., 1997.
195. Beattie, M. S., Farooqui, A. A., and Bresnahan, J. C. Review of current evidence for apoptosis after spinal cord injury. *J Neurotrauma*, 17: 915-925., 2000.
196. Fawcett, J. W. and Asher, R. A. The glial scar and central nervous system repair. *Brain Res Bull*, 49: 377-391., 1999.
197. McDonald, J. W. and Sadowsky, C. Spinal-cord injury. *Lancet*, 359: 417-425., 2002.
198. Kangas, A., Nicholson, D. W., and Holtta, E. Involvement of CPP32/Caspase-3 in c-Myc-induced apoptosis. *Oncogene*, 16: 387-398., 1998.
199. Adachi, S., Obaya, A. J., Han, Z., Ramos-Desimone, N., Wyche, J. H., and Sedivy, J. M. c-Myc is necessary for DNA damage-induced apoptosis in the G(2) phase of the cell cycle. *Mol Cell Biol*, 21: 4929-4937., 2001.
200. Hollander, M. C., Sheikh, M. S., Bulavin, D. V., Lundgren, K., Augeri-Henmueller, L., Shehee, R., Molinaro, T. A., Kim, K. E., Tolosa, E., Ashwell, J. D., Rosenberg, M. P., Zhan, Q., Fernandez-Salguero, P. M., Morgan, W. F., Deng, C. X., and Fornace, A. J., Jr. Genomic instability in Gadd45a-deficient mice. *Nat Genet*, 23: 176-184., 1999.

201. Sheikh, M. S., Hollander, M. C., and Fornace, A. J., Jr. Role of Gadd45 in apoptosis. *Biochem Pharmacol*, 59: 43-45., 2000.
202. Smith, M. L., Ford, J. M., Hollander, M. C., Bortnick, R. A., Amundson, S. A., Seo, Y. R., Deng, C. X., Hanawalt, P. C., and Fornace, A. J., Jr. p53-mediated DNA repair responses to UV radiation: studies of mouse cells lacking p53, p21, and/or gadd45 genes. *Mol Cell Biol*, 20: 3705-3714., 2000.
203. Tang, Y., Lu, A., Aronow, B. J., Wagner, K. R., and Sharp, F. R. Genomic responses of the brain to ischemic stroke, intracerebral haemorrhage, kainate seizures, hypoglycemia, and hypoxia. *Eur J Neurosci*, 15: 1937-1952, 2002.
204. Evan, G. I., Wyllie, A. H., Gilbert, C. S., Littlewood, T. D., Land, H., Brooks, M., Waters, C. M., Penn, L. Z., and Hancock, D. C. Induction of apoptosis in fibroblasts by c-myc protein. *Cell*, 69: 119-128., 1992.
205. Prendergast, G. C. Mechanisms of apoptosis by c-Myc. *Oncogene*, 18: 2967-2987., 1999.
206. Deschesnes, R. G., Huot, J., Valerie, K., and Landry, J. Involvement of p38 in apoptosis-associated membrane blebbing and nuclear condensation. *Mol Biol Cell*, 12: 1569-1582., 2001.
207. Wang, S., Nath, N., Minden, A., and Chellappan, S. Regulation of Rb and E2F by signal transduction cascades: divergent effects of JNK1 and p38 kinases. *Embo J*, 18: 1559-1570., 1999.
208. Mateyak, M. K., Obaya, A. J., and Sedivy, J. M. c-Myc regulates cyclin D-Cdk4 and -Cdk6 activity but affects cell cycle progression at multiple independent points. *Mol Cell Biol*, 19: 4672-4683., 1999.
209. Santoni-Rugiu, E., Falck, J., Mailand, N., Bartek, J., and Lukas, J. Involvement of Myc activity in a G(1)/S-promoting mechanism parallel to the pRb/E2F pathway. *Mol Cell Biol*, 20: 3497-3509., 2000.
210. Johnson, D. G., Schwarz, J. K., Cress, W. D., and Nevins, J. R. Expression of transcription factor E2F1 induces quiescent cells to enter S phase. *Nature*, 365: 349-352., 1993.
211. Shan, B. and Lee, W. H. Deregulated expression of E2F-1 induces S-phase entry and leads to apoptosis. *Mol Cell Biol*, 14: 8166-8173., 1994.
212. Henriksson, M. and Lüscher, B. Proteins of the Myc network: essential regulators of cell growth and differentiation. *Adv Cancer Res*, 68: 109-182, 1996.
213. Amati, B., Alevizopoulos, K., and Vlach, J. Myc and the cell cycle. *Front Biosci*, 3: D250-268., 1998.
214. Leone, G., Sears, R., Huang, E., Rempel, R., Nuckolls, F., Park, C. H., Giangrande, P., Wu, L., Saavedra, H. I., Field, S. J., Thompson, M. A., Yang, H., Fujiwara, Y., Greenberg, M. E., Orkin, S., Smith, C., and Nevins, J. R. Myc requires distinct E2F activities to induce S phase and apoptosis. *Mol Cell*, 8: 105-113., 2001.
215. Connell-Crowley, L., Harper, J. W., and Goodrich, D. W. Cyclin D1/Cdk4 regulates retinoblastoma protein-mediated cell cycle arrest by site-specific phosphorylation. *Mol Biol Cell*, 8: 287-301., 1997.
216. Ezhevsky, S. A., Nagahara, H., Vocero-Akbani, A. M., Gius, D. R., Wei, M. C., and Dowdy, S. F. Hypo-phosphorylation of the retinoblastoma protein (pRb) by cyclin D:Cdk4/6 complexes results in active pRb. *Proc Natl Acad Sci U S A*, 94: 10699-10704., 1997.
217. Giovanni, A., Keramaris, E., Morris, E. J., Hou, S. T., O'Hare, M., Dyson, N., Robertson, G. S., Slack, R. S., and Park, D. S. E2F1 mediates death of B-amyloid-treated cortical neurons in a manner independent of p53 and dependent on Bax and caspase 3. *J Biol Chem*, 275: 11553-11560., 2000.
218. Shivji, K. K., Kenny, M. K., and Wood, R. D. Proliferating cell nuclear antigen is required for DNA excision repair. *Cell*, 69: 367-374., 1992.
219. Freeman, R. S., Estus, S., and Johnson, E. M., Jr. Analysis of cell cycle-related gene expression in postmitotic neurons: selective induction of Cyclin D1 during programmed cell death. *Neuron*, 12: 343-355., 1994.
220. Kranenburg, O., van der Eb, A. J., and Zantema, A. Cyclin D1 is an essential mediator of apoptotic neuronal cell death. *Embo J*, 15: 46-54., 1996.

221. Boutillier, A. L., Trinh, E., and Loeffler, J. P. Caspase-dependent cleavage of the retinoblastoma protein is an early step in neuronal apoptosis. *Oncogene*, 19: 2171-2178., 2000.
222. Park, D. S., Morris, E. J., Bremner, R., Keramaris, E., Padmanabhan, J., Rosenbaum, M., Shelanski, M. L., Geller, H. M., and Greene, L. A. Involvement of retinoblastoma family members and E2F/DP complexes in the death of neurons evoked by DNA damage. *J Neurosci*, 20: 3104-3114., 2000.
223. van Lookeren Campagne, M. and Gill, R. Cell cycle-related gene expression in the adult rat brain: selective induction of cyclin G1 and p21WAF1/CIP1 in neurons following focal cerebral ischemia. *Neuroscience*, 84: 1097-1112., 1998.
224. Sakurai, M., Hayashi, T., Abe, K., Itoyama, Y., Tabayashi, K., and Rosenblum, W. I. Cyclin D1 and Cdk4 protein induction in motor neurons after transient spinal cord ischemia in rabbits. *Stroke*, 31: 200-207., 2000.
225. Padmanabhan, J., Park, D. S., Greene, L. A., and Shelanski, M. L. Role of cell cycle regulatory proteins in cerebellar granule neuron apoptosis. *J Neurosci*, 19: 8747-8756., 1999.
226. Ino, H. and Chiba, T. Cyclin-dependent kinase 4 and cyclin D1 are required for excitotoxin- induced neuronal cell death in vivo. *J Neurosci*, 21: 6086-6094., 2001.
227. Bartek, J. and Lukas, J. Pathways governing G1/S transition and their response to DNA damage. *FEBS Lett*, 490: 117-122., 2001.
228. Naeve, G. S., Ramakrishnan, M., Kramer, R., Hevroni, D., Citri, Y., and Theill, L. E. Neuritin: a gene induced by neural activity and neurotrophins that promotes neuritogenesis. *Proc Natl Acad Sci U S A*, 94: 2648-2653, 1997.
229. Corriveau, R. A., Shatz, C. J., and Nedivi, E. Dynamic regulation of cpg15 during activity-dependent synaptic development in the mammalian visual system. *J Neurosci*, 19: 7999-8008, 1999.
230. Cantalops, I., Haas, K., and Cline, H. T. Postsynaptic CPG15 promotes synaptic maturation and presynaptic axon arbor elaboration in vivo. *Nat Neurosci*, 3: 1004-1011, 2000.
231. Nedivi, E., Wu, G. Y., and Cline, H. T. Promotion of dendritic growth by CPG15, an activity-induced signaling molecule. *Science*, 281: 1863-1866, 1998.
232. Lee, W. C. and Nedivi, E. Extended plasticity of visual cortex in dark-reared animals may result from prolonged expression of cpg15-like genes. *J Neurosci*, 22: 1807-1815, 2002.
233. Nedivi, E., Javaherian, A., Cantalops, I., and Cline, H. T. Developmental regulation of CPG15 expression in Xenopus. *J Comp Neurol*, 435: 464-473, 2001.
234. Lu, X., Gunn, T. M., Shieh, K., Barsh, G. S., Akil, H., and Watson, S. J. Distribution of Mahogany/Attractin mRNA in the rat central nervous system. *FEBS Lett*, 462: 101-107, 1999.
235. Kuramoto, T., Kitada, K., Inui, T., Sasaki, Y., Ito, K., Hase, T., Kawaguchi, S., Ogawa, Y., Nakao, K., Barsh, G. S., Nagao, M., Ushijima, T., and Serikawa, T. Attractin/mahogany/zitter plays a critical role in myelination of the central nervous system. *Proc Natl Acad Sci U S A*, 98: 559-564, 2001.
236. Tang, W. and Duke-Cohan, J. S. Human secreted attractin disrupts neurite formation in differentiating cortical neural cells in vitro. *J Neuropathol Exp Neurol*, 61: 767-777, 2002.
237. Vaillant, A. R., Muller, R., Langkopf, A., and Brown, D. L. Characterization of the microtubule-binding domain of microtubule-associated protein 1A and its effects on microtubule dynamics. *J Biol Chem*, 273: 13973-13981, 1998.
238. Noiges, R., Eichinger, R., Kutschera, W., Fischer, I., Nemeth, Z., Wiche, G., and Propst, F. Microtubule-associated protein 1A (MAP1A) and MAP1B: light chains determine distinct functional properties. *J Neurosci*, 22: 2106-2114, 2002.
239. Oudega, M., Touri, F., Deenen, M. G., Riederer, B. M., and Marani, E. Microtubule-associated protein 1a is involved in the early development of the rat spinal cord. *Neurosci Lett*, 246: 81-84, 1998.

240. Cornea-Hebert, V., Watkins, K. C., Roth, B. L., Kroeze, W. K., Gaudreau, P., Leclerc, N., and Descarries, L. Similar ultrastructural distribution of the 5-HT(2A) serotonin receptor and microtubule-associated protein MAP1A in cortical dendrites of adult rat. *Neuroscience*, 113: 23-35, 2002.
241. Turnley, A. M. and Bartlett, P. F. MAG and MOG enhance neurite outgrowth of embryonic mouse spinal cord neurons. *Neuroreport*, 9: 1987-1990, 1998.
242. Coffey, J. C. and McDermott, K. W. The regional distribution of myelin oligodendrocyte glycoprotein (MOG) in the developing rat CNS: an in vivo immunohistochemical study. *J Neurocytol*, 26: 149-161, 1997.
243. Li, G., Crang, A. J., Rundle, J. L., and Blakemore, W. F. Oligodendrocyte progenitor cells in the adult rat CNS express myelin oligodendrocyte glycoprotein (MOG). *Brain Pathol*, 12: 463-471, 2002.
244. Ackley, B. D., Crew, J. R., Elamaa, H., Pihlajaniemi, T., Kuo, C. J., and Kramer, J. M. The NC1/endostatin domain of *Caenorhabditis elegans* type XVIII collagen affects cell migration and axon guidance. *J Cell Biol*, 152: 1219-1232, 2001.
245. Gallo, G. and Letourneau, P. C. Axon guidance: GTPases help axons reach their targets. *Curr Biol*, 8: R80-82, 1998.
246. Mochizuki, N., Yamashita, S., Kurokawa, K., Ohba, Y., Nagai, T., Miyawaki, A., and Matsuda, M. Spatio-temporal images of growth-factor-induced activation of Ras and Rap1. *Nature*, 411: 1065-1068, 2001.
247. Kuwamura, M., Maeda, M., Kuramoto, T., Kitada, K., Kanehara, T., Moriyama, M., Nakane, Y., Yamate, J., Ushijima, T., Kotani, T., and Serikawa, T. The myelin vacuolation (mv) rat with a null mutation in the attractin gene. *Lab Invest*, 82: 1279-1286, 2002.
248. Long, K. E. and Lemmon, V. Dynamic regulation of cell adhesion molecules during axon outgrowth. *J Neurobiol*, 44: 230-245, 2000.
249. Araki, T. and Milbrandt, J. Ninjurin, a novel adhesion molecule, is induced by nerve injury and promotes axonal growth. *Neuron*, 17: 353-361, 1996.
250. Mirza, A., Wu, Q., Wang, L., McClanahan, T., Bishop, W. R., Gheys, F., Ding, W., Hutchins, B., Hockenberry, T., Kirschmeier, P., Greene, J. R., and Liu, S. Global transcriptional program of p53 target genes during the process of apoptosis and cell cycle progression. *Oncogene*, 22: 3645-3654, 2003.
251. Bellefroid, E. J., Bourguignon, C., Hollemann, T., Ma, Q., Anderson, D. J., Kintner, C., and Pieler, T. X-MyT1, a *Xenopus* C2HC-type zinc finger protein with a regulatory function in neuronal differentiation. *Cell*, 87: 1191-1202, 1996.
252. Ashkenazi, A. and Dixit, V. M. Death receptors: signaling and modulation. *Science*, 281: 1305-1308., 1998.
253. Aravind, L., Dixit, V. M., and Koonin, E. V. The domains of death: evolution of the apoptosis machinery. *Trends Biochem Sci*, 24: 47-53., 1999.
254. Nagata, S. Apoptosis by death factor. *Cell*, 88: 355-365, 1997.
255. Boldin, M. P., Goncharov, T. M., Goltsev, Y. V., and Wallach, D. Involvement of MACH, a novel MORT1/FADD-interacting protease, in Fas/APO-1- and TNF receptor-induced cell death. *Cell*, 85: 803-815, 1996.
256. Fernandes-Alnemri, T., Armstrong, R. C., Krebs, J., Srinivasula, S. M., Wang, L., Bullrich, F., Fritz, L. C., Trapani, J. A., Tomaselli, K. J., Litwack, G., and Alnemri, E. S. In vitro activation of CPP32 and Mch3 by Mch4, a novel human apoptotic cysteine protease containing two FADD-like domains. *Proc Natl Acad Sci U S A*, 93: 7464-7469, 1996.
257. Muzio, M., Chinnaiyan, A. M., Kischkel, F. C., O'Rourke, K., Shevchenko, A., Ni, J., Scaffidi, C., Bretz, J. D., Zhang, M., Gentz, R., Mann, M., Krammer, P. H., Peter, M. E., and Dixit, V. M. FLICE, a novel FADD-homologous ICE/CED-3-like protease, is recruited to the CD95 (Fas/APO-1) death-inducing signaling complex. *Cell*, 85: 817-827, 1996.

258. Kischkel, F. C., Hellbardt, S., Behrmann, I., Germer, M., Pawlita, M., Krammer, P. H., and Peter, M. E. Cytotoxicity-dependent APO-1 (Fas/CD95)-associated proteins form a death-inducing signaling complex (DISC) with the receptor. *Embo J*, 14: 5579-5588, 1995.
259. Li, H., Zhu, H., Xu, C. J., and Yuan, J. Cleavage of BID by caspase 8 mediates the mitochondrial damage in the Fas pathway of apoptosis. *Cell*, 94: 491-501, 1998.
260. Murphy, K. M., Streips, U. N., and Lock, R. B. Bax membrane insertion during Fas(CD95)-induced apoptosis precedes cytochrome c release and is inhibited by Bcl-2. *Oncogene*, 18: 5991-5999., 1999.
261. Kudla, G., Montessuit, S., Eskes, R., Berrier, C., Martinou, J. C., Ghazi, A., and Antonsson, B. The destabilization of lipid membranes induced by the C-terminal fragment of caspase 8-cleaved bid is inhibited by the N-terminal fragment. *J Biol Chem*, 275: 22713-22718, 2000.
262. Irmeler, M., Thome, M., Hahne, M., Schneider, P., Hofmann, K., Steiner, V., Bodmer, J. L., Schroter, M., Burns, K., Mattmann, C., Rimoldi, D., French, L. E., and Tschopp, J. Inhibition of death receptor signals by cellular FLIP [see comments]. *Nature*, 388: 190-195, 1997.
263. Zou, H., Henzel, W. J., Liu, X., Lutschg, A., and Wang, X. Apaf-1, a human protein homologous to *C. elegans* CED-4, participates in cytochrome c-dependent activation of caspase-3 [see comments]. *Cell*, 90: 405-413, 1997.
264. Zou, H., Li, Y., Liu, X., and Wang, X. An APAF-1.cytochrome c multimeric complex is a functional apoptosome that activates procaspase-9. *J Biol Chem*, 274: 11549-11556., 1999.
265. Slee, E. A., Harte, M. T., Kluck, R. M., Wolf, B. B., Casiano, C. A., Newmeyer, D. D., Wang, H. G., Reed, J. C., Nicholson, D. W., Alnemri, E. S., Green, D. R., and Martin, S. J. Ordering the cytochrome c-initiated caspase cascade: hierarchical activation of caspases-2, -3, -6, -7, -8, and -10 in a caspase-9-dependent manner. *J Cell Biol*, 144: 281-292, 1999.
266. Hakem, R., Hakem, A., Duncan, G. S., Henderson, J. T., Woo, M., Soengas, M. S., Elia, A., de la Pompa, J. L., Kagi, D., Khoo, W., Potter, J., Yoshida, R., Kaufman, S. A., Lowe, S. W., Penninger, J. M., and Mak, T. W. Differential requirement for caspase 9 in apoptotic pathways in vivo. *Cell*, 94: 339-352, 1998.
267. Cecconi, F., Alvarez-Bolado, G., Meyer, B. I., Roth, K. A., and Gruss, P. Apaf1 (CED-4 homolog) regulates programmed cell death in mammalian development. *Cell*, 94: 727-737, 1998.
268. Yoshida, H., Kong, Y. Y., Yoshida, R., Elia, A. J., Hakem, A., Hakem, R., Penninger, J. M., and Mak, T. W. Apaf1 is required for mitochondrial pathways of apoptosis and brain development. *Cell*, 94: 739-750, 1998.
269. Honarpour, N., Du, C., Richardson, J. A., Hammer, R. E., Wang, X., and Herz, J. Adult Apaf-1-deficient mice exhibit male infertility. *Dev Biol*, 218: 248-258, 2000.
270. Kuida, K., Zheng, T. S., Na, S., Kuan, C., Yang, D., Karasuyama, H., Rakic, P., and Flavell, R. A. Decreased apoptosis in the brain and premature lethality in CPP32- deficient mice. *Nature*, 384: 368-372, 1996.
271. Kuida, K., Haydar, T. F., Kuan, C. Y., Gu, Y., Taya, C., Karasuyama, H., Su, M. S., Rakic, P., and Flavell, R. A. Reduced apoptosis and cytochrome c-mediated caspase activation in mice lacking caspase 9. *Cell*, 94: 325-337, 1998.
272. Pohl, D., Bittigau, P., Ishimaru, M. J., Stadthaus, D., Hubner, C., Olney, J. W., Turski, L., and Ikonomidou, C. N-Methyl-D-aspartate antagonists and apoptotic cell death triggered by head trauma in developing rat brain. *Proc Natl Acad Sci U S A*, 96: 2508-2513., 1999.
273. Hu, B. R., Liu, C. L., Ouyang, Y., Blomgren, K., and Siesjo, B. K. Involvement of caspase-3 in cell death after hypoxia-ischemia declines during brain maturation. *J Cereb Blood Flow Metab*, 20: 1294-1300., 2000.
274. de Bilbao, F., Guarin, E., Nef, P., Vallet, P., Giannakopoulos, P., and Dubois-Dauphin, M. Postnatal distribution of cpp32/caspase 3 mRNA in the mouse central nervous system: an in situ hybridization study. *J Comp Neurol*, 409: 339-357, 1999.

275. Nakajima, W., Ishida, A., Lange, M. S., Gabrielson, K. L., Wilson, M. A., Martin, L. J., Blue, M. E., and Johnston, M. V. Apoptosis has a prolonged role in the neurodegeneration after hypoxic ischemia in the newborn rat. *J Neurosci*, 20: 7994-8004., 2000.
276. Northington, F. J., Ferriero, D. M., Flock, D. L., and Martin, L. J. Delayed neurodegeneration in neonatal rat thalamus after hypoxia- ischemia is apoptosis. *J Neurosci*, 21: 1931-1938., 2001.
277. Hausmann, G., O'Reilly, L. A., van Driel, R., Beaumont, J. G., Strasser, A., Adams, J. M., and Huang, D. C. Pro-apoptotic apoptosis protease-activating factor 1 (Apaf-1) has a cytoplasmic localization distinct from Bcl-2 or Bcl-x(L). *J Cell Biol*, 149: 623-634, 2000.
278. Bruno, V., Battaglia, G., Copani, A., Casabona, G., Storto, M., Di Giorgi Gerevini, V., Ngomba, R., and Nicoletti, F. Metabotropic glutamate receptors and neurodegeneration. *Prog Brain Res*, 116: 209-221, 1998.
279. Lea, P. M. t. and Faden, A. I. Modulation of metabotropic glutamate receptors as potential treatment for acute and chronic neurodegenerative disorders. *Drug News Perspect*, 16: 513-522, 2003.
280. Conn, P. J. and Pin, J. P. Pharmacology and functions of metabotropic glutamate receptors. *Annu Rev Pharmacol Toxicol*, 37: 205-237, 1997.
281. Allen, J. W., Vicini, S., and Faden, A. I. Exacerbation of neuronal cell death by activation of group I metabotropic glutamate receptors: role of NMDA receptors and arachidonic acid release. *Exp Neurol*, 169: 449-460., 2001.
282. Gasparini, F., Lingenhohl, K., Stoehr, N., Flor, P. J., Heinrich, M., Vranesic, I., Biollaz, M., Allgeier, H., Heckendorn, R., Urwyler, S., Varney, M. A., Johnson, E. C., Hess, S. D., Rao, S. P., Saccaan, A. I., Santori, E. M., Velicelebi, G., and Kuhn, R. 2-Methyl-6-(phenylethynyl)-pyridine (MPEP), a potent, selective and systemically active mGlu5 receptor antagonist. *Neuropharmacology*, 38: 1493-1503, 1999.
283. Varney, M. A., Cosford, N. D., Jachec, C., Rao, S. P., Saccaan, A., Lin, F. F., Bleicher, L., Santori, E. M., Flor, P. J., Allgeier, H., Gasparini, F., Kuhn, R., Hess, S. D., Velicelebi, G., and Johnson, E. C. SIB-1757 and SIB-1893: selective, noncompetitive antagonists of metabotropic glutamate receptor type 5. *J Pharmacol Exp Ther*, 290: 170-181, 1999.
284. Cosford, N. D., Roppe, J., Tehrani, L., Schweiger, E. J., Seiders, T. J., Chaudary, A., Rao, S., and Varney, M. A. [3H]-methoxymethyl-MTEP and [3H]-methoxy-PEPy: potent and selective radioligands for the metabotropic glutamate subtype 5 (mGlu5) receptor. *Bioorg Med Chem Lett*, 13: 351-354, 2003.
285. Anderson, J. J., Rao, S. P., Rowe, B., Giracello, D. R., Holtz, G., Chapman, D. F., Tehrani, L., Bradbury, M. J., Cosford, N. D., and Varney, M. A. [3H]Methoxymethyl-3-[(2-methyl-1,3-thiazol-4-yl)ethynyl]pyridine binding to metabotropic glutamate receptor subtype 5 in rodent brain: in vitro and in vivo characterization. *J Pharmacol Exp Ther*, 303: 1044-1051, 2002.
286. Anderson, J. J., Bradbury, M. J., Giracello, D. R., Chapman, D. F., Holtz, G., Roppe, J., King, C., Cosford, N. D., and Varney, M. A. In vivo receptor occupancy of mGlu5 receptor antagonists using the novel radioligand [3H]3-methoxy-5-(pyridin-2-ylethynyl)pyridine. *Eur J Pharmacol*, 473: 35-40, 2003.
287. Dubois, B., Boller, F., Pillon, B., and Agid, Y. Cognitive deficits in Parkinson's disease. In: J. Grafman (ed.), *Handbook of neuropsychology*, Vol. 5, pp. 195-240. Amsterdam: Elsevier, 1991.
288. Ullman, M. T. and Gopnik, M. Inflectional morphology in a family with inherited specific language impairment. *Applied Psycholinguistics*, 20: 51-117, 1999.
289. van der Lely, H. K. J. and Christian, V. Lexical word formation in children with grammatical SLI: a grammar-specific versus an input-processing deficit? *Cognition*, 75: 33-63, 2000.
290. Ullman, M. T. and Pierpont, E. I. Specific Language Impairment is not Specific to Language: The Procedural Deficit Hypothesis. *Cortex*, In Press.
291. Hill, E. L. Non-specific nature of specific language impairment: A review of the literature with regard to concomitant motor impairments. *International Journal of Language and Communication Disorders*, 36: 149-171, 2001.
292. Leonard, L. B. *Children with specific language impairment*. Cambridge, MA: MIT Press, 1998.

293. Pinker, S. and Ullman, M. T. Combination and structure, not gradedness, is the issue. *Trends in Cognitive Sciences*, 6: 472-474, 2002.
294. Tyler, L., Randall, B., and Marslen-Wilson, W. Phonology and neuropsychology in the English past tense. *Neuropsychologia*, 40: 154-1166, 2002.
295. Goodglass, H. *Understanding aphasia*. San Diego, CA: Academic Press, 1993.
296. Alexander, M. P. Aphasia: Clinical and anatomic aspects. In: M. J. Farah (ed.), *Behavioral neurology and neuropsychology*, pp. 133-150. New York: McGraw-Hill, 1997.
297. Farah, M. J. and Grossman, M. Semantic memory impairments. In: M. J. Farah (ed.), *Behavioral neurology and neuropsychology*, pp. 473-477. New York: McGraw-Hill, 1997.
298. Embick, D. and Marantz, A. Cognitive neuroscience and the English past tense; Comments on the paper by Ullman et al. *Brain and Language*, in press.
299. Coslett, H. B. A selective morphologic impairment in writing: Evidence from a phonological dysgraphic. In: *Academy of Aphasia*, Montreal, October 1988.
300. Badecker, W. and Caramazza, A. The analysis and morphological errors in a case of acquired dyslexia. *Brain and Language*, 32: 278-305, 1987.
301. Ullman, M. T., Izvorski, R., Love, T., Yee, E., Swinney, D., and Hickok, G. Neural correlates of lexicon and grammar: Evidence from the production, reading, and judgment of inflection in aphasia. *Brain and Language*, in press.
302. Hagiwara, H., Ito, T., Sugioka, Y., Kawamura, M., and Shiota, J.-i. Neurolinguistic evidence for rule-based nominal suffixation. *Language*, 75: 739-763, 1999.
303. Penke, M., Janssen, U., and Krause, M. The representation of inflectional morphology: Evidence from Broca's aphasia. *Brain and Language*, 68: 225-232, 1999.
304. Tsapkini, K., Jarema, G., and Kehayia, E. Manifestations of morphological impairment in Greek aphasia: A case study. *Journal of Neurolinguistics*, 14: 281-296, 2001.
305. Boller, F. and Grafman, J. (eds.) *Handbook of neuropsychology*. New York: Elsevier, 1995.
306. Bird, H., Lambon Ralph, M. A., Seidenberg, M. S., McClelland, J. L., and Patterson, K. Deficits in phonology and past tense morphology: What's the connection? *Journal of Memory and Language*, 48: 502-506, 2003.
307. Marslen-Wilson, W. and Tyler, L. K. Rules, representations, and the English past tense. *Trends in Cognitive Sciences*, 2: 428-435, 1998.
308. Marslen-Wilson, W. D. and Tyler, L. K. Dissociating types of mental computation. *Nature*, 387: 592-594, 1997.
309. Tyler, L. K., de Mornay-Davies, P., Anokhina, R., Longworth, C., Randall, B., and Marslen-Wilson, W. D. Dissociations in processing past tense morphology: Neuropathology and behavioral studies. *Journal of Cognitive Neuroscience*, 14: 79-94, 2002.
310. Miozzo, M. On the processing of regular and irregular forms of verbs and nouns: Evidence from neuropsychology. *Cognition*, 87: 101-127, 2003.
311. Izvorski, R. and Ullman, M. T. Verb inflection and the hierarchy of functional categories in agrammatic anterior aphasia. *Brain and Language*, 69: 288-291, 1999.
312. Pancheva, R. and Ullman, M. T. Agrammatic aphasia and the Hierarchy Complexity Hypothesis. *Cognition*, under revision.
313. Arnold, S. E., Hyman, B. T., Flory, J., Damasio, A. R., and Hoesen, G. W. V. The topographical and neuroanatomical distribution of neurofibrillary tangles and neuritic plaques in the cerebral cortex of patients with Alzheimer's disease. *Cerebral Cortex*, 1: 103-116, 1991.
314. Boller, F. and Duyckaerts, C. Alzheimer disease: Clinical and anatomic aspects. In: M. J. Farah (ed.), *Behavioral neurology and neuropsychology*, pp. 521-544. New York: McGraw-Hill, 1997.

315. Bayles, K. A. Language function in senile dementia. *Brain and Language*, 16: 265-280, 1982.
316. Irigaray, L. *Le Langage des Déments*. The Hague: Mouton, 1973.
317. Rochon, E., Waters, G. S., and Caplan, D. Sentence comprehension in patients with Alzheimer's disease. *Brain and Language*, 46: 329-349, 1994.
318. Schwartz, M. F., Marin, O. S. M., and Saffran, E. M. Dissociations of language function in dementia : A case study. *Brain and Language*, 7: 277-306, 1979.
319. Waters, G. S., Caplan, D., and Rochon, E. Processing capacity and sentence comprehension in patients with Alzheimer's disease. *Cognitive Neuropsychology*, 12: 1-30, 1995.
320. Ullman, M. T. Evidence that lexical memory is part of the temporal lobe declarative memory, and that grammatical rules are processed by the frontal/basal-ganglia procedural system. *Brain and Language*, in press.
321. Cappa, S. and Ullman, M. T. A neural dissociation in Italian verbal morphology. *Journal of Cognitive Neuroscience, Supplement*: 63, 1998.
322. Walenski, M., Sosta, K., Cappa, S., and Ullman, M. T. Deficits on irregular verb morphology in Italian-speaking Alzheimer's disease patients: Evidence from present tense and past participle production. under review.
323. Ullman, M. T., Corkin, S., Pinker, S., Coppola, M., Locascio, J., and Growdon, J. H. Neural modularity in language: Evidence from Alzheimer's and Parkinson's diseases. *Society for Neuroscience Abstracts*, 19: 1806, 1993.
324. Ullman, M. T., Corkin, S., Pinker, S., Coppola, M., Locascio, J., and Growdon, J. The neural structures subserving language: Evidence from inflectional morphology. *In: 1st Annual Meeting of the Cognitive Neuroscience Society*, San Francisco, CA, April 1994.
325. Ullman, M. T. Naming tools and using rules: Evidence that a frontal/basal-ganglia system underlies both motor skill knowledge and grammatical rule use. *Brain and Language*, 69: 316-318, 1999.
326. Ullman, M. T., Estabrooke, I. V., Steinhauer, K., Broveto, C., Pancheva, R., Ozawa, K., Mordecai, K., and Maki, P. Sex differences in the neurocognition of language. *Brain and Language*, 83: 141-143, 2002.
327. Ullman, M. T., Corkin, S., Coppola, M., Hickok, G., Growdon, J. H., Koroshetz, W. J., and Pinker, S. A Neural Dissociation within Language: Evidence that the mental dictionary is part of declarative memory, and that grammatical rules are processed by the procedural system. *Journal of Cognitive Neuroscience*, 9: 266-276, 1997.
328. Kotz, S. A., von Cramon, D. Y., and Friederici, A. D. Regular/irregular German verb production in patients with different etiologies. *In: D. Y. von Cramon (ed.), Yearbook of the Max-Planck Institute of Cognitive Neuroscience*, pp. 34-35. Leipzig, Germany, 2003 (in press).
329. Young, A. B. and Penney, J. B. Biochemical and functional organization of the basal ganglia. *In: E. Tolosa (ed.), Parkinson's disease and movement disorders*, 2 edition, pp. 1-11. Baltimore: Williams and Wilkins, 1993.
330. Kensinger, E. A., Ullman, M. T., and Corkin, S. Bilateral medial temporal lobe damage does not affect lexical or grammatical processing: Evidence from the amnesic patient H.M. *Hippocampus*, 11: 347-360, 2001.
331. Friederici, A. D., Steinhauer, K., and Frisch, S. Lexical integration: Sequential effects of syntactic and semantic information. *Memory and Cognition*, 27: 438-453, 1999.
332. Mecklinger, A., Schriefers, H., Steinhauer, K., and Friederici, A. D. Processing relative clauses varying on syntactic and semantic dimensions: an analysis with event-related potentials. *Memory and Cognition*, 23: 477-494, 1995.
333. Steinhauer, K., Pancheva, R., Newman, A. J., and Ullman, M. T. Processing the lexical mass/count feature: ERP evidence without employing violations. *In: Proceedings of the Fourteenth Annual CUNY*

Conference on Human Sentence Processing, Vol. 14. Philadelphia, PA: CUNY Graduate School and University Center, 2001.

334. Barrett, S. E. and Rugg, M. D. Event-related potentials and the semantic matching of pictures. *Brain and Cognition*, 14: 201-212, 1990.
335. Olivares, E., Bobes, M. A., Aubert, E., and Valdes-Sosa, M. Associative ERP effects with memories of artificial faces. *Cognitive Brain Research*, 2: 39-48, 1994.
336. Hagoort, P. and Kutas, M. Electrophysiological insights into language deficits. *In: J. Grafman (ed.), Handbook of Neuropsychology*, Vol. 10, pp. 105-134. Amsterdam: Elsevier, 1995.
337. Kutas, M. and Hillyard, S. A. Reading senseless sentences: Brain potentials reflect semantic incongruity. *Science*, 207: 203-205, 1980.
338. McCarthy, G., Nobre, A. C., Bentin, S., and Spencer, D. D. Language-related field potentials in the anterior-medial temporal lobe: I. Intracranial distribution and neural generators. *The Journal of Neuroscience*, 15: 1080-1089, 1995.
339. Ni, W., Constable, R. T., Menci, W. E., Pugh, K. R., Fulbright, R. K., Shaywitz, S. E., Gore, J. C., and Shankweiler, D. An event-related neuroimaging study distinguishing form and content in sentence processing. *Journal of Cognitive Neuroscience*, 12: 120-133, 2000.
340. Segalowitz, S. J. and Chevalier, H. Event-related potential (ERP) research in neurolinguistics: Part I: Techniques and applications to lexical access. *In: H. A. Whitaker (ed.), Handbook of neurolinguistics*, pp. 95-109. San Diego, CA: Academic Press, 1998.
341. Segalowitz, S. J. and Chevalier, H. Event-related potential (ERP) research in neurolinguistics: Part II: Language processing and acquisition. *In: H. A. Whitaker (ed.), Handbook of neurolinguistics*, pp. 111-123. San Diego, CA: Academic Press, 1998.
342. Simos, P. G., Basile, L. F. H., and Papanicolaou, A. C. Source localization of the N400 response in a sentence-reading paradigm using evoked magnetic fields and magnetic resonance imaging. *Brain Research*, 762: 29-39, 1997.
343. Guillem, F., Rougier, A., and Claverie, B. Short- and long-delay intracranial ERP repetition effects dissociate memory systems in the human brain. *Journal of Cognitive Neuroscience*, 11: 437-458, 1999.
344. Halgren, E., Baudena, P., Heit, G., Clarke, M., and Marinkovic, K. Spatio-temporal stages in face and word processing. 1. Depth recorded potentials in the human occipital and parietal lobes. *Journal of Physiology*, 88: 1-50, 1994.
345. Halgren, E., Dhond, R. P., Christensen, N., Van Petten, C., Marinkovic, K., Lewine, J. D., and Dale, A. M. N400-like magnetoencephalography responses modulated by semantic context, word frequency, and lexical class in sentences. *Neuroimage*, 17: 1101-1116, 2002.
346. Kiehl, K. A., Laurens, K. R., and Liddle, P. F. Reading anomalous sentences: An event-related fMRI study of semantic processing. *Neuroimage*, 17: 842-850, 2002.
347. Ullman, M. T. The neural basis of lexicon and grammar in first and second language: the declarative/procedural model. *Bilingualism: Language and Cognition*, 4: 105-122, 2001.
348. Ullman, M. T. Contributions of memory circuits to language: The declarative/procedural model. *Cognition*, 92: 231-270, 2004.
349. Friederici, A. D., Pfeifer, E., and Hahne, A. Event-related brain potentials during natural speech processing: effects of semantic, morphological and syntactic violations. *Cognitive Brain Research*, 1: 183-192, 1993.
350. Hagoort, P., Wassenaar, M., and Brown, C. Syntax-related ERP-effects in Dutch. *Brain Research Cognitive Brain Research*, 16: 38-50, 2003.
351. Neville, H., Nicol, J. L., Barss, A., Forster, K. I., and Garrett, M. F. Syntactically based sentence processing classes: Evidence from event-related brain potentials. *Journal of Cognitive Neuroscience*, 3: 151-165, 1991.

352. Friederici, A. D., Hahne, A., and Mecklinger, A. The temporal structure of syntactic parsing: Early and late effects elicited by syntactic anomalies. *Journal of Experimental Psychology: Learning, Memory, and Cognition*, 22: 1219-1248, 1996.
353. Hahne, A. and Friederici, A. D. Electrophysiological evidence for two steps in syntactic analysis: Early automatic and late controlled processes. *Journal of Cognitive Neuroscience*, 11: 194-205, 1999.
354. Friederici, A. D., Hahne, A., and von Cramon, D. Y. First-pass versus second-pass parsing processes in a Wernicke's and a Broca's aphasic: Electrophysiological evidence for a double dissociation. *Brain and Language*, 62: 311-341, 1998.
355. Friederici, A. D., von Cramon, D. Y., and Kotz, S. A. Language related brain potentials in patients with cortical and subcortical left hemisphere lesions. *Brain*, 122: 1033-1047, 1999.
356. Friederici, A. Towards a neural basis of auditory sentence processing. *Trends in Cognitive Science*, 6: 78-84, 2002.
357. Newman, A., Izvorski, R., Davis, L., Neville, H., and Ullman, M. T. Distinct electrophysiological patterns in the processing of regular and irregular verbs. *Journal of Cognitive Neuroscience, Supplement*: 47, 1999.
358. Coulson, S., King, J. W., and Kutas, M. Expect the unexpected: Event-related brain response to morphosyntactic violations. *Language and Cognitive Processes*, 13: 21-58, 1998.
359. Friederici, A. D. and Frisch, S. Verb-argument structure processing: The role of verb-specific and argument-specific information. *Journal of Memory and Language*, 43: 476-507, 2000.
360. Kaan, E. Investigating the Effects of Distance and Number Interference in Processing Subject-Verb Dependencies: An ERP Study. *Journal of Psycholinguistic Research*, 31: 165-193., 2002.
361. Kutas, M. and Hillyard, S. A. Event-related brain potentials to grammatical errors and semantic anomalies. *Memory and Cognition*, 11: 539-550, 1983.
362. Münte, T. F., Heinze, H., and Mangun, G. R. Dissociation of brain activity related to syntactic and semantic aspects of language. *Journal of Cognitive Neuroscience*, 5: 335-344, 1993.
363. Osterhout, L. and Mobley, L. A. Event-related brain potentials elicited by failure to agree. *Journal of Memory and Language*, 34: 739-773, 1995.
364. Rosler, F., Putz, P., Friederici, A., and Hahne, A. Event-related brain potentials while encountering semantic and syntactic constraint violations. *Journal of Cognitive Neuroscience*, 5: 345-362, 1993.
365. Gunter, T. C., Stowe, L. A., and Mulder, G. When syntax meets semantics. *Psychophysiology*, 34: 660-676, 1997.
366. Friederici, A. D., Steinhauer, K., and Pfeifer, E. Brain signatures of artificial language processing: Evidence challenging the critical period hypothesis. *Proceedings of the National Academy of Sciences*, 99: 529-534, 2002.
367. Hagoort, P. and Brown, C. M. Gender electrified: ERP evidence on the syntactic nature of gender processing. *Journal of Psycholinguistic Research*, 28: 715-728, 1999.
368. Knoesche, T. R., Maess, B., and Friederici, A. D. Processing of syntactic information monitored by brain surface current density mapping based on MEG. *Brain Topography*, 12: 75-87, 2000.
369. Weber-Fox, C., Davis, L. J., and Cuadrado, E. Event-related brain potential markers of high-language proficiency in adults. *Brain and Language*, 85: 231-244, 2003.
370. Yamada, Y., Harris, A., Pakulak, E., Schacter, J., and Neville, H. J. Language proficiency in monolinguals and bilinguals reflected in ERPs during sentence processing. *In: Cognitive Neuroscience Society Annual Meeting, San Francisco, CA, 2002*, pp. 135.
371. Holcomb, P. J. and McPherson, W. B. Event-related brain potentials reflect semantic priming in an object decision task. *Brain and Cognition*, 24: 259-276, 1994.
372. Steinhauer, K., Pancheva, R., Newman, A. J., Gennari, S., and Ullman, M. T. How the mass counts: An electrophysiological approach to the processing of lexical features. *Neuroreport*, 12: 999-1005, 2001.

373. McPherson, W. B., Ackerman, P. T., Holcomb, P. J., and Dykman, R. A. Event-related brain potentials elicited during phonological processing differentiate subgroups of reading disabled adolescents. *Brain and Language*, 62: 163-185, 1998.
374. Friederici, A. D. The time course of syntactic activation during language processing: A model based on neuropsychological and neurophysiological data. *Brain and Language*, 50: 259-281, 1995.
375. Weber-Fox, C. M. and Neville, H. J. Maturational constraints on functional specializations for language processing: ERP and behavioral evidence in bilingual speakers. *Journal of Cognitive Neuroscience*, 8: 231-256, 1996.
376. Kaan, E., Harris, A., Gibson, E., and Holcomb, P. The P600 as an index of syntactic integration difficulty. *Language and Cognitive Processes*, 15: 159-201, 2000.
377. Friederici, A. D., Mecklinger, A., Spencer, K. M., Steinhauer, K., and Donchin, E. Syntactic parsing preferences and their on-line revisions: A spatio-temporal analysis of event-related brain potentials. *Cognitive Brain Research*, 11: 305-323, 2001.
378. Friederici, A. D. and Kotz, S. A. The brain basis of syntactic processes: functional imaging and lesion studies. *Neuroimage*, In Press.
379. Friederici, A. D., Kotz, S. A., Werheid, K., Hein, G., and von Cramon, D. Y. Syntactic comprehension in Parkinson's disease: investigating early automatic and late integrational processes using event-related brain potentials. *Neuropsychology*, 17: 133-142, 2003.
380. Steinhauer, K., Alter, K., and Friederici, A. D. Brain potentials indicate immediate use of prosodic cues in natural speech processing. *Nature Neuroscience*, 2: 191-196, 1999.
381. Penke, M., Weyerts, H., Gross, M., Zander, E., Munte, T. F., and Clahsen, H. How the brain processes complex words: An ERP-study of German verb inflections. *Essex Research Reports in linguistics*, 14: 1-41, 1997.
382. Weyerts, H., Penke, M., Dohrn, U., Clahsen, H., and Münte, T. F. Brain potentials indicate differences between regular and irregular German plurals. *Neuroreport*, 8: 957-962, 1997.
383. Gross, M., Say, T., Kleingers, M., Münte, T. F., and Clahsen, H. Human brain potentials to violations in morphologically complex Italian words. *Neuroscience Letters*, 241: 83-86, 1998.
384. Rodriguez-Fornells, A., Munte, T. F., and Clahsen, H. Morphological priming in Spanish verb forms: An ERP repetition priming study. *Journal of Cognitive Neuroscience*, 14: 443-454, 2002.
385. Allen, M., Badecker, W., and Osterhout, L. Morphological analysis in sentence processing: An ERP study. *Language and Cognitive Processes*, 18: 405-430, 2003.
386. Münte, T. F., Say, T., Clahsen, H., Schiltz, K., and Kutas, M. Decomposition of morphologically complex words in English: Evidence from event-related brain potentials. *Cognitive Brain Research*, 7: 241-253, 1999.
387. Ullman, M. T., Newman, A., Izvorski, R., and Neville, H. Electrophysiological correlates of lexicon and grammar: Evidence from inflectional morphology. In: *Proceedings of the Thirteenth Annual CUNY Conference on Human Sentence Processing*, Vol. 13, pp. 87. La Jolla, CA: CUNY Graduate School and University Center, 2000.
388. Newman, A. J., Ullman, M. T., Pancheva, R., Waligura, D. L., and Neville, H. J. The electrophysiology of words and rules: ERP studies of regular and irregular English past tense inflection. *Journal of Experimental Psychology: Learning, Memory and Cognition*, Under Revision.
389. Penke, M. and Krause, M. German noun plurals: a challenge to the dual-mechanism model. *Brain and Language*, in press.
390. Pinker, S. *Words and rules: The ingredients of language*. New York: Basic Books, 1999.
391. Ullman, M. T. *The computation of inflectional morphology*. Department of Brain and Cognitive Sciences, pp. 263. Cambridge, MA: Massachusetts Institute of Technology, 1993.

392. Steinhauer, K. and Ullman, M. T. Consecutive ERP effects of morph-phonology and morpho-syntax. *Brain and Language*, 83: 62-65, 2002.
393. Steinhauer, K. and Ullman, M. T. ERPs reveal consecutive effects of morpho-phonology and morpho-syntax. Under Preparation.
394. Ullman, M. T. A neurocognitive perspective on language: The declarative/procedural model. *Nature Reviews Neuroscience*, 2: 717-726, 2001.
395. Dominey, P. F., Hoen, M., Blanc, J.-M., and Lelekov-Boissard, T. Neurological basis of language and sequential cognition: Evidence from simulation, aphasia, and ERP studies. *Brain and Language*, 83: 207-225, 2003.
396. Elman, J. L. Finding structure in time. *Cognitive Science*, 14: 179-211, 1990.
397. Hoen, M. and Dominey, P. F. ERP analysis of cognitive sequencing: A left anterior negativity related to structural transformation processing. *Neuroreport*, 11: 3187-3191, 2000.
398. Newman, A. J., Pancheva, R., Ozawa, K., Neville, H. J., and Ullman, M. T. An event-related fMRI study of syntactic and semantic violations. *Journal of Psycholinguistic Research*, 30: 339-364, 2001.
399. Embick, D., Marantz, A., Miyashita, Y., O'Neil, W., and Sakai, K. L. A syntactic specialization for Broca's area. *Proceedings of the National Academy of Sciences*, 97: 6150-6154, 2000.
400. Friederici, A. D., Ruschemeyer, S. A., Hahne, A., and Fiebach, C. J. The role of left inferior frontal and superior temporal cortex in sentence comprehension: Localizing syntactic and semantic processes. *Cerebral Cortex*, 13: 170-177, 2003.
401. Kansaku, K., Yamaura, A., and Kitazawa, S. Sex differences in lateralization revealed in the posterior language areas. *Cerebral Cortex*, 10: 866-872, 2000.
402. Phillips, M. D., Lurito, J. T., Dziedzic, M., Lowe, M. J., Wang, Y., and Matthews, V. P. Temporal lobe activation demonstrates gender-based differences during passive listening. *In: 86th Scientific Assembly and Annual Meeting of the Radiological Society of North America (RSNA)*, Chicago, Illinois, 2000.
403. Price, C. J., Moore, C. J., and Friston, K. J. Getting sex into perspective. *Neuroimage*, 3: S586, 1996.
404. Rhee, J., Clark, D., Casasanto, D., Ullman, M. T., Wagner, A., and Pinker, S. Neural Substrates of English Past Tense Generation. *Journal of Cognitive Neuroscience*, *Supplement*: 131, 2001.
405. Ullman, M. T., Bergida, R., and O'Craven, K. Distinct fMRI activation patterns for regular and irregular past tense. *Neuroimage*, 5: S549, 1997.
406. Newman, A. J., Ullman, M. T., Pancheva, R., Waligura, D. L., and Neville, H. J. Regular and irregular English past tense verbs elicit distinct patterns of neural activity: an event-related fMRI study. *Journal of Cognitive Neuroscience*, *Supplement*, 2002.
407. Seidenberg, M. S. and Arnoldussen, A. The brain makes a distinction between hard and easy stimuli: comments on Beretta et al. *Brain and Language*, 85: 527-530, 2003.
408. Seidenberg, M. S. and Hoeffner, J. H. Evaluating behavioral and neuroimaging data on past tense production. *Language*, 74: 104-122, 1998.
409. Beretta, A., Campbell, C., Carr, T. H., Huang, J., Schmitt, L. M., Christianson, K., and Cao, Y. An ER-fMRI investigation of morphological inflection in German reveals that the brain makes a distinction between regular and irregular forms. *Brain and Language*, 85: 67-92, 2003.

IX. Appendices

Research report

Selective mGluR5 receptor antagonist or agonist provides neuroprotection in a rat model of focal cerebral ischemia

W.L. Bao^a, A.J. Williams^b, A.I. Faden^{a,*}, F.C. Tortella^b

^aDepartment of Neuroscience, Georgetown University Medical Center, 3970 Reservoir Road NW, Research Building, Rm. EP12, Washington, DC 20007, USA

^bDepartment of Neuropharmacology, Walter Reed Army Institute of Research, Silver Spring, MD 20910, USA

Accepted 4 September 2001

Abstract

Activation of group I metabotropic glutamate receptors (mGluR) has been implicated in the pathophysiology of acute central nervous system injury. However, the relative roles of the two group I subtypes, mGluR1 or mGluR5, in such injury has not been well examined. We compared the effects of treatment with the newly developed, selective mGluR5 antagonist 2-methyl-6-phenylethynylpyridine (MPEP) and the selective mGluR5 agonist (*R,S*)-2-chloro-5-hydroxyphenylglycine (CHPG) in a rat intraluminal filament model of temporary middle cerebral artery occlusion (MCAo). Rats were administered MPEP or CHPG i.c.v. beginning 15 or 135 min after induction of ischemia for 2 h. Infarct size was measured after either 22 or 70 h of reperfusion, and neurological function was quantified at 2, 24, 48 and 72 h. Treatment with MPEP or CHPG at 15 min reduced 24 h infarct volume by 61 and 44%, respectively. The neuroprotective effects were dose dependent. Delaying MPEP treatment until 135 min eliminated the neuroprotective effects. In other studies, using early MPEP treatment (15 min) at optimal doses, infarct volume was reduced by 44% at 72 h and this was correlated with significant neurological recovery. These data suggest that both MPEP and CHPG are neuroprotective when administered after focal cerebral ischemia. In separate, recent studies we found that although MPEP does act as an mGluR5 antagonist and blocks agonist induced phosphoinositide hydrolysis, it also serves as a non-competitive NMDA antagonist; in contrast, other results indicate that CHPG mediated neuroprotection may reflect anti-apoptotic activity. Therefore, both types of compounds may prove to have therapeutic potential for the treatment of stroke. © 2001 Elsevier Science B.V. All rights reserved.

Theme: Disorders of the nervous system

Topic: Ischemia

Keywords: Cerebral ischemia; Neuroprotection; mGluR5 receptor; Non-competitive antagonist

1. Introduction

Glutamate, a major excitatory neurotransmitter in the mammalian central nervous system, interacts with both ionotropic glutamate receptors and metabotropic glutamate receptors (mGluR). A role for ionotropic glutamate receptors in neuronal cell death following cerebral ischemia is well established [8,12]. Because such receptors play such a critical role in fast synaptic transmission, blockade of these receptors may be associated with substantial side effects. Recent evidence suggests that mGluR, which are

G-protein coupled receptors, may provide an effective alternative approach for reducing glutamate mediated cell death. Furthermore, the fact that mGluRs are primarily localized in the CNS may serve to limit certain peripheral side effects [9,20]. It should also be noted that blockade of mGluRs seems to have only a modest impact on fast excitatory transmission [7].

There are eight mGluR subtypes, which have been divided into three major groups on the basis of sequence homology, signal transduction pathways, and pharmacological sensitivities [20,21]. Group I mGluR includes mGluR1 and mGluR5; activation of these receptors causes stimulation of phospholipase C, resulting in phosphoinositide (PI) hydrolysis and intracellular calcium mobilization [20,21]. The role of group I mGluR in

*Corresponding author. Tel.: +1-202-687-0492; fax: +1-202-687-0617.

E-mail address: fadena@giccs.georgetown.edu (A.I. Faden).

neurodegeneration remains controversial. Whereas antagonists of these receptors are consistently neuroprotective, agonists have been found to either amplify or attenuate neuronal cell death [16]. Previous studies have suggested that the neurotoxic effects of putative group I ligands may be modulated primarily by the mGluR1 [6,14,15], but until recently, selective subtype specific antagonists have not been available to address this issue. The potent and selective mGluR1 antagonists (*S*)-4-carboxyphenylglycine (AIDA) reduces traumatic neuronal injury *in vivo* and *in vitro*, and attenuates the delayed degeneration of vulnerable neurons in gerbils subjected to transient global ischemia [6,19]. In addition, the selective mGluR1a antagonists (+)-2-methyl-4-carboxyphenylglycine (LY367385) and 7-hydroxyiminoclopropan[b]chromen-1a-carboxylic acid ethyl ester (CPCCOEt) have recently been described as being neuroprotective [2,6]. From these studies it may be concluded that activation of mGluR1a receptors contributes to glutamate neurotoxicity and post-ischemic cell death, conditions that largely reflect necrotic cell death. In contrast to mGluR1, mGluR5 activation may serve to attenuate apoptotic cell death [3,4]. This conclusion was partly based on studies using antisense oligonucleotides directed at mGluR5 in cerebellar granule cells cultures subjected to low levels of potassium [4]. In addition, activation of mGluR5 protects cultured granule cells against apoptotic death [1,4].

Recent development of more selective mGluR1 and mGluR5 agonists/antagonists has provided tools to further address such hypotheses. These include the mGluR5 agonist (*R,S*)-2-chloro-5-hydroxyphenylglycine (CHPG) and antagonist 6-methyl-2-(phenylethynyl)-pyridine (MPEP) [5,7]. CHPG has been shown to activate only mGluR5, but not mGluR1, in transfected cells; *in vitro* it has been shown to reduce neuronal apoptosis [5]. MPEP has been described as a selective non-competitive mGluR5 antagonist with no appreciable agonist or antagonist activity at recombinant mGluR1, group II or III mGluRs [7]. Furthermore, MPEP does not act at the extracellular glutamate binding site of mGluR5 receptors common to all known competitive mGluR antagonists. Rather it interacts with transmembrane domains III and VII of mGluR5 receptors [18], which makes MPEP less sensitive to the ambient concentration of glutamate. In the present study, we compared the effects of MPEP or CHPG treatment in a rat intraluminal filament model of temporary middle cerebral artery occlusion (MCAo).

2. Materials and methods

2.1. Surgical procedures

Male Sprague–Dawley rats (260–300 g; Charles River Lab., Raleigh, VA, USA) were used in this study. Anesthesia was induced by 5% halothane and maintained at 2%

halothane delivered in oxygen. Body temperature was maintained normothermic ($37 \pm 1^\circ\text{C}$) throughout all surgical procedures by means of a homeothermic heating system (Harvard Apparatus, South Natick, MA, USA). Food and water were provided *ad libitum* before and after surgery, and the animals were individually housed under a 12-h light–dark cycle. The facilities in which the animals were maintained and fully accredited by the American Association for the Accreditation of Laboratory Animal Care (AALAC). In conducting the research described in this report, the investigators adhered to the Guide for Care and Use of Laboratory Animals, as promulgated by the Committee on the Care and Use of Laboratory Animals of the Institute of Laboratory Resources, National Research Council.

The i.c.v. catheters were stereotactically placed into the right lateral ventricle (1.5 mm posterior and 1 mm right lateral to bregma). Two cortical electrodes (epidural stainless steel screw electrodes, $0.80 \times 1/8$ in.) were permanently implanted and fixed to the skull using dental acrylic cement [23]. At 72 h after the surgical procedure described above, rats were reanesthetized and prepared for temporary focal ischemia using the filament method of middle cerebral artery occlusion (MCAo) and reperfusion as described elsewhere [22,24]. Briefly, the right external carotid artery was isolated and its branches were coagulated. A 3-0 uncoated monofilament nylon suture with a rounded tip was introduced into the internal carotid artery via the external carotid artery and advanced (approximately 22 mm from the carotid bifurcation) until a slight resistance was observed, thus occluding the origin of the MCA. Once the filament was in place, a drop in amplitude of the cortical electroencephalographic (EEG) recording was used to indicate a successful occlusion. The endovascular suture remained in place for 2 h and then was retracted to allow reperfusion of the MCA. After surgery, animals were placed in recovery cages with ambient temperature maintained at 22°C .

Prior to MCAo, the body temperature was recorded and a neurological examination was performed (see below). EEG activity was measured in each rat under anesthesia immediately before MCAo, immediately before reperfusion at 2 h after occlusion, and again at the 24- or 72-h endpoint before euthanasia. This enabled us to establish an experimental exclusion criterion (i.e. diminution in EEG amplitude by 70% or greater at 2 h after occlusion compared with preocclusion amplitude) and to determine the effect of MPEP or CHPG on cortical EEG activity in injured rats. This exclusion criterion has been validated by us previously and used in multiple prior studies that examine neuroprotective drugs treatments [22–24]. Changes in EEG amplitude were quantified with the use of spectral analysis and data reported as percent EEG recovery compared with the 2-h reperfusion sample. At the end of each experiment (either 24 or 72 h), rats were euthanized by decapitation and their brains were removed for quantification of infarction.

2.2. Neurological examination

A neurological examination was performed on each rat immediately before MCAo, before reperfusion, and at 24, 48 and 72 h after MCAo. Neurological scores were derived using a 10-point ordinal scale. Each animal was examined for reduced resistance to lateral push (score=4), open field circling (score=3), and shoulder adduction (score=2) or contralateral forelimb flexion (score=1) when held by the tail [22,24]. Rats extending both forelimbs toward the floor and not showing any other signs of neurological impairment were scored 0. Using this procedure, maximal neurological severity was measured as a cumulative score of 10. In the present study all rats subjected to MCAo either exhibited a neurological score of 10 when examined 2 h after ischemia or immediately before reperfusion, or were excluded from the study (two of the total experimental rats).

2.3. Infarct analysis

For each rat brain, analysis of ischemic cerebral damage was performed, including total and core infarct volumes and hemispheric infarct size (calculated as percentage of infarcted tissue referenced to the corresponding contralateral uninjured cerebral hemisphere, using 2,3,5-triphenyltetrazolium chloride (TTC) staining from seven coronal sections (2-mm thick). Brain sections were taken from the region beginning 1 mm from the frontal pole and ending just rostral to the corticocerebellar junction. Computer-assisted image analysis was used to calculate infarct volumes, described in detail elsewhere [22,24]. Briefly, the posterior surface of each TTC-stained forebrain section was digitally imaged (Loats, Westminster, MD, USA) and quantified for areas (in square millimeters) of ischemic damage. Core injury was defined as brain tissue completely lacking TTC staining, whereas total injury was specified as all ipsilateral tissue showing a loss of stain compared with the contralateral, uninjured hemisphere. Sequential integration of the respective areas yielded total and core infarct volumes (in cubic millimeters). Similarly, ipsilateral and contralateral hemispheric volumes were measured where hemispheric swelling (edema) was expressed as the percentage increase in size of the ipsilateral (occluded) hemisphere over the contralateral (uninjured) hemisphere. Penumbra areas were defined as the total (green outline) minus the core (yellow outline) infarct volume, which correlated to light pink-staining brain regions (Fig. 1).

2.4. Data analysis

Data are presented as mean \pm S.E.M. Statistical analysis of single dose responses ($n=7-10$ /group) was made by comparisons using independent Student's *t* test with a modified Bonferroni correction for multiple comparisons.

2.5. Compound and treatment

MPEP was dissolved in DMSO and diluted in saline (1% final DMSO concentration). CHPG was dissolved in saline. CHPG, MPEP or vehicle (saline or DMSO 1%) were administered i.c.v. in a 5- μ l volume. All injections were given 15 min after occlusion. For the 24-h recovery studies vehicle ($n=11$), MPEP or CHPG (25–250 nmol, $n=8-9$ per dose) were injected. For the 72-h experiments vehicle ($n=8$) or MPEP (250 nmol, $n=7$) was studied. In other experiments, the injection of MPEP was delayed until 135 min after MCAo.

3. Results

3.1. 2-h MCAo in vehicle-treated rats

MCAo with 22 h reperfusion resulted in significant core infarction within the temporal/parietal cortex and underlying striatum of the ipsilateral (injured) hemisphere. Ischemic damage generally extended from the most rostral forebrain sections to the final caudal sections and was greatest in the area around the bregma (Fig. 1). Total and core infarct volumes averaged 303 ± 17 and 199 ± 14 mm³, respectively. At 2 h after MCAo, neurological function (10.0 ± 0.0) and EEG activity were markedly reduced. Neuroscores at 24 h after MCAo exhibited a significant degree of spontaneous recovery to (6.9 ± 0.7) (Table 1).

At 72 h after MCAo, the mean total and core infarct volume (364 ± 24 and 247 ± 17 mm³, respectively) were larger than those observed at 24 h. However, neurological function showed additional and significant spontaneous improvements (2.6 ± 0.4) (Table 2).

3.2. Physiological parameters

All MCAo animals lost approximately to 10–16% of body weight during the 24 h recovery period (22–27% loss at 72 h), regardless of treatment group, with no significant difference in body weight loss between groups. In vehicle-treated animals, MCAo was associated with a transient, mild increase in body temperature ($38.0 \pm 0.4^\circ\text{C}$), which returned to normal by 4–6 h post occlusion. Interestingly, at 72 h post injury, control injured animals exhibited a mild hypothermia ($35.3 \pm 0.4^\circ\text{C}$). At all time points, temperature measurements from MPEP or CHPG treated animals were not significantly different from those of the corresponding vehicle-treated animals.

3.3. Effect of early treatment of MPEP or CHPG on neuroprotection

Both MPEP and CHPG reduced the core infarct volume when administered 15 min after occlusion, as shown in Fig. 1. Although all doses of MPEP and CHPG reduced core infarct volume, only the highest dose (250 nmol)

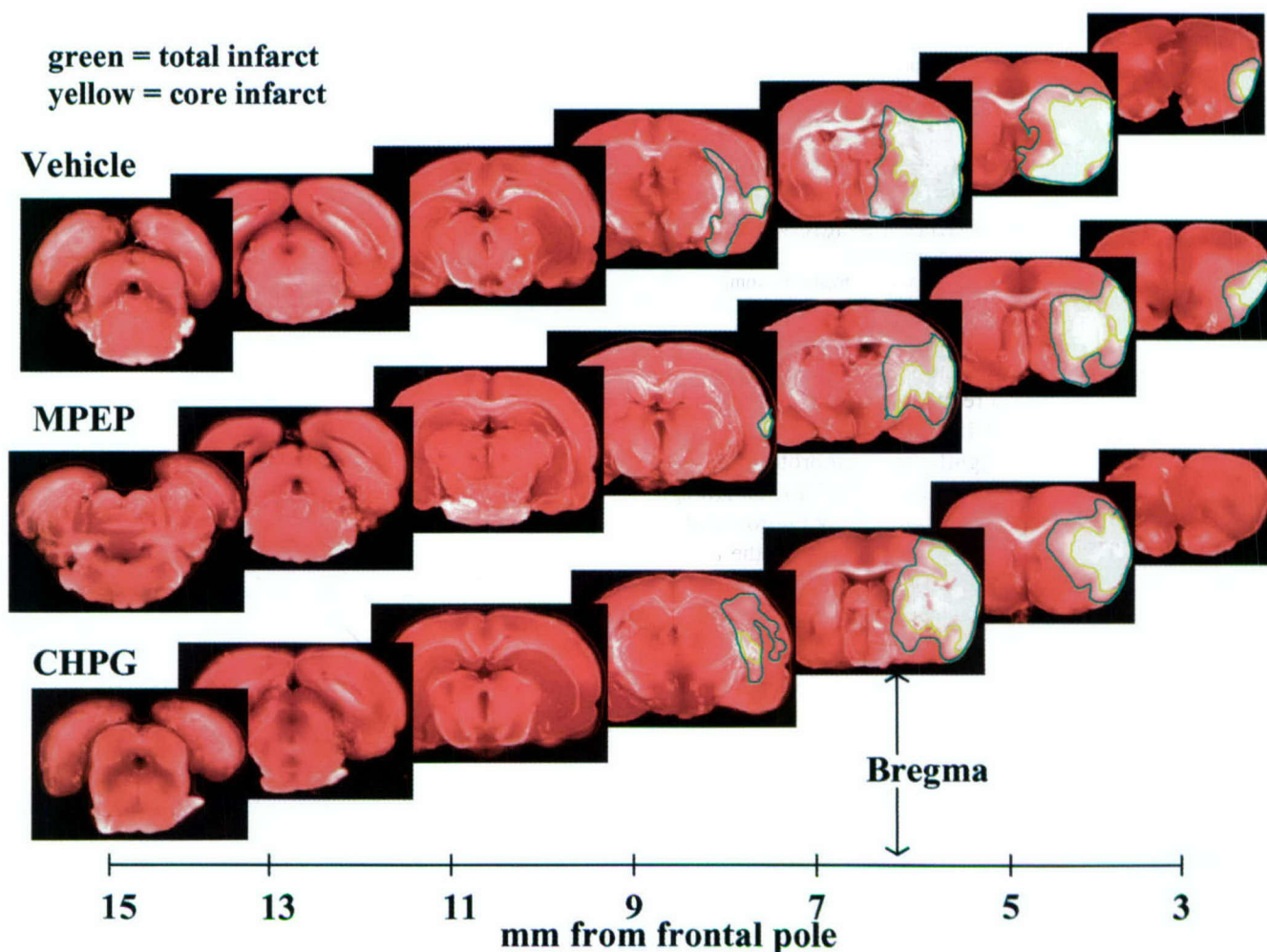


Fig. 1. Representative forebrain images of vehicle versus MPEP or CHPG (250 nmol, i.c.v.) administration after 2 h MCAo and a 22-h reperfusion. Brain sections were stained with TTC, and total infarct volume (green outline) and core infarct volume (yellow outline) were defined.

produced a significant reduction in infarct volume to 74 ± 14 mm³ (MPEP) or 104 ± 34 mm³ (CHPG) (Fig. 2). Normalization of the MPEP and CHPG infarct data to vehicle-treated rats established that at highest dose tested the neuroprotection was 61% (MPEP) and 44% (CHPG),

respectively. Examination of neurological function at 24 h in MPEP or CHPG-treated rats showed a trend toward improved neurological function, which did not reach significance (Table 1).

In separate experiments, the neuroprotective actions of

Table 1

Effect of MPEP and CHPG (administered i.c.v.) on core neuroprotection, EEG recovery and neurological function at 24 h after MCAo/reperfusion

Treatment	Dose (nmol)	n	Neuroprotection ^a (%)	EEG recovery ^b (%)	Neurological score
Vehicle		36	0	26 ± 11	6.9 ± 0.7
MPEP	25	9	14 ± 14	30 ± 13	4.8 ± 0.5
	75	8	28 ± 9	66 ± 18	5.0 ± 0.8
	250	8	60 ± 8**	50 ± 21	4.9 ± 2.8
CHPG	25	8	20 ± 6	41 ± 28	5.9 ± 2.6
	75	7	22 ± 11	31 ± 15	5.9 ± 0.7
	250	8	44 ± 14*	40 ± 20	6.8 ± 0.9

Values are presented as mean ± S.E.M.; *, $P < 0.05$, **, $P < 0.01$, compared with vehicle-treated group (independent Student's *t* test with a modified Bonferroni correction for multiple comparisons).

^a Percentage reduction of infarct volume after treatment compared with vehicle-treated group.

^b Percentage recovery of EEG power compared with pre-MCAo recording.

Table 2

Effect of MPEP and CHPG (250 nmol, i.c.v.) on core neuroprotection, EEG recovery and neurological function at 72 h after MCAo/reperfusion

Treatment	n	Neuroprotection ^a (%)	EEG recovery ^b (%)	Neurological score			
				2 h	24 h	48 h	72 h
Vehicle	6	0	9±6	9.5±0.5	7.2±1.4	3.0±0	2.6±0.4
MPEP	8	44±5**	20±8	10.0±0	5.0±0.8*	2.8±0.3	1.4±0.4*
CHPG	7	26±13	32±11	10.0±0	6.2±0.9	4.7±0.8	3.0±1.1

Values are presented as mean±S.E.M.; *, $P<0.05$, **, $P<0.01$, compared with vehicle-treated group (independent Student's *t* test with a modified Bonferroni correction for multiple comparison).

^a Percentage reduction of infarct volume after treatment compared with vehicle-treated group.

^b Percentage recovery of EEG power compared with pre-MCAo recording.

MPEP and CHPG (250 nmol) were examined at 72 h. MPEP-treated rats had a reduction in total and core infarct volumes to 245 ± 22 and 138 ± 11 mm³, respectively (Fig. 3), corresponding to a significant neuroprotection in both brain areas (total=33±6%, core=44±5%). Neurological recovery (1.4 ± 0.4) was also significantly improved at 72 h (Table 2). CHPG-treated rats had a reduction the total and core infarct volumes to 301 ± 31 and 184 ± 40 mm³ respectively (Fig. 3), but these changes did not reach significance.

3.4. Effect of delayed MPEP treatment on percent neuroprotection at 24 h

The effect of delaying treatment with 250 nmol MPEP was also examined. When rats were treated at 15 min after reperfusion (or 135 min postinjury), limited reductions in infarct volumes ($20\pm8\%$) and neuroscores (5.0 ± 0.8) were observed, which did not reach significance (Fig. 4), in contrast to the significant effects observed with treatment at 15 min post-occlusion.

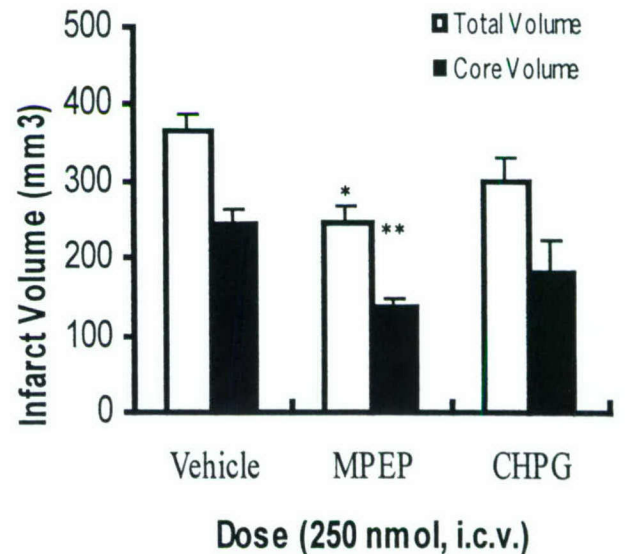


Fig. 3. Effects of MPEP or CHPG (250 nmol, i.c.v.) treatment on infarct volume at 72 h after temporary MCAo. Data are presented as mean±S.E. *, $P<0.05$, **, $P<0.01$ compared with vehicle-treated group (independent Student's *t* test with a modified Bonferroni correction for multiple comparisons).

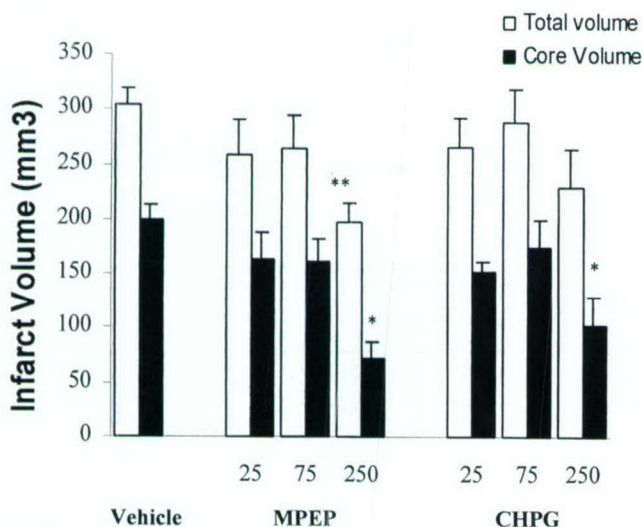


Fig. 2. Effects of increasing dose of MPEP or CHPG (nmol, i.c.v.) on infarct volume at 24 h after temporary MCAo. Data presented as mean±S.E. *, $P<0.05$, **, $P<0.01$ compared with vehicle-treated group (independent Student's *t* test with a modified Bonferroni correction for multiple comparisons).

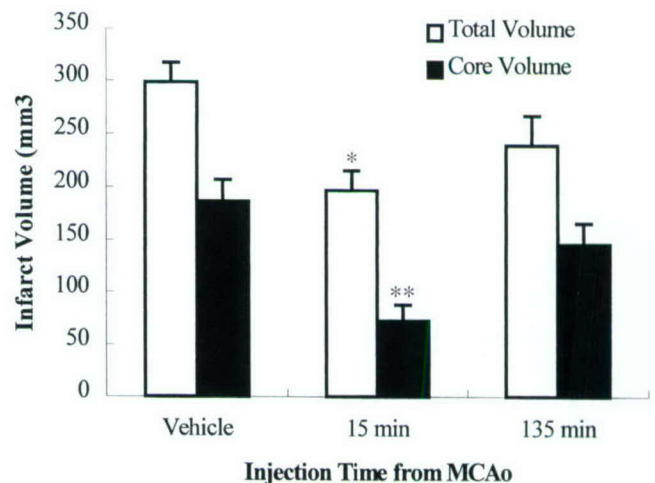


Fig. 4. Compares effect of early or delayed treatment (from time of MCAo) with MPEP (250 nmol, i.c.v.) on infarct volume at 24 h after temporary MCAo. Data are presented as mean±S.E. *, $P<0.05$, **, $P<0.01$ compared with vehicle-treated group (independent Student's *t* test with a modified Bonferroni correction for multiple comparisons).

4. Discussion

The intraluminal filament model of MCAo used in this study produces ischemia through temporary occlusion of the MCA with subsequent reperfusion at controlled time points. We have shown that both the selective mGluR5 agonist (CHPG) and antagonist (MPEP) have neuroprotective effects in this model. However, the neuroprotective mechanisms are likely to be different. Our *in vivo* observations are supported by *in vitro* results, which also showed that treatment with CHPG protects against apoptotic cell death [1]. Based on the *in vitro* results, it was suggested that CHPG may provide neuroprotection by limiting neuronal apoptosis after cerebral ischemia. Although we did not distinguish necrosis and apoptosis in our experiments, it has been reported that both can occur in response to focal cerebral ischemia [10,11].

Interestingly, our findings also demonstrated that the selective mGluR5 antagonist MPEP significantly reduces neuronal damage and improves neurological recovery induced by focal cerebral ischemia. These observations are also consistent with recent *in vitro* and *in vivo* results, which showed that MPEP and the structurally related selective mGluR5 antagonist SIB-1893 significantly attenuate post traumatic neuronal cell death and improve functional recovery [13].

Experiments from our laboratory suggest that the protective effects of MPEP may reflect non-competitive antagonism of the NMDA receptor, rather than through actions at mGluR5. For example, whereas antisense directed against mGluR1 or mGluR5 equally reduced group I mGluR-mediated increases in PI hydrolysis accumulation, only antisense against mGluR1 significantly attenuated traumatic neuronal injury in an *in vitro* model of necrotic cell death [14]. In addition, although we found that MPEP acts as an effective mGluR5 antagonist in rat cortical neuronal cultures, as shown by complete inhibition of PI hydrolysis induced by CHPG, the concentration of MPEP required to block agonist-induced PI hydrolysis was 100 times lower than that required for neuroprotection [13]. The noncompetitive NMDA receptor antagonist, (5*R*,10*S*)-(+)-5-methyl-10,11-dihydro-5*H*-dibenzo[*a,d*]cyclohepten-5,10-imine (MK801) markedly reduces glutamate or NMDA mediated neuronal cell death *in vitro*; however, no additive neuroprotective effect was observed when MPEP was applied to injured cells in presence of MK801 in our *in vitro* neurotoxic models or after mechanical injury [13]. In contrast, such additive neuroprotective effects have been shown using the mGluR1 antagonist AIDA in combination with MK801 [14]. Finally, MPEP significantly reduces steady state NMDA evoked whole-cell current at concentrations that are neuroprotective in cultured cortical neuronal cells, and also reduces the open time of the NMDA channel and the open probability of the channel [17]. This latter observation strongly suggests that MPEP acts as a non-competitive NMDA receptor antagonist.

In conclusion, as evidenced by lesion volume measurements, we have shown that both MPEP and CHPG provide neuroprotection when administered after focal cerebral ischemia. Based on *in vitro* studies, we suggest that a possible mechanism of action of CHPG may involve attenuation of apoptotic cell death, whereas MPEP appears to act as non-competitive NMDA receptor antagonist. Therefore, both types of compounds may prove to have therapeutic potential for the treatment of stroke.

Acknowledgements

This study was supported by grants from the National Institutes of Health (RO1NS37313) and the Department of Defense (DAMD-17-99-2-9007).

References

- [1] J.W. Allen, S.M. Knoblach, A.I. Faden, Activation of group I metabotropic glutamate receptors reduces neuronal apoptosis but increases necrotic cell death *in vitro*, *Cell Death Differ.* 7 (2000) 470–476.
- [2] V. Bruno, G. Battaglia, A. Kingston, M.J. O'Neill, M.V. Catania, R. Di Grezia, F. Nicoletti, Neuroprotective activity of the potent and selective mGlu1a metabotropic glutamate receptor antagonist, (+)-2-methyl-4 carboxyphenylglycine (LY367385): comparison with LY357366, a broader spectrum antagonist with equal affinity for mGlu1a and mGlu5 receptors, *Neuropharmacology* 38 (1999) 199–207.
- [3] A. Copani, V. Bruno, G. Battaglia, G. Leanza, R. Pellitteri, A. Russo, S. Stanzani, F. Nicoletti, Activation of metabotropic glutamate receptors protects cultured neurons against apoptosis induced by β -amyloid peptide, *Mol. Pharmacol.* 47 (1995) 890–897.
- [4] A. Copani, G. Casabona, V. Bruno, A. Caruso, D.F. Condorelli, A. Messina, V. Di Giorgi Gerevini, J.P. Pin, R. Kuhn, T. Knöpfel, F. Nicoletti, The metabotropic glutamate receptor mGlu5 controls the onset of developmental apoptosis in cultured cerebellar neurons, *Eur. J. Neurosci.* 10 (1998) 2173–2184.
- [5] A.J. Doherty, M.J. Palmer, J.M. Henley, G.L. Collingridge, D.E. Jane, (R,S)-2-Chloro-5-hydroxyphenylglycine (CHPG) activates mGlu5, but no mGlu1, receptors expressed in CHO cells and potentiates NMDA responses in the hippocampus, *Neuropharmacology* 36 (1997) 265–267.
- [6] A.I. Faden, D.M. O'Leary, L. Fan, W. Bao, P.G. Mullins, V.A. Movsesyan, Selective blockade of the mGluR1 receptor reduces traumatic neuronal injury *in vitro* and improves outcome after brain trauma, *Exp. Neurol.* 167 (2001) 435–444.
- [7] F. Gasparini, K. Lingenhohl, N. Stoehr, P.J. Flor, M. Heinrich, I. Vranesic, M. Biollaz, H. Allgeier, R. Heckendorn, S. Urwyler, M.A. Varney, E.C. Johnson, S.D. Hess, S.P. Rao, A.I. Sacca, E.M. Santori, G. Velicelebi, R. Kuhn, 2-Methyl-6-(phenylethynyl)-pyridine (MPEP), a potent, selective and systemically active mGlu5 receptor antagonist, *Neuropharmacology* 38 (1999) 1493–1503.
- [8] R. Gill, D. Lodge, Pharmacology of AMPA antagonists and their role in neuroprotection, *Int. Rev. Neurobiol.* 40 (1997) 197–232.
- [9] T. Knöpfel, R. Kuhn, H. Allgeier, Metabotropic glutamate receptors: novel targets for drug development, *J. Med. Chem.* 38 (1995) 1417–1426.
- [10] J.M. Lee, M.C. Grabb, G.J. Zipfel, D.W. Choi, Brain tissue responses to ischemia, *J. Clin. Invest.* 106 (2000) 723–731.
- [11] Y. Li, C. Powers, N. Jiang, M. Chopp, Intact, injured, necrotic and

- apoptotic cells after focal cerebral ischemia in the rat, *J. Neurol. Sci.* 156 (1998) 119–132.
- [12] J. McCulloch, Ischaemic brain damage — prevention with competitive and non-competitive antagonists of *N*-methyl-D-aspartate receptors, *Arzneimittelforschung* 41 (1991) 319–324.
- [13] V.A. Movsesyan, D.M. O'Leary, L. Fan, W. Bao, P.G. Mullins, S.M. Knoblach, A.I. Faden, mGluR5 antagonists 2-methyl-6-(phenylethynyl)-pyridine and (*E*)-2-methyl-6-(2-phenylethenyl)pyridine reduce traumatic neuronal injury in vitro and in vivo by antagonizing *N*-methyl-D-aspartate receptors, *J. Pharmacol. Exp. Ther.* 296 (2001) 41–47.
- [14] A. Mukhin, L. Fan, A.I. Faden, Activation of metabotropic glutamate receptor subtype mGluR1 contributes to post-traumatic neuronal injury, *J. Neurosci.* 16 (1996) 6012–6020.
- [15] A.G. Mukhin, S.A. Ivanova, A.I. Faden, mGluR modulation of post-traumatic neuronal death: role of NMDA receptors, *NeuroReport* 8 (1997) 2561–2566.
- [16] F. Nicoletti, V. Bruno, M.V. Catania, G. Battaglia, A. Copani, G. Barbagallo, V. Cena, J. Sanchez-Prieto, P.F. Spano, M. Pizzi, Group-I metabotropic glutamate receptors: hypotheses to explain their dual role in neurotoxicity and neuroprotection, *Neuropharmacology* 38 (1999) 1477–1484.
- [17] D.M. O'Leary, V. Movsesyan, S. Vicini, A.I. Faden, Selective mGluR5 antagonists MPEP and SIB-1893 decrease NMDA or glutamate-mediated neuronal toxicity through actions that reflect NMDA receptor antagonism, *Br. J. Pharmacol.* 131 (2000) 1429–1437.
- [18] A. Pagano, D. Ruegg, S. Litschig, N. Stoeckli, C. Stierlin, M. Heinrich, P. Floersheim, L. Prezeau, F. Carroll, J.P. Pin, A. Cambria, I. Vranesic, P.J. Flor, F. Gasparini, R. Kuhn, The non-competitive antagonists 2-methyl-6-(phenylethynyl)pyridine and 7-hydroxy-6-methyl-5,6,7,8-tetrahydro-2H-benzocyclopropan[b]chromen-1a-carboxylic acid ethyl ester interact with overlapping binding pockets in the transmembrane region of group I metabotropic glutamate receptors, *J. Biol. Chem.* 275 (2000) 33750–33758.
- [19] D.E. Pellegrini-Giampietro, F. Peruginelli, E. Meli, A. Cozzi, S. Albani-Torregrossa, R. Pellicciari, F. Moroni, Protection with metabotropic glutamate I receptor antagonists in models of ischemic neuronal death: time-course and mechanisms, *Neuropharmacology* 38 (1999) 1607–1619.
- [20] J.P. Pin, R. Duvoisin, The metabotropic glutamate receptors: structure and functions, *Neuropharmacology* 34 (1995) 1–26.
- [21] D.D. Schoepp, D.E. Jane, J.A. Monn, Pharmacological agents acting at subtypes of metabotropic glutamate receptors, *Neuropharmacology* 38 (1999) 1431–1476.
- [22] F.C. Tortella, P. Britton, A. Williams, X.C. Lu, A.H. Newman, Neuroprotection (focal ischemia) and neurotoxicity (electroencephalographic) studies in rats with AHN649, a 3-amino analog of dextromethorphan and low-affinity *N*-methyl-D-aspartate antagonist, *J. Pharmacol. Exp. Ther.* 291 (1999) 399–408.
- [23] F.C. Tortella, J. Rose, L. Robles, J.E. Moreton, J. Hughes, J.C. Hunter, EEG spectral analysis of the neuroprotective κ opioids enadoline and PD117302, *J. Pharmacol. Exp. Ther.* 282 (1997) 286–293.
- [24] A.J. Williams, J.R. Dave, J.B. Phillips, Y. Lin, R.T. McCabe, F.C. Tortella, Neuroprotective efficacy and therapeutic window of the high-affinity *N*-methyl-D-aspartate antagonist conantokin-G: in vitro (primary cerebellar neurons) and in vivo (rat model of transient focal brain ischemia) studies, *J. Pharmacol. Exp. Ther.* 294 (2000) 378–386.

TRAUMATIC BRAIN INJURY: DEVELOPMENTAL DIFFERENCES IN GLUTAMATE RECEPTOR RESPONSE AND THE IMPACT ON TREATMENT

Paul M. Lea IV¹ and Alan I. Faden^{*1,2,3}

¹Department of Neuroscience, Georgetown University Medical Center, Washington, DC

²Institute for Cognitive and Computational Sciences, ³Department of Pharmacology, Georgetown University Medical Center, Washington, DC

Perinatal brain injury following trauma, hypoxia, and/or ischemia represents a substantial cause of pediatric disabilities including mental retardation. Such injuries lead to neuronal cell death through either necrosis or apoptosis. Numerous *in vivo* and *in vitro* studies implicate ionotropic (iGluRs) and metabotropic (mGluRs) glutamate receptors in the modulation of such cell death. Expression of glutamate receptors changes as a function of developmental age, with substantial implications for understanding mechanisms of post-injury cell death and its potential treatment. Recent findings suggest that the developing brain is more susceptible to apoptosis after injury and that such caspase mediated cell death may be exacerbated by treatment with N-methyl-D-aspartate receptor antagonists. Moreover, group I metabotropic glutamate receptors appear to have opposite effects on necrotic and apoptotic cell death. Understanding the relative roles of glutamate receptors in post-traumatic or post-ischemic cell death as a function of developmental age may lead to novel targeted approaches to the treatment of pediatric brain injury. © 2001 Wiley-Liss, Inc. MRDD Research Reviews 2001;7:235-248.

Key Words: glutamate receptors; apoptosis; necrosis; caspase; brain injury; development

BACKGROUND

Traumatic injuries to the central nervous system is most common in younger individuals, particularly in the pediatric population [Diamond, 1996]. Moreover, perinatal brain injury associated with trauma, hypoxia and/or ischemia represents a substantial cause of pediatric disabilities including mental retardation [Delivoria-Papadopoulos and Mishra, 2000]. Brain trauma and ischemia/hypoxia cause neuronal cell death through either necrosis or apoptosis. Necrosis is a more passive process in which energy failure leads to loss of ionic homeostasis, particularly for Na⁺ and Ca²⁺, resulting in organellar (especially mitochondrial) and cellular swelling, mitochondrial membrane potential collapse, nuclear chromatin clumping, nuclear pyknosis, and activation of degradative enzymes. Collectively, these processes lead to the rupture of the plasma membrane with concomitant loss of intracellular proteins, ions, and metabolites. Necrosis is associated with inflammatory reactions and usually impacts large groups of adjacent cells [Banasiak et al., 2000]. Apoptosis is an active process, generally associated with less severe metabolic compromise (i.e., some preservation of ATP)

and de novo protein synthesis, that leads to the orderly resorption of target cells. It is both temporally and morphologically distinct from necrosis and shows structural changes consisting of nuclear chromatin clumping and mild to moderate cellular condensation. Apoptosis is generally not associated with an inflammatory response. Necrotic cell death is an earlier event, usually occurring within the first hours of injury. In contrast, apoptosis occurs later and lasts for days to weeks.

Recent studies have shown that apoptosis, as well as necrosis, contribute to cell loss and related functional deficits after acute brain injury [Colicos and Dash, 1996; Colicos et al., 1996; Conti et al., 1998; Fox and Faden, 1998; Fox et al., 1998a,b; Yakovlev et al., 2000]. Such apoptosis appears to be mediated, in part, by a class of cysteine proteases called caspases [Eldadah and Faden, 2000]. Moreover, in experimental animals, both necrosis and apoptosis may be inhibited by selective pharmacological strategies, leading to improved outcomes. Importantly, the relative roles of necrosis and apoptosis after injury appear to differ as a function of developmental age, with substantial differences between young and adult animals [Ikonomidou and Turski, 1996; Ikonomidou et al., 1999; Pohl et al., 1999]. Such differences relate to distinct patterns of protein expression (especially receptors) and signal transduction in earlier developmental periods as compared to the adult [Casabona et al., 1992; Shigemoto et al., 1992; Goto et al., 1993; Shaffer et al., 1993; Catania et al., 1994; Jiang et al., 1994; Salbego and Rodnight 1996; Casabona et al., 1997; Paupard et al., 1997; Roth 1997; Angenstein et al., 1999; Paupard et al., 2000]. Despite these differences, relatively few studies investigating head trauma in the developing brain exist. Such studies are essential if we are to recognize which developmental differences are important to our understanding and treatment of pediatric brain injury.

Grant sponsor: Department of Defense; Grant number: DAMD-17-99-2-9007; Grant sponsor: NIH; Grant numbers: R01NS37313 and P0140677.

*Correspondence to: Alan I. Faden, M.D., EP-04 Research Building, 3970 Reservoir Road N.W., Washington, DC 20007-2197. E-mail: fadena@georgetown.edu
Received 20 July 2001; Accepted 20 July 2001

NECROSIS AND EXCITOTOXICITY

Perinatal hypoxic-ischemic cerebral injury remains a major determinant of neurological mortality and morbidity. Acute disruptions in cerebral blood flow and oxygenation of the fetus and newborn may be caused by disruption of the maternal-placental-fetal system as well as by trauma [Sullivan et al., 1976]. Following injury, necrotic damage may result from multiple neurotoxic factors, including excitatory amino acids (EAA). Release of EAA after injury results in glutamate receptor mediated alterations in a number of critical ions, including Ca^{2+} , Na^+ , Cl^- and Zn^{2+} . Collectively, these disruptions in ionic homeostasis cause cell injury [Schanne et al., 1979; Jewell et al., 1982; Fleckenstein et al., 1983; Choi et al., 1988b; Koh and Choi, 1988] and intimately related neuronal cell death [Tymianski and Tator, 1996].

Cellular injury after brain trauma is caused in part by the excessive release of EAA, including glutamate, and activation of their receptors [Faden and Simon, 1988; Faden et al., 1989; Katayama et al., 1990; Panter and Faden, 1992; Bernert and Turski, 1996; Bullock et al., 1998]. Glutamate imparts its neurotoxic effects by causing decreases in both ATP levels and mitochondrial membrane potentials [Nicotera and Lipton, 1999]. Interestingly, in cerebellar granule cells, low levels of glutamate (100 $\mu\text{mol/L}$) cause necrosis when mitochondrial membrane potentials are irreversibly dissipated [Ankarcrona et al., 1995], and can lead to delayed apoptosis when there is enough ATP to allow caspase-3 activation [Green and Kroemer, 1998].

APOPTOSIS, EXCITOTOXICITY AND BRAIN INJURY

The above findings suggest that: 1) treatment with antagonists to ionotropic glutamate receptors may limit necrotic cell death; 2) treatment with caspase inhibitors can reduce apoptotic neuronal cell death; and 3) dual treatment with both glutamate receptor antagonists and inhibitors of caspase-3 activation may have additive or synergistic actions [Ma et al., 1998; Allen et al., 2000]. Indeed, many studies have shown that antagonists to the N-methyl-D-aspartate (NMDA) ionotropic glutamate receptor (iGluR) are neuroprotective in the adult brain [McIntosh et al., 1998]. Recent findings, however, suggest that treatment with NMDA antagonists alone may actually exacerbate apoptotic cell death, particularly in the developing brain [Pohl et al., 1999].

Ikonomidou and colleagues [1999] found that in rat, NMDA receptors are important for neuronal survival in late fetal or early neonatal brains. They reported that the use of NMDA receptor antagonists triggers widespread apoptotic neurodegeneration in the absence of injury. In a follow-up study, Pohl and colleagues reported that in infant rats subjected to percussive trauma, two distinct forms of brain damage could be identified: primary excitotoxic damage occurring during the first hr following trauma; and secondary damage evolving during the 6–24 hour period post-trauma. They found that giving the NMDA receptor antagonists CPP [3-(2-carboxypiperazin-4-yl)-propyl-1-phosphonate] or dizocilpine (MK-801) during the 6–24 hr period after injury exacerbated

The above findings suggest that: 1) treatment with antagonists to ionotropic glutamate receptors may limit necrotic cell death; 2) treatment with caspase inhibitors can reduce apoptotic neuronal cell death; and 3) dual treatment with both glutamate receptor antagonists and inhibitors of caspase-3 activation may have additive or synergistic actions.

secondary apoptotic damage [Pohl et al., 1999].

Hu and colleagues reported that caspase-3 involvement in cell death following hypoxia-ischemia decreases with neuronal maturation. They show that levels of active caspase-3 decreases with age in postnatal day 7, 15, and 26 rats, respectively, and that Western blot analysis indicates that levels of inactive caspase-3 also declines from high levels in young pups to minimal levels in normal adult rat forebrains. These data suggest that young animals may be more suscep-

tible to caspase-mediated apoptosis [Hu et al., 2000]. It is clear that there is an essential need for an understanding of the differences between responses in the adult versus the pediatric brain if we are to determine proper clinical treatment of head injury.

EXCITOTOXICITY/GLUTAMATE RECEPTORS

Glutamate acts through specific receptors to help maintain the balance between excitatory and inhibitory neurotransmission in the adult brain. When this balance is disrupted, either through alterations in the release of glutamate, or by pathological modulations of its receptors, glutamate can have pronounced effects that can temporarily or permanently disrupt normal functions.

A potential role for glutamate involvement in CNS injury is supported by numerous experimental and clinical studies. First, there are marked elevations in extracellular levels of excitatory amino acids (EAA), including glutamate, in both animal models and humans following trauma or ischemia to the brain or spinal cord [Faden and Simon, 1988; Faden et al., 1989; Katayama et al., 1990; Panter and Faden, 1992; Bullock et al., 1998]. Second, treatment with glutamate receptor antagonists improves behavioral and histological outcome after CNS trauma or ischemia [Meldrum, 1990; Gill, 1994; McIntosh et al., 1998]. Moreover, various in vitro models have implicated glutamate release and glutamate receptor activation as contributors to cell death in hypoxia, oxygen-glucose deprivation, glutamate exposure/toxicity, and traumatic injury [Choi et al., 1988a; Monyer et al., 1989; Choi and Rothman, 1990; Choi, 1992; Regan and Choi, 1994; Ellis et al., 1995; Gwag et al., 1995; Mukhin et al., 1997a,b; 1998]. Although the role of glutamate in the pathophysiology of TBI and other types of CNS injury has been questioned because of its inability to directly kill neurons in the intact rat brain at amounts up to 20–30 mmol [Bullock et al., 1999], many studies show that in vivo, glutamate receptor activation kills cells [Meldrum, 2000]. Moreover, under conditions of metabolic compromise, as seen after trauma, glutamate may cause cell death even at normal physiological concentrations [Di et al., 1999].

Glutamate modulates CNS function by two major classes of membrane bound receptors. Most fast excitatory synaptic transmission occurs via the ionotropic glutamate receptors (iGluRs). Slower second messenger mediated effects are seen upon activation of the

metabotropic glutamate receptors (mGluRs) [for reviews see Bleakman and Lodge, 1998; Anwyl, 1999; Dingledine et al., 1999].

IONOTROPIC GLUTAMATE RECEPTORS

The iGluRs, categorized by the pharmacological agonists to which they bind, consist of the α -amino-3-hydroxy-5-methyl-4-isoxazolepropionic acid (AMPA), high affinity kainate (KA) receptors, and the NMDA receptor. The iGluRs are ligand-gated ion channels which are permeable to potassium (K^+), sodium (Na^+), and calcium (Ca^{2+}) ions (as is the case with NMDA receptors and some AMPA receptors, see below). The subunits of the iGluRs contain three transmembrane domains (M1, M3, and M4) plus a cytoplasm-facing re-entrant membrane loop (M2) that defines the distinct ion selectivities of the ion channel [Dingledine et al., 1999].

AMPA Receptors

To date, four AMPAR members have been identified: GluR1, 2, 3, and 4 (also termed GluRA-D) [see Bleakman and Lodge, 1998 for review]. AMPARs exist in two forms, generated by alternative splicing of the primary transcript, termed "Flip" and "Flop." These forms differ in sequence at a segment which precedes the most C-terminal transmembrane region [Sommer et al., 1990]. The distribution patterns of GluR-Flip mRNA remain largely invariant during postnatal brain development, whereas the GluR-Flop mRNAs are expressed at low levels prior to postnatal day 8 and reach adult levels by postnatal day 14 [Monyer et al., 1991]. Such developmental changes may have important implications for brain injury, because the Flop variants desensitize more quickly than the Flip variants [Bleakman and Lodge, 1998]. Interestingly, the GluR2 subunit displays post-translational editing where a glutamine is altered to arginine within the M2 domain. The unedited GluR2 (Q) displays high divalent cation conductance at membrane potentials more negative or hyperpolarized than -50mV. Homo- or hetero-oligomers containing the edited GluR2 (R) display low Ca^{2+} conductance. AMPARs without the GluR2 subunit display significant Ca^{2+} conductance.

Kainate Receptors

KA receptors consist of the KA1, KA2 high-affinity kainate-binding proteins, and the GluR5-7 kainate-binding subunits [see Bleakman and Lodge, 1998

for review]. These kainate-binding proteins and subunits have limited homology with the other cloned Glu receptors and are less abundant than AMPA receptors. Neither NMDA receptor nor GluR1-4 subunits appear to co-assemble with any of the kainate-binding subunits or proteins. GluR5 and GluR6 can form homomeric channels responsive to agonists whereas KA1, KA2, and GluR7 can form functional heterooligomers with GluR5 or GluR6. The GluR5 and GluR6 subunits of KA receptors are post-transcriptionally modified by RNA editing in a similar fashion to that observed with AMPA receptors [Egebjerg and Heinemann, 1993]. The edited GluR5 (R) and GluR6 (R) produce channels with less conductance than the unedited isoforms [Swanson et al., 1996].

The expression patterns of kainate receptors may have important implications for brain injury. The different combinations of kainate receptors can influence the ligand responsiveness and desensitization kinetics of these receptors. Bahn and colleagues [1994] have shown that there are changes in kainate receptor expression patterns during development. In addition, Paschen and colleagues [1997] indicated that the unedited form of GluR5 plays a role in development of the nervous system. These data demonstrate that kainate receptors change during development, and suggest that these receptors may underlie the pathological differences found between the developing and adult brains during trauma.

NMDA Receptors

In vivo heteromeric NMDA receptor channels are formed by coassembly of two subunit families [see Dingledine et al., 1999 for review]. In the rat brain these have been named the NMDAR1 (NR1) and NMDAR2 (NR2) subunits. The NR1 subunit has only one member, and eight splice variants, whereas the NR2 subunit consists of four members (NR2A, B, C, and D). The actual number of subunits in each heteromeric NMDAR channel is unknown, although there are various estimates of 4 or 5 per receptor complex. An asparagine residue lying at the apex of the M2 reentrant loop regulates the sensitivity of the receptor to various noncompetitive antagonists.

Interestingly, the subunit composition of the NMDA receptor channel is dependent upon anatomical distribution and ontogeny [see Dingledine et al., 1999 for review]. NR1 splice variants have been shown to display distinct regional and developmental expression pat-

terns [Laurie and Seeburg, 1994; Laurie et al., 1995; Zukin and Bennett, 1995]. NR2B and 2D subunit mRNAs are expressed in the embryonic brain whereas the NR2A and NR2C mRNAs appear around birth. It is important to note that while the NR1 subunit has been implicated in binding of the coagonist glycine, the type of NR2 subunit determines the agonist affinities and antagonist sensitivities of the heteromeric NMDAR channel. Perhaps variability in the expression patterns of the NR2 subunits plays a role in the differences in NMDAR antagonist responses found in the developing brain when compared to those in the adult brain (neurotoxic versus neuroprotective, respectively) [Pohl et al., 1999]. Evidence for age-dependent functional differences in NMDA receptors have previously been reported in both the developing rat visual cortex [Carmignoto and Vicini, 1992] and in rat superior collicular neurons [Hestrin, 1992].

METABOTROPIC GLUTAMATE RECEPTORS

The mGluRs are G-protein coupled receptors which bind glutamate and utilize either inositol triphosphate and diacylglycerol or cAMP to mediate their effects, such as regulation of various ion channels and modulation of glutamate receptors [see Anwyl, 1999 for review]. Since 1991, a total of eight separate mGluR sequences and a variety of splice variants have been identified. The mGluRs are categorized into three groups based upon sequence, pharmacology, and function [see Conn and Pin, 1997; Anwyl, 1999; Schoepp et al., 1999 for reviews]. The Group I mGluRs consist of the mGluR1 and mGluR5 subtypes. They activate phospholipase C via G_q proteins and initiate an inositol triphosphate/diacylglycerol (IP_3 /DAG) second messenger cascade. The Group II mGluRs consist of the mGluR2 and mGluR3 subtypes and the Group III mGluRs consist of the mGluR4, mGluR6, mGluR7, and mGluR8 subtypes. Group II and III mGluRs inhibit adenylyl cyclase via $G_{i/o}$ proteins and block the cAMP second messenger cascade.

Similar to the iGluRs, the mGluRs are also dependent upon anatomical location [Shigemoto et al. 1992; Ohishi et al., 1993a,b; Testa et al., 1994] and ontogeny [Aronica et al., 1993; Ghosh et al., 1997; Reid et al., 1997; Simonyi et al., 1998; Berthele et al., 1999; Simonyi et al., 2000]. Additionally, expression patterns of the mGluRs appear to change during disease [Aronica et al., 1997; Al-

Ghoul et al., 1998; Oka and Takashima 1999; Simonyi et al., 1999; Blumcke et al., 2000; Richardson-Burns et al., 2000]. These findings suggest that the mGluRs may play significant roles in perinatal and adult brain injury.

CALCIUM INFLUX

It has been shown that glutamate imparts its neurotoxic effects through alterations in intracellular calcium concentration Ca^{2+} [Meldrum, 2000]. The calcium hypothesis behind neurotoxicity has been well established [Orrenius et al., 1996; Tymianski and Tator, 1996]. Factors determining whether changes in Ca^{2+} are excitotoxic include the time course and magnitude of the response. Toxicity may also be related to the concentration of glutamate present, the specific glutamate receptor subtype stimulated, and the time of receptor exposure to glutamate [Mattson and Mark, 1996] in addition to other variables such as calcium sequestering and buffering [Choi and Rothman, 1990; Orrenius et al., 1996; Tymianski and Tator, 1996]. It should be noted that the outcome of traumatic head injury is dependent upon the degree, duration, and direction of injury [Gennarelli et al., 1982] as well as the age of the patient [Eiben et al., 1984].

These differences may reflect effects of glutamate and subtype-specific receptor agonists on Ca^{2+} . For example, glutamate release after CNS trauma is highly correlated to injury severity [Faden et al., 1989]. Furthermore, the specific glutamate receptor subtypes stimulated within the mammalian CNS during head injury depend upon the location of injury and the age of the patient. Certain subtypes of glutamate receptors are expressed throughout the brain, whereas others show more regional localization. In addition, the expression of the various subunits of the glutamate receptor subtypes as well as the receptors themselves are age dependent [Zilles et al., 1991; Lee and Choi, 1992].

GLUTAMATE RECEPTORS AND CNS/NEURONAL INJURY

AMPA/KA Receptors

Some studies have suggested a limited role for AMPA/KA receptors in traumatic neuronal injury [Regan and Choi, 1994; Prehn et al., 1995]. Recently, however, both in vitro and in vivo experiments have indicated that AMPA/KA receptors may play a significant role in neuronal injury. Various in vitro models show that: 1) AMPA receptors are targets for caspase cleavage [Chan

et al., 1999]; 2) cell injury causes changes in AMPA receptor desensitization that is dependent upon activation of both NMDA receptors and CaMKII [Goforth et al., 1999; 2000]; 3) activating AMPA receptors while preventing desensitization with cyclothiazide may induce apoptosis [Cebers et al., 1997]; 4) kainate receptor activation induces cell death in neurons [Simonian et al., 1996a,b]; and 5) glutamate-induced Zn^{2+} flux through Ca^{2+} permeable AMPA receptors initiates the production of reactive oxygen species [Sensi et al., 1999a,b] known to induce cell death by either necrosis or apoptosis [Tan et al., 1998; Carmody et al., 1999; Davis and Johnson, 1999]. In vivo studies have also shown that AMPA/KA receptor modulation may have therapeutic potential. Studies in ischemia and spinal cord injury have pro-

It should be noted that the outcome of traumatic head injury is dependent upon the degree, duration, and direction of injury as well as the age of the patient. These differences may reflect effects of glutamate and subtype-specific receptor agonists on Ca^{2+} .

vided positive evidence for the use of AMPA/KA antagonists in minimizing secondary sequelae [Bullock et al., 1994; Gill 1994; Wrathall et al., 1994; Matsuoka et al., 1995; O'Neill et al., 1998; Kanellopoulos et al., 2000]. Moreover, lateral fluid percussion (LFP) injury studies in adult rats show that pretreatment with the AMPA/KA receptor antagonist NBQX reduces both cortical and hippocampal damage. Treatment after injury, however, did not protect against cortical damage. Interestingly, if NBQX was given within a therapeutic window (1–7 hr) following injury, there was a decrease in CA3 cell loss [Bernert and Turski, 1996]. However, pretreating 7-day-old rat pups with NBQX prior to LFP injury had no effect on cortical damage [Ikonomidou and Turski, 1996]. Thus, effects of AMPA/KA receptor

modulation in TBI may relate to developmental age.

NMDA Receptors (In Vivo Studies)

It is important to note that although the above studies also showed that pretreatment with NMDA receptor antagonists has neuroprotective effects in both adult [Bernert and Turski, 1996; Ikonomidou and Turski, 1996] and developing rats [Ikonomidou et al., 1996; Ikonomidou and Turski, 1996], post-injury treatment with NMDA receptor antagonists further exacerbates apoptosis in the developing rat brain [Pohl et al., 1999].

Numerous studies using primarily adult animals have found that NMDA receptor antagonists reduce post-traumatic tissue damage and associated behavioral changes (see Table 1). Many noncompetitive ion channel blockers have been effective in reducing pathological changes or improving behavioral outcome after traumatic CNS injury. For example, dextrophan, PCP, MK801, ketamine and dextromethorphan, as well as others, restore ionic homeostasis and metabolic function, reduce brain edema, or improve recovery of function after experimental TBI (Table 1). Concerns have been raised that such noncompetitive antagonists also have potentially undesirable side effects, including increased vacuolization of neurons, as well as psychotomimetic effects [Olney et al., 1989; Kornhuber and Weller, 1997]. However, it is important to note that such vacuolization does not occur in higher species, and in rodents this occurs only when doses are above those providing optimal neuroprotection. More recently developed noncompetitive antagonists have lower binding affinities within the ion channel, which may result in fewer unwanted side effects [McIntosh et al., 1998]. One example is remacemide HCl [2-amino-N-(1-methyl-1,2-diphenylethyl) acetamide hydrochloride], which reduced lesion volume in rats subjected to lateral FPI [Smith et al., 1997]. MK801 and other NMDA antagonists also produce beneficial effects in models of spinal cord trauma, suggesting that glutamate and modulation of glutamate receptors is important in spinal cord injury as well as TBI [Faden et al., 1988; Haghighi et al., 1996].

Several competitive NMDA receptor antagonists such as APV (2-amino-5-phosphovaleric acid), CPP (3-(2-carboxypiperizin-4-yl)-propyl-1-phosphonic acid), or CGS-19755, can decrease concentrations of extracellular glutamate, reduce cerebral edema, attenuate metabolic

Table 1. Glutamate Receptor Modulation in Traumatic Brain Injury¹

Site/Mechanism of Action	Compound	Conc(s) Used	Injury Model	Age	Admin. Route	Admin. Time ²	Reported Outcome	References
AMPA/KA Antagonist	NBQX	3, 30 mg/kg	LFP	A	i.p.	Pre., Post	↓ lesion volume, cell death	(Bernert and Turski, 1996)
	APV	100 μM, 1, 10 mM	CFP	A	M	Pre.	↓ glucose utilization	(Kawamata et al., 1992)
	CPP	100 μg	LFP	A, N	i.c.v.	Pre., Post	↑ motor function, ↑ apoptosis; ↓ necrosis	(Faden et al., 1989; Pohl et al., 1999)
	CGS-19755	30 mg/kg	LFP	A	i.p.	Pre.	↓ Glu release	(Pantier and Faden, 1992)
NMDA Antagonist (non-competitive)	Dextrophen	10 mg/kg	LFP	A	i.v.	Pre., Post	↓ Glu release; ↑ bioenergetic status, motor function and Mg ²⁺ homeostasis	(Faden et al., 1989; Pantier and Faden, 1992)
	Dextrothorphan	10 mg/kg	LFP	A	i.v.	Pre.	↑ bioenergetic status, motor function and Mg ²⁺ homeostasis	(Golding and Vink, 1993)
NMDA Glycine site	PCP	1, 2, 4 mg/kg	CFP	A	i.p.	Pre.	↑ motor function	(Hayes et al., 1988)
	MK801	0.3, 1, 3 mg/kg	CFP, LFP, WD	A, N	i.v., i.p.	Pre., Post	↑ bioenergetic status, motor/cognitive function and ionic homeostasis; ↓ apoptosis; ↓ edema, necrosis	(McIntosh et al., 1989; McIntosh et al., 1990; Shapira et al., 1990; Hamim et al., 1993; Pohl et al., 1999)
	Ketamine	4 mg/kg	LFP	A	i.v.	Post	↑ motor/cognitive function; ↓ edema	(Smith et al., 1993a)
	Remacemide HCl	10, 25 mg/kg	LFP	A	i.v.	Post	↑ lesion volume	(Smith et al., 1997)
NMDA Poly-amine site	CNS-1102 (Cereata)	2 mg/kg	CCI	A	i.v.	Post	↓ contusion volume, edema and H ₂ O content	(Kroppenschuetz et al., 1998)
	HU211	5, 25 mg/kg	WD	A	i.v., i.p.	Pre., Post	↑ motor/cognitive function; ↓ edema and BBB breakdown	(Shohami et al., 1993; Shohami et al., 1995)
NMDA Glycine site	Kynuremate	300 mg/kg	LFP, CFP	A	i.v.	Post	↑ motor/cognitive function, ionic homeostasis; ↓ edema and cell loss	(Kawamata et al., 1992; Smith et al., 1993b; Hicks et al., 1994)
	Indole-2-carboxylic acid	20, 50 mg/kg	LFP	A	i.v.	Post	↑ motor/cognitive function, ionic homeostasis; ↓ edema	(Smith et al., 1993b)
NMDA Mg ²⁺ site	MgCl ₂	12.5, 125 μM, 100, 300 μM/kg	LFP	A	i.v.	Post	↑ motor/cognitive function, Mg ²⁺ homeostasis; ↓ edema	(McIntosh et al., 1989b; Smith et al., 1993a; Okiyama et al., 1995; Heath and Vink, 1999)
	MgSO ₄	0.1 mEq 100, 750 μM/kg	LFP, WD	A	i.v., i.m.	Pre., Post	↑ motor/cognitive function, Mg ²⁺ homeostasis, bioenergetic status; ↓ edema	(McIntosh et al., 1988; Okiyama et al., 1995; Heath and Vink, 1998; Heath and Vink, 1999)
NMDA Poly-amine site	Eliprodil	1, 10 mg/kg	LFP	A	i.p., i.v.	Post	↑ cognitive function; ↓ lesion volume	(Toulmond et al., 1993; Hogg et al., 1998)
	CP-101, 606	6.5 + 1 mg/kg	LFP	A	i.p., sc.	Post	↑ cognitive function	(Okiyama et al., 1997)
ODC synthesis inhibitor	CP-101, 581	5 + 1 mg/kg	LFP	A	i.p., sc.	Post	↑ cognitive function	(Okiyama et al., 1997)
	CP-98, 113	5 + 1 mg/kg	LFP	A	i.p., sc.	Post	↑ cognitive function; ↓ edema	(Okiyama et al., 1997; Okiyama et al., 1998)
Group I mGluR1 antagonist	DFMO	500 mg/kg	CCI	A	i.p.	Post	↓ edema	(Bakaya et al., 1996)
	AIDA	10 nmol, 55 μg	LFP	A	i.c.v.	Pre., Post	↑ motor/cognitive function; ↓ lesion volume, cell death	(Faden et al., 2001; Lyeth et al., 2001)
Group II mGluR2/3 agonist	MPEP	55 μg	LFP	A	i.c.v.	Pre.	↑ motor/cognitive function; ↓ lesion volume	(Moresyan et al., 2001)
	LY354740	5 mg/kg	LFP	A	i.v.	Post	↑ motor function	(Allen et al., 1999a)
Group I/II antagonist	DCG-IV	500 fmol	LFP	A	i.c.v.	Post	↓ cell death	(Zwienenberg et al., 2001)
	MCPG	0.2 μM, 0.5 μmol	LFP	A	i.c.v.	Pre., Post	↑ motor/cognitive function; ↓ cell death	(Gong et al., 1995; Mukhin et al., 1996)
Inhibitors of Glu release	619C89	30 mg/kg	LFP	A	i.v.	Pre.	↑ motor/cognitive function; ↓ cell death and gliosis	(Sun and Faden, 1995a)
	BW/003C87	10 mg/kg	LFP	A	i.v.	Post	↓ edema	(Okiyama et al., 1995)
Other	Riluzole	4, 8 mg/kg	LFP	A	i.v.	Post	↑ motor/cognitive function; ↓ edema and lesion volume	(McIntosh et al., 1996; Bareyre et al., 1997; Wahl et al., 1997; Zhang et al., 1998)

¹LFP: lateral fluid percussion; CFP: central fluid percussion; WD: weight drop; BBB: blood brain barrier; M: microdialysis; A: adult; N: newborn; Pre.: pre-injury; Post: post-injury.
²Represents admin. time associated with reported outcome.

dysfunction, and improve behavioral outcome following FPI (Table 1).

NMDA Receptors (In Vitro Studies)

In vitro studies show that competitive NMDA receptor antagonists are neuroprotective against glutamate and transient oxygen-glucose deprivation [Monyer et al., 1989; Choi and Rothman, 1990; Choi, 1992; Gwag et al., 1995], as well as in various in vitro trauma models [Regan and Choi, 1994; Mukhin et al., 1997b; 1998]. In one such model, characterized by Ellis and colleagues [1995], cells cultured upon a silastic membrane are injured by stretching them with a pulse of nitrogen. This type of injury, which may replicate the shearing forces generated during TBI, decreases Mg^{2+} blockade of NMDA receptors, with concomitant increases in ionic currents and intracellular Ca^{2+} [Zhang et al., 1996]. Follow-up studies showed that: 1) 24 hr post-insult, NMDA-stimulated Ca^{2+} is increased, indicating enhanced sensitivity of the NMDA receptors following injury [Rzigalinski, 1998]; 2) AMPA receptor current is increased, via NMDA receptor and CaMKII dependent reductions in AMPA receptor desensitization [Goforth et al., 2000]; and 3) GABA release is increased via yet unidentified mechanisms [Kao et al., 2000]. Additional use of this model using septohippocampal cocultures showed that stretch injury activates both calpain and caspase-3 and leads to necrotic and apoptotic cell death [Pike et al., 2000]. Together, these studies demonstrate that in vitro, Glu and NMDA receptor activation can cause neuronal cell death.

Interestingly, in vitro work from a number of laboratories has shown that, depending upon experimental conditions, NMDA receptors may contribute to either apoptotic or necrotic cell death. For example, Glu-induced apoptosis may be unmasked by iGluR blockade [Gwag et al. 1995], and shifts from cell death into primarily necrotic or apoptotic types may be caused by alterations in underlying cellular bioenergetic state [Allen et al., 1999c; Nicotera and Lipton, 1999]. Relating to post-traumatic injury, Allen and colleagues found that cell death shifted from primarily necrotic to substantially apoptotic when mild metabolic insults (brief exposure to 3-NP and glucose deprivation) were combined with trauma.

Modulatory sites on the NMDA receptor, such as glycine, Mg^{2+} , or polyamine have also been investigated. Kynurenate (KYN) and indole-2-car-

boxylic acid (I2CA), both glycine site antagonists, reduced neurobehavioral deficits, while I2CA decreased edema, and KYN protected against hippocampal cell loss following lateral FPI in rats [Smith et al., 1993b; Hicks et al., 1994]. Although KYN is characterized as a glycine site antagonist it binds nonselectively at other Glu receptors and may be exerting its effects through other mechanisms as well. Mg^{2+} salts, such as $MgCl_2$ and $MgSO_4$, can also noncompetitively antagonize the NMDA receptor. Such treatment improves motor and cognitive recovery, decreases edema, and normalizes brain bioenergetics following lateral FPI (Table 1). Eliprodil as well as ifenprodil derivatives (e.g., CP-101,606; CP-101,581; CP-98,113) are polyamine site antagonists, which have been shown to reduce lesion volume, edema, and motor/cognitive function following lateral FPI (Table 1). Although eliprodil shows some selectivity for the NMDA receptor NR2B subunit, it may also exert its effects through the blockade of N, P and/or Q-type Ca^{2+} channels [Biton et al., 1997]. In addition, ornithine decarboxylase (ODC) inhibition decreases injury-induced edema [Baskaya et al., 1996]. ODC is an enzyme necessary for polyamine synthesis. The extended therapeutic windows for both eliprodil and $MgSO_4$ (up to 24 hr post-injury) may enhance their clinical utility (Table 1).

To address the role of NMDA receptors in the pathophysiology of post-traumatic brain injury, Wahlestedt and colleagues [1993] used an antisense oligodeoxynucleotide (as-ODN) directed against NMDAR1 subunits to inhibit the synthesis of NMDAR1. They found that reduced expression of NMDA receptors reduced the volume of focal ischaemic infarction produced by occlusion of the middle cerebral artery in the rat, and prevented NMDA-induced neurotoxicity in vitro. Similarly, Sun and Faden [1995b] found that as-ODN NMDAR1 decreased mortality, motor dysfunction, and reactive gliosis when given prior to lateral FPI.

Examples of other drugs believed to reduce injury-associated cellular and behavioral damage either via inhibition of Glu release or blockade of NMDA receptor activation include: the cannabinoid, HU-211 (7-hydroxy-tetrahydrocannabinol 1,1-dimethylheptyl), and the use-dependent sodium channel blockers Riluzole, 619C89, and BW1003C87. HU-211 has a therapeutic window of up to 4 hr and has been shown to decrease BBB breakdown, reduce edema, and enhance motor and cognitive functions fol-

lowing weight drop injury in rats, presumably via actions on the Glu receptor system (Table 1). However, this compound has multiple potential neuroprotective actions, including inhibition of TNF- α [Shohami et al., 1997]. Glutamate release is attenuated by use-dependent sodium channel blockers [Graham et al., 1994]. Recent studies provide evidence that several of these compounds, such as Riluzole, 619C89, and BW1003C87, reduce hippocampal cell loss and reactive gliosis, restore neurobehavioral function, and decrease lesion volume and edema (Table 1). It should be noted, however, that these compounds are effective after delayed treatment, when glutamate levels have returned to normal. In addition, it is important to stress that HU-211 and the use-dependent sodium channel blockers have additional mechanisms of action which may be a significant component of their observed neuroprotective effects.

NMDA Receptors (Binding and CNS Injury)

Although the NMDA receptor system is altered following traumatic injury, the actual mechanisms involved have yet to be completely elucidated. Miller and colleagues [1990] found that in rats, injury causes a significant decrease in [3H]NMDA binding to the NMDA receptor in the hippocampus (3 hr post-central FPI), and in the neocortex (5 min, 3 hr and 24 hr post-TBI). In addition, Sun and Faden [1994] found decreased [3H]MK801 receptor binding following trauma to the spinal cord. This decrease in NMDA receptor binding may reflect compensatory changes in receptor binding affinity following a post-injury excitotoxic surge of Glu. For example, Temple and colleagues [1997] found that there were decreases in immunoreactivity for hippocampal NMDAR1 subunits and NMDAR2A/B subunits 24 hr, 8 days, and 16 days following lateral FPI with the most profound decreases in the NMDAR1 subunit at 24 hr post-injury. In a recent study investigating the chronic enhancement of NMDA receptors as a possible alternative therapeutic approach to cognitive loss, Temple and Hamm [1996] found that chronic administration of a positive modulator of the NMDA-associated glycine site, D-Cycloserine (DCS; 30 mg/kg, i.p.; starting 24 hr post-injury through 15 days post-injury) significantly improved cognitive performance of rats subjected to lateral FPI to the level of sham-injured rats. Although these results suggest that chronic positive modulation at the

NMDA receptor may provide an additional therapeutic option, these positive effects due to glutamate activation beginning after subacute injury may not outweigh their potential effects on apoptosis.

Metabotropic Receptors

Until recently, the general absence of specific pharmacological agents has hindered the identification of specific mGluR subtype effects on neuronal and glial cells. Therefore, various groups have deduced effects through a myriad of experimental designs and models. The mGluRs have been shown to be regulators of various K^+ and Ca^{2+} ion channels and modulators of both AMPA and NMDA receptor currents and GABA release [see Anwyl, 1999 for review]. The mGluRs, like the iGluRs, also have distinct anatomical and ontogenetic distributions [previously referenced]. A recent study by Angenstein and colleagues [1999] showed that mGluR activation induced increases in protein kinases A and C (PKA and PKC) as well as casein kinase II substrate phosphorylation in hippocampal slices from 12-day-old rats. In contrast, they showed that in hippocampal slices from 56-day-old rats, mGluR activation only induces increases in PKA and, to a lesser extent, PKC substrate phosphorylation. Taken together, these findings suggest ontogenetic differences in the way in which mGluRs modulate the systems listed above. In addition, the known roles for these various systems in either neurotoxicity or neuroprotection, and the ability of the mGluRs to modulate them, suggests that the mGluRs are involved in neuronal injury following trauma. A number of in vivo and in vitro studies have confirmed this prediction.

Metabotropic Receptors (In Vivo Studies)

In general, a number of the in vivo studies suggest that activation of group I mGluRs is excitotoxic whereas activation of group II and III mGluRs is neuroprotectant. Early studies investigating the role of mGluRs in neuronal injury involved 1S,3R-aminocyclopentane dicarboxylate (1S,3R-ACPD), a conformationally restricted glutamate analogue, or its racemic mixture, commonly referred to as *trans*-ACPD. McDonald and Schoepp demonstrated that 1S,3R-ACPD injected intrastrially into 7-day-old rats potentiated NMDA-induced injury. In addition, they found that higher doses of 1S,3R-ACPD alone could cause seizures and neurodegeneration in both neonatal and adult rats

[Sacaan et al., 1992; McDonald et al., 1993; Schoepp et al., 1995]. More recently, Agrawal and colleagues [1998] reported that post-traumatic injury in spinal cord white matter isolated from adult rats is exacerbated by *trans*-ACPD. Orlando and colleagues [1995] showed that local injection of (S)-4C3HPG, an mGluR1 subtype specific competitive antagonist and group II mGluR agonist, prevents striatal neuron degeneration caused by the endogenous NMDA receptor agonist quinolinic acid. Similar to the early phase of Huntington's chorea, striatal infusion of quinolinic acid induces a loss of medium-sized spiny neurons with relative sparing of interneurons. When administered intracerebroventricularly either 5 min before or 15 min before and 1 hr after trauma, the group I/II mGluR antagonist MCPG improves neurological recovery, post-injury behavioral deficits, and decreases CA1 pyramidal and ipsilateral hippocampal cell loss after lateral FPI [Gong et al., 1995; Mukhin et al., 1996].

A major limitation to the conclusions of the studies listed above is the nonspecificity of the pharmacological agents used [see Schoepp et al., 1999 for review]. First, ACPD activates both group I and II mGluRs. Nevertheless, it appears that the group I mGluR mediated effects are more pronounced than those of the group II. This is probably due to group I mGluR modulation of NMDA and AMPA receptors [see Anwyl, 1999 for review]. Second, striatal neurons express both mGluR5 and mGluR3. (S)-4C3HPG has mixed activity at these receptors. Therefore, it is difficult to ascertain which group is involved. However, recent findings by Buisson and Choi [1995], showing that NMDA-induced lesions on the striatum are decreased by (S)-4C3HPG in a cAMP-dependent manner strongly suggest the involvement of group II receptors. Third, although MCPG exhibits greater antagonist effects at the mGluR1 rather than the mGluR5 subtype, it is also an antagonist at the group II mGluRs [Schoepp et al. 1999]. Recent findings by Lea and Sarvey [2000] show that the mGluR3 specific antagonist β -NAAG [Lea IV et al., 2001] can reduce epileptiform burst frequency of rat dentate granule cells suggesting that these receptors may provide a possible protective mechanism against excitotoxicity [Lea IV and Sarvey, 2000].

However, the recent development of new selective pharmacological agents has enabled us to clearly identify roles for the group I, II, and III mGluRs in injury.

In rats infused with NMDA into the caudate nucleus, and in gerbils exposed to global ischemia, intrastrially administered LY367385, a potent and selective mGluR1a antagonist, provided significant neuroprotective effects [Bruno et al., 1999]. Under similar conditions, the less specific mGluR1a and mGluR5 subtype antagonist, LY367366, also protected against injury albeit to a lesser extent. Rats infused with the selective mGluR1 antagonist AIDA, administered either 15 min prior to, or 5 min post-lateral FPI, also showed significant neuroprotection as well as improved cognitive and motor functions [Faden et al., 2001; Lyeth et al., 2001]. Together, these findings implicate a role for the group I mGluR subtype mGluR1a in neurodegeneration [Bruno et al. 1999]. Interestingly, rats given the selective mGluR5 antagonist MPEP 15 min prior to lateral FPI showed improved cognitive and motor functions and reduced lesion volume [Movsesyan et al., 2001]. In contrast, certain in vitro models show that mGluR5 subtype activation appears to be neuroprotective in certain in vitro models (see below). It appears likely that these differences are due to the ability of MPEP to directly reduce NMDA receptor current [Movsesyan et al., 2001].

In vivo studies using the gerbil model of global ischemia showed that the selective group II mGluR agonists LY354740 and LY379268, administered prior to or post-injury (respectively), provided significant neuroprotective effects [Bond et al., 1998; 2000]. Neuroprotection by LY379268 was attenuated by the selective group II antagonist LY341495 [Bond et al., 2000]. In vivo studies using lateral FPI showed that rats administered LY354740 [Allen et al., 1999a] or LY379268 [Di et al., 2000] 30 min post-injury showed improved neurological recovery 14 days after trauma. Similarly, the group II agonist DCG-IV, intracranially injected into rats immediately after lateral FPI, significantly reduced neurodegeneration [Zwienenberg et al., 2001]. Together these findings suggest that group II mGluR agonists may prove to be useful in the management of clinical head injury.

Gasparini and colleagues showed that (R,S)-4-phosphonophenylglycine (PPG), a novel, potent and selective agonist for group III mGluRs, protected against NMDA and quinolinic acid-induced striatal lesions in rats and was anticonvulsive in the maximal electroshock model in mice [Gasparini et al., 1999]. Although these findings suggest that the group III mGluRs are attractive targets

for neuroprotective and anticonvulsive therapy, Henrich-Noack and colleagues [2000] show that PPG had no effect on either focal cerebral ischemia in mice nor global cerebral ischemia in gerbils or rats. They did, however, find improved recovery of population spikes measured in acute hippocampal slices exposed to hypoxic/hypoglycemic insult. These results suggest that the group III mGluRs may be promising targets for treatment of excitotoxicity, but not ischemic-induced apoptosis.

Metabotropic Receptors (In Vitro Studies)

In contrast to the in vivo studies above, a number of in vitro studies suggest that activation of group I can be either neuroprotective or excitotoxic. This variability appears to be dependent upon the expression model and type of neuronal death (necrosis or apoptosis) under investigation. In 1991, Koh and colleagues reported that 1S,3R-ACPD reduced NMDA-induced degeneration of cultured mouse cortical neurons. Similarly, 1S,3R-ACPD reduce injury in mesencephalic neurons [Ambrosini et al., 1995], cultured rat cerebellar granule cells [Valerio et al., 1995], and rat hippocampal slices [Pizzi et al., 1996a]. Characterization of the neuroprotective effects of 1S,3R-ACPD in cultured rat cerebellar granule cells [Pizzi et al., 1993; 1996b], indicated that its ability to block increases in intracellular Ca^{2+} caused by Glu or KA, was protein kinase C (PKC) dependent [Pizzi et al., 1996b]. The involvement of PKC was supported by other findings which showed that: 1) nitric oxide (NO)-induced toxicity could be averted by 1S,3R-ACPD modulation of PKC activity [Maiese et al., 1996]; and 2) the specific group I agonist (S)-DHPG reduced necrotic cell death induced by oxygen-glucose deprivation in a PKC-dependent manner [Schroder et al., 1999]. Interestingly, the mGluR5 subtype may be responsible for the neuroprotective effects induced with these group I mGluR agonists. This is supported by the findings of Montoliu and colleagues [1997] who showed that activation of mGluR5 with the specific agonist tADA [Kozikowski et al., 1993] prevented toxicity induced by glutamate or NMDA in cultured rat cerebellar granule cells [Montoliu et al., 1997].

Group I mGluR activation was also neuroprotective against apoptotic cell death. In rat cerebellar granule cells, activation of group I mGluRs also reduce apoptosis induced by β -amyloid, a protein involved in the pathogenesis of Alz-

heimer's disease [Copani et al., 1995; Allen et al., 1999b]. In these cells, group I mGluR activation is protective whereas inhibition exacerbates cell death. This neuroprotective action may be mediated through modulation of intracellular Ca^{2+} homeostasis. Further studies by this lab show that oxygen-glucose deprivation-induced necrotic cell death, in rat cortical neuronal-glial cocultures, can be reduced by the group I mGluR antagonist AIDA. Moreover, apoptotic cell death, induced by both the nonspecific PKC inhibitor staurosporine and the topoisomerase II inhibitor etoposide, can be decreased by the group I agonist (S)-DHPG and the mGluR5 selective agonist CHPG. Interestingly, the protective effects of DHPG can be completely reversed by co-application of the group I mGluR antagonist AIDA. These data suggest that activation of group I mGluRs exacerbates necrosis, whereas both mGluR1 and mGluR5 activation play a role in the attenuation of apoptosis [Allen et al., 2000]. This prediction is supported by a recent study by Copani and colleagues [1998] which suggests that a decline in the expression of mGluR5 allows programmed cell death in cerebellar granule cells developing in culture [Copani et al., 1998]. (S)-DHPG also reduced NO-induced injury in primary hippocampal cultures presumably by preventing NO-induced decreases in pH and concomitant endonuclease activation and subsequent cell death [Vincent et al., 1999]. Interestingly, increased mechanical injury-induced cell death in cortical cultures occurred when extracellular pH was increased in association with NMDA-dependent cell loss and decreased under acidic conditions [Mukhin et al., 1998].

In cortical and spinal cord neurons, activation of group I mGluRs appears to exacerbate necrotic neurotoxicity. In mouse cortical cultures, group I mGluR agonists amplify NMDA-induced neuronal degeneration either by PKC activation [Bruno et al., 1995b], or by an enhancement of presynaptic Glu release [Strasser et al., 1998]. This effect may be mediated by the group I mGluR subtype mGluR1a, as LY367385, a potent and selective antagonist of mGluR1a, was neuroprotective in mouse cortical cultures exposed to an NMDA pulse [Bruno et al., 1999]. In rat cortical/glial cocultures, group I mGluR activation exacerbated in vitro punch injury-induced delayed neuronal injury [Mukhin et al., 1996]. The exact mechanism behind the group I mGluR effect has yet to be determined although it appears to require in part NMDA receptor modulation, as the

MK801 partly reduced exacerbation of the DHPG-induced injury [Mukhin et al., 1997b]. Modulation of NMDA receptors by group I mGluRs has been suggested to be through PKC activation and subsequent reduction of the Mg^{2+} block of NMDA receptors. However, other possible mechanisms include: 1) increased release of Ca^{2+} from intracellular stores via IP_3 -dependent mechanisms, or 2) increased production of arachidonic acid [Faden et al., 1999]. mGluR1 is most likely involved in the exacerbation of this injury, as an mGluR1 specific antisense-oligodeoxynucleotide (as-ODN) reduced injury, while an mGluR5 specific as-ODN did not [Mukhin et al., 1996]. In mouse cortical cells and in isolated spinal cord segments, where mGluR1 immunoreactivity is present, injury may also be exacerbated by activation of mGluR1 [Agrawal et al. 1998; Bruno et al. 1999].

Similar to the in vivo studies, a number of in vitro studies suggest that activation of group II mGluRs is neuroprotective. In cultured mouse cortical neurons, activation of group II mGluRs with DCG-IV, L-CCG-1, and 4C3HPG attenuates NMDA, Glu, or KA induced toxicity [Bruno et al., 1994; 1995a; Buisson and Choi, 1995; Bruno et al., 1996a; 1997; 1998b]. In addition, colchicine induced apoptosis is also protected against by activation with L-CCG-1 and trans-ACPD, possibly via both phosphoinositide activation of PKC and adenylyl cyclase inhibition [Kalda and Zharkovsky 1999; Kalda et al., 2000]. In mouse neuronal/glial cortical cocultures, NMDA-induced toxicity is reduced by the group II specific agonist 2R,4R-APDC [Battaglia et al., 1998], and the amino derivative 1-amino-APDC [Kozikowski et al., 1999]. 1-amino-APDC is a compound related to 2R,4R-APDC, which acts as a partial agonist at group II receptors. In rat cortical neuronal/glial cell cocultures injured with an in vitro punch trauma device, DCG-IV, LY354740, and 2R,4R-APDC have all been shown to reduce injury [Allen et al., 1999a]. These neuroprotective effects, found to be additive to the effects of group I mGluR and NMDA receptor antagonism, suggest that neuroprotection involves down-regulation of both the phosphoinositide and cAMP pathways. In support of a neuroprotective role via cAMP downregulation, Allen and colleagues [1999b] showed that the cAMP analogue 8-Br-cAMP exacerbates cell death while intracellular cAMP levels increase following injury [Allen et al., 1999a]. Group II mGluR agonists also cause a reduction in

the release of glutamate following trauma [Allen et al. 1999a]. Reducing pre-synaptic glutamate release is beneficial, as it limits both NMDA and group I mGluR activation; both of which have been shown to contribute to post-traumatic cell death.

Importantly, the protection provided by group II mGluR agonists may involve the interaction of glial cells. When mixed neuronal/glial cultures treated with NMDA were co-treated with medium taken from pure astrocyte cultures pre-treated with DCG-IV, L-CCG-1, or 4C3HPG for 2–20 hr, the astrocyte media was found to be neuroprotective [Bruno et al., 1997; 1998a]. One possibility is that activating group II mGluRs on astrocytes increases the formation and release of transforming growth factor beta which in turn protects neighboring neurons from excitotoxic death [Bruno et al. 1998a].

In contrast to the neuroprotective roles of various group II mGluR agonists, however, L-CCG-1 activation of group II mGluRs in primary cultures of cerebellar granule cells does not provide neuroprotection against glutamate induced toxicity [Montoliu et al., 1997]. It is important to note, however, that L-CCG-1, like DCG-IV and 4C3HPG, is not a pure group II agonist [see Schoepp et al., 1999 for review]. DCG-IV can also act as an NMDA receptor agonist [Wilsch et al., 1994] whereas L-CCG-1 has some activity at group I mGluRs at high concentrations [Nakagawa et al., 1990] with an EC₅₀ apparently less for mGluR1 than mGluR5 [Flor et al., 1996]. Additionally, L-CCG-1 has some affinity for the group III mGluR subtypes mGluR4a [Eriksen and Thomsen, 1995] and mGluR8 [Saugstad et al., 1997]. 4C3HPG acts as a group I antagonist and exhibits partial agonist activity at the group I mGluR subtype mGluR5 [Watkins and Collingridge, 1994].

Similar to the *in vivo* studies, a number of *in vitro* studies suggest that activation of group III mGluRs is neuroprotective. In mouse cerebellar granule cells (via mGluR7) and cortical neurons (via mGluR4), NMDA-induced excitotoxicity was reduced with the specific group III agonist L-AP4 [Bruno et al., 1996b; Lafon-Cazal et al., 1999]. In rat cortical cultures and hippocampal cultures, L-AP4, presumably through mGluR4 mediated protein kinase A (PKA) modulation, has also been shown to reduce NO-induced toxicity [Maiese et al., 1995; 1996]. In rat cortical neuronal/glial cocultures, L-AP4 and L-SOP provide 30% neuroprotection against *in*

vitro punch injury [Faden et al., 1997]. MAP-4 and MSOP, respective methyl-derivatives of L-AP4 and L-SOP, acting as antagonists to the group III mGluRs [Schoepp et al., 1999], exacerbate traumatic injury. Because basal cAMP levels were lower in cells treated with agonists, a role for cAMP regulation in injury was concluded. Unfortunately, the mRNA for all four group III receptors was found in these cultures, and it was not determined which specific mGluR subtype(s) mediate this effect.

The influence of mGluRs on neurotoxicity is also strongly supported by research investigating mGluR-mediated effects on high voltage activated (HVA) Ca²⁺ channels as well as K⁺ channels. Copani and colleagues [1995] reported that mGluR group II and III agonists, as well as the HVA Ca²⁺ channel blocker nimodipine, reduced β -amyloid induced toxicity in cultured cerebellar granule cells. Stefani and colleagues [1996] suggested that the mGluR-mediated effects on high voltage activated (HVA) Ca²⁺ channels may influence neurotoxicity. Activation of distinct K⁺ channels and subsequent K⁺ efflux of are believed to underlie certain forms of neuronal apoptosis [Yu et al., 1997]. The interaction of mGluRs with K⁺ channels suggests a potential role for these mGluR-mediated receptors in neuronal injury.

SUMMARY

Although there are numerous *in vivo* and *in vitro* studies implicating both iGluRs and mGluRs in neuronal injury in the adult brain, there are relatively few studies investigating their roles in neuronal injury in the developing brain. There remains the necessity to rectify this imbalance so that we may better understand the differences between the adult and developing brain which can impact the treatment of head trauma in the pediatric population. In the adult brain, the activation of AMPA/KA and NMDA ionotropic glutamate receptors can mediate cell death. These data suggest the need for a multifaceted approach to the therapeutic prevention of neuronal injury in the adult brain. Receptor antagonists directed towards the more calcium permeable AMPA receptors may provide a means to diminish the activation of reactive oxygen species, as well as the influx of presynaptically released Zn²⁺. In contrast, it appears that in the developing brain the NMDA receptor, but not the AMPA receptor, is involved, and that there is a limited temporal window of opportunity for the use of NMDA antagonists to block necrosis before they

exacerbate apoptosis. For example, in the developing brain, treatment with NMDA receptor antagonists prior to injury is neuroprotective whereas they exacerbate apoptosis if given after injury. This suggests that in the developing brain, glutamate acting through the NMDA receptor suppresses programmed cell death [Pohl et al., 1999]. Combined treatment with caspase inhibitors has shown to be more effective than treatment with either iGluR antagonists or caspase inhibitors alone. Clearly, there remains a need to identify similarities and differences in other cellular modulators of the NMDA receptors in both the developing and adult brains.

With regard to the mGluRs, the responses due to activation of group I receptors are dependent upon whether necrosis or apoptosis has been induced. For example, group I activation exacerbates necrotic injury and attenuates apoptotic cell death in cortical neurons. Group II and III mGluRs attenuate both types of injury. Although the use of mGluR agonists and antagonist will most likely provide an additional means to clinically treat TBI, especially if used in conjunction with antagonists to the various iGluRs, the contrasting effects of group I mGluRs bring into question the usefulness of group I mGluR specific compounds. In addition, the myriad of other effects of the mGluRs, especially in the modulation of cAMP and IP3/DAG levels, highlights the need to better understand ontogenic changes in the signal transduction cascades. ■

REFERENCES

- Agrawal SK, Theriault E, Fehlings MG. 1998. Role of group I metabotropic glutamate receptors in traumatic spinal cord white matter injury. *J Neurotrauma* 15:929–941.
- Al-Ghoul WM, Meeker RB, Greenwood RS. 1998. Kindled seizures increase metabotropic glutamate receptor expression and function in the rat supraproptic nucleus. *J Neurosci Res* 54:412–423.
- Allen J, Ivanova S, Fan L, et al. 1999a. Group II metabotropic glutamate receptor activation attenuates traumatic neuronal injury and improves neurological recovery after traumatic brain injury. *J Pharmacol Exp Ther* 290:112–120.
- Allen JW, Eldadah BA, Faden AI. 1999b. Beta-amyloid-induced apoptosis of cerebellar granule cells and cortical neurons: exacerbation by selective inhibition of group I metabotropic glutamate receptors. *Neuropharmacology* 38:1243–1252.
- Allen JW, Knobloch SM, Faden AI. 1999c. Combined mechanical trauma and metabolic impairment *in vitro* induces NMDA receptor-dependent neuronal cell death and caspase-3-dependent apoptosis. *FASEB J* 13:1875–1882.
- Allen JW, Knobloch SM, Faden AI. 2000. Activation of group I metabotropic glutamate receptors reduces neuronal apoptosis but in-

- creases necrotic cell death in vitro. *Cell Death Differ* 7:470-476.
- Ambrosini A, Bresciani L, Fracchia S, et al. 1995. Metabotropic glutamate receptors negatively coupled to adenylate cyclase inhibit N-methyl-D-aspartate receptor activity and prevent neurotoxicity in mesencephalic neurons in vitro. *Mol Pharmacol* 47:1057-1064.
- Angenstein F, Buchner K, Staak S. 1999. Age-dependent differences in glutamate-induced phosphorylation systems in rat hippocampal slices. *Hippocampus* 9:173-185.
- Ankarcrona M, Dypbukt JM, Bonfoco E, et al. 1995. Glutamate-induced neuronal death: a succession of necrosis or apoptosis depending on mitochondrial function. *Neuron* 15:961-973.
- Anwyl R. 1999. Metabotropic glutamate receptors: electrophysiological properties and role in plasticity. *Brain Res Rev* 29:83-120.
- Aronica E, Dell'Albani P, Condorelli DF, et al. 1993. Mechanisms underlying developmental changes in the expression of metabotropic glutamate receptors in cultured cerebellar granule cells: homologous desensitization and interactive effects involving N-methyl-D-aspartate receptors. *Mol Pharmacol* 44:981-989.
- Aronica EM, Gorter JA, Paupard MC, et al. 1997. Status epilepticus-induced alterations in metabotropic glutamate receptor expression in young and adult rats. *J Neurosci* 17:8588-8895.
- Bahn S, Volk B, Wisden W. 1994. Kainate receptor gene expression in the developing rat brain. *J Neurosci* 14:5525-5547.
- Banasik KJ, Xia Y, Haddad GG. 2000. Mechanisms underlying hypoxia-induced neuronal apoptosis. *Prog Neurobiol* 62:215-249.
- Bareyre F, Wahl F, McIntosh TK, et al. 1997. Time course of cerebral edema after traumatic brain injury in rats: effects of riluzole and mannitol. *J Neurotrauma* 14:839-849.
- Baskaya MK, Rao AM, Puckett L, et al. 1996. Effect of difluoromethylornithine treatment on regional ornithine decarboxylase activity and edema formation after experimental brain injury. *J Neurotrauma* 13:85-92.
- Battaglia G, Bruno V, Ngomba RT, et al. 1998. Selective activation of group-II metabotropic glutamate receptors is protective against excitotoxic neuronal death. *Eur J Pharmacol* 356:271-274.
- Bernert H, Turski L. 1996. Traumatic brain damage prevented by the non-N-methyl-D-aspartate antagonist 2,3-dihydroxy-6-nitro-7-sulfamoylbenzo[f] quinoxaline. *Proc Natl Acad Sci U S A* 93:5235-5240.
- Berthele A, Boxall SJ, Urban A, et al. 1999. Distribution and developmental changes in metabotropic glutamate receptor messenger RNA expression in the rat lumbar spinal cord. *Brain Res Dev Brain Res* 112:39-53.
- Biton B, Godet D, Granger P, et al. 1997. R- and L-type Ca^{2+} channels are insensitive to eliprodil in rat cultured cerebellar granule neurons. *Eur J Pharmacol* 323:277-281.
- Bleakman D, Lodge D. 1998. Neuropharmacology of AMPA and kainate receptors. *Neuropharmacology* 37:1187-1204.
- Blumcke I, Becker AJ, Klein C, et al. 2000. Temporal lobe epilepsy associated up-regulation of metabotropic glutamate receptors: correlated changes in mGluR1 mRNA and protein expression in experimental animals and human patients. *J Neuropathol Exp Neurol* 59:1-10.
- Bond A, O'Neill MJ, Hicks CA, et al. 1998. Neuroprotective effects of a systemically active group II metabotropic glutamate receptor agonist LY354740 in a gerbil model of global ischaemia. *Neuroreport* 9:1191-1193.
- Bond A, Jones NM, Hicks CA, et al. 2000. Neuroprotective effects of LY379268, a selective mGlu2/3 receptor agonist: investigations into possible mechanism of action in vivo. *J Pharmacol Exp Ther* 294:800-809.
- Bruno V, Copani A, Battaglia G, et al. 1994. Protective effect of the metabotropic glutamate receptor agonist, DCG-IV, against excitotoxic neuronal death. *Eur J Pharmacol* 256:109-112.
- Bruno V, Battaglia G, Copani A, et al. 1995a. Activation of class II or III metabotropic glutamate receptors protects cultured cortical neurons against excitotoxic degeneration. *Eur J Neurosci* 7:1906-1913.
- Bruno V, Copani A, Knöpfel T, et al. 1995b. Activation of metabotropic glutamate receptors coupled to inositol phospholipid hydrolysis amplifies NMDA-induced neuronal degeneration in cultured cortical cells. *Neuropharmacology* 34:1089-1098.
- Bruno V, Copani A, Battaglia G, et al. 1996a. Metabotropic glutamate receptors and neuronal degeneration in culture. *Adv Neurol* 71:47-51.
- Bruno V, Copani A, Bonanno L, et al. 1996b. Activation of group III metabotropic glutamate receptors is neuroprotective in cortical cultures. *Eur J Pharmacol* 310:61-66.
- Bruno V, Sureda FX, Storto M, et al. 1997. The neuroprotective activity of group-II metabotropic glutamate receptors requires new protein synthesis and involves a glial-neuronal signaling. *J Neurosci* 17:1891-1897.
- Bruno V, Battaglia G, Casabona G, et al. 1998a. Neuroprotection by glial metabotropic glutamate receptors is mediated by transforming growth factor-beta. *J Neurosci* 18:9594-9600.
- Bruno V, Battaglia G, Copani A, et al. 1998b. Metabotropic glutamate receptors and neurodegeneration. *Prog Brain Res* 116:209-221.
- Bruno V, Battaglia G, Kingston A, et al. 1999. Neuroprotective activity of the potent and selective mGlu1a metabotropic glutamate receptor antagonist, (+)-2-methyl-4 carboxyphenylglycine (LY367385): comparison with LY357366, a broader spectrum antagonist with equal affinity for mGlu1a and mGlu5 receptors. *Neuropharmacology* 38:199-207.
- Buisson A, Choi DW. 1995. The inhibitory mGluR agonist, S-4-carboxy-3-hydroxyphenylglycine selectively attenuates NMDA neurotoxicity and oxygen-glucose deprivation-induced neuronal death. *Neuropharmacology* 34:1081-1087.
- Bullock M, Lyeth B, Muizelaar J. 1999. Current status of neuroprotection trials for traumatic brain injury: lessons from animal models and clinical studies. *Neurosurgery* 45:207-220.
- Bullock R, Graham DI, Swanson S, et al. 1994. Neuroprotective effect of the AMPA receptor antagonist LY-293558 in focal cerebral ischemia in the cat. *J Cereb Blood Flow Metab* 14:466-471.
- Bullock R, Zauner A, Woodward JJ, et al. 1998. Factors affecting excitatory amino acid release following severe human head injury. *J Neurosurg* 89:507-518.
- Carmignoto G, Vicini S. 1992. Activity-dependent decrease in NMDA receptor responses during development of the visual cortex. *Science* 258:1007-1011.
- Carmody RJ, McGowan AJ, Cotter TG. 1999. Reactive oxygen species as mediators of photoreceptor apoptosis in vitro. *Exp Cell Res* 248:520-530.
- Casabona G, Genazzani AA, Di Stefano M, et al. 1992. Developmental changes in the modulation of cyclic AMP formation by the metabotropic glutamate receptor agonist 1S,3R-aminocyclopentane-1,3-dicarboxylic acid in brain slices. *J Neurochem* 59:1161-1163.
- Casabona G, Knöpfel T, Kuhn R, et al. 1997. Expression and coupling to polyphosphoinositide hydrolysis of group I metabotropic glutamate receptors in early postnatal and adult rat brain. *Eur J Neurosci* 9:12-17.
- Catania MV, Landwehrmeyer GB, Testa CM, et al. 1994. Metabotropic glutamate receptors are differentially regulated during development. *Neuroscience* 61:481-495.
- Cebers G, Zhivotovsky B, Ankarcrona M, et al. 1997. AMPA neurotoxicity in cultured cerebellar granule neurons: mode of cell death. *Brain Res Bull* 43:393-403.
- Chan SL, Griffin WS, Mattson MP. 1999. Evidence for caspase-mediated cleavage of AMPA receptor subunits in neuronal apoptosis and Alzheimer's disease. *J Neurosci Res* 57:315-323.
- Choi DW. 1992. Excitotoxic cell death. *J Neurobiol* 23:1261-1276.
- Choi DW, Rothman SM. 1990. The role of glutamate neurotoxicity in hypoxic-ischemic neuronal death. *Annu Rev Neurosci* 13:171-182.
- Choi DW, Koh JY, Peters S. 1988a. Pharmacology of glutamate neurotoxicity in cortical cell culture: attenuation by NMDA antagonists. *J Neurosci* 8:185-196.
- Choi DW, Yokoyama M, Koh J. 1988b. Zinc neurotoxicity in cortical cell culture. *Neuroscience* 24:67-79.
- Colicos MA, Dash PK. 1996. Apoptotic morphology of dentate gyrus granule cells following experimental cortical impact injury in rats: possible role in spatial memory deficits. *Brain Res* 739:120-131.
- Colicos MA, Dixon CE, Dash PK. 1996. Delayed, selective neuronal death following experimental cortical impact injury in rats: possible role in memory deficits. *Brain Res* 739:111-119.
- Conn PJ, Pin JP. 1997. Pharmacology and functions of metabotropic glutamate receptors. *Annu Rev Pharmacol Toxicol* 37:205-237.
- Conti AC, Raghupathi R, Trojanowski JQ, et al. 1998. Experimental brain injury induces regionally distinct apoptosis during the acute and delayed post-traumatic period. *J Neurosci* 18:5663-5672.
- Copani A, Bruno V, Battaglia G, et al. 1995. Activation of metabotropic glutamate receptors protects cultured neurons against apoptosis induced by beta-amyloid peptide. *Mol Pharmacol* 47:890-897.
- Copani A, Casabona G, Bruno V, et al. 1998. The metabotropic glutamate receptor mGlu5 controls the onset of developmental apoptosis in cultured cerebellar neurons. *Eur J Neurosci* 10:2173-2184.
- Davis PK, Johnson GV. 1999. Energy metabolism and protein phosphorylation during apoptosis: a phosphorylation study of tau and high-molecular-weight tau in differentiated PC12 cells. *Biochem J* 340(Pt 1):51-58.
- Delivoria-Papadopoulos M, Mishra OP. 2000. Mechanisms of perinatal cerebral injury in fetus and newborn. *Ann N Y Acad Sci* 900:159-168.
- Di X, Gordon J, Bullock R. 1999. Fluid percussion brain injury exacerbates glutamate-induced focal damage in the rat. *J Neurotrauma* 16:195-201.

- Di XZ, Mullins P, Faden AI. 2000. Novel, potent, and selective group II mGluR agonist LY379268 ameliorates cognitive and motor deficits induced by control cortical impact injury in mouse. *J Neurotrauma* 17:960.
- Diamond PT. 1996. Brain injury in the commonwealth of Virginia: an analysis of Central Registry data, 1988-1993. *Brain Inj* 10:413-419.
- Dingledine R, Borges K, Bowie D, et al. 1999. The glutamate receptor ion channels. *Pharmacol Rev* 51:7-61.
- Egebjerg J, Heinemann SF. 1993. Ca^{2+} permeability of unedited and edited versions of the kainate selective glutamate receptor GluR6. *Proc Natl Acad Sci U S A* 90:755-759.
- Eiben CF, Anderson TP, Lockman L, et al. 1984. Functional outcome of closed head injury in children and young adults. *Arch Phys Med Rehabil* 65:168-170.
- Eldadah BA, Faden AI. 2000. Caspase pathways, neuronal apoptosis, and CNS injury. *J Neurotrauma* 17:811-829.
- Ellis EF, McKinney JS, Willoughby KA, et al. 1995. A new model for rapid stretch-induced injury of cells in culture: characterization of the model using astrocytes. *J Neurotrauma* 12:325-339.
- Eriksen L, Thomsen C. 1995. [3H]-L-2-amino-4-phosphonobutrate labels a metabotropic glutamate receptor, mGluR4a. *Br J Pharmacol* 116:3279-3287.
- Faden AI, Simon RP. 1988. A potential role for excitotoxins in the pathophysiology of spinal cord injury. *Ann Neurol* 23:623-626.
- Faden AI, Lemke M, Simon RP, et al. 1988. N-methyl-D-aspartate antagonist MK801 improves outcome following traumatic spinal cord injury in rats: behavioral, anatomic, and neurochemical studies. *J Neurotrauma* 5:33-45.
- Faden AI, Demediuk P, Panter SS, et al. 1989. The role of excitatory amino acids and NMDA receptors in traumatic brain injury. *Science* 244:798-800.
- Faden AI, Ivanova SA, Yakovlev AG, et al. 1997. Neuroprotective effects of group III mGluR in traumatic neuronal injury. *J Neurotrauma* 14:885-895.
- Faden AI, O'Leary DM, Fan L, et al. 2001. Selective blockade of the mGluR1 receptor reduces traumatic neuronal injury in vitro and improves outcome after brain trauma. *Exp Neurol* 167:435-444.
- Faden AI, Allen JW, Knoblich S. 1999. Exacerbation of neuronal death by activation of group I metabotropic glutamate receptors; role of NMDA receptors and arachidonic acid release. 29th Annual Meeting of the Society for Neuroscience, Miami Beach, Fla.
- Fleckenstein A, Frey M, Fleckenstein-Grün G. 1983. Consequences of uncontrolled calcium entry and its prevention with calcium antagonists. *Eur Heart J* 4 Suppl H:43-50.
- Flor PJ, Gomez J, Tones MA, et al. 1996. The C-terminal domain of the mGluR1 metabotropic glutamate receptor affects sensitivity to agonists. *J Neurochem* 67:58-63.
- Fox GB, Faden AI. 1998. Traumatic brain injury causes delayed motor and cognitive impairment in a mutant mouse strain known to exhibit delayed Wallerian degeneration. *J Neurosci Res* 53:718-727.
- Fox GB, Fan L, LeVasseur RA. 1998a. Effect of traumatic brain injury on mouse spatial and nonspatial learning in the Barnes circular maze. *J Neurotrauma* 15:1037-1046.
- Fox GB, Fan L, LeVasseur RA, et al. 1998b. Sustained sensory/motor and cognitive deficits with neuronal apoptosis following controlled cortical impact brain injury in the mouse. *J Neurotrauma* 15:599-614.
- Gasparini F, Bruno V, Battaglia G, et al. 1999. (R,S)-4-phosphonophenylglycine, a potent and selective group III metabotropic glutamate receptor agonist, is anticonvulsive and neuroprotective in vivo. *J Pharmacol Exp Ther* 289: 1678-1687.
- Gennarelli TA, Thibault LE, Adams JH, et al. 1982. Diffuse axonal injury and traumatic coma in the primate. *Ann Neurol* 12:564-574.
- Ghosh PK, Baskaran N, van den Pol AN. 1997. Developmentally regulated gene expression of all eight metabotropic glutamate receptors in hypothalamic suprachiasmatic and arcuate nuclei—a PCR analysis. *Dev Brain Res* 102: 1-12.
- Gill R. 1994. The pharmacology of alpha-amino-3-hydroxy-5-methyl-4-isoxazole propionate (AMPA)/kainate antagonists and their role in cerebral ischaemia. *Cerebrovasc Brain Metab Rev* 6:225-256.
- Goforth P, Ellis E, Satin L. 1999. Enhancement of AMPA-mediated current after traumatic injury in cortical neurons. *J Neurosci* 19:7367-7374.
- Goforth PB, Ellis EF, Satin LS. 2000. Loss of AMPA receptor desensitization after mechanical injury of cortical neurons is dependent upon NMDA receptors and CAMKII. 30th Annual Meeting of the Society for Neuroscience, New Orleans.
- Golding EM, Vink R. 1995. Efficacy of competitive vs noncompetitive blockade of the NMDA channel following traumatic brain injury. *Mol Chem Neuropathol* 24:137-150.
- Gong QZ, Delahunty TM, Hamm RJ, et al. 1995. Metabotropic glutamate antagonist, MCPG, treatment of traumatic brain injury in rats. *Brain Res* 700:299-302.
- Goto S, Singer W, Gu Q. 1993. Immunocytochemical localization of calcineurin in the adult and developing primary visual cortex of cats. *Exp Brain Res* 96:377-386.
- Graham SH, Chen J, Lan J, et al. 1994. Neuroprotective effects of a use-dependent blocker of voltage-dependent sodium channels, BW619C89, in rat middle cerebral artery occlusion. *J Pharmacol Exp Ther* 269:854-859.
- Green D, Kroemer G. 1998. The central executioners of apoptosis: caspases or mitochondria? *Trends Cell Biol* 8: 267-271.
- Gwag BJ, Lobner D, Koh JY, et al. 1995. Blockade of glutamate receptors unmasks neuronal apoptosis after oxygen-glucose deprivation in vitro. *Neuroscience* 68:615-619.
- Haghighi SS, Johnson GC, de Vergel CF, et al. 1996. Pretreatment with NMDA receptor antagonist MK801 improves neurophysiological outcome after an acute spinal cord injury. *Neurol Res* 18:509-515.
- Hamm RJ, O'Dell DM, Pike BR, et al. 1993. Cognitive impairment following traumatic brain injury: the effect of pre- and post-injury administration of scopolamine and MK-801. *Brain Res Cogn Brain Res* 1:223-226.
- Hayes RL, Jenkins LW, Lyeth BG, et al. 1988. Pretreatment with phencyclidine, an N-methyl-D-aspartate antagonist, attenuates long-term behavioral deficits in the rat produced by traumatic brain injury. *J Neurotrauma* 5: 259-274.
- Heath DL, Vink R. 1998. Neuroprotective effects of $MgSO_4$ and $MgCl_2$ in closed head injury: a comparative phosphorus NMR study. *J Neurotrauma* 15:183-189.
- Heath DL, Vink R. 1999. Improved motor outcome in response to magnesium therapy received up to 24 hours after traumatic diffuse axonal brain injury in rats. *J Neurosurg* 90: 504-509.
- Henrich-Noack P, Flor PJ, Sabellhaus CF, et al. 2000. Distinct influence of the group III metabotropic glutamate receptor agonist (R,S)-4-phosphonophenylglycine [(R,S)-PPG] on different forms of neuronal damage. *Neuropharmacology* 39: 911-917.
- Hestrin S. 1992. Developmental regulation of NMDA receptor-mediated synaptic currents at a central synapse. *Nature* 357:686-689.
- Hicks RR, Smith DH, Gennarelli TA, et al. 1994. Kynurenate is neuroprotective following experimental brain injury in the rat. *Brain Res* 655:91-96.
- Hogg SC, Perron P, Barneoud D, et al. 1998. Neuroprotective effect of eliprodil: attenuation of a conditioned freezing deficit induced by traumatic injury of the right parietal cortex in the rat. *J Neurotrauma* 15:545-553.
- Hu BR, Liu CL, Ouyang Y, et al. 2000. Involvement of caspase-3 in cell death after hypoxia-ischemia declines during brain maturation. *J Cereb Blood Flow Metab* 20:1294-1300.
- Ikonomidou C, Turski L. 1996. Prevention of trauma-induced neurodegeneration in infant and adult rat brain: glutamate antagonists. *Metab Brain Dis* 11:125-141.
- Ikonomidou C, Qin Y, Labruyere J, et al. 1996. Prevention of trauma-induced neurodegeneration in infant rat brain. *Pediatr Res* 39: 1020-1027.
- Ikonomidou C, Bosch F, Miksa M, et al. 1999. Blockade of NMDA receptors and apoptotic neurodegeneration in the developing brain. *Science* 283:70-74.
- Jewell SA, Bellomo G, Thor H, et al. 1982. Bleb formation in hepatocytes during drug metabolism is caused by disturbances in thiol and calcium ion homeostasis. *Science* 217:1257-1259.
- Jiang X, Naik MU, Hrabec J, et al. 1994. Developmental expression of the protein kinase C family in rat hippocampus. *Dev Brain Res* 78:291-295.
- Kalda A, Zharkovsky A. 1999. Metabotropic glutamate receptor agonists protect from oxygen-glucose deprivation- and colchicine-induced apoptosis in primary cultures of cerebellar granule cells. *Neuroscience* 92:7-14.
- Kalda A, Kaasik A, Vassiljev V, et al. 2000. Neuroprotective action of group I metabotropic glutamate receptor agonists against oxygen-glucose deprivation-induced neuronal death. *Brain Res* 853:370-373.
- Kanellopoulos GK, Xu XM, Hsu CY, et al. 2000. White matter injury in spinal cord ischemia: protection by AMPA/kainate glutamate receptor antagonism. *Stroke* 31:1945-1952.
- Kao CQ, Goforth PB, Ellis EF, et al. 2000. Mechanical Injury-Induced Enhancement of GABA-A Currents in Cortical Neurons. 30th Annual Meeting of the Society for Neuroscience, New Orleans.
- Katayama Y, Becker DP, Tamura T, et al. 1990. Massive increases in extracellular potassium and the indiscriminate release of glutamate following concussive brain injury. *J Neurosurg* 73:889-900.
- Kawamata T, Katayama Y, Hovda DA, et al. 1992. Administration of excitatory amino acid antagonists via microdialysis attenuates the increase in glucose utilization seen following concussive brain injury. *J Cereb Blood Flow Metab* 12:12-24.

- Koh JY, Choi DW. 1988. Zinc alters excitatory amino acid neurotoxicity on cortical neurons. *J Neurosci* 8:2164-2171.
- Koh JY, Palmer E, Cotman CW. 1991. Activation of the metabotropic glutamate receptor attenuates N-methyl-D-aspartate neurotoxicity in cortical cultures. *Proc Natl Acad Sci U S A* 88:9431-9435.
- Kornhuber J, Weller M. 1997. Psychogenicity and N-methyl-D-aspartate receptor antagonism: implications for neuroprotective pharmacotherapy. *Biol Psychiatry* 41:135-144.
- Kozikowski AP, Tuckmantel W, Liao Y, et al. 1993. Synthesis and metabotropic receptor activity of the novel rigidified glutamate analogues (+)- and (-)-trans-azetidine-2,4-dicarboxylic acid and their N-methyl derivatives. *J Med Chem* 36:2706-2708.
- Kozikowski AP, Araldi GL, Tuckmantel W, et al. 1999. 1-amino-APDC, a partial agonist of group II metabotropic glutamate receptors with neuroprotective properties. *Bioorg Med Chem Lett* 9:1721-1726.
- Kroppenstedt SN, Schneider GH, Thomale UW, et al. 1998. Protective effects of aptiganel HCl (Cerestat) following controlled cortical impact injury in the rat. *J Neurotrauma* 15:191-197.
- Lafon-Cazal M, Fagni L, Guiraud MJ, et al. 1999. mGluR7-like metabotropic glutamate receptors inhibit NMDA-mediated excitotoxicity in cultured mouse cerebellar granule neurons. *Eur J Neurosci* 11:663-672.
- Laurie DJ, Seeburg PH. 1994. Regional and developmental heterogeneity in splicing of the rat brain NMDAR1 mRNA. *J Neurosci* 14:3180-3194.
- Laurie DJ, Putzke J, Zieglerberger W, et al. 1995. The distribution of splice variants of the NMDAR1 subunit mRNA in adult rat brain. *Brain Res Mol Brain Res* 32:94-108.
- Lea IV PM, Wroblewska B, Sarvey JM, et al. 2001. Beta-NAAG rescues LTP from blockade by NAAG in rat dentate gyrus via the type 3 metabotropic glutamate receptor. *J Neurophysiol* 85:1097-1106.
- Lea IV PM, Sarvey JM. 2000. Modulation of epileptiform burst frequency and duration by the group II metabotropic glutamate receptor subtype mGluR3. 30th Annual Meeting of the Society for Neuroscience, New Orleans.
- Lee H, Choi BH. 1992. Density and distribution of excitatory amino acid receptors in the developing human fetal brain: a quantitative autoradiographic study. *Exp Neurol* 118:284-290.
- Lyeth BG, Gong QZ, Shields S, et al. 2001. Group I metabotropic glutamate antagonist reduces acute neuronal degeneration and behavioral deficits after traumatic brain injury in rats. *Exp Neurol* 169:191-199.
- Ma J, Endres M, Moskowitz MA. 1998. Synergistic effects of caspase inhibitors and MK-801 in brain injury after transient focal cerebral ischemia in mice. *Br J Pharmacol* 124:756-762.
- Maiese K, Greenberg R, Boccone L, et al. 1995. Activation of the metabotropic glutamate receptor is neuroprotective during nitric oxide toxicity in primary hippocampal neurons of rats. *Neurosci Lett* 194:173-176.
- Maiese K, Swiriduk M, TenBroeke M. 1996. Cellular mechanisms of protection by metabotropic glutamate receptors during anoxia and nitric oxide toxicity. *J Neurochem* 66:2419-2428.
- Matsuoka Y, Kitamura Y, Tsukahara T, et al. 1995. Neuroprotective effects of NBQX on hypoxia-induced neuronal damage in rat hippocampus. *Neuroreport* 6:2205-2208.
- Mattson MP, Mark RJ. 1996. Excitotoxicity and excitoprotection in vitro. *Adv Neurol* 71:1-30.
- McDonald JW, Fix AS, Tizzano JP, et al. 1993. Seizures and brain injury in neonatal rats induced by 1S,3R-ACPD, a metabotropic glutamate receptor agonist. *J Neurosci* 13:4445-4455.
- McIntosh TK, Faden AI, Yamakami I, et al. 1988. Magnesium deficiency exacerbates and pretreatment improves outcome following traumatic brain injury in rats: 31P magnetic resonance spectroscopy and behavioral studies. *J Neurotrauma* 5:17-31.
- McIntosh TK, Vink R, Soares H, et al. 1989a. Effects of the N-methyl-D-aspartate receptor blocker MK-801 on neurologic function after experimental brain injury. *J Neurotrauma* 6:247-259.
- McIntosh TK, Vink R, Yamakami I, et al. 1989b. Magnesium protects against neurological deficit after brain injury. *Brain Res* 482:252-260.
- McIntosh TK, Vink R, Soares H, et al. 1990. Effect of noncompetitive blockade of N-methyl-D-aspartate receptors on the neurochemical sequelae of experimental brain injury. *J Neurochem* 55:1170-1179.
- McIntosh TK, Juhler M, Wieloch T. 1998. Novel pharmacologic strategies in the treatment of experimental traumatic brain injury: 1998. *J Neurotrauma* 15:731-769.
- McIntosh TK, Smith DH, Voldi M, et al. 1996. Riluzole, a novel neuroprotective agent, attenuates both neurologic motor and cognitive dysfunction following experimental brain injury in the rat. *J Neurotrauma* 13:767-780.
- Meldrum B. 1990. Protection against ischemic neuronal damage by drugs acting on excitatory neurotransmission. *Cerebrovasc Brain Metab Rev* 2:27-57.
- Meldrum B. 2000. Glutamate as a neurotransmitter in the brain: review of physiology and pathology. *J Nutr* 130:1007S-1015S.
- Miller LP, Lyeth BG, Jenkins LW, et al. 1990. Excitatory amino acid receptor subtype binding following traumatic brain injury. *Brain Res* 526:103-107.
- Montoliu C, Llansola M, Cucarella C, et al. 1997. Activation of the metabotropic glutamate receptor mGluR5 prevents glutamate toxicity in primary cultures of cerebellar neurons. *J Pharmacol Exp Ther* 281:643-647.
- Monyer H, Goldberg MP, Choi DW. 1989. Glucose deprivation neuronal injury in cortical culture. *Brain Res* 483:347-354.
- Monyer H, Seeburg PH, Wisden W. 1991. Glutamate-operated channels: developmentally early and mature forms arise by alternative splicing. *Neuron* 6:799-810.
- Movsesyan VA, O'Leary DM, Fan L, et al. 2001. mGluR5 antagonists 2-methyl-6-(phenylethynyl)-pyridine and (E)-2-methyl-6-(2-phenylethynyl)-pyridine reduce traumatic neuronal injury in vitro and in vivo by antagonizing N-methyl-D-aspartate receptors. *J Pharmacol Exp Ther* 296:41-47.
- Mukhin A, Fan L, Faden AI. 1996. Activation of metabotropic glutamate receptor subtype mGluR1 contributes to post-traumatic neuronal injury. *J Neurosci* 16:6012-6020.
- Mukhin AG, Ivanova SA, Faden AI. 1997a. mGluR modulation of post-traumatic neuronal death: role of NMDA receptors. *Neuroreport* 8:2561-2566.
- Mukhin AG, Ivanova SA, Knoblich SM, et al. 1997b. New in vitro model of traumatic neuronal injury: evaluation of secondary injury and glutamate receptor-mediated neurotoxicity. *J Neurotrauma* 14:651-666.
- Mukhin AG, Ivanova SA, Allen JW, et al. 1998. Mechanical injury to neuronal/glial cultures in microplates: role of NMDA receptors and pH in secondary neuronal cell death. *J Neurosci Res* 51:748-758.
- Nakagawa Y, Saitoh K, Ishihara T, et al. 1990. (2S,3S,4S) alpha-(carboxycyclopropyl)glycine is a novel agonist of metabotropic glutamate receptors. *Eur J Pharmacol* 184:205-206.
- Nicotera P, Lipton SA. 1999. Excitotoxins in neuronal apoptosis and necrosis. *J Cereb Blood Flow Metab* 19:583-591.
- Ohishi H, Shigemoto R, Nakanishi S, et al. 1993a. Distribution of the messenger RNA for a metabotropic glutamate receptor, mGluR2, in the central nervous system of the rat. *Neuroscience* 53:1009-1018.
- Ohishi H, Shigemoto R, Nakanishi S, et al. 1993b. Distribution of the mRNA for a metabotropic glutamate receptor (mGluR3) in the rat brain: an in situ hybridization study. *J Comp Neurol* 335:252-266.
- Oka A, Takashima S. 1999. The up-regulation of metabotropic glutamate receptor 5 (mGluR5) in Down's syndrome brains. *Acta Neuropathol (Berl)* 97:275-278.
- Okiyama K, Smith DH, Gennarelli TA, et al. 1995. The sodium channel blocker and glutamate release inhibitor BW1003C87 and magnesium attenuate regional cerebral edema following experimental brain injury in the rat. *J Neurochem* 64:802-809.
- Okiyama K, Smith DH, White WF, et al. 1997. Effects of the novel NMDA antagonists CP-98,113, CP-101,581 and CP-101,606 on cognitive function and regional cerebral edema following experimental brain injury in the rat. *J Neurotrauma* 14:211-222.
- Okiyama K, Smith DH, White WF, et al. 1998. Effects of the NMDA antagonist CP-98,113 on regional cerebral edema and cardiovascular, cognitive, and neurobehavioral function following experimental brain injury in the rat. *Brain Res* 792:291-298.
- Olney JW, Labruyere J, Price MT. 1989. Pathological changes induced in cerebrocortical neurons by phencyclidine and related drugs. *Science* 244:1360-1362.
- O'Neill MJ, Bond A, Ornstein PL, et al. 1998. Decahydroisquinolines: novel competitive AMPA/kainate antagonists with neuroprotective effects in global cerebral ischemia. *Neuropharmacology* 37:1211-1222.
- Orlando LR, Standaert DG, Penney, Jr. JB, et al. 1995. Metabotropic receptors in excitotoxicity: (S)-4-carboxy-3-hydroxyphenylglycine ((S)-4C3HPG) protects against rat striatal quinolinic acid lesions. *Neurosci Lett* 202:109-112.
- Orrenius S, Ankarcrona M, Nicotera P. 1996. Mechanisms of calcium-related cell death. *Adv Neurol* 71:137-149.
- Panter SS, Faden AI. 1992. Pretreatment with NMDA antagonists limits release of excitatory amino acids following traumatic brain injury. *Neurosci Lett* 136:165-168.
- Paschen W, Schmitt J, Gissel C, et al. 1997. Developmental changes of RNA editing of glutamate receptor subunits GluR5 and GluR6: in vivo versus in vitro. *Dev Brain Res* 98:271-280.
- Paupard MC, Friedman LK, Zukin RS. 1997. Developmental regulation and cell-specific expression of N-methyl-D-aspartate receptor splice variants in rat hippocampus. *Neuroscience* 79:399-409.

- Paupard MC, O'Connell MA, Gerber AP, et al. 2000. Patterns of developmental expression of the RNA editing enzyme rADAR2. *Neuroscience* 95:869-879.
- Pike B, Zhao X, Newcomb J, et al. 2000. Stretch injury causes calpain and caspase-3 activation and necrotic and apoptotic cell death in septo-hippocampal cell cultures. *J Neurotrauma* 17:283-298.
- Pizzi M, Fallacara C, Arrighi V, et al. 1993. Attenuation of excitatory amino acid toxicity by metabotropic glutamate receptor agonists and aniracetam in primary cultures of cerebellar granule cells. *J Neurochem* 61:683-689.
- Pizzi M, Consolandi O, Memo M, et al. 1996a. Activation of multiple metabotropic glutamate receptor subtypes prevents NMDA-induced excitotoxicity in rat hippocampal slices. *Eur J Neurosci* 8:1516-1521.
- Pizzi M, Galli P, Consolandi O, et al. 1996b. Metabotropic and ionotropic transducers of glutamate signal inversely control cytoplasmic Ca^{2+} concentration and excitotoxicity in cultured cerebellar granule cells: pivotal role of protein kinase C. *Mol Pharmacol* 49:586-594.
- Pohl D, Bittigau P, Ishimaru D, et al. 1999. N-Methyl-D-aspartate antagonists and apoptotic cell death triggered by head trauma in developing rat brain. *Proc Natl Acad Sci U S A* 96:2508-2513.
- Prehn JH, Lippert K, Kriegstein J. 1995. Are NMDA or AMPA/kainate receptor antagonists more efficacious in the delayed treatment of excitotoxic neuronal injury? *Eur J Pharmacol* 292:179-189.
- Regan RF, Choi DW. 1994. The effect of NMDA, AMPA/kainate, and calcium channel antagonists on traumatic cortical neuronal injury in culture. *Brain Res* 633:236-242.
- Reid SN, Romano C, Hughes T, et al. 1997. Developmental and sensory-dependent changes of phosphoinositide-linked metabotropic glutamate receptors. *J Comp Neurol* 389:577-583.
- Richardson-Burns SM, Haroutunian V, Davis KL, et al. 2000. Metabotropic glutamate receptor mRNA expression in the schizophrenic thalamus. *Biol Psychiatry* 47:22-28.
- Roth GS. 1997. Age changes in signal transduction and gene expression. *Mech Ageing Dev* 98:231-238.
- Rzagalinski BAW, Willoughby KA, Liang S, et al. 1998. Glutamate release and enhanced receptor sensitivity in stretch-induced neurons. *J Neurotrauma* 15:894.
- Sacaan AI, Bymaster FP, Schoepp DD. 1992. Metabotropic glutamate receptor activation produces extrapyramidal motor system activation that is mediated by striatal dopamine. *J Neurochem* 59:245-251.
- Salbego C, Rodnight R. 1996. A developmental study of protein phosphorylating systems stimulated by phorbol dibutyrate in micro-slices of rat brain. *Neurochem Int* 28:431-438.
- Saugstad JA, Kinzie JM, Shinohara MM, et al. 1997. Cloning and expression of rat metabotropic glutamate receptor 8 reveals a distinct pharmacological profile. *Mol Pharmacol* 51:119-125.
- Schanne FA, Kane AB, Young EE, et al. 1979. Calcium dependence of toxic cell death: a final common pathway. *Science* 206:700-702.
- Schoepp DD, Tizzano JP, Wright RA, et al. 1995. Reversible and irreversible neuronal injury induced by intrahippocampal infusion of the mGluR agonist 1S,3R-ACPD in the rat. *Neurodegeneration* 4:71-80.
- Schoepp DD, Jane DE, Monn JA. 1999. Pharmacological agents acting at subtypes of metabotropic glutamate receptors. *Neuropharmacology* 38:1431-1476.
- Schroder UH, Opitz T, Jager T, et al. 1999. Protective effect of group I metabotropic glutamate receptor activation against hypoxic/hypoglycemic injury in rat hippocampal slices: timing and involvement of protein kinase C. *Neuropharmacology* 38:209-216.
- Sensi SL, Yin HZ, Carriedo SG, et al. 1999a. Preferential Zn^{2+} influx through Ca^{2+} -permeable AMPA/kainate channels triggers prolonged mitochondrial superoxide production. *Proc Natl Acad Sci U S A* 96:2414-2419.
- Sensi SL, Yin HZ, Weiss JH. 1999b. Glutamate triggers preferential Zn^{2+} flux through Ca^{2+} -permeable AMPA channels and consequent ROS production. *Neuroreport* 10:1723-1727.
- Shaffer LM, Han YF, Dokas LA. 1993. Phorbol ester- and glutamate-sensitive phosphorylation of hippocampal membrane proteins from adult and neonatal rats. *Dev Brain Res* 73:133-139.
- Shapira Y, Yadid G, Cotev S, et al. 1990. Protective effect of MK801 in experimental brain injury. *J Neurotrauma* 7:131-139.
- Shigemoto R, Nakanishi S, Mizuno N. 1992. Distribution of the mRNA for a metabotropic glutamate receptor (mGluR1) in the central nervous system: an in situ hybridization study in adult and developing rat. *J Comp Neurol* 322:121-135.
- Shohami E, Novikov M, Mechoulam R. 1993. A nonpsychotropic cannabinoid, HU-211, has cerebroprotective effects after closed head injury in the rat. *J Neurotrauma* 10:109-119.
- Shohami E, Novikov M, Bass R. 1995. Long-term effect of HU-211, a novel non-competitive NMDA antagonist, on motor and memory functions after closed head injury in the rat. *Brain Res* 674:55-62.
- Shohami E, Gallily R, Mechoulam R, et al. 1997. Cytokine production in the brain following closed head injury: dexamethasone (HU-211) is a novel TNF- α inhibitor and an effective neuroprotectant. *J Neuroimmunol* 72:169-177.
- Simonian NA, Getz RL, Leveque JC, et al. 1996a. Kainate induces apoptosis in neurons. *Neuroscience* 74:675-683.
- Simonian NA, Getz RL, Leveque JC, et al. 1996b. Kainic acid induces apoptosis in neurons. *Neuroscience* 75:1047-1055.
- Simonyi A, Xia J, Igbavboa U, et al. 1998. Age differences in the expression of metabotropic glutamate receptor 1 and inositol 1,4,5-trisphosphate receptor in mouse cerebellum. *Neurosci Lett* 244:29-32.
- Simonyi A, Zhang JP, Sun GY. 1999. Changes in mRNA levels for group I metabotropic glutamate receptors following in utero hypoxia-ischemia. *Brain Res Dev Brain Res* 112:31-37.
- Simonyi A, Miller LA, Sun GY. 2000. Region-specific decline in the expression of metabotropic glutamate receptor 7 mRNA in rat brain during aging. *Brain Res* 82:101-106.
- Smith DH, Okiyama K, Gennarelli TA, et al. 1993a. Magnesium and ketamine attenuate cognitive dysfunction following experimental brain injury. *Neurosci Lett* 157:211-214.
- Smith DH, Okiyama K, Thomas MJ, et al. 1993b. Effects of the excitatory amino acid receptor antagonists kynurenic acid and indole-2-carboxylic acid on behavioral and neurochemical outcome following experimental brain injury. *J Neurosci* 13:5383-5392.
- Smith DH, Perri BR, Raghupathi R, et al. 1997. Remacemide hydrochloride reduces cortical lesion volume following brain trauma in the rat. *Neurosci Lett* 231:135-138.
- Sommer B, Keinanen K, Verdoorn TA, et al. 1990. Flip and flop: a cell-specific functional switch in glutamate-operated channels of the CNS. *Science* 249:1580-1585.
- Stefani A, Pisani A, Mercuri NB, et al. 1996. The modulation of calcium currents by the activation of mGluRs. Functional implications. *Mol Neurobiol* 13:81-95.
- Strasser U, Lobner D, Behrens MM, et al. 1998. Antagonists for group I mGluRs attenuate excitotoxic neuronal death in cortical cultures. *Eur J Neurosci* 10:2848-2855.
- Sullivan HG, Martinez J, Becker DP, et al. 1976. Fluid-percussion model of mechanical brain injury in the cat. *J Neurosurg* 45:521-534.
- Sun FY, Faden AI. 1994. High- and low-affinity NMDA receptor-binding sites in rat spinal cord: effects of traumatic injury. *Brain Res* 666:88-92.
- Sun FY, Faden AI. 1995a. Neuroprotective effects of 619C89, a use-dependent sodium channel blocker, in rat traumatic brain injury. *Brain Res* 673:133-140.
- Sun FY, Faden AI. 1995b. Pretreatment with antisense oligodeoxynucleotides directed against the NMDA-R1 receptor enhances survival and behavioral recovery following traumatic brain injury in rats. *Brain Res* 693:163-168.
- Swanson GT, Feldmeyer D, Kaneda M, et al. 1996. Effect of RNA editing and subunit co-assembly single-channel properties of recombinant kainate receptors. *J Physiol* 492:129-142.
- Tan S, Sagara Y, Liu Y, et al. 1998. The regulation of reactive oxygen species production during programmed cell death. *J Cell Biol* 141:1423-1432.
- Temple MD, Hamm RJ. 1996. Chronic, post-injury administration of D-cycloserine, an NMDA partial agonist, enhances cognitive performance following experimental brain injury. *Brain Res* 741:246-251.
- Temple MD, Hamm RJ, Delahunty TM, et al. 1997. Changes in N-Methyl-D-Aspartate Receptor (NMDAR) subunit immunohistochemistry at 1, 8, and 16 days after traumatic brain injury (TBI). *J Neurotrauma* 14:766.
- Testa CM, Standaert DG, Young AB, et al. 1994. Metabotropic glutamate receptor mRNA expression in the basal ganglia of the rat. *J Neurosci* 14:3005-3018.
- Toulmond S, Serrano A, Benavides J, et al. 1993. Prevention by eliprodil (SL 82.0715) of traumatic brain damage in the rat. Existence of a large (18 h) therapeutic window. *Brain Res* 620:32-41.
- Tymianski M, Tator CH. 1996. Normal and abnormal calcium homeostasis in neurons: a basis for the pathophysiology of traumatic and ischemic central nervous system injury. *Neurosurgery* 38:1176-1195.
- Valerio A, Alberici A, Paterlini M, et al. 1995. Opposing regulation of amyloid precursor protein by ionotropic and metabotropic glutamate receptors. *Neuroreport* 6:1317-1321.
- Vincent AM, TenBroeke M, Maiese K. 1999. Metabotropic glutamate receptors prevent programmed cell death through the modulation of neuronal endonuclease activity and intracellular pH. *Exp Neurol* 155:79-94.
- Wahl F, Renou E, Mary V, et al. 1997. Riluzole reduces brain lesions and improves neurological function in rats after a traumatic brain injury. *Brain Res* 756:247-255.
- Wahlestedt C, Golanov E, Yamamoto S, et al. 1993. Antisense oligodeoxynucleotides to

- NMDA-R1 receptor channel protect cortical neurons from excitotoxicity and reduce focal ischaemic infarctions. *Nature* 363:260-263.
- Watkins J, Collingridge G. 1994. Phenylglycine derivatives as antagonists of metabotropic glutamate receptors. *Trends Pharmacol Sci* 15:333-342.
- Wilsch VW, Pidoplichko VI, Opitz T, et al. 1994. Metabotropic glutamate receptor agonist DCG-IV as NMDA receptor agonist in immature rat hippocampal neurons. *Eur J Pharmacol* 262:287-291.
- Wrathall JR, Choiniere D, Teng YD. 1994. Dose-dependent reduction of tissue loss and functional impairment after spinal cord trauma with the AMPA/kainate antagonist NBQX. *J Neurosci* 14:6598-6607.
- Yakovlev AG, Wang G, Stoica BA, et al. 2000. A role of the $\text{Ca}^{2+}/\text{Mg}^{2+}$ -dependent endonuclease in apoptosis and its inhibition by Poly-(ADP-ribose) polymerase. *J Biol Chem* 275: 21302-21308.
- Yu SP, Yeh CH, Sensi SL, et al. 1997. Mediation of neuronal apoptosis by enhancement of outward potassium current. *Science* 278:114-117.
- Zhang C, Raghupathi R, Saatman KE, et al. 1998. Riluzole attenuates cortical lesion size, but not hippocampal neuronal loss, following traumatic brain injury in the rat. *J Neurosci Res* 52:342-349.
- Zhang L, Rzigalinski BA, Ellis EF, et al. 1996. Reduction of voltage-dependent Mg^{2+} blockade of NMDA current in mechanically injured neurons. *Science* 274:1921-1923.
- Zilles K, Qu MS, Schroder H, et al. 1991. Neurotransmitter receptors and cortical architecture. *J Hirnforsch* 32: 343-356.
- Zukin RS, Bennett MV. 1995. Alternatively spliced isoforms of the NMDAR1 receptor subunit [published erratum appears in *Trends Neurosci* 18:441]. *Trends Neurosci* 18:306-313.
- Zwienenberg M, Gong QZ, Berman RF, et al. 2001. The effect of groups II and III metabotropic glutamate receptor activation on neuronal injury in a rodent model of traumatic brain injury. *Neurosurgery* 48:1119-1127. discussion 1126-7.

Differential Expression of Apoptotic Protease-Activating Factor-1 and Caspase-3 Genes and Susceptibility to Apoptosis during Brain Development and after Traumatic Brain Injury

Alexander G. Yakovlev,¹ Katsuya Ota,² Geping Wang,¹ Vilen Movsesyan,¹ Wei-Li Bao,¹ Koichiro Yoshihara,² and Alan I. Faden¹

¹Department of Neuroscience, Georgetown University, Washington, DC 20007, and ²Department of Biochemistry, Nara Medical University, Kashihara, Nara 634–8521, Japan

Neuronal apoptosis plays an essential role in early brain development and contributes to secondary neuronal loss after acute brain injury. Recent studies have provided evidence that neuronal susceptibility to apoptosis induced by traumatic or ischemic injury decreases during brain development. However, the molecular mechanisms responsible for this age-dependent phenomenon remain unclear. Here we demonstrate that, during brain maturation, the potential of the intrinsic apoptotic pathway is progressively reduced and that such repression is associated with downregulation of apoptotic protease-activating factor-1 (Apaf-1) and caspase-3 gene expression. A similar decline in apoptotic susceptibility associated with downregu-

lation of Apaf-1 expression as a function of developmental age was also found in cultured primary rat cortical neurons. Injury-induced cytochrome *c*-specific cleavage of caspase-9 followed by activation of caspase-3 in mature brain correlated with marked increases in Apaf-1 and caspase-3 mRNA and protein expression. These results suggest that differential expression of Apaf-1 and caspase-3 genes may underlie regulation of apoptotic susceptibility during brain development, as well as after acute injury to mature brain, through the intrinsic pathway of caspase activation.

Key words: brain; development; injury; apoptosis; caspase; gene expression; Apaf-1

Apoptosis is a genetically controlled cell death that was initially recognized for its role in development. Nearly half of neural cells die by apoptosis during brain development. However, apoptosis is atypical for mature mammalian brain under normal physiological conditions (Haydar et al., 1999). Recent studies have established a role for apoptosis in neuronal loss after stroke and spinal cord or traumatic brain injury (TBI) (Gillardon et al., 1997; Yakovlev et al., 1997; Lipton, 1999; Snider et al., 1999; Beattie et al., 2000; Clark et al., 2000; Eldadah and Faden, 2000; Raghupathi et al., 2000; Yamashima, 2000). Furthermore, clinical data suggest that outcomes and mortality after acute brain injury are age-dependent, with more severe responses in infants than in adults (Brink et al., 1970; Levin et al., 1982; Adelson and Kochanek, 1998). Such differences in response to injury may be explained, in part, by differential susceptibility to apoptosis and associated caspase-3 activity in brain as a function of developmental age (Bittigau et al., 1999; Pohl et al., 1999; Hu et al., 2000). However, the molecular mechanisms underlying such age-dependent differences in apoptotic response to neuronal injury have not been identified.

Because caspase-3 appears to be the major executioner caspase involved in neuronal apoptosis (Bredesen, 2000; Eldadah and

Faden, 2000), we hypothesized that suppression of apoptotic capability during maturation of mammalian brain results from repression of genes involved in the caspase-3 activation pathway, and that injury-induced neuronal apoptosis in the mature brain results from reactivation of these genes.

Two major caspase-3-activating pathways have been identified, an extrinsic pathway involving cell surface receptors and an intrinsic pathway resulting from alterations at the level of the mitochondrion and activation of the apoptosome (Li et al., 1997; Scaffidi et al., 1998; Slee et al., 1999). A role for the extrinsic pathway in injury-induced CNS apoptosis remains to be established, whereas a role for the intrinsic pathway is supported by several recent studies (Krajewski et al., 1999; Springer et al., 1999; Kuida, 2000).

The intrinsic pathway is initiated by release of cytochrome *c* from mitochondria to the cytosol (Li et al., 1997; Zou et al., 1997, 1999; Brown and Borutaite, 1999; Richter and Ghafourifar, 1999; Kulms and Schwarz, 2000; Robertson and Orrenius, 2000). In the presence of ATP (or dATP), cytochrome *c* binds to the cytosolic adaptor protein apoptotic protease-activating factor-1 (Apaf-1) (Li et al., 1997). Binding of cytochrome *c* to Apaf-1 allows the recruitment and activation of caspase-9 within the apoptosome (Li et al., 1997). Active caspase-9, in turn, activates executioner caspases-3 and -7. Activated caspase-3 is required for the activation of four other caspases (-2, -6, -8, and -10) in this pathway and also participates in a feedback amplification loop involving caspase-9 (Li et al., 1997; Slee et al., 1999).

In the present study, we evaluated the role of the intrinsic pathway in neuronal apoptosis at different stages of rat brain development and during maturation of primary cortical neurons *in vivo* as well as in response to brain injury.

Received April 9, 2001; revised July 12, 2001; accepted July 13, 2001.

This work was supported by Grants R01 NS38941 and R01 NS36537 from the National Institute for Neurological Diseases and Stroke to A.G.Y. and A.I.F. and by Grant DAMD17-99-2-9007 from the United States Department of Defense to A.I.F. We thank Dr. Vishva M. Dixit for the dominant negative caspase-8 and caspase-9 expression constructs. We also thank Dr. Gabriel Nunez for the cDNA clone encoding human Apaf-1XL.

Correspondence should be addressed to Alexander G. Yakovlev, Georgetown University Medical Center, Research Building, WP-14, 3970 Reservoir Road Northwest, Washington, DC 20007. E-mail: yakovlev@giccs.georgetown.edu.

Copyright © 2001 Society for Neuroscience 0270-6474/01/217439-08\$15.00/0

MATERIALS AND METHODS

Tissue cultures. Cortical neuronal cultures were derived from rat embryonic cortices. Briefly, cortices from 15- to 16-d-old embryos were cleaned from their meninges and blood vessels in Krebs-Ringer's bicarbonate buffer containing 0.3% bovine serum albumin (BSA; Life Technologies, Gaithersburg, MD). Cortices were then minced and dissociated in the same buffer with 1800 U/ml trypsin (Sigma, St. Louis, MO) at 37°C for 20 min. After the addition of 200 U/ml DNase I (Sigma) and 3600 U/ml soybean trypsin inhibitor (Sigma) to the suspension, cells were triturated through a 5 ml pipette. After the tissue was allowed to settle for 5–10 min, the supernatant was collected, and the remaining tissue pellet was triturated. The combined supernatants were then centrifuged through a 4% BSA layer and the cell pellet was resuspended in neuronal seeding medium, which consisted of neurobasal medium (Life Technologies) supplemented with 1.1% 100× antibiotic-antimycotic solution (Biofluids, Rockville, MD), 25 μ M Na-glutamate, 0.5 mM L-glutamine, and 2% B27 supplement (Life Technologies). Cells were seeded at a density of 5×10^5 cells/ml onto poly-D-lysine (70–150 kDa; Sigma)-coated 96-well plates (Corning, Corning, NY) or 60 mm Petri dishes (Falcon). All experiments were performed on cultures at 1 or 14 d *in vitro* (DIV). Cell death was induced in cultured neurons by incubation with 50 μ M etoposide.

The composition of 1 and 14 DIV cortical neuronal cultures was characterized by immunostaining using the mouse monoclonal anti-neuron-specific enolase (NSE) antibodies. Briefly cultures in 96-well plates were fixed with 4% paraformaldehyde in PBS and washed twice (5 min each) with PBS. Nonspecific binding was blocked by incubation with 10% goat serum at +4°C for 16 hr. The primary anti-NSE antibodies (Chemicon, Temecula, CA) in PBS buffer (1:10) were applied for 16 hr at +4°C. Cultures were then washed three times (5 min each) with PBS and incubated with the secondary antibodies (1:100 dilution; goat anti-mouse antibodies conjugated to Texas Red; Accurate Chemicals, Westbury, NY) for 45 min. Cultures were washed three times (5 min each) again and examined using phase-contrast (to visualize all types of cells) and UV microscopy (to identify NSE-positive cells). Cells were counted in randomly selected fields in 1 and 14 DIV cultures. No significant differences were found ($n = 5$; $p = 0.475$) in the percentages of neuronal cells in 1 and 14 DIV cultures, as compared by ANOVA followed by the Student-Newman-Keuls test. One DIV cultures contained $88 \pm 4\%$ NSE-positive cells, and 14 DIV cultures contained $91 \pm 5\%$ NSE-positive cells.

Rat fluid percussion brain trauma model. This model is highly reproducible and has been extensively characterized with regard to its biochemical, physiological, morphological, and behavioral correlates (McIntosh et al., 1987; Faden et al., 1989). Briefly, male Sprague Dawley rats (400 ± 25 gm body weight) were anesthetized with sodium pentobarbital (60 mg/kg, i.p.), intubated, and implanted with femoral venous and arterial catheters. Brain temperature was assessed indirectly through a thermister in the temporalis muscle, and body temperature was maintained through a feedback-controlled heating blanket. Blood pressure was continuously monitored, and arterial blood gases were analyzed periodically. A small craniotomy (2 mm), located midway between the lambda and bregma sutures over the left parietal cortex, allowed insertion of a Leur-Loc that was cemented in place. The fluid percussion head injury device, manufactured by the Medical College of Virginia, consists of a Plexiglas cylindrical reservoir filled with 37°C isotonic saline; one end includes a transducer that is mounted and connected to a 5 mm tube that attaches through a male Leur-Loc fitting to the female Leur-Loc cemented at the time of surgery. A pendulum strikes a piston at the opposite end of the device, producing a pressure pulse of ~22 msec duration, leading to the deformation of underlying brain. The degree of injury is related to the pressure pulse expressed in atmospheres; a pulse of 2.4 ± 0.1 atmospheres produces moderately severe injury that permits evaluation of pharmacological interventions. Animals were maintained on anesthetics (sodium pentobarbital, 15 mg \cdot kg $^{-1}$ \cdot hr $^{-1}$) and artificially ventilated. All animal experiments were in compliance with Georgetown University Animal Care and Use Committee guidelines and the National Institutes of Health *Guide for the Care and Use of Laboratory Animals* (National Institutes of Health publication 85-23).

Assay for caspase-3 activation. Sham-operated and injured rat cortices or pellets of primary cortical neurons were homogenized in a Dounce homogenizer in 20 mM HEPES-KOH, pH 7.5, 10 mM KCl, 1.5 mM MgCl₂, 1 mM EDTA, 1 mM EGTA, 1 mM dithiothreitol (DTT), 1 mM phenylmethylsulfonyl fluoride (PMSF), 10 μ M leupeptin, 10 μ M aprotinin, 10 μ M pepstatin A, and 250 mM sucrose. Homogenates were

centrifuged at $13,000 \times g$ for 30 min. Supernatants were transferred to new tubes and stored at -80°C until used. Protein concentration was estimated by the Bradford method (Bio-Rad, Hercules, CA) according to recommendations by the manufacturer. Twenty to 80 μ g aliquots of the cytosolic extracts were incubated in the presence or absence of 1 mM dATP and 10 μ M cytochrome *c* at 37°C for 1 hr in a final volume of 20 μ l of caspase activation buffer (10 mM HEPES, pH 7.4, 5 mM EGTA, 2 mM MgCl₂, 5 mM DTT, 1 mM ATP, 1 mM PMSF, 10 μ M leupeptin, 10 μ M aprotinin, 10 μ M pepstatin A, 10 mM phosphocreatinin, and 150 μ M creatine kinase). At the end of the incubation, aliquots of reaction mixtures (20 μ g of protein in 100 μ l of caspase-3 assay buffer consisting of 50 mM HEPES, pH 7.4, 100 mM NaCl, 0.1% 3-[(3-cholamidopropyl)dimethylammonio]-1-propanesulfonic acid, 10 mM DTT, 1 mM EDTA, and 10% glycerol) were mixed with equal volumes of 40 μ M fluorescent tetrapeptide substrate [Ac-DEVD-aminomethylcoumarin (AMC); Bachem] in the same buffer solution. Caspase-3-like activity was measured using a CytoFluor 4000 fluorometer (PerSeptive Biosystems) as described below.

Assay for caspase activity. Aliquots of cytosolic extracts (20 μ g of protein in 100 μ l of caspase-3 assay buffer) were mixed with equal volumes of 40 μ M Ac-DEVD-AMC in the same buffer. Free AMC accumulation, which resulted from cleavage of the aspartate-AMC bond, was monitored continuously in each sample over 30 min in 96-well microtiter plates using a CytoFluor 4000 fluorometer at 360 nm excitation and 460 emission wavelengths. The emission from each well was plotted against time. Linear regression analysis of the initial velocity (slope) of each curve yielded an activity for each sample.

Assessment of cell viability. Cell viability was measured by retention and deesterification of calcein AM (Eldadah et al., 1997). For the calcein AM retention assay, culture media in 96-well plates were replaced with 5 μ M calcein AM (Molecular Probes, Eugene, OR) in Locke's buffer containing (in mM): 154 NaCl, 5.6 KCl, 3.6 NaHCO₃, 2.3 CaCl₂, 1.2 MgCl₂, 5.6 glucose, and 5 HEPES, pH 7.4. After incubation at 37°C for 30 min, fluorescence was measured using a CytoFluor 4000 fluorometer at 485 nm excitation and 560 nm emission wavelengths.

Immunoblot analysis. Brain tissue or primary neurons were harvested, washed once with ice-cold PBS, and lysed on ice in a solution containing 50 mM Tris-HCl, pH 7.5, 150 mM NaCl, 1 mM EGTA, 1 mM PMSF, 0.5% NP-40, 0.25% SDS, 5 μ M leupeptin, and 5 μ M aprotinin. After removal of cell debris by centrifugation, the protein concentration of the cell lysate was determined with the Bio-Rad protein assay reagent. A portion of the lysate (50–80 μ g of protein) was then fractionated by SDS-PAGE, and the separated proteins were transferred to a nitrocellulose filter. The filter was stained with Ponceau S to confirm equal loading and transfer of samples and was then probed with specific antibodies. Immune complexes were detected with appropriate secondary antibodies and chemiluminescence reagents (Pierce, Rockford, IL). A polyclonal rabbit antibody to caspase-3 (H-277) was obtained from Santa Cruz Biotechnology (Santa Cruz, CA); a polyclonal rabbit antibody to active caspase-3 (9661) was obtained from Cell Signaling Technology (New England Biolabs, Beverly, MA); a monoclonal mouse antibody to caspase-9 (clone 5B4) was obtained from Medical and Biological Laboratories (MBL); and a polyclonal rabbit antibody to Apaf-1 (AB16941) was obtained from Chemicon.

Reverse transcription-PCR. The levels of mRNA were analyzed using a reverse transcription (RT)-PCR approach as previously described (Yakovlev et al., 1997). In brief, total RNA was isolated by acidic phenol extraction (Chomczynski and Sacchi, 1987), and 10 μ g of it was reverse transcribed with Moloney murine leukemia virus RT (Life Technologies) in 30 μ l reaction mixture. The resulting cDNA (3 μ l) was amplified by PCR. Numbers of cycles and reaction temperature conditions were estimated to be optimal to provide a linear relationship between the amount of input template and the amount of PCR product generated over a wide concentration range: from 1 to 20 μ g of total RNA, as described in detail previously (Yakovlev and Faden, 1994). Primers to amplify the rat caspase-3 cDNA were 5'-GGTATTGAGACAGACAGTGG-3' (sense primer) and 5'-CATGGGATCTGTTTCTTTGC-3' (antisense primer). Primers to amplify the rat caspase-9 cDNA were 5'-ACAAGCCCTTCGACAGTG-3' (sense primer) and 5'-GTACCAGGAACCGCTCTT-3' (antisense primer). Primers to amplify the rat Apaf-1 cDNA were 5'-GATATGGAATGTCTCAGATGGCC-3' (sense primer) and 5'-GGTCTGTGAGGACTCCCCA-3' (antisense primer). Amplified cDNA was analyzed in agarose electrophoretic gels. After staining with ethidium bromide, UV light gel images were captured and analyzed using the Image 1.59 program. Levels of individual mRNA were expressed in

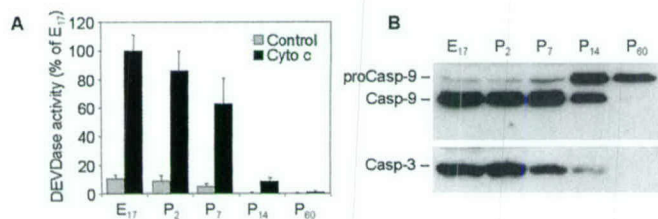


Figure 1. Age-dependent susceptibility of cytosolic protein extracts from rat cortex to cytochrome *c*- and dATP-dependent activation of caspase-3. **A**, Fifty microgram aliquots of cytosolic protein extracts isolated from cortex of E17 or P2, P7, P14, and P60 rat brains were incubated in the presence or absence of cytochrome *c* (*Cyto c*) and dATP in caspase activation buffer as described in Materials and Methods. Caspase-3-like activity in treated and control extracts was assayed fluorometrically by measuring the accumulation of free AMC resulting after cleavage of Ac-DEVD-AMC. Protease activity is expressed as percentage of E17 (mean value) \pm SD ($n = 5$). **B**, Fifty microgram aliquots of cytosolic extracts were treated as described in **A**, subjected to 12% SDS-PAGE, and transferred to nitrocellulose filters. The filters were probed with a monoclonal anti-caspase-9 (*Casp-9*) antibody (clone 5B4; MBL) or with a rabbit polyclonal antibody against p17 cleaved form of caspase-3 (*Casp-3*; Cell Signaling Technology). The antigen–antibody complexes were visualized by an ECL method as described in Materials and Methods. These experiments were repeated in four occasions with similar results.

arbitrary units as the proportion of individual PCR product mean optical density (inverted image) to a control product mean optical density obtained from the same RNA sample. The cDNA for glyceraldehyde-3-phosphate dehydrogenase (GAPDH) was used as the internal control, because its levels remain constant in different models tested. Primers to amplify rat GAPDH cDNA were 5'-TAAAGGGCATCTGGGCTACACT-3' (sense primer) and 5'-TTACTCCTTGGAGGCCATGTAGG-3' (antisense primer). The identity of a PCR-generated product to a corresponding cDNA was confirmed by the sequencing of the PCR products.

Production of recombinant Apaf-1XL. Recombinant human Apaf-1XL was purified essentially as it was described by us earlier (Yakovlev et al., 2000). The full-length coding cDNA clone was kindly provided by Dr. Gabriel Nunez. A pET21c(+) expression vector (Novagen, Madison, WI) containing the coding region for Apaf-1XL was used for the production of the His-tagged protein. The expression plasmid was transformed into a BL21(DE3)pLysS *Escherichia coli* strain. After induction with 1 mM isopropyl-1-thio- β -D-galactopyranoside, Apaf-1XL was isolated from bacterial inclusion bodies using Ni-nitrilotriacetic acid agarose (Qiagen, Hilden, Germany) according to the manufacturer's protocol. The yield of recombinant Apaf-1XL was as low as a few micrograms of protein per liter of bacterial culture, probably because of high toxicity of this protein.

Data analysis. Changes in mRNA content, activity for caspase-3, and neuronal viability were analyzed using ANOVA, followed by Dunnett's test; $p < 0.05$ was considered statistically significant.

RESULTS

To assess effectiveness of the cytochrome *c*-dependent caspase-3 activation pathway in rat brain at different stages of development, we used a well-established assay of reconstitution of cytochrome *c*-dependent caspase-3 activation *in vitro*. Cytochrome *c* and dATP are necessary for the oligomerization and binding of Apaf-1 to procaspase-9 followed by autoactivation of this caspase. Active caspase-9, in turn, cleaves and activates downstream caspases, including caspase-3. Therefore, we incubated cell-free cytosolic extracts isolated from rat brain cortex on embryonic day 17 (E17) or postnatal day 2 (P2), P7, P14, and P60 in the absence or presence of cytochrome *c* and dATP. As an outcome, we used a fluorogenic substrate assay to measure caspase-3-like (DEV-Dase) enzyme activity levels in the cortical extracts (Fig. 1A).

High levels of cytochrome *c*-induced DEV-Dase activity were found in extracts from E17 and P2 rat cortex with no considerable

difference between these two age groups. In contrast, activity of DEV-Dase in P7 protein extracts decreased to ~65% of embryonic and neonatal levels. DEV-Dase activity in P14 extracts decreased further, reaching nearly 10% of E17, and was not detected in extracts from mature (P60) brain. No DEV-Dase activity was detected also in extracts preincubated in the absence of cytochrome *c* (Fig. 1A).

Because cytochrome *c*-dependent activation of caspase-3 requires activation of caspase-9, we next examined cleavage of these two caspases by Western blot analysis. Using a monoclonal 5B4 anti-caspase-9 antibody (MBL) that recognizes both rat procaspase-9 and its large subunit, we observed nearly complete cleavage of procaspase-9 in E17, P2, and P7 extracts (Fig. 1B). The degree of caspase-9 cleavage was markedly decreased in P14 extracts and was not detected in P60 extracts. Using a polyclonal anti-caspase-3 antibody from Cell Signaling Technology that recognizes p17 cleaved fragments, we found that, consistent with results of DEV-Dase activity assay, caspase-3 was cleaved to its active form in E17, P2, and P7 extracts and to lesser extent in P14 extracts, but such cleavage was not detected in P60 extracts (Fig. 1B). Similar age-dependent changes in cytochrome *c*-dependent apoptotic susceptibility were found in developing mouse brain (data not shown).

To identify a potential molecular basis for the observed age-dependent change in cytochrome *c*-dependent apoptotic potential, we examined expression of each component of the apoptosome during rat brain development at mRNA and protein levels. mRNA levels were estimated by RT-PCR analysis. These experiments were based on the available rat Apaf-1, caspase-3, and caspase-9 mRNA sequences (GenBank accession numbers NM023979, U58656, and AF262319, respectively). RT-PCR experiments revealed that Apaf-1 and caspase-3 mRNA levels decreased markedly in the rat cortex between 1 and 2 weeks after birth and were sustained at these levels in the mature brain (Fig. 2A). In contrast, caspase-9 mRNA expression was not significantly changed during development.

To examine whether the observed decrease of caspase-3 and Apaf-1 mRNA correlated with decreased expression of the corresponding proteins, we estimated Apaf-1, procaspase-3, and procaspase-9 protein expression in rat cortex at the same times in rat brain development. Protein expression was assayed by Western blot analysis. Identification of procaspase-3 and procaspase-9 was performed by staining with H-277 and 5B4 antibodies (Santa Cruz Biotechnology and MBL, respectively), which, in each case, recognized a major protein band of a predicted molecular weight. Among a number of anti-Apaf-1 antibodies tested in this study, only a polyclonal rabbit antibody (AB16941; Chemicon) recognized a band of ~140 kDa, corresponding to predicted molecular weight of rat Apaf-1 (140 kDa), whereas the rest of tested antibodies stained a ~110 kDa protein of unknown origin. The specificity of this antibody was confirmed in preliminary experiments in which immunostaining of Apaf-1 in rat brain samples was compared with staining of human recombinant Apaf-1 and Apaf-1 preparations purified from bovine thymus (Fig. 3).

As shown in Figure 2B, levels of both Apaf-1 and caspase-3 proteins in cortical extracts were markedly decreased after 1 week of age and were minimal in the mature tissue. In contrast, no significant changes in caspase-9 protein expression were detected in this experiment.

To investigate further age-dependent changes in neuronal susceptibility to apoptosis, we analyzed the level of Apaf-1 protein expression, cytochrome *c*-mediated caspase-3 activation, and

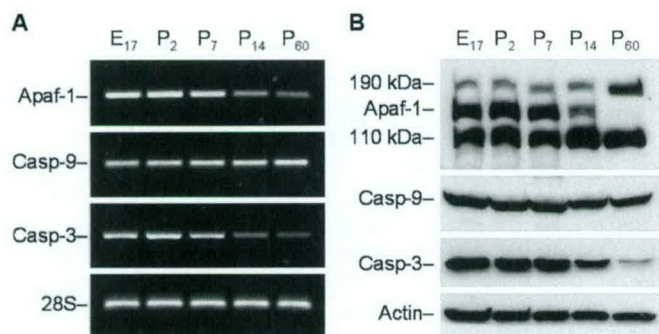


Figure 2. Analysis of age-dependent expression of Apaf-1, caspase-9, and caspase-3 mRNA and proteins in rat cortex. *A*, RT-PCR analysis of the abundance of transcripts encoding rat Apaf-1, caspase-9 (*Casp-9*), and caspase-3 (*Casp-3*) in cortex of E17 or P2, P7, P14, and P60 rat brains. Total RNA from rat cortex on the indicated days of development was subjected to RT-PCR with primers specific for Apaf-1, caspase-9, and caspase-3. Amplification of 28S rRNA was used as an internal control. The PCR products were analyzed by electrophoresis through an agarose gel and visualized after staining with ethidium bromide. *B*, Western blot analysis of the abundance of Apaf-1 and procaspases-9 and -3 in the protein extracts isolated from rat cortex on the indicated days of rat development. Eighty microgram aliquots of cytosolic protein extracts isolated from rat brain cortex at indicated developmental stages were subjected to 5% (*Apaf-1*) or 12% SDS-PAGE and transferred to a nitrocellulose filter. The filters were probed with a polyclonal anti-Apaf-1 antibody (AB16941; Chemicon), a monoclonal anti-caspase-9 antibody (clone 5B4; MBL), or a rabbit polyclonal antibody against caspase-3 (H-277, Santa Cruz Biotechnology). The antigen–antibody complexes were visualized by an ECL method as described in Materials and Methods. β -Actin protein abundance was used as an additional control for gel loading and transfer. These experiments were repeated four times with similar results.

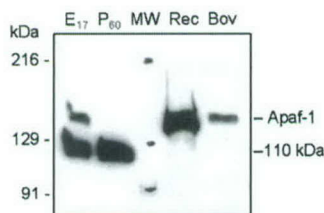


Figure 3. Analysis of anti-Apaf-1 antibody specificity. Fifty micrograms of cytosolic proteins from E17 and P60 rat cortex, 20 ng of recombinant human Apaf-1 (*Rec*), 10 ng of Apaf-1 purified from bovine thymus (*Bov*), and 5 μ l of prestained standards (*MW*; Bio-Rad, catalog #161-0324) were separated in 5% SDS-PAGE followed by staining with a polyclonal antibody (AB16941; Chemicon). The preparation of purified bovine Apaf-1 demonstrated Apaf-1 activity in the *in vitro* reconstitution system with cytochrome *c* (data not shown). Results show the location of the Apaf-1 protein band above the extensively stained 110 kDa protein of unknown origin.

etoposide-induced cell death in primary rat cortical neurons cultured for 1, 7, or 14 DIV. Western analysis showed that Apaf-1 expression was clearly decreased in 14 DIV primary neurons compared with 1 DIV cells, a result consistent with Apaf-1 protein expression in developing rat cortex (Fig. 4*A*). The difference in expression levels of Apaf-1 in 1 and 7 DIV cells was not obvious (data not shown). Incubation of cytosolic extracts from 1 DIV primary neurons in the presence of cytochrome *c* and dATP led to marked activation of caspase-3; in contrast, activation of caspase-3 in extracts from 7 DIV cells was $\sim 30\%$ lower and in 14 DIV neurons was approximately fivefold lower than in 1 DIV extracts (Fig. 4*B*). Similar differences in levels of caspase-3 activity were observed in the cytosol from primary neurons treated

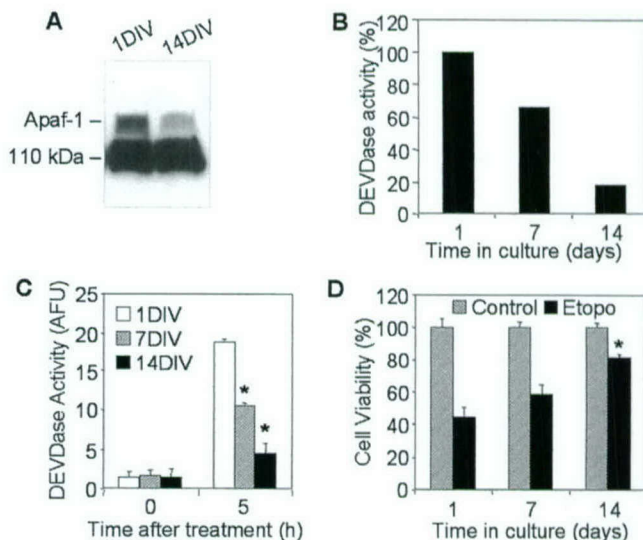


Figure 4. Analyses of Apaf-1 expression, cytochrome *c*-inducible apoptotic potential, and cell viability in primary cultures of rat cortical neurons. *A*, One hundred micrograms of cytosolic proteins from 1 or 14 DIV primary rat cortical neurons were separated in 5% SDS-PAGE followed by staining with an Apaf-1 antibody (Chemicon). *B*, Protein extracts from 1, 7, or 14 DIV primary rat cortical neurons were incubated in the presence of cytochrome *c* and dATP as described in Materials and Methods. Caspase-3-like activity was assayed fluorometrically by measuring the accumulation of free AMC resulting after cleavage of Ac-DEVD-AMC. Data are expressed as percentage of 1 DIV-induced caspase activity. *C*, One, 7, or 14 DIV primary rat cortical neurons were treated with 50 μ M etoposide for 5 hr. Control cultures (0 hr) served as negative controls. Caspase-3-like activity in cytosolic extracts from treated or control cells was assayed fluorometrically. Protease activity is expressed in arbitrary fluorescence units \pm SD ($n = 6$). $*p < 0.001$, compared with caspase-3 activity in etoposide-treated 1 DIV cells, by ANOVA, followed by Dunnett's test. *D*, One, 7, or 14 DIV primary neurons were treated with 50 μ M etoposide (*Etopo*) for 24 hr, and cell viability was analyzed by measurement of calcein AM fluorescence. Data are expressed as a percentage of the value for control cells not exposed to etoposide \pm SD ($n = 6$). $*p < 0.001$, compared with viability of 1 DIV cells after 24 hr etoposide treatment, by ANOVA, followed by Dunnett's test.

with etoposide: 5 hr treatment of 1 DIV cells resulted in activity of caspase-3 corresponding to 18.7 ± 0.4 arbitrary units of fluorescence (AUF); in contrast, activity in 14 DIV extracts was only 4.7 ± 0.1 AUF (Fig. 4*C*). Changes in caspase-3 activity in the etoposide-treated neurons correlated inversely with the degree of cell survival. After 24 hr incubation of 1 DIV neurons with etoposide, $45 \pm 6\%$ of cells survived, whereas in 7 DIV cultures, $55 \pm 5\%$ of cells survived, and in 14 DIV cultures, $79 \pm 3\%$ of cells were viable (Fig. 4*D*).

Our previous report suggested that brain trauma in rats results in activation of caspase-3 (Yakovlev et al., 1997). Because activation of caspase-3 results from specific cleavage of the precursor protein, we examined such cleavage of caspase-3 using Western analysis as a function of time after TBI. Consistent with previous findings, low levels of the cleaved forms of caspase-3 were detected beginning 4 hr after trauma but increased markedly at 48 hr after injury (Fig. 5).

Because the apoptotic potential in mature brain tissue is repressed, and such repression may be predetermined by downregulation of both Apaf-1 and caspase-3 gene expression, we hypothesized that elevation of caspase-3 activity after TBI may require reactivation of these genes in the mature brain. In part, this hypothesis is supported by results of our previous studies in which

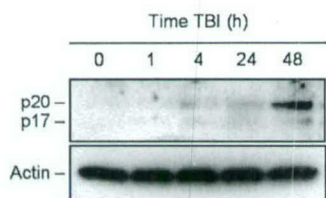


Figure 5. TBI-induced specific cleavage of procaspase-3 in rat brain cortex. Eighty microgram aliquots of cytosolic protein extracts isolated from sham control or traumatized rat cortex at indicated times after TBI were subjected to 12% SDS-PAGE and transferred to a nitrocellulose filter. The filter was probed with a rabbit polyclonal antibody against a p17 cleaved form of procaspase-3 (Cell Signaling Technology). To control protein loading, membranes were stripped and reprobed with an antibody against β -actin. A significant increase in caspase-3 cleavage was observed 48 hr after injury.

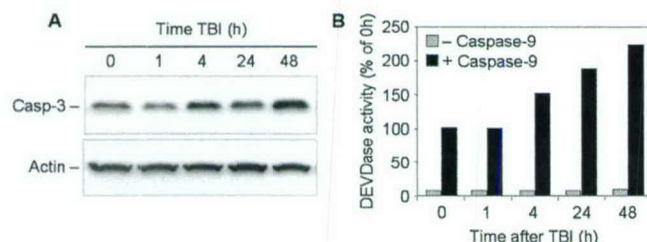


Figure 6. Time course of procaspase-3 protein expression in rat brain cortex after TBI. *A*, Fifty microgram aliquots of cytosolic protein extracts isolated from sham control or traumatized rat cortex at indicated times after TBI were subjected to 12% SDS-PAGE and transferred to a nitrocellulose filter. The filter was probed with a rabbit polyclonal antibody against caspase-3 (*Casp-3*; H-277; Santa Cruz Biotechnology). The antigen-antibody complexes were visualized by an ECL method as described in Materials and Methods. To control protein loading, membranes were stripped and reprobed with an antibody against β -actin. *B*, Fifty microgram aliquots of cytosolic protein extracts isolated from sham control or traumatized rat cortex at indicated times after TBI were incubated with or without active recombinant human caspase-9 (20 U; Biomol, Plymouth Meeting, PA) in 50 μ l of caspase activation buffer at 37°C for 1 hr. Caspase-3-like activity was assayed fluorometrically by measuring the accumulation of free AMC. Protease activity is expressed as a percentage of the activity in sham-operated control extracts.

we found that TBI results in an early increase in caspase-3 mRNA content in the injured brain regions (Yakovlev et al., 1997). In this study, we examined protein expression of procaspase-3 in injured cortex as a function of time after brain trauma. Using Western blot analysis, we found that procaspase-3 protein levels were elevated in injured cortex by 4–48 hr after TBI (Fig. 6*A*).

Because of the limitations of Western blot for quantitative analysis of protein expression, we examined whether the apparent increase in procaspase-3 after TBI leads to an increase in corresponding caspase activity after experimental cleavage by active recombinant caspase-9. As shown in Figure 6*B*, TBI induced a significant elevation of caspase-9-mediated caspase-3 activity in extracts from injured cortex. A 1.5-fold increase in caspase-9-dependent caspase-3 activation was observed in extracts isolated from injured cortex 4 hr after TBI. This induced activity was further increased at later time points after TBI, exceeding twice control levels by 2 d after injury. No such changes in caspase-3 activity were detected in contralateral brain regions (data not shown).

Injury-induced increases in caspase-3 protein expression observed in this study are consistent with increases in activity of this caspase after TBI. On the other hand, activation of caspase-3

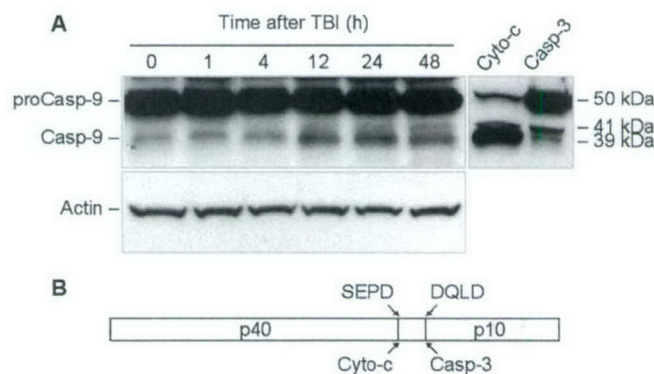


Figure 7. TBI induces time-dependent cleavage of procaspase-9 in rat brain cortex. *A*, Eighty microgram aliquots of cytosolic protein extracts isolated from sham control or traumatized rat cortex at indicated times after TBI were subjected to 10% SDS-PAGE and transferred to a nitrocellulose filter. As a positive control for cleavage specificity, 80 μ g aliquots of protein extracts from 2-d-old rat cortex were preincubated in the presence of either recombinant active rat caspase-3 (*Casp-3*; 20 U; Alexis) or cytochrome *c* (*Cyto-c*) and dATP for 1 hr at 37°C. The filter was probed with a monoclonal antibody against caspase-9 (*Casp-9*; clone 5B4; MBL). The antigen-antibody complexes were visualized by an ECL method as described in Materials and Methods. To control protein loading, membranes were stripped and reprobed with an antibody against β -actin. *B*, Schematic diagram illustrating processing of procaspase-9. Procaspase-9 is processed preferentially at the SEP site within the apoptosome and at the DQLD site by caspase-3 to generate the large subunit (*p40*) and small subunit (*p10*) of mature caspase-9.

requires previous activation of caspase-9 within the apoptosome. We found that in the mature brain this pathway is repressed, in part, because of downregulation of Apaf-1 expression. Therefore, we hypothesized that neuronal injury may lead to reactivation of the intrinsic pathway of apoptosis via reactivation of Apaf-1 gene expression. To test this hypothesis at the functional level, we first examined whether specific cleavage of caspase-9 could be detected after TBI. This was assessed by Western analysis of cortical protein extracts in the time course after trauma.

Amino acid sequence analysis of rat procaspase-9 revealed that, like human procaspase-9, it contains an SEP potential autoactivation cleavage site and a DQLD caspase-3 recognition site. Correspondingly, cytochrome *c*-mediated autoactivation is expected to produce a 39 kDa large subunit recognizable by the antibodies, whereas, a 41 kDa large fragment is expected after cleavage with caspase-3 (Fig. 7). Indeed, treatment of P2 cortical extracts with cytochrome *c* and dATP resulted in cleavage of caspase-9 corresponding to the 39 kDa subunit, whereas treatment of the extracts with recombinant active rat caspase-3 (Alexis) primarily resulted in appearance of the 41 kDa fragment. Notably, processing of procaspase-9 by caspase-3 was less efficient compared with that by cytochrome *c* treatment (Fig. 7).

Western blot analysis of protein samples of injured cortex showed accumulation of the 39 kDa caspase-9 subunit after TBI. At 48 hr after injury, the 41 kDa caspase-9 fragment also became apparent, reflecting increased caspase-3 activity in the samples at this time point (Fig. 7).

Injury-induced cleavage of procaspase-9 at autoactivation-specific sites presumes that injury reactivates the apoptosome complex, which, as we show here, is normally repressed in the mature brain. Therefore, we next examined whether expression of Apaf-1 mRNA and protein are affected by TBI.

Results of semiquantitative RT-PCR showed that Apaf-1 mRNA content increased in the injured cortex, reaching 143 \pm

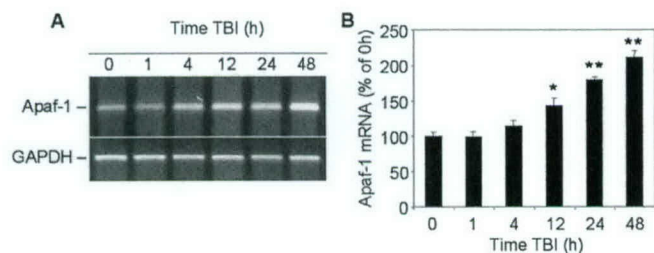


Figure 8. Time course of Apaf-1 mRNA expression in rat cortex at indicated times after TBI or in sham-operated controls (0 hr). *A*, Levels of mRNA were measured by using semiquantitative RT-PCR as indicated in Materials and Methods. *B*, Levels of Apaf-1 mRNA are expressed as the proportion of individual RT-PCR product mean optical density to GAPDH RT-PCR product optical density of the same RNA sample. mRNA content is expressed as a percentage of sham controls \pm SEM ($n = 5$). * $p < 0.05$; ** $p < 0.005$, compared with control, by ANOVA, followed by Dunnett's test.



Figure 9. TBI induces a time-dependent increase in Apaf-1 protein content in rat brain cortex. Eighty microgram aliquots of cytosolic protein extracts isolated from rat brain cortex at E17 or from sham control (0 hr) or traumatized rat cortex at indicated times after TBI were subjected to 5% SDS-PAGE and transferred to a nitrocellulose filter. The filter was probed with a rabbit polyclonal antibody against human Apaf-1 (AB16941; Chemicon). To control protein loading, the same samples were subjected to 10% SDS-PAGE, transferred to a nitrocellulose filter, and probed with an antibody against β -actin. The antigen-antibody complexes were visualized by an ECL method as described in Materials and Methods. This experiment was repeated three times with similar results.

10% of control (sham) levels by 12 hr, $180 \pm 5\%$ by 24 hr, and $211 \pm 9\%$ by 48 hr after TBI (Fig. 8*A,B*). Furthermore, Western blot revealed increased intensity of the Apaf-1 protein band in cortical extracts isolated 24 hr after injury, with a peak expression at 48 hr (Fig. 9).

DISCUSSION

Activation of caspase-3 appears to be a critical event in the execution of neuronal apoptosis in the brain during development and after acute injury (Kuida et al., 1996; Bredesen, 2000; Eldadah and Faden, 2000). In the intrinsic pathway of caspase-3 activation, Apaf-1, caspase-9, and cytochrome *c* work together forming the apoptosome complex (Li et al., 1997; Zou et al., 1997, 1999), which, in the presence of dATP, leads to activation of caspase-9 (Li et al., 1997). Active caspase-9, in turn, activates caspase-3.

A role for the apoptosome-mediated pathway of neuronal apoptosis in brain development has been established through transgenic studies (Cecconi et al., 1998; Hakem et al., 1998; Yoshida et al., 1998; Honarpour et al., 2000). Recently, a functional role for this pathway in injury-induced neuronal apoptosis also was demonstrated in models of brain (Krajewski et al., 1999) and spinal cord injury (Springer et al., 1999). This suggests that the same pathway may be functional in physiological apoptosis during

brain development and in pathological processes related to CNS injury.

In the present study, we examined the intrinsic pathway of caspase-3 activation in rat brain cortex and in primary rat cortical neurons as a function of developmental age and as a function of time after traumatic injury to mature brain. We also investigated expression of Apaf-1, caspase-9, and caspase-3 genes at mRNA and protein levels, given the role of these proteins in developmental and injury-induced neuronal apoptosis.

Using an *in vitro* system, we demonstrated that the ability of cytochrome *c* to induce activation of caspase-3 was decreased during maturation of rat brain and was undetectable by the caspase activity assay and by Western blot in rat (and mouse; data not shown) brain samples after 2 weeks of age. This observation is consistent with recent reports on age-dependent differences in injury-induced caspase-3 activation and susceptibility to apoptosis in mammalian brain (Bittigau et al., 1999; Pohl et al., 1999; Hu et al., 2000).

Results of Western blot experiments showed that age-dependent declines in cytochrome *c*-dependent activation of caspase-3 in rat brain cortex paralleled the extent of procaspase-9 processing in the *in vitro* assay. This suggests that repression of cytochrome *c*-dependent apoptotic potential might be regulated at the level of the apoptosome. To address this issue, we analyzed Apaf-1, caspase-9, and caspase-3 gene expression as a function of developmental age.

We found that mRNA and protein expression for both Apaf-1 and caspase-3 were markedly decreased in rat cortex during brain development. The age-dependent decrease in caspase-3 mRNA content in rat brain tissue is consistent with previously published data (Zou et al., 1997; de Bilbao et al., 1999). Profiles of both Apaf-1 and caspase-3 gene expression were comparable with the developmental profile of cytochrome *c*-mediated caspase-3 activation in rat brain. Interestingly, caspase-9 gene activity, at both mRNA and protein levels, did not change notably during brain development, suggesting that activation of this caspase in the brain may depend on the Apaf-1-mediated pathway. Developmental downregulation of caspase-3 gene activity may serve as a supplementary mechanism that protects the mature brain from apoptosis initiated by other caspases, such as caspase-8, -11, or -12 (Ivins et al., 1999; Raoul et al., 1999; Sanchez et al., 1999; Matsushita et al., 2000; Nakagawa et al., 2000).

Because of the poor specificity of the available anti-Apaf-1 antibodies, we were not able to examine directly whether downregulation of Apaf-1 during brain maturation occurs in neurons. Therefore, we examined Apaf-1 protein expression, cytochrome *c*-dependent activation of caspase-3, and etoposide-induced apoptosis in primary rat cortical neurons cultured for 1 or 14 DIV. Both Apaf-1 expression and apoptosome-mediated activation of caspase-3 were markedly decreased in 14 DIV neurons. Decreased levels of caspase-3 activity and highly significant reduction of associated apoptosis were also found in neurons at 14 DIV (vs 1 DIV) treated with etoposide. In transfection studies using dominant negative mutant constructs of caspase-8 and -9, we have demonstrated that etoposide-induced apoptosis in rat primary cortical neurons, as well as in the SH-SY5Y neuroblastoma cell line, proceeds through a caspase-9-dependent pathway (data not shown). Collectively these data support the hypothesis that neuronal maturation *in vitro* leads to repression of cytochrome *c*-dependent apoptotic susceptibility and that this process parallels the decrease in Apaf-1 protein expression in rat cortical neurons.

Given the present findings and previous observations that brain injury causes activation of caspase-3 and related neuronal apoptosis, we examined whether TBI recapitulates apoptotic potential via coordinated reactivation of caspase-3 and Apaf-1 genes. Increased caspase-3 mRNA levels after neuronal injury have been demonstrated previously in various models of apoptosis, including TBI (Yakovlev et al., 1997; Clark et al., 2000); however, changes in procaspase-3 protein levels have not been reported. Therefore, we examined expression of procaspase-3 protein as a function of time after brain trauma, using Western analysis and by measuring caspase-9-induced caspase-3 activity in extracts from injured cortex. Both techniques showed a marked increase in procaspase-3 after TBI.

Preliminary analysis of caspase-8 cleavage and activation in cortical protein extracts after brain injury did not suggest a role for caspase-8 in TBI-induced cell death (data not shown). In contrast, brain trauma resulted in accumulation of cleavage fragments of caspase-9 in rat cortex after injury that paralleled activation-specific cleavage of caspase-3.

Given the repression of Apaf-1 in normal mature brain cortex, we examined whether its levels were increased after brain injury. RT-PCR and Western blot showed that Apaf-1 mRNA and protein content were substantially increased after fluid percussion-induced TBI compared with sham-injured controls.

A role for Apaf-1 gene regulation in apoptosis has been suggested recently by *in vitro* studies. Robles et al. (1999) demonstrated that downregulation of Apaf-1 protein expression in granulosa cells by treatment with gonadotropin completely suppressed apoptotic cell death via the intrinsic procaspase-3 processing pathway. Soengas et al. (2001) reported that metastatic melanomas often lose Apaf-1 expression. Moreover, Apaf-1-negative cells are consistently chemoresistant and are unable to undergo apoptosis in response to p53 activation. The authors showed that loss of Apaf-1 expression can be recovered by treatment with the methylation inhibitor 5-aza-2'-deoxycytidine. Restoring physiological levels of Apaf-1 rescued the apoptotic defects associated with Apaf-1 loss. These authors suggested that inactivation of the Apaf-1 gene may result from methylation of an enhancer or other regulatory elements outside the Apaf-1 core promoter (Soengas et al., 2001). We do not exclude that methylation may also contribute to downregulation of Apaf-1 during brain development.

In addition, Moroni et al. (2001) recently reported that the expression of Apaf-1 gene can be directly regulated by E2F1 transcription factor and that Apaf-1 is a direct transcriptional target of the tumor suppressor p53. The previous studies demonstrated that p53 is upregulated in vulnerable cells in response to lateral fluid percussion brain injury in the rat (Napieralski et al., 1999). These observations suggest that injury-induced p53 expression might sensitize cells to apoptosis by increasing Apaf-1 levels.

Taken together, our findings are consistent with previous observations on differential susceptibility to apoptosis and associated caspase-3 activity in developing and mature brain tissues (Bittigau et al., 1999; Pohl et al., 1999; Hu et al., 2000). In addition, this report suggests a potential molecular mechanism underlying such age-dependent differences and indicates that Apaf-1 and caspase-3 gene expression is normally repressed in the adult brain. Acute brain injury appears to recapitulate earlier expression patterns for these proapoptotic genes that lead to apoptosis. Development of specific antibodies and inhibitors of Apaf-1 will help clarify the role of this protein in developmental

neuronal apoptosis as well as in injury-induced apoptotic cell death.

REFERENCES

- Adelson PD, Kochanek PM (1998) Head injury in children. *J Child Neurol* 13:2–15.
- Beattie MS, Farooqui AA, Bresnahan JC (2000) Review of current evidence for apoptosis after spinal cord injury. *J Neurotrauma* 17:915–925.
- Bittigau P, Siffringer M, Pohl D, Stadthaus D, Ishimaru M, Shimizu H, Ikeda M, Lang D, Speer A, Olney JW, Ikonomidou C (1999) Apoptotic neurodegeneration following trauma is markedly enhanced in the immature brain. *Ann Neurol* 45:724–735.
- Bredesen DE (2000) Apoptosis: overview and signal transduction pathways. *J Neurotrauma* 17:801–810.
- Brink JD, Garrett AL, Hale WR, Nickel VL, Woo-Sam J (1970) Recovery of motor and intellectual function in children sustaining severe head injuries. *Dev Med Child Neurol* 12:565–571.
- Brown GC, Borutaite V (1999) Nitric oxide, cytochrome *c* and mitochondria. *Biochem Soc Symp* 66:17–25.
- Cecconi F, Alvarez-Bolado G, Meyer BI, Roth KA, Gruss P (1998) Apaf1 (CED-4 homolog) regulates programmed cell death in mammalian development. *Cell* 94:727–737.
- Chomczynski P, Sacchi N (1987) Single-step method of RNA isolation by acid guanidinium thiocyanate-phenol-chloroform extraction. *Anal Biochem* 162:156–159.
- Clark RS, Kochanek PM, Watkins SC, Chen M, Dixon CE, Seidberg NA, Melick J, Loeffert JE, Nathaniel PD, Jin KL, Graham SH (2000) Caspase-3 mediated neuronal death after traumatic brain injury in rats. *J Neurochem* 74:740–753.
- de Bilbao F, Guarín E, Nef P, Vallet P, Giannakopoulos P, Dubois-Dauphin M (1999) Postnatal distribution of cyp32/caspase 3 mRNA in the mouse central nervous system: an *in situ* hybridization study. *J Comp Neurol* 409:339–357.
- Eldadah BA, Faden AI (2000) Caspase pathways, neuronal apoptosis, and CNS injury. *J Neurotrauma* 17:811–829.
- Eldadah BA, Yakovlev AG, Faden AI (1997) The role of CED-3-related cysteine proteases in apoptosis of cerebellar granule cells. *J Neurosci* 17:6105–6113.
- Faden AI, Demediuk P, Panter SS, Vink R (1989) The role of excitatory amino acids and NMDA receptors in traumatic brain injury. *Science* 244:798–800.
- Gillardon F, Bottiger B, Schmitz B, Zimmermann M, Hossmann KA (1997) Activation of CPP-32 protease in hippocampal neurons following ischemia and epilepsy. *Brain Res Mol Brain Res* 50:16–22.
- Hakem R, Hakem A, Duncan GS, Henderson JT, Woo M, Soengas MS, Elia A, de la Pompa JL, Kagi D, Khoo W, Potter J, Yoshida R, Kaufman SA, Lowe SW, Penninger JM, Mak TW (1998) Differential requirement for caspase 9 in apoptotic pathways *in vivo*. *Cell* 94:339–352.
- Haydar TF, Kuan CY, Flavell RA, Rakic P (1999) The role of cell death in regulating the size and shape of the mammalian forebrain. *Cereb Cortex* 9:621–626.
- Honarpour N, Du C, Richardson JA, Hammer RE, Wang X, Herz J (2000) Adult Apaf-1-deficient mice exhibit male infertility. *Dev Biol* 218:248–258.
- Hu BR, Liu CL, Ouyang Y, Blomgren K, Siesjö BK (2000) Involvement of caspase-3 in cell death after hypoxia-ischemia declines during brain maturation. *J Cereb Blood Flow Metab* 20:1294–1300.
- Ivins KJ, Thornton PL, Rohn TT, Cotman CW (1999) Neuronal apoptosis induced by beta-amyloid is mediated by caspase-8. *Neurobiol Dis* 6:440–449.
- Krajewski S, Krajewska M, Ellerby LM, Welsh K, Xie Z, Deveraux QL, Salvesen GS, Bredesen DE, Rosenthal RE, Fiskum G, Reed JC (1999) Release of caspase-9 from mitochondria during neuronal apoptosis and cerebral ischemia. *Proc Natl Acad Sci USA* 96:5752–5757.
- Kuida K (2000) Caspase-9. *Int J Biochem Cell Biol* 32:121–124.
- Kuida K, Zheng TS, Na S, Kuan C, Yang D, Karasuyama H, Rakic P, Flavell RA (1996) Decreased apoptosis in the brain and premature lethality in CPP32-deficient mice. *Nature* 384:368–372.
- Kulms D, Schwarz T (2000) Molecular mechanisms of UV-induced apoptosis. *Photodermatol Photoimmunol Photomed* 16:195–201.
- Levin HS, Eisenberg HM, Wigg NR, Kobayashi K (1982) Memory and intellectual ability after head injury in children and adolescents. *Neurosurgery* 11:668–673.
- Li P, Nijhawan D, Budihardjo I, Srinivasula SM, Ahmad M, Alnemri ES, Wang X (1997) Cytochrome *c* and dATP-dependent formation of Apaf-1/caspase-9 complex initiates an apoptotic protease cascade. *Cell* 91:479–489.
- Lipton P (1999) Ischemic cell death in brain neurons. *Physiol Rev* 79:1431–1568.
- Matsushita K, Wu Y, Qiu J, Lang-Lazdunski L, Hirt L, Waeber C, Hyman BT, Yuan J, Moskowitz MA (2000) Fas receptor and neuronal cell death after spinal cord ischemia. *J Neurosci* 20:6879–6887.

- McIntosh TK, Noble L, Andrews B, Faden AI (1987) Traumatic brain injury in the rat: characterization of a midline fluid-percussion model. *Cent Nerv Syst Trauma* 4:119–134.
- Moroni MC, Hickman ES, Denchi EL, Caprara G, Colli E, Cecconi F, Muller H, Helin K (2001) Apaf-1 is a transcriptional target for E2F and p53. *Nat Cell Biol* 3:552–558.
- Nakagawa T, Zhu H, Morishima N, Li E, Xu J, Yankner BA, Yuan J (2000) Caspase-12 mediates endoplasmic-reticulum-specific apoptosis and cytotoxicity by amyloid-beta. *Nature* 403:98–103.
- Napieralski JA, Raghupathi R, McIntosh TK (1999) The tumor-suppressor gene, p53, is induced in injured brain regions following experimental traumatic brain injury. *Brain Res Mol Brain Res* 71:78–86.
- Pohl D, Bittigau P, Ishimaru MJ, Stadthaus D, Hubner C, Olney JW, Turski L, Ikonomidou C (1999) *N*-Methyl-D-aspartate antagonists and apoptotic cell death triggered by head trauma in developing rat brain. *Proc Natl Acad Sci USA* 96:2508–2513.
- Raghupathi R, Graham DI, McIntosh TK (2000) Apoptosis after traumatic brain injury. *J Neurotrauma* 17:927–938.
- Raoul C, Henderson CE, Pettmann B (1999) Programmed cell death of embryonic motoneurons triggered through the Fas death receptor. *J Cell Biol* 147:1049–1062.
- Richter C, Ghafourifar P (1999) Ceramide induces cytochrome *c* release from isolated mitochondria. *Biochem Soc Symp* 66:27–31.
- Robertson JD, Orrenius S (2000) Molecular mechanisms of apoptosis induced by cytotoxic chemicals. *Crit Rev Toxicol* 30:609–627.
- Robles R, Tao XJ, Trbovich AM, Maravel DV, Nahum R, Perez GI, Tilly KI, Tilly JL (1999) Localization, regulation and possible consequences of apoptotic protease-activating factor-1 (Apaf-1) expression in granulosa cells of the mouse ovary. *Endocrinology* 140:2641–2644.
- Sanchez I, Xu CJ, Juo P, Kakizaka A, Blenis J, Yuan J (1999) Caspase-8 is required for cell death induced by expanded polyglutamine repeats. *Neuron* 22:623–633.
- Scaffidi C, Fulda S, Srinivasan A, Friesen C, Li F, Tomaselli KJ, Debatin KM, Krammer PH, Peter ME (1998) Two CD95 (APO-1/Fas) signaling pathways. *EMBO J* 17:1675–1687.
- Slee EA, Harte MT, Kluck RM, Wolf BB, Casiano CA, Newmeyer DD, Wang HG, Reed JC, Nicholson DW, Alnemri ES, Green DR, Martin SJ (1999) Ordering the cytochrome *c*-initiated caspase cascade: hierarchical activation of caspases-2, -3, -6, -7, -8, and -10 in a caspase-9-dependent manner. *J Cell Biol* 144:281–292.
- Snider BJ, Gottron FJ, Choi DW (1999) Apoptosis and necrosis in cerebrovascular disease. *Ann NY Acad Sci* 893:243–253.
- Soengas MS, Capodieci P, Polsky D, Mora J, Esteller M, Opitz-Araya X, McCombie R, Herman JG, Gerald WL, Lazebnik YA, Cordon-Cardo C, Lowe SW (2001) Inactivation of the apoptosis effector Apaf-1 in malignant melanoma. *Nature* 409:207–211.
- Springer JE, Azbill RD, Knapp PE (1999) Activation of the caspase-3 apoptotic cascade in traumatic spinal cord injury. *Nat Med* 5:943–946.
- Yakovlev AG, Faden AI (1994) Sequential expression of *c-fos* protooncogene, TNF-alpha, and dynorphin genes in spinal cord following experimental traumatic injury. *Mol Chem Neuropathol* 23:179–190.
- Yakovlev AG, Knobloch SM, Fan L, Fox GB, Goodnight R, Faden AI (1997) Activation of CPP32-like caspases contributes to neuronal apoptosis and neurological dysfunction after traumatic brain injury. *J Neurosci* 17:7415–7424.
- Yakovlev AG, Wang G, Stoica BA, Boulares HA, Spoonde AY, Yoshida K, Smulson ME (2000) A role of the $\text{Ca}^{2+}/\text{Mg}^{2+}$ -dependent endonuclease in apoptosis and its inhibition by poly(ADP-ribose) polymerase. *J Biol Chem* 275:21302–21308.
- Yamashita T (2000) Implication of cysteine proteases calpain, cathepsin and caspase in ischemic neuronal death of primates. *Prog Neurobiol* 62:273–295.
- Yoshida H, Kong YY, Yoshida R, Elia AJ, Hakem A, Hakem R, Penninger JM, Mak TW (1998) Apaf1 is required for mitochondrial pathways of apoptosis and brain development. *Cell* 94:739–750.
- Zou H, Henzel WJ, Liu X, Lutschg A, Wang X (1997) Apaf-1, a human protein homologous to *C. elegans* CED-4, participates in cytochrome *c*-dependent activation of caspase-3. *Cell* 90:405–413.
- Zou H, Li Y, Liu X, Wang X (1999) An APAF-1-cytochrome *c* multimeric complex is a functional apoptosome that activates procaspase-9. *J Biol Chem* 274:11549–11556.

Ceramide-Induced Cell Death in Primary Neuronal Cultures: Upregulation of Ceramide Levels During Neuronal Apoptosis

Rachelle E. Toman,^{1,2} Vilen Movsesyan,³ Shvetha K. Murthy,² Sheldon Milstien,⁴ Sarah Spiegel,² and Alan I. Faden^{3*}

¹Interdisciplinary Program in Neuroscience, Georgetown University Medical Center, Washington, DC

²Department of Biochemistry and Molecular Biology, Georgetown University Medical Center, Washington, DC

³Department of Neuroscience, Georgetown University Medical Center, Washington, DC

⁴Laboratory of Cellular and Molecular Communication, NIMH, Bethesda, Maryland

Ceramide is a sphingolipid that has been implicated both in apoptosis and protection from cell death. We show that in both rat cerebellar granule cells and cortical neuronal cultures application of C₂-ceramide causes cell death in a dose- and time-dependent manner. Similar effects were observed with the exogenous application of bacterial sphingomyelinase, which hydrolyzes sphingomyelin located on the outer leaflet of the plasma membrane and leads to endogenous ceramide accumulation. Furthermore, endogenous ceramide levels were increased during apoptosis induced by nutrient deprivation or etoposide treatment. These findings suggest that upregulation of ceramide levels, which may be generated through activation of sphingomyelinase, contributes to neuronal apoptosis. © 2002 Wiley-Liss, Inc.

Key words: apoptosis; ceramide; cerebellar granule cells; cortical neurons; sphingolipid

Apoptosis, a form of programmed cell death, is a key physiological response that occurs during development of the nervous system, resulting in the death of nearly half of the embryonic neuronal population (Oppenheim, 1991; Raff et al., 1993; Pettmann and Henderson, 1998). This intrinsic cell suicide program, which is morphologically distinguished from necrosis, is characterized by cell shrinkage, chromatin condensation, membrane blebbing, and internucleosomal DNA fragmentation (Arends and Wylie, 1991; Oppenheim, 1991; Krueger et al., 1995). Activation of apoptotic pathways in adults appears to be involved in both acute and chronic neurodegeneration (Cotman and Anderson, 1995; Barinaga, 1998; Hutchins and Barger, 1998).

Ceramide has been implicated in the regulation of various cellular functions, such as cell growth, differentiation, and death (Spiegel and Merrill, 1996). It is an evolutionarily conserved sensor of cell stress (Hannun, 1996). Structurally, ceramide consists of a long-chain sphingoid base with an amide-linked fatty acid component of 16–24 carbons in length. There are two potential

pathways for intracellular ceramide formation: *de novo* synthesis via the condensation of serine and palmitoyl-CoA, followed by conversion to dihydroceramide and finally to ceramide and/or the breakdown of sphingomyelin through sphingomyelinase (Futerman et al., 1990; Bielawska et al., 1993; Hannun, 1994; Kolesnick and Kronke, 1998).

A role for ceramide in apoptosis was originally described in U397 monoclonal leukemia cells, where the addition of C₂-ceramide (a cell permeable ceramide analogue) resulted in apoptosis (Obeid et al., 1993). Subsequently, it was found that many agents causing apoptosis also activate sphingomyelinase, leading to increased ceramide formation; moreover, the degree of apoptosis induced appears to be closely correlated to the amount of ceramide produced (Hannun, 1996). Such stimuli include environmental agents like radiation (Haimovitz-Friedman et al., 1994), IL-1 (Yao et al., 1995), TNF- α (Jarvis et al., 1994; Obeid and Hannun, 1995), or Fas binding (Cifone et al., 1994).

In cells of neural origin, the effects of ceramide are more controversial, either killing or protecting cells depending on the concentration and experimental paradigm. Exogenous addition of ceramide has been found to induce apoptosis in a variety of neuronally derived cells, including PC12 cells, mesencephalic neurons, and human neuroblastoma cells (Brugg et al., 1996; Marcora et al., 1996; France-Lanord et al., 1997; Hartfield et al., 1997). In

Contract grant sponsor: DOD; Contract grant number: DAMD 17-99-2-9007.

Rachelle E. Toman and Vilen Movsesyan contributed equally to this article.

*Correspondence to: Alan I. Faden, MD, Departments of Neuroscience, Neurology, and Pharmacology, Georgetown University, 3970 Reservoir Road, NW, Room EP-12, Washington, DC 20007.

E-mail: fadena@gicc.georgetown.edu

Received 10 October 2001; Revised 18 December 2001; Accepted 27 December 2001

embryonic chick neurons derived from the cerebral hemispheres, the addition of ceramide-induced caspase-3 activation and apoptosis in a time- and dose-dependent manner (Wiesner and Dawson, 1996a, b). Moreover, the proapoptotic agents staurosporine, wortmannin or LY294002 were reported to induce cell death through activation of sphingomyelinase and intracellular ceramide accumulation (Dawson et al., 1998). Similar processes were observed with hypoxia induced death of both naive and NGF-differentiated PC12 (Yoshimura et al., 1999). In primary oligodendrocyte culture, ceramide has also been found to mediate cell death through an increase of c-jun amino terminal kinase activity, following NGF binding to its low affinity receptor (Dobrowsky et al., 1994; Casaccia-Bonnel et al., 1996).

Opposite actions, however, have been reported in other primary cultures. In both spinal motor neurons and hippocampal neurons, low concentrations of ceramide ($>3 \mu\text{M}$) were found to increase survival and differentiation of immature cells, whereas higher concentrations resulted in cell death (Furuya et al., 1998; Irie and Hirabayashi, 1998). Moreover, addition of C_2 -ceramide or sphingomyelinase prevented apoptosis induced by NGF deprivation in primary sympathetic neurons (Ito and Horigome, 1995). It also seems that ceramide must be present at critical levels for the survival and differentiation of cerebellar Purkinje cells, as either the depletion of sphingolipids or the inhibition of ceramide synthesis can cause apoptotic death of these neurons (Furuya et al., 1998).

Growing importance attributed to sphingolipid signaling in the control of neuronal survival, differentiation, and death, led us to examine the effects of ceramide in cell death of cerebellar granule cells and cortical neurons. Although it has been shown previously that exogenous ceramide addition may result in neuronal apoptosis (Saito et al., 1998) and an increase in caspase-3 activation (Marks et al., 1998), few studies have compared such effects with evaluation of changes in intracellular levels of ceramide in apoptosis. We report that exogenous addition of either C_2 -ceramide or bacterial sphingomyelinase results in a time- and dose-dependent increase in cell death of primary cultured neurons. Additionally, we found that the extent of cell death induced by trophic withdrawal or etoposide treatment correlated with increases in endogenous ceramide levels.

MATERIALS AND METHODS

Cell Cultures

Cerebellar granule cells (CGC) cultures were prepared as previously described (Eldadah et al., 1997). Briefly, the meninges and blood vessels were removed from cerebella of 7-day-old Sprague-Dawley rat pups (Taconic) while in Krebs-Ringer's bicarbonate buffer containing 0.3% bovine serum albumin (BSA, Gibco BRL, Gaithersburg, MD). The cerebella were dissociated at 37°C for 20 min in the same buffer with the addition of 1,800 U/ml trypsin (Sigma Chemical Company, St. Louis, MO). The dissociated cells were triturated through a 5 ml pipet following the addition of 200 U/ml DNase I (Sigma) and 3,600 U/ml soybean trypsin inhibitor (Sigma). The supernatant

was collected after the tissue settled for 5–10 min; the pellet was re triturated as noted above. The supernatants were combined and centrifuged through a 4% BSA solution. The pellet was resuspended in seeding medium (basal medium Eagle (BME, Gibco), 2 mM L-glutamine (Biofluids, Rockville, MD), 50 $\mu\text{g}/\text{ml}$ gentamicin sulfate (Biofluids), 10% fetal bovine serum (FBS) (HyClone Laboratories, Inc., Logan, UT), and 25 mM KCl (Sigma). Cells were seeded at 3.5×10^5 cells/ml onto 96-well tissue culture plates or 60 mm Petri dishes (Corning, Corning, NY) pre-coated with poly-D-lysine (70–150 kDa, Sigma). After 24 hr at 37°C in 5% CO_2 , 10 μM cytosine arabinoside (Sigma) was added. Alternatively, cells were seeded at the same density in neurobasal medium (Gibco) containing 25 mM KCL, 0.5 mM L-glutamine, 50 $\mu\text{g}/\text{ml}$ gentamicin, and 2% B27 supplement (Gibco). Incubation continued for 6 more days. All experiments were performed at Day 7 in vitro (DIV).

Rat cortical neuronal cultures (RCN) were derived from rat embryonic cortices (Taconic, Germantown, NY) with modifications of our previously described method (Mukhin et al., 1998). Briefly, cortices from 17–18-day-old Sprague-Dawley rat embryos were cleaned from their meninges and blood vessels in Krebs-Ringer's bicarbonate buffer containing 0.3% bovine serum albumin (BSA, Gibco BRL). Cortices were then minced and dissociated in the same buffer with 1,800 U/ml trypsin (Sigma) at 37°C for 20 min. Following the addition of 200 U/ml DNase I (Sigma) and 3,600 U/ml soybean trypsin inhibitor (Sigma) to the suspension, cells were triturated through a 5 ml pipet. After the tissue was allowed to settle for 5–10 min, the supernatant was collected, and the remaining tissue pellet was re triturated. The combined supernatants were then centrifuged through a 4% BSA layer and the cell pellet was resuspended in neuronal seeding medium (NSM), which consisted of neurobasal medium (Gibco), supplemented with 1.1% 100 \times antibiotic-antimycotic solution (Biofluids), 25 μM Na-glutamate, 0.5 mM L-glutamine, and 2% B27 Supplement (Gibco). Cells were seeded at a density of 5×10^5 cells/ml onto 96-well tissue culture plates or 60 mm Petri dishes (Corning) pre-coated with poly-D-lysine (70–150 kD, Sigma). On 4 DIV, feeding media (NSM without Na-glutamate and B27 supplement) in 1:2 proportion was added to cultures. All experiments were performed on cultures at 7 DIV.

Induction of Cell Death in Neuronal Cultures

C_2 -ceramide was obtained from Biomol (Plymouth Meeting, PA). Stock solution of C_2 -ceramide in methanol was dried down using N_2 gas and resuspended in a 4% BSA (Sigma, Fatty Acid Free) solution. In all experiments, control cultures received the same volume of vehicle alone. CGC were incubated overnight in serum-free BME with 25 mM KCl before application of C_2 -ceramide. In experiments using sphingomyelinase-induced apoptosis, cerebellar granule cells or cortical neurons preincubated overnight in serum-free BME with 25 mM KCl or B27-free neurobasal medium respectively were treated with the indicated concentrations of sphingomyelinase diluted in the relevant serum-free medium. Sphingomyelinase from *B. cereus* or *S. aureus* (both from Sigma) were used. Both preparations showed similar effects on neuronal cell viability in CGC and RCN cultures (data not shown). Apoptosis was also induced in cultured neuronal cells either by incubation with apoptosis-inducing agents or by trophic support with-

drawal. In experiments using trophic support withdrawal, CGCs cultured in BME with 10% FBS and 25 mM KCl were washed once in BME and placed in serum-free BME containing 5 mM KCl; RCN were deprived of B27 supplement by being washed three times with neurobasal medium following incubation in B27-free Neurobasal medium. In experiments using drug-induced apoptosis, 50 μ M of etoposide diluted in the relevant serum-free medium was administered to cell cultures. This dose of etoposide was previously shown to induce apoptosis in neuronal cultures (Movsesyan et al., 2001).

Assessment of Cell Viability

Cell viability was measured by retention and de-esterification of calcein AM as described previously (Eldadah et al., 1997). Culture medium in 96-well plates was replaced with 5 μ M calcein AM (Molecular Probes, Eugene, OR) in Locke's buffer containing 154 mM NaCl, 5.6 mM KCl, 3.6 mM NaHCO_3 , 2.3 mM CaCl_2 , 1.2 mM MgCl_2 , 5.6 mM glucose, and 5 mM HEPES, pH 7.4. After incubation at 37°C for 30 min, fluorescence was measured using a CytoFluor II fluorometer (PerSeptive Biosystems, Framingham, MA) at 485 nm excitation and 560 nm emission wavelengths.

Hoechst Staining

Cells were washed in PBS and stained for 10 min at room temperature in PBS containing 4% paraformaldehyde and 10 μ g/ml Hoechst 33258 (Sigma). Morphological evaluation of nuclear condensation and fragmentation was performed immediately after staining using a Nikon TE300 fluorescent microscope.

Measurement of Endogenous Ceramide

Lipids were extracted and mass amounts of ceramide in cellular extracts were measured by the DAG kinase enzymatic method (Olivera and Spiegel, 1992). Briefly, an aliquot (10–50 nmol of total phospholipid) of the chloroform phase from cellular lipid extracts was dried under nitrogen gas. The lipids or standard bovine brain type IV ceramides were resuspended in 40 μ l of 7.5% (w/v) octyl-D-glucopyranoside/5 mM cardiolipin in 1 mM DETPAC/10 mM imidazole, pH 6.6, and solubilized by freeze-thawing and subsequent sonication. The enzymatic reaction was started by the addition of 20 μ l of DTT (20 mM), 10 μ l of *E. coli* diacylglycerol kinase (0.88 U/ml), 20 μ l of [32 P]ATP (10–20 μ Ci, 10 mM), and 100 μ l of reaction buffer (100 mM imidazole, pH 6.6, 100 mM NaCl, 25 mM MgCl_2 , and 2 mM EGTA). After incubation for 1 hr at room temperature, lipids were extracted with 1 ml of chloroform/methanol/concentrated HCl (100:200:1, v/v) and 0.17 ml of 1 M KCl. Labeled phosphatidic acid and ceramide-1-phosphate were resolved by TLC with chloroform/acetone/methanol/acetic acid/water (10:4:3:2:1, v/v). Bands corresponding to ceramide were quantified with a Molecular Dynamics (Sunnyvale, CA) Storm PhosphorImager.

Data Analysis

Changes in cell viability were analyzed by Kruskal-Wallis ANOVA. Data on alterations in intracellular ceramide levels were analyzed using two-tailed Student's *t*-test. A *P*-value <0.05 was considered statistically significant.

RESULTS

C_2 -Ceramide and Sphingomyelinase Induce Neuronal Apoptosis

In the presence of serum, addition of C_2 -ceramide has little effect on viability of neuronal cultures (Brugg et al., 1996). This is likely due to the strong interaction of C_2 -ceramide with serum components that prevents its uptake (Spiegel and Merrill, 1996). Cultures grown in serum-free medium and exposed to ceramide exhibited time- and dose-dependent decreases in viability as measured by Calcein AM de-esterification (Fig. 1A,B). Cerebellar granule cells grown in serum-free BME contained 25 M KCl were resistant to the low-level ceramide exposure (10 μ M), but showed substantial increases in cell death starting at 24 hr of incubation with higher concentrations of C_2 -ceramide (20 μ M and 40 μ M; Fig. 1A). Application of C_2 -ceramide to CGC cultured in the presence of B27 supplement caused cell death at doses similar to those observed in our experiments performed in the serum deprived cultures. Administration of C_2 -ceramide in concentrations of 20 and 40 μ M for 24 hr reduced cell viability to 84.2 ± 4.03 and $50.2 \pm 6.68\%$ of the control levels respectively, as measured by the calcein AM assay. Low doses of C_2 -ceramide (1, 2.5, and 5 μ M) had no effect on cell viability of 7 DIV CGC, cultured in the presence of B27 and 25 mM KCl, and did not provide neuroprotection in the cultures subjected to B27 and potassium deprivation for 24 or 48 hr (data not shown). Cortical neuronal cultures grown in neurobasal medium with B27 supplement had a very similar response, showing minimal toxicity at 10 μ M and substantial increases in cell death with extended time and dose (Fig. 1B). Similarly to results obtained for CGC, low doses of C_2 -ceramide (1, 2.5, and 5 μ M) were not protective against cell death induced in 7 DIV cortical cultures by 24 or 48 hr of trophic support (B27) withdrawal, and had no effect on the cells growing under normal conditions (data not shown).

Similarly, treatment with bacterial sphingomyelinase, which hydrolyzes membrane sphingomyelin to form endogenous ceramide, resulted in a time- and dose-dependent decrease in viability of both types of cultured neurons (Fig. 2A,B). After 48 hr, at sphingomyelinase concentrations greater than 50 mU/mL, both cerebellar granule cells (Fig. 2A) and cortical neurons (Fig. 2B) exhibited a 50% or greater decrease in cell viability. Viability in both types of neuronal cultures decreased by more than 80% and remained at this low level for several days. To confirm that ceramide-induced cell death was indeed due to apoptosis, cells were stained with Hoechst 33258 to visualize condensed apoptotic nuclei. Both cerebellar granule cells and cortical neuronal cultures treated with 100 mU/mL sphingomyelinase for 48 hr had a significantly increased number of nuclei with apoptotic morphology ($239.3 \pm 25.8\%$ and $267.46 \pm 47.7\%$ respectively) when compared to relevant control cultures. It should be noted that the apoptotic effect of sphingomyelinase in cortical neuronal cultures was abolished by the

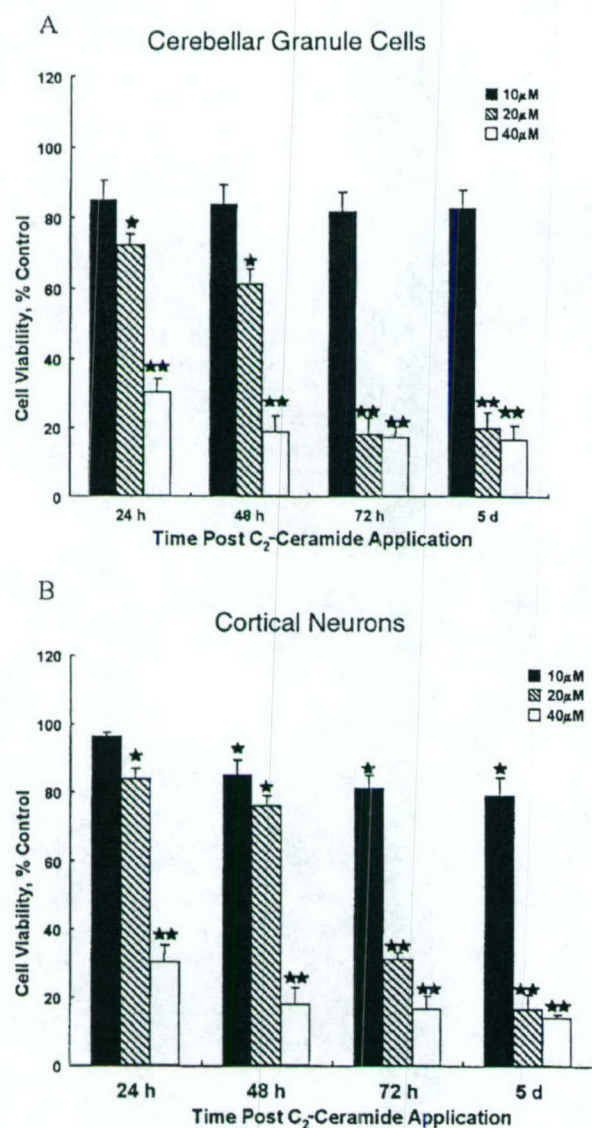


Fig. 1. C₂-ceramide reduces viability of cerebellar granule cells (A) and cortical neurons (B). Seven DIV cultures were treated with the indicated concentrations of C₂-ceramide and viability was measured after the indicated time periods by the calcein AM method. Each point is the mean \pm SE of eight wells. The data is representative of three to five separate experiments. * P < 0.05; ** P < 0.01 vs. control (ANOVA, Kruskal-Wallis post-hoc).

presence of B27 supplement in the medium (data not shown).

Exogenous Sphingomyelinase Upregulates Intracellular Ceramide Levels in Primary Neuronal Cultures

Because sphingomyelinase treatment markedly increased apoptosis of both cerebellar granule cells and cor-

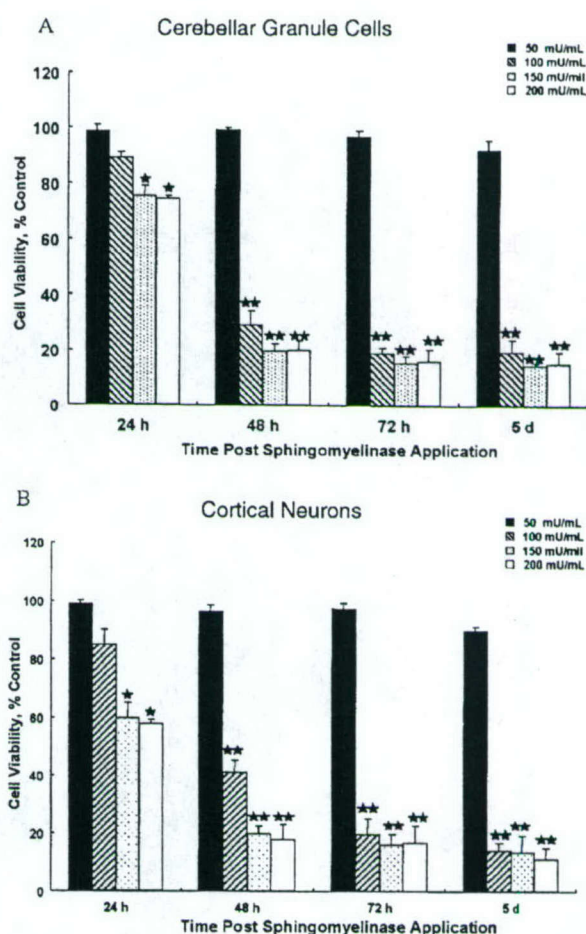


Fig. 2. Effect of sphingomyelinase treatment on viability of cerebellar granule cells (A) and cortical neurons (B). Seven DIV cortical neurons or cerebellar granule cells preincubated overnight in B27-free or serum-free medium with 25 mM KCl respectively were treated with the indicated concentrations of sphingomyelinase and viability was measured after the indicated time periods by the calcein AM method. Each point is the mean \pm SE of eight wells. The data is representative of three to five separate experiments. * P < 0.05; ** P < 0.01 vs. control (ANOVA, Kruskal-Wallis post-hoc).

tical neurons, we examined the effect of sphingomyelinase on the accumulation of intracellular ceramide. Although basal ceramide levels were markedly different in these two type of neurons, cerebellar granule cells having much higher basal levels of ceramide than cortical neurons, treatment with bacterial sphingomyelinase significantly increased ceramide accumulation in both types of cultures (Fig. 3). Ceramide accumulation also increased continuously in both cell types after exposure to sphingomyelinase for several days. Treatment with 100 mU/mL sphingomyelinase for 72 hr, which caused marked apoptosis in cortical neurons and cerebellar granule cells, increased ceramide levels in these cultures by three- and nine-fold, respectively (Fig. 3A,B).

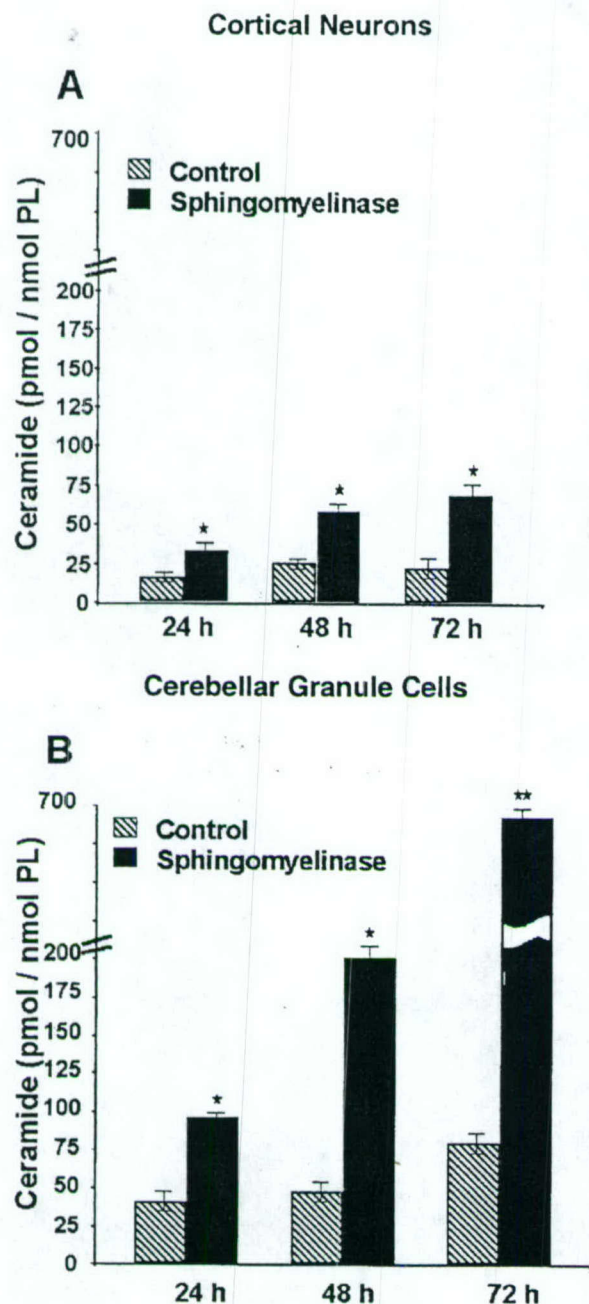


Fig. 3. Treatment of cortical neurons (A) and cerebellar granule cells (B) with sphingomyelinase increases endogenous ceramide levels. Seven DIV cortical neurons or cerebellar granule cells preincubated overnight in B27-free or serum-free medium with 25 mM KCl respectively were treated with 100 mU/mL of sphingomyelinase and intracellular ceramide was measured at the indicated times as described in Materials and Methods. The data are expressed as pmol ceramide per nmol total phospholipids. Each point is the mean \pm SE of triplicates. Similar results were obtained in two additional experiments. * $P < 0.05$; ** $P < 0.01$ vs. control, compared by two-tailed Student's *t*-test.

Intracellular Ceramide Accumulation in Primary Neuronal Cultures Subjected to Apoptotic Stimuli

We also examined whether stress stimuli, such as trophic factor withdrawal or etoposide, both of which induce apoptosis in these cultures (Eldadah et al., 1997; Movsesyan et al., 2001), are associated with ceramide accumulation. Trophic withdrawal involved removal of the B27 supplement for cortical cultures or serum and potassium deprivation for cerebellar granule cells. Although there was some time-dependent increase in ceramide production in the control cultures, there was a remarkable enhancement of ceramide accumulation following trophic withdrawal (Fig. 4). Trophic support withdrawal in RCN induced significant and stable upregulation in ceramide levels (Fig. 4A). Although serum withdrawal in CGC in the presence of 25 mM KCl resulted in increased ceramide levels after 72 hr, removal of both serum and potassium from culture medium caused significantly greater and more rapid ceramide accumulation in these cultures, albeit less than with sphingomyelinase treatment (Fig. 4B). Upregulation of ceramide levels correlated with cell death induced by serum/potassium deprivation in CGC or by B27 withdrawal in RCN. Thus, serum/potassium withdrawal for 48 hr reduced CGC viability to 37.4 ± 4.3 % of control, while B27 deprivation for 48 hr decreased RCN viability to 52.3 ± 2.7 % of control levels, as measured by the calcein AM assay.

Etoposide, a topoisomerase II inhibitor, known to induce apoptosis in neurons (Nakajima et al., 1994; Movsesyan et al., 2001), also induced accumulation of ceramide in a time-dependent manner in both cerebellar granule cells and cortical neurons (Fig. 5). Treatment with 50 μ M of etoposide for 48 hr also decreased CGC and RCN viability to 38.3 ± 3.9 % and 36 ± 6.2 % of control respectively, as measured by the calcein AM assay.

DISCUSSION

The different roles of ceramide in neuronal physiology and pathology is underscored by the apparent contradictory results that have been reported with respect to the effects of ceramide on survival, differentiation, and cell death. Although, the exogenous addition of ceramide analogues has been demonstrated to kill certain neuron-derived cell lines (Marcora et al., 1996; Hartfield et al., 1997; Lievremon et al., 1999), mesencephalic rat neurons (Brugg et al., 1996), and embryonic chick neurons (Wiesner and Dawson, 1996b), ceramide has been shown to have a bimodal effect on hippocampal neurons, protecting them at low concentrations and causing cell death at higher concentrations (Goodman and Mattson, 1996). In other reports, exogenous ceramide has been shown to have neuroprotective effects against hypoxic injury (Liu et al., 2000; Chen et al., 2001) and to enhance differentiation (Ito and Horigome, 1995). Using both primary cortical neurons and cerebellar granule cells, we observed dose dependent cell death induced by C_2 -ceramide with no evidence of protection at low concentrations. Similar observations were made after application of sphingomyelin-

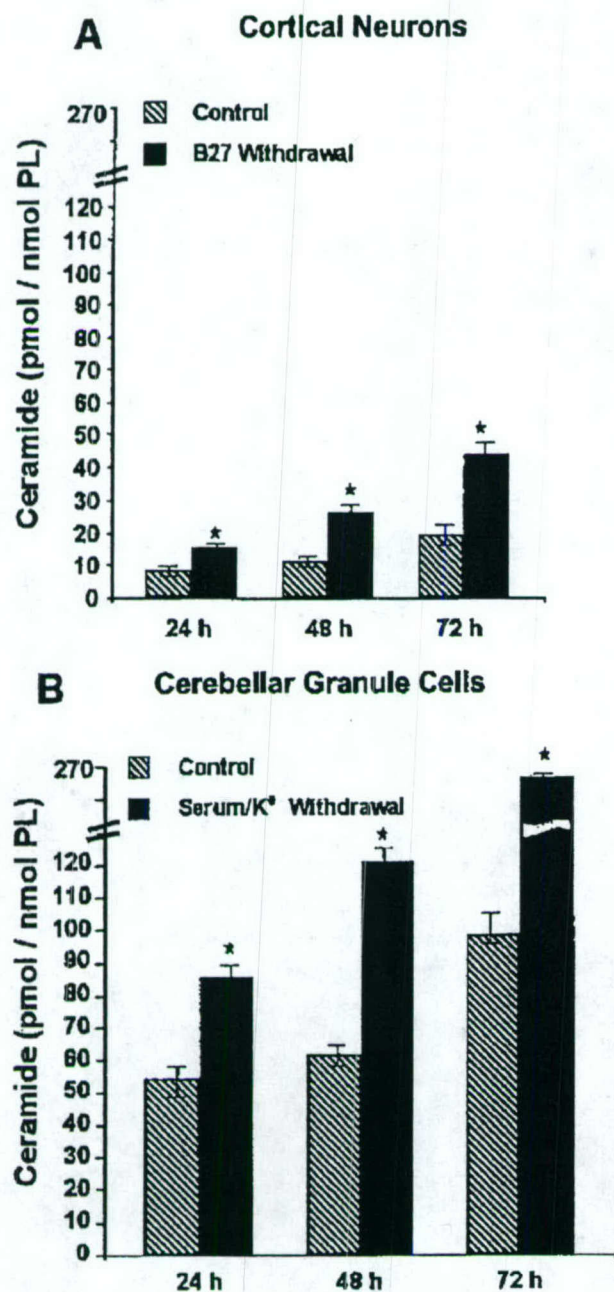


Fig. 4. Trophic withdrawal markedly enhances ceramide accumulation. Cortical neurons (A) and cerebellar granule cells (B) were cultured in serum free medium in the presence or absence of B27 or 25 mM KCl, respectively. Intracellular ceramide levels were measured at the indicated times as described in Materials and Methods. The data are expressed as pmol ceramide per nmol total phospholipids. Each point is the mean \pm SE of triplicate samples and similar results were obtained in two additional experiments. * $P < 0.05$ vs. control, compared by two-tailed Student's *t*-test.

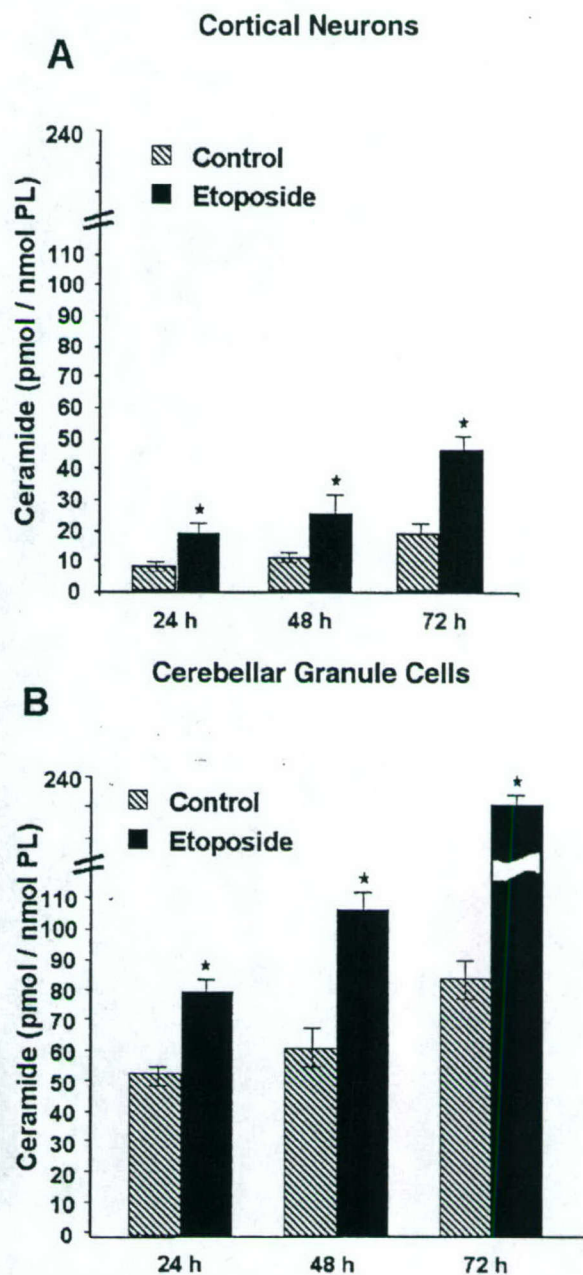


Fig. 5. Time-dependent increase in endogenous ceramide accumulation following etoposide addition to cortical neurons (A) and cerebellar granule cells (B). Cells were treated with 50 μ M etoposide and intracellular ceramide levels measured at the indicated times. Each point is the mean \pm SE of triplicate determinations. Similar results were obtained in two additional experiments. * $P < 0.05$ vs. control, compared by two-tailed Student's *t*-test.

ase, which was shown to increase endogenous ceramide levels. Moreover, in two classical models of neuronal apoptosis, trophic withdrawal and application of etoposide, apoptotic cell death was associated with marked increases in the level of ceramide.

Ceramide may modulate cell death through a number of enzymatic and signaling pathways. It is known that ceramide acts upon proline-directed kinases, such as mitogen activated protein kinase (Raines et al., 1993), stress activated protein kinase (Verheij et al., 1996), ceramide activated kinase (Liu et al., 1994), Raf-1 (Yao et al., 1995), ceramide activated phosphatase (Bielawska et al., 1993), protein kinase C (Yao and Cooper, 1995; Sawai et al., 1997), reactive oxygen species (France-Lanord et al., 1997; Lambeng et al., 1999), and platelet-activating factor (Perry et al., 1998), as well as several phospholipases (Gomez-Munoz et al., 1994), transcription factors, and caspases (Hannun, 1996). In addition to enhancing pathways associated with neuronal death, like the activation of the transcription factor c-jun and the downregulation of c-myc, ceramide can also inhibit neuronal survival signals. Akt, a kinase with a prosurvival role, is inhibited during C₂-ceramide induced apoptosis of neuronal cell lines (Zhou et al., 1998; Salinas et al., 2000). Specifically, ceramide appears to induce Akt dephosphorylation and subsequent activation of BAD, a proapoptotic Bcl-2 family member (Basu et al., 1998). Although numerous publications suggest that caspases are involved in the ceramide signaling cascade (Hannun, 1996; Gamard et al., 1997; Kolesnick and Kronke, 1998; Lievreumont et al., 1999; Gill and Windebank, 2000), it has not been clearly determined whether ceramide acts up- or downstream to, or independently of caspases. Recent work in cerebellar granule cells suggests that caspase activation was not crucial for the morphological alterations and cell death triggered by prolonged ceramide exposure (Monti et al., 2001). Preliminary studies from our own laboratory suggest, however, that a caspase 9/caspase 3 pathway is involved in ceramide induced cell death (Movsesyan et al., unpublished observation).

One dilemma that often arises with the use of exogenously added agents is whether or not the concentrations used to induce cell death in cultures is relevant to the endogenous levels found in physiological or pathological conditions. This question is difficult to address, in part, because ceramide levels may fluctuate rapidly. Indeed, a ten-fold variation in ceramide concentration has been recently reported in normal brain tissue (Herr et al., 1999). Additionally, the requirements for intracellular ceramide may vary considerably. It has been suggested that cerebellar granule cells have higher endogenous levels of ceramide than other neuronal cell types (Riboni et al., 1999). The fact that 100 mU/mL sphingomyelinase had similar proapoptotic effects on both cortical neurons and cerebellar granule cells, but induced markedly different levels of ceramide production, supports this idea. In addition, the similarity of the increases in ceramide levels induced in these neuronal cultures by several apoptotic stimulators

suggests that this may be a more general characteristic of the apoptosis.

In conclusion, the present results suggest that cell death in primary cultures of both cortical neurons and cerebellar granule cells involves the intracellular accumulation of ceramide. It is possible that this accumulation may occur by the conversion of membrane sphingomyelin to ceramide through the activation of sphingomyelinase. These observations suggest that ceramide accumulation may be a more generalized feature of many types of neuronal cell death, and that ceramide may play a role in certain forms of acute and chronic neurodegeneration associated with neuronal loss.

ACKNOWLEDGMENT

We thank Ms. Elvira Dabaghyan for technical assistance in preparation of cell cultures, cell viability assays, and Hoechst 33258 staining.

REFERENCES

- Arends MJ, Wyllie AH. 1991. Apoptosis: mechanisms and roles in pathology. *Int Rev Exp Pathol* 32:223-254.
- Barinaga M. 1998. Stroke-damaged neurons may commit cellular suicide. *Science* 281:1302-1303.
- Basu S, Bayoumy S, Zhang Y, Lozano J, Kolesnick R. 1998. BAD enables ceramide to signal apoptosis via Ras and Raf-1. *J Biol Chem* 273:30419-30426.
- Bielawska A, Crane HM, Liotta D, Obeid LM, Hannun YA. 1993. Selectivity of ceramide-mediated biology: lack of activity of erythrodiacylglyceramide. *J Biol Chem* 268:26222-26232.
- Brugg B, Michel PP, Agid Y, Ruberg M. 1996. Ceramide induces apoptosis in cultured mesencephalic neurons. *J Neurochem* 66:733-739.
- Casaccia-Bonnel P, Carter BD, Dobrowsky RT, Chao MV. 1996. Death of oligodendrocytes mediated by the interaction of nerve growth factor with its receptor p75. *Nature* 383:716-719.
- Chen Y, Ginis I, Hallenbeck JM. 2001. The protective effect of ceramide in immature rat brain hypoxia-ischemia involves upregulation of bcl-2 and reduction of TUNEL-positive cells. *J Cereb Blood Flow Metab* 21:34-40.
- Cifone MG, De Maria R, Roncalioli P, Rippo MR, Azuma M, Lanier LL, Santoni A, Testi R. 1994. Apoptotic signaling through CD95 (Fas/Apo-1) activates an acidic sphingomyelinase. *J Exp Med* 180:1547-1552.
- Cotman CW, Anderson AJ. 1995. A potential role for apoptosis in neurodegeneration and Alzheimer disease. *Mol Neurobiol* 10:19-45.
- Dawson G, Goswami R, Kilus J, Wiesner D, Dawson S. 1998. The formation of ceramide from sphingomyelin is associated with cellular apoptosis. *Acta Biochim Pol* 45:287-297.
- Dobrowsky R, Werner M, Castellino A, Chao M, Hannun Y. 1994. Activation of the sphingomyelin cycle through the low affinity neurotrophin receptor. *Science* 265:1596-1599.
- Eldadah BA, Yakovlev AG, Faden AI. 1997. The role of CED-3-related cysteine proteases in apoptosis of cerebellar granule cells. *J Neurosci* 17:6105-6113.
- France-Lanord V, Brugg B, Michel PP, Agid Y, Ruberg M. 1997. Mitochondrial free radical signal in ceramide-dependent apoptosis: a putative mechanism for neuronal death in Parkinson disease. *J Neurochem* 69:1612-1621.
- Furuya S, Mitoma J, Makino A, Hirabayashi Y. 1998. Ceramide and its interconvertible metabolite sphingosine function as indispensable lipid factors involved in survival and dendritic differentiation of cerebellar Purkinje cells. *J Neurochem* 71:366-377.
- Futerman AH, Stieger B, Hubbard AL, Pagano RE. 1990. Sphingomyelin synthesis in rat liver occurs predominantly at the cis and medial cisternae of the Golgi apparatus. *J Biol Chem* 265:8650-8657.

- Garnard CJ, Dbaibo GS, Liu B, Obeid LM, Hannun YA. 1997. Selective involvement of ceramide in cytokine-induced apoptosis. Ceramide inhibits phorbol ester activation of NF κ B. *J Biol Chem* 272:16474-16481.
- Gill JS, Windebank AJ. 2000. Ceramide initiates NF κ B-mediated caspase activation in neuronal apoptosis. *Neurobiol Dis* 7:448-461.
- Gomez-Munoz A, Martin A, O'Brien L, Brindley DN. 1994. Cell-permeable ceramides inhibit the stimulation of DNA synthesis and phospholipase D activity by phosphatidate and lysophosphatidate in rat fibroblasts. *J Biol Chem* 269:8937-8943.
- Goodman Y, Mattson M. 1996. Ceramide protects hippocampal neurons against excitotoxic and oxidative results, and amyloid B-peptide toxicity. *J Neurochem* 66:869-872.
- Haimovitz-Friedman A, Kan CC, Ehleiter D, Persaud RS, McLoughlin M, Fuks Z, Kolesnick R. 1994. Ionizing radiation acts on cellular membranes to generate ceramide and initiate apoptosis. *J Exp Med* 180:525-535.
- Hannun YA. 1996. Functions of ceramide in coordinating cellular responses to stress. *Science* 274:1855-1859.
- Hannun YA. 1994. The sphingomyelin cycle and the second messenger function of ceramide. *J Biol Chem* 269:3125-3128.
- Hartfield PJ, Mayne GC, Murray AW. 1997. Ceramide induces apoptosis in PC12 cells. *FEBS Lett* 401:148-152.
- Herr I, Martin-Villalba A, Kurz E, Roncaioli P, Schenkel J, Cifone MG, Debatin KM. 1999. FK506 prevents stroke-induced generation of ceramide and apoptosis signaling. *Brain Res* 826:210-219.
- Hutchins JB, Barger SW. 1998. Why neurons die: cell death in the nervous system. *Anat Rec* 253:79-90.
- Irie F, Hirabayashi Y. 1998. Application of exogenous ceramide to cultured rat spinal motoneurons promotes survival or death by regulation of apoptosis depending on its concentrations. *J Neurosci Res* 54:475-485.
- Ito A, Horigome K. 1995. Ceramide prevents neuronal programmed cell death induced by nerve growth factor deprivation. *J Neurochem* 65:463-466.
- Jarvis W, Kolesnick R, Fornari F, Traylor R, Gerwitz D, Grant S. 1994. Induction of apoptotic DNA damage and cell death by activation of the sphingomyelin pathway. *Proc Natl Acad Sci USA* 91:73-77.
- Kolesnick RN, Kronke M. 1998. Regulation of ceramide production and apoptosis. *Annu Rev Physiol* 60:643-665.
- Krueger BK, Burne JF, Raff MC. 1995. Evidence for large-scale astrocyte death in the developing cerebellum. *J Neurosci* 15:3366-3374.
- Lambert N, Michel PP, Brugg B, Agid Y, Ruberg M. 1999. Mechanisms of apoptosis in PC12 cells irreversibly differentiated with nerve growth factor and cyclic AMP. *Brain Res* 821:60-68.
- Lievremont JP, Sciorati C, Morandi E, Paolucci C, Bunone G, Della Valle G, Meldolesi J, Clementi E. 1999. The p75(NTR)-induced apoptotic program develops through a ceramide-caspase pathway negatively regulated by nitric oxide. *J Biol Chem* 274:15466-15472.
- Liu J, Ginis I, Spatz M, Hallenbeck JM. 2000. Hypoxic preconditioning protects cultured neurons against hypoxic stress via TNF- α and ceramide. *Am J Cell Physiol* 278:C144-153.
- Liu J, Mathias S, Yang Z, Kolesnick RN. 1994. Renaturation and tumor necrosis factor- α stimulation of a 97-kDa ceramide-activated protein kinase. *J Biol Chem* 269:3047-3052.
- Marcora E, Mariotti A, Mancini M, Morandi E, Mazzoli F, Politi K, Valle GD. 1996. C₂-Ceramide induces apoptosis in human neuroblastoma cells. *Found Clin Immunol* 4:11-13.
- Marks N, Berg MJ, Guidotti A, Saito M. 1998. Activation of caspase-3 and apoptosis in cerebellar granule cells. *J Neurosci Res* 52:334-341.
- Monti B, Zanghellini P, Contestabile A. 2001. Characterization of ceramide-induced apoptotic death in cerebellar granule cells in culture. *Neurochem Int* 39:11-18.
- Movsesyan VA, Yakovlev AG, Fan L, Faden AI. 2001. Effect of serine protease inhibitors on posttraumatic brain injury and neuronal apoptosis. *Exp Neurol* 167:366-375.
- Mukhin AG, Ivanova SA, Allen JW, Faden AI. 1998. Mechanical injury to neuronal/glial cultures in microplates: role of NMDA receptors and pH in secondary neuronal cell death. *J Neurosci Res* 51:748-758.
- Nakajima M, Kashiwagi K, Ohta J, Furukawa S, Hayashi K, Kawashima T, Hayashi Y. 1994. Etomidate induces programmed death in neurons cultured from the fetal rat central nervous system. *Brain Res* 641:350-352.
- Obeid LM, Hannun YA. 1995. Ceramide: a stress signal and mediator of growth suppression and apoptosis. *J Cell Biochem* 58:191-198.
- Obeid LM, Lindaric CM, Karolak LA, Hannun YA. 1993. Programmed cell death induced by ceramide. *Science* 259:1769-1771.
- Olivera A, Spiegel S. 1992. Ganglioside GM1 and sphingolipid breakdown products in cellular proliferation and signal transduction pathways. *J Glycoconj* 9:109-117.
- Oppenheim RW. 1991. Cell death during development of the nervous system. *Annu Rev Neurosci* 14:453-501.
- Perry SW, Hamilton JA, Tjoelker LW, Dbaibo G, Dzenko KA, Epstein LG, Hannun Y, Whittaker JS, Dewhurst S, Gelbard HA. 1998. Platelet-activating factor receptor activation. An initiator step in HIV-1 neuropathogenesis. *J Biol Chem* 273:17660-17664.
- Pettmann B, Henderson CE. 1998. Neuronal cell death. *Neuron* 20:633-647.
- Raff MC, Barres BA, Burne JF, Coles HS, Ishizaki Y, Jacobson MD. 1993. Programmed cell death and the control of cell survival: lessons from the nervous system. *Science* 262:695-700.
- Raines MA, Kolesnick RN, Golde DW. 1993. Sphingomyelinase and ceramide activate mitogen-activated protein kinase in myeloid HL-60 cells. *J Biol Chem* 268:14572-14575.
- Riboni L, Bassi R, Prinetti A, Viani P, Tettamanti G. 1999. Predominance of the acylation route in the metabolic processing of exogenous sphingosine in neural and extraneural cells in culture. *Biochem J* 338:147-151.
- Saito M, Guidotti A, Berg MJ, Marks N. 1998. The semisynthetic glycosphingolipid LIGA20 potentially protects neurons against apoptosis. *Ann NY Acad Sci* 845:253-262.
- Salinas M, Lopez-Valdaliso R, Martin D, Alvarez A, Cuadrado A. 2000. Inhibition of PKB/Akt1 by C₂-ceramide involves activation of ceramide-activated protein phosphatase in PC12 cells. *Mol Cell Neurosci* 15:156-169.
- Sawai H, Okazaki T, Takeda Y, Tashima M, Sawada H, Okuma M, Kishi S, Umehara H, Domae N. 1997. Ceramide-induced translocation of protein kinase C- δ and - ϵ to the cytosol. Implications in apoptosis. *J Biol Chem* 272:2452-2458.
- Spiegel S, Merrill AH Jr. 1996. Sphingolipid metabolism and cell growth regulation. *FASEB J* 10:1388-1397.
- Verheij M, Bose R, Lin XH, Yao B, Jarvis WD, Grant S, Birrer MJ, Szabo E, Zon LI, Kyriakis JM, Haimovitz-Friedman A, Fuks Z, Kolesnick RN. 1996. Requirement for ceramide-initiated SAPK/JNK signaling in stress-induced apoptosis. *Nature* 380:75-79.
- Wiesner DA, Dawson G. 1996a. Programmed cell death in neurotumor cells involves the generation of ceramide. *Glycoconj J* 13:327-333.
- Wiesner DA, Dawson G. 1996b. Staurosporine induces programmed cell death in embryonic neurons and activation of the ceramide pathway. *J Neurochem* 66:1418-1425.
- Yao B, Zhang Y, Dellkat S, Mathias S, Basu S, Kolesnick R. 1995. Phosphorylation of raf by ceramide-activated protein kinase. *Nature* 378:307-310.
- Yao R, Cooper GM. 1995. Requirement for phosphatidylinositol-3 kinase in the prevention of apoptosis by nerve growth factor. *Science* 267:2003-2006.
- Yoshimura S, Banno Y, Nakashima S, Hayashi K, Yamakawa H, Sawada M, Sakai N, Nozawa Y. 1999. Inhibition of neutral sphingomyelinase activation and ceramide formation by glutathione in hypoxic PC12 cell death. *J Neurochem* 73:675-683.
- Zhou H, Summers SA, Birnbaum MJ, Pittman RN. 1998. Inhibition of Akt kinase by cell-permeable ceramide and its implications for ceramide-induced apoptosis. *J Biol Chem* 273:16568-16575.



ELSEVIER

Pharmacology, Biochemistry and Behavior 73 (2002) 287–298

**PHARMACOLOGY
BIOCHEMISTRY
AND
BEHAVIOR**

www.elsevier.com/locate/pharmbiochembeh

Neuronal and glial mGluR5 modulation prevents stretch-induced enhancement of NMDA receptor current

Paul M. Lea^a, Stephanie J. Custer^a, Stefano Vicini^{a,b}, Alan I. Faden^{a,c,d,*}^aDepartment of Neuroscience, Georgetown University Medical Center, Washington, DC 20007-2197, USA^bDepartment of Physiology, Georgetown University Medical Center, Washington, DC 20007-2197, USA^cInstitute for Cognitive and Computational Sciences, Georgetown University Medical Center, Washington, DC 20007-2197, USA^dDepartment of Pharmacology, Georgetown University Medical Center, Washington, DC 20007-2197, USA

Received 5 October 2001; received in revised form 18 January 2002; accepted 12 February 2002

Abstract

Neuronal stretching in culture has been used to model diffuse axonal injury caused by head trauma, and activation of *N*-methyl-D-aspartate receptors (NMDARs) has been implicated in the pathophysiology of such injury. Here we report the effects of modulating injury severity and the metabotropic glutamate receptor subtype 5 (mGluR5) on NMDAR activity after stretch injury. Following mild stretch, cortical neurons plated upon a confluent layer of astrocytes (NG) exhibited both increased maximal current (I_{NMDA}) and reduction in the voltage-dependent Mg^{2+} block. In contrast, neurons grown without an astrocyte monolayer (PN) only exhibited increased I_{NMDA} . In NG, surprisingly, pretreatment with either the mGluR5 agonist CHPG or the mGluR5 antagonist MPEP decreased the enhancement of I_{NMDA} . In contrast, in PN, MPEP similarly limited I_{NMDA} changes, but CHPG was without effect. In both culture conditions, MPEP, but not CHPG, limited the stretch-reduced Mg^{2+} block. Severe stretch had no effect on I_{NMDA} or the Mg^{2+} block in either culture condition, despite a correlation between injury severity and the release of lactose dehydrogenase measured postinjury. Neither CHPG nor MPEP had any direct effects upon the NMDA receptor. We conclude that mGluR5 regulates NMDAR activity during mild stretch injury, but not severe injury, by modulating both the Mg^{2+} block and I_{NMDA} . © 2002 Elsevier Science Inc. All rights reserved.

Keywords: Glutamate receptor; Excitotoxicity; Stretch injury; Head trauma; Cortical neurons; Neuronal–glial interaction

1. Introduction

Glutamate regulates CNS function through two major classes of receptors: the ionotropic (iGluR) and the metabotropic (mGluR) glutamate receptors. Most fast excitatory synaptic transmissions occur via the iGluRs, whereas slower second messenger-mediated affects occur following activation of the mGluRs (for reviews, see Anwyl, 1999; Bleakman and Lodge, 1998; Dingledine et al., 1999). The iGluRs, categorized by the pharmacological agonists to which they bind, include α -amino-3-hydroxy-5-methyl-4-isoxazolepropionic acid (AMPA), kainate (KA) and *N*-methyl-D-aspartate receptors (NMDARs). The iGluRs are ligand-gated ion channels, permeable to potassium (K^+), sodium (Na^+), and,

in the case of NMDA receptors and some AMPA receptors, calcium (Ca^{2+}) ions. In contrast, the mGluRs are G-protein-coupled receptors that either utilize inositol triphosphate, diacylglycerol, or cAMP to mediate their actions, which include regulation of ion channels or modulation of glutamate receptors, among others (for a review, see Anwyl, 1999). The mGluRs are categorized into three groups based upon sequence, pharmacology, and function (for reviews, see Anwyl, 1999; Conn and Pin, 1997; Schoepp et al., 1999). Group I mGluRs (mGluR1 and 5) activate phospholipase C via G_q proteins and initiate an inositol triphosphate/diacylglycerol (IP_3/DAG) second messenger cascade, whereas Group II mGluRs (mGluR2 and 3) and the Group III mGluRs (mGluR4, 6, 7, and 8) inhibit adenylylcyclase via $\text{G}_{i/o}$ proteins.

Multiple *in vivo* and *in vitro* studies support a role for iGluR and mGluR in cell death following traumatic neuronal injury (for a review, see Temple et al., 2001). Whereas inhibition of iGluRs provides protection against both cell

* Corresponding author. EP-04 Research Building, 3970 Reservoir Road Northwest, Washington, DC 20007-2197, USA. Tel.: +1-202-687-0492; fax: +1-202-687-0617.

E-mail address: fadena@georgetown.edu (A.I. Faden).

injury and neurological dysfunction (Faden et al., 1989; Gill, 1994; McIntosh et al., 1998), the role of the mGluRs is less clear. Inhibition of mGluR1 appears to be neuroprotective (Faden et al., 2001; Nicoletti et al., 1999). However, activation of Group I mGluRs may either protect or exacerbate injury depending upon the model and type of cell death (Allen et al., 2000).

Multiple lines of evidence suggest that Group I mGluRs can modulate NMDA receptor activity through several potential mechanisms: PKC-mediated enhancement of NMDA receptor activity, or changes in the polymerization state of the actin cytoskeleton via alterations in $[Ca^{2+}]_i$, or through a calcium/calmodulin pathway (Anwyl, 1999; Ehlers et al., 1996; Hisatsune et al., 1997; Holohean et al., 1999; Krupp et al., 1999; Rosenmund and Westbrook, 1993; Zhang et al., 1998). Moreover, Group I mGluR1 and mGluR5 subtypes may differentially utilize these mechanisms to affect changes in NMDA receptor current (Kawabata et al., 1996, 1998; Ugolini et al., 1997, 1999).

An in vitro neuronal stretch injury model has been used to study NMDA receptor modulation after trauma. Previous characterization of this model showed a significant correlation between amplitude of injury and the release of lactose dehydrogenase (LDH) or the uptake of propidium iodide, the latter being indicators of neuronal cell death (Ellis et al., 1995). Studies using this model found that a mild level of stretch causes an enhancement of NMDA receptor current and a reduced voltage-dependent Mg^{2+} block in neurons grown in the presence of glia (Zhang et al., 1996). In light of the above observations, we investigated whether there are correlations among the stretch-induced increases in NMDA receptor current, increasing amplitudes of stretch, and the release of LDH. Zhang et al. (1996) also showed that treatment with the PKC inhibitor, calphostin C, partially reversed the stretch-mediated reduction in the voltage-dependent Mg^{2+} block. Because Group I mGluR activation results in the upregulation of PKC through a phospholipase C pathway, we also examined the effect of modulating one Group I mGluR subtype (mGluR5) on stretch-induced enhancement of NMDA receptor current. Studies investigating effects of various compounds on either the voltage-dependent Mg^{2+} block of the NMDA receptor, or NMDA receptor current, have differed according to whether experiments were performed in either the presence or absence of extracellular magnesium. As there have been differing results with regard to the effects of mGluR modulation of NMDA receptor activity, we examined whether such differences may be due to the levels of $MgCl_2$ present. Moreover, because it has been suggested that certain modulatory affects of mGluR5 may result from actions in glial cells (Nicoletti et al., 1999), we also compared the affects of stretch on NMDA receptor current in cultures consisting of neurons grown in the absence or presence of a monolayer of glia.

2. Materials and methods

2.1. Drugs

The following drugs were obtained from Tocris Cookson (St. Louis, MO): *selective Group I mGluR agonist*—(*S*)-3,5-dihydroxyphenylglycine (DHPG); *selective mGluR5 agonist*—(*R,S*)-2-chloro-5-hydroxyphenylglycine (CHPG); *selective mGluR1 antagonist*—7-(hydroxyimino)cyclopropa[*b*]chromen-1a-carboxylate ethyl ester (CPCCoEt); *selective mGluR5 antagonists*—(*R,S*)-1-aminoindan-1,5-dicarboxylic acid (AIDA), 2-methyl-6-(phenylethynyl)pyridine (MPEP); *L-type calcium channel blocker*—1,4-dihydro-2,6-dimethyl-4-(3-nitrophenyl)-3,5-pyridinedicarboxylic acid 2-methoxyethyl 1-methylethyl ester (nimodipine); *NMDA receptor agonist*—NMDA. The reversible sodium channel blocker, tetrodotoxin (TTX), was obtained from Sigma (St. Louis, MO). All drugs were prepared and stored according to the manufacturer's guidelines.

Selection of doses used for the mGluR5 compounds was based upon published EC_{50} and IC_{50} values (Schoepp et al., 1999), in addition to previous experience by this laboratory (Movsesyan et al., 2001; O'Leary et al., 2000) as well as others (Ugolini et al., 1999).

2.2. Neuronal–glial cultures

Glia were prepared from 1- to 3-day-old Sprague–Dawley rat cortices (Taconic Farms, Germantown, NY) and neurons were prepared from 17- to 18-day-old Sprague–Dawley rat embryonic cortices. For both glial and neuronal cultures, cortical hemispheres were isolated and minced in Krebs–Ringer bicarbonate buffer containing 0.3% bovine serum albumin (BSA; Life Technologies, Gaithersburg, MD). The cells were dissociated in 1800 U/ml trypsin (Sigma) at 37 °C for 20 min. Following dissociation, trypsinisation was halted by the addition of 200 U/ml DNase I and 3600 U/ml soybean trypsin inhibitor (Sigma). Individual cells were obtained by trituration and subsequent centrifugation through a 4% BSA layer. Glia were seeded in six-well silastic membrane stretch plates (Flex I Untreated Culture Plates; Flexcell International Hillsborough, NC) treated with poly-D-lysine and allowed to grow to confluency in minimal essential medium (MEM) with Earle's salts sans glutamine supplemented with 10% fetal bovine serum, 10% horse serum, 2.5% 1 M HEPES (pH 7.2), 1% 200 mM glutamine stock, 1% 2 M glucose stock, and 1% antibiotic–antimycotic. Neuronal cell suspension volume was adjusted with Hank's balanced salt solution without calcium or magnesium (Mediatech–CellGro, Herndon, VA) to $2\text{--}2.5 \times 10^6$ cells/ml and then diluted to 1:10 immediately before plating with neuronal seeding media [NSM; MEM with Earle's salts sans glutamine supplemented with 5% fetal bovine serum, 5% horse serum, 2.5% 1 M HEPES (pH 7.2), 1% 200 mM glutamine stock, 1% 2 M glucose stock,

and 1% antibiotic–antimycotic]. Neurons were plated onto the confluent layer of glial cells (DIV 10). Cultures were fed twice per week by replacement of one-half of media with MEM with Earle's salts (Mediatech-CellGro, Herndon, VA) supplemented with 10% equine serum, 2.5% 1 M HEPES (pH 7.2), 1% 200 mM glutamine (Biofluids, Rockville, MD), 1% 2 M glucose (Biofluids, Rockville, MD), and 1% antibiotic–antimycotic solution (Biofluids Rockville, MD; feeding solution A). Cytosine- β -D-arabino-furanoside (10 μ M; Sigma) was added during the first feeding to stop further glial proliferation (feeding solution B). Subsequent feedings, alternating between feeding Media A and B, were done twice per week until cells were used (14–25 DIV). Cell cultures were maintained at 37 °C in humid atmosphere with 5% CO₂.

2.3. Neuronal cultures

Cortical neurons were derived similar to the methods outlined above. Following centrifugation through the 4% BSA layer, however, the cell pellet was resuspended in NSM consisting of Neurobasal Medium (Invitrogen-Gibco, Carlsbad, CA), supplemented with 1.1% 100 \times antibiotic–antimycotic solution (Biofluids, Rockville, MD), 25 μ M Na-glutamate, 0.5 mM L-glutamine, and 2% B27 Supplement (Invitrogen-Gibco, Carlsbad, CA). Cells (2.5×10^5 cells/ml) were seeded onto six-well silastic membrane stretch plates (Flex I Untreated Culture Plates; Flexcell International) pretreated with poly-D-lysine. On Day 4, the seeding media was replaced with feeding media (NSM without Na-glutamate and B27 supplement) in a 1:2 proportion. Subsequent feedings using the same feeding media were done twice per week until cells were used (14–25 DIV). Cell cultures were maintained at 37 °C in humid atmosphere with 5% CO₂.

2.4. Stretch model and electrophysiology

Cells cultured upon a deformable membrane can be stretched with compressed gas at known durations and pressures equating to varying levels of injury (Ellis et al., 1995). On the day of the experiment, growth media was replaced by a recording solution consisting of: 145 mM NaCl, 5 mM KCl, 1 mM CaCl₂, 1 mM MgCl, 5 mM HEPES, 5 mM glucose, and 2 mM glycine. Osmolarity was adjusted to 325 mOsm with sucrose, and pH adjusted to 7.4 with NaOH prior to media substitution. After switching the media, cells were returned to the incubator for at least 20 min prior to injury in the absence or presence of various Group I mGluR group- and subtype-specific compounds. Stretch (5.7 or 7.5 mm deformations of the membrane; 50 ms duration) was applied to the cells using a Cell Injury Controller (Biomedical Engineering Facility, Medical College of Virginia). Following the stretch, cells were returned to the incubator for an additional hour prior to recording. At the time of recording, a portion of the silastic membrane was trans-

ferred to a recording chamber undergoing continuous perfusion of recording solution on the stage of an inverted microscope (Zeiss Axiovert 135). Electrophysiological recordings were performed at room temperature (20–22 °C). Electrodes were pulled from a Wiretrol II capillary glass (Drummond Scientific, Broomall, PA) in three stages on a horizontal pipette puller (Mecanex, Nyon, Switzerland). Typical pipette resistance was 4–11 M Ω . The recording pipette contained (mM) 145 K-gluconate, 5 MgCl₂, 11 ethylene glycol bis (β -aminoethylether)-*N,N,N',N'*-tetraacetic acid (EGTA), 5 Na-adenosine-5'-triphosphate (ATP), 0.2 guanosine-5'-triphosphate (GTP), and 10 4-(2-hydroxyethyl)-1-piperazineethanesulfonic acid (HEPES) at pH 7.2 with KOH. Whole cell recordings were performed with a patch-clamp amplifier (Axopatch 1D; Axon Instruments, Foster City, CA) after capacitance and series resistance compensation. Cultured cortical neurons were voltage-clamped at a –60 mV holding potential. Access and input resistances were monitored intermittently during recordings by giving a 10-mV hyperpolarizing pulse. Application of drugs to the cells was via Y tubing controlled by a BPS-4 valve control system (Scientific Instruments, New York, NY). The recording solution (see above) used for wash and for drug application was supplemented with 10 μ M nimodipine and 0.6 μ M TTX. Electrophysiological recordings were both digitized and analyzed using pClamp 8 software (Axon Instruments).

2.5. Assays

Stretch injury-induced release of LDH was measured 24 h postinjury. Growth media was replaced with extracellular recording solution (ERS; see above) prior to mild and severe stretch injury. One six-well stretch plate was used for each treatment group (control, 5.7 mm stretch, 7.5 mm stretch). Twenty-four hours poststretch injury (see above), aliquots of ERS were removed from each well ($n=6$) and frozen (–20 °C) until assayed. LDH was measured using a CytoTox-96 nonradioactive cytotoxicity assay kit (Promega, Madison, WI) according to the manufacturer's protocol. Relative absorbance was measured at 490 nm using a Multiskan Ascent microplate reader (Labsystems Oy, Helsinki, Finland). Following the subtraction of background LDH levels measured in uninjured cells, 5.7- and 7.5-mm injury-induced LDH levels were compared.

2.6. Data analysis

Data were analyzed using Clampfit 8.0 (Axon Instruments), Excel (Microsoft Corp., Redmond, WA), and Statview 5.0.1 (SAS Institute, Cary, NC). Studies were performed in cortical neurons cultured in the presence (NG) or absence (PN) of a monolayer of glial cells. All currents were measured at the peak of the response. Average cell capacitance (pF) was estimated from the transient

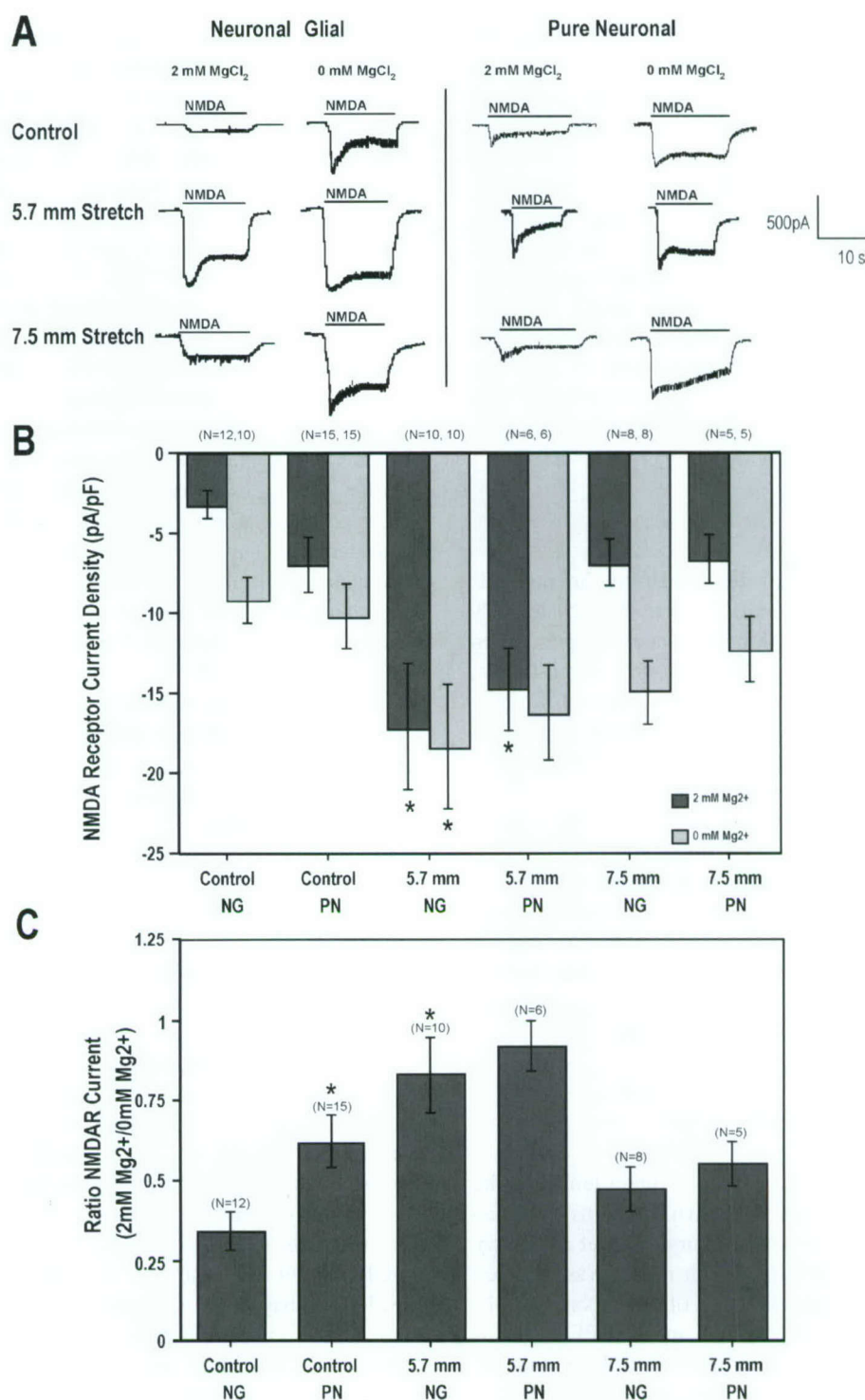


Fig. 1. Effects of stretch injury on NMDA receptor activity. (A) Representative traces of NMDA-evoked whole cell currents in the absence of stretch injury, and after 5.7 and 7.5 mm stretch of the silastic membrane. Whole cell currents were recorded from 14 to 25 DIV cultured cortical neurons voltage clamped at -60 mV. (B) The 5.7-mm, but not 7.5-mm, stretch significantly increased the current through the NMDA receptor in both the presence ($P < .05$; ANOVA) and absence ($P < .05$; ANOVA) of 2 mM extracellular MgCl₂ and in both rat cortical neurons cultured on top of a monolayer of glial cells (neuronal glial; NG) and in the absence of the glial monolayer (pure neuronal; PN). (C) In NG neurons, the 5.7-mm stretch significantly increased the ratio of I_{NMDA} measured in the presence to that measured in the absence of 2 mM extracellular MgCl₂ ($P < .05$; ANOVA). The ratio in PN neurons did not reach significance ($P > .05$; ANOVA). Ratios in control PN neurons were significantly different from control NG neurons ($P < .05$; ANOVA). Ratios in both NG and PN neurons were similar to those measured in control after the 7.5-mm stretch ($P > .05$; ANOVA). * Significant differences from NG controls.

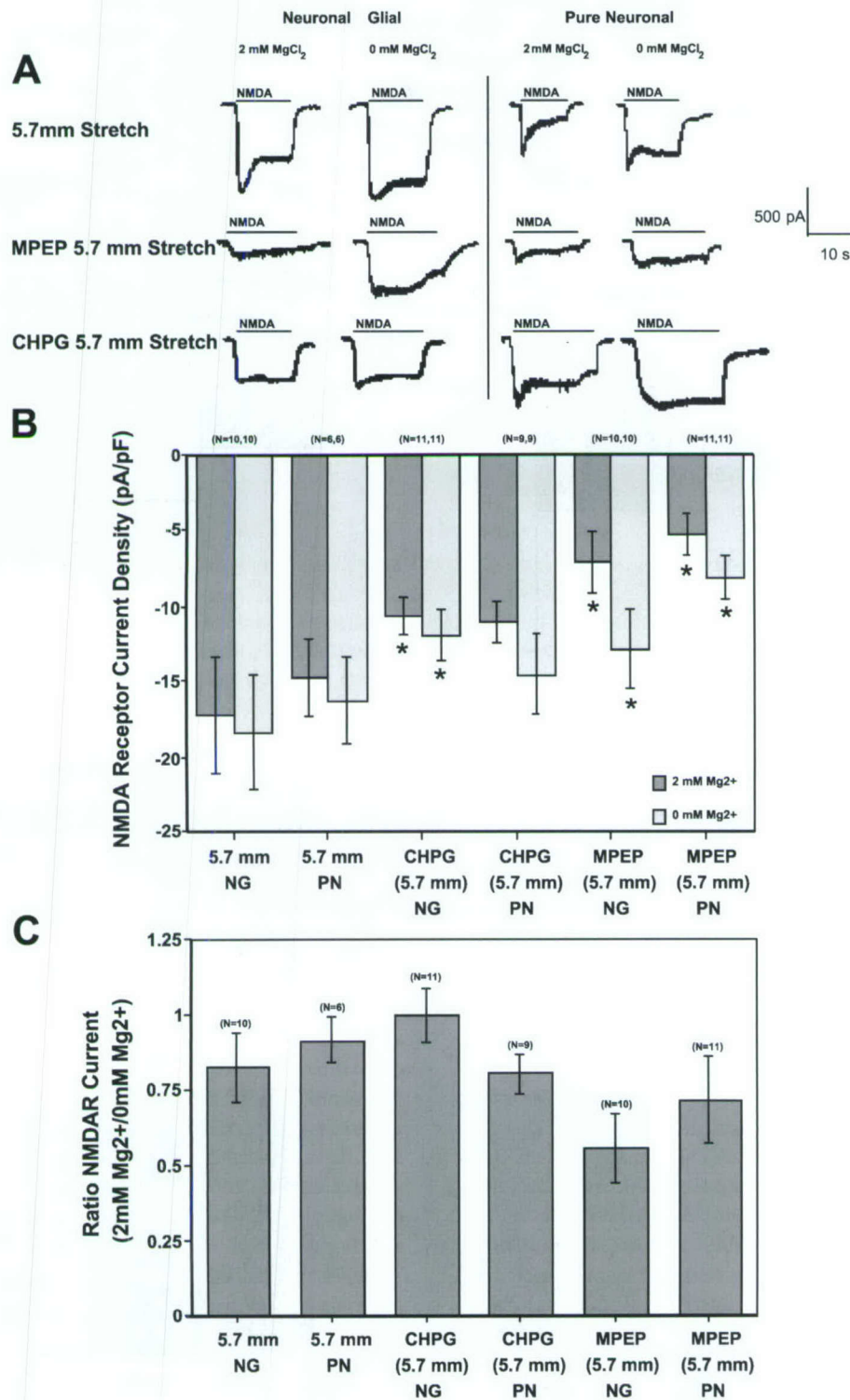


Fig. 2. Effects of mGluR5 modulation prior to the 5.7-mm stretch injury. (A) Representative traces of NMDA-evoked whole cell currents measured after the 5.7-mm stretch with and without pretreatment using either the mGluR5 antagonist, MPEP (2 μ M), or the agonist, CHPG (1 mM). Whole cell currents were recorded from 14 to 25 DIV cultured cortical neurons voltage clamped at -60 mV. (B) Pretreatment of NG, but not PN, cortical neurons with the mGluR5 agonist, CHPG (1 mM), caused a significant reduction in the enhanced NMDA inward current seen after the 5.7-mm stretch ($P < .05$; ANOVA). Pretreatment of both NG and PN cortical neurons with the mGluR5 antagonist, MPEP (2 μ M), caused a significant reduction in the enhanced NMDA inward current seen after the 5.7-mm stretch ($P < .05$; ANOVA). (C) Neither pretreatment with CHPG nor MPEP had any significant effect on the ratio of I_{NMDA} measured after the 5.7-mm stretch ($P > .05$; ANOVA), although significant differences were found between CHPG- and MPEP-treated NG neurons ($P < .05$; ANOVA). * Significant differences from the 5.7-mm stretched neurons.

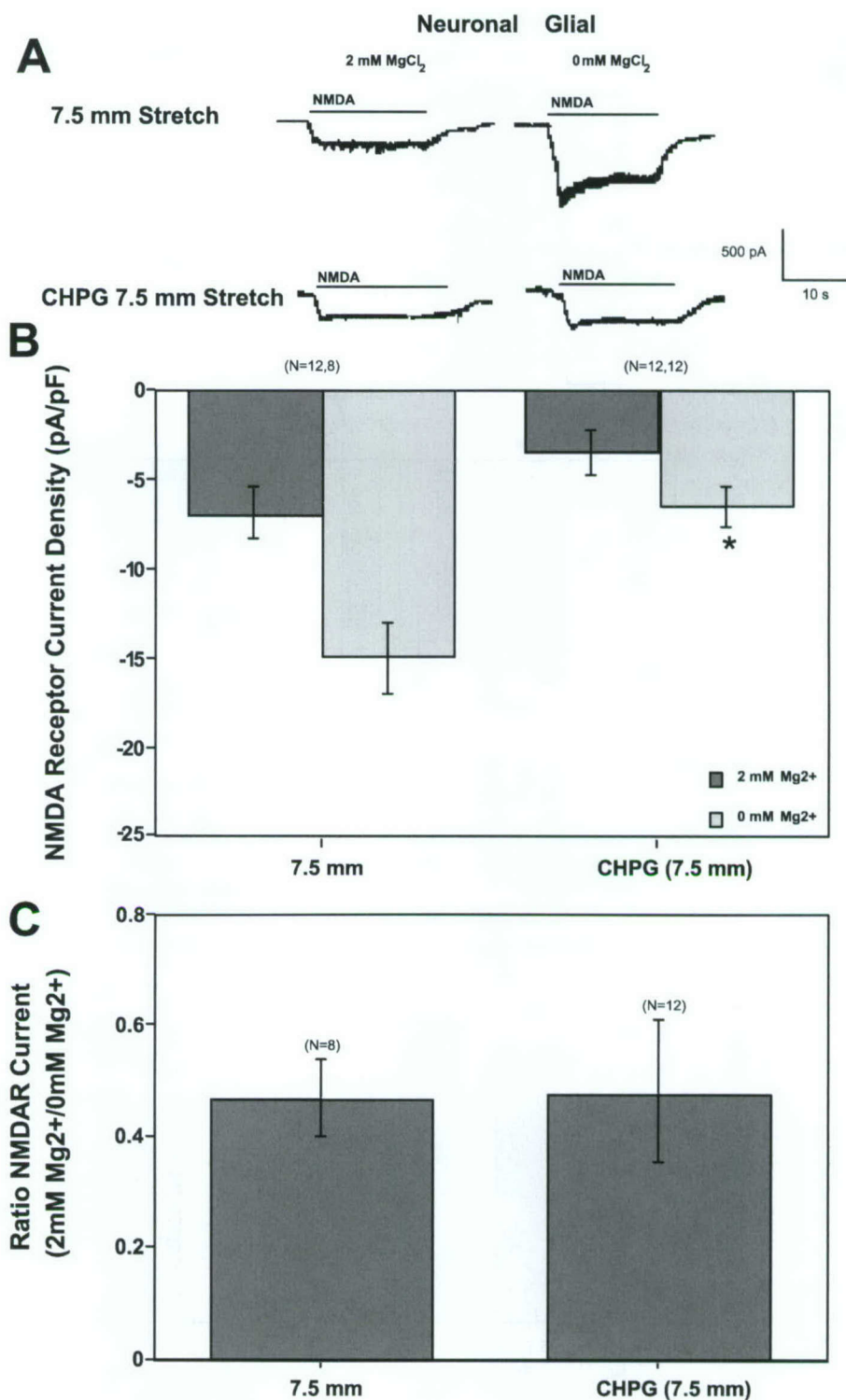


Fig. 3. Effects of the mGluR5 agonist, CHPG, on NMDA receptor current and current ratio in NG neurons following the 7.5-mm stretch. (A) Representative traces of NMDA-evoked whole cell currents measured after the 7.5-mm stretch of NG neurons with and without CHPG (1 mM) pretreatment. Whole cell currents were recorded from 14 to 25 DIV cultured cortical neurons voltage clamped at -60 mV. (B) Pretreatment of NG cortical neurons with the mGluR5 agonist, CHPG (1 mM), caused a significant reduction in NMDA receptor inward current measured in the absence of 2 mM extracellular MgCl₂ ($P < .05$; ANOVA), but not in the presence of 2 mM extracellular MgCl₂ ($P > .05$; ANOVA). (C) Pretreatment of NG cortical neurons with the mGluR5 agonist, CHPG (1 mM), prior to the 7.5-mm stretch did not significantly change the ratio of I_{NMDA} from levels measured after the 7.5-mm stretch ($P > .05$; ANOVA). * Significant difference from current density measured in the 7.5-mm stretched neurons in the absence of 2 mM extracellular Mg²⁺.

relaxation currents produced by the 10-mV hyperpolarizing voltage pulses given at the beginning of recording in each cell (Corsi et al., 1998). NMDA receptor currents (pA) were normalized to cell capacitance (pF) to provide a measure of current density (pA/pF). Current densities (pA/pF) and the 2 mM Mg^{2+} /0 mM Mg^{2+} ratios were analyzed using a one-way ANOVA followed by Fischer's PLSD. Significance was accepted at an $\alpha < .05$.

3. Results

3.1. Stretch injury, NMDA receptor activity, and cell death

NMDA receptor current density (I_{NMDA}), determined by the responses to application of 200 μ M NMDA in both the presence and absence of 2 mM extracellular $MgCl_2$, was similar (Fig. 1B; $P > .05$; ANOVA) in both NG cortical neurons (-3.25 pA/pF \pm 0.87 S.E.M., -9.17 ± 1.48 S.E.M., respectively; $n = 12$) and PN cortical neurons (-6.95 pA/pF \pm 1.85 S.E.M., -10.21 ± 1.98 S.E.M., respectively; $n = 15$). The 5.7-mm stretch significantly enhanced I_{NMDA} (Fig. 1B; $P < .05$; ANOVA) in the presence of 2 mM extracellular $MgCl_2$ in both NG cortical neurons

(-17.10 pA/pF \pm 3.97 S.E.M.) and PN cortical neurons (-15.08 pA/pF \pm 3.03 S.E.M.). In the absence of 2 mM extracellular $MgCl_2$, however, significant increases in I_{NMDA} following the 5.7-mm stretch were observed in NG cortical neurons (-18.34 ± 3.86 S.E.M.; $n = 10$; $P < .05$; ANOVA), but not PN cortical neurons (-16.27 pA/pF \pm 2.91 S.E.M.; $n = 6$; $P > .05$; ANOVA; Fig. 1B). A 7.5-mm stretch injury had no effect on I_{NMDA} (Fig. 1B; $P > .05$; ANOVA) in either NG cortical neurons (-6.88 pA/pF \pm 1.46 S.E.M., -14.93 ± 1.94 S.E.M., respectively; $n = 8$) or PN cortical neurons (-6.63 pA/pF \pm 1.46 S.E.M., -12.33 ± 2.04 S.E.M., respectively; $n = 5$), whether or not $MgCl_2$ (2 mM) was present. Responses due to activation of the NMDA receptor after stretch injury did not have consistently altered profiles; however, large response variability was found between cells in all paradigms.

The absence of a monolayer of glia caused a significant difference between the ratios of NMDA receptor inward currents measured in 2 mM extracellular $MgCl_2$ to inward currents measured in 0 mM extracellular $MgCl_2$ (2 mM Mg^{2+} /0 mM Mg^{2+} ratios) observed in control NG and PN cortical neurons (0.34 ± 0.06 S.E.M., $n = 12$; 0.62 ± 0.08 S.E.M., $n = 15$; respectively; $P < .05$; ANOVA; Fig. 1C). A mild 5.7-mm stretch

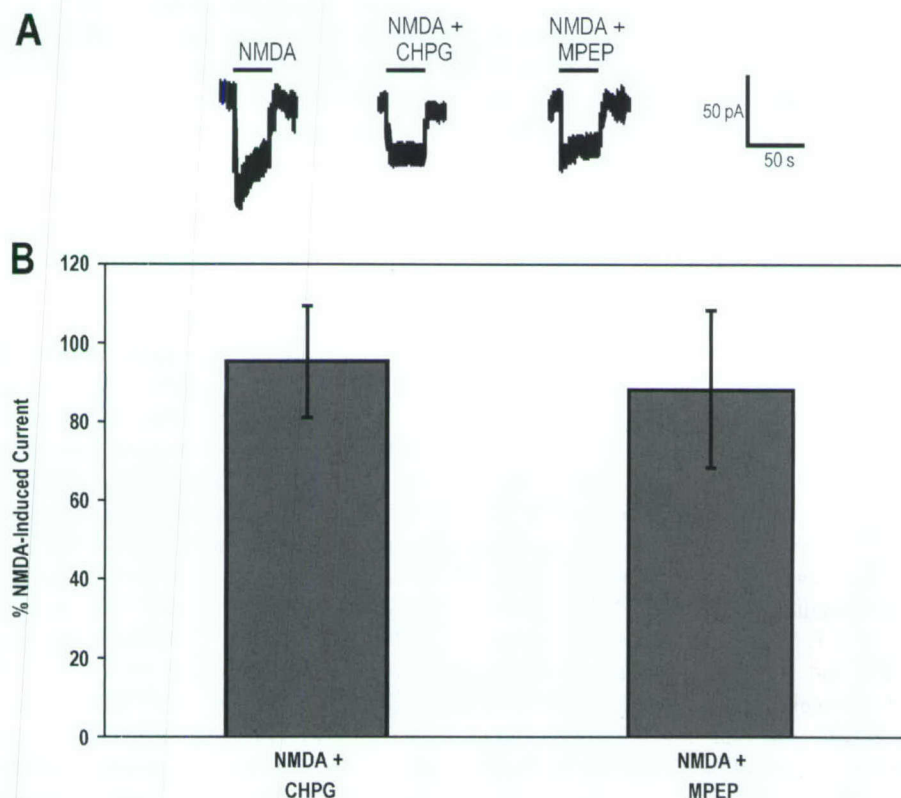


Fig. 4. Effects of CHPG and MPEP on NMDA-induced inward current in NG cortical neurons. (A) Representative traces of NMDA (200 μ M)-induced inward current with or without coapplication of the mGluR5 agonist, CHPG (1 mM), or the mGluR5 antagonist, MPEP (2 μ M). (B) Normalized to NMDA-induced currents, inward currents induced by NMDA (200 μ M) and either CHPG (1 mM; $n = 7$) or MPEP (2 μ M; $n = 6$) show no significant effects of these mGluR5-specific compounds on NMDA-evoked inward current ($P > .05$; ANOVA).

significantly increased the 2 mM Mg^{2+} /0 mM Mg^{2+} ratios from control values in NG cortical neurons (0.83 ± 0.12 S.E.M.; $n=10$; $P<.05$; ANOVA), but not in PN cortical neurons (0.92 ± 0.08 S.E.M.; $n=6$; $P>.05$; ANOVA; Fig. 1C). A more severe 7.5-mm stretch did not significantly alter the 2 mM Mg^{2+} /0 mM Mg^{2+} ratios from control values in either NG (0.47 ± 0.07 S.E.M.; $n=8$) or PN (0.55 ± 0.07 S.E.M.; $n=5$) cortical neurons (Fig. 1C; $P>.05$; ANOVA). In PN neurons, stretch injury caused an injury dose-dependent release of LDH. Injury-induced LDH measured 24 h postinjury was $360 \pm 124\%$ (S.E.M.) greater in 7.5-mm stretched neurons as compared to levels measured after the 5.7-mm stretch (taken as 100%).

3.2. Modulation by mGluR5 compounds

Pretreatment with the mGluR5 antagonist, MPEP, limited the 5.7-mm stretch-induced increases in I_{NMDA} measured in the presence or absence of 2 mM extracellular $MgCl_2$ in both NG (-7.06 ± 1.99 S.E.M., -12.76 ± 2.61 S.E.M., respectively; $n=10$) and PN (-5.51 ± 1.49 S.E.M., -8.00 ± 1.47 S.E.M., respectively; $n=11$) cortical neurons (Fig. 2B; $P<.05$; ANOVA). I_{NMDA} measurements were similar to control levels ($P>.05$; ANOVA). In contrast, pretreatment with the mGluR5 agonist, CHPG (1 mM), limited the 5.7-mm stretch-induced increases in I_{NMDA} measured in the presence or absence of 2 mM extracellular $MgCl_2$ in NG (-10.79 ± 1.41 S.E.M., -11.83 ± 1.75 S.E.M., respectively; $n=11$; $P<.05$; ANOVA), but not PN (-10.96 ± 1.49 S.E.M., -14.46 ± 2.69 S.E.M., respectively; $n=9$; $P>.05$; ANOVA) cortical neurons (Fig. 2B). CHPG reduced the 5.7-mm stretch-induced increases in I_{NMDA} measured in the absence, but not presence, of 2 mM extracellular $MgCl_2$ back to control levels ($P>.05$; ANOVA). Neither MPEP, nor CHPG, had any significant effect on the 5.7-mm stretch-induced increases in the 2 mM Mg^{2+} /0 mM Mg^{2+} ratios measured in both NG (0.56 ± 0.12 S.E.M., $n=10$; 1.00 ± 0.09 S.E.M., $n=11$; respectively) and PN (0.72 ± 0.15 S.E.M., $n=11$; 0.81 ± 0.07 S.E.M., $n=9$; respectively) cortical neurons (Fig. 2C; $P>.05$; ANOVA), although, in both culture conditions, MPEP appears to reduce the ratio back towards control levels ($P>.05$; ANOVA). Pretreatment with CHPG prior to the 7.5-mm stretch had no significant effect on I_{NMDA} measured in the presence of 2 mM extracellular $MgCl_2$ in NG cortical neurons (-3.43 ± 1.18 S.E.M., $P>.05$; ANOVA; Fig. 3B). In contrast, CHPG did reduce I_{NMDA} measured in the absence of 2 mM extracellular $MgCl_2$ in NG cortical neurons (6.47 ± 1.04 S.E.M.; $n=12$; $P<.05$; ANOVA). However, the data were not significantly different from controls ($P>.05$; ANOVA). Pretreatment with CHPG prior to the 7.5-mm stretch had no significant effect on the 2 mM Mg^{2+} /0 mM Mg^{2+} ratio in NG cortical neurons (0.48 ± 0.13 S.E.M.; $n=12$; $P>.05$; ANOVA; Fig. 3C).

3.3. Direct effects of Group I mGluR compounds on NMDA receptor activity

Fig. 4 shows that when coapplied under saturating conditions (i.e., 200 μ M NMDA and 2 μ M glycine) in the presence of 2 mM extracellular $MgCl_2$, neither 2 μ M MPEP ($n=6$) nor 1 mM CHPG ($n=7$) had any significant effects on NMDA-evoked I_{NMDA} in our NG cortical neurons ($P>.05$; ANOVA). The amplitude of the responses to NMDA alone (Fig. 4) was comparable with the NG control traces in Fig. 1A measured in the presence of 2 mM extracellular $MgCl_2$.

4. Discussion

Multiple lines of evidence show that NMDA receptors are intimately involved in the process of cell death following traumatic injury (for a review, see Temple et al., 2001). In addition to activation of the NMDA receptor by trauma-induced release of glutamate, injury-induced enhancement of NMDA receptor activity can occur by modulatory changes such as a reduced voltage-dependent Mg^{2+} block of the NMDA receptor, a change in the expression of NMDA receptors, an increased peak open probability, or a change in receptor subtype expression with different open probabilities (Chen et al., 1999). The latter three possibilities reflect a change in NMDA current density. Under normal resting conditions, the maintenance of the NMDA receptor voltage-dependent Mg^{2+} block prevents the inward movement of extracellular calcium through the NMDA receptor pore. When this Mg^{2+} block is relieved, either through a positive change in membrane potential or through a modification of the receptor by endogenous effectors, the inward movement of calcium can have profound effects, such as enhanced release of neurotransmitter or the induction of cell death.

An in vitro stretch trauma model developed by Ellis et al. (1995), thought to parallel the stretch forces generated during diffuse axonal injury (Tomei et al., 1990), is well suited for studying trauma-induced changes in NMDA receptor activity. Previous use of this model using various cell types has demonstrated significant alterations in membrane, receptor, and mitochondrial properties, which can lead to the activation of both necrotic and apoptotic pathways (Ahmed et al., 2000; Ellis et al., 1995; Goforth et al., 1999; Hoffman et al., 2000a,b; Lamb et al., 1997; Pike et al., 2000; Rzigalinski et al., 1997, 1998; Tavalin et al., 1997; Weber et al., 1999, 2001; Zhang et al., 1996). One such study showed that mild injury to rat cortical neurons, grown in coculture with glia, caused an enhancement of NMDA-evoked inward current via a reduction of the NMDA receptor voltage-dependent Mg^{2+} block (Zhang et al., 1996). This conclusion was supported by whole cell patch recordings of NMDA receptor currents measured while sequentially changing the cell membrane potential: cur-

rent–voltage (I – V) relationships showed that at +40 mV, there was no difference in NMDA inward current between control and stretched neurons. Taken together, their results indicate that mild stretch injury has no effect on maximal NMDA receptor current and, therefore, stretch-induced changes in NMDA receptor current are due to the reduction of the voltage-dependent Mg^{2+} block and not alterations in NMDA current density.

The above findings, combined with studies showing that activation of NMDA receptors is intimately involved with cell death (Mukhin et al., 1997a,b), lead us to the hypothesis that increases in levels of stretch injury would cause a corresponding increase in NMDA receptor activity. To test this hypothesis, we compared the effects of a mild (5.7 mm) and severe (7.5 mm) stretch injury on NMDA receptor current density, as well as on the ratio of NMDA receptor inward currents measured in 2 versus 0 mM extracellular $MgCl_2$. In the original work characterizing the stretch model, the terms ‘mild,’ ‘moderate,’ and ‘severe’ were used to define 5.5, 6.5, and 7.5 mm levels of stretch, respectively (Ellis et al., 1995). The 2 mM Mg^{2+} /0 mM Mg^{2+} ratio can provide an indication of the extent of the NMDA receptor voltage-dependent Mg^{2+} block so long as the alterations measured at a –60 mV holding potential are physiological and not due to possible errors in voltage clamping at one potential. Zhang et al. (1996) used standard current–voltage relationships to demonstrate that at a –60 mV holding potential stretch-induced enhancement of NMDA receptor is physiological. In support of their findings, we found that a mild level of stretch injury to rat cortical neurons, grown in the presence or absence of a monolayer of glia, and in the presence of extracellular $MgCl_2$ induced significant increases NMDA receptor activity and reduced the voltage-dependent Mg^{2+} block. In contrast, however, we observed significant increases in NMDA receptor current measured in the absence of extracellular $MgCl_2$, suggesting that in addition to the reduced voltage-dependent Mg^{2+} block, mild stretch injury also increases maximal NMDA receptor current through alterations in NMDA current density. These findings are supported by previous studies showing injury-induced changes in NMDA receptor subunit composition (Kreutz et al., 1998; Sun and Faden, 1995). Potential explanations for the differences between our findings and those of Zhang et al. (1996) include differences in culture conditions (Condorelli et al., 1993; Daniels and Brown, 2001) and the age of the cells (Zhong et al., 1994). Both of these conditions can influence the expression pattern of the NMDA receptor subtypes. Additionally, the age of the cells can influence the coupling of mGluR and iGluR to different phosphorylation systems (Angenstein et al., 1999).

In contrast to the 5.7-mm stretch injury, increasing the level of stretch to a more severe level (7.5 mm) had no effect on either the inward current or voltage-dependent Mg^{2+} block of the NMDA receptor, despite more elevated

levels of LDH measured 24 h postsevere injury. These results suggest that the increased levels of LDH at higher levels of stretch do not reflect NMDA receptor-dependent cell death. It is possible that more severe stretch injury may cause calcium-dependent desensitization of the NMDA receptor (for a review, see McBain and Mayer, 1994), or inhibition of NMDA receptor activity by injury-induced release of redox-related congeners of nitric oxide or anandamide (Hampson et al., 1998; Kim et al., 1999; Lipton and Stamler, 1994). A possibility remains that at higher levels of stretch, cell death may be primarily due to other factors, such as activation of calpain and/or caspase-3 (Pike et al., 2000). Because the goal of this study was to look at stretch-enhanced NMDA receptor activity, we focused on the 5.7-mm model of injury for the pharmacological studies.

Group I mGluR activation has been shown to modulate NMDA receptor activity in multiple *in vitro* systems (Allen et al., 2000; Awad et al., 2000; Bortolotto and Collingridge, 1995; Colwell et al., 1996; Contractor et al., 1998; Holohan et al., 1999; Kinney and Slater, 1993; Skeberdis et al., 2001; Ugolini et al., 1997, 1999; Yu et al., 1997), suggesting a likely role for Group I mGluR-mediated enhancement of NMDA receptors in excitotoxicity following neuronal injury. Indeed, in mouse cortical neurons, Bruno et al. (1995, 1999) showed that Group I mGluR agonists amplify NMDA-induced neuronal degeneration through PKC activation and that LY367385, a potent and selective antagonist of mGluR1a, was neuroprotective in cultures exposed to an NMDA pulse. In rat cortical/glia cocultures, Mukhin et al. (1996, 1997b) showed that Group I mGluR activation exacerbates *in vitro* punch injury-induced delayed neuronal cell death and that MK801 partly reduced injury exacerbation caused by the Group I mGluR agonist, DHPG.

To test the prediction that mGluR5 modulates both mild (5.7 mm) stretch-induced increases in NMDA receptor activity and reductions in the voltage-dependent Mg^{2+} block of the NMDA receptor, we pretreated our cells with either the mGluR5 agonist, CHPG (1 mM), or antagonist, MPEP (2 μ M), prior to injury. MPEP limited mild stretch-induced changes in NMDA current density and the voltage-dependent Mg^{2+} block in cortical neurons grown in the presence or absence of a glial monolayer. These findings are consistent with studies showing mGluR5-mediated enhancement of NMDA receptor activity (Awad et al., 2000; Ugolini et al., 1999), and a reciprocal positive feedback interaction between these two glutamate receptor subtypes (Alagarsamy et al., 1999). Previous data from this laboratory (O’Leary et al., 2000), as well as others (Contractor et al., 1998), suggest that the reduced NMDA receptor inward current may be due to direct interactions of MPEP on the NMDA receptor. However, we do not believe this to be the case here, as all of our experiments utilized saturating concentrations of NMDA and glycine. In addition, neither MPEP (2 μ M) nor CHPG (1 mM) had any effects on NMDA-evoked inward currents in cells not subjected to stretch.

Surprisingly, the mGluR5 agonist, CHPG, also prevented mild stretch-induced increases in NMDA current density in cortical neurons cultured in the presence of a monolayer of glia. These findings are in contrast to the studies noted above, in which mGluR5 activation enhanced NMDA receptor currents in subthalamic nucleus (Awad et al., 2000) and spinal cord (Ugolini et al., 1999) neurons. It may be that these differences are dependent upon the source of neurons for culture (Bruno et al., 1996, 1998), or due to pretreating with the mGluR5 agonist prior to injury. Studies show that activation of mGluR5 can lead to rapid desensitization of the receptor (Gereau and Heinemann, 1998), or a switch from 'neurotoxic' to 'neuroprotective' activity (Bruno et al., 2001). However, we believe that the ability of CHPG to exert its effects is predominately due to glial mGluR5 receptors, as pretreatment with CHPG had no effect on mild stretch-induced increases in NMDA current density in our cultured neurons grown in the absence of a glial monolayer. Although it is possible that the presence of the monolayer of glia alone significantly alters the NMDA receptor expression in such a way as to make the two culture conditions noncomparable (Daniels and Brown, 2001), a statistical comparison between mean NMDA receptor currents of the two populations argues against such a possibility. Combined, our data suggest a significant role for neuronal mGluR5 receptors in regulating mild stretch-induced enhancement of NMDA current density, and a significant role for glial mGluR5 receptors in regulating neuronal NMDA current density.

Previous reports from this laboratory, as well as others, show that Group I mGluR compounds can directly affect the NMDA receptor (Contractor et al., 1998; Movsesyan et al., 2001; O'Leary et al., 2000). It is postulated that this may be due to the use of low concentrations of NMDA and glycine (Contractor et al., 1998), or to the concentration of extracellular Mg^{2+} . Indeed, a previous study showed that the modulatory effect of the Group I/II mGluR agonist, *trans*-ACPD, on NMDA receptor activity in frog spinal cord is dependent upon extracellular Mg^{2+} concentration (Holohean et al., 1999). We show that the presence or absence of extracellular magnesium influences whether the observed mGluR-induced enhancement of NMDA receptor activity occurs through alterations in the voltage-dependent Mg^{2+} block of the NMDA receptor, or through changes in NMDA current density.

As discussed, neither MPEP nor CHPG significantly altered NMDA-evoked inward currents measured in the presence of $MgCl_2$ in cells not subjected to stretch injury. These results suggest that the effects of the mGluR compounds were not due to direct interactions with the NMDA receptor. Combined, our results indicate that inhibition of neuronal mGluR5 prior to stretch injury reduces injury-induced increases in maximal NMDA-evoked inward currents by significantly altering NMDA current density and by limiting the stretch-induced reductions of the voltage-dependent Mg^{2+} block of the NMDA receptor. Further-

more, our data suggest that activation of glial mGluR5 prior to stretch injury reduces stretch-induced increases in maximal NMDA-evoked inward currents by significantly altering neuronal NMDA current density through an as yet unidentified neuronal/glial interaction. Although glial mGluR5 activation did not significantly alter the stretch-reduced voltage-dependent Mg^{2+} block of the NMDA receptor, there appeared to be a trend for CHPG to exacerbate stretch-induced reductions in the 2 mM Mg^{2+} /0 mM ratios. The ability of glial mGluR5 to regulate the voltage-dependent Mg^{2+} block of neural NMDA receptors is also supported by our data, as we found a significant difference between the 2 mM Mg^{2+} /0 mM ratios measured after CHPG and MPEP in the cocultures. These data suggest that studies looking at the protective/excitotoxic effects of mGluR5, particularly in relation to NMDA receptor-induced cell death, need to differentiate between the effects due to activation of glial and/or neuronal mGluR5.

References

- Ahmed SM, Rzigalinski BA, Willoughby KA, Sitterding HA, Ellis EF. Stretch-induced injury alters mitochondrial membrane potential and cellular ATP in cultured astrocytes and neurons. *J Neurochem* 2000; 74:1951–60.
- Alagarsamy S, Marino MJ, Rouse ST, Gereau RWT, Heinemann SF, Conn PJ. Activation of NMDA receptors reverses desensitization of mGluR5 in native and recombinant systems. *Nat Neurosci* 1999;2:234–40.
- Allen JW, Knoblach SM, Faden AI. Activation of group I metabotropic glutamate receptors reduces neuronal apoptosis but increases necrotic cell death in vitro. *Cell Death Differ* 2000;7:470–6.
- Angenstein F, Buchner K, Staak S. Age-dependent differences in glutamate-induced phosphorylation systems in rat hippocampal slices. *Hippocampus* 1999;9:173–85.
- Anwyl R. Metabotropic glutamate receptors: electrophysiological properties and role in plasticity. *Brain Res Brain Res Rev* 1999;29:83–120.
- Awad H, Hubert GW, Smith Y, Levey AI, Conn PJ. Activation of metabotropic glutamate receptor 5 has direct excitatory effects and potentiates NMDA receptor currents in neurons of the subthalamic nucleus (In process citation) *J Neurosci* 2000;20:7871–9.
- Bleakman D, Lodge D. Neuropharmacology of AMPA and kainate receptors. *Neuropharmacology* 1998;37:1187–204.
- Bortolotto ZA, Collingridge GL. On the mechanism of long-term potentiation induced by (1S,3R)-1-aminocyclopentane-1,3-dicarboxylic acid (ACPD) in rat hippocampal slices. *Neuropharmacology* 1995;34: 1003–14.
- Bruno V, Copani A, Knopfel T, Kuhn R, Casabona G, Dell'Albani P, Condorelli DF, Nicoletti F. Activation of metabotropic glutamate receptors coupled to inositol phospholipid hydrolysis amplifies NMDA-induced neuronal degeneration in cultured cortical cells. *Neuropharmacology* 1995;34:1089–98.
- Bruno V, Copani A, Battaglia G, Dell'Albani P, Condorelli DF, Nicoletti F. Metabotropic glutamate receptors and neuronal degeneration in culture. *Adv Neurol* 1996;71:47–51.
- Bruno V, Battaglia G, Copani A, Casabona G, Storto M, Di Giorgi Ger-evini V, Ngomba R, Nicoletti F. Metabotropic glutamate receptors and neurodegeneration. *Prog Brain Res* 1998;116:209–21.
- Bruno V, Battaglia G, Kingston A, O'Neill MJ, Catania MV, Di Grezia R, Nicoletti F. Neuroprotective activity of the potent and selective mGluR1a metabotropic glutamate receptor antagonist, (+)-2-methyl-4 carboxy-phenylglycine (LY367385): comparison with LY357366, a broader

- spectrum antagonist with equal affinity for mGlu1a and mGlu5 receptors. *Neuropharmacology* 1999;38:199–207.
- Bruno V, Battaglia G, Copani A, Cespedes VM, Galindo MF, Cena V, Sanchez-Prieto J, Gasparini F, Kuhn R, Flor PJ, Nicoletti F. An activity-dependent switch from facilitation to inhibition in the control of excitotoxicity by group I metabotropic glutamate receptors. *Eur J Neurosci* 2001;13:1469–78.
- Chen N, Luo T, Raymond LA. Subtype-dependence of NMDA receptor channel open probability. *J Neurosci* 1999;19:6844–54.
- Colwell CS, Altemus KL, Cepeda C, Levine MS. Regulation of *N*-methyl-D-aspartate-induced toxicity in the neostriatum: a role for metabotropic glutamate receptors? *Proc Natl Acad Sci USA* 1996;93:1200–4.
- Condorelli D, Dell'Albani P, Aronica E, Genazzani A, Casabona G, Corsaro M, Balazs R, Nicoletti F. Growth conditions differentially regulate the expression of alpha-amino-3-hydroxy-5-methylisoxazole-4-propionate (AMPA) receptor subunits in cultured neurons. *J Neurochem* 1993;61:2133–9.
- Conn PJ, Pin JP. Pharmacology and functions of metabotropic glutamate receptors. *Annu Rev Pharmacol Toxicol* 1997;37:205–37.
- Contractor A, Gereau RWT, Green T, Heinemann SF. Direct effects of metabotropic glutamate receptor compounds on native and recombinant *N*-methyl-D-aspartate receptors. *Proc Natl Acad Sci USA* 1998;95:8969–74.
- Corsi L, Li JH, Krueger KE, Wang YH, Wolfe BB, Vicini S. Up-regulation of NR2B subunit of NMDA receptors in cerebellar granule neurons by Ca^{2+} /calmodulin kinase inhibitor KN93. *J Neurochem* 1998;70:1898–906.
- Daniels M, Brown D. Astrocytes regulate *N*-methyl-D-aspartate receptor subunit composition increasing neuronal sensitivity to excitotoxicity. *J Biol Chem* 2001;276:22446–52.
- Dingledine R, Borges K, Bowie D, Traynelis SF. The glutamate receptor ion channels. *Pharmacol Rev* 1999;51:7–61.
- Ehlers MD, Zhang S, Bernhardt JP, Haganir RL. Inactivation of NMDA receptors by direct interaction of calmodulin with the NR1 subunit. *Cell* 1996;84:745–55.
- Ellis EF, McKinney JS, Willoughby KA, Liang S, Povlishock JT. A new model for rapid stretch-induced injury of cells in culture: characterization of the model using astrocytes. *J Neurotrauma* 1995;12:325–39.
- Faden AI, Demediuk P, Panter SS, Vink R. The role of excitatory amino acids and NMDA receptors in traumatic brain injury. *Science* 1989;244:798–800.
- Faden AI, O'Leary DM, Fan L, Bao W, Mullins PG, Movsesyan VA. Selective blockade of the mGluR1 receptor reduces traumatic neuronal injury in vitro and improves outcome after brain trauma. *Exp Neurol* 2001;167:435–44.
- Gereau RWT, Heinemann SF. Role of protein kinase C phosphorylation in rapid desensitization of metabotropic glutamate receptor 5. *Neuron* 1998;20:143–51.
- Gill R. The pharmacology of alpha-amino-3-hydroxy-5-methyl-4-isoxazole propionate (AMPA)/kainate antagonists and their role in cerebral ischaemia. *Cerebrovasc Brain Metab Rev* 1994;6:225–56.
- Goforth P, Ellis E, Satin L. Enhancement of AMPA-mediated current after traumatic injury in cortical neurons. *J Neurosci* 1999;19:7367–74.
- Hampson A, Bornheim L, Scanziani M, Yost C, Gray A, Hansen B, et al. Dual effects of anandamide on NMDA receptor-mediated responses and neurotransmission. *J Neurochem* 1998;70:671–6.
- Hisatsune C, Umemori H, Inoue T, Michikawa T, Kohda K, Mikoshiba K, Yamamoto T. Phosphorylation-dependent regulation of *N*-methyl-D-aspartate receptors by calmodulin. *J Biol Chem* 1997;272:20805–10.
- Hoffman S, Rzigalinski B, Willoughby K, Ellis E. Astrocytes generate isoprostanes in response to trauma or oxygen radicals. *J Neurotrauma* 2000a;17:415–20.
- Hoffman SW, Rzigalinski BA, Willoughby KA, Ellis EF. Astrocytes generate isoprostanes in response to trauma or oxygen radicals. *J Neurotrauma* 2000b;17:415–20.
- Holohean AM, Hackman JC, Davidoff RA. Mechanisms involved in the metabotropic glutamate receptor-enhancement of NMDA-mediated motoneuron responses in frog spinal cord. *Br J Pharmacol* 1999;126:333–41.
- Kawabata S, Tsutsumi R, Kohara A, Yamaguchi T, Nakanishi S, Okada M. Control of calcium oscillations by phosphorylation of metabotropic glutamate receptors. *Nature* 1996;383:89–92.
- Kawabata S, Kohara A, Tsutsumi R, Itahana H, Hayashibe S, Yamaguchi T, Okada M. Diversity of calcium signaling by metabotropic glutamate receptors. *J Biol Chem* 1998;273:17381–5.
- Kim W, Choi Y, Rayudu P, Das P, Asaad W, Arnelle D, Stamler J, Lipton S. Attenuation of NMDA receptor activity and neurotoxicity by nitroxyl anion, NO^- . *Neuron* 1999;24:461–9.
- Kinney GA, Slater NT. Potentiation of NMDA receptor-mediated transmission in turtle cerebellar granule cells by activation of metabotropic glutamate receptors. *J Neurophysiol* 1993;69:585–94.
- Kreutz MR, Bockers TM, Bockmann J, Seidenbecher CI, Kracht B, Vorwerk CK, Weise J, Sabel BA. Axonal injury alters alternative splicing of the retinal NR1 receptor: the preferential expression of the NR1b isoforms is crucial for retinal ganglion cell survival. *J Neurosci* 1998;18:8278–91.
- Krupp JJ, Vissel B, Thomas CG, Heinemann SF, Westbrook GL. Interactions of calmodulin and alpha-actinin with the NR1 subunit modulate Ca^{2+} -dependent inactivation of NMDA receptors. *J Neurosci* 1999;19:1165–78.
- Lamb RG, Harper CC, McKinney JS, Rzigalinski BA, Ellis EF. Alterations in phosphatidylcholine metabolism of stretch-injured cultured rat astrocytes. *J Neurochem* 1997;68:1904–10.
- Lipton S, Stamler J. Actions of redox-related congeners of nitric oxide at the NMDA receptor. *Neuropharmacology* 1994;33:1229–33.
- McBain CJ, Mayer ML. *N*-methyl-D-aspartic acid receptor structure and function. *Physiol Rev* 1994;74:723–60.
- McIntosh TK, Juhler M, Wieloch T. Novel pharmacologic strategies in the treatment of experimental traumatic brain injury. *J Neurotrauma* 1998;15:731–69.
- Movsesyan VA, O'Leary DM, Fan L, Bao W, Mullins PG, Knoblach SM, Faden AI. mGluR5 antagonists 2-methyl-6-(phenylethynyl)-pyridine and (*E*)-2-methyl-6-(2-phenylethenyl)-pyridine reduce traumatic neuronal injury in vitro and in vivo by antagonizing *N*-methyl-D-aspartate receptors. *J Pharmacol Exp Ther* 2001;296:41–7.
- Mukhin A, Fan L, Faden AI. Activation of metabotropic glutamate receptor subtype mGluR1 contributes to post-traumatic neuronal injury. *J Neurosci* 1996;16:6012–20.
- Mukhin AG, Ivanova SA, Faden AI. mGluR modulation of post-traumatic neuronal death: role of NMDA receptors. *NeuroReport* 1997a;8:2561–6.
- Mukhin AG, Ivanova SA, Knoblach SM, Faden AI. New in vitro model of traumatic neuronal injury: evaluation of secondary injury and glutamate receptor-mediated neurotoxicity. *J Neurotrauma* 1997b;14:651–63.
- Nicoletti F, Bruno V, Catania MV, Battaglia G, Copani A, Barbagallo G, Cena V, Sanchez-Prieto J, Spano PF, Pizzi M. Group-I metabotropic glutamate receptors: hypotheses to explain their dual role in neurotoxicity and neuroprotection. *Neuropharmacology* 1999;38:1477–84.
- O'Leary DM, Movsesyan V, Vicini S, Faden AI. Selective mGluR5 antagonists MPEP and SIB-1893 decrease NMDA or glutamate-mediated neuronal toxicity through actions that reflect NMDA receptor antagonism. *Br J Pharmacol* 2000;131:1429–37.
- Pike B, Zhao X, Newcomb J, Glenn C, Anderson D, Hayes R. Stretch injury causes calpain and caspase-3 activation and necrotic and apoptotic cell death in septo-hippocampal cell cultures. *J Neurotrauma* 2000;17:283–98.
- Rosenmund C, Westbrook GL. Calcium-induced actin depolymerization reduces NMDA channel activity. *Neuron* 1993;10:805–14.
- Rzigalinski BA, Liang S, McKinney JS, Willoughby KA, Ellis EF. Effect of Ca^{2+} on in vitro astrocyte injury. *J Neurochem* 1997;68:289–96.
- Rzigalinski BA, Weber JT, Willoughby KA, Ellis EF. Intracellular free calcium dynamics in stretch-injured astrocytes. *J Neurochem* 1998;70:2377–85.
- Schoepp DD, Jane DE, Monn JA. Pharmacological agents acting at sub-

- types of metabotropic glutamate receptors. *Neuropharmacology* 1999; 38:1431–76.
- Skeberdis VA, Lan J, Opitz T, Zheng X, Bennett MV, Zukin RS. mGluR1-mediated potentiation of NMDA receptors involves a rise in intracellular calcium and activation of protein kinase C. *Neuropharmacology* 2001;40:856–65.
- Sun FY, Faden AI. Pretreatment with antisense oligodeoxynucleotides directed against the NMDA-R1 receptor enhances survival and behavioral recovery following traumatic brain injury in rats. *Brain Res* 1995; 693:163–8.
- Tavalin SJ, Ellis EF, Satin LS. Inhibition of the electrogenic Na pump underlies delayed depolarization of cortical neurons after mechanical injury or glutamate. *J Neurophysiol* 1997;77:632–8.
- Temple M, O'Leary D, Faden A. The role of glutamate receptors in the pathophysiology of traumatic central nervous system injury. In: Miller LA, Hayes RL, Newcomb JK, editors. *Head trauma: basic, preclinical and clinical directions*. New York: Wiley, 2001. pp. 87–113.
- Tomei G, Spagnoli D, Ducati A, Landi A, Villani R, Fumagalli G, Sala C, Gennarelli T. Morphology and neurophysiology of focal axonal injury experimentally induced in the guinea pig optic nerve. *Acta Neuropathol* 1990;80:506–13.
- Ugolini A, Corsi M, Bordi F. Potentiation of NMDA and AMPA responses by group I mGluR in spinal cord motoneurons. *Neuropharmacology* 1997;36:1047–55.
- Ugolini A, Corsi M, Bordi F. Potentiation of NMDA and AMPA responses by the specific mGluR5 agonist CHPG in spinal cord motoneurons. *Neuropharmacology* 1999;38:1569–76.
- Weber JT, Rzigalinski BA, Willoughby KA, Moore SF, Ellis EF. Alterations in calcium-mediated signal transduction after traumatic injury of cortical neurons. *Cell Calcium* 1999;26:289–99.
- Weber JT, Rzigalinski BA, Ellis EF. Traumatic injury of cortical neurons causes changes in intracellular calcium stores and capacitative calcium influx. *J Biol Chem* 2001;276:1800–7.
- Yu SP, Sensi SL, Canzoniero LM, Buisson A, Choi DW. Membrane-delimited modulation of NMDA currents by metabotropic glutamate receptor subtypes 1/5 in cultured mouse cortical neurons. *J Physiol (London)* 1997;499:721–32.
- Zhang L, Rzigalinski BA, Ellis EF, Satin LS. Reduction of voltage-dependent Mg^{2+} blockade of NMDA current in mechanically injured neurons. *Science* 1996;274:1921–3.
- Zhang S, Ehlers MD, Bernhardt JP, Su CT, Huganir RL. Calmodulin mediates calcium-dependent inactivation of *N*-methyl-D-aspartate receptors. *Neuron* 1998;21:443–53.
- Zhong J, Russell S, Pritchett D, Molinoff P, Williams K. Expression of mRNAs encoding subunits of the *N*-methyl-D-aspartate receptor in cultured cortical neurons. *Mol Pharmacol* 1994;45:846–53.



Pergamon

Bioorganic & Medicinal Chemistry 10 (2002) 3043–3048

BIOORGANIC &
MEDICINAL
CHEMISTRY

Synthesis and Biological Activity of Novel Neuroprotective Diketopiperazines

K. R. C. Prakash,^a Y. Tang,^a Alan P. Kozikowski,^{a,*} Judith L. Flippen-Anderson,^b Susan M. Knoblach^c and Alan I. Faden^c

^a*Drug Discovery Program, Department of Neurology, Georgetown University Medical Center, 3900 Reservoir Road, N. W., Washington, DC 20007-2197, USA*

^b*Laboratory for the Structure of Matter, Code 6030, Naval Research Laboratory, 4555 Overlook Ave., S. W., Washington, DC 20375-5000, USA*

^c*Department of Neuroscience, Georgetown University Medical Center, 3900 Reservoir Road, N. W., Washington, DC 20007, USA*

Received 22 October 2001; accepted 5 February 2002

Abstract—The cyclic dipeptide cyclo[His-Pro] (CHP) is synthesized endogenously de novo and as a breakdown product of thyrotropin-releasing hormone (TRH), a tripeptide with known neuroprotective activity. We synthesized two isomeric compounds based on the structure of CHP, in which the histidine residue was replaced by 3,5-di-*tert*-butyltyrosine (DBT), a phenolic amino acid that traps reactive oxygen species. These novel diketopiperazines prevented neuronal death in an in vitro model of traumatic injury. In addition, they dose-dependently prevented death caused by the direct induction of free radicals, and by calcium mobilization through an agent that evokes rapid, necrotic death. The drugs showed activity in the latter system at picomolar concentrations. The neuroprotective profile of these compounds suggests that they may be useful as treatments for neuronal degeneration in vivo, potentially through several different mechanisms. © 2002 Elsevier Science Ltd. All rights reserved.

Introduction

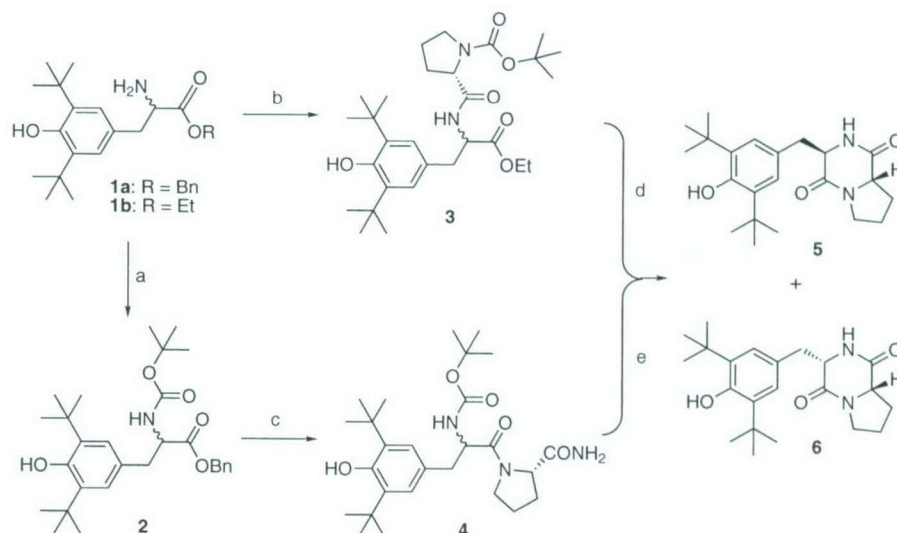
Thyrotropin-releasing hormone (TRH)¹ is a tripeptide present in the central nervous system (CNS) as well as in the periphery. Its best-described role is that of a hypothalamic neuroendocrine hormone. Exogenous administration of TRH elicits a variety of behavioral responses. Among these are changes in sleep/arousal,² temperature,³ autonomic outflow,⁴ and interactions with many physiological effects of opioids/opiates.⁵

TRH and its analogues have been investigated as potential treatments for a variety of disorders, including CNS trauma, where they showed substantial beneficial effects. Continuous infusion of TRH or bolus injections of analogues with intact C-termini and longer half-lives improved recovery across species in models of traumatic injury to the brain or spinal cord.⁶ Such benefits may be

related to reversal of pathophysiological secondary events (i.e., release of glutamate, generation of free radicals) that are initiated by the insult and evolve from minutes to days later. For example, TRH or TRH analogues stabilize levels of catecholamines, restore cationic imbalances, and antagonize the pathophysiological effects of endogenous opioids, leukotrienes and platelet-activating factor that occur after injury.⁷

Whether synthesized endogenously or injected, TRH is rapidly metabolized in blood and CNS tissue. The cyclic dipeptide cyclo[His-Pro] (CHP) is generated by primary cleavage of the pyroglutamyl residue from TRH by the abundant and relatively non-specific enzyme pyroglutamyl aminopeptidase.⁸ CHP is also synthesized de novo endogenously, where it is both detectable in CNS tissue by radioimmunoassay and has demonstrable bioactivity. Because CHP and TRH share similarities in biological activity, and exogenous administration of TRH can increase CHP, it has been hypothesized that at least some of the effects of TRH administration may occur through CHP.⁹ Therefore, we designed a novel

*Corresponding author. Tel.: +1-202-687-0686; fax: +1-202-687-5065; e-mail: kozikowa@georgetown.edu



Scheme 1. Reagents and conditions: (a) (BOC)₂O, ⁱPr₂NEt, rt; (b) DCC, HOBT, *N*-(*tert*-butoxycarbonyl)-L-proline; (c) (i) H₂/Pd/C; (ii) L-prolinamide, DCC, HOBT; (d) (i) CF₃COOH, CH₂Cl₂ (ii) NaCN, MeOH; (e) (i) CF₃COOH, CH₂Cl₂ (ii) Et₃N, CH₂Cl₂.

cyclic dipeptide related to CHP in which the imidazole moiety is replaced by a di-*tert*-butylphenol (i.e., the histidine residue is replaced by 3,5-di-*tert*-butyltyrosine). Our rationale was that the known structure of CHP, combined with the ability of certain phenols to act as scavengers for reactive oxygen species (ROS) might yield compounds with novel neuroprotective potential. We report the route of synthesis of the two diastereomeric cyclic dipeptides, cyclo[(di-*tert*-Bu)Tyr-Pro], together with details of their action in several different *in vitro* models of neuronal injury. These molecules appear to provide an interesting profile of action that warrants further study.

Chemistry

The diketopiperazines **5** and **6** were prepared in optically pure form starting from the benzyl or ethyl ester of 3',5'-di-*tert*-butyltyrosine (**1a/1b**)¹⁰ in two different ways (Scheme 1). Compound **1a** was prepared in racemic form by reaction of the anion of benzyl *N*-(diphenylmethylene)glycinate with 4-(bromomethyl)-2,6-di-*tert*-butylphenol followed by HCl workup. Next, the free amine **1a** was treated with (BOC)₂O in the presence of diisopropylethylamine to afford the amino-protected tyrosine derivative **2**. The benzyl ester group of **2** was cleaved by hydrogenolysis over Pd/C to obtain the free acid, which was then coupled with L-prolinamide in presence of HOBT and DCC to give **4** as a diastereomeric mixture. Compound **4** was further converted to **5** and **6** by treatment with trifluoroacetic acid followed by triethylamine. The two diastereomers (**5** and **6**) were separated by column chromatography.

As an alternative and shorter route to the same cyclic peptides, the ethyl ester **1b** was coupled with the *N*-(*tert*-butoxycarbonyl)-L-proline in the presence of HOBT and DCC in CH₂Cl₂ to yield the dipeptide **3** in 80% yield. This intermediate was then treated with TFA in methylene chloride followed by NaCN in MeOH to provide

the diketopiperazines **5** and **6** in good yield. Chromatographic purification of the crude diastereomeric mixture gave equal amounts of **5** and **6**. The structures of compounds **5** and **6** were established by NMR analysis, and additionally, a single-crystal X-ray analysis was carried out on **6** (Fig. 1). The second route is the more efficient one of the two, as only three synthetic steps are required from the starting amino acid **1b**.

Biological studies — activity in a model of CNS injury

To evaluate whether **5** and **6** showed neuroprotective activity we tested them in several models of cell death. 3,5-Di-*tert*-butyltyrosine (DBT) and cyclo(Gly-Pro) (CGP),¹¹ the components of the new drugs **5** and **6**, were used as controls. The *in vitro* mechanical punch model has been used by our group and others to mimic both acute cell destruction and secondary loss associated with traumatic injury *in vivo*.¹² In this model, neuronal-glial co-cultures are subjected to physical

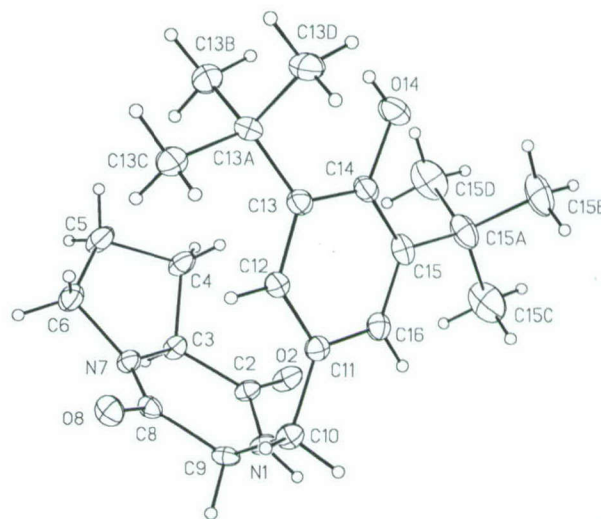


Figure 1. Single-crystal X-ray structure of the diketopiperazine **6**.

disruption with a device that rapidly deploys a series of 28 parallel blades to the culture surface. Cells under the blades are destroyed on contact, and the cultures are then washed to remove resultant debris. However, over the course of the ensuing 24 h after impact, neurons throughout the culture slowly begin to die; calcein staining reveals that the highest proportion of cell death occurs at and near the site of impact, with progressively lower and more delayed cell death/injury taking place as the distance from impact increases. Because this injury is both delayed and indirect, it serves as a useful model of secondary injury mechanisms that contribute to impairment *in vivo*.¹² In our co-culture system, activity of the enzyme lactate dehydrogenase in the culture media correlates with total neuronal death. Treatment with either **5** or **6** reduced cell death in this model (Fig. 2); this activity followed an inverted U-shaped dose-response curve. Neither DBT nor CGP prevented cell death in this model, suggesting that neither the 3,5-di-*tert*-butyltyrosine nor the cyclo(Gly-Pro) components of **5** and **6** were singularly involved in their neuroprotective activity.

Multiple factors have been implicated in the secondary injury response. They include free radicals, glutamate, influx and cellular dysregulation of sodium and calcium, breakdown of phospholipids with the generation of toxic by-products, activation of inflammatory cascades and alterations in signal transduction (i.e., protein kinase C and others), and induction of programmed (apoptotic)^{13,14} cell death cascades. Therefore, to characterize the neuroprotective activity of **5** and **6** further, we evaluated whether they would prevent cell death induced by several of these injury-associated factors/mechanisms.

Calcium-induced necrosis

Maitotoxin is a marine, algal, polyether type neurotoxin that induces cell death via external calcium influx and mobilization of intracellular calcium stores.¹⁵ It produces rapid deterioration and necrotic morphology, as well as activation of enzymes associated with necrotic cell death.¹⁵ Compounds **5** and **6** were very effective at preventing death induced by a maitotoxin pulse (Fig. 3). High concentrations of DBT and CGP also showed

some neuroprotection in this model, but it was 4-fold less than that provided by equal concentrations of **5** or **6**. These data suggest that both the DBT and CGP moieties of **5** and **6** may each contribute, albeit minimally, to the observed neuroprotective properties of **5** and **6** against cell death induced by maitotoxin. MK-801 showed no activity.

Excitotoxic cell death

The next objective was to determine whether **5** and **6** prevented excitotoxic cell death induced by a glutamate pulse. Neither compound prevented this type of cell death. Higher concentrations of these drugs also had no effect (data not shown). MK-801, a selective inhibitor of the NMDA subtype of glutamate receptors, served as a positive control.

Apoptotic death

Staurosporine induces apoptotic death and activation of enzymes (caspases) specifically associated with this type of cell self-destruction in cultured neurons.¹⁴ Therefore we examined whether **5** and **6** could prevent this type of cell death in our culture system. The drugs had no effect on death induced by 0.1 μ M staurosporine at concentrations of 0.1–100 μ M (data not shown). MK-801 was also ineffective in this model.

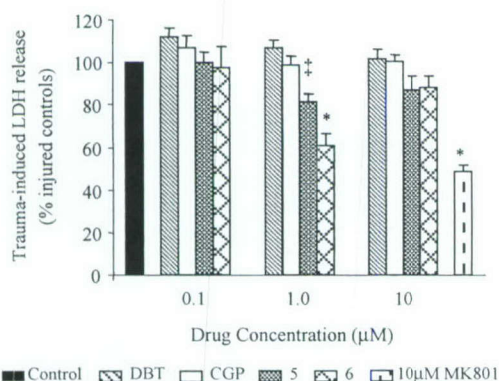


Figure 2. Bars represent the mean \pm SEM for $n=40$ –46 wells per condition. $^{\dagger}p < 0.01$, $^*p < 0.0001$ for *t*-test with Bonferroni correction.

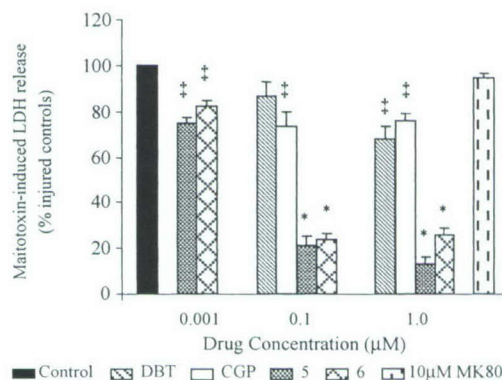


Figure 3. Bars represent the mean \pm SEM for $n=40$ –46 wells per condition. $^{\dagger}p < 0.01$, $^*p < 0.0001$ for *t*-test with Bonferroni correction.

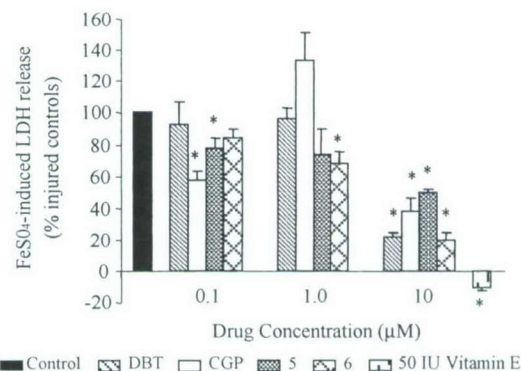


Figure 4. Bars represent the mean \pm SEM for $n=40$ –46 wells per condition. $^{\dagger}p < 0.05$, $^{\ddagger}p < 0.01$, $^*p < 0.0001$ for *t*-test with Bonferroni correction.

Free-radical-induced death

As anticipated based upon the presence of the di-*tert*-butylphenol group in these cyclic dipeptides, both compounds **5** and **6** increased survival in a model of free radical induced cell death¹⁶ initiated by FeSO₄ (Fig. 4). However, in contrast to the results seen with the mechanical punch, the neuroprotective efficacy in this model followed a dose-dependent activity curve. DBT and CGP showed neuroprotective activity as well, with DBT and **6** providing the best protection at the highest concentrations tested. As glycine itself is known in the literature¹⁷ to serve as an antioxidant, it was not surprising to find that CGP, a cyclic derivative of glycine, shows significant neuroprotection even at a concentration of 0.1 μ M in this model. These data indicate that not only does the DBT moiety contribute to the free-radical scavenging properties of **5** and **6**, but that the CGP moiety may do so as well. Vitamin E, a well-described anti-oxidant, was utilized as a positive control.

Conclusion

In summary, the novel cyclic dipeptides reported herein show neuroprotective properties in a neuronal-glial model of trauma, which involves activation of multiple secondary injury factors. They are also able to block calcium-induced necrotic cell death initiated by maitotoxin as well as death induced by FeSO₄, a free radical generator. Secondary tissue damage and associated cell death after acute CNS insults thought to reflect a multifactorial biochemical process that together cause cellular necrosis or apoptosis.¹⁸ Development of compounds **5** and **6**, like other diketopiperazines or related tripeptides,¹⁹ was based upon the concept that effective treatment of CNS injury requires either use of multiple neuroprotective agents with complementary mechanisms or use of single compounds (like TRH) with multifactorial actions. In the present studies, compounds **5** and **6** attenuated both trauma and maitotoxin induced cell death *in vitro*; each of these models causes almost exclusively necrotic cell death. Data from the DBT and CGP controls suggest that each of these components contributes to the neuroprotective effects of **5** and **6**. In contrast, the compounds did not inhibit glutamate induced cell death, which can cause either necrotic or apoptotic cell death, depending upon concentration, duration of treatment or age of cultures. They also did not inhibit a classical apoptotic cell death model. Free radicals may cause either necrotic or apoptotic cell death through different mechanisms.²⁰ Taken together, the ability of compounds **5** or **6** to modify three different *in vitro* models, all of which may be associated with cellular necrosis, suggests that the protective actions reflect antinecrotic properties. Yet their inability to modify glutamate induced changes indicates that other pro-necrotic factors may be involved, such as free radical induced lipid peroxidation²⁰ or effects of calpains.¹⁵ Thus, the unique combination of these moieties yields compounds with a pharmacological profile that indicates an action through several different secondary injury mechanisms. When tested at concentrations as

high as 100 μ M, these compounds failed to show any cytotoxicity. Therefore, these agents may have potential utility as treatments for acute CNS injuries such as stroke and trauma.

Experimental

Chemical methods

General. Starting materials were obtained from the Aldrich Chemical Co. or from other commercial suppliers. Solvents were purified as follows: diethyl ether was distilled from phosphorus pentoxide; THF was freshly distilled under nitrogen from sodium/benzophenone. ¹H and ¹³C NMR spectra were obtained with a Varian Unity Inova instrument at 300 and 75.46 MHz, respectively. ¹H chemical shifts (δ) are reported in ppm downfield from internal TMS. ¹³C chemical shifts are referenced to CDCl₃ (central peak, δ = 77.0 ppm). NMR assignments were made with the help of COSY, NOESY, DEPT, and HETCOR experiments. Melting points were determined in Pyrex capillaries with a Thomas-Hoover Unimelt apparatus and are uncorrected. Mass spectra were measured in the EI mode at an ionization potential of 70 eV. TLC was performed on Merck silica gel 60F₂₅₄ glass plates; column chromatography was performed using Merck silica gel (60–200 mesh). Abbreviations: THF, tetrahydrofuran; LDA, lithium diisopropylamide; DCC, dicyclohexylcarbodiimide; DMF, dimethylformamide; HOBt, 1-hydroxybenzotriazole.

3',5'-Di-*tert*-butyltyrosine benzyl ester (1a).¹⁰ To a solution of benzyl *N*-(diphenylmethylene)glycinate¹⁸ (1.3 g, 4.0 mmol) in THF (20 mL) at –78 °C was added under a N₂ atmosphere LiHMDS (5.0 mL, 1.0 M solution in THF, 5.0 mmol). After stirring for 15 min at –78 °C, 4-(bromomethyl)-2,6-di-*tert*-butylphenol (1.2 g, 4.0 mmol) was added dropwise, and the resulting mixture was stirred for an additional 8 h. The solvent was removed under reduced pressure, and the residue was stirred with ether/1 N HCl (20 mL, 1:1 mixture) overnight at rt. The reaction mixture was neutralized to pH 7.0 and extracted with ether (3 \times 100 mL). The combined ether layers were washed with brine, dried (Na₂SO₄), and concentrated. The residue on purification by flash chromatography (hexane/ethyl acetate 1:1) yielded the ester **1a** (0.84 g) in 54% yield: ¹H NMR (CDCl₃) δ 1.43 (s, 18H), 2.88 (dd, *J* = 7.5, 13.5 Hz, 1H), 3.05 (dd, *J* = 5.7, 13.5 Hz, 1H), 3.79 (dd, *J* = 5.7, 7.2 Hz, 1H), 5.13 and 5.19 (ABq, *J* = 12.3 Hz, 2H), 7.00 (s, 2H), 7.33 (m, 5H). ¹³C NMR (CDCl₃) δ 30.51, 34.47, 41.27, 56.29, 66.83, 125.99, 127.70, 128.28, 128.49, 128.77, 135.75, 136.20, 152.90, 175.40. MS (EI) *m/z* 383 (M⁺, 3%), 219 (100%).

3',5'-Di-*tert*-butyltyrosine ethyl ester (1b).¹⁰ To a solution of ethyl *N*-(diphenylmethylene)glycinate¹⁸ (1.3 g, 3.9 mmol) in THF (20 mL) at –78 °C was added LDA (5.0 mL, 1.0 M solution in THF, 5.0 mmol) under a N₂ atmosphere. After stirring for 15 min at –78 °C, a solution of 4-(bromomethyl)-2,6-di-*tert*-butylphenol (1.2 g,

4.0 mmol) in THF (5 mL) was added. The resulting mixture was stirred for an additional 5 h at -78°C . The solvent was removed. To the resulting residue was added ether (10 mL) followed by HCl (1 N, 10 mL), and the mixture was stirred at room temperature overnight. The reaction mixture was neutralized to pH 7.0 and extracted with ether (3×100 mL). The combined ether layers were washed with brine, dried (Na_2SO_4), and concentrated. The residue was purified by column chromatography on silica gel (EtOAc/MeOH 15:1) to give the ester **1b**. Yield: 1.0 g (65%). ^1H NMR (CDCl_3) δ 1.27 (t, $J=7.2$ Hz, 3H), 1.43 (s, 18H), 2.84 (dd, $J=7.8$, 13.8 Hz, 1H), 3.02 (dd, $J=5.4$, 13.8 Hz, 1H), 3.70 (dd, $J=5.4$, 7.5 Hz, 1H), 4.18 (q, $J=7.2$ Hz, 2H), 7.00 (s, 2H). ^{13}C NMR (CDCl_3) δ 14.37, 30.46, 34.43, 41.16, 56.12, 60.98, 125.95, 127.75, 136.13, 152.80, 175.43. MS (EI) m/z 321 (M^+ , 1%), 219 (100%).

***N*-(*tert*-Butoxycarbonyl)-3',5'-di-*tert*-butyltyrosine benzyl ester (2).** To a solution of compound **1a** (0.42 g, 1.09 mmol) in CH_3CN (10 mL) was added at room temperature under N_2 , $^i\text{Pr}_2\text{NEt}$ (0.18 g, 1.4 mmol), followed by $(\text{BOC})_2\text{O}$ (0.305 g, 1.4 mmol). The mixture was stirred overnight. The solvent was removed under reduced pressure, and the residue was purified by flash chromatography (hexane/ethyl acetate 15:1) to give the pure product (**2**, 0.48 g) in 90% yield: ^1H NMR (CDCl_3) δ 1.44 (s, 18H), 1.47 (s, 9H), 3.06 (m, 2H), 4.65 (dd, $J=6.3$, 14.1 Hz, 1H), 5.13 (m, 4H), 6.95 (s, 2H), 7.27 (m, 2H), 7.35 (m, 3H). ^{13}C NMR (CDCl_3) δ 28.52, 30.48, 34.43, 54.82, 67.08, 79.94, 126.04, 126.54, 128.10, 128.47, 128.74, 135.39, 136.11, 153.01, 155.17, 172.24. MS (EI) m/z 483 (M^+ , 5%), 219 (100%).

***N*-[*N*-(*tert*-Butoxycarbonyl)prolyl]-3',5'-di-*tert*-butyltyrosine ethyl ester (3).** To a solution of *N*-(*tert*-butoxycarbonyl)proline (53 mg, 0.24 mmol) in DMF (3 mL) was added HOBt (35 mg, 0.26 mmol), followed by DCC (50 mg, 0.24 mmol). The mixture was stirred for 2 h, then a solution of 3,5-di-*tert*-butyltyrosine ethyl ester (**1b**) (80 mg, 0.29 mmol) and triethylamine (0.3 mL) in DMF (5 mL) was added, and the resulting mixture was stirred for 12 h at room temperature. The solvent was pumped off, and the residue was purified by flash chromatography on silica gel (hexane/ethyl acetate 1:1) to give **3** (125 mg, 97%) as a white foam. ^1H NMR (CDCl_3) δ 1.10–1.14 (dt, $J=7.2$ Hz, 3H), 1.39 (s, 27H), 1.90 (m, 4H), 3.00 (m, 2H), 3.36 (m, 3H), 4.18 (m, 2H), 4.76 (m, 1H), 5.16 (s, 1H), 6.36 (br s, 1H), 6.95 (s, 1H), 7.00 (s, 1H).

Cyclo[(*R*)-3',5'-di-*tert*-butyl-Tyr-L-Pro] (5) and cyclo[(*S*)-3',5'-di-*tert*-butyl-Tyr-L-Pro] (6). From compound **2**. To a solution of compound **2** (480 mg, 1.0 mmol) in *tert*-butyl alcohol (20 mL) was added 10% Pd/C (40 mg). The resulting mixture was stirred at room temperature under an H_2 atmosphere for 2 h, and the catalyst was filtered off. After removal of the solvent, the residue was dissolved in DMF/EtOAc (1:5, 12 mL), and to this solution was added HOBt (162 mg, 1.2 mmol), followed by DCC (254 mg, 1.23 mmol). The resulting solution was stirred for 2 h, and then prolinamide (124 mg, 1.08 mmol) was added. The mixture was stirred overnight at room temperature. The precipitate was filtered off, and

the solution was diluted with CH_2Cl_2 (500 mL), washed with water, dried (Na_2SO_4), and concentrated. The residue was passed through a short column of silica gel to give the crude product **4** (470 mg, 97%). This material was dissolved in $\text{CH}_2\text{Cl}_2/\text{CF}_3\text{COOH}$ (10:1, 5 mL) at 0°C , and the solution was stirred for 2 h at the same temperature. The solvent was removed under reduced pressure, the residue was dissolved in CH_2Cl_2 /triethylamine (5:1, 10 mL), and the resulting mixture was stirred overnight. The reaction mixture was diluted with CH_2Cl_2 , washed with saturated NaHCO_3 , dried (Na_2SO_4), and concentrated to give an oil. Purification by column chromatography on silica gel [$\text{CHCl}_3/\text{MeOH}$ (9:1)] gave the pure compounds **5** (80 mg, 21% yield) and **6** (121 mg, 32% yield).

From compound 3. A solution of compound **3** (16 mg, 0.03 mmol) in $\text{CH}_2\text{Cl}_2/\text{CF}_3\text{COOH}$ (10:1, 5 mL) was stirred for 2 h at 0°C . The reaction mixture was diluted with CH_2Cl_2 , washed with saturated NaHCO_3 , dried (Na_2SO_4), and concentrated to give an oil. The residue was dissolved in MeOH (5 mL), NaCN (2 mg) was added, and the resulting mixture was stirred at 45°C overnight. The solvent was removed under reduced pressure, and the residue was purified by column chromatography on silica gel [$\text{CHCl}_3/\text{MeOH}$ (9:1)] to give the compounds **5** and **6** (5 mg, 43%, and 5.2 mg, 45%, respectively).

5: $[\alpha]_{\text{D}}^{25} -137^{\circ}$ (c 0.93, CHCl_3). Mp $194\text{--}197^{\circ}\text{C}$. ^1H NMR (CDCl_3) δ 1.45 (s, 18H), 1.98 (m, 3H), 2.37 (m, 1H), 2.69 (dd, $J=10.8$, 14.4 Hz, 1H), 3.59 (m, 3H), 4.12 (t, $J=7.2$ Hz, 1H), 4.27 (d, $J=8.7$ Hz, 1H), 5.21 (s, 1H), 5.68 (s, 1H), 7.00 (s, 2H). ^{13}C NMR (CDCl_3) δ 22.70, 28.62, 30.41, 34.52, 37.12, 45.53, 56.58, 59.34, 125.73, 126.37, 136.94, 153.33, 165.46, 169.48. Anal. calcd for $\text{C}_{22}\text{H}_{32}\text{N}_2\text{O}_3$: C, 70.92; H, 8.66; N, 7.52. Found: C, 71.13; H, 8.50; N, 7.63.

6: $[\alpha]_{\text{D}}^{25} -23^{\circ}$ (c 1.07, CHCl_3). Mp $216\text{--}218^{\circ}\text{C}$. ^1H NMR (CDCl_3) δ 1.44 (s, 18H), 1.76 (m, 2H), 1.95 (m, 1H), 2.16 (m, 1H), 2.64 (dd, $J=6.6$, 10.5 Hz, 1H), 2.93 (dd, $J=3.9$, 13.8 Hz, 1H), 3.13 (dd, $J=5.7$, 13.5 Hz, 1H), 3.42 (m, 1H), 3.63 (m, 1H), 4.23 (q, $J=5.1$ Hz, 1H), 5.23 (s, 1H), 5.80 (s, 1H), 6.99 (s, 2H). ^{13}C NMR (CDCl_3) δ 21.95, 29.11, 30.49, 34.43, 40.54, 45.27, 57.90, 59.43, 125.55, 126.83, 136.65, 153.50, 165.21, 169.39. Anal. calcd for $\text{C}_{22}\text{H}_{32}\text{N}_2\text{O}_3$: C, 70.92; H, 8.66; N, 7.52. Found: C, 70.66; H, 8.45; N, 7.65.

Acknowledgements

We are indebted to the Department of Defense (DAMD 17-99-2-9007) for the support of this work.

References and Notes

- De La Pena, P.; Delgado, L. M.; Del Camino, D.; Barros, F. *Biochem. J.* **1992**, *284*, 891.
- (a) Breese, G. R.; Cott, J. M.; Cooper, B. R.; Prange, A. J., Jr; Lipton, M. A. *J. Pharmacol. Exp. Ther.* **1975**, *193*, 11(b);

- Stanton, T. L.; Winokur, A.; Bechman, A. L.; *Brain Res.* **1980**, *181*, 470.
3. (a) Metcalf, G. *Nature* **1974**, 252, 310. (b) Lahti, H.; Koskinen, M.; Pyomilla, A.; Hissa, R. *Experientia* **1983**, *39*, 1338.
4. (a) Kolvasulo, F. I.; Paakkari, J.; Leppauloto, J.; Karppanen, H. *Acta Physiol. Scand.* **1979**, *106*, 83. (b) Tache, Y.; Lesiege, D.; Bale, W.; Collu, R. *Eur. J. Pharmacol.* **1985**, *107*, 146.
5. (a) Reny-Palasse, V.; Constans, M.; Rips, R. *Br. J. Pharmacol.* **1989**, *97*, 197. (b) Ramarao, P.; Bhargava, H. N. *Neuropeptides* **1990**, *15*, 213.
6. (a) Behrmann, D. L.; Bresnahan, J. C.; Beattie, M. S. *Exp. Neurol.* **1994**, *126*, 61. (b) Faden, A. I.; Labroo, V. M.; Cohen, L. A. *J. Neurotrauma* **1993**, *10*, 101. (c) Faden, A. I.; Jacobs, T. P.; Holaday, J. W. *N. Engl. J. Med.* **1981**, *305*, 1063.
7. (a) Tanaka, K.; Ogawa, N.; Asanuma, M.; Kondo, Y. *Regul. Pept.* **1997**, *70*, 173. (b) Vink, R.; McIntosh, T. K.; Faden, A. I. *Brain Res.* **1988**, *460*, 184. (c) Koenig, M. L.; Yourick, D. L.; Meyerhoff, J. L. *Brain Res.* **1996**, *730*, 143. (d) Faden, A. I.; Vink, R.; McIntosh, T. K. *Ann. N.Y. Acad. Sci.* **1989**, *553*, 380.
8. (a) Prasad, C. *Neurosci. Biobehav. Rev.* **1988**, *12*, 19. (b) Prasad, C. *Ann. N.Y. Acad. Sci.* **1989**, *553*, 232. (c) Peterkofsky, A.; Battaini, F.; Koch, Y.; Takahara, Y.; Dannies, P. *Mol. Cell. Biochem.* **1982**, *42*, 45.
9. (a) Prasad, C.; Jayaraman, A.; Robertson, H. H.; Rao, J. K. *Neurochem. Res.* **1987**, *12*, 767. (b) Prasad, C. *Thyroid* **1998**, *8*, 969.
10. (a) O'Donnell, M. J.; Bennett, W. D.; Bruder, W. A.; Jacobsen, W. N.; Knuth, K.; LeClef, B.; Polt, R. L.; Bordwell, F. G.; Mrozack, S. R.; Cripe, T. A. *J. Am. Chem. Soc.* **1988**, *110*, 8520. (b) O'Donnell, M. J.; Wu, S.; Huffman, J. C. *Tetrahedron* **1994**, *50*, 4507.
11. Cyclo[Gly-Pro] (CGP) was synthesized in the same way as reported for compounds **5** and **6**, starting from glycine ethyl ester and prolinamide. Mp 171–173 °C. ¹H NMR (CDCl₃) δ 1.87–2.15 (m, 3H), 2.31–2.43 (m, 1H), 3.52–3.69 (m, 2H), 3.89 (dd, *J* = 4.2, 16.5 Hz, 1H), 4.08–4.13 (m, 2H), 6.16 (br s, 1H). ¹³C NMR (CDCl₃) δ 22.82, 28.88, 45.76, 47.11, 58.92, 163.73, 169.97.
12. (a) Mukhin, A. G.; Ivanova, S. A.; Allen, J. W.; Faden, A. I. *J. Neurosci. Res.* **1998**, *51*, 748. (b) Tecoma, E. S.; Monyer, H.; Goldberg, M. P.; Choi, D. W. *Neuron* **1989**, *2*, 1541.
13. (a) Graham, D. I.; McIntosh, T. K.; Maxwell, W. L.; Nicoll, J. A. *J. Neuropathol. Exp. Neurol.* **2000**, *59*, 641. (b) McIntosh, T. K.; Saatman, K. E.; Ragupathi, R.; Graham, D. I.; Smith, D. H.; Lee, V. M.; Trojanowski, J. Q. *Neuropathol. Appl. Neurobiol.* **1998**, *24*, 251.
14. Koh, J.-Y.; Wie, M. B.; Gwag, B. J.; Sensi, S. L.; Canzoniero, L. M.; Demaro, J.; Csernansky, C.; Choi, D. W. *Exp. Neurol.* **1995**, *135*, 153.
15. Zhao, X.; Pike, B. R.; Newcomb, J. K.; Wang, K. K.; Posmantur, R. M.; Hayes, R. L. *Neurochem. Res.* **1999**, *24*, 371.
16. Mattson, M. P.; Barger, S. W.; Begley, J. G.; Mark, R. J. *Methods Cell Biol.* **1995**, *46*, 187.
17. (a) Shaikh, Z. A.; Tang, W. *Toxicology* **1999**, *132*, 139. (b) Rauk, A.; Armstrong, A. A.; Fairlie, D. P. *J. Am. Chem. Soc.* **2000**, *122*, 9761.
18. Faden, A. I. *Arch. Neurol.* **2001**, *58*, 1553.
19. Faden, A. I.; Fox, G. B.; Fan, L.; Araldi, G. L.; Qiao, L.; Wang, S.; Kozikowski, A. P. *Am. J. Physiol.* **1999**, *277*, 1196.
20. Lewen, A.; Matz, P.; Chan, P. K. *J. Neurotrauma* **2000**, *17*, 871.

Administration of Either Anti-Intercellular Adhesion Molecule-1 or a Nonspecific Control Antibody Improves Recovery after Traumatic Brain Injury in the Rat

S.M. KNOBLACH and A.I. FADEN

ABSTRACT

Intercellular adhesion molecule-1 (ICAM-1) is an endothelial protein that facilitates invasion of leukocytes into the CNS in response to injury or inflammation. ICAM-1 expression correlates with the severity of clinical head injuries, but its importance in secondary injury events is not fully understood. Therefore, we evaluated ICAM-1 expression and the effect of anti-ICAM-1 treatment on motor recovery and neutrophil invasion after traumatic brain injury induced via the lateral fluid-percussion method in the rat. ICAM-1 was expressed in large and small blood vessels within the injured cortex at 10 and 24 h after injury. Repeated administration of anti-ICAM-1 antibody (clone 1A29) at 1, 10, and again at 24 h after injury significantly improved performance in two of three motor tests, compared to saline controls. Equal doses of nonspecific control antibody (IgG) also significantly improved motor test scores, compared to saline controls. Cortical myeloperoxidase activity, an indicator of neutrophil invasion, was significantly reduced 26 h after injury in animals treated with anti-ICAM-1. Animals treated with IgG showed a trend toward reduction that did not reach significance. These data suggest that ICAM-1 may be involved in neutrophil invasion and neurological dysfunction after TBI, but also implicate a role for a nonspecific antibody effect in improved functional outcome.

Key words: antibody; anti-ICAM-1; CNS; expression; function; head injury; IgG

INTRODUCTION

INTERCELLULAR ADHESION MOLECULE-1 (ICAM-1) is an adhesion molecule involved in the migration of neutrophils from cerebral vasculature to the brain parenchyma after CNS injuries. ICAM-1 is normally constitutively expressed at low levels in cerebral endothelium, but it is upregulated in response to ischemia or contusion injury (Carlos et al., 1997; Isaksson et al., 1997; Grady et al., 1999; Jean et al., 1998; Feuerstein et al., 1998). In clinical studies of head-injured patients, elevations in ICAM-1 positively correlate with increased severity of injury

and worsened neurological outcome (Whalen et al., 1998; McKeating et al., 1998b,c; Pleines et al., 1998).

Delineation of a precise role for ICAM-1 in injury-induced neutrophil invasion and subsequent secondary damage is not straightforward, in part because leukocyte extravasation and migration occurs in several steps that involve different classes of adhesion molecules (for reviews, see Dunon et al., 1996; Kochanek et al., 1992; McKeating et al., 1998a). Initially, endothelial L-, P-, or E-selectins bind sialyl-Lewis^x carbohydrate ligands present on leukocytes to promote reversible attachment and rolling along the intravascular wall. Rolling leukocytes

express several $\beta 2$ -integrins (CD11a/LFA-1, CD11b/Mac-1/CR3, CD11c/p150,95), which attach firmly to vessels through binding to the endothelial adhesion molecules ICAM-1/CD54, vascular adhesion molecule-1 (VCAM-1/CD106) and/or platelet-endothelial adhesion molecule-1 (PECAM-1/CD31). Firm attachment is a key step in leukocyte invasion, because it results in a commitment to extravasation and activation. The importance of ICAM-1 in this process is supported by studies in which systemic administration of anti-ICAM-1 antibodies reduced neutrophil accumulation in damaged CNS tissue (Carlos et al., 1997; Clark et al., 1996).

Extravasation of activated neutrophils is linked to several injury-induced secondary events. Among these are the release of free radicals, degradative proteases, and proinflammatory chemokines and/or cytokines (for review, see Palmer, 1995; Scapini et al., 2000; Jaeschke et al., 1996; Mazzoni et al., 1996). In addition, neutrophil influx correlates with blood-brain barrier damage and the development of cerebral edema, though it is difficult to isolate causal factors linking these events (Carlos et al., 1997; Whalen et al., 1999b, 2000; Clark et al., 1996; Uhl et al., 1994; Kochanek et al., 1992).

In contrast to secondary factors that contribute to neurological dysfunction within minutes after injury (e.g., changes in glutamate), the relatively delayed and prolonged time course associated with neutrophil invasion (hours to days after injury) may permit a larger window of opportunity for therapeutic intervention. In support of this, ICAM-1 inhibitors significantly reduced tissue damage and improved neurological outcome in models of focal cerebral ischemia (Zhang et al., 1994; Clark et al., 1991; Bowes et al., 1993). Anti-ICAM-1 treatment was also beneficial after experimental spinal cord injury (Hamada et al., 1996). However, to our knowledge, no study has yet addressed whether this strategy may improve functional outcome after traumatic brain injury (TBI). Thus, the objective of the present work was to evaluate the effect of an ICAM-1 antagonist on neurological recovery after TBI. In addition, we verified whether ICAM-1 expression is increased in the lateral fluid-percussion model of traumatic brain injury and assessed the effect of the ICAM-1 antagonist on neutrophil extravasation. We focused on the cerebral cortex, because in this model this region typically shows leukocyte infiltration concomitant with neuronal degeneration (Soares et al., 1995).

MATERIALS AND METHODS

Traumatic Brain Injury

Individual immunocytochemical, behavioral, and biochemical studies were performed utilizing 16, 40, and 14

rats, respectively. To produce TBI, a craniotomy was performed over the left parietal cortex of anesthetized (70 mg/kg Sodium Pentobarbital, i.p.), intubated, male Sprague-Dawley rats (400 ± 25 g; Harlan Sprague-Dawley, Frederick, MD) ventilated on room air. Injury was induced by a brief, pressurized (2.5–2.6 atm), saline pulse delivered through the craniotomy to the intact dura as previously detailed (McIntosh et al., 1989). This level of injury produces moderate chronic neurological dysfunction and histopathological alterations. Sham controls were subjected to identical surgical procedures, with the exception that no fluid pulse was delivered. The caudal artery was cannulated to monitor blood gas and pressure throughout the procedure. Body (rectal; 37.5–38.5°C) and brain temperature (lateralis muscle; 36.5–37.5°C) were monitored and maintained within normal ranges during the experiment. Normal core temperature was maintained until 10 h after injury. All procedures involving live animals were approved by the Georgetown University Animal Care and Use Committee, and were performed according to principles enumerated in the Guide for the Care and Use of Laboratory Animals, prepared by the Committee on the Care and Use of Laboratory Animals of the Institute of Laboratory Resources, National Research Council (DHEW publication no. NIH 85-23-2985).

Immunocytochemistry

Rats were killed either 1, 10, or 24 h ($n = 4$ per group) after injury. Sham controls were killed at either 10 or 24 h ($n = 2$ per group) after sham injury. The injured hemisphere was removed, frozen, and sectioned (10 μ m) from approximately -2.3 to -3.7 AP relative to Bregma (Paxinos et al., 1986). This region contains the cortical area that deteriorates to a cavitation lesion by 2 weeks after TBI. One section out of every 10 cut serially through the lesion was mounted on a glass slide. One out of every five slides counted serially was stained and evaluated for ICAM-1 expression. This yielded about three to four sections per animal, distributed through the lesion. Sections were fixed in acetone (4°C, 4–5 min) and methanol (4°C, 30 sec), rinsed briefly, and blocked with 10% goat serum (30 min, room temperature). Blocking solution was then tapped off, the primary antibody applied (anti-ICAM-1 monoclonal antibody [clone 1A29], 1:500 dilution; Genzyme, Cambridge, MA), and the sections incubated overnight (16–18 h) in a humidified chamber (4°C). The next day, sections were rinsed (3×3 min each), and incubated with secondary antibody (1:200) for 30 min at room temperature. Sections were then rinsed once again and coverslipped with fluorescent mounting medium (Johnson et al., 1981). Hoescht 33258 was applied for 5 min as a fluorescent counterstain to some sections. Pri-

mary or secondary antibodies were deleted in procedural controls. PBS, pH 7.4, was used for all rinses and for dilution of Hoechst dye. Blocking solution, and primary and secondary antibodies were prepared in Dulbecco's PBS (with magnesium and calcium), pH 7.4. Affinity purified, rat adsorbed fluorescein (FITC)-conjugated goat anti-mouse IgG no. JGM095100 (Accurate Chemicals, Westbury, NY) was used as the secondary antibody.

Drug Treatment

Anti-ICAM-1 (1 mg/kg in 0.5 mL of saline) was injected in a repeated administration schedule at 1, 10, and 24 h after TBI ($n = 15$). Controls received either equivalent volume injections of murine IgG (1 mg/kg in saline; $n = 7$) or saline only ($n = 7$). Treatment groups that received either equivalent doses/volumes of IgG or saline were prepared as nonspecific antibody control and vehicle control groups, respectively. The initial design of the experiment anticipated that these two control groups would perform similarly, and data from these groups could later be combined. However, because preliminary results indicated that IgG appeared to be improving recovery, both control groups were enlarged ($n = 11$ – 14 each) to allow separate statistical comparisons of IgG and anti-ICAM-1, relative to saline vehicle.

Murine IgG (no. I5381) was purchased commercially (Sigma, St. Louis, MO). The murine monoclonal anti-ICAM-1 antibody (clone 1A29) was kindly provided by Dr. Robert Rothlein (Boehringer Ingelheim, Ridgefield, CT). Synthesis and purification of the 1A29 antibody has been previously described (Tamatani and Miyasaka, 1993). This antibody recognizes the 85–89-kD epitope of ICAM-1 expressed by cytokine activated rat endothelial cells and inhibits homotypic aggregation of T-cell blasts induced by phytohemagglutinin (Tamatani and Miyasaka, 1993). In addition, it specifically recognizes Chinese hamster ovary cells transfected with rat ICAM-1 cDNA (Kita et al., 1992). Note that, though antibodies used for the treatment and immunocytochemical studies were obtained through different sources (Boehringer Ingelheim vs. Genzyme), both were derived from the 1A29 clone.

To inject drugs, a 23-gauge angiocath was inserted into the lateral tail vein after injury. The angiocath was then sealed with an injection cap, and stabilized with surgical tape. A 0.5-cc saline flush was immediately delivered to ensure that no leakage occurred and that the angiocath was patent. Each injection of anti-ICAM-1, IgG, or saline was followed by a 0.5-cc flush to ensure that the drugs entered the circulation and that the angiocath was still patent. Two hours after the last drug injection, the angiocath was removed, pressure was briefly applied to stop any residual bleeding, and the site was cleansed with surgical soap.

Neurological Evaluation

Neurological examinations were performed by an individual blinded to treatment at 1, 7, and 14 days after trauma, as previously detailed (McIntosh et al., 1989). Briefly, scores were derived from three separate motor tests as follows: (1) flexion test—measures forelimb and paw (left and right) extension and placement in response to a perceived fall; (2) lateral pulsion test—measures body and leg resistance (left and right) to a lateral push; and (3) inclined plane test—assesses the ability to maintain balance (in the vertical, left lateral, and right lateral positions) on a progressively inclined surface. Scores for each limb on the individual tests range from 0 (maximal deficit) to 5 (no deficit).

Myeloperoxidase Assay

Injured rats treated with either anti-ICAM-1, IgG, or saline ($n = 5$ – 6 /group) were anesthetized (sodium pentobarbital, 100 mg/kg, i.p.) and perfused with heparinized saline (200 mL) at 26 h after injury. The injured cortex was then quickly removed, frozen (-70°C), and later homogenized (1:6 w/v) in 50 mM KPO₄ buffer with 0.5% hexadecyltrimethylammonium bromide (Sigma Chemicals, St. Louis, MO) as previously described (Bradley et al., 1982; Matsuo et al., 1994). Homogenates were sonicated, subjected to freeze-thaw, and centrifuged ($13,000 \times g$). The supernatant was collected, frozen, and later resuspended in 0.1 M KPO₄ buffer with *o*-diansidine and 0.05% H₂O₂. Absorbance at 460 nm was recorded every 30 sec for 4 min. The rate of decomposition of H₂O₂ by peroxidase in each sample was determined by the rate of change of absorbance at 460 nm. Purified myeloperoxidase (donor: hydrogen-peroxide oxidoreductase [EC 1.11.1.7]; peroxidase; Sigma Chemicals) was included separately in the assay as a standard control. One unit of enzyme activity is that amount of enzyme that decomposes 1 μM of peroxide per minute at 25°C (Worthington, 1993).

Data Analyses

Motor test scores of animals that survived the 14-day test period were expressed as median and individual scores, and analyzed by one-tailed Kruskal-Wallis ANOVA with significance set at $p < 0.05$. One-tailed Mann-Whitney *U* tests (adjusted for ties) were used for post-hoc comparisons. The significance level of the Mann-Whitney *U* tests was set at $p < 0.025$ ($p < 0.05/2$) to correct for multiple comparisons (anti-ICAM-1 vs. saline, and IgG vs. saline). Assay data were expressed as means and standard errors and analyzed by ANOVA, with post-hoc *t* tests with Bonferroni correction for multiple comparisons. For assay data, the significance level was set at $p < 0.05$.

RESULTS

ICAM-1 was expressed by a few large and small blood vessels in the cortex of sham animals and at 1 h after injury. However, ICAM-1-positive vessels were more frequently observed at 10 and 24 h after injury (Figs. 1 and 2). The level of ICAM-1 expression also appeared to be increased at these times, as determined by the intensity of the fluorescent signal. ICAM-1 expression was mainly confined to the area of the cortical lesion and, to some extent, the ipsilateral hippocampus. An abrupt decrease in ICAM-1 expression could be visualized moving from areas proximal to the lesion to areas more distal (Fig. 2). ICAM-1 was not expressed by cortical neurons or in the pyramidal/granule cell layers of the hippocampus. No obvious glial expression patterns were detected.

To assess the effect of injury-induced ICAM-1 expression on neurological outcome, a separate behavioral study was performed. For this study, either anti-ICAM-1 (1 mg/kg), IgG (1 mg/kg), or saline was injected into the tail vein three times—at 1, 12, and 24 h after TBI. Mortality (deaths/subjects prepared) in each group was

as follows: anti-ICAM-1 = 1/15, IgG = 1/11, and saline = 4/14. Motor function was evaluated by three separate motor tests (flexion, pulsion, inclined plane) at 1, 7, and 14 days after injury. Data from the flexion and pulsion tests revealed significant treatment-related improvements in neuroscores (Fig. 3). Results from the pulsion test showed a trend toward improved performance in anti-ICAM-1 and IgG treated groups vs. saline at all times. This trend was more pronounced in the anti-ICAM-1 treated group at 7 days after injury (Mann-Whitney *U* comparison for saline vs. IgG, $p = 0.052$; for saline versus anti-ICAM-1, $p = 0.042$). Treatment effects were significant by Kruskal-Wallis analysis ($p = 0.03$) at 14 days after injury. Both anti-ICAM-1 and IgG significantly improved pulsion scores (Mann-Whitney *U* comparison for saline vs. IgG, $p = 0.017$; for saline vs. anti-ICAM-1, $p = 0.007$).

Similar trends were evident in scores for the flexion test (Mann-Whitney *U* comparison at 7 days—saline vs. IgG, $p = 0.248$; saline vs. anti-ICAM-1, $p = 0.045$). However, this test just missed reaching statistical significance by Kruskal-Wallis analysis ($p = 0.05$) at 14 days

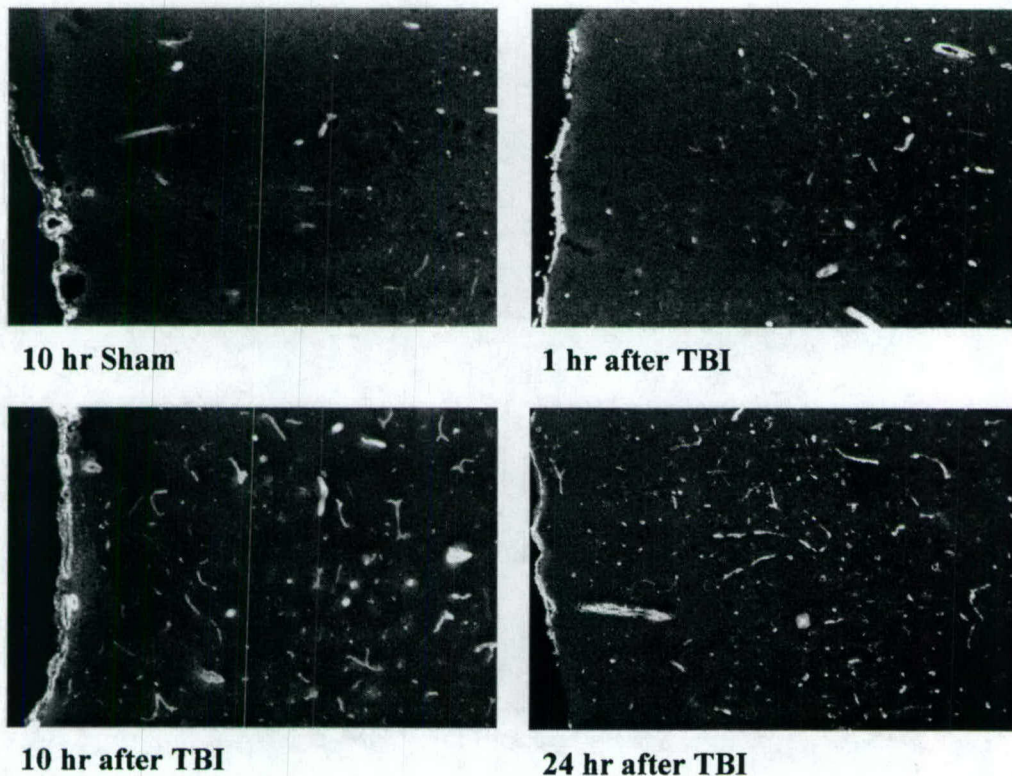


FIG. 1. ICAM-1 expression in the injured cortex from 1 to 24 h after moderate (2.5–2.6 atm) traumatic brain injury (TBI). Representative photomicrographs (25 \times) from $n = 4$ per time point are shown. For sham, animals were anesthetized and prepared surgically, but no injury was performed. The number of ICAM-1-positive vessels and intensity of ICAM-1 staining was increased at 10 and 24 h after TBI relative to 10 h after sham or 1 h after TBI.

ANTI-ICAM-1 AND RECOVERY AFTER TBI IN THE RAT

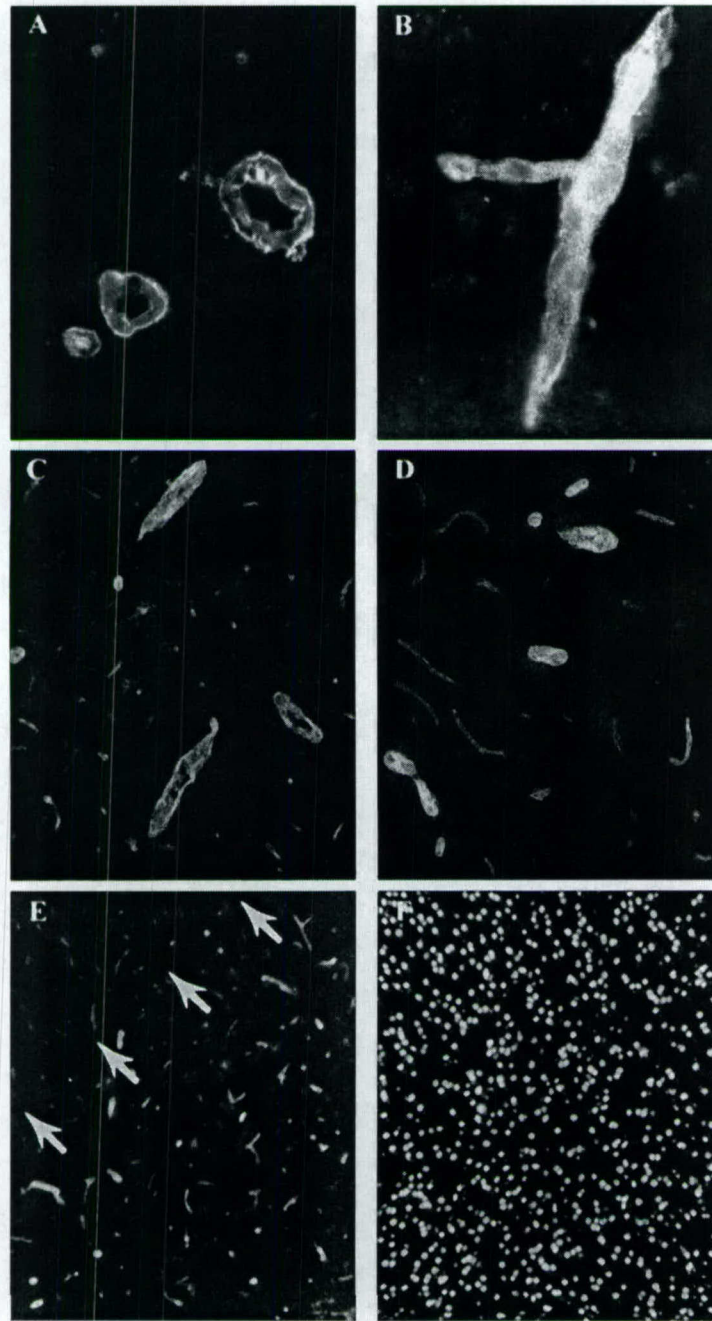


FIG. 2. ICAM-1 expression in blood vessels of the injured cortex 24 h after TBI. ICAM-1 was expressed in both large and small vessels visualized in transverse (**A**, $\times 125$; **C**, $\times 50$) or longitudinal (**B**, $\times 125$; **D**, $\times 50$) orientation. Enhanced expression of ICAM-1 was confined to a discrete cortical area. Arrows circumscribe an abrupt transition zone at the perimeter of the injured region (**E**) where ICAM-1 expression was not increased after injury ($\times 25$). Hoechst 33258 counterstain shows that tissue is present in the cortical region that does not show ICAM-1 increases after injury (**F**; $\times 25$).

after injury. Nevertheless, Mann-Whitney *U* comparisons at this time indicated that both anti-ICAM-1 ($p = 0.014$) and IgG ($p = 0.016$) significantly improved flexion scores, compared to saline controls. Overall, anti-ICAM-

1 treated animals scored somewhat better than IgG treated animals in both flexion and pulsion tests at 7 and 14 days after injury, as *p* values versus saline controls for this group were, in the majority of cases, lower than for IgG.

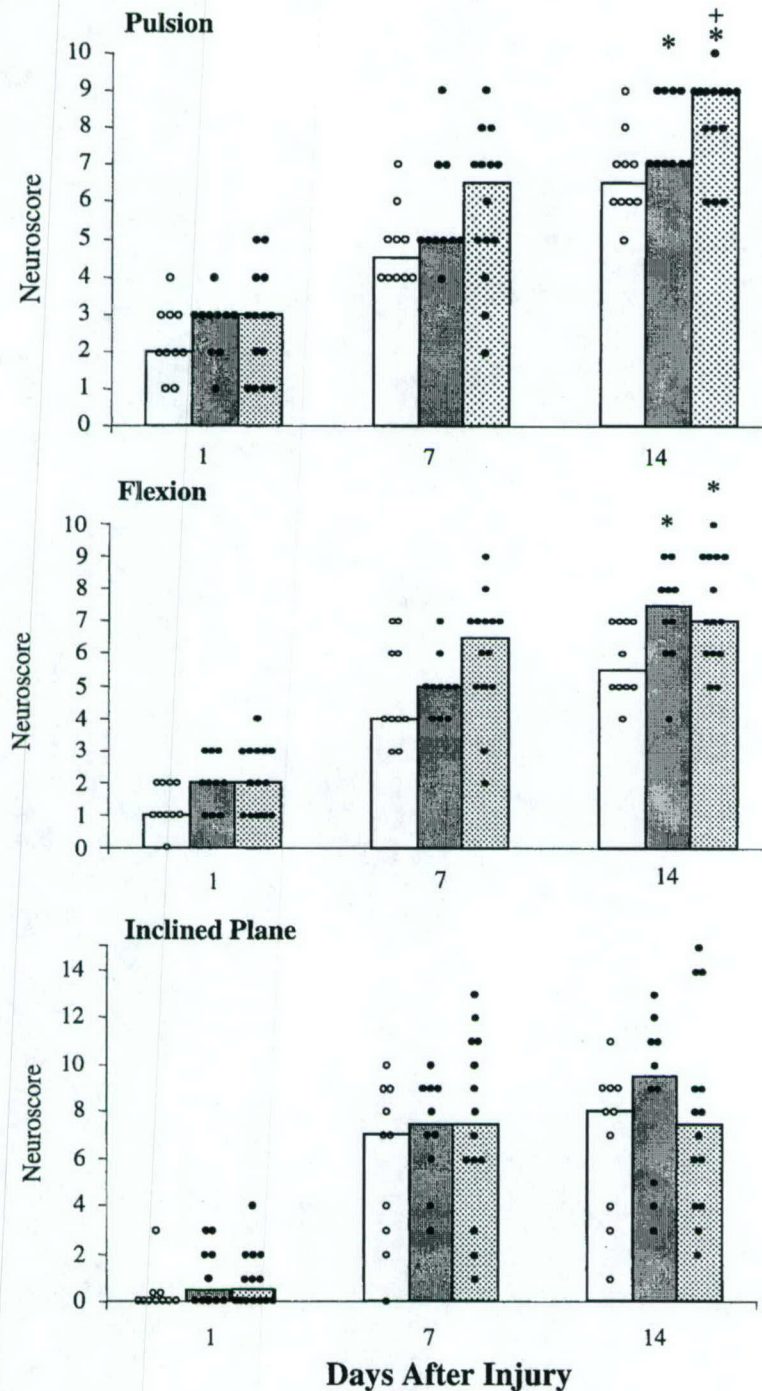


FIG. 3. Effect of intravenous administration of anti-ICAM-1 antibody on neurological recovery as assessed by individual motor scores. Anti-ICAM-1 antibody (1 mg/kg in saline), IgG (1mg/kg in saline), or saline was injected into the lateral tail vein at 1, 10, and 24 h after moderate (2.5–2.6 atm) lateral fluid-percussion brain injury. Histograms represent median neuroscores for each group of 14 day survivors on each of three individual motor tests: clear bars/clear dots = saline controls ($n = 10$), gray bars/black dots = IgG ($n = 10$), dotted bars/black dots = anti-ICAM-1 ($n = 14$). Single dots represent scores of individual animals. $^+p < 0.05$ by Kruskal-Wallis ANOVA; $*p < 0.025$ versus control using one-tailed Mann-Whitney U comparisons (adjusted for ties). To adjust for multiple Mann-Whitney U comparisons, only $p < 0.025$ ($0.05/2$) were considered statistically significant.

In contrast to the pulsion and flexion data, a wide range of scores, with no treatment effect for either anti-ICAM-1 or IgG, was observed on the inclined plane test (Fig. 3).

To determine the effect of anti-ICAM-1 or IgG treatment on neutrophil invasion within the injured cortex, an additional study was performed. For this, separate groups of animals were prepared that were treated as detailed for the neurobehavioral study, with the exception that their brains were removed at 26 h after injury. Myeloperoxidase (MPO) activity, which serves as an indirect measure of neutrophil invasion (Bradley et al., 1982), was assayed in cortical extracts prepared from these animals. MPO activity was significantly reduced in the cortex of injured animals treated with anti-ICAM-1, in comparison to samples from injury alone or injury + saline treated controls (Fig. 4). Anti-ICAM-1 treatment reduced MPO activity to one-third of the level observed in controls. Treatment with IgG resulted in a trend toward lower MPO activity, but this was not significantly different from controls.

DISCUSSION

ICAM-1 expression has not yet been evaluated after lateral fluid-percussion injury; thus, it was necessary to our hypothesis to first determine whether ICAM-1 is increased in this model of traumatic injury. ICAM-1 expression increased relatively late (10 and 24 h), in both large and small blood vessels restricted to the site of injury. These results verify that ICAM-1 is elevated after lateral fluid-percussion injury, and indicate that the distribution and time course of this increase resembles that previously reported in models of contusive injury and cerebral ischemia (Carlos et al., 1997; Isaksson et al., 1997; Okada et al., 1994; Wang et al., 1994). This same time course also approximates cortical PMN accumulation (Soares et al., 1995). Elevated expression of ICAM-1 in microvessels indicates that it may potentially contribute to "no-reflow" phenomena and associated blood flow reductions after TBI, as previously described in association with transient, focal ischemia (Mori et al., 1992; Palmer, 1995; Del Zoppo, 1997).

Endothelial cells express ICAM-1 in response to cytokines, free radicals, and physical disruption, all of which are known factors in the pathophysiology of TBI (Hubbard et al., 2000; McKeating et al., 1998a; Feuerstein et al., 1998). Our data suggest that ICAM-1 expression is primarily confined to the vascular system after TBI, although we did not perform cell-type specific double-labeling studies that would conclusively prove this. Such a distinct association with the vascular system is similar to observations from models of stroke, and contrasts with findings from certain neuroinflammatory dis-

eases (multiple sclerosis, meningitis, HIV-induced neuropathy) in which ICAM-1 is expressed by glia (Seilhean et al., 1997; Lewczuk et al., 1998). Therefore, the role of this molecule in traumatic injuries may be significantly different from these other conditions. Indeed, many *in vitro* studies show that neurons, astrocytes, oligodendrocytes, and microglia all express ICAM-1 in culture, and that ICAM-1-associated signal transduction cascades appear to be cell-type specific (Shrikant et al., 1995; Birdsall, 1991; Hery et al., 1995; Zielasek et al., 1993; Lee et al., 1999).

The present results are the first to show a beneficial effect of anti-ICAM-1 therapy on neurological recovery after injury. However, this effect appears to be relatively modest. Anti-ICAM-1 treatment significantly improved function on the flexion and pulsion tests 14 days after injury, compared to saline controls. Treated animals also showed strong trends toward improvement at most other times after injury. Nonetheless, these trends are not statistically different from controls because of the conservative correction factor ($p < 0.05/2$) used to protect against a type I error due to multiple post-hoc nonparametric comparisons.

The dosage, timing, and route of administration of anti-ICAM-1 used for this study (1 mg/kg at 1, 10, and 24 h after TBI) was based on previous use of a similar multiple administration protocol for this antibody (1A29) in stroke models, as well as the present data showing the time course of ICAM-1 expression in our model. Anti-ICAM-1 reduced lesion volume after transient focal

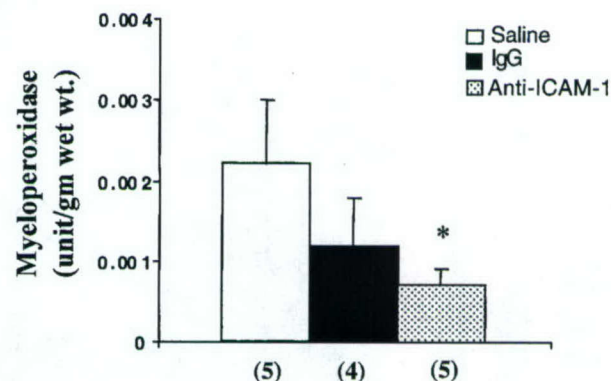


FIG. 4. Myeloperoxidase activity in the injured cortex 26 h after TBI: effects of treatment with anti-ICAM-1, IgG, or saline. Treatments (1 mg/kg in saline) or saline control were given intravenously at 1, 10, and 24 h after moderate TBI (2.5–26 atm) as described for Figure 3. Histograms indicate means \pm SEM for groups as indicated in the legend. Numbers beneath the x-axis indicate the number of animals/group. * $p < 0.05$ versus injured control using *t* tests with Bonferroni correction.

stroke when given twice intravenously, first at a dose of 1 mg/kg upon reperfusion and again at a dose of 0.5 mg/kg, 22 h later (Zhang et al. 1994). In a subsequent study, the dosages were increased to 2 mg/kg and 1 mg/kg, respectively, but treatment began at 1 h after reperfusion (Zhang et al., 1995). Equal levels of protection were seen in both studies, though direct comparisons are not valid because of the delay in treatment used in the latter. We selected a dose within this range and also utilized multiple administrations, as the half-life of the antibody has not been reported. Because our immunocytochemical data indicated that ICAM-1 was elevated at 10 and 24 h after TBI, anti-ICAM-1 was given at these times, as well as 1 h after TBI, to antagonize increases in ICAM-1 that may have occurred between 1 and 10 h after injury. Although this administration scheme was sufficient to show that anti-ICAM-1 may improve outcome and reduce neutrophil accumulation after TBI, additional studies are necessary to determine whether different treatment schedules/dosages would provide more substantial improvement.

Though not the only repository, neutrophils are the major source of MPO in both blood and brain (Bradley et al., 1982; Barone et al., 1991). Thus, MPO assays serve as estimates for the presence of neutrophils, but do not provide direct information about their actual number and individual activation states. Nonetheless, taking these considerations into account, the amount of MPO activity in tissue homogenates has been used extensively as a measure of neutrophil accumulation (Zhang et al., 1995; Hamada et al., 1996; Clark et al., 1996; Matsuo et al., 1994). By this method, we found that anti-ICAM-1 treatment decreased neutrophil accumulation by ~60% in the injured cortex 26 h after injury. A similar reduction in parenchymal neutrophil influx by anti-ICAM-1 was observed after cortical contusion injury (Carlos et al., 1997), although, in that study, functional status was not evaluated. However, both neurological recovery and neutrophil invasion after anti-ICAM-1 treatment have been assessed in models of focal cerebral ischemia and spinal cord trauma, where functional improvement coincided with 25–40% reductions in tissue neutrophil accumulation (Zhang et al., 1994; Hamada et al., 1996). The present data are in agreement with these observations. Taken together, these studies suggest that anti-ICAM-1 treatment need not completely block neutrophil extravasation for functional improvement to be observed after ischemic or traumatic CNS injuries.

Partial blockade of neutrophil accumulation by anti-ICAM-1 may indicate that other independent mechanisms contribute to invasion in these models of CNS injury. Complete exclusion of leukocytes may require inhibition of several adhesion molecules and/or their

counter-receptors because of the functional redundancy displayed by adhesion molecules, in general (Dunon et al., 1996; McKeating et al., 1998a; Kochanek et al., 1992). Apart from this, some leukocyte infiltration after CNS injury may occur directly, without the involvement of adhesion molecules, or the paradigm of rolling, sticking, and diapedesis (Dunon et al., 1996). Alternative routes of entry such as this may contribute a subpopulation of neutrophils within the parenchyma that would be expected to be unresponsive to any antiadhesion treatment strategy.

Additionally, though the present data implicate neutrophil accumulation as a secondary injury event that may contribute to neurological deterioration, it is worth noting that neurological deficits and ICAM-1 elevations occur after traumatic axonal injury, without concomitant neutrophil accumulation (Rancan et al., 2001). Thus, ICAM-1 may also be involved in neutrophil-independent responses, likely mediated through glia and/or endothelium (Shrikant et al., 1996; Etienne et al., 1998), whose role in injury remains to be defined.

In contrast to the present results, recent studies in a contusive model of TBI did not show any improvements in neurological recovery, tissue sparing, or neutrophil influx in either ICAM-1 $-/-$ or ICAM-1 $/P$ -selectin $-/-$ mice, when compared to their respective wild type controls (Whalen et al., 1999a, 2000). Similar inconsistencies have been reported after spinal cord trauma, where an anti-ICAM-1 antagonist improved neurological recovery and reduced both neutrophil invasion and lesion size (Hamada et al., 1996), whereas ICAM-1 knock-out mice showed no significant change in function or lesion size, and reductions of neutrophil infiltration only in white matter (Isaksson et al., 2000). The reasons for such discrepancies are difficult to pinpoint. Expression profiles of knock-out mice have revealed concurrent alterations in inflammatory components other than ICAM-1 (Sligh et al., 1993; Whalen et al., 2000), and these may be influencing the results in ways that are not yet understood. However, it is notable that in studies of focal transient ischemia, which are more numerous than those of traumatic injuries, data from both genetic models and pharmacological strategies uniformly support an important role for ICAM-1 in neutrophil invasion, secondary injury and neurological dysfunction (Connolly et al., 1996; Bowes et al., 1993; Zhang et al., 1994; Soriano et al., 1996; Clark et al., 1991). Therefore, it seems more likely that the discrepancies evident in trauma work may relate to specific characteristics of traumatic injury, such as whether a significant ischemic/reperfusion component exists in the particular model and level of traumatic injury employed. In this regard, it is also worth pointing out that, at least in the fluid-percussion model, a signif-

icant amount of neurodegeneration occurs in regions apart from areas of neutrophil invasion (i.e., subcortical) (Soares et al., 1995), and thus may be unrelated to ICAM-1 associated events.

Pharmacological adhesion molecule blockade strategies are complex, especially when treatment involves antibodies as antagonists. Antibody-based anti-ICAM-1 treatments may initiate undesirable secondary side effects, including reaction to the foreign antibody protein, activation of complement by the Fc portion of antibody clusters bound to ICAM-1, and activation of ICAM-1-mediated cascades by antibody, rather than $\beta 2$ integrin cross-linking. These possible complications of antibody therapy have recently been summarized (DeGraba, 1998) and implicated (Vuorte et al., 1999; Furuya et al., 2001) as potential explanations for a lack of benefit, and adverse side effects, noted after an anti-ICAM-1 regimen in a recent stroke trial (Schneider, 1998). The use of F(ab₂') fragments, or other alternatives, may resolve such complications.

Some of the generalized responses to antibody administration may also be induced by antibodies utilized as "nonspecific" controls, because of common structural components (i.e., Fc portion) present in all antibody proteins. Therefore, we included matched antibody controls in the present study and found, surprisingly, that this treatment also significantly improved neurological function in comparison to treatment with the saline vehicle. Statistically, the effect of IgG was as good as anti-ICAM-1, although anti-ICAM-1 showed much better trends toward improved function than did IgG at 1 week after injury (shown in Fig. 3 and supported by lower *p* values for relevant Mann-Whitney *U* tests). In addition, although anti-ICAM-1 significantly reduced neutrophil accumulation, but IgG did not, small sample sizes may have contributed to this conclusion, as both anti-ICAM-1 and IgG reduced myeloperoxidase by at least 50%. The observation that a nonspecific antibody improved function suggests that at least some of the effects of anti-ICAM-1 may not reflect interaction with ICAM-1, but rather, general properties of antibodies, or an effect specifically associated with injection of mouse IgG into the rat. In previous studies, either saline or IgG have been used as controls, but not both, which precluded such an observation. The present data indicate that results from antibody controls should be approached with caution, and that additional controls for a potential nonspecific antibody effect should be incorporated in studies utilizing antibodies as antagonists. These findings are similar to those recently demonstrating neuroprotection and improved function after injection of albumin, another protein which had previously been used as a nonspecific control for injection of protein (Belayev et al., 1999). In that case, additional

studies have shown that albumin may act through mechanisms previously unconsidered (Ginsberg et al., 2001). Such may be true with IgG, as well.

Though it is beyond the scope of this work to determine what may account for the IgG effect, speculative explanations might include the following: (1) a host inflammatory/acute phase reaction to the mouse challenge that either counteracts or modulates TBI-induced inflammation in favor of repair/recovery; (2) contamination of the IgG preparation with aggregates that have anticomplement activity (Lundblad et al., 1986), and thus may influence recovery (Kaczorowski et al., 1995); and (3) the administration schedule and/or dose of IgG may have altered colloid oncotic pressure, which has been controversially associated with hemodynamic changes and/or edema after injury (Cole et al., 1996; Zhuang et al., 1995).

Lastly, with regard to the IgG effect, it is worth noting that many studies in models of cerebral ischemia demonstrated beneficial effects of anti-ICAM-1 compared to nonspecific antibody controls only, which leaves open the possibility that the positive effects of anti-ICAM-1 treatment may be more substantial in such models than has actually been appreciated.

In conclusion, the present data show that ICAM-1 expression is increased in cerebral vasculature at 10–24 h after lateral fluid-percussion brain injury. Intravenous injection of anti-ICAM-1 at 1, 10, and again at 24 hr after injury reduced neutrophil influx and improved outcome in two of three neurological tests. However, similar treatment with a nonspecific mouse IgG antibody control also improved outcome. Though these data implicate a potential role for ICAM-1 in neurological dysfunction and neutrophil invasion after TBI, they also suggest that antibody treatment strategies may nonspecifically alter outcome, as well.

ACKNOWLEDGMENTS

The anti-ICAM-1 antibody was generously provided by Dr. Robert Rothlein (Boehringer Ingelheim, Ridgefield, CT). We thank Susan Wishner and Randi Goodnight for technical assistance. This work was supported by R49CCR306634-07 from the Centers for Disease Control to A.I.F. S.M.K. was supported in part by NIH 5T32HD07459.

REFERENCES

- BARONE, F.C., HILLEGASS, L.M., PRICE, W.J., et al. (1991). Polymorphonuclear leukocyte infiltration into cere-

- bral focal ischemic tissue: myeloperoxidase activity assay and histologic verification. *J. Neurosci. Res.* **29**, 336–345.
- BELAYEV, L., ALONSO, O.F., HUH, P.W., et al. (1999). Posttreatment with high-dose albumin reduces histopathological damage and improves neurological deficit following fluid percussion brain injury in rats. *J. Neurotrauma* **16**, 445–453.
- BIRDSALL, H.H. (1991). Induction of ICAM-1 on human neural cells and mechanisms of neutrophil-mediated injury. *Am. J. Pathol.* **139**, 1341–1350.
- BOWES, M.P., ZIVIN, J.A., and ROTHLEIN, R. (1993). Monoclonal antibody to the ICAM-1 adhesion site reduces neurological damage in a rabbit cerebral embolism stroke model. *Exp. Neurol.* **119**, 215–219.
- BOWES, M.P., ROTHLEIN, R., FAGAN, S.C., et al. (1995). Monoclonal antibodies preventing leukocyte activation reduce experimental neurologic injury and enhance efficacy of thrombolytic therapy. *Neurology* **45**, 815–819.
- BRADLEY, P.P., PRIEBAT, D.A., CHRISTENSEN, R.A., et al. (1982). Measurement of cutaneous inflammation: estimation of neutrophil content with an enzyme marker. *J. Invest. Derm.* **78**, 206–209.
- CARLOS, T.M., CLARK, R.B.S., FRANCIOLA-HIGGINS, D., et al. (1997). Expression of endothelial adhesion molecules and recruitment of neutrophils after traumatic brain injury in rats. *J. Leukoc. Biol.* **61**, 279–285.
- CLARK, R.S., CARLOS, T.M., SCHIDING, J.K., et al. (1996). Antibodies against Mac-1 attenuate neutrophil accumulation after traumatic brain injury in rats. *J. Neurotrauma* **13**, 333–341.
- CLARK, W.M., MADDEN, K.P., ROTHLEIN, et al. (1991). Reduction of central nervous system ischemic injury by monoclonal antibody to intercellular adhesion molecule. *J. Neurosurg.* **75**, 623–627.
- COLE, D.J., DRUMMOND, J.C., PATEL, P.M., et al. (1996). Effect of oncotic pressure of diaspirin cross-linked hemoglobin (DCLHb) on brain injury after temporary focal cerebral ischemia in rats. *Anesth. Analg.* **83**, 342–347.
- CONNOLLY, E.S., JR., WINFREE, C.J., SPRINGER, T.A., et al. (1996). Cerebral protection in homozygous null ICAM-1 mice after middle cerebral artery occlusion. *J. Clin. Invest.* **97**, 209–216.
- DEGRABA, T.J. (1998) The role of inflammation after acute stroke. *Neurology* **51** (Suppl 3), S62–S68.
- DEL ZOPPO, G.J. (1997). Microvascular responses to cerebral ischemia/inflammation. *Ann. NY Acad. Sci.* **823**, 132–147.
- DUNON, D., PIALI, L., and IMHOF, B.A. (1996). To stick or not to stick: the new leukocyte homing paradigm. *Curr. Opin. Cell Biol.* **8**, 714–723.
- ETIENNE, S., ADAMSON, P., GREENWOOD, J., et al. (1998). ICAM-1 signaling pathways associated with Rho activation in microvascular brain endothelial cells. *J. Immunol.* **161**, 5755–5761.
- FEUERSTEIN, G.Z., WANG, X., and BARONE, F.C. (1998). The role of cytokines in the neuropathology of stroke and neurotrauma. *Neuroimmunomod.* **5**, 143–159.
- FURUYA, K., TAKEDA, H., AZHAR, S., et al. (2001). Examination of several potential mechanisms for the negative outcome in a clinical stroke trial of Enlimomab, a murine anti-human intercellular adhesion molecule-1 antibody. *Stroke* **32**, 2665–2674.
- GRADY, M.S., CODY JR., R.F., Maris, D.O., et al. (1999). P-Selectin blockade following fluid-percussion injury: behavioral and immunochemical sequelae. *J. Neurotrauma* **16**, 13–25.
- GINSBERG, M.D., ZHAO, W., BELAYEV, L., et al. (2001). Diminution of metabolism/blood flow uncoupling following traumatic brain injury in rats in response to high-dose human albumin treatment. *J. Neurosurg.* **94**, 499–509.
- HAMADA, Y., IKATA, T., KATOH, S., et al. (1996). Involvement of an intercellular adhesion molecule 1-dependent pathway in the pathogenesis of secondary changes after spinal cord injury in rats. *J. Neurochem.* **66**, 1525–1531.
- HERY, C., SEBIRE, G., PEUDENIER, S., et al. (1995). Adhesion to human neurons and astrocytes of monocytes: the role of interaction of CR3 and ICAM-1 and modulation by cytokines. *J. Neuroimmunol.* **57**, 101–109.
- HUBBARD, A.K., and ROTHLEIN, R. (2000). Intercellular adhesion molecule-1 (ICAM-1) expression and cell signaling cascades. *Free Radic. Biol. Med.* **28**, 1379–1386.
- ISAKSSON, J., LEWEN, A., HILLERED, L., et al. (1997). Up-regulation of intercellular adhesion molecule 1 in cerebral microvessels after cortical contusion trauma in a rat model. *Acta Neuropathol.* **94**, 16–20.
- ISAKSSON, J., FAROOQUE, M., and OLSSON, Y. (2000). Spinal cord injury in ICAM-1 deficient mice: assessment of functional and histopathological outcome. *J. Neurotrauma* **17**, 333–344.
- JAESCHKE, H., SMITH, C.W., CLEMENS, M.G., et al. (1996). Mechanisms of inflammatory liver injury: adhesion molecules and cytotoxicity of neutrophils. *Toxicol. Appl. Pharmacol.* **139**, 213–226.
- JEAN, W.C., SPELLMAN, S.R., NUSSBAUM, E.S., et al. (1998). Reperfusion injury after focal cerebral ischemia: the role of inflammation and the therapeutic horizon. *Neurosurgery* **43**, 1382–1397.
- JOHNSON, G.D., and NOGUIERA ARAUJO, G.M. (1981). A simple method of reducing the fading of immunofluorescence during microscopy. *J. Immunol. Meth.* **43**, 349–350.
- KACZOROWSKI, S.L., SCHIDING, J.K., TOTTH, C.A., et al. (1995). Effect of soluble complement receptor-1 on neutrophil accumulation after traumatic brain injury in rats. *J. Cereb. Blood Flow Metab.* **15**, 860–854.

ANTI-ICAM-1 AND RECOVERY AFTER TBI IN THE RAT

- KITA, Y., TAKASHI, T., IIGO, Y., et al. (1992). Sequence and expression of rat ICAM-1. *Biochim Biophys Acta* **1131**, 108–110.
- KOCHANNEK, P.M., and HALLENBECK, J.M. (1992). Polymorphonuclear leukocytes and monocytes/macrophages in the pathogenesis of cerebral ischemia and stroke. *Stroke* **23**, 1367–1379.
- LEE, S.J., and BENVENISTE, E.N. (1999). Adhesion molecule expression and regulation on cells of the nervous system. *J. Neuroimmunol.* **98**, 77–88.
- LEWCZUK, P., REIBER, H., and TUMANI, H. (1998). Inter-cellular adhesion molecule-1 in cerebrospinal fluid—the evaluation of blood-derived and brain-derived fractions in neurological diseases. *J. Neuroimmunol.* **87**, 156–161.
- LUNDBLAD, J.L., MITRA, G., STERNBERG, M.M., et al. (1986). Comparative studies of impurities in intravenous immunoglobulin preparations. *Rev. Infect. Dis.* **8 Suppl 4**, S382–S390.
- MATSUO, Y., ONODERA, H., SHIGA, Y., et al. (1994). Correlation between myeloperoxidase-quantified neutrophil accumulation and ischemic brain injury in the rat. *Stroke* **25**, 1469–1475.
- MAZZONI, M.C., and SCHMID-SCHONBEIN, G.W. (1996). Mechanisms and consequences of cell activation in the microcirculation. *Cardiovasc. Res.* **32**, 709–719.
- MCINTOSH, T.K., VINK, R., NOBLE, L., et al. (1989). Traumatic brain injury in the rat: characterization of a lateral fluid-percussion model. *Neuroscience* **28**, 233–244.
- McKeating, E.G., and ANDREWS, P.J. (1998a). Cytokines and adhesion molecules in acute brain injury. *Br. J. Anaesth.* **80**, 77–84.
- McKEATING, E.G., ANDREWS, P.J., and MASCIA, L. (1998b) The relationship of soluble adhesion molecule concentrations in systemic and jugular venous serum to injury severity and outcome after traumatic brain injury. *Anesth. Analg.* **86**, 759–765.
- McKEATING, E.G., ANDREWS, P.J., and MASCIA, L. (1998c). Leukocyte adhesion molecule profiles and outcome after traumatic brain injury. *Acta Neurochir. Suppl.* **71**, 200–202.
- MORI, E., DEL ZOPPO, G.J., CHAMBERS, J.D., et al. (1992). Inhibition of polymorphonuclear leukocyte adherence suppresses no-reflow after focal cerebral ischemia in baboons. *Stroke* **23**, 712–718.
- OKADA, Y., COPELAND, B.R., MORI, E., et al. (1994). P-selectin and intercellular adhesion molecule-1 expression after focal brain ischemia and reperfusion. *Stroke* **25**, 202–211.
- PALMER, C. (1995). Hypoxic-ischemic encephalopathy. Therapeutic approaches against microvascular injury, and the role of neutrophils, PAF, and free radicals. *Clin. Perinatol.* **22**, 481–517.
- PAXINOS, G., and WATSON, C. (1986). *The Rat Brain in Stereotaxic Coordinates*. Academic Press: San Diego.
- PLEINES, U.E., STOVER, J.F., KOSSMANN, T., et al. (1998). Soluble ICAM-1 in CSF coincides with the extent of cerebral damage in patients with severe traumatic brain injury. *J. Neurotrauma* **15**, 399–409.
- RANCAN, M., OTTO, V.I., HANS, V.H.J., et al. (2001). Up-regulation of ICAM-1 and MCP-1 but not of MIP-2 and sensorimotor deficit in response to traumatic axonal injury in rats. *J. Neurosci. Res.* **63**, 438–446.
- SCAPINI, P., LAPINET-VERA, J.A., GASPERINI, S., et al. (2000). The neutrophil as a cellular source of chemokines. *Immunol. Rev.* **177**, 195–203.
- SEILHEAN, D., DZIA-LEPFOUNDZOU, A., SAZDOVITCH, V., et al. (1997). Astrocytic adhesion molecules are increased in HIV-1-associated cognitive/motor complex. *Neuropathol. App. Neurobiol.* **23**, 83–92.
- SCHNEIDER, D., BERROUSCHOT, J., BRANDT, T., et al. (1998). Safety, pharmacokinetics and biological activity of enlimomab (anti-ICAM-1 antibody): an open-label, dose escalation study in patients hospitalized for acute stroke. *Eur. Neurol.* **40**, 78–83.
- SHRIKANT, P., and BENVENISTE, E.N. (1996). The central nervous system as an immunocompetent organ: role of glial cells in antigen presentation. *J. Immunol.* **157**, 1819–1822.
- SHRIKANT, P., WEBER, E., JILLING, T., et al. (1995). Intercellular adhesion molecule-1 gene expression by glial cells. *J. Immunol.* **155**, 1489–1501.
- SLIGH, J.E., BALLANTYNE, C.M., RICH, S.S., et al. (1993). Inflammatory and immune responses are impaired in mice deficient in intercellular adhesion molecule-1. *Proc. Natl. Acad. Sci. USA* **90**, 8529–8533.
- SOARES, H.D., HICKS, R.R., SMITH, D., et al. (1995). Inflammatory leukocytic recruitment and diffuse neuronal degeneration are separate pathological processes resulting from traumatic brain injury. *J. Neurosci.* **15**, 8223–8233.
- SORIANO, S.G., LIPTON, S.A., WANG, Y.F., et al. (1996). Intercellular adhesion molecule-1-deficient mice are less susceptible to cerebral ischemia-reperfusion injury. *Ann. Neurol.* **39**, 618–624.
- TAMATANI, T., and MIYASAKA, M. (1993). Identification of monoclonal antibody reactive with the rat homologue of ICAM-1, and evidence for differential involvement of ICAM-1 in the adherence of resting versus activated lymphocytes to high endothelial cells. *Int. Immunol.* **2**, 166–172.
- UHL, M.W., BIAGAS, K.V., GRUNDL, P.D., et al. (1994). Effects of neutropenia on edema, histology, and cerebral blood flow after traumatic brain injury in rats. *J. Neurotrauma* **11**, 303–315.
- VUORTE, J., LINDSBERG, P.J., KASTE, M., et al. (1999). Anti-ICAM-1 monoclonal antibody R6.5 (Enlimomab) pro-

- motes activation of neutrophils in whole blood. *J. Immunol.* **162**, 2353-2357.
- WANG, X., SIREN, A.-L., LIU, Y., et al. (1994). Upregulation of intercellular adhesion molecule 1 (ICAM-1) on brain microvascular endothelial cells in rat ischemic cortex. *Mol. Brain Res.* **26**, 61-68.
- WHALEN, M.J., CARLOS, T.M., KOCHANNEK, P. M., et al. (1998). Soluble adhesion molecules in CSF are increased in children with severe head injury. *J. Neurotrauma* **15**, 777-787.
- WHALEN, M.J., CARLOS, T.M., DIXON, C.E., et al. (1999a). Effect of traumatic brain injury in mice deficient in intercellular adhesion molecule-1: assessment of histopathologic and functional outcome. *J. Neurotrauma* **16**, 299-309.
- WHALEN, M.J., CARLOS, T.M., KOCHANNEK, P.M., et al. (1999b). Neutrophils do not mediate blood-brain barrier permeability early after controlled cortical impact in rats. *J. Neurotrauma* **16**, 583-594.
- WHALEN, M.J., CARLOS, T.M., DIXON, C.E., et al. (2000). Reduced brain edema after traumatic brain injury in mice deficient in P-selectin and intercellular adhesion molecule-1. *J. Leukoc. Biol.* **67**, 160-168.
- WORTHINGTON, V. (1993). *Worthington Enzyme Manual*. Worthington Biochemical Corporation: Freehold, NJ.
- ZHANG, R.L., CHOPP, M., LI, Y., et al. (1994). Anti-ICAM-1 antibody reduces cell damage after transient middle cerebral artery occlusion in the rat. *Neurology* **44**, 1747-1751.
- ZHANG, R.L., CHOPP, M., JIANG, N., et al. (1995). Anti-intercellular adhesion molecule-1 antibody reduces ischemic cell damage after transient but not permanent middle cerebral artery occlusion in the Wistar rat. *Stroke* **26**, 1438-1443.
- ZHUANG, J., SHACKFORD, S.R., SCHMOKER, J.D., et al. (1995). Colloid infusion after brain injury: effect on intracranial pressure, cerebral blood flow, and oxygen delivery. *Crit. Care Med.* **23**, 140-148.
- ZIELASEK, J., ARCHELOS, J.J., TOYKA, K.V., et al. (1993). Expression of intercellular adhesion molecule-1 on rat microglial cells. *Neurosci. Lett.* **153**, 136-139.

Address reprint requests to:
 Susan M. Knobloch, Ph.D.
 Georgetown University Medical Center
 3970 Reservoir Rd. NW
 Washington, DC 20007

E-mail: knobblachs@giccs.georgetown.edu

Ceramide induces neuronal apoptosis through the caspase-9/caspase-3 pathway

Vilen A. Movsesyan, Alexander G. Yakovlev, Elvira A. Dabaghyan, Bogdan A. Stoica, and Alan I. Faden*

Department of Neuroscience, Georgetown University Medical Center, 3970 Reservoir Road, N.W., Research Building, Rm. EP12, Washington, DC 20057, USA

Received 11 October 2002

Abstract

C₂-ceramide, a cell-permeable analog of ceramide, caused cell death in cultured rat cortical neuronal cells. C₂-ceramide-induced neuronal loss was accompanied by upregulation of caspase-3 activity, measured by cleavage of its fluorogenic substrate Ac-DEVD-AMC. Similar results were obtained when cortical neuronal cultures were treated with sphingomyelinase, an enzyme responsible for ceramide formation in the cell. Morphological evaluation of C₂-ceramide-treated cortical neurons showed nuclear condensation and fragmentation as visualized by Hoechst 33258 staining. Co-administration of the selective caspase-3 inhibitor z-DEVD-fmk or caspase-9 inhibitor z-LEHD-fmk significantly reduced C₂-ceramide-induced cell death, while co-application of the caspase-8, inhibitor z-IETD-fmk, was without effect. Immunoblot analysis of protein extracts from C₂-ceramide-treated cortical neuronal cultures revealed upregulation of active caspase-9 and caspase-3 protein levels, whereas presence of active caspase-8 immunoreactivity was undetectable in this system. Administration of C₂-ceramide to SH-SY5Y human neuroblastoma cells also caused apoptotic cell death. Moreover, ceramide-induced cell death was significantly decreased in caspase-9 dominant-negative SH-SY5Y cells, while both caspase-8 dominant-negative cultures and mock-transfected cells showed equally high levels of cell death following C₂-ceramide treatment. Taken together, these data suggest that neuronal death induced by ceramide may be linked to the caspase-9/caspase-3 regulated intrinsic pathway of cellular apoptosis.

© 2002 Elsevier Science (USA). All rights reserved.

Keywords: Caspases; Ceramide; Neuronal death; Cortical neurons; SH-SY5Y

Ceramide, an evolutionally conserved sphingolipid, has been implicated as a second messenger in the regulation of cell cycle arrest, cell differentiation, or cellular apoptosis (for review see [1–4]). Intracellular levels of ceramide can be modulated via several pathways, including de novo synthesis, enzymatic transformation from sphingomyelin by sphingomyelinases, or by regulation of ceramide degradation [5]. Involvement of the ceramide pathway has been suggested for a variety of neurological disorders such as epilepsy, Alzheimer's and Parkinson's diseases, and cerebral ischemia. [6–9]. However, the precise role for ceramide in processes of neuronal death and survival remains uncertain, as effects

of ceramide on cell viability appear to depend on model system and experimental conditions. Thus, protective effects have been reported following intraventricular injections of C₂-ceramide in an immature rat brain hypoxia-ischemia model [9,10]. In contrast, Yu et al. [11] demonstrated beneficial effects of ceramide downregulation in mice subjected to cerebral ischemia, both in acidic sphingomyelinase knockouts and after pharmacological sphingomyelinase inhibition. Upregulation of ceramide levels was observed in cultured rat cerebellar granule cells (CGC), and in cortical neurons associated with apoptosis induced by trophic support withdraw or treatment with etoposide [12]. It was also shown that serum deprivation caused an increase in ceramide levels with concomitant apoptosis in an HN9.10e neuronal cell line [13]. Administration of cell-permeable ceramide analogs or sphingomyelinase causes neuronal cell death

* Corresponding author. Fax: 1-202-687-0617.

E-mail address: fadena@georgetown.edu (A.I. Faden).

in various neuronal culture systems, such as CGC, cortical neurons, HMN1 motor neuron cells, and hippocampal neurons [12,14–18]. However, despite growing evidence suggesting a role for ceramide in neuronal apoptosis, specific intracellular pathways of ceramide-induced neuronal death remain to be identified.

In the present study, we examine the mechanisms of ceramide-induced cell death using rat cortical neuronal cultures and SH-SY5Y human neuroblastoma cells. Our results show caspase-3 activation and nuclear fragmentation in ceramide-treated cells and provide further evidence in support of a role for ceramide in neuronal apoptosis. We also demonstrate involvement of the intrinsic caspase-9 pathway, but not the extrinsic caspase-8 pathway in ceramide-induced neuronal apoptosis.

Materials and methods

Cell cultures

Rat cortical neuronal cultures. Cortical neuronal cultures were derived from rat embryonic cortices (Taconic, Germantown, NY) as previously described [19]. Briefly, cortices from 17–18-day-old Sprague–Dawley rat embryos were cleaned from meninges and blood vessels in Krebs–Ringer's bicarbonate buffer containing 0.3% bovine serum albumin (BSA, Gibco, Gaithersburg, MD). Cortices were minced and dissociated in the same buffer with 1800 U/ml trypsin (Sigma, St. Louis, MO) at 37 °C for 20 min. Following the addition of 200 U/ml DNase I (Sigma) and 3600 U/ml soybean trypsin inhibitor (Sigma) to the suspension, cells were titrated through a 5 ml pipette. After the tissue was allowed to settle for 5–10 min, the supernatant was collected and the remaining tissue pellet was retitrated. The combined supernatants were centrifuged through a 4% BSA layer and the cell pellet was resuspended in neuronal seeding medium (NSM), which consisted of neurobasal medium (Gibco), supplemented with 1.1% 100× antibiotic–antimycotic solution (Biofluids), 25 µM Na-glutamate, 0.5 mM L-glutamine, and 2% B27 Supplement (Gibco). Cells were seeded at a density of 5×10^5 cells/ml onto 96-well tissue culture plates (Corning, Corning, NY) pre-coated with poly-D-lysine (70–150 kDa, Sigma), on 100 mm petri dishes (Corning) pre-coated with poly-D-lysine. On day 4 in vitro (DIV), feeding media (NSM without Na-glutamate and B27 supplement) in 1:2 proportion was added to cultures. All experiments were performed on cultures at 7–9 DIV. C₂-ceramide or C₂-dihydro-ceramide (Biomol), diluted in ethanol, was directly administered to the cultures (1 µL/300 µL). Sphingomyelinase from *B. cereus* (Sigma), diluted in culture medium, was added to cortical neurons, preincubated overnight in B27-free Neurobasal medium. Control cultures received vehicle alone.

SH-SY5Y cells. SH-SY5Y human neuroblastoma cells were routinely cultured in DMEM (Gibco) supplemented with 10% FBS (Hyclone Laboratories, Logan, UT), 50 U/ml penicillin/streptomycin, and 5 µg/ml fungizone (Biofluids) in 250 ml flasks (Corning). For experiments, cells were detached from the surface by trypsin–EDTA solution (Gibco), resuspended in fresh media, and seeded at 2×10^5 cells/ml onto 96-well tissue culture plates (Corning, Corning, NY) pre-coated with poly-D-lysine (70–150 kDa, Sigma) or at 5×10^5 cells/ml on 100 mm petri dishes. C₂-Ceramide (Biomol) diluted in ethanol was directly administered to the cultures (1 µL/300 µL). Control cultures received the same volume of vehicle alone.

Development of stable SH-SY5Y lines expressing dominant-negative caspase forms. SH-SY5Y neuroblastoma cells were stably transfected with pcDNA3 vector expressing dominant-negative forms of human

caspases-8 or -9. Transfections were performed using lipofectamine reagent (Gibco) and stable transfectants were pooled after selection for 2 weeks in the presence of G418 (1 mg/ml). Constructs expressing dominant-negative forms of human caspases-8 and -9 were kindly provided by Dr. Vishva M. Dixit. In the inactive mutant form of caspase-8 cysteine residue at its active site QACQG was changed to serine. In the dominant-negative form of caspase-9 cysteine residue at its active site QACGG was changed to alanine. In addition, both mutants were fused with a FLAG epitope at their C-termini. Previous studies by Dr. Dixit's group have demonstrated that expression of these mutants in mammalian cells potently and specifically inhibits activation of caspases-8 or -9 [20]. Expression of the recombinant mutant caspases was confirmed by immunoblotting using the anti-FLAG antibodies (data not shown). Stable cell clones transfected with the empty pcDNA3 vector served as a negative control.

Cell viability assays

Cell viability was measured by LDH release assay [21] or by Alamar blue assay [22]. LDH release was measured using CytoTox 96 non-radioactive cytotoxicity assay kit (Promega) according to manufacturer's protocol. Relative absorbance was measured at 490 nm at Ceres 9000 plate reader (Bio-Tek Instruments, Winooski, VT). Background LDH release determined in intact control cultures was subtracted from all experimental values. Alamar blue fluorometric cell viability assays were performed as recommended by manufacturer (BioSource International, Camarillo, CA). Fluorescence was measured using a CytoFluor II fluorometer (PerSeptive Biosystems,) at 530 nm excitation and 590 nm emission wavelengths.

Hoechst staining

Cells were washed in PBS and stained for 10 min at room temperature in PBS containing 4% paraformaldehyde and 10 µg/ml Hoechst 33258 (Sigma). Morphological evaluation of nuclear condensation and fragmentation was performed immediately after staining using a Nikon TE300 fluorescent microscope.

Assay for caspase activity

Aliquots of cytosolic extracts (20 µg protein in 100 µl caspase-3 assay buffer consisting of 50 mM Hepes, pH 7.4, 100 mM NaCl, 0.1% CHAPS, 10 mM DTT, 1 mM EDTA, and 10% glycerol) were mixed with equal volumes of 40 µM fluorescent tetrapeptide substrate (Ac-DEVD-AMC, Bachem) in the same buffer solution. Free aminomethylcoumarin (AMC) accumulation, which resulted from cleavage of the aspartate–AMC bond, was monitored continuously in each sample over 30 min in 96-well microtiter plates using a CytoFluor 4000 fluorometer (PerSeptive Biosystems) at 360 nm excitation and 460 emission wavelengths. The emission from each well was plotted against time. Linear regression analysis of the initial velocity (slope) of each curve yielded an activity for each sample.

Immunoblot analysis

Cells were harvested, washed once with ice-cold phosphate-buffered saline, and lysed on ice in a solution containing 50 mM Tris–HCl, pH 7.5, 150 mM NaCl, 1 mM EGTA, 1 mM PMSF, 0.5% NP-40, 0.25% sodium deoxycholate, 0.1% SDS, leupeptin (5 mg/ml), and aprotinin (5 mg/ml). After removal of cell debris by centrifugation, the protein concentration of the cell lysate was determined with the Bio-Rad protein assay reagent. A portion of the lysate (50–80 µg of protein) was then fractionated by SDS–polyacrylamide gel electrophoresis (PAGE) and the separated proteins were transferred to a nitrocellulose membrane. The membrane was stained with Ponceau S (Sigma) to confirm equal loading and transfer of samples, and then probed with specific antibodies. Immune complexes were detected with appropriate secondary antibodies and chemiluminescence reagents (Pierce). A

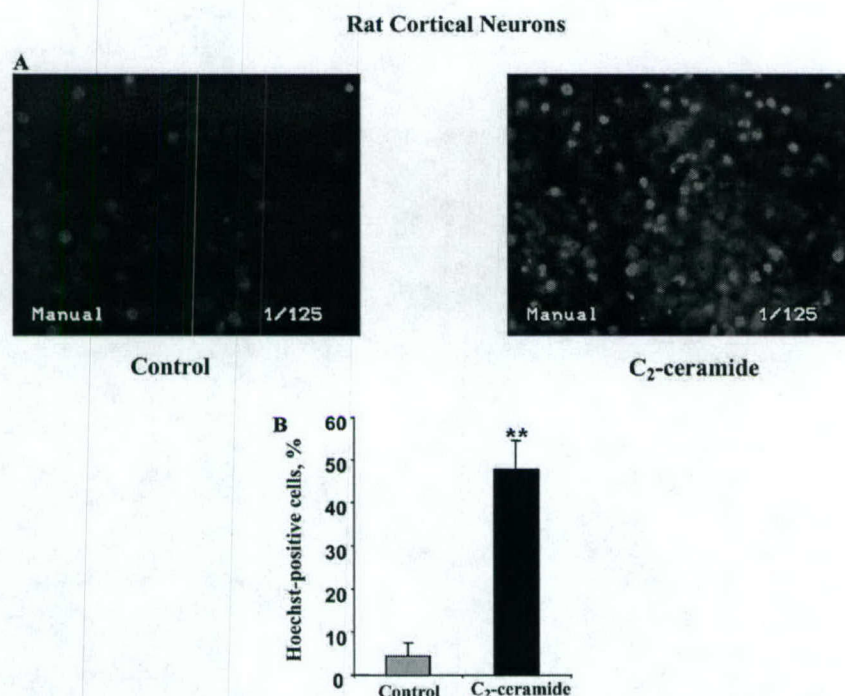


Fig. 1. Treatment with C₂-ceramide significantly increases the number of cells with apoptotic morphology in rat cortical neuronal cultures. After 24 h of incubation with 40 μ M C₂-ceramide, cells were stained by Hoechst 33258 and examined using fluorescent microscopy. (A) Representative images of control and C₂-ceramide-treated cells. (B) Histograms indicate percentage of apoptotic cells \pm SD; ** P < 0.01 versus control compared by ANOVA, followed by Dunnett's test.

polyclonal rabbit antibody to active caspase-3 was obtained from Cell Signaling Technology (Beverly, MA); a monoclonal mouse antibody to caspase-9 from Medical and Biological Laboratories (Naka-ku Nagoya, Japan); a polyclonal rabbit antibody to caspase-8—a gift from SmithKline Beecham (King of Prussia, PA); and a monoclonal mouse antibody to β -actin—from Sigma. Cell lysates prepared from cultures treated with 50 μ M etoposide (Sigma) for 8 h were utilized as a positive control for caspase-3 and caspase-9 activation. Cell lysates obtained from Jurkat cells treated with anti-Fas antibody (Kamya Biomedical, Seattle, WA) for 6 h were used as a positive control for anti-caspase-8 antibody.

Data analysis

Changes in cell viability were analyzed by ANOVA, followed by Dunnett's test. A P value less than 0.05 was considered statistically significant.

Results

Ceramide-induced apoptosis in rat cortical neuronal cells

To examine whether ceramide-induced cell death in cortical neuronal cultures was apoptotic, we evaluated two characteristic features of apoptosis, morphological (nuclear condensation and fragmentation) and biochemical (caspase activity). Morphological evaluation of cortical neuronal cultures using Hoechst 33258 staining and fluorescent microscopy revealed marked increase in

the number of cells with nuclear condensation and fragmentation after 24 h of treatment with 40 μ M C₂-ceramide, as compared to control cultures (Fig. 1). This dose of C₂-ceramide, based upon previous dose-response studies [12], caused a significant reduction in rat cortical neuronal cell viability, as measured by calcein AM assay at 24 h of treatment. In contrast, a similar dose of the inactive ceramide analog, C₂-dihydro-ceramide, had no effect on rat cortical neuronal cell viability, as assessed by calcein AM or LDH release methods (data not shown).

Caspase-3-like activity was examined in cytosolic protein extracts from cortical neuronal cells treated with 40 μ M C₂-ceramide for 1–24 h and compared to that in sister control cultures. The fluorometric assay, using DEVD-AMC as a substrate, showed an 8-fold elevation of caspase-3-like activity in the extracts from C₂-ceramide-treated cells at 16 h of treatment. Caspase-3-like activity was further upregulated at 24 h of the treatment to a level approximately 16-times higher than in untreated control extracts (Fig. 2A). Significant elevation of caspase-3-like activity was also observed in cortical neuronal cultures subjected to 24 h of treatment with 100 mU/ml sphingomyelinase, an enzyme involved in ceramide formation in cells (Fig. 2B). It was shown by us previously that treatment with the same dose of sphingomyelinase upregulates intracellular ceramide

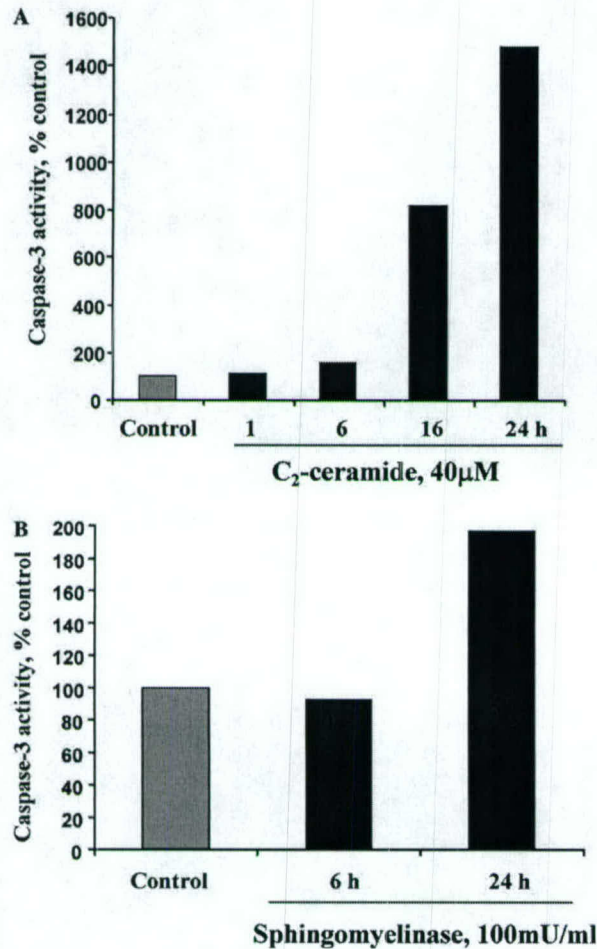


Fig. 2. Treatment with C₂-ceramide or sphingomyelinase significantly upregulates caspase-3-like activity in rat cortical neuronal cells. At 7 DIV, cultures were treated with 40 μM C₂-ceramide (A) or 100 mU/ml sphingomyelinase (B); after indicated periods of time cells were harvested and caspase-3-like activity was measured fluorometrically as described in Materials and methods. Histograms represent caspase-3-like activity as a percentage of the activity in control cells.

levels and causes apoptotic cell death in cortical neuronal cultures [12].

Caspase-9 and caspase-3, but not caspase-8, activity is correlated with ceramide-induced apoptosis

Given the above-described indications of apoptotic nature of ceramide-induced neuronal cell death, we examined the effect of various selective caspase inhibitors on C₂-ceramide-stimulated neuronal loss. As shown on Fig. 3, pretreatment with the selective caspase-3 inhibitor z-DEVD-fmk or the caspase-9 inhibitor z-LEHD-fmk significantly decreased cell death induced in cortical neuronal cultures by treatment with 40 μM C₂-ceramide, as assessed by LDH release at 24 h. However, application of the selective caspase-8 inhibitor z-IETD-fmk had

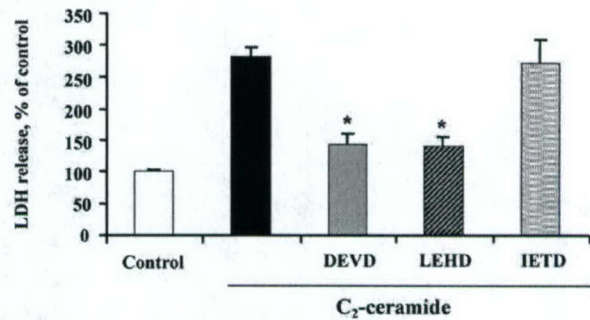


Fig. 3. Pretreatment with the caspase-3 inhibitor z-DEVD-fmk, or the caspase-9 inhibitor, z-LEHD-fmk, but not the caspase-8 inhibitor z-IETD-fmk, significantly reduced C₂-ceramide induced cell death in rat cortical neuronal cultures. Cell death was measured by LDH release assay after 24 h of incubation with 40 μM C₂-ceramide with or without 1 h pretreatment with selective caspase inhibitors (each at 150 μM). Histograms indicate LDH release as percentage of controls ±SD; *n* = 8–16 cultures per condition; **P* < 0.01 versus C₂-ceramide-injured cells compared by ANOVA, followed by Dunnett's test.

no protective effect on C₂-ceramide-induced cell loss in the same experimental system (Fig. 3). Immunoblot analysis of protein extracts from C₂-ceramide-treated cortical neuronal cultures demonstrated significant up-regulation in protein levels for active forms of both caspase-9 and caspase-3 (Fig. 4). Moreover, increased active caspase-9 immunoreactivity was evident at 6 h of C₂-ceramide treatment, while elevation of active caspase-3 protein level appeared later (after 16 h of the treatment). Presence of active caspase-8 immunoreactivity was undetectable in this system (data not shown).

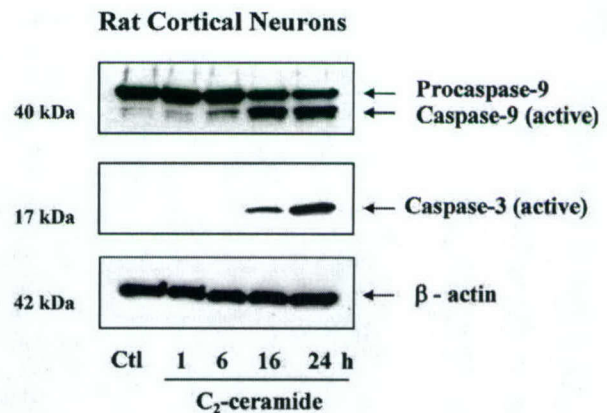


Fig. 4. Immunoblot analysis of C₂-ceramide-treated rat cortical neuronal cultures revealed upregulation of active caspase-3 and caspase-9 protein levels. Active caspase-8 immunoreactivity was undetectable in this system (data not shown). At 7 DIV, cultures were treated with 40 μM C₂-ceramide; after indicated periods of time cells were harvested and subjected to immunoblot analysis as described in Materials and methods. β-Actin was used as an internal control.

C₂-ceramide-induced apoptosis in SH-SY5Y human neuroblastoma cells: caspase-9- but not caspase-8 dominant-negative SH-SY5Y cells are significantly more resistant to C₂-ceramide-induced cell death

Administration of C₂-ceramide caused apoptotic cell death in cultured human neuroblastoma SH-SY5Y cells,

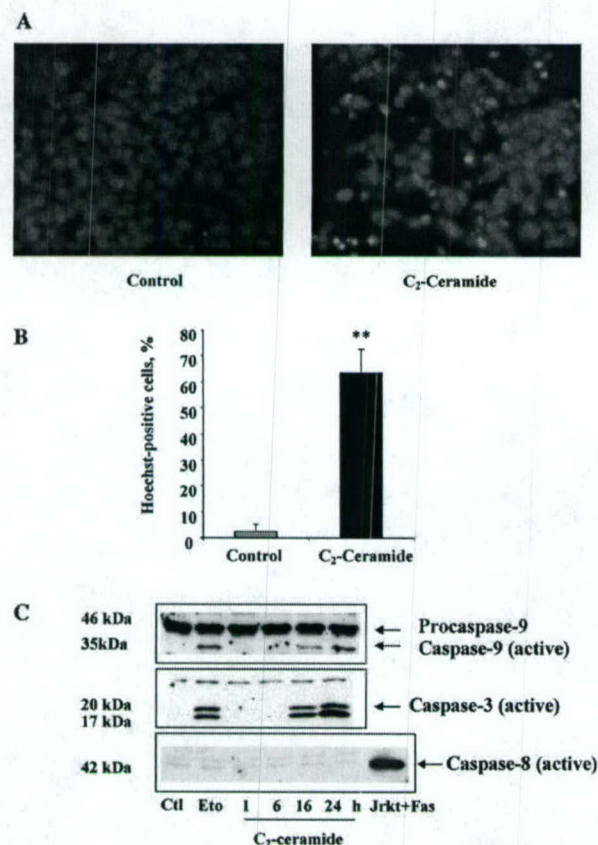


Fig. 5. Treatment with C₂-ceramide significantly increases the number of cells with apoptotic morphology and upregulates caspase-3 levels in SH-SY5Y cells. Representative images of control and C₂-ceramide-treated SH-SY5Y cells, stained by Hoechst 33258 shown. (A) Cultures were treated with 50 μ M C₂-ceramide for 36 h; cells were fixed in 4% formaldehyde, stained with Hoechst 33258, and visualized by fluorescent microscopy. Hoechst 33258 staining revealed many condensed, fragmented, brightly stained nuclei after C₂-ceramide treatment, which is suggestive of apoptosis. The number of apoptotic cells was assessed using Hoechst 33258 staining and fluorescent microscopy. (B) Histograms indicate percentage of cells with apoptotic morphology \pm SD; $n = 300$ –500 cells per condition. ** $P < 0.01$ versus intact cells compared by ANOVA, followed by Dunnett's test. Immunoblot analysis of C₂-ceramide-treated SH-SY5Y cells revealed upregulation of active caspase-3 and caspase-9 protein levels. Active caspase-8 immunoreactivity was undetectable in this system. (C) Cultures were treated with 50 μ M C₂-ceramide. After indicated periods of time cells were harvested and subjected to immunoblot analysis as described in Materials and methods. SH-SY5Y cells treated with 50 μ M etoposide (Eto) were utilized as a positive control for caspase activation. Anti-Fas-treated Jurkat cells (Jrkt + Fas) were used as a positive control for anti-caspase-8 antibody.

as showed by both Hoechst 33258 staining and immunoblot assay (Fig. 5). Morphological assessment of SH-SY5Y cells using Hoechst 33258 staining revealed significantly higher number of cells with nuclear condensation and fragmentation after 36 h of treatment with 50 μ M C₂-ceramide, as compared to control cultures (Figs. 5A and B).

Immunoblot analysis of protein extracts from SH-SY5Y cells treated with C₂-ceramide showed significant upregulation in protein levels of active forms of caspase-3 and caspase-9. In the same system, active caspase-8 immunoreactivity was not detected, although the antibody used was able to recognize active caspase-8 in the anti-Fas-treated Jurkat cell lysate, utilized as a positive control (Fig. 5C). Increased active caspase-3 immunoreactivity appeared after 16 h of C₂-ceramide treatment, when elevation of active caspase-9 protein level was also apparent.

We have also prepared dominant-negative caspase-9 and caspase-8 SH-SY5Y cells stably transfected with mutant caspase-9 and caspase-8 constructs (see Materials and methods). We further examined the effects of C₂-ceramide on caspase-9- and caspase-8 dominant-negative SH-SY5Y cell viability in comparison to that in cells transfected with empty vector. For this particular experiment, we chose Alamar blue assay instead of LDH release measurement, since SH-SY5Y cells are grown in the presence of serum, which may contribute to high background in the LDH assay. As shown in Fig. 6, C₂-ceramide-induced cell death in SH-SY5Y cells in a dose-dependent manner, as measured by Alamar blue assay after 36 h of treatment. However, cell death caused by C₂-ceramide was significantly reduced in caspase-9 dominant-negative SH-SY5Y cells, whereas both caspase-8 dominant-negative cultures and SH-SY5Y cells

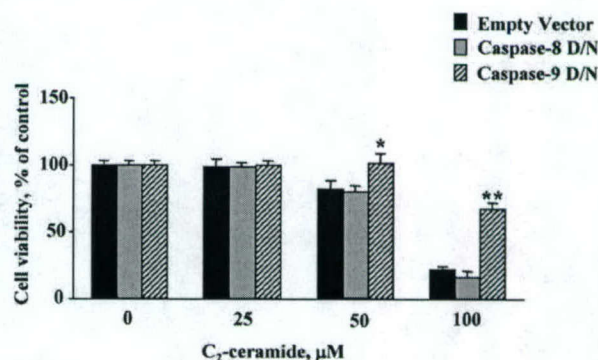


Fig. 6. Caspase-9 dominant-negative, but not caspase-8 dominant-negative, SH-SY5Y cells are significantly less sensitive to treatment with C₂-ceramide. After 36 h of incubation with indicated concentrations of C₂-ceramide cell viability was measured by Alamar blue assay. Histograms indicate cell viability as percentage of intact controls \pm SD; $n = 8$ to 16 cultures per condition. * $P < 0.05$, ** $P < 0.01$ versus cells transfected with empty vector compared by ANOVA, followed by Dunnett's test.

transfected with empty vector showed equally high levels of cell death following C₂-ceramide treatment (Fig. 6).

Discussion

An important role for ceramide in apoptosis was initially established in lymphoid cell lines using ceramide analogs. Increased activity of ceramide-producing enzymes and associated upregulation of intracellular ceramide levels were significantly correlated to the degree of apoptosis induced by different stimuli [5,23]. Nevertheless, in cells of neuronal origin, reports regarding a role for ceramide in cell death or survival have been less consistent; both protective and destructive functions for ceramide have been suggested, depending upon the doses of ceramide used and the developmental stage of the cells. Thus, low doses of ceramide in certain models have positive effects on survival, differentiation, or arborization, particularly when administered to immature neuronal cells; both hippocampal neurons and spinal motoneurons showed such effects at low doses of ceramide analogs (<3 μ M) during early days of culturing [24,25]. However, these protective effects were not observed in mature neurons either by us [12] or others [24]. In contrast, administration of high doses of ceramide analogs, or treatment with sphingomyelinase, caused neuronal loss in different neuronal culture systems [12,14,16,17,26]. A recent study by Pelled et al. [18] showed that C₆-ceramide induces neuronal apoptosis in hippocampal neurons, which is associated with upregulation of DAP kinase levels. Moreover, intracellular ceramide levels were significantly increased in cortical neurons [12] or HN9.10e cells [13] subjected to apoptotic stimuli, including treatment with etoposide or serum deprivation, which correlated with the degree of neuronal cell death.

In the present study, we found that administration of a cell-permeable ceramide analog or sphingomyelinase caused apoptotic cell death in cultured rat cortical neurons, as shown by Hoechst staining. This was associated with increased caspase-3-like activity and co-treatment with the selective caspase-3 inhibitor z-DEVD-fmk provided significant neuroprotection in cultures given C₂-ceramide. A similar time course for caspase-3 activation was shown by Willaime et al. [26] in C₂-ceramide-treated mouse cortical neurons. However, these authors could not reduce ceramide-induced cell death by co-application of the pan-caspase inhibitor z-VAD-fmk, from which they concluded that caspase-3 independent mechanisms were involved in ceramide-induced neuronal apoptosis. These differences from our findings may be explained, in part, by different culture models used or by differences in doses of the inhibitors utilized (50 μ M in Willaime et al. work versus 150 μ M in our study). Our previous studies showed that caspase inhibitors, such as z-DEVD-fmk or

z-VAD-fmk, required doses of 150 μ M and higher to reduce cell death in cultured primary neurons subjected to apoptotic stimuli [27,28]. In our hands the same high doses of ZVAD-fmk (150 μ M and higher) inhibited caspase-3 cleavage/activation induced by C₂-ceramide, whereas 50 μ M was not effective, as assessed by immunoblot analysis (data not shown). This requirement for such high doses, most likely, reflects limited cell permeability of these drugs, as 50 μ M z-VAD is sufficient for inhibition of caspase-3 activity in cell-free system (data not shown).

Caspase-3 is a major “executioner” caspase involved in neuronal apoptosis. It is also widely accepted that caspase-3 activity is controlled by upstream regulatory caspases, such as caspase-8 or caspase-9, which modulate the extrinsic or intrinsic pathways of neuronal apoptosis, respectively [29–32]. To address which of these pathways might be involved in ceramide-induced apoptosis, we conducted parallel studies using cortical neuronal and SH-SY5Y cells in culture. Inhibition of caspase-9, but not caspase-8, using selective inhibitors was protective against ceramide-induced neuronal loss in rat cortical cultures. Immunoblot analysis of C₂-ceramide-treated rat cortical neuronal cells showed marked upregulation of active caspase-3 and caspase-9, but not active caspase-8 protein levels. It should be noted that elevation in active caspase-9 protein in cortical neuronal cultures preceded changes in active caspase-3 immunoreactivity or caspase-3-like activity measured using specific fluorogenic substrate, suggesting that caspase-9 is most probably acting upstream of caspase-3 in this system. Upregulation of active caspase-3 and caspase-9 immunoreactivity, without changes in active caspase-8 protein levels, was also observed in ceramide-treated SH-SY5Y cells. Moreover, caspase-9 dominant-negative SH-SY5Y cells showed significantly higher resistance to C₂-ceramide treatment than either caspase-8 dominant-negative, or mock-transfected cells, as shown by cell viability assay. Together, these observations indicate a regulatory role for caspase-9 in ceramide-induced neuronal apoptosis and suggest that ceramide contributes to neuronal apoptosis by activating intrinsic caspase-9/caspase-3 controlled pathway.

Acknowledgments

This study was supported by grants from the National Institutes of Health (NS 36537-03) and the Department of Defense (DAMD17-2-9007). We thank Dr. Renee Ren-Patterson and Ms. Geping Wang for technical assistance.

References

- [1] R.E. Toman, S. Spiegel, A.I. Faden, Role of ceramide in neuronal cell death and differentiation, *J. Neurotrauma* 17 (2000) 891–898.

- [2] Y.A. Hannun, C. Luberto, Ceramide in the eukaryotic stress response, *Trends Cell Biol.* 10 (2000) 73–80.
- [3] R. Goswami, G. Dawson, Does ceramide play a role in neural cell apoptosis?, *J. Neurosci. Res.* 60 (2000) 141–149.
- [4] Y.A. Hannun, L.M. Obeid, The ceramide-centric universe of lipid-mediated cell regulation: stress encounters of the lipid kind, *J. Biol. Chem.* 277 (2002) 13.
- [5] Y. Hannun, Functions of ceramide in coordinating cellular responses to stress, *Science* 274 (1996) 1855–1859.
- [6] A.L. Rose, P.M. Farmer, N. Mitra, K.E. Wisniewski, R.K. Pullarkat, Clinical, pathologic, and neurochemical studies of an unusual case of neuronal storage disease with lamellar cytoplasmic inclusions: a new genetic disorder?, *J. Child Neurol.* 14 (1999) 123–129.
- [7] V. France-Lanord, B. Brugg, P.P. Michel, Y. Agid, M. Ruberg, Mitochondrial free radical signal in ceramide-dependent apoptosis: a putative mechanism for neuronal death in Parkinson's disease, *J. Neurochem.* 69 (1997) 1612–1621.
- [8] I. Herr, A. Martin-Villalba, E. Kurz, P. Roncaioli, J. Schenkel, M.G. Cifone, K.M. Debatin, FK506 prevents stroke-induced generation of ceramide and apoptosis signaling, *Brain Res.* 826 (1999) 210–219.
- [9] Y. Chen, I. Ginis, J.M. Hallenbeck, The protective effect of ceramide in immature rat brain hypoxia-ischemia involves up-regulation of bcl-2 and reduction of TUNEL-positive cells, *J. Cereb. Blood Flow Metab.* 21 (2001) 34–40.
- [10] K. Furuya, I. Ginis, H. Takeda, Y. Chen, J.M. Hallenbeck, Cell permeable exogenous ceramide reduces infarct size in spontaneously hypertensive rats supporting in vitro studies that have implicated ceramide in induction of tolerance to ischemia, *J. Cereb. Blood Flow Metab.* 21 (2001) 226–232.
- [11] Z.F. Yu, M. Nikolova-Karakashian, D. Zhou, G. Cheng, E.H. Schuchman, M.P. Mattson, Pivotal role for acidic sphingomyelinase in cerebral ischemia-induced ceramide and cytokine production, and neuronal apoptosis, *J. Mol. Neurosci.* 15 (2000) 85–97.
- [12] R. Toman, V. Movsesyan, S. Murthy, S. Miltien, S. Spiegel, A.I. Faden, Ceramide-induced cell death in primary neuronal cultures: upregulation of ceramide levels during neuronal apoptosis, *J. Neurosci. Res.* 68 (2002) 323–330.
- [13] L. Colombari, L.M. Frago, I. Varela-Nieto, R. Pesi, M. Garcia-Gil, Serum deprivation increases ceramide levels and induces apoptosis in undifferentiated HN9.10e cells, *Neurochem. Int.* 40 (2002) 327–336.
- [14] N. Marks, M.J. Berg, A. Guidotti, M. Saito, Activation of caspase-3 and apoptosis in cerebellar granule cells, *J. Neurosci. Res.* 52 (1998) 334–341.
- [15] M. Saito, A. Guidotti, M.J. Berg, N. Marks, The semisynthetic glycosphingolipid LIGA20 potently protects neurons against apoptosis, *Ann. NY Acad. Sci.* 845 (1998) 253–262.
- [16] T. Taniwaki, T. Yamada, H. Asahara, Y. Ohyagi, J. Kira, Ceramide induces apoptosis to immature cerebellar granule cells in culture, *Neurochem. Res.* 24 (1999) 685–690.
- [17] H. Zhou, S.A. Summers, M.J. Birnbaum, R.N. Pittman, Inhibition of Akt kinase by cell-permeable ceramide and its implications for ceramide-induced apoptosis, *J. Biol. Chem.* 273 (1998) 16568–16575.
- [18] D. Pelled, T. Raveh, C. Riebeling, M. Fridkin, H. Berissi, A.H. Futerman, A. Kimchi, Death-associated protein (DAP) kinase plays a central role in ceramide-induced apoptosis in cultured hippocampal neurons, *J. Biol. Chem.* 277 (2002) 1957–1961.
- [19] V.A. Movsesyan, D.M. O'Leary, L. Fan, W. Bao, P.G. Mullins, S.M. Knoblach, A.I. Faden, mGluR5 antagonists 2-methyl-6-(phenylethynyl)-pyridine and (E)-2-methyl-6-(2-phenylethenyl)-pyridine reduce traumatic neuronal injury in vitro and in vivo by antagonizing N-methyl-D-aspartate receptors, *J. Pharmacol. Exp. Ther.* 296 (2001) 41–47.
- [20] G. Pan, K. O'Rourke, V.M. Dixit, Caspase-9, Bcl-XL, and Apaf-1 form a ternary complex, *J. Biol. Chem.* 273 (1998) 5841–5845.
- [21] M.C. Sinensky, A.L. Leiser, H. Babich, Oxidative stress aspects of the cytotoxicity of carbamide peroxide: in vitro studies, *Toxicol. Lett.* 75 (1995) 101–109.
- [22] S.A. Back, R. Khan, X. Gan, P.A. Rosenberg, J.J. Volpe, A new Alamar blue viability assay to rapidly quantify oligodendrocyte death, *J. Neurosci. Methods* 91 (1999) 47–54.
- [23] L.M. Obeid, C.M. Lindaric, L.A. Karolak, Y.A. Hannun, Programmed cell death induced by ceramide, *Science* 259 (1993) 1769–1771.
- [24] J. Mitoma, M. Ito, S. Furuya, Y. Hirabayashi, Bipotential roles of ceramide in the growth of hippocampal neurons: promotion of cell survival and dendritic outgrowth in dose- and developmental stage-dependent manners, *J. Neurosci. Res.* 51 (1998) 712–722.
- [25] F. Irie, Y. Hirabayashi, Application of exogenous ceramide to cultured rat spinal motoneurons promotes survival or death by regulation of apoptosis depending on its concentrations, *J. Neurosci. Res.* 54 (1998) 475–485.
- [26] S. Willaime, P. Vanhoutte, J. Caboche, Y. Lemaigre-Dubreuil, J. Mariani, B. Brugg, Ceramide-induced apoptosis in cortical neurons is mediated by an increase in p38 phosphorylation and not by the decrease in ERK phosphorylation, *Eur. J. Neurosci.* 13 (2001) 2037–2046.
- [27] B.A. Eldadah, A.G. Yakovlev, A.I. Faden, The role of CED-3-related cysteine proteases in apoptosis of cerebellar granule cells, *J. Neurosci.* 17 (1997) 6105–6113.
- [28] V.A. Movsesyan, A.G. Yakovlev, L. Fan, A.I. Faden, Effect of serine protease inhibitors on posttraumatic brain injury and neuronal apoptosis, *Exp. Neurol.* 167 (2001) 366–375.
- [29] N. Noshita, A. Lewen, T. Sugawara, P.H. Chan, Evidence of phosphorylation of Akt and neuronal survival after transient focal cerebral ischemia in mice, *J. Cereb. Blood Flow Metab.* 21 (2001) 1442–1450.
- [30] M. Dubois-Dauphin, Y. Pfister, P.G. Vallet, A. Savioz, Prevention of apoptotic neuronal death by controlling procaspases? A point of view, *Brain Res. Brain Res. Rev.* 36 (2001) 196–203.
- [31] A.G. Yakovlev, K. Ota, G. Wang, V. Movsesyan, W.L. Bao, K. Yoshihara, A.I. Faden, Differential expression of apoptotic protease-activating factor-1 and caspase-3 genes and susceptibility to apoptosis during brain development and after traumatic brain injury, *J. Neurosci.* 21 (2001) 7439–7446.
- [32] H. Zhou, X.M. Li, J. Meinkoth, R.N. Pittman, Akt regulates cell survival and apoptosis at a postmitochondrial level, *J. Cell Biol.* 151 (2000) 483–494.

Caspase-Dependent Apoptotic Pathways in CNS Injury

Alexander G. Yakovlev and Alan I. Faden*

*Department of Neuroscience, Georgetown University Medical Center,
3970 Reservoir Rd., Room EP-12, Washington, DC 20007*

Abstract

Recent studies have suggested a role for neuronal apoptosis in cell loss following acute CNS injury as well as in chronic neurodegeneration. Caspases are a family of cysteine requiring aspartate proteases with sequence similarity to Ced-3 protein of *Caenorhabditis elegans*. These proteases have been found to contribute significantly to the morphological and biochemical manifestations of apoptotic cell death. Caspases are translated as inactive zymogens and become active after specific cleavage. Of the 14 identified caspases, caspase-3 appears to be the major effector of neuronal apoptosis induced by a variety of stimuli. A role for caspase-3 in injury-induced neuronal cell death has been established using semispecific peptide caspase inhibitors. This article reviews the current literature relating to pathways regulating caspase activation in apoptosis associated with acute and chronic neurodegeneration, and suggests that identification of critical upstream caspase regulatory mechanisms may permit more effective treatment of such disorders.

Index Entries: Caspases; apoptosis; Bcl-2; traumatic brain injury; spinal cord injury; cerebral ischemia; development.

Introduction

Tissue damage following brain injury results from both direct mechanical injury and secondary autodestructive reactions (1). Secondary injury involves a cascade of biochemical changes that contribute to delayed tissue damage and cell death (1). Although the focus of

research on secondary brain injury has historically been on mechanisms related to necrosis (2), recent studies have suggested a role for apoptosis in cell loss following stroke, spinal-cord injury or traumatic brain injury (TBI) (3-8), as well in chronic degenerative conditions such as Alzheimer's disease (AD) (9), Huntington's disease (HD) (10), Parkinson's disease (PD) (11,12), and Amyotrophic Lateral Sclerosis (ALS) (13-15).

Apoptosis and necrosis have been defined on histological criteria (16). Tissue necrosis is

* Author to whom all correspondence and reprint requests should be addressed. E-mail: fadena@gicc.s.georgetown.edu

typified by loss of membrane integrity, morphological signs of organelle damage, nuclear flocculation, loss of lysosomal contents, cellular swelling, and uncontrolled cell lysis (17). Apoptosis is characterized by preservation of membrane integrity, cytoplasmic and nuclear condensation, diminution of cellular volume, plasma-membrane bleb formation, and morphological preservation of organelle structure. The cell eventually fragments into apoptotic bodies, which are engulfed by neighboring cells and degraded. During apoptosis, morphological changes are often accompanied by internucleosomal cleavage of genomic DNA (18). In contrast to necrosis, apoptosis does not result in a loss of cellular content and does not initiate an inflammatory response.

Apoptosis is a genetically controlled type of cell death. The key apoptotic genes were originally identified in *Caenorhabditis elegans*. Approximately 1 out of 10 cells that are generated during development of this nematode undergo apoptosis. Among 15 genes that control this process, at least three are critical: *ced-3* and *ced-4* are both required for cell death, whereas *ced-9* is inhibitory (19). It has been revealed that Ced-3 is a type of cysteine proteases (caspase) whose activation is the major cause of apoptosis in *C. elegans* (20). Activation of Ced-3 is mediated by the Ced-4 and inhibited in the presence of Ced-9 (21,22). These three proteins physically interact forming the apoptosome complex (23).

The apoptotic machinery identified in *C. elegans* is evolutionarily conserved. Thus, *ced* genes have their mammalian homologs, and the interactions described for nematode Ced proteins have also been detected in mammals (23,24). However, regulatory mechanisms of apoptosis in mammals appear much more complex than those in *C. elegans*.

Caspase Family of Cysteine Proteases

The term "caspase" refers for cysteine requiring aspartate proteases with sequence similarity to Ced-3 (25). These proteases share from about 30–50% sequence identity in a 115 residue segment around the putative active site

cysteine: QAC(R/A/G)G. The protease activity of caspases is unique in that they all have an absolute substrate requirement for aspartate at the P1 (amino acid 1) and cleave following this residue (D-X). The requirement for D-X at P1 position in the recognition sequence for cleavage by caspases is absolute; however, there is some variability in the P2-4 region that determines substrate specificity for different caspases. Based on their preferential substrate specificity, caspases are divided into three distinct groups. Members of Group I (caspases -1, -4, and -5) all prefer the tetrapeptide sequence WEHD. In contrast, the optimal peptide recognition motif for Group II caspases (-2, -3, and -7) is DEXD. The caspases in Group III (-6, -8, and -9) prefer the sequence (L/V)EXD (26).

Caspases are translated as inactive zymogens and become active after specific cleavage. They are composed of an N-terminal prodomain, a large subunit, and a C-terminal small subunit, which are separated by specific caspase recognition sites. This means that active caspases can activate other caspases following an initial stimulus. Active caspases are heterotetramers consisting of two large and two small subunits from the cleaved pro-enzymes. Upon activation they may cleave their own precursors or other procaspases.

Based on their activation during progression of apoptosis, caspases can be divided into at least two subgroups: initiator and effector caspases (27). The initiator caspases, such as caspase-8 and -9, begin the disassembly process and activate the downstream effector caspases, such as caspase-3, -6, and -7, leading to an amplified caspase cascade (28–30). Activated effector caspases contribute most significantly to the morphological and biochemical manifestation of apoptotic death such as membrane blebbing, condensation or margination of chromatin and nuclear fragmentation, as well as alterations in activity of numerous nuclear and cytosolic enzymes.

Unlike effector caspases, initiator caspases have a long N-terminal prodomain, do not undergo autoactivation, and do not cleave each other. For activation they require additional proteins such as death domain-contain-

ing receptors (type I apoptosis) or functional apoptosomes (type II apoptosis).

A third group of caspases, which includes caspases -1, -4, -5, -11, -12, and -13, has been defined in terms of their function as pro-inflammatory enzymes. In contrast to the effector caspases that are involved in the execution of the apoptotic process, pro-inflammatory caspases are poor substrates for other caspases, and their apical activation pathways are less well-understood. Caspase-1 was the first identified member of the caspase family (20). Also known as, ICE (for interleukin-1 β -converting enzyme), caspase-1 is responsible for processing of 31 kDa pre-interleukin-1 β to its mature 17 kDa active form by cleaving the precursor protein at two target sites (FEAD and YVHD) (31).

Of the 14 caspases identified in mammals, caspase-3 appears to have the greatest degree of homology with Ced-3 (32). Caspase-3 is the major effector in neuronal apoptosis triggered by various stimuli. The first strong evidence supporting the specific role for this protease in neuronal apoptosis in the brain came from studies on mice deficient in caspase-3, in which brain development is profoundly altered, including cellular hyperplasia and disorganized cell deployment (33). A role for caspase-3 in injury-induced neuronal death was subsequently established using semispecific peptide caspase inhibitors in various models of apoptosis triggered by ischemic or traumatic injury *in vivo* and *in vitro* (3-5,34-39).

Because activation of caspases, and caspase-3 in particular, appears to be a major factor for execution of neuronal apoptosis in brain, evaluation of upstream modulatory mechanisms is important for understanding the regulation of the apoptotic process. Thus, caspase-3 can be activated by at least two mechanisms: an extrinsic pathway involving cell-surface receptors and an intrinsic pathway resulting from alterations at the level of the mitochondrion (40-42).

Pathways of Caspase Activation

Initiation and progression of apoptosis are often stimulus-specific. Thus, in a variety of cell

types, apoptosis can be regulated by extracellular death factors. These factors are members of the tumor necrosis factor (TNF) family of cytokines and include Fas ligand (Apo-1/CD95 ligand), TNF- α , TNF related apoptosis-induced ligand (TRAIL)/Apo-2 ligand, and TNF-related weak inducer of apoptosis (TWEAK) (43,44). The pathway involves transduction mechanisms, where an important role has been attributed to a "death domain" sequence motif in the cytoplasmic segments of corresponding receptors (45). Caspase-8 appears to play the major role in the initiation of caspase cascade (46-48). Stimulation of death receptors by their respective ligands induces oligomerization of the receptors and the formation of a death-inducing signaling complex (DISC) (49). The intracellular domain of the death receptor binds to the adaptor molecule Fas-associating protein with death domain (FADD), which in turn recruits procaspase-8 allowing its autocleavage and activation. The released active caspase-8 activates downstream executioner caspases-3 and -7 (45). In addition, activated caspase-3 may cleave procaspase-8 (42,50), thereby amplifying the death process.

Active caspase-8 can initiate also downstream cleavage of executioner caspases by mitochondrial-dependent mechanisms. Thus, recent studies suggest that cell-death receptors may amplify their suicide signal by activating the apoptosome. In this pathway, caspase-8 cleaves Bid, a BH3 domain-containing proapoptotic Bcl2 family member (51). C-terminal cleavage product of Bid translocates from cell cytosol to mitochondria and interacts with Bax, thus triggering its translocation from cytosol to mitochondrial membranes followed by the release of cytochrome c, and activation of caspase-9 and downstream executioner caspases (52,53). In addition, Bid fragments can act as a membrane-destabilizing agent, increasing release of cytochrome c (54). The cytochrome c releasing activity of Bid is antagonized by Bcl2 (53) and effectively inhibited by the protein FLICE inhibitory protein (FLIP) (for FADD-like caspase, or caspase-8 [FLICE]-inhibitory protein): two alternatively spliced forms of FLIP interact with the adaptor protein

FADD and the caspase-8, thus potentially inhibiting apoptosis induced by death receptors (55).

While studying the biochemical mechanism of caspase activation, Xiaodong Wang's group had discovered that cell extracts contained three major protein factors that worked together to activate caspase-3 and induce apoptosis (41,56,57). Identification of those factors revealed an intrinsic cell-death pathway that is initiated by release of cytochrome c from mitochondria to the cytosol (41). It is important to note that release of cytochrome c from mitochondria can be initiated by a variety of proapoptotic stimuli (58–61).

In the presence of ATP (or dATP), cytochrome c binds to the cytosolic adaptor protein Apaf-1 (41). The N-terminal 85 amino acids of Apaf-1 show 53% similarity to the N-terminal pro-domain of the *C. elegans* Ced-3. This is followed by 320 amino acids that show 48% similarity to Ced-4. The C-terminal region of Apaf-1 comprises multiple WD repeats, which are proposed to mediate protein-protein interactions (56). Binding of cytochrome c to Apaf-1 allows the recruitment and activation of caspase-9 within the apoptosome (41). Caspase-9 and Apaf-1 bind to each other via their respective N-terminal Ced-3 homologous domains. This event leads to caspase-9 activation (41). Active caspase-9, in turn, activates executioner caspases-3 and -7. Activated caspase-3 is required for the activation of four other caspases (-2, -6, -8, and -10) in this pathway and also participates in a feedback amplification loop involving caspase-9 (41,42).

Similarly to null mutants of caspase-3, both Apaf-1 and caspase-9 knockout mice demonstrate a variety of hyperplasias and disorganized cell deployment in the brain leading to death during embryonic development (62–65). This suggests that activation of caspase-3 by apoptosome-mediated caspase-9 activation has a critical role in the developing central nervous system (CNS) (33,62,66).

Modulation of Caspase Activation

The complexity of caspase-activation mechanisms is increased by the fact that they can be

modulated in different ways at almost every critical step. Thus, Bcl-2 was the first identified mammalian homolog of the *ced* genes. It is homologous to Ced-9 and is involved in inhibiting apoptosis. Bcl-2 was first identified in B-cell lymphoma as a result of a chromosomal translocation, which leads to high expression of Bcl-2 in these tumors. Since the discovery of Bcl-2, an entire gene family has been identified. There are several different ways in which Bcl-2 members may function. Members of this protein family may serve as either positive or negative regulators of apoptosis. Among the anti-apoptotic proteins, Bcl-xL is predominantly expressed in mammalian brain (67), and acts as a major inhibitor of the cytochrome c-mediated pathway of caspase activation in neurons. Mice lacking *bcl-x* die as embryos, showing massive death of postmitotic neurons (68).

Initially, it was proposed that Bcl-xL directly binds to Apaf-1, thus preventing activation of caspase-9 (69). However, more recent studies have not confirmed this hypothesis (70) and have demonstrated that Apaf-1 has a cytoplasmic localization distinct from Bcl-xL (71). Thus, it appears that Bcl-xL, like other anti-apoptotic members of Bcl-2 family, controls mitochondrial-membrane permeability and redistribution of cytochrome c from the inter-membrane space to the cytosol during apoptosis via interaction with Bax (72). On the other hand, Bcl-xL can be cleaved by caspases, and the resulting C-terminal fragment of Bcl-xL potentially induces apoptosis (73).

Bax is another member of the bcl-2 family found to promote apoptosis. Under normal conditions, Bax predominantly localizes in the cytosol but translocates to mitochondrial and other membranes early in apoptosis (74–76). Once been translocated to mitochondria, Bax forms homodimers leading to loss of mitochondrial membrane potential, cytochrome c release, formation of the apoptosome complex, and caspase activation (77–80). Although Bax deficiency does not cause hyperplasia or malformations of the nervous system, it decreases apoptosis in the developing CNS and prevents

increased neuronal death caused by Bcl-x disruption (81–84).

Apoptosome-mediated apoptosis also may be regulated by more complicated mechanisms. Thus, numerous alternatively spliced isoforms of certain apoptosis regulators, such as Bcl-x (85,86), caspase-9 (87), and Apaf-1 (88), have been shown to play opposing roles in regulating apoptosis (89). Furthermore, growth factors can promote cell survival by activating the phosphatidylinositolide-3'-OH kinase and its downstream target, the serine-threonine kinase Akt. Cardone and collaborators recently reported that active Akt can phosphorylate recombinant human caspase-9 on serine-196 and inhibit its activity (90). However, the corresponding Akt phosphorylation site was not found in the cloned mouse ortholog (91). A more recent report suggests that Akt may inhibit activation of caspase-9 and -3 by post-translational modification of a cytosolic factor downstream of cytochrome c and before activation of caspase-9 (92). On the other hand, it has also been demonstrated that growth factor-induced activation of the PI3'K/Akt signaling pathway results in the phosphorylation of BAD, another member of BCL-2 family (93), thereby altering its pro-apoptotic function. Various proapoptotic stimuli lead to increased intracellular Ca^{2+} concentrations, resulting in activation of the protein phosphatase calcineurin, which can dephosphorylate BAD (94). In other models, dephosphorylation of BAD can be achieved by Ras-dependent activation of the protein phosphatase 1 alpha (95). Dephosphorylated BAD forms heterodimer with BCL-XL displacing BAX that lead to release of cytochrome c and activation of downstream caspases, promoting apoptosis (96). When caspase-3 is active, it can specifically cleave Akt, thereby amplifying the death process (97).

Release of cytochrome c from mitochondria to cytosol does not necessarily determine cell fate, since activation of the apoptosome is controlled by other factors. Thus, the cellular stress response can lead to cellular protection by inducing heat-shock proteins (Hsp). Two

members of Hsp family, Hsp70 and Hsp90, prevent cytochrome c/dATP-mediated caspase activation by direct association with Apaf-1, thereby preventing recruitment of caspases to the apoptosome complex (98,99). A third member of the family, Hsp27, also inhibits cytochrome c-mediated activation of caspases by binding to cytochrome c and thus prevents the interaction of Apaf-1 with procaspase-9 (100).

Another regulatory mechanism that parallels the proapoptotic action of cytochrome c involves a novel mitochondrial protein, Smac, which is released into the cytosol when cells undergo apoptosis. Smac promotes caspase-9 activation by binding to inhibitor of apoptosis proteins, IAPs (101), removing their inhibitory activity (102).

Recently Nakagawa et al. (103) showed that the caspase cascade can also be initiated by caspase-12. Caspase-12-deficient mice were resistant to endoplasmic reticulum stress-induced apoptosis and caspase-12-deficient cortical neurons were resistant to apoptosis induced by β -amyloid ($A\beta$) (103). Caspase-12 is able to activate caspase-3 in the A549 cell line and antisense-mediated inhibition of caspase-12 reduces apoptosis (104). It has been proposed that disturbance to intracellular Ca^{2+} storage as a result of ischemic injury or $A\beta$ cytotoxicity may induce apoptosis through calpain-mediated caspase-12 activation and Bcl-xL inactivation (105).

Caspase-11, another member of the murine caspase family, which serves as an upstream activator of caspase-1 (106), is a critical initiator caspase responsible for the activation of caspase-3. Caspase-11-deficient mice have a reduced number of apoptotic cells and a defect in caspase-3 activation after middle cerebral-artery occlusion (107). Caspase-11 has been shown to be activated by cathepsin B (108), which, in turn, can be activated by calpain (8).

Although it is unclear whether all discovered regulatory mechanisms of the apoptosome-mediated pathway (Fig. 1) are functional during neuronal apoptosis in the mammalian brain, mitochondrial alterations accompanied by release of cytochrome c and caspase-3 acti-

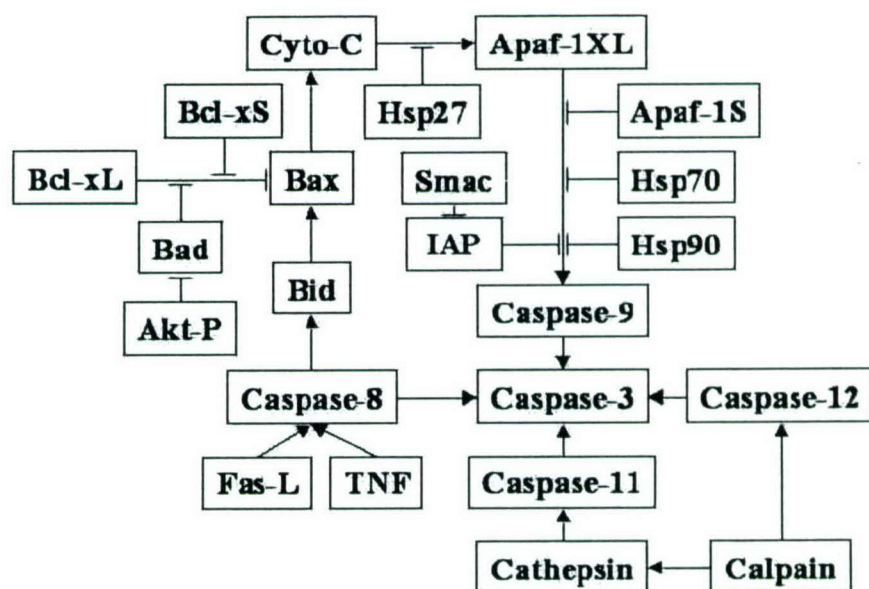


Fig. 1. Modulation of caspase activation.

vation have been almost universally seen in models of CNS injury (109–115).

Pathways of Caspase Activation in Acute Neuronal Injury

The ability of caspase inhibitors to block neuronal cell death has established a crucial role of caspases (caspase-3, in particular) in various models of apoptosis triggered by ischemic or traumatic injury in vivo and in vitro (3–5,34–39).

Thus, we have previously demonstrated that fluid percussion-induced TBI in rats results in induction of neuronal apoptosis with high frequency in both traumatized rat cortex and hippocampus. In this model, we have identified post-traumatic increase in mRNA for both caspase-1 and caspase-3 in affected brain regions; however, increased enzymatic activity was detected for caspase-3-like, but not caspase-1-like proteases. Intracerebroventricular administration of z-DEVD-fmk, a somewhat selective tetrapeptide inhibitor of caspase-3, before and

after injury markedly reduced post-traumatic apoptosis, as demonstrated by DNA electrophoresis and terminal deoxynucleotidyl-transferase d UTP Nick End Labeling (TUNEL) staining. Such treatment also significantly improved neurological recovery (3). The participation of caspase-3 activation in neuronal death after TBI in rats was also suggested by Clark et al. (4). These authors observed cleavage of procaspase-3 in cytosolic cellular fractions and an increase in caspase-3-like enzyme activity in injured brain, as well as neuroprotective effect of DEVD-fmk after TBI (4).

Preliminary data from Knobloch et al. (116) showed that activation of caspases-3 and -9 contributes to the secondary injury response after moderate lateral fluid-percussion TBI in rats. In contrast, caspase-8 cleavage fragments were not detected in this study at any time after injury. Immunohistochemistry for active forms of caspases-3 and -9 showed that they are expressed by both neurons and glia, and in TUNEL-positive cells that have morphologic features of apoptosis. Postinjury treatment with the pan-caspase inhibitor z-VAD-fmk sig-

nificantly improved both composite motor neuroscores and spatial learning in a Morris water-maze task (116).

Namura et al. (37) examined the expression, activation, and cellular localization of caspase-3 in adult mouse brain after temporary middle cerebral-artery occlusion. They found that procaspase-3, but not its cleavage products, was expressed in neurons throughout brain. Activation of caspase-3-like enzymes was detected in brain homogenate as early as 20 min after reperfusion (37).

In a similar murine model of brain ischemia, Endres and colleagues (117) examined the neuroprotective effects of two caspase family inhibitors, z-VAD-fmk and z-DEVD-fmk, and the N-methyl-D-aspartate (NMDA) receptor antagonist, MK-801, administered intracerebroventricularly. Both caspase inhibitors decreased infarct size, oligonucleosomal DNA laddering, and neurologic deficits when administered 6 after reperfusion. By contrast, the therapeutic window for MK-801 did not extend beyond the time of occlusion, probably because it does not inhibit apoptotic cell death (117). Our own preliminary studies showed that of z-DEVD-fmk has neuroprotective effects in a mouse model of brain trauma, even when administered *icv* as late as 8 h after injury (unpublished observations).

A role for caspase-3 in "ischemic" injury was further explored *in vitro*, using cultured neurons from embryonic rat forebrain subjected to 6 h hypoxia. Neuronal expression of the active cleavage product and proteolytic activity of caspase-3 was increased after hypoxia to nearly 10-fold over control values at 96 h postinsult. In this model, caspase-3 activity was also blocked dose-dependently by Asp-glu-val-Asp-aldehyde (DEVD-CHO); this peptide inhibitor reduced the number of apoptotic cells and prevented the hypoxia-induced decrease in cell viability, even when given 24 h postinsult (118).

Recent studies have implicated activation of caspase-3 in apoptotic processes in seizure-related neuronal injury. Using a model of status epilepticus in rats induced by kainic acid, Kondratyev and Gale (119) demonstrated

expression of caspase-3 activity in rhinal cortex and amygdala at 24 h. Intracerebroventricular administration of z-DEVD-fmk caspase-3 inhibitor prior to and following status epilepticus substantially attenuated apoptotic cell death, both in hippocampus and cortex, as evaluated by analysis of internucleosomal DNA fragmentation and neuronal nuclear morphology (119).

Kermer and co-authors investigated whether caspase inhibition provides long-term neuroprotection of adult rat retinal ganglion cells following optic-nerve transection and demonstrated that treatment for 2 wk with z-DEVD-cmk increased the number of surviving cells 4 wk postlesion from 11 to 24%. However, treatment with this inhibitor over the entire experimental period of 4 wk had no additional effect (120).

Since activation of caspases, and caspase-3 in particular, appears to be a major event in the execution of neuronal apoptosis in the brain, analysis of upstream mechanisms in the injured neurons is important. The apoptosis-mediated pathway of neuronal apoptosis has been investigated in detail using a model of traumatic spinal-cord injury in rats. Springer and collaborators reported that the upstream and downstream components of the cytochrome c-dependent apoptotic pathway are activated in injured spinal cord, and are found in neurons and in oligodendroglia (121).

Krajewski et al. have reported that caspase-9 may be found in mitochondria of several cell types, including brain neurons, and that it is released by exposure to Ca^{2+} or Bax *in vitro* (110). These authors also observed that, in an animal model of transient global cerebral ischemia, caspase-9 was released early from mitochondria and accumulated in neuronal nuclei within hippocampus and other vulnerable regions of postischemic brain (110).

Despite the fact that Fas-ligand and TNF- α are widely expressed in the nervous system, the potential role of caspase-8-mediated apoptotic pathway in neurons has received limited attention. Recently, caspase-8 activation has been investigated using *in vitro* models of HD and AD (122,123). Sanchez and co-authors

demonstrated that death of primary rat neurons resulted after overexpression of polyglutamine repeat (Q79) was preceded by activation of caspase-8. Inhibition of this caspase blocked Q79-induced cell death. Co-expression of Q79 with the caspase inhibitor CrmA, a dominant-negative mutant of FADD, Bcl-2, or Bcl-xL prevented the recruitment of caspase-8 and inhibited cell death. In addition, this study reports the presence of activated caspase-8 in affected brain regions from HD patients but not in normal controls (122). Ivins et al. provided evidence that A β also might initiate apoptosis by cross-linking death receptors of the Fas/TNFR family (123). They showed that the caspase-8 inhibitor peptide, IETD-fmk, inhibited neuronal death induced by A β and that neurons expressing dominant-negative FADD were protected from apoptosis in this model of AD (123).

Recently, caspase-8 activity was also attributed to neuronal apoptosis following hypoxic-ischemic injury to the developing brain (124) and transient spinal-cord ischemia (125). On the other hand, Velier and collaborators reported that after permanent focal stroke in rats, active forms of caspase-8 and caspase-3 were found differentially expressed in lamina V and lamina II/III, respectively (126). The authors suggested that the molecular mechanisms of cell death differ among the populations of neurons comprising the cerebral cortex.

Developmental Changes in Caspase-3 Activation

Clinical observations suggest that age influences outcomes and mortality after brain injury; however, why the same insult results in different response to injury in adults and in infants remained unclear. Using different models of experimental brain injury, recent reports suggest age-dependent differences in susceptibility to apoptosis. Bittigau et al. (127) reported age dependency of apoptotic neurodegeneration in the developing rat brain after head trauma. In 7-

d-old rats, mechanical trauma triggered widespread apoptosis in the hemisphere ipsilateral to the trauma site. This was accompanied by elevation of caspase-3 activity and DNA fragmentation in vulnerable brain regions. Severity of trauma-triggered apoptosis in the brains of 3- to 30-d-old rats was age-dependent, was highest in 3- and 7-d-old animals, and demonstrated a subsequent rapid decline.

Pohl et al. also reported that susceptibility to apoptotic death after TBI is dependent on age (128), with 3- and 7 d-old rats showing the highest vulnerability. By 10 and 14 d, the severity of apoptotic cell loss had markedly decreased; by 30 d of age, damage was minimal and limited to the site of impact.

These results may be explained, in part, by another report showing that the expression of caspase-3 mRNA in the brain is highly regulated during the postnatal period (129). De Bilbao and colleagues investigated the expression of caspase-3 mRNA by *in situ* hybridization in the mouse brain from birth to adulthood. From 1 postnatal d to 12 postnatal d, caspase-3 mRNA was expressed ubiquitously in all brain nuclei, including areas where neurogenesis occurred; this expression decreased substantially after day 12. The authors also found a positive correlation between areas displaying high levels of mRNA and apoptotic nuclei. In the adult brain, caspase-3 mRNA was restricted to the piriform and entorhinal cortices, to the neocortex, and to areas where neurogenesis is observed (129).

The involvement of caspase-3 in cell death after hypoxia-ischemia (HI) was also studied during brain maturation. Unilateral HI was produced in rats at postnatal days 7–60 by a combination of left carotid-artery ligation and systemic hypoxia. Activation of caspase-3 and cell death was examined *in situ* by confocal microscopy and by biochemical analysis. Active caspase-3 positive neurons was identified in more than 90% HI damaged striatal and neocortical neurons in 7-d-old pups; this number was reduced to approx 65% in striatum and 34% in the neocortex of 15-d-old pups, and to approx 26% in striatum and 2% in neocortex

of 26-d-old rats. In 60-d-old rats, less than 4% of the damaged neurons in striatum and less than 1% in neocortex were positive for active caspase-3. Western-blot analysis demonstrated that the level of inactive caspase-3 in normal forebrain tissue gradually declined from a high level in young pups to very low levels in adult rats. Concomitantly, HI-induced active caspase-3 was reduced from a relatively high level in young to a barely detectable level in mature rats (130).

Conclusion and Future Directions

Collectively, these studies suggest that apoptosis of CNS cells may play an important pathophysiological role in acute and chronic neurodegeneration. Both intrinsic and extrinsic caspase pathways appear to be activated in association with such apoptosis. Because apoptosis occurs later and over a longer postinjury time frame than necrosis, pharmacological inhibition of apoptosis may offer substantial therapeutic advantages over traditional therapies. Identification of critical upstream caspase regulatory pathways may permit even more effective interventions. Potential targets may include modulation of Akt, IAPs, or Smac.

Apoptotic pathways appear to play a greater role in perinatal brain injury than in adults. This may have important implications for understanding and treating such conditions as cerebral palsy.

Acknowledgments

This work was supported by NIH 1RO1NS-38941, NIH 1RO1NS36537, and DAMD 17-99-2-9007.

References

1. Faden A. I. (1996) Pharmacological treatment of central nervous system trauma. *Pharmacol. Toxicol.* **78**, 12–17.

2. Trump B. F. and Bulger R. E. (1967) Studies of cellular injury in isolated flounder tubules. I. Correlation between morphology and function of control tubules and observations of autophagocytosis and mechanical cell damage. *Lab. Invest.* **16**, 453–482.
3. Yakovlev A. G., Knoblach S. M., Fan L., Fox G. B., Goodnight R., and Faden A. I. (1997) Activation of CPP32-like caspases contributes to neuronal apoptosis and neurological dysfunction after traumatic brain injury. *J. Neurosci.* **17**, 7415–7424.
4. Clark R. S., Kochanek P. M., Watkins S. C., et al. (2000) Caspase-3 mediated neuronal death after traumatic brain injury in rats. *J. Neurochem.* **74**, 740–753.
5. Gillardon F., Bottiger B., Schmitz B., Zimmermann M., Hossmann K. A. (1997) Activation of CPP-32 protease in hippocampal neurons following ischemia and epilepsy. *Brain Res. Mol. Brain Res.* **50**, 16–22.
6. Lipton P. (1999) Ischemic cell death in brain neurons. *Physiol. Rev.* **79**, 1431–1568.
7. Snider B. J., Gottron F. J., Choi D. W. (1999) Apoptosis and necrosis in cerebrovascular disease. *Ann. NY Acad. Sci.* **893**, 243–253.
8. Yamashima T. (2000) Implication of cysteine proteases calpain, cathepsin and caspase in ischemic neuronal death of primates. *Prog. Neurobiol.* **62**, 273–295.
9. Selznick L. A., Holtzman D. M., Han B. H., et al. (1999) In situ immunodetection of neuronal caspase-3 activation in Alzheimer disease. *J. Neuropathol. Exp. Neurol.* **58**, 1020–1026.
10. Portera-Cailliau C., Hedreen J. C., Price D. L., Koliatsos V. E. (1995) Evidence for apoptotic cell death in Huntington disease and excitotoxic animal models. *J. Neurosci.* **15**, 3775–3787.
11. Jellinger K. A. (2000) Cell death mechanisms in Parkinson's disease. *J. Neural. Transm.* **107**, 1–29.
12. Hartmann A., Hunot S., Michel P. P., et al. (2000) Caspase-3: a vulnerability factor and final effector in apoptotic death of dopaminergic neurons in Parkinson's disease. *Proc. Natl. Acad. Sci. USA* **97**, 2875–2880.
13. Martin L. J. (1999) Neuronal death in amyotrophic lateral sclerosis is apoptosis: possible contribution of a programmed cell death mechanism. *J. Neuropathol. Exp. Neurol.* **58**, 459–471.
14. Honig L. S. and Rosenberg R. N. (2000) Apoptosis and neurologic disease. *Am. J. Med.* **108**, 317–330.
15. Wellington C. L. and Hayden M. R. (2000) Caspases and neurodegeneration: on the cutting

- edge of new therapeutic approaches. *Clin. Genet.* **57**, 1–10.
16. Kerr J. F., Wyllie A. H., and Currie A. R. (1972) Apoptosis: a basic biological phenomenon with wide-ranging implications in tissue kinetics. *Br. J. Cancer* **26**, 239–257.
 17. Bredesen D. E. (1995) Neural apoptosis. *Ann. Neurol.* **38**, 839–851.
 18. Wyllie A. H., Kerr J. F., and Currie A. R. (1980) Cell death: the significance of apoptosis. *Int. Rev. Cytol.* **68**, 251–306.
 19. Horvitz H. R. (1999) Genetic control of programmed cell death in the nematode *Caenorhabditis elegans*. *Cancer Res.* **59**, 1701s–1706s.
 20. Yuan J., Shaham S., Ledoux S., Ellis H. M., and Horvitz H. R. (1993) The *C. elegans* cell death gene *ced-3* encodes a protein similar to mammalian interleukin-1 beta-converting enzyme. *Cell* **75**, 641–652.
 21. Yuan J. and Horvitz H. R. (1992) The *Caenorhabditis elegans* cell death gene *ced-4* encodes a novel protein and is expressed during the period of extensive programmed cell death. *Development* **116**, 309–320.
 22. Hengartner M. O. and Horvitz H. R. (1994) Programmed cell death in *Caenorhabditis elegans*. *Curr. Opin. Genet. Dev.* **4**, 581–586.
 23. Hengartner M. O. (1999) Programmed cell death in the nematode *C. elegans*. *Recent Prog. Horm. Res.* **54**, 213–222.
 24. Hengartner M. (1998) Apoptosis. Death by crowd control [comment]. *Science* **281**, 1298–1299.
 25. Alnemri E. S., Livingston D. J., Nicholson D. W., et al. (1996) Human ICE/CED-3 protease nomenclature [letter]. *Cell* **87**, 171.
 26. Thornberry N. A., Rano T. A., Peterson E. P., et al. (1997) A combinatorial approach defines specificities of members of the caspase family and granzyme B. Functional relationships established for key mediators of apoptosis. *J. Biol. Chem.* **272**, 17,907–17,911.
 27. Thornberry N. A. and Lazebnik Y. (1998) Caspases: enemies within. *Science* **281**, 1312–1316.
 28. Martin S. J. and Green D. R. (1995) Protease activation during apoptosis: death by a thousand cuts? *Cell* **82**, 349–352.
 29. Zhivotovsky B., Burgess D. H., and Orrenius S. (1996) Proteases in apoptosis. *Experientia* **52**, 968–978.
 30. Cohen G. M. (1997) Caspases: the executioners of apoptosis. *Biochem. J.* **326**, 1–16.
 31. Miura M., Zhu H., Rotello R., Hartwig E. A., and Yuan J. (1993) Induction of apoptosis in fibroblasts by IL-1 beta-converting enzyme, a mammalian homolog of the *C. elegans* cell death gene *ced-3*. *Cell* **75**, 653–660.
 32. Fernandes-Alnemri T., Litwack G., and Alnemri E. S. (1994) CPP32, a novel human apoptotic protein with homology to *Caenorhabditis elegans* cell death protein *Ced-3* and mammalian interleukin-1 beta-converting enzyme. *J. Biol. Chem.* **269**, 30,761–30,764.
 33. Kuida K., Zheng T. S., Na S., et al. (1996) Decreased apoptosis in the brain and premature lethality in CPP32-deficient mice. *Nature* **384**, 368–372.
 34. Gottron F. J., Ying H. S., and Choi D. W. (1997) Caspase inhibition selectively reduces the apoptotic component of oxygen-glucose deprivation-induced cortical neuronal cell death. *Mol. Cell Neurosci.* **9**, 159–169.
 35. Fink K., Zhu J., Namura S., et al. (1998) Prolonged therapeutic window for ischemic brain damage caused by delayed caspase activation. *J. Cereb. Blood Flow Metab.* **18**, 1071–1076.
 36. Eldadah B. A., Yakovlev A. G., and Faden A. I. (1997) The role of CED-3-related cysteine proteases in apoptosis of cerebellar granule cells. *J. Neurosci.* **17**, 6105–6113.
 37. Namura S., Zhu J., Fink K., et al. (1998) Activation and cleavage of caspase-3 in apoptosis induced by experimental cerebral ischemia. *J. Neurosci.* **18**, 3659–3668.
 38. Clark R. S., Kochanek P. M., Chen M., et al. (1999) Increases in Bcl-2 and cleavage of caspase-1 and caspase-3 in human brain after head injury. *FASEB J.* **13**, 813–821.
 39. Allen J. W., Knoblach S. M., and Faden A. I. (1999) Combined mechanical trauma and metabolic impairment in vitro induces NMDA receptor-dependent neuronal cell death and caspase-3-dependent apoptosis. *FASEB J.* **13**, 1875–1882.
 40. Scaffidi C., Fulda S., Srinivasan A., et al. (1998) Two CD95 (APO-1/Fas) signaling pathways. *EMBO J.* **17**, 1675–1687.
 41. Li P., Nijhawan D., Budihardjo I., et al. (1997) Cytochrome c and dATP-dependent formation of Apaf-1/caspase-9 complex initiates an apoptotic protease cascade. *Cell* **91**, 479–489.
 42. Slee E. A., Harte M. T., Kluck R. M., et al. (1999) Ordering the cytochrome c-initiated caspase cascade: hierarchical activation of caspases-2, -3, -6, -7, -8, and -10 in a caspase-9-dependent manner. *J. Cell Biol.* **144**, 281–292.

43. Ashkenazi A. and Dixit V. M. (1998) Death receptors: signaling and modulation. *Science* **281**, 1305–1308.
44. Aravind L., Dixit V. M., and Koonin E. V. (1999) The domains of death: evolution of the apoptosis machinery. *Trends Biochem Sci.* **24**, 47–53.
45. Nagata S. (1997) Apoptosis by death factor. *Cell* **88**, 355–365.
46. Boldin M. P., Goncharov T. M., Goltsev Y. V., and Wallach D. (1996) Involvement of MACH, a novel MORT1/FADD-interacting protease, in Fas/APO-1- and TNF receptor-induced cell death. *Cell* **85**, 803–815.
47. Fernandes-Alnemri T., Armstrong R. C., Krebs J., et al. (1996) In vitro activation of CPP32 and Mch3 by Mch4, a novel human apoptotic cysteine protease containing two FADD-like domains. *Proc. Natl. Acad. Sci. USA* **93**, 7464–7469.
48. Muzio M., Chinnaiyan A. M., Kischkel F. C., et al. (1996) FLICE, a novel FADD-homologous ICE/CED-3-like protease, is recruited to the CD95 (Fas/APO-1) death-inducing signaling complex. *Cell* **85**, 817–827.
49. Kischkel F. C., Hellbardt S., Behrmann I., et al. (1995) Cytotoxicity-dependent APO-1 (Fas/CD95)-associated proteins form a death-inducing signaling complex (DISC) with the receptor. *EMBO J.* **14**, 5579–5588.
50. Woo M., Hakem A., Elia A. J., et al. (1999) In vivo evidence that caspase-3 is required for Fas-mediated apoptosis of hepatocytes. *J. Immunol.* **163**, 4909–4916.
51. Li H., Zhu H., Xu C. J., and Yuan J. (1998) Cleavage of BID by caspase 8 mediates the mitochondrial damage in the Fas pathway of apoptosis. *Cell* **94**, 491–501.
52. Murphy K. M., Streips U. N., and Lock R. B. (1999) Bax membrane insertion during Fas(CD95)-induced apoptosis precedes cytochrome c release and is inhibited by Bcl-2. *Oncogene* **18**, 5991–5999.
53. Luo X., Budihardjo I., Zou H., Slaughter C., and Wang X. (1998) Bid, a Bcl2 interacting protein, mediates cytochrome c release from mitochondria in response to activation of cell surface death receptors. *Cell* **94**, 481–490.
54. Kudla G., Montessuit S., Eskes R., et al. (2000) The destabilization of lipid membranes induced by the C-terminal fragment of caspase 8-cleaved bid is inhibited by the N-terminal fragment. *J. Biol. Chem.* **275**, 22,713–22,718.
55. Irmeler M., Thome M., Hahne M., et al. (1997) Inhibition of death receptor signals by cellular FLIP [see comments]. *Nature* **388**, 190–195.
56. Zou H., Henzel W. J., Liu X., Lutschg A., and Wang X. (1997) Apaf-1, a human protein homologous to C. elegans CED-4, participates in cytochrome c-dependent activation of caspase-3 [see comments]. *Cell* **90**, 405–413.
57. Zou H., Li Y., Liu X., and Wang X. (1999) An APAF-1, cytochrome c multimeric complex is a functional apoptosome that activates procaspase-9. *J. Biol. Chem.* **274**, 11,549–11,556.
58. Kulms D. and Schwarz T. (2000) Molecular mechanisms of UV-induced apoptosis. *Photo-dermatol. Photoimmunol. Photomed.* **16**, 195–201.
59. Robertson J. D. and Orrenius S. (2000) Molecular mechanisms of apoptosis induced by cytotoxic chemicals. *Crit. Rev. Toxicol.* **30**, 609–627.
60. Richter C. and Ghafourifar P. (1999) Ceramide induces cytochrome c release from isolated mitochondria. *Biochem. Soc. Symp.* **66**, 27–31.
61. Brown G. C. and Borutaite V. (1999) Nitric oxide, cytochrome c and mitochondria. *Biochem. Soc. Symp.* **66**, 17–25.
62. Hakem R., Hakem A., Duncan G. S., et al. (1998) Differential requirement for caspase 9 in apoptotic pathways in vivo. *Cell* **94**, 339–352.
63. Cecconi F., Alvarez-Bolado G., Meyer B. I., Roth K. A., and Gruss P. (1998) Apaf1 (CED-4 homolog) regulates programmed cell death in mammalian development. *Cell* **94**, 727–737.
64. Yoshida H., Kong Y. Y., Yoshida R., et al. (1998) Apaf1 is required for mitochondrial pathways of apoptosis and brain development. *Cell* **94**, 739–750.
65. Honarpour N., Du C., Richardson J. A., Hammer R. E., Wang X., and Herz J. (2000) Adult Apaf-1-deficient mice exhibit male infertility. *Dev. Biol.* **218**, 248–258.
66. Kuida K., Haydar T. F., Kuan C. Y., et al. (1998) Reduced apoptosis and cytochrome c-mediated caspase activation in mice lacking caspase 9. *Cell* **94**, 325–337.
67. Gonzalez-Garcia M., Perez-Ballesteros R., Ding L., et al. (1994) bcl-XL is the major bcl-x mRNA form expressed during murine development and its product localizes to mitochondria. *Development* **120**, 3033–3042.
68. Motoyama N., Wang F., Roth K. A., et al. (1995) Massive cell death of immature hematopoietic cells and neurons in Bcl-x- deficient mice. *Science* **267**, 1506–1510.

69. Pan G., O'Rourke K., and Dixit V. M. (1998) Caspase-9, Bcl-XL, and Apaf-1 form a ternary complex. *J. Biol. Chem.* **273**, 5841–5845.
70. Moriishi K., Huang D. C., Cory S., and Adams J. M. (1999) Bcl-2 family members do not inhibit apoptosis by binding the caspase activator Apaf-1. *Proc. Natl. Acad. Sci. USA* **96**, 9683–9688.
71. Hausmann G., O'Reilly L. A., van Driel R., et al. (2000) Pro-apoptotic apoptosis protease-activating factor 1 (Apaf-1) has a cytoplasmic localization distinct from Bcl-2 or Bcl-x(L). *J. Cell. Biol.* **149**, 623–634.
72. Shimizu S., Konishi A., Kodama T., and Tsujimoto Y. (2000) BH4 domain of antiapoptotic Bcl-2 family members closes voltage-dependent anion channel and inhibits apoptotic mitochondrial changes and cell death [published erratum appears in *Proc. Natl. Acad. Sci. USA* 2000 Aug 1;97(16):9347]. *Proc. Natl. Acad. Sci. USA* **97**, 3100–3105.
73. Fujita N., Nagahashi A., Nagashima K., Rokudai S., and Tsuruo T. (1998) Acceleration of apoptotic cell death after the cleavage of Bcl-XL protein by caspase-3-like proteases. *Oncogene* **17**, 1295–1304.
74. Hsu Y. T., Wolter K. G., and Youle R. J. (1997) Cytosol-to-membrane redistribution of Bax and Bcl-X(L) during apoptosis. *Proc. Natl. Acad. Sci. USA* **94**, 3668–3672.
75. Wolter K. G., Hsu Y. T., Smith C. L., Nechustan A., Xi X. G., and Youle R. J. (1997) Movement of Bax from the cytosol to mitochondria during apoptosis. *J. Cell Biol.* **139**, 1281–1292.
76. Goping I. S., Gross A., Lavoie J. N., et al. (1998) Regulated targeting of BAX to mitochondria. *J. Cell Biol.* **143**, 207–215.
77. Chinnaiyan A. M. (1999) The apoptosome: heart and soul of the cell death machine. *Neoplasia* **1**, 5–15.
78. Eskes R., Antonsson B., Osen-Sand A., et al. (1998) Bax-induced cytochrome C release from mitochondria is independent of the permeability transition pore but highly dependent on Mg^{2+} ions. *J. Cell Biol.* **143**, 217–224.
79. Priault M., Chaudhuri B., Clow A., Camougrand N., and Manon S. (1999) Investigation of bax-induced release of cytochrome c from yeast mitochondria permeability of mitochondrial membranes, role of VDAC and ATP requirement. *Eur. J. Biochem.* **260**, 684–691.
80. Gross A., Jockel J., Wei M. C., and Korsmeyer S. J. (1998) Enforced dimerization of BAX results in its translocation, mitochondrial dysfunction and apoptosis. *EMBO J.* **17**, 3878–3885.
81. Shindler K. S., Latham C. B., and Roth K. A. (1997) Bax deficiency prevents the increased cell death of immature neurons in bcl-x-deficient mice. *J. Neurosci.* **17**, 3112–3119.
82. Sedlak T. W., Oltvai Z. N., Yang E., et al. (1995) Multiple Bcl-2 family members demonstrate selective dimerizations with Bax. *Proc. Natl. Acad. Sci. USA* **92**, 7834–7838.
83. Knudson C. M., Tung K. S., Tourtellotte W. G., Brown G. A., and Korsmeyer S. J. (1995) Bax-deficient mice with lymphoid hyperplasia and male germ cell death. *Science* **270**, 96–99.
84. Deckwerth T. L., Elliott J. L., Knudson C. M., Johnson E. M., Jr., Snider W. D., and Korsmeyer S. J. (1996) BAX is required for neuronal death after trophic factor deprivation and during development. *Neuron* **17**, 401–411.
85. Minn A. J., Boise L. H., and Thompson C. B. (1996) Bcl-x(S) antagonizes the protective effects of Bcl-x(L). *J. Biol. Chem.* **271**, 6306–6312.
86. Yang X. F., Weber G. F., and Cantor H. (1997) A novel Bcl-x isoform connected to the T cell receptor regulates apoptosis in T cells. *Immunity* **7**, 629–639.
87. Srinivasula S. M., Ahmad M., Guo Y., et al. (1999) Identification of an endogenous dominant-negative short isoform of caspase-9 that can regulate apoptosis. *Cancer Res.* **59**, 999–1002.
88. Benedict M. A., Hu Y., Inohara N., and Nunez G. (2000) Expression and functional analysis of Apaf-1 isoforms. Extra Wd-40 repeat is required for cytochrome c binding and regulated activation of procaspase-9. *J. Biol. Chem.* **275**, 8461–8468.
89. Jiang Z. H. and Wu J. Y. (1999) Alternative splicing and programmed cell death. *Proc. Soc. Exp. Biol. Med.* **220**, 64–72.
90. Cardone M. H., Roy N., Stennicke H. R., et al. (1998) Regulation of cell death protease caspase-9 by phosphorylation [see comments]. *Science* **282**, 1318–1321.
91. Fujita E., Jinbo A., Matuzaki H., Konishi H., Kikkawa U., and Momoi T. (1999) Akt phosphorylation site found in human caspase-9 is absent in mouse caspase-9. *Biochem. Biophys. Res. Commun.* **264**, 550–555.
92. Zhou H., Li X. M., Meinkoth J., and Pittman R. N. (2000) Akt regulates cell survival and apoptosis at a postmitochondrial level [In Process Citation]. *J. Cell Biol.* **151**, 483–494.

93. Datta S. R., Dudek H., Tao X., et al. (1997) Akt phosphorylation of BAD couples survival signals to the cell-intrinsic death machinery. *Cell* **91**, 231–241.
94. Wang H. G., Pathan N., Ethell I. M., et al. (1999) Ca^{2+} -induced apoptosis through calcineurin dephosphorylation of BAD. *Science* **284**, 339–343.
95. Ayllon V., Martinez A. C., Garcia A., Cayla X., and Rebollo A. (2000) Protein phosphatase 1 α is a Ras-activated Bad phosphatase that regulates interleukin-2 deprivation-induced apoptosis. *EMBO J.* **19**, 2237–2246.
96. Yang E., Zha J., Jockel J., Boise L. H., Thompson C. B., and Korsmeyer S. J. (1995) Bad, a heterodimeric partner for Bcl-XL and Bcl-2, displaces Bax and promotes cell death. *Cell* **80**, 285–291.
97. Francois F. and Grimes M. L. (1999) Phosphorylation-dependent Akt cleavage in neural cell in vitro reconstitution of apoptosis. *J. Neurochem.* **73**, 1773–1776.
98. Pandey P., Saleh A., Nakazawa A., et al. (2000) Negative regulation of cytochrome c-mediated oligomerization of apaf-1 and activation of procaspase-9 by heat shock protein 90 [In Process Citation]. *EMBO J.* **19**, 4310–4322.
99. Beere H. M., Wolf B. B., Cain K., et al. (2000) Heat-shock protein 70 inhibits apoptosis by preventing recruitment of procaspase-9 to the Apaf-1 apoptosome. *Nat. Cell Biol.* **2**, 469–475.
100. Bruey J. M., Ducasse C., Bonniaud P., et al. (2000) Hsp27 negatively regulates cell death by interacting with cytochrome c. *Nat. Cell Biol.* **2**, 645–652.
101. Hay B. A. (2000) Understanding IAP function and regulation: a view from *Drosophila*. *Cell Death Differ* **7**, 1045–1056.
102. Du C., Fang M., Li Y., Li L., and Wang X. (2000) Smac, a mitochondrial protein that promotes cytochrome c-dependent caspase activation by eliminating IAP inhibition. *Cell* **102**, 33–42.
103. Nakagawa T., Zhu H., Morishima N., et al. (2000) Caspase-12 mediates endoplasmic-reticulum-specific apoptosis and cytotoxicity by amyloid- β . *Nature* **403**, 98–103.
104. Bitko V. and Barik S. (2001) An endoplasmic reticulum-specific stress-activated caspase (caspase-12) is implicated in the apoptosis of A549 epithelial cells by respiratory syncytial virus. *J. Cell Biochem.* **80**, 441–454.
105. Nakagawa T. and Yuan J. (2000) Cross-talk between two cysteine protease families. Activation of caspase-12 by calpain in apoptosis. *J. Cell Biol.* **150**, 887–894.
106. Wang S., Miura M., Jung Y. K., Zhu H., Li E., and Yuan J. (1998) Murine caspase-11, an ICE-interacting protease, is essential for the activation of ICE. *Cell* **92**, 501–509.
107. Kang S. J., Wang S., Hara H., et al. (2000) Dual role of caspase-11 in mediating activation of caspase-1 and caspase-3 under pathological conditions. *J. Cell Biol.* **149**, 613–622.
108. Schotte P., Van Crielinge W., Van de Craen M., et al. (1998) Cathepsin B-mediated activation of the proinflammatory caspase-11. *Biochem. Biophys. Res. Commun.* **251**, 379–387.
109. Hall K. E. and Wiley J. W. (1998) Neural injury, repair and adaptation in the GI tract. I. New insights into neuronal injury: a cautionary tale. *Am. J. Physiol.* **274**, G978–983.
110. Krajewski S., Krajewska M., Ellerby L. M., et al. (1999) Release of caspase-9 from mitochondria during neuronal apoptosis and cerebral ischemia. *Proc. Natl. Acad. Sci. USA* **96**, 5752–5757.
111. Morita-Fujimura Y., Fujimura M., Kawase M., Chen S. F., and Chan P. H. (1999) Release of mitochondrial cytochrome c and DNA fragmentation after cold injury-induced brain trauma in mice: possible role in neuronal apoptosis. *Neurosci. Lett.* **267**, 201–205.
112. Buki A., Okonkwo D. O., Wang K. K., and Povlishock J. T. (2000) Cytochrome c release and caspase activation in traumatic axonal injury. *J. Neurosci.* **20**, 2825–2834.
113. Tamatani M., Mitsuda N., Matsuzaki H., et al. (2000) A pathway of neuronal apoptosis induced by hypoxia/reoxygenation: roles of nuclear factor- κ B and Bcl-2. *J. Neurochem.* **75**, 683–693.
114. Ouyang Y. B., He Q. P., Li P. A., Janelidze S., Wang G. X., and Siesjo B. K. (2000) Is neuronal injury caused by hypoglycemic coma of the necrotic or apoptotic type? [In Process Citation]. *Neurochem. Res.* **25**, 661–667.
115. Deshmukh M., Kuida K., and Johnson E. M., Jr. (2000) Caspase inhibition extends the commitment to neuronal death beyond cytochrome c release to the point of mitochondrial depolarization. *J. Cell Biol.* **150**, 131–143.
116. Knoblach S. M., Fan L., Huang X., Krajewski S., Reed J. C., and Faden A. I. (2000) Activation of caspases 3 and 9 after traumatic brain injury in the rat: treatment with a pan-caspase inhibitor improves outcome. *Soc. Neurosci. Abst.*

117. Endres M., Namura S., Shimizu-Sasamata M., et al. (1998) Attenuation of delayed neuronal death after mild focal ischemia in mice by inhibition of the caspase family. *J. Cereb. Blood Flow Metab.* **18**, 238–247.
118. Bossenmeyer-Pourie C., Koziel V., and Daval J. L. (1999) CPP32/CASPASE-3-like proteases in hypoxia-induced apoptosis in developing brain neurons. *Brain Res. Mol. Brain Res.* **71**, 225–237.
119. Kondratyev A. and Gale K. (2000) Intracerebral injection of caspase-3 inhibitor prevents neuronal apoptosis after kainic acid-evoked status epilepticus. *Brain Res. Mol. Brain Res.* **75**, 216–224.
120. Kermer P., Klocker N., and Bahr M. (1999) Long-term effect of inhibition of ced 3-like caspases on the survival of axotomized retinal ganglion cells in vivo. *Exp. Neurol.* **158**, 202–205.
121. Springer J. E., Azbill R. D., and Knapp P. E. (1999) Activation of the caspase-3 apoptotic cascade in traumatic spinal cord injury. *Nat. Med.* **5**, 943–946.
122. Sanchez I., Xu C. J., Juo P., Kakizaka A., Blenis J., and Yuan J. (1999) Caspase-8 is required for cell death induced by expanded polyglutamine repeats [see comments]. *Neuron* **22**, 623–633.
123. Ivins K. J., Thornton P. L., Rohn T. T., and Cotman C. W. (1999) Neuronal apoptosis induced by beta-amyloid is mediated by caspase-8. *Neurobiol. Dis.* **6**, 440–449.
124. Felderhoff-Mueser U., Taylor D. L., Greenwood K., et al. (2000) Fas/CD95/APO-1 can function as a death receptor for neuronal cells in vitro and in vivo and is upregulated following cerebral hypoxic-ischemic injury to the developing rat brain. *Brain Pathol.* **10**, 17–29.
125. Matsushita K., Wu Y., Qiu J., et al. (2000) Fas receptor and neuronal cell death after spinal cord ischemia. *J. Neurosci.* **20**, 6879–6887.
126. Velier J. J., Ellison J. A., Kikly K. K., Spera P. A., Barone F. C., and Feuerstein G. Z. (1999) Caspase-8 and caspase-3 are expressed by different populations of cortical neurons undergoing delayed cell death after focal stroke in the rat. *J. Neurosci.* **19**, 5932–5941.
127. Bittigau P., Siffringer M., Pohl D., et al. (1999) Apoptotic neurodegeneration following trauma is markedly enhanced in the immature brain. *Ann. Neurol.* **45**, 724–735.
128. Pohl D., Bittigau P., Ishimaru M. J., et al. (1999) N-Methyl-D-aspartate antagonists and apoptotic cell death triggered by head trauma in developing rat brain. *Proc. Natl. Acad. Sci. USA* **96**, 2508–2513.
129. de Bilbao F., Guarin E., Nef P., Vallet P., Giannakopoulos P., and Dubois-Dauphin M. (1999) Postnatal distribution of cpp32/caspase 3 mRNA in the mouse central nervous system: an in situ hybridization study. *J. Comp. Neurol.* **409**, 339–357.
130. Hu B. R., Liu C. L., Ouyang Y., Blomgren K., and Siesjo B. K. (2000) Involvement of caspase-3 in cell death after hypoxia-ischemia declines during brain maturation. *J. Cereb. Blood Flow Metab.* **20**, 1294–1300.

Small Shifts in Craniotomy Position in the Lateral Fluid Percussion Injury Model Are Associated with Differential Lesion Development

ROBERT VINK, PAUL G.M. MULLINS, MEREDITH D. TEMPLE, WEILI BAO,
and ALAN I. FADEN

ABSTRACT

Previous studies have shown that location and direction of injury may affect outcome in experimental models of traumatic brain injury. Significant variability in outcome data has also been noted in studies using the lateral fluid percussion brain injury model (FPI) in rats. In recent studies from our laboratory, we observed considerable variability in localization and severity of tissue damage as a function of small changes in craniotomy position. To further address this issue, we examined the relationship between craniotomy position and brain lesion size/location in rats subjected to moderate FPI (2.28 ± 0.18 atmospheres). With placement of a 5-mm craniotomy adjacent to the sagittal suture, there was both ipsilateral and contralateral damage as detected at 3 weeks posttrauma using T₂-weighted magnetic resonance imaging (MRI). The MRI lesions were generally restricted to the hippocampus and subcortical layers. Shifting of the craniotomy site laterally was associated with increased ipsilateral tissue damage and a greater cortical component that correlated with distance from the sagittal suture. In contrast, the contralateral MRI lesion did not change significantly in size or location unless the center of the craniotomy was placed more than 3.5 mm from the sagittal suture, under which condition contralateral damage could no longer be detected. Ipsilateral tissue damage as determined from the MRI scans was linearly correlated to motor outcome but not with cognitive outcome as assessed by the Morris Water Maze. We conclude that craniotomy position is critical in determining extent and location of tissue injury produced during the lateral FPI model in rats. Addressing such potential variability is essential for studies that address either injury mechanisms or therapeutic treatments.

Key words: behavioral outcome; lesions; magnetic resonance imaging; neurotrauma

INTRODUCTION

A NUMBER of experimental brain injury models have been developed to mimic certain features of clinical brain trauma (Gennarelli, 1994). One of the most widely used is the lateral (parasagittal) fluid percussion injury

(FPI) model in rats. This model was originally developed by McIntosh et al. (1989) to induce a more focal, unilateral injury in rats with less brainstem involvement than midline FPI models (Dixon et al., 1987, 1988; McIntosh et al., 1987b). As originally described, lateral FPI showed good rates of survival, even in nonventilated animals, and

induced substantial cortical and subcortical lesions that were limited to the parietal lobe of the injured hemisphere (McIntosh et al., 1989). As a result, this adaptation facilitated the study of mechanisms of posttraumatic tissue damage and evaluation of experimental pharmacotherapies.

Various adaptations of the lateral FPI model have been developed to better parallel certain features characteristic of clinical trauma. These include induction of injury with either an open dura, a second craniotomy over the contralateral hemisphere, or a combination of trauma plus a secondary insult such as hypoxia, hypotension, or hemorrhage, amongst others (Bramlett et al., 1999; Gennarelli, 1994; Glass et al., 1999). Despite introducing a higher degree of variability, these adaptations have established that secondary and combination insults result in a more widespread injury encompassing both hemispheres, with exacerbation of injury deficits. Recent reports, however, have suggested that the lateral FPI model may have an inherent variability that may lead to widespread, bilateral injury rather than the unilateral injury that has most commonly been reported in this model. Floyd et al. (1997) have suggested that both outcome and mortality can be variable in the lateral FPI model depending on the location of the craniotomy. In studies from our laboratory, we have observed considerable variability in localization and severity of tissue damage as a function of small changes in craniotomy position using this model. Thus, alterations of the craniotomy position in lateral FPI may result in variable formation of lesions and variable biochemical changes, both ipsilaterally and contralaterally.

Magnetic resonance imaging (MRI) offers a noninvasive means by which to characterize the relationship between craniotomy position and lesion size/location. Lesions following traumatic brain injury (TBI) can be readily identified using standard T₂-weighted imaging techniques (Qian et al., 1996), and the images also provide an accurate means by which to pinpoint the craniotomy position. Moreover, because of the noninvasive nature of MRI techniques, neurological assessment of posttraumatic motor and cognitive performance can be determined in the same animals. The present study used MRI techniques to examine the relationship between craniotomy position, lesion location/size and motor/cognitive outcome in rats subjected to lateral fluid percussion-induced TBI. We demonstrate that lesion variability, both in location and size, can be caused by very small lateral shifts in craniotomy position, and that these changes may account for some of the variability noted in this model of TBI.

MATERIALS AND METHODS

Induction of Injury

All experiments were conducted according to the National Research Council Guide for the Care and Use of Laboratory Animals, and were approved by the Georgetown University Animal Care Committee.

Lateral FPI was induced in rats as previously described (Faden et al., 1999; McIntosh et al., 1989). Briefly, male Sprague-Dawley rats ($n = 21$; 385–410 g) were fed and watered *ad libitum* before being anesthetized with 70 mg/kg sodium pentobarbital i.p. An arterial line (PE50) was then inserted into either the femoral or tail artery for continuous monitoring of blood pressure and periodic sampling of arterial blood gases throughout the surgical procedures. After exposing the skull by midline incision and reflection of the scalp and temporalis muscle, a 5-mm craniotomy was placed over the left parietal cortex midway between the lambda and bregma sutures, but varying in lateral location between the sagittal suture and the temporal ridge. A female Leur-Loc was then glued within the craniotomy to facilitate connection to the injury device and fixed in place using dental cement. The dura was left intact at the opening. After the dental cement had dried, injury was induced using a lateral fluid percussion injury device (Faden et al., 1999; McIntosh et al., 1989). This device results in an isotonic saline pressure pulse generated within a Plexiglas tube and rapidly injected (~22 msec) into the extradural space of the rat via the Leur-Loc connection. This causes a brief and transient deformation of the brain tissue resulting in the formation of lesions and the associated development of neurologic deficits. The pressure of the saline pulse is measured in atmospheres (atm) using a force transducer placed immediately prior to the Leur-Loc connection, and then recorded on an oscilloscope. The pulse pressure in the present experiments was between 2.10 and 2.46 atm, which is consistent with what has been described as moderate injury. After injury, the dental cement and Leur-Loc were removed, the incisions sutured, and the animals allowed to recover on a heating pad used to maintain animal rectal temperature at 37°C throughout the surgery and induction of injury. Upon recovery, animals were returned to their home cages.

Magnetic Resonance Imaging

At three weeks after injury, all animals were reanesthetized with sodium pentobarbital (70 mg/kg i.p.) and subjected to MRI examination using a Bruker 7.0-tesla magnetic resonance spectrometer/imager as previously described (Albensi et al., 2000). Briefly, animals were

placed in a Plexiglas holder in which a heating pad warmed to 37°C was fixed to maintain the animal's temperature. A respiratory motion detector was positioned over the thorax to facilitate respiratory gating. The plexiglas holder was then positioned in the center of the magnet bore where a proton tuned birdcage coil had been positioned. Field homogeneity across the brain was then optimized and sagittal and coronal scout images obtained to orient the transverse slices throughout the brain region of interest. A T₂-weighted, multislice, multiecho imaging sequence was then initiated to obtain eight contiguous slices using the following parameters: field of view, 3.0 × 3.0 cm; slice thickness, 2 mm; resolution, 128 × 128; repetition time, 1.5 sec; echo time, 20 msec; number of echoes, 4. Respiratory gating was used throughout the acquisition of the T₂-weighted images making total imaging time approximately 8 min. Lesion volumes and craniotomy position were determined independently by two different observers directly off the MRI slices using the resident Bruker Paravision imaging software.

Neurological Assessment

Motor scoring was performed on days 7 and 14 after TBI using three separate tests (Faden et al., 1999), each of which is scored via an ordinal scale ranging from zero (no function) to five (normal function). Tests include the ability to maintain position on an inclined plane in the vertical and two horizontal positions, forelimb flexion and forced lateral pulsion. Forelimb flexion measures the reflex extension of the forelimb to break a fall when suspended by the tail. Lateral pulsion measures the degree of resistance to a lateral push. Each of seven individual scores (vertical angle, right and left horizontal angle, right and left forelimb flexion, right and left lateral pulsion) were added to yield a composite neurological score ranging from 0 to 35.

Cognitive outcome (spatial learning) was determined using the hidden platform version of the Morris water maze (MWM) as previously described (Faden et al., 1999). Briefly, rats are trained to locate a hidden, submerged platform using constant extramaze visual information. The apparatus consists of a large, white circular pool (900 mm diameter, 500 mm high, water temperature 24 ± 1°C) with a Plexiglas platform 76 mm in diameter painted white and submerged 15 mm below the surface of the water (225 mm high). The surface of the water is rendered opaque with the addition of dilute, white, nontoxic paint (Crayola, Tempura paint). During training, the platform remained in a constant location hidden in one quadrant 14 cm from the side wall. The rat was gently placed in the water facing the wall at one of

four randomly chosen locations separated by 90°. The latency to find the hidden platform within a 90-sec criterion time was recorded by a blinded observer. Four trials per day were conducted on days 14, 15, 16, and 17 postinjury.

Histology

At the conclusion of neurologic assessments and MRI studies at 3 weeks after injury, all rats were euthanized, their brains removed, embedded in OCT and frozen with isopentane in dry ice. Coronal 20-μm sections through the injury site were then cut with a cryostat and mounted on glass slides. Sections were then defatted, stained with cresyl violet, dehydrated and coverslipped. Sections were observed for morphological damage at the light microscopic level (Olympus).

Statistical Analysis

Correlations between craniotomy position and neurological outcome measures were analyzed using the non-parametric Spearman rank test for linear regression. All other data were analyzed by parametric Pearson linear regression tests.

RESULTS

Induction of lateral fluid percussion injury always resulted in development of hyperintense lesions on T₂-weighted MRI scans obtained 3 weeks after trauma (Fig. 1). When the craniotomy was centered more than 3.5 mm from the sagittal suture, such tissue damage could be clearly identified on MRI in the ipsilateral hemisphere (Fig. 1A,B). The MRI lesions were typically large and were located in the cortex and hippocampus, extending into other subcortical regions. At this craniotomy distance from the midline, FPI did not result in any identifiable hyperintense lesions in the contralateral hemisphere. Locating the center of the craniotomy nearer than 3.5 mm to the sagittal suture resulted in smaller ipsilateral MRI lesions throughout the whole hemisphere as well as the consistent appearance of contralateral MRI enhancement (Fig. 1C,D). The ipsilateral hyperintensity was limited to the hippocampus and subcortical layers with little involvement of the cortex. The contralateral hyperintensity uniformly involved the hippocampus, with occasional subcortical involvement. There was no significant cortical involvement in the contralateral hemisphere.

Histological examination at 3 weeks posttrauma confirmed that the hyperintense lesions observed by MRI demonstrated evidence of tissue damage. In the ipsilat-

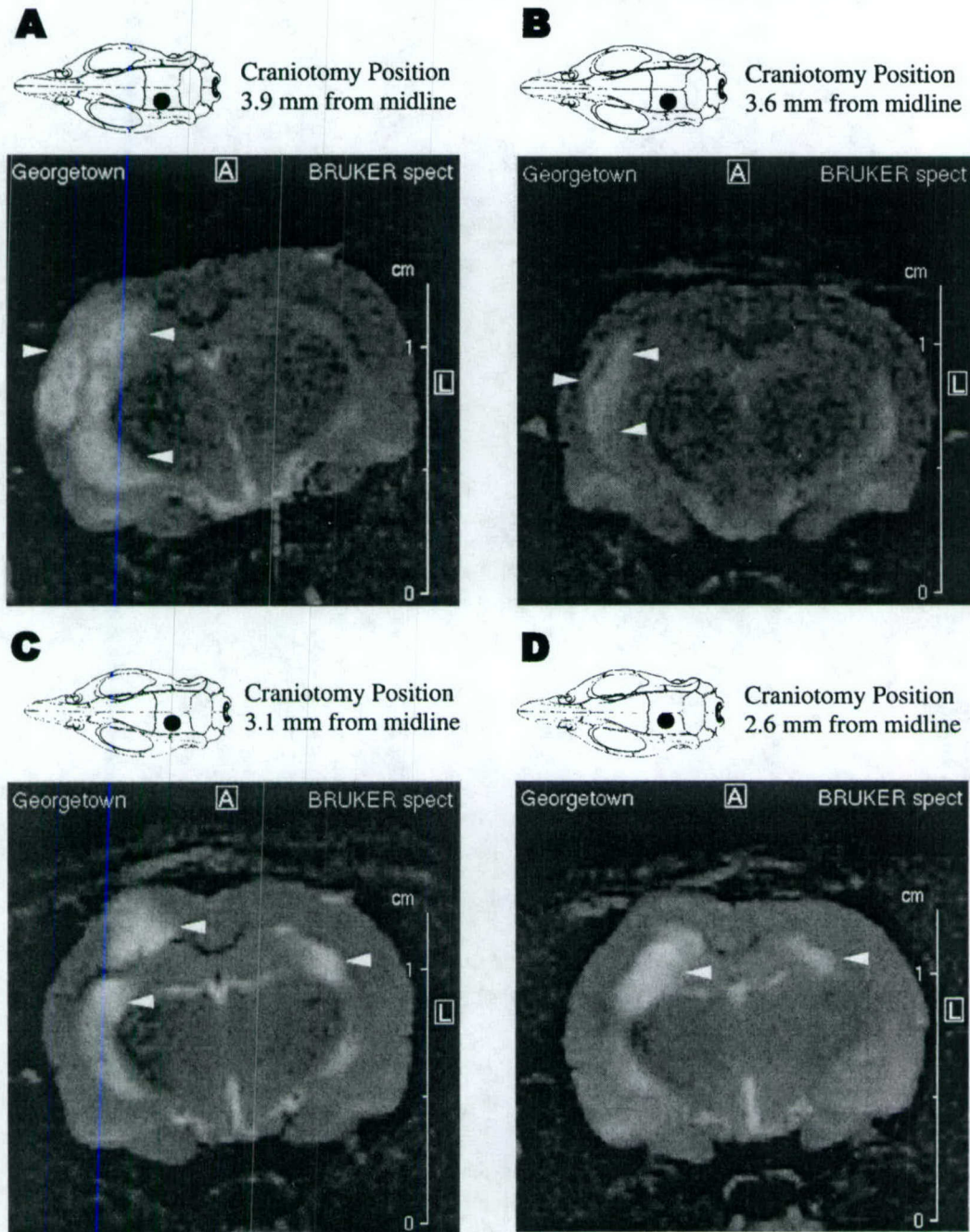


FIG. 1. T₂-weighted magnetic resonance images of a rat brain 21 days after lateral fluid percussion injury. The craniotomy was centered between 3.9 and 2.6 mm from the midline. The location of the craniotomy in the individual animals is shown as a black circle on the skull immediately above each magnetic resonance image: (A) 3.9 mm from the midline. (B) 3.6 mm from the midline. (C) 3.1 mm from the midline. (D) 2.6 mm from the midline. The gray circle on each skull represents the craniotomy position of 2.6 mm from midline and is included for comparison. Arrows indicate regions of hyperintensity that are indicative of tissue damage.

eral hemisphere, there was a clear loss of cortical and subcortical tissue (Fig. 2). There was also evidence of hippocampal CA3 region neuronal cell loss (Fig. 2B), although this varied between animals. In the contralateral hemisphere, the appearance of MRI hyperintensity was

associated with the consistent enlargement of the lateral ventricle with surrounding gliosis (Fig. 2C). Thus, the hyperintense T₂-weighted MRI lesions identified in the present study represent compromised tissue demonstrating histologically identified neuronal cell loss and/or, de-

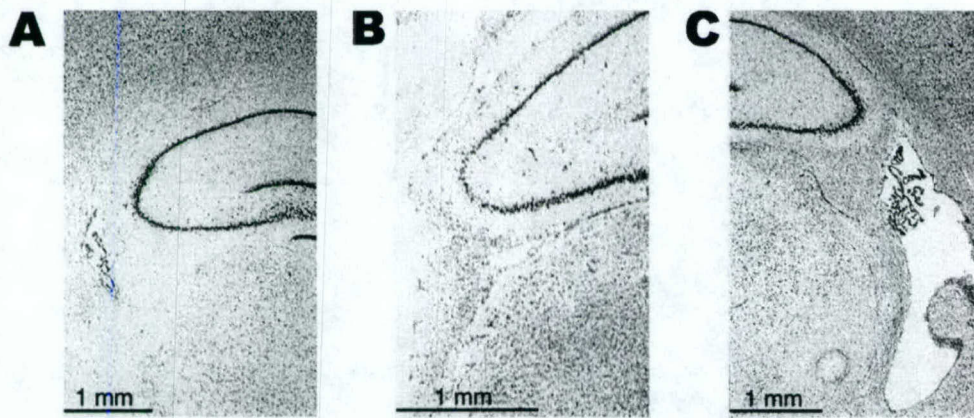


FIG. 2. Cresyl violet-stained sections of a sham animal (A), and the ipsilateral (B) and contralateral (C) injury regions as identified from the magnetic resonance images. The injured sections are taken from the same animal. Note the extensive tissue damage and CA3 loss in the ipsilateral section, while the contralateral section shows ventricular enlargement with periventricular gliosis.

pending on the location of the hyperintensity, ventricular enlargement with periventricular gliosis.

When examining craniotomy position versus appearance of contralateral MRI lesions (Fig. 3), there was no contralateral injury when the center of the craniotomy was located more than 3.5 mm from the midline. As the craniotomy was moved to between 3.3 and 3.5 mm from midline, contralateral MRI injury was frequently observed; when located less than 3.3 mm from the midline, a contralateral hyperintense lesion was always present. There was no dependence of this contralateral MRI lesion size on craniotomy position. Thus, it appears that a consistent injury affecting both the ipsilateral and contralateral hemispheres is produced when the center of the craniotomy is located within 3.5 mm of the midline. Over this range, the ipsilateral MRI lesion volume was linearly related to the craniotomy position ($r = 0.54$, $p < 0.05$; Fig. 4). The closer to the midline the craniotomy was positioned, the smaller the ipsilateral MRI lesion volume. Moreover, within this range there was also a linear correlation between craniotomy position and 2-week motor scores ($r = 0.62$, $p < 0.01$; Fig. 5). The closer to the midline the craniotomy was positioned, the smaller the degree of resultant neurologic motor deficit. There was no correlation between MRI lesion volume or craniotomy position with results of the cognitive testing in the Morris water maze (results not shown). This may be a reflection of consistent disruption of the ipsilateral hippocampus observed in the present study. Moreover, there was no correlation between the magnitude of the fluid percussion pressure pulse and MRI lesion volume ($r = 0.02$, $p = 0.94$; results not shown), confirming that differing injury magnitude between 2.10 and 2.46 atm could

not account for the observed differences in MRI lesion volume.

DISCUSSION

The present study has shown that small shifts in the location of injury site using the lateral FPI model of brain injury results in marked differences in tissue injury as indicated by lesion location, size, and associated neurologic

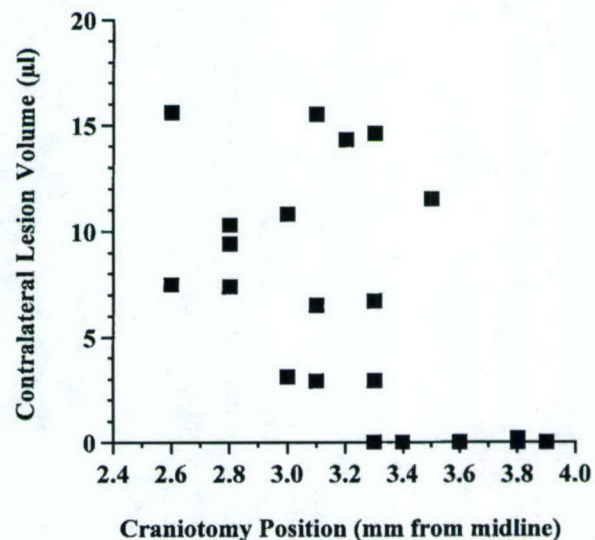


FIG. 3. Craniotomy position versus contralateral lesion size in rats following lateral fluid percussion injury. At distances greater than 3.5 mm from the midline, no contralateral lesions could be identified from the magnetic resonance images.

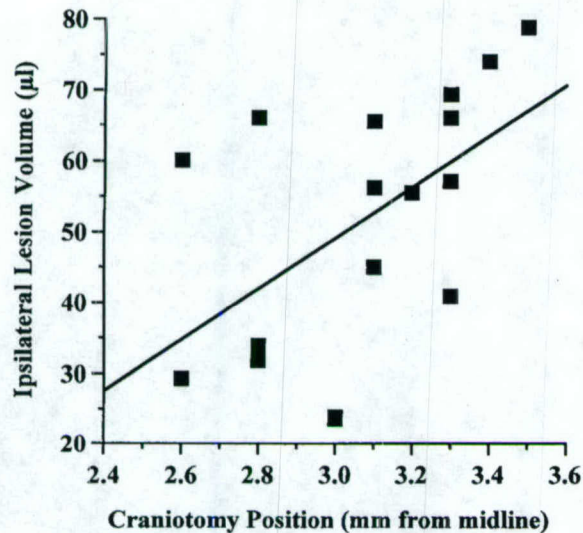


FIG. 4. Relationship between craniotomy position and ipsilateral size over the range 2.6 to 3.5 mm from midline where uniform contralateral injury was consistently present ($r = 0.54$; $p < 0.05$).

outcome. A more lateral craniotomy position as originally proposed by McIntosh et al. (1989) resulted in unilateral injury with significant MRI lesions located in the ipsilateral cortex, hippocampus and other subcortical structures. A more medial craniotomy position (but still over the same, single hemisphere) resulted in bilateral MRI lesions to the hippocampus with reduced involvement of cortical tissue in the ipsilateral hemisphere, and no identifiable damage in the contralateral cortex. Craniotomy position was correlated to both ipsilateral MRI lesion size and motor outcome. These results indicate that even 1-mm shifts in craniotomy position can markedly alter the resultant injury profile following lateral FPI.

The original lateral FPI model was developed by McIntosh et al. (1989) in the late 1980s. At that time, the central FPI model was widely used (Dixon et al., 1987, 1988). At moderate injury levels, central FPI produced little, if any, contusion (Gennarelli, 1994), whereas at more severe injury levels it caused scattered brainstem axonal damage (Dixon et al., 1987; Shima and Marmarou, 1991). There was, however, significant bilateral disruption of the blood-brain barrier (Jiang et al., 1992), including both hippocampi (Schmidt and Grady, 1993). Relocating the injury site laterally resulted in less brainstem damage (Thibault et al., 1992) and an associated improvement in survival in nonventilated animals. Moreover, it also produced obvious lesions beneath the impact site with associated cell loss in the ipsilateral cortex and hippocampus (Schmidt and Grady, 1993). No contralateral injury was associated with these initial studies (Smith

et al., 1991). The occurrence of a cortical lesion with this lateral model facilitated the noninvasive magnetic resonance studies of biochemical changes following lateral FPI-induced TBI (Vink et al., 1987).

Later studies, however, utilizing the same lateral model of FPI have reported bilateral injury. Significant bilateral changes in edema and cations were first reported by Soares et al. (1992). This observation of bilateral damage was supported in a later publication reporting that significant accumulations of amyloid precursor proteins occur in the ipsilateral hemisphere with changes sometimes observed in the contralateral hemisphere as well (Pierce et al., 1996). Smith et al. (1994) reported that persistent cognitive dysfunction in lateral FPI was associated with bilateral hippocampal damage. This bilateral hippocampal damage was not detected in earlier studies by the same group (Smith et al., 1991). Biochemical changes have also been reported to occur bilaterally. Prasad et al. (1994) showed transient changes in basal levels of second messengers in the contralateral hippocampus following lateral FPI. Changes in receptor-coupled second messenger systems in both the ipsilateral and contralateral hippocampus at acute postinjury time points and out to 15 days following lateral FPI have been reported by Delahunty et al. (1995). These contralateral biochemical changes occurred in the absence of any overt neuronal cell loss. Thus, since 1989, the degree of involvement of the contralateral hemisphere following lateral FPI model has been reported to range from no involvement, to occasional involvement without overt cell

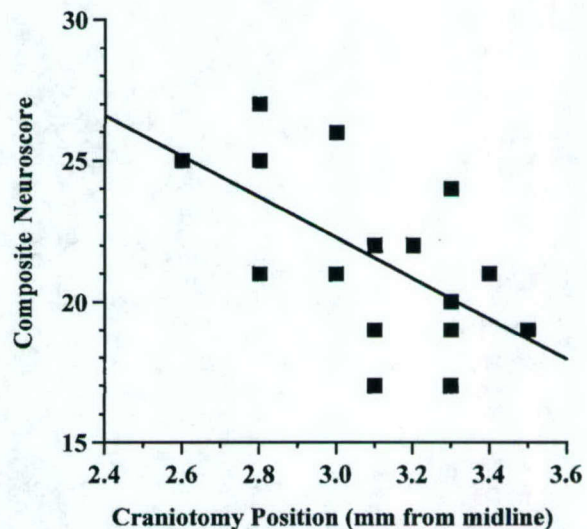


FIG. 5. Relationship between craniotomy position and 2-week motor neuroscore over the range 2.6 to 3.5 mm from midline where uniform contralateral injury was consistently present ($r = 0.62$; $p < 0.01$).

CRANIOTOMY POSITION IN FPI AND LESION DEVELOPMENT

TABLE 1. SEVERITY OF DAMAGE AND IMPAIRMENT AS A FUNCTION OF CRANIOTOMY POSITION AFTER LATERAL FLUID PERCUSSION INJURY

<i>Center of craniotomy</i>	<i>Ipsilateral lesion</i>	<i>Contralateral lesion</i>	<i>Motor deficit</i>	<i>Cognitive deficit</i>
Medial craniotomy (<3.3 mm from midline)	+	+	+	++
Central craniotomy (3.3–3.5 mm from midline)	++	+	++	+
Lateral craniotomy (>3.5 mm from midline)	+++	–	+++	+

loss, to consistent involvement with cell loss. The findings of the current study suggest that craniotomy position may be one contributing factor to this observed variability in contralateral involvement, a proposal previously suggested by Floyd et al. (1997) with respect to cognitive outcome and mortality following lateral FPI.

Hyperintensity on T_2 -weighted magnetic resonance images largely reflects increased tissue water content. Previous studies have demonstrated that, after FPI, these T_2 -weighted hyperintense lesions are correlated to histopathologic evidence of neuronal damage (Qian et al., 1996). In the present study, ipsilateral MRI hyperintensity was associated with clear neuronal cell loss. However, on the contralateral side, we did not observe overt cell loss, but rather ventricular enlargement with periventricular gliosis. Increase in the size of the lateral ventricle may be due to normal pressure hydrocephalus perhaps caused by a blockage of CSF reabsorption subsequent to trauma-induced hemorrhage. Alternatively, tissue atrophy may account for an enlargement of the lateral ventricle. The periventricular gliosis observed in the current study would suggest that some periventricular damage has occurred and may account for the enlarged ventricle. Given that the T_2 -weighted MRI clearly demonstrated contralateral hyperintensity involving the ventricles and hippocampal regions, it may be that such hyperintensity is detecting tissue that has been compromised, yet does not demonstrate overt cell loss histologically.

In the current study, we have evaluated animals at 21 days postinjury, thus permitting the identification of MRI lesions that could be correlated with the presence of persistent neurologic deficits. The persistence of such deficits was confirmed in outcome studies that identified significant motor and cognitive deficits in all animals at 2 weeks after trauma. Consistent with previous studies of lateral FPI (Albensi et al., 2000; Perri et al., 1997), increased ipsilateral lesion size following TBI was associated with an increase in motor deficits. Moreover, in the present study, the MRI-identified lesion size was corre-

lated to the position of the craniotomy. In contrast, there were no correlations in the present study between craniotomy position/lesion size and cognitive outcome. This lack of association may be a consequence of MRI lesion size in the present study being dependent on the degree of cortical involvement and not any change in hippocampal involvement. Indeed, any increase in ipsilateral MRI lesion volume with increasing distance of the craniotomy from the midline was a reflection of increasing cortical involvement, not an alteration of hippocampal involvement. The hippocampus in the ipsilateral hemisphere always showed an MRI hyperintense lesion irrespective of the craniotomy position. Since cognitive outcome in the Morris water maze is known to be associated with hippocampal function (Hamm et al., 1993), the lack of correlation between MRI-determined lesion volume and cognitive outcome supports this conclusion. Nonetheless, shifting the craniotomy position medially reduced the degree of cortical injury identified by MRI throughout the ipsilateral hemisphere but increased the incidence of MRI hyperintensity in and surrounding the contralateral hippocampus. Once induced, the contralateral MRI lesion size in the hippocampal region never changed in volume with shifting craniotomy position. Thus, the bilateral hippocampal damage in this model, as determined by MRI, was an all or none phenomenon depending on craniotomy position. Consistent bilateral injury was produced when the craniotomy was centered no more than 3.5 mm from the midline. This may have ramifications in terms of maximizing cognitive deficits using the lateral FPI model. For example, medial placement of the craniotomy will induce bilateral hippocampal damage, and presumably maximal cognitive deficits, at the expense of motor deficits, which will be reduced with any decrease in ipsilateral cortical involvement. In contrast, more lateral placement of the craniotomy will increase the degree of cortical involvement and associated motor deficits yet will reduce bilateral hippocampal damage (Table 1).

Another significant observation pertaining to the dif-

ferential involvement of the cortex in lesion development concerns studies of cortical parameters following lateral FPI. Earlier magnetic resonance studies of lateral FPI reported by the developers of the lateral FPI model (McIntosh et al., 1987a; Vink et al., 1987, 1988) demonstrated significant changes in ipsilateral metabolism following induction of injury. These included alterations in phosphate-containing metabolites, pH, free magnesium, and lactate, and were present irrespective of injury severity. These initial observations have since been replicated by a number of investigators using FPI models of brain injury (Anderson et al., 1988; Headrick et al., 1994; Heath and Vink, 1996; Ishige et al., 1988; Rubin et al., 1997). More recently, however, Golding et al. (1996) failed to demonstrate any biochemical changes in the ipsilateral hemisphere in their magnetic resonance studies of lateral FPI in rats. Because they used a small 5-mm surface coil in their studies, it is likely that the spectra these authors acquired were mostly representative of cortical tissue. In the present study, we show that small medial shifts in craniotomy position can result in a decrease in MRI-detected cortical injury in the ipsilateral hemisphere in this model. The cortical damage in the ipsilateral hemisphere detected by T₂-weighted MRI is very small when the craniotomy site is placed adjacent to the sagittal suture. Accordingly, the negative results of Golding et al. (1996) may well have represented FPI induced using a medial craniotomy position. We recommend that any results obtained using technologies that sample mostly cortical parameters following lateral FPI must therefore be interpreted with great caution.

A dependence on injury position has previously been shown in other models of injury. Cortical impact injury has been shown to result in differential development of injury depending on the location of injury (Hamm et al., 1992; Sutton et al., 1993). Indeed, the changes in injury profile with central versus lateral cortical impact injury were similar to that reported in studies comparing midline versus lateral FPI (Delahunty et al., 1995). Furthermore, the inertial acceleration model of brain injury has been shown to result in different degrees of injury depending upon the direction of injury (Kotapka et al., 1991). In the present study, we show that changes in craniotomy position as small as 1 mm result in a very different lesion location and size as identified by MRI following lateral FPI. This difference has important implications with respect to model reproducibility. It is critical that investigators using this model take this effect into account. Indeed, if this craniotomy dependence is taken into account, we find that the model does result in highly reproducible outcomes.

ACKNOWLEDGMENTS

This work was supported, in part, by the Centers for Disease Control grant CCR 306634 and the Department of Defense grant DAMD 17-93-V-3018 to A.I.F. R.V. is supported by the Australian National Health and Medical Research Council.

REFERENCES

- ALBENSI, B.C., KNOBLACH, S.M., CHEW, B.G., et al. (2000). Diffusion and high resolution MRI of traumatic brain injury in rats: time course and correlation with histology. *Exp. Neurol.* **162**, 61–72.
- ANDERSON, B.J., UNTERER, A.W., CLARKE, G.D., et al. (1988). Effect of posttraumatic hypoventilation on cerebral energy metabolism. *J. Neurosurg.* **68**, 601–607.
- BRAMLETT, H.M., DIETRICH, W.D., and GREEN, E.J. (1999). Secondary hypoxia following moderate fluid percussion brain injury in rats exacerbates sensorimotor and cognitive deficits. *J. Neurotrauma* **16**, 1035–1047.
- DELAHUNTY, T.M., JIANG, J.Y., GONG, Q.Z., et al. (1995). Differential consequences of lateral and central fluid percussion brain injury on receptor coupling in rat hippocampus. *J. Neurotrauma* **12**, 1045–1057.
- DIXON, C.E., LYETH, B.G., POVLISHOCK, J.T., et al. (1987). A fluid percussion model of experimental brain injury in the rat. *J. Neurosurg.* **67**, 110–119.
- DIXON, C.E., LIGHTHALL, J.W., and ANDERSON, T.T. (1988). Physiologic, histopathologic, and cineradiographic characterization of a new fluid-percussion model of experimental brain injury in the rat. *J. Neurotrauma* **5**, 99–104.
- FADEN, A.I., FOX, G.B., FAN, L., et al. (1999). Novel TRH analog improves motor and cognitive recovery after traumatic brain injury in rodents. *Am. J. Physiol.* **277**, R1196–R1204.
- FLOYD, C.L., LYETH, G.B., HAMM, R.J., et al. (1997). Small differences in fluid percussion craniectomy position affects Morris Water Maze performance following injury. *J. Neurotrauma* **14**, 766.
- GENNARELLI, T.A. (1994). Animate models of human head injury. *J. Neurotrauma* **11**, 357–368.
- GLASS, T.F., FABIAN, M.J., SCHWEITZER, J.B., et al. (1999). Secondary neurologic injury resulting from nonhypotensive hemorrhage combined with mild traumatic brain injury. *J. Neurotrauma* **16**, 771–782.
- GOLDING, E.M., DOBSON, G.P., and GOLDING, R.M. (1996). A critical assessment of noise-induced errors in ³¹P MRS: application to the measurement of free intracellular magnesium *in vivo*. *Magn. Reson. Med.* **35**, 174–185.
- HAMM, R.J., DIXON, C.E., GBADEBO, D.M., et al. (1992).

CRANIOTOMY POSITION IN FPI AND LESION DEVELOPMENT

- Cognitive deficits following traumatic brain injury produced by controlled cortical impact. *J. Neurotrauma* **9**, 11–20.
- HAMM, R.J., LYETH, B.G., JENKINS, L.W., et al. (1993). Selective cognitive impairment following traumatic brain injury in rats. *Behav. Brain Res.* **59**, 169–173.
- HEADRICK, J.P., BENDALL, M.R., FADEN, A.I., et al. (1994). Dissociation of adenosine levels from bioenergetic state in experimental brain trauma: potential role in secondary injury. *J. Cereb. Blood Flow Metab.* **14**, 853–861.
- HEATH, D.L., and VINK, R. (1996). Traumatic brain axonal injury produces sustained decline in intracellular free magnesium concentration. *Brain Res.* **738**, 150–153.
- ISHIGE, N., PITTS, L.H., BERRY, I., et al. (1988). The effects of hypovolemic hypotension on high-energy phosphate metabolism of traumatized brain in rats. *J. Neurosurg.* **68**, 129–136.
- JIANG, J.Y., LYETH, B.G., KAPASI, M.Z., et al. (1992). Moderate hypothermia reduces blood–brain barrier disruption following traumatic brain injury in the rat. *Acta Neuropathol. Berl.* **84**, 495–500.
- KOTAPKA, M.J., GENNARELLI, T.A., GRAHAM, D.I., et al. (1991). Selective vulnerability of hippocampal neurons in acceleration-induced experimental head injury. *J. Neurotrauma* **8**, 247–258.
- McINTOSH, T.K., FADEN, A.I., BENDALL, M.R., et al. (1987a). Traumatic brain injury in the rat: alterations in brain lactate and pH as characterized by ^1H and ^{31}P nuclear magnetic resonance. *J. Neurochem.* **49**, 1530–1540.
- McINTOSH, T.K., NOBLE, L., ANDREWS, B., et al. (1987b). Traumatic brain injury in the rat: characterization of a midline fluid-percussion model. *CNS Trauma* **4**, 119–134.
- McINTOSH, T.K., VINK, R., NOBLE, L.J., et al. (1989). Traumatic brain injury in the rat: characterization of a lateral fluid percussion injury model. *Neuroscience* **28**, 233–244.
- PERRI, B.R., SMITH, D.H., MURAI, H., et al. (1997). Metabolic quantification of lesion volume following experimental traumatic brain injury in the rat. *J. Neurotrauma* **14**, 15–22.
- PIERCE, J.E., TROJANOWSKI, J.Q., GRAHAM, D.I., et al. (1996). Immunohistochemical characterisation of alterations in the distribution of amyloid precursor proteins and beta-amyloid peptide after experimental brain injury in the rat. *J. Neurosci.* **16**, 1083–1090.
- PRASAD, M.R., DHILLON, H.S., CARBARY, T., et al. (1994). Enhanced phosphodiesteric breakdown of phosphatidylinositolbiphosphate after experimental brain injury. *J. Neurochem.* **63**, 773–776.
- QIAN, L., NAGAOKA, T., OHNO, K., et al. (1996). Magnetic resonance imaging and pathologic studies on lateral fluid percussion injury as a model of focal brain injury in rats. *Bull. Tokyo Med. Dent. Univ.* **43**, 53–66.
- RUBIN, Y., CECIL, K., WEHRLI, S., et al. (1997). High-resolution H-1 NMR spectroscopy following experimental brain trauma. *J. Neurotrauma* **14**, 441–449.
- SCHMIDT, R.H., and GRADY, M.S. (1993). Regional patterns of blood–brain barrier breakdown following central and lateral fluid percussion injury in rodents. *J. Neurotrauma* **10**, 415–430.
- SHIMA, K., and MARMAROU, A. (1991). Evaluation of brainstem dysfunction following severe fluid-percussion head injury to the cat. *J. Neurosurg.* **74**, 270–277.
- SMITH, D.H., OKIYAMA, K., THOMAS, M.J., et al. (1991). Evaluation of memory dysfunction following experimental brain injury using the Morris water maze. *J. Neurotrauma* **8**, 259–269.
- SMITH, D.H., LOWENSTEIN, D.H., GENNARELLI, T.A., et al. (1994). Persistent memory dysfunction is associated with bilateral hippocampal damage following experimental brain injury. *Neurosci. Lett.* **168**, 151–154.
- SOARES, H.D., THOMAS, M., CLOHERTY, K., et al. (1992). Development of prolonged focal cerebral edema and regional cation changes following experimental brain injury in the rat. *J. Neurochem.* **58**, 1845–1852.
- SUTTON, R.L., LESCAUDRON, L., and STEIN, D.G. (1993). Unilateral cortical contusion injury in the rat: vascular disruption and temporal development of cortical necrosis. *J. Neurotrauma* **10**, 135–149.
- THIBAUT, L.E., MEANEY, D.F., ANDERSON, B.J., et al. (1992). Biomechanical aspects of a fluid percussion model of brain injury. *J. Neurotrauma* **9**, 311–322.
- VINK, R., McINTOSH, T.K., WEINER, M.W., et al. (1987). Effects of traumatic brain injury on cerebral high energy phosphates and intracellular pH: a ^{31}P magnetic resonance spectroscopy study. *J. Cereb. Blood Flow Metab.* **7**, 563–571.
- VINK, R., McINTOSH, T.K., DEMEDIUK, P., et al. (1988). Decline in intracellular free magnesium concentration is associated with irreversible tissue injury following brain trauma. *J. Biol. Chem.* **263**, 757–761.

Address reprint requests to:
Robert Vink, Ph.D.
Department of Pathology
Adelaide University
Adelaide, SA 5005
Australia

E-mail: Robert.Vink@adelaide.edu.au

Neuroprotection and Traumatic Brain Injury

The Search Continues

Alan I. Faden, MD

During the last decade, experimental studies of traumatic brain injury (TBI) have provided important new insights into the pathophysiological mechanisms leading to post-traumatic tissue damage and associated neurological dysfunction. The concept of delayed or secondary tissue injury has strong experimental support and a cascade of secondary injury factors has been delineated.^{1,2} These observations have led to the application of targeted pharmacotherapies, whose aim is to block specific pathobiological pathways.^{2,3} Such research has been aided by the development of rodent models of head injury that simulate critical components of clinical neurotrauma, as well as by the development of novel neuroprotective agents.^{3,4} These experimental studies have identified mechanisms of delayed tissue damage and have demonstrated the effectiveness of a number of pharmacological treatment strategies.¹⁻⁴ However, despite this enormous experimental promise, the clinical studies to date have been disappointing.^{5,6} Here we explore the conceptual and methodological issues that have contributed to this discrepancy between preclinical and clinical studies.

SECONDARY INJURY AND NEUROPROTECTION: PRECLINICAL STUDIES

Although earlier studies focused on brain injury models in higher species such as the sheep, cat, and primate, most studies during the past decade have used rodent models.⁷ Such models have been designed to reflect certain components of clinical head injury, such as contusion, hematoma, and/or diffuse axonal injury.^{6,7} Nonetheless, there are significant questions as to how adequately these animal models reflect human brain injury, which is a highly heterogeneous disorder. Moreover, rodent models generally use highly inbred strains of one sex in an effort to minimize intersubject variability. Despite these limitations, a variety of biochemical changes have been consistently identified across experimental models and across laboratories; these include changes in ionic homeostasis (calcium, potassium, sodium,

magnesium), release of excitatory amino acids, induction of free radicals, inflammatory/immune changes, and alterations of multiple neurotransmitter systems,^{1,2} among others. It has also been established that TBI leads to apoptotic as well as necrotic cell death, and that both forms of cell death may be pharmacologically modulated.⁸⁻¹⁰ These observations have led to the evaluation of numerous pharmacological strategies, including calcium channel blockers, corticosteroids and other antioxidants, glutamate receptor antagonists, opioid receptor antagonists, thyrotropin-releasing hormone analogs, and magnesium administration, as well as various anti-inflammatory and immune modulatory treatments.^{3,4} Some of these approaches, such as the use of *N*-methyl-D-aspartate receptor antagonists, have particularly strong experimental support.^{8,11} More recently, it has also been shown that modulation of apoptotic cell death by inhibiting caspases also improves outcome after TBI.⁹ Another strategy that has gained increasing experimental support but that has not yet been

From the Departments of Neuroscience, Neurology, and Pharmacology, Georgetown University, Washington, DC.

translated into well-designed clinical trials is the use of either combination therapies that block different components of the secondary injury cascade or administration of single agents (such as thyrotropin-releasing hormone or HU-211) that modulate multiple components of the cascade.^{12,13}

NEUROPROTECTION AND TBI: CLINICAL STUDIES

During the past 50 years, numerous clinical trials of neuroprotective agents have been conducted. In general, these have not shown significant beneficial effects.^{5,6} Negative trials have included evaluation of corticosteroids, barbiturates, calcium channel antagonists, antioxidants/free radical scavengers, and glutamate antagonists, among others.^{5,6,14,15} Why has it been so difficult to demonstrate effective drug treatments for clinical head injury in contrast to recent studies of stroke or spinal cord injury? Moreover, why are there such substantial discrepancies between animal head injury studies and related clinical studies? There are various potential explanations for such failures.

HETEROGENEITY OF POPULATIONS BEING STUDIED

As noted above, patients with severe brain trauma include a heterogeneous population with regard to underlying mechanisms of secondary injury, with the latter including varying degrees of hypoxia, ischemia, contusion, diffuse axonal injury, edema, and the presence of associated hematoma.⁶ Therefore, in evaluating potential therapeutic strategies, investigators may need to better define or stratify subpopulations of patients being studied. For example, although 2 earlier clinical trials of nimodipine treatment in head injury were negative,^{16,17} subgroup analysis suggested a potential benefit in patients demonstrating traumatic subarachnoid hemorrhage. A subsequent small study that focused on patients with traumatic hemorrhage did report a significant treatment effect.¹⁸ The latter will need to be repeated with larger numbers of patients but it does suggest the possibility that clearer delineation of classes of patients with head injuries may increase the likelihood that significant neuroprotective effects may be observed.

INJURY SEVERITY

Clinical trials have generally included patients with severe head injuries. However, animal studies have shown that moderate head injury may provide a better target for evaluation of neuroprotective treatments. Subjects with severe injuries may be incapable of demonstrating a treatment effect because of the severity of the primary insult or associated injuries. On the other hand, inclusion of only mildly injured patients may lead to a ceiling effect, in which case it is unlikely that a treatment effect can be observed unless very large populations are studied.

RELEVANCE OF ANIMAL MODELS

Animal models are usually designed to model a component of clinical head injury, such as concussion or con-

tusion, to improve consistency across subjects and reduce outcome variability. Despite inherent difficulties, it would be desirable to develop more complex animal models that may include hypoxia, ischemia, or other potentially relevant components of clinical head injury (hemorrhage, hematoma, etc).

END POINTS

End points in clinical and experimental studies often differ significantly. Experimental studies generally use behavioral assessment and lesion volume measurements, whereas clinical studies may examine combined death/disability or use surrogate markers such as intracranial pressure changes.

TIME POINTS/THERAPEUTIC WINDOWS

In experimental studies, pharmacotherapies are often administered either as pretreatment or as very early post-treatment (ie, 15-30 minutes). In contrast, clinical studies can rarely enter a brain trauma patient into a study sooner than 3 to 6 hours after injury, particularly in view of difficulties in obtaining informed consent. More clinically relevant treatment times should be examined in animal studies before they are moved into the clinic. It is also important to develop clinical treatment approaches that permit earlier treatment times.

PHARMACOLOGY IN EXPERIMENTAL MODELS

In animal studies, it is rare that pharmacokinetic or pharmacodynamic studies are performed. Moreover, studies examining central penetration of systemically administered compounds are rarely conducted. More detailed pharmacological profiles, as well as optimization of treatment protocols, should be conducted in animals before moving such studies into clinical trials.

COMBINATION OR MULTIPOTENTIAL TREATMENT STRATEGIES

Experimental studies have established that both necrotic and apoptotic cell death occur after TBI.⁸⁻¹⁰ Moreover, it has been shown that treatment strategies aimed at necrosis may enhance apoptotic cell death.¹⁹ Importantly, combination treatment with agents directed to each type of cell death have shown additive, if not synergistic, treatment effects.²⁰ Further studies are needed to examine whether such combination treatment strategies can improve outcomes in more clinically relevant animal model systems.

OTHER METHODOLOGICAL DIFFERENCES

Another major difference between clinical and preclinical studies is that the former generally use an intent-to-treat methodology; that is, patients are included in the treatment group even if by mistake they did not receive the effective treatment dose. In contrast, with animal experimentation, investigators routinely exclude an animal that fails to receive adequate treatment; in many cases,

subjects are excluded based on other criteria, such as inadequacy of trauma, etc.

LESSONS LEARNED: CAN THEY BE APPLIED?

Many important lessons have been learned during the past few years regarding clinical trial design in head injury/neuroprotection studies. In many reported studies there has been concern about adequacy of sample size and some recent studies suggest substantial increases in proposed sample size.²¹ Future clinical studies should identify more appropriate target populations, ideally focusing on moderate as opposed to mild or severe injury. It will be important to better stratify these populations, for example, with regard to the presence or absence of significant hemorrhage or other confounding factors. Future trials should also await more complete preclinical investigation, in particular with regard to such issues as therapeutic window, pharmacokinetics, and central nervous system drug penetration. Finally, more emphasis should be placed on evaluating either drugs with multipotential treatment actions (ie, altering multiple components of the secondary injury cascade) or combination treatment strategies.

Accepted for publication June 7, 2001.

Corresponding author: Alan I. Faden, MD, Department of Neuroscience, EP-12 Research Bldg, 3970 Reservoir Rd NW, Washington, DC 20007 (e-mail: fadena@giccs.georgetown.edu).

REFERENCES

1. Panter S, Faden A. Biochemical changes and secondary injury from stroke and trauma. In: Young RR, Delwade PJ, eds. *Principles and Practice of Restorative Neurology*. New York, NY: Butterworths; 1992:32-52.
2. McIntosh TK. Neurochemical sequelae of traumatic brain injury: therapeutic implications. *Cerebrovasc Brain Metab Rev*. 1994;6:109-162.
3. Faden AI. Pharmacological treatment of central nervous system trauma. *Pharmacol Toxicol*. 1996;78:12-17.
4. McIntosh TK, Juhler M, Wieloch T. Novel pharmacologic strategies in the treatment of experimental traumatic brain injury: 1998. *J Neurotrauma*. 1998;15:731-769.
5. Faden AI. Pharmacologic treatment of acute traumatic brain injury. *JAMA*. 1996; 276:569-570.
6. Bullock M, Lyeth B, Muizelaar J. Current status of neuroprotection trials for traumatic brain injury: lessons from animal models and clinical studies. *Neurosurgery*. 1999;45:207-217.
7. Povlishock J. An overview of brain injury models. In: Narayan RJ, Wilberger JE, Povlishock J, eds. *Neurotrauma*. New York, NY: McGraw Hill Co; 1996:1325-1336.
8. Temple M, O'Leary D, Faden A. The role of glutamate receptors in the pathophysiology of traumatic brain injury. In: L Miller, R Hayes, J Newcomb, eds. *Head Trauma*. New York, NY: John Wiley & Sons; 2001:87-113.
9. Yakovlev AG, Knoblach SM, Fan L, Fox GB, Goodnight R, Faden AI. Activation of CPP32-like caspases contributes to neuronal apoptosis and neurological dysfunction after traumatic brain injury. *J Neurosci*. 1997;17:7415-7424.
10. Rink A, Fung KM, Trojanowski JQ, Lee VM, Neugebauer E, McIntosh TK. Evidence of apoptotic cell death after experimental traumatic brain injury in the rat. *Am J Pathol*. 1995;147:1575-1583.
11. Faden AI, Demediuk P, Panter SS, Vink R. The role of excitatory amino acids and NMDA receptors in traumatic brain injury. *Science*. 1989;244:798-800.
12. Faden AI. Comparison of single and combination drug treatment strategies in experimental brain trauma. *J Neurotrauma*. 1993;10:91-100.
13. Bieganski A and Joseph AB. Development of HU-211 as a neuroprotectant for ischemic brain damage. *Neuro Res*. 1995;17:275-280.
14. Young B, Runge JW, Waxman KS, et al. Effects of pegorgotein on neurologic outcome of patients with severe head injury: a multicenter, randomized controlled trial. *JAMA*. 1996;276:538-543.
15. Morris GF, Bullock R, Marshall SB, Marmarou A, Maas A, Marshall LF. Failure of the competitive N-methyl-D-aspartate antagonist Selfotel (CGS 19755) in the treatment of severe head injury: results of two phase III clinical trials. *J Neurosurg*. 1999;91:737-743.
16. Teasdale G, Bailey I, Bell A, et al. The effect of nimodipine on outcome after head injury: a prospective randomised control trial: the British/Finnish Co-operative Head Injury Trial Group. *Acta Neurochir Suppl*. 1990;51:315-316.
17. The European Study Group on Nimodipine in Severe Head Injury. A multicenter trial of the efficacy of nimodipine on outcome after severe head injury. *J Neurosurg*. 1994;80:797-804.
18. Harders A, Kakarieka A, Braakman A, German tSAH Study Group. Traumatic subarachnoid hemorrhage and its treatment with nimodipine. *J Neurosurg*. 1996; 85:82-89.
19. Pohl D, Bittigau P, Ishimaru MJ, et al. N-Methyl-D-aspartate antagonists and apoptotic cell death triggered by head trauma in developing rat brain. *Proc Natl Acad Sci U S A*. 1999;96:2508-2513.
20. Allen JW, Knoblach SM, Faden AI. Combined mechanical trauma and metabolic impairment in vitro induces NMDA receptor-dependent neuronal cell death and caspase-3-dependent apoptosis. *FASEB J*. 1999;13:1875-1882.
21. Dickinson K, Bunn F, Wentz R, Edwards P, Roberts I. Size and quality of randomised controlled trials in head injury: review of published studies. *BMJ*. 2000; 320:1308-1311.

Exacerbation of Neuronal Cell Death by Activation of Group I Metabotropic Glutamate Receptors: Role of NMDA Receptors and Arachidonic Acid Release

Jason W. Allen,*† Stefano Vicini,†‡ and Alan I. Faden*†§¹

*Institute for Cognitive and Computational Sciences, †Interdisciplinary Program in Neuroscience, ‡Department of Physiology and Biophysics, and §Department of Neuroscience, Georgetown University, Washington, DC 20007

Received August 31, 2000; accepted February 22, 2001

Both ionotropic and metabotropic glutamate receptors have been implicated in the pathogenesis of neuronal injury. Activation of group I metabotropic glutamate receptors (mGluR) exacerbates neuronal cell death, whereas inhibition is neuroprotective. However, the mechanisms involved remain unknown. Activation of group I mGluR modulates multiple signal transduction pathways including stimulation of phosphoinositide hydrolysis, potentiation of NMDA receptor activity, and release of arachidonic acid. Here we demonstrate that whereas activation of group I mGluR by (S)-3,5-dihydroxyphenylglycine (DHPG) potentiates NMDA-induced currents and intracellular calcium increases in rat cortical neuronal cultures, partial effects of group I mGluR activation or inhibition on neuronal injury induced by oxygen–glucose deprivation remain despite NMDA receptor blockade. DHPG stimulation also increases basal arachidonic acid release from rat neuronal–glial cultures and potentiates injury-induced arachidonic acid release in these cultures. Thus, activation of group I mGluR may exacerbate neuronal injury through multiple mechanisms, which include positive modulation of NMDA receptors and enhanced release of arachidonic acid.

© 2001 Academic Press

Key Words: CNS injury; ischemia; trauma; calcium; neuronal–glial culture; signal transduction.

INTRODUCTION

CNS injury is characterized by activation of both ionotropic and metabotropic glutamate receptors. The former are directly linked to cation channels, whereas the latter are coupled to G-proteins (48). Numerous reports have demonstrated the neuroprotective effects

of ionotropic glutamate receptor antagonists following trauma or ischemia, both *in vitro* (35, 42) and *in vivo* (21, 22, 55). Modulation of metabotropic glutamate receptors (mGluR) also affects neuronal survival following injury, with the result depending upon the mGluR group involved and the type of injury model used (1, 9, 23, 26, 41, 47, 51).

A role for group I mGluR in neuronal injury has been established in a variety of *in vitro* and *in vivo* models. *In vitro*, activation of group I mGluR exacerbates, whereas inhibition of group I mGluR attenuates, neuronal injury induced by application of NMDA (8, 9), oxygen–glucose deprivation (OGD) (3, 9, 47), or mechanical trauma (41, 43). Similar results have been described *in vivo*, including models of ischemia–reperfusion (51) and traumatic brain injury (26, 41).

Much early work relating to signal transduction pathways activated by group I mGluR focused on phospholipase C, activation of which results in phosphoinositide (PI) hydrolysis, liberation of intracellular calcium stores, and stimulation of protein kinase C (13, 48). Yet it has been recognized that other pathways may also be induced by group I mGluR; these include activation of adenylyl cyclase, release of arachidonic acid, stimulation of phospholipase D, potentiation of NMDA receptors, and modulation of calcium and potassium channels (13, 48). However, many of these earlier studies were performed before the advent of subtype selective agonists and antagonists, utilizing transfection studies in cell lines to isolate each receptor subtype. Thus, the role of such signal transduction pathways in mediating effects of group I mGluR in neurons or during neuronal injury remains largely unexplored.

We have previously demonstrated that activation of group I mGluR increased phosphoinositides in neuronal–glial cultures and that antisense oligonucleotides directed against both mGluR1 and mGluR5 attenuated this response (41). Interestingly, antisense directed against mGluR1, but not mGluR5, selectively attenu-

¹ To whom correspondence should be addressed at Department of Neuroscience, EP-12b Research Building, 3970 Reservoir Road, NW, Washington, DC 20007. Fax: (202) 687-0617. E-mail: fadena@giccs.georgetown.edu.



ated neuronal injury following mechanical trauma *in vitro* (41), despite similar functional effects of each oligonucleotide on PI hydrolysis. This finding suggests that activation of phospholipase C may not be a primary mechanism underlying the modulation of neuronal injury by group I mGluR. In the present studies, two possible mechanisms by which group I mGluR may exacerbate neuronal injury were evaluated. Using rat cortical neuronal and neuronal-glial cultures, we examined the effects of group I mGluR activation on NMDA receptor-mediated responses and arachidonic acid release.

MATERIALS AND METHODS

Neuronal-Glial Cultures

Glia were prepared from 1- to 3-day-old Sprague-Dawley rat cortices (Taconic Farms) and neurons were prepared from 18-day-old Sprague-Dawley rat embryonic cortices as previously described in detail (44). Briefly, cortices dissociated from 1- to 3-day-old rats were seeded in 96-well Primaria microplates (Falcon) and resulting glia were allowed to grow to confluency. Cortices were dissociated from 18-days-old rat embryos and individual cells ($2\text{--}2.5 \times 10^6$ cells/ml) were plated on a layer of confluent glial cells; they were then dissociated in Hanks' balanced salt solution without calcium or magnesium (Mediatech) supplemented with 10 mM Hepes (pH 7.0; Biofluids) and 1 mM sodium pyruvate (Biofluids). Cultures were fed twice per week by replacement of one-third of medium with minimal essential medium with Earle's salts (Mediatech) supplemented with 10% equine serum (HyClone Laboratories), 27.5 mM Hepes (pH 7.2), 2 mM glutamine (Biofluids), 20 mM glucose (Biofluids), and 1% antibiotic-antimycotic solution (Biofluids). Cytosine- β -D-arabinofuranoside (10 μ M; Sigma) was added during the first feeding to stop further glial proliferation. After 10 days *in vitro* (DIV), glutamine concentration was reduced to 1 mM and equine serum was omitted. Cultures were incubated at 37°C in humid atmosphere with 4% CO₂. Neuronal-glial cultures were used at 19–21 DIV.

Cortical Neuronal Cultures

Neocortices from 18-day-old Sprague-Dawley rat embryos (Taconic Farms) were used to prepare neuronal cultures. Individual neurons were obtained as detailed above. After dissociation, cell suspension was diluted with Neurobasal medium (NBM; Life Technologies) supplemented with 25 μ M glutamate (Sigma), 0.5 mM glutamine, 1% antibiotic-antimycotic, and 2% B27 supplement (Life Technologies). Cells were seeded at 1×10^6 cells per milliliter onto microplates (96-well; Corning) or circular coverslips (12 or 25 mm; Fisher

Scientific) precoated with 10 μ g/ml poly-D-lysine (Sigma). Pure neuronal cultures were fed on day 4 *in vitro* by the addition of an equal volume of NBM supplemented with 0.5 mM glutamine, 1% antibiotic-antimycotic, and 2% B27 supplement. Medium volume was then adjusted to 100 μ l. Mature neuronal cultures were used at 11–14 DIV.

Qualitative Reverse-Transcription Polymerase Chain Reaction (RT-PCR)

The expression profiles for mGluR1, mGluR5, and NMDA NR1 mRNA were analyzed in neuronal (11 DIV) and neuronal-glial (18 DIV) cultures in 96-well microplates by qualitative RT-PCR. Cells were lysed using TRIzol reagent (Life Technologies) and chloroform (Sigma) was added to lysates. Samples were centrifuged at 13,000g at 4°C for 15 min and an equal volume of isopropanol (Sigma) was added to the aqueous phase. After incubation at –20°C, RNA was subjected to ethanol (Sigma) precipitation and RNA concentration was determined spectrophotometrically for each sample.

Complementary DNA (cDNA) was generated for each sample. Twenty micrograms of RNA was ethanol precipitated and resuspended in deionized water. DNA present in the sample was degraded by incubation with 0.2 U/ μ g RNA of RNase-free DNase I (Promega) in cDNA synthesis buffer (Life Technologies) at 37°C for 1 h. cDNA was produced by adding the following to each sample: 5 mM DTT (Life Technologies), 500 μ M dNTPs (Sigma), 4 μ M oligo(dT) primer (15-mer; Life Technologies), 4 μ M random primer (10-mer; Life Technologies), and 2 μ l Moloney murine leukemia virus reverse transcriptase (Life Technologies). Reactions were incubated at 37°C for 2 h, and reverse transcriptase was inactivated by incubating samples at 70°C for 10 min.

PCR was performed using 1/10 of the cDNA volume and 30 pmol of the following specific primer pairs: for mGluR1, 5'-CCCCTGTTCTGCTGATTC-3' and 5'-AAAGGAGAAGGAGGCGTCAG-3'; for mGluR5, 5'-GCTTCACAGCCAACATCTCC-3' and 5'-TTTGGGAGAGGATGGGATGC-3'; and for NMDA NR1, 5'-GGCCGTGCTGGAGTTTGAGG-3' and 5'-CCCCGGTGCTCGTGTCTTTG-3'. The following program was used: initial denaturing at 95°C for 2 min, subsequent denaturing at 94°C for 2 s, annealing at 55°C for 15 s, primer extension at 72°C for 45 s, and final primer extension at 72°C for 2 min. One-third of the reaction volume was loaded onto a 1.5% agarose gel containing 0.5 μ g/ml ethidium bromide. Electrophoresis was performed at 5 mV/cm. DNA was visualized by ultraviolet transillumination at 300 nm. Images were captured using Speedlight gel documentation system (Hoefer).

To confirm the sequence of RT-PCR results, each product was cloned into PCR 2.1 plasmid using a TA

cloning kit (Invitrogen). Resulting plasmids were transfected into competent NM522 *Escherichia coli*. Positive clones were picked and plasmid DNA was isolated using Wizard *Plus* miniprep DNA purification system (Promega) and sequenced using ABI Prism dye terminator cycle sequencing ready reaction kit (Perkin Elmer) following manufacturer's guidelines.

Electrophysiology

Neuronal cultures grown on 12-mm coverslips were used for electrophysiological studies. Borosilicate glass recording pipettes were pulled to a resistance of 6–8 M Ω . Coverslips containing neurons were transferred to a stage of an inverted microscope and placed into a perfusion bath of extracellular recording solution (ERS) containing 145 mM NaCl, 5 mM KCl, 1 mM CaCl₂, 10 μ M MgCl₂, 0.02 mM glycine, 5 mM glucose, and 5 mM Hepes at pH 7.2 with NaOH. Osmolarity of ERS was adjusted to 325 mOsm with sucrose. The culture dish in the recording chamber was continuously perfused at a rate of 5 ml/min. Phase-contrast bright neurons were voltage-clamped at –60 mV in the whole-cell configuration using the patch-clamp technique (28) with a recording pipette containing 145 mM K-gluconate, 5 mM EGTA, 5 mM MgCl₂, 5 mM NaATP, 0.2 mM NaGTP, and 10 mM Hepes at pH 7.2 with KOH. NMDA and DHPG were applied directly through a gravity-fed Y-tubing delivery system placed within 100 μ m of the recorded cell (45). Currents were monitored with a patch amplifier (EPC-7; List Electronics), filtered at 1.5 kHz (eight-pole low-pass Bessel; Frequency Devices), and digitized with the use of an IBM-PC computer with pCLAMP 6 software.

Calcium Imaging

NMDA-induced increases in intracellular calcium levels were monitored using an established method (31). Neuronal cultures grown on 25-mm coverslips were used for calcium imaging. Cultures were washed with ERS. Neurons were loaded with a calcium-sensitive fluorescent probe by incubating cells with 1 μ M fura-2 AM (Molecular Probes) at 37°C for 1 h in 1 ml ERS supplemented with 1 mM MgCl₂ (ERSM). After loading, cultures were washed three times with ERSM. Coverslips containing neurons were then transferred to an inverted Zeiss microscope and baseline measurements were obtained in ERSM. Addition of an equal volume of ERSM had no effect on basal levels of intracellular calcium (data not shown). DHPG or vehicle was diluted in ERSM and added to cultures. After 2 min, NMDA diluted in ERSM was added to cultures. Fluorescent images were acquired at 334 and 380 nm at a rate of 1 ratio image per second using a Zeiss-Attofluor ratio arc imaging system (Zeiss) and a 40 \times Zeiss Fluor oil immersion objective lens.

Induction of in Vitro Mechanical Trauma

The induction of injury and the cellular response to this trauma model has been previously described in detail (2, 44). This model has been modified as outlined below. All drugs were added 30 min prior to injury. Media from neuronal–glial plates was replaced with a balanced salt solution (BSS) containing 116 mM NaCl, 5.4 mM KCl, 0.8 mM MgSO₄, 1.8 mM CaCl₂, 1.0 mM NaH₂PO₄, 26.2 mM NaHCO₃, 0.01 mM glycine, and 10 mg/L phenol red. Control uninjured and trauma cultures were supplemented with 5.5 mM glucose. Ten millimolar 3-nitropropionic acid (3NP) was added to cultures used for trauma with 3NP and glucose deprivation (trauma + 3NP/GD) injury. Injury was induced by a specially designed punch device that produces 28 parallel cuts 1.2 mm in length at 0.5 mm intervals. Immediately following injury, cultures were returned to 37°C and 5% CO₂ and incubated for 60 min. Cultures were then washed seven times with BSS and the medium volume was adjusted to 100 μ l by the addition of BSS containing 1% antibiotic–antimycotic. Glucose was added to a final concentration of 5.5 mM and cultures were incubated at 37°C for 24 h. Control uninjured sister cultures were treated identically with the exception of trauma and were used to estimate basal cell death.

Induction of Oxygen–Glucose Deprivation Injury

OGD injury was performed following an established protocol with minimal modifications (3, 25). In brief, atmosphere was evacuated from anaerobic system Model 1025 (Forma Scientific) and replaced with 5% CO₂, 10% H₂, and 85% N₂. Deoxygenated BSS was prepared by bubbling with the anaerobic gas mixture prior to starting experiments. Neuronal–glial cultures in 96-well microplates were transferred into the anaerobic chamber and washed with deoxygenated BSS. All drugs were diluted with deoxygenated BSS in the chamber. Control cultures were treated with vehicle diluted in deoxygenated BSS. After adding compounds to appropriate wells, cultures were placed in an incubator at 37°C within the chamber. Cultures were removed from incubator and washed with deoxygenated BSS and then removed from the chamber. "Reperfusion" was performed by immediately adding an equal volume of oxygenated BSS supplemented with 5.5 mM glucose, 1% antibiotic–antimycotic and vehicle or drug where appropriate. Cultures were then placed at 37°C for 24 h before cell death assessment.

Cell Death Assessment

Total cell death was estimated using lactate dehydrogenase (LDH) released into the culture medium as a biochemical marker. LDH release in these models correlates well with other markers of cell death including

trypan blue counts and increases in ethidium homodimer fluorescence (42, 44). LDH activity measurements were performed following an established protocol (41). Twenty-four hours after injury, medium was transferred to a 96-well microplate and diluted with LDH assay reagent containing 5 mM β -NAD (Sigma), 25 mM lactic acid (Sigma), 0.03% bovine serum albumin (Sigma), 100 mM Trizma (Sigma), and 0.9% NaCl, pH 8.45. Spectrophotometric analysis was performed at room temperature using a Ceres 900 microplate reader (Biotek Instruments, Inc.) measuring optical density at 340 nm over 250 s at 5-s intervals (50 readings per sample). Linear regression analysis provided an estimate of LDH activity. Basal or control LDH activity levels were subtracted from treatments prior to analysis.

Measurement of [3 H]Arachidonic Acid Release

Release of [3 H]arachidonic acid ([3 H]AA) was quantified following an established protocol (60) with minor modifications. Neuronal–glial cultures were incubated with 0.1 μ Ci/ml of [3 H]AA (Amersham; sp act 216 Ci/mmol) at 37°C for 24 h and then washed seven times with BSS. Cultures were incubated for 10 min with fatty acid-free bovine serum albumin (BSA) at a final concentration of 5 μ g/ml to trap released [3 H]AA. Some experiments were performed in the presence of 50 μ M thimerosal to prevent reacylation of released [3 H]AA. Cultures were then exposed to drug or vehicle or subjected to trauma + 3NP/GD as described below. Medium was collected at various time points and centrifuged at 12,000g for 5 min to remove cellular debris. Supernatants were transferred to scintillation tubes and released radioactivity was measured by liquid scintillation counting.

Drugs

(*R,S*)-1-Aminoindan-1,5-dicarboxylic acid (AIDA), (*S*)-4-carboxyphenylglycine (4CPG), dizocilpine (MK801), and (*S*)-3,5-dihydroxyphenylglycine (DHPG) were all purchased from Tocris Cookson. Tetrodotoxin (TTX) was purchased from Calbiochem.

RESULTS

Cortical Neurons Express both NMDA Receptors and Group I mGluR

We have previously demonstrated that neuronal–glial cultures express both NMDA NR1 and group I mGluR using RT-PCR and Western blot techniques (41, 44). The presence of NMDA receptors was confirmed in rat cortical neuronal and neuronal–glial cultures by qualitative RT-PCR using primers specific for NR1 (Fig. 1). NR1 expression is required for the assembly of functional NMDA receptors (39). Qualitative RT-PCR was also used to demonstrate the expression of

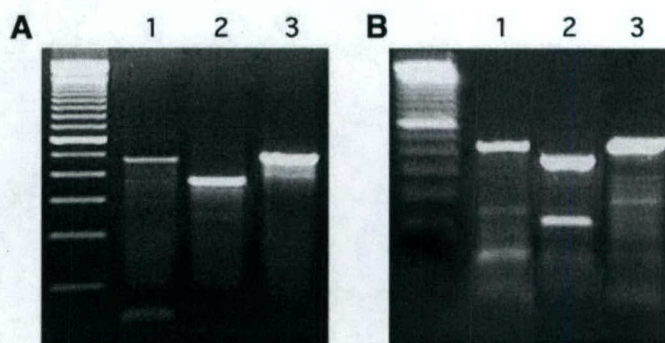


FIG. 1. Qualitative RT-PCR analysis of mRNA extracted from 18 DIV neuronal–glial (A) and 11 DIV neuronal (B) cultures using primers specific for group I mGluR (mGluR1 and mGluR5) or NMDA receptors (NR1). Both neuronal–glial (A) and neuronal cultures (B) express mGluR1 (lane 1), mGluR5 (lane 2), and NR1 (lane 3) mRNA. The specificity of all bands was confirmed by subcloning and sequencing as detailed under Materials and Methods.

mGluR1 and mGluR5 in both of these cultures (Fig. 1). The presence of NMDA receptors and group I mGluR were confirmed in cortical neuronal cultures by immunohistochemistry using antibodies specific for NMDA NR1, mGluR1, and mGluR5 (data not shown).

Group I mGluR-Mediated Potentiation of NMDA Receptor Function

Cortical neurons grown on glass coverslips were transferred to a perfusion bath of BSS containing 0.5 μ M TTX to inhibit synaptic currents. NMDA applied via Y-tubing to neurons in whole-cell configuration induced a large inward current that exhibited rapid desensitization (Fig. 2A). Cells that did not exhibit this response to NMDA receptor stimulation were not considered for further study. Selective activation of group I mGluR by DHPG via Y-tubing for 2 min did not generate any detectable current (Fig. 2A). Reapplication of NMDA after incubation with DHPG for 2 min induced a larger current compared with the initial NMDA response (Fig. 2A). The currents induced by NMDA after DHPG application exhibited no gross differences in kinetics or desensitization from NMDA currents generated before DHPG (Fig. 2A). Quantitation revealed a significant potentiation of maximal NMDA response after DHPG compared with currents induced by NMDA alone (Fig. 2B). NMDA receptor-mediated steady-state currents did not exhibit statistically significant enhancement by application of NMDA following incubation with DHPG (Fig. 2C).

Cortical neurons were loaded with the calcium-sensitive dye fura-2 AM. NMDA application in the presence of 0.5 μ M TTX significantly increased intracellular calcium levels in these cells (Fig. 3A). Application of DHPG for 2 min did not appreciably alter intracellular calcium levels (Fig. 3A). Similar to the potentiation of NMDA receptor-mediated currents by activation of group I mGluR,

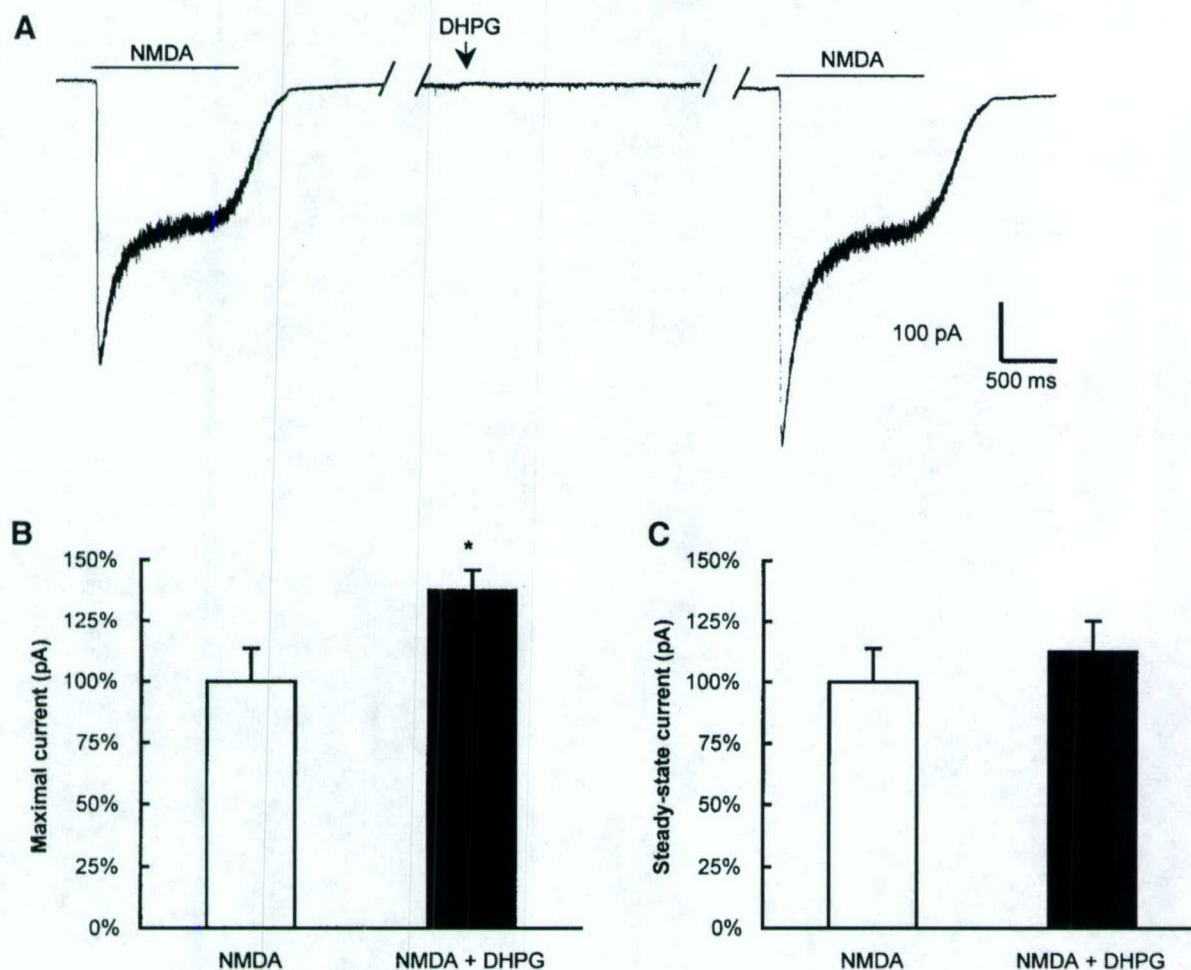


FIG. 2. Group I mGluR activation potentiates NMDA-mediated currents in 11 DIV neuronal cultures. (A) Representative current trace recorded from a single neuron voltage-clamped at a holding potential of -60 mV. After recording a baseline, NMDA ($200 \mu\text{M}$) was applied via Y-tubing. DHPG ($200 \mu\text{M}$) applied for 2 min did not generate any current (partial tracing shown). Reapplication of NMDA ($200 \mu\text{M}$) immediately after discontinuing DHPG application induced a larger current. (B) Maximal NMDA-induced current was significantly potentiated following administration of $200 \mu\text{M}$ DHPG for 2 min (filled bar) compared with NMDA alone (open bar). (C) Control NMDA-mediated steady-state current was unaffected by DHPG application. To block synaptic activity, $0.5 \mu\text{M}$ TTX was added to the extracellular recording solution during all experiments. All recordings were performed in the presence of $10 \mu\text{M}$ Mg^{2+} . Bars, mean \pm SEM, $n = 6$. Data are expressed as a percentage of NMDA-induced current before application of DHPG. * $P < 0.05$, Student's t test.

DHPG significantly potentiated NMDA-induced increases in intracellular calcium (Fig. 3B).

Effects of Group I mGluR Modulation in the Presence of MK801 during Neuronal Injury

To determine whether group I mGluR-mediated potentiation of NMDA receptor function is important in the setting of neuronal injury, neuronal–glial cultures were subjected to OGD in the presence of NMDA receptor blockade. We have previously generated a dose-response curve for MK801 in the setting of mechanical trauma in these neuronal–glial cultures and found an EC_{50} of 10 – 50 nM (43, 44). Administration of MK801 completely inhibits NMDA toxicity (43) and blocks OGD toxicity (3, 25). We have also demonstrated that group I mGluR activation exacerbates OGD injury

whereas group I mGluR inhibition protects against this injury (3). Blockade of group I mGluR by either AIDA or 4CPG provided significant protection against OGD-induced LDH release in the presence of a maximally effective dose of MK801 (Fig. 4A). In addition, activation of group I mGluR by DHPG significantly exacerbated OGD-induced injury in the presence of MK801 (Fig. 4B).

Effects of Group I mGluR Modulation on Trauma + 3NP/GD-Induced Injury

We have recently developed a novel injury model that combines mechanical trauma with “ischemic” conditions, which is characterized by both necrotic and apoptotic neuronal cell death (2). We examined whether modulation of group I mGluR had similar

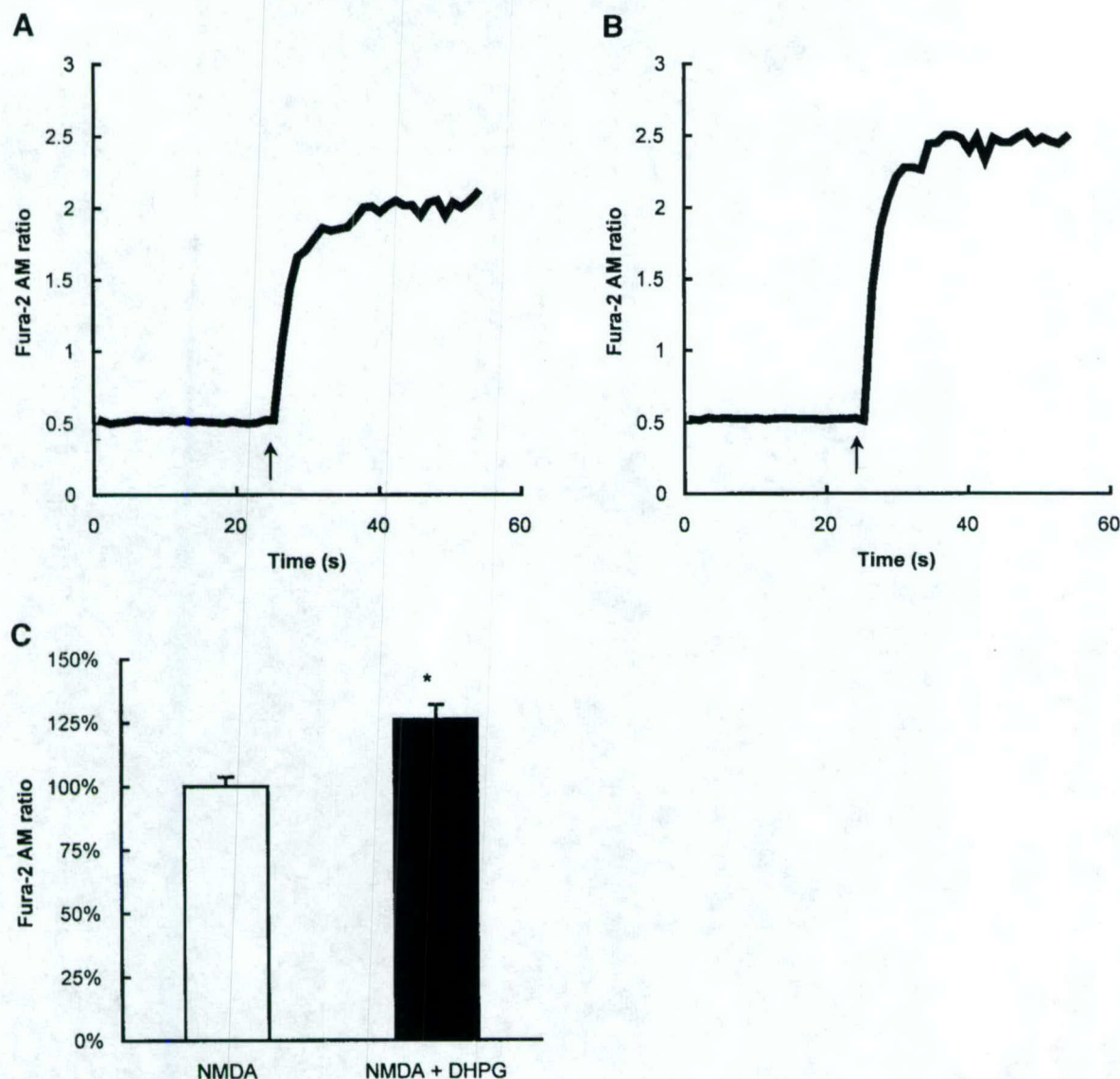


FIG. 3. Group I mGluR activation potentiates NMDA-induced increases in intracellular calcium in 11 DIV neurons. (A) Representative trace of average change in fura-2 AM ratio values after addition of 200 μ M NMDA (arrow). (B) Preincubation with 200 μ M DHPG for 2 min did not appreciably alter baseline intracellular calcium levels (partial tracing shown), but potentiated control NMDA-mediated rise in intracellular calcium. Values represent mean fura-2 AM ratio for 15–17 cells. (C) Quantitation demonstrates that DHPG (200 μ M) significantly potentiated NMDA-induced fura-2 AM ratio values. Bars, means \pm SEM, $n = 5$ –6 cultures (15–25 cells analyzed per culture). Data are expressed as a percentage of NMDA response. * $P = 0.012$ vs control (two-tailed Mann–Whitney U test). TTX (0.5 μ M) and 1 mM Mg^{2+} were included in the extracellular solution during all experiments.

effects in this injury model compared to either OGD or mechanical trauma. Inhibition of group I mGluR by AIDA provided significant protection against trauma + 3NP/GD, as indicated by LDH release at 24 h (Fig. 5A). Stimulation of group I mGluR by DHPG significantly exacerbated this injury at 24 h (Fig. 5B).

Potentiation of Basal- and Trauma + 3NP/GD-Induced Release of Arachidonic Acid by Group I mGluR Activation

Neuronal–glial cultures were preloaded with [3 H]AA as described above. Application of DHPG induced sig-

nificant liberation of [3 H]AA into the culture medium compared with basal release (Fig. 6A). [3 H]AA levels began to return to basal levels after 30 min of stimulation with DHPG, which was the latest time point examined (Fig. 6A).

Release of [3 H]AA into medium of neuronal–glial cultures was significantly increased immediately following trauma + 3NP/GD injury (Fig. 6B). Increased levels of [3 H]AA were still detectable at 50 min (Fig. 6B). Application of DHPG during trauma + 3NP/GD significantly potentiated [3 H]AA release at both 30 and 60 min postinjury (Fig. 7). Similarly, OGD injury sig-

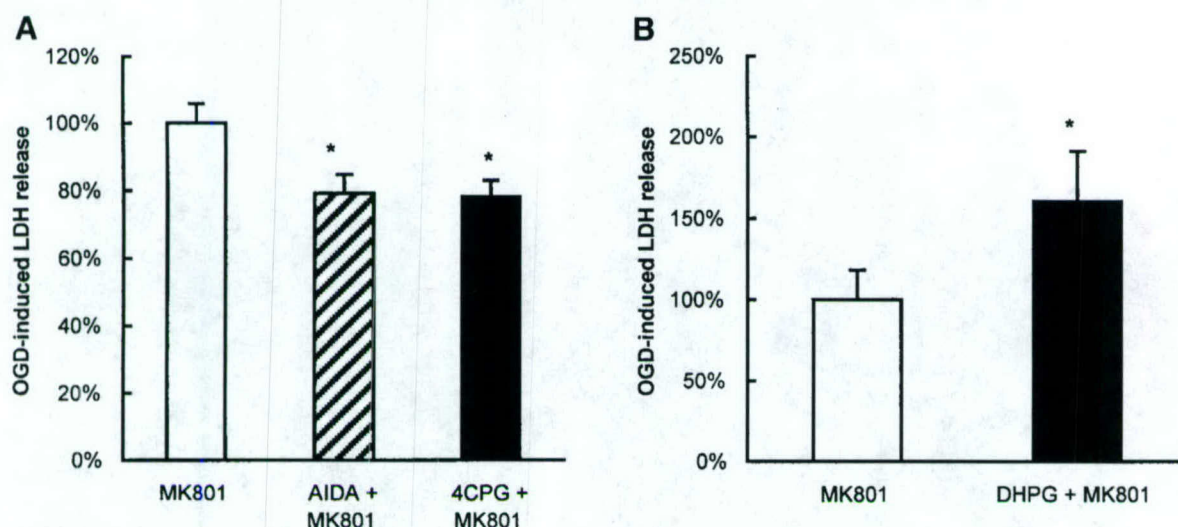


FIG. 4. Effects of group I mGluR modulation of OGD injury persist in the presence of NMDA receptor blockade. (A) Inhibition of group I mGluR by AIDA (200 μ M; hatched bar) or 4CPG (30 μ M; filled bar) in the presence of 10 μ M MK801 induced significant protection over that produced by MK801 alone (open bar) 24 h after OGD. * P < 0.05 vs control (ANOVA followed by Student–Newman–Keuls test). (B) Group I mGluR activation by DHPG (20 μ M; filled bar) in the presence of MK801 significantly exacerbated OGD-induced LDH release at 24 h compared with MK801 alone (open bar). * P < 0.05 vs control (Student's t test). Bars, means + SEM after basal LDH release subtraction, n = 22–31. Data are expressed as a percentage of OGD with MK801 treatment.

nificantly increased [3 H]AA at 60 min postinjury (control 100 ± 4 versus OGD 187 ± 35 ; n = 6–10; P < 0.05, Student's t test), and application of DHPG (20 μ M) significantly potentiated this release at 60 min postinjury (OGD 100 ± 18 versus OGD + DHPG 149 ± 13 ; n = 6–10; P < 0.05, Student's t test).

DISCUSSION

The present studies demonstrate that the effects of group I mGluR stimulation include both potentiation of

NMDA-induced responses and increases in arachidonic acid release from rat cortical cultures. In addition, we report that the exacerbating and neuroprotective effects of group I mGluR modulation following OGD injury partially persist in the presence of NMDA receptor blockade. These effects of group I mGluR modulation are consistent across injury models as similar effects were also observed following trauma + 3NP/GD injury. Taken together, our data suggest that multiple second messenger systems may be involved in group I mGluR modulation of neuronal injury.

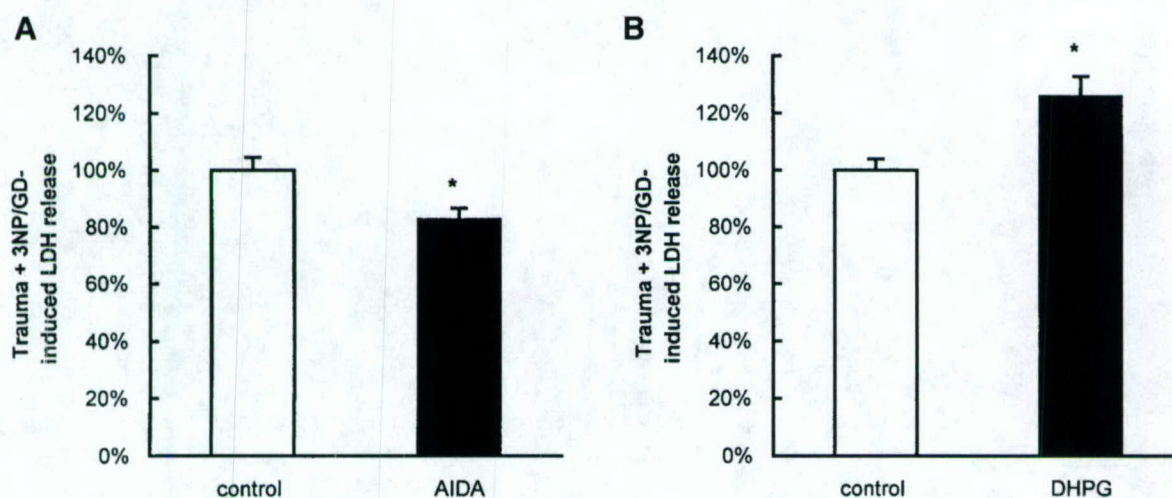


FIG. 5. Effects of group I mGluR modulation on trauma + 3NP/GD injury. (A) Group I mGluR inhibition by AIDA (200 μ M) significantly decreased trauma + 3NP/GD-induced LDH release 24 h after injury. (B) Application of DHPG (20 μ M) significantly worsened this injury. These effects are similar to those observed after group I mGluR modulation of OGD injury. Bars, means + SEM, n = 19–21. Data are expressed as a percentage of trauma + 3NP/GD (control). * P < 0.005 vs trauma + 3NP/GD (Student's t test).

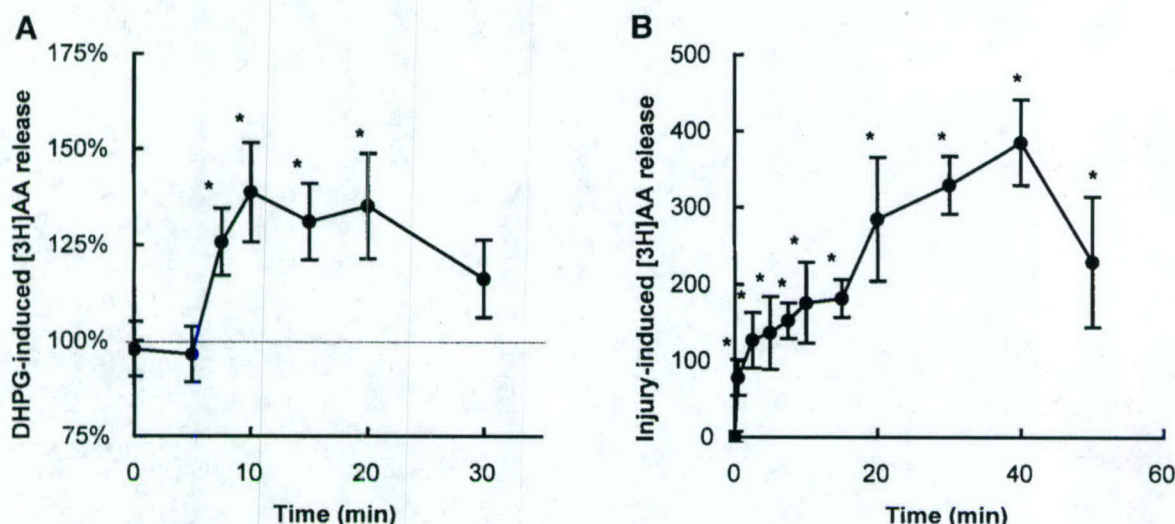


FIG. 6. Group I mGluR activation and trauma + 3NP/GD increase [^3H]arachidonic acid ([^3H]AA) release from neuronal-glial cultures. (A) Application of DHPG (20 μM) to 18 DIV neuronal-glial cultures significantly increases [^3H]AA detected in culture medium by 7.5 min. The dashed line indicates the level of basal release from control sister cultures. Values represent means \pm SEM, $n = 8$. Data are expressed as a percentage of basal release. $*P < 0.05$ vs basal levels (Student's t test). Experiments were performed in the presence of thimerosal to prevent reacylation of released [^3H]AA. (B) Trauma + 3NP/GD induces [^3H]AA release from neuronal-glial cultures. [^3H]AA levels are significantly increased in culture media immediately following trauma + 3NP/GD induction and remain significantly elevated at all time points examined. Values represent [^3H]AA detected in culture medium minus basal release in sister control cultures, $n = 3$. $*P < 0.05$ vs basal release (Student's t test).

Early studies using *trans*(\pm)-1-amino-1,3-cyclopentanedicarboxylic acid (ACPD), a relatively nonselective agonist, demonstrated that activation of mGluR potentiated NMDA-mediated currents in brain slices or cultured neurons from the hippocampus (4, 29), spinal cord (6, 57), striatum (49), or cortex (50). In contrast,

two studies from independent laboratories have reported that ACPD attenuates NMDA receptor-mediated currents (12, 62). More recently, potentiation of NMDA-induced currents was attributed to activation of group I mGluR because the selective agonists DHPG and CHPG mimicked this effect when applied to brain slices or cultures from the hippocampus (24), spinal cord (32, 57, 58), striatum (49), or cortex (17).

We were particularly interested in whether activation of group I mGluR would modulate NMDA receptors in rat cortical neurons, as this species has been used in many studies by us and others investigating the role of group I mGluR in neuronal injury. Application of DHPG significantly potentiated the maximal response induced by NMDA in whole-cell recordings of these neurons. This effect was not due to increased synaptic activity as a result of increased glutamate release, as all experiments were performed in the presence of TTX. Consistent with other studies, application of DHPG in the absence of NMDA did not generate any detectable current (62). Potentiation of NMDA-induced currents by DHPG did not appreciably alter the kinetics of NMDA receptor-mediated currents and this potentiation persisted up to 5 min after DHPG application, the latest time point examined. This is consistent with the report that enhancement of NMDA-generated currents by mGluR in rat spinal dorsal horn neurons persists up to 75 min (10).

Potentiation of NMDA receptor-mediated currents in rat cortical neurons was confirmed by calcium-imaging studies using fura-2 AM. No change in intracellular

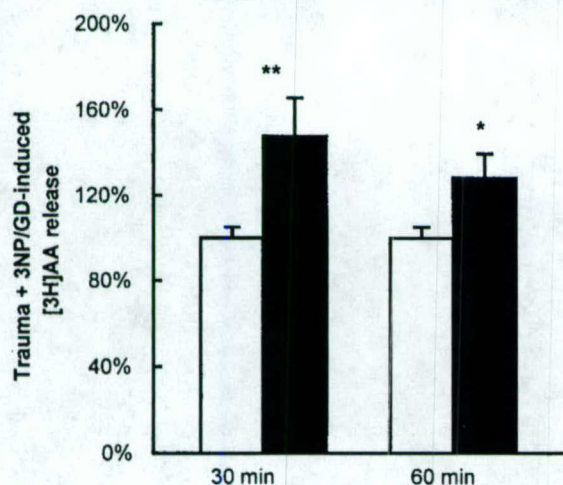


FIG. 7. Group I mGluR activation potentiates trauma + 3NP/GD-induced [^3H]arachidonic acid ([^3H]AA) release from neuronal-glial cultures. Treatment with 20 μM DHPG (filled bars) induced significant increases in [^3H]AA released into the culture medium at 30 and 60 min compared with trauma + 3NP/GD alone (open bars). Values represent means \pm SEM after subtraction of basal values, $n = 18-21$. Data are expressed as a percentage of trauma + 3NP/GD. $*P < 0.05$ vs trauma + 3NP/GD; $**P < 0.01$ vs trauma + 3NP/GD (Student's t test).

calcium levels was detected after DHPG administration, indicating that group I mGluR activation alone does not lead to detectable increases in intracellular calcium in these neurons. However, increases in NMDA-induced intracellular calcium levels were observed after preincubation with DHPG. Again, all experiments were performed in the presence of TTX; thus, this increase was not a result of increases in synaptic transmission. As group I mGluR may enhance calcium channel activation in other cell types, such as cerebellar granule cells (11), a similar effect in cortical neurons cannot be excluded. Nonetheless, this appears unlikely given a lack of rise in intracellular calcium levels following the addition of DHPG alone, as well as the many reports indicating that the primary effect of group I mGluR activation on calcium channels is inhibition (37, 53, 54, 56).

In contrast to the data presented here, Yu *et al.* (62) reported a reversible attenuation of NMDA currents by selective group I mGluR agonists in cultured mouse cortical neurons. They also noted reduction of NMDA-induced increases in intracellular calcium in these cells by the addition of (*S*)-3-hydroxyphenylglycine (3HPG), a selective group I mGluR agonist. The differing results reported in the current study may be attributable to differences in experimental design, including the use of a different species as a basis for cultured cortical neurons. However, another explanation may relate to the presence or absence of Mg^{2+} in the extracellular solution. Our experiments were performed in the presence of $10 \mu M Mg^{2+}$, as this ion is normally present *in vivo*, whereas Yu and colleagues utilized a nominally free Mg^{2+} extracellular solution. Recently, it has been reported that the group I mGluR-mediated potentiation of NMDA-induced currents in frog motoneurons requires a minimum Mg^{2+} concentration; no effect on these currents was observed in a nominally free Mg^{2+} extracellular solution (32). However, earlier studies have reported potentiation of NMDA receptor-mediated currents by ACPD in rat spinal dorsal horn neurons (10) and rat hippocampal slices (29) even in nominally free Mg^{2+} extracellular solution. Thus, the effects of Mg^{2+} on modulation of NMDA receptors by group I mGluR remains unclear and may depend on the cell type and preparation under study.

Studies using transfected human embryonic kidney (HEK) 293 cells, which lack native mGluR, demonstrated that the effects of group I mGluR stimulation on NMDA-induced currents depends upon the composition of the NMDA receptor complex and the concentrations of NMDA and glycine used (14). DHPG may directly inhibit, potentiate, or have no effect on NMDA-induced currents depending upon the NMDA subunits expressed (14). Direct potentiation of NMDA-induced currents by DHPG was only observed with reduced NMDA ($50 \mu M$) and glycine ($100 nM$) concentrations (14). It is unlikely that the potentiation reported in the

present study is due to a direct action at the NMDA receptor as the concentrations of NMDA and glycine (200 and $20 \mu M$, respectively) were similar to experimental conditions in which DHPG had no effect on or inhibited NMDA-induced currents in transfected HEK293 cells (14).

Nicoletti *et al.* (46) recently hypothesized that the variability in effects found with group I mGluR activation, at least in the setting of neuronal injury, may be due to differing subunits in the NMDA receptor complex. The composition of the NMDA receptor complex in the rat cortical neurons used in the present study was not studied and could conceivably differ from the composition found in the mouse cortical neurons used by Yu and colleagues. Regardless, both the calcium imaging and the electrophysiology studies presented here provide consistent evidence of group I mGluR-induced potentiation of NMDA currents in rat cortical neurons. These findings are consistent with the hypothesis that potentiation of NMDA receptors by group I mGluR may contribute to neuronal injury, at least in rat cortical neuronal cultures.

The mechanism whereby group I mGluR potentiate NMDA receptor-mediated currents is unknown. It has been reported in other cell types that this effect may be mediated through a PKC-dependent pathway (4, 49), although others have failed to block group I mGluR-mediated potentiation using PKC inhibitors (29, 50). Recently, it has been suggested that the mechanism may involve a calmodulin-dependent reduction of the Mg^{2+} blockade of NMDA receptors (32). Another possibility may relate to the release of arachidonic acid after stimulation of group I mGluR. Arachidonic acid also potentiates NMDA-generated currents (40). In the present study we demonstrate that activation of group I mGluR leads to arachidonic acid release, suggesting a possible alternative mechanism whereby group I mGluR may potentiate NMDA currents.

However, enhancement of NMDA receptor currents cannot be the sole mechanism whereby group I mGluR mediate injury. We have previously reported that the modulatory effects of group I mGluR activation/inhibition on *in vitro* mechanical trauma of neuronal-glial cultures persist in the presence of NMDA receptor blockade (43). In the present study, we were interested in whether this phenomenon was restricted to traumatic injury or would be a feature of other injurious stimuli. Similar to our results with traumatic injury, exacerbation of injury by group I mGluR activation or protection by group I mGluR inhibition in the presence of MK801 was also observed after OGD-induced injury. Thus, at least under conditions of NMDA receptor blockade, group I mGluR may act through other signal transduction pathways to exacerbate neuronal injury.

Nonetheless, these studies do not exclude the possibility that NMDA receptor potentiation may be an important mechanism for injury modulation by group I

mGluR in the absence of NMDA receptor blockade. The presence of MK801 may alter the characteristics of injury, as has been suggested for the OGD model of neuronal injury (27). It has also recently been reported that potentiation of NMDA-mediated currents by ACPD in frog motoneurons occurs even in the presence of open channel blockers such as MK801 (32). However, the dose of MK801 used here has been shown by us to completely block NMDA-induced cell death in neuronal-glial cultures and is 1 order of magnitude greater than the maximally effective dose against traumatic injury in these cultures (42, 43).

We have previously detailed a novel injury model, in which mechanical trauma is coupled with a brief period of "ischemic-like" conditions (2). This model may more accurately predict traumatic brain injury (TBI) *in vivo*, because TBI is frequently accompanied by ischemia (7, 38, 63). In addition, this model induces both necrotic cell death and caspase-dependent apoptotic cell death, which is similar to findings after *in vivo* TBI (2). Consistent with our results using OGD, mechanical trauma and *in vivo* TBI (3, 43), DHPG exacerbates, whereas AIDA inhibits, cell death following trauma + 3NP/GD.

Liberation of arachidonic acid occurs after *in vivo* trauma (15, 20, 34, 61) or following stimulation *in vitro* with glutamate analogues (52, 59). Phospholipid hydrolysis generates free radicals (15) and arachidonic acid or its metabolites may contribute to injury *in vivo* through a variety of mechanisms (16, 20, 33). In transfection studies using Chinese hamster ovary cells, activation of mGluR1 induces release of arachidonic acid (5). Arachidonic acid release also occurs in cultured neurons after stimulation with a nonselective mGluR agonist (19). However, the specific mGluR group involved in this arachidonic acid release is unknown. In the present study, we demonstrate selective activation of group I mGluR in neuronal-glial cultures releases [³H]AA into the culture medium.

A direct coupling between group I mGluR and phospholipase A₂ (PLA₂) may not necessarily be the mechanism underlying DHPG-induced [³H]AA release. Activation of NMDA receptors also leads to the liberation of arachidonic acid, possibly by increasing intracellular calcium levels that subsequently induce PLA₂ activity (18, 36). Thus, group I mGluR activation may result in release of arachidonic acid indirectly through potentiation of NMDA receptors or through release of calcium from intracellular stores.

Significant liberation of [³H]AA occurred after trauma + 3NP/GD injury to neuronal-glial cultures, and this release was potentiated by administration of DHPG during trauma. Similar results were observed for OGD injury at 60 min; however, this model exhibited significantly more variability in [³H]AA release (unpublished observations). In the present study, we were unable to successfully inhibit PLA₂ in our cul-

tures due to the toxic effects of prolonged exposure to all of the PLA₂ inhibitors tested, including arachidonyl trifluoromethyl ketone (AACOCF₃), quinacrine, and 7,7-dimethyl-(5Z,8Z)-eicosadienoic acid (unpublished observations). Although the data presented here only support a correlation between increased injury-induced arachidonic acid release and cell death by DHPG, the findings are consistent with the conclusion that arachidonic acid release may contribute, at least in part, to group I mGluR-mediated injury.

As noted above, in addition to its other well-known toxic effects, arachidonic acid potentiates NMDA receptor-mediated currents (40). This suggests a possible mechanism whereby group I mGluR may exacerbate injury via increases in arachidonic acid release. Furthermore, potentiation of glutamate release by group I mGluR is most pronounced in the presence of arachidonic acid (30), allowing for a possible positive feedback loop, wherein group I mGluR stimulation releases arachidonic acid, which in turn increases glutamate release. Such glutamate release may serve to further activate both NMDA receptors and group I mGluR.

In summary, group I mGluR-mediated exacerbation of neuronal injury may occur as a result of activation of multiple parallel and possibly serial pathways. Potentiation of NMDA receptors by group I mGluR remains an attractive hypothesis because of the central role that NMDA receptors play in neuronal injury (21, 22, 55). However, the results presented here indicate that other signal transduction pathways may also be involved, such as release of arachidonic acid, and that these alternate pathways may become more important during therapeutic interventions such as blockade of NMDA receptors.

ACKNOWLEDGMENTS

This study was supported by a cooperative research agreement Department of Defense Grant (DAMD-17-93-V-3018) and NIH Grant R01NS37313.

REFERENCES

1. Allen, J. W., S. A. Ivanova, L. Fan, M. G. Espey, A. S. Basile, and A. I. Faden. 1999. Group II metabotropic glutamate receptor activation attenuates traumatic neuronal injury and improves neurological recovery after traumatic brain injury. *J. Pharmacol. Exp. Ther.* **290**: 112-120.
2. Allen, J. W., S. M. Knoblach, and A. I. Faden. 1999. Combined mechanical trauma and metabolic impairment *in vitro* induces NMDA receptor-dependent neuronal cell death and caspase-3-dependent apoptosis. *FASEB J.* **13**: 1875-1882.
3. Allen, J. W., S. M. Knoblach, and A. I. Faden. 2000. Activation of group I metabotropic glutamate receptors reduces neuronal apoptosis but increases necrotic cell death *in vitro*. *Cell Death Differ.* **7**: 470-476.
4. Aniksztejn, L., S. Otani, and Y. Ben-Ari. 1992. Quisqualate metabotropic receptors modulate NMDA currents and facilitate

- induction of long-term potentiation through protein kinase C. *Eur. J. Neurosci.* **4**: 500–505.
5. Aramori, I., and S. Nakanishi. 1992. Signal transduction and pharmacological characteristics of a metabotropic glutamate receptor, mGluR1, in transfected CHO cells. *Neuron* **8**: 757–765.
 6. Bleakman, D., K. I. Rusin, P. S. Chard, S. R. Glaum, and R. J. Miller. 1992. Metabotropic glutamate receptors potentiate ionotropic glutamate responses in the rat dorsal horn. *Mol. Pharmacol.* **42**: 192–196.
 7. Bouma, G. J., and J. P. Muizelaar. 1992. Cerebral blood flow, cerebral blood volume, and cerebrovascular reactivity after severe head injury. *J. Neurotrauma* **9**: S333–S348.
 8. Bruno, V., A. Copani, T. Knöpfel, R. Kuhn, G. Casabona, P. Dell'Albani, D. F., and F. Nicoletti. 1995. Activation of metabotropic glutamate receptors coupled to inositol phospholipid hydrolysis amplifies NMDA-induced neuronal degeneration in cultured cortical cells. *Neuropharmacology* **34**: 1089–1098.
 9. Buisson, A., and D. W. Choi. 1995. The inhibitory mGluR agonist, *s*-4-carboxy-3-hydroxy-phenylglycine selectively attenuates NMDA neurotoxicity and oxygen–glucose deprivation-induced neuronal death. *Neuropharmacology* **34**: 1081–1087.
 10. Cerne, R., and M. Randic. 1992. Modulation of AMPA and NMDA responses in rat spinal dorsal horn neurons by *trans*-1-aminocyclopentane-1,2-dicarboxylic acid. *Neurosci. Lett.* **144**: 180–184.
 11. Chavis, P., J. M. Nooney, J. Bockaert, L. Fagni, A. Feltz, and J.-L. Bossu. 1995. Facilitatory coupling between a glutamate metabotropic receptor and dihydropyridine-sensitive calcium channels in cultured cerebellar granule cells. *J. Neurosci.* **15**: 135–143.
 12. Colwell, C. S., and M. S. Levine. 1994. Metabotropic glutamate receptors modulate *N*-methyl-D-aspartate receptor function in neostriatal neurons. *Neuroscience* **61**: 497–507.
 13. Conn, P. J., and J.-P. Pin. 1997. Pharmacology and functions of metabotropic glutamate receptors. *Annu. Rev. Pharmacol. Toxicol.* **37**: 205–237.
 14. Contractor, A., R. W. Gereau IV, T. Green, and S. F. Heinemann. 1998. Direct effects of metabotropic glutamate receptor compounds on native and recombinant *N*-methyl-D-aspartate receptors. *Proc. Natl. Acad. Sci. USA* **95**: 8969–8974.
 15. Demediuk, P., R. D. Saunders, N. R. Clenenon, E. D. Means, D. K. Anderson, and L. A. Horrocks. 1985. Changes in lipid metabolism in traumatized spinal cord. *Prog. Brain Res.* **63**: 211–226.
 16. Demediuk, P., and A. I. Faden. 1988. Traumatic spinal cord injury in rats causes increases in tissue thromboxane but not peptidoleukotrienes. *J. Neurosci. Res.* **20**: 115–121.
 17. Doherty, A. J., M. J. Palmer, J. M. Henley, G. L. Collingridge, and D. E. Jane. 1997. (*RS*)-2-Chloro-5-hydroxyphenylglycine (CHPG) activates mGlu5, but not mGlu1, receptors expressed in CHO cells and potentiates NMDA responses in the hippocampus. *Neuropharmacology* **36**: 265–267.
 18. Dumuis, A., M. Sebben, L. Haynes, J.-P. Pin, and J. Bockaert. 1988. NMDA receptors activate the arachidonic acid cascade system in striatal neurons. *Nature* **336**: 68–70.
 19. Dumuis, A., M. Sebben, L. Fagni, L. Prezeau, O. Manzoni, E. J. Cragoe Jr., and J. Bockaert. 1993. Stimulation of arachidonic acid release by glutamate receptors depends on $\text{Na}^+/\text{Ca}^{2+}$ exchange in neuronal cells. *Mol. Pharmacol.* **43**: 976–981.
 20. Faden, A. I., P. H. Chan, and S. Longar. 1987. Alterations in lipid metabolism, (Na^+ , K^+)-ATPase activity, and tissue water content of spinal cord following experimental traumatic injury. *J. Neurochem.* **48**: 1809–1816.
 21. Faden, A. I., and R. P. Simon. 1988. A potential role for excitotoxins in the pathophysiology of spinal cord injury. *Ann. Neurol.* **23**: 623–636.
 22. Faden, A. I., P. Demediuk, S. S. Panter, and R. Vink. 1989. The role of excitatory amino acids and NMDA receptors in traumatic brain injury. *Science* **244**: 798–800.
 23. Faden, A. I., S. A. Ivanova, A. G. Yakovlev, and A. G. Mukhin. 1998. Neuroprotective effects of group III mGluR in traumatic neuronal injury. *J. Neurotrauma* **14**: 885–895.
 24. Fitzjohn, S. M., A. J. Irving, M. J. Palmer, J. Harvey, D. Lodge, and G. L. Collingridge. 1996. Activation of group I mGluRs potentiates NMDA responses in rat hippocampal slices. *Neurosci. Lett.* **203**: 211–213.
 25. Goldberg, M. P., and D. W. Choi. 1993. Combined oxygen and glucose deprivation in cortical cell culture: Calcium-dependent and calcium-independent mechanisms of neuronal injury. *J. Neurosci.* **13**: 3510–3524.
 26. Gong, Q.-Z., T. M. Delahunty, R. J. Hamm, and B. G. Lyeth. 1995. Metabotropic glutamate antagonist, MCPG, treatment of traumatic brain injury in rats. *Brain Res.* **700**: 299–302.
 27. Gwag, B. J., D. Lobner, J. Y. Koh, M. B. Wie, and D. W. Choi. 1995. Blockade of glutamate receptors unmasks neuronal apoptosis after oxygen-glucose deprivation *in vitro*. *Neuroscience* **68**: 615–619.
 28. Hamill, O. P., A. Marty, E. Neher, B. Sakmann, and F. J. Sigworth. 1981. Improved patch-clamp technique for high-resolution current recording from cell and cell-free membrane patches. *Pflügers Arch.* **391**: 85–91.
 29. Harvey, J., and G. L. Collingridge. 1993. Signal transduction pathways involved in the acute potentiation of NMDA responses by *1S,3R*-ACPD in rat hippocampal slices. *Br. J. Pharmacol.* **109**: 1085–1090.
 30. Herrero, I., T. Miras-Portugal, and J. Sanchez-Prieto. 1992. Positive feedback of glutamate exocytosis by metabotropic presynaptic stimulation. *Nature* **360**: 163–166.
 31. Hirashima, N., R. Etcheberrigaray, S. Bergamaschi, M. Racchi, F. Battaini, G. Binetti, S. Govoni, and D. L. Alkon. 1996. Calcium responses in human fibroblasts: A diagnostic molecular profile for Alzheimer's disease. *Neurobiol. Aging* **17**: 549–555.
 32. Holohean, A. M., J. C. Hackman, and R. A. Davidoff. 1999. Mechanisms involved in the metabotropic glutamate receptor-enhancement of NMDA-mediated motoneurone responses in frog spinal cord. *Br. J. Pharmacol.* **126**: 333–341.
 33. Hsu, C. Y., P. V. Halushka, E. L. Hogan, N. L. Banik, W. A. Lee, and P. L. Perot, Jr. 1985. Alteration of thromboxane and prostacyclin levels in experimental spinal cord injury. *Neurology* **35**: 1003–1009.
 34. Ikeda, M., S. Yoshida, R. Buso, M. Santiso, and M. D. Ginsberg. 1986. Polyphosphoinositides as a probable source of brain free fatty acids accumulated at the onset of ischemia. *J. Neurochem.* **44**: 465–472.
 35. Kaku, D. A., R. G. Giffard, and D. W. Choi. 1993. Neuroprotective effects of glutamate antagonists and extracellular acidity. *Science* **260**: 1516–1518.
 36. Lazarewicz, J. W., J. T. Wroblewski, and E. Costa. 1990. *N*-Methyl-D-aspartate-sensitive glutamate receptors induce calcium-mediated arachidonic acid release in primary cultures of cerebellar granule cells. *J. Neurochem.* **55**: 1875–1881.
 37. Lester, R. A. J., and C. E. Jahr. 1990. Quisqualate receptor-mediated depression of calcium currents in hippocampal neurons. *Neuron* **4**: 741–749.
 38. Marion, D. W., J. Darby, and H. Yonas. 1991. Acute regional cerebral blood flow changes caused by severe head injuries. *J. Neurosurg.* **74**: 407–414.

39. McBain, C. J., and M. L. Mayer. 1994. *N*-Methyl-D-aspartic acid receptor structure and function. *Physiol. Rev.* **74**: 723-760.
40. Miller, B., M. Sarantis, S. F. Traynelis, and D. Attwell. 1992. Potentiation of NMDA receptor currents by arachidonic acid. *Nature* **355**: 722-725.
41. Mukhin, A., L. Fan, and A. I. Faden. 1996. Activation of metabotropic glutamate receptor subtype mGluR1 contributes to post-traumatic neuronal injury. *J. Neurosci.* **16**: 6012-6020.
42. Mukhin, A. G., S. A. Ivanova, S. M. Knoblach, and A. I. Faden. 1997. New *in vitro* model of traumatic neuronal injury: Evaluation of secondary injury and glutamate receptor mediated neurotoxicity. *J. Neurotrauma* **14**: 651-663.
43. Mukhin, A. G., S. A. Ivanova, and A. I. Faden. 1997. mGluR modulation of post-traumatic neuronal death: Role of NMDA receptors. *NeuroReport* **8**: 2561-2566.
44. Mukhin, A. G., S. A. Ivanova, J. W. Allen, and A. I. Faden. 1998. Mechanical injury to neuronal/glial cultures in microplates: Role of NMDA receptors and pH in secondary neuronal cell death. *J. Neurosci. Res.* **51**: 748-758.
45. Murase, K., P. D. Ryu, and M. Randic. 1989. Excitatory and inhibitory amino acids and peptide-induced responses in acutely isolated rat spinal dorsal horn neurons. *Neurosci. Lett.* **103**: 56-63.
46. Nicoletti, F., V. Bruno, M. V. Catania, G. Battaglia, A. Copani, G. Barbagallo, V. Cena, J. Sanchez-Prieto, P. F. Spano, and M. Pizzi. 1999. Group-I metabotropic glutamate receptors: Hypotheses to explain their dual role in neurotoxicity and neuroprotection. *Neuropharmacology* **38**: 1477-1484.
47. Opitz, T., R. Richter, and K. G. Reymann. 1994. The metabotropic glutamate receptor antagonist (+)- α -methyl-4-carboxyphenylglycine protects hippocampal CA1 neurons of the rat from *in vitro* hypoxia/hypoglycemia. *Neuropharmacology* **33**: 715-717.
48. Pin, J.-P., and R. Duvoisin. 1995. Review: neurotransmitter receptors I: the metabotropic glutamate receptors: structure and functions. *Neuropharmacology* **34**: 1-26.
49. Pisani, A., P. Calabresi, D. Centonze, and G. Bernardi. 1997. Enhancement of NMDA responses by group I metabotropic glutamate receptor activation in striatal neurones. *Br. J. Pharmacol.* **120**: 1007-1014.
50. Rahman, S., and R. S. Neuman. 1996. Characterization of metabotropic glutamate receptor-mediated facilitation of *N*-methyl-D-aspartate depolarization of neocortical neurones. *Br. J. Pharmacol.* **117**: 675-683.
51. Riedel, G., T. Opitz, and K. G. Reymann. 1996. Blockade of metabotropic glutamate receptors protects hippocampal neurons from hypoxia-induced cell death in rat *in vivo*. *Prog. Neuro-Psychopharmacol. Biol. Psychiat.* **20**: 1253-1263.
52. Sanfeliu, C., A. Hunt, and A. J. Patell. 1990. Exposure to *N*-methyl-D-aspartate increases release of arachidonic acid in primary cultures or rat hippocampal neurons and not in astrocytes. *Brain Res.* **526**: 241-248.
53. Sayer, R. J., P. C. Schwindt, and W. E. Crill. 1992. Metabotropic glutamate receptor-mediated suppression of L-type calcium current in acutely isolated neocortical neurons. *J. Neurophysiol.* **68**: 833-842.
54. Sayer, R. J. 1998. Group I metabotropic glutamate receptors mediate slow inhibition of calcium current in neocortical neurons. *J. Neurophysiol.* **80**: 1981-1988.
55. Simon, R. P., J. H. Swan, T. Griffith, and B. S. Meldrum. 1984. Blockade of *N*-methyl-D-aspartate receptors may protect against ischemic damage in the brain. *Science* **226**: 850-852.
56. Swartz, K. J., A. Merrit, B. P. Bean, and D. M. Lovinger. 1993. Protein kinase C modulates glutamate receptor inhibition of Ca^{2+} channels and synaptic transmission. *Nature* **361**: 165-168.
57. Ugolini, A., M. Corsi, and F. Bordi. 1997. Potentiation of NMDA and AMPA responses by group I mGluR in spinal cord motoneurons. *Neuropharmacology* **36**: 1047-1055.
58. Ugolini, A., M. Corsi, and F. Bordi. 1999. Potentiation of NMDA and AMPA responses by the specific mGluR5 agonist CHPG in spinal cord motoneurons. *Neuropharmacology* **38**: 1569-1576.
59. Verity, M. A. 1993. Mechanisms of phospholipase A2 activation and neuronal injury. *Ann. N. Y. Acad. Sci.* **679**: 110-120.
60. Viu, E., A. Zapata, J. L. Capdevila, L. H. Fossom, P. Skolnick, P., and R. Trullas. 1998. Glycine site antagonists and partial agonists inhibit *N*-methyl-D-aspartate receptor-mediated [3 H]arachidonic acid release in cerebellar granule cells. *J. Pharmacol. Exp. Ther.* **285**: 527-532.
61. Yoshida, S., S. Inoh, T. Asano, K. Sano, M. Kubota, H. Shmazaki, and N. Ueta. 1980. Effect of transient ischemia on free fatty acids and phospholipids in the gerbil brain. *J. Neurosurg.* **53**: 323-331.
62. Yu, S. P., S. L. Sensi, L. M. T. Canzoniero, A. Buisson, and D. W. Choi. 1997. Membrane-delimited modulation of NMDA currents by metabotropic glutamate receptor subtypes 1/5 in cultured mouse cortical neurons. *J. Physiol.* **499**: 721-732.
63. Yuan, X.-Q., D. S. Prough, T. L. Smith, and D. S. DeWitt. 1988. The effects of traumatic brain injury on regional cerebral blood flow in rats. *J. Neurotrauma* **5**: 289-301.

Multiple Caspases Are Activated after Traumatic Brain Injury: Evidence for Involvement in Functional Outcome

SUSAN M. KNOBLACH,¹ MARIA NIKOLAEVA,¹ XIULING HUANG,¹ LEI FAN,¹
STANISLAW KRAJEWSKI,² JOHN C. REED,² and ALAN I. FADEN¹

ABSTRACT

Caspase-3 is a cysteine protease that is strongly implicated in neuronal apoptosis. Activation of caspase-3 may be induced by at least two major initiator pathways: a caspase-8-mediated pathway activated through cell surface death receptors (extrinsic pathway), and a caspase-9-mediated pathway activated by signals from the mitochondria that lead to formation of an apoptosomal complex (intrinsic pathway). In the present studies, we compare the activation of caspases-3, -8, and -9 after lateral fluid-percussion traumatic brain injury (TBI) in rats. Immunoblot analysis identified cleaved forms of caspases-3 and -9, but not caspase-8, at 1, 12, and 48 h after injury. Immunocytochemistry specific for cleaved caspases-3 and -9 revealed their expression primarily in neurons. These caspases were also frequently localized in TUNEL-positive cells, some of which demonstrated morphological features of apoptosis. However, caspases-3 and -9 were also found in neurons that were not TUNEL-positive, and other TUNEL-positive cells did not show activated caspases. In contrast to caspases-3 or -9, caspase-8 expression was only minimally changed by injury. An increase in expression of this caspase was undetectable by immunoblotting methods, and appeared as positive immunostaining restricted to a few cells within the injured cortex. Treatment with the pan-caspase inhibitor z-VAD-fmk at 15 min after TBI improved performance on motor and spatial learning tests. These data suggest that several caspases may be involved in the pathophysiology of TBI and that pan-caspase inhibition strategies may improve neurological outcomes.

Key words: brain injury; caspase; cysteine protease; mitochondria; neuron; trauma

INTRODUCTION

TRAUMATIC BRAIN INJURY (TBI) initiates physiological and cellular secondary injury responses that ultimately lead to neuronal death and neurological dysfunction. Although necrosis has long been acknowledged as a major cell death mechanism after TBI, a significant role for apoptotic cell death has recently been described (Rink et al., 1995; Yakovlev et al., 1997; Fox et al., 1998; Clark et al., 1999; Newcomb et al., 1999; Ng et al., 2000).

Activation of caspase proteases has been strongly implicated in apoptosis after CNS injuries, including TBI (Yakovlev et al., 1997; Namura et al., 1998; Clark et al., 1999, 2000; Fink et al., 1999; Krajewski et al., 1999; Springer et al., 1999; Beer et al., 2000b; Buki et al., 2000; Li et al., 2000; Lu et al., 2000). Caspases are cysteine proteases that are expressed as inactive pro-forms (zymogens) that, upon activation, are cleaved into large and small subunits that form heterotetramers with enzymatic activity (for caspase review, see Eldadah and Faden,

¹Department of Neuroscience, Georgetown University, Washington, D.C.

²The Burnham Institute, La Jolla, California.

2000; Reed, 2000). Caspases have been categorized into three groups, based on function: (1) initiator/apical caspases (caspases -2, -8, -9, -10); (2) executioner/effector caspases (caspases-3, -6, -7); (3) inflammatory caspases (caspases-1, -4, -5, -11). Initiator/apical caspases are so-named because of their relative position upstream of other caspases in putative apoptotic pathways. Executioner/effector caspases primarily function downstream of apical caspases, and directly cleave various substrate proteins responsible for apoptosis. Inflammatory caspases play dual roles as both cell-death proteins and processors of pro-inflammatory cytokines.

To date, two major routes of caspase activation have been described. An extrinsic pathway involves binding of cell surface receptors by specific ligands, that directly trigger caspase activation through adaptor proteins. Thus, apoptosis is induced through signals received at the cell surface. This pathway is utilized by members of the tumor necrosis factor (TNF) superfamily. Examples include binding of TNF receptor I by TNF/lymphotoxin, and binding of Fas by Fas ligand (Chinnaiyan et al., 1995; Juo et al., 1998; Varfolomeev et al., 1998). Either of these events can serve to activate pro-caspase-8, which subsequently activates pro-caspase-3 (Stennicke et al., 1998). In contrast, the intrinsic pathway is triggered by intracellular activation through signals derived from mitochondria. Cytochrome c is released from mitochondria and, in turn, binds the caspase-activating protein Apaf-1, which oligomerizes and binds pro-caspase-9, resulting in its cleavage/activation (Li et al., 1997; Hakem et al., 1998; Saleh et al., 1999; Zou et al., 1999). Subsequently, caspase-9 activates pro-caspase-3 (Slee et al., 1999). Although this classification of extrinsic and intrinsic pathways has proved generally useful, it should be noted that the scheme is somewhat oversimplified, as evidenced by cross-talk and feed-forward amplification of these pathways (Saleh et al., 1999; Zou et al., 1999; Reed, 2000).

Activated caspases cleave a diverse group of substrates, including other enzymes, and proteins involved in cell structure, signal transduction, transcription and DNA repair (reviewed in Eldadah and Faden, 2000). Effector caspases, in particular, cleave proteins that maintain the integrity of nucleic acids (ICAD, PARP) and cell structure (lamins, α -fodrin). Degradation of such proteins leads to membrane blebbing, nuclear fragmentation or condensation, cell shrinkage and/or formation of apoptotic bodies, all of which are morphological hallmarks of apoptotic demise.

Information about caspase activation, and its potential effect on neurological recovery and tissue loss after traumatic brain injury is primarily confined to caspases-1, -2, and -3 (Yakovlev et al., 1997; Beer et al., 2000b; Buki

et al., 2000; Clark et al., 2000). Recently, the activation of caspases-8 and -9, was described in models of cerebral ischemia and traumatic spinal cord injury (Krajewski et al., 1999; Springer et al., 1999; Velier et al., 1999; Keane et al., 2001b). As these caspases are initiators of well-described intrinsic and extrinsic apoptotic pathways, respectively, information about them provides particular insight into the type of apoptotic mechanisms that may be important in secondary injury responses. To address this issue, we evaluated the activation of caspase-8, -9, and -3 after TBI induced by the rat lateral fluid-percussion model via temporal immunoblot analysis of cleaved fragments of caspases-3, -8, and -9. In addition, we performed immunocytochemistry utilizing antibodies specific for active caspases, to determine their relative distribution and cell-type specific expression, as well as their association with a late event associated with apoptotic cell death—namely, DNA fragmentation as assessed by the TUNEL assay. Lastly, we evaluated the effect of treatment with a broad-spectrum caspase inhibitor on motor and cognitive function over time after injury.

MATERIALS AND METHODS

Traumatic Brain Injury

The lateral fluid-percussion model of rat brain injury has been previously detailed (McIntosh et al., 1989). Briefly, a craniotomy was performed over the left parietal cortex of anesthetized (70 mg/kg sodium pentobarbital, i.p.), intubated, male Sprague-Dawley rats (400 \pm 25 g, Harlan) ventilated on room air. Injury was induced by a brief, pressurized (2.5–2.6 atm), saline pulse delivered through the craniotomy to the intact dura. Sham controls were subjected to identical surgical procedures, with the exception that no fluid pulse was delivered. The caudal artery was cannulated to monitor blood gas and pressure throughout the procedure. Body (rectal) (37.5–38.5°C) and brain temperature (lateralis muscle) (36.5–37.5°C) were assessed and maintained within normal ranges. Three different sets of animals were prepared: (1) for immunoblot and activity assay studies, rats were subjected to the brain injury procedure and then sacrificed either 1, 12, 48, or 168 h later ($n = 5$ –6/group); naïve rats were used as controls ($n = 5$ –6); (2) for immunocytochemical studies, rats were subjected to brain injury and then sacrificed either 4 or 24 h later ($n = 3$ /group); controls were sacrificed either 4 or 24 h after sham injury performed as described above ($n = 3$ /group); (3) for the drug treatment study, 25 mM z-VAD-fmk was dissolved in DMSO and injected intracerebroventricularly (5 μ L/2 min) at 15 min after injury ($n = 12$); con-

trols received equi-volume injections of DMSO vehicle ($n = 13$).

All procedures involving live animals were approved by the Georgetown University Animal Care and Use Committee, and were performed according to principles enumerated in the Guide for the Care and Use of Laboratory Animals, prepared by the Committee on the Care and Use of Laboratory Animals of the Institute of Laboratory Resources, National Research Council (DHEW publication NIH 85-23-2985).

Preparation of Tissue Homogenates and Immunoblotting

After decapitation, rat cortices were resected on ice and immediately frozen (-70°C). Later, the samples were weighed and homogenized in a 5:1 (wt/v) ratio of RIPA buffer (1% Na deoxycholate, 0.1% SDS, 1% Triton X-100, 0.01 M Tris HCl, pH 8.0, 0.14 M NaCl, 1 mM iodoacetamide, 1 mM AEBSF, 1 mM Aprotinin). Homogenates were centrifuged ($10,000 \times g$, 4°C) for 15 min and the resulting supernatant removed and frozen in 50- μL aliquots. One aliquot was used to determine protein concentration via the method of Bradford (Bradford, 1976). Protein lysates were normalized for total protein content (50 $\mu\text{g}/\text{lane}$) and loaded into 16% (caspase-3) or 4–20% (caspases-9 or -8) Tris-glycine gels and electrophoresed at 100 V for 2–3 h in a Tris/glycine/SDS running buffer. Proteins were transferred to PVDF membranes (25 V for 2 h, 4°C) in Tris/glycine buffer. The membrane was blocked for 2 h with 5% dried milk in Tris/borate/1% Tween 20 buffer at room temperature, then incubated overnight with primary polyclonal rabbit antisera. The next day, membranes were washed three times for 10 min each in Tris/borate buffer, and the protein bands were detected by enhanced chemiluminescence-based ECL methods using Hyperfilm (Amersham). The following primary antibodies were used: caspase-3 (Bur1797, 1:2,000; Burnham Institute, La Jolla, CA); caspase-9 (Bur81, 1:2,000); and caspase-8 (SK440, 1:2,000; SmithKline Beecham, King of Prussia, PA). The specificity of these antibodies has been demonstrated previously (Velier et al., 1999; Krajewski et al., 1999), except for Bur81, which was prepared and specificity demonstrated as described below. Recombinant active caspases and/or cells that are known to highly express caspases were used as positive controls. All blots were directly re-probed with anti- β -actin antibody as an internal control for loading and transfer of proteins (Liao et al., 2000). Blots shown are representative of experiments that were repeated on samples taken from three to five different animals/timepoint.

Production and Specificity of Bur81 Antibody

Anti-caspase-9 serum B81 was produced using recombinant human caspase-9 full-length His 6 protein as an immunogen. Recombinant C9/B81 was produced as a fusion protein with a C-terminal his 6 tag. This protein was expressed in BL21 (DE3) cells by induction with 1 mM IPTG. Following cell growth and lysis, the clarified cell lysate was applied to a Ni-NTA column and eluted with an imidazole gradient. The pooled C9 fractions were dialyzed against 50 mM Tris at pH 8.8 and applied to a 10/10 FPLC mono Q column (Pharmacia, Piscataway, NJ) and eluted with a NaCl gradient. New Zealand white female rabbits were injected subcutaneously with a mixture of recombinant protein (0.1–0.25 mg protein per immunization) and 0.5 mL of Freund's complete adjuvant (dose divided over 10 injections sites) and then boosted three times at weekly intervals, followed by another 3–20 boostings at monthly intervals of recombinant protein immunogens in Freund's incomplete adjuvant, before collecting blood and obtaining immune serum. Specificity of the antisera was tested for reactivity to *in vitro* translated caspases as follows. Caspase-3, -6, -7, -8, -9, and -10 cDNAs subcloned into pcDNA-3 (Invitrogen, Carlsbad, CA) were transcribed and translated *in vitro* using 1 μg of plasmid DNA, T7 RNA polymerase and TNT reticulocyte lysates (Promega, Madison, WI), according to the manufacturer's protocol, in the presence of [^{35}S]-labeled L-methionine ($\sim 1 \text{ mCi}/\text{mmole}$) (Amersham, Piscataway, NJ). The *in vitro* translated caspase proteins were then subjected to SDS-PAGE/immunoblot analysis using Bur81 antisera.

Immunocytochemistry

Animals were anesthetized and intracardially perfused with saline and 4% paraformaldehyde at selected times after injury. Brains were removed, protected in sucrose, frozen in O.C.T. media, sectioned serially (40 μm), and stored free-floating in 2% paraformaldehyde. Approximately four to six sections distributed evenly within the area of the lesion (approximately -2.3 to -3.9 relative to Bregma) (Paxinos and Watson, 1986) were used for staining.

For immunocytochemistry, sections were placed in 4% paraformaldehyde for 5 min, rinsed twice in phosphate-buffered saline (PBS) and blocked in 10% goat serum/0.3% triton for 1 h at room temperature. Primary antibodies specific for cleaved forms of either caspase-3 or -9 (9661S, 9501S; Cell Signaling, Beverly, MA) were diluted 1:100 in PBS containing 2% goat serum/0.2% triton. Antibody 9661S detects only the 17–20-kDa fragment of caspase-3 in human, rat and mouse. Antibody

9501S detects only 37- and 17-kDa fragments of caspase-9 in human and rat. Neither antibody recognizes full-length forms of these caspases. Alternatively, some sections were incubated with SK398 (anti-cleaved caspase-3), SK440 (anti-cleaved caspase-8) (both from SmithKline Beecham), or Bur81 (anti-caspase-9) (Burnham Institute) at a dilution of 1:1000. Antibody SK398 is a neo-epitope peptide antibody generated to the C terminus of the p20 subunit of caspase-3 (GIETD). It detects only an 18-kDa fragment of caspase-3 in rodents. Antibody SK440 was raised against a p20/p10 fusion protein purified from *E. coli*. It recognizes epitopes in the p20 fragment of caspase-8. It does not react with endogenous caspase-8 expressed by Jurkat cells, or with recombinant full-length caspase-8-spiked Jurkat extracts (Velier et al., 1999). Bur81 reacts preferentially with 32–33- and 15-kDa fragments of caspase-9, but also detects the 48-kDa proform of this caspase, as shown in Figure 2 below. Sections were incubated in these solutions overnight (16 h/4°C). In some cases, mouse monoclonal antibodies against neuronal nuclear protein (NeuN) (Chemicon, Temecula, CA) or glial fibrillary acidic protein (GFAP) (Sigma, St. Louis, MO) were diluted at 1:100 in solution with caspase primary antibodies to serve as cell-type specific markers. After incubation, sections were rinsed twice (5 min each) in PBS (4°C) and then incubated with secondary antibodies (1:50) for 1 h (room temperature). Either goat anti-rabbit FITC (Sigma) or goat anti-mouse Texas Red (Accurate Chemicals, Westbury, NY) served as secondary antibodies. Finally, the sections were rinsed twice (5 min each), mounted, covered with anti-fade mounting medium, sealed with glass coverslips, and visualized with a confocal microscope. Confocal parameters were kept constant to allow valid comparisons between experimental groups. Method controls omitted either primary or secondary antibodies.

For sections co-labeled with TUNEL, Tdt reaction mix was applied for 1 h (37°C) after rinsing off primary antibodies. Tdt reaction mix consisted of dNTPs, Tdt buffer, and Tdt enzyme (Life Technologies, Rockville, MD) in sterile, ultrapure H₂O. The TUNEL reaction was stopped in 0.1 M EDTA, pH 8.0 for 2–5 min. Sections were rinsed twice in PBS (5 min each), and incubated with secondary antibody + DN-Avidin-FITC (Vector Labs, Burlingame, CA) for 1 h (room temperature). Thereafter, sections were rinsed, sealed with coverslips, and viewed with a Nikon TE300 inverted fluorescent microscope.

Neurological Evaluation

All neurological examinations were performed by an individual blinded to treatment. Complete methods for motor and cognitive testing have previously been de-

scribed (McIntosh et al., 1989; Fox et al., 1998). Motor testing was performed at 7 and 14 days after trauma (McIntosh et al., 1989). Composite scores were derived from three separate motor tests: (1) flexion test—measures forelimb and paw (left and right) extension and placement in response to a perceived fall, (2) lateral pul- sion test—measures body and leg resistance (left and right) to a lateral push, (3) inclined plane test—assesses the ability to maintain balance (in the vertical, left lateral and right lateral positions) on a progressively inclined surface. Scores for each limb on the individual tests range from 0 (maximal deficit) to 5 (no deficit). These were combined for a possible total maximal composite neuro-score of 35.

Morris water maze training began at day 14 after injury, and concluded after a total of 16 trials were completed in blocks of 4/day. For each trial, rats were gently placed into a tank of opaque water that had extramaze visual cues. The latency, or time required to locate a hidden, submerged, platform was recorded. After reaching the platform, animals were allowed to remain on it for 10 sec before they were removed, dried and kept in a warm environment until the next trial. Animals that failed

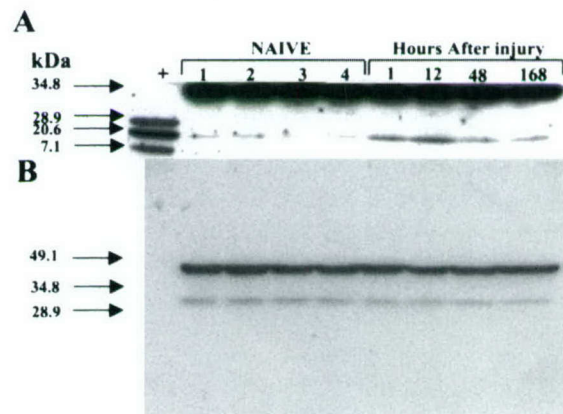


FIG. 1. Temporal expression of caspase-3 cleavage fragments in injured cortex after traumatic brain injury (TBI). Anesthetized rats ($n = 5-6$ /group) were subjected to lateral fluid-percussion trauma (2.5–2.6 ATM). Injured cortex was analyzed by immunoblot at various times after injury (1–168 h). (A) A blot shows results from one animal at each time point, which is representative of results obtained from all animals in each group. The molecular weight of each cleavage fragment appears on the left. Bands corresponding to a 32-kDa proform and a 17-kDa cleavage fragment are present; expression of the 17-kDa fragment increased after trauma. Recombinant active caspase-3 was used as a positive control. Naive rats served as injury controls. (B) β -actin was directly assessed as an internal methods control. As β -actin may itself be cleaved by caspases, some control blots were overexposed, revealing a ~31 kDa cleaved fragment of β -actin which was unchanged by trauma.

to reach the platform within 2 min after placement in the tank, were gently placed on the platform for 10 sec before removal. Data are presented as the average latencies for the treated or untreated groups on each individual day of training.

Data Analysis

Densitometric immunoblot analysis data were assessed by ANOVA followed by post-hoc Dunnett's test. Motor neuroscores were analyzed by nonparametric Mann-Whitney *U* tests. Morris water maze data were analyzed by repeated measures ANOVA followed by multiple two-tailed *t* tests with Bonferroni (Dunn's) correction. A *p* value of <0.05 was considered statistically significant.

RESULTS

Immunoblot analysis of caspase-3 indicated the presence of a 32-kDa proform in all brain samples (Fig. 1A), but not in a recombinant active caspase-3-positive control. A 17-kDa cleavage fragment of caspase-3 was evident at 1, 12, and 48 h after injury. Blots were directly reprobed with β -actin antibody (without stripping) (Liao et al., 2000) which served as an internal control for protein loading and transfer. Loading and transfer of proteins was equal in all wells, as shown by equivalent signal intensity of a 42-kDa β -actin internal control (Fig. 1B; also see Fig. 3C below). However, because caspases are known to cleave β -actin, some control blots were overexposed to determine whether cleavage fragments of this protein were present. In some cases, a 30-kDa β -actin cleavage fragment was detected under this condition, but it was neither robust, nor trauma-dependent (Fig. 1B), thus verifying that β -actin was a suitable internal control.

Specificity studies showed that antibody Bur-81 did not react with either full-length or cleaved forms of caspases-3, -6, -7, -8, or -10, expressed by *in vitro* translation. Bur-81 preferentially reacted with the 32–33- or 15-kDa cleaved forms of caspase-9, but also detected the 48-kDa pro-form of this caspase (Fig. 2A). Similarly, the antibody detected the 48-kDa pro-form of caspase-9 in all brain extracts, as well as 32–33-kDa cleaved fragment (Fig. 2B). Expression of the 15-kDa cleavage fragment was low in naive controls, but increased after TBI. Densitometric analysis of the 15-kDa subunit revealed significant elevations over uninjured controls at 1 and 12 h after injury (Fig. 2C). The appearance of the 32–33-kDa cleaved fragment in both naive and injured cortex is consistent with observations that caspase-9 is auto-processed in brain and peripheral nerve (Krajewski et al., 1999).

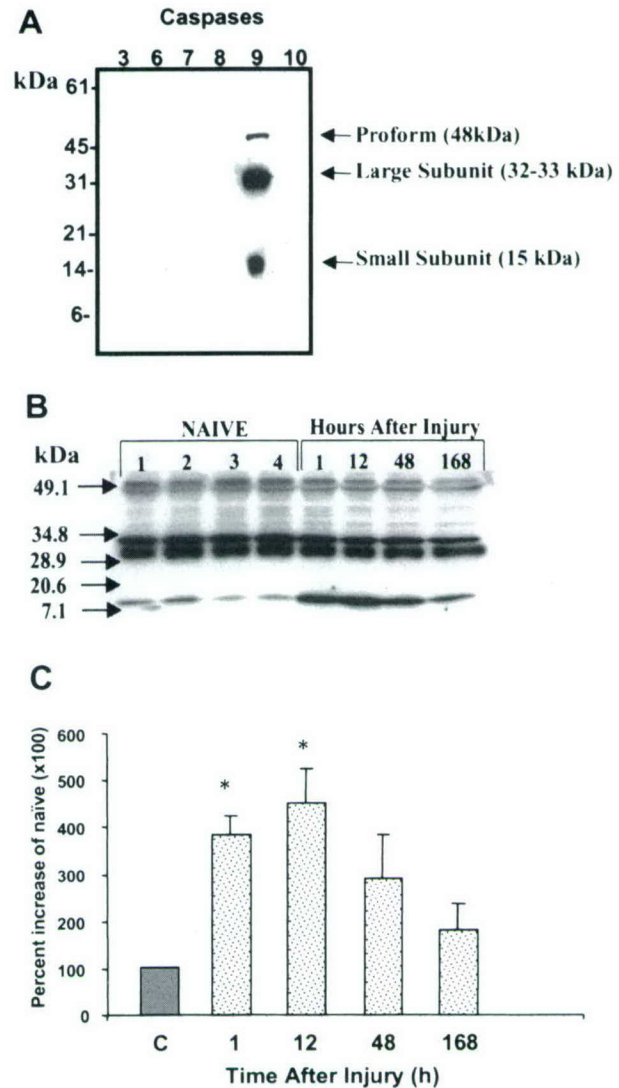


FIG. 2. Specificity of the Bur81 anti-caspase-9 antibody and temporal expression of caspase-9 cleavage fragments in cytosolic extracts of injured cortex after traumatic brain injury (TBI). (A) Immunoblots utilizing extracts from cells expressing *in vitro* translated caspases-3, -6, -7, -8, -9, and -10 show that Bur81 reacts primarily with the ~32–33 and 15-kDa processed (cleaved) forms of caspase-9, and also with the 48-kDa pro-caspase-9. (B,C) Rats ($n = 5$ –6/group) were subjected to lateral fluid-percussion trauma, and the injured cortex assessed by immunoblotting with Bur81 as described for Fig. 1. A representative immunoblot is shown in B. Bands corresponding to a 48-kDa proform and 32–33- or 15-kDa cleavage fragments are present; expression of the 15-kDa fragment increased after trauma. A 32–33-kDa subunit of processed caspase-9 is known to be present in naive cortex and in peripheral nerve. (C) Immunoreactivity of the 15-kDa cleavage fragment is expressed as arbitrary densitometric units. Data were transformed to the percentage of densitometric levels from naive animals visualized on the same scanned blot. Bars indicate means \pm SEM for each timepoint. * $p < 0.05$ versus controls by ANOVA and Dunnett's post-hoc test.

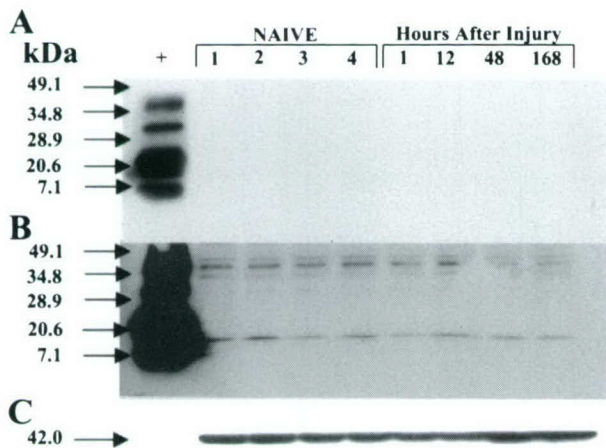


FIG. 3. Temporal expression of caspase-8 cleavage fragments in cytosolic extracts of injured cortex after traumatic brain injury (TBI). Rats ($n = 5-6$ /group) were subjected to lateral fluid-percussion trauma, and the injured cortex assessed by immunoblotting as described for Fig. 1. (A–C) The blot shows results from one animal at each time point, which is representative of results obtained from all animals in each group. The molecular weight of each cleavage fragment appears on the left. In A, the blot was exposed for 15 sec to detect cleaved products present in the recombinant caspase-8 control, which undergoes auto-processing. In B, the same blot was exposed for 8 min to determine whether caspase-8 cleavage fragments were present. At this exposure, bands corresponding to 38–40- or 14-kDa cleavage fragments were detected, although a p55-kDa proform was not. Expression of the 38–40- or 14-kDa cleavage fragments was unchanged by trauma. The β -actin internal control is shown in C.

There was no evidence for injury-induced cleavage of caspase-8, despite the fact that antibody SK440 detected several cleavage fragments in recombinant active caspase-8–positive control samples run on the same gels (Fig. 3A). Blots were subjected to multiple exposures, the longest of which revealed the presence of 38–40- and 14-kDa cleavage fragments in all brain samples, regardless of injury status (Fig. 3B).

To determine the distribution and cell-type expression patterns of caspases within the injured cortex and hippocampus we performed qualitative immunocytochemistry. Four to six sections distributed evenly within the extent of the lesion were chosen and stained for caspases-3, -9, or -8. For caspases-3 and -9, commercially available (Cell Signaling) antibodies, designated 9661S and 9501S, respectively, were used. The antibodies do not detect pro-forms of these caspases; they are specific for cleaved forms, and thus can be used as a cellular marker of caspase activation. Cleaved forms of caspases-3 and -9 were expressed mainly in the inner cortex along the border of the corpus callosum at 4 h after injury (Fig. 4), but were distributed widely throughout the entire region of injured cortex by 24 h after injury (Fig. 5). Active forms of caspases-3 and -9 were also expressed in the CA3 and CA2 regions of the hippocampus, particularly at 24 h after injury (Fig. 6). Selective cell loss was also evident in the CA3 region at this time.

In contrast to the relatively widespread distribution of active caspases-3 and -9 at 4 and 24 h after injury, expression of caspase-8 was limited to only a few cells within the injured cortex at either time (Fig. 7A). These

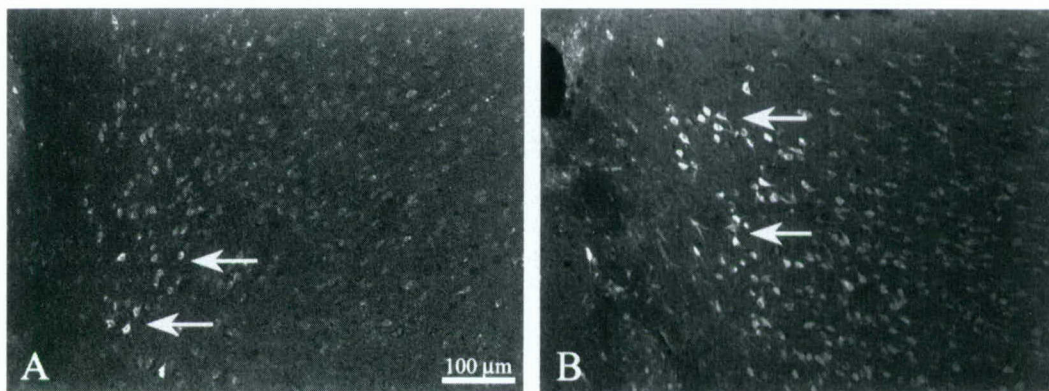


FIG. 4. Distribution of active caspase-3 (A) or caspase-9 (B) (antibodies 9661S or 9501S, respectively) in the inner cortex after lateral fluid-percussion injury, as visualized by fluorescent immunohistochemistry. Injury was produced as described in Fig. 1. At 4 or 24 h after injury, sham-injury brains were removed and stained as described in methods. Low-power images ($\times 10$) of the inner injured cortex at 4 h after injury are shown. Arrows indicate positively stained cells near the border of the corpus callosum. Images are representative of data obtained from $n = 3$ rats/group.

INTRINSIC APOPTOTIC PATHWAYS AFTER BRAIN INJURY

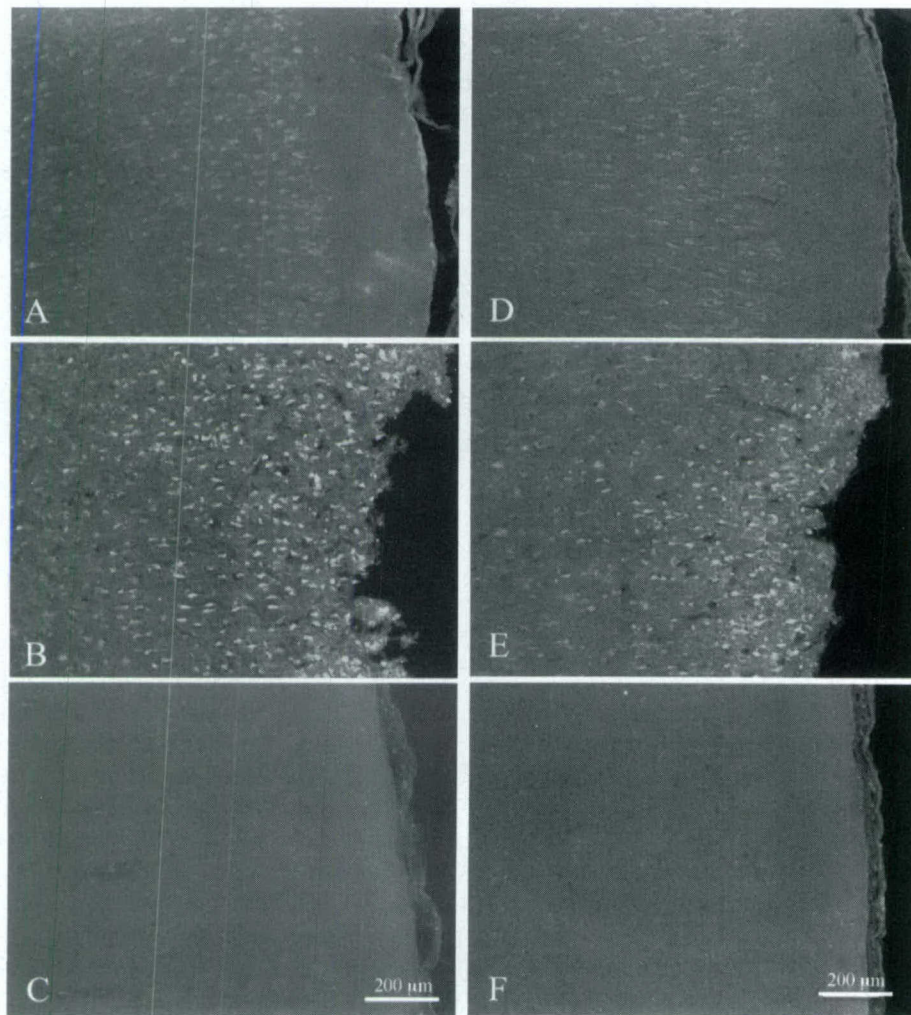


FIG. 5. Distribution of active caspase-3 (A–C) (antibody 9661S) or -9 (D–F) (antibody 9501S) in the outer cortex after lateral fluid-percussion injury. Data were obtained from the same rats described in Fig. 4. Low-power images ($\times 10$) of outer injured cortex were obtained at 4 h (A,D) and 24 h (B,E) after TBI, or 24 h after sham-TBI (C,F).

cells morphologically resembled neurons and glia. Even though few cells stained positively, such staining was associated with injury, as sham-injury controls showed no evidence of any positive staining (Fig. 7B).

Double-label immunocytochemistry revealed that cleaved caspases-3 and -9 were expressed by neurons, but not astrocytes of the injured cortex (Figs. 8 and 9). Staining in neurons was diffuse, cytosolic and present in the soma as well as what appeared to be dendrites, on some occasions (Figs. 5, 8, and 9). Caspase-9 and the cleaved fragment of caspase-3 were also colocalized to some extent with TUNEL-positive cortical cells that showed apoptotic-like condensed or punctate nuclear morphology (Fig. 10). However, this colocalization was not exclusive, as many TUNEL-positive and TUNEL-

positive cells with apoptotic-like phenotypes did not express active subunits of either caspase, and some caspase positive cells were not TUNEL-positive.

To evaluate the effect of caspase inhibition on functional recovery after injury, animals were treated 15 min after injury with z-VAD-fmk, a pan-caspase inhibitor. This treatment significantly improved performance on a series of three separate motor tests administered 2 weeks later (Fig. 11A). In addition, in daily comparisons, z-VAD-fmk treated animals performed significantly better than controls in the Morris water maze test on days 2 and 4 of training (Fig. 11B). There was no significant difference in latencies on the first day of training, indicating that swim speeds were not significantly different between treated and control groups.

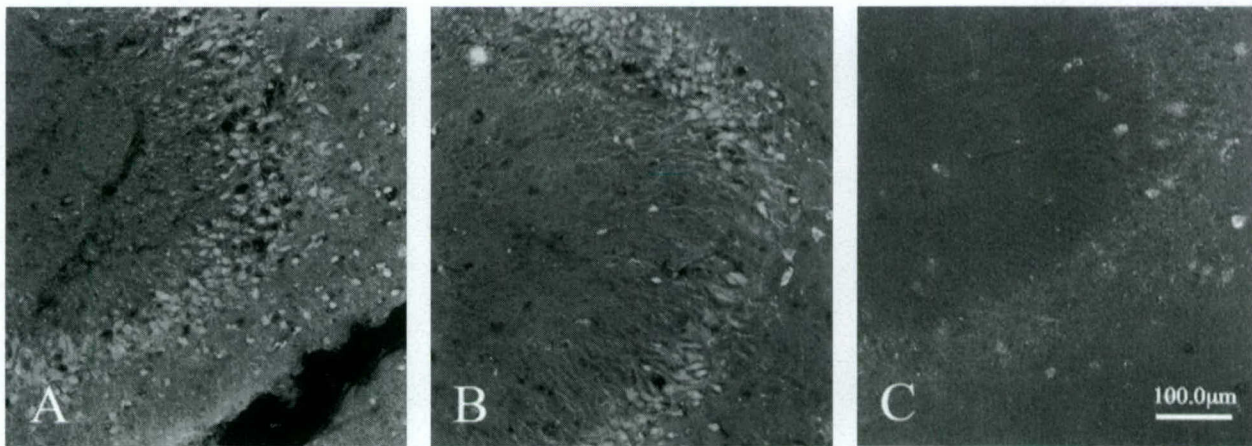


FIG. 6. Distribution of active caspase-3 (A) (9661S) or caspase-9 (B) (9501S) in the hippocampus 24 h after TBI. Many CA3 pyramidal cells stained positively for caspase-3 (A) or caspase-9 (B). Note that some cell loss is also visible in the CA3 region. The majority of CA2 cells at the junction with CA1 were caspase-3 or -9 positive, although most CA1 cells were not (data not shown). Few caspase-positive cells were observed in the hippocampus at 2 h after sham-TBI (C) or at 4 h after injury (data not shown).

DISCUSSION

Our studies show that caspases-3 and -9 are activated in injured cortex and hippocampus after traumatic injury. Cleavage products of these caspases were expressed throughout the cortex, primarily in neurons, and frequently co-localized with TUNEL-positive labeling. The latter associates these caspases with neuronal cell death that is likely to be, at least in part, apoptotic. In contrast, the presence of active caspase-8 was more difficult to detect than either caspase-3 or -9. Cleavage fragments for this caspase were not observed on immunoblots, and were only localized to a few cells by immunocytochemistry.

Caspase activation after brain injury has been assessed by a variety of methods, ranging from accumulation of degraded downstream substrates unique to a particular caspase (Pike et al., 1998; Beer et al., 2000b; Clark et al., 2000), to direct activity measurements utilizing oligopeptide substrates tagged with a fluorogen that produces an optical change upon cleavage (Yakovlev et al., 1997; Clark et al., 2000). In preliminary experiments, we found that, in the case of caspases-8 and -9, such fluorescence-based activity assays were nonspecific. In assays with Ac-LETD-afc (caspase-8) and Ac-LEHD-afc (caspase-9), the recognized substrate sequences for these caspases (Talanian et al., 1997; Thornberry et al., 1997), submicro-

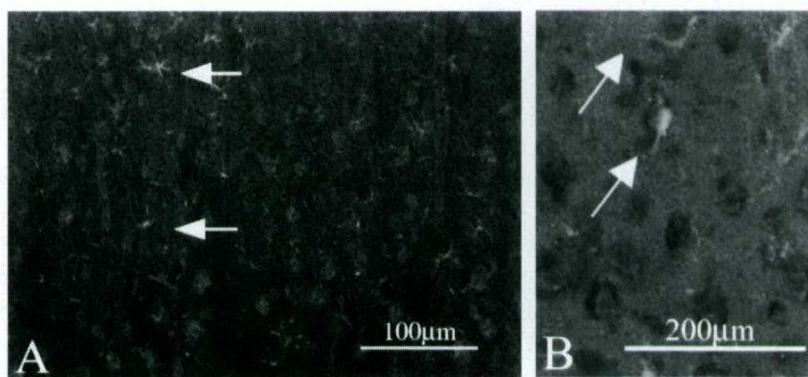


FIG. 7. Distribution of caspase-8 (antibody SK440) in the injured parietal cortex at 24 h after TBI. Low-power image shows that only a few cells distributed within the cortex expressed caspase-8 after injury (A; some positive cells indicated by arrows). Under higher power magnification, such cells resembled glia or neurons (B; cells indicated by arrows). Results are representative of $n = 3$ animals. Sections from 4 h after injury were also evaluated (including sections adjacent to those which showed positive staining for caspases-9 and -3), and showed a distribution of staining similar to that shown in A.

INTRINSIC APOPTOTIC PATHWAYS AFTER BRAIN INJURY

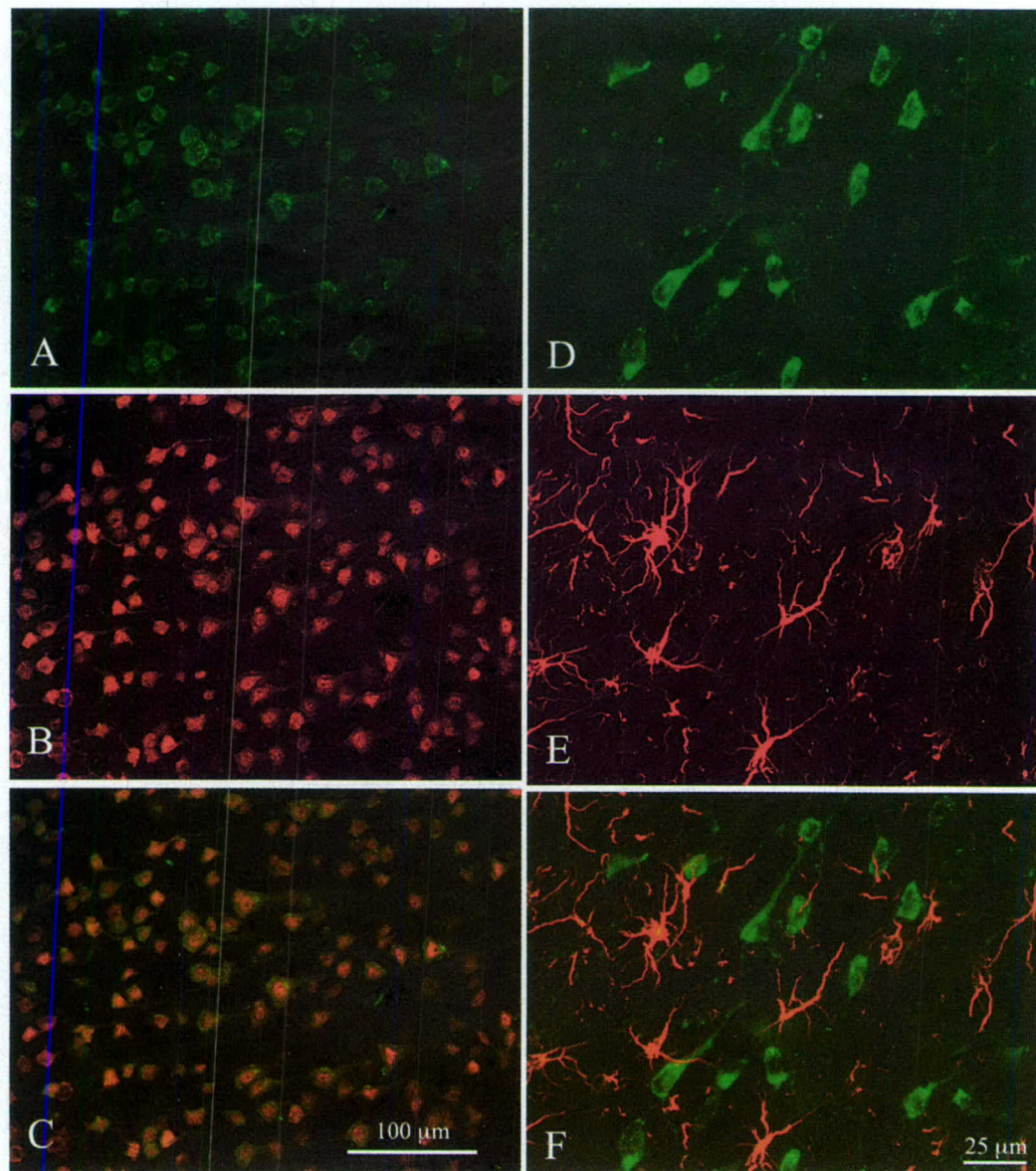


FIG. 8. Double-label immunocytochemistry for active caspase-3 (A,D) (antibody 9661S) combined with either NeuN, a neuronal marker (B) or GFAP (E), a marker for astrocytes. Staining for active caspase-3 was diffuse, cytosolic (A), and was localized to neuronal cell bodies (B,C), and in some instances, dendrites (A). Active caspase-3 was not frequently expressed by astrocytes (E,F). Images were taken from the injured parietal cortex at 24 h after TBI. They are representative of data from $n = 3$ animals.

molar concentrations of either recombinant caspase-3 or z-DEVD added to control (sham) samples respectively markedly increased or decreased apparent caspase-8 or -9 activity. Therefore, this method was replaced with detection of active caspases via immunoblot.

Our data indicated that caspases-3 and -9 were activated from 1 to at least 12 h after lateral fluid-percussion injury. These results are consistent with both the time-course for activation of caspase-3 we reported previously

using a fluorogenic activity assay (Yakovlev et al., 1997), and with recently reported time-courses for caspases-3 or -9 utilizing immunoblotting methods (Beer et al., 2000b; Clark et al., 2000). Together, such findings suggest that cortical apoptosis occurs over an extended time-course, in agreement with studies which showed increased TUNEL-staining in the same model from 24 to 168 h after injury (Rink et al., 1995; Conti et al., 1998). These results are also consistent with the time course for acti-

vation of caspase-3 and apoptotic cell death reported in cortical contusion models (Yakovlev et al., 1997; Fox et al., 1998; Newcomb et al., 1999; Beer et al., 2000b; Clark et al., 2000).

In undisturbed neurons, the location of procaspase-9 is frequently mitochondrial, giving rise to a distinct organellar staining pattern (Krajewski et al., 1999). After ischemic injury, caspase-9 translocates from the mitochondria to the cytosol and nucleus, resulting in diffuse staining throughout the cell (Krajewski et al., 1999), which resembles that pattern we observed, suggesting that a similar translocation of caspase-9 occurs in both ischemic and traumatic injuries. Caspase-3 primarily resides in the cytosol (Krajewska et al., 1997), and thus staining for this caspase is usually diffuse, as seen here, and reported previously in other models of trauma (Beer et al., 2000b; Clark et al., 2000) or ischemia (Namura et al., 1998). Apart from visualization in the soma, we observed some expression of caspase-9 (and caspase-3) in what appeared to be dendrites. Dendritic expression of active caspase has been associated with synaptic loss and cell death due to excessive glutamate stimulation (Mattson et al., 1998). Thus, it is possible that caspase activation through this route could be a factor in traumatic injury. Expression of cytochrome c, calpain and active caspase-3 have also been observed in cortical axons, where they are hypothesized to contribute to neuronal demise in models of axonal injury (Buki et al., 2000). Together, these data suggest that activated caspases are not limited to somatic expression in injured neurons, and may reflect several different local routes through which neuronal death or synaptic reorganization could be initiated.

Qualitatively, the regional and cell-type distributions of active caspases-3 and -9 appeared similar, as they were evident in all layers of injured cortex, albeit somewhat preferentially in the inner cortex adjacent to the corpus callosum at 4 h after injury, but distributed throughout the region at 24 h after injury. Both caspases were expressed primarily by neurons rather than astrocytes, in agreement with findings from cortical contusion models, which also mainly located active caspase-3 expression to neurons trauma (Beer et al., 2000b; Clark et al., 2000). Caspase-3 appeared to be expressed in more cells than caspase-9 at both 4 and 24 h after injury. In this regard, it is worth noting that caspase-3 may be activated not only through extrinsic and intrinsic cascades, but also by additional factors, including granzyme B, caspase-11, and others, whose role in injury, if any, is uncertain (Yang et al., 1998; Kang et al., 2000).

We could not use antibodies 9661S or 9501S in the TUNEL double-label study, because these antibodies did not perform well on thin, mounted sections, but TUNEL-

staining did not work well on thick free-floating sections. Therefore, antibodies SK398 and Bur81 were used in the TUNEL double-label experiments. In this regard, it is worth noting that SK398 is specific only for active caspase-3, whereas Bur81 preferentially stains cleaved fragments of caspase-9, but also reacts to a lesser extent with the pro-form of this caspase. Data from this experiment indicate that active caspase-3, and likely, active caspase-9, are expressed by either type I or type II TUNEL-labeled cells, but this association was not complete, as noted previously for caspase-3 by others (Beer et al., 2000b; Clark et al., 2000). This result may reflect the fact that active caspases are short-lived, and their temporal expression may not completely overlap the DNA fragmentation that gives rise to the TUNEL signal, but rather (and particularly in the case of caspase-9) precede it. Other factors may also contribute to the discrepancy. These would include observations that: some TUNEL positive cells are actually necrotic (Rink et al., 1995; de Torres et al., 1997); there may be a mixed apoptotic-necrotic phenotype (Allen et al., 1999); there is likely to be cross-talk between cell death mechanisms, and/or activation of certain apoptotic pathways may not be mediated by caspases (Susin et al., 2000; Thomas et al., 2000).

Presumptive involvement of the extrinsic apoptotic pathway in TBI is supported by evidence that Fas and Fas ligand are increased after TBI (Ertel et al., 1997; Beer et al., 2000a), as is TNF (Shohami et al., 1996; Knoblich et al., 1999). Yet, the present data show only limited caspase-8 activation. It is unlikely that our findings are due to antibody specificity issues. This antibody, which has previously been extensively characterized (Velier et al., 1999), strongly detected a positive caspase-8 control. In addition, we have utilized the antibody in an identical protocol to evaluate active caspase-8 expression after spinal cord injury (Huang et al., 2000), and others have used it in models of spinal ischemia and focal stroke (Velier et al., 1999; Matsushita et al., 2000). In all these studies, substantial expression of active caspase-8 was detected. More likely, the data reflect injury level or model issues. Caspase-8 activation was recently shown after more moderate fluid percussion injury (1.7–2.2 atm), where its temporal elevation correlated well with the time course of TNF α we observed after severe injury (2.6–2.7 atm) (Keane et al., 2001a). In our hands, more moderate injury (2.0 atm) did not consistently elevate TNF α . Thus, there are apparent differences in actual injury levels between laboratories, and it is possible that our severe injury level may be required to induce substantial caspase-8 activation. This is supported indirectly by a recent study in the cortical impact injury model, which demonstrated increases in both caspase-8 mRNA and activation, and in

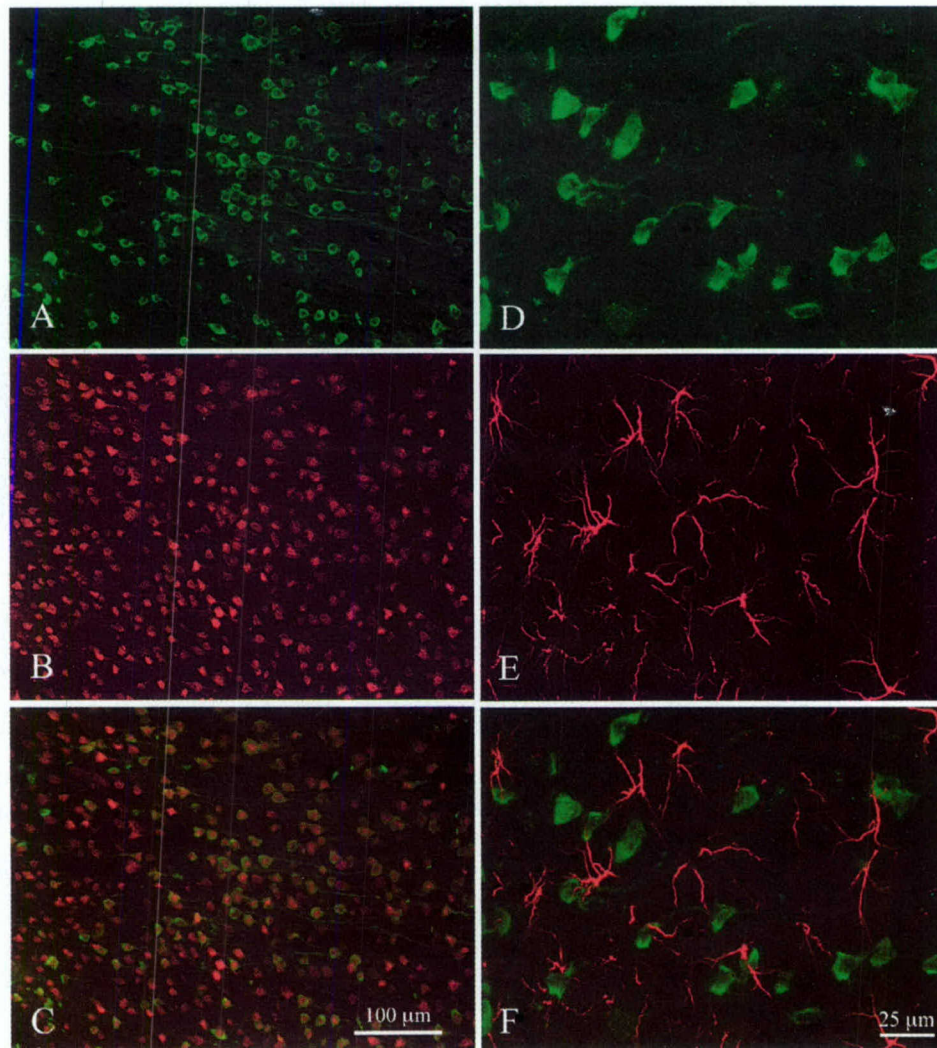


FIG. 9. Double-label immunocytochemistry for active caspase-9 (**A,D**) (antibody 9501S) combined with either NeuN, a neuronal marker (**B**) or GFAP (**E**), a marker for astrocytes. As with caspase-3, staining was diffuse, cytosolic and was localized to neuronal bodies and in some instances, dendrites (**A,D,C**). Active caspase-9 was not frequently expressed by astrocytes (**F**). Images were taken from the injured parietal cortex 24 h after TBI. They are representative of data from $n = 3$ animals.

addition, associated caspase-8 with neurons and glia (Beer et al., 2001). This injury model is known to invoke an ischemic response that may only be present at severe levels of fluid percussion injury (Bryan et al., 1995).

Our caspase-9 data are the first to show the cortical distribution of this caspase after injury, as well as to evaluate its expression in specific cell-types, or in conjunction with TUNEL staining. The results are consistent with reports of increased expression of apaf-1 and cytochrome c after trauma (Yakovlev et al., 2001), as well as alterations of endogenous inhibitors of this pathway, such as bcl-2 or XIAP (Clark et al., 1999; Lu et al., 2000; Keane et al., 2001a,b). Together, these data collectively provide

strong support for the intrinsic pathway of apoptotic cell death after TBI.

Treatment with the pan-caspase inhibitor z-VAD-fmk improved motor and cognitive function, compared to vehicle controls. This likely relates to caspase expression both in cortex and hippocampus, as shown here for caspase-9 and previously for caspase-3 (Yakovlev et al., 1997). Z-VAD-fmk was also neuroprotective in a mouse model of controlled cortical impact, where it reduced lesion volume (Fink et al., 1999), and in mouse and rat models of ischemia, where it both reduced lesion volume and improved neurological function (Loddick et al., 1996; Hara et al., 1997; Fink et al., 1998; Ma et al., 1998).

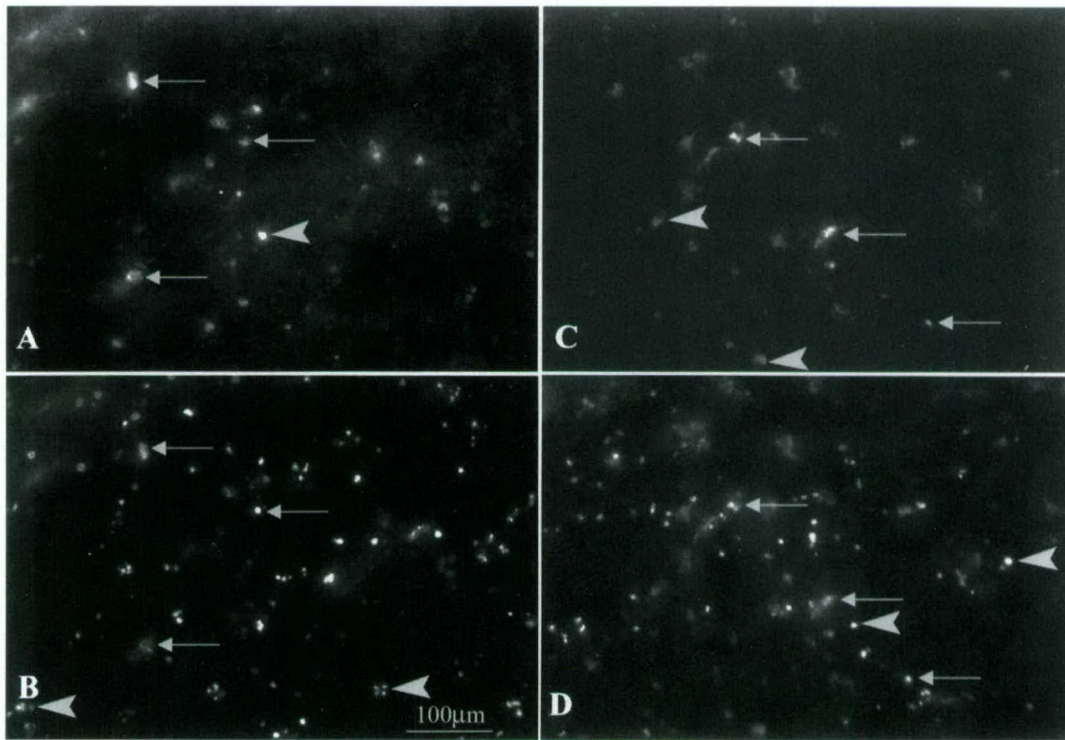


FIG. 10. Colocalization of caspases and TUNEL staining in rat cortex at 24 h after TBI. Fluorescent immunostaining was used to detect either active caspase-3 (SK398 antibody) (A) or caspase-9 (Bur81 antibody) (C) as indicated in representative fields ($\times 40$). (B,D) Images show TUNEL-positive staining observed in the same fields as A and C, respectively. Arrows denote cells positive for caspase as well as TUNEL labeling. Chevrons denote cells positive for either caspase or TUNEL labeling, but not both.

Z-VAD-fmk is an irreversible inhibitor of most caspases, showing greatest inhibition of caspases-1, -5, -8, and -9, but also significant inhibition of caspases-3, -4, -6, and -7 (Thornberry et al., 1997). Of these, caspases-4, -5, -6, and -7 have not yet been associated with TBI, and may not even be present in the CNS (Eldadah and Faden, 2000). However, we previously observed improved neurological recovery concurrent with reductions in TUNEL-labeled cells and DNA laddering after selective inhibition of caspase-3 with z-DEVD-fmk in our model (Yakovlev et al., 1997), implicating this caspase in tissue damage and functional deterioration. Similar findings were reported after caspase-3 inhibition in a model of controlled cortical impact, although behavioral status was unchanged (Clark et al., 2000). The parenchymal injection scheme employed in the latter study may have led to local tissue preservation, but prevented diffusion of z-DEVD-fmk to brain regions (cortex, hippocampus) that are represented in behavioral outcome measures. Caspase-1 has also been implicated in TBI, but here again, the data are mixed. The selective caspase-1 inhibitor z-YVAD-fmk reduced lesion volume in a mouse cortical contusion model, and dominant-negative caspase-1 mu-

tant mice showed improved neurological function and reduced lesion volumes (Fink et al., 1999). However, activation of caspase-1 was not significantly elevated after lateral fluid-percussion injury, though mRNA for the pro-form did increase (Yakovlev et al., 1997). Nonetheless, caspase-1 activation has been observed after clinical head injury (Clark et al., 1999). Whether such discrepancies reflect potential ischemic/metabolic complications associated with clinical head injury and/or model specific anomalies remains to be determined. Specific proof of an important role for caspases-8 or -9 awaits additional studies, perhaps with ribozyme constructs, given issues with the specificity of currently available selective inhibitors for these caspases.

In addition to inhibition of caspases, z-VAD-fmk was recently found to inhibit calpains (Wolf et al., 1999; Blomgren et al., 2001), enzymes which are independently recognized as important mediators of necrotic cell death, tissue loss and dysfunction in both traumatic and ischemic injuries (Kampfl et al., 1996; Saatman et al., 1996; Pike et al., 1998; McCracken et al., 1999; Zhao et al., 1999; Buki et al., 2000). The IC₅₀ of z-VAD is actually lower for m- and u-calpain (15 μ M) than for caspase-3

INTRINSIC APOPTOTIC PATHWAYS AFTER BRAIN INJURY

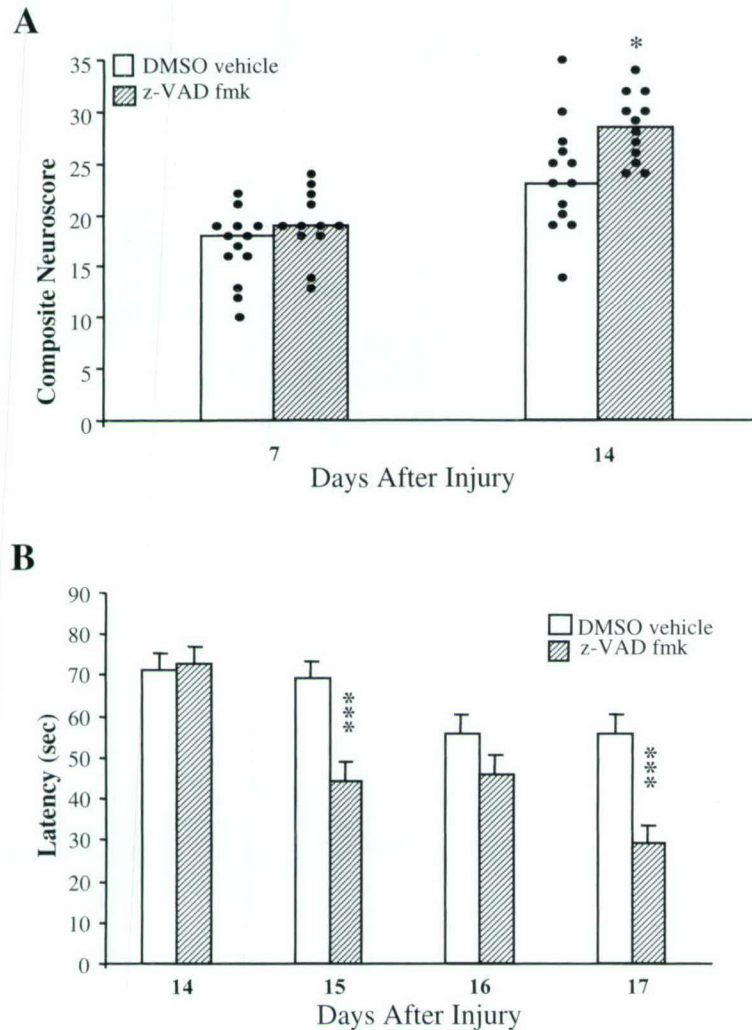


FIG. 11. Pan-caspase inhibitor z-VAD-fmk improves neurological recovery after traumatic brain injury. Z-VAD-fmk (25 mM in 5 μ L), was injected intracerebroventricularly 15 min after lateral fluid-percussion-induced brain injury. **(A)** Bars represent median combined score on three separate tests of motor function (flexion, pulsion, and inclined plane). Dots represent scores of individual animals (z-VAD-fmk, $n = 12$; vehicle [DMSO], $n = 13$). The best possible combined score is 35. Animals treated with z-VAD-fmk scored significantly better than DMSO controls 14 days after injury. * $p < 0.05$ versus vehicle by Mann-Whitney U comparison. **(B)** Bars represent the daily mean \pm SEM of latency to find a hidden platform for each group over four trials of a Morris water maze visuospatial learning paradigm. Four consecutive days of training (for a total of 16 trials) commenced 14 days after traumatic brain injury. Data are from the same animals/experiment shown in A. Z-VAD-fmk-treated animals performed significantly better on days 2 and 4 of water maze testing than did vehicle (DMSO)-treated controls. *** $p < 0.001$ for z-VAD-fmk versus vehicle from the same day. Maze data were analyzed by repeated measures ANOVA followed by post-hoc t tests with Bonferroni correction.

(60 μ M) (Blomgren et al., 2001); thus, it is possible that some of the beneficial effects of z-VAD-fmk may reflect inhibition of calpains. From a treatment perspective, an agent which inhibits both calpains and caspases may be optimal for clinical use, as it would target both necrotic and apoptotic cell death. This may be particularly important, since evidence suggests that prevention of either necrosis or apoptosis may shunt the injury response toward the alternate death pathway (Pohl et al., 1999;

Lewen et al., 2001; Susin et al., 1998). In addition, calpain- and caspase-mediated cell death pathways appear to share points of intersection as well as common features (reviewed in Wang, 2000). Illustrative examples include that the endogenous calpain inhibitor calpastatin is degraded by active caspases (Wang et al., 1998a), and that both enzymes degrade spectrin, a major component of cytoskeleton (Wang et al., 1998b).

In summary, we show evidence for the activation of

several caspases after TBI. Activation of caspases-3 and -9 was significantly elevated from hours to days after injury, in contrast to active caspase-8, which was expressed in only a few cells. In addition, the pan-caspase inhibitor z-VAD-fmk improved motor and cognitive neurological dysfunction after TBI. Together, these data support an involvement of several caspases in secondary cell death and neurological dysfunction after TBI, and suggest that anti-caspase treatment strategies may be potentially useful after traumatic brain injury in humans.

ACKNOWLEDGMENTS

We thank Sadia Aden, Anu Singh, and Tong Zhang for technical assistance. Grant support was provided by NIH NS36537 and DAMD17-99-2-9007 to A.I.F., KA1-9905-02 from the Christopher Reeve Paralysis Foundation to S.M.K., and NIH NS36821 to S. Krajewski.

REFERENCES

- ALLEN, J.W., KNOBLACH, S.M., and FADEN, A.I. (1999). Combined mechanical trauma and metabolic impairment *in vitro* induces NMDA receptor-dependent neuronal cell death and caspase-3-dependent apoptosis. *FASEB J.* **13**, 1875-1882.
- BEER, R., FRANZ, G., KRAJEWSKI, S., et al. (2001). Temporal and spatial profile of caspase 8 expression and proteolysis after experimental traumatic brain injury. *J. Neurochem.* **78**, 862-873.
- BEER, R., FRANZ, G., SCHOPF, M., et al. (2000a). Expression of Fas and Fas ligand after experimental traumatic brain injury in the rat. *J. Cereb. Blood Flow Metab.* **20**, 669-677.
- BEER, R., FRANZ, G., SRINIVASAN, A., et al. (2000b). Temporal profile and cell subtype distribution of activated caspase-3 following experimental traumatic brain injury. *J. Neurochem.* **75**, 1264-1273.
- BLOMGREN, K., ZHU, C., WANG, X., et al. (2001). Synergistic activation of caspase-3 by m-calpain after neonatal hypoxia-ischemia: a mechanism of "pathological apoptosis"? *J. Biol. Chem.* **276**, 10191-10198.
- BRADFORD, M.M. (1976). A rapid and sensitive method for the quantitation of microgram quantities of protein utilizing the principle of protein-dye binding. *Anal. Biochem.* **72**, 248-254.
- BRYAN, R.M., JR., CHERIAN, L., and ROBERTSON, C. (1995). Regional cerebral blood flow after controlled cortical impact injury in rats. *Anesth. Analg.* **80**, 687-695.
- BUKI, A., OKONKWO, D., WANG, K., et al. (2000). Cytochrome c release and caspase activation in traumatic axonal injury. *J. Neurosci.* **20**, 2825-2834.
- CHINNAIYAN, A.M., O'ROURKE, K., TEWARI, M., et al. (1995). FADD, a novel death domain-containing protein, interacts with the death domain of Fas and initiates apoptosis. *Cell* **81**, 505-512.
- CLARK, R., KOCHANNEK, P., CHEN, M., et al. (1999). Increases in Bcl-2 and cleavage of caspase-1 and caspase-3 in human brain after head injury. *FASEB J.* **13**, 813-821.
- CLARK, R., KOCHANNEK, P., WATKINS, S., et al. (2000). Caspase-3-mediated neuronal death after traumatic brain injury in rats. *J. Neurochem.* **74**, 740-753.
- CONTI, A.C., RAGHUPATHI, R., TROJANOWSKI, J.Q., et al. (1998). Experimental brain injury induces regionally distinct apoptosis during the acute and delayed post-traumatic period. *J. Neurosci.* **18**, 5663-5672.
- DE TORRES, C., MUNELL, F., FERRER, I., et al. (1997). Identification of necrotic cell death by the TUNEL assay in the hypoxic-ischemic neonatal rat brain. *Neurosci. Lett.* **230**, 1-4.
- ELDADAH, B.A., and FADEN, A.I. (2000). Caspase pathways, neuronal apoptosis, and CNS injury. *J. Neurotrauma* **17**, 811-829.
- ERTEL, W., KEEL, M., STOCKER, R., et al. (1997). Detectable concentrations of Fas ligand in cerebrospinal fluid after severe head injury. *J. Neuroimmunol.* **80**, 93-96.
- FINK, K., ZHU, J., NAMURA, S., et al. (1998). Prolonged therapeutic window for ischemic brain damage caused by delayed caspase activation. *J. Cereb. Blood Flow Metab.* **18**, 1071-1076.
- FINK, K., ANDREWS, L., BUTLER, W., et al. (1999). Reduction of post-traumatic brain injury and free radical production by inhibition of the caspase-1 cascade. *Neuroscience* **94**, 1213-1218.
- FOX, G.B., FAN, L., LEVASSEUR, R.A., et al. (1998). Sustained sensory/motor and cognitive deficits with neuronal apoptosis following controlled cortical impact brain injury in the mouse. *J. Neurotrauma* **15**, 599-614.
- HAKEM, R., HAKEM, A., DUNCAN, G.S., et al. (1998). Differential requirement for caspase 9 in apoptotic pathways *in vivo*. *Cell* **94**, 339-352.
- HARA, H., FRIEDLANDER, R.M., GAGLIARDINI, V., et al. (1997). Inhibition of interleukin 1beta converting enzyme family proteases reduces ischemic and excitotoxic neuronal damage. *Proc. Natl. Acad. Sci. U.S.A.* **94**, 2007-2012.
- HUANG, X., VAN GELDEREN, J., CALVA-CERQUIERA, D., et al. (2000). Differential activation of caspases after traumatic spinal cord injury in the rat. In: *Society for Neuroscience. Society for Neuroscience, 30th Annual Meeting, New Orleans, LA.*
- JUO, P., KUO, C.J., YUAN, J., et al. (1998). Essential requirement for caspase-8/FLICE in the initiation of the Fas-induced apoptotic cascade. *Curr. Biol.* **8**, 1001-1008.

- KAMPFL, A., POSMANTUR, R., NIXON, R., et al. (1996). μ -Calpain activation and calpain-mediated cytoskeletal proteolysis following traumatic brain injury. *J. Neurochem.* **67**, 1575–1583.
- KANG, S.J., WANG, S., HARA, H., et al. (2000). Dual role of caspase-11 in mediating activation of caspase-1 and caspase-3 under pathological conditions. *J. Cell Biol.* **149**, 613–622.
- KEANE, R.W., KRAYDIEH, S., LOTOCKI, G., et al. (2001a). Apoptotic and antiapoptotic mechanisms after traumatic brain injury. *J. Cereb. Blood Flow Metab.* **21**, 1189–1198.
- KEANE, R.W., KRAYDIEH, S., LOTOCKI, G., et al. (2001b). Apoptotic and anti-apoptotic mechanisms following spinal cord injury. *J. Neuropathol. Exp. Neurol.* **60**, 422–429.
- KNOBLACH, S., FAN, L., and FADEN, A. (1999). Early neuronal expression of tumor necrosis factor- α after experimental brain injury contributes to neurological impairment. *J. Neuroimmunol.* **95**, 115–125.
- KRAJEWSKA, M., WANG, H.G., KRAJEWSKI, S., et al. (1997). Immunohistochemical analysis of *in vivo* patterns of expression of CPP32 (Caspase-3), a cell death protease. *Cancer Res.* **57**, 1605–1613.
- KRAJEWSKI, S., KRAJEWSKA, M., ELLERBY, L.M., et al. (1999). Release of caspase-9 from mitochondria during neuronal apoptosis and cerebral ischemia. *Proc. Natl. Acad. Sci. U.S.A.* **96**, 5752–5757.
- LEWEN, A., SKOGLOSA, Y., CLAUSEN, F., et al. (2001). Paradoxical increase in neuronal DNA fragmentation after neuroprotective free radical scavenger treatment in experimental traumatic brain injury. *J. Cereb. Blood Flow Metab.* **21**, 344–350.
- LI, M., ONA, V.O., CHEN, M., et al. (2000). Functional role and therapeutic implications of neuronal caspase-1 and -3 in a mouse model of traumatic spinal cord injury. *Neuroscience* **99**, 333–342.
- LI, P., NIJHAWAN, D., BUDIHARDJO, I., et al. (1997). Cytochrome c and dATP-dependent formation of Apaf-1/caspase-9 complex initiates an apoptotic protease cascade. *Cell* **91**, 479–489.
- LIAO, J., XU, X., and WARGOVICH, M.J. (2000). Direct reprobating with anti- β -actin antibody as an internal control for western blotting analysis. *Biotechniques* **28**, 216–218.
- LODDICK, S.A., MacKENZIE, A., and ROTHWELL, N.J. (1996). An ICE inhibitor, z-VAD-DCB attenuates ischaemic brain damage in the rat. *Neuroreport* **7**, 1465–1468.
- LU, J., MOOCHHALA, S., KAUR, C., et al. (2000). Changes in apoptosis-related protein (p53, Bax, Bcl-2 and Fos) expression with DNA fragmentation in the central nervous system in rats after closed head injury. *Neurosci. Lett.* **290**, 89–92.
- MA, J., ENDRES, M., and MOSKOWITZ, M.A. (1998). Synergistic effects of caspase inhibitors and MK-801 in brain injury after transient focal cerebral ischaemia in mice. *Br. J. Pharmacol.* **124**, 756–762.
- MATSUSHITA, K., WU, Y., QIU, J., et al. (2000). Fas receptor and neuronal cell death after spinal cord ischemia. *J. Neurosci.* **20**, 6879–6887.
- MATTSON, M.P., KELLER, J.N., and BEGLEY, J.G. (1998). Evidence for synaptic apoptosis. *Exp. Neurol.* **153**, 35–48.
- MCCRACKEN, E., HUNTER, A., PATEL, S., et al. (1999). Calpain activation and cytoskeletal protein breakdown in the corpus callosum of head-injured patients. *J. Neurotrauma.* **16**, 749–761.
- McINTOSH, T.K., VINK, R., NOBLE, L., et al. (1989). Traumatic brain injury in the rat: characterization of a lateral fluid-percussion model. *Neuroscience* **28**, 233–244.
- NAMURA, S., ZHU, J., FNK, K., et al. (1998). Activation and cleavage of caspase-3 in apoptosis induced by experimental cerebral ischemia. *J. Neurosci.* **18**, 3659–3668.
- NEWCOMB, J., ZHAO, X., PIKE, B., et al. (1999). Temporal profile of apoptotic-like changes in neurons and astrocytes following controlled cortical impact injury in the rat. *Exp. Neurol.* **158**, 76–88.
- NG, I., YEO, T., TANG, W., et al. (2000). Apoptosis occurs after cerebral contusions in humans. *Neurosurgery* **46**, 949–956.
- PAXINOS, G., and WATSON, C. (1986). *The Rat and Brain in Stereotaxic Coordinates*. Academic Press: Sydney.
- PIKE, B.R., ZHAO, X., NEWCOMB, J.K., et al. (1998). Regional calpain and caspase-3 proteolysis of α -spectrin after traumatic brain injury. *Neuroreport* **9**, 2437–2442.
- POHL, D., BITTIGAU, P., ISHIMARU, M.J., et al. (1999). N-Methyl-D-aspartate antagonists and apoptotic cell death triggered by head trauma in developing rat brain. *Proc. Natl. Acad. Sci. U.S.A.* **96**, 2508–2513.
- REED, J.C. (2000). Mechanisms of apoptosis. *Am. J. Pathol.* **157**, 1415–1430.
- RINK, A., FUNG, K.M., TROJANOWSKI, J.Q., et al. (1995). Evidence of apoptotic cell death after experimental traumatic brain injury in the rat. *Am. J. Pathol.* **147**, 1575–1583.
- SAATMAN, K.E., MURAI, H., BARTUS, R.T., et al. (1996). Calpain inhibitor AK295 attenuates motor and cognitive deficits following experimental brain injury in the rat. *Proc. Natl. Acad. Sci. U.S.A.* **93**, 3428–3433.
- SALEH, A., SRINIVASULA, S.M., ACHARYA, S., et al. (1999). Cytochrome c and dATP-mediated oligomerization of Apaf-1 is a prerequisite for procaspase-9 activation. *J. Biol. Chem.* **274**, 17941–17945.
- SHOHAMI, E., BASS, R., WALLACH, D., et al. (1996). Inhibition of tumor necrosis factor α (TNF α) activity in rat brain is associated with cerebroprotection after closed head injury. *J. Cereb. Blood Flow Metab.* **16**, 378–384.

- SLEE, E.A., HARTE, M.T., KLUCK, R.M., et al. (1999). Ordering the cytochrome c-initiated caspase cascade: hierarchical activation of caspases-2, -3, -6, -7, -8, and -10 in a caspase-9-dependent manner. *J. Cell Biol.* **144**, 281-292.
- SPRINGER, J.E., AZBILL, R.D., and KNAPP, P.E. (1999). Activation of the caspase-3 apoptotic cascade in traumatic spinal cord injury. *Nat. Med.* **5**, 943-946.
- STENNICKE, H.R., JURGENSMEIER, J.M., SHIN, H., et al. (1998). Pro-caspase-3 is a major physiologic target of caspase-8. *J. Biol. Chem.* **273**, 27084-27090.
- SUSIN, S.A., DAUGAS, E., RAVAGNAN, L., et al. (2000). Two distinct pathways leading to nuclear apoptosis. *J. Exp. Med.* **192**, 571-580.
- SUSIN, S.A., ZAMZAMI, N., and KROEMER, G. (1998). Mitochondria as regulators of apoptosis: doubt no more. *Biochim. Biophys. Acta* **1366**, 151-165.
- TALANIAN, R.V., QUINLAN, C., TRAUTZ, S., et al. (1997). Substrate specificities of caspase family proteases. *J. Biol. Chem.* **272**, 9677-9682.
- THOMAS, D.A., DU, C., XU, M., et al. (2000). DFF45/ICAD can be directly processed by granzyme B during the induction of apoptosis. *Immunity* **12**, 621-632.
- THORNBERRY, N.A., RANO, T.A., PETERSON, E.P., et al. (1997). A combinatorial approach defines specificities of members of the caspase family and granzyme B. Functional relationships established for key mediators of apoptosis. *J. Biol. Chem.* **272**, 17907-17911.
- VARFOLOMEEV, E.E., SCHUCHMANN, M., LURIA, V., et al. (1998). Targeted disruption of the mouse caspase 8 gene ablates cell death induction by the TNF receptors, Fas/Apo1, and DR3 and is lethal prenatally. *Immunity* **9**, 267-276.
- VELIER, J.J., ELLISON, J.A., KIKLY, K.K., et al. (1999). Caspase-8 and caspase-3 are expressed by different populations of cortical neurons undergoing delayed cell death after focal stroke in the rat. *J. Neurosci.* **19**, 5932-5941.
- WANG, K.K. (2000). Calpain and caspase: can you tell the difference? *Trends Neurosci.* **23**, 20-26.
- WANG, K.K., POSMANTUR, R., NATH, R., et al. (1998b). Simultaneous degradation of alphaII- and betaII-spectrin by caspase 3 (CPP32) in apoptotic cells. *J. Biol. Chem.* **273**, 22490-22497.
- WANG, K.K., POSMANTUR, R., NADIMPALLI, R., et al. (1998a). Caspase-mediated fragmentation of calpain inhibitor protein calpastatin during apoptosis. *Arch. Biochem. Biophys.* **356**, 187-196.
- WOLF, B.B., GOLDSTEIN, J.C., STENNICKE, H.R., et al. (1999). Calpain functions in a caspase-independent manner to promote apoptosis-like events during platelet activation. *Blood* **94**, 1683-1692.
- YAKOVLEV, A.G., KNOBLACH, S.M., FAN, L., et al. (1997). Activation of CPP32-like caspases contributes to neuronal apoptosis and neurological dysfunction after traumatic brain injury. *J. Neurosci.* **17**, 7415-7424.
- YANG, X., STENNICKE, H.R., WANG, B., et al. (1998). Granzyme B mimics apical caspases. Description of a unified pathway for trans-activation of executioner caspase-3 and -7. *J. Biol. Chem.* **273**, 34278-34283.
- ZHAO, X., PIKE, B.R., NEWCOMB, J.K., et al. (1999). Maitotoxin induces calpain but not caspase-3 activation and necrotic cell death in primary septo-hippocampal cultures. *Neurochem. Res.* **24**, 371-382.
- ZOU, H., LI, Y., LIU, X., et al. (1999). An APAF-1/cytochrome c multimeric complex is a functional apoptosome that activates procaspase-9. *J. Biol. Chem.* **274**, 11549-11556.

Address reprint requests to:

Susan M. Knoblach, Ph.D.

Georgetown University Medical Center

EP-16, New Research Building

3970 Reservoir Rd. NW

Washington, DC 20007

E-mail: knoblachs@giccs.georgetown.edu

Neuroprotection and traumatic brain injury: theoretical option or realistic proposition

Alan I. Faden

Purpose of review

Preclinical studies have shown that treatment to limit secondary cell damage can significantly improve outcome after traumatic brain injury. In contrast, neuroprotection trials in human traumatic brain injury have failed to convincingly demonstrate therapeutic benefit. Recent literature has begun to address this discrepancy between preclinical and clinical trials.

Recent findings

Perhaps the most important recent observations relate to the potential role of apoptosis in secondary brain injury. Because apoptosis peaks more than 24 h after injury, concepts about the therapeutic window for traumatic brain injury treatment have changed. Apoptosis and necrosis are in delicate balance and inhibition of one cell death pathway may enhance the other. This raises questions about the ultimate effectiveness of treatment strategies directed toward a single injury mechanism. In contrast to clinical head injury, which reflects a complex multifactorial disorder, animal models are generally designed to address only a single injury component and are performed in genetically inbred animals of a single sex. Moreover, animal studies usually employ pretreatment or early posttreatment administration, examine moderate rather than severe injury, fail to examine brain drug levels or treatment optimization, and do not use an intent-to-treat methodology.

Summary

Recognition of these methodological differences between animal and human studies has led to new trial design proposals. For clinical studies, there should be better stratification of patients, a focus on moderate injury and earlier treatment, and larger sample sizes. Animal experiments should better parallel clinical studies and address therapeutic window and treatment optimization. Recognition of multiple cell death pathways should lead to new treatment strategies – including both combination drug treatment and drugs that affect multiple components of the secondary injury cascade.

Keywords

traumatic brain injury, neuroprotection, apoptosis, necrosis, trial design

Curr Opin Neurol 15:707–712. © 2002 Lippincott Williams & Wilkins.

Department of Neuroscience, Georgetown University Medical Center, Washington DC, USA

Correspondence to Alan I. Faden MD, Department of Neuroscience, Georgetown University Medical Center, 3970 Reservoir Rd, NW, Room EP-12, Washington, DC 20057, USA

Tel: +1 202 687 0492; fax: +1 202 687 0617; e-mail: fadena@georgetown.edu

Current Opinion in Neurology 2002, 15:707–712

DOI: 10.1097/01.wco.0000044767.39452.bf

Abbreviations

Apaf-1	apoptotic protease-activating factor
CNS	central nervous system
TBI	traumatic brain injury

© 2002 Lippincott Williams & Wilkins
1350-7540

Introduction

Experimental studies of traumatic brain injury (TBI) over the past 5 years have helped to elucidate pathophysiological mechanisms related to posttraumatic cell death and associated neurological impairment. Recognition that delayed biochemical reactions contribute substantially to tissue damage after head injury has led to the development of targeted neuroprotective strategies to limit such secondary posttraumatic cell death and improve neurological recovery [1•]. A number of experimental models of central nervous system (CNS) trauma have been developed, both *in vivo* and *in vitro* [2,3], in an attempt to isolate or define critical pathophysiological mechanisms involved. These models have been used in numerous preclinical TBI studies that demonstrated neuroprotective actions for various classes of compounds [4]. Despite this considerable experimental promise, however, clinical studies of neuroprotection in TBI, as for stroke, have been disappointing [1•,5•,6•]. There are important methodological differences between the experimental and clinical studies that have undoubtedly contributed to the many failed clinical trials [1•,7•]. In addition, a number of potential flaws in the design of the clinical studies have been recognized [6•–8•]. Together, recent experimental and clinical studies have helped to delineate key methodological pitfalls that may have contributed to these unsuccessful clinical trials.

Animal traumatic brain injury models: how relevant are they?

TBI in humans is a highly heterogeneous disorder that includes variable combinations of contusion, hematoma, axonal injury, hypoxia and ischemia [1•,5•,6•]. In contrast, experimental trauma models have been designed for simplicity and tend, in most cases, to reflect only single components of this complex process, such as contusion or axonal injury. Moreover, whereas studies prior to 1995 preferentially used higher species, such as sheep, cat, or primate, most recent studies have utilized rodents [2,3]. Using such models, investigators have

demonstrated that trauma induces a cascade of secondary biochemical changes over a period of minutes to days after the insult; these include alterations of ionic homeostasis, induction of inflammatory and immune responses, release of excitatory amino acids and neurotransmitters, and the generation of free radicals, among others [4].

By targeting individual components of this cascade, animal studies have shown clear improvement in outcome after TBI, using behavioral and/or histological endpoints [4]. It should be noted, however, that in most cases, such studies have been performed using pretreatment or very early treatment times, and have utilized tightly controlled injury models in highly inbred strains of a single sex. Moreover, several hours after trauma there appear to be complex multifactorial metabolic and biochemical changes. Adding to this complexity, recent studies have demonstrated that both necrotic and apoptotic cell death occur after injury [9–11], and that strategies that inhibit one pathway of cell death may enhance cell death through the other [11,12]. Importantly, recent studies have also suggested that cell death mechanisms may differ as a function of developmental age, and this may have important implications for potential neuroprotective treatment of brain injury in the prenatal or early postnatal period, which may differ from that in adolescents or adults [11]. Thus, in moving from relatively simplistic early treatment studies in animals to more delayed, heterogeneous injury in humans, it may be critical to simultaneously target multiple components of the secondary injury cascade, including both necrotic and apoptotic pathways.

Mechanism studies in animals and humans: implications for treatment

A variety of approaches have been utilized to address potential mechanisms of secondary injury in experimental animal models. These have included pharmacological treatment to modify specific factors, receptors, or transmitter systems, or use of genetically manipulated animals (including knockout and transgenic models). Most recent studies have confirmed that secondary injury causes changes involving genes or gene products for neurotransmitters, neurotransmitter receptors, hormones, and inflammatory/immune responses, among others [13•,14,15,16•–18•]. Whereas such studies may suggest potential avenues for therapeutic treatment in humans [19–22], they have substantial limitations in providing substantive experimental support for potential clinical trials. In many of these preclinical neuroprotection studies, there is a serious question about specificity of the treatment effects. For example, most proclaimed 'specific' modulators of a particular system are apt to have additional, and sometimes unexpected, effects on other receptors or factors. Certain experimental strategies

can be employed to address this concern, such as the use of structurally different modulators that share similar modulatory functions on a particular pathway, or parallel use of knockouts and pharmacological antagonists of a particular protein. However, such complementary studies are not commonly performed [23,24]. Another potential problem is the use of outcome measures in animals that may have limited relevance to effects in humans, such as acute measurements of cerebral edema or early functional changes, without examining chronic neurological function or histopathology.

Pharmacological studies in animals rarely provide the type of detailed evaluation to justify or properly design clinical trials. Extensive dose–response studies in animals, in combination with both chronic behavioral outcome and histopathology, are rarely performed. Moreover, animal studies rarely examine the brain levels of drugs administered, attempt to optimize drug treatment, or examine the therapeutic window. The latter issue may be particularly important. For example, use of glutamate receptor antagonists in animals has consistently been shown to improve therapeutic outcome across various injury models [17•]. Such treatment, however, is usually effective only if administered within the first several hours of injury, consistent with the early pattern of posttraumatic glutamate release. In contrast, clinical TBI studies rarely can enter patients into a trial before 3–4 h and usually not before 6 h after trauma. This has been the case with previous negative trials using glutamate receptor antagonists [5•,6•,25]. Finally, neuroprotection studies in animals rarely examine profiles across different experimental models or species. Such studies, if performed in conjunction with detailed evaluation of therapeutic window and drug optimization experiments, would probably enhance the likelihood of identifying neuroprotective strategies that may work in humans.

One of the more important observations made during the past several years, both experimentally and in humans, relates to the activation of signal transduction pathways associated with neuronal apoptosis after TBI. Caspase-3 is a cysteine protease whose activation can cause neuronal apoptotic cell death (for review, see [26]). Caspase activation, in association with morphological evidence of apoptosis, has been demonstrated both in animal and human models of TBI [26,27•]. Recent studies have extended these observations by demonstrating that both Fas receptor signaling [28•,29•] and apoptotic protease-activating factor (Apaf-1) signaling [30•] are induced by trauma. Fas/Fas ligand binding is a key component of the so-called 'extrinsic' caspase pathway that involves caspase-8 as an upstream regulator [26]. Qiu *et al.* [28•] demonstrated that there is upregulation of the Fas receptor death-inducing signal-

ing complex after TBI in both mice and in humans, and Lenzlinger *et al.* [29•] demonstrated prolonged release of soluble Fas in cerebrospinal fluid after TBI in humans. Apaf-1 is the homolog to the *Ced-4* death-promoting gene in *Caenorhabditis elegans* and has been linked to caspase-9 and the 'intrinsic' mitochondrial-related caspase pathway [26]. Yakovlev *et al.* [30•] found that Apaf-1 expression is substantially inhibited in adult as compared with young animals, and is upregulated strongly after TBI in the adult animal. Other recent experimental studies have identified changes in other signal transduction pathways that have been implicated in neuronal apoptosis, including mitogen-activated protein kinases [31] and nuclear factor κ B [32]. Because apoptotic cell death occurs at far later time points than does necrosis [9,10], it raises the possibility that pharmacological inhibition of caspase-3, or of upstream regulators of this effector caspase, may offer more effective treatments than traditional therapies aimed at modulating necrosis. Indeed, Fink *et al.* [33] have shown that treatment with a caspase-3 inhibitor can be delayed up to 9 h after middle cerebral artery occlusion in mice, and yet still produce a striking reduction in lesion volumes after injury. We have recently replicated such studies following fluid-percussion-induced TBI in rats [34].

Sex differences in traumatic brain injury: implications for treatment

It has long been known that sex differences may significantly affect outcomes after CNS injury. Several groups have recently extended such observations. Bramlett and Dietrich [35•] compared lesion volumes following TBI across intact female rats, ovariectomized females or males. Intact female rats showed significantly lower lesion volumes than did ovariectomized females or males, the latter two groups being insignificantly different from one another. Igarashi *et al.* [36] demonstrated gender differences with regard to the regional vulnerability after TBI in mice that over express human copper, zinc superoxide dismutase. Cortical lesion volumes were significantly reduced in transgenic males as compared with non-transgenic males; such differences were not observed between the transgenic and non-transgenic female animals [36]. Because most experimental brain injury studies examine only a single sex, these reports raise questions about the general applicability of observations from such restricted animal model systems to humans.

Cellular transplantation/neurotrophic factors and neuroprotection in traumatic brain injury

Experimental TBI studies have investigated the effectiveness of delayed treatment approaches, using cellular transplantation to express neurotrophic factors or growth factor infusions [37,38•]. Kim *et al.* [37] reported

neuroprotective effects, following infusions of glial cell line-derived neurotrophic factor, on hippocampal neurons after TBI in rats. Philips *et al.* [38•] showed neuroprotection and behavioral efficacy of hippocampal progenitor cell transplants transfected with growth factor after rat TBI. Use of stem cells in brain plasticity and repair after CNS injury is an active research area, with potential therapeutic implications for improving recovery after CNS insults, including TBI [39•]. Mahmood *et al.* [40•] have recently examined the use of delayed intravenous treatment (24 h) with bone marrow stromal cells in animals subjected to TBI. The transplanted cells were shown to be preferentially engrafted into the parenchyma of injured brain, and treatment was associated with significantly improved motor function at 7 and 14 days. This study raises the possibility that injections of neural precursor cells may be able to modify brain function after injury with a considerably delayed therapeutic window.

Neuroprotection and traumatic brain injury: clinical studies

During the last five decades, there have been many neuroprotective treatment trials in humans. None of these trials to date has shown convincing clinical efficacy in the overall population being studied [1,5•]. Two recent reports have reviewed the neuroprotective treatment after TBI in humans and provide suggestions for potentially improving clinical design for such trials in the future [5•,6•]. Some of the issues that may explain the discrepancy between animal and human studies have already been addressed, but these reports provide additional possible explanations for such differences.

Heterogeneity of studied populations

Most clinical studies have focused on patients with severe brain injuries. Such patients are highly heterogeneous and include different degrees of contusion, hematoma, brain edema, axonal injury, hypoxia and ischemia [5•,6•]. A number of investigators have called for better stratification in order to define more suitable subsets of patients for a particular clinical study. For example, two major randomized clinical trials of treatment with the calcium channel antagonist nimodipine in human head injury were negative, yet subgroup analysis suggested a potentially beneficial effect in a subset of patients showing traumatic subarachnoid hemorrhage [41,42]. Subsequently, a small randomized study examined nimodipine treatment only in patients showing traumatic subarachnoid hemorrhage and reported a significant treatment effect [43]. Although the latter will need to be repeated with a larger sample size, it suggests that better delineation of study populations may be more likely to demonstrate a potential neuroprotective effect.

The fact that severely injured patients have been preferentially studied is problematic for other reasons, including the fact that such injury may cause widespread early necrosis that is not amenable to treatment at later treatment times. This has been long recognized in animal models, which preferentially utilize a moderate injury severity. In contrast, inclusion of patients with relatively mild injury may lead to a ceiling effect in which it may be difficult to show significant therapeutic effects unless very large populations are examined [44]. These issues have been increasingly recognized by clinical investigators who have recommended that future clinical trials be preferentially directed at those with moderate brain injury [1•,5•].

Methodological differences between clinical and experimental studies

As indicated above, animal models are designed to emphasize a particular component of clinical brain injury, such as concussion, contusion, or diffuse axonal injury. In order to make such models consistent and limit inter-animal variability, these studies have utilized genetically identical animals of a single sex, well-controlled injury levels, and generally excluded animals with associated ischemia or hypoxia. Because such animal models only parallel the human condition in limited ways, it may be necessary to develop more complex animal model systems that more closely mimic the human condition.

Human neuroprotection studies generally employ an intent to treat paradigm; that is, patients are included in the analysis even if the wrong dose has been administered or administered at the wrong treatment time. Alternatively, most animal studies exclude animals that fail to meet prescribed experimental conditions, such as demonstration of the appropriate level of impact energy, or the absence of hematoma, or posttraumatic seizures.

Endpoints for treatment in animals and humans also may differ considerably. Clinical studies often use such endpoints as combined death/disability, or such surrogate markers as changes in intracranial pressure. In contrast, most animal studies have utilized cognitive or motor assessment or measurements of lesion volumes.

Relatively few animal studies have performed extensive therapeutic window studies and rarely have they demonstrated neuroprotective effects following delayed treatment periods that correlate to likely treatment times in humans. Indeed, most animal studies generally employ either a pretreatment or very early posttreatment paradigm (i.e. 1–2 h). In contrast, it is difficult to enter TBI patients into clinical trials before 6 h, in part because of the informed consent issues. It is also extremely rare in animal studies for investigators to examine the pharmacokinetic or pharmacodynamic

profiles of drugs being studied, and they virtually never measure brain levels of drugs in relation to therapeutic actions.

Laser-targeted versus multipotential treatment strategies

As described above, it has been increasingly recognized that both necrotic and apoptotic cell death may contribute to neurological deficits after experimental or clinical brain injury [11,27•–30•]. It has also been increasingly demonstrated that modulation of one cell death pathway may lead to enhanced cell death through the other pathway [11,12]. This raises questions about the likelihood of demonstrating therapeutic effects by employing highly targeted ('laser-targeted') strategies that serve to modulate a single receptor or transmitter pathway. Rather, what may be required are combination treatment strategies such as those being employed in the treatment of cancer and infectious diseases [6•,45]. An alternative may be the use of multipotential treatments, that is, the use of single agents that have actions on multiple secondary injury factors [1•]. Examples of the latter group of drugs include such agents as the cannabinoid HU-211 [46] and thyrotropin-releasing hormone or related peptides [47].

Design issues and future clinical trials

Recent neuroprotection treatment failures in humans have included hypothermia, as well as pharmacotherapies [48•,49•]. A number of authors have recently commented on neuroprotection failures in stroke or TBI and have proposed modification in study design [5•,6•–8•]. It has been suggested that entry criteria for clinical trials be tightened. This has included emphasis on including only patients treated at more limited treatment times, perhaps less than 4 h after injury, in order to optimize likely effects on secondary injury [5•,6•,7•]. Although this may considerably limit the ability to include patients in clinical trials, it may substantially enhance the likelihood of treatment success, as has been found for tissue plasminogen activating factor in the treatment of acute stroke [7•]. The therapeutic dose in humans is often chosen to be the maximum tolerated dose without recognizing that many drugs show an inverted U-shaped dose-response curve [8•]. It has been suggested that new trials examine potentially smaller benefits by incorporating much larger patient populations [44]. In addition, newer methods need to be introduced to improve the balance between treatment and control populations [7•,8•]. In recent clinical trials, there has been increased consideration for the use of surrogate markers, such as changes in imaging outcome to monitor neuroprotection [8•]. Taken together, such design changes would likely enhance the probability of identifying a potential neuroprotective effect in TBI.

Conclusion

Despite promising preclinical studies of neuroprotection in TBI, clinical trials have been disappointing. There are important methodological differences between the animal and human studies that may help to explain this discrepancy.

Most clinical studies have preferentially included patients with severe injuries and treatment is rarely initiated within 4 h of trauma. Under such conditions, considerable necrotic cell death has already occurred before treatment has begun. Moreover, such patients are highly heterogeneous with regard to underlying pathobiology – including varying degrees of hypoxia, ischemia, hemorrhage, and axonal injury. In contrast, most preclinical studies involve highly controlled injury models that primarily reflect only a single component of clinical trauma, utilize very early treatment times, and examine moderate rather than severe injuries. Importantly, most experimental neuroprotection strategies are intended to modify only one secondary injury factor, despite the fact that TBI initiates a complex multifactorial biochemical process that contributes to tissue damage. In addition, both apoptotic and necrotic cell death are precipitated by trauma, and experimental work indicates that strategies intended to block one pathway of cell death may amplify the other.

Further trials should aim to better match preclinical and clinical design, with particular emphasis on the therapeutic window, drug pharmacokinetics/pharmacodynamics, and underlying pathophysiology. Better patient stratification, focus on moderate injury, and larger sample sizes would be beneficial. Finally, more attention must be given to multidrug strategies or to use of multipotential drugs, that is drugs that may modify multiple components of secondary injury.

Acknowledgements

This work was supported by the National Institutes of Health Grants R01 NS 36537-04 (Faden) and R01 NS 41119-02 (Faden).

References and recommended reading

Papers of particular interest, published within the annual period of review, have been highlighted as:

- of special interest
- of outstanding interest

- 1 Faden AI. Neuroprotection and traumatic brain injury: the search continues. *Arch Neurol* 2001; 58:1553–1555.
Reviews methodological differences between preclinical and clinical studies of TBI and discusses reasons for failed clinical trials.
- 2 Povlishock JT. An overview of brain injury models. In: Narayan RK, Wilberger JE, Povlishock JT, editors. *Neurotrauma*. New York: McGraw-Hill; 1996. pp. 1325–1336.
- 3 Morrison B III, Saatman KE, Meaney DF, McIntosh TK. In vitro central nervous system models of mechanically induced trauma: a review. *J Neurotrauma* 1998; 15:911–928.

- 4 Faden AI. Pharmacological treatment approaches for brain and spinal cord trauma. In: Narayan RK, Wilberger JE, Povlishock JT, editors. *Neurotrauma*. New York: McGraw-Hill; 1996. pp. 1479–1490.
- 5 Maas AI. Neuroprotective agents in traumatic brain injury. *Expert Opin Investig Drugs* 2001; 10:753–767.
This review critically assesses recent phase III trials in TBI and argues that such failures do not establish that the drugs studied were ineffective, but rather may reflect problems in trial design or analysis. Better targeting of the most appropriate treatment population is emphasized.
- 6 Clausen T, Bullock R. Medical treatment and neuroprotection in traumatic brain injury. *Curr Pharm Des* 2001; 7:1517–1532.
Reviews recent clinical and preclinical studies with emphasis on glutamate receptor antagonists, calcium channel blockers, free radical scavengers, and cyclosporin A. Emphasizes the potential benefits in combining neuroprotection strategies.
- 7 Grotta J. Neuroprotection is unlikely to be effective in humans using current trial designs. *Stroke* 2002; 33:306–307.
Critiques current trial design for evaluation of neuroprotective agents in stroke and provides suggestions for improving study design.
- 8 Lees KR. Neuroprotection is unlikely to be effective in humans using current trial designs: an opposing view. *Stroke* 2002; 33:308–309.
Reviews flaws in the trial design of recent neuroprotection studies of stroke and suggests changes to improve future studies.
- 9 Rink A, Fung KM, Trojanowski JQ, et al. Evidence of apoptotic cell death after experimental traumatic brain injury in the rat. *Am J Pathol* 1995; 147:1575–1583.
- 10 Yakovlev AG, Knoblach SM, Fan L, et al. Activation of CPP32-like caspases contributes to neuronal apoptosis and neurological dysfunction after traumatic brain injury. *J Neurosci* 1997; 17:7415–7424.
- 11 Pohl D, Bittigau P, Ishimaru MJ, et al. N-Methyl-D-aspartate antagonists and apoptotic cell death triggered by head trauma in developing rat brain. *Proc Natl Acad Sci U S A* 1999; 96:2508–2513.
- 12 Glazner GW, Chan SL, Lu C, Mattson MP. Caspase-mediated degradation of AMPA receptor subunits: a mechanism for preventing excitotoxic necrosis and ensuring apoptosis. *J Neurosci* 2000; 20:3641–3649.
- 13 Frantseva MV, Kokorotseva L, Naus CG, et al. Specific gap junctions enhance the neuronal vulnerability to brain traumatic injury. *J Neurosci* 2002; 22:644–653.
Modulation of gap junctional channels, formed by connexins, was studied in organotypic hippocampal slices subjected to trauma. Cultures from connexin knockout animals or with antisense treatment showed less cell death.
- 14 Lynch JR, Pineda JA, Morgan D, et al. Apolipoprotein E affects the central nervous system response to injury and the development of cerebral edema. *Ann Neurol* 2002; 51:113–117.
- 15 Kumar A, Zou L, Yuan X, et al. N-methyl-D-aspartate receptors: transient loss of NR1/NR2A/NR2B subunits after traumatic brain injury in a rodent model. *J Neurosci Res* 2002; 67:781–786.
- 16 Matzilevich DA, Rall JM, Moore AN, et al. High-density microarray analysis of hippocampal gene expression following experimental brain injury. *J Neurosci Res* 2002; 67:646–663.
This is the first study to report diverse changes in messenger RNA expression after experimental TBI using high-density microarray. Conclusions were limited because of the small number of time points examined and the fact that few of the changes were validated by other established procedures.
- 17 Temple M, O'Leary D, Faden A. The role of glutamate receptors in the pathophysiology of traumatic brain injury. In: Miller L, Hayes R, Newcomb J, editors. *Head trauma*. New York: John Wiley & Sons; 2001. pp. 87–113.
This is a detailed review of the role of both ionotropic and metabotropic glutamate receptors in modulating secondary tissue damage after TBI.
- 18 Golarai G, Greenwood AC, Feeney DM, Connor JA. Physiological and structural evidence for hippocampal involvement in persistent seizure susceptibility after traumatic brain injury. *J Neurosci* 2001; 21:8523–8537.
The authors utilize an experimental TBI model to show how injury may lead to structural tissue changes that may underlie posttraumatic epilepsy.
- 19 Zwienerberg M, Gong QZ, Berman RF, et al. The effect of groups II and III metabotropic glutamate receptor activation on neuronal injury in a rodent model of traumatic brain injury. *Neurosurgery* 2001; 48:1119–1126; discussion 1126–1127.
- 20 Cerami A, Brines M, Ghezzi P, et al. Neuroprotective properties of epoetin alfa. *Nephrol Dial Transplant* 2002; 17:8–12.
- 21 Kline AE, Yu J, Horvath E, et al. The selective 5-HT(1A) receptor agonist repinotan HCl attenuates histopathology and spatial learning deficits following traumatic brain injury in rats. *Neuroscience* 2001; 106:547–555.

- 22 Suehiro E, Singleton RH, Stone JR, Povlishock JT. The immunophilin ligand FK506 attenuates the axonal damage associated with rapid rewarming following posttraumatic hypothermia. *Exp Neurol* 2001; 172:199-210.
- 23 Mukhin A, Fan L, Faden AI. Activation of metabotropic glutamate receptor subtype mGluR1 contributes to post-traumatic neuronal injury. *J Neurosci* 1996; 16:6012-6020.
- 24 Sun FY, Faden AI. Pretreatment with antisense oligodeoxynucleotides directed against the NMDA-R1 receptor enhances survival and behavioral recovery following traumatic brain injury in rats. *Brain Res* 1995; 693:163-168.
- 25 Morris GF, Bullock R, Marshall SB, et al. Failure of the competitive N-methyl-D-aspartate antagonist Selfotel (CGS 19755) in the treatment of severe head injury: results of two phase III clinical trials. The Selfotel Investigators. *J Neurosurg* 1999; 91:737-743.
- 26 Eldadah BA, Faden AI. Caspase pathways, neuronal apoptosis, and CNS injury. *J Neurotrauma* 2000; 17:811-829.
- 27 Harter L, Keel M, Hentze H, et al. Caspase-3 activity is present in cerebrospinal fluid from patients with traumatic brain injury. *J Neuroimmunol* 2001; 121:76-78.
Caspase-3 activity was found in more than 25% of cerebrospinal fluid samples from 27 patients with severe TBI. Highest levels were observed between 2 and 5 days after injury.
- 28 Qiu J, Whalen MJ, Lowenstein P, et al. Upregulation of the Fas receptor death-inducing signaling complex after traumatic brain injury in mice and humans. *J Neurosci* 2002; 22:3504-3511.
Fas-Fas ligand binding was upregulated after controlled cortical impact TBI in mice and after TBI in humans. This was associated with the activation and cleavage of pro-caspase-8.
- 29 Lenzinger PM, Marx A, Trentz O, et al. Prolonged intrathecal release of soluble Fas following severe traumatic brain injury in humans. *J Neuroimmunol* 2002; 122:167-174.
Identified prolonged release of soluble Fas in the cerebrospinal fluid following severe TBI in humans, for up to 15 days following injury.
- 30 Yakovlev AG, Ota K, Wang G, et al. Differential expression of apoptotic protease-activating factor-1 and caspase-3 genes and susceptibility to apoptosis during brain development and after traumatic brain injury. *J Neurosci* 2001; 21:7439-7446.
Showed suppression of caspase-3 and Apaf-1 in adult versus young rats, but these were upregulated following TBI.
- 31 Mori T, Wang X, Jung JC, et al. Mitogen-activated protein kinase inhibition in traumatic brain injury: in vitro and in vivo effects. *J Cereb Blood Flow Metab* 2002; 22:444-452.
- 32 Sanz O, Acarin L, Gonzalez B, Castellano B. NF-kappaB and IkappaBalpha expression following traumatic brain injury to the immature rat brain. *J Neurosci Res* 2002; 67:772-780.
- 33 Fink K, Zhu J, Namura S, et al. Prolonged therapeutic window for ischemic brain damage caused by delayed caspase activation. *J Cereb Blood Flow Metab* 1998; 18:1071-1076.
- 34 Knoblach S, Fan L, Huang X, et al. Activation of caspase 3 and 9 after traumatic brain injury in the rat: treatment with a pan-caspase inhibitor improves outcome. In Society for Neuroscience 2000; 26:2300.
- 35 Bramlett HM, Dietrich WD. Neuropathological protection after traumatic brain injury in intact female rats versus males or ovariectomized females. *J Neurotrauma* 2001; 18:891-900.
Intact female rats showed smaller lesion volumes following TBI as compared with ovariectomized females or male animals.
- 36 Igarashi T, Huang TT, Noble LJ. Regional vulnerability after traumatic brain injury: gender differences in mice that overexpress human copper, zinc superoxide dismutase. *Exp Neurol* 2001; 172:332-341.
- 37 Kim BT, Rao VL, Sailor KA, et al. Protective effects of glial cell line-derived neurotrophic factor on hippocampal neurons after traumatic brain injury in rats. *J Neurosurg* 2001; 95:674-679.
- 38 Philips MF, Mattiasson G, Wieloch T, et al. Neuroprotective and behavioral efficacy of nerve growth factor-transfected hippocampal progenitor cell transplants after experimental traumatic brain injury. *J Neurosurg* 2001; 94:765-774.
Cellular transplants of progenitor cells transfected with nerve growth factor were transplanted stereotactically into three sites adjacent to the trauma site 24 h after TBI in rats. Treated animals showed improved motor and cognitive recovery and reduced CA3 cell loss.
- 39 Peterson DA. Stem cells in brain plasticity and repair. *Curr Opin Pharmacol* 2002; 2:34-42.
Reviews adult neurogenesis and the potential role of stem cells in plasticity and repair after injury.
- 40 Mahmood A, Lu D, Wang L, et al. Treatment of traumatic brain injury in female rats with intravenous administration of bone marrow stromal cells. *Neurosurgery* 2001; 49:1196-1203; discussion 1203-1204.
Bone marrow stromal cells were injected intravenously at 24 h in female rats subjected to TBI. Treatment improved functional recovery at 15 days as compared with controls.
- 41 Teasdale G, Bailey I, Bell A, et al. The effect of nimodipine on outcome after head injury: a prospective randomised control trial. The British/Finnish Co-operative Head Injury Trial Group. *Acta Neurochir Suppl* 1990; 51:315-316.
- 42 The European Study Group on Nimodipine in Severe Head Injury. A multicenter trial of the efficacy of nimodipine on outcome after severe head injury. *J Neurosurg* 1994; 80:797-804.
- 43 Harders A, Kakarieka A, Braakman R. Traumatic subarachnoid hemorrhage and its treatment with nimodipine. German ISAH Study Group. *J Neurosurg* 1996; 85:82-89.
- 44 Dickinson K, Bunn F, Wentz R, et al. Size and quality of randomised controlled trials in head injury: review of published studies. *BMJ* 2000; 320:1308-1311.
- 45 Allen JW, Knoblach SM, Faden AI. Combined mechanical trauma and metabolic impairment in vitro induces NMDA receptor-dependent neuronal cell death and caspase-3-dependent apoptosis. *FASEB J* 1999; 13:1875-1882.
- 46 Eshhar N, Striem S, Kohen R, et al. Neuroprotective and antioxidant activities of HU-211, a novel NMDA receptor antagonist. *Eur J Pharmacol* 1995; 283:19-29.
- 47 Faden AI, Fox GB, Fan L, et al. Novel TRH analog improves motor and cognitive recovery after traumatic brain injury in rodents. *Am J Physiol Regul Integr Comp Physiol* 1999; 277:R1196-R1204.
- 48 Gupta AK, Al-Rawi PG, Hutchinson PJ, Kirkpatrick PJ. Effect of hypothermia on brain tissue oxygenation in patients with severe head injury. *Br J Anaesth* 2002; 88:188-192.
Shows that reducing brain temperature below 35°C may impair brain tissue oxygenation in patients with severe head injury.
- 49 Clifton GL, Miller ER, Choi SC, et al. Lack of effect of induction of hypothermia after acute brain injury. *N Engl J Med* 2001; 344:556-563.
Randomized trial of hypothermia in 392 patients with traumatic coma after closed head injury. There were no differences in mortality or poor outcome between the groups. Although fewer patients in the hypothermia group had high intracranial pressure, they had longer hospital stays and more complications than controls.

Neuroprotective and Nootropic Actions of a Novel Cyclized Dipeptide After Controlled Cortical Impact Injury in Mice

*Alan I. Faden, *Gerard B. Fox, *Xiao Di, *Susan M. Knoblach, *Ibolja Cernak, *Paul Mullins, *Maria Nikolaeva, and †Alan P. Kozikowski

Departments of *Neuroscience and †Neurology, Georgetown University Medical Center, Washington, DC, U.S.A.

Summary: 1-ARA-35b (35b) is a cyclized dipeptide that shows considerable neuroprotective activity *in vitro* and improves neurologic recovery after fluid percussion-induced traumatic brain injury in rats. The authors evaluated the effects of treatment with 35b in mice subjected to controlled cortical impact brain injury. Animals treated with intravenous 35b after traumatic injury showed significantly enhanced recovery of beam walking and place learning functions compared with vehicle-treated controls, in addition to reduced lesion volumes. Beneficial effects were dose related and showed an inverted U-shaped dose-response curve between 0.1 and 10 mg/kg. Pro-

tective actions were found when the drug was administered initially at 30 minutes or 1, 4, or 8 hours, but not at 24 hours, after trauma. In separate experiments, rats treated with 35b on days 7 through 10 after injury showed remarkably improved place learning in comparison with injured controls. These studies confirm and extend the neuroprotective effects of this diketopiperazine in traumatic brain injury. In addition, they show that 35b has a relatively wide therapeutic window and improves cognitive function after both acute and chronic injury. **Key Words:** TRH analogs—Traumatic brain injury—Neuroprotection—Behavior—Diketopiperazine.

The concept of secondary injury after CNS trauma has been firmly established on the basis of experimental studies (Panter and Faden, 1992). Traumatic CNS injury initiates a complex series of metabolic and other biochemical changes that begin within seconds of injury and may continue for days to weeks after the insult (Faden, 1996; McIntosh, 1994). Collectively, these changes ultimately cause death of neuronal cells adjoining the area of immediate physical insult.

Based on this concept of secondary biochemical injury, many potential treatments have been proposed and tested experimentally (Faden, 1996; McIntosh et al., 1998). Most of these strategies have been directed toward inhibiting a single component or factor in the secondary injury cascade. Although there is considerable experimental support for the use of these kinds of targeted strategies to reduce histologic damage and improve neurologic outcome after CNS trauma in experimental

animal models, beneficial effects in humans have proved quite limited. For example, methylprednisone and naloxone have shown comparable and significant protective effects when administered within the first 8 hours after spinal cord trauma in humans (Bracken and Holford, 1993). These beneficial effects, however, are relatively modest and their therapeutic window is relatively narrow. Treatment of human brain trauma has proved less effective in several recent clinical trials, despite promising experimental results (Faden, 2002; Maas, 2001). Given the fact that tissue injury after neurotrauma is thought to be highly multifactorial, it may not be surprising that strategies aimed at only a single injury component have shown limited effectiveness.

Optimal treatment for traumatic CNS injury may therefore require either single drugs that modulate multiple factors within the secondary injury cascade or the use of combination drug-treatment strategies (Faden AI, 2001). Thyrotropin-releasing hormone (TRH), a tripeptide named for its hypophysiotropic function, has considerable neuroprotective properties and has been found to modulate a number of proposed secondary injury factors (Faden, 1996; Faden et al., 1999b). However, TRH and traditional TRH analogs have several physiologic actions—autonomic, analeptic, and endocrine (Yar-brough, 1979)—that may limit their clinical utility. We

Received April 15, 2002; final version received October 21, 2002; accepted October 22, 2002.

This work was supported by Department of Defense Cooperative Agreement DAMD17-99-2-9007 and National Institutes of Health grant R01 NS41119.

Address correspondence and reprint requests to Alan I. Faden, M.D., Department of Neuroscience, Georgetown University Medical Center, 3970 Reservoir Road NW, Room EP-12, Washington, DC 20057, U.S.A.; e-mail: fadena@georgetown.edu

have developed a series of tripeptide derivatives of TRH (Faden et al., 1999a) and related cyclic dipeptides, which are devoid of autonomic, analeptic, and endocrine actions, yet have striking neuroprotective actions. Among these, 35b, a cyclohexyl diketopiperazine, has shown good neuroprotective activity in *in vivo* and *in vitro* rat models (Faden et al., 2003). The present studies were designed to examine the effects of 35b in a different head injury model (controlled cortical impact [CCI]) in a different species (mouse). Dose-response and therapeutic-window studies were examined, with both behavioral and lesion volume outcomes. In addition, the potential cognitive-enhancing effect of the compound was examined relatively late after injury (7 to 10 days). 35b was found to have striking neuroprotective effect, with a relatively large therapeutic window of at least 8 hours, as well as nootropic actions in chronic injured animals.

MATERIALS AND METHODS

Animals

Male C57Bl/6 mice (20 to 25 g) were obtained from Taconic Farms (Germantown, NY, U.S.A.) and housed in an area directly adjoining surgical and behavioral rooms for at least 1 week before any procedures. A constant temperature ($22^{\circ}\text{C} \pm 2^{\circ}\text{C}$) and 12-hour light/dark-cycle environment were maintained, and all behavioral testing was performed during the light cycle (6 A.M. to 6 P.M.). All mice had free access to food and water.

Controlled cortical impact device

Our injury device was designed and built at the Georgetown Institute for Cognitive and Computational Sciences and consists of a microprocessor-controlled pneumatic impactor with a 3.5-mm-diameter tip (Fox et al., 1998). The impactor is vertically mounted on a mill table (Sherline, Vista, CA, U.S.A.) and allows for precise adjustment in the vertical plane above the mouse head, which is secured in a stereotaxic apparatus (David Kopf Instruments, Tujunga, CA, U.S.A.). The core rod of a linear voltage differential transducer (Serotec, Raleigh, NC, U.S.A.) is attached to the lower end of the impactor to allow measurement of velocities between 3.0 and 9.0 m/s. Velocity of the impactor is controlled by fine tuning both positive and negative (back) air pressures. An oscilloscope (Tektronix, Beaverton, OR, U.S.A.) records the time-displacement curve produced by the downward force on the linear voltage differential transducer, allowing precise measurement of the impactor velocity.

Surgery

Surgical anesthesia was induced and maintained with 4% and 2% isoflurane, respectively, using a flow rate of 1.0 to 1.5 L/min oxygen. Depth of anesthesia was assessed by monitoring respiration rate and palpebral and pedal-withdrawal reflexes. The animal was then placed on a heated pad and core body temperature was monitored and maintained at $38^{\circ}\text{C} \pm 0.2^{\circ}\text{C}$. The head was mounted in a stereotaxic frame and the surgical site clipped and cleansed before surgery. A 10-mm midline incision was made over the skull, the skin and fascia were reflected, and a craniotomy was performed (4 mm) on the central aspect of the left parietal bone (Roboz, Gaithersburg, MD, U.S.A.). Great care was taken during removal of the pa-

rietal bone to avoid injury to the underlying dura mater, which was continuously bathed in sterile normal saline warmed to 37.5°C . The impounder tip of the pneumatic injury device was sterilized, extended its full stroke distance (44 mm), positioned to the surface of the exposed dura, and reset to impact the cortical surface at a moderate level (6.0-m/s velocity, 1-mm tissue deformation). After injury, the incision was closed with interrupted 6-0 silk sutures, anesthesia was discontinued, and the mouse was placed in a heated cage to maintain normothermia during a 45-minute recovery period. All animals were monitored carefully for at least 4 hours after surgery and then daily. To minimize variation between animals due to anesthesia during acute neurologic testing, 20 minutes was allowed for surgery and 5 minutes for suturing for each animal.

Acute and chronic neurologic evaluation

After cessation of anesthesia, each mouse was placed into a heated cage in the supine position. Acute neurologic recovery was assessed in all mice by recording the time to recovery of hind paw flexion after application of pressure, an indicator of simple somatomotor function. Similarly, latency to recovery of the righting reflex, an indicator of somatosensory function, was recorded for each animal.

Chronic neurologic recovery was evaluated for all animals using a beam-walking task, a method which is particularly good at discriminating fine motor coordination differences between injured and sham-operated animals (Fox et al., 1998). The device consists of a narrow wooden beam 6-mm wide and 120-mm long suspended 300 mm above a 60-mm-thick foam rubber pad. The mouse was placed on one end of the beam and the number of foot faults for the right hind limb recorded during 50 steps counted in either direction on the beam. A basal level of competence at this task was established before surgery with an acceptance level of <10 faults per 50 steps.

Spatial learning and memory function

A Morris water maze paradigm was used to access spatial learning and working memory by training mice to locate a hidden submerged platform using extramaze visual information, as previously detailed (Fox et al., 1998). The apparatus consists of a large, white, circular pool (900-mm diameter, 500-mm high, water temperature of $24^{\circ}\text{C} \pm 1^{\circ}\text{C}$) with a 76-mm-diameter plexiglas platform painted white and submerged 15 mm below the surface of the water (225-mm high), which was rendered opaque with the addition of white nontoxic paint. During training, the platform was hidden in one quadrant of the maze 14 inches from the side wall. The mouse was gently placed into the water facing the wall at one of four randomly chosen quadrants separated by 90 degrees. The time required (latency) to find the hidden platform with a 90-second limit was recorded by a blinded observer. Mice failing to find the platform within 90 seconds were assisted to the platform. Animals were allowed to remain on the platform for 15 seconds on the first trial and 10 seconds on all subsequent trials. There was an intertrial interval of 30 minutes, during which time the mice were towel-dried and placed under a heat lamp. A total of 16 training trials were conducted in blocks of four per day on days 7 to 10 (studies 1 and 4) or 14 to 17 (study 3) after surgery. To control for visual discriminative ability, animals were subjected to an additional four visuomotor trials 2 hours after the last training trial (trial 16). For visuomotor trials, a clearly visible black platform, raised 5 mm above the water surface, was placed at a different location than that for the submerged platform. Time required to find the visible platform was recorded.

Drug administration

Conscious mice were placed in a mouse restrainer and injected via the lateral tail vein with normal saline or 35b at various doses and times after CCI injury. The investigators were blinded to drug treatment, both at the time of surgery and for neurologic and behavioral scoring. Four separate studies were performed: (1) administration of a single intravenous bolus (1.0 mg/kg) of 35b thirty minutes after trauma; (2) dose-response evaluation of 35b, administered as a single intravenous bolus injection (0.1, 1, or 10 mg/kg) 1 hour after trauma; (3) time-course (therapeutic window) study with 35b (1.0 mg/kg) administered as a single intravenous bolus injection 1, 4, 8, or 24 hours after trauma; and (4) daily injection of an intravenous bolus of 35b (1.0 mg/kg) administered 30 minutes before mice were subjected to four place-learning trials on days 7, 8, 9, and 10 after injury.

Magnetic resonance imaging measurement

Proton density and T_2 -weighted magnetic resonance imaging (MRI) has been shown to be a reliable method of measuring lesion volume in other models of brain injury, most notably ischemia (Hockings et al., 1995; Loubinoux et al., 1997) where lesion size at 24 hours correlated well with histologic measures of damage. Diffusion and perfusion imaging have also been performed at 24 hours and 7 days after TBI (Assaf et al., 1999). We used T_2 -weighted MRI at 21 days to measure lesion volume after TBI, as previously detailed (Faden et al., 2001).

Twenty-one days after TBI, all animals were anesthetized with sodium pentobarbital (70 mg/kg, intraperitoneally) and subjected to MRI using a Bruker 7T/21 cm Biospec-Avance system (Bruker, Karlsruhe, Germany). Briefly, animals were placed within a Plexiglas animal bed with a 37°C heating pad to maintain body temperature. Respiratory gating to reduce motion artifacts was achieved using a respiratory monitor as described previously (Albensi et al., 2000). The animal bed was positioned with the head in the center of the magnet within a 72-mm ^1H birdcage resonator (Bruker). Field homogeneity across the brain was optimized and a sagittal scout image was acquired (RARE [rapid acquisition relaxation enhancement pulse sequence] image, field of vision, 4×4 cm; 128×128 resolution; repetition time (TR) to echo time (TE), 1,500/10 milliseconds with a RARE factor of 8, making the effective TE 40 milliseconds). Multislice T_2 -weighted images were then acquired to obtain eight contiguous slices commencing at the end of the olfactory bulb and working caudally (field of vision, 3×3 cm; slice thickness, 2 mm; 128×128 resolution; TR/TE, 1,500/20 milliseconds; four echo images and two averages). Each scan took approximately 8 minutes. Lesion volume was estimated from the summation of areas of hyperintensity on each slice, multiplied by slice thickness, for both the ipsilateral and contralateral hemispheres. Average lesion volume (\pm SEM in μL) was calculated for each treatment group.

Histologic evaluation

Twenty-one days after injury, animals were killed with an overdose of sodium pentobarbital (100 mg/kg body weight) and perfused transcardially with physiologic saline and heparin followed by 4% paraformaldehyde in phosphate-buffered saline. The brains were removed, postfixed in the same fixative for 24 hours, dehydrated in a graded series of ethanols, and embedded in a series of celloidin (2% to 12%) dissolved in a 50:50 mixture of ethanol and ethyl ether. Embedded brains were exposed to chloroform vapors and then submerged in ethanol until serial (40- μ) sections were cut coronally on a microtome. Every fifth section was stained with modified Giemsa stain. A 0.4% w/v Giemsa stock was prepared in buffered methanol at a pH of 6.

The stock was diluted 1:4 with water, and six drops of 1% glacial acetic acid were added per 100 mL diluted stain. Sections were stained in Giemsa (60 minutes) and rinsed in 95% (45 minutes) and 100% (2 minutes) ethanol. Sections were then immersed in isopropyl ethanol (20 minutes) and cedar wood oil (5 minutes), washed in xylene, mounted on slides, and cover-slipped with permount. The lesion volume was assessed blindly with respect to treatment group using a systematic sampling principle (Gundersen and Jensen, 1987). On average, 15 sections per animal were used for lesion volume measurement: section periodicity was 5, the space between used sections was 200 microns. In selected sections, the area that contained damaged tissue or cavity was carefully circumscribed at low magnification (1.5 \times objective lens) using the Neurolucida program (MicroBrightField, Williston, VT, U.S.A.).

Data analysis

Beam-walking and Morris water maze data were analyzed by two-way repeated measures ANOVA, followed by *post hoc* one-tailed Dunnett tests with CCI + vehicle-treated animals serving as controls. In the dose-response and therapeutic-window studies, raw beam-walk scores were not normally distributed; these data were normalized with a square root transformation and then assessed as described previously. Data are expressed as mean \pm SEM, except for beam-walk scores in the therapeutic window study (which are expressed as individual animal scores and medians for each group). Data points greater than three standard errors from the mean were considered outliers and not included for statistical analysis. Lesion volume data were analyzed by one-tailed *t*-tests and regression ANOVA, and graphed as mean \pm SEM. Histologic data were analyzed with GB-Stat Version 6 statistical package (Dynamic Microsystems, Silver Spring, MD, U.S.A.). The relation between lesion volume measured by MRI and histologic assessment was analyzed by linear regression.

RESULTS

Physiology and acute recovery

There was no significant difference in body weight and core temperature among groups. After cessation of anesthesia, no significant differences in either pedal withdrawal or righting reflexes were found in any of the treated groups when compared with the control group (data not shown).

Beam walking

Treatment with 35b (1.0 mg/kg) 30 minutes after injury (study 1; Fig. 1) significantly reduced the number of foot faults compared with vehicle-treated controls at 14 and 21 days after injury ($P < 0.05$ for CCI + 35b vs. CCI + saline on days 14 and 21). In addition, when given over a range of doses (0.1 to 10 mg/kg) at 1 hour after injury (study 2; Fig. 2), 35b improved beam walking 21 and 28 days later ($P < 0.05$ for 0.1, 1.0, or 10 mg/kg 35b vs. control scores from the same day on days 21 or 28). The 1.0-mg/kg dose was most robust, and significantly reduced foot faults 7, 14, 21, and 28 days after injury ($P < 0.05$ for CCI + 1.0 mg/kg 35b vs. control scores from the same day). This dose was therefore selected for a therapeutic-window study (study 3; Fig. 3), where long-term improvement in beam walking was observed when

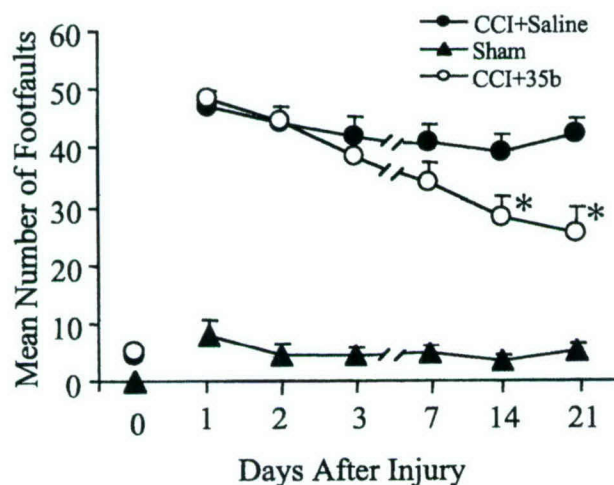


FIG. 1. Effect of 35b on motor recovery over time after controlled cortical impact (CCI) in the mouse. 35b (1.0 mg/kg) or an equivalent volume of saline vehicle was injected intravenously at 30 minutes after injury. Animals were tested to determine the number of errors (foot faults) on a beam-walking task 1 to 21 days later. The 0 indicates beam scores before injury. Sham mice received surgery but no injury. Dots represent the mean \pm SEM number of foot faults for each group as shown in the legend (* P < 0.05 vs. CCI + saline scores from the same day).

treatment was delayed as long as 4 or 8 hours after injury (on day 14, P < 0.05 for CCI + 35b at 1 or 4 hours after injury vs. saline at 1 hour after injury; on day 21, P < 0.05 for CCI + 35b at 1, 4, or 8 hours after injury vs. saline at 1 hour after injury).

Place learning

The effect of 35b on cognitive recovery (study 1; Fig. 4) was assessed by comparing the time required to find a submerged resting platform in a Morris water maze task (goal latencies). Treatment with 35b (1.0 mg/kg) 30 minutes after injury significantly reduced mean latencies on

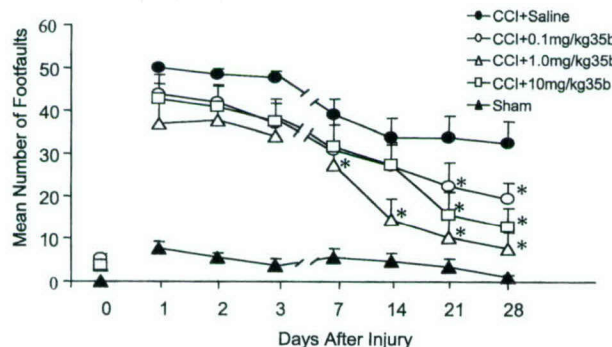


FIG. 2. Dose-response of 35b on motor recovery after controlled cortical impact (CCI) in the mouse. Either 0.1, 1.0, or 10 mg/kg 35b or an equivalent volume of saline was injected intravenously 1 hour after CCI. Beam-walking ability was tested 1 to 28 days later (x-axis). Sham mice received surgery but no injury. The 0 indicates beam scores before injury. Dots represent the mean \pm SEM number of foot faults for each group, as shown in the legend. * P < 0.05 versus CCI + saline scores from the same day.

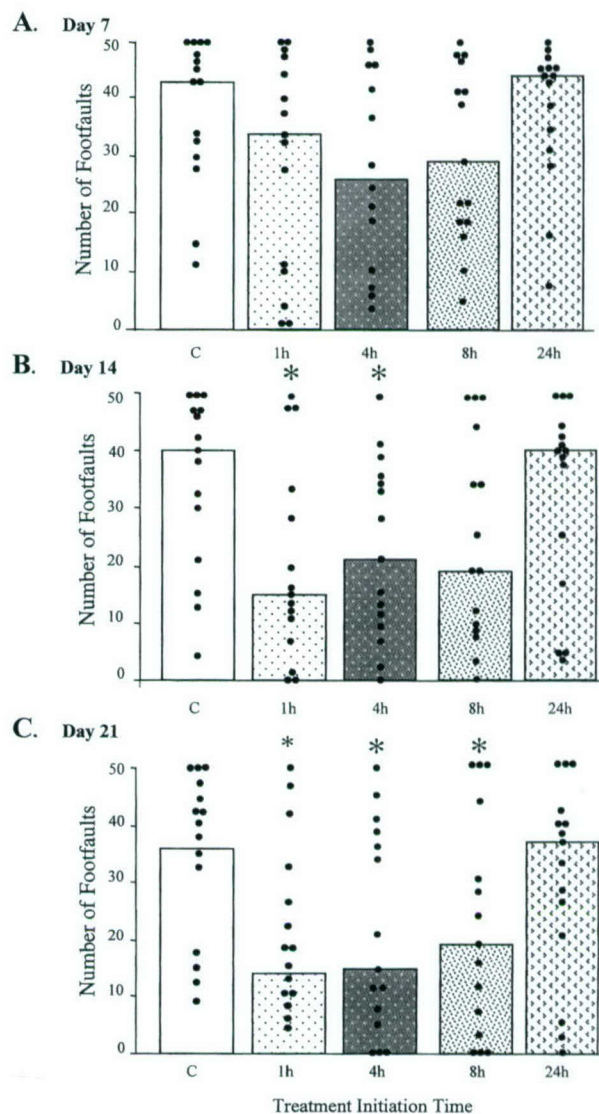


FIG. 3. Therapeutic window of 35b effect on motor recovery after controlled cortical impact (CCI) in the mouse. A single dose of 35b (1.0 mg/kg) was injected intravenously 1, 4, 8, or 24 hours after injury. Controls received equivalent injections of saline 1 hour after injury. The number of foot faults for each individual animal is represented as a dot, whereas bars represent the median score for each treatment group. A, B, and C show scores 7, 14, and 21 days after injury, respectively. * P < 0.05 versus control scores from the same day.

three of four test days (P < 0.05 for CCI + 35b vs. control scores on the same day on days 8, 9, or 10). This performance was similar to that seen in sham animals. Delayed administration of 35b was associated with similar improvements. Treatment at 1 or 4 hours after injury (study 3; Fig. 5) reduced mean latencies on two of four test days (P < 0.05 for CCI + 35b at 1 or 4 hours after injury vs. saline at 1 hour after injury, scores from the same day on days 16 and 17). Treatment delayed as long as 8 hours after injury (Fig. 5) significantly reduced latencies on one day of testing, and showed strong trends toward reduction on three of four test days (on day 16, P

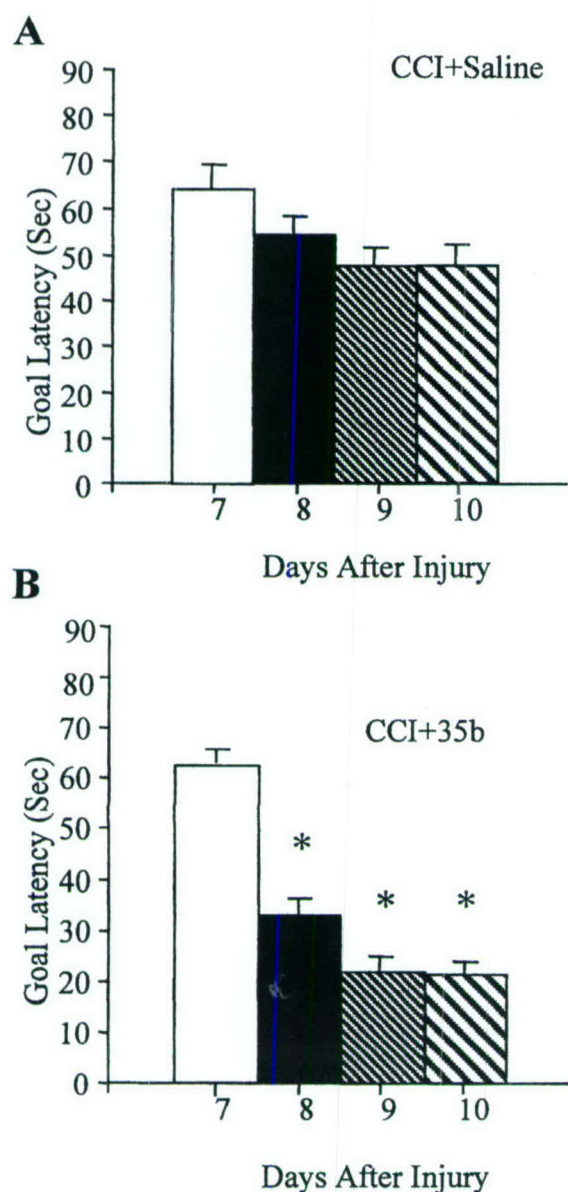


FIG. 4. Effect of 35b (**B**) or an equivalent volume of saline vehicle (**A**) on a Morris water maze test of cognitive recovery over time after controlled cortical impact (CCI) in the mouse. Data are from the same mice injured and treated as described in Fig. 1. Animals experienced four training trials 30 minutes apart on days 7 to 10 after injury, as indicated on the x-axis. Bars represent the mean \pm SEM time required to find a hidden platform (goal latency) averaged from the four trials. * $P < 0.05$ versus CCI + saline scores from the same day.

< 0.05 for CCI + 35b at 8 hours after injury vs. saline at 1 hour after injury scores from the same day). Trends were also observed in mice treated 24 hours after injury (Fig. 5).

In a study designed to test the effect of 35b on cognition in animals with an established brain lesion (study 4; Fig. 6), 35b (1.0 mg/kg) was administered once daily before water maze testing on each of four consecutive days, beginning 1 week after injury. This treatment re-

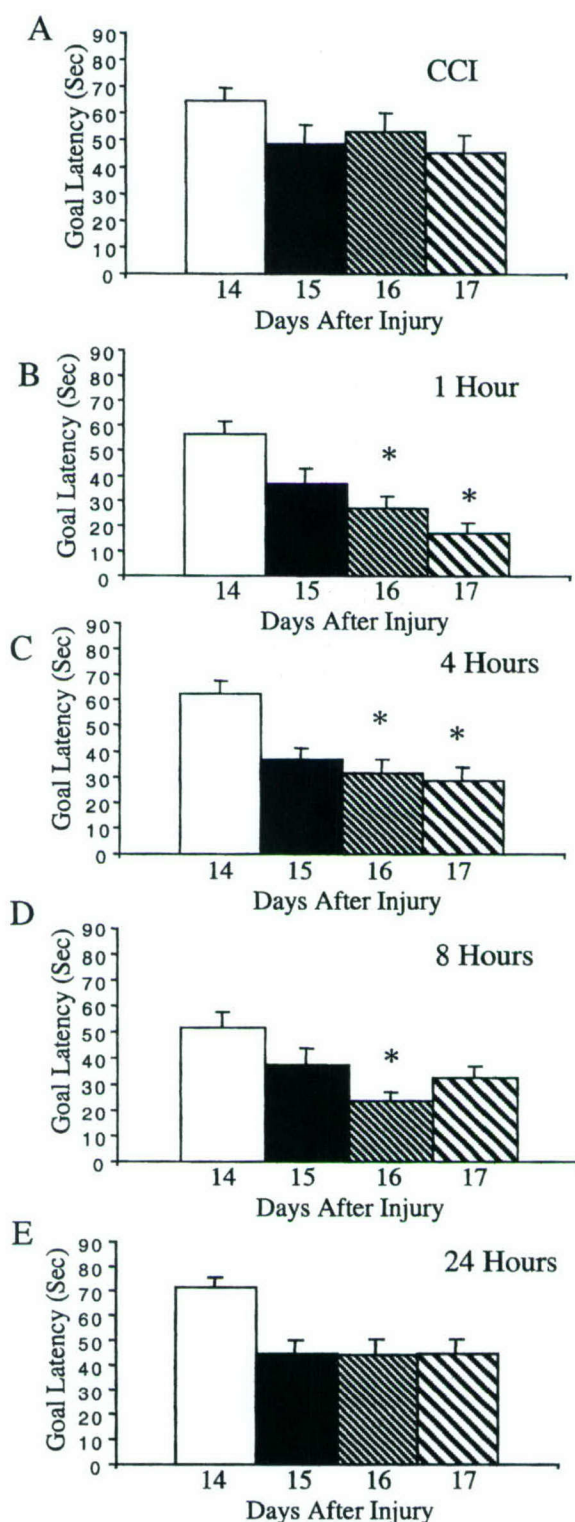


FIG. 5. Therapeutic window of 35b effect on cognitive recovery after controlled cortical impact (CCI) in the mouse. Data are from the same mice injured and treated as described in Fig. 3. Animals experienced 4 training trials 30 minutes apart on days 14 through 17 after injury, as indicated on the x-axis. **A** through **E** show data for various treatment times. Bars represent the mean \pm SEM time required to find a hidden platform (goal latency) averaged from the 4 trials. * $P < 0.05$ versus CCI (controls) scores from the same day.

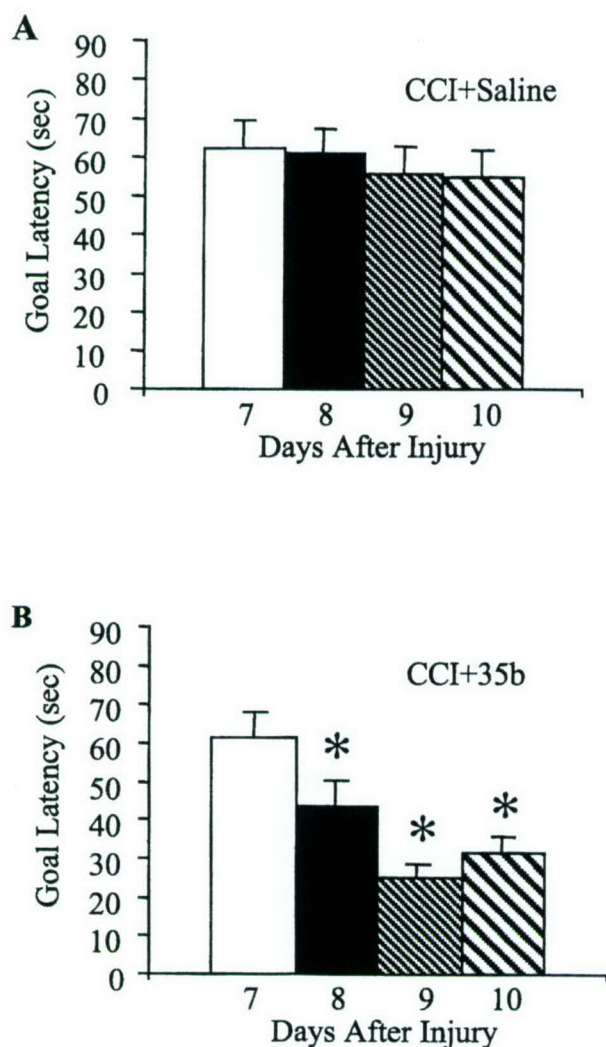


FIG. 6. Effect of 35b on Morris water maze performance in mice with an established controlled cortical impact (CCI) lesion. Mice were injured and allowed to recover. Seven to 10 days after injury, a single dose of 35b was injected intravenously (1.0 mg/kg) on each day 30 minutes before four trials of water maze testing began. Blocks represent the mean \pm SEM score across the four trials for each day. Treatment with saline or 35b is shown in **A** and **B**, respectively. * $P < 0.05$ versus CCI + saline scores from the same day. On visuomotor trials, when animals could identify a visible platform above the water surface, there were no differences between 35b- and vehicle-treated controls.

duced latencies in the water maze task compared with saline-treated injured controls on three of four testing days ($P < 0.05$ for CCI + 35b vs. CCI + saline on days 8, 9, and 10). There was no difference in swimming ability between the treated and saline groups on the visuomotor test because both groups had similar latencies to find a visible platform (mean latency \pm SEM for CCI + 35b or CCI + saline groups was 19.6 ± 3.78 and 20.2 ± 4.14 , respectively).

Lesion volume measurements

The T_2 -weighted MRI images used to assess lesion volume 21 days after injury showed a trend toward re-

duced lesion size in animals treated with 35b one hour after injury compared with vehicle-treated controls, though this reduction just missed significance cutoff value ($P = 0.06$; Fig. 7A). Histologic assessment of lesion volume in the same animals (Figs. 7B and 8), however, showed a similar decrease in lesion volume that was statistically significant ($P < 0.05$). Plotted together, the MRI and histologic data were highly correlated (correlation coefficient 0.7529, $P = 0.0012$, by simple regression ANOVA; Fig. 7C).

DISCUSSION

Thyrotropin-releasing hormone and closely related peptides have substantial neuroprotective actions across

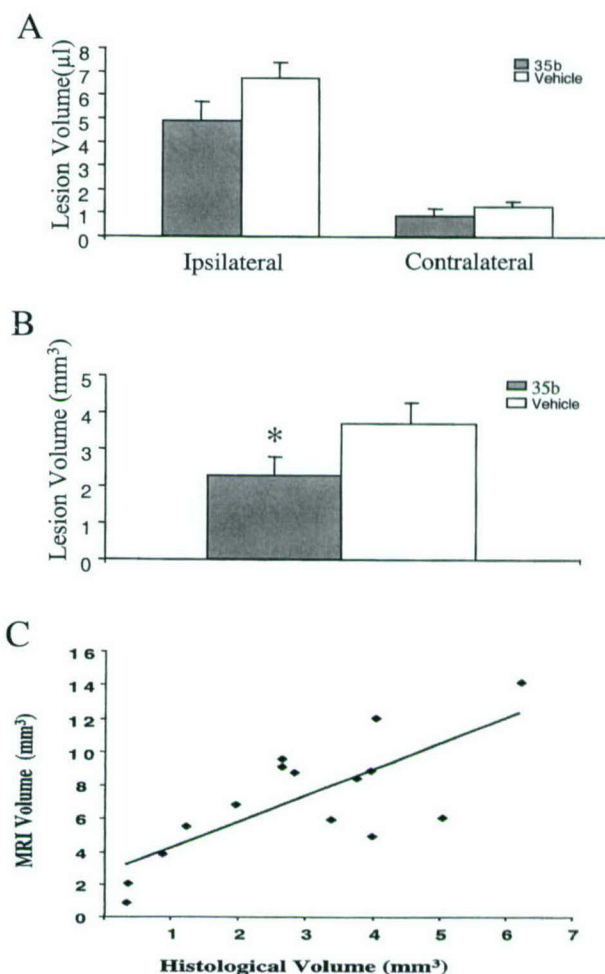


FIG. 7. Effect of 35b on controlled cortical impact (CCI)-induced lesion volume 21 days after injury in the mouse. Data are from the same mice treated 1 hour after injury with 35b or saline vehicle, as detailed in Fig. 3. **(A)** Lesion volume in the injured ipsilateral or injured contralateral hemisphere (x-axis) as assessed by magnetic resonance imaging (MRI). **(B)** Lesion volume as detected by histologic assessment in the injured ipsilateral hemisphere from the same animals. * $P < 0.05$ versus vehicle. **(C)** A significant correlation was detected between lesion volume values obtained with the two methods ($P < 0.05$, regression ANOVA).

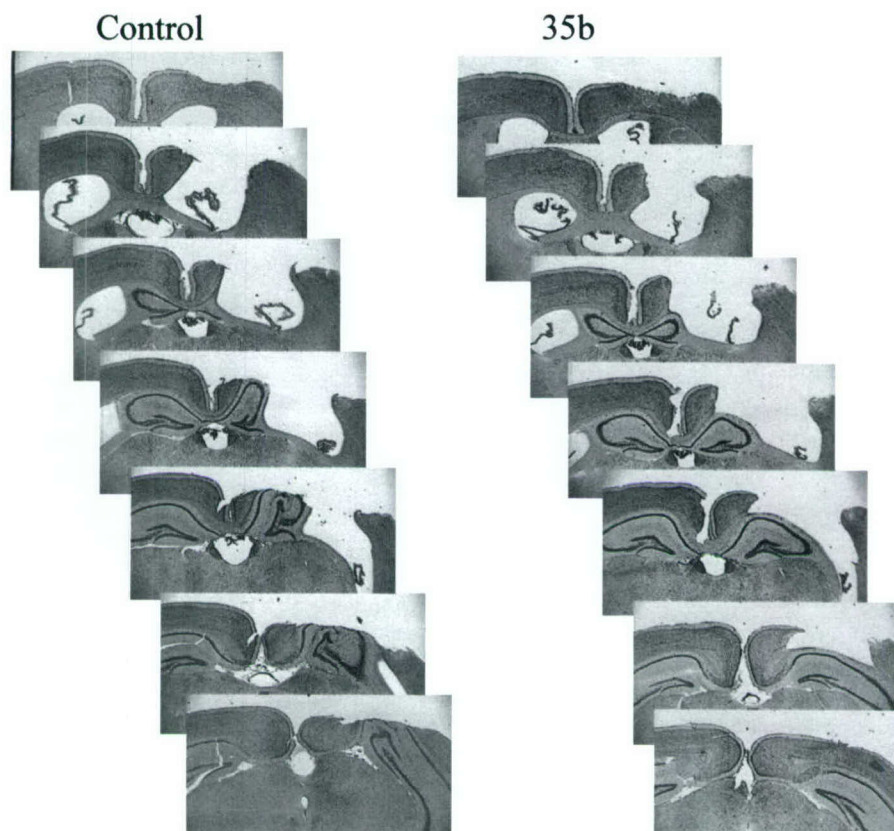


FIG. 8. Cresyl violet-stained sections through the anterior to posterior aspect of the lesion from representative mice in the control and 35b treatment groups. Data are from animals treated 1 hour after injury in the therapeutic-window study.

a variety of experimental models of CNS trauma in a number of species (Akdemir et al., 1993; Arias MJ, 1987; Behrmann et al., 1994; Ceylan et al., 1990, 1992; Faden, 1989, 1993; Faden et al., 1981, 1990; Fukuda et al., 1979; Puniak et al., 1991; Takami et al., 1991; Wang and Zhu, 1991). A small clinical study confirmed these beneficial effects in human spinal cord injury (Pitts et al., 1995). However, TRH and traditional TRH analogs have other physiologic actions that may limit their clinical utility (Faden et al., 1999b). For example, pressor actions may be undesirable in a head-injured patient with significant intraparenchymal hemorrhage. Euthermic actions may preclude the use of hypothermia and may serve to elevate body temperature above desirable levels. Analeptic effects may antagonize the effects of sedatives (e.g., barbiturate coma) or anesthetics required for surgical intervention. Finally, endocrine interactions may be problematic if longer-term administration is considered.

Compound 35b was identified as part of a drug-discovery effort to develop peptide and nonpeptide analogs of TRH that preserve its neuroprotective actions but eliminate the other major physiologic actions of this hormone (Faden et al., 2003). Previously, we reported a novel tripeptide analog that showed considerable neuroprotection and was devoid of autonomic or analeptic effects, although it possessed some endocrine actions (Faden et al., 1999b). Thyrotropin-releasing hormone is

metabolized to a cyclized dipeptide (cyclo-his-pro) that retains some physiologic activity, although it has not been reported to be neuroprotective (Prasad, 1995). Other cyclized dipeptides (diketopiperazines) have also been shown to have physiologic activity (Prasad, 1995).

Compound 35b is a relatively lipophilic diketopiperazine that has structural similarities to cyclo-his-pro. The partition coefficient for 35b between *n*-octanol and water (logP), calculated using the Hint program (eduSoft, Ashland, VA, U.S.A.), was 1.17; thus it is several orders of magnitude more hydrophobic than TRH or previous TRH analogs. This superior hydrophobicity would be expected to enhance its cellular permeability, thereby improving its accessibility to the brain. 35b has no autonomic, analeptic, or endocrine activity and, indeed, does not have appreciable activity at either of the two identified, high-affinity TRH receptors (Faden et al., 2003). In parallel studies, this compound showed considerable neuroprotective activity *in vitro*—including models of trauma, apoptosis, and necrosis. Moreover, rats subjected to lateral fluid percussion-induced TBI and treated with a single intravenous bolus infusion of 35b thirty minutes after trauma showed significantly improved motor and cognitive recovery (Faden et al., 2003).

In the present studies we sought determine (1) whether 35b had neuroprotective actions in another model of TBI

(CCI) and in another species (mouse); (2) whether it had an inverted U-shaped dose–response curve like TRH or classical TRH analogs; (3) the therapeutic window of 35b; and (4) whether it had cognitive-enhancing properties (nootropic effects) in injured animals with an established lesion. We used a well-characterized CCI model in mice, which differs pathologically from fluid percussion injury. Dose–response studies showed a relatively flat, inverted U-shaped dose–response curve between 0.1 and 10 mg/kg, with the most effective dose being 1 mg/kg. These dose–response characteristics are similar to those we have reported for the N-terminal–substituted TRH analog YM14673, which shows potent neuroprotection in rat TBI and spinal cord injury models (Faden, 1989). The fact that significant neuroprotective effects were observed at 10 times the optimal dose, without apparent toxicity, suggests that 35b may have a good therapeutic index. Significantly improved functional recovery was observed even when initial treatment was delayed until 8 hours after trauma, which indicates a long therapeutic window for the compound. These improved behavioral effects were associated with a substantial reduction in lesion volumes, determined both histologically and with T₂-weighted MRI.

To our knowledge, this is the first TBI study to directly compare histologic lesion volume measurements with those obtained using MRI; the results of these two methods were highly correlated. Use of MRI to measure lesion volumes has several potential advantages over standard histology: (1) lesion volumes can be followed noninvasively over time, so that one can examine effects of pharmacological interventions over the course of secondary injury development and longer-term tissue loss; (2) behavioral assessment and tissue loss can be correlated over time in the same animals; (3) potential post-mortem artifacts are avoided; and (4) assessment can be done quite rapidly. In other studies, we have shown the utility of MRI application to evaluate both secondary injury and pharmacological actions (Faden et al., 2001). Whether this can be used as a surrogate marker for clinical head injury or pharmacological studies remains to be determined.

Importantly, administration of 35b before each water maze trial, on days 7 to 10 after trauma, resulted in remarkably improved spatial learning, with treated animals recovering to a level similar to uninjured (sham-injured) controls. This suggests that 35b may have nootropic properties and thus may have a role in the treatment of chronic head injury. The chemical structure of 35b suggests that it may also be administered orally—a highly desirable quality for chronic administration. It should be noted that some other diketopiperazines have shown cognitive-enhancing properties, although the TRH derivative cyclo-his-pro does not (Prasad, 1995).

The mechanisms by which 35b produces its therapeutic actions have not been identified, although it can attenuate *in vitro* models of both necrotic neuronal cell death (*in vitro* trauma, maitotoxin) and apoptotic cell death (staurosporine) (Faden et al., 2003). The class of compound also reduces glutamate or free radical–induced toxicity *in vitro* (S. Knoblich and A. I. Faden, unpublished observations, 2002), which suggests multi-potential neuroprotective actions. Moreover, it attenuates the neuronal toxicity of β -amyloid *in vitro* (V. Movsesyan and A. I. Faden, unpublished observations, 2002), which, combined with its nootropic properties, may make this diketopiperazine a candidate for the treatment of Alzheimer disease.

Using the NIMH screening profile for receptor binding, 35b has shown very modest binding to various muscarinic receptors and no significant binding to a large number of classical neurotransmitter receptors or transporters. However, TRH has been shown to physiologically antagonize a number of factors implicated in secondary injury (endogenous opioids platelet activity factor, leukotrienes, glutamate), without having appreciable activity at their respective receptors (Faden, 1996). It is also possible that 35b may alter the regulation of genes or gene products involved in secondary injury. Such studies are now feasible using micro-array technology.

CONCLUSIONS

In summary, we report the neuroprotective and nootropic effects of a novel diketopiperazine. Its relatively large therapeutic window and its ability to attenuate necrotic and apoptotic neuronal cell death suggest that this compound may have utility for the treatment of acute head injury. Moreover, its ability to improve cognitive function in animals with established lesions suggests that drugs of this class may also have a role in the treatment of chronic head-injured patients.

Acknowledgments: The authors thank Sadia Aden and Anu Singh for their expert technical assistance.

REFERENCES

- Akdemir H, Pasaoglu H, Arman F, Coksevim B, Pasaoglu A (1993) Effects of TRH and high-dose corticosteroid therapy on evoked potentials, and tissue Na⁺, K⁺ and water content in experimental spinal injury. *Res Exp Med* 193:297–304
- Albensi BC, Knoblich SM, Chew BG, O'Reilly MP, Faden AI, Pekar JJ (2000) Diffusion and high resolution MRI of traumatic brain injury in rats: time course and correlation with histology. *Exp Neurol* 162:61–72
- Arias MJ (1987) Treatment of experimental spinal cord injury with TRH, naloxone, and dexamethasone. *Surg Neurol* 28:335–338
- Assaf Y, Holokovsky A, Berman E, Shapira Y, Shohami E, Cohen Y (1999) Diffusion and perfusion magnetic resonance imaging following closed head injury in rats. *J Neurotrauma* 16:1165–1176
- Behrmann DL, Bresnahan JC, Beattie MS (1994) Modeling of acute

- spinal cord injury in the rat: neuroprotection and enhanced recovery with methylprednisolone, U-74006F and YM-14673. *Exp Neurol* 126:61-75
- Bracken MB, Holford TR (1993) Effects of timing of methylprednisolone or naloxone administration on recovery of segmental and long-tract neurological function in NASCIS 2. *J Neurosurg* 79: 500-507
- Ceylan S, Kalelioglu M, Akturk G, Akturk F (1990) Medical treatment of acute spinal cord injuries. *Res Exp Med* 190:111-119
- Ceylan S, Ilbay K, Baykal S, Sener U, Ozmenoglu M, Kalelioglu M, Akturk F, Komsuoglu SS, Ozoran A (1992) Treatment of acute spinal cord injuries: comparison of thyrotropin-releasing hormone and nimodipine. *Res Exp Med* 192:23-33
- Faden AI (1989) TRH analog YM-14673 improves outcome following traumatic brain and spinal cord injury in rats: dose-response studies. *Brain Res* 486:228-235
- Faden AI (1993) Comparison of single and combination drug treatment strategies in experimental brain trauma. *J Neurotrauma* 10:91-100
- Faden AI (1996) Pharmacological treatment approaches for brain and spinal cord trauma. In: *Neurotrauma* (Narayan RK, Wilberger JE, Povlishock JT, eds), New York: McGraw-Hill, pp 1479-1490
- Faden AI (2001) Neuroprotection and traumatic brain injury: the search continues. *Arch Neurol* 58:1553-1555
- Faden AI (2002) Neuroprotection and traumatic brain injury: theoretical option or realistic proposition. *Curr Opin Neurol* 15:707-712
- Faden AI, Jacobs TP, Holaday JW (1981) Thyrotropin-releasing hormone improves neurologic recovery after spinal trauma in cats. *N Engl J Med* 305:1063-1067
- Faden AI, Yum SW, Lemke M, Vink R (1990) Effects of TRH-analog treatment on tissue cations, phospholipids and energy metabolism after spinal cord injury. *J Pharmacol Exp Ther* 255:608-614
- Faden AI, Fox G, Fan L, Knoblich S, Araldi GL, Kozikowski AP (1999a) Neuroprotective and cognitive enhancing effects of novel small peptides. *Ann N Y Acad Sci* 890:120
- Faden AI, Fox GB, Fan L, Araldi GL, Qiao L, Wang S, Kozikowski AP (1999b) Novel TRH analog improves motor and cognitive recovery after traumatic brain injury in rodents. *Am J Physiol* 277:R1196-1204
- Faden AI, O'Leary DM, Fan L, Bao W, Mullins PG, Movsesyan VA (2001) Selective blockade of the mGluR1 receptor reduces traumatic neuronal injury *in vitro* and improves outcome after brain trauma. *Exp Neurol* 167:435-444
- Faden AI, Knoblich SM, Cernak I, Fan L, Vink R, Araldi GL, Fricke ST, Roth B, Kozikowski AP (2003) Novel diketopiperazine enhances motor and cognitive recovery after traumatic brain injury in rats and shows neuroprotection *in vitro* and *in vivo*. *J Cereb Blood Flow Metab* 23:
- Fox GB, Fan L, Levasseur RA, Faden AI (1998) Sustained sensory/motor and cognitive deficits with neuronal apoptosis following controlled cortical impact brain injury in the mouse. *J Neurotrauma* 15:599-614
- Fukuda N, Saji Y, Nagawa Y (1979) [Behavioral and EEG alterations with brain stem compression and effect of thyrotropin-releasing hormone (TRH) in chronic cats (author's translation)]. *Nippon Yakurigaku Zasshi* 75:321-331
- Gundersen HJ, Jensen EB (1987) The efficiency of systematic sampling in stereology and its prediction. *J Microsc* 147:229-263
- Hockings PD, Middleton DA, Patel S, Samson NA, Reid DG, Rose SE, Crozier S, Roffman W, Rothaul AL, Hunter JA, et al (1995) Correlation between high-field T₂-weighted MR imaging and histology of ischemic lesions in gerbil brain. *J Magn Reson Imaging* 5:437-442
- Loubinoux I, Volk A, Borredon J, Guirimand S, Tiffon B, Seylaz J, Meric P (1997) Spreading of vasogenic edema and cytotoxic edema assessed by quantitative diffusion and T₂ magnetic resonance imaging. *Stroke* 28:419-426; discussion 426-427
- Maas AI (2001) Neuroprotective agents in traumatic brain injury. *Expert Opin Invest Drugs* 10:753-767
- McIntosh TK (1994) Neurochemical sequelae of traumatic brain injury: therapeutic implications. *Cerebrovasc Brain Metab Rev* 6:109-162
- McIntosh TK, Juhler M, Wieloch T (1998) Novel pharmacologic strategies in the treatment of experimental traumatic brain injury: 1998. *J Neurotrauma* 15:731-769
- Panter SS, Faden AI (1992) Pretreatment with NMDA antagonists limits release of excitatory amino acids following traumatic brain injury. *Neurosci Lett* 136:165-168
- Pitts LH, Ross A, Chase GA, Faden AI (1995) Treatment with thyrotropin-releasing hormone (TRH) in patients with traumatic spinal cord injuries. *J Neurotrauma* 12:235-243
- Prasad C (1995) Bioactive cyclic dipeptides. *Peptides* 16:151-164
- Puniak MA, Freeman GM, Agresta CA, Van Newkirk L, Barone CA, Salzman SK (1991) Comparison of a serotonin antagonist, opioid antagonist, and TRH analog for the acute treatment of experimental spinal trauma. *J Neurotrauma* 8:193-203
- Takami K, Hashimoto T, Shino A, Fukuda N (1991) Effect of thyrotropin-releasing hormone (TRH) in experimental spinal cord injury: a quantitative histopathologic study. *Jpn J Pharmacol* 57:405-417
- Wang GL, Zhu C (1991) Effects of thyrotropin-releasing hormone on acute experimental traumatic head injury in cats. *Chin Med J (Engl)* 104:939-944
- Yarbrough GG (1979) On the neuropharmacology of thyrotropin releasing hormone (TRH). *Prog Neurobiol* 12:291-312

Novel Diketopiperazine Enhances Motor and Cognitive Recovery After Traumatic Brain Injury in Rats and Shows Neuroprotection *In Vitro* and *In Vivo*

*Alan I. Faden, *Susan M. Knoblach, *Ibolja Cernak, *Lei Fan, †Robert Vink,
‡Gian Luca Araldi, *Stanley T. Fricke, ‡Bryan L. Roth, and †Alan P. Kozikowski

Departments of *Neuroscience and †Neurology, Georgetown University Medical Center, Washington, DC, and ‡NIMH Psychoactive Drug Screening Program and Department of Biochemistry, Case Western Reserve University Medical School, Cleveland, Ohio, U.S.A.

Summary: The authors developed a novel diketopiperazine that shows neuroprotective activity in a variety of *in vitro* models, as well as in a clinically relevant experimental model of traumatic brain injury (TBI) in rats. Treatment with 1-ARA-35b (35b), a cyclized dipeptide derived from a modified thyrotropin-releasing hormone (TRH) analog, significantly reduced cell death associated with necrosis (maitotoxin), apoptosis (staurosporine), or mechanical injury in neuronal-glia cocultures. Rats subjected to lateral fluid percussion-induced TBI and then treated with 1 mg/kg intravenous 35b thirty minutes after trauma showed significantly improved motor recovery and spatial learning compared with vehicle-treated controls. Treatment also significantly reduced lesion volumes as shown by magnetic resonance imaging, and decreased the

number of TUNEL-positive neurons observed in ipsilateral hippocampus. Unlike TRH or traditional TRH analogs, 35b treatment did not change mean arterial pressure, body temperature, or thyroid-stimulating hormone release, and did not have analeptic activity. Moreover, in contrast to TRH or typical TRH analogs, 35b administration after TBI did not alter free-magnesium concentration or cellular bioenergetic state. Receptor-binding studies showed that 35b did not act with high affinity at 50 classical receptors, channels, or transporters. Thus, 35b shows none of the typical physiologic actions associated with TRH, but possesses neuroprotective actions *in vivo* and *in vitro*, and appears to attenuate both necrotic and apoptotic cell death. **Key Words:** TRH analogs—Neuroprotection—Traumatic brain injury—Necrosis—Apoptosis.

Traumatic brain injury (TBI) remains a leading cause of neurologic disability and causes approximately 75,000 deaths and 350,000 hospitalizations in the United States annually (Krause et al., 1996). Experimental head injury models have been developed in rodents to study pathophysiologic mechanisms that may relate to clinical head injury as well as to examine potential pharmacological therapies. The motor and cognitive impairments that are found in these models parallel those observed clinically

(Dixon et al., 1991; Fox et al., 1998; Hamm et al., 1992; McIntosh et al., 1989; Povlishock, 1996; Smith et al., 1995). Such deficits result, in part, from delayed secondary tissue damage resulting from altered metabolic and biochemical processes that are induced by injury (Faden, 1996b; Raghupathi et al., 2000; Vink et al., 1987; Yakovlev et al., 1997). Proposed injury factors include changes in ionic homeostasis, excitatory amino acids, free radicals, proteases, and inflammatory-immune responses, among others; together, they form an interactive cascade that may lead to a reduction in local blood flow, decrease in metabolism, damage to cell membranes, and/or the initiation apoptosis (Faden, 1996b; Raghupathi et al., 2000; Yakovlev et al., 1997; Yamakami et al., 1995).

Many pharmacological treatment strategies have been proposed that are intended to interrupt or inhibit a particular component of this secondary injury cascade. Although several experimental studies have reported improved functional outcome in treated animals (for

Received July 5, 2002; final version received October 21, 2002; accepted October 23, 2002.

This work was supported by Department of Defense Cooperative Agreement DAMD17-99-2-9007, National Institutes of Health grants R01 NS41119-01 (to A.I.F.) and KO2MH01366 (to B.L.R.), and the NIMH Psychoactive Drug Screening Program Contract (to B.L.R.).

Address correspondence and reprint requests to Alan I. Faden, MD, Department of Neuroscience, Georgetown University Medical Center, 3970 Reservoir Road NW, Room EP-12, Washington, DC 20057, U.S.A.; e-mail: fadena@georgetown.edu

Abbreviations used: TUNEL, terminal deoxynucleotidyl transferase-mediated 2'-deoxyuridine 5'-triphosphate-biotin nick end labeling.

review, see Faden, 1996b; McIntosh et al., 1998), neuroprotective treatment after clinical TBI has been disappointing (Faden, 2002; Maas, 2001). This failure may reflect the highly multifactorial nature of tissue damage after trauma, which includes varying combinations of ischemia or hypoxia, hematoma, contusion, diffuse axonal injury, and edema (Bullock et al., 1999), as well as issues relating to injury severity, sample size, or lack of appropriate stratification (Faden, 2002; Maas, 2001). Therefore, effective clinical treatment may require either combination drug strategies or the use of single drugs that modulate multiple injury factors (Faden, 2001, 2002).

Thyrotropin-releasing hormone (TRH) and certain TRH analogs have shown neuroprotective effects across species in various CNS injury models, through mechanisms that are believed to be multifactorial (Faden, 1996b). For example, TRH can modulate the effects of endogenous opioids, leukotrienes, platelet-activating factor, glutamate, and sodium channel activity, as well as improve cerebral blood flow and cellular bioenergetic state after CNS trauma (Faden, 1996b). Moreover, TRH has a large therapeutic window (Faden et al., 1984) and is well tolerated in humans (Pitts et al., 1995). Cognitive-enhancing properties have also been demonstrated for TRH and certain TRH analogs (Olson et al., 1995).

However, TRH or conventional TRH analogs have other physiologic effects that may limit their potential utility for the treatment of TBI (Faden et al., 1993; Metcalf, 1982). For example, pressor actions may serve to exacerbate posttraumatic hemorrhage. Temperature regulating effects may limit the potential use of hypothermia as a treatment. Analeptic actions may preclude the implementation of pharmacological coma or inhibit anesthesia required for surgery. In addition, endocrine effects could limit chronic treatment, as may be desired for its possible nootropic actions.

Structure-activity studies have suggested that the neuroprotective actions of TRH do not relate to effects at its classical high-affinity receptor (Faden et al., 1988, 1993, 1999) and may be separable from its other major physiologic actions. Thyrotropin-releasing hormone is rapidly metabolized through the action of endopeptidases (Bassiri and Utiger, 1973; Metcalf, 1982). Its metabolic product, the cyclic dipeptide cyclo(his-pro) (CHP) or histidyl-proline diketopiperazine, has considerable physiologic activity, as do other naturally occurring diketopiperazines (Prasad, 1995). We have developed a series of diketopiperazines related to derivatives of TRH analogs and have examined them for neuroprotective effects as well as for other pharmacological actions. One such compound, 35b, shows considerable neuroprotective activity *in vivo* and *in vitro*, but is devoid of many of the other physiologic actions of TRH.

In the present studies, we used both *in vivo* and *in vitro* injury models to examine the effects of 35b treatment. Neuronal-glial cocultures subjected to necrotic (maitotoxin), apoptotic (staurosporine), or traumatic insults were used to evaluate the potential neuroprotective actions of the diketopiperazine. Potential autonomic, endocrine, and analeptic effects were examined in uninjured animals and compared with a classical TRH analog (YM-14673) with established neuroprotective properties. Using a lateral fluid percussion TBI model, effects of 35b treatment or vehicle on motor and cognitive recovery and lesion volumes were compared using T₂-weighted magnetic resonance imaging (MRI). Numbers of TUNEL-positive neurons were also compared in ipsilateral hippocampus between treated/injured animals and controls. ³¹P magnetic resonance spectroscopy (MRS) was used to evaluate possible actions of 35b on posttraumatic bioenergetics. Finally, receptor-binding profiles were performed with regard to classical neurotransmitters and transporters.

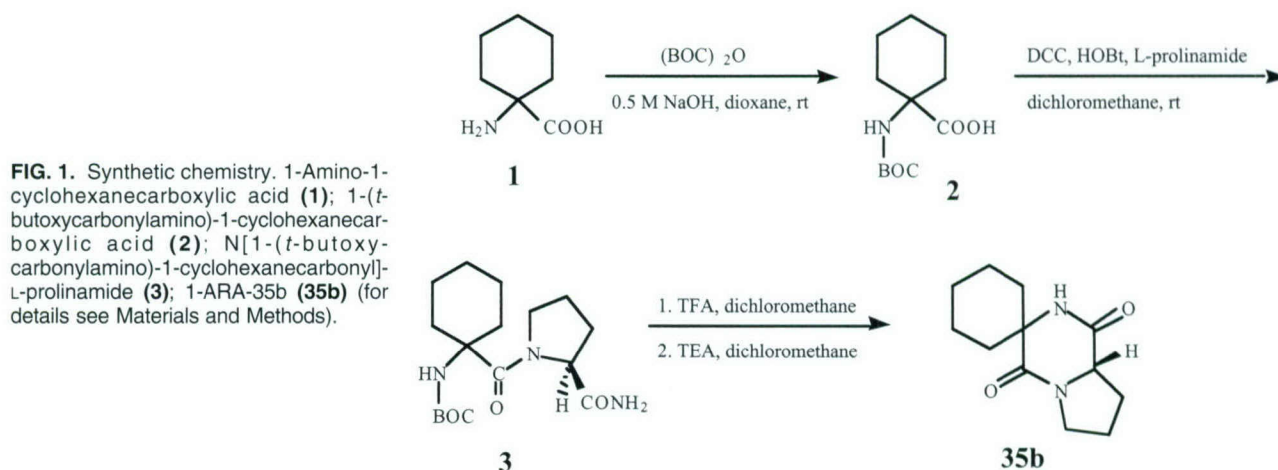
MATERIALS AND METHODS

Synthetic chemistry

1-(*t*-Butoxycarbonylamino)-1-cyclohexanecarboxylic acid: 1-amino-1-cyclohexanecarboxylic acid (1.0 g, 6.98 mmol) was dissolved in a mixture of dioxane (15 mL) and NaOH (0.5 mol/L, 15 mL). To this solution was added di-*tert*-butyl dicarbonate (1.6 g, 7.33 mmol) and the resulting mixture was stirred at room temperature for 15 hours. The reaction mixture was concentrated under reduced pressure and diluted with ethyl acetate (EtOAc; 50 mL). The aqueous solution was extracted with EtOAc (3 × 50 mL), and the collected organic phase was washed with brine (50 mL), dried over sodium sulfate, and concentrated under reduced pressure to yield the title compound 2 (0.98 g, 60%) as a white solid; melting point (mp) 175°C to 177°C; ¹H NMR (CD₃OD) δ 1.08 to 1.19 (multiplet [m], 2H), 1.40 (singlet [s], 9H), 1.42 to 1.58 (m, 4H), 1.59 to 1.66 (m, 2H), 1.80 to 1.98 (broad singlet, 2H), 6.88 (s, 1H), 12.08 (s, 1H) (Fig. 1).

N[1-(*t*-Butoxycarbonylamino)-1-cyclohexanecarbonyl]-L-prolinamide in dry dichloromethane (20 mL) was dissolved at 0°C 1-(*t*-butoxycarbonylamino)-1-cyclohexanecarboxylic acid (0.60 g, 2.47 mmol), L-prolinamide (0.28 g, 2.47 mmol), and dicyclohexylcarbodiimide (0.51 g, 2.47 mmol). The resulting mixture was stirred at 0°C for 10 minutes, and HOBt (4.93 mL of 0.5-mol/L solution in DMF, 2.47 mmol) was added and the mixture stirred overnight at room temperature. Insoluble matters were filtered off, and the filtrate was concentrated under reduced pressure. The crude residue was washed with hexane/EtOAc (9:1, 20 mL) to yield the title compound 3 (0.50 g, 60%) as a white solid; mp: 220°C; ¹H NMR (CD₃OD) δ 1.02 to 1.90 (m, 12H), 1.42 (s, 9H), 1.91 to 2.10 (m, 2H), 3.36 to 3.41 (m, 1H), 3.72 to 3.82 (m, 1H), 4.08 to 4.14 (m, 1H), 6.85 (doublet, 2H), 7.50 (s, 1H) (Fig. 1).

Diketopiperazine 35b. Trifluoroacetic acid (5 mL) was added to an ice-cold solution of N[1-(*t*-butoxycarbonylamino)-1-cyclohexanecarbonyl]-L-prolinamide (0.50 g, 1.47 mmol) in dichloromethane (5 mL), and the resulting solution was stirred



for 4 hours at room temperature. The reaction mixture was concentrated under reduced pressure. The residue was dissolved in dichloromethane (5 mL), 5 mL triethylamine was added, and the resulting solution was stirred at room temperature overnight. The reaction mixture was diluted with dichloromethane and washed with saturated NaHCO_3 solution (2×20 mL) followed by brine (20 mL). The organic layer was dried (Na_2SO_4) and concentrated under reduced pressure. The residue was purified by column chromatography to yield the title compound **35b** (0.23 g, 70%) as a crystalline solid; mp. 173°C to 174°C ; $[\alpha]_D^{25}$: -115° (c 0.5, CHCl_3); ^1H NMR (CDCl_3) δ 1.25 to 2.05 (m, 12H), 2.20 to 2.31 (m, 1H), 2.37 to 2.43 (m, 1H), 3.48 to 3.68 (m, 2H), 4.1 to 4.18 (m, 1H), 6.48 (s, 1H); ^{13}C NMR (CDCl_3) δ 21.1, 21.2, 22.6, 24.9, 29.2, 32.2, 34.5, 46.0, 58.7, 59.4, 169.0, 169.6 (Fig. 1).

Fluid percussion-induced traumatic brain injury

Fluid percussion-induced TBI was induced as previously described (McIntosh et al., 1989; Yakovlev et al., 1997). Male Sprague-Dawley rats (350 ± 50 g) were anesthetized with sodium pentobarbital (70 mg/kg, intraperitoneally), intubated, and implanted with femoral venous and arterial catheters (studies 1 and 3); in studies 2 and 4, the tail artery was cannulated and the tail vein was used for injection of drug or vehicle. Brain temperature was assessed indirectly through a thermistor in the temporalis muscle and body temperature was maintained at normal levels through a feedback-controlled heating blanket. Blood pressure was continuously monitored, and arterial blood gases were analyzed periodically. After the animal was placed in a stereotaxic frame, the scalp and temporal muscle were reflected; a small craniotomy (5 mm), located midway between the lambda and bregma sutures over the left parietal cortex, allowed insertion of a Leur-Loc that was cemented in place. The fluid-percussion head injury device, manufactured by the Medical College of Virginia (Richmond, VA, U.S.A.), consists of a plexiglas cylindrical reservoir filled with isotonic saline; one end includes a transducer that is mounted and connected to a 5-mm tube that attaches through a male Leur-Loc fitting to the female Leur-Loc cemented at the time of surgery. A pendulum strikes a piston at the opposite end of the device, producing a ~ 22 -millisecond pressure pulse, leading to the deformation of underlying brain. The degree of injury is related to the pressure pulse expressed in atmospheres (atm): 2.6 or 2.7 atm in our laboratory produces a moderately severe injury with regard to neurologic and histologic deficits. Sham (control) animals were subjected to anesthesia and surgery without fluid percussion brain injury.

Motor scores

Standardized motor scoring was performed at 1, 7, and 14 days after TBI, by persons unaware of treatment (Yakovlev et al., 1997). Motor function was evaluated using three separate tests, each of which is scored via an ordinal scale ranging from 0 (severely impaired) to 5 (normal function). Tests measure the ability to maintain position on an inclined plane in a vertical and two horizontal positions for 5 seconds, forelimb flexion (suspension by the tail), and forced lateral pulsion. Each of seven individual scores (vertical angle, right and left horizontal angle, right and left forelimb flexion, right and left lateral pulsion) was added to yield a composite neurologic score ranging from 0 to 35. This scoring method, which has been used in our laboratory extensively during the last 10 years, shows high interrater reliability ($>93\%$) and is very sensitive to pharmacological manipulations (McIntosh et al., 1989).

Cognitive assessment: Morris water maze

Learning and memory deficits in laboratory models of brain injury can be detected using a water maze paradigm similar to that originally described by Morris (Morris, 1984), as previously described by us for experimental TBI (Faden et al., 1999; Fox et al., 1998). Spatial learning was assessed by training the animals to locate a hidden, submerged platform using extramaze visual cues. The apparatus used consisted of a large, white circular pool (165-cm diameter, water temperature $24^\circ\text{C} \pm 1^\circ\text{C}$) with a plexiglas platform (110 mm^2) painted white and submerged (20 mm) below the surface of water that was rendered opaque with the addition of white, nontoxic paint. During training, the platform was hidden in one quadrant, and the animal was gently placed into the water facing the wall at one of four randomly chosen locations separated by 90 degrees. The latency to find the hidden platform within a 90-second period was recorded by a blinded observer. On the first trial, rats failing to find the platform within 90 seconds were assisted to the platform. Animals were allowed to remain on the platform for 15 seconds on the first trial and 10 seconds on all subsequent trials. There was an intertrial interval of 30 minutes, during which time the animals were towel-dried and placed under a heat lamp. A series of 16 training trials administered in blocks of 4 were conducted on days 14 to 17 after injury. To control for visual discriminative ability or motor impairment, the same animals were required to locate a clearly visible black platform (placed in a different location) raised 5 mm above the water surface at least 2 hours after the last training trial.

Study 1 was performed in association with motor testing. Because lesion volumes were not evaluated in this study, a

second study was performed using a more recently acquired computerized analytical system. In study 2, a PC-controlled video system (AccuScan Instruments, Inc., Columbus, OH, U.S.A.) was used to examine swim speed, distance, latency necessary to find a submerged resting platform, and time spent in the periphery versus the central zone adjacent to the platform. The swimming pool was monitored by a video camera (Sony CCD-TR517) equipped with a wide-angle objective. The signal was digitized (50 half-frame/s) and data were buffered in the computer's (Pentium-IV) main memory. The software (EZ-Video version 2.50, Automated Tracking System with Accu-Trak version 2.40, AccuPlot version 2.40, SerSwit 1.00, and ZoneMapper version 2.30) acquired, compressed, stored, and analyzed real-time pictures of animal movement. Swim speed was calculated by dividing path length by latency for each trial for each rat, and expressed as centimeters per second. The periphery was defined as a circular zone (zone 1) with a diameter of 20 cm (of 165 cm total). The remaining inner circle was divided into four equal parts (zones 2, 3, 4, and 5), with the platform located in the central zone 5 (Fig. 2). The mean latency and time periods spent in periphery and central zone adjacent to the platform were expressed in seconds. The effect of 35b on cognitive outcome was analyzed by comparison among groups (sham-operated controls, injured group without therapy, and injured group with 35b).

Analeptic and autonomic assessment

Additional groups of uninjured rats were tested for autonomic and analeptic responses immediately before and up to 60 minutes after drug administration. For the analeptic study, rats were first anesthetized with 40 mg/kg sodium pentobarbital intraperitoneally and placed onto an unheated pad on the laboratory bench top at room temperature (22°C + 2°C). A thermistor probe was placed in the rectum to measure core body temperature. After a 10-minute period, vehicle or drug was administered via the tail vein. Time to recovery of the righting

reflex was subsequently determined while temperature was recorded at 5-minute intervals for all animals.

To assess mean arterial pressure responses to the novel TRH analogs, a separate group of rats was anesthetized with 4% isoflurane (1.5 L/min). Catheters were then placed into the right carotid artery and internal jugular vein and exteriorized through the back of the neck. Rats were separated in individual cages and allowed to recover from anesthesia. Mean arterial blood pressure was continuously recorded via a transducer connected directly to the arterial catheter for the duration of the study. One hour after catheter placement, vehicle or drug was administered via the venous catheter.

Endocrine assessment

A radioimmunoassay for rat (r) TSH was used to assess endocrine function. Saline or 35b was administered intravenously via a chronically implanted catheter in anesthetized rats (70 mg/kg sodium pentobarbital; $n = 6$ /group) at time 0, and 5 mL whole blood was collected 30 minutes after injection. Blood plasma was subsequently obtained, frozen at -70°C, and shipped to Covance Laboratories (Vienna, VA, U.S.A.) for appropriate analyses. The rTSH assay is a specific double-antibody radioimmunoassay using antiserum prepared in the rabbit against purified rTSH antigens (Kieffer et al., 1974). The assay is standardized against purified rTSH.

Drugs and design

Four separate TBI studies were performed. In all four studies, rats were injected with 1.0 mg/kg 35b or vehicle 30 minutes after injury. In study 1, cognitive and motor functions were assessed in animals treated with vehicle ($n = 11$) and 35b ($n = 12$), and all injections were made through the femoral vein. In study 2, vehicle-treated ($n = 11$) and 35b-treated ($n = 11$) animals were subjected to cognitive testing as assessed by multiple outcomes (i.e., distance swum, search strategy) and lesion volume measurements via MRI, and all injections were made via the tail vein. In study 3, vehicle-treated ($n = 5$) and 35b-treated ($n = 5$) animals were used for MRS analysis of bioenergetic status after injury, and all injections were made via the femoral vein. In study 4, vehicle-treated ($n = 6$) and 35b-treated ($n = 5$) animals were killed 24 hours after injury and their brains removed for TUNEL analysis. The numbers of animals given are those that survived the intended experimental period. The level of mortality in all studies was less than 20% and was not affected by treatment. Investigators were blinded as to treatment.

For autonomic, analeptic, or endocrine studies, rats were given normal saline ($n = 6$), YM-14673 ($n = 6$), or 35b ($n = 6$) at the times indicated previously. YM-14673 was used for comparison purposes because previous work showed that the TRH analog significantly improves outcome after CNS injury (Faden, 1989, 1993). Different anesthetic protocols were used in the various studies, as required by the different models and durations of measurement, but in all cases, nontreated vehicle controls were used for comparisons.

TUNEL studies

Rats were anesthetized with sodium pentobarbital (100 mg/kg) 24 hours after TBI and then killed by decapitation. Their brains were quickly removed and submerged in OCT (OCT Tissue-Tek; Andwin Scientific, Warner Center, CA, U.S.A.) media and frozen in cooled isopentane (-70°C). Later, 16- μ mol/L sections were taken from -3.2 to -3.7 relative to bregma as described previously (Knobloch et al., 1999). Every tenth section was saved, and four of these sections (each at least 500 μ m apart) were selected for analysis. Tissue was stained

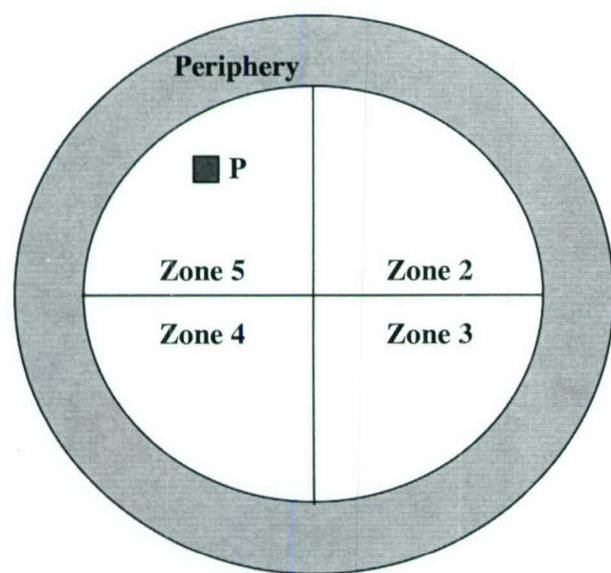


FIG. 2. Diagrammatic representation of the map generated by a software used to analyze animal performance during the Morris water maze test. The periphery is defined as a circular zone (zone 1) with a diameter of 20 cm (of 165 cm total), whereas the remaining inner circle is divided into four equal parts. The hidden, submerged platform (P) is located in zone 5 (central zone).

using the ApopTag Fluorescein-based indirect immunofluorescence staining kit (Serologicals Corporation, Norcross, GA, U.S.A.) with minor modifications. Some sections were double-labeled with anti-NeuN neuronal-specific marker antibody as detailed previously (Knobloch et al., 1999). Sections were viewed with a Nikon TE300 microscope, and all TUNEL-positive cells within the dentate granule cell layer (upper and lower blades) and CA3 region were counted at high magnification. Cell counts for all slides from each animal were averaged, and averages from each animal were combined and represented as the mean \pm SEM for the group.

Magnetic resonance imaging

Three weeks after injury, animals included in study 2 were reanesthetized with sodium pentobarbital (70 mg/kg, intraperitoneally) and an MRI examination using a Bruker 7.0-T magnetic resonance spectrometer/imager was performed as described elsewhere (Albensi et al., 2000). Animals ($n = 11/\text{group}$) were placed in a plexiglas holder with a heating pad warmed to 37°C, and a respiratory motion detector was fastened over the thorax to facilitate respiratory gating. The plexiglas holder was then slid into proton-tuned birdcage coil, located in the center of the magnet bore. Field homogeneity across the brain was optimized, and sagittal and coronal scout images were collected to position the transverse slices throughout the brain region of interest. Multislice, multiecho T_2 -weighted images were acquired to obtain eight contiguous slices of cerebrum (field of vision, 4×4 cm; slice thickness, 2 mm; resolution, 256×256 ; repetition time to echo time, 2,000/20 milliseconds; four echo images and two averages). Lesion volumes were estimated from the summation of areas of hyperintensity in cerebrum on each slice, multiplied by slice thickness, for both ipsilateral and contralateral hemispheres, using Bruker Paravision 2.1 imaging software. Average lesion volume for each group (\pm SEM in μL) was calculated. A comparison was made between injured animals treated with 35b and those receiving vehicle after injury.

Magnetic resonance spectroscopy

Magnetic resonance spectra were obtained as detailed elsewhere (Vink et al., 1990). Briefly, animals were placed in a specially constructed, temperature-controlled plexiglas holder and a 5×9 -mm surface coil was placed centrally around the craniotomy site. Skin and muscle were retracted away from the coil to prevent contributions from these tissues. The animals were inserted into the center of a 7.0-T magnet interfaced with a Bruker spectrometer, and field homogeneity was optimized on the water signal before acquisition of phosphorus spectra. Phosphorus spectra were obtained in 30-minute blocks before and for 4 hours after induction of fluid percussion-induced TBI using a 90° pulse calibrated for a 2-mm cortical depth, a 700-millisecond delay time, and a 4,000-Hz spectral width containing 2,048 data points. Rectal temperature and respiration were monitored at all times. Anesthesia was maintained via intravenous sodium pentobarbital ($15 \text{ mg} \cdot \text{kg}^{-1} \cdot \text{h}^{-1}$). At the conclusion of the 4-hour acquisition period, animals were removed from the magnet and returned to their cages after their wounds were closed.

Phosphorus magnetic resonance spectra were analyzed using a Bruker computer software program. Following convolution difference (400/20 Hz), chemical shifts and integrals of the individual peaks were determined after line fitting. Intracellular pH, brain free-magnesium concentration, and cytosolic phosphorylation potential were then determined as described in detail elsewhere (Vink et al., 1990). Briefly, intracellular pH was determined from the chemical shift of the inorganic phosphate

peak (δP_i) relative to phosphocreatine in the magnetic resonance spectra using the following equation:

$$\text{pH} = 6.77 + \log \left(\frac{\delta P_i - 3.29}{5.68 - \delta P_i} \right) \quad (1)$$

Similarly, free-magnesium concentration was determined from the chemical shift difference between the α and β peaks of ATP (Gupta et al., 1978) using the following equation:

$$[\text{Mg}^{2+}] = K_d \left(\frac{10.82 - \delta_{\alpha-\beta}}{\delta_{\alpha-\beta} - 8.35} \right) \quad (2)$$

where X is the chemical shift difference between the α and β peaks of ATP. The K_d for MgATP was initially assumed to be 50 $\mu\text{mol/L}$ at a pH 7.2 and an ionic strength of 0.15 mol/L, and was corrected for pH according to the method described by Bock et al. (1987).

Cytosolic phosphorylation potential (PP) was determined according to the following equation:

$$\text{PP} = \frac{[\Sigma \text{ATP}]}{[\Sigma \text{ADP}][\Sigma P_i]} \quad (3)$$

where Σ represents all the ionic forms of the free species. The concentration of ADP was calculated from the creatine kinase equilibrium equation after correcting the equilibrium constant for pH and free-magnesium concentration as described in detail elsewhere (Vink et al., 1994). Concentrations of the other metabolites were determined from the integrated peak areas of the respective MRS peaks, assuming that the normal, preinjury values for phosphocreatine and ATP were 4.72 and 2.59 $\mu\text{mol/g}$, respectively, and that the total creatine pool remained constant at 10.83 $\mu\text{mol/g}$ (Siesjo, 1981; Veech et al., 1979). Brain water content was assumed to be 80%, with the intracellular compartment accounting for 78% of the total water (Siesjo, 1981).

In vitro studies

Preparation of neuronal–glial cocultures. The preparation of neuronal–glial cocultures and description of the traumatic injury model have been previously detailed (Mukhin et al., 1998). Briefly, glial cells were obtained from neonatal Sprague-Dawley (Taconic, Germantown, NY, U.S.A.) rat cortices. After decapitation and removal of meninges, the cortices were minced with scissors and triturated in magnesium and calcium-free Hank balanced salt solution supplemented with 1% 1 mol/L HEPES (pH 7.0) and 1% 100 mmol/L sodium pyruvate. The dissociated cell preparation was seeded (0.25 hemisphere/plate) on 96-well plates (#831835300; Sarstedt, Newton, NC, U.S.A.) in minimal essential Eagle medium with Earle salts (MEM) containing 10% each of fetal bovine and equine serums, 25 mmol/L HEPES (pH 7.2), 2 mmol/L glutamine, 20 mmol/L glucose, 10 ng/mL epidermal growth factor, and 1% antibiotic–antimycotic. At 9 days *in vitro* (DIV), a new neuronal layer was prepared from cortices of day 18 gestation rat embryos dissociated as described for glia. Cells from this dissociation were seeded (2 to 2.5×10^6 cells/plate) on the glial cultures. Solutions were identical to those used for glial culture preparation with the exception that the seeding media contained 5% each of bovine and equine serums, but no epidermal growth factor. At 4 DIV after the second seeding, 3 mmol/L cytosine arabinoside was added to the feeding medium to stop proliferation of nonneuronal cells. Cultures were fed twice weekly until used for experiments 18 to 21 DIV. Cultures were fed by replacing one third of the media with fresh media. Feeding

media was identical to that used for the second seeding with the exception that only equine serum (5%) was added until 11 DIV, after which time serum was excluded.

Radioligand binding assays. 35b was screened at a total of 50 receptors, channels, and transporters using the resources of the NIMH Psychoactive Drug Screening Program at a concentration of 10 $\mu\text{mol/L}$ in quadruplicate (see online protocols at: <http://pdsp.cwru.edu/nimh/binding.htm>). Where >50% inhibition was measured, K_i determinations were done using concentrations spanning 1 to 10,000 nmol/L with replicate determinations done in duplicate. K_i values were calculated using GraphPad Prism (GraphPad Software, San Diego, CA, U.S.A.).

Injury in vitro. Before each experiment, the culture medium was replaced with incubation media (IM) containing MEM plus 10 mmol/L HEPES (pH 7.2 to 7.4), 1 mmol/L glutamine, and 20 mmol/L glucose. For staurosporine-induced injury, a 100 mmol/L stock solution of staurosporine (Sigma, St. Louis, MO, U.S.A.) in dimethyl sulfoxide was diluted with IM, with or without 35b, and added to cultures at a final concentration of 0.1 $\mu\text{mol/L}$. For maitotoxin injury, cells were incubated with maitotoxin (Alexis Biochemicals, San Diego, CA, U.S.A.) dissolved in IM at a final concentration of 0.1 nmol/L with or without 35b. Before induction of injury via mechanical trauma, cultures were pretreated with or without 35b in IM for 15 minutes. For trauma, cells were then injured with a mechanical punch device that delivered 28 parallel, uniformly distributed cuts to the surface of the culture. This *in vitro* trauma model has been well characterized by us and causes secondary neuronal cell death that is largely necrotic and which can be attenuated with a variety of neuroprotective strategies that parallel effects in animal TBI models (Mukhin et al., 1996, 1998). Thirty minutes after mechanical injury, or 1 hour after incubation with maitotoxin, IM media was replaced with fresh IM plus 1% antibiotic-antimycotic with or without 35b, as appropriate. Sixteen to 18 hours after all injuries, 50% of the media (75 μL) was removed and analyzed for the presence of lactate dehydrogenase (LDH) activity as an index of cell death, as previously described (Gupta et al., 1978).

Lactate dehydrogenase activity measurements. The LDH reagent (5 mmol/L β -NAD, 25 mmol/L lactic acid, 0.3% bovine serum albumin, 100 mmol/L Tris, 0.9% NaCl, final pH 8.45, room temperature) was added to each well (4:1 volume) and optical density (340 nm) was measured on a Ceres 900 microplate reader (Biotek Instruments, Winooski, VT, U.S.A.) at 5-second intervals over a 5-minute period. The slope of the curve of absorbance measurements over 250 seconds represented LDH activity. Lactate dehydrogenase measurements correlate in this model to other measures of cell death (viability including trypan blue and ethidium homodimer [Mukhin et al., 1997, 1998]).

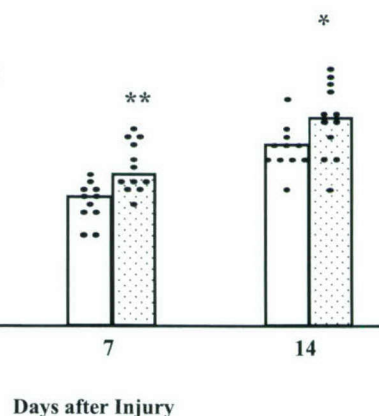
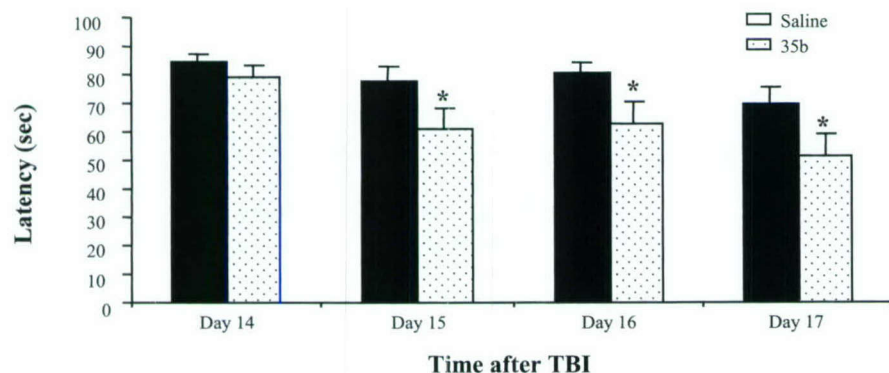


FIG. 3. Effect of 35b on motor recovery after moderately severe (2.6 to 2.7 atmospheres) lateral fluid percussion injury in the rat. 35b (1 mg/kg, intravenously, $n = 12$) or saline vehicle ($n = 11$) was administered 30 minutes after injury. Columns represent median values for each treatment group, whereas each dot represents an individual animal score. * $P < 0.05$, ** $P < 0.01$ versus saline group.

Data analysis. Continuous variables compared across groups were examined using an analysis of variance (ANOVA) followed by Bonferroni correction (acute reflexes). Continuous variables subjected to repeated measurements over a period of time (cardiovascular and core temperature measurements and water maze studies) were analyzed using a repeated-measures ANOVA followed by Tukey pairwise comparison at each time point. Ordinal measurements (composite neurologic scores) were evaluated using the nonparametric Kruskal-Wallis ANOVA with individual, nonparametric Mann-Whitney U tests corrected for multiple comparisons. TUNEL data were analyzed with a t -test. For *in vitro* studies, data were expressed as the percentage of LDH release in treated cultures compared with that induced by injury alone, with LDH from uninjured controls subtracted from all values. Bars represent the mean \pm SD for measurements for $n = 25$ to 30 wells per condition. Analysis of variance followed by t -tests with Bonferroni corrections for multiple comparisons were used for comparisons of treated, injured groups and untreated, injured groups; $P < 0.05$ was considered to reflect a statistically significant difference.

RESULTS

Neurologic outcome after traumatic brain injury

Study 1 examined the effects of 35b administration on motor and cognitive deficits induced by lateral fluid

FIG. 4. Latency to find the hidden platform in a version of the Morris water maze (study 1). Results are expressed as daily mean \pm SEM for each group over four trials. * $P < 0.05$ versus saline group. TBI, traumatic brain injury.

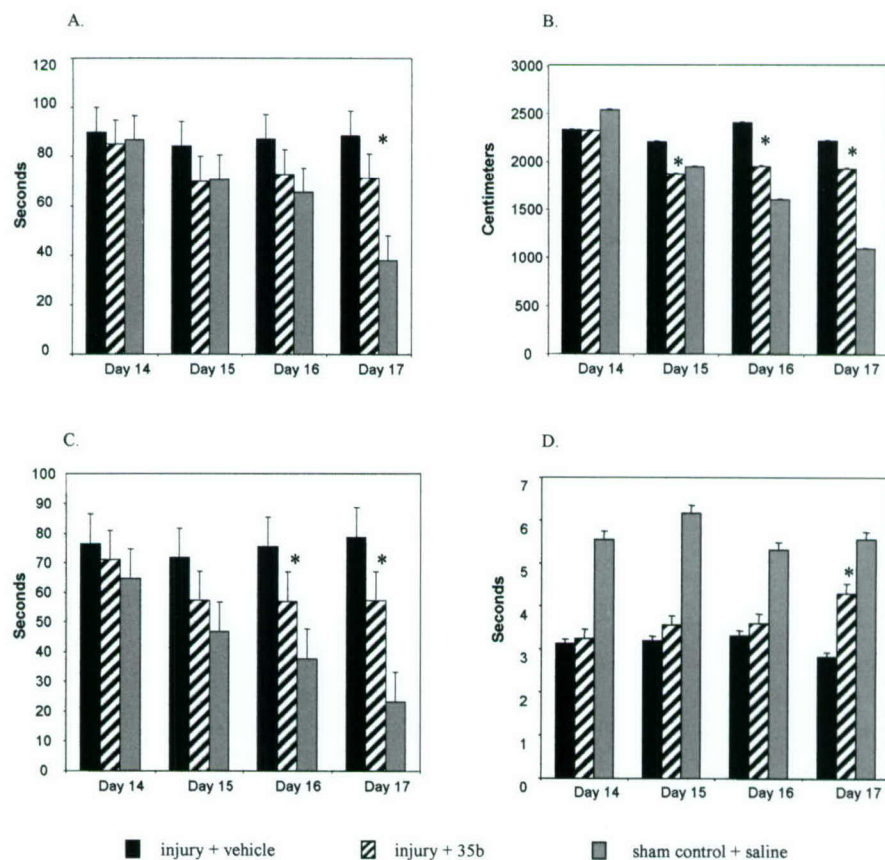


FIG. 5. The effects of 35b on Morris water maze performance after traumatic brain injury as assessed using a computerized video system to acquire data on multiple outcomes. Bars represent the mean \pm SEM averaged from the four trials. * $P < 0.05$ versus fluid percussion injury (injury + vehicle) from the same day. (A) Latency required to find a hidden platform (goal latency). (B) Distance covered to find the hidden platform. (C) Time spent in periphery while searching for the platform. (D) Time spent in the zone encompassing the platform.

percussion injury. Significantly improved composite neurologic scores were observed 7 and 14 days after trauma in 35b-treated animals compared with vehicle-treated controls (Fig. 3). For spatial learning, the latency to find the submerged platform was significantly reduced on all testing days after the initial training day (Fig. 4).

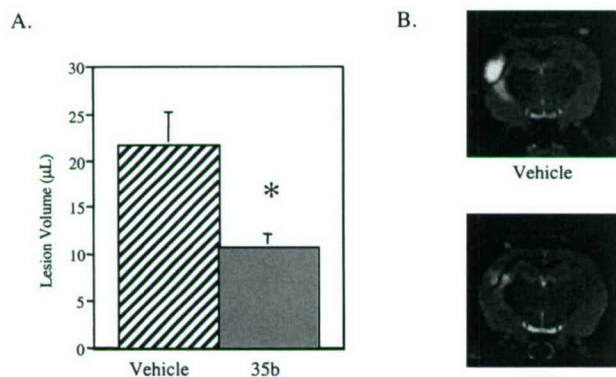


FIG. 6. Effect of 35b on lateral fluid percussion-induced lesion volume 21 days after injury in the rat. Data are from rats treated 1 hour after injury with 35b or saline vehicle. (A) Lesion volumes (mean \pm SEM) and (B) representative T_2 -weighted magnetic resonance imaging of vehicle- and 35b-treated rats. Regions of marked hyperintensity are evident in the hippocampus, cortex, and corpus callosum. * $P < 0.05$ versus vehicle.

Study 2 examined the effects of 35b injection on trauma-induced cognitive deficits, measured and analyzed in detail using the aforementioned PC-controlled video system for tracking and analyzing animal behavior. Parameters such as latency required to find a submerged resting platform, swim speed and distance, and time spent in periphery and in the central zone adjacent to the platform were evaluated and compared in 35b-treated injured, vehicle-treated injured, and sham-control animals (Fig. 5). The swim speed was similar in both 35b- and vehicle-treated injured groups (27 ± 6 vs. 25 ± 5 cm/s; data not shown). The latency necessary to find the platform in sham-operated controls was 38 ± 5 seconds. Administration of 35b significantly ($P < 0.05$) reduced mean latency on the fourth test day (day 17 after trauma) compared with the vehicle-treated injured group (71 ± 7 vs. 89 ± 8 seconds; Fig. 5A). Furthermore, 35b-treated animals covered less distance to the platform ($1,948 \pm 21$ and $1,927 \pm 18$ cm vs. $2,407 \pm 17$ and $2,214 \pm 15$ cm, respectively; $P < 0.05$) than the nontreated animals on postinjury days 16 and 17, respectively (Fig. 5B). At the same time points, injured animals receiving 35b spent less time in periphery compared with the traumatized vehicle-treated group (57 ± 6 and 57 ± 8 seconds vs. 76 ± 8 and 79 ± 7 seconds; $P < 0.05$; Fig. 5C). Additionally, the 35b group spent more time in the central zone than the

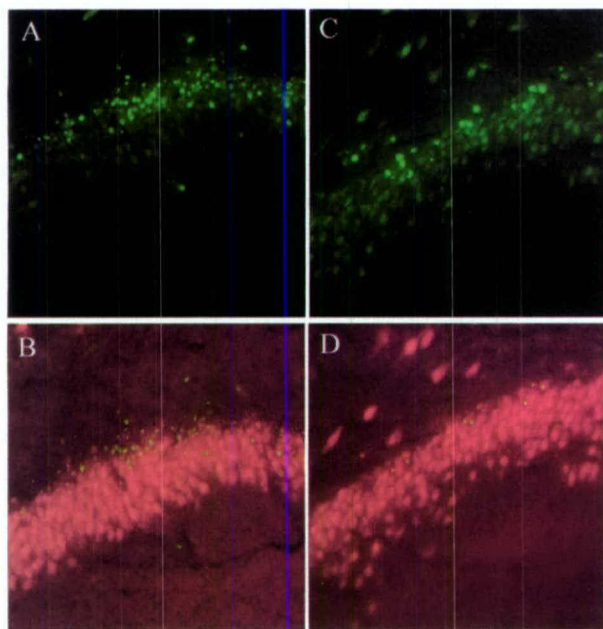
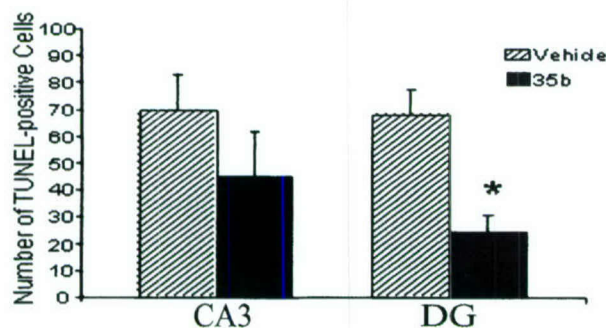
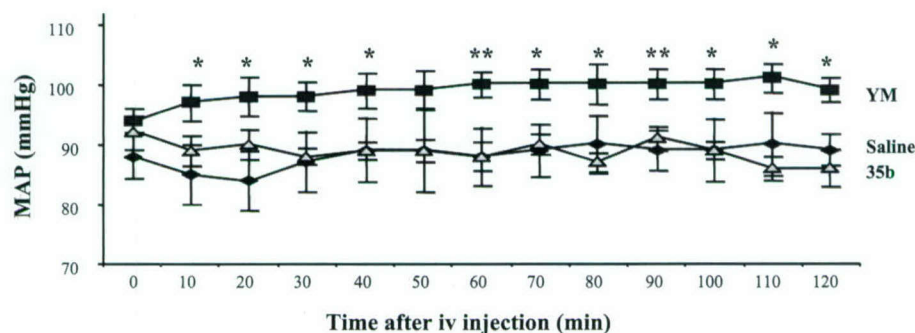


FIG. 7. Effect of 35b on apoptotic cell death after traumatic brain injury. 35b (1.0 mg/kg or vehicle) was injected 30 minutes after moderately severe lateral fluid percussion injury. The number of TUNEL-positive cells in the ipsilateral hippocampus was then quantified 24 hours later. Bars on graph indicate the mean \pm SEM of TUNEL-positive cells in the CA3 and dentate granule (DG) cell layers for each treatment group as indicated. (A and C) Images of TUNEL-positive cells in the DG cell layer in vehicle- and 35b-treated groups, respectively. (B and D) Images of TUNEL-positive cells in the DG cell layer in vehicle- and 35b-treated groups, respectively, showing double-label staining of TUNEL together with anti-NeuN, a neuronal marker antibody colabel. TUNEL-positive-only cells are green, anti-NeuN-only cells are red, and TUNEL-positive anti-NeuN colabeled cells are yellow.

FIG. 8. Graph of mean arterial blood pressure (MAP) up to 120 minutes after vehicle or drug administration (1 mg/kg) in the fully conscious and unrestrained rat. Rats treated with 35b ($n = 6$) did not differ significantly from saline-treated controls ($n = 6$). Rats treated with YM-14673 ($n = 6$), however, maintained a significantly higher MAP over the 120-minute testing period ($P < 0.05$).



vehicle-treated group on the fourth day of testing (4.30 ± 0.30 vs. 2.83 ± 0.19 seconds; $P < 0.05$) (Fig. 5D).

Magnetic resonance imaging lesion volume measurement

T_2 -weighted images were used to assess lesion volume by MRI at 21 days after injury. Changes in magnetic resonance signal in injured animals were evident as increases in pixel intensity. Regions of hyperintensity were observed principally in the ipsilateral hemisphere, encompassing not only cortex and hippocampus but also the subcortical white matter tracts such as corpus callosum. Administration of 35b significantly ($P < 0.05$) reduced lesion volumes compared with the injured vehicle-treated animals (10.77 ± 1.39 vs. 21.75 ± 3.56 μ L; Fig. 6).

TUNEL staining after traumatic brain injury

The TUNEL-positive cells were distributed throughout the ipsilateral cortex of all animals 24 hours after TBI. In addition, TUNEL-positive cells were observed in the CA3, CA4/hilus and granule cell layer of the hippocampus. However, the number of TUNEL-positive cells in the granule cell layer of the hippocampus was significantly lower in 35b-treated rats compared with vehicle-treated controls ($P < 0.05$ for treated vs. control; Fig. 7).

Autonomic and analeptic studies

After 35b treatment, there were no significant effects on blood pressure, body temperature, TSH activity, or latency to recover the righting reflex (Figs. 8 to 11). Blood pressures were indistinguishable between 35b- and vehicle-treated, uninjured animals examined over a 2-hour period, whereas YM-16743 caused a rapid (<10 -minute) and sustained (>2 -hour) pressor effect. Animals subjected to TBI showed a transient pressor response (30–50 mm Hg for 10–20 seconds), followed by a transient drop in pressure below the original baseline (20–40 mm Hg for 5–15 minutes). In all TBI studies, drugs were injected 30 minutes after injury, when the initial TBI-induced changes had stabilized. Nevertheless, the blood pressure was monitored for an additional 30 minutes after injection in approximately one third of the animals (selected at random). Only one of these animals, a vehicle-treated injured control, showed transient pressor

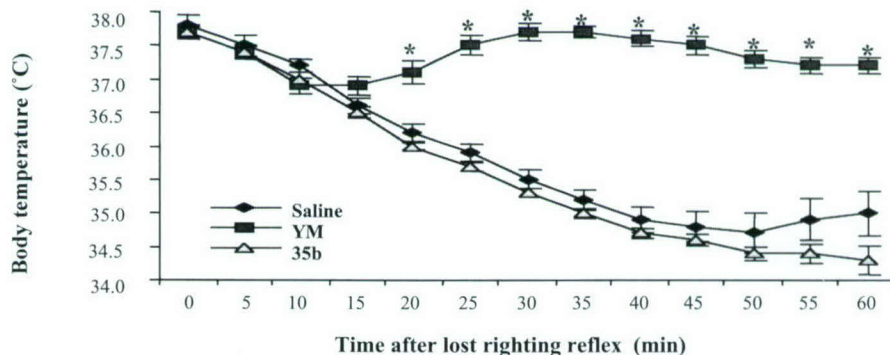


FIG. 9. Effect of vehicle and thyrotropin-releasing hormone analogs (1 mg/kg; $n = 6$ for each group) on core body temperature in the lightly anesthetized rat. All treatment groups, with the exception of animals receiving YM-14673, exhibited a pronounced decrease in body temperature up to 60 minutes after loss of righting reflex. The YM-14673-treated group maintained normothermia for the duration of testing, with temperatures differing significantly from vehicle- or 35b-treated animals 20 to 60 minutes after loss of righting reflex ($P < 0.01$).

response (5 minutes) after injection. It was not possible to assess the effect of 35b on core body or brain temperature after TBI, because injured animals were routinely maintained on feedback-controlled heating pads to exclude the effect of temperature on TBI-associated outcomes.

Magnetic resonance spectroscopy studies

After injury, there were no significant changes in pH or ATP concentration as determined from the magnetic resonance spectra (Fig. 12), which is consistent with previous results using this severity of injury (Vink et al., 1996). There was, however, a marked decline in brain free-magnesium concentration after injury in both groups. Before injury, brain free-magnesium in all animals ($n = 10$) was 0.47 ± 0.05 mmol/L. After injury, magnesium levels declined in both groups to reach a minimum value of 0.30 ± 0.04 ($P < 0.05$) by 2 hours after trauma. The free-magnesium concentration did not change significantly from this value for the remainder of the 4-hour magnetic resonance monitoring period. Similarly, cytosolic phosphorylation potential declined in both treatment groups from a preinjury value of 41 ± 5 mmol/L $^{-1}$ ($n = 10$) to 21 ± 4 mmol/L $^{-1}$ ($P < 0.05$) by 2 hours after trauma. There was no significant change from this value for the remainder of the magnetic resonance monitoring period. At no point was there a significant difference between the two treatment groups.

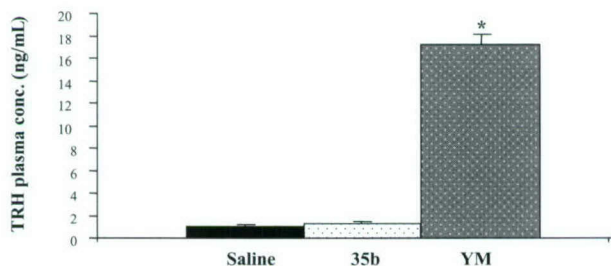


FIG. 10. Graph of mean (\pm SEM) plasma thyrotropin-releasing hormone (TRH) levels 30 minutes after saline or drug (1 mg/kg) administration. Rats treated with YM-14673 exhibited significantly elevated levels of TRH when compared with saline controls. TRH levels in 35b-treated rats did not differ significantly from those of saline controls ($*P < 0.0001$ versus saline control).

In vitro studies

As shown in Fig. 13, 1 μ mol/L 35b significantly attenuated cell death, as reflected by LDH release in three different models of neuronal cell death. Greatest neuroprotective actions (approximately 5%) were found with maitotoxin-induced neuronal death, a model of cellular necrosis (Zhao et al., 1999). Lactate dehydrogenase release was reduced by approximately 30% after mechanical trauma in a model that causes predominantly necrotic cell death (Mukhin et al., 1998). Approximately 30% protection was also found for treatment of staurosporine in cleaved cell death, a classical model of neuronal apoptosis (Koh et al., 1995).

Receptor-binding profiles for 35b

35b was screened at a total of 50 receptors, channels, and transporters using the resources of the NIMH Psychoactive Drug Screening Program (Table 1) at a 10- μ mol/L concentration. At only three cloned receptor preparations (M_1 , M_3 , and M_4 -muscarinic receptors) was significant inhibition measured, though the K_i values for 35b were still quite low (Table 1) and likely to be insignificant. These results indicate that 35b does not interact with high affinity at any of the tested receptors, channels, or transporters.

DISCUSSION

The present studies show that a novel diketopiperazine, derived from a modified TRH analog, exhibits

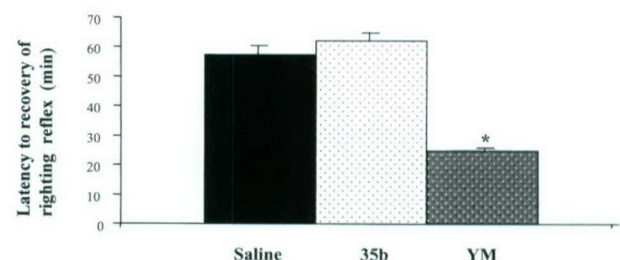


FIG. 11. Effect of vehicle and thyrotropin-releasing hormone (TRH) analogs (1 mg/kg) on latency to recovery of righting reflex after light anesthesia. Rats treated with YM-14673 recovered this function significantly earlier than any of the other treatment groups ($*P < 0.0001$). Rats treated with 35b did not differ significantly from saline treated controls.

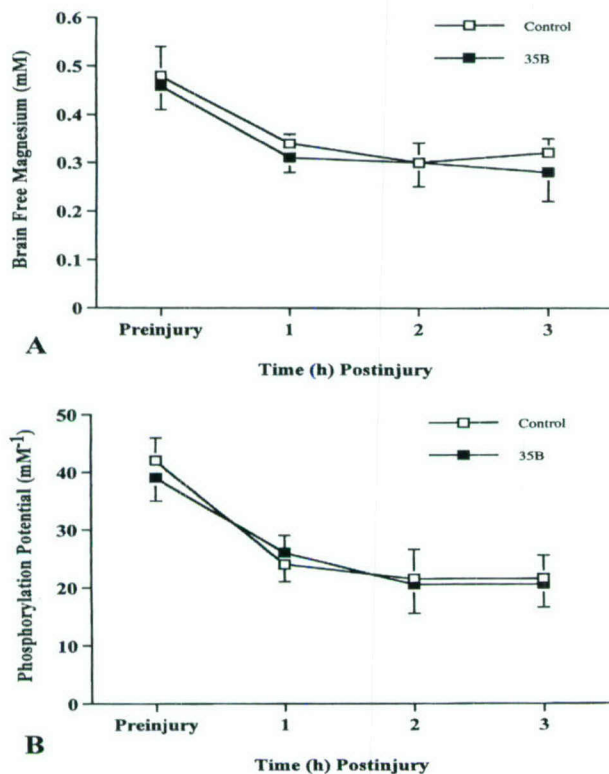


FIG. 12. Effect of 35b on cerebral metabolism and free magnesium after moderately severe (2.6 to 2.7 atmospheres) traumatic brain injury (TBI). Change in cytosolic phosphorylation potential from before injury up to 3 hours immediately after TBI is shown in **A**. Filled squares represent mean values for rats treated with 35b (1 mg/kg, intravenously) at 30 minutes after injury ($n = 5$). Unfilled squares represent data from saline controls ($n = 5$). The change in cerebral intracellular free-magnesium concentration after TBI is shown in **B**. These data are from the same animals and experiment described in **A**.

substantial neuroprotective effects *in vitro* and *in vivo*. Fluid percussion-induced TBI models certain components of human head injury (McIntosh et al., 1987) and has been used extensively both to study pathobiologic mechanisms and to evaluate neuroprotective treatment strategies (Faden, 1996a). Treatment with 35b, administered systemically after the insult, significantly enhanced both motor and cognitive recovery in rats subjected to TBI. Using the Morris water maze as an assessment tool, 35b-treated rats showed reduced latencies to find the submerged platform, decreased path length, and greater swim time near the platform. These findings did not reflect differences in swim speed, which did not differ between groups. Treatment with 35b reduced lesion volumes, as shown by T₂-weighted MRI, and decreased the number of TUNEL-positive neurons in ipsilateral hippocampus, which indicate the 35b is neuroprotective *in vivo*. Such neuroprotective effects were reproduced *in vitro* using a well-characterized trauma (punch) model in rat neuronal–glial cocultures (Mukhin et al., 1996, 1998).

Compound 35b is one of a class of diketopiperazines derived from modified TRH analogs. Thyrotropin-releasing hormone itself is metabolized to form CHP, a diketopiperazine that has been shown to have considerable physiologic activity (Metcalf, 1982). It has been reported to have thermoregulatory actions, anorectic effects, and analgesic activity; some of these properties may reflect opioid and dopaminergic mechanisms (Prasad, 1995). Although there are no reports that CHP has neuroprotective activity, it is not clear to what extent this issue has been directly addressed. Interestingly, CHP

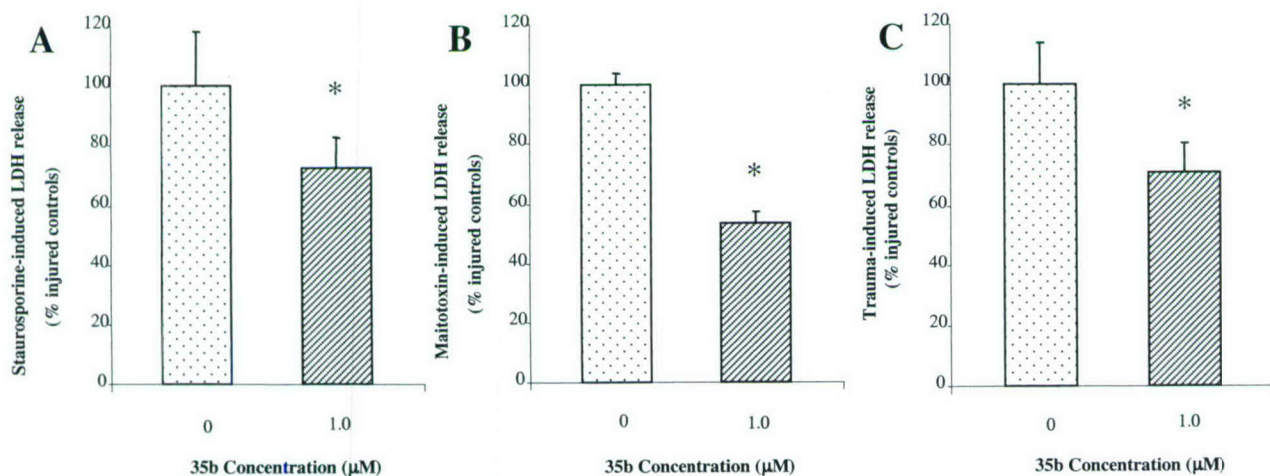


FIG. 13. Effect of 35b on lactate dehydrogenase (LDH) release in three different *in vitro* models of cell death: apoptotic death induced by staurosporine (**A**); necrotic death induced by maitotoxin (**B**); traumatic death induced by a punch model that produces both initial physical disruption and later secondary death (**C**). Bars represent means and standard deviations for LDH released 16 to 18 hours after injury in untreated injured cultures (dots) or injured cultures treated with 35b (diagonal lines) ($n = 25$ to 30 wells per condition). In **A**, cultures were incubated with 0.3-μmol/L staurosporine for 16 to 18 hours in the presence or absence of 35b. In **B**, cultures were incubated with 0.1-nmol/L maitotoxin for 1 hour in the presence or absence of 35b. Cultures were then washed and incubated for 16 to 18 hours with or without 35b, as appropriate. In **C**, 35b or media vehicle was present for 30 minutes before injury. Cells were then injured with a mechanical punch that delivered 28 parallel, uniformly distributed cuts to the surface of the cell layer. Thirty minutes after injury, cultures were washed again and incubated with 35b or vehicle, as appropriate, for 16 to 18 hours.

TABLE 1. Receptor-binding profile of 35b

Receptor	Cold ligand	³ H ligand	kd (nmol/L)	Assay concentration (nmol/L)	Ki value
5HT _{1A}	WAY 100,635	8-OH-DPAT	1	0.5	>10,000
5HT _{1B}	Ergotamine	GR125743	0.3	0.3	>10,000
5HT _{1D}	Ergotamine	GR125743	0.3	0.3	>10,000
5HT _{1E}	5HT	5HT	7.2	3	>10,000
r5HT _{2A}	Chlorpromazine	Ketanserine	0.8	0.5	>10,000
r5HT _{2C}	Chlorpromazine	Mesulergine	1.2	0.5	>10,000
5HT _{5A}	Ergotamine	LSD	1.6	1	>10,000
5HT ₆	Chlorpromazine	LSD	1.5	1	>10,000
5HT ₇	Chlorpromazine	LSD	2	1	>10,000
D ₁	SKF38393/fluphenazine	SCH23390	0.35	0.2	>10,000
D _{2L}	Haloperidol	N-Methylspiperone	0.5	0.2	>10,000
D ₃	Chlorpromazine	N-Methylspiperone	0.4	0.2	>10,000
D ₄	Chlorpromazine	N-Methylspiperone	0.5	0.2	>10,000
D ₅	SKF38393/olazapine	SCH23390	0.3	0.2	>10,000
M ₁ -muscarinic	Atropine	Quinuclidinyl benzilate	0.2	0.7	7,649 ± 2,475
M ₂ -muscarinic	Atropine	Quinuclidinyl benzilate	0.2	0.7	>10,000
M ₃ -muscarinic	Atropine	Quinuclidinyl benzilate	0.2	0.7	4,695 ± 2,105
M ₄ -muscarinic	Atropine	Quinuclidinyl benzilate	0.2	0.7	4,302 ± 1,854
M ₅ -muscarinic	Atropine	Quinuclidinyl benzilate	0.2	0.7	>10,000
α _{1A} -Adrenergic	Prazosin	[¹²⁵ I]-HEAT	0.02	0.02	>10,000
α _{1B} -Adrenergic	Prazosin	[¹²⁵ I]-HEAT	0.02	0.02	>10,000
α _{1D} -Adrenergic	Prazosin	[¹²⁵ I]-HEAT	0.02	0.02	>10,000
α _{2A} -Adrenergic	Epinephrine	[¹²⁵ I]-Iodoclonidine	0.2	0.1	>10,000
α _{2B} -Adrenergic	Epinephrine	[¹²⁵ I]-Iodoclonidine	0.2	0.1	>10,000
α _{2C} -Adrenergic	Epinephrine	[¹²⁵ I]-Iodoclonidine	0.2	0.1	>10,000
β ₁ -Adrenergic	Isoproterenol	[¹²⁵ I]-Iodopindolol	0.1	0.05	>10,000
β ₂ -Adrenergic	Isoproterenol	[¹²⁵ I]-Iodopindolol	0.1	0.05	>10,000
MOR	Naloxone	Diprenorphine	0.2	0.2	>10,000
DOR	Naltrindole	Diprenorphine	0.2	0.2	>10,000
KOR	Naloxone	Bremazocine	4	2	>10,000
SERT	Fluoxetine	Citalopram	0.8	0.5	>10,000
NET	Nortriptyline/imipramine	Nisoxetine	1.2	0.5	>10,000
bDAT	4',4''-Difluoro-3α-(diphenylmethoxy)tropane HCL	GBR12935	1	0.5	>10,000
H1	Chlorpheniramine	Pyrimilamine	3.6	1	>10,000
rNMDA (PCP site 1)	MK801	MK801	4.6	1	>10,000
rBZP	Diazepam	RO 15-1788	0.8	0.4	>10,000
rGABA _A	GABA	Muscimol		3	>10,000
rGABA _B	GABA	Baclofen		15	>10,000
Vasopressin-V ₁	Vasopressin	Vasopressin	2	1	>10,000
Vasopressin-V ₂	Vasopressin	Vasopressin	2	1	>10,000
Vasopressin-V ₃	Vasopressin	Vasopressin	2	1	>10,000
α ₂ /β ₂	(-)-Nicotine	(+)-Epibatidine	0.02	0.1	>10,000
α ₂ /β ₄	(-)-Nicotine	(+)-Epibatidine	0.08	0.1	>10,000
α ₃ /β ₂	(-)-Nicotine	(+)-Epibatidine	0.03	0.1	>10,000
α ₃ /β ₄	(-)-Nicotine	(+)-Epibatidine	0.3	0.1	>10,000
α ₄ /β ₂	(-)-Nicotine	(+)-Epibatidine	0.04	0.1	>10,000
α ₄ /β ₂	(-)-Nicotine	(+)-Epibatidine	0.05	0.1	>10,000
α ₄ /β ₄	(-)-Nicotine	(+)-Epibatidine	0.09	0.1	>10,000
OT	Oxytocin	Oxytocin	0.89		>10,000
rPCP	PCP/ketamine	TCP	1	0.5	>10,000

Ki values represent mean ± SEM of 2 to 3 separate determinations, each performed in duplicate, and are given in nanomoles per liter. Radioligands, unless otherwise specified, were tritium (³H) labeled. All receptor preparations represent human cloned receptors unless otherwise specified (r, rat; b, bovine).

may increase cerebral blood flow (Koskinen, 1986; Prasad, 1995), and it may have antioxidant activity (Prasad, 1995; Shvachkin et al., 1989). This dipeptide, however, does not appear to have any nootropic activity and may even disrupt some forms of learning (Andrews and Sahgal, 1983, 1984; Prasad, 1995).

In our studies, 35b did not alter hypothermia associated with pentobarbital administration, nor did it show analeptic or endocrine actions exhibited by TRH or tra-

ditional TRH analogs. These observations are consistent with the finding that 35b does not bind to high-affinity TRH receptors (M. Gershengorn, unpublished observation, 2001) and indicates that this diketopiperazine may have substantial advantages over TRH or traditional TRH analogs as potential neuroprotective agents. For example, the absence of pressor effects may be an advantage in a patient with significant posttraumatic hemorrhage, and the absence of eutermic actions would

permit associated hypothermia treatment. Moreover, the lack of analeptic actions would permit the use of sedative or anesthetic agents.

It is noteworthy that 35b administration significantly attenuated both necrosis-related and apoptosis-related neuronal cell death *in vitro*. It strongly antagonized the neurotoxic effects of maitotoxin, a marine toxin that causes a marked influx of calcium and has recently been used as a model of neuronal necrosis *in vitro* (Zhao et al., 1999). Significant neuroprotective effects for 35b were also found in our mechanical trauma culture model (Mukhin et al., 1998), which causes necrotic cell death that is largely mediated by glutamate receptors (Mukhin et al., 1997, 1998). In contrast, staurosporine has been commonly used to induce apoptotic cell death in cultured neurons (Koh et al., 1995). In our staurosporine-treated cultures, neurons showed morphologic features of apoptosis. Treatment with 35b significantly reduced such cell death. Both necrosis and apoptosis occur after TBI and appear to contribute to the subsequent neurologic dysfunction. Moreover, studies *in vitro* and *in vivo* suggest that attenuation of posttraumatic necrosis may exacerbate apoptosis (Pohl et al., 1999) and that blockade of both cell death pathways may have additive or synergistic neuroprotective effects (Allen et al., 1999). Therefore, the ability of 35b to attenuate each type of cell death may explain its striking neuroprotective activity.

Unlike TRH or traditional TRH analogs, 35b did not affect cellular bioenergetic state or magnesium homeostasis, and does not affect cerebral blood flow (L. O. Koskinen, unpublished observation, 2001). The lack of effect on blood flow may relate to its lack of pressor action in a subject that has lost its autoregulatory ability. That 35b did not modulate magnesium homeostasis or cellular bioenergetic after trauma was unexpected because these have been postulated to be major mechanisms by which TRH/TRH analogs exert their neuroprotective activity (Faden et al., 1990; McIntosh et al., 1988; Vink et al., 1988).

35b did not show appreciable receptor binding to a large number of other classical neurotransmitter or neuromodulator receptors, including glutamate, opioid, cholinergic, adrenergic, or serotonergic receptors (Table 1). Many of these receptors have been implicated in secondary injury after trauma. The ability, however, of TRH to antagonize the effects of many factors linked to secondary injury (e.g., endogenous opioids, platelet-activating factor, leukotrienes, and perhaps glutamate) may reflect so-called physiologic antagonism and has not been linked to specific receptor systems. Another possibility that should be addressed is whether these diketopiperazines modulate the regulation of genes or gene products associated with necrotic or apoptotic cell death.

In summary, we report the development of a novel cyclic dipeptide that has substantial neuroprotective ac-

tions *in vitro* and that enhances both motor and cognitive recovery *in vivo*. Neuroprotective mechanisms associated with this compound are likely to be multifactorial and may involve attenuation of both necrotic and apoptotic pathways of cell death.

Acknowledgments: The authors thank Mike O'Reilly, Elena Kazanova, Alejandro Hidalgo, and Svetlana Ivanova for technical assistance.

REFERENCES

- Albensi BC, Knobloch SM, Chew BG, O'Reilly MP, Faden AI, Pekar JJ (2000) Diffusion and high resolution MRI of traumatic brain injury in rats: time course and correlation with histology. *Exp Neurol* 162:61–72
- Allen JW, Knobloch SM, Faden AI (1999) Combined mechanical trauma and metabolic impairment *in vitro* induces NMDA receptor-dependent neuronal cell death and caspase-3-dependent apoptosis. *FASEB J* 13:1875–1882
- Andrews JS, Sahgal A (1983) Central administration of thyrotropin-releasing hormone and histidyl-proline-diketopiperazine disrupts the acquisition of a food rewarded task by a non-aversive action. *Regul Pept* 7:373–383
- Andrews JS, Sahgal A (1984) The effects of thyrotropin-releasing hormone on a visual discrimination task in rats. *Pharmacol Biochem Behav* 21:715–719
- Bassiri RM, Utiger RD (1973) Metabolism and excretion of exogenous thyrotropin-releasing hormone in humans. *J Clin Invest* 52:1616–1619
- Bock JL, Wenz B, Gupta RK (1987) Studies on the mechanism of decreased NMR-measured free magnesium in stored erythrocytes. *Biochim Biophys Acta* 928:8–12
- Bullock M, Lyeth B, Muizelaar J (1999) Current status of neuroprotection trials for traumatic brain injury: lessons from animal models and clinical studies. *Neurosurgery* 45:207–220
- Dixon CE, Clifton GL, Lighthall JW, Yaghmai AA, Hayes RL (1991) A controlled cortical impact model of traumatic brain injury in the rat. *J Neurosci Methods* 39:253–262
- Faden AI (1989) TRH analog YM-14673 improves outcome following traumatic brain and spinal cord injury in rats: dose-response studies. *Brain Res* 486:228–235
- Faden AI (1993) Comparison of single and combination drug treatment strategies in experimental brain trauma. *J Neurotrauma* 10:91–100
- Faden AI (1996a) Pharmacologic treatment of acute traumatic brain injury [editorial]. *JAMA* 276:569–570
- Faden AI (1996b) Pharmacological treatment approaches for brain and spinal cord trauma. In: *Neurotrauma* (Narayan RK, Wilberger JE, Povlishock JT, eds), New York, NY: McGraw-Hill, pp 1479–1490
- Faden AI (2001) Neuroprotection and traumatic brain injury: the search continues. *Arch Neurol* 58:1553–1555
- Faden AI (2002) Neuroprotection and traumatic brain injury: theoretical option or realistic proposition. *Curr Opin Neurol* 15:702–712
- Faden AI, Jacobs TP, Smith MT (1984) Thyrotropin-releasing hormone in experimental spinal injury: dose response and late treatment. *Neurology* 34:1280–1284
- Faden AI, Sacksen I, Noble LJ (1988) Structure-activity relationships of TRH analogs in rat spinal cord injury. *Brain Res* 448:287–293
- Faden AI, Ellison JA, Noble LJ (1990) Effects of competitive and noncompetitive NMDA receptor antagonists in spinal cord injury. *Eur J Pharmacol* 175:165–174
- Faden AI, Labroo VM, Cohen LA (1993) Imidazole-substituted analogues of TRH limit behavioral deficits after experimental brain trauma. *J Neurotrauma* 10:101–108
- Faden AI, Fox GB, Fan L, Araldi GL, Qiao L, Wang S, Kozikowski AP (1999) Novel TRH analog improves motor and cognitive recovery after traumatic brain injury in rodents. *Am J Physiol* 277:R1196–R1204
- Fox GB, Fan L, Levasseur RA, Faden AI (1998) Sustained

- sensory/motor and cognitive deficits with neuronal apoptosis following controlled cortical impact brain injury in the mouse. *J Neurotrauma* 15:599-614
- Gupta RK, Benovic JL, Rose ZB (1978) The determination of the free magnesium level in the human red blood cell by ^{31}P NMR. *J Biol Chem* 253:6172-6176
- Hamm RJ, Dixon CE, Gbadebo DM, Singha AK, Jenkins LW, Lyeth BG, Hayes RL (1992) Cognitive deficits following traumatic brain injury produced by controlled cortical impact. *J Neurotrauma* 9:11-20
- Kieffer JD, Weintraub BD, Baigelman W, Leeman S, Maloof F (1974) Homologous radioimmunoassay of thyrotrophin in rat plasma. *Acta Endocrinol (Copenh)* 76:495-505
- Knoblauch SM, Fan L, Faden AI (1999) Early neuronal expression of tumor necrosis factor- α after experimental brain injury contributes to neurological impairment. *J Neuroimmunol* 95:115-125
- Koh JY, Wie MB, Gwag BJ, Sensi SL, Canzoniero LM, Demaro J, Csernansky C, Choi DW (1995) Staurosporine-induced neuronal apoptosis. *Exp Neurol* 135:153-159
- Koskinen LO (1986) Effect of low intravenous doses of TRH, acid-TRH and cyclo(His-Pro) on cerebral and peripheral blood flows. *Br J Pharmacol* 87:509-519
- Krause JF, McArthur DL, Silverman TA, Jayaraman M (1996) Epidemiology of brain injury. In: *Neurotrauma* (Narayan RK, Wilberger JE, Povlishock JT, eds), New York, NY: McGraw-Hill, pp 13-30
- Maas AI (2001) Neuroprotective agents in traumatic brain injury. *Expert Opin Invest Drugs* 10:753-767
- McIntosh TK, Noble L, Andrews B, Faden AI (1987) Traumatic brain injury in the rat: characterization of a midline fluid-percussion model. *Cent Nerv Sys Trauma* 4:119-134
- McIntosh TK, Vink R, Faden AI (1988) An analogue of thyrotrophin-releasing hormone improves outcome after brain injury: ^{31}P NMR studies. *Am J Physiol* 254:R785-R792
- McIntosh TK, Vink R, Noble L, Yamakami I, Fernyak S, Soares H, Faden AI (1989) Traumatic brain injury in the rat: characterization of a lateral fluid-percussion model. *Neuroscience* 28:233-244
- McIntosh TK, Juhler M, Wieloch T (1998) Novel pharmacologic strategies in the treatment of experimental traumatic brain injury: 1998. *J Neurotrauma* 15:731-769
- Metcalf G (1982) Regulatory peptides as a source of new drugs—the clinical prospects for analogues of TRH which are resistant to metabolic degradation. *Brain Res* 257:389-408
- Morris R (1984) Developments of a water-maze procedure for studying spatial learning in the rat. *J Neurosci Methods* 11:47-60
- Mukhin A, Fan L, Faden AI (1996) Activation of metabotropic glutamate receptor subtype mGluR1 contributes to post-traumatic neuronal injury. *J Neurosci* 16:6012-6020
- Mukhin AG, Ivanova SA, Knoblauch SM, Faden AI (1997) New *in vitro* model of traumatic neuronal injury: evaluation of secondary injury and glutamate receptor-mediated neurotoxicity. *J Neurotrauma* 14:651-663
- Mukhin AG, Ivanova SA, Allen JW, Faden AI (1998) Mechanical injury to neuronal/glia cultures in microplates: role of NMDA receptors and pH in secondary neuronal cell death. *J Neurosci Res* 51:748-758
- Olson GL, Cheung HC, Chiang E, Madison VS, Sepinwall J, Vincent GP, Winokur A, Gary KA (1995) Peptide mimetics of thyrotrophin-releasing hormone based on a cyclohexane framework: design, synthesis, and cognition-enhancing properties. *J Med Chem* 38:2866-2879
- Pitts LH, Ross A, Chase GA, Faden AI (1995) Treatment with thyrotrophin-releasing hormone (TRH) in patients with traumatic spinal cord injuries. *J Neurotrauma* 12:235-243
- Pohl D, Bittigau P, Ishimaru MJ, Stadthaus D, Hubner C, Olney JW, Turski L, Ikonomidou C (1999) *N*-Methyl-D-aspartate antagonists and apoptotic cell death triggered by head trauma in developing rat brain. *Proc Natl Acad Sci U S A* 96:2508-2513
- Povlishock JT (1996) An overview of brain injury models. In: *Neurotrauma* (Narayan RK, Wilberger JE, Povlishock JT, eds), New York, NY: McGraw-Hill, pp 1325-1336
- Prasad C (1995) Bioactive cyclic dipeptides. *Peptides* 16:151-164
- Raghupathi R, Graham DI, McIntosh TK (2000) Apoptosis after traumatic brain injury. *J Neurotrauma* 17:927-938
- Shvachkin IP, Korshunova GA, Bavykina NI, Guliaeva NV, Dupin AM (1989) The antioxidant activity of cyclohistidylproline. *Biull Eksp Biol Med* 108:671-673
- Siesjo BK (1981) Measurements of cerebral oxygen consumption: advantages and limitations. *Eur Neurol* 20:194-199
- Smith DH, Soares HD, Pierce JS, Perlman KG, Saatman KE, Meaney DF, Dixon CE, McIntosh TK (1995) A model of parasagittal controlled cortical impact in the mouse: cognitive and histopathologic effects. *J Neurotrauma* 12:169-178
- Veech RL, Lawson JW, Cornell NW, Krebs HA (1979) Cytosolic phosphorylation potential. *J Biol Chem* 254:6538-6547
- Vink R, McIntosh TK, Weiner MW, Faden AI (1987) Effects of traumatic brain injury on cerebral high-energy phosphates and pH: a ^{31}P magnetic resonance spectroscopy study. *J Cereb Blood Flow Metab* 7:563-571
- Vink R, McIntosh TK, Faden AI (1988) Treatment with the thyrotrophin-releasing hormone analog CG3703 restores magnesium homeostasis following traumatic brain injury in rats. *Brain Res* 460:184-188
- Vink R, McIntosh TK, Rhomhanyi R, Faden AI (1990) Opiate antagonist nalmefene improves intracellular free Mg^{2+} , bioenergetic state, and neurologic outcome following traumatic brain injury in rats. *J Neurosci* 10:3524-3530
- Vink R, Golding EM, Headrick JP (1994) Bioenergetic analysis of oxidative metabolism following traumatic brain injury in rats. *J Neurotrauma* 11:265-274
- Vink R, Heath DL, McIntosh TK (1996) Acute and prolonged alterations in brain free magnesium following fluid percussion-induced brain trauma in rats. *J Neurochem* 66:2477-2483
- Yakovlev AG, Knoblauch SM, Fan L, Fox GB, Goodnight R, Faden AI (1997) Activation of CPP32-like caspases contributes to neuronal apoptosis and neurological dysfunction after traumatic brain injury. *J Neurosci* 17:7415-7424
- Yamakami I, Vink R, Faden AI, Gennarelli TA, Lenkinski R, McIntosh TK (1995) Effects of acute ethanol intoxication on experimental brain injury in the rat: neurobehavioral and phosphorus-31 nuclear magnetic resonance spectroscopy studies. *J Neurosurg* 82:813-821
- Zhao X, Pike BR, Newcomb JK, Wang KK, Posmantur RM, Hayes RL (1999) Maitotoxin induces calpain but not caspase-3 activation and necrotic cell death in primary septo-hippocampal cultures. *Neurochem Res* 24:371-382



ACADEMIC
PRESS

Available online at www.sciencedirect.com

SCIENCE @ DIRECT®

MCN
Molecular and Cellular
Neuroscience

Molecular and Cellular Neuroscience 22 (2003) 365–382

www.elsevier.com/locate/ymcne

Ceramide-induced neuronal apoptosis is associated with dephosphorylation of Akt, BAD, FKHR, GSK-3 β , and induction of the mitochondrial-dependent intrinsic caspase pathway

Bogdan A. Stoica, Vilen A. Movsesyan, Paul M. Lea IV, and Alan I. Faden*

Department of Neuroscience, Georgetown University Medical Center, Washington, DC 20057, USA

Received 4 August 2002; revised 10 October 2002; accepted 8 November 2002

Abstract

Neuronal apoptosis has been implicated as an important mechanism of cell death in acute and chronic neurodegenerative disorders. Ceramide is a product of sphingolipid metabolism which induces neuronal apoptosis in culture, and ceramide levels increase in neurons during various conditions associated with cell death. In this study we investigate the mechanism of ceramide-induced apoptosis in primary cortical neuronal cells. We show that ceramide treatment initiates a cascade of biochemical alterations associated with cell death: earliest signal transduction changes involve Akt dephosphorylation and inactivation followed by dephosphorylation of proapoptotic regulators such as BAD (proapoptotic Bcl-2 family member), Forkhead family transcription factors, glycogen synthase kinase 3- β , mitochondrial depolarization and permeabilization, release of cytochrome *c* into the cytosol, and caspase-3 activation. Bongkreikic acid, an agent that inhibits mitochondrial depolarization, significantly reduces ceramide-induced cell death and correlated caspase-3 activation. Together, these data demonstrate the importance of the mitochondrial-dependent intrinsic pathway of caspase activation for ceramide-induced neuronal apoptosis.

© 2003 Elsevier Science (USA). All rights reserved.

Introduction

Apoptotic neuronal cell death has been implicated in the pathology of head injury, spinal cord injury, and cerebral ischemia, as well as in chronic neurodegenerative disorders such as Alzheimer's disease and Huntington's disease (Bredesen, 2000; Eldadah and Faden, 2000). Caspases are a class of proteases which play a critical role in many models of neuronal apoptosis, both *in vitro* and *in vivo* (Benchoua et al., 2001; Eldadah and Faden, 2000; Oppenheim et al., 2001; Troy et al., 2001; Yakovlev and Faden, 2001). There are at least two major caspase pathways: an intrinsic pathway initiated by the release of cytochrome *c* from mitochondria resulting in the activation of caspase-9, and an extrinsic pathway initiated by ligation of receptors of the

TNFR superfamily, resulting in the activation of caspase-8 (Chinnaiyan and Dixit, 1997; Li et al., 1997; Zou et al., 1997, 1999). One of the mechanisms proposed for initiation of apoptosis through the intrinsic pathway is activation of proapoptotic Bcl-2 family members, such as BAD, followed by mitochondrial permeabilization and cytochrome *c* release (Luo et al., 1998; Zha et al., 1996).

Ceramide is a product of sphingolipid metabolism which induces a variety of cellular changes, including cell death and differentiation. A number of known apoptotic initiators, such as growth factor withdrawal, cytokines (Cifone et al., 1994; Hannun, 1996), and cytotoxic agents (e.g., chemotherapeutic agents), activate sphingolipid metabolism causing increased ceramide levels correlated to subsequent cell death (Hannun, 1996). Exogenous application of ceramide analogs causes apoptosis in primary cerebellar granule cell (CGC) cultures as indicated by DNA fragmentation assays (Saito et al., 1998), as well as increased caspase-3 activity (Marks et al., 1998). Inhibition of either transcription or translation prevents these effects, suggesting that both RNA

* Corresponding author. Department of Neuroscience, Georgetown University Medical Center, 3970 Reservoir Road, N.W., Research Building, Rm. EP12, Washington, DC 20057, USA. Fax: +1-202-687-0617.

E-mail address: fadena@georgetown.edu (A.I. Faden).

and protein synthesis are required for ceramide-induced apoptosis (Taniwaki et al., 1999). Application of ceramide increases intracellular caspase-3 levels and causes apoptosis of both cortical neurons and astrocytes (Keane et al., 1997). We have also found that increased ceramide levels are associated with induction of apoptosis by trophic withdrawal or etoposide, both in CGCs and in cortical neurons (Toman et al., 2002).

Ceramide may act through a variety of signaling molecules to modulate cell death (Goswami and Dawson, 2000; Hannun and Luberto, 2000), inhibiting the PI3K antiapoptotic/prosurvival pathway by modulating the activity of Akt. The ability of Akt to promote cell survival is based on its ability to phosphorylate on residues necessary for their inactivation several proapoptotic proteins, including BAD (Cardone et al., 1998; del Peso et al., 1997), Forkhead family transcription factor (FKHR) (Brunet et al., 1999), and—in some species—caspase-9, leading to inhibition of caspase-3 activation (Cardone et al., 1998; Datta et al., 1997).

Mitochondria represent another potential target for ceramide-induced signaling pathways (Kroesen et al., 2001). Release of cytochrome *c* from the intermembrane space of mitochondria is critical for the activation of the intrinsic caspase pathway (Li et al., 1997). Such a release may reflect opening of the mitochondrial permeability transition pore, decreasing mitochondrial membrane potential and subsequent swelling/disruption of mitochondrial membranes. In a model of ceramide-dependent apoptosis, both extensive mitochondrial swelling and a decrease in the mitochondrial membrane potential have been demonstrated (Kroesen et al., 2001).

Here, we examine the mechanism of ceramide-induced apoptosis in primary cultures of rat cortical neurons. We show that changes in Akt activity and mitochondrial membrane potential were induced early after ceramide treatment, leading to activation of the intrinsic caspase pathway, and that inhibition of such mitochondrial changes reduces ceramide-induced apoptosis.

Results

The short acyl-chain C_2 ceramide induces neuronal cell death and caspase-3-like activation. The effects of C_2 ceramide on cell death and caspase activity are specific, as we could detect no changes when the cells were treated with the inactive ceramide analog (Figs. 1A and 1B, respectively). Long-chain ceramides such as C_{16} ceramide are also able to induce cell death and caspase-3-like activity to a degree similar to that of C_2 ceramide (Figs. 1C and 1D).

During a time course of C_2 treatment the earliest time point with detectable presence of the p17 cleaved fragment of procaspase-3 was 6 h (Fig. 2A). The p17 reactivity was weak before 15 h. In Fig. 2B, we confirmed these findings using a sensitive fluorometric caspase-3 enzymatic assay.

Although indications of weak caspase-3 activity were present at the 7- and 8-h time points, the earliest time point that showed intense activity was 12 h.

Following C_2 treatment, the phosphorylation of Akt on the Ser 473 residue, which is essential for its activity, was rapidly and markedly decreased (Fig. 3A). As early as 1 h, a significant decrease in phospho-Akt levels was evident. Akt Ser473 phosphorylation was progressively reduced until 8 h, subsequently returning toward normal by 15 h. Ceramide treatment had a much smaller effect on the phosphorylation of the other residue critical for Akt activity, Thr308 (Fig. 3B). Quantitative analysis by densitometry of multiple Western immunoblot data (at least three independent experiments) strongly confirmed these observations (Fig. 3C). C_2 treatment had no effect on the cellular expression of total Akt, as shown using an antibody that recognizes Akt irrespective of its phosphorylation state (Fig. 3D). Akt activation requires simultaneous phosphorylation of both Ser473 and Thr308. Therefore, loss of phosphorylation of Ser473 alone would be expected to significantly decrease Akt kinase activity. This is confirmed in Fig. 4A; Akt kinase activity is decreased after ceramide treatment following a time course consistent with the loss of phosphorylation on Ser473. The level of phosphorylation of Ser473 is determined by a balance between the kinase that phosphorylates the residue and phosphatases that dephosphorylate it. In order to determine the involvement of a ceramide-activated phosphatase, we used okadaic acid, a specific inhibitor, at concentrations below 1 μ M, of phosphatases from the protein phosphatase 2A (PP2A) family. As shown in Fig. 4B, pretreatment with low doses of okadaic acid (5–10 nM, left panel) results in significant reduction of dephosphorylation of Ser473 caused by ceramide. At higher concentrations (10 nM) the level of Ser473 phosphorylation after ceramide treatment is even higher than the control level. Calyculin-A, an inhibitor of both PP2A and protein phosphatase 1 (PP1), has a similar effect at the same concentrations (Fig. 4B, right panel). The level of Thr308 phosphorylation was unchanged compared to control after treatment with ceramide with or without Okadaic acid or calyculin-A (1–10 nM, Fig. 4C, left and right panels, respectively). Pretreatment with okadaic acid at concentrations of 100–500 nM resulted in increased levels of Thr308 phosphorylation both in ceramide-treated and untreated samples (Fig. 4D). This indicates that PP2A family members are responsible for dephosphorylation of Ser473 and Thr308, both in untreated and ceramide-treated cells. Fig. 5 illustrates the effect of C_2 treatment on the phosphorylation of FKHR (A), glycogen synthase kinase 3- β (GSK-3 β) (B), and BAD (C). FKHR, GSK-3 β , and BAD phosphorylation decreased as early as 1 h, and remains depressed for at least 24 h. Quantitative analysis by densitometry of multiple Western immunoblot data (at least three independent experiments) was consistent with these observations (Fig. 5C). No decrease in total levels of FKHR, GSK-3, and BAD were detectable over a comparable time course of C_2 treatment (Fig. 5E). We conclude that a very

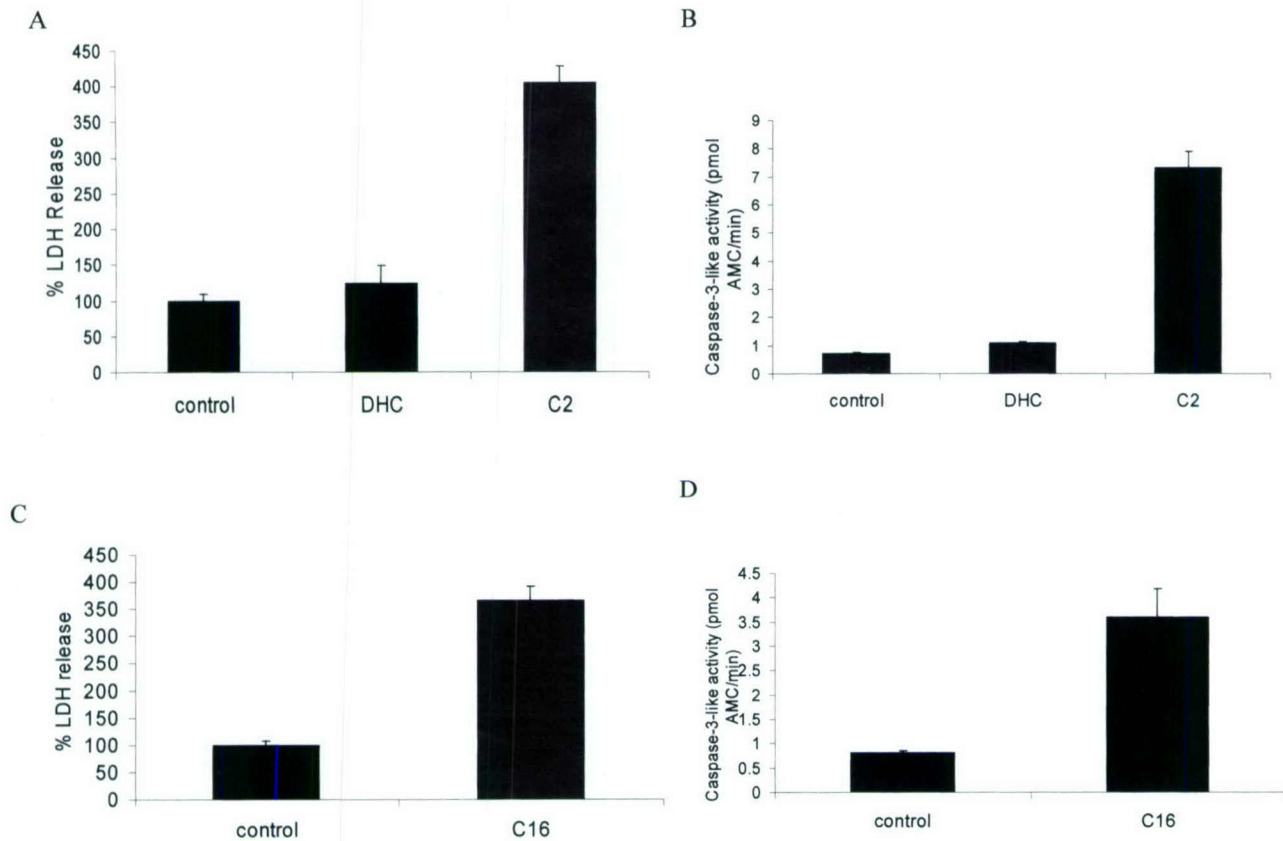


Fig. 1. Short acyl-chain C_2 ceramide and long-acyl chain C_{16} ceramide induce neuronal cell death and caspase activation while the inactive ceramide analog dihydroceramide (DHC) has no effect on cell viability or caspase activation. Rat primary cortical neurons were treated with $50 \mu\text{M}$ C_2 ceramide (C2) or dihydroceramide (DHC) for 24 h. Cell death was evaluated by measuring LDH release in the culture media (A). The same neuronal plates were then assayed for caspase-3 activity with the Ac-DEVD-AMC fluorogenic caspase-3 substrate as described under Experimental methods (B). Similar results were obtained when rat primary cortical neurons were treated with $5 \mu\text{M}$ C_{16} ceramide (C16) for 24 h. Cell death was evaluated by measuring LDH release in the culture media (C). The same neuronal plates were then assayed for caspase-3 activity with the Ac-DEVD-AMC fluorogenic caspase-3 substrate (D).

early effect of C_2 treatment is dephosphorylation and resultant inactivation of Akt. Among the molecular consequences of such actions are dephosphorylation of proapoptotic Akt targets, such as BAD, FKHR, and GSK-3 β , a step necessary for their activation; the latter two proteins stimulate the transcription of genes coding for proteins with proapoptotic function.

The importance of the PI3K pathway for neuronal survival in our model is demonstrated using a widely used PI3K inhibitor, LY 294002. Treatment for 24 h with a concentration of $50 \mu\text{M}$ LY 294002 results in cell death (Fig. 6A) and caspase-3 activation (Fig. 6B). In contrast, no effects were found when the ERK1/2 pathway was inhibited with the MEK inhibitor, PD-98059. We obtained similar results using another ERK1/2 inhibitor, U-0126 (data not shown). As presented in Figs. 6C and 6D, an inhibitor of translation, such as cycloheximide, can significantly decrease ceramide-induced cell death and markedly decreases ceramide-induced caspase-3 activity. Cycloheximide alone did not cause cell death and caspase activation in our model. BAD is known to cause mitochondrial dysfunction associ-

ated with cytochrome *c* release into the cytosol and initiation of the intrinsic caspase activation pathway. Cytochrome *c* is released into the cytosol after 3 h of C_2 treatment (Fig. 7A). These findings are consistent with the data in Fig. 5C, which show earlier BAD dephosphorylation which is required for the mitochondrial translocation of BAD. Once in the cytoplasm, cytochrome *c*, together with APAF-1, contributes to the formation of the apoptosome and activation of caspase-9. As shown in Fig. 7B, the cleavage of procaspase-9 (51 kDa, in rat) into the 40 kDa active fragment becomes detectable as early as 4 h. The 38 kDa cleavage fragment becomes detectable at later time points.

One of the mechanisms thought to mediate cytochrome *c* release from the mitochondrial intermembrane space involves opening of the permeabilization transition pore complex (PTPC). PTPC is a mitochondrial structure whose opening can result in mitochondrial swelling followed by rupture of mitochondrial membranes and release of cytochrome *c* into the cytosol. One of the markers of the opening of PTPC is a decrease in the mitochondrial membrane

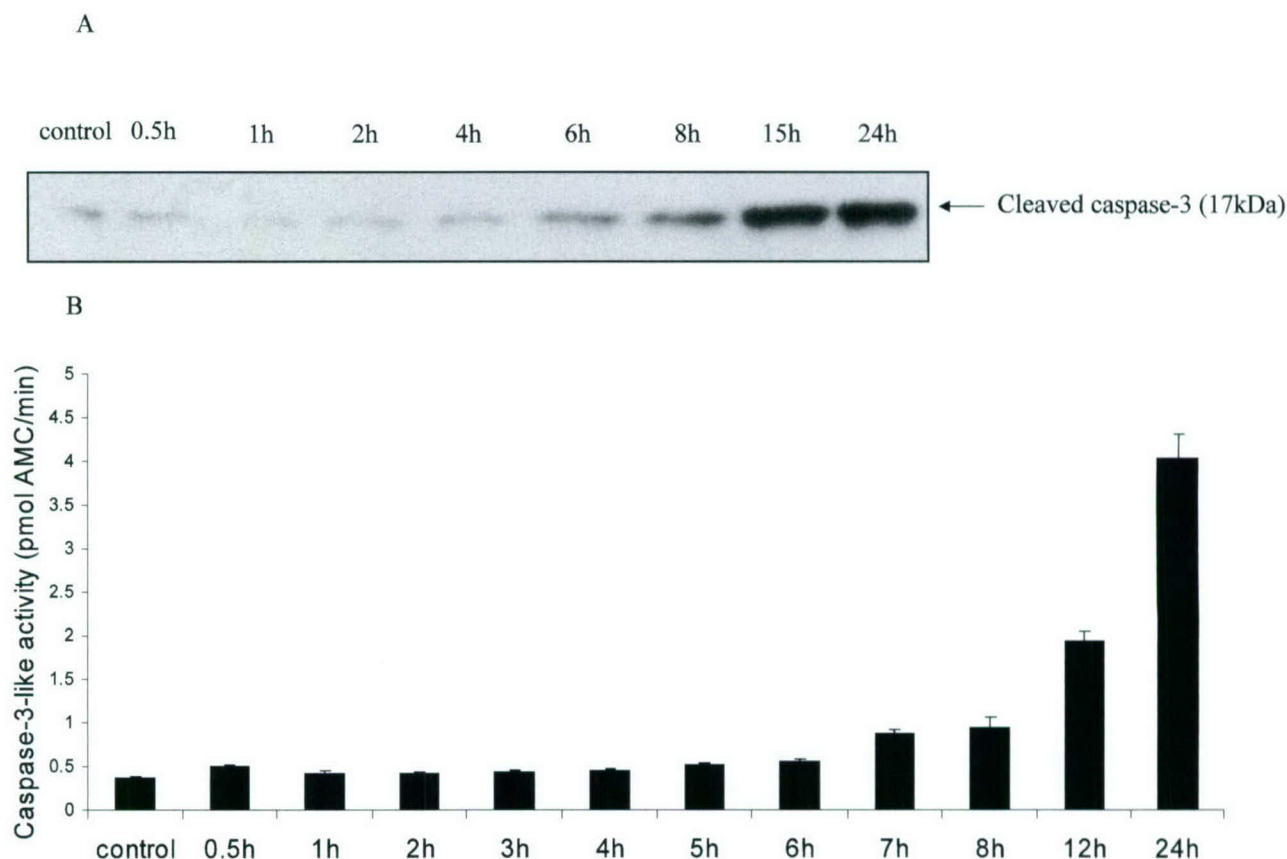


Fig. 2. C_2 ceramide induces caspase-3 activation. Cortical neurons were treated with a concentration of $50 \mu\text{M}$ C_2 ceramide. After various time intervals the cells were harvested and lysed as described under Experimental methods. Protein concentration was measured and $50 \mu\text{g}$ of protein was separated on SDS gels and transferred to nitrocellulose membranes and active caspase-3 was identified with antibodies specific for the 17-kDa cleaved fragment of caspase-3 (A). Cortical neurons were cultured in 96-well plates and treated with $50 \mu\text{M}$ C_2 ceramide for the indicated times. The in-plate caspase-3-like activity assay with Ac-DEVD-AMC fluorogenic substrate was performed as described under Experimental methods (B). Similar results were obtained in at least three separate experiments.

potential ($\Delta\psi_m$). As illustrated in Fig. 8A, using cytofluorometric analysis a decrease in the mitochondrial membrane potential was detectable as early as 2 h and continued until the 6 h time point. Although we were especially interested in early changes in the mitochondrial membrane potential that can play a part in apoptosis initiation, ceramide induced decreases in ($\Delta\psi_m$) continue until at least 24 h (data not shown). The effect of C_2 ceramide on mitochondrial potential was specific because the inactive ceramide analog dihydroceramide produced no depolarization (Fig. 8B).

Inhibitors of the PTPC pore, such as Bongkrekic acid (BA), represent a useful tool to explore the role of PTPC in induction of apoptosis in this model. Pretreatment with $25 \mu\text{M}$ of BA significantly inhibits cell death induced by C_2 ceramide (Fig. 9A) and is associated with a marked decrease in caspase-3-like activity (Fig. 9B). In order to verify that these results are not caused by a nonspecific effect, we incubated recombinant caspase-3 with BA, and then estimated the activity with the fluorometric assay. No inhibition of caspase-3 activity was detected at any of the BA con-

centrations used in this study (data not shown). Fig. 10A confirms the previous observation by demonstrating that the p17 caspase fragment reactivity is decreased in a dose-dependent fashion by BA. The $25 \mu\text{M}$ concentration causes a large decrease in p17 levels; at $50 \mu\text{M}$ there is nearly complete disappearance of p17. Fig. 10B shows that BA ($50 \mu\text{M}$) very significantly reduces the ceramide-induced cleavage of caspase-9 and partially blocks the ceramide-induced mitochondrial depolarization (Fig. 10C). Furthermore, pretreatment with 25 – $50 \mu\text{M}$ concentrations of BA almost completely blocks the development of chromatin condensation, one of the most characteristic features of apoptosis, and dependent on caspase-3 activity (Fig. 11). We estimated the apoptotic index (the percentage of cell with apoptotic nuclei) in the samples presented in Fig. 11. The control, C_2 , $C_2 + \text{BA } 25 \mu\text{M}$, $C_2 + \text{BA } 50 \mu\text{M}$ had an apoptotic index of 3.3, 34.2, 2.6, and 3.2%, respectively. Finally, as shown in Fig. 12, pretreatment with $50 \mu\text{M}$ BA reduces the cleavage of caspase-3 substrate poly(ADP-ribose) polymerase (PARP), which is a characteristic biochemical feature of apoptosis.

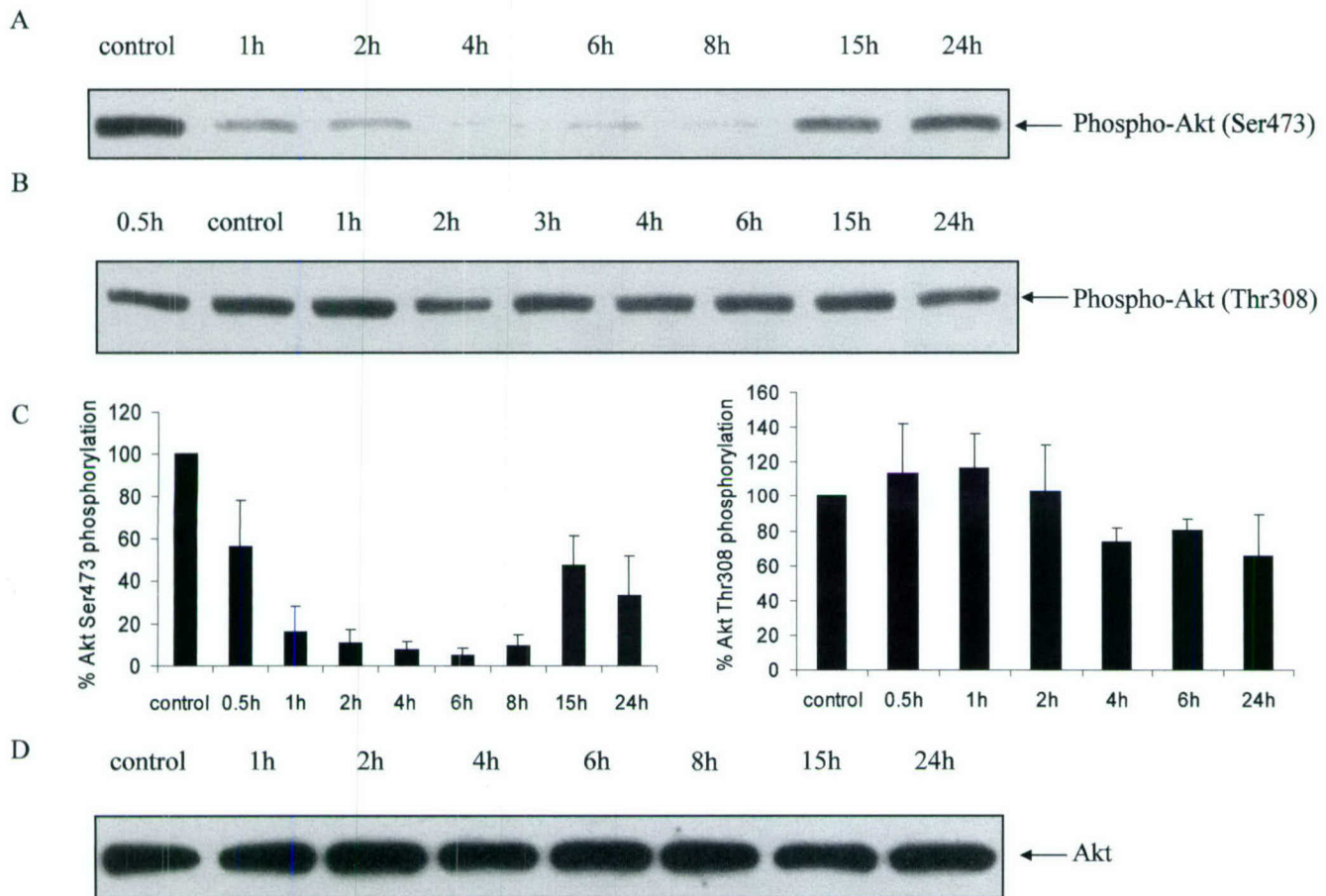


Fig. 3. C_2 ceramide induces rapid and extensive dephosphorylation of Ser473 but only moderately affects the phosphorylation status of Thr308 of Akt. Rat primary cortical neurons were treated with 50 μ M C_2 ceramide for different time intervals, as indicated. Protein concentration was measured and 25 μ g of protein was separated on SDS gels and transferred to nitrocellulose membranes and levels of Akt phosphorylated on Ser473 (A) and Thr308 (B) were probed with phosphorylation-specific antibodies as described under Experimental methods. Similar results were obtained in at least three independent experiments. (C) Quantitative analysis of the level of Ser473 and Thr308 phosphorylation in cortical neurons treated with 50 μ M C_2 ceramide for various time intervals was performed using Western immunoblot and densitometry, as indicated under Experimental methods and confirms the data presented in (A) and (B). Treatment with C_2 ceramide did not cause any significant change in the total levels of Akt protein (D).

Discussion

Ceramide consists of a long-chain sphingoid base with an amide-linked fatty acid component and can be synthesized via a *de novo* pathway by a multistep process that takes place in the endoplasmic reticulum (Futerman, 1998). Ceramide can also be generated from the degradation of sphingomyelin, complex sphingolipids and sphingosine by sphingomyelinases (SMases), cerebrosidases, and ceramidases, respectively. Due to its extremely hydrophobic nature, naturally occurring ceramide is difficult to use in *in vitro* experiments. Instead, it is replaced by short-acyl chain ceramide analogs such as C_2 ceramide, which is much more soluble. Although questions have been raised regarding the significance of findings using short-acyl chain ceramides, these results have been confirmed using various inhibitors or recombinant constructs of enzymes of ceramide metabolism that cause endogenous ceramide accumulation (Luberto and Hannun, 2000). Moreover, C_2 ceramide appears to

be naturally generated by cells (Luberto and Hannun, 2000). Using a recently described method to deliver long-chain ceramides in solution (Luberto and Hannun, 2000), we replicated the cell death and caspase-3-like activity induced by C_2 ceramide using C_{16} ceramide. We show that treatment with exogenous sphingomyelinase, an enzyme that results in ceramide accumulation from sphingomyelin, has similar effects on neuronal cell viability and caspase-3 activation with C_2 ceramide (Toman et al., 2002). The present study shows that treatment with C_2 ceramide initiates a cascade of biochemical changes associated with apoptosis, including activation of caspase-3. The earliest detectable events included dephosphorylation and inactivation of Akt, reduction in the mitochondrial membrane potential, and release of cytochrome *c* into the cytosol, leading to activation of the intrinsic caspase pathway.

Release of cytochrome *c* occurred relatively early, approximately 3 h after ceramide treatment. One mechanism proposed to induce cytochrome *c* release is physical disruption

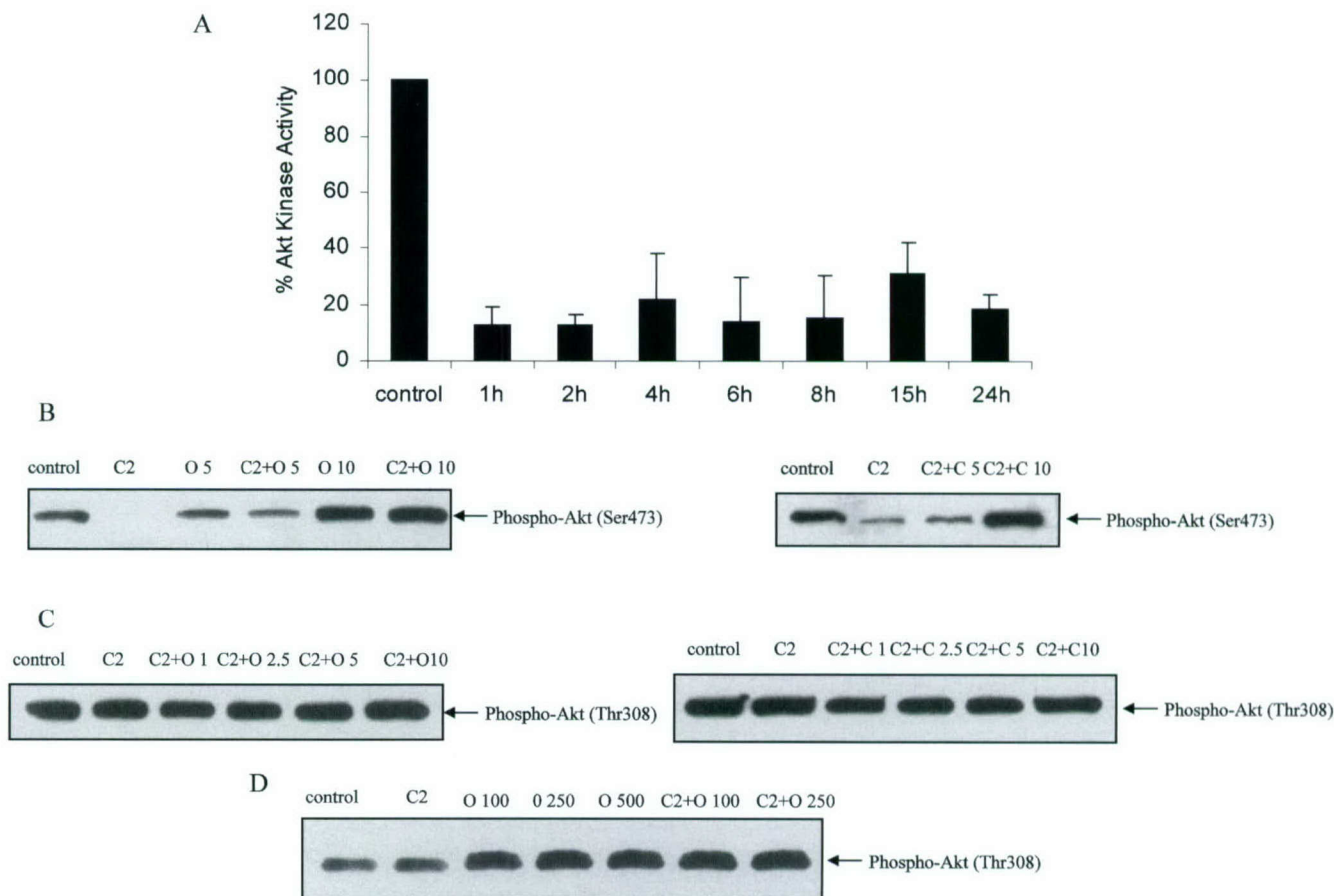


Fig. 4. C_2 ceramide treatment results in decrease in Akt kinase activity (A). Rat primary cortical neurons were treated with $50 \mu M$ C_2 ceramide for the indicated time intervals. Akt kinase activity was measured from Akt immunoprecipitated from cell extracts as described under Experimental methods. The figure includes data from three independent experiments. Okadaic acid and calyculin-A reverses ceramide-induced dephosphorylation of Ser473 (B). Primary rat cortical neurons were treated with $50 \mu M$ C_2 ceramide (3 h) with or without pretreatment with the indicated (nM) concentrations of okadaic acid (o) or calyculin-A (c). The phosphorylation of Akt at Ser473 (B) and Thr308 (C, D) was evaluated with phosphorylation-specific antibodies.

tion of the mitochondrial outer membrane. Such disruption may reflect osmotic swelling caused by mitochondrial permeability transition (MPT). This phenomenon occurs when the PTPC opens and the ions and water flow freely between the mitochondrial matrix and the cytosol (Bernardi, 1999; Crompton, 1999; Lemasters et al., 1999). One consequence is mitochondrial membrane depolarization, along with swelling of the mitochondrial matrix, followed by rupture of mitochondrial membranes and release of cytochrome *c* (Bradham et al., 1998; Pastorino et al., 1998).

However, there are also indications that in some cell death models, MPT is not required for cytochrome *c* release (Bossy-Wetzel et al., 1998; Eskes et al., 1998). Studies involving isolated mitochondria have confirmed that MPT is capable of causing the release of cytochrome *c* (Andreyev and Fiskum, 1999; Kowaltowski et al., 2000), but the potential to undergo MPT varies across tissues (Andreyev et al., 1998; Andreyev and Fiskum, 1999). Neuronal mitochondria may be less prone to undergo MPT compared to other cell types and can release cytochrome *c* independently

of MPT (Andreyev et al., 1998; Andreyev and Fiskum, 1999).

Once present in the cytosol, cytochrome *c*, together with APAF1 and caspase-9, forms the "apoptosome" resulting in activation of caspase-9 and subsequently caspase-3 (Li et al., 1997). Our data are consistent with the induction of such a pathway and show that depolarization of the mitochondria was detectable between 2–4 h after ceramide treatment. Thus, mitochondria may represent an early target of ceramide. BA is an inhibitor of adenine nucleotide translocator (ANT), which is a component of the PTPC (Lauquin et al., 1976; Marchetti et al., 1996; Zamzami et al., 1996). ANT prevents mitochondrial depolarization, redistributes cytochrome *c* from the mitochondria to the cytosol, causes caspase activation, and ultimately blocks cell death in several apoptosis models (Pastorino and Hoek, 2000; Scarlett et al., 2000).

Bongkreikic acid was an effective inhibitor of ceramide-induced apoptosis in our model. Treatment with Bongkreikic acid not only reduced mitochondrial membrane potential

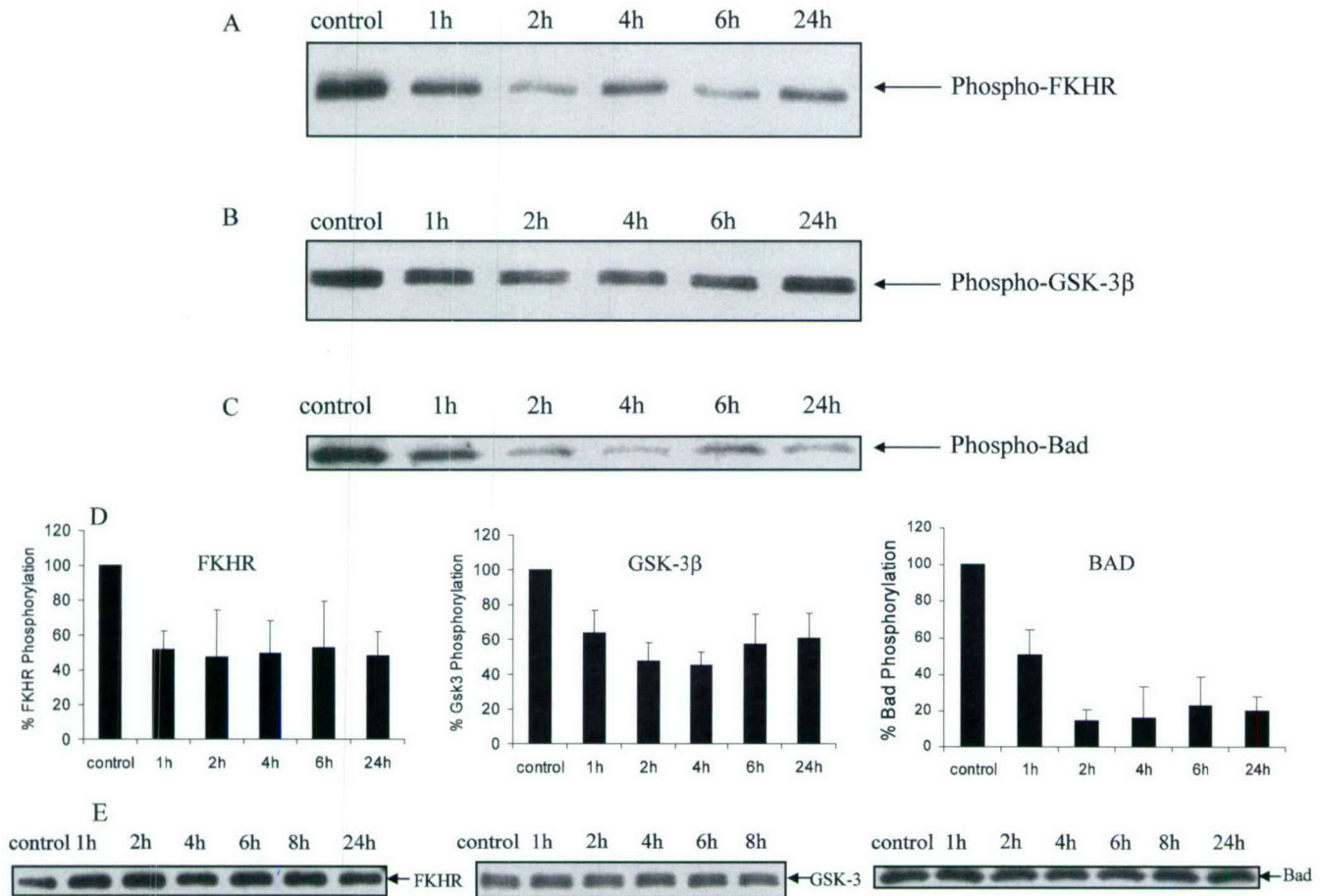


Fig. 5. C_2 ceramide induces dephosphorylation of FKHR on Thr24 (A), GSK-3 β on Ser9 (B), and BAD on Thr112 (C). Rat primary cortical neurons were treated with 50 μ M C_2 ceramide for different time intervals, as indicated. Protein concentration was measured and 25 μ g of protein was separated on SDS gels and transferred to nitrocellulose membranes and phosphorylation levels of FKHR Thr24, GSK-3 β Ser9, and BAD Thr112 were probed with phosphorylation-specific antibodies as described under Experimental methods. (D) Quantitative analysis using Western Immunoblot and densitometry confirms the data presented in (A), (B), and (C). The totals levels of FKHR, GSK-3, and BAD do not decrease after C_2 ceramide treatment.

changes and ceramide-induced caspase-9 and caspase-3 activation, but also inhibited hallmark manifestations of apoptosis (chromatin condensation, PARP cleavage) and reduced cell death (LDH release). Bongkreikic acid appeared to act downstream of Akt, because it did not reverse the Akt Ser473 dephosphorylation induced by ceramide (data not shown). However, Bongkreikic acid did not modify the translocation of cytochrome *c* into the cytosol (data not shown). How can this fact be reconciled with previous reports on the role of Bongkreikic acid and with our own findings showing its capacity to block apoptosis? Bongkreikic acid was reported to have neuroprotective actions in a model of NMDA-induced neuronal cell death (Budd et al., 2000). This antiapoptotic effect was associated with inhibition of caspase-3 activity and preservation of mitochondrial potential, even though cytochrome *c* was released into the cytosol; these features were also present in our model. Budd speculated that the ability of Bongkreikic acid to block ANT might mimic the interaction of Bcl-2 with ANT (Vander Heiden et al., 1999) and that the most important effect of such interactions would be to regulate the exchange of ATP

for ADP. As dATP is a cofactor for caspase activation, modulation of its levels might be sufficient to prevent apoptosis. On the other hand, BA was not able to prevent apoptosis and caspase activation induced by staurosporine which is associated with cytochrome *c* release but not with decrease in mitochondrial transmembrane potential (Budd et al., 2000) (Stoica and Faden, unpublished observations). Therefore, it is more likely that BA can block apoptosis only when induced by stimuli that activate pathways that are regulated by BA. The primary targets are mechanisms controlled by the decrease in mitochondrial transmembrane potential such as NAD(P)H oxidation/depletion (Gendron et al., 2001). A very recent study (Siskind et al., 2002) found that ceramide can form channels in mitochondria membranes which allow cytochrome *c* to permeate. Although there are differences between using purified mitochondria (Siskind et al., 2002) and using cells as in our case, the formation of such channels might explain why the release of cytochrome *c* in the cytosol is not inhibited by Bongkreikic acid.

Another potential explanation for the anti-apoptotic ef-

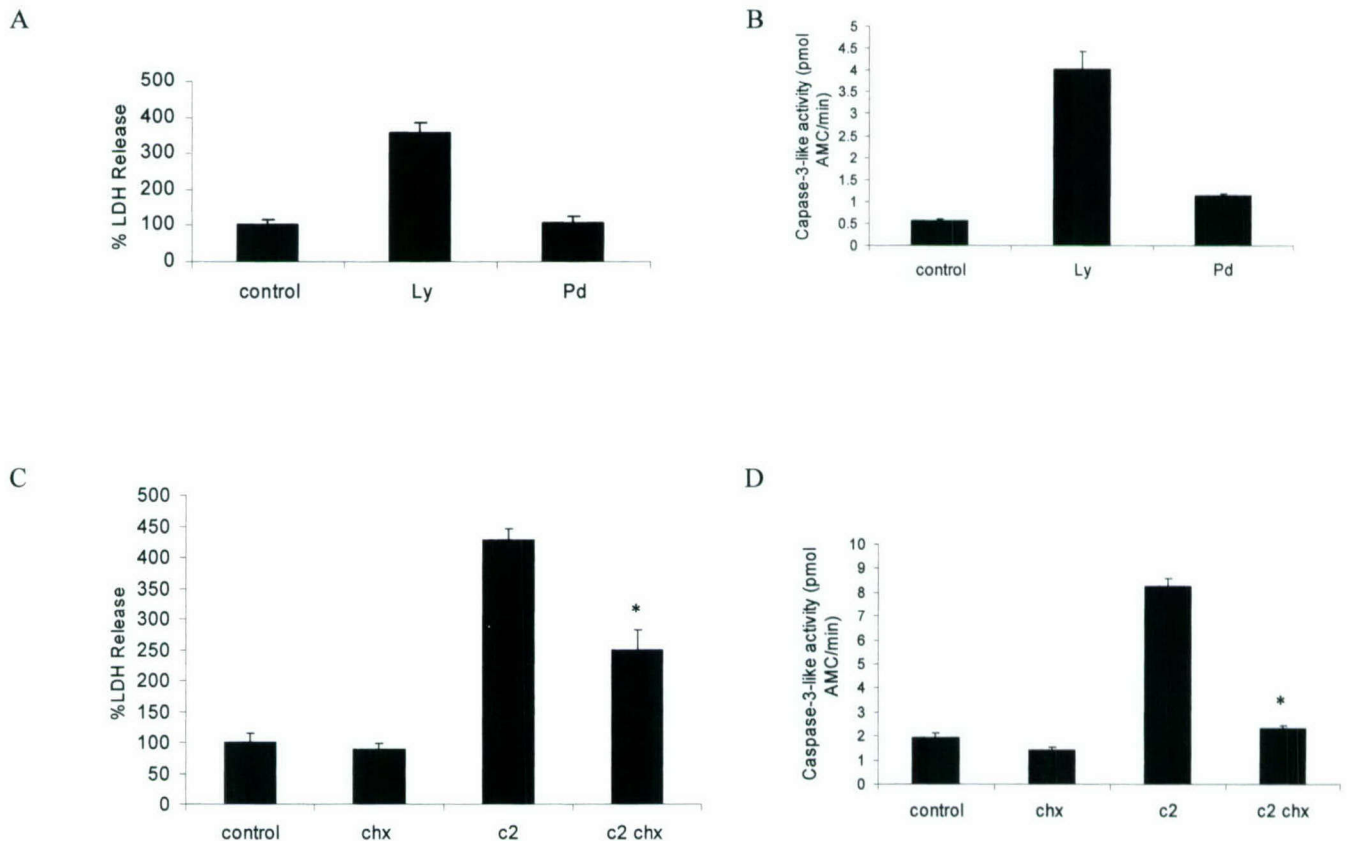


Fig. 6. Inhibitors of the PI3K pathway, but not the ERK1/2 pathway, cause neuronal cell death and caspase-3 activation. Cortical neurons were treated with 50 μ M PD-98059 (inhibitor of ERK1/2 pathway) (Pd) or LY 294002 (inhibitor of PI3K) (Ly) for 24 h and cell death was evaluated by detection of release of LDH into the medium as described under Experimental methods (A). The same neuronal cultures were probed for caspase-3-like activity with the Ac-DEVD-AMC substrate (B). Blocking protein translation with cycloheximide prevents both cell death and caspase-3 activation induced by C₂ ceramide. Rat primary cortical neurons cultured in 96-well plates were treated with 1 μ g/ml cycloheximide or with 50 μ M C₂ ceramide for 24 h with (C2 chx) or without (C2) cycloheximide. Cell death was evaluated by measuring LDH release in the culture media (C). The same neuronal plates were then assayed for caspase-3 activity with the Ac-DEVD-AMC fluorogenic caspase-3 substrate as described under Experimental methods (D). Similar results were obtained in three independent experiments. *Significant difference between the C2 and the C2 chx samples ($n = 6$ per treatment, unpaired t test, $P < 0.05$).

fects of Bongkreikic acid may be related to pro-apoptotic proteins, such as caspase-9, AIF, and Smac/DIABLO, normally located in the mitochondrial intermembrane space and released into the cytosol at the initiation of apoptosis (Chai et al., 2000; Joza et al., 2001; Krajewski et al., 1999; Srinivasula et al., 2000; Susin et al., 1999). Smac is a mitochondrial protein that induces caspase activation and apoptosis by neutralizing one or more members of the IAP family of apoptosis inhibitory proteins (Liu et al., 2000). Release of Smac and cytochrome *c* from the mitochondria may occur independently (Adrain et al., 2001; Chauhan et al., 2001), raising the possibility that different mechanisms may be involved. Furthermore, in at least some instances, the presence of cytochrome *c* in the cytosol is insufficient for caspase activation and apoptosis, which also requires the presence of Smac (Carson et al., 2002). One possibility is that Bongkreikic acid may interfere with the release of Smac, and under such conditions, cytochrome *c* release might not result in caspase activation and apoptosis.

What mechanisms might be responsible for ceramide-

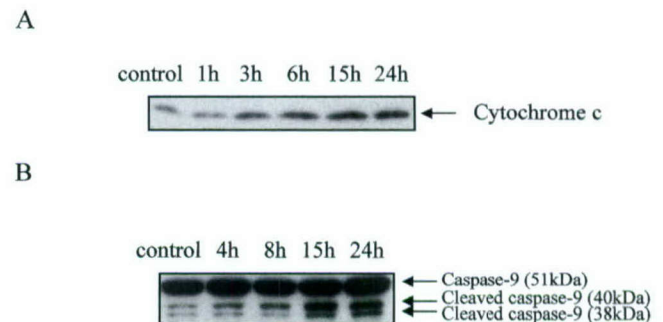


Fig. 7. C₂ ceramide induces the activation of the intrinsic caspase pathway. Rat primary cortical neurons were treated with 50 μ M C₂ ceramide for different time intervals. (A) Cytosolic fractions were prepared as described under Experimental methods. Twenty-five micrograms of cytosolic extract was separated on SDS gels, transferred to nitrocellulose membranes, and probed with specific anti-cytochrome *c* antibodies. (B) Cells were harvested and lysed to prepare total cell extracts. Protein concentration was measured and 25 μ g of protein was separated on SDS gels and transferred to nitrocellulose membranes and full-length (51 kDa) and cleaved (38/40 kDa) caspase-9 fragments were identified with a specific antibody as indicated under Experimental methods. Similar results were obtained in two independent experiments.

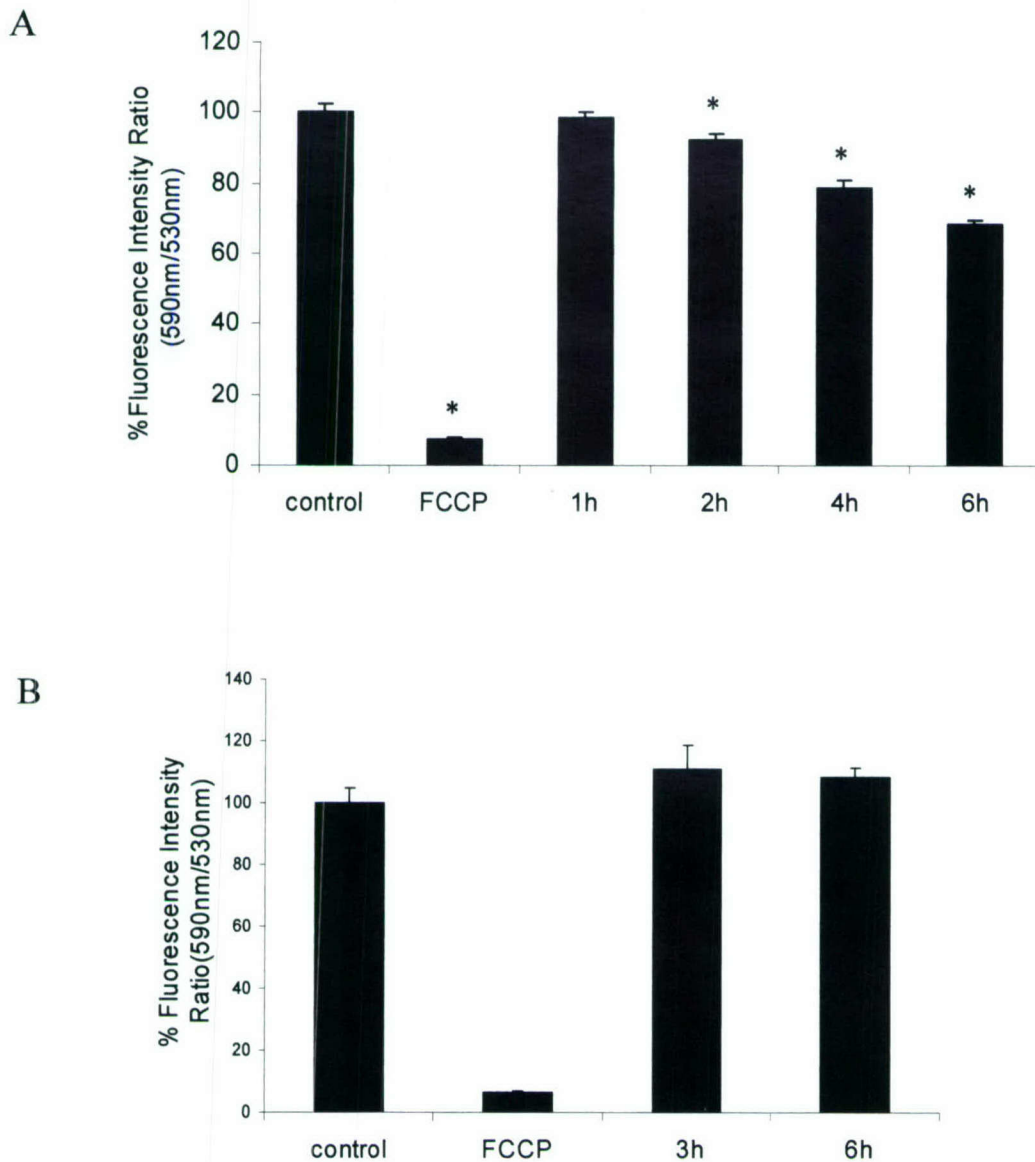


Fig. 8. C_2 ceramide causes rapid mitochondrial depolarization. Rat primary cortical neurons were treated with $50 \mu M$ C_2 ceramide for different time intervals. The mitochondrial membrane potential was evaluated by JC-1 staining followed cytofluorometric readings (A) as described under Experimental methods. To demonstrate that dihydroceramide, an inactive ceramide analog, had no effect on mitochondrial depolarization, rat primary cortical neurons were treated with $50 \mu M$ dihydroceramide for the indicated time intervals and mitochondrial membrane potential was evaluated with the cytofluorometric method (B). Carbonyl cyanide *p*-(trifluoromethoxy) phenylhydrazone (FCCP) was used as a positive control for complete mitochondrial depolarization. Similar results were obtained in two independent experiments. *Significant difference from control ($n = 4$ per treatment, $P < 0.05$, ANOVA).

induced mitochondrial dysfunction? The PI3-kinase (PI3K) and the ERK1/2 (p44/42 MAP kinase) pathways promote cell growth and development, as well as inhibiting apoptosis in many cell types. Treatment with PD-98059 or U-0126 (inhibitors of ERK1/2 pathway) had no effect on cell viability, whereas treatment with LY 294002 (inhibitor of PI3K pathway) caused activation of caspase-3 and cell death in our cultures. Thus, the PI3K pathway, but not the ERK1/2 pathway, may be involved in neuronal survival in our model.

One of the most important survival factors in the PI3K pathway is Akt, which depends on PI3K for its activation.

Once active, Akt may phosphorylate and inactivate several pro-apoptotic proteins, such as the Bcl-2 family member, BAD, the transcription factors of the FKHR family, or signaling molecules like GSK- β . Results obtained in other model systems support an important role for Akt inhibition in ceramide-induced apoptosis. For example, in motor neurons, application of $50 \mu M$ C_2 -ceramide causes apoptosis and decreases both basal and stimulated Akt activity (Zhou et al., 1998). Overexpression of Akt also blocks ceramide-induced apoptosis in F-11 cells (Goswami et al., 1999). One of the earliest detectable events (30 min–2 h) in our model was a decrease in the phosphorylation of Akt on the critical

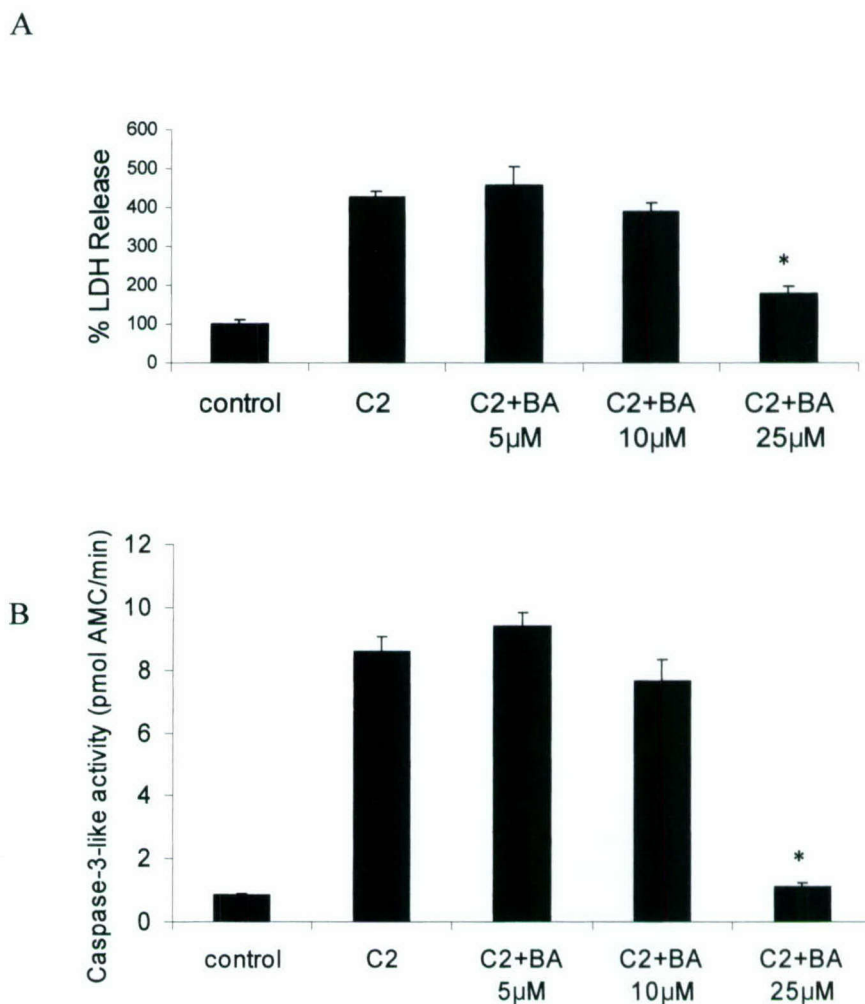


Fig. 9. Bongkreikic acid prevents both the cell death and the caspase-3 activation induced by C_2 ceramide. Rat primary cortical neurons were treated with $50 \mu M$ C_2 ceramide (C2) for 24 h in the presence of various concentrations of Bongkreikic acid (C2+BA). Cell death was evaluated by measuring LDH release in the culture media (A). The same neuronal plates were then assayed for caspase-3 activity with the Ac-DEVD-AM fluorogenic caspase-3 substrate. *Significant difference from control ($n = 6$ per treatment, $P < 0.05$ Bonferroni/Dunn). Similar results were obtained in three independent experiments.

Ser473 residue. Akt activity was rapidly inhibited after ceramide treatment and phosphorylation of the proteins BAD, FKHR, and GSK3 β was also reduced at approximately the same time. There was a modest recovery in the level of phosphorylation on Ser473 at 15–24 h after ceramide treatment. Published reports have shown that C_2 -ceramide can be metabolized in cells (Abe et al., 1996; Lee et al., 1996). One explanation may be that by 15–24 h cellular metabolism degrades C_2 -ceramide into less active metabolites. Akt activity may not have recovered significantly at this time probably because of dephosphorylation on Thr308. However, by the time phosphorylation on Ser473 partially recovers, the apoptotic process (cytochrome *c* release, caspase activation) is well under way; therefore, it is probably too late to be inhibited.

Once BAD is phosphorylated by Akt, it is recognized and bound by members of the 14-3-3 protein family, resulting in sequestration of BAD into the cytoplasm and its effective inactivation (del Peso et al., 1997; Zha et al.,

1996). The interaction between BAD and 14-3-3 is dependent upon the specific recognition by 14-3-3 of Akt-phosphorylated residues in BAD. Dephosphorylated BAD loses its ability to form a complex with 14-3-3 and is believed to exert its pro-apoptotic effects following translocation from the cytosol to the mitochondria, where it can promote cytochrome *c* release. BAD was shown to bind and inhibit the actions of anti-apoptotic proteins, such as Bcl-2 and Bcl-x_L (Zha et al., 1997). BAD can also promote the translocation of another pro-apoptotic Bcl-2 family member, Bax, to the mitochondria (Tafani et al., 2001). Bcl-2 and Bax may interact directly with components of PTPC, such as ANT, preventing or inducing, respectively, its permeabilization (Zamzami and Kroemer, 2001).

In neurons, apoptosis may require active transcription and translation (D'Mello et al., 1993; Mesner et al., 1992; Pittman et al., 1993). We found that cycloheximide, which inhibits protein synthesis in eukaryotes by interfering with the translocation step, suppresses ceramide-induced

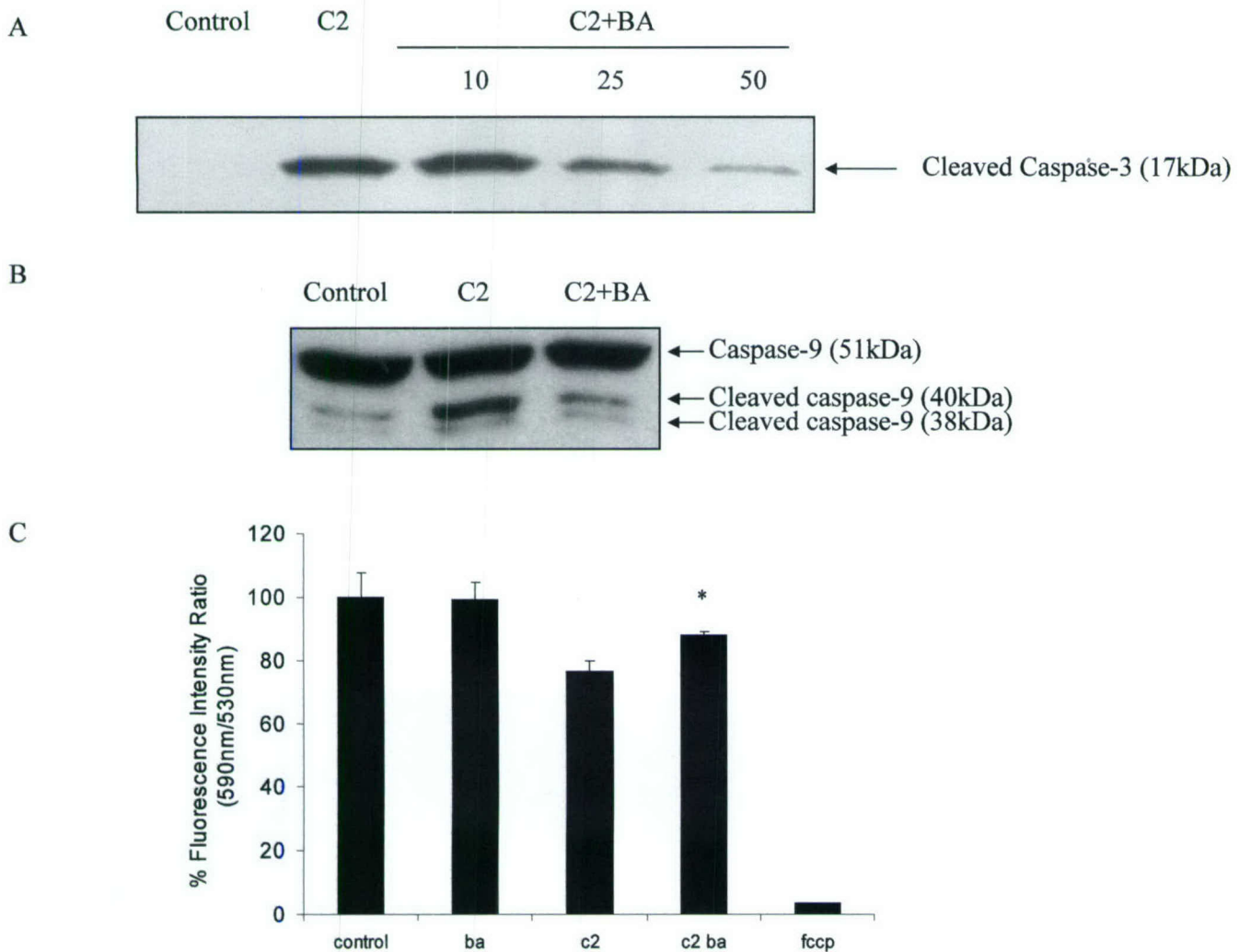


Fig. 10. Bongkreikic acid prevents the cleavage of caspase-3 induced by C_2 ceramide. Rat primary cortical cells were treated for 24 h with 50 μ M C_2 ceramide with (C2+BA) or without (C2) various concentrations of Bongkreikic acid; 25 μ g of cell lysate was resolved on SDS gels, transferred to nitrocellulose membranes, and probed with antibodies specific for the cleaved fragment of caspase-3 (A). Rat primary cortical cells were treated for 24 h with 50 μ M C_2 ceramide (C2) or with 50 μ M C_2 ceramide in the presence of 50 μ M Bongkreikic acid (C2+BA); 25 μ g of cell lysate was resolved on SDS gels and transferred to nitrocellulose membranes and full-length (51 kDa) and cleaved (38/40 kDa) caspase-9 fragments were identified with a specific antibody, as indicated under Experimental methods (B). Similar results were obtained in two independent experiments. Rat primary cortical neurons were treated with 50 μ M C_2 ceramide (C2), 50 μ M Bongkreikic acid (ba) or with the same concentration of ceramide and Bongkreikic acid in combination (c2 ba) for 6 h. The mitochondrial membrane potential was evaluated by JC-1 staining followed by cytofluorometric readings (C). Carbonyl cyanide *p*-(trifluoromethoxy) phenylhydrazone (fccp) is used as a positive control for complete mitochondrial depolarization. *Significant difference between c2 and c2 ba samples ($n = 4$ per treatment, $P < 0.05$, ANOVA).

caspase-3 activation and inhibits cell death. Among the best described nuclear substrates of Akt are the transcription factors from the Forkhead family (FKHR, FKHR-L1, and AFX) (Brunet et al., 2001; Shin et al., 2001; Tang et al., 1999). This family of transcription factors induces cell cycle arrest and apoptosis (Dijkers et al., 2000a, 2000b, 2002; Nakamura et al., 2000). Recently, it was found that AFX transcriptionally activates p27kip1 resulting in increased protein levels (Medema et al., 2000). Akt phosphorylates FKHR-L1 at key regulatory residues, promoting its exit from the nucleus and blocking of FKHR-mediated transcription. A requirement for new protein transcription might explain the time interval between the appearance of cyto-

chrome *c* in the cytoplasm (3 h after ceramide exposure) and the activation of caspase-3 (6–8 h at the earliest).

Several studies have identified a pro-apoptotic role for GSK-3 (Cross et al., 2001; Culbert et al., 2001; Li et al., 2000; Pap and Cooper, 1998). GSK-3 phosphorylates many substrates that have important roles in neuronal survival, such as the initiation factor eIF2B (Pap and Cooper, 2002), the microtubule-associated protein tau, and the transcription factors CREB, c-myc, c-jun, and β -catenin (Li et al., 2000). GSK3 β itself is phosphorylated and inactivated by Akt (Pap and Cooper, 1998, 2002). Ceramide-induced suppression of Akt and subsequent dephosphorylation of GSK-3 β , as demonstrated, would be expected to provide a pro-apoptotic stimulus.

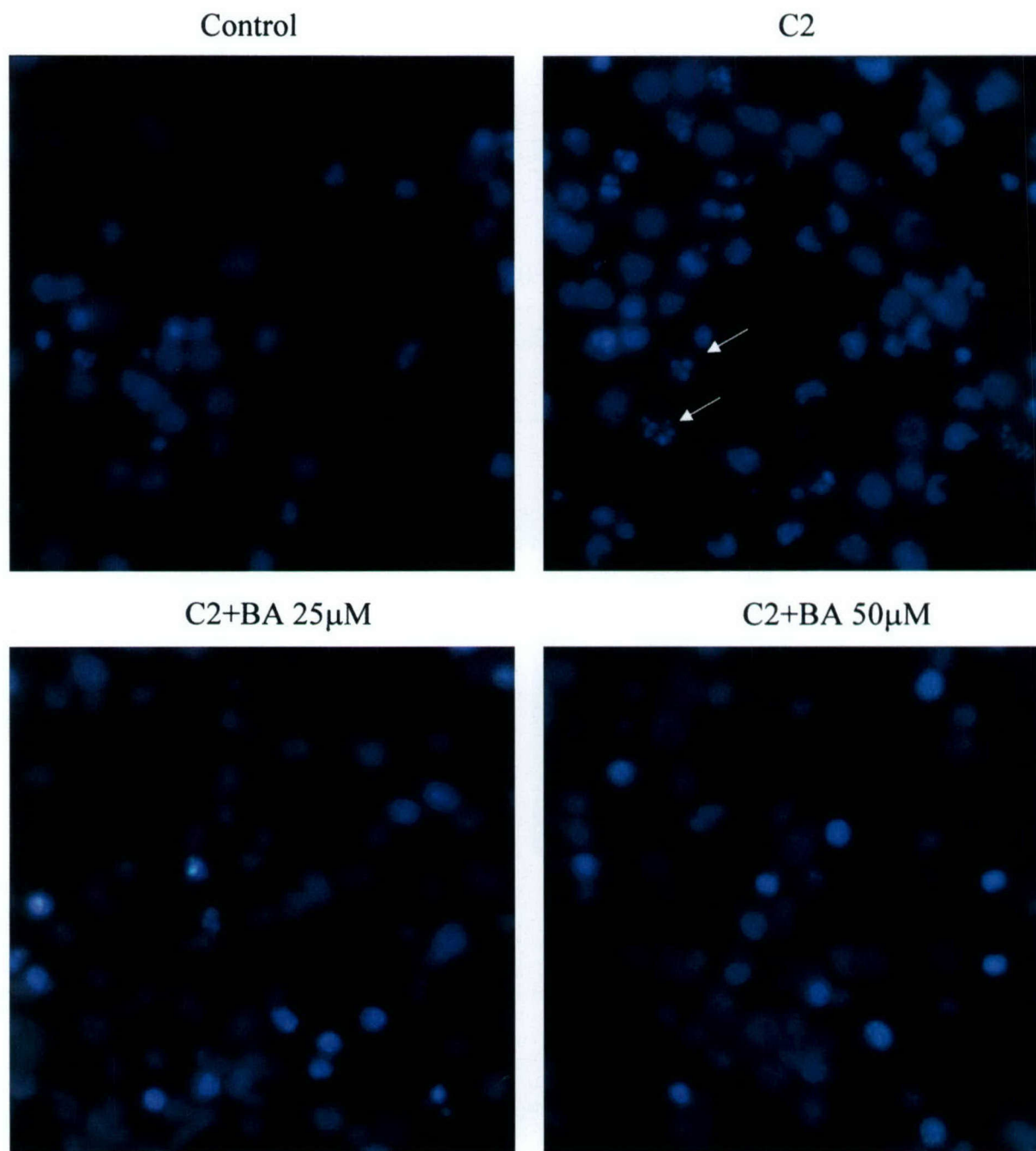


Fig. 11. Bongkreikic acid prevents chromatin condensation induced by C_2 ceramide. Rat primary cortical cells were treated with $50 \mu\text{M}$ C_2 ceramide (C2) or with the same concentration of C_2 ceramide in the presence of $25\text{--}50 \mu\text{M}$ Bongkreikic acid (C2+BA). Chromatin condensation status was evaluated after staining with Hoechst 33258. Nuclei presenting at least two chromatin bodies intensely stained were considered apoptotic. Such nuclei were counted; some are indicated with arrows for exemplification.

The fact that phosphorylation of Thr308 residue of Akt is less affected by ceramide treatment suggests that ceramide acts mainly downstream of PI3K. Phosphoinositide-dependent protein kinase 1 (PDK1), which is PI3K dependent, plays a central role in many signal transduction pathways (Belham et al., 1999; Toker and Newton, 2000; Williams et al., 2000). PDK1 regulates the phosphorylation of Thr308 in

Akt, whereas the phosphorylation of Ser473 is dependent on an as yet to be characterized PDK2.

Previous studies have indicated that in different models PI3K may be inhibited (Zundel and Giaccia, 1998), activated (Hanna et al., 1999), or unaffected (Zhou et al., 1998) by ceramide. Based on our present findings, we believe that PDK1 and the PI3K pathway upstream of it are not affected

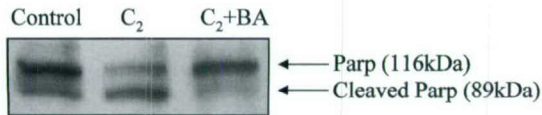


Fig. 12. Bongkreikic acid prevents the ceramide-induced cleavage of caspase-3 substrate PARP. Rat primary cortical cells were treated for 24 h with 50 μ M C_2 ceramide (C_2) or with the same concentration of ceramide in the presence of 50 μ M Bongkreikic acid (C_2 +BA). Twenty-five micrograms of cell lysate was resolved on SDS gels, transferred to nitrocellulose membranes, and probed with antibodies specific for full-length and cleaved PARP (B).

by ceramide in our model. Ceramide-induced inactivation of PDK2 or the activation of a specific serine phosphatase (Cazzoli et al., 2001; Schubert et al., 2000), are two possible mechanisms that may explain selective Ser473 dephosphorylation. Our results showing that pretreatment with okadaic acid (5 nM) prevents the Ser473 dephosphorylation indicate that a PP2A family member is activated by ceramide and responsible, in considerable part, for Akt dephosphorylation in primary cortical neurons exposed to ceramide. At higher concentrations of okadaic acid (10 nM), we observed that the level of Akt Ser473 phosphorylation of ceramide-treated and nontreated samples was identical, but increased compared to control indicating that PP2A inhibition reverses ceramide-induced Ser473 dephosphorylation and also that PP2A modulates the basal level of Akt Ser473 phosphorylation. Previous studies have indicated that Ser473 represents a better substrate for protein phosphatases than does Thr308 (Andjelkovic et al., 1999), possibly providing an explanation for our findings. One recent study investigating an erythroleukemic cell line stimulated with GM-CSF (Schubert et al., 2000) also reported that the phosphorylation of Thr308 is not changed by ceramide treatment but, significantly, found that okadaic acid and calyculin-A by themselves reduced the phosphorylation at Thr308. Other recent studies (Salinas et al., 2000; Zinda et al., 2001) found that ceramide reduced the phosphorylation on both Ser473 and Thr308 induced by NGF in PC12 or in basal U87MG glioblastoma cells (PTEN negative) and that okadaic acid reversed these changes. Differences between these studies and the present one include critical elements such as the use of growth factor or genetic alteration-induced versus basal state Akt phosphorylation and the use of cell lines versus primary neurons and indicate that different mechanism control Akt phosphorylation in different systems. We believe that our model using primary cortical neurons in their basal state provides a critical link to uncovering the mechanism responsible for regulating Akt function in the brain.

In conclusion, we find that ceramide inhibits the Akt pathway, resulting in mitochondrial dysfunction followed by caspase activation and apoptosis. Reducing such mitochondrial changes using Bongkreikic acid suppressed these latter effects. Our observations suggest that Bongkreikic acid or related compounds might have neuroprotective effects in

vivo for conditions in which ceramide has been implicated as a pathological factor, such as cerebral ischemia or head injury.

Experimental methods

Materials

The following chemicals were used: Bongkreikic acid (Sigma-Aldrich, St. Louis, MO, USA, No. B6179), PD-98059 (Biomol Research Laboratories, Plymouth Meeting, PA, USA, No. EI-360), C_2 -ceramide (Biomol, No. SL-100), C_2 -dihydroceramide (Biomol, No. SL-101), and LY-294002 (Biomol, No. ST-420). The following antibodies, obtained from Cell Signaling Technology (Beverly, MA, USA), were used: Cleaved caspase-3 No. 9661, Phospho-Akt (Ser473) No. 9271, Phospho-Akt (Thr308) No. 9275, Phospho-BAD (Ser112) 7E11 monoclonal antibody No. 9296, Phospho-FKHR (Thr24) No. 9464, Phospho-GSK-3 β (Ser9) No. 9336, and caspase-9 (No. 9506). The antibody recognizing PARP (No. sc-7150) is from Santa Cruz Biotechnology (Santa Cruz, CA, USA). The antibodies recognizing FKHR No. 9462 and GSK-3 No. 9332 are from Cell Signaling Technology (Beverly, MA, USA) and the antibody recognizing BAD No. sc-943 is from Santa Cruz.

Tissue cultures

Cortical neuronal cultures were derived from rat embryonic cortices, as described (Mukhin et al., 1997, 1998; Yakovlev et al., 2001). Briefly, cortices from 15- to 16-day-old embryos were cleaned from their meninges and blood vessels in Krebs'-Ringer's bicarbonate buffer containing 0.3% bovine serum albumin (BSA; Life Technologies, Gaithersburg, MD, USA). Cortices were then minced and dissociated in the same buffer with 1800 U/ml trypsin (Sigma, St. Louis, MO, USA); at 37°C for 20 min. After the addition of 200 U/ml DNase I (Sigma) and 3600 U/ml soybean trypsin inhibitor (Sigma) to the suspension, cells were triturated through a 5-ml pipette. After the tissue settled for 5–10 min, the supernatant was collected, and the remaining tissue pellet was re triturated. The combined supernatants were then centrifuged through a 4% BSA layer, and the cell pellet was resuspended in neuronal seeding medium which consisted of neurobasal medium (Life Technologies) supplemented with 1.1% 100 \times antibiotic-antimycotic solution (Biofluids, Rockville, MD, USA), 25 μ M Na-glutamate, 0.5 mM L-glutamine, and 2% B27 supplement (Life Technologies). Cells were seeded at a density of 5×10^5 cells/ml onto poly-D-lysine-(70- to 150-kDa; Sigma)-coated 96-well plates (Corning, Corning, NY, USA) or 100-mm Petri dishes (Falcon). All experiments were performed on cultures at 7 days in vitro (DIV). The cellular composition of the cultures is approximately 90% neurons (Yakovlev et al., 2001).

Treatments

We investigated the mechanism of ceramide-induced apoptosis in neurons by treating rat primary cortical neurons with the soluble ceramide analogue C_2 -ceramide. Through dose–response experiments we have established (Toman et al., 2002) that 50 μ M is one of the lowest concentrations of C_2 -ceramide capable of inducing a significant degree of apoptosis in these neurons after 24 h of treatment, and therefore, this C_2 ceramide concentration was used throughout this study. In order to control for nonspecific changes in the lipid composition of cells after C_2 treatment, we used a related molecule devoid of biological effects—dihydro- C_2 -ceramide. Using this control, we observed no effects on cell viability, caspase activation, or mitochondrial depolarization. The delivery of the long-chain ceramide C_{16} was performed as a 2% (v/v) dodecane solution in ethanol (Luberto and Hannun, 2000).

Immunoblot

After various times of treatment, the cells were harvested by scraping with a cell scraper and maintained on ice. Samples were washed once with ice-cold DPBS (GIBCO BRL) and the cellular pellet was resuspended in lysis buffer (60 mM Tris–HCl, pH 7.8, containing 150 mM NaCl, 5 mM EDTA, 10% glycerol, 2 mM Na_3VO_4 , 25 mM NaF, 10 μ g/ml leupeptin (Sigma), 10 μ g/ml aprotinin (Sigma), 1 mM AEBSF (Sigma), 1 mM Pepstatin (Sigma), 1 μ M Microcystin LR (Sigma), and 1% Triton X-100 (Calbiochem, La Jolla, CA, USA). The samples were incubated on ice for at least 30 min and centrifuged at 20,000g for 15 min. The soluble fraction representing total cell extracts was recovered and stored at -80°C until use. Protein concentration in the samples was determined with the Micro-BCA assay kit (Pierce). Equal protein aliquots (25–50 μ g) were resolved by SDS–PAGE and transferred to nitrocellulose membranes (Hybond-C super, Amersham, Arlington Heights, IL, USA). After transfer the gels were stained with GelCode blue stain reagent (Pierce, Rockford, IL, USA) to verify equal protein loading. The membranes were probed with specific primary antibodies and the immune-complexes were detected using appropriate horseradish peroxidase-like secondary antibodies chemiluminescence reagents (Super Signal West-Dura, Pierce), and Kodak Biomax MR-1 films (Sigma). The quantification of signal intensity was performed as indicated below.

Measurement of mitochondrial membrane potential ($\Delta\psi_m$)

Rat primary cortical neurons were cultured in 24-well plates. After various treatments 5,5',6,6'-tetrachloro-1,1',3,3'-tetraethyl-benzimidazolylcarbocyanine iodide (JC-1) was added to each well at a final concentration of 2.5 μ M. The plates were kept in the incubator for an additional 30 min, and the tissue culture supernatant was

removed and replaced with 1 ml of HBSS. The plate fluorescence was sequentially measured at λ emission at 530 nm and 590 nm with λ excitation at 480 nm in a CytoFluor 4000 fluorometer. JC-1 has a potential-dependent accumulation in the mitochondria demonstrated by a fluorescence emission shift from green (λ_{em} 530 nm) to red (λ_{em} 590 nm). A decrease in mitochondrial membrane potential ($\Delta\psi_m$) is associated with a decrease in the red/green fluorescence intensity ratio. We calculated the ratio between fluorescence intensity at 590 and 530 nm for each well and expressed the ratio in treated samples as percentage control as previously described (Gomez et al., 2001). Each individual treatment/time point reflects four replicates.

Assessment of cell viability and in-plate fluorometric caspase-3 assay

Rat primary cortical neurons were cultured in 96-well plates. After treatment, 50 μ l of tissue culture media was removed and used for the LDH release. This assay was performed using the CytoTox 96 assay kit (Promega) according to the manufacturer's protocol. Relative absorbance was measured at 492 nm on a Labsystems Multiskan Ascent plate reader. After removal of the tissue culture media for LDH release, the remaining media was aspirated and 50 μ l of caspase assay buffer (10 mM Hepes/KOH, pH 7.4, 2 mM EDTA, 0.1% Chaps, 5 mM dithiothreitol, 1 mM AEBSF, 10 μ g/ml pepstatin A, 20 μ g/ml leupeptin, and 10 μ g/ml aprotinin) containing 20 μ M Ac-DEVD-AMC (Biomol No. P411) was added to each well. The plate was introduced into a CytoFluor 4000 fluorometer and free AMC accumulation which resulted from cleavage of the aspartate–AMC bond was monitored continuously in each well over 1 h at 360-nm excitation and 460-nm emission wavelengths. The emission from each well was plotted against time. Linear regression analysis of the initial velocity (slope) of each curve yielded an activity for each sample. A standard curve was established using known concentrations of free AMC and the results were normalized based on the standard curve and expressed as picomoles (pmol) AMC per minute. Each individual treatment/time point reflects six replicates for all assays performed on cortical neurons cultured in 96-well plates. The interpretation of the in-plate assay is based on the fact that all wells were plated with and contain the same number of cells.

Hoechst staining

Nuclear morphology was assessed after Hoechst staining. Briefly, cells were harvested and fixed for 1 h at room temperature in PBS containing 4% formaldehyde. The cells were washed twice with PBS and stained with Hoechst 33342 (24 μ g/ml) (Molecular Probes) in PBS for 1 h. Nuclear morphology was observed under a fluorescence

microscope (Nikon Eclipse TE 200) and photographed with a Sony DKC5000 digital camera.

Assay of cytochrome *c* release

Cytochrome *c* release in the cytosol was assessed after subcellular fractionation. In short, after harvesting the cell pellet was resuspended in 5 Vol of a hypotonic buffer [20 mM Hepes–KOH (pH 7.5), 10 mM KCl, 1.5 mM MgCl₂, 1 mM EDTA, 1 mM EGTA, 1 mM DTT, 0.1 mM AEBSF, 20 µg/ml leupeptin, 10 µg/ml aprotinin, 250 mM sucrose] and incubated for 15 min on ice. Cells were homogenized by 15–20 passages through a 22-gauge needle, 1.5 inches long. The lysate was centrifuged at 1000g for 5 min at 4°C to pellet nuclei and unbroken cells. Supernatant was recovered and further centrifuged at 12,000g for 15 min at 4°C. The resulting mitochondrial pellet was suspended in lysis buffer. Supernatant was transferred to a new tube and centrifuged again at 12,000g for 15 min and the resulting supernatant representing the cytosolic fraction was recovered. Twenty-five micrograms of protein from the cytosolic fraction was analyzed by immunoblotting using an anti-cytochrome *c* monoclonal antibody, clone 7H8.2C12 (BD Biosciences, San Diego, CA, USA, No. 65981A).

Akt activity assay

Assay was performed using the Akt kinase assay kit (No. 9840) from Cell Signaling Technology following the manufacturer's instructions. In short, 250 µg of cellular lysate was incubated with 20 µl of immobilized Akt antibody slurry for 2 h with gentle rocking at 4°C. The pellet was washed twice with lysis buffer and twice with 1× kinase buffer. The kinase assay was performed by resuspending the pellet in 40 µl of 1× kinase buffer containing 200 µM ATP and 1 µg GSK-3 fusion protein and incubating for 30 min at 30°C with vigorous mixing. The reaction was terminated by adding 10 µl of 5× sample buffer to each tube and boiling at 100°C for 5 min. Thirty microliters of each sample were loaded on 12% SDS–polyacrylamide gels and then the samples were analyzed by Western immunoblotting with Phospho-Gsk-3α/β antibody. The quantification of the phosphorylated GSK-3 band on films was performed as indicated below.

Quantitative analysis

Measurement of signal intensity on Kodak Biomax MR-1 films after Western immunoblotting with various antibodies was performed using a GS-710 calibrated densitometer with Quantity One software (Bio-Rad Laboratories). The films used for analysis did not contain saturated pixels. All figures showing quantitative analysis include data from at least three independent experiments. All values were expressed as percentage of control.

Statistical analysis

All statistical analyses were performed using Statview 5.0 software (SAS Institute, Inc.). Data were analyzed and compared using either an *F* test followed by an unpaired *t* test, or a one-way ANOVA followed by a Fischer's PLSD. A probability of 0.05 was selected as the level of statistical significance for all data.

Acknowledgments

This work was supported by NIH RO1 NS36537, DAMD17-99-2-9007, and NIH HD40677. The authors thank Dr. Fen-Yang Sun at the Shanghai Medical Center for input during the early development of the project and Elvira Dabaghyan for expert technical support.

References

- Abe, A., Shayman, J.A., Radin, N.S., 1996. A novel enzyme that catalyzes the esterification of *N*-acetyl sphingosine. Metabolism of C2-ceramides. *J. Biol. Chem.* 271, 14383–14389.
- Adrain, C., Creagh, E.M., Martin, S.J., 2001. Apoptosis-associated release of Smac/DIABLO from mitochondria requires active caspases and is blocked by Bcl-2. *EMBO J.* 20, 6627–6634.
- Andjelkovic, M., Maira, S.M., Cron, P., Parker, P.J., Hemmings, B.A., 1999. Domain swapping used to investigate the mechanism of protein kinase B regulation by 3-phosphoinositide-dependent protein kinase 1 and Ser473 kinase. *Mol. Cell. Biol.* 19, 5061–5072.
- Andreyev, A., Fiskum, G., 1999. Calcium induced release of mitochondrial cytochrome *c* by different mechanisms selective for brain versus liver. *Cell Death Differ.* 6, 825–832.
- Andreyev, A.Y., Fahy, B., Fiskum, G., 1998. Cytochrome *c* release from brain mitochondria is independent of the mitochondrial permeability transition. *FEBS Lett.* 439, 373–376.
- Belham, C., Wu, S., Avruch, J., 1999. Intracellular signalling: PDK1—a kinase at the hub of things. *Curr. Biol.* 9, R93–R94.
- Benchoua, A., Guegan, C., Couriaud, C., Hosseini, H., Sampaio, N., Morin, D., Onteniente, B., 2001. Specific caspase pathways are activated in the two stages of cerebral infarction. *J. Neurosci.* 21, 7127–7134.
- Bernardi, P., 1999. Mitochondrial transport of cations: channels, exchangers, and permeability transition. *Physiol. Rev.* 79, 1127–1155.
- Bossy-Wetzel, E., Newmeyer, D.D., Green, D.R., 1998. Mitochondrial cytochrome *c* release in apoptosis occurs upstream of DEVD-specific caspase activation and independently of mitochondrial transmembrane depolarization. *EMBO J.* 17, 37–49.
- Bradham, C.A., Qian, T., Streetz, K., Trautwein, C., Brenner, D.A., Lemasters, J.J., 1998. The mitochondrial permeability transition is required for tumor necrosis factor alpha-mediated apoptosis and cytochrome *c* release. *Mol. Cell. Biol.* 18, 6353–6364.
- Bredesen, D.E., 2000. Apoptosis: overview and signal transduction pathways. *J. Neurotrauma* 17, 801–810.
- Brunet, A., Bonni, A., Zigmond, M.J., Lin, M.Z., Juo, P., Hu, L.S., Anderson, M.J., Arden, K.C., Blenis, J., Greenberg, M.E., 1998. Akt promotes cell survival by phosphorylating and inhibiting a Forkhead transcription factor. *Cell* 96, 857–868.
- Brunet, A., Park, J., Tran, H., Hu, L.S., Hemmings, B.A., Greenberg, M.E., 2001. Protein kinase SGK mediates survival signals by phosphorylating the forkhead transcription factor FKHL1 (FOXO3a). *Mol. Cell. Biol.* 21, 952–965.

- Budd, S.L., Tenneti, L., Lishnak, T., Lipton, S.A., 2000. Mitochondrial and extramitochondrial apoptotic signaling pathways in cerebrocortical neurons. *Proc. Natl. Acad. Sci. USA* 97, 6161–6166.
- Cardone, M.H., Roy, N., Stennicke, H.R., Salvesen, G.S., Franke, T.F., Stanbridge, E., Frisch, S., Reed, J.C., 1998. Regulation of cell death protease caspase-9 by phosphorylation. *Science* 282, 1318–1321.
- Carson, J.P., Behnam, M., Sutton, J.N., Du, C., Wang, X., Hunt, D.F., Weber, M.J., Kulik, G., 2002. Smac is required for cytochrome c-induced apoptosis in prostate cancer LNCaP cells. *Cancer Res.* 62, 18–23.
- Cazzoli, R., Carpenter, L., Biden, T.J., Schmitz-Peiffer, C., 2001. A role for protein phosphatase 2A-like activity, but not atypical protein kinase C ζ , in the inhibition of protein kinase B/Akt and glycogen synthesis by palmitate. *Diabetes* 50, 2210–2218.
- Chai, J., Du, C., Wu, J.W., Kyin, S., Wang, X., Shi, Y., 2000. Structural and biochemical basis of apoptotic activation by Smac/DIABLO. *Nature* 406, 855–862.
- Chauhan, D., Hideshima, T., Rosen, S., Reed, J.C., Kharbanda, S., Anderson, K.C., 2001. Apaf-1/cytochrome c-independent and Smac-dependent induction of apoptosis in multiple myeloma (MM) cells. *J. Biol. Chem.* 276, 24453–24456.
- Chinnaiyan, A.M., Dixit, V.M., 1997. Portrait of an executioner: the molecular mechanism of FAS/APO-1-induced apoptosis. *Semin. Immunol.* 9, 69–76.
- Cifone, M.G., De Maria, R., Roncalioli, P., Rippo, M.R., Azuma, M., Lanier, L.L., Santoni, A., Testi, R., 1994. Apoptotic signaling through CD95 (Fas/Apo-1) activates an acidic sphingomyelinase. *J. Exp. Med.* 180, 1547–1552.
- Crompton, M., 1999. The mitochondrial permeability transition pore and its role in cell death. *Biochem. J.* 341 (Pt 2), 233–249.
- Cross, D.A., Culbert, A.A., Chalmers, K.A., Facci, L., Skaper, S.D., Reith, A.D., 2001. Selective small-molecule inhibitors of glycogen synthase kinase-3 activity protect primary neurones from death. *J. Neurochem.* 77, 94–102.
- Culbert, A.A., Brown, M.J., Frame, S., Hagen, T., Cross, D.A., Bax, B., Reith, A.D., 2001. GSK-3 inhibition by adenoviral FRAT1 overexpression is neuroprotective and induces Tau dephosphorylation and beta-catenin stabilisation without elevation of glycogen synthase activity. *FEBS Lett.* 507, 288–294.
- Datta, S.R., Dudek, H., Tao, X., Masters, S., Fu, H., Gotoh, Y., Greenberg, M.E., 1997. Akt phosphorylation of BAD couples survival signals to the cell-intrinsic death machinery. *Cell* 91, 231–241.
- del Peso, L., Gonzalez-Garcia, M., Page, C., Herrera, R., Nunez, G., 1997. Interleukin-3-induced phosphorylation of BAD through the protein kinase Akt. *Science* 278, 687–689.
- Dijkers, P.F., Birkenkamp, K.U., Lam, E.W., Thomas, N.S., Lammers, J.W., Koenderman, L., Coffey, P.J., 2002. FKHR-L1 can act as a critical effector of cell death induced by cytokine withdrawal: protein kinase B-enhanced cell survival through maintenance of mitochondrial integrity. *J. Cell Biol.* 156, 531–542.
- Dijkers, P.F., Medema, R.H., Lammers, J.W., Koenderman, L., Coffey, P.J., 2000a. Expression of the pro-apoptotic Bcl-2 family member Bim is regulated by the forkhead transcription factor FKHR-L1. *Curr. Biol.* 10, 1201–1204.
- Dijkers, P.F., Medema, R.H., Pals, C., Banerji, L., Thomas, N.S., Lam, E.W., Burgering, B.M., Raaijmakers, J.A., Lammers, J.W., Koenderman, L., Coffey, P.J., 2000b. Forkhead transcription factor FKHR-L1 modulates cytokine-dependent transcriptional regulation of p27(KIP1). *Mol. Cell. Biol.* 20, 9138–9148.
- D'Mello, S.R., Galli, C., Ciotti, T., Calissano, P., 1993. Induction of apoptosis in cerebellar granule neurons by low potassium: inhibition of death by insulin-like growth factor I and cAMP. *Proc. Natl. Acad. Sci. USA* 90, 10989–10993.
- Eldadah, B.A., Faden, A.I., 2000. Caspase pathways, neuronal apoptosis, and CNS injury. *J. Neurotrauma* 17, 811–829.
- Eskes, R., Antonsson, B., Osen-Sand, A., Montessuit, S., Richter, C., Sadoul, R., Mazzei, G., Nichols, A., Martinou, J.C., 1998. Bax-induced cytochrome C release from mitochondria is independent of the permeability transition pore but highly dependent on Mg²⁺ ions. *J. Cell Biol.* 143, 217–224.
- Futerman, A.H., 1998. The roles of ceramide in the regulation of neuronal growth and development. *Biochemistry (Moscow)* 63, 74–83.
- Gendron, M.C., Schrantz, N., Metivier, D., Kroemer, G., Maciorowska, Z., Sureau, F., Koester, S., Petit, P.X., 2001. Oxidation of pyridine nucleotides during Fas- and ceramide-induced apoptosis in Jurkat cells: correlation with changes in mitochondria, glutathione depletion, intracellular acidification and caspase 3 activation. *Biochem. J.* 353, 357–367.
- Gomez, C., Reiriz, J., Pique, M., Gil, J., Ferrer, I., Ambrosio, S., 2001. Low concentrations of 1-methyl-4-phenylpyridinium ion induce caspase-mediated apoptosis in human SH-SY5Y neuroblastoma cells. *J. Neurosci. Res.* 63, 421–428.
- Goswami, R., Dawson, G., 2000. Does ceramide play a role in neural cell apoptosis? *J. Neurosci. Res.* 60, 141–149.
- Goswami, R., Kilus, J., Dawson, S.A., Dawson, G., 1999. Overexpression of Akt (protein kinase B) confers protection against apoptosis and prevents formation of ceramide in response to pro-apoptotic stimuli. *J. Neurosci. Res.* 57, 884–893.
- Hanna, A.N., Chan, E.Y., Xu, J., Stone, J.C., Brindley, D.N., 1999. A novel pathway for tumor necrosis factor- α and ceramide signaling involving sequential activation of tyrosine kinase, p21 (ras), and phosphatidylinositol 3-kinase. *J. Biol. Chem.* 274, 12722–12729.
- Hannun, Y.A., 1996. Functions of ceramide in coordinating cellular responses to stress. *Science* 274, 1855–1859.
- Hannun, Y.A., Luberto, C., 2000. Ceramide in the eukaryotic stress response. *Trends Cell Biol.* 10, 73–80.
- Joza, N., Susin, S.A., Daugas, E., Stanford, W.L., Cho, S.K., Li, C.Y., Sasaki, T., Elia, A.J., Cheng, H.Y., Ravagnan, L., Ferri, K.F., Zamzami, N., Wakeham, A., Hakem, R., Yoshida, H., Kong, Y.Y., Mak, T.W., Zuniga-Pflucker, J.C., Kroemer, G., Penninger, J.M., 2001. Essential role of the mitochondrial apoptosis-inducing factor in programmed cell death. *Nature* 410, 549–554.
- Keane, R.W., Srinivasan, A., Foster, L.M., Testa, M.P., Ord, T., Nonner, D., Wang, H.G., Reed, J.C., Bredesen, D.E., Kayalar, C., 1997. Activation of CPP32 during apoptosis of neurons and astrocytes. *J. Neurosci. Res.* 48, 168–180.
- Kowaltowski, A.J., Vercesi, A.E., Fiskum, G., 2000. Bcl-2 prevents mitochondrial permeability transition and cytochrome c release via maintenance of reduced pyridine nucleotides. *Cell Death Differ.* 7, 903–910.
- Krajewski, S., Krajewska, M., Ellerby, L.M., Welsh, K., Xie, Z., Deveraux, O.L., Salvesen, G.S., Bredesen, D.E., Rosenthal, R.E., Fiskum, G., Reed, J.C., 1999. Release of caspase-9 from mitochondria during neuronal apoptosis and cerebral ischemia. *Proc. Natl. Acad. Sci. USA* 96, 5752–5757.
- Kroesen, B.J., Pettus, B., Luberto, C., Busman, M., Sietsma, H., de Leij, L., Hannun, Y.A., 2001. Induction of apoptosis through B-cell receptor cross-linking occurs via de novo generated C16-ceramide and involves mitochondria. *J. Biol. Chem.* 276, 13606–13614.
- Lauquin, G.J., Duplaa, A.M., Klein, G., Rousseau, A., Vignais, P.V., 1976. Isobongkrekic acid, a new inhibitor of mitochondrial ADP-ATP transport: radioactive labeling and chemical and biological properties. *Biochemistry* 15, 2323–2327.
- Lee, T.C., Ou, M.C., Shinozaki, K., Malone, B., Snyder, F., 1996. Biosynthesis of *N*-acetyl sphingosine by platelet-activating factor: sphingosine CoA-independent transacylase in HL-60 cells. *J. Biol. Chem.* 271, 209–217.
- Lemasters, J.J., Qian, T., Bradham, C.A., Brenner, D.A., Cascio, W.E., Trost, L.C., Nishimura, Y., Nieminen, A.L., Herman, B., 1999. Mitochondrial dysfunction in the pathogenesis of necrotic and apoptotic cell death. *J. Bioenerg. Biomembr.* 31, 305–319.

- Li, M., Wang, X., Meintzer, M.K., Laessig, T., Birnbaum, M.J., Heidenreich, K.A., 2000. Cyclic AMP promotes neuronal survival by phosphorylation of glycogen synthase kinase 3 β . *Mol. Cell. Biol.* 20, 9356–9363.
- Li, P., Nijhawan, D., Budihardjo, I., Srinivasula, S.M., Ahmad, M., Alnemri, E.S., Wang, X., 1997. Cytochrome c and dATP-dependent formation of Apaf-1/caspase-9 complex initiates an apoptotic protease cascade. *Cell* 91, 479–489.
- Liu, Z., Sun, C., Olejniczak, E.T., Meadows, R.P., Betz, S.F., Oost, T., Herrmann, J., Wu, J.C., Fesik, S.W., 2000. Structural basis for binding of Smac/DIABLO to the XIAP BIR3 domain. *Nature* 408, 1004–1008.
- Luberto, C., Hannun, Y.A., 2000. Use of short-chain ceramides. *Methods Enzymol.* 312, 407–420.
- Luo, X., Budihardjo, I., Zou, H., Slaughter, C., Wang, X., 1998. Bid, a Bcl2 interacting protein, mediates cytochrome c release from mitochondria in response to activation of cell surface death receptors. *Cell* 94, 481–490.
- Marchetti, P., Castedo, M., Susin, S.A., Zamzami, N., Hirsch, T., Macho, A., Haeflner, A., Hirsch, F., Geuskens, M., Kroemer, G., 1996. Mitochondrial permeability transition is a central coordinating event of apoptosis. *J. Exp. Med.* 184, 1155–1160.
- Marks, N., Berg, M.J., Guidotti, A., Saito, M., 1998. Activation of caspase-3 and apoptosis in cerebellar granule cells. *J. Neurosci. Res.* 52, 334–341.
- Medema, R.H., Kops, G.J., Bos, J.I., Burgering, B.M., 2000. AFX-like Forkhead transcription factors mediate cell-cycle regulation by Ras and PKB through p27kip1. *Nature* 404, 782–787.
- Mesner, P.W., Winters, T.R., Green, S.H., 1992. Nerve growth factor withdrawal-induced cell death in neuronal PC12 cells resembles that in sympathetic neurons. *J. Cell Biol.* 119, 1669–1680.
- Mukhin, A.G., Ivanova, S.A., Allen, J.W., Faden, A.I., 1998. Mechanical injury to neuronal/glial cultures in microplates: role of NMDA receptors and pH in secondary neuronal cell death. *J. Neurosci. Res.* 51, 748–758.
- Mukhin, A.G., Ivanova, S.A., Knoblach, S.M., Faden, A.I., 1997. New in vitro model of traumatic neuronal injury: evaluation of secondary injury and glutamate receptor-mediated neurotoxicity. *J. Neurotrauma* 14, 651–663.
- Nakamura, N., Ramaswamy, S., Vazquez, F., Signoretti, S., Loda, M., Sellers, W.R., 2000. Forkhead transcription factors are critical effectors of cell death and cell cycle arrest downstream of PTEN. *Mol. Cell. Biol.* 20, 8969–8982.
- Oppenheim, R.W., Flavell, R.A., Vinsant, S., Prevette, D., Kuan, C.Y., Rakic, P., 2001. Programmed cell death of developing mammalian neurons after genetic deletion of caspases. *J. Neurosci.* 21, 4752–4760.
- Pap, M., Cooper, G.M., 1998. Role of glycogen synthase kinase-3 in the phosphatidylinositol 3-kinase/Akt cell survival pathway. *J. Biol. Chem.* 273, 19929–19932.
- Pap, M., Cooper, G.M., 2002. Role of translation initiation factor 2B in control of cell survival by the phosphatidylinositol 3-kinase/Akt/glycogen synthase kinase 3 β signaling pathway. *Mol. Cell. Biol.* 22, 578–586.
- Pastorino, J.G., Chen, S.T., Tafani, M., Snyder, J.W., Farber, J.L., 1998. The overexpression of Bax produces cell death upon induction of the mitochondrial permeability transition. *J. Biol. Chem.* 273, 7770–7775.
- Pastorino, J.G., Hoek, J.B., 2000. Ethanol potentiates tumor necrosis factor- α cytotoxicity in hepatoma cells and primary rat hepatocytes by promoting induction of the mitochondrial permeability transition. *Hepatology* 31, 1141–1152.
- Pittman, R.N., Wang, S., DiBenedetto, A.J., Mills, J.C., 1993. A system for characterizing cellular and molecular events in programmed neuronal cell death. *J. Neurosci.* 13, 3669–3680.
- Saito, M., Guidotti, A., Berg, M.J., Marks, N., 1998. The semisynthetic glycosphingolipid LIGA20 potentially protects neurons against apoptosis. *Ann. N.Y. Acad. Sci.* 845, 253–262.
- Salinas, M., Lopez-Valdaliso, R., Martin, D., Alvarez, A., Cuadrado, A., 2000. Inhibition of PKB/Akt1 by C2-ceramide involves activation of ceramide-activated protein phosphatase in PC12 cells. *Mol. Cell. Neurosci.* 15, 156–169.
- Scarlett, J.L., Sheard, P.W., Hughes, G., Ledgerwood, E.C., Ku, H.H., Murphy, M.P., 2000. Changes in mitochondrial membrane potential during staurosporine-induced apoptosis in Jurkat cells. *FEBS Lett.* 475, 267–272.
- Schubert, K.M., Scheid, M.P., Duronio, V., 2000. Ceramide inhibits protein kinase B/Akt by promoting dephosphorylation of serine 473. *J. Biol. Chem.* 275, 13330–13335.
- Shin, I., Bakin, A.V., Rodeck, U., Brunet, A., Arteaga, C.L., 2001. Transforming growth factor β enhances epithelial cell survival via Akt-dependent regulation of FKHL1. *Mol. Biol. Cell* 12, 3328–3339.
- Siskind, L.J., Kolesnick, R.N., Colombini, M., 2002. Ceramide channels increase the permeability of the mitochondrial outer membrane to small proteins. *J. Biol. Chem.* 10, 10.
- Srinivasula, S.M., Datta, P., Fan, X.I., Fernandes-Alnemri, T., Huang, Z., Alnemri, E.S., 2000. Molecular determinants of the caspase-promoting activity of Smac/DIABLO and its role in the death receptor pathway. *J. Biol. Chem.* 275, 36152–36157.
- Susin, S.A., Lorenzo, H.K., Zamzami, N., Marzo, I., Snow, B.E., Brothers, G.M., Mangion, J., Jacotot, E., Costantini, P., Loeffler, M., Larochette, N., Goodlett, D.R., Aebersold, R., Siderovski, D.P., Penninger, J.M., Kroemer, G., 1999. Molecular characterization of mitochondrial apoptosis-inducing factor. *Nature* 397, 441–446.
- Tafani, M., Minchenko, D.A., Serroni, A., Farber, J.L., 2001. Induction of the mitochondrial permeability transition mediates the killing of HeLa cells by staurosporine. *Cancer Res.* 61, 2459–2466.
- Tang, E.D., Nunez, G., Barr, F.G., Guan, K.L., 1999. Negative regulation of the forkhead transcription factor FKHR by Akt. *J. Biol. Chem.* 274, 16741–16746.
- Taniwaki, T., Yamada, T., Asahara, H., Ohyagi, Y., Kira, J., 1999. Ceramide induces apoptosis to immature cerebellar granule cells in culture. *Neurochem. Res.* 24, 685–690.
- Toker, A., Newton, A.C., 2000. Cellular signaling: pivoting around PDK-1. *Cell* 103, 185–188.
- Toman, R.E., Movsesyan, V., Murthy, S.K., Miltien, S., Spiegel, S., Faden, A.I., 2002. Ceramide-induced cell death in primary neuronal cultures: upregulation of ceramide levels during neuronal apoptosis. *J. Neurosci. Res.* 68, 323–330.
- Troy, C.M., Rabacchi, S.A., Hohl, J.B., Angelastro, J.M., Greene, L.A., Shelanski, M.L., 2001. Death in the balance: alternative participation of the caspase-2 and -9 pathways in neuronal death induced by nerve growth factor deprivation. *J. Neurosci.* 21, 5007–5016.
- Vander Heiden, M.G., Chandel, N.S., Schumacker, P.T., Thompson, C.B., 1999. Bcl-xL prevents cell death following growth factor withdrawal by facilitating mitochondrial ATP/ADP exchange. *Mol. Cell* 3, 159–167.
- Williams, M.R., Arthur, J.S., Balendran, A., van der Kaay, J., Poli, V., Cohen, P., Alessi, D.R., 2000. The role of 3-phosphoinositide-dependent protein kinase 1 in activating AGC kinases defined in embryonic stem cells. *Curr. Biol.* 10, 439–448.
- Yakovlev, A.G., Faden, A.I., 2001. Caspase-dependent apoptotic pathways in CNS injury. *Mol. Neurobiol.* 24, 131–144.
- Yakovlev, A.G., Ota, K., Wang, G., Movsesyan, V., Bao, W.L., Yoshihara, K., Faden, A.I., 2001. Differential expression of apoptotic protease-activating factor-1 and caspase-3 genes and susceptibility to apoptosis during brain development and after traumatic brain injury. *J. Neurosci.* 21, 7439–7446.
- Zamzami, N., Kroemer, G., 2001. The mitochondrion in apoptosis: how Pandora's box opens. *Nat. Rev. Mol. Cell. Biol.* 2, 67–71.
- Zamzami, N., Susin, S.A., Marchetti, P., Hirsch, T., Gomez-Monterrey, I., Castedo, M., Kroemer, G., 1996. Mitochondrial control of nuclear apoptosis. *J. Exp. Med.* 183, 1533–1544.
- Zha, I., Harada, H., Osipov, K., Jockel, J., Waksman, G., Korsmeyer, S.J., 1997. BH3 domain of BAD is required for heterodimerization

- with BCL-XL and pro-apoptotic activity. *J. Biol. Chem.* 272, 24101–24104.
- Zha, J., Harada, H., Yang, E., Jockel, J., Korsmeyer, S.J., 1996. Serine phosphorylation of death agonist BAD in response to survival factor results in binding to 14-3-3 not BCL-X(L). *Cell* 87, 619–628.
- Zhou, H., Summers, S.A., Birnbaum, M.J., Pittman, R.N., 1998. Inhibition of Akt kinase by cell-permeable ceramide and its implications for ceramide-induced apoptosis. *J. Biol. Chem.* 273, 16568–16575.
- Zinda, M.J., Vlahos, C.J., Lai, M.T., 2001. Ceramide induces the dephosphorylation and inhibition of constitutively activated Akt in PTEN negative U87mg cells. *Biochem. Biophys. Res. Commun.* 280, 1107–1115.
- Zou, H., Henzel, W.J., Liu, X., Lutschg, A., Wang, X., 1997. Apaf-1, a human protein homologous to *C. elegans* CED-4, participates in cytochrome c-dependent activation of caspase-3. *Cell* 90, 405–413.
- Zou, H., Li, Y., Liu, X., Wang, X., 1999. An APAF-1/cytochrome c multimeric complex is a functional apoptosome that activates procaspase-9. *J. Biol. Chem.* 274, 11549–11556.
- Zundel, W., Giaccia, A., 1998. Inhibition of the anti-apoptotic PI(3)K/Akt/Bad pathway by stress. *Genes Dev.* 12, 1941–1946.

Gene Expression Profile Changes Are Commonly Modulated across Models and Species after Traumatic Brain Injury

JOANNE E. NATALE,^{1,2} FARID AHMED,^{1,2} IBOLJA CERNAK,²
BOGDAN STOICA,² and ALAN I. FADEN²

ABSTRACT

Brain trauma is a major cause of morbidity and mortality, both in adult and pediatric populations. Much of the functional deficit derives from delayed cell death resulting from induction of neurotoxic factors that overwhelm endogenous neuroprotective responses. To identify the potential molecular mechanisms underlying such delayed responses, we compared gene expression patterns using high-density oligonucleotide arrays at 4, 8, 24, and 72 h after moderate levels of lateral fluid percussion-induced brain injury in rats and lateral controlled cortical impact injury in mice (a total of 47 profiles). Expression of 82 genes in 12 functional categories was significantly changed in both species after trauma. The largest number of gene expression changes were found in the functional groups related to inflammation (17%), transcription regulation (16%), and cell adhesion/extracellular matrix (15%). Fifty percent of genes similarly altered across models had not been previously implicated in traumatic brain injury. Of particular interest were expression changes in genes linked to neurodegeneration, such as ATF3 and lysosomal membrane glycoprotein 2, and to neuroprotection including lipocortin 1, calponin 3, gelsolin, Id-1, and p45 NF-E2. Gene expression profiling across species and models may help identify candidate molecular pathways induced by brain injury, some of which may provide novel targets for therapeutic intervention.

Key words: controlled cortical impact; fluid percussion; gene expression; mRNA

INTRODUCTION

TRAUMATIC BRAIN INJURY (TBI) induces a cascade of biochemical responses, both neurotoxic and neuroprotective that substantially determine subsequent tissue loss and associated functional deficits. However, molecular mechanisms underlying such delayed responses are not fully understood. Moreover, although it has long been recognized that TBI causes changes in gene expression patterns, until recently such studies have examined relatively small numbers of genes and/or their protein products (for review, see Marciano et al., 2002).

Microarray-based technologies can evaluate gene expression changes in a highly parallel manner, allowing the measurement of changes of thousands of genes and/or expressed sequence tags as a function of time after injury. Several groups have recently utilized microarray technology to examine gene expression changes following controlled cortical impact injury in rodents (Kobori et al., 2002; Matzilevich et al., 2002; Long et al., 2003; Raghavendra Rao et al., 2003). The two studies using rats examined alterations during the first 24 h following injury in either hippocampus (Matzilevich et al., 2002) or cerebral cortex (Raghavendra Rao et al., 2003). Both

¹Research Centers for Genetic Medicine and Neuroscience, Children's National Medical Center, Washington, D.C.

²Department of Neuroscience, Georgetown University School of Medicine, Washington, D.C.

found up-regulation of genes associated with inflammatory responses (e.g., interleukin-1 β , monocyte inhibitory protein-2, P-selectin, monocyte inhibitory protein-1 α [MIP-1 α]), oxidative stress (e.g., heme oxygenase-1, [HO-1]), and transcription regulation (e.g., interferon regulator factor-1, ICER, c-fos, neuronal activity-regulated pentraxin). In addition, both studies observed down-regulation of glutamate receptor subtypes (e.g., GLURK3, GLUR3). Examining a more extended post-injury period, cortical responses were also analyzed in a mouse model (Kobori et al., 2002). Comparison of these studies showed a subset of genes commonly regulated across both species, specifically genes associated with inflammatory processes (e.g., MIP-1 α , monocyte inhibitory protein-1 β , Fc receptor gamma), cell growth (e.g., brain derived growth factor), cell cycle regulation, and oxidative stress (e.g., GADD45, HO-1, metallothionein 1).

These common gene expression changes suggest that it is possible to identify consistent transcriptional responses to traumatic brain injury. However, comparing across experimental platforms and experimental systems may introduce considerable variability, due to the use of different controls (sham-injured vs. normal portions of the brain), platforms (oligonucleotide or cDNA microarrays), time-points, or analytical methods employed. Therefore, observed changes may in part reflect such methodological differences.

The purpose of the present study was to identify common gene expression changes across different injury models (fluid percussion vs. controlled cortical impact) and species (rat vs. mouse) in order to address the hypothesis that common changes across pathobiologically different models and species may help to identify the more important secondary injury responses. Importantly, we examined the same brain regions (parietal cortex directly underlying cortical impact site) in both models and compared injured to sham-injured tissue at all time points. We also studied multiple time points (4, 8, 24, 72 h), used replicate samples in order to conduct statistical analyses while holding constant the ratio of sham to experimental chips (2:3), conducted all expression profiling on the Affymetrix platform, and consistently applied normalization and filtering criteria prior to stringent statistical analyses.

MATERIALS AND METHODS

Experimental Injury Models

All protocols involving animals were approved by the Georgetown University Institutional Animal Use and Care Committee and were in compliance with the stan-

dards stated in the *Committee on Care and Use of Laboratory Animals of the Institute of Laboratory Resources*, National Research Council (DHEW pub. no. [NIH] 85-23, 1985). We employed pathobiologically different models in the rat and mouse. However, both reflect frequently used models of TBI and show many common mechanisms of secondary injury and cell death (Yakovlev et al., 1997; Fox et al., 1998).

Rat lateral fluid percussion trauma model. During the past 15 years we have developed and evaluated a lateral fluid percussion-induced traumatic brain injury model in rats. This model has been extensively characterized with regard to physiologic, biochemical, metabolic, behavioral and histological changes (Faden, 1989, 1993; McIntosh et al., 1989; Faden et al., 1993; Yakovlev et al., 1997). Briefly, male Sprague-Dawley rats (400 \pm 25 g) housed in a 12-h light, 12-h dark cycle with free access to standard rodent chow and water, were anesthetized with sodium pentobarbital (60 mg/kg i.p.), intubated, and implanted with tail vein and artery catheters. Brain temperature was assessed indirectly through a thermister in the temporalis muscle and maintained at 36–37°C through a feedback-controlled heating system. A small craniotomy (5 mm) located midway between the lambda and bregma sutures over the left parietal cortex allowed insertion of a female Leur-Loc that was cemented in place. The fluid-percussion head injury device consisted of a Plexiglas cylindrical reservoir filled with isotonic saline; one end included a transducer that was mounted and connected to a 5 mm tube attached through a male Leur-Loc fitting. A pendulum struck a piston at the opposite end of the device, producing a brief 2.5 atmosphere pressure pulse leading to the deformation of underlying brain and causing moderate brain injury as defined by behavioral changes and histopathology (McIntosh et al., 1989). Three rats were injured for each time point (4, 8, 24, and 72 h). Sham rats (four rats at the 4-h time point and two rats/time point at 8, 24, and 72 h) were subjected to the surgery but were not injured. Three strain- and age-matched rats, not subjected to any surgery/injury, served as the naive group. At predetermined times after surgery (4, 8, 24, and 72 h), sham and injured rats were anesthetized with pentobarbital (100 mg/kg i.p.) and decapitated with a sharp, small animal guillotine. The brain was rapidly removed and placed on an iced dissection plate. A 7-mm disk of parieto-occipital cortex, centered on the point of impact of the injury and containing the contusion area, was removed and immediately frozen in chilled 2-methylbutane and then stored at –80°C. For naive and sham rats, the same size cortical region was sampled and stored.

Mouse controlled cortical impact (CCI) model. We have also extensively characterized a mouse CCI model with regard to biochemical, behavioral and histological changes (Fox and Faden, 1998; Fox et al., 1999; Yakovlev et al., 2001; Faden et al., 2003). Male C57BL/6 mice (20–25 g) were housed in a 12-h light, 12-h dark cycle with free access to standard rodent chow and water. Surgical anesthesia was induced and maintained in freely breathing mice with 4% and 1.5% isoflurane respectively, using a flow rate of 1–1.5 L/minute oxygen. The depth of anesthesia was assessed by response of the palpebral and pedal-withdrawal reflexes, and by monitoring the respiration rate of the mouse. The mouse was placed on a heated pad and rectal temperature was maintained at $38 \pm 0.2^\circ\text{C}$. The head was mounted in the stereotaxic frame of the device and a 4-mm craniotomy, between lambda and bregma on the central aspect of the left parietal bone, was made using a tissue puncher.

The mouse controlled cortical impact injury device consisted of a microprocessor-controlled pneumatic impactor with an interchangeable tip. The core rod of a linear variable differential transducer (LVDT) was attached to the lower end of the impactor. An oscilloscope recorded the time/displacement curve produced by the downward force on the LVDT, allowing precise measurement of the impactor velocity. The impounder tip of the pneumatic injury device was positioned on the surface of the exposed dura, and then withdrawn to create a 44-mm stroke distance. A 6 m/sec impact velocity and 1.5-mm deformation depth produced a moderate level of injury as defined by behavioral and histological outcomes (Fox et al., 1998). After the injury, anesthesia was discontinued and each mouse placed in a heated cage for 45 min during recovery from anesthesia. Sham mice (6/time-point) were subjected to the same surgery, but not injured. Naive mice ($n = 6$) were not subjected to any surgery/injury. At predetermined times after surgery \pm injury (4, 8, 24, and 72 h), mice were anesthetized with pentobarbital (100 mg/kg i.p.) and decapitated with a sharp, small animal guillotine. The brain was rapidly removed and placed on an iced dissection plate. A 4-mm-diameter disk of parieto-occipital cortex, centered on the point of impact of the injury and containing the contusion area, was removed and immediately frozen in chilled 2-methylbutane then stored at -80°C . For naive and sham mice, the same size cortical region was sampled and stored.

RNA Extraction, Amplification, and Hybridization to Microarrays

To ensure adequate tissue for RNA extraction (~ 100 mg), three mouse cortex disks were pooled prior to RNA extraction. Pooling produced two naive (from six mice)

samples, and for each experimental time point two sham (from six mice) and three injured samples (from nine mice) were obtained ($n = 22$ profiles). However, cortical tissue from one rat provided sufficient RNA without the need for pooling ($n = 25$ profiles). Frozen brain tissue was rapidly homogenized using a Polytron (Brinkmann Instruments, Westbury, NY) in TRIzol reagent (Invitrogen Corp., Carlsbad, CA), then RNA extracted with chloroform, and precipitated in isopropyl alcohol. Total RNA was purified using an RNeasy kit (Qiagen Inc., Valencia, CA) prior to quantification. To detect extensive degradation, purified RNA was run on an agarose gel prior to cDNA synthesis. Degraded RNA was not used for hybridization. Procedures for cRNA preparation and GeneChip processing were performed as previously described. Briefly, seven micrograms of total RNA from each tissue sample were converted into double-stranded cDNA with an oligo-dT primer containing T7 RNA polymerase promoter. Purified double-stranded cDNA was converted to biotin-labeled cRNA. Each fragmented cRNA sample was hybridized to rat U34A or mouse Mu74Av2 oligonucleotide microarrays (Affymetrix Inc., Santa Clara, CA) for 16 h at 60 rpm at 45°C . The mouse Mu74Av2 microarray contains $\sim 12,500$ full-length sequences and expressed sequence tags (referred to as probe sets or genes throughout this text), while the rat U34A microarray contains ~ 8800 probe sets. After hybridization, each microarray was then washed and stained on the Affymetrix Fluidics Station 400 using instructions and reagents provided by Affymetrix. Raw intensity data were captured, and the Affymetrix GeneChip[®] software MAS 5.0 was used to calculate signal intensity values for each oligonucleotide probe set in each genome (mouse or rat). A scaling factor, with a target intensity of microarray sector fluorescence to 800, was automatically applied to each microarray by the MAS 5.0 algorithm, permitting reproducible interarray comparisons. Probe sets hybridization performance (pairs of 20 perfect match and mismatch 25mer oligonucleotides per probe sets) identified signal intensities that were reliably detected as present, and eliminated most non-specific cross-hybridization signals, as previously described (Chen et al., 2000; Bakay et al., 2002).

Microarray Quality Control, Correction for Saturated Probe Sets, and Normalization

Within both species, each microarray underwent a stringent quality control evaluation as previously described (Chen et al., 2000; Di Giovanni et al., 2003). The following parameters were considered: cRNA fold changes (amount of cRNA obtained from starting total RNA); scaling factor; percentage of probe sets reliably

detected (present); mean signal value indicating the relative abundance of a probe set; and correlation coefficient of mean signal values for each transcript between microarrays at the same experimental time point. In addition, control charts were generated using scaling factor and percentage present probe sets to identify systematic errors in the expression profiling process. Identification of microarrays with scaling factor or percent present ≥ 2 standard deviations above or below the mean, as shown in Figure 1, alerted us to the possibility of significant errors in laboratory methods.

We used a high setting for the microarray scanner photomultiplier tube to maximize sensitivity of low abundant transcripts at the expense of intensity saturation of high abundant transcripts. Therefore, for the chips in the mouse genome, we used an algorithm to detect probe sets that became saturated by the biotin/streptavidin/phycoerythrin amplification (T. Teslovich, unpublished data). For each of these probe sets, the saturated intensity value was replaced with non-saturated intensity signal generated by the initial streptavidin/phycoerythrin scan across all microarrays in the mouse experiment. This saturated probe set procedure was repeated for the microarrays in the rat experiment.

Data Filtering and Statistical Analysis

We based all further analysis only on those probe sets that were detected in 40% or more of the microarrays

comprising the complete microarray series for each experimental model. This data scrubbing retained the probe sets with the most reliable and consistent performance between multiple measurements among arrays of the same experimental group (Di Giovanni et al., 2003).

Experiment normalization and statistical analysis were performed using GeneSpring software, version 5.0 (Silicon Genetics, Redwood, CA). For each probe set, signal intensity from injured and sham controls were normalized to the mean signal intensity generated from the same cortical region from three naive rats or mice. We identified significantly regulated genes using two methods. For method 1, normalized signal intensities for each probe set were compared between sham ($n = 8$ or 10) and injured ($n = 12$) microarrays within each experimental model. Two criteria were then applied in order for a response to be significant: (1) at least a two-fold change in signal intensity and (2) meeting a criterion p -value < 0.05 using a Welch t -test, without correction for multiple comparisons. Method 1 pooled chips from all time points and was therefore more stringent because it was less likely to detect mRNA levels that were variably expressed when compared to sham at only one time point. To improve identification of probe sets that may have been significantly regulated at only one point post-injury, we also identified genes as "significant" if they met these same two criteria when samples (sham versus injured) were compared within each time point (method 2). The combination of fold change threshold and p values serves to eliminate most false positives, producing a more strin-

TABLE 1. OLIGONUCLEOTIDE SEQUENCES FOR REVERSE TRANSCRIPTASE-PCR

Gene name	Sequence	Product size
RPL-19	5'-ggctactgccaacgctcgat-3'	325
RPL-19	5'-ccttgacagagtcttgat-3'	
Peripheral-type benzodiazepine receptor	5'-ctctacactggcagctggctc-3'	309
Peripheral-type benzodiazepine receptor	5'-acctgatgcctggctggcag-3'	
C-C chemokine receptor 5	5'-cacattgtcaaacgcttctgcca-3'	308
C-C chemokine receptor 5	5'-ttactgtctcatcaataattctc-3'	
Metallothionein-1	5'-cctgcacctgctccagctcc-3'	287
Metallothionein-1	5'-tggaggtgtacggcaagactc-3'	
Myelin-associated glycoprotein	5'-gattgccattgtctgtacatca-3'	326
Myelin-associated glycoprotein	5'-actcagccagctcctgtgca-3'	
Neurokinin	5'-catgtgcagatctctcacaag-3'	300
Neurokinin	5'-tagaattacaatgcttattggcac-3'	
Cathepsin D	5'-atgaactacaccagagaagtaca-3'	313
Cathepsin D	5'-agcaactactaggcagtgatga-3'	
Hemoglobin beta	5'-ctgctgattgtctacccttga-3'	320
Hemoglobin beta	5'-tggaaggcagcctgtgact-3'	
TMP21-I	5'-gagatcgcaaaagttagaact-3'	296
TMP21-I	5'-agcgatgttctgctgctcca-3'	

PRL-19, ribosomal protein (housekeeping gene).

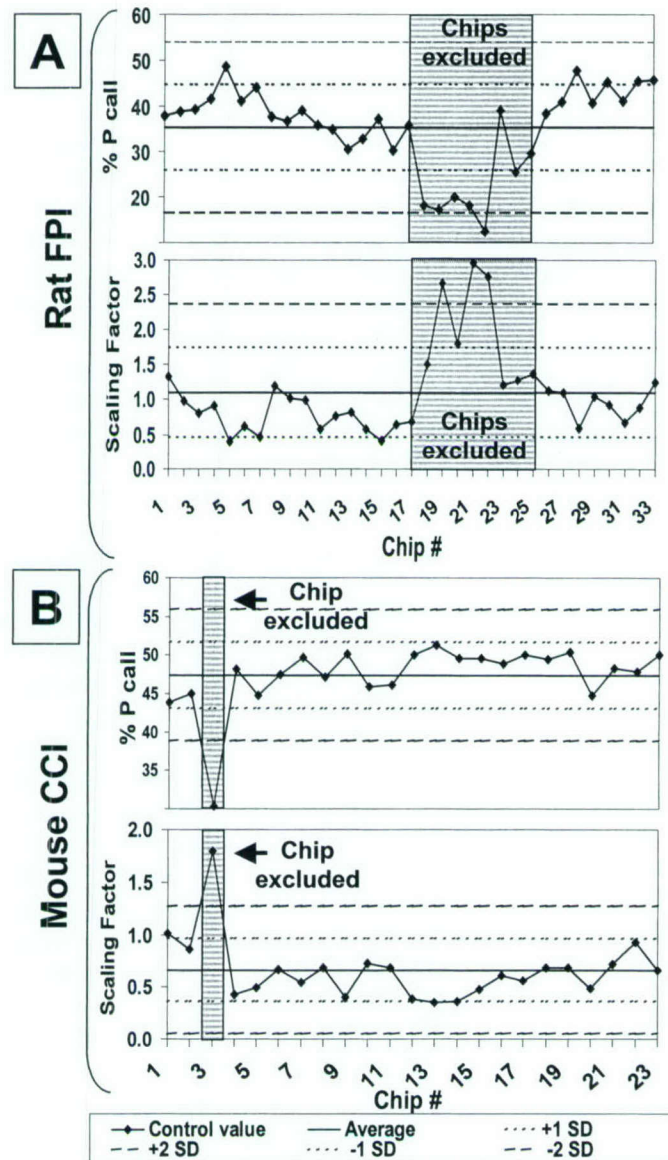


FIG. 1. Control charts showing variability in microarray processing across each experiment. **(A)** Rat fluid percussion injury experiment. Percentage present call (upper panel) and scaling factor (lower panel) are plotted for each chip in the order that chips were hybridized. Mean and standard deviation for percentage present call or scaling factor were calculated for all chips in the experiment. Horizontal lines indicated the mean (solid line), one standard deviation (dotted lines), and two standard deviations (dashed lines) above and below the mean. Chips with control values falling outside 2 standard deviations from the mean are flagged (chips 20, 22, 23). All chips processed under the same conditions as flagged chips are excluded (gray region) from further analysis. **(B)** Mouse controlled cortical impact. Same as A. One chip, 3, failed to meet control standards and was excluded.

gent list. To accurately identify significantly regulated genes shared by both species, cross species probe set matches were identified using UniGene and the Program in Genomic Applications web site <http://pga.tigr.org/tigr-scripts/xref/list.pl>. Furthermore, each match was verified by direct sequence matching of significantly regulated rat and mouse genes.

Microarray Validation: Semi-Quantitative Reverse Transcriptase-Polymerase Chain Reaction

One μg of total RNA was used for cDNA synthesis using SuperScript reverse transcriptase and oligo (dT)-primer (Invitrogen Corp., Carlsbad, CA). The amount of synthesized cDNA was evaluated by PCR using primers

specific for ribosomal protein RPL19. Polymerase chain reactions (PCR) were performed in a PTC-225 Thermal Cycler (MJ Research, Waltham, MA) using AmpliTaq polymerase (Applied Biosystems, Foster City, CA). Each PCR reaction was repeated at least twice. The thermal cycling parameters were as follows: 1 min 30 sec at 94°C followed by 30 cycles of 30 sec at 94°C, 1 min 30 sec at 59°C, 1 min at 72°C and final incubation for 5 min at 72°C. PCR reaction products were analyzed by agarose gel-electrophoresis. Intensity of sham ($n = 2$) and injured (two samples randomly selected from three samples at each time point) cDNA was adjusted with 2 randomly selected naive samples using the housekeeping gene RPL19. Normalized cDNA was then used to estimate the relative abundance of C-C chemokine receptor 5 (CCR5), cathepsin D, hemoglobin beta, metallothionein 1 (Mt 1), myelin-associated glycoprotein (MAG), neurokinin, peripheral benzodiazepine receptor (PBR), tissue inhibitor of metalloproteinase 1 (TIMP-1), and transmembrane protein Tmp21-I. Primers (Invitrogen Corp., Carlsbad, CA) for each gene were located in different exons (Table 1). Different dilutions of cDNA samples were used for different genes to provide a linear range for PCR. The intensity of DNA bands was measured using UN-SCAN-IT gel digitizing software (Silk Scientific Inc., Orem, UT).

Functional Classification of Genes

The 82 differentially expressed genes were assigned functional annotations based on information in publicly available sources including Gene Ontology and PubMed. It is recognized that a given gene may have multiple functions and that a variety of assignment systems can be constructed. For these analyses, each gene was assigned to only one functional class.

RESULTS

Stringent Quality Assurance Improves Reliability of Microarray Results

We applied stringent quality control standards and data filtering using methods previously reported by our labo-

ratory (Di Giovanni et al., 2003). As shown in Table 2, these included an evaluation of the scaling factor, proportion of present probe sets, mean signal value, and observed correlation between signal values for each gene between microarrays obtained at the same experimental time point and from the same experimental model. We obtained highly reliable gene expression profile data in both the rat and mouse model. Furthermore, since the microarrays used in this study were processed over a five-month period, we used control charts to demonstrate that our process remained in statistical control over the course of the experiment (Brassard, 1996). Figure 1 displays control charts of present calls and scaling factor versus chip number assigned sequentially by the order in which they were hybridized. Data for both the rat and the mouse are displayed. Quality control standards (values within two standard deviations above or below the mean value for all chips in the experiment) were not achieved for three rat microarrays (chips 20, 22, 23). We subsequently identified reagent contamination during the fragmentation step as the cause, and then successfully repeated the expression profiling for these and five additional chips (18–19, 21, 24–25) that were processed under the same conditions. Quality control standards (values within two standard deviations above or below the mean value for all chips in the experiment) were not achieved for one mouse microarrays (chip 3). The nine chips that failed to meet quality control criteria (gray regions) were not used in subsequent analyses. Thus, these quality control methods permit identification of aberrant individual chips that might not have been detected in statistical analyses.

Temporal Profiling Demonstrates Serial Gene Regulation after TBI

Approximately half of the probe sets fulfilled the requirement of >40% of the microarrays showing a "present" call for each gene (3751 probe sets from the 8800 represented on the rat U34A chip [43%]; 6216 probe sets from the 12,488 represented on the mouse Mu74Av2 chip [50%]). Of the 3751 rat probe sets analyzed, we found that 266 (7%) showed a significant change in expression

TABLE 2. QUALITY CONTROL VALUES (MEAN AND RANGE) FOR 33 U34A AND 24 MU74AV2 GENE CHIPS

	U34A (rat)		Mu74Av2 (mouse)	
	Mean \pm SD	Range	Mean \pm SD	Range
Scaling factor	0.83 \pm 0.3	0.42–1.33	0.66 \pm 0.3	0.40–1.01
% Present	39.5 \pm 4.9	30.4–48.6	48.1 \pm 2.2	43.8–51.3
Signal value	2327 \pm 217	1824–2752	1865 \pm 112	1703–2013
Signal correlation ^a	0.89 \pm 0.1	0.73–0.96	0.95 \pm 0.03	0.88–0.98

^aMean between chip pair-wise correlation of signal intensities.

GENE PROFILES MODULATED AFTER BRAIN TRAUMA

level after injury using Method 1 (pooling across time points for identifying genes significantly changed by >two-fold after injury). Of these changes, 181 had increased expression while 85 had decreased. Similarly, in our mouse model a total of 506 (8%) genes showed significant changes in expression, of which 350 were up-regulated and 156 downregulated using the same criteria described for rat.

Next we determined the time points when these genes were at least two-fold up or down regulated (Fig. 2A for rat; Fig. 2B for mouse). The number of upregulated genes generally increased over the 72-h time period from 44 at 4 h to 130 at 72 h in the rat and from 64 to 260 in the mouse. While the absolute numbers are without biological significance, these data demonstrate serial upregula-

tion of relevant genes during the first 72 h after brain injury. We also note the large proportion of genes at 72 h that are *only* induced at that one time point (53% of all rat genes induced at 72 h are not present at any of the earlier time points; 37% of all mouse genes induced at 72 h are similarly not present at 4–24 h after injury). This contrasts sharply with each of the other time points at which 10–24% of the expressed genes are confined to a single time point.

Comparison across the Two Models Identifies Commonly Expressed Genes

Our analyses focused on identification across species and models of “essential” genes consistently responding

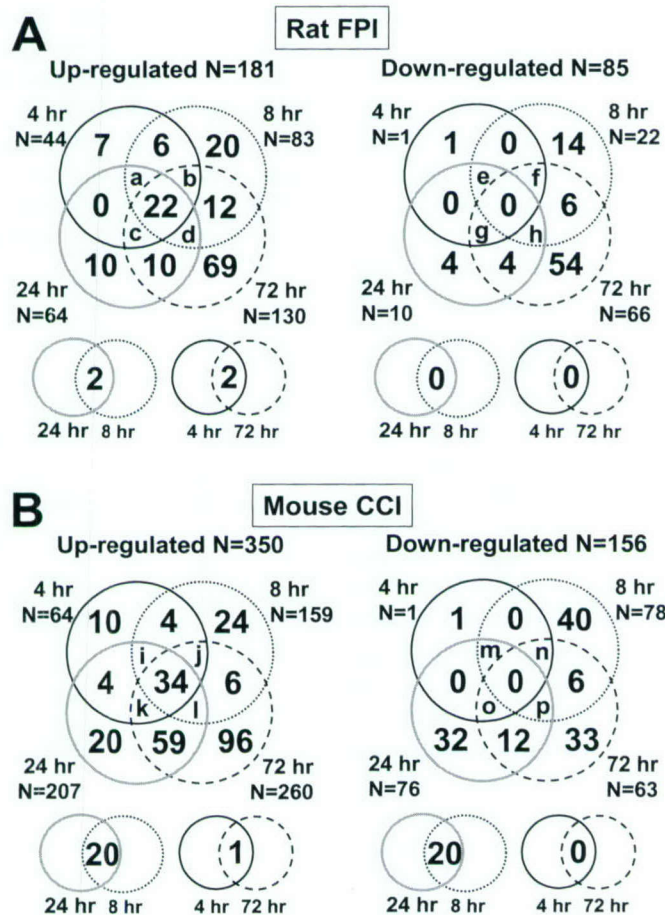


FIG. 2. Venn diagrams showing numbers of genes significantly upregulated or downregulated in each species. Numbers of genes regulated at more than one time point are found in the cells encircled by intersection of those time points. **(A)** Numbers of genes that were upregulated (left panel) or downregulated (right panel) in parietal cortex at 4 h (solid line), 8 h (dotted line), 24 h (gray line), and 72 h (dashed line) after fluid percussion injury in rats. Number of genes in cells: a, 6; b, 1; c, 0; d, 14; e–g, 0; h, 2. **(B)** Numbers of genes that were upregulated (left panel) or downregulated (right panel) in parietal cortex at 4 h (solid line), 8 h (dotted line), 24 h (gray line), and 72 h (dashed line) after controlled cortical impact injury in mice. Number of genes in cells: i, 8; j, 2; k, 1; l, 61; m–o, 0; p, 12.

to the stress of traumatic injury. Sequence matching identified 67 genes significantly regulated across both species using method 1. Method 2, which compared gene expression levels between experimental and sham tissue within each time point, identified 192 (5%) and 416 (7%) significantly regulated genes in the rat and mouse experiments, respectively. Of these, we found 15 genes not identified by Method 1 to be significantly regulated by method 2.

Overall, 82 genes identified using method 1 and/or method 2 were significantly regulated across *both* models and all subsequent analyses focus on this subset of genes. The 82 genes regulated in common across the two models were categorized with respect to known functions, as displayed in Figure 3. The highest proportion of genes commonly altered between the two models reflected inflammation (17%) or transcription regulation (16%). However, we identified numerous genes related to cell adhesion/extracellular matrix, cytoskeleton, and RBC-related, which have previously received little attention in TBI molecular pathobiology.

Gene functions were broadly grouped into those involved in biological processes or cellular functions. As shown in Figure 4, we examined the proportion of genes in each biological process class that was regulated at each time point and within each model. For example, of the genes regulated at 4 h after fluid percussion injury in the rat, 8% were in the apoptosis/cell cycle class. These data demonstrate expression of genes regulating cell adhesion, inflammation, and oxidative stress in both models by 4–8 h. By 8 h, genes associated with apoptosis/cell cycle are upregulated in the mouse injured cortex. Similarly, Figure 5 shows the relative contribution of the seven cellular functional classes that were regulated at each time point and within each model. Expression of RBC-related genes occurred rapidly, suggesting mRNA release from damaged RBC quickly after injury. Genes associated with the actin cytoskeleton and cellular motility were upregulated 8–72 h after cortical injury. Genes related to proteolysis were markedly upregulated at 72 h. Taken together, these results indicate that inflammation and oxidative stress, as well as changes in transcriptional regulation and calcium binding, participate in the brain's response to injury. Furthermore, the induction of genes related to cell adhesion/ECM, cytoskeleton, and proteolysis appear to reflect more delayed components of the secondary injury response.

The 82 genes regulated in common in both of the rodent models are shown in Table 3, grouped by function into the 12 categories provided above. Within these categories, genes are displayed by the temporal onset of their expression following injury in the rat model, permitting a direct comparison of results between the rat and mouse

models. In addition, as shown in Table 3, we identified 42 genes not previously reported as regulated following traumatic brain injury (indicated by \checkmark). These are distributed across the 11 categories of previously identified genes but also contribute a new category of genes (red blood cell-related) not previously identified in models of TBI. In addition, to identify additional genes or processes that may contribute to TBI pathobiology, we selected two of the genes not previously implicated in TBI as anchor genes for coordinate clustering. With the transcription factor p45 NF-E2 (Nrf2) as an anchor gene, we imposed Pearson coordinate clustering across the 3751 genes that fulfilled the requirement of >40% of the microarrays showing a "present" call for each gene in the rat experiment (Fig. 6A). A branch of eight genes among the 59 genes highly coordinately regulated to Nrf2 ($R = 0.99$) contained the oxidative stress response genes glutathione peroxidase, ferritin, and ceruloplasmin. Similarly, lysosomal membrane glycoprotein 2 (Lamp2) served as the anchor for clustering across the 6216 genes in the mouse experiment (Fig. 6B). A branch of nine genes highly coordinately regulated to Lamp2 ($R = 0.99$) contained genes with function related to cell adhesion/ECM including junctional adhesion molecule, lumican, and secreted acidic cysteine rich glycoprotein (SPARC).

Microarray Result Validation: RT-PCR

To validate our microarray results, we used semi quantitative RT-PCR with nine genes representing most functional categories. RT-PCR confirmed the direction and relative magnitude of change in gene expression between sham and injured samples (Fig. 7). Between comparison of the magnitude of the microarray and the RT-PCR expression results, these two independent methods show the same general pattern of expression for all genes studied.

DISCUSSION

Patterns of gene expression changes that are conserved across species and TBI models may help to identify factors involved in secondary injury response, both neurotoxic and neuroprotective. The 82 genes showing consistent expression changes across these models are likely to contain critical modulators of cell death and/or regeneration following trauma. Among these are numerous genes that have not been previously implicated in the pathobiology of traumatic brain injury, including genes implicated in neuronal regeneration and neurite outgrowth.

GENE PROFILES MODULATED AFTER BRAIN TRAUMA

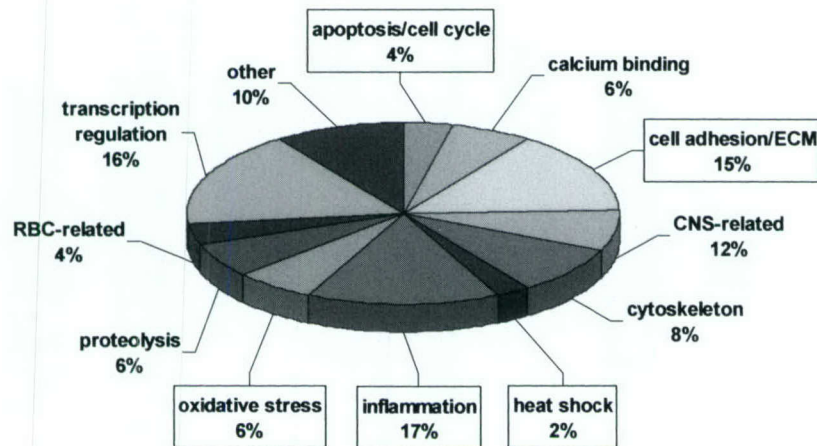


FIG. 3. Functional classes of the 82 genes regulated in both models and across both species. Genes were assigned to a functional class based on their reported function. Pie chart showing percentage of genes assigned to each functional category. Both up and downregulated genes are shown. Five functional classes (box surrounding name) are involved in biological processes while the remaining seven relate to cellular functions. CNS, central nervous system; ECM, extracellular matrix; RBC, red blood cell.

Secondary Brain Injury: Novel Gene Expression Patterns Suggestive of Degeneration or Regeneration

TBI expression profiling revealed altered regulation of processes linked both to neural degeneration and regeneration. In the injured cortex we observed altered regulation of numerous genes that have been associated with

neurodegenerative or restorative processes in a variety of models of CNS disease or injury. Several genes identified in this study but not previously implicated in TBI that have been associated with tissue degeneration: the transcription factor ATF3 (member of ATF/CREB family of transcription factors induced by stress in neurons), myelin associated glycoprotein, and lysosomal membrane glycoprotein 2 (receptor for substrate proteins of

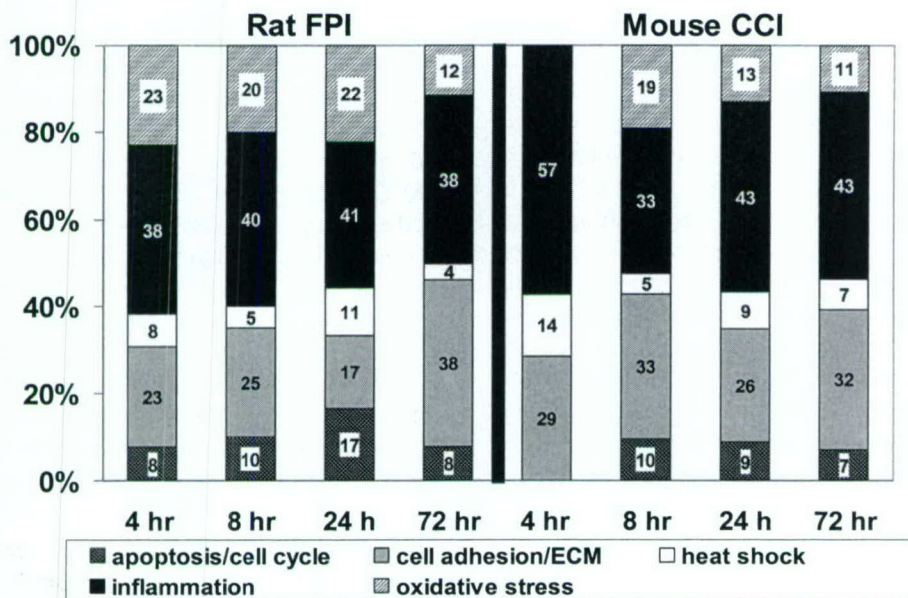


FIG. 4. Relative contribution of the five biological processes to overall gene expression at each time point. Numbers in each segment corresponds to the proportion of genes in each biological process class regulated at each time point. Left panel: Rat fluid percussion injury (FPI). Right panel: Mouse controlled cortical impact (CCI). ECM, extracellular matrix.

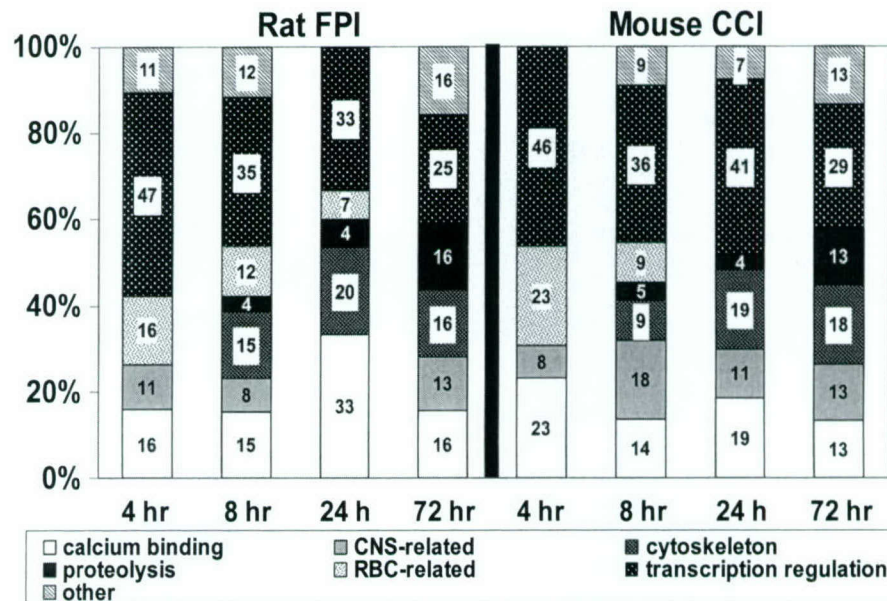


FIG. 5. Relative contribution of the seven cellular functional classes to overall gene expression at each time point. Numbers in each segment corresponds to the proportion of genes in each cellular functional class regulated at each time point. Left panel: Rat fluid percussion injury (FPI). Right panel: Mouse controlled cortical impact (CCI). CNS, central nervous system; RBC, red blood cell.

chaperone mediated autophagy). Other previously unreported gene changes may reflect endogenous neuroprotective mechanisms such as lipocortin 1 (an anti-inflammatory calcium binding protein); calponin 3 (an actin-binding protein enriched at neuronal growth cones); gelsolin (an actin severing protein that mediates calcium influx in neurons by altering mobility of NMDA receptor subunits); Id-1 (a helix-loop-helix transcription factor expressed during neuronal proliferation and differentiation); and p45 NF-E2 (Nrf2, a bZIP transcription factor that regulates phase 2 antioxidant genes by binding to the antioxidant response element in their promoters). It is, however, not always possible to clearly differentiate genes contributing to neurodegenerative versus neuroprotective processes. For example, cathepsin B is a proteolytic enzyme that can cause cellular degeneration or, when released in the extracellular matrix, can enhance remodeling to promote neurite growth (Hill et al., 1997; Felbor et al., 2002). Given the important balance between neurodegenerative and regenerative processes following traumatic brain injury, future studies might profitably examine the contribution of genes identified here.

Microarray Result Validation: Comparison to Other Injury Studies

A second approach to independently confirm microarray findings (Chuaqui et al., 2002; Rhodes et al., 2002) is to compare our work to other studies of acute CNS in-

jury. Selected genes from each functional category are briefly discussed using this method and novel genes are identified as well.

Apoptosis/cell cycle. Both models of TBI studied demonstrate neuronal apoptosis and upregulation of proapoptotic genes (reviewed by Raghupathi et al., 2000). However, relatively few genes associated with apoptosis were found to be differentially regulated, and all had been previously identified in TBI or by our group in spinal cord injury (Kaya et al., 1999; Raghavendra Rao et al., 2000; Di Giovanni et al., 2003). This may reflect the fact that the percentage of cells showing apoptosis at any single time point is relatively small, and thus any related gene changes were likely to be washed out given the tissue sampling process and the twofold change requirement for identifying genes of interest. Consistent with the observations of Raghavendra Rao et al. (2000), there is upregulation of mRNA for the peripheral benzodiazepine receptor, whose ligands may promote neuronal survival after axotomy (Banati et al., 1997; Casellas et al., 2002).

Calcium binding. Calcium influx into neurons is known to produce neuronal cell death following injury (reviewed by Young, 1992). We found five genes linked to calcium binding proteins with altered expression following injury. Of these, three had not been previously identified in this setting (lipocortin 1, annexin 2 and

TABLE 3. GENES REGULATED AFTER TRAUMATIC BRAIN INJURY IN BOTH SPECIES GROUPED BY GENE FUNCTION

Gene symbol	GenBank	Rat FPI				Mouse CCI			
		Fold change ^a				Fold change ^a			
		4 h	8 h	24 h	72 h	4 h	8 h	24 h	72 h
Biological process									
Apoptosis/cell cycle									
Myc	Y00396	3.52	2.33	2.73	1.95				
Bzip	J05122	1.27	2.06	2.67	3.37	1.95	3.72	2.08	4.24
Gadd45a	A1070295	1.51	1.85	3.35	4.74	1.01	1.09	1.28	2.04
Cell adhesion/ECM						1.29	2.59	2.71	1.12
Plat	M23697	2.09	1.73	1.68	-1.10	1.46	1.69	1.84	2.68
Spp1	M14656	8.56	34.72	52.53	133.35	-1.00	3.10	13.56	36.79
Icam1	D00913	4.04	3.64	1.28	2.23	3.45	5.32	1.55	2.23
Timp	A1169327	3.57	5.89	5.86	3.44	1.89	7.57	5.31	4.25
Dab2	U95178	1.04	2.53	1.93	2.89	1.65	2.49	4.25	5.75
Fnl	X05834	1.06	1.40	2.98	3.40	1.14	1.16	1.56	2.20
Coll1a1	A1231472	-1.87	-1.10	1.30	2.14	-2.22	-1.21	1.46	6.56
Itgb1	A1177366	1.04	1.24	1.46	2.76	1.44	1.32	2.19	1.98
Lum	X84039	-1.06	1.18	1.23	3.57	1.03	1.10	1.99	3.30
Ptprz	U04998	1.08	-1.73	-1.15	2.40	1.01	-2.00	-1.66	1.14
Mglap	A1012030	1.07	1.37	1.95	3.37	-1.13	2.31	2.08	2.45
Alcam	AB008538	-1.07	-2.04	-1.69	-1.73	-1.09	-2.89	-2.90	-1.94
Heat shock									
Hsp70-2	Z75029	6.71	10.88	21.38	3.11	-1.20	-1.42	-2.32	-2.00
Hsp70	X15705	-1.02	1.11	3.47	1.49	1.52	2.31	4.31	5.95
Inflammation									
C3ar1	U86379	2.24	1.56	1.34	2.88	1.79	2.03	3.19	5.02
Cmkbr5	Y12009	2.45	3.19	2.22	1.54	1.31	2.96	3.25	3.36
Ifi1	X61381	2.05	2.34	3.70	2.38	1.41	1.96	1.65	2.15
Scya2	X17053	16.96	23.21	7.07	13.20	5.13	61.73	89.24	44.17
Lcn2	AA946503	2.80	17.73	19.46	8.22	5.02	15.20	38.25	7.38
Il1r2	Z22812	1.51	3.20	1.68	1.57	1.21	2.34	2.16	2.10
Cd53	M57276	1.50	2.99	1.91	7.77	2.16	3.15	5.00	7.68
Cd9	X76489	-1.18	2.44	1.38	2.32	-1.11	1.17	2.07	4.63
Lgals3	J02962	1.99	4.27	5.86	33.78	7.89	34.59	50.69	121.32
Cd63	X61654	1.73	1.87	2.58	3.06	1.24	1.42	3.00	3.70
C1qb	X71127	1.05	-1.08	1.31	5.17	1.00	1.61	2.56	5.60
Ii	X13044	1.56	1.79	1.77	4.95	1.43	1.43	1.74	3.47

(continued)

S100A11). Calgranulin A is member of the superfamily of S-100 proteins characterized by two calcium binding sites and is known to have an intracellular role during calcium-dependent signaling (Rammes et al., 1997), being preferentially expressed by activated microglia as reviewed by Schafer and Heizmann (1996). Calgranulin A mRNA expression is increased in humans following both cerebral ischemia (Postler et al., 1997) and traumatic brain injury (Engel et al., 2000). Lipocortin 1, a glucocorticoid-inducible protein with anti-inflammatory properties expressed by microglia (McKanna, 1993), is induced by interleukin-1 after CNS injury and may provide trophic support to neurons (Miyachi et al., 2001).

Cell adhesion/extracellular matrix. After CNS injury, extracellular matrix (ECM) molecules secreted by cells in the glial scar participate in both the inhibition and promotion of neuronal regeneration (Fawcett and Asher, 1999; Jones and Tuszynski, 2002; Morgenstern et al., 2002). In spinal cord injury, modulating the ECM may enhance axonal growth and regeneration (Bradbury et al., 2002), but the ECM has received less attention in TBI. Consistent with findings in spinal cord injury, we found induction of the inhibitory ECM molecule keratin sulfate proteoglycan lumican 72 h after TBI. Similarly, the chondroitin sulphate proteoglycan phosphacan, an inhibitor of axon outgrowth after spinal cord injury (Bradbury et al., 2002), was upregulated at 72 h after FPI. Tissue plasminogen activator (tPA) also has both neuroprotective and neurotoxic activity after CNS injury. Although tPA is a serine protease that is used for thrombolysis in stroke treatment (NINDS 1995), in cerebral ischemia and traumatic brain injury tPA may directly mediate neuronal death by potentiating NMDA-receptor-mediated excitotoxicity (Wang et al., 1998; Mori et al., 2001; Nicole et al., 2001). Furthermore, degradation of ECM molecules by tPA-generated plasmin can prevent axonal outgrowth and limit regeneration. In contrast, regeneration may be enhanced by modulation of metalloproteinases, including TIMP-1 (Jaworski, 2000). Moreover, two important components of the extracellular matrix, fibronectin and collagen, are upregulated 72 h after injury; they have been proposed to have a role in neurite outgrowth and regeneration after injury (Carri et al., 1992; Sakai et al., 2001). Taken together, the commonly altered regulation of this class of genes implicates cell adhesion/ECM as an important secondary injury response.

CNS-related genes. We also observed altered regulation of CNS-related genes, a broad category generally consisting of synaptic or myelin genes and neuropeptides. As might be expected in the face of neuronal loss, there is down-regulation of the glutamate receptor, AMPA,

and the synaptic protein, HPC-1/syntaxin (Fujino et al., 1997). The 2–6-fold upregulation of myelin-associated glycoprotein (MAG) noted in both our injury models may inhibit axonal regeneration (Mukhopadhyay et al., 1994) and limit recovery.

Cytoskeleton. An intact cytoskeleton is required for inflammatory cell migration to the region of injury (Meyer and Feldman, 2002) and is important for neurite extension during regeneration. However, brain injury leads to the secondary loss of cytoskeletal integrity and changes in tissue structure. We found the induction of six cytoskeleton-related genes after brain injury. Actin-related protein complex, implicated in the control of actin polymerization in cells (Meyer and Feldman, 2002) and calponin 3, an actin binding protein enriched in neuronal growth cones and mature astroglia (Plantier et al., 1999), may each be involved in neuronal plasticity after TBI. Gelsolin, a protein that prevents actin polymerization, was upregulated at 72 h after injury; it may have a neuroprotective role because it reduces calcium conductance through NMDA channels by altering their subunit conformation through its effects on actin polymerization (Endres et al., 1999).

Heat shock proteins. Heat shock proteins (HSP), a highly conserved family of stress-response proteins, help restore function to damaged proteins within the cell (Beckmann et al., 1990; Hightower, 1991; Sharp et al., 1999). The HSP70 gene is induced in the brain by processes such as ischemia that denature proteins. Overproduction of HSP70 in transgenic mice or by viral gene transfer protects neurons from degeneration in several models of injury (as reviewed by Yenari et al., 1999). We found increased expression of HSP70 after TBI, consistent with earlier reports in human cerebral cortex (Dutcher et al., 1998; Truettner et al., 1999).

RBC-related genes. Three red blood cell-related genes (hemoglobin alpha-1, hemoglobin beta-1, and delta ALA synthetase) showed increased expression at 4 h after injury. Changes in the expression for these genes have not been previously reported in TBI. However, their biological significance in this context is unknown and it is possible that these mRNAs arise from release of injured erythrocytes rather than active induction.

Oxidative stress. Oxidative stress is a component of secondary injury after TBI and we identified five antioxidant genes that were commonly upregulated. Metallothionein I and II (Mt-1, Mt-2) and heme oxygenase 1 (HO-1) had been identified by other investigators (Raghavendra Rao et al., 2003), whereas changes in ceru-

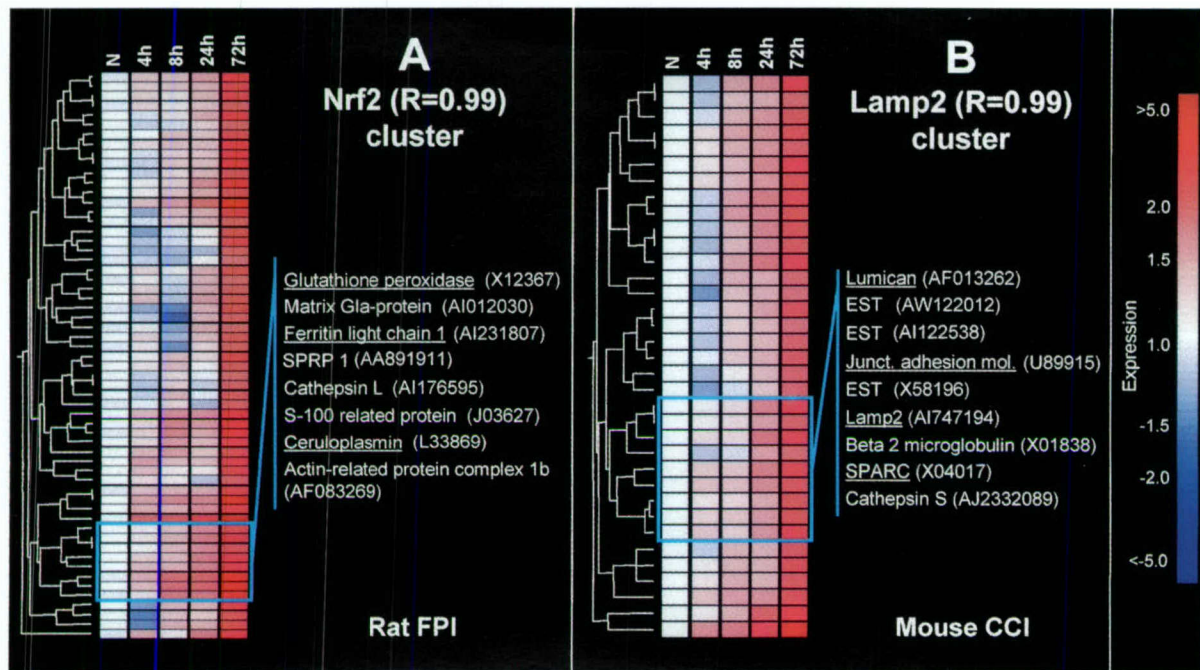


FIG. 6. Hierarchical cluster of genes coordinately regulated to two genes not previously implicated in traumatic brain injury pathophysiology. Upregulated genes (red) and downregulated genes (blue) in injured parietal cortex at 4, 8, 24, and 72 h after fluid percussion injury (FPI) in rat (**A**) or controlled cortical impact (CCI) in mouse (**B**). Expression level after injury normalized to expression level in parietal cortex at same time point after sham injury. Panel A: Genetree containing 59 genes with expression pattern highly correlated (Pearson correlation, $R = 0.99$) with NF-E2-related factor 2 (Nrf2) after FPI. White box encloses a tree sub-branch containing 3 oxidative stress response genes (names underlined) that share a similar expression pattern. Panel B: Gene tree containing 35 genes with expression pattern highly correlated (Pearson correlation, $R = 0.99$) with lysosomal membrane glycoprotein 2 (Lamp2). White box encloses a tree sub-branch containing three cell adhesion/extracellular matrix genes (names underlined) that share a similar expression pattern. EST, expressed sequence tag; Junct. Adhesion mol., junctional adhesion molecule; SPARC, secreted acidic cysteine rich glycoprotein; SPRP 1, small proline-rich protein 1.

loplasmin and ferritin expression had not been previously reported in these models. Metallothioneins are a family of small, cysteine-rich proteins that donate metals to target metalloproteins (particularly zinc finger protein and enzymes), act as metal chelators (specifically of cadmium and zinc), and scavenge superoxide (Hussain et al., 1996). Interleukin-1, interleukin-6, antioxidant response element, and glucocorticoids regulate Mt transcription (Andrews, 2000). Mice over expressing Mt-1 are partially protected from focal cerebral ischemia (van Lookeren Campagne et al., 1999). Similarly, Mt-1 and Mt-2 deficient mice demonstrate decreased astrogliosis and increased neuronal apoptosis after traumatic brain injury (Penkowa et al., 2001). Thus, Mt-1 and Mt-2 may play an important role in protecting the CNS from oxidative stress.

Proteolysis. Another family showing gene changes is related to proteolysis, including these three previously

identified genes (lysozyme C, cathepsin D, and cathepsin L) and two genes (cathepsin B and lysosomal membrane glycoprotein 2) whose expression changes were not previously noted. All are maximally regulated 72 h following injury, consistent with their documented role in cellular degradation and removal of debris (Leist and Jaattela, 2001). Cathepsin B and L provide examples of genes that may be required for neuronal survival (Felbor et al., 2002), yet contribute to neuronal degradation when released from lysosomes (Hill et al., 1997).

Transcriptional regulation. Genes participating in transcription regulation composed the largest group of commonly altered genes after TBI. This broad category of genes includes five subgroups: (1) the immediate early genes (c-fos, jun-B, v-jun, ATF3); (2) genes involved in antioxidant response (p45 NF-E2); (3) genes implicated in inflammatory responses (IRF1, C/EBP beta, C/EBP delta, LPS-induced TNF-alpha factor); (4) growth-related

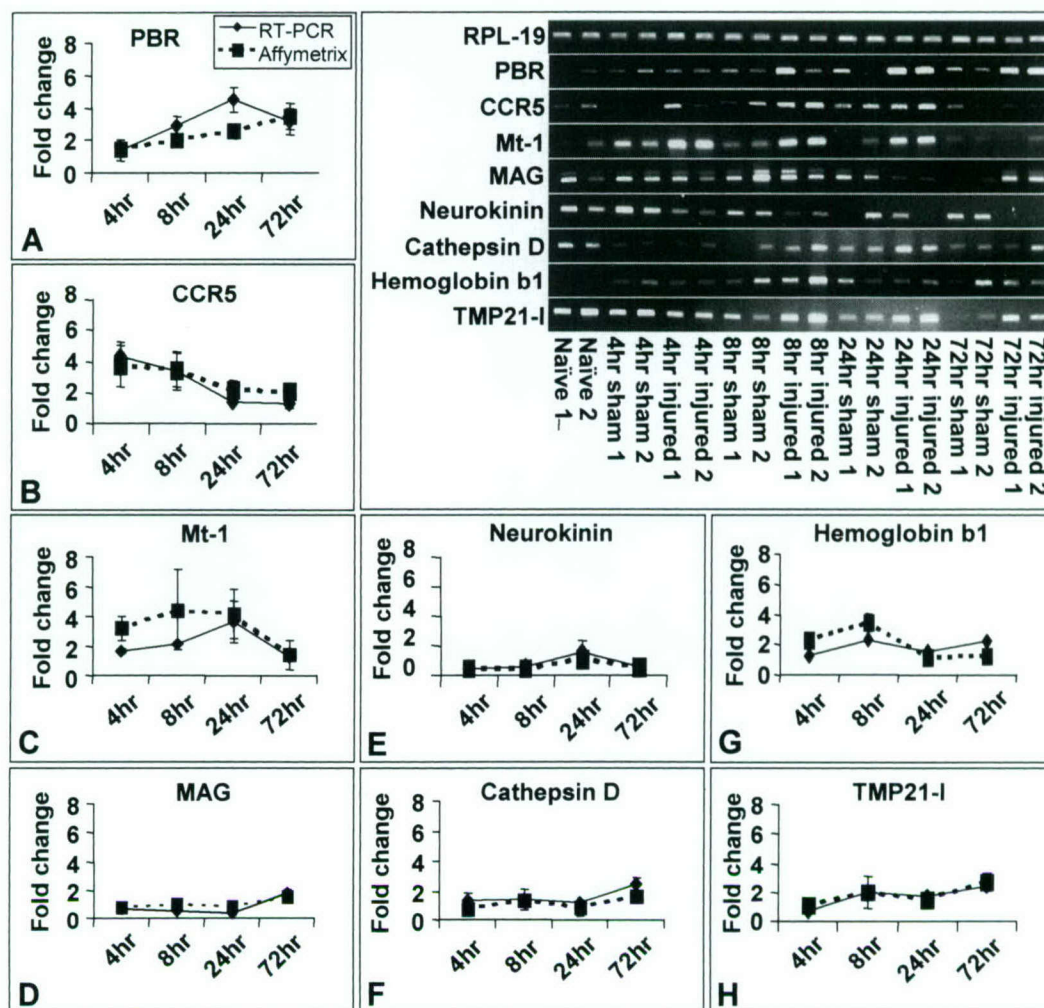


FIG. 7. Validation of expression changes observed by microarray with RT-PCR in nine genes across four time points after experimental TBI. Magnitude and pattern of gene expression of eight genes shows significant induction. (A) Peripheral benzodiazepine receptor (PBR), (B) C-C chemokine receptor 5 (CCR5), (C) metallothionein I (Mt-1), (D) myelin-associated glycoprotein (MAG), (E) neurokinin, (F) cathepsin D, (G) hemoglobin b1, (H) transmembrane protein (TMP21-I).

genes (c-myc, butyrate response factor 2, HMG box 2); (5) CNS development-related genes (Id-1, Id-3, COUP-TF). Of these, c-fos, jun-B, v-jun, IRF1, Id-3, and C/EBP beta have been shown by others to be altered following brain injury (Kobori et al., 2002; Marciano et al., 2002; Matzilevich et al., 2002; Raghavendra Rao et al., 2003). Several of these genes (jun-B, c-myc) have been implicated in the induction of programmed cell death (Di Giovanni et al., 2003).

Molecular Evidence for Microglial Activation after TBI

Injury to the brain or spinal cord is accompanied by cellular responses dominated by the activation and pro-

liferation of microglia (Prewitt et al., 1997; Koshinaga et al., 2000). Once activated, microglia play a major role in the general neuroinflammatory response of the CNS, including phagocytosis of bacterial pathogens and cellular debris, and release of cytotoxic (nitric oxide, superoxide, tumor necrosis factor α) and neuroprotective (brain derived neurotrophic factor) factors (for review, see Kreutzberg, 1996). Although microglial activation has been linked to neurotoxicity, there is evolving evidence suggesting that microglia may also provide protective and restorative functions that promote recovery from injury (Bruce-Keller, 1999).

Consistent with known characteristic microglial response to brain injury, we found that genes related to immune response and specifically to activated microglia

dominated expression in the cortical impact region. For example, Fukuda et al. (1995) showed sustained expression of HO-1 as long as 5 days after fluid percussion injury in the injured cortex of rats. In addition, HO-1 expression co-localized with microglia at 72 h after injury, suggesting that transcription in microglia may have contributed to the upregulation of HO-1 we found in both models at 72 h. Our gene expression profiling results suggest a predominant role for microglia/brain macrophages in the transcriptional response to experimental TBI.

Analysis of Sequential Gene Expression

IRF1 was the first nuclear transacting factor demonstrated to contribute directly to cerebral ischemic damage (Iadecola et al., 1999) and its binding to the interferon response factor element is known to be essential for interferon gamma-induced MHC class II expression (O'Keefe et al., 2001). Furthermore, Matzilevich also found IRF1 to be upregulated following traumatic brain injury. It is, therefore, not surprising that in our experiments MHC class II expression consistently followed the expression of IRF1 (Matzilevich et al., 2002). This was true even though the exact timing of these events was not the same in the mouse and rat models.

Over half of genes upregulated at 72 hours were not expressed at earlier time points, suggesting that a new set of molecular and cellular responses are initiated relatively late after injury. These include factors related to inflammation, oxidative stress, cytoskeleton and proteolysis, among others (Table 3). For example, the bZip transcription factor Nrf2, an essential activator of genes encoding antioxidant enzymes and phase II detoxifying enzymes through the antioxidant response element (Venugopal and Jaiswal, 1998; Gong et al., 2002), was among genes showing initial upregulation at 72 h. The Nrf2-regulated genes HO-1 and ferritin were also upregulated at 72 h. Furthermore, the expression patterns of an additional two oxidative stress response genes, glutathione peroxidase and ceruloplasmin, were highly correlated ($R = 0.99$) with the pattern of Nrf2. The coordinated regulation of Nrf2 with oxidative stress sensitive genes suggests a delayed oxidative stress to which a transcriptional response is mounted. Increased F_2 -isoprostane-containing lipids in cerebrospinal fluid 5–7 days after TBI in children support the presence of such a late oxidative stress (Bayir et al., 2002).

Limitations and Strengths

It is important to recognize both the methodological limitations and strengths of this work. We performed RNA extraction from brain tissue at four-time points following traumatic brain injury. Therefore, we describe

a heterogeneous cell population that is tissue-specific rather than cell-specific. Furthermore, the distribution of particular cell types is likely to differ at the four time points. Because the methods that we employ provide sensitivity that is affected by the relative distributions of various transcripts, rare transcripts were less likely to be detected. Subsequent work using cell-specific profiling would address some of these limitations.

Our experimental approach does, however, also contribute significant strengths. First, we examined expression of almost 9000 genes/ESTs at four time points over 72 h, thus improving our ability to understand the alterations induced by injury. Second, our sampling in both the experimental and sham animals was regionally specific and included extraction of the same tissue sample volume. This provided a consistent and directly comparable source of RNA for analysis. Third, we have reduced the rate of false positive results, a prevailing concern in microarray experiments, by eliminating microarray results that fail to meet high quality control standards and by imposing stringent statistical criteria for identification of differentially regulated genes. Moreover, we identified a group of consistently regulated genes from two species and two injury models that are dissimilar in a number of ways, suggesting that the molecular pathways reported here may be characteristic of the genomic response to CNS injury.

Previously Described mRNA Changes following CNS Injury Are Corroborated

Many of the genes we identified as regulated using our two experimental models were also identified in other models of brain injury (Tang et al., 2002, 2003). Tang also used a comparative strategy to characterize the genomic response of the brain to ischemic stroke, intracerebral hemorrhage, induced seizures, hypoglycemia, and hypoxia in adult rats (Tang et al., 2002). They identified 45 genes regulated in common across these diverse models. Of these, many were also identified (matched by GenBank accession number) in our two experimental models. These included genes related to apoptosis (PBR), calcium binding (annexin 2, S100A11, and S100A4), cellular adhesion/ECM (TIMP-1, osteopontin, and matrix gla-protein), cytoskeleton (actin-related protein complex, GFAP, and calponin 3), heat shock protein (HSP70.2), inflammation (monocyte chemoattractant protein, MHC class II, galectin-3, lipocalin 2), oxidative stress (heme oxygenase, ceruloplasmin, Mt-1 and -2), proteolysis (lysozyme C), and transcription regulation (C/EBP delta). These data, reflecting non-traumatic brain injury, both support our current findings as well as the concept that microarray approaches can successfully identify common molecular processes associated with brain injury.

Furthermore, using the same data filtering, normalization, and statistical analyses to select significantly-regulated genes (probes present on 40% of microarrays in the experiment and both statistically significant and twofold change in signal intensity vs. time-matched sham), we compared the 82 commonly regulated after brain injury to significantly-regulated genes 4 h, 24 h, or 7 days after mild spinal cord injury in rats (Di Giovanni et al., 2003). When gene expression was compared between these different tissues (thoracic spinal cord and parietal cortex) and using different post-injury time periods, 34 of 82 genes appeared to be commonly regulated. These included all genes classified as apoptosis/cell cycle and calcium binding. Additionally, genes altered across the spinal cord and cortical injury models included those related to cell adhesion/ECM (tPA, osteopontin, ICAM-1, disabled homolog 2, and fibronectin), cytoskeleton (actin-related protein complex, gelsolin, and tropomyosin 4), immune response (C3a anaphylatoxin chemotactic receptor, monocyte chemoattractant protein-1, CD53, galectin-3, and complement C1q B chain), oxidative stress (ceruloplasmin), proteolysis (lysozyme C and cathepsin L), transcription regulation (c-fos, IRF-1, ATF-3, butyrate response factor 2, C/EBP beta, C/EBP delta, and v-jun), and others (thromboplastin, granulin). In addition to providing methodological validation, these shared results can further refine identification of candidate molecular pathways involved in CNS injury, and suggest that the CNS generates a partially stereotypic molecular response to a wide variety of insults. Most importantly, these highly consistent pathways may serve as a starting point for development of therapies that may more successfully limit neurotoxicity and enhance recovery.

ACKNOWLEDGMENTS

We acknowledge Maria Idalia Cruz, Xiao Di, Jill MacLeod, and Fiona Patricio for their outstanding technical assistance, along with Simone Di Giovanni and Eric Hoffman for their thoughtful comments and suggestions. This work was supported by NINDS 1K08 NS41273 (J.E.N.), DAMD17-2-99-9007 (A.I.F.), Mental Retardation and Developmental Disabilities Research Center at Children's National Medical Center, NICHD 1P30HD40677-01 (A.I.F. and J.E.N.), and NIH NS36537 (A.I.F.).

REFERENCES

ANDREWS, G.K. (2000). Regulation of metallothionein gene expression by oxidative stress and metal ions. *Biochem. Pharmacol.* **59**, 95–104.

- BAKAY, M., ZHAO, P., CHEN, J., et al. (2002). A web-accessible complete transcriptome of normal human and DMD muscle. *Neuromuscul. Disord.* **12**, Suppl 1, S125–S141.
- BANATI, R.B., MYERS, R., and KREUTZBERG, G.W. (1997). PK ('peripheral benzodiazepine')—binding sites in the CNS indicate early and discrete brain lesions: microautoradiographic detection of [³H]PK11195 binding to activated microglia. *J. Neurocytol.* **26**, 77–82.
- BAYIR, H., KAGAN, V.E., TYURINA, Y.Y., et al. (2002). Assessment of antioxidant reserves and oxidative stress in cerebrospinal fluid after severe traumatic brain injury in infants and children. *Pediatr. Res.* **51**, 571–578.
- BECKMANN, R.P., MIZZEN, L.E., and WELCH, W.J. (1990). Interaction of Hsp 70 with newly synthesized proteins: implications for protein folding and assembly. *Science* **248**, 850–854.
- BRADBURY, E.J., MOON, L.D., POPAT, R.J., et al. (2002). Chondroitinase ABC promotes functional recovery after spinal cord injury. *Nature* **416**, 636–640.
- BRASSARD, M. (1996). Control chart. The Memory Jogger Plus+. GOAL/QPC 288–297.
- BRUCE-KELLER, A.J. (1999). Microglial–neuronal interactions in synaptic damage and recovery. *J. Neurosci. Res.* **58**, 191–201.
- CARRI, N.G., RUBIN, K., GULLBERG, D., et al. (1992). Neuriteogenesis on collagen substrates. Involvement of integrin-like matrix receptors in retinal fibre outgrowth on collagen. *Int. J. Dev. Neurosci.* **10**, 393–405.
- CASELLAS, P., GALIEGUE, S., and BASILE, A.S. (2002). Peripheral benzodiazepine receptors and mitochondrial function. *Neurochem. Int.* **40**, 475–486.
- CHEN, Y.W., ZHAO, P., BORUP, R., et al. (2000). Expression profiling in the muscular dystrophies: identification of novel aspects of molecular pathophysiology. *J. Cell Biol.* **151**, 1321–1336.
- CHUAQUI, R.F., BONNER, R.F., BEST, C.J., et al. (2002). Post-analysis follow-up and validation of microarray experiments. *Nat. Genet.* **32**, Suppl, 509–514.
- DI GIOVANNI, S., KNOBLACH, S.M., BRANDOLI, C., et al. (2003). Gene profiling in spinal cord injury shows role for cell cycle in neuronal death. *Ann. Neurol.* **53**, 454–468.
- DUTCHER, S.A., UNDERWOOD, B.D., WALKER, P.D., et al. (1998). Patterns of heat-shock protein 70 biosynthesis following human traumatic brain injury. *J. Neurotrauma* **15**, 411–420.
- ENDRES, M., FINK, K., ZHU, J., et al. (1999). Neuroprotective effects of gelsolin during murine stroke. *J. Clin. Invest.* **103**, 347–354.
- ENGEL, S., SCHLUESENER, H., MITTELBRONN, M., et al. (2000). Dynamics of microglial activation after human traumatic brain injury are revealed by delayed expression of

GENE PROFILES MODULATED AFTER BRAIN TRAUMA

- macrophage-related proteins MRP8 and MRP14. *Acta Neuropathol. (Berl.)* **100**, 313–322.
- FADEN, A.I. (1989). TRH analog YM-14673 improves outcome following traumatic brain and spinal cord injury in rats: dose-response studies. *Brain Res.* **486**, 228–235.
- FADEN, A.I. (1993). Comparison of single and combination drug treatment strategies in experimental brain trauma. *J. Neurotrauma* **10**, 91–100.
- FADEN, A.I., LABROO, V.M., and COHEN, L.A. (1993). Imidazole-substituted analogues of TRH limit behavioral deficits after experimental brain trauma. *J. Neurotrauma* **10**, 101–108.
- FADEN, A.I., X, D., SM, K., et al. (2003). Neuroprotective and nootropic actions of a novel cyclized dipeptide following controlled cortical impact in mice. *J. Cereb. Blood Flow Metab.* **23**, 355–363.
- FAWCETT, J.W., and ASHER, R.A. (1999). The glial scar and central nervous system repair. *Brain Res. Bull.* **49**, 377–391.
- FELBOR, U., KESSLER, B., MOTHES, W., et al. (2002). Neuronal loss and brain atrophy in mice lacking cathepsins B and L. *Proc. Natl. Acad. Sci. USA* **99**, 7883–7888.
- FOX, G.B., and FADEN, A.I. (1998). Traumatic brain injury causes delayed motor and cognitive impairment in a mutant mouse strain known to exhibit delayed Wallerian degeneration. *J. Neurosci. Res.* **53**, 718–727.
- FOX, G.B., FAN, L., LEVASSEUR, R.A., et al. (1998). Sustained sensory/motor and cognitive deficits with neuronal apoptosis following controlled cortical impact brain injury in the mouse. *J. Neurotrauma* **15**, 599–614.
- FOX, G.B., LEVASSEUR, R.A., and FADEN, A.I. (1999). Behavioral responses of C57BL/6, FVB/N, and 129/SvEMS mouse strains to traumatic brain injury: implications for gene targeting approaches to neurotrauma. *J. Neurotrauma* **16**, 377–389.
- FUJINO, I., FUJIWARA, T., and AKAGAWA, K. (1997). Transient decrease of HPC-1/syntaxin-1A mRNA in the rat hippocampus by kainic acid. *Neurosci. Res.* **28**, 243–247.
- FUKUDA, K., PANTER, S.S., SHARP, F.R., et al. (1995). Induction of heme oxygenase-1 (HO-1) after traumatic brain injury in the rat. *Neurosci. Lett.* **199**, 127–130.
- GONG, P., STEWART, D., HU, B., et al. (2002). Activation of the mouse heme oxygenase-1 gene by 15-deoxy-Delta(12,14)-prostaglandin J(2) is mediated by the stress response elements and transcription factor Nrf2. *Antioxid. Redox Signal* **4**, 249–257.
- HIGHTOWER, L.E. (1991). Heat shock, stress proteins, chaperones, and proteotoxicity. *Cell* **66**, 191–197.
- HILL, I.E., PRESTON, E., MONETTE, R., et al. (1997). A comparison of cathepsin B processing and distribution during neuronal death in rats following global ischemia or decapitation necrosis. *Brain Res.* **751**, 206–216.
- HUSSAIN, S., SLIKKER, W., JR., and ALI, S.F. (1996). Role of metallothionein and other antioxidants in scavenging superoxide radicals and their possible role in neuroprotection. *Neurochem. Int.* **29**, 145–152.
- IADECOLA, C., SALKOWSKI, C.A., ZHANG, F., et al. (1999). The transcription factor interferon regulatory factor 1 is expressed after cerebral ischemia and contributes to ischemic brain injury. *J. Exp. Med.* **189**, 719–727.
- JAWORSKI, D.M. (2000). Differential regulation of tissue inhibitor of metalloproteinase mRNA expression in response to intracranial injury. *Glia* **30**, 199–208.
- JONES, L.L., and TUSZYNSKI, M.H. (2002). Spinal cord injury elicits expression of keratan sulfate proteoglycans by macrophages, reactive microglia, and oligodendrocyte progenitors. *J. Neurosci.* **22**, 4611–4624.
- KAYA, S.S., MAHMOOD, A., LI, Y., et al. (1999). Apoptosis and expression of p53 response proteins and cyclin D1 after cortical impact in rat brain. *Brain Res.* **818**, 23–33.
- KOBORI, N., CLIFTON, G.L., and DASH, P. (2002). Altered expression of novel genes in the cerebral cortex following experimental brain injury. *Brain Res. Mol. Brain Res.* **104**, 148–158.
- KOSHINAGA, M., KATAYAMA, Y., FUKUSHIMA, M., et al. (2000). Rapid and widespread microglial activation induced by traumatic brain injury in rat brain slices. *J. Neurotrauma* **17**, 185–192.
- KREUTZBERG, G.W. (1996). Microglia: a sensor for pathological events in the CNS. *Trends Neurosci.* **19**, 312–318.
- LEIST, M., and JAATTELA, M. (2001). Triggering of apoptosis by cathepsins. *Cell Death Differ.* **8**, 324–326.
- LONG, Y., ZOU, L., LIU, H., et al. (2003). Altered expression of randomly selected genes in mouse hippocampus after traumatic brain injury. *J. Neurosci. Res.* **71**, 710–720.
- MARCIANO, P.G., EBERWINE, J.H., RAGUPATHI, R., et al. (2002). Expression profiling following traumatic brain injury: a review. *Neurochem. Res.* **27**, 1147–1155.
- MATZILEVICH, D.A., RALL, J.M., MOORE, A.N., et al. (2002). High-density microarray analysis of hippocampal gene expression following experimental brain injury. *J. Neurosci. Res.* **67**, 646–663.
- McINTOSH, T.K., VINK, R., NOBLE, L., et al. (1989). Traumatic brain injury in the rat: characterization of a lateral fluid-percussion model. *Neuroscience* **28**, 233–244.
- McKANNA, J.A. (1993). Lipocortin 1 immunoreactivity identifies microglia in adult rat brain. *J. Neurosci. Res.* **36**, 491–500.
- MEYER, G., and FELDMAN, E.L. (2002). Signaling mechanisms that regulate actin-based motility processes in the nervous system. *J. Neurochem.* **83**, 490–503.
- MİYACHI, T., ASAI, K., TSUIKI, H., et al. (2001). Interleukin-1_{beta} induces the expression of lipocortin 1 mRNA in cultured rat cortical astrocytes. *Neurosci. Res.* **40**, 53–60.

- MORGENSTERN, D.A., ASHER, R.A., and FAWCETT, J.W. (2002). Chondroitin sulphate proteoglycans in the CNS injury response. *Prog. Brain Res.* **137**, 313–332.
- MORI, T., WANG, X., KLINE, A.E., et al. (2001). Reduced cortical injury and edema in tissue plasminogen activator knockout mice after brain trauma. *Neuroreport* **12**, 4117–4120.
- MUKHOPADHYAY, G., DOHERTY, P., WALSH, F.S., et al. (1994). A novel role for myelin-associated glycoprotein as an inhibitor of axonal regeneration. *Neuron* **13**, 757–767.
- NATIONAL INSTITUTE OF NEUROLOGICAL DISORDERS AND STROKE rt-PA STROKE STUDY GROUP. (1995). Tissue plasminogen activator for acute ischemic stroke. *N. Engl. J. Med.* **333**, 1581–1587.
- NICOLE, O., DOCAGNE, F., ALI, C., et al. (2001). The proteolytic activity of tissue-plasminogen activator enhances NMDA receptor-mediated signaling. *Nat. Med.* **7**, 59–64.
- O'KEEFE, G.M., NGUYEN, V.T., PING TANG, L.L., et al. (2001). IFN-gamma regulation of class II transactivator promoter IV in macrophages and microglia: involvement of the suppressors of cytokine signaling-1 protein. *J. Immunol.* **166**, 2260–2269.
- PENKOWA, M., GIRALT, M., THOMSEN, P.S., et al. (2001). Zinc or copper deficiency-induced impaired inflammatory response to brain trauma may be caused by the concomitant metallothionein changes. *J. Neurotrauma* **18**, 447–463.
- PLANTIER, M., FATTOUM, A., MENN, B., et al. (1999). Acidic calponin immunoreactivity in postnatal rat brain and cultures: subcellular localization in growth cones, under the plasma membrane and along actin and glial filaments. *Eur. J. Neurosci.* **11**, 2801–2812.
- POSTLER, E., LEHR, A., SCHLUESENER, H., et al. (1997). Expression of the S-100 proteins MRP-8 and -14 in ischemic brain lesions. *Glia* **19**, 27–34.
- PREWITT, C.M., NIESMAN, I.R., KANE, C.J., et al. (1997). Activated macrophage/microglial cells can promote the regeneration of sensory axons into the injured spinal cord. *Exp. Neurol.* **148**, 433–443.
- RAGHAVENDRA RAO, V.L., DHODDA, V.K., SONG, G., et al. (2003). Traumatic brain injury-induced acute gene expression changes in rat cerebral cortex identified by GeneChip analysis. *J. Neurosci. Res.* **71**, 208–219.
- RAGHAVENDRA RAO, V.L., DOGAN, A., BOWEN, K.K., et al. (2000). Traumatic brain injury leads to increased expression of peripheral-type benzodiazepine receptors, neuronal death, and activation of astrocytes and microglia in rat thalamus. *Exp. Neurol.* **161**, 102–114.
- RAGHUPATHI, R., GRAHAM, D.I., and MCINTOSH, T.K. (2000). Apoptosis after traumatic brain injury. *J. Neurotrauma* **17**, 927–938.
- RAMMES, A., ROTH, J., GOEBELER, M., et al. (1997). Myeloid-related protein (MRP) 8 and MRP14, calcium-binding proteins of the S100 family, are secreted by activated monocytes via a novel, tubulin-dependent pathway. *J. Biol. Chem.* **272**, 9496–9502.
- RHODES, D.R., BARRETTE, T.R., RUBIN, M.A., et al. (2002). Meta-analysis of microarrays: interstudy validation of gene expression profiles reveals pathway dysregulation in prostate cancer. *Cancer Res.* **62**, 4427–4433.
- SAKAI, T., JOHNSON, K.J., MUROZONO, M., et al. (2001). Plasma fibronectin supports neuronal survival and reduces brain injury following transient focal cerebral ischemia but is not essential for skin-wound healing and hemostasis. *Nat. Med.* **7**, 324–330.
- SCHAFER, B.W., and HEIZMANN, C.W. (1996). The S100 family of EF-hand calcium-binding proteins: functions and pathology. *Trends Biochem. Sci.* **21**, 134–140.
- SHARP, F.R., MASSA, S.M., and SWANSON, R.A. (1999). Heat-shock protein protection. *Trends Neurosci.* **22**, 97–99.
- TANG, Y., LU, A., ARONOW, B.J., et al. (2002). Genomic responses of the brain to ischemic stroke, intracerebral haemorrhage, kainate seizures, hypoglycemia, and hypoxia. *Eur. J. Neurosci.* **15**, 1937–1952.
- TANG, Y., NEE, A.C., LU, A., et al. (2003). Blood genomic expression profile for neuronal injury. *J. Cereb. Blood Flow Metab.* **23**, 310–319.
- TRUETTNER, J., SCHMIDT-KASTNER, R., BUSTO, R., et al. (1999). Expression of brain-derived neurotrophic factor, nerve growth factor, and heat shock protein HSP70 following fluid percussion brain injury in rats. *J. Neurotrauma* **16**, 471–486.
- VAN LOOKEREN CAMPAGNE, M., THIBODEAUX, H., VAN BRUGGEN, N., et al. (1999). Evidence for a protective role of metallothionein-1 in focal cerebral ischemia. *Proc. Natl. Acad. Sci. USA* **96**, 12870–12875.
- VENUGOPAL, R., and JAISWAL, A.K. (1998). Nrf2 and Nrf1 in association with Jun proteins regulate antioxidant response element-mediated expression and coordinated induction of genes encoding detoxifying enzymes. *Oncogene* **17**, 3145–3156.
- WANG, Y.F., TSIRKA, S.E., STRICKLAND, S., et al. (1998). Tissue plasminogen activator (tPA) increases neuronal damage after focal cerebral ischemia in wild-type and tPA-deficient mice. *Nat. Med.* **4**, 228–231.
- YAKOVLEV, A.G., DI, X., MOVSESYAN, V., et al. (2001). Presence of DNA fragmentation and lack of neuroprotective effect in DFF45 knockout mice subjected to traumatic brain injury. *Mol. Med.* **7**, 205–216.

GENE PROFILES MODULATED AFTER BRAIN TRAUMA

- YAKOVLEV, A.G., KNOBLACH, S.M., FAN, L., et al. (1997). Activation of CPP32-like caspases contributes to neuronal apoptosis and neurological dysfunction after traumatic brain injury. *J. Neurosci.* **17**, 7415-7424.
- YENARI, M.A., GIFFARD, R.G., SAPOLSKY, R.M., et al. (1999). The neuroprotective potential of heat shock protein 70 (HSP70). *Mol. Med. Today.* **5**, 525-531.
- YOUNG, W. (1992). Role of calcium in central nervous system injuries. *J. Neurotrauma* **9**, Suppl 1, S9-S25.

Address reprint requests to:
JoAnne E. Natale, M.D., Ph.D.
Research Centers for Genetic Medicine and
Neuroscience
Children's National Medical Center
111 Michigan Ave., NW
Washington, DC 20010

E-mail: jnatale@cnmcresearch.org

Mechanisms of Neural Cell Death: Implications for Development of Neuroprotective Treatment Strategies

Alexander G. Yakovlev and Alan I. Faden

Department of Neuroscience, Georgetown University Medical Center, Washington, DC 20057

Summary: It has been increasingly recognized that cell death phenotypes and their molecular mechanisms are highly diverse. Necrosis is no longer considered a single entity, passively mediated by energy failure. Moreover, caspase-dependent apoptosis is not the only pathway involved in programmed cell death or even the only apoptotic mechanism. Recent experimental work emphasizes the diverse and interrelated nature of cell death mechanisms. Thus, there are both caspase-dependent and caspase-independent forms of apoptosis, which may differ morphologically as well as mechanistically. There are also necrotic-like phenotypes that require *de novo* protein synthesis and are, therefore, forms of programmed cell death. In addition,

forms of cell death showing certain morphological features of both necrosis and apoptosis have been identified, leading to the term *aponecrosis*. Considerable experimental evidence also shows that modulation of one form of cell death may lead to another. Together, these observations underscore the need to substantially revise our conceptions about neuroprotection strategies. Use of multiple treatments that target different cell death cascades, or single agents that moderate multiple cell death pathways, is likely to lead to more effective neuroprotection for clinical disorders. **Key Words:** Apoptosis, necrosis, caspase, calpain, AIF.

INTRODUCTION

Neuronal loss occurs as an essential feature of normal CNS development, as well as in acute or chronic neurodegenerative disorders.¹⁻⁴ It has long been recognized that a variety of factors can trigger secondary auto-destructive reactions within the CNS, including free radicals, excitatory amino acids, eicosanoids, lipid degradation products, tissue cations, inflammation, and immune responses.^{5,6} These secondary injury factors are released or activated over a period from seconds (e.g., lipid, cation changes) to days (e.g., inflammatory, immune responses) after the primary insult and may act either sequentially or in parallel to cause delayed or expanding cell death. Detailed reviews of delayed injury processes/mechanisms can be found elsewhere.^{5,6} Depending on developmental age, injury severity, or a specific cell type, injury factors can trigger alternative mechanisms of cell death.⁷

The focus of research on secondary brain injury has historically been on mechanisms related to necrosis. This

has led to the evaluation of numerous pharmacological strategies, including calcium channel blockers, corticosteroids and antioxidants, glutamate receptor antagonists, opioid receptor antagonists, thyrotropin-releasing hormone analogs, and magnesium administration, as well as various anti-inflammatory and immune modulatory treatments.⁸ Although several of these strategies have shown modest benefits in the treatment of acute spinal cord injury in humans,^{9,10} neuroprotection studies in head injury and stroke have been disappointing. In part, this may reflect flaws in trial design or failure to more directly parallel pre-clinical and clinical studies^{11,12}; however, to a significant degree, such negative trials may result from conceptual difficulties, namely a failure to appreciate the complexity of cell death phenotypes and mechanisms.

CELL DEATH PHENOTYPES

Nomenclature relating to the cell death phenotypes has been confusing. One of the early attempts to classify cell death phenotypes, based upon morphological analyses in developmental models, was made by Schweichel and Merker,¹³ who identified three types of cell death (types 1, 2, and 3). Type 1 is manifested by nuclear condensa-

Address correspondence and reprint requests to Alan I. Faden, M.D., Department of Neuroscience, Georgetown University Medical Center, 3970 Reservoir Road NW, Room EP-12, Washington, DC 20057. E-mail: fadena@georgetown.edu.

tion and pyknosis, reduced cytoplasmic volume, late cell fragmentation, and phagocytosis. Type 2, or autophagic degeneration, is characterized by substantial autophagic vacuolization in the cytoplasm. Type 3, or cytoplasmic cell death, is characterized by general disintegration and deletion of organelles. Features of type 1 cell death appear identical to those classically identified by Kerr as apoptosis.¹⁴ Types 2 and 3 show features associated with necrosis¹⁵; in 1990, this classification was recapitulated and refined by Clarke,¹⁶ who distinguished two subtypes of cytoplasmic cell death, 3A non-lysosomal disintegration and 3B cytoplasmic. Additional morphological forms have been described, but it has been suggested that these may reflect different cell types or initiating stimuli rather than fundamentally different cellular mechanisms.¹⁷ Further details regarding these morphological classifications can be found in several excellent reviews.^{15,17,18}

More recent studies have focused on the roles of apoptosis *versus* necrosis in neuronal loss associated with acute or chronic neurodegenerative disorders. Apoptosis and necrosis have been distinguished by various histological and biochemical criteria. Thus, necrosis is characterized by loss of membrane integrity and cellular swelling, damage to organelles, lysosomal disruption, and uncontrolled cell lysis that often leads to tissue inflammation.¹⁹ In contrast, typical features of apoptotic cells include preserved membrane integrity and cell shrinkage, cytoplasmic and nuclear condensation, and plasma membrane blebbing. At later stages of apoptosis, cells may disintegrate into apoptotic bodies, which are engulfed by neighboring cells. Moreover, it does not lead to an inflammatory response.¹⁹

Although such morphological differences have been widely used to distinguish these two types of cell death, some pathologists have suggested a modified nomenclature. Thus, the Society of Toxicologic Pathologists proposed use of the term "necrosis" to describe cell death independent of a specific pathway, with "oncosis" used to reflect cell swelling as may occur with acute ischemia and "apoptotic" as a modifier of cell death ("necrosis") showing apoptotic features as described above.²⁰ However, apoptosis and necrosis may, in fact, share certain common signal transduction pathways and cooperate in cell death.²¹ Indeed, apoptosis and necrosis may be induced by the same insult, with the magnitude of the insult determining the decision of the cell to undergo one of the alternative cell death pathways.²² Intracellular ATP levels appear to be an important factor in the initiation of apoptotic or necrotic execution programs.^{23,24} Moreover, inhibition of one of these cell death pathways may increase cell loss through the other.^{7,25}

Recent studies have further complicated the classification of cell death phenotypes, as well as the mechanisms involved.²¹ Careful morphological analyses of dy-

ing neurons in mouse models of Huntington's disease and amyotrophic lateral sclerosis failed to identify either classical necrosis or apoptosis^{24,26} but rather revealed features more consistent with an alternative type of neuronal cell death that has been termed paratosis.²⁷ This type of neuronal death requires gene expression, displays non-apoptotic morphology with vacuolization, and is independent of caspase activation. Whether this form of cell death should be characterized within the existing nomenclature as type 2 or 3B is uncertain,²⁸ but many descriptions of non-apoptotic cell death showing cytoplasmic vacuolization appear to be most closely related to type 3B.²⁷ In addition, forms of apoptosis with non-classical morphological features and different biochemical markers have been identified.²⁹ Thus, there appear to be multiple forms of programmed cell death, with different morphological features and likely distinct molecular mechanisms (FIG. 1). Recognition of this diversity has substantial implications for the development of more effective neuroprotective strategies.

CASPASE-DEPENDENT APOPTOSIS

The apoptotic machinery initially identified in *Caenorhabditis elegans* is evolutionarily conserved in higher organisms.³⁰ Programmed cell death in this nematode is largely controlled by two pro-apoptotic genes (*ced-3* and *ced-4*) and one anti-apoptotic gene (*ced-9*). Although molecular mechanisms controlling apoptosis in mammals are far more complex, homologs for *ced-3* (caspases), *ced-4* [apoptosis protease activating factor-1 (*apaf-1*)], and *ced-9* (*bcl-2*) have been identified.²⁹ The term "caspase" refers to cysteinyl aspartic acid-proteases.³¹ Caspases share considerable sequence identity around the putative active site cysteine: QAC(R/A/G)G.³¹ These enzymes are translated as zymogen proforms that include an N-terminal prodomain, a large subunit, and a C-terminal small subunit, which are separated by specific caspase recognition sites. Processing of caspase precursors at these sites leads to their activation. Active caspases are heterotetramers consisting of two large and two small subunits. Upon activation, caspases may cleave their own precursors or other procaspases, resulting in a caspase activation cascade.

Most caspase substrates are cleaved by these proteases after aspartate at P1; however, some exceptions to the rule have also been reported.³² Variability in the P2-P4 region determines substrate specificity for individual members of the family. Based on their substrate specificity, caspases have been divided into group I (caspase-1, -4, and -5, which prefer the tetrapeptide sequence WEHD), group II (caspase-2, -3, and -7, which preferentially cleave DEXD), and group III (caspase-6, -8, and -9, which prefer (L/V)EXD).³¹

Based on mechanisms of activation, caspases have

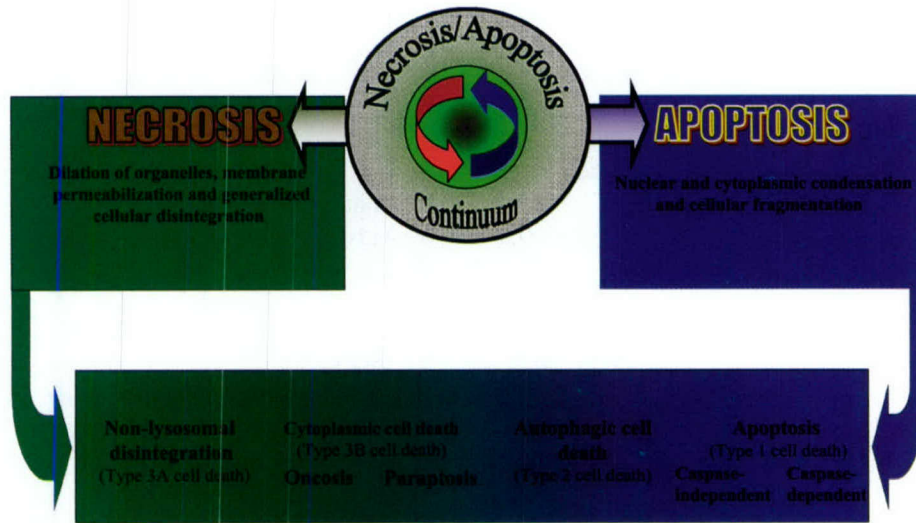


FIG. 1. Apoptosis-necrosis continuum. Cell death includes morphologically distinct types that have been characterized in various ways. No single classification encompasses all of the variant descriptions in the literature. Clearly, there is a continuum of cell death variants, with multiple variants coexisting in both clinical disorders and clinically relevant experimental models. Here we depict an apoptosis-necrosis continuum leading to cell death with different morphological features.

been divided into initiators and effectors. The initiator caspases, such as caspase-8 and -9, begin the disassembly process and activate downstream effector caspase-3, -6, and -7, leading to an amplified caspase cascade.³³ Active effector caspases contribute to the morphological and biochemical manifestation of apoptotic death, such as membrane blebbing, condensation or margination of chromatin and nuclear fragmentation, as well as alterations in activity of numerous nuclear and cytosolic enzymes. Unlike effector caspases, initiator caspases have a long N-terminal prodomain, do not undergo autoactivation, and do not cleave one another. For activation they require additional proteins, such as death domain-containing receptors (type I apoptosis) or functional apoptosomes (type II apoptosis).¹

A third group of mammalian caspases, which includes caspase-1, -4, -5, -11, -12, and -13, has been defined in terms of their function as pro-inflammatory enzymes. In contrast to the effector caspases that are involved in the execution of the apoptotic process, pro-inflammatory caspases are poor substrates for other caspases, and their apical activation pathways are poorly understood.

Pathways of caspase-3 activation

Of the 14 caspases identified in mammals, caspase-3 appears to be the major effector in neuronal apoptosis triggered by various stimuli. Strong evidence supporting the specific role for this protease comes from studies on caspase-3 knockout mice, in which brain development is profoundly altered.³⁴ A role for caspase-3 in injury-induced neuronal loss was subsequently established using semi-specific peptide caspase inhibitors *in vivo* and *in vitro*.³⁵

Two major caspase-3 activating pathways have been

identified: an extrinsic pathway involving cell-surface receptors, and an intrinsic pathway resulting from alterations at the level of the mitochondrion and activation of the apoptosome.¹ The extrinsic pathway requires oligomerization of "death" receptors and the formation of death-inducing signaling complex.³⁵ This process is regulated by members of the tumor necrosis factor (TNF) family of cytokines that include Fas ligand (Apo-1/CD95 ligand), TNF- α , TNF-related apoptosis-inducing ligand, and TNF-related weak inducer of apoptosis.^{35,36} Oligomerization of a death receptor leads to binding of its intracellular domain to the adaptor molecule Fas-associated death domain or caspase and RIP adaptor with death domain, which recruits initiator procaspase-8 and triggers its activation. The released active caspase-8 activates downstream executioner caspases-3 and -7. In addition, activated caspase-3 may cleave procaspase-8,³⁷ thereby amplifying the death process. Initiation of apoptosis through the extrinsic pathway does not usually require new mRNA or protein synthesis.

In some cell types caspase-8 triggers the intrinsic apoptotic pathway by cleaving cytosolic Bid, a pro-apoptotic member of the Bcl-2 family. The C-terminal portion of Bid translocates to the outer mitochondrial membrane and triggers the release of cytochrome *c* from mitochondria to the cytoplasm.³⁸ In the presence of ATP or dATP, cytochrome *c* binds to Apaf-1 and allows the recruitment and activation of procaspase-9 within the apoptosome.³⁵ Caspase-9 cleaves and activates executioner caspases-3 and -7. Active caspase-3 can cleave and activate at least four other caspases (-2, -6, -8, and -10) and also participates in a feedback amplification loop involving caspase-9.³⁷

In contrast to the extrinsic pathway, initiation of the intrinsic apoptotic cascade in specific cell types often requires gene induction and protein synthesis, where an essential role has been attributed to p53 and pro-apoptotic members of Bcl-2 family.^{35,39} However, precise mechanisms by which gene activation signals Bcl-2 family proteins remain to be elucidated.

Numerous reports support an essential role for the intrinsic caspase pathway in neuronal apoptosis after cerebral ischemia, brain trauma, spinal cord injury, Huntington's disease, Alzheimer's disease, and seizures.^{1,4,35,40} Moreover, similar to caspase-3 knockout mice, null mutants of caspase-9 show severe defects of programmed cell death in the nervous system.⁴¹ The majority of these mutants are embryonic lethal or die shortly after birth. A general reduction of neuronal death is found in their embryonic brain tissue; however, the phenotype of caspase-9^{-/-} mice is more severe than that of caspase-3^{-/-}, which suggests that caspases other than caspase-3 (such as caspase-7) may also function downstream from caspase-9.⁴¹ Furthermore, insertional mutagenesis or targeted disruption of *apaf-1* gene also produces perinatal lethality that is associated with marked developmental abnormalities. Apaf-1^{-/-} cells fail to activate caspase-3 through the intrinsic pathway of apoptosis *in vivo* or *in vitro*, which presumably accounts for similar developmental abnormalities seen in Apaf-1-, caspase-9-, and caspase-3-deficient embryos.^{34,41} This suggests that activation of procaspase-3 by the apoptosome-mediated pathway plays a critical role in neuronal apoptosis at early stages of brain development.

Modulation of caspase activation

Caspase activation can be modulated at many critical steps. For example, the anti-apoptotic Bcl-xL protein⁴² acts as a major inhibitor of cytochrome *c*-mediated caspase activation; transgenic mice lacking *bcl-x* die in embryonic development and show increased death of post-mitotic neurons.⁴³

Initially, it has been suggested that Bcl-xL directly binds to Apaf-1, thus preventing activation of caspase-9. However, recent studies demonstrate that intracellular localization of Apaf-1⁴⁴ differs from that of Bcl-xL⁴⁵ and indicate that Bcl-xL, like other anti-apoptotic members of the Bcl-2 family, is involved in the control of permeability of mitochondrial membranes and the release of cytochrome *c* via interaction with Bax.⁴⁶ On the other hand, Bcl-xL can be cleaved by caspases, and the resulting C-terminal fragment of Bcl-xL potently induces apoptosis.⁴⁷

Bax is another member of the Bcl-2 family found to promote apoptosis. Under normal conditions, Bax predominantly localizes in the cytosol but translocates to mitochondrial and other membranes early in apoptosis.⁴⁸ Once translocated to mitochondria, Bax forms homo-

oligomers, leading to loss of mitochondrial membrane potential, cytochrome *c* release, formation of the apoptosome complex, and caspase activation.⁴⁹ Bax deficiency does not cause hyperplasia or malformations of the nervous system, but it decreases apoptosis in the developing CNS and reduces neuronal death caused by Bcl-x disruption.⁵⁰ Recent findings by Scorrano and co-workers⁵¹ suggest that Bax and another "multidomain" pro-apoptotic protein, Bak, are required to maintain homeostatic concentrations of Ca²⁺ in the endoplasmic reticulum (ER). The authors found that mouse embryonic fibroblasts deficient for both these proteins had a reduced resting concentration of calcium in the ER that results in decreased uptake of Ca²⁺ by mitochondria after Ca²⁺ release from the ER. Hence, this function of Bax and Bak may control the apoptotic fate of cells responding to Ca²⁺-dependent stimuli, such as oxidative stress.

Cytochrome *c* release can be induced by members of the caspase family.^{52,53} Of particular interest are recent reports that suggest involvement of caspase-2 in mitochondria-dependent apoptosis by inducing the release of cytochrome *c* and other mitochondrial apoptogenic factors into the cell cytoplasm.^{53,54} However, other studies show that initiation of the intrinsic pathway is mediated before caspase activation.⁵⁵

Apoptosome-mediated apoptosis may additionally be regulated by more complicated mechanisms. Thus, numerous alternatively spliced isoforms of certain apoptosis regulators, such as Bcl-x,⁵⁶ caspase-9,⁵⁷ and Apaf-1⁵⁸ have been shown to play opposing roles in regulating apoptosis.⁵⁹ Furthermore, growth factors can promote cell survival by activating the phosphatidylinositol-3'-OH kinase and its downstream target, the serine-threonine kinase Akt. Cardone and collaborators⁶⁰ found that active Akt can phosphorylate recombinant human caspase-9 on serine-196 and inhibit its activity. However, the corresponding Akt phosphorylation site was not found in the cloned mouse ortholog.⁶¹ Akt may inhibit activation of caspases-9 and -3 by posttranslational modification of a cytosolic factor downstream of cytochrome *c* and before activation of caspase-9.⁶² Activation of the PI3'/K/Akt signaling pathway by growth factors leads to phosphorylation of pro-apoptotic Bad⁶³, thereby altering its function. On the other hand, an increase in intracellular Ca²⁺ concentration results in activation of the protein phosphatase calcineurin, which can dephosphorylate Bad.⁶⁴ In other models, dephosphorylation of Bad can be achieved by Ras-dependent activation of the protein phosphatase 1 α .⁶⁵ Dephosphorylated Bad forms a heterodimer with Bcl-xL, displacing Bax; this leads to the release of cytochrome *c* and activation of downstream caspases, promoting apoptosis.⁶⁶ Active caspase-3 can specifically cleave Akt and, thus, amplify the death process.⁶⁷

Other regulatory mechanisms that parallel the pro-

Mitochondrial Factors and Apoptosis

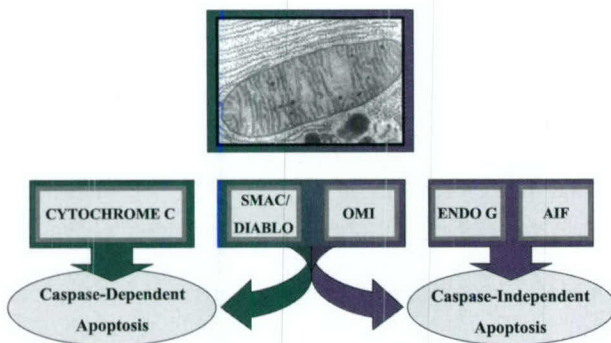


FIG. 2. A variety of mitochondrial proteins have been identified, whose translocation precipitates or contributes to apoptotic cell death. These include those leading primarily to caspase-dependent apoptosis (cytochrome *c*), to caspase-independent cell death (AIF, endonuclease G), or to both (Smac/DIABLO, Omi/HtrA₂).

apoptotic action of cytochrome *c* involve the mitochondrial proteins Smac/DIABLO and Omi/HtrA₂, which are also released into the cytosol when cells undergo apoptosis (FIG. 2). These proteins promote caspase-9 activation by modulating inhibitors of apoptosis proteins (IAPs),⁶⁸ removing their inhibitory activity.^{69,70} Initially identified as baculoviral suppressors of apoptosis in host cells, seven IAP genes have been found in mammalian genomes.⁷¹ Anti-apoptotic activity of corresponding proteins has been attributed to the conserved baculovirus IAP repeat (BIR) domain.⁷² Members of this protein family, XIAP, c-IAP-1, and c-IAP-2 bind procaspase-9 and prevent its activation within the apoptosome and can also inhibit active caspases-3 and -9.⁷³

Smac seems to function as a general neutralizer of IAPs by binding to the BIR2 and BIR3 domains of c-IAP1, c-IAP2, and XIAP.⁶⁹ This could presumably prevent interactions of the IAPs with caspases, therefore releasing their inhibition of caspase activation and caspase activities.⁶⁹ The serine protease Omi/HtrA₂ is also released from mitochondria and inhibits the function of XIAP by direct binding in a way similar to Smac/DIABLO.⁷⁴

Recently, Wang and co-workers⁷⁵ identified two additional proteins that regulate mitochondrial cell death: the oncoprotein prothymosin- α , which inhibits assembly of the apoptosome, and tumor suppressor putative HLA-DR-associated proteins (PHAPs), which stimulate activation of apoptosome. Previous studies have demonstrated that PHAPs can interact with the protein ataxin-1, suggesting that these proteins may contribute to a polyglutamine repeat disorder such as spinocerebellar ataxia type I.⁷⁶

The release of cytochrome *c* from mitochondria to cytosol does not necessarily determine cell fate, since activation of the apoptosome is controlled by other factors. Thus, the cellular stress response can lead to cellular

protection by inducing heat-shock proteins (Hsp). Two members of this family, Hsp70 and Hsp90, prevent cytochrome *c*/dATP-mediated caspase activation by direct association with Apaf-1, thereby preventing recruitment of caspases to the apoptosome complex.^{77,78} A third member of the family, Hsp27, also inhibits cytochrome-*c*-mediated activation of caspases by binding to cytochrome *c* and thus prevents the interaction of Apaf-1 with procaspase-9.⁷⁹

Other caspases

Nakagawa et al.⁸⁰ showed that the caspase cascade can also be initiated by caspase-12. Caspase-12-knockout mice are resistant to apoptosis induced by cellular stress, and caspase-12-deficient cortical neurons are resistant to apoptosis induced by β -amyloid. In this stress-induced pathway caspase-12 activates caspase-3, and this process can be reversed by antisense-mediated inhibition of caspase-12.⁸¹ It has been proposed that increased intracellular Ca^{2+} , resulting from ischemic injury or β -amyloid cytotoxicity, may induce apoptosis through simultaneous activation of caspase-12 and inactivation of Bcl-xL by calpain.⁸²

Furthermore, in other models, an upstream activator of caspase-1,⁸³ caspase-11 is able to cleave and activate caspase-3. Caspase-11-deficient mice demonstrate reduced caspase-3 activity and cell death caused by brain ischemia.⁸⁴ This caspase has also been shown to be activated by cathepsin B⁸⁵ that, in turn, can be activated by calpains.⁸⁶

Results of several studies suggest that activation of caspase-2 plays a critical role in initiation and progression of apoptosis. Thus, diminished expression of this caspase in PC12 cells and sympathetic neurons mediated by antisense oligonucleotides rescues them from death caused by trophic factor deprivation.⁸⁷ More recently, Lassus and collaborators⁵³ demonstrated that caspase-2 is required for the permeabilization of mitochondria, the release of cytochrome *c* and Smac, and translocation of Bax from the cytoplasm to mitochondria in response to cytotoxic stress.

In contrast, results of knockout studies show that death of motor neurons during development is accelerated in caspase-2-deficient mice, and that caspase-2-deficient sympathetic neurons undergo apoptosis more effectively than wild-type neurons when deprived of nerve growth factor.⁸⁸ Thus, caspase-2 may serve either as a positive or negative regulator of apoptosis.

Developmental changes

Clinical data suggest that outcomes and mortality after acute brain injury are age-dependent, with more severe responses in infants than in adults.⁸⁹ Such differences in response to injury may be explained, in part, by differential susceptibility to apoptosis and associated caspase-3 activity in brain as a function of developmen-

tal age.^{90,92} During brain maturation, the potential of the intrinsic apoptotic pathway is progressively reduced; such repression is associated with down-regulation of Apaf-1 and caspase-3 gene expression.⁴⁰ Injury-induced cytochrome *c*-specific cleavage of procaspase-9, followed by activation of caspase-3 in mature brain, correlated with marked increases in Apaf-1 and caspase-3 mRNA and protein expression.⁴⁰ These results suggest that differential expression of Apaf-1 and caspase-3 genes may underlie regulation of apoptotic susceptibility during brain development, as well as after acute injury to mature brain, through the intrinsic pathway of caspase activation.

CASPASE-INDEPENDENT APOPTOSIS

Although caspases have been recognized as important mediators of apoptosis, there is accumulating evidence suggesting the existence of caspase-independent mechanisms of neuronal death (FIG. 2).^{29,93} Blockade of the caspase execution machinery may only temporarily rescue damaged neurons, and classical apoptotic features can still appear in caspase-inhibited neurons and other cell types.⁹⁴ In experimental models of stroke, caspase inhibition affords protection in certain neuronal populations but not in others.⁹⁵ These results are consistent with the idea that the involvement of specific caspase-dependent and caspase-independent mechanisms of cell death may depend on brain region, cell type, and age.⁹⁶ Although there has been extensive investigation of caspase-mediated cell death processes, much less is known about molecular mechanisms involved in the regulation of caspase-independent apoptosis and their role in brain development.

Specific mitochondrial factors appear to play a central role in both caspase-dependent and caspase-independent apoptosis. Thus, cytochrome *c*, Smac/DIABLO, and HtrA2/Omi are released from mitochondria during initiation of apoptosis and control activation or activity of caspases.^{29,69,74,93} In contrast, apoptosis-inducing factor (AIF) and endonuclease G promote caspase-independent cell death.^{29,93} However, Smac/DIABLO and HtrA2/Omi may also contribute to caspase-independent apoptosis.⁹³

AIF

AIF normally localizes in mitochondria; however, after an apoptotic insult, it translocates to the cytosol and the nucleus, where it induces peripheral chromatin condensation and high molecular weight DNA fragmentation.^{93,97} Nuclear translocation of AIF has been observed under a wide variety of cell death inducing conditions such as protein kinase inhibition, c-Myc overexpression, ceramide exposure, or *in vitro* chemotherapy.^{93,97} Importantly, AIF translocation also occurs after ATP depletion that leads to inhibition of apoptosis and promotion of necrotic cell death.⁹⁷ Intracellular redistribution of AIF

correlates with large-scale DNA fragmentation and chromatin condensation, which occurs even in cells lacking Apaf-1 or caspase-3.⁹⁸ This suggests that AIF may be responsible for the caspase-independent features of apoptosis. Kinetic analyses revealed that release of AIF from mitochondria does not correspond to that of cytochrome *c* that has been explained by differential localization of these proteins within mitochondria.⁹⁷

AIF possesses a second, oxidoreductase, enzymatic activity different from its apoptotic potential.⁹⁹ The cellular targets of AIF remain elusive. However, heat shock protein 70 (Hsp70) physically interacts with AIF and inhibits its apoptotic effects both *in vitro* and in intact cells.¹⁰⁰ Overexpression of Bcl-2 also blocks the AIF redistribution.²⁹

A recent study on Harlequin (*Hq*) mice has suggested a vital role for AIF in neuron survival in the aging mouse brain.¹⁰¹ In this report, Klein and co-authors¹⁰¹ found that *Hq* mutation caused an approximately 80% reduction in AIF expression and associated progressive degeneration of terminally differentiated cerebellar and retinal neurons in mice after 3 months of age. Reduced levels of AIF in mutant cells increased their susceptibility to exogenous and endogenous peroxide-mediated apoptosis that was inhibited by AIF overexpression. Furthermore, terminally differentiated neurons in the cerebellum and retina (but not in other neural tissues) undergo unscheduled cell cycle reentry, providing another molecular mechanism by which free-radical damage can lead to neuronal death.¹⁰¹ A pathway involving redistribution of AIF has been reported after acute brain injury in rats.¹⁰²

In our preliminary studies, we demonstrated that in contrast to Apaf-1 and procaspase-3 proteins, AIF is up-regulated during brain development in rats (Yakovlev, unpublished observation). This observation suggests that developmentally orchestrated regulation of Apaf-1, caspase-3, and AIF expression may determine the relative roles of caspase-dependent and caspase-independent mechanisms of neuronal cell loss in the course of brain maturation and brain injury.

Endonuclease G

Endonuclease G was identified as the mitochondrial nuclease involved in mitochondrial DNA replication.¹⁰³ It can be specifically activated by apoptotic stimuli, such as TNF- α , anti-Fas antibodies, and UV irradiation, and, as for many other nucleases, induces internucleosomal fragmentation of nuclear DNA.¹⁰⁴ Once released into the cytosol and translocated to the nucleus, this nuclease generates oligonucleosomal DNA fragmentation even in the presence of caspase inhibitors or absence of DNA fragmentation factor (DFF40).¹⁰⁴ Another apoptotic endonuclease that is activated by caspase-3 and digests genomic DNA into oligonucleosomal fragments.² DFF40 is a 40-kDa protein that is translated in the pres-

ence of its inhibitor (DFF45), which functions as a specific chaperone and forms a heterodimer with DFF40 in proliferating cells. Unlike endonuclease G, DFF45 is cleaved by caspase-3, releasing the nuclease activity of DFF40 from inhibitory control and triggering DNA fragmentation.¹⁰⁵

In contrast to Li et al.,¹⁰⁴ who reported DNA laddering resulting from endonuclease G activity, Van Loo et al.¹⁰⁶ only observed higher-order (~50 kb) DNA degradation. Furthermore, in comparison to DFF40, much higher concentrations of endonuclease G are required for DNA degradation,⁹³ suggesting a requirement for other co-factors, such as DNase I,¹⁰⁷ to induce effective DNA fragmentation.

Omi/HtrA2

Protein analysis of supernatants isolated from mitochondria exposed to recombinant tBid, a pro-apoptotic Bcl-2 member, revealed the presence of the serine protease Omi, also called HtrA2.⁷⁰ The autoprocessed amino-terminal domain of HtrA2/Omi demonstrates homology to Smac/DIABLO and Reaper family proteins.²⁹ Processed Omi/HtrA2 is released to the cytoplasm upon induction of apoptosis where it binds XIAP resulting in caspase-9 activation.^{29,70,93} This function of Omi is similar to that of Smac/DIABLO, which also binds IAPs and activates caspase-9¹⁰⁸; however, HtrA2/Omi can also induce apoptosis in a caspase-independent manner.^{29,93} When overexpressed extramitochondrially, it induces cell death, which is neither accompanied by significant caspase activation nor prevented by caspase inhibitors. This effect of HtrA2/Omi appears to depend on its serine protease activity, since its catalytically inactive mutant does not induce cell death.^{70,74}

Smac/DIABLO

Smac/DIABLO is also able to induce cell death independently of its binding to IAPs. Thus, Roberts and coworkers¹⁰⁹ have demonstrated that a short splice variant of Smac/DIABLO (Smac β) that lacks the mitochondria targeting and IAPs binding domains potentiates apoptosis induced by death receptor and chemical stimuli. Furthermore, expression of a NH(2)-terminally truncated Smac mutant (Delta75), which lacks the entire IAP-interacting domain, potentiates apoptosis to the same extent as Smac/DIABLO and Smac β .¹⁰⁹

Although expression of Smac/DIABLO is undetectable in adult mouse brain under normal conditions, Shibata and collaborators¹¹⁰ reported its induction after transient focal ischemia in mice. However, it is still unclear whether this mitochondrial protein plays an essential role in neuronal death *in vivo*, since the knockout mice are viable and do not demonstrate any obvious phenotypic abnormality; moreover, Smac/DIABLO^{-/-} cells undergo typical apoptosis induced by a variety of stimuli.¹¹¹

MOLECULAR PATHWAYS OF CELL NECROSIS

Neuronal necrosis is often observed under severe pathophysiological conditions, such as hypoxia, ischemia, hypoglycemia, exposure to reactive oxygen metabolites and toxins, among others. This type of cell death has also been described in such neurodegenerative disorders as Alzheimer's, Huntington's, Parkinson's diseases, amyotrophic lateral sclerosis, and epilepsy.^{112,113} Moreover, autophagic and cytoplasmic types represent alternative necrosis-like forms of programmed cell death that normally occur during development.¹¹⁴

In contrast to apoptosis, necrosis has been considered a passive and disordered process leading to accidental and unavoidable death of cells exposed to extreme insults. However, new findings have revised this concept. Thus, execution of necrotic death depends on activation of Ca²⁺-dependent proteolysis that employs proteases different from caspases. Moreover, similar morphological and ultrastructural features of necrotic cells of different origin suggests existence of a conserved execution program. Recent studies on genetic mechanisms of excitotoxic degeneration of the six touch receptor neurons in *C. elegans* established a role for CLP-1 and TRA-3 calpain-like proteases and aspartyl proteases ASP-3 and ASP-4, two orthologs of mammalian cathepsins.¹¹⁵ The authors demonstrated that overexpression of ASP-3 and -4 can induce spontaneous vacuolization and death of neurons in the ventral nerve cord. RNAi-mediated inhibition of ASP-3 and -4 expression resulted in neuroprotection.

According to the "calpain-cathepsin" hypothesis, activation of cathepsins occurs as a result of Ca²⁺-dependent activation of calpains. In agreement with this hypothesis, inhibition of calpain activity in worms by z-Val-Phe-CHO markedly reduced the number of degenerating neurons. RNAi-mediated knockdown of six of 17 *C. elegans* calpain homologs revealed an essential role for *clp-1* and *tra-3* genes in neuronal loss. Simultaneous repression of both calpain or both cathepsin genes by RNAi resulted in an enhanced suppression of neurodegeneration. However, no synergy was observed between aspartyl proteases and calpain, suggesting their contribution to the same pathway of neurodegeneration in *C. elegans*. Overall, results of this study indicate that diverse death-initiating conditions lead to Ca²⁺-dependent activation of calpains and a subsequent increase in cathepsins activity, leading to cell destruction.¹¹⁵

Calpains

Mammalian calpains compose a large family of constitutively expressed intracellular cysteine proteases.⁸⁶ Two major groups of these enzymes are known as μ - and m-calpains (also called calpains I and II, respectively). The enzymes of both groups require Ca²⁺ for their ac-

tivation. While μ -calpains are active at micromolar Ca^{2+} concentrations *in vitro*, active m-calpains require millimolar Ca^{2+} . Although a large number of calpain substrates have been demonstrated, including cytoskeletal proteins, growth factor receptors, and transcription- and cell-cycle-related proteins, the precise function of calpains *in vivo* remains unclear.⁸⁶

Calpains have been proposed to play a role in regulating normal signal transduction processes by cleaving cytoskeletal proteins such as talin and α -actinin, membrane proteins such as the epidermal growth factor receptor, integrin, N-CAM, and cadherin, and enzymes such as protein kinase C and calmodulin-dependent kinase.¹¹⁶ Constitutive expression of calpains in mammalian CNS and the property of activation by Ca^{2+} indicate that these proteases can also contribute to neurodegeneration. Activation of calpains has been proposed to contribute to neuronal cell death in ischemic brain injury,¹¹⁷ brain trauma,¹¹⁸ and Alzheimer's disease.¹¹⁹ Moreover, calpain inhibitors show neuroprotective effects in animal models of cerebral ischemia¹¹⁷ and traumatic brain injury.¹¹⁸

Cathepsins

Like calpains, cathepsins also belong to the papain superfamily of cysteine proteases. They are synthesized as inactive precursors and undergo proteolytic activation. Cathepsins are localized predominantly to the lysosomes, but have also been found in cell nuclei and cytosol.⁸⁶ Neuronal lysosomes are known to contain at least cathepsins B, D, and L; activity of these enzymes has been implicated neuronal injury,⁸⁶ and cathepsin inhibitors such as CA-074 and E-64c have been demonstrated to significantly inhibit neuronal death.¹²⁰

The cytosolic activity of cathepsin D increases significantly from 2 to 6 months in the rat brain, and by 36 months it shows twice the activity of the lysosomal/mitochondrial fraction.¹²¹ Our preliminary data, on the other hand, suggest that in contrast to the pro-apoptotic genes, such as procaspase-3 and Apaf-1, m-calpain protein expression is up-regulated during rat brain development (unpublished observations). Taken together, regulatory mechanisms that control expression of key apoptotic and necrotic genes during brain development appear to predetermine different types of injury-induced neuronal death.

COOPERATION OF CELL DEATH PROGRAMS

As indicated previously, morphological descriptions of apoptosis and necrosis do not describe all variations of cell death. There are many examples when biochemical and morphological features of more than one type of programmed death can be found in the same cell,¹¹³ and inhibition of one form of cell death can lead to domina-

tion of another.⁷ These experimental studies support the existence of a spectrum of death programs in cells.²¹ Thus, Formigli and collaborators²¹ found that antimycin A, a metabolic poison that affects mitochondrial respiratory chain complex III, induced a type of cell death that shared dynamic, molecular, and morphological features with both apoptosis and necrosis, which they called aponecrosis. Inhibition of caspase-3 caused a shift from aponecrosis to necrosis, and higher doses of antimycin A induced necrosis. The analysis of the cellular energetic stores showed that the levels of ATP were a primary determinant in directing toward active cell death (apoptosis), aponecrosis, or necrosis. These and other recent data indicate that apoptosis and necrosis may not necessarily be two independent pathways, but rather may share some common events, at least with regard to signal transduction pathways and early phases of the cell death process. This idea is consistent with observations that anti-apoptotic genes, such as *bcl-2*, are able to inhibit both apoptotic and necrotic cell death.¹²²

Furthermore, it is becoming increasingly clear that various types of cell death can share pathways of their execution. For example, recent data suggest a cross-talk between calpains and caspases. Thus, m-calpain can cleave and activate procaspase-12, leading to the caspase cascade.⁸² In addition, calpain may be responsible for cleaving the loop region in Bcl-xL, thereby transforming an anti-apoptotic molecule into a pro-apoptotic one.⁸²

CELL DEATH MECHANISMS: IMPLICATIONS FOR TREATMENT

The existence of multiple cell death pathways with both overlapping and distinct molecular mechanisms, combined with the observation that inhibition of one such pathway may enhance alternative ones, suggest that treatment strategies should optimally be directed at multiple targets/mechanisms. Traditionally, neuroprotection treatment approaches have focused on single receptors or injury factors, and have been primarily aimed at reducing necrotic cell death.¹¹ Because necrosis is an early event, and it is often not possible to treat patients until many hours after acute injuries, such strategies are not likely to be effective. Indeed, virtually all neuroprotective treatment trials in stroke or traumatic brain injury have failed.^{11,123} Alternatively, many recent experimental studies have attempted to modulate caspase-mediated apoptosis. Such studies may make more conceptual sense, as apoptosis is a more delayed event, and use of caspase inhibitors has proved effective in experimental stroke, head injury, and spinal cord injury.³⁵ However, this approach is potentially problematic for several reasons. First, there is evidence that inhibition of apoptosis may enhance necrotic cell death.²¹ Second, the effectiveness of peptide caspase inhibitors may relate to their ability to reduce necrotic cell

death, possibly mediated by calpains (Knobloch and Faden, unpublished observations).

These observations suggest that optimal neuroprotective approaches should include either combination treatment strategies directed toward multiple cell death pathways or the use of single compounds that may inhibit more than one cell death mechanism (multipotential agents). We have previously shown in a cell culture model of traumatic neuronal cell death, which induces both apoptotic and necrotic cell death, that combination treatment with an NMDA antagonist and a caspase inhibitor has additive, if not synergistic, neuroprotective actions.¹²⁴

A prototypic multipotential agent is thyrotropin-releasing hormone (TRH). TRH serves as a physiologic antagonist for endogenous opioids, peptidyl leukotrienes, and platelet-activating factor, all of which have been implicated in secondary tissue injury; it also improves cerebral blood flow, cellular bioenergetic state, and ionic homeostasis.¹²⁵ TRH has substantial neuroprotective actions in brain and spinal cord injury models,¹²⁶ and has shown effectiveness in human spinal cord injury.⁹

During the past several years, a number of other neuroprotective agents have been evaluated that have multipotential actions. Dexanabol (HU-211) is an NMDA antagonist that also has antioxidant and anti-TNF properties; it has good neuroprotective activity in experimental models of stroke and head injury.¹²⁷ AM36 has actions as a sodium channel blocker, NMDA antagonist and free radical scavenger.¹²⁸ It has been shown to have neuroprotective actions *in vivo* and *in vitro*, as well as anti-apoptotic effects.^{128,129} 35b is a cyclized dipeptide, somewhat related to a metabolic product of TRH, which blocks both apoptotic (caspase-dependent) and necrotic cell death in primary neuronal cell cultures, and shows striking neuroprotective actions following traumatic brain injury in rats and mice.^{130,131}

As molecular mechanisms of non-caspase-dependent programmed cell death are defined, other types of combined treatment or multipotential treatment approaches should be developed. Because multiple cell death pathways may have common upstream initiators, or share signal transduction cascades, new drug development strategies directed at such common targets should be considered for the treatment of both acute and chronic neurodegenerative disorders.

Acknowledgments: This work was supported by Department of Defense Cooperative Agreement DAMD17-99-2-9007, NIH Grants R01 NS36537 and R01 NS41119 to A. I. F., NIH Grant P30 HD40677 Core Subcontract to A. I. F., and NIH Grant R01 NS38941 to A.G.Y.

REFERENCES

- Eldadah BA, Faden AI. Caspase pathways, neuronal apoptosis, and CNS injury. *J Neurotrauma* 17:811–829, 2000.
- Snider BJ, Gottron FJ, Choi DW. Apoptosis and necrosis in cerebrovascular disease. *Ann NY Acad Sci* 893:243–253, 1999.
- Graeber MB, Moran LB. Mechanisms of cell death in neurodegenerative diseases: fashion, fiction, and facts. *Brain Pathol* 12:385–390, 2002.
- Honig LS, Rosenberg RN. Apoptosis and neurologic disease. *Am J Med* 108:317–330, 2000.
- Panter SS, Faden AI. Biochemical changes and secondary injury from stroke and trauma. In: Principles and practice of restorative neurology, Chap 5 (Young RR, Delwade PJ, eds), pp 32–52. New York: Butterworth's, 1992.
- McIntosh TK. Neurochemical sequelae of traumatic brain injury: therapeutic implications. *Cerebrovasc Brain Metab Rev* 6:109–162, 1994.
- Pohl D, Bittigau P, Ishimaru MJ, Stadthaus D, Hubner C, Olney JW et al. N-methyl-D-aspartate antagonists and apoptotic cell death triggered by head trauma in developing rat brain. *Proc Natl Acad Sci USA* 96:2508–2513, 1999.
- Faden AI. Pharmacological treatment of central nervous system trauma. *Pharmacol Toxicol* 78:12–17, 1996.
- Pitts LH, Ross A, Chase GA, Faden AI. Treatment with thyrotropin-releasing hormone (TRH) in patients with traumatic spinal cord injuries. *J Neurotrauma* 12:235–243, 1995.
- Bracken MB, Holford TR. Effects of timing of methylprednisolone or naloxone administration on recovery of segmental and long-tract neurological function in NASCIS 2. *J Neurosurg* 79:500–507, 1993.
- Faden AI. Neuroprotection and traumatic brain injury: theoretical option or realistic proposition. *Curr Opin Neurol* 15:707–712, 2002.
- Lees KR. Neuroprotection is unlikely to be effective in humans using current trial designs: an opposing view. *Stroke* 33:308–309, 2002.
- Schweichel JU, Merker HJ. The morphology of various types of cell death in prenatal tissues. *Teratology* 7:253–266, 1973.
- Kerr JF, Wyllie AH, Currie AR. Apoptosis: A basic biological phenomenon with wide-ranging implications in tissue kinetics. *Br J Cancer* 26:239–257, 1972.
- Kitanaka C, Kuchino Y. Caspase-independent programmed cell death with necrotic morphology. *Cell Death Differ* 6:508–515, 1999.
- Clarke PG. Developmental cell death: morphological diversity and multiple mechanisms. *Anat Embryol (Berl)* 181:195–213, 1990.
- Van Cruchten S, Van Den Broeck W. Morphological and biochemical aspects of apoptosis, oncosis and necrosis. *Anat Histol Embryol* 31:214–223, 2002.
- Bursch W. The autophagosomal-lysosomal compartment in programmed cell death. *Cell Death Differ* 8:569–581, 2001.
- Bredesen DE. Neural apoptosis. *Ann Neurol* 38:839–851, 1995.
- Levin S, Bucci TJ, Cohen SM, Fix AS, Hardisty JF, LeGrand EK et al. The nomenclature of cell death: recommendations of an *ad hoc* Committee of the Society of Toxicologic Pathologists. *Toxicol Pathol* 27:484–490, 1999.
- Formigli L, Papucci L, Tani A, Schiavone N, Tempestini A, Orlandini GE et al. Aponecrosis: morphological and biochemical exploration of a synthetic process of cell death sharing apoptosis and necrosis. *J Cell Physiol* 182:41–49, 2000.
- Bonfoco E, Krainc D, Ankarcrona M, Nicotera P, Lipton SA. Apoptosis and necrosis: two distinct events induced, respectively, by mild and intense insults with N-methyl-D-aspartate or nitric oxide/superoxide in cortical cell cultures. *Proc Natl Acad Sci USA* 92:7162–7166, 1995.
- Eguchi Y, Shimizu S, Tsujimoto Y. Intracellular ATP levels determine cell death fate by apoptosis or necrosis. *Cancer Res* 57:1835–1840, 1997.
- Turnmaine M, Raza A, Mahal A, Mangiarini L, Bates GP, Davies SW. Nonapoptotic neurodegeneration in a transgenic mouse model of Huntington's disease. *Proc Natl Acad Sci USA* 97:8093–8097, 2000.
- Fiskum G. Mitochondrial participation in ischemic and traumatic neural cell death. *J Neurotrauma* 17:843–855, 2000.

26. Dal Canto MC, Gurney ME. Development of central nervous system pathology in a murine transgenic model of human amyotrophic lateral sclerosis. *Am J Pathol* 145:1271-1279, 1994.
27. Sperandio S, de Belle I, Bredesen DE. An alternative, nonapoptotic form of programmed cell death. *Proc Natl Acad Sci USA* 97:14376-14381, 2000.
28. Castro-Obregon S, Del Rio G, Chen SF, Swanson RA, Frankowski H, Rao RV et al. A ligand-receptor pair that triggers a non-apoptotic form of programmed cell death. *Cell Death Differ* 9:807-817, 2002.
29. Ravagnan L, Roumier T, Kroemer G. Mitochondria, the killer organelles and their weapons. *J Cell Physiol* 192:131-137, 2002.
30. Hengartner MO. Programmed cell death in the nematode *C. elegans*. *Recent Prog Horm Res* 54:213-222, 1999.
31. Alnemri ES, Livingston DJ, Nicholson DW, Salvesen G, Thornberry NA, Wong WW et al. Human ICE/ced-3 protease nomenclature [letter]. *Cell* 87:171, 1996.
32. Ethell DW, Bossy-Wetzel E, Bredesen DE. Caspase 7 can cleave tumor necrosis factor receptor-I (p60) at a non-consensus motif, in vitro. *Biochim Biophys Acta* 1541:231-238, 2001.
33. Cohen GM. Caspases: the executioners of apoptosis. *Biochem J* 326:1-16, 1997.
34. Kuida K, Zheng TS, Na S, Kuan C, Yang D, Karasuyama H et al. Decreased apoptosis in the brain and premature lethality in CPP32-deficient mice. *Nature* 384:368-372, 1996.
35. Yakovlev AG, Faden AI. Caspase-dependent apoptotic pathways in CNS injury. *Mol Neurobiol* 24:131-144, 2001.
36. Aravind L, Dixit VM, Koonin EV. The domains of death: evolution of the apoptosis machinery. *Trends Biochem Sci* 24:47-53, 1999.
37. Slee EA, Harte MT, Kluck RM, Wolf BB, Casiano CA, Newmeyer DD et al. Ordering the cytochrome c-initiated caspase cascade: hierarchical activation of caspases-2, -3, -6, -7, -8, and -10 in a caspase-9-dependent manner. *J Cell Biol* 144:281-292, 1999.
38. Luo X, Budihardjo I, Zou H, Slaughter C, Wang X. Bid, a Bcl2 interacting protein, mediates cytochrome c release from mitochondria in response to activation of cell surface death receptors. *Cell* 94:481-490, 1998.
39. Cory S, Adams JM. The Bcl2 family: Regulators of the cellular life-or-death switch. *Nat Rev Cancer* 2:647-656, 2002.
40. Yakovlev AG, Ota K, Wang G, Movsesyan V, Bao WL, Yoshihara K et al. Differential expression of apoptotic protease-activating factor-1 and caspase-3 genes and susceptibility to apoptosis during brain development and after traumatic brain injury. *J Neurosci* 21:7439-7446, 2001.
41. Kuida K, Haydar TF, Kuan CY, Gu Y, Taya C, Karasuyama H et al. Reduced apoptosis and cytochrome c-mediated caspase activation in mice lacking caspase 9. *Cell* 94:325-337, 1998.
42. Gonzalez-Garcia M, Perez-Ballesteros R, Ding L, Duan L, Boise LH, Thompson CB et al. Bcl-XL is the major Bcl-x mRNA form expressed during murine development and its product localizes to mitochondria. *Development* 120:3033-3042, 1994.
43. Motoyama N, Wang F, Roth KA, Sawa H, Nakayama K, Negishi I et al. Massive cell death of immature hematopoietic cells and neurons in Bcl-x-deficient mice. *Science* 267:1506-1510, 1995.
44. Moriishi K, Huang DC, Cory S, Adams JM. Bcl-2 family members do not inhibit apoptosis by binding the caspase activator Apaf-1. *Proc Natl Acad Sci USA* 96:9683-9688, 1999.
45. Hausmann G, O'Reilly LA, van Driel R, Beaumont JG, Strasser A, Adams JM et al. Pro-apoptotic apoptosis protease-activating factor 1 (Apaf-1) has a cytoplasmic localization distinct from Bcl-2 or Bcl-x(L). *J Cell Biol* 149:623-634, 2000.
46. Shimizu S, Konishi A, Kodama T, Tsujimoto Y. Bcl4 domain of antiapoptotic Bcl-2 family members closes voltage-dependent anion channel and inhibits apoptotic mitochondrial changes and cell death [Erratum 1:97:9347, 2000]. *Proc Natl Acad Sci USA* 97:3100-3105, 2000.
47. Fujita N, Nagahashi A, Nagashima K, Rokudai S, Tsuruo T. Acceleration of apoptotic cell death after the cleavage of Bcl-XL protein by caspase-3-like proteases. *Oncogene* 17:1295-1304, 1998.
48. Hsu YT, Wolter KG, Youle RJ. Cytosol-to-membrane redistribution of Bax and Bcl-X(L) during apoptosis. *Proc Natl Acad Sci USA* 94:3668-3672, 1997.
49. Gross A, Jockel J, Wei MC, Korsmeyer SJ. Enforced dimerization of Bax results in its translocation, mitochondrial dysfunction and apoptosis. *EMBO J* 17:3878-3885, 1998.
50. Shindler KS, Latham CB, Roth KA. Bax deficiency prevents the increased cell death of immature neurons in bcl-x-deficient mice. *J Neurosci* 17:3112-3119, 1997.
51. Scorrano L, Oakes SA, Opferman JT, Cheng EH, Sorcinelli MD, Pozzan T et al. Bax and Bak regulation of endoplasmic reticulum Ca2+: a control point for apoptosis. *Science* 300:135-139, 2003.
52. Bossy-Wetzel E, Green DR. Caspases induce cytochrome c release from mitochondria by activating cytosolic factors. *J Biol Chem* 274:17484-17490, 1999.
53. Lassus P, Opitz-Araya X, Lazebnik Y. Requirement for caspase-2 in stress-induced apoptosis before mitochondrial permeabilization. *Science* 297:1352-1354, 2002.
54. Guo Y, Srinivasula SM, Druihe A, Fernandes-Alnemri T, Alnemri ES. Caspase-2 induces apoptosis by releasing proapoptotic proteins from mitochondria. *J Biol Chem* 277:13430-13437, 2002.
55. Schuler M, Bossy-Wetzel E, Goldstein JC, Fitzgerald P, Green DR. P53 induces apoptosis by caspase activation through mitochondrial cytochrome c release. *J Biol Chem* 275:7337-7342, 2000.
56. Minn AJ, Boise LH, Thompson CB. Bcl-x(S) antagonizes the protective effects of Bcl-x(L). *J Biol Chem* 271:6306-6312, 1996.
57. Srinivasula SM, Ahmad M, Guo Y, Zhan Y, Lazebnik Y, Fernandes-Alnemri T et al. Identification of an endogenous dominant-negative short isoform of caspase-9 that can regulate apoptosis. *Cancer Res* 59:999-1002, 1999.
58. Benedict MA, Hu Y, Inohara N, Nunez G. Expression and functional analysis of Apaf-1 isoforms. Extra Wd-40 repeat is required for cytochrome c binding and regulated activation of procaspase-9. *J Biol Chem* 275:8461-8468, 2000.
59. Jiang ZH, Wu JY. Alternative splicing and programmed cell death. *Proc Soc Exp Biol Med* 220:64-72, 1999.
60. Cardone MH, Roy N, Stennicke HR, Salvesen GS, Franke TF, Stanbridge E et al. Regulation of cell death protease caspase-9 by phosphorylation. *Science* 282:1318-1321, 1998.
61. Fujita E, Jinbo A, Matuzaki H, Konishi H, Kikkawa U, Momoi T. Akt phosphorylation site found in human caspase-9 is absent in mouse caspase-9. *Biochem Biophys Res Commun* 264:550-555, 1999.
62. Zhou H, Li XM, Meinkoth J, Pittman RN. Akt regulates cell survival and apoptosis at a postmitochondrial level. *J Cell Biol* 151:483-494, 2000.
63. Datta SR, Dudek H, Tao X, Masters S, Fu H, Gotoh Y et al. Akt phosphorylation of BAD couples survival signals to the cell-intrinsic death machinery. *Cell* 91:231-241, 1997.
64. Wang HG, Pathan N, Ethell IM, Krajewski S, Yamaguchi Y, Shibasaki F et al. Ca2+-induced apoptosis through calcineurin dephosphorylation of BAD. *Science* 284:339-343, 1999.
65. Ayllon V, Martinez AC, Garcia A, Cayla X, Rebollo A. Protein phosphatase 1 α is a Ras-activated Bad phosphatase that regulates interleukin-2 deprivation-induced apoptosis. *EMBO J* 19:2237-2246, 2000.
66. Yang E, Zha J, Jockel J, Boise LH, Thompson CB, Korsmeyer SJ. Bad, a heterodimeric partner for Bcl-XL and Bcl-2, displaces Bax and promotes cell death. *Cell* 80:285-291, 1995.
67. Francois F, Grimes ML. Phosphorylation-dependent Akt cleavage in neural cell in vitro reconstitution of apoptosis. *J Neurochem* 73:1773-1776, 1999.
68. Hay BA. Understanding IAP function and regulation: a view from drosophila. *Cell Death Differ* 7:1045-1056, 2000.
69. Du C, Fang M, Li Y, Li L, Wang X. Smac, a mitochondrial protein that promotes cytochrome c-dependent caspase activation by eliminating IAP inhibition. *Cell* 102:33-42, 2000.
70. Hegde R, Srinivasula SM, Zhang Z, Wassell R, Mukattash R, Cilenti L et al. Identification of Omi/HtrA2 as a mitochondrial apoptotic serine protease that disrupts inhibitor of apoptosis protein-caspase interaction. *J Biol Chem* 277:432-438, 2002.

71. Deveraux QL, Reed JC. IAP family proteins—suppressors of apoptosis. *Genes Dev* 13:239–252, 1999.
72. Takahashi R, Deveraux Q, Tamm I, Welsh K, Assa-Munt N, Salvesen GS et al. A single BIR domain of XIAP sufficient for inhibiting caspases. *J Biol Chem* 273:7787–7790, 1998.
73. Deveraux QL, Roy N, Stennicke HR, Van Arsedale T, Zhou Q, Srinivasula SM et al. IAPs block apoptotic events induced by caspase-8 and cytochrome c by direct inhibition of distinct caspases. *EMBO J* 17:2215–2223, 1998.
74. Suzuki Y, Imai Y, Nakayama H, Takahashi K, Takio K, Takahashi R. A serine protease, HtrA2, is released from the mitochondria and interacts with XIAP, inducing cell death. *Mol Cell* 8:613–621, 2001.
75. Jiang X, Kim HE, Shu H, Zhao Y, Zhang H, Kofron J et al. Distinctive roles of PHAP proteins and prothymosin- α in a death regulatory pathway. *Science* 299:223–226, 2003.
76. Matilla A, Koshy BT, Cummings CJ, Isobe T, Orr HT, Zoghbi HY. The cerebellar leucine-rich acidic nuclear protein interacts with ataxin-1. *Nature* 389:974–978, 1997.
77. Pandey P, Saleh A, Nakazawa A, Kumar S, Srinivasula SM, Kumar V et al. Negative regulation of cytochrome c-mediated oligomerization of Apaf-1 and activation of procaspase-9 by heat shock protein 90. *EMBO J* 19:4310–4322, 2000.
78. Beere HM, Wolf BB, Cain K, Mosser DD, Mahboubi A, Kuwana T et al. Heat-shock protein 70 inhibits apoptosis by preventing recruitment of procaspase-9 to the Apaf-1 apoptosome. *Nat Cell Biol* 2:469–475, 2000.
79. Bruey JM, Ducasse C, Bonniaud P, Ravagnan L, Susin SA, Diaz-Latoud C et al. Hsp27 negatively regulates cell death by interacting with cytochrome c. *Nat Cell Biol* 2:645–652, 2000.
80. Nakagawa T, Zhu H, Morishima N, Li E, Xu J, Yankner BA et al. Caspase-12 mediates endoplasmic-reticulum-specific apoptosis and cytotoxicity by amyloid- β . *Nature* 403:98–103, 2000.
81. Bitko V, Barik S. An endoplasmic reticulum-specific stress-activated caspase (caspase-12) is implicated in the apoptosis of A549 epithelial cells by respiratory syncytial virus. *J Cell Biochem* 80:441–454, 2001.
82. Nakagawa T, Yuan J. Cross-talk between two cysteine protease families. Activation of caspase-12 by calpain in apoptosis. *J Cell Biol* 150:887–894, 2000.
83. Wang S, Miura M, Jung YK, Zhu H, Li E, Yuan J. Murine caspase-11, an ICE-interacting protease, is essential for the activation of ICE. *Cell* 92:501–509, 1998.
84. Kang SJ, Wang S, Hara H, Peterson EP, Namura S, Amin-Hanjani S et al. Dual role of caspase-11 in mediating activation of caspase-1 and caspase-3 under pathological conditions. *J Cell Biol* 149:613–622, 2000.
85. Schotte P, Van Crielinge W, Van de Craen M, Van Loo G, Desmedt M, Grooten J et al. Cathepsin B-mediated activation of the proinflammatory caspase-11. *Biochem Biophys Res Commun* 251:379–387, 1998.
86. Yamashita T. Implication of cysteine proteases calpain, cathepsin and caspase in ischemic neuronal death of primates. *Prog Neurobiol* 62:273–295, 2000.
87. Troy CM, Stefanis L, Greene LA, Shelanski ML. Nedd2 is required for apoptosis after trophic factor withdrawal, but not superoxide dismutase (SOD1) downregulation, in sympathetic neurons and PC12 cells. *J Neurosci* 17:1911–1918, 1997.
88. Bergeron L, Perez GI, Macdonald G, Shi L, Sun Y, Jurisicova A et al. Defects in regulation of apoptosis in caspase-2-deficient mice. *Genes Dev* 12:1304–1314, 1998.
89. Adelson PD, Kochanek PM. Head injury in children. *J Child Neurol* 13:2–15, 1998.
90. de Bilbao F, Guarín E, Nef P, Vallet P, Giannakopoulos P, Dubois-Dauphin M. Postnatal distribution of cyp32/caspase 3 mRNA in the mouse central nervous system: an in situ hybridization study. *J Comp Neurol* 409:339–357, 1999.
91. Bittigau P, Siffringer M, Pohl D, Stadthaus D, Ishimaru M, Shimizu H et al. Apoptotic neurodegeneration following trauma is markedly enhanced in the immature brain. *Ann Neurol* 45:724–735, 1999.
92. Hu BR, Liu CL, Ouyang Y, Blomgren K, Siesjö BK. Involvement of caspase-3 in cell death after hypoxia-ischemia declines during brain maturation. *J Cereb Blood Flow Metab* 20:1294–1300, 2000.
93. van Loo G, Saelens X, van Gurp M, MacFarlane M, Martin SJ, Vandenberghe P. The role of mitochondrial factors in apoptosis: a Russian roulette with more than one bullet. *Cell Death Differ* 9:1031–1042, 2002.
94. Volbracht C, Leist M, Kolb SA, Nicotera P. Apoptosis in caspase-inhibited neurons. *Mol Med* 7:36–48, 2001.
95. Zhan RZ, Wu C, Fujihara H, Taga K, Qi S, Naito M et al. Both caspase-dependent and caspase-independent pathways may be involved in hippocampal CA1 neuronal death because of loss of cytochrome c from mitochondria in a rat forebrain ischemia model. *J Cereb Blood Flow Metab* 21:529–540, 2001.
96. Oppenheim RW, Flavell RA, Vinsant S, Prevette D, Kuan CY, Rakic P. Programmed cell death of developing mammalian neurons after genetic deletion of caspases. *J Neurosci* 21:4752–4760, 2001.
97. Daugas E, Susin SA, Zamzami N, Ferri KF, Irinopoulou T, Larochette N et al. Mitochondrio-nuclear translocation of AIF in apoptosis and necrosis. *FASEB J* 14:729–739, 2000.
98. Loeffler M, Daugas E, Susin SA, Zamzami N, Metivier D, Néménin AL et al. Dominant cell death induction by extramitochondrially targeted apoptosis-inducing factor. *FASEB J* 15:758–767, 2001.
99. Susin SA, Lorenzo HK, Zamzami N, Marzo I, Snow BE, Brothers GM et al. Molecular characterization of mitochondrial apoptosis-inducing factor. *Nature* 397:441–446, 1999.
100. Ravagnan L, Gurbuxani S, Susin SA, Maisse C, Daugas E, Zamzami N et al. Heat-shock protein 70 antagonizes apoptosis-inducing factor. *Nat Cell Biol* 3:839–843, 2001.
101. Klein JA, Longo-Guess CM, Rossmann MP, Seburn KL, Hurd RE, Frankel WN et al. The harlequin mouse mutation downregulates apoptosis-inducing factor. *Nature* 419:367–374, 2002.
102. Zhang X, Chen J, Graham SH, Du L, Kochanek PM, Draviam R et al. Intracellular localization of apoptosis-inducing factor (AIF) and large scale DNA fragmentation after traumatic brain injury in rats and in neuronal cultures exposed to peroxynitrite. *J Neurochem* 82:181–191, 2002.
103. Cote J, Ruiz-Carrillo A. Primers for mitochondrial DNA replication generated by endonuclease G. *Science* 261:765–769, 1993.
104. Li LY, Luo X, Wang X. Endonuclease G is an apoptotic DNase when released from mitochondria. *Nature* 412:95–99, 2001.
105. Liu X, Zou H, Slaughter C, Wang X. DFF, a heterodimeric protein that functions downstream of caspase-3 to trigger DNA fragmentation during apoptosis. *Cell* 89:175–184, 1997.
106. van Loo G, Schotte P, van Gurp M, Demol H, Hoorelbeke B, Gevaert K et al. Endonuclease G: a mitochondrial protein released in apoptosis and involved in caspase-independent DNA degradation. *Cell Death Differ* 8:1136–1142, 2001.
107. Widlak P, Li LY, Wang X, Garrard WT. Action of recombinant human apoptotic endonuclease G on naked DNA and chromatin substrates: cooperation with exonuclease and DNase I. *J Biol Chem* 276:48404–48409, 2001.
108. Srinivasula SM, Datta P, Fan XJ, Fernandes-Alnemri T, Huang Z, Alnemri ES. Molecular determinants of the caspase-promoting activity of Smac/DIABLO and its role in the death receptor pathway. *J Biol Chem* 275:36152–36157, 2000.
109. Roberts DL, Merrison W, MacFarlane M, Cohen GM. The inhibitor of apoptosis protein-binding domain of Smac is not essential for its proapoptotic activity. *J Cell Biol* 153:221–228, 2001.
110. Shibata M, Hattori H, Sasaki T, Gotoh J, Hamada J, Fukuuchi Y. Subcellular localization of a promoter and an inhibitor of apoptosis (Smac/DIABLO and XIAP) during brain ischemia/reperfusion. *Neuroreport* 13:1985–1988, 2002.
111. Okada H, Suh WK, Jin J, Woo M, Du C, Elia A et al. Generation and characterization of Smac/DIABLO-deficient mice. *Mol Cell Biol* 22:3509–3517, 2002.
112. Syntichaki P, Tavernarakis N. Death by necrosis. Uncontrollable catastrophe, or is there order behind the chaos? *EMBO Rep* 3:604–609, 2002.
113. Proskuryakov SY, Konoplyannikov AG, Gabai VL. Necrosis: a specific form of programmed cell death? *Exp Cell Res* 283:1–16, 2003.

114. Kitanaka C, Kuchino Y. Caspase-independent programmed cell death with necrotic morphology. *Tanpakushitsu Kakusan Koso* 44:2091–2100, 1999.
115. Syntichaki P, Xu K, Driscoll M, Tavernarakis N. Specific aspartyl and calpain proteases are required for neurodegeneration in *C. elegans*. *Nature* 419:939–944, 2002.
116. Saido TC, Sorimachi H, Suzuki K. Calpain: new perspectives in molecular diversity and physiological- pathological involvement. *FASEB J* 8:814–822, 1994.
117. Bartus RT, Hayward NJ, Elliott PJ, Sawyer SD, Baker KL, Dean RL et al. Calpain inhibitor AK295 protects neurons from focal brain ischemia. Effects of postocclusion intra-arterial administration. *Stroke* 25:2265–2270, 1994.
118. Kampfl A, Posmantur RM, Zhao X, Schmutzhard E, Clifton GL, Hayes RL. Mechanisms of calpain proteolysis following traumatic brain injury: implications for pathology and therapy: a review and update. *J Neurotrauma* 14:121–134, 1997.
119. Saito K, Elce JS, Hamos JE, Nixon RA. Widespread activation of calcium-activated neutral proteinase (calpain) in the brain in Alzheimer disease: a potential molecular basis for neuronal degeneration. *Proc Natl Acad Sci USA* 90:2628–2632, 1993.
120. Yoshida M, Yamashita T, Zhao L, Tsuchiya K, Kohda Y, Tonchev AB et al. Primate neurons show different vulnerability to transient ischemia and response to cathepsin inhibition. *Acta Neuropathol (Berl)* 104:267–272, 2002.
121. Nakamura Y, Takeda M, Suzuki H, Morita H, Tada K, Hariguchi S et al. Age-dependent change in activities of lysosomal enzymes in rat brain. *Mech Ageing Dev* 50:215–225, 1989.
122. Shimizu S, Eguchi Y, Kamiike W, Waguri S, Uchiyama Y, Matsuda H et al. Retardation of chemical hypoxia-induced necrotic cell death by Bcl-2 and ICE inhibitors: possible involvement of common mediators in apoptotic and necrotic signal transductions. *Oncogene* 12:2045–2050, 1996.
123. Maas AI. Neuroprotective agents in traumatic brain injury. *Expert Opin Investig Drugs* 10:753–767, 2001.
124. Allen JW, Knoblach SM, Faden AI. Combined mechanical trauma and metabolic impairment in vitro induces NMDA receptor-dependent neuronal cell death and caspase-3-dependent apoptosis. *FASEB J* 13:1875–1882, 1999.
125. Faden AI, Fox GB, Fan L, Araldi GL, Qiao L, Wang S et al. Novel TRH analog improves motor and cognitive recovery after traumatic brain injury in rodents. *Am J Physiol (Lond)* 277: R1196–R1204, 1999.
126. Faden AI. Pharmacotherapeutic treatment approaches for brain and spinal cord trauma. In: Neurotrauma (Narayan RK, Wilberger J, Povlishock JT, eds), pp 1479–1490. New York: McGraw-Hill, 1996.
127. Lavie G, Teichner A, Shohami E, Ovadia H, Leker RR. Long-term cerebroprotective effects of dexanabol in a model of focal cerebral ischemia. *Brain Res* 901:195–201, 2001.
128. Callaway JK, Beart PM, Jarrott B, Giardina SF. Incorporation of sodium channel blocking and free radical scavenging activities into a single drug, AM-36, results in profound inhibition of neuronal apoptosis. *Br J Pharmacol* 132:1691–1698, 2001.
129. Callaway JK, Knight MJ, Watkins DJ, Beart PM, Jarrott B. Delayed treatment with AM-36, a novel neuroprotective agent, reduces neuronal damage after endothelin-1-induced middle cerebral artery occlusion in conscious rats. *Stroke* 30: 2704–2712, 1999.
130. Faden AI, Fox GB, Di X, Knoblach SM, Cernak I, Mullins P et al. Neuroprotective and nootropic actions of a novel cyclized dipeptide following controlled cortical impact injury in mice. *J Cereb Blood Flow Metab* 23:355–363, 2003.
131. Faden AI, Knoblach SM, Cernak I, Fan L, Vink R, Roth BL et al. Novel diketopiperazine enhances motor and cognitive recovery after traumatic brain injury in rats and shows neuroprotection in vitro. *J Cereb Blood Flow Metab* 23:342–354, 2003.



Further development and validation of empirical scoring functions for structure-based binding affinity prediction

Renxiao Wang^a, Luhua Lai^b & Shaomeng Wang^{a,*}

^aMedical Chemistry and Comprehensive Cancer Center, University of Michigan, 1500 E. Medical Center Drive, Ann Arbor, MI 48109-0934, U.S.A.; ^bInstitute of Physical Chemistry, Peking University, Beijing 100871, P.R. China

Received 27 August 2001; Accepted 7 February 2002

Key words: binding affinity prediction, consensus scoring, empirical scoring molecular docking, structure-based drug design

Summary

New empirical scoring functions have been developed to estimate the binding affinity of a given protein-ligand complex with known three-dimensional structure. These scoring functions include terms accounting for van der Waals interaction, hydrogen bonding, deformation penalty, and hydrophobic effect. A special feature is that three different algorithms have been implemented to calculate the hydrophobic effect term, which results in three parallel scoring functions. All three scoring functions are calibrated through multivariate regression analysis of a set of 200 protein-ligand complexes and they reproduce the binding free energies of the entire training set with standard deviations of 2.2 kcal/mol, 2.1 kcal/mol, and 2.0 kcal/mol, respectively. These three scoring functions are further combined into a consensus scoring function, X-CSCORE. When tested on an independent set of 30 protein-ligand complexes, X-CSCORE is able to predict their binding free energies with a standard deviation of 2.2 kcal/mol. The potential application of X-CSCORE to molecular docking is also investigated. Our results show that this consensus scoring function improves the docking accuracy considerably when compared to the conventional force field computation used for molecular docking.

Introduction

Considerable advances in structure-based drug design have made a significant impact on drug discovery processes in the past decade [1–5]. By utilizing the essential structural properties of the target macromolecule, a variety of methods now exist for suggesting potential ligand molecules either by screening large chemical databases [6–10] or by assembling molecular fragments inside the binding site [11–18]. These methods usually suggest a large number of molecules rapidly, far too many for organic synthesis and biological experiments. Therefore, a structure-based drug design approach tends to arrive at the bottleneck where it is necessary to select only the most promising can-

didates for further experimental characterization. The basic assumption underlying structure-based drug design is that a good ligand molecule should bind tightly to its target. Thus, it is extremely valuable to predict the binding affinity of a given ligand to its target and use it as a criterion for selection. This is known as the 'scoring problem' and has attracted great interests in developing methods for binding affinity calculation [19–21].

A large group of methods calculate binding affinities through force fields. In early years, attempts have been made to calculate the direct interactions, e.g. steric and electrostatic interactions, between a ligand and its target molecule and relate the force field energies to binding affinities [22]. This method is still popular nowadays especially among molecular docking studies. However, as many researchers have pointed out, the interaction energy computed in this

*To whom correspondence should be addressed. E-mail: shaomeng@med.umich.edu

way is only an approximation to the enthalpy change in the binding process, therefore the application of this method is usually restricted to the analysis of a congeneric series of ligands. Some researchers have supplemented standard force fields with an additional term to address the solvation effect with either PB/SA or GB/SA method [23]. More ambitious methods, such as free energy perturbation [24] and linear response approximation [25, 26], try to consider solvent molecules explicitly and deal with ensemble averages. In theory these methods are expected to give more accurate predictions. However, in practice they do not always meet this expectation due to the deficiency in the force field as well as in the sampling procedure. In addition, these methods are still computationally expensive even for today's computers, which has limited their popularity in structure-based drug design practice.

Following the pioneering work of Böhm [27], a number of so-called empirical scoring functions have emerged as an alternative [28–32]. These approaches assume that the overall receptor-ligand binding free energy can be decomposed into basic components, which can be written out conceptually as:

$$\Delta G_{\text{bind}} = \Delta G_{\text{motion}} + \Delta G_{\text{interaction}} + \Delta G_{\text{desolvation}} + \Delta G_{\text{configuration}}$$

Usually those factors which are known to be important for the binding process are included in the above function. Unlike force fields, empirical scoring functions are not derived from 'first principle'. Instead, they are directly calibrated with a set of protein-ligand complexes with experimentally determined structures and binding affinities through multivariate regression analysis. Empirical scoring functions have several appealing features. Firstly, since they are calibrated with diverse protein-ligand complexes, their applications are not limited to a certain congeneric series of ligands or a particular target receptor. Secondly, each term in an empirical scoring function has a clear physical meaning. Studying the regression coefficients before each term sheds lights on the understanding of the receptor-ligand binding process. Thirdly, at a lightning speed, the accuracy level (~ 2 kcal/mol) that a current empirical scoring function can achieve in binding affinity prediction is acceptable for structure-based drug design approaches. In recent years, empirical scoring functions have become more and more popular among structure-based drug design applications in which very accurate binding affinity predictions are

not necessary, such as virtual database screening and *de novo* ligand generation.

We have extensive experience in applying several empirical scoring functions, including Böhm's scoring function [27], ChemScore [30] and SCORE [32], to structure-based drug design projects. Despite of all the encouraging results we have obtained with these empirical scoring functions, it is clear that there is still plenty of room for improvement in terms of accuracy as well as robustness. In this paper, we will describe our work on further development and validation of empirical scoring functions. Firstly, we have derived three scoring functions, each of which has only five adjustable parameters. These scoring functions are calibrated with a diverse set of 200 protein-ligand complexes, which is the largest one ever used by an empirical scoring function approach. Secondly, inspired by the consensus scoring strategy [33], we combine these three scoring functions into a consensus scoring function, X-CSCORE, to ensure converged results in binding affinity prediction. This consensus scoring function is tested on an independent set of 30 protein-ligand complexes. Thirdly, we have also explored the potential application of X-CSCORE to molecular docking. When compared to conventional force field computation, this consensus scoring function performs considerably better in identifying the experimentally determined protein-ligand complex structures.

Methods and results

Training set construction

Developing an empirical scoring function requires a set of receptor-ligand complexes for calibration. Both the size and the quality of the training set will affect the final form of the scoring function. In our selection of receptor-ligand complexes, we used the following five criteria to ensure the quality of the training set. (1) Only protein-ligand complexes are considered. Complexes involving other types of receptors, such as nucleic acids, are not included. (2) The ligand molecule should be a 'normal' organic compound and bind to the receptor non-covalently. Therefore, complexes containing covalently bound ligands, complex ligands (such as Heme), or large ligands (MW > 1000) are excluded. (3) There should be no cofactor binding beside the ligand. (4) Crystal structure of the complex with a resolution better than 3.0 Å should be available from the Protein Data Bank (PDB) [34]. Complex

structures solved by NMR techniques are currently not included in our selection. (5) The dissociation equilibrium constant (K_i or K_d) of the complex has been determined experimentally and can be found in literature. Complexes with only IC_{50} values are not accepted.

The resulting training set has 200 protein-ligand complexes, which comprises more than 70 different types of proteins. Basically, this training set is an assembly of the training sets used by other empirical scoring functions [27–32] plus our own collections. The experimentally determined binding affinities are cited either from those previous approaches or the references listed in the relevant PDB files. All binding affinities are expressed in the negative logarithms of dissociation constants, i.e. pK_d , for convenience. In this training set, the pK_d values range from 1.48 to 11.42, covering nearly 10 orders of magnitude. Here we neglect the potential inconsistency in the dissociation constants related to experiment conditions, such as pH level, temperature, and salt concentration. A complete list of the training set can be found in the *supplementary material* section in this paper.

Coordinates of the complex structure in the training set are downloaded from PDB. No minimization is performed to further adjust the structure. For the convenience of processing, each complex structure is processed in SYBYL [35]. First, the ligand is extracted from the complex, assigned proper atom and bond types, and then written out as a separate file in the MOL2 format. The remaining part of the complex, i.e. the protein, is written out into another file in the PDB format. Metal ions located inside the binding site are left with the protein and treated as part of it. All crystallographic water molecules and other cofactors are removed.

Scoring functions

We assume that the overall free energy change in a protein-ligand binding process can be dissected into the following terms:

$$\Delta G_{\text{bind}} = \Delta G_{\text{vdw}} + \Delta G_{\text{H-bond}} + \Delta G_{\text{deformation}} + \Delta G_{\text{hydrophobic}} + \Delta G_0. \quad (1)$$

Here, ΔG_{vdw} accounts for the van der Waals interaction between the ligand and the protein; $\Delta G_{\text{H-bond}}$ accounts for the hydrogen bonding between the ligand and the protein; $\Delta G_{\text{deformation}}$ accounts for the deformation effect; $\Delta G_{\text{hydrophobic}}$ accounts for the hydrophobic effect; ΔG_0 is the regression constant

which implicitly includes the effects due to the translational and rotational entropy loss in the binding process. Detailed algorithms for calculating each term will be described below.

(1) Atom classification. Besides element type and hybridization state, both ligand and protein atoms need to be classified to compute some of the terms in our scoring functions. The atom types defined in our study are: (i) H-bond donor. Oxygen and nitrogen atoms bonded to hydrogen atom(s) and metal ions located inside the binding site of the protein. (ii) H-bond acceptor. Oxygen and sp^2 or sp hybridized nitrogen atoms with lone pair(s). (iii) H-bond donor/acceptor. Oxygen and nitrogen atoms which may act as either H-bond donor or H-bond acceptor, such as the oxygen atom in a hydroxyl group. (iv) Polar atom. Oxygen and nitrogen atoms that are neither H-bond donor nor H-bond acceptor, sulfur and phosphorus atoms, and carbon atoms bonded to hetero-atom(s). (v) Hydrophobic atom. Carbon atoms that do not belong to the 'polar atom' group and halogen atoms.

The following set of atomic radii are used in computation: carbon, 1.9 Å; nitrogen, 1.8 Å; oxygen, 1.7 Å; sulfur, 2.0 Å; phosphorus, 2.1 Å; fluorine, 1.5 Å; chlorine, 1.8 Å; bromine, 2.0 Å; iodine, 2.2 Å; metals, 1.2 Å. This radii set is applied to both ligands and proteins.

(2) Van der Waals interaction. The van der Waals interaction is one of the essential non-covalent interactions. We employ the Lennard-Jones equation to reflect the balance between the short-range repulsion and the long-range attractive dispersion force:

$$VDW = \sum_i^{\text{ligand}} \sum_j^{\text{protein}} VDW_{ij} \\ = \sum_i^{\text{ligand}} \sum_j^{\text{protein}} \left[\left(\frac{d_{ij,0}}{d_{ij}} \right)^8 - 2 \times \left(\frac{d_{ij,0}}{d_{ij}} \right)^4 \right] \quad (2)$$

Here VDW denotes for the van der Waals interaction energy, which is calculated by considering all the atom pairs between the ligand and the protein; d_{ij} denotes for the distance between the ligand atom i and the protein atom j ; $d_{ij,0} = r_i + r_j$, i.e. the sum of van der Waals radius of atom i and j . Note that we use a 'softer' form in Equation 2 instead of the standard 12–6 equation. Furthermore, in our algorithm, (i) only heavy atoms contribute. Hydrogen atoms are neglected. (ii) All heavy atoms are weighted equally. No weight factor is used to differentiate them. (iii) To avoid the huge repulsion raised by overlapped atom

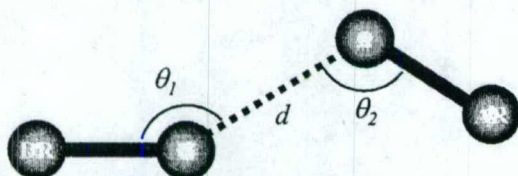


Figure 1. Illustration of the three geometric parameters used in characterizing a hydrogen bond.

pairs, we set an upper limit of 100 for VDW_{ij} in Equation 2. For any pair of atoms, if VDW_{ij} exceeds this limit, it will be cut flat to 100.

(3) Hydrogen bonding. Hydrogen bonding is perhaps the most important factor for the specific binding of a ligand to its receptor. Such interaction happens when two atoms get close enough and form a donor-acceptor pair. The geometry of a hydrogen bond, $D-H \cdots A$, is typically described by the bond length, i.e. the distance between the hydrogen atom (H) and the acceptor (A), and the bond angle, i.e. $\angle DHA$. However, hydrogen atoms are normally not revealed in X-ray crystallography analysis. Although hydrogen atoms can be added later, energy minimization is usually required to set them into position. This practice could become problematic especially when the hydrogen atoms can take multiple low-energy positions, such as the one in a hydroxyl group. Furthermore, minimized structures will depend on force field parameters and they may be incompatible with the initial experimentally determined ones. Therefore, we choose not to consider hydrogen atoms explicitly. Here we introduce the concept of 'root': the root of an atom is its non-hydrogen neighboring atom. When an atom bonds with more than one non-hydrogen atom, its root locates at the geometric center of all its non-hydrogen neighboring atoms. Let DR denotes for the donor's root and AR for the acceptor's root. In our algorithm, the geometry of a hydrogen bond is described by: (i) the distance (d) between D and A; (ii) the angle (θ_1) between DR, D and A; and (iii) the angle (θ_2) between D, A and AR (Figure 1).

We assume that a hydrogen bond has an ideal geometry and any deviation from it will weaken the strength of the hydrogen bond. The strength of a hydrogen bond is then computed by considering these three geometric descriptors:

$$HB_{ij} = f(d_{ij}) f(\theta_{1,ij}) f(\theta_{2,ij}). \quad (3)$$

The distance function $f(d)$ and the angular functions $f(\theta_1)$ and $f(\theta_2)$ in Equation 3 are written in the

following simple linear fuzzy forms:

$$\begin{aligned} f(d) &= 1.0 & d_0 \leq d_0 - 0.7 \text{ \AA} \\ &= (1/0.7) \times (d_0 - d) & d_0 - 0.7 \text{ \AA} < d \leq d_0 \\ &= 0.0 & d > d_0 \\ f(\theta_1) &= 1.0 & \theta_1 \geq 120^\circ \\ &= (1/60) \times (\theta_1 - 60) & 120^\circ > \theta_1 \geq 60^\circ \\ &= 0.0 & \theta_1 < 60^\circ \\ f(\theta_2) &= 1.0 & \theta_2 \geq 120^\circ \\ &= (1/60) \times (\theta_2 - 60) & 120^\circ > \theta_2 \geq 60^\circ \\ &= 0.0 & \theta_2 < 60^\circ \end{aligned}$$

Here $d_0 = r_i + r_j$, i.e. the van der Waals distance between the donor and the acceptor. These functions are derived from the analysis of all the potential hydrogen bonding pairs presented in the training set. The observed distribution of the donor-acceptor distance (d) is shown in Figure 2a. In this figure, one can see that the peak value appears around 2.8 Å, which can be interpreted as the ideal length of a hydrogen bond. As d increases, the population decreases. But after d exceeds 3.4 ~ 3.5 Å, it passes the bottom and begins to rise again, which can be interpreted as the turning point from a hydrogen bond to a normal van der Waals contact. Therefore, it is reasonable to define that $f(d) = 1.0$ when $d = 2.8$ Å while $f(d) = 0.0$ when $d = 3.5$ Å. Considering the atomic radii of oxygen and nitrogen atoms, 2.8 Å corresponds to $d_0 - 0.7$ Å while 3.5 Å corresponds to d_0 , approximately. By assuming that the distance dependence of the strength of a hydrogen bond is linear within this range, one will obtain the function listed above. The angular functions $f(\theta_1)$ and $f(\theta_2)$ are also derived similarly by interpreting the observed distributions of θ_1 and θ_2 from the training set (Figures 2b and 2c).

The hydrogen bonding interaction between the ligand and the protein is calculated by summing up all the hydrogen bonds:

$$HB = \sum_i^{ligand} \sum_j^{protein} HB_{ij} \quad (4)$$

All types of hydrogen bonds, i.e. O-O, O-N, and N-N, are equally weighted so that no extra parameter is necessary. Special attention has been paid to the saturation in hydrogen bonding if one donor or acceptor atom contacts with multiple donor or acceptor atoms. For a given donor or acceptor atom, we define that (i) the maximal number of hydrogen bonds that a donor atom can form should not exceed the number of hydrogen atoms on that donor atom; and (ii) the maximal number of hydrogen bonds that an acceptor atom can

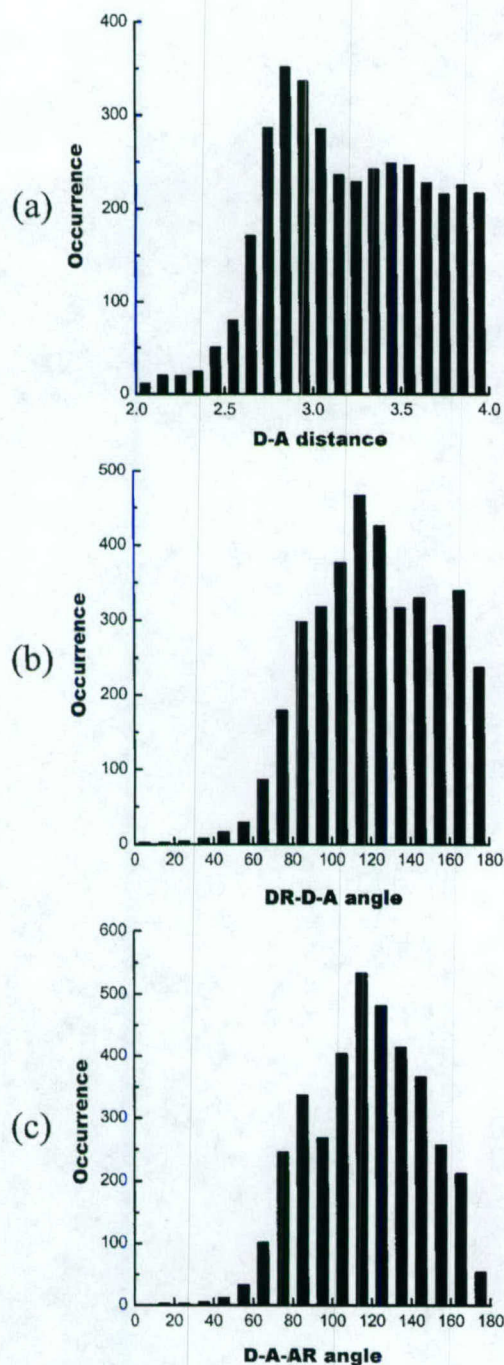


Figure 2. Distribution of the three geometric parameters in a hydrogen bond observed in the training set: (a) the donor-acceptor distance (in angstroms); (b) the DR-D-A angle (in degrees); (c) the D-A-AR angle (in degrees).

form should not exceed the number of lone pairs on that acceptor atom. If an atom could be a donor and an acceptor at the same time, such as the oxygen atom in a hydroxyl group, both rules apply.

As implied above, charged and neutral hydrogen bonds are not treated separately in our scoring functions since we find that the improvement of *our scoring functions* in the training set regression is totally negligible by separating them.

In some cases, metal ions are found inside the binding site of the protein. They may form coordinated bonds with atoms with lone pairs in the ligand and thus also contribute to the binding affinity. We include this kind of interaction in the hydrogen bonding term since it is the same as hydrogen bonding in nature, i.e. Lewis acid-base pair. Note that technically we define metal ions as 'donor' so that the metal-ligand coordinated bonds are calculated with exactly the same distance and angular functions of hydrogen bonding.

(4) Deformation effect. Upon binding, both the ligand and the protein will be constrained in conformation as compared to their free states in solvent. This will raise adverse entropic changes, which is a negative effect that must be overcome during the binding process. In other empirical scoring functions, the deformation effect of the ligand is often estimated by counting the number of rotatable bonds (rotors) that become frozen during the binding process, assuming that each rotor is associated with a discrete number of low-energy conformations and thus a certain amount of conformational entropy. If there are more than one rotor in the ligand, their contributions are assumed to be additive. This assumption is reasonable when all the rotors are isolated and free to rotate, so the low-energy conformations associated with each rotor will multiply to build up the entire conformational space. However, when two or more rotors cross, apparently this assumption is no longer valid because now the rotation of any of them will interfere with the others and this will result in a reduction in the total number of possible low-energy conformations (Figure 3). Therefore, simply counting the number of rotors often overestimates the conformational flexibility of certain kinds of molecules, such as oligo-peptides.

In our algorithm, rotor is defined as acyclic sp^3 - sp^3 or sp^3 - sp^2 single bond between two non-hydrogen atoms. Terminal groups, such as $-CH_3$, $-NH_2$, $-OH$, and $-X$ ($X = F, Cl, Br, I$), whose rotation does not produce any new conformation of heavy atoms are not counted as rotors. The potential flexibility of cyclic portions of the ligand is ignored. The deformation

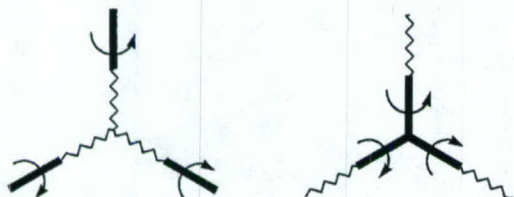


Figure 3. Illustration of 'isolated' (on the left) and 'crossed' rotors (on the right).

effect of the ligand is then expressed as the contribution of all the rotors with proper weight factors. For the convenience of computation, rotors are counted by summing the share of each ligand atom:

$$RT = \sum_i^{ligand} RT_i, \quad (5)$$

where $RT_i = 0$ if atom i is not involved in any rotor; $RT_i = 0.5$ if atom i is involved in one rotor; and $RT_i = 1.0$ if atom i is involved in two rotors. However, if atom i is involved in more than two rotors, then $RT_i = 0.5$. Note that, according to the conventional rotor-counting algorithm, RT_i should be 1.5 (in three rotors) or 2.0 (in four rotors) in this case. This reduction in the RT_i value reflects our consideration for offsetting the overestimation of conformational flexibility in the conventional algorithm. Although very crude, we found that our algorithm improves the accuracy of our scoring functions.

In our algorithm, the deformation effect of the protein is neglected. We have attempted to count the number of rotors presented in the side chains of the binding site residues and include it as a term in our scoring functions. However, such attempt did not improve the result. It is not surprising since the side chains of the binding site residues are generally immobilized even in the unbound state due to the stacking of neighboring residues. A more reasonable algorithm needs to be developed to account for the flexibility of the protein.

(5) Hydrophobic effect. Binding of the ligand and the protein is accompanied by the desolvation process that undergoes changes in entropy as well as in enthalpy. One of the results is that non-polar groups tend to favor each other, which is also referred to as 'hydrophobic effect'. This effect is very difficult for accurate characterization since it involves complicated ligand-water, protein-water, and water-water interactions before and after binding. Different algorithms have been used in other empirical scoring functions

to calculate this term. We have implemented three representative algorithms in our scoring functions.

(i) Hydrophobic surface algorithm. The hydrophobic effect is assumed to be proportional to the buried hydrophobic surface of the ligand (Equation 6). This algorithm was adopted by Bohm's scoring function [27]. It should be pointed out that technically there are several types of molecular surfaces. Here we choose to use the solvent-accessible surface (SAS).

$$HS = \sum_i^{ligand} SAS_i. \quad (6)$$

The radius of the solvent probe is set to 1.5 Å. The solvent-accessible surface of the ligand is represented by evenly distributed dots in a spacing of 0.5 Å. Numerical integration is used to calculate the surface area. The surface areas of hydrogen atoms are attributed to their root atoms. Any part of the ligand surface is considered buried if it penetrates into the solvent-accessible surface of the protein. Note that only hydrophobic atoms are considered in Equation 6. The total amount of buried surface area is expressed in square Angstrom.

(ii) Hydrophobic contact algorithm. The hydrophobic effect is calculated by summing up the hydrophobic atom pairs formed between the ligand and the protein. This algorithm was adopted by ChemScore [30]. In our algorithm, it is calculated as:

$$HC = \sum_i^{ligand} \sum_j^{protein} f(d_{ij}), \quad (7)$$

where

$$f(d) = \begin{cases} 1.0 & d \leq d_0 + 0.5 \text{ Å} \\ (1/1.5) \times (d_0 + 2.0 - d) & d_0 + 0.5 \text{ Å} < d \leq d_0 + 2.0 \text{ Å} \\ 0.0 & d > d_0 + 2.0 \text{ Å} \end{cases}$$

This distance function reflects the intuition that the strength of 'hydrophobic interaction' will reach the maximum when two hydrophobic atoms form van der Waals contact and diminish gradually with the increase in the inter-atomic distance. We find that this distance function needs to be fairly long-ranged in order to work well.

(iii) Hydrophobic matching algorithm. This algorithm was adopted by SCORE [32]. According to this method, different parts of the ligand sense the protein differently because of the heterogeneous nature of the binding site. If a hydrophobic ligand atom is placed at a hydrophobic site of the protein, then it is

expected to be favorable to the binding process. The overall hydrophobic matching between the ligand and the protein is calculated as:

$$HM = \sum_i^{\text{ligand}} \log P_i \times HM_i. \quad (8)$$

Here HM_i is an indicator variable. It is set to 1 if a hydrophobic atom i is placed in a hydrophobic environment; otherwise it is set to 0. $\log P_i$ refers to the hydrophobic scale of atom i , which is the contribution of atom i to the n-octanol/water partition coefficient ($\log P$) of the molecule. In our algorithm, the hydrophobic scales for all kinds of atoms are cited from XLOGP2 [36]. They are introduced as weight factors here to ensure that more hydrophobic atoms contribute more to the hydrophobic effect. The 'environment' of a given ligand atom is defined to consist of all the atoms on the protein which are within 6 Å from the ligand atom. The hydrophobicity of the environment is determined by summing up the hydrophobic scales of all its member atoms. Our investigation of the training set shows that the average hydrophobicity of an environment surrounding a hydrophobic ligand atom is $-0.50 \log P$ units. Therefore, in our algorithm an environment is defined as hydrophobic if its hydrophobicity is greater than $-0.50 \log P$ units.

Finally, we summarize our scoring functions below. The binding affinity of a given protein-ligand complex, as expressed in pK_d unit, is calculated by summing up all the terms described above. Since three different algorithms for modeling the hydrophobic effect have been implemented, we have three resulting scoring functions:

$$pK_{d,1} = C_{0,1} + C_{VDW,1} \times VDW + C_{H-bond,1} \times HB + C_{rotor,1} \times RT + C_{hydrophobic,1} \times HS, \quad (9)$$

$$pK_{d,2} = C_{0,2} + C_{VDW,2} \times VDW + C_{H-bond,2} \times HB + C_{rotor,2} \times RT + C_{hydrophobic,2} \times HC, \quad (10)$$

$$pK_{d,3} = C_{0,3} + C_{VDW,3} \times VDW + C_{H-bond,3} \times HB + C_{rotor,3} \times RT + C_{hydrophobic,3} \times HM. \quad (11)$$

It should be emphasized that, except for the hydrophobic effect term, all the other terms in these

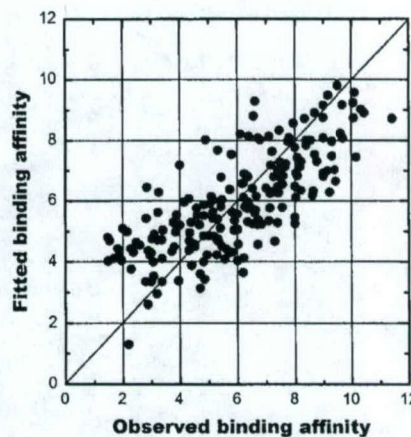


Figure 4. Correlation between the observed binding affinities of the 200 protein-ligand complexes in the training set and the fitted values given by X-CSCORE (in pK_d units).

three scoring functions are calculated using identical algorithms. The consensus scoring function, which is named as X-CSCORE, is the arithmetical average of Equations 9–11:

$$X-CSCORE = (pK_{d,1} + pK_{d,2} + pK_{d,3})/3 \quad (12)$$

Regression analyses

Coefficients before each term in Equations 9–11 are derived through standard least-square multivariate regression analyses of the training set. They are listed in Table 1 together with other related information. Correlation coefficients (r^2) and standard deviations (s) obtained from regression are listed in Table 2. The correlation between the observed binding affinities and the fitted values given by X-CSCORE is shown in Figure 4. Leave-one-out cross-validations are performed to judge the quality of the regression models. The resulting q^2 and s_{press} are listed in Table 2. Both the regression and the cross-validation are performed with the QSAR module in SYBYL.

Validation

(1) Test set. An independent test set is usually needed to validate a regression model. When constructing the training set, we deliberately separate all the complexes released by the Protein Data Bank after 1998 from the others. These complexes, 30 in total, are used as a test set in our study. A complete list of the test set can

Table 1. Regression models of Equations 9–11

Term	Coefficient ^a	Mean value ^b	Contribution fraction ^c
(Equation 9)			
VDW	$-2.01 \times 10^{-3} (\pm 1.81 \times 10^{-3})$	-6.00×10^2	16.5%
H-Bond	$0.307 (\pm 0.137)$	4.21	19.8 %
Rotor	$-0.159 (\pm 0.079)$	7.28	25.3 %
Hydrophobic surface	$7.10 \times 10^{-3} (\pm 2.50 \times 10^{-3})$	$2.74 \times 10^2 \text{ \AA}^2$	38.4%
Constant	$2.69 (\pm 0.66)$	–	–
(Equation 10)			
VDW	$-0.96 \times 10^{-3} (\pm 1.91 \times 10^{-3})$	-6.00×10^2	8.6%
H-Bond	$0.412 (\pm 0.149)$	4.21	29.4%
Rotor	$-0.100 (\pm 0.074)$	7.28	17.5%
Hydrophobic contact	$3.73 \times 10^{-2} (\pm 1.12 \times 10^{-2})$	43.1	44.5%
Constant	$2.78 (\pm 0.65)$	–	–
(Equation 11)			
VDW	$-2.14 \times 10^{-3} (\pm 1.65 \times 10^{-3})$	-6.00×10^2	16.4%
H-Bond	$0.311 (\pm 0.131)$	4.21	18.8%
Rotor	$-0.169 (\pm 0.078)$	7.28	25.2%
Hydrophobic matching	$0.602 (\pm 0.159)$	2.51	39.6%
Constant	$3.10 (\pm 0.65)$	–	–

^a All coefficients are presented in pK_d units. They can be converted into binding free energies at 298 K in kcal/mol by multiplying a factor of -1.36 . The values in brackets are 95% confidence intervals in regression.

^b Mean values of each term are calculated over the entire training set.

^c Contribution fractions are calculated by using the QSAR/PLS module in SYBYL.

Table 2. Statistical results of Equations 9–11 and X-CSCORE

	Equation 9	Equation 10	Equation 11	X-CSCORE
R^2	0.504	0.546	0.571	0.591
S^a	1.58	1.53	1.43	1.47
$F(4, 195)$	49.6	58.7	70.4	–
Q^2	0.480	0.522	0.551	–
S_{press}	1.62	1.57	1.47	–
R^2_{pred}	0.318	0.319	0.249	0.356
S_{pred}	1.51	1.61	1.63	1.58

^a All the standard deviations, including S , S_{press} and S_{pred} , are presented in pK_d units. They can be converted into binding free energies at 298 K in kcal/mol by multiplying a factor of -1.36 .

be found in the *supplementary material* section in this paper.

All the scoring functions, including Equations 9–12, are used to predict the binding affinities of the 30 protein-ligand complexes in the test set. The root-

mean-squared deviation (s_{pred}) is used to measure the quality of prediction:

$$s_{\text{pred}} = \sqrt{\sum (pK_{d,\text{pred}} - pK_{d,\text{obs}})^2 / (N - 1)}. \quad (13)$$

The statistical results are shown in Table 2. The correlation between the experimentally observed binding affinities and the predicted values given by X-CSCORE is shown in Figure 5.

(2) Evolutionary regression. We have adopted an iterative regression procedure to further validate the internal consistency of our scoring functions, which was originally proposed in our previous work SCORE [32]. The central idea of this procedure, called evolutionary regression, is to test a given regression model with training sets of different sizes. In our study, this procedure starts from constructing a subset of 50 complexes which are randomly selected from the training set without duplication. This subset is used to perform multivariate regression and leave-one-out cross-validation for the scoring function under inves-

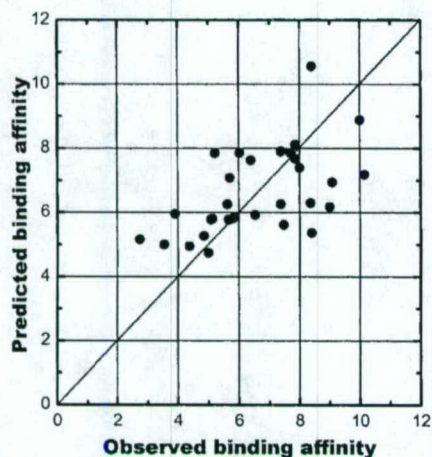


Figure 5. Correlation between the observed binding affinities of the 30 protein-ligand complexes in the test set and the predicted values given by X-CSCORE (in pK_d units).

tigation. All the regression results, including r^2 , s , q^2 , s_{press} , and the coefficients for each term in the scoring function, are recorded. This regression model is then used to predict the K_d values of the test set. The resulting r^2_{pred} and s_{pred} are also recorded. Since the subset is constructed randomly, the entire procedure, i.e. construction of the subset, multivariate regression, cross-validation, and calculation of the test set, is repeated for 10 times to reduce the noises in all the statistical results. Only the averaged results are used for analysis. At the next step, the size of the subset is increased by 10, and the regression model is re-evaluated with this new subset. This procedure is repeated until the size of the subset reached the full size of the training set. We have performed evolutionary regression for Equations 9–11. The standard deviations observed during the evolutionary regression procedure of Equations 9–11 are shown in Figure 6a–c, respectively.

(3) Molecular docking. We have also tested the performance of X-CSCORE in molecular docking experiments. We select 10 samples from the training set, including the L-arabinose binding protein/L-arabinose complex (PDB code 1ABE), the alcohol dehydrogenase/CNAD complex (PDB code 1ADB), the adenosine deaminase/DAA complex (PDB code 1ADD), the cytidine deaminase/uridine complex (PDB code 1AF2), the maltodextrin binding protein/maltose complex (PDB code 1ANF), the carboxypeptidase A/L-benzylsuccinate complex (PDB code 1CBX), the antibody DB3/progesterone analogue complex

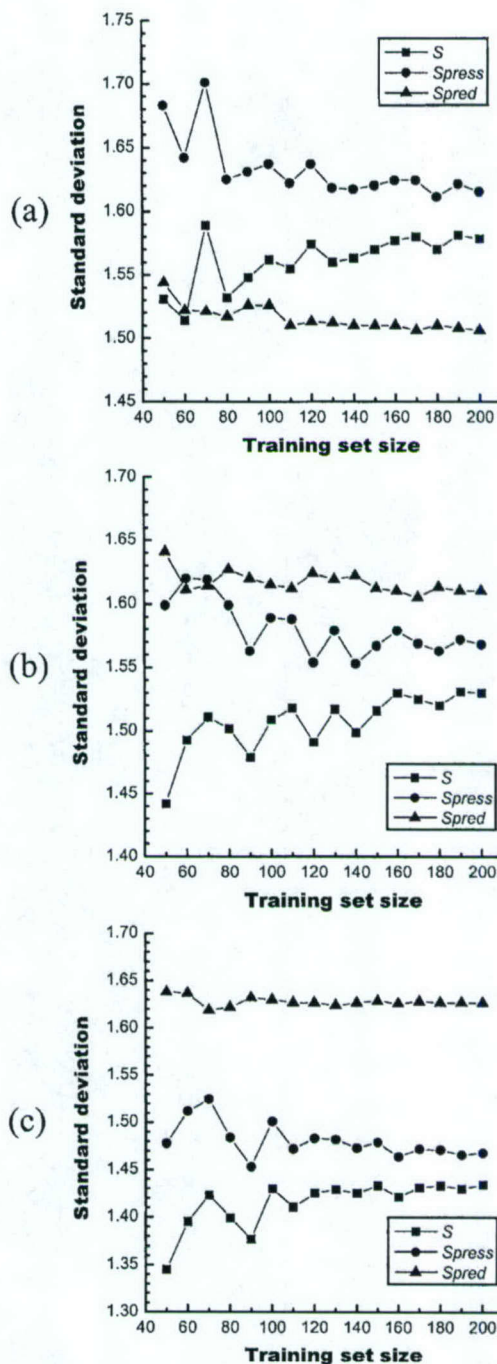


Figure 6. Standard deviations (in pK_d units) observed in the evolutionary regression procedure. (a) Equation 9; (b) Equation 10; (c) Equation 11.

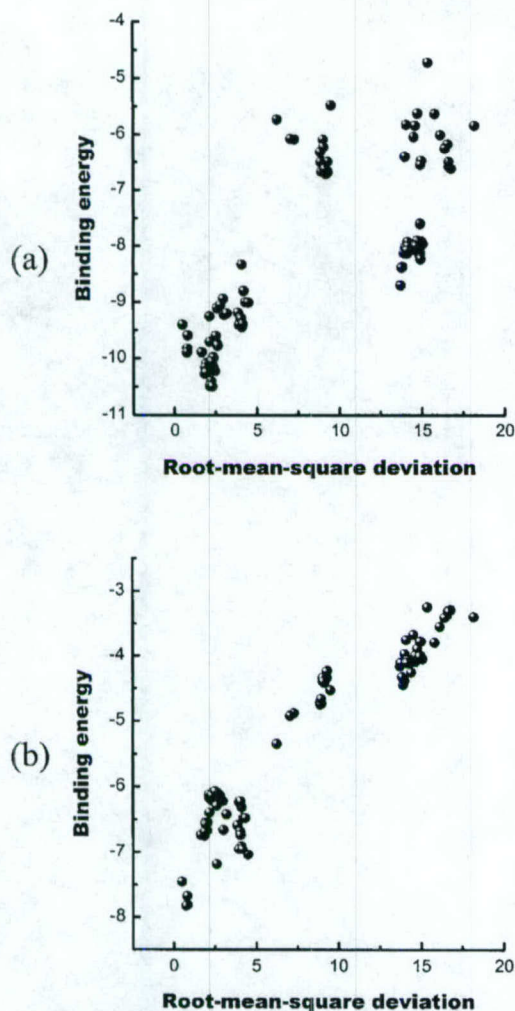


Figure 7. Relationship between the RMSD values (\AA) and the binding energies (kcal/mol) of 100 conformations of L-benzylsuccinate in complex with carboxypeptidase A (PDB code 1CBX). (a) Binding energies calculated by AutoDock. (b) Binding energies calculated by X-CSCORE.

(PDB code 1DBM), the dihydrofolate reductase/folate complex (PDB code 1DHF), the glutathione S-transferase/glutathione complex (PDB code 1GST), and the HIV-1 protease/VX-478 complex (PDB code 1HPV). The selection of these 10 samples emphasizes the diversity of the ligands and the proteins. For each complex, the AutoDock 3.0 program [8] is employed to perform a molecular docking run. In each case, the experimentally determined complex structure is al-

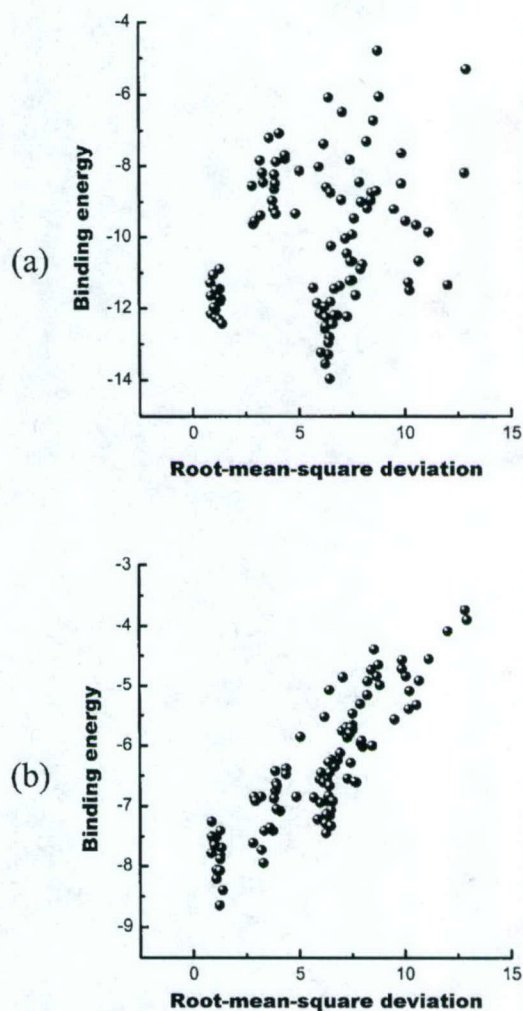


Figure 8. Relationship between the RMSD values (\AA) and the binding energies (kcal/mol) of 100 conformations of folate in complex with dihydrofolate reductase (PDB code 1DHF). (a) Binding energies calculated by AutoDock. (b) Binding energies calculated by X-CSCORE.

ways used as the starting point. The ligand is treated flexible while the protein is kept rigid. The searching steps in the conformational sampling for translation, quaternion, and torsion are set to 0.5 \AA , 15° and 15° , respectively. Fifty thousand genetic algorithm generations are run with a population of 100 conformations. The final 100 best-scored conformations are saved and their root-mean-squared deviations (RMSD), as calculated by using the observed bound conformation as the reference, are recorded. Then the binding

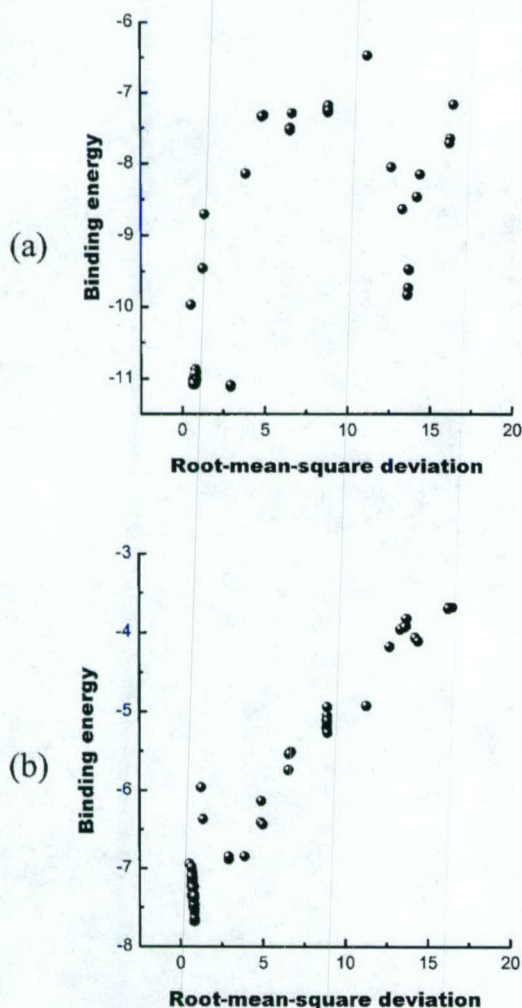


Figure 9. Relationship between the RMSD values (Å) and the binding energies (kcal/mol) of 100 conformations of 1-deaza-adenosine in complex with adenosine deaminase (PDB code 1ADD). (a) Binding energies calculated by AutoDock. (b) Binding energies calculated by X-CSCORE.

energies of these conformations are re-calculated by X-CSCORE. RMSD values of the best-scored conformations, picked by AutoDock and X-CSCORE, of all 10 complexes are summarized in Table 3. For complex 1CBX, 1DHF, and 1ADD, RMSD values of the final 100 conformations are plotted against the binding energies of these conformations in Figures 7–9, respectively.

Program description

We have developed a program, X-CSCORE, to implement the three scoring functions described by Equations 9–11. Here 'CSCORE' means consensus scoring; while the prefix 'X' indicates that it is part of our in-house drug design toolkit X-TOOL. This program is written in ANSI C++ and has been tested on UNIX and LINUX platforms. The required inputs include the three-dimensional structure of the protein in PDB format and the pre-docked ligand molecule(s) in MOL2 format. The user is allowed to enable or disable any of the three scoring functions in computation and the final predicted binding affinities are based on the arithmetic average of all the enabled scoring functions. If all three scoring functions are enabled, typically this program is able to process around 10 000 ligand molecules for a given protein target in an hour on a SGI O2/R5000/180MHz workstation.

Discussion

Accuracy and robustness

As shown in Table 2, Equations 9–11 are able to reproduce the binding affinities of the entire training set with standard deviations (s) of 1.58, 1.53 and 1.43 pK_d units, respectively. Their standard deviations in leave-one-out cross-validation (s_{press}) are at the same level, which are 1.62, 1.57 and 1.47 pK_d units, respectively. More importantly, these scoring functions perform almost equally well for the independent test set: the standard deviations in the predicted binding affinities (s_{pred}) are 1.51, 1.61 and 1.63 pK_d units, respectively. These values correspond to 2.1–2.2 kcal/mol in binding free energy at room temperature. Considering the diversity of the test set, such accuracy in binding affinity prediction is encouraging. Compared to other existing empirical scoring functions, our scoring functions have achieved better or comparable statistical results. If taking the Fisher significant ratio (F) as an objective criterion for comparing different regression models, the values are 32.1, 44.5 and 57.8 for Bohm's scoring function [27], ChemScore [30], and SCORE [32], respectively. In comparison, the F values of our scoring functions are 49.6, 58.7 and 70.4 for Equations 9–11, respectively.

When building a regression model, over-fitting of the regression equation should be avoided because it may fail to give reasonable predictions for samples

Table 3. Results from the molecular docking studies of 10 protein-ligand complexes

PDB code	Resolution (Å)	RMSD (Å) ^a		pK_d	
		AutoDock	X-CSCORE	Exp. ^b	X-CSCORE ^c
1ABE	1.7	0.62	0.73	6.52	5.14 (5.25)
1ADB	2.4	2.74	2.74	8.40	6.71 (8.01)
1ADD	2.4	2.93	0.83	6.74	5.63 (5.36)
1AF2	2.3	0.88	0.88	3.10	5.26 (4.90)
1ANF	1.67	0.60	0.54	5.46	6.16 (6.03)
1CBX	2.0	2.30	0.77	6.35	5.74 (5.74)
1DBM	2.7	1.31	1.13	9.44	6.84 (6.65)
1DHF	2.3	6.44	1.24	7.40	6.34 (5.27)
1GST	2.2	0.74	1.21	4.68	5.92 (5.21)
1HPV	1.9	1.73	1.16	9.22	6.47 (6.28)

^aRMSD value of the best scored conformation in reference to the observed bound conformation.

^bExperimentally determined binding affinity.

^cCalculated binding affinity for the best scored conformation. The values in brackets are the calculated one for the observed bound conformation.

outside the training set. For this reason, only a minimal number of adjustable parameters are included in our scoring functions to achieve maximal N/M ratio in regression analysis. For example, we do not assign additional weighting factors to different types of atoms when calculating the van der Waals interaction. When calculating the hydrogen bonding, we do not differentiate charged and neutral hydrogen bonds. No differentiation in aliphatic and aromatic atoms was made in calculating the hydrophobic effect. Besides the regression constant, there are only four coefficients in each of our scoring functions. As shown in Table 1, they are all significant in regression analysis. Here the van der Waals interaction term in Equation 10 seems to be an exception, which contributes only a relative small fraction. However, it is not surprising since the hydrophobic effect term in Equation 10 is also calculated by counting atom pairs, therefore it overlaps with the van der Waals term partially and 'grabs' some contributions from the van der Waals term.

The N/M ratio issue deserves a little more discussion. It is reasonable to expect that statistically converged results can only be obtained by using a large training set. But how large is large? What is the proper size of the training set for deriving an empirical scoring function like ours? To answer this question, we have adopted the evolutionary regression procedure to look for the answer. The idea of evolutionary regression is to test a given regression model with training sets in different sizes and monitor the quality of the regression model during this procedure. Several trends

can be seen in the evolutionary regression experiments of Equations 9–11 (Figure 6). (i) The standard deviation in the whole set fitting (s) gradually increases when the training set grows larger. This can be understood because the scoring function under regression is kept fixed during the whole procedure. A larger training set represents more complexity and thus is more difficult to reconcile. (ii) The predictive ability of the regression model, as indicated by the standard deviations in leave-one-out cross-validation (s_{press}) and test set computation (s_{pred}), is gradually improved when the training set grows larger. This indicates that a larger training set indeed helps our scoring functions achieve better predictive ability. (iii) When the training set is relatively small, the regression model is generally unstable. The final regression model depends very sensitively on the contents of the training set, which may lead to chance correlation in regression and poor predictive ability. When the training set grows larger, the regression model becomes more stable and tends to converge to a certain level. As suggested by our evolutionary regression experiments, a training set containing at least 160 samples is required to derive a stable empirical scoring function with four terms, i.e. a minimal N/M ratio of 40. Unfortunately, the N/M ratios of other existing empirical scoring functions are generally much lower than this, e.g. LUDI (N/M = 45/6 = 9) [27], ChemScore (N/M = 82/4 = 20) [30], and SCORE (N/M = 170/10 = 17) [32]. In our case, the N/M ratio is 200/4 = 50. Therefore, we believe our scoring functions are, if not much more accurate, more

robust in binding affinity prediction for a wider range of protein-ligand complexes.

Consensus scoring

A unique feature of our study is that three different algorithms have been implemented for modeling the hydrophobic effect. As described in the Methods section, hydrophobic effect is calculated either by the buried solvent-accessible molecular surface (Equation 9), or by the number of hydrophobic contacts between the protein and the ligand (Equation 10), or by the hydrophobic matching of the ligand with the binding site (Equation 11). All three algorithms are conceptually acceptable and actually they represent three typical algorithms adopted by empirical scoring functions for modeling the hydrophobic effect. However, it is not a good idea to include all three terms together in one scoring function since they account for the same effect and thus are highly correlated to each other. Therefore, they have to be accommodated in three scoring functions. As indicated by our regression results (Table 2), all three scoring functions perform reasonably well and are basically comparable to each other. However, since these three algorithms utilize different geometric features of the given protein-ligand complex structure in computation, their results differ. We have found that, for 40.0% of the samples in the training set, the difference between the lowest and the highest calculated binding affinity by these three scoring functions is less than 0.50 pK_d units; for 40.5% of the samples, the difference is between 0.50 and 1.00 pK_d units; while for the remaining 19.5% of the samples, the difference is larger than 1.00 pK_d units. One can see that such difference is not trivial at all in many cases. Conceivably, if one can predict which scoring function will be the best for a given protein-ligand complex, the accuracy in binding affinity prediction will be improved greatly. Indeed, if the experimental values are correlated to the best fitted values (each of them is chosen from three hits), the standard deviation in the training set fitting will drop by half to about 0.7 pK_d units. We have attempted to find out which scoring function may perform better for certain classes of ligands or families of proteins. Unfortunately this attempt ended without much success.

Based on the fact that there is no reason to bias towards any one of the three scoring functions, we simply combine them together (Equation 12). This practice is consistent with the idea of consensus scoring which has been demonstrated to be an effective

way of improving the hit-rates in virtual database screening [33]. As shown in Table 2, the performance of a single scoring function may vary and is not predictable. For example, among the three scoring functions, Equation 9 is the worst one for the training set but the best one for the test set. In contrast, Equation 11 is the best one for the training set but the worst one for the test set. By averaging these scoring functions, i.e. X-CSCORE, the result is not always the closest one to the true value (in fact it is always between the best one and the worst one). However, the advantages are: (i) it provides a clear indication of what level of accuracy these three scoring functions can achieve. Obtaining a converged result in binding affinity prediction is certainly important for structure-based drug design practice; and (ii) large errors in binding affinity prediction can be reduced. Recently we have pointed out that the nature of consensus scoring is multiple sampling [37]. By applying multiple scoring functions in combination, the positive and the negative errors have a chance to cancel each other and that is why consensus scoring generally performs better than any single scoring procedure.

Application to molecular docking

Our scoring function is developed primarily for estimating the binding affinity of a given complex with known structure ('scoring'). We also expect it to be useful for identifying the correct 'pose' of a ligand to its receptor ('docking'). Although some disputes still exist in whether 'docking' or 'scoring' should use the same type of function, we believe that ideally a 'scoring' function should also be able to serve as a 'docking' function. This is very important because in practice 'docking' and 'scoring' are often inseparable, such as in a virtual database screening study.

As described in the *Methods* section, we have investigated the potential application of X-CSCORE in molecular docking with 10 samples. Since we have not implemented this consensus scoring function into any molecular docking program directly, we employ the AutoDock program as a tool to generate possible bound conformations of the given ligand. All the conformations are then re-evaluated by X-CSCORE. RMSD values of the best scored conformations of these 10 protein-ligand complexes are listed in Table 3, where the results of X-CSCORE and the force field calculation in AutoDock are compared side by side. As one can see, if using the force field calculation in AutoDock as the scoring engine, 4 out

of the total 10 samples have RMSD values larger than 2.0 Å; while if using X-CSCORE as the scoring engine, only one sample, i.e. the alcohol dehydrogenase/CNAD complex (PDB code 1ADB), shows a RMSD value larger than 2.0 Å. In this case, we have checked all the 100 conformations generated by AutoDock and we found that the lowest RMSD value is 2.74 Å. This indicates that, with the parameters we were using, AutoDock has not generated any conformation close enough to the observed one. In fact, X-CSCORE predicts a much higher pK_d value of 8.01 for the observed one. The RMSD versus energy relationships observed in our docking tests for the Carboxypeptidase A/L-benzylsuccinate complex (PDB code 1CBX), the Dihydrofolate reductase/folate complex (PDB code 1DHF), and the adenosine deaminase/DAA complex (PDB code 1ADD) are shown in Figures 7–9, respectively. For these three samples, the best RMSD values given by AutoDock are 2.30 Å, 6.44 Å and 2.93 Å; while the corresponding ones given by X-CSCORE are 0.77 Å, 1.24 Å and 0.83 Å. It is very interesting to notice that, in the case of 1DHF, AutoDock has apparently chosen a wrong class of conformations while the correct one is somehow scored about 2 kcal/mol higher. In contrast, X-CSCORE has no problem in identifying the correct conformation.

It is very encouraging that our scoring functions are also applicable to molecular docking. Our scoring functions have all the necessary elements that correspond to the non-covalent interactions in a conventional force field, such as the van der Waals interaction and the electrostatic interaction (replaced by the hydrogen bonding term in our scoring functions). Besides that, our scoring functions also consider the hydrophobic effect and thus provide a better estimation of binding free energies. This is suggested in Figures 7b, 8b and 9b. In these cases, there is always a clear correlation between the RMSD values of the conformations and their binding energies calculated by X-CSCORE. Generally, the smaller is the RMSD value, the lower is the binding energy. The importance of this feature should not be underestimated. Molecular docking is a conformational sampling procedure which is performed on the potential energy surface defined by a certain scoring function. It is important that this potential energy surface does not contain a large number of false minima since such frustration will probably lead to poor convergence or wrong binding modes. The potential energy surface defined by an ideal scoring function should shape like a funnel, on which all the paths finally go down to

the right position. As indicated by the RMSD versus energy relationships shown in Figures 7b, 8b and 9b, our consensus scoring function may have such an appealing feature. We expect that if a molecular docking program adopts our consensus scoring function as its scoring engine, its accuracy and efficiency in finding the correct bound structure will be improved considerably.

Considering that in practice our consensus scoring function will be applied in conjunction with molecular docking programs, it is highly desirable that all our scoring functions are able to tolerate at least a small amount of uncertainty in the input structure. For this reason, we have designed our scoring functions in such a way that they are not too sensitive to atomic coordinates. For example, we avoid the explicit use of hydrogen atoms in our algorithms. The reason is that predicting the position of a hydrogen atom precisely could be problematic when the hydrogen atom is bonded to a terminal rotatable group, such as a hydroxyl group. This uncertainty will lead to large deviation if hydrogen atoms have to be included explicitly in the calculation. Secondly, all the terms in our scoring functions are calculated with relatively large tolerances. For example, a 'softer' 8–4 equation is adopted in the van der Waals interaction term; loose criteria for distance and angular dependence are adopted in the hydrogen bonding term; long-distance cutoff is adopted in the hydrophobic effect terms. All these efforts are dedicated to emphasize on the overall fitness of the ligand to the binding site rather than trivial structural details. As shown in Table 3, by applying X-CSCORE, if a conformation is close to the reference conformation, then indeed it will get a score close to the one of the reference conformation.

Strength and weakness

Our scoring functions are developed to provide fast binding affinity estimations for a wide range of proteins and ligands. As demonstrated by the training set and the test set, the average accuracy of our consensus scoring function in calculating absolute binding free energies is approximately 2 kcal/mol. This level of accuracy is acceptable for structure-based lead discovery in which very accurate prediction of binding free energies may not be necessary, such as virtual database screening or *de novo* structure generation. The speed of our consensus scoring function is also perfectly suitable for such approaches.

We have implemented our scoring functions in a user-friendly program and have already applied it to several on-going structure-based drug design projects in our group. In these projects, large chemical databases are screened first by a standard docking program, such as DOCK, to pick out the top 10% compounds. These compounds are then re-evaluated by X-CSCORE. The best compounds selected by X-CSCORE, usually less than 0.1% of the original database, are then tested in biological assays. Very promising compounds have been identified since the application of this approach.

However, the accuracy of our consensus scoring function in binding affinity prediction is still not totally satisfactory: an error of 2 kcal/mol in binding free energy equals to approximately 50 folds in dissociation constant. Several drawbacks in our approach may have contributed to this inaccuracy. Firstly, since our scoring functions are derived from regression, they tend to characterize only the "common" interactions that are exhibited by a large population in the training set. Some other types of interactions, such as cation- π interaction and π - π stacking, are not included in our scoring functions simply because they have rare occurrences and thus do not contribute much to the regression model. It is thus expected that a general-type scoring function like ours could fail to give reasonable predictions when these types of interactions are playing an important role in protein-ligand binding. Secondly, there are also some factors which are common but we do not really have reasonable methods to take them into account. One example is the water molecules existing on the protein-ligand interface. Such water molecules are quite common and in some cases are thought to play an important role in the ligand binding. However, it remains unclear how to consider water molecules explicitly with an empirical scoring function. If water molecules need to be considered explicitly, maybe the entire algorithm for modeling the so-called 'hydrophobic effect' needs to be replaced as well.

Our scoring functions also tend to give large positive errors for complexes with very low affinities and large negative errors for complexes with very high affinities (Figure 4). This phenomenon contributes to the significant positive intercept (~ 3 pK_d units) observed in all three scoring functions. Given the fact that most of the samples in the training set (80%) have pK_d values between 3.00 and 9.00, our scoring functions are calibrated better for binding affinities at this range. In fact, if only the samples within this affinity

range are chosen to derive our scoring functions, the standard deviations in regression will drop to 1.2–1.3 pK_d units (~ 1.7 kcal/mol in binding free energy).

Another major problem is the quality of the training set. Ideally, each protein-ligand complex in the training set should have a known high-resolution three-dimensional structure together with a reliably measured binding affinity value accessible to the public. Obtaining protein-ligand complex structures is not a problem since the Protein Data Bank provides an excellent resource for such information. However, collecting the binding affinities for these complexes is a tedious job since they all scatter in various literatures. So far, no appreciable database for such information has been established. The training set used in our study is a compilation of the training sets published in others' work plus our own collections from the literature. Containing 200 samples, it is already the largest set published to date in an empirical scoring function approach. As demonstrated in our evolutionary regression test, the size of this training set is sufficient for calibrating our scoring functions. However, the binding affinity data presented in this training set still need careful examination because a large portion of them are cited directly from others' work without further confirmation. Besides, some of the dissociation constants could have been measured under different experimental conditions, such as pH level, temperature, and salt concentration. The uncertainties in the binding affinity data have certainly placed an intrinsic limit on the accuracy of our scoring functions.

It should be mentioned that all the drawbacks we have discussed above are shared by other empirical scoring functions as well. Despite of all these drawbacks, empirical scoring functions remain a valuable and indispensable means for structure-based drug design. Constructing a better training set will not be a problem in the future because more and more structural and binding affinity data are becoming available. We are also optimistic that better algorithms will appear to account for the binding process. All these efforts will lead to a substantial improvement in the performance of future empirical scoring functions.

Conclusion

We have developed a consensus empirical scoring function, X-CSCORE, for estimating the binding affinity of a given protein-ligand complex with a known three-dimensional structure. The framework

of our study is very similar to Böhm's pioneering work. However, we have presented our works on designing better algorithms for the contributing terms and calibrating the scoring functions against a larger training set. As shown in this paper, our consensus scoring function is able to predict the binding free energies with an average accuracy of approximately 2 kcal/mol. Its potential application to molecular docking is demonstrated with a number of protein-ligand complexes. When compared to the conventional force field calculation, X-CSCORE performs considerably better in identifying the correct bound conformations. Considering the reasonable accuracy, the wide applicability, and the respectable speed, we expect that X-CSCORE will become a valuable tool for structure-based drug design.

Supplementary material

Tables of the training set (200 protein-ligand complexes) and the test set (30 protein-ligand complexes). The program, X-CSCORE, is available by contacting the authors.

Acknowledgements

This work is financially supported by the Cap CURE Foundation (2001 Young Investigator Award to Dr Renxiao Wang) and the Department of Defense (Grant No. DOD DAMP17-93-V-3018 to Dr Shaomeng Wang). The authors are grateful to Dr John B. O. Mitchell at University of Cambridge for providing some of the binding affinity data used in this study. The authors are also grateful to Dr Chao-Yie Yang at University of Michigan Medical School for his many thoughtful suggestions.

References

- Kuntz, I.D., *Science*, 257 (1992) 1078.
- Greer, J., Erickson, J.W., Baldwin, J.J. and Varney, M.D., *J. Med. Chem.*, 37 (1994) 1035.
- Verlinde C.L.M.J. and Hol W.G.J., *Structure*, 2 (1994) 577.
- Babine, R.E. and Bender, S.L., *Chem. Rev.*, 97 (1997) 1359.
- Gane, P.J. and Dean, P.M., *Curr. Opin. Struct. Biol.*, 10 (2000) 401.
- Walters, W.P., Stahl, M.T. and Murcko, M.A., *Drug Discovery Today*, 3 (1998) 160.
- Makino, S. and Kuntz, I.D., *J. Comp. Chem.*, 18 (1997) 1812.
- Morris, G.M., Goodsell, D.S., Halliday, R., Huey, R., Hart, W.E., Belew, R.K. and Olson, A.J., *J. Comput. Chem.*, 19 (1998) 1639.
- Jones, G., Wilett, P., Glen, R.C., Leach, A.R. and Taylor, R., *J. Mol. Biol.*, 267 (1997) 727.
- Rarey, M., Kramer, B., Lengauer, T. and Klebe, G., *J. Mol. Biol.*, 261 (1996) 470.
- Böhm, H.J., *Curr. Opin. Biotech.*, 7 (1996) 433.
- Miranker, A. and Karplus, M., *Proteins*, 11 (1991) 29.
- Böhm, H.J., *J. Comput. Aid. Mol. Des.*, 6 (1992) 61.
- Gillet, V., Johnson, P. and Mata, P., *J. Comput. Aid. Mol. Des.*, 7 (1993) 127.
- Clark, D.E., Frenkel, D. and Levy, S.A., *J. Comput. Aid. Mol. Des.*, 5 (1995) 13.
- Pearlman, D.A. and Murcko, M.A., *J. Med. Chem.*, 39 (1996) 1651.
- Wang, R., Gao, Y., Lai, L., *J. Mol. Model.*, 6(2000) 498-516.
- Schneider, G., Lee, M.L., Stahl, M. and Schneider, P., *J. Comput. Aid. Mol. Des.*, 14 (2000) 487.
- Kollman, P.A., *Curr. Opin. Struct. Biol.*, 4 (1994) 240.
- Ajay and Murcko, M.A., *J. Med. Chem.*, 38 (1995) 4953.
- Tame, J.R.H., *J. Comput. Aid. Mol. Des.*, 13 (1999) 99.
- Goodford, P.J.A., *J. Med. Chem.*, 28 (1985) 849.
- Massova, I. and Kollman, P., *Perspect. Drug Disc. Des.*, 18 (2000) 113.
- Kollman, P., *Chem. Rev.*, 7 (1993) 2395.
- Aqvist, J., Medina, C. and Samuelsson, J.E., *Protein Eng.*, 7 (1994) 385.
- Carlson, H.A. and Jorgensen, W.L., *J. Phys. Chem.*, 99 (1995) 10667.
- Böhm, H.J., *J. Comput. Aid. Mol. Des.*, 8 (1994) 243.
- Jain, A.N., *J. Comput. Aid. Mol. Des.*, 10 (1996) 427.
- Head, R.D., Smythe, M.L., Oprea, T.I., Waller, C.L., Green, S.M. and Marshall, G.R., *J. Am. Chem. Soc.*, 118 (1996) 3959.
- Eldridge, M.D., Murray, C.W., Auton, T.R., Paolini, G.V. and Mee, R.P., *J. Comput. Aid. Mol. Des.*, 11 (1997) 425.
- Böhm, H.J., *J. Comput. Aid. Mol. Des.*, 12 (1998) 309.
- Wang, R., Gao, Y. and Lai, L., *J. Mol. Model.*, 4 (1998) 379.
- Charifson, P.S., Corkery, J.J., Murcko, M.A. and Walters, W.P., *J. Med. Chem.*, 42 (1999) 5100.
- Berman, H.M., Westbrook, J., Feng, Z., Gilliland, G., Bhat, T.N., Weissig, H., Shindyalov, I.N. and Bourne, P.E., *Nucleic Acids Res.*, 28 (2000) 235, <http://www.rcsb.org/pdb/>.
- SYBYL v6.2, Tripos Inc. St. Louis, MO, U.S.A. <http://www.tripos.com/>
- Wang, R., Gao, Y. and Lai, L., *Perspect. Drug Disc. Des.*, 19 (2000) 47.
- Wang, R. and Wang, S., *J. Chem. Inf. Comput. Sci.*, 41 (2001) 1422.

Noting this circularity, Ramscar [6] repeated the Kim *et al.* study, taking truly independent ratings to see which verbs participants considered to be denominal or deverbal (i.e. exocentric or not). The results of this new experiment were clear. The semantic similarity (or otherwise) of verbs-in-context to ordinary irregular usage predicted the acceptability of past-tense forms. Whether or not verbs were perceived to be exocentric was irrelevant to this. It is worth noting that these results were obtained using the verbs put forward by Kim *et al.* [5] to try to demonstrate their theory. The theory that homophone verb processing can be explained by exocentricity fails completely in the face of examples like *shoe-shoo*, where it is the denominal verb that is irregular (*shoe-shod*) and the deverbal verb regular (*shoo-shooed*). (Further support for these findings comes from on-line studies that have shown that semantics – and not exocentric form – predict comprehension time for homophone verbs [7].)

What is the relevance of these data to the past-tense debate? First, they demonstrate that the 'in-principle' objection to single-route models supposedly posed by homophone verbs is wrong. Inflections of homophone verbs are determined by complex semantic and phonological patterns, not grammatical status. Second, they show that children's ability to process homophone verbs is not indicative of their innate sensitivity to nouns and verbs [8], but rather is indicative of children's ability to learn

languages. Finally, because the exocentricity thesis is false, the dual-route theory itself cannot account for the processing of homophone verbs. Providing an account of homophone-verb inflection is vital to explaining past-tense processing [1–4]; the evidence suggests that it is two routes that this phenomenon rules out, not one.

References

- 1 Pinker, S. and Ullman, M. (2002) The past and future of the past tense. *Trends Cogn. Sci.* 6, 456–463
- 2 Pinker, S. and Ullman, M. (2002) Combination and structure, not gradedness, is the issue. Reply to McClelland and Patterson. *Trends Cogn. Sci.* 6, 472–474
- 3 Pinker, S. (1999) *Words and Rules*, HarperCollins
- 4 Pinker, S. and Prince, A. (1988) On language and connectionism: analysis of a parallel distributed processing model of language acquisition. *Cognition* 28, 73–193
- 5 Kim, J.J. *et al.* (1991) Why no mere mortal has ever flown out to center field. *Cogn. Sci.* 15, 173–218
- 6 Ramscar, M.J.A. (2002) The role of meaning in inflection: why the past tense doesn't require a rule. *Cogn. Psychol.* 45, 45–94
- 7 Ramscar, M.J.A. (2002) When the fly flied and when the fly flew: the effects of semantics on the comprehension of past tense inflections. *Proc. 24th Annu. Conf. Cogn. Sci. Soc.*, pp. 768–773, Erlbaum
- 8 Kim, J.J. *et al.* (1994) Sensitivity of children's inflection to grammatical structure. *J. Child Lang.* 21, 179–209

1364-6613/03/\$ - see front matter © 2003 Elsevier Science Ltd. All rights reserved.
doi:10.1016/S1364-6613(03)00019-6

Letters Response

Beyond one model per phenomenon

Steven Pinker¹ and Michael T. Ullman²

¹Department of Brain and Cognitive Sciences, NE20-413, Massachusetts Institute of Technology, Cambridge, MA 02139, USA

²Department of Neuroscience, Research Building EP-04, Georgetown University, 3900 Reservoir Rd, NW, Washington DC 20007, USA

Reply to Seidenberg and Joanisse

We would be the last to claim that the Joanisse and Seidenberg model (JSM) is the same as the Words and Rules theory. 'Crude implementation' refers to an earlier model [1] with units encoding the relatedness of a verb to its noun root (a surrogate for morphological structure), not to JSM. Our noting that JSM contains a lexicon is not a failure to distinguish theoretical commitments from implementational details: Joanisse and Seidenberg themselves justified their decision to represent words, not semantic features, by pointing out that semantic similarity, 'although... crucial for other phenomena,... is not important for the past tense.' Our point exactly.

As for the differences, current evidence indicates that deficits on irregulars in anomia cannot, as J&S predicted, be reduced to semantic deficits [2]; nor can deficits with regulars be reduced to phonological deficits either in agrammatic aphasia [3] or in SLI [4]. We disagree that regular-irregular differences in agrammatic aphasia are as rare as in occasional random simulation runs selected post hoc [5]: the difference has been reported in eight studies

(see [6,7]), and has survived several attempts to eliminate it by controlling for factors such as phonology ([3,7,8]; this includes Bird *et al.*'s reading data [9]).

Although J&S protest our observation that recent connectionist models are tailored to a single phenomenon, Seidenberg's past-tense models are an example. One of them addressed frequency effects in reaction time, and had no lexical or semantic nodes, which might have created an unwanted frequency effect [10]. Another addressed systematic regularization, and built in verb-noun-relatedness units [1]. A third (JSM) addressed double dissociations, and had distinct sub-networks of lexical and phonological units (but no relatedness units). Yes, the parallels between morphology and spelling are noteworthy. But they were first addressed by dual-route models [11], and the successes of connectionist models in both domains derive from a feature we readily acknowledge: the sensitivity of superpositional memory to frequency and similarity.

Reply to Ramscar

In noting the unimportance of semantic similarity for the past tense, J&S are on our side, against Ramscar. Ramscar is incorrect in claiming that Kim *et al.* [12] defined the

Corresponding authors: Steven Pinker (steve@psyche.mit.edu),
Michael T. Ullman (michael@georgetown.edu).

denominal status circularly. Our first set of denominal items were existing verbs that had been independently categorized as denominal and judged as regular by linguists; because some skeptics had dismissed the judgments, we tested them to verify that naïve subjects preferred the regular forms. The second set presented nouns to participants, followed by a novel denominal verb usage. As this was an experimental manipulation that defined denominal status *a priori*, rather than a correlational study, the absence of ratings of denominal status does not create a logical circle.

Ramscar's findings differ from ours because his instructions stacked the deck against finding an effect of morphology. Sensitivity to morphology was measured by asking participants whether a target verb was similar to a single example: a novel usage of *fly* meaning 'to greet customers while wearing a fly costume'. This complex metalinguistic judgment – whether the target verb is crucially similar to the one in this odd scenario – is an insensitive measure of people's perception of whether a verb is based on a noun, as can be seen in anomalous data such as participants indicating little perceived relationship between 'to brake' and *brakes*.

Conversely, the measure of semantic similarity was confounded with headedness: subjects were asked whether the activity described by the target word 'reminded' them of the base word and to 'consider all the possible things [they] associated with [the] use of the word.' If two words share a root, one will certainly remind people of the other, and trigger associations with the other. This is distinct from whether the two words share semantic features, the mechanism invoked in connectionist accounts.

The pair *shod*–*shoed* does not contrast headless and headed verbs. Both are headless: dictionaries define *to shoos* 'to say *shoo*.' In any case, *shod* is a dubious example of people irregularizing headless verbs. It is an archaic form (the fossil of a defunct phonological rule) that today is used most often as

a participial adjective. Many people are unaware that it is the preterite of *to shoe*, as can be seen in errors such as *to shod* [13]. That Ramscar had to reach for this as his counter-example shows that the overwhelming tendency is for headless verbs to get regular past-tense forms.

References

- 1 Daugherty, K.G. *et al.* (1993) Why no mere mortal has ever flown out to center field but people often say they do. *15th Annu. Conf. Cogn. Sci. Soc.*, pp. 383–388, Erlbaum
- 2 Miozzo, M. (2003) On the processing of regular and irregular forms of verbs and nouns: evidence from neuropsychology. *Cognition* (in press)
- 3 Tyler, L.K. *et al.* (2002) Phonology and neuropsychology of the English past tense. *Neuropsychologia* 40, 1154–1166
- 4 van der Lely, H.K. and Christian, V. (2000) Lexical word formation in Grammatical SLI children: a grammar-specific or input-processing deficit? *Cognition* 75, 33–63
- 5 Joanisse, M.F. and Seidenberg, M.S. (1999) Impairments in verb morphology after brain injury: a connectionist model. *Proc. Natl. Acad. Sci. U. S. A.* 96, 7592–7597
- 6 Pinker, S. and Ullman, M.T. (2002) Combination and structure, not gradedness, is the issue. *Trends Cogn. Sci.* 6, 472–474
- 7 Ullman, M.T. *et al.* (2003) Neural correlates of lexicon and grammar: evidence from the production, reading, and judgment of inflection in aphasia. *Brain Lang.* (in press)
- 8 Ullman, M. *et al.* (1997) A neural dissociation within language: evidence that the mental dictionary is part of declarative memory, and that grammatical rules are processed by the procedural system. *J. Cogn. Neurosci.* 9, 289–299
- 9 Bird, H. (2003) Deficits in phonology and past tense morphology: what is the connection? *J. Mem. Lang.* (in press)
- 10 Daugherty, K. and Seidenberg, M. (1992) Rules or connections? The past tense revisited. *14th Annu. Conf. Cogn. Sci. Soc.*, pp. 259–264, Erlbaum
- 11 Coltheart, M. (1985) Cognitive neuropsychology and the study of reading. In *Functions of the Right Cerebral Hemisphere* (Young, A., ed.), pp. 3–37, Academic Press
- 12 Kim, J.J. *et al.* (1991) Why no mere mortal has ever flown out to center field. *Cogn. Sci.* 15, 173–218
- 13 Pinker, S. (1999) *Words and Rules: The Ingredients of Language*, HarperCollins

1364-6613/03/\$ - see front matter © 2003 Elsevier Science Ltd. All rights reserved.
doi:10.1016/S1364-6613(03)00021-4

Letters

Mental imagery: against the nihilistic hypothesis

Stephen M. Kosslyn^{1,2}, Giorgio Ganis^{1,3} and William L. Thompson¹

¹Harvard University, Department of Psychology, 830 William James Hall, 33 Kirkland Street, Cambridge, MA 02138, USA

²Massachusetts General Hospital, Department of Neurology, 55 Fruit Street, Boston, MA 02114, USA

³Massachusetts General Hospital, Department of Radiology, 55 Fruit Street, Boston, MA 02114, USA

We begin with a summary of central elements of our depictive theory, which will allow the reader to decide whether it is 'grotesque' (to use Pylyshyn's term [1]). The theory hinges on the facts that: (i) the occipital lobe contains numerous topographically mapped areas that support depictive representations; and (ii) most cortical areas used in visual perception are also used in imagery [2], including early visual cortex [3–5]. In perception, the occipital topographic areas provide input to two major

visual pathways. One, running down the inferior temporal lobe, is involved in object recognition. Visual memories are stored in this pathway, but in a non-topographic form [6]. The other, running up to the posterior parietal lobe, is involved in specifying locations and orientations in space. According to our theory, a mental image of a shape is created when a visual memory is activated top-down, inducing a pattern of activation in the topographically mapped areas; backward connections from higher-level to lower-level visual areas are well-documented [7]. Similarly, images of spatial relations are created when a spatial

Corresponding author: Stephen M. Kosslyn (smk@wjh.harvard.edu).

<http://tics.trends.com>



Available online at www.sciencedirect.com

SCIENCE @ DIRECT®

COGNITION

Cognition 92 (2004) 231–270

www.elsevier.com/locate/COGNIT

Contributions of memory circuits to language: the declarative/procedural model

Michael T. Ullman*

*Brain and Language Laboratory, Departments of Neuroscience, Linguistics, Psychology and Neurology,
Georgetown University, Washington, DC, USA*

Received 12 December 2001; revised 13 December 2002; accepted 29 October 2003

Abstract

The structure of the brain and the nature of evolution suggest that, despite its uniqueness, language likely depends on brain systems that also subserve other functions. The declarative/procedural (DP) model claims that the mental lexicon of memorized word-specific knowledge depends on the largely temporal-lobe substrates of declarative memory, which underlies the storage and use of knowledge of facts and events. The mental grammar, which subserves the rule-governed combination of lexical items into complex representations, depends on a distinct neural system. This system, which is composed of a network of specific frontal, basal-ganglia, parietal and cerebellar structures, underlies procedural memory, which supports the learning and execution of motor and cognitive skills, especially those involving sequences. The functions of the two brain systems, together with their anatomical, physiological and biochemical substrates, lead to specific claims and predictions regarding their roles in language. These predictions are compared with those of other neurocognitive models of language. Empirical evidence is presented from neuroimaging studies of normal language processing, and from developmental and adult-onset disorders. It is argued that this evidence supports the DP model. It is additionally proposed that “language” disorders, such as specific language impairment and non-fluent and fluent aphasia, may be profitably viewed as impairments primarily affecting one or the other brain system. Overall, the data suggest a new neurocognitive framework for the study of lexicon and grammar.

© 2004 Elsevier B.V. All rights reserved.

Keywords: Language; Lexicon; Grammar; Declarative memory; Procedural memory; Syntax; Morphology; Regular; Irregular; Basal ganglia; Neostriatum; Caudate nucleus; Cerebellum; Broca's area; Dorsal stream; Ventral stream; Working memory; Sequence learning; Specific language impairment; Dyslexia; Attention deficit hyperactivity disorder; Autism; Aphasia; Parkinson's disease; Alzheimer's disease; Huntington's disease; Semantic dementia; Functional magnetic resonance imaging; Positron emission tomography; Event-related potential

* Department of Neuroscience, Georgetown University, Box 571464, Washington, DC 20057-1464, USA.
E-mail address: michael@georgetown.edu (M.T. Ullman).

1. Introduction

The study of language has focused largely on language itself. That is, in order to understand the representation, processing, development, neural correlates and other aspects of language, most theories and investigations have directed their attention to language. This is unsurprising, and not only because of the obvious point that directly investigating a domain generally elucidates it. Additionally, the apparent uniqueness of human language has drawn attention away from evidence suggesting the existence of biological and computational substrates that are shared between language on the one hand, and non-language domains in humans and animals on the other.

Brain organization and evolutionary principles both lead to an expectation of commonalities between language and non-language domains. First, a number of brain structures seem to be organized topographically, with sub-regions performing analogous computations on different domains of information, as a function of each sub-region's particular set of inputs and outputs. This type of brain organization has been claimed for the cerebellum, for various sub-cortical structures, including the basal ganglia, and for certain cortical regions, in particular in frontal cortex (Alexander, DeLong, & Strick, 1986; Middleton & Strick, 2000a; Shimamura, 1995). This suggests that analogous computations may underlie a range of cognitive domains, including language. Second, commonalities between language and non-language domains are not surprising from an evolutionary perspective, given the well-established pattern that biological structures tend to evolve from already-existing structures (Maynard Smith, 1975/1993; Mayr, 1963).

So, whether or not there are aspects of the neurocognition of language that are unique to this faculty and to our species, much and perhaps most aspects of language are likely to *not* be unique. Importantly, other cognitive domains are much better understood than language in a number of respects, including their neuroanatomy, physiology, biochemistry, evolution, development, and neural computation. This follows from the fact that most other domains have benefited from the development of animal models which allow for invasive and highly informative techniques that are not permissible to perform on humans.

A reasonable research program would thus be to identify domains that share commonalities with language: their underlying neural and computational systems will be promising candidates for those subserving language. Importantly, if the systems underlying the target domains are well understood, they should yield clear predictions about language, based solely on non-language theories and data. This should provide far greater predictive power about language than research restricted to language, whose theories and predictions are generally if not always derived from evidence solely related to language itself. Since the research tools we have at our disposal to understand language are quite impoverished compared to those available for the investigation of other domains, a research program limited to language necessarily restricts language theories and their predictions. In contrast, theories that are motivated by non-language domains as well as language have a much wider potential predictive range for language, and thus are likely to lead to important advances in our understanding of this faculty. This should be particularly likely for areas of research that have been given greater attention in non-language than language domains, such as functional neuroanatomy, physiology, biochemistry,

neuroendocrinology, and pharmacology. Importantly, the converse holds as well. That is, our understanding of many aspects of the representation, computation, and processing of language has progressed far beyond that of many other cognitive domains. So, the demonstration of neurocognitive links between language and other domains should also improve our understanding of the latter. Note that I am *not* arguing that research programs directed solely at language should be replaced by those examining language in the context of other cognitive domains. Rather I am maintaining that the latter type of research program must crucially complement the former.

It is in this general spirit that my colleagues and I have proposed and explored the declarative/procedural (DP) model of language (Ullman, 2001a,c; Ullman et al., 1997). The basic premise of the DP model is that important aspects of the distinction between the mental lexicon and the mental grammar in language are tied to the distinction between declarative and procedural memory – two memory systems which have been implicated in non-language functions in humans and other animals (Eichenbaum & Cohen, 2001; Mishkin, Malamut, & Bachevalier, 1984; Schacter & Tulving, 1994; Squire & Knowlton, 2000). That is, lexical memory depends largely on the declarative memory system, whereas aspects of grammar depend on the procedural memory system. Importantly, multiple characteristics of these two systems, including their computational, neuro-anatomical, physiological and biochemical substrates, have been quite well studied, and thus should lead to important predictions about language.

2. Lexicon and grammar

Language depends upon a memorized “mental lexicon” and a computational “mental grammar” (Chomsky, 1965, 1995; de Saussure, 1959; Pinker, 1994).¹ The mental lexicon is a repository of all idiosyncratic word-specific information. Thus, it includes all words whose phonological forms and meanings cannot be derived from each other (i.e. their sound–meaning pairings are arbitrary), such as the non-compositional (“simple”) word *cat*. It also contains other irregular—i.e. not entirely derivable—word-specific information, such as the particular arguments that must accompany a given verb (e.g. *hit* takes a direct object), and any unpredictable forms that a word takes (e.g. *teach* takes the irregular past-tense *taught*). The mental lexicon may comprise other distinctive information as well, smaller or larger than words: bound morphemes (e.g. the *-ed* or *-ness* suffixes, as in *walked* or *happiness*), and representations of complex linguistic structures whose meanings cannot be transparently derived from their parts (e.g. idiomatic phrases, such as *kick the bucket*).

¹ A terminological distinction must be made between the notion of a “mental lexicon”, which is simply a storage place, and the way the term “lexicon” is often used in linguistic theories. Most linguistic theories assume an organization in which syntactic computations draw words from the “lexicon” (Anderson, 1992; Chomsky, 1965, 1970; Di Sciullo & Williams, 1987; Jackendoff, 1997; Lieber, 1992). However, the nature of this “linguistic” lexicon is controversial, as to whether it is a simple storage place (the mental lexicon) or whether, in addition, rule-based computations are carried out there (Anderson, 1992; Chomsky, 1970; Di Sciullo & Williams, 1987; Lieber, 1992; Spencer, 1991). In this paper the term “lexicon” is used solely to refer to the “mental lexicon”—that is, a repository of stored information.

Many regularities can also be found in language. These regularities can be captured by rules of grammar. The rules constrain how lexical forms and abstract symbols or features (e.g. *walk*, *-ed*, *Verb*, *Past-Tense*) can combine to make complex representations. The rules crucially allow us to interpret the meanings of complex forms even if we have not heard or seen them before. Thus, in the sentence “*Clementina glicked the plag*”, we know that Clementina did something in the past to some entity. The rules specify not only the sequential order (precedence) of lexical items, but also their hierarchical relations, e.g. that a verb phrase (*glicked the plag*) can contain a noun phrase (*the plag*). Such rule-governed behavior is found at various levels in language, including in the structure of phrases and sentences (syntax), and of complex words such as *walked* or *glicked* (morphology). Importantly, the rules and constraints are a type of mental knowledge in that they underlie our individual mental capacity to produce and comprehend complex forms. It is often argued that aspects of the ability to learn, represent and compute the rules and constraints that underlie grammar depend on innately-specified mental constructs (Chomsky, 1995). The learning of grammatical knowledge, and the knowledge itself, are generally not available to conscious access (Fodor, 1983); that is, they are implicit. It has been argued that grammatical processing is not influenced by other cognitive domains; that is, the underlying system is “straight-through”, or “informationally encapsulated” (Fodor, 1983; Frazier & Fodor, 1978). Moreover, at least certain aspects of grammatical processing are fast as well as automatic, in that they are not under conscious control but are rather triggered by the linguistic stimulus (Fodor, 1983; Friederici, 2002).

The two language capacities interact in a number of ways. First, the grammar combines lexical items into complex structures. Second, even though certain representations of complex linguistic structures that have idiosyncratic meanings (e.g. idioms) may be stored in the lexicon, their structures still generally follow the rules of grammar. Third, although “regular” (i.e. transparent; derivable) complex representations (e.g. *walked*; *the cat*) could be computed anew each time they are used (e.g. *walk* + *-ed*), and must be if they are new (e.g. *glicked*), they could in principle also be stored in the mental lexicon after being encountered. Finally, a general pattern observed in languages is that idiosyncratic, exceptional forms and meanings are selected preferentially over general, derivable ones (the “Elsewhere” principle; Halle & Marantz, 1993; Kiparsky, 1982; Pinker, 1984), suggesting that stored lexical items take precedence over those composed by the mental grammar.

3. Declarative and procedural memory

The declarative and procedural memory systems have been intensively studied in humans and in several animal models, including monkeys and rodents. The demonstration of numerous double dissociations has shown that the two systems are largely independent from each other, though they interact in a number of ways (Eichenbaum & Cohen, 2001; Mishkin et al., 1984; Poldrack & Packard, 2003; Schacter & Tulving, 1994; Squire & Knowlton, 2000). As will be seen, the two memory systems share a number of characteristics with the two language capacities. Importantly, research has begun to elucidate the specific computational, developmental, anatomical, cellular, molecular and

other aspects of these two systems across species. These findings lead to highly specific predictions about language.

3.1. *Declarative memory*

The “declarative” memory system (Eichenbaum & Cohen, 2001; Mishkin et al., 1984; Schacter & Tulving, 1994; Squire & Knowlton, 2000) has been implicated in the learning, representation, and use of knowledge about facts (“semantic knowledge”) and events (“episodic knowledge”). It is important for the very rapid learning (e.g. based on a single stimulus presentation) of arbitrarily-related information – that is, for the associative binding of information (Cohen, Poldrack, & Eichenbaum, 1997; Eichenbaum & Cohen, 2001; Squire & Knowlton, 2000). It has been argued that the information learned by this system is not informationally encapsulated, being accessible to multiple mental systems (Squire & Zola, 1996). Moreover, at least part of this knowledge can be consciously (“explicitly”) recollected.

Declarative memory depends, first of all, on medial temporal lobe structures: the hippocampal region (the dentate gyrus, the subicular complex, and the hippocampus itself), entorhinal cortex, perirhinal cortex, and parahippocampal cortex (Squire & Knowlton, 2000; Suzuki & Eichenbaum, 2000). The hippocampus projects to midline diencephalic nuclei, in particular the mammillary bodies and portions of the thalamus. These structures also play an important role in declarative memory, though they are less well studied than the medial-temporal lobe. The medial temporal structures are hierarchically organized: evidence from non-human primates indicates that the hippocampal region is heavily connected with entorhinal cortex, which is strongly connected with both the perirhinal and parahippocampal cortices, which are in turn connected extensively with temporal and parietal neocortical regions (Suzuki & Amaral, 1994).

The medial-temporal complex appears to subserve several related memory functions, including the encoding, consolidation and retrieval of new memories (Buckner & Wheeler, 2001; Eichenbaum & Cohen, 2001; Squire & Knowlton, 2000). Memories eventually (in humans, over months to years) become largely independent of the medial temporal lobe structures, and dependent upon neocortical regions, particularly in the temporal lobes (Hodges & Patterson, 1997; Squire, Clark, & Knowlton, 2001). Different regions of the temporal lobes may be specialized for different types of knowledge (Damasio, Grabowski, Tranel, Hichwa, & Damasio, 1996; Martin, Ungerleider, & Haxby, 2000). It has been posited that medial temporal lobe structures associate or “bind” inputs from cortical regions, which together store an entire memory (Alvarez & Squire, 1994; McClelland, McNaughton, & O'Reilly, 1995).

The term “declarative memory system” is used here to refer to the entire system involved in the learning, representation and use of the relevant information (Eichenbaum, 2000), not just to those brain structures underlying the learning of new memories. Indeed, other brain structures also play a role in this system, although the precise regions and functions are still not entirely clear. First of all, prefrontal regions have been implicated in numerous studies (Buckner & Wheeler, 2001; Tulving, Kapur, Craik, Moscovitch, & Houle, 1994). Ventrolateral prefrontal cortex (VL-PFC), which corresponds to the inferior frontal gyrus and Brodmann's areas (BA) 44, 45 and 47 (Damasio, 1995), plays a role in the encoding of

new memories and the selection or retrieval of declarative knowledge (Buckner & Wheeler, 2001; Thompson-Schill, D'Esposito, Aguirre, & Farah, 1997; Wagner et al., 1998). Two functionally and anatomically distinct sub-regions have been implicated: posterior/dorsal inferior frontal cortex (BA 6/44) is strongly implicated in aspects of phonology, whereas anterior/ventral inferior frontal cortex (BA 45/47) is more important for semantics (Fiez, 1997; Poldrack, Wagner et al., 1999). Their precise roles may be closely related to working memory (Buckner & Wheeler, 2001; Moscovitch, 1992). Indeed, neuroimaging studies show that VL-PFC is consistently activated in working memory tasks (Smith & Jonides, 1999), and, within the same subjects, in both retrieval and working memory tasks (Braver et al., 2001). Additionally, anterior frontal-polar cortex (BA 10) is implicated in the retrieval of memories, or in the monitoring of that retrieval (Buckner & Wheeler, 2001). This area is also associated with working memory (Braver et al., 2001; McLeod, Plunkett, & Rolls, 1998). Finally, evidence suggests that portions of the cerebellum are involved in searching, retrieving or otherwise processing declarative memories (Desmond & Fiez, 1998; Ivry & Fiez, 2000).

The declarative memory system is closely related to the "ventral" stream system (Goodale & Milner, 1992; Ungerleider & Mishkin, 1982). This system is rooted in inferior and lateral temporal-lobe structures. It underlies the formation of perceptual representations of objects and their relations. These representations underlie the recognition and identification of objects and the long-term storage of knowledge about objects (Goodale, 2000). The ventral system is thus a memory-based system, feeding representations into long-term (declarative) memory, and comparing those representations with new ones. It has also been argued that humans are conscious of aspects of ventral stream functioning (Norman, 2002).

The declarative memory system has been intensively studied not only at functional and neuroanatomical levels, but also at cellular and molecular levels (Curran, 2000; Lynch, 2002). Acetylcholine in particular plays an important role in declarative memory and hippocampal function (Freo, Pizzolato, Dam, Ori, & Battistin, 2002; Packard, 1998). Thus, levels of choline acetyl transferase, the synthesizing enzyme for acetylcholine, correlate with declarative memory abilities (Baskin et al., 1999). Pharmacological manipulations of the cholinergic system in normal, healthy adults have also implicated acetylcholine in declarative memory (Nissen, Knopman, & Schacter, 1987; Rammsayer, Rodewald, & Groh, 2000). For example, acetylcholine esterase inhibitors, which prolong the activity of acetylcholine at the synapse, improve declarative memory (Ballard, 2002; Hammond, Meador, Aung-Din, & Wilder, 1987).

Evidence also suggests that the declarative memory system is affected by estrogen (Phillips & Sherwin, 1992; Sherwin, 1988), perhaps via the modulation of acetylcholine (Packard, 1998; Shughrue, Scrimo, & Merchenthaler, 2000). Declarative memory abilities and medial temporal-lobe function are linked to estrogen, via organizational effects in utero, and/or activational effects later on. Estrogen improves declarative memory in women (Maki & Resnick, 2000; Sherwin, 1998) and men (Kampen & Sherwin, 1996; Miles, Green, Sanders, & Hines, 1998), and strengthens the cellular and molecular correlates of long-term hippocampal learning (McEwen, Alves, Bulloch, & Weiland, 1998; Woolley & Schwartzkroin, 1998). Testosterone, which is the main source of estrogen in men, also improves their memory (Cherrier et al., 2001). Women with Turner's

syndrome, who do not produce estrogen, have worse declarative memory (which improves with estrogen therapy; Ross, Roeltgen, Feuillan, Kushner, & Cutler, 2000) and smaller hippocampi than control subjects (Murphy et al., 1993). During declarative memory tasks, increased estrogen (i.e. hormone replacement therapy) in healthy post-menopausal women leads to greater blood flow activation changes in medial temporal lobe regions, including the hippocampus (Maki & Resnick, 2000; Resnick, Maki, Golski, Kraut, & Zonderman, 1998).

3.2. *Procedural memory*

The “procedural memory” system (Eichenbaum & Cohen, 2001; Mishkin et al., 1984; Schacter & Tulving, 1994; Squire & Knowlton, 2000) subserves the learning of new, and the control of established, sensori-motor and cognitive “habits”, “skills”, and other procedures, such as riding a bicycle and skilled game playing. The system is commonly referred to as an “implicit memory system” because both the learning of the knowledge, and the knowledge itself, are generally not available to conscious access. Note that I use the term “procedural memory” to refer *only* to one type of implicit, non-declarative, memory system (Squire & Knowlton, 2000), *not* all non-declarative or implicit memory systems. Moreover, and analogously to how I use the term “declarative memory”, the term “procedural memory” is used here to refer to the entire system involved in the learning, representation and use of the relevant knowledge, not just to those parts of the system underlying the learning of new memories.

Although procedural memory is less well understood than declarative memory, its functional characteristics and neural bases are beginning to be revealed. Functionally, the system may be characterized as subserving aspects of the learning and processing of context-dependent stimulus-response rule-like relations (Knowlton, Mangels, & Squire, 1996; Packard & Knowlton, 2002; Poldrack, Prabhakaran, Seger, & Gabrieli, 1999; White, 1997; Wise, Murray, & Gerfen, 1996). The system seems to be especially important for learning and processing these relations in the context of real-time sequences – whether the sequences are serial or abstract, or sensori-motor or cognitive (Aldridge & Berridge, 1998; Boecker et al., 2002; Doyon et al., 1997; Graybiel, 1995; Howard & Howard, 1997; Saint-Cyr, Taylor, & Lang, 1988; Willingham, 1998). Learning in the system is gradual, in that it occurs on an ongoing basis during multiple presentations of stimuli and responses – unlike the fast learning subserved by the declarative memory system. The relations are rule-like in that they are rigid, inflexible, and not influenced by other mental systems (Mishkin et al., 1984; Squire & Zola, 1996). Thus, this system, unlike declarative memory, appears to be informationally encapsulated (Squire & Zola, 1996). The rules apply quickly and automatically, in that the response is triggered by the stimulus rather than being under conscious control. The procedural system plays a role not only in learning and processing new sequences but also in the coordination of innate ones, such as “grooming sequences” in rodents, which follow a stereotyped sequence of “syntactic chains” that combine up to dozens of actions into a predictable order (Aldridge & Berridge, 1998). Intriguingly, although fixed linear sequences and possibly probabilistic sequences can be learned by monkeys, apes and humans, hierarchical structure is apparently commonly used and easily learned only by humans, though it has been observed in apes (Conway & Christiansen, 2001).

The procedural memory system is composed of a network of brain structures. The system is rooted in frontal/basal-ganglia circuits, with a likely role for portions of parietal cortex, superior temporal cortex and the cerebellum (De Renzi, 1989; Heilman, Watson, & Rothi, 1997; Hikosaka et al., 2000; Mishkin et al., 1984; Rizzolatti, Fogassi, & Gallese, 2000; Schacter & Tulving, 1994; Squire & Zola, 1996).

The basal ganglia are a set of sub-cortical structures, including the neostriatum, globus pallidus, sub-thalamic nucleus, and substantia nigra (Wise et al., 1996). In primates the neostriatum is composed of two structures: the putamen and the caudate nucleus. The putamen is particularly important for motor functions, whereas the caudate appears to underlie aspects of cognition (Alexander et al., 1986; Middleton & Strick, 2000a). Dorsal aspects of these structures (the dorsal striatum) play an important role in procedural memory, whereas ventral aspects (the ventral striatum) may be more important in affective (emotional) memory (Packard & Knowlton, 2002). The basal ganglia have been implicated in a number of functions, including implicit procedural learning in general (Eichenbaum & Cohen, 2001; Mishkin et al., 1984; Schacter & Tulving, 1994; Squire & Knowlton, 2000); stimulus-response learning (Packard & Knowlton, 2002; White, 1997), in particular of egocentric (body-centered) sensori-motor relations (White, 1997); probabilistic rule learning (Knowlton et al., 1996; Poldrack, Prabhakaran et al., 1999); sequence learning (Aldridge & Berridge, 1998; Boecker et al., 1998; Doyon et al., 1997; Graybiel, 1995; Peigneux et al., 2000; Willingham, 1998); reinforcement learning (in the dorsal striatum; cf. reward-based, in the ventral striatum) (Doya, 2000; Packard & Knowlton, 2002; White, 1997); real-time motor planning and control (Wise et al., 1996), particularly that which involves precise timing (Penhune, Zattore, & Evans, 1998) and the selection or switching among multiple motor programs (Haaland, Harrington, O'Brien, & Hermanowicz, 1997); mental rotation (Podzebenko, Egan, & Watson, 2002); interval timing and rhythm (Meck & Benson, 2002; Schubotz & von Cramon, 2001); and the context-dependent rule-based selection (Peigneux et al., 2000; Wise et al., 1996) and maintenance in working memory (Menon, Anagnoson, Glover, & Pfefferbaum, 2000) of and the real-time shifting (of attention, or focus) between sets, functions or programs. Importantly, these apparently disparate functions appear to be quite intimately related (Meck & Benson, 2002; Wise et al., 1996), although the precise nature of their relations and interactions are not yet understood.

The basal ganglia, in particular the neostriatum, receive input projections from multiple cortical areas, especially in frontal cortex, but also from other structures, including the medial temporal lobe (Alexander & Crutcher, 1990; Middleton & Strick, 2000b; Wise et al., 1996). The basal ganglia send outputs via the thalamus to neocortex, largely in frontal regions (Middleton & Strick, 2000b). The basal ganglia structures themselves are highly interconnected. Perhaps most importantly, the neostriatum projects to both the "direct" and the "indirect" pathways within the basal ganglia. The two pathways have opposing effects on the basal ganglia's outputs to frontal cortex via the thalamus. The direct pathway inhibits, whereas the indirect pathway disinhibits, the *inhibitory* projections from the basal ganglia to the thalamus. Thus, the direct pathway ultimately results in the *disinhibition*, and the indirect pathway in the *inhibition*, of the excitatory projections from thalamus to frontal cortex. So, frontal cortical activity is disinhibited by the direct pathway, and inhibited by the indirect pathway. The posited selection and set

shifting functions of the basal ganglia may be attributed to the interaction between the direct and indirect pathways: a given cortical “set” or “program” can be disinhibited, while the rest are inhibited (Young & Penney, 1993). Imbalances between the two pathways can lead to the excessive inhibition or disinhibition of the functions that depend on the frontal cortical regions to which the basal ganglia project. This is thought to explain the inhibited/suppressed and disinhibited/unsuppressed motor and other behaviors found in Parkinson’s, Huntington’s and other diseases affecting the basal ganglia (Young & Penney, 1993). The two pathways are modulated by dopaminergic projections from the substantia nigra to the neostriatum. Indeed, it is this bundle of neurons which degenerates in Parkinson’s disease. These nigrostriatal dopaminergic neurons appear to have a role not only in the real-time modulation of the direct and indirect pathways, but also in the reinforcement learning functions of the basal ganglia, specifically in memory consolidation (Doya, 2000; Packard & Knowlton, 2002; White, 1997).

Importantly, the various connections within the basal ganglia contain parallel and largely functionally segregated “circuits” (i.e. channels) (Alexander & Crutcher, 1990; Alexander et al., 1986; Middleton & Strick, 2000a,b). Each circuit receives projections at the neostriatum – some circuits primarily at the caudate, others at the putamen – from a particular set of cortical and sub-cortical structures. Each circuit then follows the split between the direct and indirect pathways, and projects via the thalamus to a particular cortical region, largely in frontal cortex. This cortical output area in turn projects back to the portion of the neostriatum that receives inputs for that circuit. Thus, there is at least in part a closed loop with feedback. For example, a basal ganglia “motor circuit” projects to frontal motor areas, a “prefrontal” circuit projects to prefrontal regions, and other circuits project to other frontal areas. The different basal ganglia circuits have similar synaptic organizations, suggesting that similar neuronal operations might be performed at comparable stages of each circuit (Alexander, Crutcher, & DeLong, 1990; Middleton & Strick, 2000b). Thus, the various parallel circuits of the basal ganglia seem to perform analogous computations; these are applied to different sets of information from different domains, depending on the particular set of input regions and frontal cortical output destinations of a given circuit (Middleton & Strick, 2000b). So, if the basal ganglia play a role in grammar, that role should be computationally analogous to that which the structures play in other domains, with the grammar-subserving circuits possibly projecting to somewhat different frontal cortical regions (e.g. in Broca’s area) than other circuits.

Certain frontal cortical regions are also critical for procedural memory, in a manner which seems to be closely related to the functions of the basal ganglia. In the macaque, the basal ganglia project via the thalamus to pre-motor regions, including the supplementary motor area (SMA) and the general region of area F5 (Middleton & Strick, 2000a,b). F5 is a well-studied ventral pre-motor region that is a likely homologue of human BA 44 in Broca’s area (Rizzolatti, Fadiga, Gallese, & Fogassi, 1996) (Broca’s area is defined here as a portion of human inferior frontal cortex, including and perhaps limited to cortex corresponding to BA 44 – pars opercularis – and BA 45 – pars triangularis; Amunts et al., 1999). Each of these frontal regions plays an important role in the procedural memory system.

First of all, pre-motor regions (Harrington et al., 2000; Jenkins, Brooks, Nixon, Frackowiak, & Passingham, 1994), including SMA (Jenkins et al., 1994) and pre-SMA

(rostral SMA) (Boecker et al., 1998; Hikosaka et al., 1996), are implicated in motor sequence learning in humans. Motor sequence learning in macaques also depends on SMA and pre-SMA (Hikosaka et al., 2000). Lateral pre-motor cortex and SMA are also involved in mental rotation (Jordan, Heinze, Lutz, Kanowski, & Jancke, 2001; Kosslyn, Di, Thompson, & Alpert, 1998; Podzebenko et al., 2002), and lateral pre-motor and pre-SMA regions are implicated in aspects of timing or rhythm (Schubotz & von Cramon, 2001).

Broca's area is another critical component of the procedural memory system. Evidence suggests that motor sequence learning depends on left inferior frontal cortex (Peigneux et al., 1999), including Broca's area (Conway & Christiansen, 2001; Dominey, Hoen, Blanc, & Lelekov-Boissard, *in press*), and its right homologue (Doyon, Owen, Petrides, Sziklas, & Evans, 1996). Broca's area in humans seems particularly important for learning sequences which contain abstract and potentially hierarchical structure, as opposed to fixed linear sequences (Conway & Christiansen, 2001; Dominey et al., 2003; Goschke, Friederici, Kotz, & van Kampen, 2001). Broca's area has also been implicated in mental rotation tasks (Jordan et al., 2001; Podzebenko et al., 2002), the processing of non-motor sequences, including musical sequences (Maess, Koelsch, Gunter, & Friederici, 2001), and sequences of phonological material in working memory (Smith & Jonides, 1999). A recent study suggests that the manipulation of sequential information engages posterior Broca's area, independent of the type of information that is manipulated (Gelfand & Bookheimer, 2003). More generally, evidence suggests a close link between working memory and sequence learning and processing. These two functions share much of their circuitry: like sequence learning and processing, working memory involves Broca's area, SMA, and other pre-motor regions (Ivry & Fiez, 2000; Smith & Jonides, 1999), as well as regions in other structures (see below). It has been suggested that Broca's area, and perhaps VL-PFC more generally, may subserve particular functions that are important for working memory, including the selection and comparison of maintained information (Petrides, 1996; Petrides, Alivisatos, & Evans, 1995), or the maintenance of information over a delay (D'Esposito et al., 1998; Smith & Jonides, 1997). Similarly, it has been argued that the role of this region in working memory is to recall or select and maintain information that is actually stored in temporal and temporo-parietal regions (Cowan, 1999; Ruchkin, Grafman, Cameron, & Berndt, *in press*). These functions appear to be closely related to the role of this region in the selection of declarative knowledge (see above). The functions also appear to be related to the view that frontal cortex underlies the inhibition of, excitation of, and switching between (and possibly learning of) sets, programs and rules (Knight & Grabowecky, 2000; Shimamura, 1995; Wise et al., 1996), and the inhibitory and excitatory control of posterior brain regions (Knight & Grabowecky, 2000; also see Passingham, 1993). It has additionally been suggested that these attentional set shifting and sequence coordination roles may depend upon the timing functions of frontal cortex (Knight & Grabowecky, 2000; Meck & Benson, 2002; Wise et al., 1996). Indeed, Broca's area also appears to play an important role in timing and rhythm (Fiez et al., 1995; Schubotz & von Cramon, 2001; Szelag, von Steinbüchel, & Poppel, 1997).

Within Broca's area, BA 44 plays an especially important role in a number of the functions described above. This region is also implicated in the observation of motor skills, and in the mental imagery of motion (Binkofski et al., 2000; Rizzolatti & Arbib,

1998; Rizzolatti et al., 2000). Intriguingly, F5 – the monkey homologue of BA 44 – contains “mirror neurons”, which fire not only at the execution of particular learned sequential motor skills (i.e. each neuron discharges with specific goal-oriented movement sequences), but also during the observation of (and even the sound of) the same action sequences (Kohler et al., 2002; Rizzolatti, Fogassi, & Gallese, 2001). Evidence suggests that human BA 44 also has this mirror function (Rizzolatti et al., 2001). It has been suggested that in humans such neurons may play a role in language, in particular in language comprehension (Rizzolatti & Arbib, 1998).

Portions of parietal cortex also play an important role in the procedural system. Anatomical studies of macaques show that parietal cortex projects heavily to, and reciprocally receives projections from, frontal cortex, with specific parietal regions connecting to specific frontal regions (Petrides & Pandya, 1984; Wise, Boussaoud, Johnson, & Caminiti, 1997). Macaque area F5, which corresponds to the BA 44 area in humans (see above), receives strong input from a number of parietal regions (Matelli, Camarda, Glickstein, & Rizzolatti, 1986; Petrides & Pandya, 1984), especially macaque area AIP (Gallese, Fogassi, Fadiga, & Rizzolatti, 2001; Matelli, Luppino, Murata, & Sakata, 1994) – which is a probable homologue of human anterior intraparietal sulcus (Culham & Kanwisher, 2001) – and macaque area PF (also referred to as area 7b) (Matelli et al., 1986; Petrides & Pandya, 1984; Rizzolatti, Luppino, & Matelli, 1998) – which is likely homologous to the human anterior inferior parietal lobule (supramarginal gyrus; BA 40) (Nishitani, Uutela, Shibasaki, & Hari, 1999), or possibly to part of the superior parietal lobule (BA 7) (Culham & Kanwisher, 2001; Milner, 1996).

In monkeys, AIP neurons discharge during hand movements, with the majority of neurons preferring specific types of hand grips (Sakata, Taira, Mine, & Murata, 1992). AIP neurons also contains neurons that are tuned to the specific shapes to be grasped (Sakata & Taira, 1994). Similarly, AIP's human homologue, the anterior intraparietal sulcus, is activated during visually-guided grasping (Binkofski et al., 1998; Faillenot, Toni, Decety, Gregoire, & Jeannerod, 1997) and reaching (Culham & Kanwisher, 2001), by the physical manipulation of objects (Binkofski et al., 1999), by mental rotation (Harris et al., 2000; Podzebenko et al., 2002), by the observation of hand movements made by others (Iacoboni et al., 1999), and by passively looking at manipulable objects, namely tools (Chao & Martin, 2000).

Monkey area PF is connected not only with frontal area F5, but also with parietal area AIP (Nishitani et al., 1999). Area PF is related to hand manipulation and eye movements, and may code the orientation of body parts (Nishitani et al., 1999). Like frontal area F5, area PF contains mirror neurons (Gallese et al., 2001; Rizzolatti et al., 2001). Human superior parietal lobule (BA 7), one possible homologue of PF, is strongly related to attention (Perry & Zeki, 2000). Human inferior parietal lobule, and the supramarginal gyrus (BA 40) in particular, another likely homologue of PF, has been implicated in a number of functions, including attention (Perry & Zeki, 2000), mental rotation (Harris et al., 2000; Podzebenko et al., 2002), and the execution and recognition of motor skills (Heilman et al., 1997). According to one view, inferior parietal regions may serve as a repository of stored knowledge of motor skills, including information of stored sequences (Heilman et al., 1997). This region has also been strongly implicated in phonological processing, including in working memory tasks (Ivry & Fiez, 2000).

Intriguingly, circumscribed portions of the temporal lobes also appear to play a role in the procedural memory system. In macaques neurons that respond to the observation of movement, though *not* to movement itself (that is, they are not mirror neurons), are found in the anterior superior temporal sulcus – a region which is connected to both frontal area F5 and parietal area PF (Rizzolatti et al., 2001). In humans, superior temporal regions in more posterior areas, including the superior temporal sulcus, have been implicated in the storage of information about motion, in contrast to more ventral temporal regions, which appear to underlie the storage of information about visual form (Martin et al., 2000).

The cerebellum has traditionally been implicated in the coordination of skilled movement and in the control of balance, as well as in motor learning (Ivry & Fiez, 2000). More recent evidence suggests that portions of the cerebellum subserve procedural memory, in particular in motor sequencing (Desmond & Fiez, 1998; Eichenbaum & Cohen, 2001; Hikosaka et al., 2000; Ivry & Fiez, 2000; Mostofsky, Goldberg, Landa, & Denckla, 2000; Squire & Knowlton, 2000). Some evidence suggests that the cerebellum may be involved in the modification of performance of learned sequences, rather than in the learning of those sequences (Seidler et al., 2002). Within the cerebellum, the dentate nucleus (Hikosaka et al., 2000) as well as portions of the cerebellar hemispheres and the vermis (Desmond & Fiez, 1998) play important roles in learning procedures, especially of motor sequences. The cerebellar hemispheres and vermis, especially regions at least partly overlapping those that also underlie sequence learning, have also been implicated in verbal working memory and in the retrieval or search of information from declarative memory (Desmond & Fiez, 1998). The cerebellum has additionally been implicated in imaged hand movements and in mental rotation (Ivry & Fiez, 2000; Podzebenko et al., 2002). The cerebellum has important timing functions, and seems to be involved in mental coordination and the control of attention, and in error detection and error-based learning (Doya, 2000; Ivry & Fiez, 2000). Studies of macaques have shown that, analogously to the basal ganglia, the cerebellum projects via the thalamus to frontal cortex, with each cerebellar region projecting (via the thalamus) to particular frontal regions. Intriguingly, in macaques the dentate nucleus projects via the thalamus to ventral pre-motor cortex (Middleton & Strick, 2000a), suggesting that in humans it might project to BA 44 in Broca's area.

The procedural system, and parietal cortex in particular, is closely related to the "dorsal" stream system (Goodale & Milner, 1992; Ungerleider & Mishkin, 1982). This system is rooted in posterior parietal structures, and the frontal pre-motor regions to which they are heavily connected. The system underlies the transformation of visual information into an egocentric framework that enables the execution of motor programs, such as grasping and otherwise manipulating an object. It has been argued that the main function of this system is the analysis of visual input for visually-guided motor behavior.

3.3. Interaction of the two memory systems

The declarative and procedural memory systems interact in a number of ways. In sum, together the systems form a dynamically interacting network which yields both cooperative and competitive learning and processing, such that memory function may be optimized (Poldrack & Packard, 2003).

First, brain structures which underlie procedural memory also perform context-dependent selection and maintenance (in working memory) of knowledge stored in declarative memory. Note that it is only a terminological issue as to whether we consider these structures to be part of the procedural system which plays a role in declarative memory, or vice versa, or simply (and most reasonably) brain structures that play particular roles in both systems.

Second, although there appear to be striking separations of function among the different brain areas involved in the two brain systems, it does not appear to be the case that all parts of each lobe subserve only one or the other system. In particular, we have seen that superior aspects of the temporal lobe may play some function in the procedural system, perhaps as a storage repository of procedural knowledge, and that the same or nearby areas of VL-PFC play related roles in declarative and procedural memory.

Third, the two systems can complement each other in acquiring the same or analogous knowledge, including knowledge of sequences. As was initially shown in patient H.M., the declarative memory system need not be intact for the procedural memory system to learn (Corkin, 1984; Eichenbaum & Cohen, 2001; Squire & Knowlton, 2000). However, when both systems are undamaged they can complement each other. Thus, in motor sequence learning in humans, both systems can be used cooperatively to learn the task, optimizing learning in some cases (Willingham, 1998). When the declarative memory system is able to acquire knowledge, it may do so initially, thanks to its rapid learning abilities, while the procedural system gradually learns the same or analogous knowledge (Packard & McGaugh, 1996; Poldrack & Packard, 2003). Note that if a given sequence that is normally learned and processed by the procedural system is memorized in declarative memory, its structure will likely be constrained by the rules governing the sequence in procedural memory. Interestingly, the time-course of this shift from declarative to procedural memory can be modulated pharmacologically (Packard, 1999).

Fourth, animal and human studies suggest that the two systems can also interact competitively (for reviews, see Packard & Knowlton, 2002; Poldrack & Packard, 2003). This leads to what one might call a “see-saw effect”, such that a dysfunction of one system leads to *enhanced* learning in the other, or that learning in one system depresses functionality of the other. Animal studies show that damage to medial-temporal lobe structures, including the hippocampus, can enhance basal-ganglia-based procedural learning (McDonald & White, 1993; Packard, Hirsh, & White, 1989; Schroeder, Wingard, & Packard, 2002). Conversely, damage to the neostriatum in the basal ganglia can facilitate learning in declarative memory (Mitchell & Hall, 1988). A similar pattern has been found in human lesion (Halbig et al., 2002) and neuroimaging studies (Dagher, Owen, Boecker, & Brooks, 2001; Jenkins et al., 1994; Poldrack & Packard, 2003; Poldrack et al., 2001; Poldrack, Prabhakaran et al., 1999).

The see-saw effect may be explained by a number of factors. In rodents there are direct anatomical projections from the medial temporal lobe (entorhinal cortex) to the dorsal striatum (Sorensen & Witter, 1983). Stimulation of both entorhinal and hippocampal neurons leads to mainly inhibitory responses in both the dorsal and ventral striatum (Finch, 1996; Finch, Gigg, Tan, & Kosoyan, 1995). Conversely, stimulation of the caudate (in cats) reduces the occurrence of hippocampal spikes (La Grutta & Sabatino, 1988; Sabatino, Ferraro, Liberti, Vella, & La, 1985). Several studies have suggested that lesions

to the hippocampus can result in increased dopamine transmission in the portion of the striatum to which the hippocampus projects (Jaskiw, Karoum, & Weinberger, 1990; Lipska, Jaskiw, Chrapusta, Karoum, & Weinberger, 1992). Neurochemically, acetylcholine appears to play a role in the interaction (Packard & Knowlton, 2002), perhaps by enhancing function of the hippocampus (see above), which could in turn inhibit function of the striatum via the projections described above. Moreover, acetylcholine can also directly inhibit the function of the neostriatum (Calabresi, Centonze, Gubellini, Pisani, & Bernardi, 2000). Because acetylcholine function can be enhanced by estrogen, particularly in the hippocampus (see above), it is plausible that estrogen may also contribute to the see-saw effect.

A recent and quite elegant series of neuroimaging experiments of healthy adults nicely demonstrates interactions between the two brain memory systems (Poldrack et al., 2001; Poldrack, Prabhakaran et al., 1999). Procedural learning – probabilistic rule learning – was shown to yield not only activation in the caudate nucleus, but also *deactivation* in the medial temporal lobe. Moreover, across subjects, the degree of activity in the caudate nucleus correlated negatively with the degree of activity in the medial temporal lobe. That is, subjects with higher caudate activity had lower medial-temporal activity, and vice versa. This suggests that individuals vary with respect to their relative dependence on the two systems. Moreover, this relationship changed over the course of learning. During early training the medial temporal lobe structures were activated while the caudate was not, whereas as learning progressed, the medial temporal structures became deactivated, while caudate activation increased. These experiments suggest some sort of competitive interaction between the two systems. Moreover, they strengthen the view that early in learning declarative memory can play a particularly important role compared to procedural learning, and that over time this balance shifts to the opposite direction. Thus, with increased dependence on procedural memory for a given function, there may be a decreased dependence on declarative memory, even if that system played a role initially in the same function. As we will see below, evidence suggests a similar pattern in language learning.

4. The declarative/procedural model

We have seen above that there are a number of striking commonalities between the functional characteristics of grammar/lexicon on the one hand, and of declarative/procedural (DP) memory and their underlying brain structures on the other. These commonalities lead to the basic claim of the DP model: the brain systems which subserve declarative and procedural memory play analogous roles in language as in their non-language functions. So, the DP model predicts common or related computational, processing, anatomic, physiological and biochemical substrates for the language and non-language functions.

4.1. The lexical/declarative memory system

According to the DP model, the brain system underlying declarative memory also underlies the mental lexicon. This system subserves the acquisition, representation and use not only of knowledge about facts and events, but also about words. It stores all arbitrary, idiosyncratic word-specific knowledge, including word meanings, word sounds, and

abstract representations such as word category. It includes, among other things, representations of simple (non-derivable) words such as *cat*, bound morphemes such as the past-tense suffixed *-ed*, “irregular” morphological forms, verb complements, and idioms. It can also contain stored complex forms and abstract structures that are “regular” in that they can *also* be composed or derived by the grammatical/procedural system. As with idiosyncratic knowledge, the likelihood of these “regular” representations being memorized should increase with item-related factors such as their frequency, and subject-related factors such as the individual’s lexical/declarative memory abilities. The system supports a superpositional associative memory, which allows for generalizations across representations. For example, the memorization of phonologically similar stem-irregular past tense pairs (e.g. *spring–sprang*, *sing–sang*) may allow for memory-based generalization to new irregularizations, either from real words (*bring–brang*) or from novel ones (*spling–splang*). This ability to generalize could underlie some degree of productivity within the memory system.

The brain structures that subserve declarative memory play analogous roles in lexical memory. Thus, medial temporal lobe structures underlie the encoding, consolidation and access or retrieval of new memories, which eventually rely instead on neocortical regions, especially in temporal and temporo-parietal areas. Inferior and ventral temporal regions are particularly important for representing non-linguistic conceptual knowledge and word meanings. They may also contain abstract lexical representations (Damasio et al., 1996). Superior temporal cortex may be particularly important for storing phonological representations, and perhaps other grammatical (syntactic, morphological) representations. Thus, this region may be related to both the procedural and declarative memory systems. Other brain structures, particularly those related to the procedural memory system, also play roles in declarative memory. These are described below. Acetylcholine and estrogen have important functions in lexical/declarative memory, likely in the learning and/or retrieval of new lexical knowledge.

4.2. *The grammatical/procedural memory system*

The brain system underlying procedural memory subserves the mental grammar. This system underlies the learning of new, and the computation of already-learned, rule-based procedures that govern the regularities of language—particularly those procedures related to combining items into complex structures that have precedence (sequential) and hierarchical relations. Thus, the system is hypothesized to have an important role in rule-governed structure building; that is, in the sequential and hierarchical combination – “merging” (Chomsky, 1995), or concatenation – of stored forms and abstract representations into complex structures. Procedural memory is assumed to play a role in all sub-domains of grammar which depend on these functions, including syntax; inflectional and derivational morphology – at least for default “regulars” (Pinker, 1999; Ullman, 2001a,c), but also for irregulars that appear to be affixed (Ullman, Hartshorne, Estabrooke, Brovetto, & Walenski, submitted); aspects of phonology (the combination of sounds); and possibly non-lexical (compositional) semantics (the interpretive, i.e. semantic, aspects of the composition of words into complex structures). Moreover, the computational nature of the system is likely to be similar across grammatical sub-domains – although this does not preclude the

possibility that these sub-domains maintain a certain degree of independence (see discussion below).

The system is a network composed of several brain structures. These are functionally related, highly inter-connected, and dynamically interactive: the basal ganglia, especially the caudate nucleus; frontal cortex, in particular Broca's area and pre-motor regions (including SMA and pre-SMA); parietal cortex, particularly the supramarginal gyrus (BA 40) and possibly the superior parietal lobule (BA 7); superior temporal cortex, probably in close relation with the declarative memory system; and the cerebellum, including the cerebellar hemispheres, the vermis, and the dentate nucleus.

The language-related functions of each of these structures is expected to be highly related to its non-language functions. Thus, the basal ganglia are posited to play a role in one or more aspects of the real-time selection and maintenance in working memory of, and switching between, sequentially and hierarchically structured elements in complex linguistic representations, and in the learning of rules over those representations. Grammar is learned and processed by one or more channels that run throughout the basal ganglia to the thalamus and thence to frontal cortex. These channels are parallel to and largely functionally segregated from other channels that undergo analogous computations but subserve other domains. The channel(s) subserving grammar might also subserve other domains, such as non-linguistic sequence learning; that is, they may be at least somewhat domain-independent. Alternatively, there may be one or more channels dedicated to grammar, and perhaps distinct (sub)channels for distinct grammatical sub-domains (e.g. syntax, morphology). Such channels and their frontal outputs may be considered domain-specific "modules" dedicated to grammar or its sub-domains. Though these hypothesized grammatical (sub)channels are domain-specific in that they underlie only grammatical processing, they are part of a domain-general procedural system, in which the same or analogous computations are performed on parallel and largely functionally segregated channels subserving other domains. This is a somewhat different view of modularity than is traditionally discussed in the study of language (Fodor, 1983).

The frontal cortical areas to which the basal ganglia project – in particular Broca's area, SMA and pre-SMA – also underlie aspects of grammar. Broca's area or portions thereof – especially BA 44 – may play an especially important role. Based on the functions of Broca's area in non-linguistic domains, this region is expected to subserve aspects of the selection and maintenance in working memory of elements in complex linguistic structures, and the learning and processing of rule-governed sequential and hierarchical patterns over those structures. These functions are, not surprisingly, quite related to the hypothesized functions of the basal ganglia in language, though Broca's area and the basal ganglia likely differ at least somewhat in their specific functions (Ullman, 2003; Ullman and Pierpont, *in press*).

Although the other structures that constitute the procedural system network are also expected to subserve language, their functional roles are perhaps less clear than those of the structures discussed above. Following evidence from their non-linguistic functions, the supramarginal gyrus and/or the superior parietal lobule may each play a role in attentional selection, which could be related to the selection functions described above. Parietal cortex may also play a role not only in sensori-motor transformations, but also in transforming structured representations stored in superior temporal regions to the dynamic

representations created by Broca's area. The cerebellum is expected to be involved in the search of lexical items, and possibly in the error-based learning of the rules that underlie the regularities of complex structures.

4.3. Interactions between the systems

The lexical/declarative memory system and the grammatical/procedural system are hypothesized to interact in several ways. First, the procedural system is hypothesized to build complex structures, and learn rule-governed patterns over those structures, by selecting lexical items from declarative memory, and maintaining and structuring those items together in working memory. Second, superior aspects of the temporal lobe may play a role in the storage of knowledge about procedural memory related relations of structured representations. Third, the same or similar types of knowledge can in at least some cases be acquired by both systems. The rapid lexical/declarative storage of sequences of lexical forms should provide a database from which grammatical rules can gradually and implicitly be abstracted by the procedural memory system. Moreover, in some cases explicit knowledge of the rules themselves may help guide processing, perhaps enhancing the procedural rule acquisition. Fourth, the two systems interact competitively in a number of ways. Access to a stored representation which has similar mappings to one which could be composed compositionally by the procedural system (e.g. an irregular vs. a regular past-tense form of the same verb) would block completion of the latter computation. Damage to the declarative system is expected to lead to enhanced learning and processing by the procedural system, and vice versa. Moreover, learning in one system may depress functionality of the other. It is possible that, at least under certain circumstances, enhancing acetylcholine or estrogen function in medial temporal lobe structures may result not only in improved lexical/declarative memory function, but also in suppressed grammatical/procedural function.

4.4. Further clarifications

The DP model is motivated by a set of commonalities between language functions on the one hand, and the functions of the memory brain systems on the other. However, the commonalities do *not* suggest, and indeed it is not the claim, that there are isomorphic (one-to-one) relations between lexicon and declarative memory, or between grammar and procedural memory. That is, it is *not* expected that all parts of the brain system underlying procedural memory subserve all aspects of the mental grammar, and similarly for declarative memory and the mental lexicon. First, there may be parts of each system that subserve non-language functions but which play no role in language, or a minimal role, or perhaps a role only in special circumstances (e.g. after breakdown). Indeed, this seems likely. For example, the declarative memorization of visual images clearly depends in part on cortical regions which may be specialized for and perhaps dedicated to visual processing, and thus are unlikely to be involved in the memorization of phonological word forms. Second and conversely, the DP model does *not* claim that *all* aspects of language depend upon the two brain memory systems. Other neural structures and other cognitive or computational components, perhaps even dedicated to language, may play an important role

in the two language capacities. Third, as we have seen above, structures with topographically segregated sub-regions (i.e. the basal ganglia, cerebellum, and possibly frontal cortex) may contain distinct sub-regions or circuits that subserve language and non-language functions (see above). On this view, the procedural memory system may be domain-independent in that it subserves many functions, but is also domain-specific in that each function is subserved by parallel and functionally segregated sub-components or modules. Fourth, as discussed above, even in the context of such topographic organization, there may be anatomical and functional specialization of sub-regions, such as in Broca's area.

4.5. Predictions

The predictions follow from the model described above. Most fundamentally, language and non-language functions that are posited to depend on the same brain systems should pattern together, showing similar computational, anatomic, physiological, biochemical and other characteristics. Moreover, this should apply not only to normal functioning, but also to the breakdown of these brain systems, and to recovery from this breakdown.

5. Comparison with other models

The DP model is proposed in the same spirit as, and is similar in a number of respects to, several other models and proposals (Dominey, 1997; Dominey et al., in press; Friederici, 1990; Greenfield, 1991; Lieberman et al., 1992; Rizzolatti & Arbib, 1998). These focus on the relation between grammar on the one hand, and implicit procedural memory, motor sequencing and hierarchical structure on the other. Some of these proposals are quite well-specified in certain respects. For example, Dominey and his colleagues have developed a computational model of the type of sequencing that may underlie both grammar and non-linguistic sequencing (Dominey et al., 2003). These models complement the DP model, specifying some aspects to a greater depth than the DP model, which in turn provides further specification in other dimensions, in particular the anatomical, physiological and biochemical substrates, and the functional roles in language played by those substrates.

The DP model is also largely, though not completely, compatible with many “dual-system” (“dual-mechanism”) or multiple-system linguistic and psycholinguistic models of language (Bever, Sanz, & Townsend, 1998; Chomsky, 1995; Fodor, 1983; Fodor, Bever, & Garrett, 1974; Frazier & Fodor, 1978; Pinker, 1994, 1999). On these views, language is subserved by separable components. At the very least, the mental lexicon is assumed to be distinct from a “computational” mental grammar, which moreover is often claimed to be composed of several components (Chomsky, 1995). These theories also claim or assume that at least the grammatical component or components are domain-specific. As can be seen from the discussion above, all of these claims are compatible with the DP model. Thus, the DP model can be thought of as a neurocognitive model of aspects of these linguistic and psycholinguistic proposals. The neurocognitive model provides further specification in certain respects, particularly of the underlying brain structures and their functions, whereas the linguistic and psycholinguistic models provide much greater specification at the level of representation, computation and processing.

In contrast, the DP model is at least partially inconsistent with certain claims about the domain specificity of the neural basis of grammar. Thus, the DP model is not consistent with the particular claim (Grodzinsky, 2000) that Broca's area is dedicated to language and performs a different set of linguistic computations than are claimed by the DP model. The DP model is also not consistent with the claims made by certain connectionist models, in particular connectionist models that deny grammatical composition (Bates & MacWhinney, 1989; Joanisse & Seidenberg, 1999; MacDonald, Pearlmutter, & Seidenberg, 1994; Rumelhart & McClelland, 1986). These models also do not predict empirical associations among grammatical domains and procedural memory, or dissociations between these and lexical and declarative memory.

6. Empirical evidence

Here I examine neurocognitive evidence pertaining to the claims and predictions of the DP model in native (first) language. I focus on the relation between brain and cognition. For a discussion of purely behavioral (psycholinguistic) evidence from cognitively unimpaired individuals, see Pinker (1999), Ullman (2001a), or Pinker and Ullman (2002), among others. Three broad types of evidence are examined here. First, I provide brief overviews of hemodynamic (PET, fMRI) and electrophysiological (ERP) evidence from normal processing (i.e. in cognitively unimpaired individuals). For more in-depth reviews of this evidence, see, among others, Kaan and Swaab (2002), Kaan and Stowe (2002), and Friederici (2002). Second, I present evidence from developmental and adult-onset disorders that have traditionally been viewed as "language" disorders. I argue that the evidence suggests that these may be viewed as disorders affecting the brain structures of one or the other of the two brain memory systems. Third, evidence is presented that suggests that developmental and adult-onset disorders that have traditionally not been associated with language impairments in fact do affect language, and can also be profitably considered to be disorders of one or the other brain memory system.

6.1. Neuroimaging evidence from normal processing

6.1.1. Hemodynamics: PET and fMRI

Activation in temporal/temporo-parietal regions, including the hippocampus and other medial temporal lobe structures, is strongly linked to the representation and processing of both non-linguistic conceptual-semantic knowledge and lexical knowledge (Damasio et al., 1996; Martin et al., 2000; Newman, Pancheva, Ozawa, Neville, & Ullman, 2001). Activation in VL-PFC, and Broca's area in particular, has been elicited not only in a range of tasks related to procedural memory (see above), but also numerous tasks designed to probe syntactic processing, in both receptive and expressive language (Caplan, Alpert, & Waters, 1998; Embick, Marantz, Miyashita, O'Neil, & Sakai, 2000; Friederici, 2002; Indefrey, Hagoort, Herzog, Seitz, & Brown, 2001; Moro et al., 2001; Ni et al., 2000; Stromswold, Caplan, Alpert, & Rauch, 1996). Intriguingly, many of these studies have implicated BA 44 (pars opercularis) and the adjacent frontal operculum, suggesting that these regions play a particularly important role in grammatical processing, possibly related to aspects of

working memory (Friederici, 2002). Syntactic processing has been shown to elicit activation in SMA/pre-SMA (Caplan et al., 1998; Newman et al., 2001), the basal ganglia, specifically the caudate nucleus (Moro et al., 2001), and anterior superior temporal gyrus (Dapretto & Bookheimer, 1999; Meyer, Friederici, & von Cramon, 2000; Ni et al., 2000). Interestingly, processing of lexically stored syntactic knowledge (i.e. word-specific knowledge regarding which arguments a verb takes) has yielded inferior temporal lobe activation (Kuperberg et al., 2000).

6.1.2. *Electrophysiology: event-related potentials (ERPs)*

Event-related potentials (ERPs) reflect the real-time electrophysiological brain activity of cognitive processes that are time-locked to the presentation of target stimuli. Difficulties in lexical processing as well as non-linguistic conceptual-semantic processing elicit central/posterior bilateral negativities that peak about 400 ms post-stimulus ("N400s") (Kutas & Hillyard, 1980; Olivares, Bobes, Aubert, & Valdes-Sosa, 1994). Evidence from several empirical approaches suggests that N400s depend especially on temporal lobe structures, including in the medial temporal lobe (Kiehl, Laurens, & Liddle, 2002; Nobre, Allison, & McCarthy, 1994; Simos, Basile, & Papanicolaou, 1997), and possibly VL-PFC as well (Halgren et al., 2002; Kiehl et al., 2002). The N400 is posited to reflect declarative memory processes (Ullman, 2001b,c).

Anomalies in rule-governed syntax, morpho-syntax, or morpho-phonology can yield relatively early (150–500 ms) left anterior negativities ("LANs") (Friederici, Pfeifer, & Hahne, 1993; Neville, Nicol, Barss, Forster, & Garrett, 1991; Penke et al., 1997; Weyerts, Penke, Dohrn, Clahsen, & Münte, 1997). These LANs have been linked to rule-based automatic computations (Friederici, 2002; Friederici, Hahne, & Mecklinger, 1996) and left frontal structures (Friederici, Hahne, & von Cramon, 1998). LANs have also been elicited by difficulties in non-linguistic sequencing (Hoen & Dominey, 2000), and by the observation of incorrect tool use (e.g. incorrect positioning of a screwdriver with respect to the screw) (Bach, Gunter, Knoblich, Prinz, & Friederici, 2002). LANs are posited to reflect procedural memory processes (Ullman, 2001b,c). Syntactic processing difficulties also tend to elicit late (600 ms) centro-parietal positivities ("P600s") (Hagoort, Brown, & Groothusen, 1993; Osterhout & Holcomb, 1992). These are associated with controlled processing (Friederici et al., 1996), and are posited to not reflect automatic aspects of procedural memory. Intriguingly, difficulties in processing word-specific syntactic knowledge (about verb arguments) can elicit an N400 rather than an LAN (Friederici & Frisch, 2000).

6.2. "Language" disorders

6.2.1. *Developmental "language" disorders*

6.2.1.1. *Specific Language Impairment.* The term Specific Language Impairment (SLI) is often assigned to developmental language disorders that do not have any apparent social, psychological or neurological cause (Leonard, 1998). SLI has generally been explained as an impairment specific to grammar (Clahsen, 1989; Rice & Oetting, 1993; van der Lely & Stollwerck, 1996) or as a processing deficit (Leonard, McGregor, & Allen, 1992),

specifically of working memory (Gathercole & Baddeley, 1993) or of brief stimuli and rapid sequences (Merzenich, Schreiner, Jenkins, & Wang, 1993; Tallal & Piercy, 1978). However, SLI may best be viewed as an impairment of procedural memory, resulting from the dysfunction of the brain structures underlying this system (Ullman & Gopnik, 1999; Ullman & Pierpont, in press).

SLI is strongly associated with grammatical impairments, including of syntax (Clahsen, Bartke, & Göllner, 1997; van der Lely, 1996), morphology (both morpho-syntax and morpho-phonology) (Leonard, Bortolini, Caselli, McGregor, & Sabbadini, 1992; Rice & Oetting, 1993; van der Lely & Ullman, 2001) and phonology (Gathercole & Baddeley, 1993). Lexical knowledge is relatively spared in SLI, as evidenced by spared recognition and comprehension in word learning tasks (Leonard, 1982; Weismer & Hesketh, 1996). In contrast, retrieval of lexical knowledge (word finding) is often difficult for people with SLI (Rapin & Wilson, 1978; Weckerly, Wulfeck, & Reilly, 2001), as might be expected if structures underlying procedural memory are involved in this function.

Contrary to traditional perspectives, SLI is also strongly associated with impairments of procedural memory (see Ullman & Pierpont, in press). First, motor deficits are widely observed in children and adults with SLI (Bishop, 2002; Hill, 2001; Owen & McKinlay, 1997). These include impairments of oral or facial praxis, limb praxis/coordination, and fine motor skills. People with SLI have particular difficulty on motor tasks involving complex sequences of movements, such as moving pegs, sequential finger opposition, rapid finger tapping and stringing beads. SLI is also associated with deficits of a number of other functions which depend upon the brain structures underlying procedural memory, including working memory (Gathercole & Baddeley, 1993), processing rapidly-presented sequences (Merzenich et al., 1993; Tallal, Stark, & Mellits, 1985), and mental rotation (Johnston & Weismer, 1983) and other “dynamic” mental imagery tasks involving the mental manipulation of images (Leonard, 1998). In contrast, “static” mental imagery appears to be spared in the disorder (Leonard, 1998). SLI is linked to abnormalities of the brain structures underlying procedural memory, especially Broca’s area, the basal ganglia (particularly the caudate nucleus), SMA and the cerebellum (Gauger, Lombardino, & Leonard, 1997; Jernigan, Hesselink, Sowell, & Tallal, 1991; Oki, Takahashi, Miyamoto, & Tachibana, 1999; Tallal, Jernigan, & Trauner, 1994; Vargha-Khadem et al., 1998). In contrast, declarative memory abilities often remain intact in SLI (Dewey & Wall, 1997; Merritt & Liles, 1987; also see Ullman & Pierpont, in press).

Evidence suggests that people with SLI may shift their reliance from the impaired procedural memory system to the relatively spared declarative memory (for further discussion see Ullman & Pierpont, in press). For example, whereas in normally developing children and adults, frequency effects (indicating storage) for regular inflected forms are absent, inconsistent or weak, they have been consistently demonstrated in children and adults with SLI, in both past-tense and plural production (Oetting & Horohov, 1997; Ullman & Gopnik, 1999; van der Lely & Ullman, 2001). Moreover, children with SLI produce compounds with regular as well as irregular plurals in them (e.g. *mice-eater* and *rats-eater*), whereas normal children only produce compounds with irregular plurals (e.g. *mice-eater* vs. *rat-eater*) (van der Lely & Christian, 2000). These data suggest that while normal children retrieve only irregular past-tense forms from memory, children with SLI retrieve both past-tense types.

6.2.2. Adult-onset “language” disorders

6.2.2.1. Aphasia. The term “aphasia” generally refers to language impairments resulting from one or more focal lesions in the brain. Clusters of symptoms tend to co-occur in types (syndromes) of aphasia. Although there are a number of different adult-onset aphasia syndromes, several of these can be grouped into either of two larger categories, which are often referred to as non-fluent and fluent aphasia (Alexander, 1997; Damasio, 1992; Goodglass, 1993). It is argued here that non-fluent aphasia reflects, at least in part, damage to the brain structures underlying procedural memory. In contrast, it is posited that fluent aphasia entails damage to brain structures underlying long-term representations in declarative memory, although the damage also often extends to posterior areas involved in procedural memory, resulting in the accompaniment of particular types of impairments of the grammatical/procedural system.

Non-fluent aphasia is associated with lesions of left inferior (ventro-lateral) frontal regions, in particular Broca’s area and nearby cortex, as well as the basal ganglia, portions of inferior parietal cortex, and anterior superior temporal cortex (Alexander, 1997; Damasio, 1992; Dronkers, Redfern, & Knight, 2000). Characteristic of anterior aphasia is “agrammatism”: syntactic and morphological impairments in production and comprehension, and especially in the use of free and bound grammatical morphemes (e.g. auxiliaries, determiners, and affixes such as *-ed*) (Goodglass, 1993). Agrammatics have been shown to have more trouble with regular than irregular morphology, holding constant word frequency, length, and other factors, in both expressive and receptive language tasks (Pinker & Ullman, 2002; Ullman et al., 1997, in press). Agrammatism is also strongly associated with phonological impairments (Goodglass, 1993). Agrammatic speech can follow focal lesions that are relatively circumscribed to the left basal ganglia (Fabbro, Clarici, & Bava, 1996) or right cerebellum (Silveri, Leggio, & Molinari, 1994; Zettin et al., 1997). Non-fluent aphasics are relatively spared in their recognition and comprehension of non-compositional (simple) content words (e.g. nouns, adjectives) (Goodglass, 1993). As would be expected with damage to Broca’s area and the basal ganglia if these structures play a role in lexical retrieval, agrammatics generally have difficulty retrieving content words, despite the spared recognition of these words (Alexander, 1997; Damasio, 1992; Dronkers et al., 2000; Goodglass, 1993).

Non-fluent aphasia is strongly associated with impairments of non-linguistic functions that depend on procedural memory and its underlying brain structures. Non-fluent aphasics typically have a range of motor impairments, from articulation to the execution of complex learned motor skills, particularly those involving sequences (ideomotor apraxia) (Alexander, 1997; De Renzi, 1989; Dronkers et al., 2000; Goodglass, 1993; Heilman et al., 1997). Non-fluent aphasics have also been shown to have impairments learning new motor sequences, especially sequences containing abstract structure (Conway & Christiansen, 2001; Dominey et al., 2003; Goschke et al., 2001). Non-fluent aphasia is also linked to deficits of working memory and impairments of timing in speech production and perception, (Goodglass, 1993; Szelag et al., 1997).

Fluent aphasia is linked to damage of left temporal and temporo-parietal regions, often extending to inferior parietal structures. Fluent aphasia is associated with impairments in

the production, reading, and recognition of the sounds and meanings of content words, as well as of conceptual knowledge (Alexander, 1997; Damasio, 1992; Dronkers et al., 2000; Farah & Grossman, 1997). In contrast, fluent aphasics tend to produce syntactically well-structured sentences, and to not omit morphological affixes (e.g. the past tense *-ed* suffix). Intriguingly, damage in and around inferior parietal cortex in fluent aphasia can lead to certain types of grammatical impairments (Goodglass, 1993), supporting a role for this region in the mental grammar. Nevertheless, in direct comparisons of regular and irregular morphology, fluent aphasics show the opposite pattern to that of non-fluent aphasics, with worse performance at irregulars (Ullman et al., 1997, in press).

6.3. "Non-language" disorders

6.3.1. Developmental "non-language" disorders

A number of developmental disorders are associated with impairments of procedural memory related functions, and with abnormalities of the brain structures underlying this system. These include dyslexia, Attention Deficit Hyperactivity Disorder (ADHD) and autism spectrum disorder. According to the DP model, in these disorders one should observe both grammatical difficulties and lexical retrieval impairments, though the particular characteristics of these language deficits may differ depending on the specific procedural memory dysfunction in each disorder.

Dyslexia and ADHD are both linked to impairments of motor function (Denckla, Rudel, Chapman, & Krieger, 1985; Diamond, 2000; Wolff, Cohen, & Drake, 1984) and working memory (Denckla, 1996; Gathercole & Baddeley, 1993). Both disorders yield deficits in the ability to accurately reproduce time intervals (Barkley, Koplowitz, Anderson, & McMurray, 1997; Goswami et al., 2002) and to maintain motor timing control (Diamond, 2000; Wolff et al., 1984). The cerebellum has been implicated in dyslexia (Nicolson, Daum, Schugens, Fawcett, & Schulz, 2002) and ADHD (Berquin et al., 1998; Castellanos, 2001). The basal ganglia, especially the caudate nucleus, is abnormal in ADHD (Castellanos, 2001; Diamond, 2000), and possibly in dyslexia (Georgiewa et al., 2002). Dyslexia and ADHD show high co-morbidity with SLI and with each other (Cohen et al., 2000; Denckla, 1996; Snowling, 2000). According to one study, approximately 55% of children with a specific reading disorder were found to have impaired oral language, and 51% of children with SLI had a reading disability (McArthur, Hogben, Edwards, Heath, & Mengler, 2000). Some studies document as high as a 45% rate of language impairment among children with ADHD (Tirosh & Cohen, 1998). Indeed, the most frequent psychiatric diagnosis among children with language impairments is ADHD (Cohen et al., 2000).

Autism spectrum disorder is associated with cerebellar abnormalities (Courchesne, Yeung-Courchesne, Press, Hesselink, & Jernigan, 1988; Rumsey, 1996) and with deficits of motor function (Bauman, 1992; Ohta, 1987), working – but not declarative – memory (Bennetto, Pennington, & Rogers, 1996), and procedural learning, especially of sequences (Mostofsky et al., 2000; Sigman & Ungerer, 1984). One of the defining characteristics of autism is a deficit in language (Rutter, 1978). In many cases expressive language ability never develops at all (Bailey, Phillips, & Rutter, 1996). Deficits have been reported in syntax (Ramondo & Milech, 1984; Van Meter, Fein, Morris, Waterhouse, & Allen, 1997) and morphology (Bartolucci, Pierce, & Streiner, 1980; Howlin, 1984; Pierce & Bartolucci,

1977). In contrast, knowledge of words and concepts are apparently not impaired (Tager-Flusberg, 1985; Whitehouse & Harris, 1984), though there may be impairments in the recall of this knowledge (Tager-Flusberg, 1985).

6.3.2. Adult-onset “non-language” disorders

6.3.2.1. Alzheimer’s disease. Alzheimer’s disease (AD) affects medial and neocortical temporal-lobe structures, leaving frontal cortex – particularly Broca’s area and motor cortex – and basal-ganglia structures relatively intact (Arnold, Hyman, Flory, Damasio, & Hoesen, 1991). The temporal lobe dysfunction may explain AD patients’ impairments in learning new and using established lexical and conceptual knowledge (Grossman et al., 1998; Nebes, 1997; Sagar, Cohen, Sullivan, Corkin, & Growdon, 1988). AD patients are relatively spared at acquiring and expressing motor and cognitive skills (Beatty et al., 1994; Gabrieli, Corkin, Mickel, & Growdon, 1993; Nebes, 1997; Saint-Cyr et al., 1988), and at aspects of syntactic processing (Bayles, 1982; Schwartz, Marin, & Saffran, 1979). AD patients with severe deficits at object naming or fact retrieval make more errors at producing past-tense forms of irregulars than of regulars or *-ed*-suffixes novel verbs. Across AD patients, error rates at object naming and at fact retrieval correlate with error rates at producing irregular but not regular or *-ed*-suffixes novel past tenses (Ullman, in press; Ullman et al., 1997). Similarly, Italian AD patients have greater difficulty producing Italian irregular than regular present tense and past participle forms (Cappa & Ullman, 1998; Walenski, Sosta, Cappa & Ullman, submitted).

6.3.2.2. Semantic dementia. Semantic dementia is associated with the progressive and severe degeneration of inferior and lateral temporal lobe regions. The disorder results in the loss of non-linguistic conceptual and lexical knowledge (Bozeat, Lambon Ralph, Patterson, Garrard, & Hodges, 2000), with spared motor, syntactic and phonological abilities (Graham, Patterson, & Hodges, 1999). Patients with semantic dementia yield a pattern like that of AD patients: they have more trouble producing and recognizing irregular than regular and *-ed*-suffixes novel past tenses, and the degree of their impairment on irregulars correlates with their performance on an independent lexical memory task (Patterson, Lambon Ralph, Hodges, & McClelland, 2001).

6.3.2.3. Parkinson’s disease. Parkinson’s disease (PD) is associated with the degeneration of dopaminergic neurons, especially in the basal ganglia (i.e. the substantia nigra). This causes high levels of inhibition in the motor and other frontal cortical areas to which the basal ganglia project. It is thought to explain why PD patients show suppression of motor activity (hypokinesia) and have difficulty expressing motor sequences (Dubois, Boller, Pillon, & Agid, 1991; Willingham, 1998; Young & Penney, 1993). It may also account for their impairments at acquiring motor and cognitive skills (Harrington, Haaland, Yeo, & Marder, 1990; Saint-Cyr et al., 1988), and at grammatical processing (Grossman, Carvell, & Peltzer, 1993; Illes, Metter, Hanson, & Iritani, 1988; Lieberman et al., 1992). PD patients also have trouble retrieving words (Dubois et al., 1991). In contrast, temporal-lobe regions remain relatively undamaged and the recognition of words and facts remains relatively intact in low- or non-demented PD patients (Dubois et al., 1991; Sagar et al.,

1988; Saint-Cyr et al., 1988). Severely hypokinetic PD patients show a pattern opposite to that found among AD patients, making more errors when producing regular and *-ed*-suffixed novel past-tenses than irregular past-tenses. Across PD patients, the level of right-side hypokinesia, which reflects left basal ganglia degeneration, correlates with error rates at the production of regular and *-ed*-suffixed novel forms but not irregular forms. Intriguingly, left-side hypokinesia, which reflects right basal ganglia degeneration, does not show the analogous correlations with error rates in the production of any past tense type, underscoring the role of left frontal/basal-ganglia structures in grammatical rule use (Ullman, in press; Ullman et al., 1997). Across PD patients, error rates at regular and *-ed*-suffixed novel past-tenses correlate with error rates at naming manipulated objects (e.g. tools), but not non-manipulated objects, suggesting a common neural basis for manipulated objects and *-ed*-affixation, as expected by the DP model (Ullman, 1999).

6.3.2.4. Huntington's disease. Although Huntington's disease (HD) is like PD in causing degeneration of the basal ganglia, it strikes different portions of these structures. Unlike in PD, this damage affects the indirect pathway, resulting in the disinhibition of frontal areas receiving basal ganglia projections (Young & Penney, 1993). This is thought to explain the unsuppressible movements (chorea, a type of hyperkinesia) found in patients with HD. Patients with HD show the opposite pattern to those with PD not only in the type of movement impairment (the suppressed movements of hypokinesia vs. the unsuppressed movements of hyperkinesia), but also in the type of errors on *-ed*-suffixed forms (Ullman, in press; Ullman et al., 1997). HD patients produce forms like *walkeded*, *plaggeded*, and *dugged*, but not analogous errors on irregulars like *dugug* or *keptet*, suggesting that these errors are not attributable to articulatory or motor deficits. Rather the data suggest unsuppressed *-ed*-suffixation. This conclusion is strengthened by the finding that the production rate of these over-suffixed forms correlates with the degree of chorea, across patients. These contrasting findings in PD and HD, linking movement and *-ed*-suffixation in two distinct types of impairments related to two types of basal ganglia damage, strongly implicate frontal/basal-ganglia circuits in *-ed*-suffixation. They support the hypothesis that these structures underlie the expression of grammatical rules as well as movement, and suggest that they play similar roles in the two domains.

6.3.2.5. Amnesia. Bilateral damage to medial temporal lobe structures leads to an inability to learn new information about facts, events, and words (Schacter & Tulving, 1994). Importantly, neither phonological nor semantic lexical knowledge is acquired (Gabrieli, Cohen, & Corkin, 1988; Postle & Corkin, 1998), supporting the DP hypothesis that these structures underlie the learning of word forms as well as word meanings. This "anterograde amnesia" is typically accompanied by the loss of this type of information for a period preceding the damage. However, knowledge acquired substantially before lesion onset tends to be spared (Schacter & Tulving, 1994). Thus, even though medial temporal lobe structures are posited to underlie the learning of new lexical information, knowledge of words learned during childhood should be largely intact in adult-onset amnesia. As expected, the examination of the well-studied amnesic H.M. (Kensinger, Ullman, & Corkin, 2001) revealed that he did not differ from normal age- and education-matched

control subjects at syntactic processing tasks, or at his production of regular or irregular forms in past-tense, plural and derivational morphology.

7. Conclusion

According to the DP model, the brain systems underlying two well-studied memory capacities, declarative and procedural memory, also subserve aspects of the mental lexicon and the mental grammar. Both brain systems play similar functional roles across language and non-language domains, which depend on common anatomical, physiological, and biochemical substrates. Evidence from neuroimaging (fMRI, PET, ERPs) and from developmental and adult-onset disorders supports this claim. Moreover, I have argued that certain developmental and adult-onset “language” disorders may be best viewed as disorders that affect brain structures underlying the memory systems.

The DP model has a number of implications in addition to those discussed above. First, our understanding of the two memory systems should lead to further predictions about language. For example, sex differences in language acquisition and processing can be predicted by independent knowledge of declarative memory. Women show an advantage over men at remembering verbal information in declarative memory (Golomb et al., 1996; Kimura, 1999). This effect is modulated by estrogen (see above). These data lead to the prediction that girls and women tend to memorize complex forms (*walked*) in lexical/declarative memory that boys and men tend to compose (*walk* + *-ed*) in the grammatical/procedural system (Ullman et al., 2002). Preliminary evidence supports this contention, and implicates estrogen in the effect (Estabrooke, Mordecai, Maki, & Ullman, 2002; Ullman et al., 2002, submitted).

Second, aspects of our existing understanding of language can be reinterpreted in the context of the DP model. For example, evidence suggests that in late second language learning – particularly after puberty – grammar is more difficult to learn than lexical knowledge (Birdsong, 1999; Johnson & Newport, 1989). Under the DP model, this suggests that at later ages, especially after puberty, the grammatical/procedural system is less available than lexical/declarative memory (Ullman, 2001b). This may result from the attenuation of procedural memory, possibly due to increasing estrogen levels at puberty (directly or via testosterone; see above), which would be expected to enhance declarative memory, and possibly suppress the procedural system through the “see-saw” competition mechanism. The availability of the lexical/declarative system should allow it to compensate for the dysfunctional grammatical/procedural system, as has been found in SLI (see above). However, since practice should increase performance in procedural memory, late-language learners should tend to become native like with experience, showing an increased dependence on the grammatical/procedural system. Previous studies are consistent with this view of second language acquisition and processing (Ullman, 2001b). Moreover, a recent fMRI study examining the acquisition of an artificial language in adulthood (Opitz & Friederici, in press) found that early during acquisition (i.e. at low proficiency) syntactic processing involves the hippocampus and cortical areas in the temporal lobe. Activation in these brain structures decreased across the experiment (as proficiency increased), while activation increased in Broca’s area. This finding

suggests a shift from the declarative to the procedural system during late second language learning, similar to the non-linguistic procedural learning experiments discussed above (Poldrack et al., 2001; Poldrack, Prabhakaran et al., 1999).

Third, because language is a relatively well-understood cognitive domain, it is likely that linguistic theory and related language disciplines will shed light on aspects of the declarative and procedural memory systems. For example, the Elsewhere Principle (see above) suggests that even in non-language domains, declarative memory may hold precedence in certain contexts over procedural memory.

Fourth, the DP model suggests the feasibility of the development of animal models for the study of language: the model predicts that significant advances in our understanding of language can be made by investigating non-language functions, in particular by using a range of highly informative methods available only in animal models. Therefore, a reasonable and desirable research program would be to develop animal models of non-linguistic functions whose computational and neural substrates are expected to be shared with those of linguistic functions.

Fifth, the model has direct educational and clinical implications. For example, the neuropharmacology of declarative memory and its underlying neural substrates (Curran, 2000) should pertain to language as well. Moreover, as discussed above, people with disorders of the grammatical/procedural system may recover through the memorization of complex forms (e.g. *walked*) in lexical/declarative memory. Such recovery could presumably be encouraged with neuropharmacological and other therapeutic approaches motivated by existing knowledge of the memory systems (Ullman & Pierpont, in press). Finally, the existence of brain systems that subserve language and are homologous to systems in other animals has implications for the evolution of language.

Acknowledgements

Support was provided to MTU by a McDonnell-Pew grant in Cognitive Neuroscience, a research grant from the National Alliance For Autism Research, NSF SBR-9905273, NIH MH58189, and Army DAMD-17-93-V-3018/3019/3020 and DAMD-17-99-2-9007. I would like to thank all the members of the Brain and Language Laboratory, especially Claudia Bonin, John Drury, Ivy Estabrooke, Joshua Hartshorne, Matthew Moffa, Rene Pierpont, Karsten Steinhauer, and Matthew Walenski, for lively discussions and for helpful comments.

References

- Aldridge, J. W., & Berridge, K. C. (1998). Coding of serial order by neostriatal neurons: a "natural action" approach to movement sequence. *Journal of Neuroscience*, 18(7), 2777–2787.
- Alexander, G. E., & Crutcher, M. D. (1990). Functional architecture of basal ganglia circuits: neural substrates of parallel processing. *Trends in Neuroscience*, 13(7), 266–271.
- Alexander, G. E., Crutcher, M. D., & DeLong, M. R. (1990). Basal ganglia-thalamocortical circuits: parallel substrates for motor oculomotor 'prefrontal' and 'limbic' functions. In H. B. M. Uylings, C. G. Van Eden, J. P. C. DeBruin, M. A. Corner, & M. G. P. Feenstra (Eds.), (85) (pp. 119–146). *Progress in brain research*, New York: Elsevier Science.

- Alexander, G. E., DeLong, M. R., & Strick, P. L. (1986). Parallel organization of functionally segregated circuits linking basal ganglia and cortex. *Annual Review of Neuroscience*, 9, 357–381.
- Alexander, M. P. (1997). Aphasia: clinical and anatomic aspects. In T. E. Feinberg, & M. J. Farah (Eds.), *Behavioral neurology and neuropsychology* (pp. 133–150). New York: McGraw-Hill.
- Alvarez, P., & Squire, L. R. (1994). Memory consolidation and the medial temporal lobe: a simple network model. *Proceedings of the National Academy of Sciences USA*, 91(15), 7041–7045.
- Amunts, K., Schleicher, A., Burgel, U., Mohlberg, H., Uylings, H., & Zilles, K. (1999). Broca's region revisited: cytoarchitecture and intersubject variability. *Journal of Comparative Neurology*, 412(2), 319–341.
- Anderson, S. R. (1992) (62). *A-morphous morphology*. New York: Cambridge University Press.
- Arnold, S. E., Hyman, B. T., Flory, J., Damasio, A. R., & Hoesen, G. W. V. (1991). The topographical and neuroanatomical distribution of neurofibrillary tangles and neuritic plaques in the cerebral cortex of patients with Alzheimer's disease. *Cerebral Cortex*, 1, 103–116.
- Bach, P., Gunter, T. C., Knoblich, G., Prinz, W., & Friederici, A. D. (2002). Conceptual and structural relations in action comprehension. In A. D. Friederici, & D. Y. von Cramon (Eds.), *Annual report of the Max Planck Institute of Cognitive Neuroscience* (pp. 34–35). Leipzig: Max Planck Institute of Cognitive Neuroscience.
- Bailey, A., Phillips, W., & Rutter, M. (1996). Autism: towards an integration of clinical, genetic, neuropsychological and neurobiological perspectives. *Journal of Child Psychology and Psychiatry*, 37, 89–126.
- Ballard, C. (2002). Advances in the treatment of Alzheimer's disease: benefits of dual cholinesterase inhibition. *European Journal of Neurology*, 47(1), 64–70.
- Barkley, R. A., Koplowitz, S., Anderson, T., & McMurray, M. B. (1997). Sense of time in children with ADHD: effects of duration, distraction, and stimulant medication. *Journal of the International Neuropsychological Society*, 3(4), 359–369.
- Bartolucci, G., Pierce, S. J., & Streiner, D. (1980). Cross-sectional studies of grammatical morphemes in autistic and mentally retarded children. *Journal of Autism and Developmental Disorders*, 10(1), 39–50.
- Baskin, D. S., Browning, J. L., Pirozzolo, F. J., Korporeal, S., Baskin, J. A., & Appel, S. H. (1999). Brain choline acetyltransferase and mental function in Alzheimer disease. *Archives of Neurology*, 56(9), 1121–1123.
- Bates, E., & MacWhinney, B. (1989). Functionalism and the competition model. In B. MacWhinney, & E. Bates (Eds.), *The crosslinguistic study of sentence processing* (pp. 3–73). Cambridge: Cambridge University Press.
- Bauman, M. L. (1992). Motor dysfunction in autism. In A. Joseph, & R. Young (Eds.), (1) (pp. 658–661). *Movement disorders in neurology and psychiatry*, Boston, MA: Blackwell.
- Bayles, K. A. (1982). Language function in senile dementia. *Brain and Language*, 16, 265–280.
- Beatty, W. W., Winn, P., Adams, R. L., Allen, E. W., Wilson, D. A., Prince, J. R., Olson, K. A., Dean, K., & Littleford, D. (1994). Preserved cognitive skills in dementia of the Alzheimer type. *Archives of Neurology*, 51, 1040–1046.
- Bennetto, L., Pennington, B. F., & Rogers, S. J. (1996). Intact and impaired memory functions in autism. *Child Development*, 67, 1816–1835.
- Berquin, P. C., Giedd, J. N., Jacobsen, L. K., Hamburger, S. D., Krain, A. L., Rapoport, J. L., & Castellanos, F. X. (1998). Cerebellum in attention-deficit hyperactivity disorder: a morphometric MRI study. *Neurology*, 50(4), 1087–1093.
- Bever, T. G., Sanz, M., & Townsend, D. J. (1998). The emperor's psycholinguistics. *Journal of Psycholinguistic Research*, 27(2), 261–284.
- Binkofski, F., Amunts, K., Stephan, K., Posse, S., Schormann, T., Freund, H., Zilles, K., & Seitz, R. (2000). Broca's region subserves imagery of motion: a combined cytoarchitectonic and fMRI study. *Human Brain Mapping*, 11(4), 273–285.
- Binkofski, F., Buccino, G., Stephan, K., Rizzolatti, G., Seitz, R., & Freund, H. (1999). A parieto-premotor network for object manipulation: evidence from neuroimaging. *Experimental Brain Research*, 128(1–2), 210–213.
- Binkofski, F., Dohle, C., Posse, S., Stephan, K., Hefter, H., Seitz, R., & Freund, H. (1998). Human anterior intraparietal area subserves prehension: a combined lesion and functional MRI activation study. *Neurology*, 50(5), 1253–1259.
- Birdsong, D. (Ed.). (1999). *Second language acquisition and the critical period hypothesis*. Mahwah, NJ: Lawrence Erlbaum Associates.

- Bishop, D. V. (2002). Motor immaturity and specific speech and language impairment: evidence for a common genetic basis. *American Journal of Medical Genetics*, 114(1), 56–63.
- Boecker, H., Ceballos-Baumann, A. O., Bartenstein, P., Dagher, A., Forster, K., Haslinger, B., Brooks, D. J., Schwaiger, M., & Conrad, B. (2002). A H2150 positron emission tomography study on mental imagery of movement sequences – the effect of modulating sequence length and direction. *Neuroimage*, 17, 999–1009.
- Boecker, H., Dagher, A., Ceballos-Baumann, A. O., Passingham, R. E., Samuel, M., Friston, K. J., Poline, J., Dettmers, C., Conrad, B., & Brooks, D. J. (1998). Role of the human rostral supplementary motor area and the basal ganglia in motor sequence control: investigations with H2 15O PET. *Journal of Neurophysiology*, 79(2), 1070–1080.
- Bozeat, S., Lambon Ralph, M. A., Patterson, K., Garrard, P., & Hodges, J. R. (2000). Non-verbal impairment in semantic dementia. *Neuropsychologia*, 38, 1207–1214.
- Braver, T. S., Barch, D. M., Kelley, W. M., Buckner, R. L., Cohen, N. J., Miezin, F. M., Snyder, A. Z., Ollinger, J. M., Akbudak, E., Conturo, T. E., & Petersen, S. E. (2001). Direct comparison of prefrontal cortex regions engaged by working and long-term memory tasks. *Neuroimage*, 14(1 Pt 1), 48–59.
- Buckner, R. L., & Wheeler, M. E. (2001). The cognitive neuroscience of remembering. *Nature Review Neuroscience*, 2(9), 624–634.
- Calabresi, P., Centonze, D., Gubellini, P., Pisani, A., & Bernardi, G. (2000). Acetylcholine-mediated modulation of striatal function. *Trends in Neurosciences*, 23(3), 120–126.
- Caplan, D., Alpert, N., & Waters, G. (1998). Effects of syntactic structure and propositional number on patterns of regional cerebral blood flow. *Journal of Cognitive Neuroscience*, 10(4), 541–552.
- Cappa, S., & Ullman, M. T. (1998). A neural dissociation in Italian verbal morphology. *Journal of Cognitive Neuroscience, Supplement*, 63.
- Castellanos, F. X. (2001). Neural substrates of attention-deficit hyperactivity disorder. *Advances in Neurology*, 85, 197–206.
- Chao, L., & Martin, A. (2000). Representation of manipulable man-made objects in the dorsal stream. *Neuroimage*, 12(4), 478–484.
- Cherrier, M. M., Asthana, S., Plymate, S., Baker, L., Matsumoto, A. M., Peskind, E., Raskind, M. A., Brodtkin, K., Bremner, W., Petrova, A., La Tendre, S., & Craft, S. (2001). Testosterone supplementation improves spatial and verbal memory in healthy older men. *Neurology*, 57(1), 80–88.
- Chomsky, N. (1965). Aspects of the theory of syntax. Cambridge, MA: MIT Press.
- Chomsky, N. (1970). Remarks on nominalization. In R. Jacobs, & P. Rosenbaum (Eds.), *Readings in English transformational grammar* (pp. 184–221). Waltham, MA: Ginn.
- Chomsky, N. (1995). The minimalist program. Cambridge, MA: MIT Press.
- Clahsen, H. (1989). The grammatical characterization of developmental dysphasia. *Linguistics*, 27, 897–920.
- Clahsen, H., Bartke, S., & Göllner, S. (1997). Formal features in impaired grammars: a comparison of English and German SLI children. *Essex Research Reports in Linguistics*, 14, 42–75.
- Cohen, N. J., Poldrack, R. A., & Eichenbaum, H. (1997). Memory for items and memory for relations in the procedural/declarative memory framework. *Memory*, 5(1–2), 131–178.
- Cohen, N. J., Vallance, D. D., Barwick, M., Im, N., Menna, R., Horodezky, N. B., & Isaacson, L. (2000). The interface between ADHD and language impairment: an examination of language, achievement, and cognitive processing. *Journal of Child Psychology and Psychiatry*, 41(3), 353–362.
- Conway, C., & Christiansen, M. (2001). Sequential learning in non-human primates. *Trends in Cognitive Sciences*, 5(12), 539–546.
- Corkin, S. (1984). Lasting consequences of bilateral medial temporal lobectomy: clinical course and experimental findings in H.M. *Seminars in Neurology*, 4(2), 249–259.
- Courchesne, E., Yeung-Courchesne, R., Press, G. A., Hesselink, J. R., & Jernigan, T. L. (1988). Hypoplasia of cerebellar vermal lobules VI and VII in autism. *New England Journal of Medicine*, 318(21), 1349–1354.
- Cowan, N. (1999). An embedded-process model of working memory. In A. Miyake, & P. Shah (Eds.), *Models of working memory* (pp. 62–101). Cambridge: Cambridge University Press.
- Culham, J. C., & Kanwisher, N. G. (2001). Neuroimaging of cognitive functions in human parietal cortex. *Current Opinion in Neurobiology*, 11(2), 157–163.
- Curran, H. V. (2000). Psychopharmacological approaches to human memory. In M. S. Gazzaniga (Ed.), *The new cognitive neurosciences* (pp. 797–804). Cambridge, MA: MIT Press.

- Dagher, A., Owen, A., Boecker, H., & Brooks, D. (2001). The role of the striatum and hippocampus in planning: a PET activation study in Parkinson's disease. *Brain*, 124(Pt 5), 1020–1032.
- Damasio, A. R. (1992). Aphasia. *New England Journal of Medicine*, 326(8), 531–539.
- Damasio, H. (1995). Human brain anatomy in computerized images. New York: Oxford University Press.
- Damasio, H., Grabowski, T., Tranel, D., Hichwa, R., & Damasio, A. (1996). A neural basis for lexical retrieval. *Nature*, 380(6574), 499–505.
- Dapretto, M., & Bookheimer, S. Y. (1999). Form and content: dissociating syntax and semantics in sentence comprehension. *Neuron*, 24(2), 427–432.
- Denckla, M. B. (1996). Biological correlates of learning and attention: what is relevant to learning disability and attention-deficit hyperactivity disorder. *Developmental and Behavioral Pediatrics*, 17(2), 114–119.
- Denckla, M. B., Rudel, R. G., Chapman, C., & Krieger, J. (1985). Motor proficiency in dyslexic children with and without attentional disorders. *Archives of Neurology*, 42(3), 228–231.
- De Renzi, E. (1989). Apraxia. In F. Boller, & J. Grafman (Eds.), (2) (pp. 245–263). *Handbook of neuropsychology*, New York: Elsevier Science.
- de Saussure, F. (1959). A course in general linguistics. London: Peter Owen.
- Desmond, J. E., & Fiez, J. A. (1998). Neuroimaging studies of the cerebellum: language, learning, and memory. *Trends in Cognitive Sciences*, 2(9), 355–362.
- D'Esposito, M., Aguirre, G. K., Zarahn, E., Ballard, D., Shin, R. K., & Lease, J. (1998). Functional MRI studies of spatial and nonspatial working memory. *Brain Research: Cognitive Brain Research*, 7(1), 1–13.
- Dewey, D., & Wall, K. (1997). Praxis and memory deficits in language-impaired children. *Developmental Neuropsychology*, 13(4), 507–512.
- Diamond, A. (2000). Close interrelation of motor development and cognitive development and of the cerebellum and prefrontal cortex. *Child Development*, 71(1), 44–56.
- Di Sciullo, A. M., & Williams, E. (1987) (14). *On the definition of word*, Cambridge, MA: MIT Press.
- Dominey, P. F. (1997). An anatomically structured sensory-motor sequence learning system displays some general linguistic capacities. *Brain and Language*, 59, 50–75.
- Dominey, P. F., Hoen, M., Blanc, J.-M., & Lelekov-Boissard, T. (2003). Neurological basis of language and sequential cognition: evidence from simulation, aphasia, and ERP studies. *Brain and Language*, 83, 207–225.
- Doya, K. (2000). Complementary roles of basal ganglia and cerebellum in learning and motor control. *Current Opinion in Neurology*, 10, 732–739.
- Doyon, J., Gaudreau, D., Laforce, R., Castonguay, M., Bedard, P. J., Bedard, F., & Bouchard, J. P. (1997). Role of the striatum, cerebellum, and frontal lobes in the learning of a visuomotor sequence. *Brain and Cognition*, 34(2), 218–245.
- Doyon, J., Owen, A. M., Petrides, M., Sziklas, V., & Evans, A. C. (1996). Functional anatomy of visuomotor skill learning in human subjects examined with positron emission tomography. *European Journal of Neuroscience*, 8(4), 637–648.
- Dronkers, N. F., Redfern, B. B., & Knight, R. T. (2000). The neural architecture of language disorders. In M. S. Gazzaniga (Ed.), *The new cognitive neurosciences* (pp. 949–958). Cambridge, MA: MIT Press.
- Dubois, B., Boller, F., Pillon, B., & Agid, Y. (1991). Cognitive deficits in Parkinson's disease. In F. Boller, & J. Grafman (Eds.), (5) (pp. 195–240). *Handbook of neuropsychology*, Amsterdam: Elsevier.
- Eichenbaum, H. (2000). A cortical-hippocampal system for declarative memory. *Nature Review Neuroscience*, 1(1), 41–50.
- Eichenbaum, H., & Cohen, N. J. (2001). From conditioning to conscious recollection: memory systems of the brain. New York: Oxford University Press.
- Embick, D., Marantz, A., Miyashita, Y., O'Neil, W., & Sakai, K. L. (2000). A syntactic specialization for Broca's area. *Proceedings of the National Academy of Sciences USA*, 97, 6150–6154.
- Estabrooke, I. V., Mordecai, K., Maki, P., & Ullman, M. T. (2002). The effect of sex hormones on language processing. *Brain and Language*, 83, 143–146.
- Fabbro, F., Clarici, A., & Bava, A. (1996). Effects of left basal ganglia lesions on language production. *Perceptual and Motor Skills*, 82(3 Pt 2), 1291–1298.
- Faillenot, I., Toni, I., Decety, J., Gregoire, M. C., & Jeannerod, M. (1997). Visual pathways for object-oriented action and object recognition: functional anatomy with PET. *Cerebral Cortex*, 7, 77–85.

- Farah, M. J., & Grossman, M. (1997). Semantic memory impairments. In T. E. Feinberg, & M. J. Farah (Eds.), *Behavioral neurology and neuropsychology* (pp. 473–477). New York: McGraw-Hill.
- Fiez, J. A. (1997). Phonology, semantics, and the role of the left inferior prefrontal cortex. *Human Brain Mapping*, 5, 79–83.
- Fiez, J. A., Tallal, P., Raichle, M. E., Miezin, F. M., Katz, W. F., Dobmeyer, S., & Peterson, S. E. (1995). PET studies of auditory and phonological processing: effects of stimulus characteristics and task demands. *Journal of Cognitive Neuroscience*, 7(3), 357–375.
- Finch, D., Gigg, J., Tan, A., & Kosoyan, O. (1995). Neurophysiology and neuropharmacology of projections from entorhinal cortex to striatum in the rat. *Brain Research*, 670(2), 233–247.
- Finch, D. M. (1996). Neurophysiology of converging synaptic inputs from the rat prefrontal cortex, amygdala, midline thalamus, and hippocampal formation onto single neurons of the caudate/putamen and nucleus accumbens. *Hippocampus*, 6(5), 495–512.
- Fodor, J. A. (1983). *The modularity of mind: an essay on faculty psychology*. Cambridge, MA: MIT Press.
- Fodor, J. A., Bever, T. G., & Garrett, M. F. (1974). The psychological reality of grammatical structures. In R. P. Rainer, & S. Gamer (Eds.), *The psychology of language: an introduction to psycholinguistics and generative grammar* (pp. 221–274). New York: McGraw-Hill.
- Frazier, L., & Fodor, J. D. (1978). The sausage machine: a new two-stage parsing model. *Cognition*, 6, 291–325.
- Preo, U., Pizzolato, G., Dam, M., Ori, C., & Battistin, L. (2002). A short review of cognitive and functional neuroimaging studies of cholinergic drugs: implications for therapeutic potentials. *Journal of Neural Transmission*, 109(5–6), 857–870.
- Friederici, A. (2002). Towards a neural basis of auditory sentence processing. *Trends in Cognitive Sciences*, 6(2), 78–84.
- Friederici, A. D. (1990). On the properties of cognitive modules. *Psychological Research*, 52(2–3), 175–180.
- Friederici, A. D., & Frisch, S. (2000). Verb-argument structure processing: the role of verb-specific and argument-specific information. *Journal of Memory and Language*, 43, 476–507.
- Friederici, A. D., Hahne, A., & Mecklinger, A. (1996). The temporal structure of syntactic parsing: early and late effects elicited by syntactic anomalies. *Journal of Experimental Psychology: Learning, Memory, and Cognition*, 22(5), 1219–1248.
- Friederici, A. D., Hahne, A., & von Cramon, D. Y. (1998). First-pass versus second-pass parsing processes in a Wernicke's and a Broca's aphasic: electrophysiological evidence for a double dissociation. *Brain and Language*, 62(3), 311–341.
- Friederici, A. D., Pfeifer, E., & Hahne, A. (1993). Event-related brain potentials during natural speech processing: effects of semantic, morphological and syntactic violations. *Cognitive Brain Research*, 1(3), 183–192.
- Gabrieli, J. D. E., Cohen, N. J., & Corkin, S. (1988). The impaired learning of semantic knowledge following bilateral medial temporal-lobe resection. *Brain and Cognition*, 7, 157–177.
- Gabrieli, J. D. E., Corkin, S., Mickel, S. F., & Growdon, J. H. (1993). Intact acquisition and long-term retention of mirror-tracing skill in Alzheimer's disease and in global amnesia. *Behavioral Neuroscience*, 107(6), 899–910.
- Gallese, V., Fogassi, L., Fadiga, L., & Rizzolatti, G. (2001). Action representation and the inferior parietal lobule. In W. Prinz, & B. Hommel (Eds.), *Common mechanisms in perception and action (XIX). Attention and performance*. Oxford: Oxford University Press.
- Gathercole, S. E., & Baddeley, A. D. (1993). *Working memory and language*. Hillsdale, NJ: Lawrence Erlbaum Associates.
- Gauger, L. M., Lombardino, L. J., & Leonard, C. M. (1997). Brain morphology in children with specific language impairment. *Journal of Speech, Language, and Hearing Research*, 40(6), 1272–1284.
- Gelfand, J. R., & Bookheimer, S. Y. (2003). Dissociating neural mechanisms of temporal sequencing and processing phonemes. *Neuron*, 38, 831–842.
- Georgiewa, P., Rzanny, R., Gaser, C., Gerhard, U. J., Vieweg, U., Freesmeyer, D., Mentzel, H. J., Kaiser, W. A., & Blanz, B. (2002). Phonological processing in dyslexic children: a study combining functional imaging and event related potentials. *Neuroscience Letters*, 318(1), 5–8.
- Golomb, J., Kluger, A., de Leon, M. J., Ferris, S. H., Mittelman, M., Cohen, J., & George, A. E. (1996). Hippocampal formation size predicts declining memory performance in normal aging. *Neurology*, 47(3), 810–813.

- Goodale, M. A. (2000). Perception and action in the human visual system. In M. S. Gazzaniga (Ed.), *The new cognitive neurosciences* (pp. 365–378). Cambridge, MA: MIT Press.
- Goodale, M. A., & Milner, A. D. (1992). Separate visual pathways for perception and action. *Trends in Neuroscience*, 15(1), 20–25.
- Goodglass, H. (1993). Understanding aphasia. San Diego, CA: Academic Press.
- Goschke, T., Friederici, A., Kotz, S. A., & van Kampen, A. (2001). Procedural learning in Broca's aphasia: dissociation between the implicit acquisition of spatio-motor and phoneme sequences. *Journal of Cognitive Neuroscience*, 13(3), 370–388.
- Goswami, U., Thompson, J., Richardson, U., Stainthorpe, R., Hughes, D., Rosen, S., & Scott, S. K. (2002). Amplitude envelope onsets and developmental dyslexia: a new hypothesis. *Proceedings of the National Academy of Sciences USA*, 99(16), 10911–10916.
- Graham, K. S., Patterson, K., & Hodges, J. R. (1999). Episodic memory: new insights from the study of semantic dementia. *Current Opinion in Neurobiology*, 9, 245–250.
- Graybiel, A. M. (1995). Building action repertoires: memory and learning functions of the basal ganglia. *Current Opinion in Neurobiology*, 5, 733–741.
- Greenfield, P. M. (1991). Language, tools, and brain: the ontogeny and phylogeny of hierarchically organized sequential behavior. *Behavioral and Brain Sciences*, 14, 531–595.
- Grodzinsky, Y. (2000). The neurology of syntax: language use without Broca's area. *Behavioral and Brain Sciences*, 23(1), 1–71.
- Grossman, M., Carvell, S., & Peltzer, L. (1993). The sum and substance of it: the appreciation of mass and count qualifiers in Parkinson's disease. *Brain and Language*, 44, 351–384.
- Grossman, M., Payer, F., Onishi, K., D'Esposito, M., Morrison, D., Sadek, A., & Alavi, A. (1998). Language comprehension and regional cerebral defects in frontotemporal degeneration and Alzheimer's disease. *Neurology*, 50, 157–163.
- Haaland, K., Harrington, D., O'Brien, S., & Hermanowicz, N. (1997). Cognitive-motor learning in Parkinson's disease. *Neuropsychology*, 11(2), 180–186.
- Hagoort, P., Brown, C., & Groothusen, J. (1993). The syntactic positive shift (SPS) as an ERP measure of syntactic processing. *Language and Cognitive Processes*, 8(4), 439–483.
- Halbig, T. D., Gruber, D., Scherer, P., Kopp, U. A., Trottenberg, T., & Kupsch, A. (2002). *Subthalamic high frequency stimulation differentially modulates declarative and nondeclarative memory*. Paper presented at the Society for Neuroscience annual meeting, Orlando, FL.
- Halgren, E., Dhond, R. P., Christensen, N., Van Petten, C., Marinkovic, K., Lewine, J. D., & Dale, A. M. (2002). N400-like magnetoencephalography responses modulated by semantic context, word frequency, and lexical class in sentences. *Neuroimage*, 17, 1101–1116.
- Halle, M., & Marantz, A. (1993). Distributed morphology and the pieces of inflection. In K. Hale, & S. J. Keyser (Eds.), *The view from building 20*. Cambridge, MA: MIT Press.
- Hammond, E. J., Meador, K. J., Aung-Din, R., & Wilder, B. J. (1987). Cholinergic modulation of human P3 event-related potentials. *Neurology*, 37(2), 346–350.
- Harrington, D., Rao, S., Haaland, K., Bobholz, J., Mayer, A., Binderx, J., & Cox, R. (2000). Specialized neural systems underlying representations of sequential movements. *Journal of Cognitive Neuroscience*, 12(1), 56–77.
- Harrington, D. L., Haaland, K. Y., Yeo, R. A., & Marder, E. (1990). Procedural memory in Parkinson's disease: impaired motor but not visuoperceptual learning. *Journal of Clinical and Experimental Neuropsychology*, 12(2), 323–339.
- Harris, I., Egan, G., Sonkkila, C., Tochon-Danguy, H., Paxinos, G., & Watson, J. (2000). Selective right parietal lobe activation during mental rotation: a parametric PET study. *Brain*, 123(Pt 1), 65–73.
- Heilman, K. M., Watson, R. T., & Rothi, L. G. (1997). Disorders of skilled movements: limb apraxia. In T. E. Feinberg, & M. J. Farah (Eds.), *Behavioral neurology and neuropsychology* (pp. 227–235). New York: McGraw-Hill.
- Hikosaka, O., Sakai, K., Miyauchi, S., Takino, R., Sasaki, Y., & Putz, B. (1996). Activation of human presupplementary motor area in learning of sequential procedures: a functional MRI study. *Journal of Neurophysiology*, 76(1), 617–621.

- Hikosaka, O., Sakai, K., Nakahara, H., Lu, X., Miyachi, S., Nakamura, K., & Rand, M. K. (2000). Neural mechanisms for learning of sequential procedures. In M. S. Gazzaniga (Ed.), *The new cognitive neurosciences* (pp. 553–572). Cambridge, MA: MIT Press.
- Hill, E. L. (2001). Non-specific nature of specific language impairment: a review of the literature with regard to concomitant motor impairments. *International Journal of Language and Communication Disorders*, 36(2), 149–171.
- Hodges, J. R., & Patterson, K. (1997). Semantic memory disorders. *Trends in Cognitive Sciences*, 1(2), 68–72.
- Hoen, M., & Dominey, P. F. (2000). ERP analysis of cognitive sequencing: a left anterior negativity related to structural transformation processing. *NeuroReport*, 11(14), 3187–3191.
- Howard, J. H., & Howard, D. V. (1997). Age differences in implicit learning of higher-order dependencies in serial patterns. *Psychology and Aging*, 12(4), 634–656.
- Howlin, P. (1984). The acquisition of grammatical morphemes in autistic children: a critique and replication of the findings of Bartolucci, Pierce, and Streiner, 1980. *Journal of Autism and Developmental Disorders*, 14(2), 127–136.
- Iacoboni, M., Woods, R. P., Brass, M., Bekkering, H., Mazziotta, J. C., & Rizzolatti, G. (1999). Cortical mechanisms of human imitation. *Science*, 286, 2526–2528.
- Illes, J., Metter, E. J., Hanson, W. R., & Iritani, S. (1988). Language production in Parkinson's disease: acoustic and linguistic considerations. *Brain and Language*, 33, 146–160.
- Indefrey, P., Hagoort, P., Herzog, H., Seitz, R., & Brown, C. (2001). Syntactic processing in left prefrontal cortex is independent of lexical meaning. *Neuroimage*, 14(3), 546–555.
- Ivry, R. B., & Fiez, J. A. (2000). Cerebellar contributions to cognition and imagery. In M. S. Gazzaniga (Ed.), *The new cognitive neurosciences* (pp. 999–1011). Cambridge, MA: MIT Press.
- Jackendoff, R. (1997). *The architecture of the language faculty*. Cambridge, MA: MIT Press.
- Jaskiw, G. E., Karoum, F. K., & Weinberger, D. R. (1990). Persistent elevations of dopamine and its metabolites in the nucleus accumbens after mild subchronic stress in rats with ibotenic acid lesions of the medial prefrontal cortex. *Brain Research*, 534, 321–323.
- Jenkins, I. H., Brooks, D. J., Nixon, P. D., Frackowiak, R. S., & Passingham, R. E. (1994). Motor sequence learning: a study with positron emission tomography. *Journal of Neuroscience*, 14(6), 3775–3790.
- Jernigan, T. L., Hesselink, J. R., Sowell, E., & Tallal, P. A. (1991). Cerebral structure on magnetic resonance imaging in language- and learning-impaired children. *Archives of Neurology*, 48, 539–545.
- Joanisse, M. F., & Seidenberg, M. S. (1999). Impairments in verb morphology after brain injury: a connectionist model. *Proceedings of the National Academy of Sciences USA*, 96(13), 7592–7597.
- Johnson, J. S., & Newport, E. L. (1989). Critical period effects in second language learning: the influence of maturational state on the acquisition of English as a second language. *Cognitive Psychology*, 21(1), 60–99.
- Johnston, J. R., & Weismer, S. E. (1983). Mental rotation abilities in language-disordered children. *Journal of Speech and Hearing Research*, 26(3), 397–403.
- Jordan, K., Heinze, H. J., Lutz, K., Kanowski, M., & Jancke, L. (2001). Cortical activations during the mental rotation of different visual objects. *Neuroimage*, 13(1), 143–152.
- Kaan, E., & Stowe, L. (2002). Storage and computation in sentence processing: a neuroimaging perspective. In S. Nooteboom, F. Weerman, & F. Wijnen (Eds.), *Storage and computation in the language faculty* (pp. 257–295). Dordrecht: Kluwer.
- Kaan, E., & Swaab, T. (2002). The brain circuitry of syntactic comprehension. *Trends in Cognitive Sciences*, 6(8), 350–356.
- Kampen, D. L., & Sherwin, B. B. (1996). Estradiol is related to visual memory in healthy young men. *Behavioral Neuroscience*, 110(3), 613–617.
- Kensinger, E. A., Ullman, M. T., & Corkin, S. (2001). Bilateral medial temporal lobe damage does not affect lexical or grammatical processing: evidence from the amnesic patient H.M. *Hippocampus*, 11(4), 347–360.
- Kiehl, K. A., Laurens, K. R., & Liddle, P. F. (2002). Reading anomalous sentences: an event-related fMRI study of semantic processing. *Neuroimage*, 17, 842–850.
- Kimura, D. (1999). *Sex and cognition*. Cambridge, MA: MIT Press.
- Kiparsky, P. (1982). From cyclic phonology to lexical phonology. In H. v. d. Hulst, & N. Smith (Eds.), (1) (pp. 131–175). *The structure of phonological representations*, Dordrecht: Foris.

- Knight, R. T., & Grabowecky, M. (2000). Prefrontal cortex, time, and consciousness. In M. S. Gazzaniga (Ed.), *The new cognitive neurosciences* (pp. 1319–1340). Cambridge, MA: MIT Press.
- Knowlton, B. J., Mangels, J. A., & Squire, L. R. (1996). A neostriatal habit learning system in humans. *Science*, 273, 1399–1402.
- Kohler, E., Keysers, C., Umiltà, M. A., Fogassi, L., Gallese, V., & Rizzolatti, G. (2002). Hearing sounds, understanding actions: action representation in mirror neurons. *Science*, 297(5582), 846–848.
- Kosslyn, S., Di, G. G., Thompson, W., & Alpert, N. (1998). Mental rotation of objects versus hands: neural mechanisms revealed by positron emission tomography. *Psychophysiology*, 35(2), 151–161.
- Kuperberg, G. R., McGuire, P. K., Bullmore, E. T., Brammer, M. J., Rabe-Hesketh, S., Wright, I. C., Lythgoe, D. J., Williams, S. C. R., & David, A. S. (2000). Common and distinct neural substrates for pragmatic, semantic, and syntactic processing of spoken sentences: an fMRI study. *Journal of Cognitive Neuroscience*, 12, 321–341.
- Kutas, M., & Hillyard, S. A. (1980). Reading senseless sentences: brain potentials reflect semantic incongruity. *Science*, 207(1), 203–205.
- La Grutta, V., & Sabatino, M. (1988). Focal hippocampal epilepsy: effect of caudate stimulation. *Experimental Neurology*, 99(1), 38–49.
- Leonard, L., Bortolini, U., Caselli, M., McGregor, K., & Sabbadini, L. (1992). Morphological deficits in children with specific language impairment: the status of features in the underlying grammar. *Language Acquisition*, 2(2), 151–179.
- Leonard, L., McGregor, K., & Allen, G. (1992). Grammatical morphology and speech perception in children with specific language impairment. *Journal of Speech and Hearing Research*, 35, 1076–1085.
- Leonard, L. B. (1982). Early lexical acquisition in children with specific language impairment. *Journal of Speech and Hearing Research*, 25, 554–564.
- Leonard, L. B. (1998). Children with specific language impairment. Cambridge, MA: MIT Press.
- Lieber, R. (1992). Deconstructing morphology: word formation in syntactic theory. Chicago, IL: University of Chicago Press.
- Lieberman, P., Kako, E., Friedman, J., Tajchman, G., Feldman, L. S., & Jimenez, E. B. (1992). Speech production, syntax comprehension, and cognitive deficits in Parkinson's disease. *Brain and Language*, 43, 169–189.
- Lipska, B. K., Jaskiw, G. E., Chrapusta, S., Karoum, F., & Weinberger, D. (1992). Ibotenic acid lesion of the ventral hippocampus differentially affects dopamine and its metabolites in the nucleus accumbens and prefrontal cortex in the rat. *Brain Research*, 585, 1–6.
- Lynch, G. (2002). Memory enhancement: the search for mechanism-based drugs. *Nature Neuroscience*, 5(Supplement), 1035–1038.
- MacDonald, M. C., Pearlmutter, N. J., & Seidenberg, M. S. (1994). Lexical nature of syntactic ambiguity resolution. *Psychological Review*, 101(4), 676–703.
- Maess, B., Koelsch, S., Gunter, T. C., & Friederici, A. D. (2001). Musical syntax is processed in Broca's area: an MEG study. *Nature Neuroscience*, 4(5), 540–545.
- Maki, P. M., & Resnick, S. M. (2000). Longitudinal effects of estrogen replacement therapy on PET cerebral blood flow and cognition. *Neurobiology of Aging*, 21(2), 373–383.
- Martin, A., Ungerleider, L. G., & Haxby, J. V. (2000). Category specificity and the brain: the sensory/motor model of semantic representations of objects. In M. S. Gazzaniga (Ed.), *The cognitive neurosciences* (pp. 1023–1036). Cambridge, MA: MIT Press.
- Matelli, M., Camarda, R., Glickstein, M., & Rizzolatti, G. (1986). Afferent and efferent projections of the inferior area 6 in the macaque monkey. *Journal of Comparative Neurology*, 251(3), 281–298.
- Matelli, M., Luppino, G., Murata, M., & Sakata, H. (1994). Independent anatomical circuits for reaching and grasping linking the inferior parietal sulcus and inferior area 6 in macaque monkey. *Society for Neuroscience Abstracts*, 20, 404.4.
- Maynard Smith, J. (1975/1993). The theory of evolution. New York: Cambridge University Press.
- Mayr, E. (1963). Animal species and evolution. Cambridge, MA: Harvard University Press.
- McArthur, G. M., Hogben, J. H., Edwards, V. T., Heath, S. M., & Mengler, E. D. (2000). On the "specifics" of specific reading disability and specific language impairment. *Journal of Child Psychology and Psychiatry*, 41(7), 869–874.

- McClelland, J. L., McNaughton, B. L., & O'Reilly, R. C. (1995). Why there are complementary learning systems in the hippocampus and neocortex: insights from the successes and failures of connectionist models of learning and memory. *Psychological Review*, 102(3), 419–457.
- McDonald, R., & White, N. (1993). A triple dissociation of memory systems: hippocampus, amygdala, and dorsal striatum. *Behavioral Neuroscience*, 107(1), 3–22.
- McEwen, B. S., Alves, S. E., Bulloch, K., & Weiland, N. G. (1998). Clinically relevant basic science studies of gender differences and sex hormone effects. *Psychopharmacology Bulletin*, 34(3), 251–259.
- McLeod, P., Plunkett, K., & Rolls, E. T. (1998). Introduction to connectionist modeling of cognitive processes. New York: Oxford University Press.
- Meck, W. H., & Benson, A. M. (2002). Dissecting the brain's internal clock: how frontal-striatal circuitry keeps time and shifts attention. *Brain and Cognition*, 48(1), 195–211.
- Menon, V., Anagnoson, R. T., Glover, G. H., & Pfefferbaum, A. (2000). Basal ganglia involvement in memory-guided movement sequencing. *NeuroReport*, 11(16), 3641–3645.
- Merritt, D. D., & Liles, B. Z. (1987). Story grammar ability in children with and without language disorder: story generation, story retelling, and story comprehension. *Journal of Speech and Hearing Research*, 30, 539–552.
- Merzenich, M. M., Schreiner, C., Jenkins, W. M., & Wang, X. Q. (1993). Neural mechanisms underlying temporal integration, segmentation, and input sequence representation: some implications for the origin of learning disabilities. *Annals of the New York Academy of Sciences*, 682, 1–22.
- Meyer, M., Friederici, A. D., & von Cramon, D. Y. (2000). Neurocognition of auditory sentence comprehension: event related fMRI reveals sensitivity to syntactic violations and task demands. *Cognitive Brain Research*, 9, 19–33.
- Middleton, F. A., & Strick, P. L. (2000a). Basal ganglia and cerebellar loops: motor and cognitive circuits. *Brain Research Reviews*, 31(2–3), 236–250.
- Middleton, F. A., & Strick, P. L. (2000b). Basal ganglia output and cognition: evidence from anatomical, behavioral, and clinical studies. *Brain and Cognition*, 42(2), 183–200.
- Miles, C., Green, R., Sanders, G., & Hines, M. (1998). Estrogen and memory in a transsexual population. *Hormones and Behavior*, 34(2), 199–208.
- Milner, A. D. (1996). Neglect, extinction, and the cortical streams of visual processing. In P. Thier, & H.-O. Karnath (Eds.), *Parietal lobe contributions to orientation in 3D space* (pp. 3–22). Heidelberg: Springer-Verlag.
- Mishkin, M., Malamut, B., & Bachevalier, J. (1984). Memories and habits: two neural systems. In G. Lynch, J. L. McGaugh, & N. W. Weinburger (Eds.), *Neurobiology of learning and memory* (pp. 65–77). New York: Guilford Press.
- Mitchell, J. A., & Hall, G. (1988). Caudate-putamen lesions in the rat may impair or potentiate maze learning depending upon availability of stimulus cues and relevance of response cues. *Quarterly Journal of Experimental Psychology B*, 40(3), 243–258.
- Moro, A., Tettamanti, M., Perani, D., Donati, C., Cappa, S. F., & Fazio, F. (2001). Syntax and the brain: disentangling grammar by selective anomalies. *Neuroimage*, 13(1), 110–118.
- Moscovitch, M. (1992). Memory and working-with-memory: a component process model based on modules and central systems. *Journal of Cognitive Neuroscience*, 4, 257–267.
- Mostofsky, S. H., Goldberg, M. C., Landa, R. J., & Denckla, M. B. (2000). Evidence for a deficit in procedural learning in children and adolescents with autism: implications for cerebellar contribution. *Journal of the International Neuropsychological Society*, 6(7), 752–759.
- Murphy, D. G., De Carli, C., Daly, E., Haxby, J. V., Allen, G., White, B. J., McIntosh, A. R., Powell, C. M., Horwitz, B., Rapoport, S. I., & Schapiro, M. B. (1993). X-Chromosome effects on female brain: a magnetic resonance imaging study of Turner's syndrome. *Lancet*, 342(8881), 1197–1200.
- Nebes, R. D. (1997). Alzheimer's disease: cognitive neuropsychological aspects. In T. E. Feinberg, & M. J. Farah (Eds.), *Behavioral neurology and neuropsychiatry* (pp. 545–550). New York: McGraw-Hill.
- Neville, H., Nicol, J. L., Barss, A., Forster, K. I., & Garrett, M. F. (1991). Syntactically based sentence processing classes: evidence from event-related brain potentials. *Journal of Cognitive Neuroscience*, 3(2), 151–165.
- Newman, A. J., Pancheva, R., Ozawa, K., Neville, H. J., & Ullman, M. T. (2001). An event-related fMRI study of syntactic and semantic violations. *Journal of Psycholinguistic Research*, 30(3), 339–364.

- Ni, W., Constable, R. T., Menci, W. E., Pugh, K. R., Fulbright, R. K., Shaywitz, S. E., Gore, J. C., & Shankweiler, D. (2000). An event-related neuroimaging study distinguishing form and content in sentence processing. *Journal of Cognitive Neuroscience*, 12(1), 120–133.
- Nicolson, R. I., Daum, I., Schugens, M. M., Fawcett, A. J., & Schulz, A. (2002). Eyeblink conditioning indicates cerebellar abnormality in dyslexia. *Experimental Brain Research*, 143(1), 42–50.
- Nishitani, N., Uutela, K., Shibasaki, H., & Hari, R. (1999). Cortical visuomotor integration during eye pursuit and eye-finger pursuit. *Journal of Neuroscience*, 19(7), 2647–2657.
- Nissen, M. J., Knopman, D. S., & Schacter, D. L. (1987). Neurochemical dissociation of memory systems. *Neurology*, 37(5), 789–794.
- Nobre, A. C., Allison, T., & McCarthy, G. (1994). Word recognition in the human inferior temporal lobe. *Nature*, 372, 260–263.
- Norman, J. (2002). Two visual systems and two theories of perception: an attempt to reconcile the constructivist and ecological approaches. *Behavioral and Brain Sciences*, 25, 73–96.
- Oetting, J. B., & Horohov, J. E. (1997). Past tense marking by children with and without specific language impairment. *Journal of Speech and Hearing Research*, 40, 62–74.
- Ohta, M. (1987). Cognitive disorders of infantile autism: a study employing the WISC, spatial relationships, conceptualization, and gesture imitations. *Journal of Autism and Developmental Disorders*, 17, 45–62.
- Oki, J., Takahashi, S., Miyamoto, A., & Tachibana, Y. (1999). Cerebellar hypoperfusion and developmental dysphasia in a male. *Pediatric Neurology*, 21(4), 745–748.
- Olivares, E., Bobes, M. A., Aubert, E., & Valdes-Sosa, M. (1994). Associative ERP effects with memories of artificial faces. *Cognitive Brain Research*, 2(1), 39–48.
- Opitz, B., & Friederici, A. D. (in press). Interactions of the hippocampal system and the prefrontal cortex in learning language-like rules. *Neuroimage*.
- Osterhout, L., & Holcomb, P. J. (1992). Event-related brain potentials elicited by syntactic anomaly. *Journal of Memory and Language*, 31, 785–806.
- Owen, S., & McKinlay, I. (1997). Motor difficulties in children with developmental disorders of speech and language. *Child: Care, Health and Development*, 23(4), 315–325.
- Packard, M., Hirsh, R., & White, N. (1989). Differential effects of fornix and caudate nucleus lesions on two radial maze tasks: evidence for multiple memory systems. *Journal of Neuroscience*, 9(5), 1465–1472.
- Packard, M., & Knowlton, B. (2002). Learning and memory functions of the basal ganglia. *Annual Review of Neuroscience*, 25, 563–593.
- Packard, M., & McGaugh, J. (1996). Inactivation of hippocampus or caudate nucleus with lidocaine differentially affects expression of place and response learning. *Neurobiology of Learning and Memory*, 65(1), 65–72.
- Packard, M. G. (1998). Posttraining estrogen and memory modulation. *Hormones and Behavior*, 34(2), 126–139.
- Packard, M. G. (1999). Glutamate infused posttraining into the hippocampus or caudate-putamen differentially strengthens place and response learning. *Proceedings of the National Academy of Sciences USA*, 96(22), 12881–12886.
- Passingham, R. (1993) (21). *The frontal lobes and voluntary action*, New York: Oxford University Press.
- Patterson, K., Lambon Ralph, M. A., Hodges, J. R., & McClelland, J. L. (2001). Deficits in irregular past-tense verb morphology associated with degraded semantic knowledge. *Neuropsychologia*, 39, 709–724.
- Peigneux, P., Maquet, P., Meulemans, T., Destrebecqz, A., Laureys, S., Degueldre, C., Delfiore, G., Aerts, J., Luxen, A., Franck, G., Van der Linden, M., & Cleeremans, A. (2000). Striatum forever, despite sequence learning variability: a random effect analysis of PET data. *Human Brain Mapping*, 10(4), 179–194.
- Peigneux, P., Maquet, P., Van der Linden, M., Meulemans, T., Degueldre, C., Delfiore, G., Luxen, A., Cleeremans, A., & Franck, G. (1999). Left inferior frontal cortex is involved in probabilistic serial reaction time learning. *Brain and Cognition*, 40(1), 215–219.
- Penhune, V. B., Zatorre, R. J., & Evans, A. C. (1998). Cerebellar contributions to motor timing: a PET study of auditory and visual rhythm reproduction. *Journal of Cognitive Neuroscience*, 10(6), 752–765.
- Penke, M., Weyerts, H., Gross, M., Zander, E., Munte, T. F., & Clahsen, H. (1997). How the brain processes complex words: an ERP-study of German verb inflections. *Essex Research Reports in Linguistics*, 14, 1–41.
- Perry, R., & Zeki, S. (2000). The neurology of saccades and covert shifts in spatial attention: an event-related fMRI study. *Brain*, 123(Pt 11), 2273–2288.

- Petrides, M. (1996). Specialized systems for the processing of mnemonic information within the primate frontal cortex. *Philosophical Transactions of the Royal Society of London. Series B, Biological Sciences*, 351(1346), 1455–1462.
- Petrides, M., Alivisatos, B., & Evans, A. C. (1995). Functional activation of the human ventrolateral frontal cortex during mnemonic retrieval of verbal information. *Proceedings of the National Academy of Sciences USA*, 92(13), 5803–5807.
- Petrides, M., & Pandya, D. (1984). Projections to the frontal cortex from the posterior parietal region in the rhesus monkey. *Journal of Comparative Neurology*, 228(1), 105–116.
- Phillips, S. M., & Sherwin, B. B. (1992). Effects of estrogen on memory function in surgically menopausal women. *Psychoneuroendocrinology*, 17(5), 485–495.
- Pierce, S., & Bartolucci, G. (1977). A syntactic investigation of verbal autistic, mentally retarded, and normal children. *Journal of Autism and Childhood Schizophrenia*, 7(2), 121–134.
- Pinker, S. (1984) (7). *Language learnability and language development*, Cambridge, MA: Harvard University Press.
- Pinker, S. (1994). *The language instinct*. New York: William Morrow.
- Pinker, S. (1999). *Words and rules: the ingredients of language*. New York: Basic Books.
- Pinker, S., & Ullman, M. T. (2002). The past and future of the past tense. *Trends in Cognitive Sciences*, 6(11), 456–463.
- Podzebenko, K., Egan, G. F., & Watson, J. D. G. (2002). Widespread dorsal stream activation during a parametric mental rotation task, revealed with functional magnetic resonance imaging. *Neuroimage*, 15, 547–558.
- Poldrack, R., & Packard, M. G. (2003). Competition among multiple memory systems: converging evidence from animal and human brain studies. *Neuropsychologia*, 41(3), 245–251.
- Poldrack, R. A., Clark, J., Pare-Blagoev, E. J., Shohamy, D., Moyano, J. C., Myers, C., & Gluck, M. A. (2001). Interactive memory systems in the human brain. *Nature*, 414, 546–550.
- Poldrack, R. A., Prabhakaran, V., Seger, C. A., & Gabrieli, J. D. (1999). Striatal activation during acquisition of a cognitive skill. *Neuropsychology*, 13(4), 564–574.
- Poldrack, R. A., Wagner, A. D., Prull, M. W., Desmond, J. E., Glover, G. H., & Gabrieli, J. D. (1999). Functional specialization for semantic and phonological processing in the left inferior prefrontal cortex. *Neuroimage*, 10(1), 15–35.
- Postle, B. R., & Corkin, S. (1998). Impaired word-stem completion priming but intact perceptual identification priming with novel words: evidence from the amnesic patient H.M. *Neuropsychologia*, 15, 421–440.
- Rammesayer, T. H., Rodewald, S., & Groh, D. (2000). Dopamine-antagonistic, anticholinergic, and GABAergic effects on declarative and procedural memory functions. *Cognitive Brain Research*, 9(1), 61–71.
- Ramondo, N., & Milech, D. (1984). The nature and specificity of the language coding deficit in autistic children. *British Journal of Psychology*, 75, 95–103.
- Rapin, I., & Wilson, B. C. (1978). Children with developmental language disability: neuropsychological aspects and assessment. In M. A. Wyke (Ed.), *Developmental dysphasia* (pp. 13–41). London: Academic Press.
- Resnick, S., Maki, P., Golski, S., Kraut, M., & Zonderman, A. (1998). Effects of estrogen replacement therapy on PET cerebral blood flow and neuropsychological performance. *Hormones and Behavior*, 34(2), 171–182.
- Rice, M., & Oetting, J. B. (1993). Morphological deficits of SLI children: evaluation of number marking and agreement. *Journal of Speech and Hearing Research*, 36(6), 1249–1257.
- Rizzolatti, G., & Arbib, M. A. (1998). Language within our grasp. *Trends in Neuroscience*, 21(5), 188–194.
- Rizzolatti, G., Fadiga, L., Gallese, V., & Fogassi, L. (1996). Premotor cortex and the recognition of motor actions. *Cognitive Brain Research*, 3(2), 131–141.
- Rizzolatti, G., Fogassi, L., & Gallese, V. (2000). Cortical mechanisms subserving object grasping and action recognition: a new view on the cortical motor functions. In M. S. Gazzaniga (Ed.), *The new cognitive neurosciences* (pp. 539–552). Cambridge, MA: MIT Press.
- Rizzolatti, G., Fogassi, L., & Gallese, V. (2001). Neurophysiological mechanisms underlying the understanding and imitation of action. *Nature Review Neuroscience*, 2(9), 661–670.
- Rizzolatti, G., Luppino, G., & Matelli, M. (1998). The organization of the cortical motor system: new concepts. *Electroencephalography and Clinical Neurophysiology*, 106(4), 283–296.
- Ross, J. L., Roeltgen, D., Feuillan, P., Kushner, H., & Cutler, G. B., Jr. (2000). Use of estrogen in young girls with Turner syndrome: effects on memory. *Neurology*, 54(1), 164–170.

- Ruchkin, D. S., Grafman, J., Cameron, K., & Berndt, R. S. (in press). Working memory retention systems: a state of activated long-term memory. *Behavioral and Brain Sciences*.
- Rumelhart, D. E., & McClelland, J. L. (1986). On learning the past tenses of English verbs. In J. L. McClelland, D. E. Rumelhart, & PDP Research Group (Eds.), (2) (pp. 216–271). *Parallel distributed processing: explorations in the microstructures of cognition*, Cambridge, MA: Bradford/MIT Press.
- Rumsey, J. M. (1996). Neuroimaging studies of autism. In G. R. Lyon, & J. Rumsey (Eds.), *Neuroimaging: a window in to the neurological foundations of learning and behavior in children* (pp. 119–146). Baltimore, MD: Brookes.
- Rutter, M. (1978). Diagnosis and definition. In M. Rutter, & E. Schopler (Eds.), *Autism: a reappraisal of concepts and treatment* (pp. 1–25). New York: Plenum.
- Sabatino, M., Ferraro, G., Liberti, G., Vella, N., & La, G. V. (1985). Striatal and septal influence on hippocampal theta and spikes in the cat. *Neuroscience Letters*, 61(1–2), 55–59.
- Sagar, H. J., Cohen, N. J., Sullivan, E. V., Corkin, S., & Growdon, J. H. (1988). Remote memory function in Alzheimer's and Parkinson's disease. *Brain*, 111, 185–206.
- Saint-Cyr, J. A., Taylor, A. E., & Lang, A. E. (1988). Procedural learning and neostriatal dysfunction in man. *Brain*, 111(4), 941–959.
- Sakata, H., & Taira, M. (1994). Parietal control of hand action. *Current Opinion in Neurobiology*, 4(6), 847–856.
- Sakata, H., Taira, M., Mine, S., & Murata, A. (1992). Hand-movement related neurons of the posterior parietal cortex of the monkey: their role in visual guidance of hand movements. In R. Caminiti, P. B. Johnson, & Y. Burnod (Eds.), *Control of arm movement in space* (pp. 185–198). Berlin: Springer-Verlag.
- Schacter, D. L., & Tulving, E. (Eds.), (1994). *Memory systems 1994*. Cambridge, MA: MIT Press.
- Schroeder, J. A., Wingard, J., & Packard, M. G. (2002). Post-training reversible inactivation of the dorsal hippocampus reveals interference between multiple memory systems. *Hippocampus*, 12, 280–284.
- Schubotz, R. I., & von Cramon, D. Y. (2001). Interval and ordinal properties of sequences are associated with distinct premotor areas. *Cerebral Cortex*, 11(3), 210–222.
- Schwartz, M. F., Marin, O. S. M., & Saffran, E. M. (1979). Dissociations of language function in dementia: a case study. *Brain and Language*, 7, 277–306.
- Seidler, R. D., Purushotham, A., Kim, S. G., Ugurbil, K., Willingham, D., & Ashe, J. (2002). Cerebellum activation associated with performance change but not motor learning. *Science*, 296(5575), 2043–2046.
- Sherwin, B. B. (1988). Estrogen and/or androgen replacement therapy and cognitive functioning in surgically menopausal women. *Psychoneuroendocrinology*, 13(4), 345–357.
- Sherwin, B. B. (1998). Estrogen and cognitive functioning in women. *Proceedings of the Society for Experimental Biology and Medicine*, 217(1), 17–22.
- Shimamura, A. P. (1995). Memory and frontal lobe function. In M. S. Gazzaniga (Ed.), *The cognitive neurosciences* (pp. 803–813). Cambridge, MA: MIT Press.
- Shughrue, P. J., Scrimo, P. J., & Merchenthaler, I. (2000). Estrogen binding and estrogen receptor characterization (ERalpha and ERbeta) in the cholinergic neurons of the rat basal forebrain. *Neuroscience*, 96(1), 41–49.
- Sigman, M., & Ungerer, J. A. (1984). Cognitive and language skills in autistic, mentally retarded, and normal children. *Developmental Psychology*, 20(2), 293–302.
- Silveri, M. C., Leggio, M. G., & Molinari, M. (1994). The cerebellum contributes to linguistic production: a case of agrammatic speech following a right cerebellar lesion. *Neurology*, 44, 2047–2050.
- Simos, P. G., Basile, L. F. H., & Papanicolaou, A. C. (1997). Source localization of the N400 response in a sentence-reading paradigm using evoked magnetic fields and magnetic resonance imaging. *Brain Research*, 762(1–2), 29–39.
- Smith, E. E., & Jonides, J. (1997). Working memory: a view from neuroimaging. *Cognitive Psychology*, 33(1), 5–42.
- Smith, E. E., & Jonides, J. (1999). Storage and executive processes in the frontal lobes. *Science*, 283(5408), 1657–1661.
- Snowling, M. (2000). *Dyslexia* (2nd ed.). Oxford: Blackwell.
- Sorensen, K., & Witter, M. (1983). Entorhinal efferents reach the caudato-putamen. *Neuroscience Letters*, 35(3), 259–264.
- Spencer, A. (1991). *Morphological theory*. Cambridge, MA: Basil Blackwell.

- Squire, L. R., Clark, R. E., & Knowlton, B. J. (2001). Retrograde amnesia. *Hippocampus*, 11(1), 50–55.
- Squire, L. R., & Knowlton, B. J. (2000). The medial temporal lobe, the hippocampus, and the memory systems of the brain. In M. S. Gazzaniga (Ed.), *The new cognitive neurosciences* (pp. 765–780). Cambridge, MA: MIT Press.
- Squire, L. R., & Zola, S. M. (1996). Structure and function of declarative and nondeclarative memory systems. *Proceedings of the National Academy of Sciences USA*, 93, 13515–13522.
- Stromswold, K., Caplan, D., Alpert, N., & Rauch, S. (1996). Localization of syntactic comprehension by positron emission tomography. *Brain and Language*, 52, 452–473.
- Suzuki, W. A., & Amaral, D. G. (1994). Perirhinal and parahippocampal cortices of the macaque monkey: cortical afferents. *Journal of Comparative Neurology*, 350(4), 497–533.
- Suzuki, W. A., & Eichenbaum, H. (2000). The neurophysiology of memory. *Annals of the New York Academy of Sciences*, 911, 175–191.
- Szelag, E., von Steinbüchel, N., & Poppel, E. (1997). Temporal processing disorders in patients with Broca's aphasia. *Neuroscience Letters*, 235, 33–36.
- Tager-Flusberg, H. (1985). The conceptual basis for referential word meaning in children with autism. *Child Development*, 56(5), 1167–1178.
- Tallal, P., Jernigan, T. L., & Trauner, D. (1994). Developmental bilateral damage to the head of the caudate nuclei: implications for speech-language pathology. *Journal of Medical Speech-Language Pathology*, 2, 23–28.
- Tallal, P., & Piercy, M. (1978). Defects of auditory perception in children with developmental dysphasia. In M. A. Wyke (Ed.), *Developmental dysphasia* (pp. 63–84). New York: Academic Press.
- Tallal, P., Stark, R., & Mellits, E. (1985). Identification of language-impaired children on the basis of rapid perception and production skills. *Brain and Language*, 25(2), 314–322.
- Thompson-Schill, S. L., D'Esposito, M., Aguirre, G. K., & Farah, M. J. (1997). Role of left inferior prefrontal cortex in retrieval of semantic knowledge: a reevaluation. *Proceedings of the National Academy of Sciences USA*, 94(26), 14792–14797.
- Tirosh, E., & Cohen, A. (1998). Language deficit with an attention-deficit disorder: a prevalent comorbidity. *Journal of Child Neurology*, 13(10), 493–497.
- Tulving, E., Kapur, S., Craik, F. I. M., Moscovitch, M., & Houle, S. (1994). Hemispheric encoding/retrieval asymmetry in episodic memory: positron emission tomography findings. *Proceedings of the National Academy of Sciences USA*, 91, 2016–2020.
- Ullman, M. T., (1999). Naming tools and using rules: evidence that a frontal/basal-ganglia system underlies both motor skill knowledge and grammatical rule use. *Brain and Language*, 69, 316–318.
- Ullman, M. T. (2001a). The declarative/procedural model of lexicon and grammar. *Journal of Psycholinguistic Research*, 30(1), 37–69.
- Ullman, M. T. (2001b). The neural basis of lexicon and grammar in first and second language: the declarative/procedural model. *Bilingualism: Language and Cognition*, 4(1), 105–122.
- Ullman, M. T. (2001c). A neurocognitive perspective on language: the declarative/procedural model. *Nature Reviews Neuroscience*, 2, 717–726.
- Ullman, M. T. (2003). *Is Broca's area part of a frontal/basal-ganglia procedural memory circuit?* Paper presented at Perception, Action, Syntax and the Brain, Max Planck Institute of Cognitive Neuroscience, Leipzig, Germany.
- Ullman, M. T. (in press). Evidence that lexical memory is part of the temporal lobe declarative memory, and that grammatical rules are processed by the frontal/basal-ganglia procedural system. *Brain and Language*.
- Ullman, M. T., Corkin, S., Coppola, M., Hickok, G., Growdon, J. H., Koroshetz, W. J., & Pinker, S. (1997). A neural dissociation within language: evidence that the mental dictionary is part of declarative memory, and that grammatical rules are processed by the procedural system. *Journal of Cognitive Neuroscience*, 9(2), 266–276.
- Ullman, M. T., Estabrooke, I. V., Steinhauer, K., Brovotto, C., Pancheva, R., Ozawa, K., Mordecai, K., & Maki, P. (2002). Sex differences in the neurocognition of language. *Brain and Language*, 83, 141–143.
- Ullman, M. T., & Gopnik, M. (1999). Inflectional morphology in a family with inherited specific language impairment. *Applied Psycholinguistics*, 20(1), 51–117.

- Ullman, M. T., Hartshorne, J. K., Estabrooke, I. V., Broveto, C., & Walenski, M. (submitted). Sex, regularity, frequency and consistency: a study of factors predicting the storage of inflected forms. Manuscript submitted for publication.
- Ullman, M. T., Izvorski, R., Love, T., Yee, E., Swinney, D., & Hickok, G. (in press). Neural correlates of lexicon and grammar: evidence from the production, reading, and judgment of inflection in aphasia. *Brain and Language*.
- Ullman, M. T., & Pierpont, E. I. (in press). Specific language impairment is not specific to language: the procedural deficit hypothesis. *Cortex*.
- Ungerleider, L. G., & Mishkin, M. (1982). Two cortical visual systems. In D. J. Ingle, M. A. Goodale, & R. J. W. Mansfield (Eds.), *Analysis of visual behavior* (pp. 549–587). Cambridge, MA: MIT Press.
- van der Lely, H. K. J. (1996). Specifically language impaired and normally developing children: verbal passive vs. adjectival passive sentence interpretation. *Lingua*, 98, 243–272.
- van der Lely, H. K. J., & Christian, V. (2000). Lexical word formation in children with grammatical SLI: a grammar-specific versus an input-processing deficit? *Cognition*, 75, 33–63.
- van der Lely, H. K. J., & Stollwerck, L. (1996). A grammatical specific language impairment in children: an autosomal dominant inheritance? *Brain and Language*, 52, 484–504.
- van der Lely, H. K. J., & Ullman, M. T. (2001). Past tense morphology in specifically language impaired and normally developing children. *Language and Cognitive Processes*, 16(2), 177–217.
- Van Meter, L., Fein, D., Morris, R., Waterhouse, L., & Allen, D. (1997). Delay versus deviance in autistic social behavior. *Journal of Autism and Developmental Disorders*, 27(5), 557–569.
- Vargha-Khadem, F., Watkins, K. E., Price, C. J., Ashburner, J., Alcock, K. J., Connelly, A., Frackowiak, R. S., Friston, K. J., Pembrey, M. E., Mishkin, M., Gadian, D. G., & Passingham, R. E. (1998). Neural basis of an inherited speech and language disorder. *Proceedings of the National Academy of Sciences USA*, 95(21), 12695–12700.
- Wagner, A. D., Schacter, D. L., Rotte, M., Koutstaal, W., Maril, A., Dale, A. M., Rosen, B. R., & Buckner, R. L. (1998). Building memories: remembering and forgetting of verbal experiences as predicted by brain activity. *Science*, 281(5380), 1188–1191.
- Walenski, M., Sosta, K., Cappa, S., & Ullman, M. T. Deficits on irregular verbal morphology in Italian-speaking Alzheimer's disease participants. Manuscript submitted for publication.
- Weckerly, J., Wulfeck, B., & Reilly, J. (2001). Verbal fluency deficits in children with specific language impairment: slow rapid naming or slow to name? *Child Neuropsychology*, 7(3), 142–152.
- Weismer, S. E., & Hesketh, L. J. (1996). Lexical learning by children with specific language impairment: effects of linguistic input presented at varying speaking rates. *Journal of Speech and Hearing Research*, 39, 177–190.
- Weyerts, H., Penke, M., Dohrn, U., Clahsen, H., & Münte, T. F. (1997). Brain potentials indicate differences between regular and irregular German plurals. *NeuroReport*, 8(4), 957–962.
- White, N. M. (1997). Mnemonic functions of the basal ganglia. *Current Opinion in Neurobiology*, 7, 164–169.
- Whitehouse, D., & Harris, J. C. (1984). Hyperlexia in infantile autism. *Journal of Autism and Developmental Disorders*, 14(3), 281–289.
- Willingham, D. B. (1998). A neuropsychological theory of motor skill learning. *Psychological Review*, 105(3), 558–584.
- Wise, S. P., Boussaoud, D., Johnson, P. B., & Caminiti, R. (1997). Premotor and parietal cortex: corticocortical connectivity and combinatorial computations. *Annual Review of Neuroscience*, 20, 25–42.
- Wise, S. P., Murray, E. A., & Gerfen, C. R. (1996). The frontal cortex-basal ganglia system in primates. *Critical Reviews in Neurobiology*, 10(3–4), 317–356.
- Wolff, P. H., Cohen, C., & Drake, C. (1984). Impaired motor timing control in specific reading retardation. *Neuropsychologia*, 22(5), 587–600.
- Woolley, C. S., & Schwartzkroin, P. A. (1998). Hormonal effects on the brain. *Epilepsia*, 39(8), S2–S8.
- Young, A. B., & Penney, J. B. (1993). Biochemical and functional organization of the basal ganglia. In J. Jankovic, & E. Tolosa (Eds.), *Parkinson's disease and movement disorders* (2nd ed.) (pp. 1–11). Baltimore, MD: Williams and Wilkins.
- Zettin, M., Cappa, S. F., D'Amico, A., Rago, R., Perino, C., Perani, D., & Fazio, F. (1997). Agrammatic speech production after a right cerebellar haemorrhage. *Neurocase*, 3, 375–380.

A NEUROCOGNITIVE PERSPECTIVE ON LANGUAGE: THE DECLARATIVE/PROCEDURAL MODEL

Michael T. Ullman

What are the psychological, computational and neural underpinnings of language? Are these neurocognitive correlates dedicated to language? Do different parts of language depend on distinct neurocognitive systems? Here I address these and other issues that are crucial for our understanding of two fundamental language capacities: the memorization of words in the mental lexicon, and the rule-governed combination of words by the mental grammar. According to the declarative/procedural model, the mental lexicon depends on declarative memory and is rooted in the temporal lobe, whereas the mental grammar involves procedural memory and is rooted in the frontal cortex and basal ganglia. I argue that the declarative/procedural model provides a new framework for the study of lexicon and grammar.

Language depends on two mental capacities: a memorized 'mental lexicon' and a computational 'mental grammar'^{1,2}. The mental lexicon is a repository of stored information, including all idiosyncratic, word-specific information. It includes those words with arbitrary sound-meaning pairings, such as the non-compositional word 'cat'. It is also thought to contain other irregular word-specific information, such as any arguments that must accompany a verb ('devour' must be accompanied by a direct object), and any unpredictable forms that a word takes ('teach' takes 'taught' as its past tense). The mental lexicon might also comprise complex linguistic structures, such as phrases and sentences, the meanings of which cannot be derived transparently from their parts (for example, idiomatic phrases such as 'kick the bucket').

But language also consists of regularities, which can be captured by the rules of grammar. The rules constrain how lexical forms can combine to make complex representations, and allow us to interpret the meanings of complex forms even if we have not heard or seen them before. For example, in the sentence 'Clementina glicked the plag', we know that Clementina did something in the past to some entity. The meaning can be derived from rules that underlie not only the sequential

order of lexical items, but also their hierarchical relations. In this example, an abstract representation for the verb phrase 'glicked the plag' contains a representation for the noun phrase 'the plag'. This grammatical ability to derive meaning from any well-formed complex structure underlies the incredible productivity and creativity of human language. Such rule-governed behaviour is found at various levels in language; for example, in phrases and sentences (syntax), and in complex words such as 'walked' or 'glicked' (morphology). Importantly, the rules are a form of mental knowledge, in that they underlie our individual capacity to produce and comprehend complex forms. Moreover, the rules underlie mental operations that manipulate words and abstract representations in the composition of complex structures. The learning and use of the rules and operations of grammar are generally implicit (subconscious), and it has been argued that such grammatical knowledge is not available to other cognitive operations — it is 'informationally encapsulated'³. Last, although complex representations ('walked') could be computed anew each time they are used ('walk' + '-ed'), and certainly must be if they have not been previously encountered ('glicked'), they could, in principle, also be stored in the mental lexicon after being constructed.

*Departments of
Neuroscience, Linguistics,
Psychology and Neurology,
Georgetown University,
Research Building, 3900
Reservoir Road North West,
Washington DC 20007, USA.
e-mail:
michael@georgetown.edu*

The declarative/procedural model

The neurocognitive bases of the mental lexicon and the mental grammar have been the focus of many studies^{2,4-7}, which have concentrated on several issues including separability (do lexicon and grammar depend on distinct or shared neurocognitive correlates?), computation (what computational mechanisms underlie the learning, representation and processing of the two language capacities, and how is linguistic knowledge represented?), domain specificity (are the neurocognitive correlates of lexicon and grammar dedicated only to language, or do they subserve other functions?), and the identification of their neural correlates (can we localize their neural circuitry to particular brain structures; what is the temporal order in which these structures participate during language processing, and how do they interact?).

Several models have attempted to address these issues. Here I focus on one model — the declarative/procedural model — and compare its claims and predictions with those of competing models. The basic premise of the declarative/procedural model is that aspects of the lexicon/grammar distinction are tied to the distinction between two well-studied brain memory systems — declarative and procedural memory — that have been implicated in non-language functions in humans and other animals^{8,9}.

The declarative memory system¹⁰⁻¹² has been implicated in the learning, representation and use of knowledge about facts (semantic knowledge) and events (episodic knowledge). This memory system seems to be closely related to the ventral visual stream¹³. It might be particularly important for learning arbitrarily related items — that is, for the associative/contextual binding of information. The knowledge might be explicitly (consciously) recollected, and might not be informationally encapsulated, but accessible to multiple mental systems¹¹. Declarative memory is subserved by regions of the medial temporal lobe — in particular, the hippocampus — which are largely connected with temporal and temporoparietal neocortical regions¹⁴. The medial temporal lobe is required to consolidate (and possibly to retrieve) new memories, although they eventually become independent of the medial temporal lobe and depend on neocortical regions, particularly those in the temporal lobe^{15,16}. Other brain structures are also part of this system. Anterior prefrontal cortex might underlie the selection or retrieval^{17,18} of declarative memories, whereas portions of the right cerebellum might be involved in searching for this knowledge¹⁸.

The procedural memory system¹⁰⁻¹² has been implicated in learning new, and controlling well-established, motor and cognitive skills. Learning and remembering these procedures is largely implicit. It has been argued that the procedural system is informationally encapsulated, having relatively little access to other mental systems¹¹. (Note that I use the term 'procedural memory' to refer to only one particular brain memory system¹¹ and not to all non-declarative or implicit memory systems.) The system is rooted in portions of the frontal

cortex (including Broca's area and the supplementary motor area), the basal ganglia, parietal cortex and the dentate nucleus of the cerebellum^{10-12,19-22}. This system might be related to the dorsal visual stream¹³ and is important for learning or processing skills that involve action sequences²³. The execution of these skills seems to be guided in real time by the posterior parietal cortex, which is densely connected to frontal regions¹³. Inferior parietal regions might serve as a repository for knowledge of skills, including information about stored sequences²⁰. Similarly, the basal ganglia are also densely connected to the frontal cortex²⁴. Basal ganglia circuits seem to be arranged in parallel and are functionally segregated; each of them projects through the thalamus to a particular cortical region, largely in the frontal cortex²⁴.

According to the declarative/procedural model, the declarative memory system underlies the mental lexicon, whereas the procedural system subserves aspects of mental grammar. So, declarative memory is an associative memory that stores not only facts and events, but also lexical knowledge, including the sounds and meanings of words. Learning new words relies largely on medial temporal lobe structures. Eventually, the knowledge of words becomes independent of the medial temporal lobe and dependent on other neocortical areas, particularly those in temporal and temporoparietal regions. The temporal lobe might be particularly important for storing word meanings, whereas temporoparietal regions might be more important in storing word sounds. Lexical memory is not informationally encapsulated, but is accessible to multiple mental systems.

On the other hand, procedural memory subserves the implicit learning and use of a symbol-manipulating grammar across subdomains that include syntax, morphology and possibly phonology (how sounds are combined). The system might be especially important in grammatical-structure building — that is, in the sequential and hierarchical combination of stored forms ('walk' + '-ed') and abstract representations into complex structures. The learning of rules should depend on parts of the system that are involved in procedural learning. One or more circuits between the basal ganglia and particular frontal regions might subserve grammatical processing and perhaps even finer distinctions, such as morphology versus syntax. From this point of view, the frontal cortex and basal ganglia are 'domain general', in that they subserve non-linguistic and linguistic processes, but contain parallel, 'domain-specific' circuits.

It is important to note that the model does not assume that all parts of the two memory systems subserve language. At least in the procedural system, and probably also in the declarative system, parallel circuits are posited to have analogous computational functions in language and in other domains. Similarly, the model does not assume that these two memory systems are the only systems that underlie lexicon and grammar. Other neural structures and other cognitive or computational components might be important for both capacities.

INFLECTIONAL MORPHOLOGY

The modification of a word to fit its grammatical role. For example, 'sang' and 'walked' are inflected in the past tense.

DERIVATIONAL MORPHOLOGY

The creation of new words. For example, the nouns 'solemnity' and 'toughness' are derived from the adjectives solemn and tough, respectively.

Comparison with other models

The declarative/procedural model is similar in certain respects to other 'dual-system' models^{1,2,25}. These models hold that lexicon and grammar are separable and subserved by distinct cognitive systems^{1,2,26}. The learning, representation and processing of words and other arbitrary information in a rote or associative memory is subserved by one or more systems that might be specialized for and dedicated to these functions^{1,3,27}. It has been claimed that the use of stored words might depend on left temporal and temporoparietal structures⁷. The learning, knowledge and processing of grammar are also subserved by one or more systems that are dedicated to their linguistic functions. The grammar manipulates symbols

representing lexical forms and abstract representations, combining them to construct complex linguistic structures. These structures are often suggested to be composed from their parts every time they are used^{12,28,29}. Grammar has been claimed to depend on the left frontal cortex, particularly on Broca's area and adjacent anterior regions^{30,31}. So, the declarative/procedural model shares several features with other dual-system models. Their differences will become clearer when I discuss the specific predictions made by each of them.

'Single-system' theories posit that the learning and use of the words and rules of language depend on a single computational system that has a broad anatomical distribution^{32,33}. According to this view, there is no categorical distinction between non-compositional and compositional forms. Instead, rules are only descriptive entities, and the system gradually learns the entire statistical structure of language, from the arbitrary mappings in non-compositional forms to the rule-like mappings of compositional forms. Modern connectionist theory has offered a computational framework for the single-system view. It has been argued that the learning, representation and processing of grammatical rules and lexical items take place over many interconnected, simple processing units. Learning occurs by adjustments to the weights of connections on the basis of statistical contingencies in the environment^{4,34}.

Deciding between these competing perspectives has been problematic, partly because tasks that probe for lexicon or grammar usually differ in ways other than their use of the two capacities. For example, it is difficult to match measures of grammatical processing in sentence comprehension with measures of lexical memory. For this reason, much recent research has focused on the distinction between regular and irregular morphology, especially in English past tense^{9,25,34,35}. This offers a comparison between two otherwise well-matched types of linguistic form. The application and construction of irregular past-tense forms is not entirely predictable (compare, for example, bring-brought, sing-sang and come-came), and must therefore depend on memorized representations^{9,25,29}. Regular past tenses follow a simple rule, the affixation of '-ed', which is the default transformation for the past tense. Regular past tenses could therefore be rule products. This distinction between regular and irregular forms is found across languages, in both INFLECTIONAL MORPHOLOGY and DERIVATIONAL MORPHOLOGY. So, the irregular/regular distinction offers a relatively simple and well-studied cross-linguistic approach for examining the neurocognitive correlates of lexicon and grammar.

Predictions of the models

Dual-system models predict that representations of irregulars are stored in lexical memory, whereas regulars are grammatical rule products (BOX 1). Single-system models argue that all forms are learned, represented and processed in an associative memory, which can be modelled by a connectionist network. Whereas early connectionist models focused on the phonological mappings between stem and past tense^{34,36}, a recent

Box 1 | Dual-system models and regular/irregular morphology

All dual-system models assume that regular (default) forms are computed by rules that manipulate symbols representing their parts, whereas the use of irregular (non-default) forms involves form-specific stored representations. However, the models differ in the specific aspects of these claims.

Regular forms

'Piece-based' theories, such as the declarative/procedural model, assume that affixes are stored lexical items that are combined with stems^{25,29,134}. Some piece-based theories assume that pieces are put together anew each time they are used^{9,25,29,134}. For example, 'walked' is the real-time product of a function combining two arguments — 'walk' and '-ed'. Other piece-based theories posit that forms are combined from pieces and then stored as whole words¹³⁵, with or without more-specific representation of part-whole structure. So, 'walked' is listed as a whole word but could also contain information specifying its constituent parts 'walk' and '-ed'.

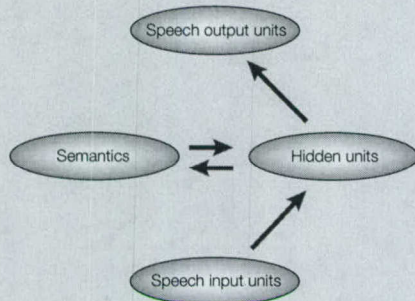
Other dual-system theories deny the piece-based computation of complex words. These posit that, unlike phrases and sentences, the parts of complex words do not exist as separate pieces, but are specified by relations that capture regularities among words. For example, 'walked' is related to 'walk' by an affixation function that takes 'walk' as its only argument. The controversy between real-time computation and memorized representations also exists among these theories. Although it is sometimes assumed that regular complex words are computed anew whenever they are used¹³⁶, it is alternatively claimed that the representations of existing forms are stored^{137,138}.

Irregular forms

Because the application of an irregular transformation is, by definition, arbitrary, all dual-system models claim that each word is associated with some type of stored information regarding any irregular transformations. Theories differ as to how the information is represented, what type of information is stored, and with which irregular items it is stored. Some models suggest that any memorized irregulars are stored as symbols in a rote memory^{29,48}. All such models admit that 'suppletive' forms (utterly idiosyncratic, as in go-went) must be stored. However, it has been argued that subregularities that are found among many irregular transformations (for example, the shared pattern in sing-sang, spring-sprang and ring-rang) can be captured by rules of grammar^{29,139}. Although memorized representations that link the stems of irregulars to their individual rules must exist, the irregular morphological forms themselves are suggested to be rule products that are computed anew each time they are used. These rule products can be computed by morphophonological 'stem-readjustment rules' for forms that undergo stem changes (dig-dug or sing-sang) and/or affixation rules. Last, several dual-system models, including the declarative/procedural model, claim that irregulars are represented and processed in a distributed associative memory that is at least partially productive, therefore allowing the generation of new irregulars (for example, spling-splang). So, the system learns the mappings of individual morphologically complex forms (sing-sang), learns patterns common to the mappings of different forms (sing-sang, spring-sprang, ring-rang), and can then generalize these patterns to new forms (spling-splang). Moreover, some of these models²⁵, including the declarative/procedural model, assume that the representations of forms can be structured, reflecting the morphophonological and phonological part-whole structures of words.

Box 2 | A single-system model of regular/irregular morphology

Double dissociations between regular and irregular forms have posed a problem for single-system language models, but a recent model³⁵ has tried to go beyond this limitation. The model contains distinct representations for semantics, and for input and output phonology, each being subserved by a separate set of units. These units (ellipses), and the pathways between



them (arrows), are assumed to be neuroanatomically distinct, and can therefore be lesioned independently. Although the model claims distinct representations and pathways, it is a single-system model in that it assumes a uniformity of processing mechanisms. All representations and pathways underlie the computation of both regular and irregular morphological forms. It is suggested that the inconsistent phonological patterns of irregulars result in their computation relying more on semantics than on phonology. Regulars, by contrast, do not show this bias, and novel verbs actually show the opposite pattern, relying for their computation on phonology but not on semantics.

Simulations of damage to the semantic representation led to worse performance in producing irregular rather than regular or novel past tenses. Simulations of damage to output phonology led to worse performance in producing novel rather than regular and irregular past tenses, but no difference between regulars and irregulars. So, the model revealed double dissociations between irregular and novel verbs but, crucially, not between irregular and regular forms, even from lesions to output phonology. The results from this simulation do not fit the empirical data from patients. For example, several reports^{8,68–72,74} have revealed a consistent pattern of worse performance by patients with anterior aphasia in processing regular than irregular past tenses over five classes of task: production, reading, judgement, writing and repetition.

single-system model attempted to integrate semantic and phonological knowledge, which are assumed to be linked to temporal lobe and frontal lobe structures, respectively³⁵ (BOX 2).

The declarative/procedural model predicts that irregular forms are stored in declarative memory. This is an associative memory of distributed representations, over which the phonological and semantic mappings of the transformations are learned, stored and computed (BOX 1). The procedural system, by contrast, is suggested to subserve the composition of regular forms from their parts in real time ('walk' + '-ed'). The computation of a morphologically complex form involves the parallel activation of the two systems; the declarative system tries to compute a form in associative memory, while the procedural system attempts to compute a rule product in real time³⁷. As the memory-based computation proceeds, a continuous signal is sent to the rule-processing system, indicating the probability of the successful retrieval of a form from declarative memory. This signal prevents the procedural system from carrying out its computation. So the computation of 'dug' blocks the computation of 'digged'. If a memorized form is not retrieved, then the rule can apply, resulting in over-regularization errors such as 'digged'^{8,37–40}. In addition, the successful computation

of a form by the procedural system should inhibit the memorization of that form in declarative memory, therefore decreasing the likelihood of memorizing regular forms. However, any regular form can, in principle, be memorized. The likelihood of memorization should increase with factors such as the frequency with which the item is encountered or individual variation in learning abilities of the declarative memory system.

The different theoretical perspectives make specific predictions about the issues that I have discussed above, allowing the theories to be distinguished empirically.

Separability. The declarative/procedural model and other dual-system models posit that lexicon and grammar are subserved by separable cognitive systems, with at least partially distinct neural correlates. So, these models predict DOUBLE DISSOCIATIONS between the two language capacities. Single-system models do not invoke separate underpinnings for lexicon and grammar, and therefore do not predict such double dissociations.

Computation. The declarative/procedural model assumes that language involves an associative memory system and a symbol-manipulation system. This assumption is consistent with other dual-system models, although many such models adopt the distinct perspective that lexical memory is a rote list of words (BOX 1). According to the declarative/procedural model, psychological markers of associative memory, such as FREQUENCY EFFECTS and phonological-similarity effects^{40–43}, should be found with memorized lexical items including irregular forms, but not with regular and other complex linguistic forms that are rule-computed in real time. By contrast, single-system models predict associative memory effects for all linguistic forms.

Domain generality. According to the declarative/procedural model, but not to other dual- or single-system models, lexicon and grammar are subserved by distinct systems, each of which underlies a specific set of non-language functions. Only the declarative/procedural model predicts associations in learning, representation and processing, among irregular forms, non-compositional lexical items, facts and events. Similarly, only this model predicts associations between regular forms, aspects of syntax and other domains of grammar, and motor and cognitive skills.

Localization. The declarative/procedural model makes specific claims about links between the two language capacities and sets of specific brain structures on the basis of the roles of these structures in the two memory systems. Certain dual-system models predict similar links, but they do not make the particular neuro-anatomical claims of the declarative/procedural model. Single-system models do not predict the same function-structure associations.

As I discuss next, these predictions are supported by evidence from several languages, obtained using a range of methodological approaches in children and adults.

DOUBLE DISSOCIATION

A double dissociation is observed when two different tasks lead to complementary patterns in behaviour or brain activation. Task X is normal in patient A but not patient B, whereas task Y is normal in patient B but not in A. Similarly, in scanning healthy subjects, task X leads to activation in one brain area but not another, whereas task Y shows the opposite pattern.

FREQUENCY EFFECTS

Words stored in memory are remembered better and faster if they have been more frequently encountered.

Psycholinguistic evidence

Frequency effects⁵ are expected for representations stored in the lexicon, but not for representations that are constructed by mental rules in real time. Several studies have found frequency effects for irregular but not for regular past-tense forms^{40,41,43–45}. A similar contrast has been found between irregular and regular plurals in German^{46,47}. These data indicate that the representations of irregular but not regular past tenses are retrieved from memory^{9,43}. However, frequency effects for some regular past tenses, such as those in which stems rhyme with the stems of irregulars (for example, glide–glided; compare with hide–hid and ride–rode), indicate that at least some regular forms can be stored^{9,40}.

If multiple stored representations share distributed memory traces, then strengthening one representation will strengthen all of them (BOX 1). Such distributed-frequency (phonological-similarity) effects have been found for real and novel irregular past tenses (for example, spring–sprang and spling–spling), but not for real or novel regular past tenses (walk–walked and grock–grocked)^{40,42,43,48}. Analogous contrasts between regular and irregular forms have been found for adjectival past-tense inflection in Japanese⁴⁹. These contrasting phonological-similarity effects support the declarative/procedural and other dual-system models in which irregulars, but not regulars, are represented in a distributed associative memory.

These effects indicate that representations of irregular, but not regular, forms are generally memorized. However, real-time rule processing can also be examined directly. One widely used method is PRIMING⁵. Studies of English past tense, and German participles and plurals, have consistently shown that a target word stem ('walk') is consistently primed as much by its regular inflected form ('walked') as by itself ('walk'); this is not the case for irregulars^{50–52}. This indicates that regulars but not irregulars are decomposed into their stems, as predicted by dual-system models.

The real-time composition of regulars has also been tested by examining the limited storage capacity of working memory. The number of items that it is possible to hold actively in mind is relatively small. If regular complex words ('walked') are composed in real time from multiple independent pieces ('walk' and '-ed'), then maintaining them in working memory would involve maintaining each of their constituent pieces. By contrast, for forms that are associated with a single memorized representation (irregulars), one should need to maintain only one element. It should therefore be possible to retain fewer forms that are composed from two or more independent pieces than forms that are not. Indeed, performance in a working memory task was worse for regular than for irregular past tenses⁵³. The results support the real-time composition of regulars from their stems and affixes.

Evidence from developmental disorders

Specific language impairment. This term is often assigned to developmental language disorders that do not have any other apparent social, psychological or neurological cause⁵⁴. Although specific language impairment (SLI) is a

heterogeneous disorder, homogeneous groups of people with SLI have been identified⁵⁴, including groups with a hereditary form of the disorder that is accompanied by syntactic deficits^{55,56}. Processing of past tense was examined in two such groups^{45,57,58}, both of which failed to produce novel regular forms (for example, plam–plammed) and over-regularizations (dig–digged), indicating that they were unable to apply the '-ed' suffix productively. Both groups showed frequency effects for regular as well as irregular past-tense forms^{45,57,58}. These data indicate that subjects with SLI had difficulty in learning grammatical rules and were therefore forced to memorize regular as well as irregular forms^{45,57,58}. Motor-skill performance and brain abnormalities were probed in one of the groups. Consistent with an underlying deficit of the procedural memory system, they showed impairments in performing motor sequences⁵⁹ and abnormalities in frontal cortical regions, including the left supplementary motor area and Broca's area, and in the caudate nucleus of the basal ganglia⁶⁰. These findings link the rule of '-ed' affixation for regular verbs to syntax and procedural memory.

Williams' syndrome. People with WILLIAMS' SYNDROME might have spared syntactic abilities but abnormal lexical retrieval^{61,62}. Children and adults with the disorder have more difficulty producing irregular than regular past tenses (dig–dug versus look–looked) and plurals (mouse–mice versus rat–rats). Most of their errors are over-regularizations (digged, mouses)^{62,63}. These results help to dissociate irregular from regular forms, and link irregulars to lexical memory and regulars to syntactic abilities.

Neurological evidence

Aphasia. There are at least two fundamental classes of APHASIA — anterior and posterior^{64–66}. Anterior aphasia is associated with damage to left frontal regions — in particular, to Broca's area and nearby cortex — the basal ganglia and portions of inferior parietal cortex^{64,65}. People with anterior aphasia typically show AGRAMMATISM, but are relatively spared in their use of non-compositional words. Anterior aphasia is also linked to IDEOMOTOR APRAXIA^{6,20}. Posterior aphasia, in turn, is associated with damage to left temporal and temporoparietal regions. People with posterior aphasia show impairments in the production, reading and recognition of word sounds and meanings. These patients tend to produce syntactically well-structured sentences and do not omit morphological affixes such as '-ed'⁶. Posterior aphasia is also linked with semantic impairments in non-language domains, but not with motor deficits^{64,67}.

People with anterior aphasia are worse at producing^{8,68}, reading out loud^{8,68–73}, writing to dictation⁷⁴, repeating⁷¹ and judging⁶⁸ regular versus irregular past-tense forms. These patients also have more difficulty in reading^{69,70} and writing⁷⁴ regular compared with irregular plurals. Patients with posterior aphasia show the opposite pattern: worse production^{8,68}, reading⁶⁸ and judgement⁶⁸ of irregular past tenses. Similar double dissociations have been found with a priming task^{75,76}. In Japanese, the

PRIMING

A word is recognized faster if it has been primed by an earlier presentation of the same word.

WILLIAMS' SYNDROME

A hereditary developmental disorder characterized by cognitive impairment (usually mild mental retardation), distinctive facial features and cardiovascular disease.

APHASIA

Language impairments acquired as a result of stroke or other brain injury.

AGRAMMATISM

Syntactic and morphological impairments in production and comprehension, including those in the use of free and bound grammatical morphemes (auxiliaries, determiners, and affixes such as '-ed').

IDEOMOTOR APRAXIA

An impairment in the expression of motor skills. Patients with ideomotor apraxia have problems with imitation, pantomime and tool use.



Figure 1 | Haemodynamic responses to syntactic and lexical/semantic violations detected by fMRI. Haemodynamic responses averaged over 14 subjects in a functional magnetic resonance imaging (fMRI) study. **a** | Syntactic violations elicited greater blood-oxygen-level-dependent (BOLD) activations than semantic violations, primarily in bilateral superior frontal gyrus, corresponding to Brodmann areas (BA) 6 and 8, including the supplementary motor area. Additional activations were observed in the left insula and right anterior superior temporal sulcus. **b** | Semantic anomalies yielded a different pattern of activation, with substantially more temporal and temporoparietal involvement than syntactic anomalies, in the angular gyri bilaterally (BA 39), the right middle temporal gyrus (BA 21), and left hippocampus and parahippocampal gyrus. Additional activations were found in dorsolateral prefrontal cortex and medial foci. Reproduced with permission from REF. 103 © 2001 Plenum Publishing Corporation.

double dissociation between people with anterior and posterior aphasia has been found in a judgement task of regular and irregular forms in derivational morphology⁷⁷. The findings link irregular forms to lexical and non-linguistic semantic memory, and to temporal/temporoparietal cortex, and link regular forms to syntax, motor skills, and left frontal cortex and the basal ganglia.

Neurodegenerative disease. Alzheimer's disease largely affects structures in the temporal lobe, leaving frontal cortex (particularly Broca's area and motor regions) and the basal ganglia relatively spared⁷⁸. Temporal-lobe dysfunction might explain the impairments of patients with Alzheimer's disease in learning new and using established lexical and conceptual knowledge^{79–81}. These patients are relatively spared at acquiring and expressing motor and cognitive skills^{79,82–84}, and aspects of syntactic processing^{85,86}. In the morphology domain, investigations of past

tense have found that error rates in object naming and in fact retrieval correlate with error rates in producing irregular but not regular forms^{84,87}. Patients with severe deficits in object naming or fact retrieval make more errors in producing irregular than regular past tenses. Similarly, Italian patients with Alzheimer's disease have greater difficulty in producing irregular than regular present tense and past participle forms in Italian⁸⁸.

Semantic dementia is associated with severe degeneration of inferior and lateral regions of the temporal lobe. The disorder results in the loss of lexical and non-linguistic conceptual knowledge⁸⁹, with spared motor, syntactic and phonological abilities⁹⁰. Patients with semantic dementia yield a pattern like that of patients with Alzheimer's disease. They have more trouble producing and recognizing irregular than regular past tenses, and the degree of their impairment on irregular forms correlates with their performance on an independent lexical memory task⁹¹. The data link irregular forms to stored words and conceptual knowledge, and to inferior and lateral temporal lobe regions.

Parkinson's disease is associated with the degeneration of dopamine neurons, especially in the substantia nigra of the basal ganglia. Loss of dopamine leads to the suppression of motor activity (hypokinesia) and difficulty in expressing motor sequences^{19,92,93}. It might also account for the impairments of patients with Parkinson's disease in acquiring motor and cognitive skills^{83,94}, and in grammatical processing^{95–97}. By contrast, the temporal lobe remains relatively undamaged in these patients, and the use of words and facts remains relatively intact, if dementia is not present^{80,83,93}. In fact, non-demented patients with Parkinson's disease that suffer from severe hypokinesia show a pattern opposite to that found among patients with Alzheimer's disease, making more errors when producing regular versus irregular past tenses. The level of right-side hypokinesia, which reflects degeneration of the left basal ganglia, correlates with error rates in the production of regular but not irregular forms. Intriguingly, left-side hypokinesia is not accompanied by the analogous correlations with error rates in the production of any type of past tense, underscoring the role of left structures in the use of grammatical rules⁸⁷.

Although Huntington's disease is also associated with degeneration of the basal ganglia, it involves different structures than those affected in Parkinson's disease; in particular, regions of the caudate nucleus. This degeneration leads to unsuppressible movements (hyperkinesia) instead of the hypokinesia that characterizes people with Parkinson's disease⁹². In the language domain, patients with Huntington's disease also show the opposite pattern of abnormalities to that found in Parkinson's disease⁸⁷. Patients with Huntington's produce forms like 'walked-ed' and 'dugged', but not analogous errors on irregular verbs like 'dugug' or 'keptet', indicating that these errors are not attributable to articulatory or motor deficits. Instead, the data point to unsuppressed '-ed' suffixation. The finding that the production rate of these over-suffixed forms correlates with the degree of chorea, across patients, strengthens this conclusion. The findings in Parkinson's and Huntington's diseases strongly implicate

frontal cortex and the basal ganglia in '-ed' suffixation. More generally, they support the hypothesis that these structures underlie the expression of grammatical rules, as well as movement, and indicate that they have a similar function in the two domains.

Amnesia. Bilateral damage to medial temporal lobe structures leads to an inability to learn new information about facts, events and words¹². Importantly, neither phonological nor semantic lexical knowledge is acquired^{98,99}, supporting the hypothesis that these structures underlie the learning of word forms, as well as meanings. The ANTEROGRADE AMNESIA seen after damage to the temporal lobe is accompanied by variable degrees of RETROGRADE AMNESIA. However, knowledge acquired a long time before the lesion tends to be spared¹². So, although medial temporal lobe structures underlie the learning of new lexical information, knowledge of words learned during childhood should be intact in adult-onset amnesia. As expected, our examination of the well-studied global amnesic H.M.¹⁰⁰ revealed that he did not differ from normal age- and education-matched subjects in syntactic processing tasks, or in the production of regular and irregular forms in past-tense, plural and derivational morphology.

ANTEROGRADE AMNESIA

The inability to store new information in long-term memory.

RETROGRADE AMNESIA

Loss of or inability to recall information that was previously stored in long-term memory.

H.M.

Arguably the best-studied patient in the literature on memory, H.M. became amnesic after the bilateral resection of large parts of the temporal lobe in an attempt to treat epilepsy episodes. The analysis of H.M.'s amnesia provided a clear dissociation between declarative and procedural memory.

MAGNETOENCEPHALOGRAPHY

A non-invasive technique that allows the detection of the changing magnetic fields that are associated with brain activity. As the magnetic fields of the brain are very weak, extremely sensitive magnetic detectors known as superconducting quantum interference devices, which work at very low, superconducting temperatures (-269°C), are used to pick up the signal.

DIPOLE MODELLING

A method to determine the location of the sources that underlie the responses measured in a magnetoencephalographic experiment. It provides an estimate of the location, orientation and strength of the source as a function of time after the stimulus was presented.

Neuroimaging evidence

Haemodynamics. Several studies using positron emission tomography (PET) and functional magnetic resonance imaging (fMRI) have investigated the pattern of brain activation during language processing. Lexical and semantic processing is strongly associated with activation in temporal/temporoparietal regions, including the medial temporal lobe (FIG. 1)^{16,101–104}. In addition, selection or retrieval of lexical and semantic knowledge leads to activation in anterior prefrontal cortex¹⁷. By contrast, several tasks that are designed to probe syntactic processing preferentially elicit activation of Broca's area, the supplementary motor area (FIG. 1) and the left basal ganglia (caudate nucleus)^{102,105–109}. Interestingly, the processing of lexically stored syntactic knowledge (for example, word-specific knowledge about what arguments a verb takes) is accompanied by activation of the temporal lobe¹⁰⁴.

Imaging studies have examined the production of regular and irregular forms in the English past tense^{110–112}, and in the German past tense and past participle¹¹³. These studies have found differential activation in frontal and temporal regions for the two forms, although the specific regions have varied across the studies⁹. A study of Finnish, a morphologically very rich and productive language, reported greater activation in Broca's area for regular morphologically complex words than for non-compositional words¹¹⁴, strengthening the view that this region underlies rule-based morphological processing.

Electrophysiology. Event-related potentials (ERPs) reflect the real-time electrophysiological activity of the brain elicited by cognitive processes that are time-locked to the presentation of target stimuli. Difficulties in semantic processing with lexical or non-linguistic stimuli elicit central/posterior bilateral negativities that peak

about 400 ms post stimulus (N400s), and depend on bilateral temporal lobe structures^{115–117}. Difficulties in rule-governed syntactic processing can yield early (150–500 ms) left anterior negativities (LANs)^{118,119}, which have been linked to rule-based automatic computations¹²⁰ and left frontal structures¹²¹. Intriguingly, difficulties in processing word-specific syntactic knowledge can elicit an N400 rather than a LAN¹²². Syntactic processing difficulties also tend to elicit late (600 ms) centroparietal positivities (P600s)¹²³. However, these positivities are associated with controlled processing¹²⁰ and posterior brain regions, and are not suggested to depend on the procedural system.

Several ERP studies have examined regular and irregular inflectional morphology in German^{124,125}, Italian¹²⁶ and English^{127–129}. All of these studies have found distinct ERP patterns for regular and irregular morphology. Although the specific results have varied, a trend has emerged. Whereas inappropriate regular affixation (anomalous addition^{124,125} or omission^{128,129} of the affix) can lead to a LAN, modification of irregular inflection tends to elicit a more central, N400-like negativity^{124,128,129}. Moreover, this LAN does not seem to differ in topography from the LAN that is elicited by syntactic anomalies^{128,129}, underscoring common neural mechanisms for regular morphology and syntax.

Whereas most ERP studies examine language during comprehension, a recent experiment probed regular and irregular past-tense production, and examined cortical localization of the scalp-recorded potentials¹³⁰. Regular past tenses elicited more frontal activation than irregular verbs, but irregular forms yielded more activity in left temporal lobe regions, strengthening the temporal lobe/frontal lobe dichotomy that is predicted by the declarative/procedural model.

Magnetoencephalography. In a MAGNETOENCEPHALOGRAPHIC investigation of regular and irregular past-tense production, DIPOLE MODELLING was used to localize sources of brain activity¹³¹. Dipoles were localized to a single left temporal/parietal region for both regular and irregular verbs, 250–310 ms after verb-stem presentation. Dipoles in left frontal regions were found only for regular verbs and only for times immediately after the left temporal/parietal dipoles (310–330 ms). No dipoles were found in the right hemisphere. These results are consistent with a dual-system model in which temporal/parietal-based memory is searched for an irregular form, the successful retrieval of which blocks the application of a frontal-based suffixation rule⁸.

Conclusion

In summary, studies using different methodologies have examined the acquisition, computation, processing and neural bases of lexicon and grammar, focusing on irregular and regular morphology in several languages. These studies have tested the predictions of different single- and dual-system language models. The data largely conform to the dissociations and associations that are predicted by the declarative/procedural model, supporting its validity (BOX 3).

Box 3 | Some open questions

Although I argue that most of the available evidence supports the declarative/procedural model, the data are not uniform in this regard. Even the relatively simple approach of studying regular and irregular morphology has failed to yield entirely consistent results, particularly in other languages, in which the contrast is not as well understood as in English²⁵.

Moreover, several issues remain to be further specified by the declarative/procedural model, including the following.

- What is the exact computational role of the procedural system and its parts? What particular functions do the different brain structures in the system underlie? Is the system involved in both structure building and learning rules?
- What specific regions in frontal and parietal cortex subserve these functions? Are inferior parietal structures involved in lexical as well as grammatical functions?
- The declarative/procedural model does not claim that these two brain systems are the only circuits underlying lexicon and grammar, let alone other aspects of language. What other circuits underlie these two language capacities, and how do they relate to the declarative and procedural systems?
- What types of regular and other complex structures are stored? What form do their representations take?
- Are there individual differences (for example, corresponding to sex differences) in the storage of complex forms?
- How similar are the linguistic and non-linguistic computations in each of the two systems? Do the similarities extend to the non-linguistic computations in other animals, such as non-human primates? Would this enable the development of an animal model of aspects of language?

The declarative/procedural model has several implications. First, the numerous studies of the declarative and procedural memory systems in animals and humans are expected to help to elucidate the computational and neural bases of learning, representation and processing of lexicon and grammar. For example, the neuropharmacology of declarative memory and its underlying neural substrates¹³² should also pertain to language. Second, because language is a relatively well-understood cognitive domain, linguistic theory and related language disciplines will probably shed light on the workings of declarative and procedural memory. Third, the model has direct clinical implications. People with developmental or adult-onset disorders of the grammatical/procedural system should recover through the memorization of complex forms using lexical/declarative memory. Indeed, this is what subjects with SLI seem to do (see above)^{45,57,58}. In addition, preliminary evidence indicates that people with anterior (but not posterior) aphasia memorize regular forms after the onset of their lesion¹³³. Such recovery could be stimulated with pharmacological and other therapeutic approaches derived from our current knowledge of the two memory systems. Last, the existence of brain systems that subserve language in humans, but are homologous to systems that are present in other animals, has implications for the evolution of language.

1. Chomsky, N. *The Minimalist Program* (MIT Press, Cambridge, Massachusetts, 1995).
Extends the influential Government and Binding framework in theoretical linguistics.
2. Pinker, S. *The Language Instinct* (William Morrow, New York, 1994).
A highly readable overview of language, arguing that it is dependent on innate mental constructs.
3. Fodor, J. A. *The Modularity of Mind: an Essay on Faculty Psychology* (MIT Press, Cambridge, Massachusetts, 1983).
A clearly reasoned claim that there are distinct mental 'modules' dedicated to different mental capacities.
4. Elman, J. et al. *Rethinking Innateness: a Connectionist Perspective on Development* (MIT Press, Cambridge, Massachusetts, 1996).
An overview of modern connectionism, arguing that traditional views of cognitive innateness are flawed.
5. Gleason, J. B. & Ratner, N. B. (eds) *Psycholinguistics* (Harcourt Brace College Publishers, Fort Worth, 1998).
6. Goodglass, H. *Understanding Aphasia* (Academic, San Diego, California, 1993).
7. Damasio, A. R. & Damasio, H. Brain and language. *Sci. Am.* **267**, 88–95 (1992).
An important perspective on the relation between brain and language.
8. Ullman, M. T. et al. A neural dissociation within language: evidence that the mental dictionary is part of declarative memory, and that grammatical rules are processed by the procedural system. *J. Cogn. Neurosci.* **9**, 266–276 (1997).
Based on evidence from anterior and posterior aphasia, and from Alzheimer's, Parkinson's and Huntington's diseases, it is argued that grammatical rules depend on a frontal/basal ganglia procedural system, whereas lexical items are stored in a temporal lobe declarative memory system.
9. Ullman, M. T. The declarative/procedural model of lexicon and grammar. *J. Psycholinguist. Res.* **30**, 37–69 (2001).
10. Mishkin, M., Malamut, B. & Bachevalier, J. In *Neurobiology of Learning and Memory* (eds Lynch, G., McGaugh, J. L. & Weinburger, N. W.) 65–77 (Guilford, New York, 1984).
A proposal that there are distinct memory systems.
11. Squire, L. R. & Zola, S. M. Structure and function of declarative and nondeclarative memory systems. *Proc. Natl Acad. Sci. USA* **93**, 13515–13522 (1996).
12. Schacter, D. L. & Tulving, E. (eds) *Memory Systems* (MIT Press, Cambridge, Massachusetts, 1994).
13. Goodale, M. A. In *The New Cognitive Neurosciences* (ed. Gazzaniga, M. S.) 365–378 (MIT Press, Cambridge, Massachusetts, 2000).
A proposal that 'dorsal' and 'ventral' visual streams underlie distinct types of visual processing.
14. Suzuki, W. A. & Amaral, D. G. Perirhinal and parahippocampal cortices of the macaque monkey: cortical afferents. *J. Comp. Neurol.* **350**, 497–533 (1994).
15. Hodges, J. R. & Patterson, K. Semantic memory disorders. *Trends Cogn. Sci.* **1**, 68–72 (1997).
16. Martin, A., Ungerleider, L. G. & Haxby, J. V. In *The New Cognitive Neurosciences* (ed. Gazzaniga, M. S.) 1023–1036 (MIT Press, Cambridge, Massachusetts, 2000).
17. Buckner, R. L. In *The New Cognitive Neurosciences* (ed. Gazzaniga, M. S.) 817–828 (MIT Press, Cambridge, Massachusetts, 2000).
18. Desmond, J. E., Gabrieli, J. D. E. & Glover, G. H. Dissociation of frontal and cerebellar activity in a cognitive task: evidence for a distinction between selection and search. *Neuroimage* **7**, 368–376 (1998).
19. De Renzi, E. In *Handbook of Neuropsychology* Vol. 2 (eds Bolter, F. & Grafman, J.) 245–263 (Elsevier, New York, 1989).
20. Heilman, K. M., Watson, R. T. & Rothi, L. G. In *Behavioral Neurology and Neuropsychology* (eds Feinberg, T. E. & Farah, M. J.) 227–235 (McGraw-Hill, New York, 1997).
21. Hikosaka, O. et al. In *The New Cognitive Neurosciences* (ed. Gazzaniga, M. S.) 553–572 (MIT Press, Cambridge, Massachusetts, 2000).
22. Rizzolatti, G., Fogassi, L. & Gallese, V. In *The New Cognitive Neurosciences* (ed. Gazzaniga, M. S.) 539–552 (MIT Press, Cambridge, Massachusetts, 2000).
23. Willingham, D. B. A neuropsychological theory of motor skill learning. *Psychol. Rev.* **105**, 558–584 (1998).
24. Alexander, G. E., Crutcher, M. D. & DeLong, M. R. In *Progress in Brain Research* Vol. 85 (eds Uylings, H. B. M., Van Eden, C. G., DeBruin, J. P. C., Corner, M. A. & Feenstra, M. G. P.) 119–146 (Elsevier, New York, 1990).
A discussion of evidence that the basal ganglia are composed of parallel circuits that subserve distinct domains, and project to distinct frontal cortical regions.
25. Pinker, S. *Words and Rules: the Ingredients of Language* (Basic Books, New York, 1999).
Focusing on evidence from regular and irregular morphology, especially in English past tense, it is argued that the mental lexicon and the mental grammar are distinct systems in the mind and brain.
26. Bresnan, J. *Lexical-Functional Syntax* (Blackwell, Oxford, 2001).
27. Levelt, W. J. M. *Speaking: from Intention to Articulation* (MIT Press, Cambridge, Massachusetts, 1989).
28. Frazier, L. In *Attention and Performance* Vol. 12 (ed. Coltheart, M.) 559–586 (Lawrence Erlbaum, Hillsdale, New Jersey, 1987).
29. Halle, M. & Marantz, A. In *The View from Building 20* (MIT Press, Cambridge, Massachusetts, 1993).
30. Caramazza, A., Berndt, R. S., Basili, A. G. & Koller, J. J. Syntactic processing deficits in aphasia. *Cortex* **17**, 333–348 (1981).
31. Grodzinsky, Y. The neurology of syntax: language use without Broca's area. *Behav. Brain Sci.* **23**, 1–71 (2000).
32. MacDonald, M. C., Pearlmutter, N. J. & Seidenberg, M. S. Lexical nature of syntactic ambiguity resolution. *Psychol. Rev.* **101**, 676–703 (1994).
33. Bates, E. & MacWhinney, B. In *The Crosslinguistic Study of Sentence Processing* (eds MacWhinney, B. & Bates, E.) 3–73 (Cambridge Univ. Press, Cambridge, UK, 1989).
34. Rumelhart, D. E. & McClelland, J. L. In *Parallel Distributed Processing: Explorations in the Microstructures of Cognition* Vol. 2 (eds McClelland, J. L., Rumelhart, D. E. & PDP Research Group) 216–271 (Bradford/MIT Press, Cambridge, Massachusetts, 1986).
A seminal proposal that regular and irregular past tense forms are learned, represented and processed in a single connectionist network.
35. Joanisse, M. F. & Seidenberg, M. S. Impairments in verb morphology after brain injury: a connectionist model. *Proc. Natl Acad. Sci. USA* **96**, 7592–7597 (1999).
A connectionist model that attempts to simulate previous empirically-demonstrated neurological double dissociations between regular and irregular past tense forms.
36. Plunkett, K. & Marchand, V. U-shaped learning and frequency effects in a multi-layered perceptron: implications for child language acquisition. *Cognition* **38**, 43–102 (1991).

37. Pinker, S. & Prince, A. Regular and irregular morphology and the psychological status of rules of grammar. *Berkeley Linguist. Soc.* **17**, 230–251 (1991).
38. Pinker, S. Rules of language. *Science* **253**, 530–535 (1991).
39. Marcus, G. F. et al. Overregularization in language acquisition. *Monogr. Soc. Res. Child Dev.* **57**, 1–165 (1992).
40. Ullman, M. T. *The Computation of Inflectional Morphology*. Thesis, Massachusetts Inst. Technol. (1993).
41. Prasada, S., Pinker, S. & Snyder, W. Some evidence that irregular forms are retrieved from memory but regular forms are rule-generated. *31st Annu. Meet. Psychonom. Soc.* (New Orleans, 1990).
42. Prasada, S. & Pinker, S. Generalization of regular and irregular morphological patterns. *Lang. Cogn. Processes* **8**, 1–56 (1993).
43. Ullman, M. T. Acceptability ratings of regular and irregular past tense forms: evidence for a dual-system model of language from word frequency and phonological neighbourhood effects. *Lang. Cogn. Processes* **14**, 47–67 (1999).
44. Sternberger, J. P. & MacWhinney, B. In *Theoretical Morphology: Approaches in Modern Linguistics* (eds Hammond, M. & Noonan, M.) 101–116 (Academic Press, New York, 1988).
45. Van der Lely, H. K. J. & Ullman, M. T. Past tense morphology in specifically language impaired and normally developing children. *Lang. Cogn. Processes* **16**, 177–217 (2001).
46. Clahsen, H., Eisenbeiss, S. & Sonnenstuhl, I. Morphological structure and the processing of inflected words. *Theor. Linguist.* **23**, 201–249 (1997).
47. Penke, M. & Krause, M. German noun plurals: a challenge to the dual-mechanism model. *Brain Lang.* (in the press).
48. Bybee, J. L. & Moravcsik, E. L. Morphological classes as natural categories. *Language* **59**, 251–270 (1983).
49. Fujiwara, M. & Ullman, M. T. In *Proc. 12th Annu. CUNY Conf. Hum. Sentence Process.* Vol. 12, 88 (CUNY Graduate School and University Center, CUNY, New York, 1999).
50. Stanners, R. F., Neiser, J. J., Hemon, W. P. & Hall, R. Memory representation for morphologically related words. *J. Verb. Learn. Verb. Behav.* **18**, 399–412 (1979).
51. Marslen-Wilson, W., Hare, M. & Older, L. In *Proc. 15th Annu. Conf. Cogn. Sci. Soc.* 1–6 (Hillsdale, New Jersey, 1993).
52. Sonnenstuhl, I., Eisenbeiss, S. & Clahsen, H. Morphological priming in the German mental lexicon. *Cognition* **72**, 203–236 (1999).
53. Ullman, M. T., Walenski, M., Prado, E., Ozawa, K. & Steinhilber, K. In *Proc. 14th Annu. CUNY Conf. Hum. Sentence Process.* Vol. 14, 64 (CUNY Graduate School and University Center, Philadelphia, 2001).
54. Leonard, L. B. *Children with Specific Language Impairment* (MIT Press, Cambridge, Massachusetts, 1998).
55. Gopnik, M. Feature-blind grammar and dysphasia. *Nature* **344**, 715 (1990).
56. Van der Lely, H. K. J. & Stollwerck, L. A grammatical specific language impairment in children: an autosomal dominant inheritance? *Brain Lang.* **52**, 484–504 (1996).
57. Ullman, M. T. & Gopnik, M. In *The McGill Working Papers in Linguistics: Linguistic Aspects of Familial Language Impairment* Vol. 10 (ed. Matthews, J.) 81–118 (McGill, Montreal, 1994).
58. Ullman, M. T. & Gopnik, M. Inflectional morphology in a family with inherited specific language impairment. *Appl. Psycholinguist.* **20**, 51–117 (1999).
59. Vargha-Khadem, F., Watkins, K., Alcock, K., Fletcher, P. & Passingham, R. Praxic and nonverbal cognitive deficits in a large family with genetically transmitted speech and language disorder. *Proc. Natl Acad. Sci. USA* **92**, 930–933 (1995).
60. Vargha-Khadem, F. et al. Neural basis of an inherited speech and language disorder. *Proc. Natl Acad. Sci. USA* **95**, 12695–12700 (1998).
61. Bellugi, U., Bihler, A., Jernigan, T., Trauner, D. & Doherty, S. Neuropsychological, neurological, and neuroanatomical profile of Williams syndrome. *Am. J. Med. Genet.* **6** (Suppl.), 115–125 (1990).
62. Clahsen, H. & Almazan, M. Syntax and morphology in Williams syndrome. *Cognition* **68**, 167–198 (1998).
63. Bromberg, H. et al. In *Proc. 18th Annu. Boston Univ. Conf. Lang. Dev.* (Boston, Massachusetts, 1994).
64. Alexander, M. P. In *Behavioral Neurology and Neuropsychology* (eds Feinberg, T. E. & Farah, M. J.) 133–150 (McGraw-Hill, New York, 1997).
65. Damasio, A. R. Aphasia. *N. Engl. J. Med.* **326**, 531–539 (1992).
66. Tyler, L. K., Ostrin, R. K., Cooke, M. & Moss, H. E. Automatic access of lexical information in Broca's aphasia: against the automaticity hypothesis. *Brain Lang.* **48**, 131–162 (1995).
67. Farah, M. J. & Grossman, M. In *Behavioral Neurology and Neuropsychology* (eds Feinberg, T. E. & Farah, M. J.) 473–477 (McGraw-Hill, New York, 1997).
68. Ullman, M. T. et al. Neural correlates of lexicon and grammar: evidence from the production, reading, and judgement of inflection in aphasia. *Brain Lang.* (in the press).
69. Marin, O. S. M., Saffran, E. M. & Schwartz, M. F. Dissociations of language in aphasia: implications for normal function. *Ann. NY Acad. Sci.* **280**, 868–884 (1976).
70. Coslett, H. B. Dissociation between reading of derivational and inflectional suffixes in two phonological dyslexics. *Academy of Aphasia* (Nashville, 1986).
71. Badecker, W. & Caramazza, A. The analysis and morphological errors in a case of acquired dyslexia. *Brain Lang.* **32**, 278–305 (1987).
72. Badecker, W. & Caramazza, A. Morphological composition in the lexical output system. *Cogn. Neuropsychol.* **8**, 335–367 (1991).
73. Ullman, M. T., Hickok, G. & Pinker, S. Irregular and regular inflectional morphology in an aphasic. *Brain Cogn.* **28**, 88–99 (1995).
74. Coslett, H. B. A selective morphological impairment in writing: evidence from a phonological dysgraphic. *Academy of Aphasia* (Montreal, 1988).
75. Marslen-Wilson, W. D. & Tyler, L. K. Dissociating types of mental computation. *Nature* **387**, 592–594 (1997).
76. Marslen-Wilson, W. & Tyler, L. K. Rules, representations, and the English past tense. *Trends Cogn. Sci.* **2**, 428–435 (1998).
77. Hagiwara, H., Ito, T., Sugioka, Y., Kawamura, M. & Shiota, J.-I. Neurolinguistic evidence for rule-based nominal suffixation. *Language* **75**, 739–763 (1999).
78. Boller, F. & Doykaerts, C. In *Behavioral Neurology and Neuropsychology* (eds Feinberg, T. E. & Farah, M. J.) 521–544 (McGraw-Hill, New York, 1997).
79. Nebes, R. D. In *Behavioral Neurology and Neuropsychiatry* (eds Feinberg, T. E. & Farah, M. J.) 545–550 (McGraw-Hill, New York, 1997).
80. Sagar, H. J., Cohen, N. J., Sullivan, E. V., Corkin, S. & Growdon, J. H. Remote memory function in Alzheimer's and Parkinson's disease. *Brain* **111**, 185–206 (1988).
81. Grossman, M. et al. Language comprehension and regional cerebral defects in frontotemporal degeneration and Alzheimer's disease. *Neurology* **50**, 157–163 (1998).
82. Gabrieli, J. D. E., Corkin, S., Mickel, S. F. & Growdon, J. H. Intact acquisition and long-term retention of mirror-tracing skill in Alzheimer's disease and in global amnesia. *Behav. Neurosci.* **107**, 899–910 (1993).
83. Saint-Cyr, J. A., Taylor, A. E. & Lang, A. E. Procedural learning and neostriatal dysfunction in man. *Brain* **111**, 941–959 (1988).
84. Beatty, W. W. et al. Preserved cognitive skills in dementia of the Alzheimer type. *Arch. Neurol.* **51**, 1040–1046 (1994).
85. Bayles, K. A. Language function in senile dementia. *Brain Lang.* **16**, 265–280 (1982).
86. Schwartz, M. F., Marin, O. S. M. & Saffran, E. M. Dissociations of language function in dementia: a case study. *Brain Lang.* **7**, 277–306 (1979).
87. Ullman, M. T. Evidence that lexical memory is part of the temporal lobe declarative memory, and that grammatical rules are processed by the frontal/basal-ganglia procedural system. *Brain Lang.* (in the press).
88. Cappa, S. & Ullman, M. T. A neural dissociation in Italian verbal morphology. *Abstr. Cogn. Neurosci. Soc.* **5**, 63 (1998).
89. Bozeat, S., Lambon Ralph, M. A., Patterson, K., Garrard, P. & Hodges, J. R. Non-verbal impairment in semantic dementia. *Neuropsychologia* **38**, 1207–1214 (2000).
90. Graham, K. S., Patterson, K. & Hodges, J. R. Episodic memory: new insights from the study of semantic dementia. *Curr. Opin. Neurobiol.* **9**, 245–250 (1999).
91. Patterson, K., Lambon Ralph, M. A., Hodges, J. R. & McClelland, J. L. Deficits in irregular past-tense verb morphology associated with degraded semantic knowledge. *Neuropsychologia* **39**, 709–724 (2001).
92. Young, A. B. & Penney, J. B. In *Parkinson's Disease and Movement Disorders* (eds Jankovic, J. & Tolosa, E.) 1–11 (Williams & Wilkins, Baltimore, Maryland, 1993).
93. Dubois, B., Boller, F., Pillon, B. & Agid, Y. In *Handbook of Neuropsychology* Vol. 5 (eds Boller, F. & Grafman, J.) 195–240 (Elsevier, Amsterdam, 1991).
94. Harrington, D. L., Haaland, K. Y., Yeo, R. A. & Marder, E. Procedural memory in Parkinson's disease: impaired motor but not visuospatial learning. *J. Clin. Exp. Neuropsychol.* **12**, 323–339 (1990).
95. Grossman, M., Carvill, S. & Peltzer, L. The sum and substance of it: the appreciation of mass and count qualifiers in Parkinson's disease. *Brain Lang.* **44**, 351–384 (1993).
96. Iles, J., Metter, E. J., Hanson, W. R. & Iritani, S. Language production in Parkinson's disease: acoustic and linguistic considerations. *Brain Lang.* **33**, 146–160 (1988).
97. Lieberman, P. et al. Speech production, syntax comprehension, and cognitive deficits in Parkinson's disease. *Brain Lang.* **43**, 169–189 (1992).
98. Gabrieli, J. D. E., Cohen, N. J. & Corkin, S. The impaired learning of semantic knowledge following bilateral medial temporal-lobe resection. *Brain Cogn.* **7**, 157–177 (1988).
99. Postle, B. R. & Corkin, S. Impaired word-stem completion priming but intact perceptual identification priming with novel words: evidence from the amnesic patient H. M. *Neuropsychologia* **15**, 421–440 (1998).
100. Kensinger, E. A., Ullman, M. T. & Corkin, S. Bilateral medial temporal lobe damage does not affect lexical or grammatical processing: evidence from the amnesic patient H. M. *Hippocampus* **11**, 347–360 (2001).
101. Damasio, H., Grabowski, T. J., Tranel, D., Hichwa, R. D. & Damasio, A. R. A neural basis for lexical retrieval. *Nature* **380**, 499–505 (1996).
102. Bookheimer, S. Y., Zeffiro, T. A., Gaillard, W. & Theodore, W. Regional cerebral blood flow changes during the comprehension of syntactically varying sentences. *Soc. Neurosci. Abstr.* **19**, 843 (1993).
103. Newman, A. J., Pancheva, R., Ozawa, K., Neville, H. J. & Ullman, M. T. An event-related fMRI study of syntactic and semantic violations. *J. Psycholinguist. Res.* **30**, 339–364 (2001).
104. Kuperberg, G. E. et al. Common and distinct neural substrates for pragmatic, semantic, and syntactic processing of spoken sentences: an fMRI study. *J. Cogn. Neurosci.* **12**, 321–341 (2000).
105. Stromswold, K., Caplan, D., Alpert, N. & Rauch, S. Localization of syntactic comprehension by positron emission tomography. *Brain Lang.* **52**, 452–473 (1996).
106. Ni, W. et al. An event-related neuroimaging study distinguishing form and content in sentence processing. *J. Cogn. Neurosci.* **12**, 120–133 (2000).
107. Embick, D., Marantz, A., Miyashita, Y., O'Neil, W. & Sakai, K. L. A syntactic specialization for Broca's area. *Proc. Natl Acad. Sci. USA* **97**, 6150–6154 (2000).
108. Indefrey, P. et al. In *Proc. 12th Annu. CUNY Conf. Hum. Sentence Process.* Vol. 12, 93 (CUNY Graduate School and University Center, CUNY, New York, 1999).
109. Moro, A. et al. Syntax and the brain: disentangling grammar by selective anomalies. *Neuroimage* **13**, 110–118 (2001).
110. Jaeger, J. J. et al. A positron emission tomographic study of regular and irregular verb morphology in English. *Language* **72**, 451–497 (1996).
111. Ullman, M. T., Bergida, R. & O'Craven, K. Distinct fMRI activation patterns for regular and irregular past tense. *Neuroimage* **5**, S549 (1997).
112. Rhee, J. et al. Neural substrates of English past tense generation. *Abstr. Cogn. Neurosci. Soc.* **8**, 131 (2001).
113. Indefrey, P. et al. A PET study of cerebral activation patterns induced by verb inflection. *Neuroimage* **5**, S548 (1997).
114. Laine, M., Rinne, J. O., Krause, B. J., Teras, M. & Sipila, H. Left hemisphere activation during processing of morphologically complex word forms in adults. *Neurosci. Lett.* **271**, 85–88 (1999).
115. Barrett, S. E. & Rugg, M. D. Event-related potentials and the semantic matching of pictures. *Brain Cogn.* **14**, 201–212 (1990).
116. Nobre, A. C., Allison, T. & McCarthy, G. Word recognition in the human inferior temporal lobe. *Nature* **372**, 260–263 (1994).
117. Segalowitz, S. J. & Chevalier, H. In *Handbook of Neurolinguistics* (eds Stemmer, B. & Whitaker, H. A.) 95–109 (Academic, San Diego, California, 1998).
118. Neville, H., Nicol, J. L., Bars, A., Forster, K. I. & Garrett, M. F. Syntactically based sentence processing classes: evidence from event-related brain potentials. *J. Cogn. Neurosci.* **3**, 151–165 (1991).
119. Friederici, A. D., Pfeifer, E. & Hahne, A. Event-related brain potentials during natural speech processing: effects of semantic, morphological and syntactic violations. *Brain Res. Cogn. Brain Res.* **1**, 183–192 (1993).
120. Friederici, A. D., Hahne, A. & Mecklinger, A. The temporal structure of syntactic parsing: early and late effects elicited by syntactic anomalies. *J. Exp. Psychol. Learn. Mem. Cogn.* **22**, 1219–1248 (1996).
121. Friederici, A. D., Hahne, A. & Von Cramon, D. Y. First-pass versus second-pass parsing processes in a Wernicke's and a Broca's aphasia: electrophysiological evidence for a double dissociation. *Brain Lang.* **62**, 311–341 (1998).
122. Friederici, A. D. & Frisch, S. Verb-argument structure processing: the role of verb-specific and argument-specific information. *J. Mem. Lang.* **43**, 476–507 (2000).
123. Osterhout, L. & Holcomb, P. J. Event-related brain potentials elicited by syntactic anomaly. *J. Mem. Lang.* **31**, 785–806 (1992).
124. Veyerts, H., Penke, M., Dohm, U., Clahsen, H. & Münte, T. F. Brain potentials indicate differences between regular and irregular German plurals. *Neuroreport* **8**, 957–962 (1997).
125. Penke, M. et al. How the brain processes complex words: an event-related potential study of German verb inflections. *Brain Res. Cogn. Brain Res.* **6**, 37–52 (1997).

REVIEWS

126. Gross, M., Say, T., Kleingers, M., Münte, T. F. & Clahsen, H. Human brain potentials to violations in morphologically complex Italian words. *Neurosci. Lett.* **241**, 83–86 (1998).
127. Münte, T. F., Say, T., Clahsen, H., Schiltz, K. & Kutas, M. Decomposition of morphologically complex words in English: evidence from event-related brain potentials. *Brain Res. Cogn. Brain Res.* **7**, 241–253 (1999).
128. Newman, A., Izvorski, R., Davis, L., Neville, H. & Ullman, M. T. Distinct electrophysiological patterns in the processing of regular and irregular verbs. *Abstr. Cogn. Neurosci. Soc.* **6**, 47 (1999).
129. Ullman, M. T., Newman, A., Izvorski, R. & Neville, H. in *Proc. 13th Annu. CUNY Conf. Hum. Sentence Process.* Vol. 13, 87 (CUNY Graduate School and University Center, La Jolla, California, 2000).
130. Lavric, A., Pizzagalli, D., Forstmeier, S. & Rippon, G. Mapping dissociations in verb morphology. *Trends Cogn. Sci.* **5**, 301–308 (2001).
131. Rhee, J., Pinker, S. & Ullman, M. T. A magnetoencephalographic study of English past tense production. *Abstr. Cogn. Neurosci. Soc.* **6**, 47 (1999).
132. Curran, H. V. in *The New Cognitive Neurosciences* (ed. Gazzaniga, M. S.) 797–804 (MIT Press, Cambridge, Massachusetts, 2000).
133. Ullman, M. T. Neural plasticity and morphological processing in agrammatic aphasia: implications for recovery. *Abstr. Cogn. Neurosci. Soc.* **7**, 53 (2000).
134. Dell, G. S. A spreading-activation theory of retrieval in sentence production. *Psychol. Rev.* **93**, 283–321 (1986).
135. Halle, M. Prolegomena to a theory of word formation. *Linguistic Inq.* **4**, 3–16 (1973).
136. Anderson, S. R. *A-morphous morphology* (Cambridge Univ. Press, New York, 1992).
137. Jackendoff, R. S. Morphological and semantic regularities in the lexicon. *Language* **51**, 639–671 (1975).
138. Aronoff, M. *Word Formation in Generative Grammar* (MIT Press, Cambridge, Massachusetts, 1976).
139. Ling, C. X. & Marinov, M. A symbolic model of the nonconscious acquisition of information. *Cogn. Sci.* **18**, 595–621 (1994).

Acknowledgements

Support was provided by a McDonnell-Pew grant in Cognitive Neuroscience, and by grants from the National Institutes of Health and the, the National Science Foundation and the Department of Defence.

Online links

DATABASE LINKS

The following terms in this article are linked online to: MIT Encyclopedia of Cognitive Sciences:

<http://cognet.mit.edu/MITECS/>
magnetic resonance imaging | positron emission tomography
OMIM: <http://www.ncbi.nlm.nih.gov/Omim/>
Alzheimer's disease | Huntington's disease | Parkinson's disease

FURTHER INFORMATION

MIT Encyclopedia of Cognitive Sciences:
<http://cognet.mit.edu/MITECS/>
grammar, neural basis of | language, neural basis of | lexicon,
neural basis of | linguistics and language | psycholinguistics

Database links

MIT Encyclopedia of Cognitive Sciences
<http://cognet.mit.edu/MITECS/>

magnetic resonance imaging
<http://cognet.mit.edu/MITECS/Entry/ugurbil>

positron emission tomography
<http://cognet.mit.edu/MITECS/Entry/raichle>

OMIM
<http://www.ncbi.nlm.nih.gov/Omim/>

Alzheimer's disease
<http://www.ncbi.nlm.nih.gov/htbin-post/Omim/dispim?104300>

Huntington's disease
<http://www.ncbi.nlm.nih.gov/htbin-post/Omim/dispim?143100>

Parkinson's disease
<http://www.ncbi.nlm.nih.gov/htbin-post/Omim/dispim?168600>

Further information

MIT Encyclopedia of Cognitive Sciences
<http://cognet.mit.edu/MITECS/>

grammar, neural basis of
<http://cognet.mit.edu/MITECS/Entry/caplan>

language, neural basis of
<http://cognet.mit.edu/MITECS/Entry/dronkers>

lexicon, neural basis of
<http://cognet.mit.edu/MITECS/Entry/caramazza>

linguistics and language
<http://cognet.mit.edu/MITECS/Entry/ling.intro>

psycholinguistics
<http://cognet.mit.edu/MITECS/Entry/clark>

Biography

Michael Ullman is a faculty member of the Department of Neuroscience and at the Georgetown Institute for Cognitive and Computational Sciences at Georgetown University, Washington DC. He holds secondary appointments in Linguistics, Psychology and Neurology. He received his Ph.D. from the Department of Brain and Cognitive Sciences at the Massachusetts Institute of Technology. His group examines the neural, psychological and computational underpinnings of language, focusing on the mental lexicon of memorized words and the mental grammar, which underlies rule-governed behaviour. He uses various methodological approaches, including neuroimaging, neuropsychology and psycholinguistics, to probe the structure of words (morphology), and phrases and sentences (syntax), in several languages, including English, Italian, Spanish and Japanese.

At a glance

- Several models have been proposed to account for the neurocognitive basis of the mental lexicon (a repository of stored words) and the mental grammar (which captures the regularities of language). The declarative/procedural model argues that lexicon and language depend on two neural systems that are intensively studied in the context of memory: declarative and procedural memory.
- The declarative/procedural model links lexicon with the declarative system and with brain structures in temporal/temporoparietal regions. On the other hand, the model links grammar with the procedural system, and with structures in the basal ganglia and frontal cortex.
- The declarative/procedural model makes a set of specific predictions about the neurocognitive basis of lexicon and grammar, regarding their separability, computation, domain generality and localization. These predictions, which have been thoroughly tested in the context of the use of regular versus irregular word forms (walk-walked versus go-went), have been helpful in contrasting this model with other competing perspectives.
- Several lines of evidence support the declarative/procedural model over alternative views. This evidence has come from psycholinguistic studies, the analysis of developmental disorders of language, neurological cases, haemodynamic studies and neurophysiological observations. Collectively, the data show a double dissociation. On the one hand, there is a link between lexicon, associative-memory markers, the knowledge of facts and events, and temporal/temporoparietal regions. On the other, there is a link between grammar, motor and cognitive skills, and structures in the frontal lobe and the basal ganglia.
- The declarative/procedural model has several implications. First, studies of declarative and procedural memory should help to elucidate the neural bases of lexicon and grammar, and vice versa. Second, the model has clinical implications for people with developmental or adult-onset disorders of grammar, as they might recover through the memorization of complex forms using the declarative system. Last, the existence of systems that subserve language in humans and are homologous to systems present in other animals has implications for the evolution of language.

How Does Consensus Scoring Work for Virtual Library Screening? An Idealized Computer Experiment

Renxiao Wang and Shaomeng Wang*

Institute of Cognitive and Computational Science and Lombardi Cancer Center, Departments of Oncology and Neuroscience, Georgetown University Medical Center, 4000 Reservoir Road, Washington, D.C. 20007

Received March 15, 2001

It has been reported recently that consensus scoring, which combines multiple scoring functions in binding affinity estimation, leads to higher hit-rates in virtual library screening studies. This method seems quite independent to the target receptor, the docking program, or even the scoring functions under investigation. Here we present an idealized computer experiment to explore how consensus scoring works. A hypothetical set of 5000 compounds is used to represent a chemical library under screening. The binding affinities of all its member compounds are assigned by mimicking a real situation. Based on the assumption that the error of a scoring function is a random number in a normal distribution, the predicted binding affinities were generated by adding such a random number to the "observed" binding affinities. The relationship between the hit-rates and the number of scoring functions employed in scoring was then investigated. The performance of several typical ranking strategies for a consensus scoring procedure was also explored. Our results demonstrate that consensus scoring outperforms any single scoring for a simple statistical reason: the mean value of repeated samplings tends to be closer to the true value. Our results also suggest that a moderate number of scoring functions, three or four, are sufficient for the purpose of consensus scoring. As for the ranking strategy, both the rank-by-number and the rank-by-rank strategy work more effectively than the rank-by-vote strategy.

INTRODUCTION

Structure-based virtual screening of chemical libraries has become an extremely valuable tool for identifying lead compounds in the case that the three-dimensional structure of the target has been determined.¹ This approach helps to narrow the size of the chemical library under investigation and thus results in a generally improved efficiency in drug discovery. With the completeness of the human genome sequencing, the number of potential pharmaceutical targets will increase dramatically.² Undoubtedly this technique will become even more useful in the drug discovery processes in the future.

Flexible docking programs are usually adopted in virtual library screening approaches to predict the receptor-ligand binding modes. Examples of the most popular docking programs are DOCK,³ AutoDock,⁴ GOLD,⁵ and FlexX.⁶ Although the conformational searching is usually addressed adequately in a docking program, the scoring method remains as a weakness. A scoring method implemented in a docking program is expected to meet two different purposes: during the docking process, it is used to detect the correct bound conformation among the false ones; after the completion of docking, it is used to estimate the binding affinities of the candidate molecules. Furthermore, since library screening usually needs to process hundreds of thousands of compounds in a relatively short time period, the scoring method has to be fast enough. The scoring methods used in docking programs nowadays are based on either force field calculations,³⁻⁵ empirical scoring functions,⁶⁻⁹ or knowledge-based potential of mean force.¹⁰⁻¹² It is true that these scoring methods have been applied successfully to many drug discovery projects. However, due to the inadequate understanding of the elegant physics embedded in the receptor-ligand binding process, these scoring methods are still far from accurate. Finding better scoring methods are still a haunting goal for the researchers who are working on structure-based drug design.

A very interesting method called consensus scoring appeared recently.¹³ In such an approach, a docking program is still employed to fit compounds to the target receptor. However, the best docked conformer of each compound is reevaluated with multiple scoring functions. Only the top scored compounds common to each scoring function will be identified as candidates for bioassay. Compared to single scoring procedure, it was shown that false positives in virtual library screening were largely reduced and hence the hit-rates were improved. More applications of consensus scoring have begun to appear in the literature.^{14,15} It seems that this method is quite independent to the target receptor, the docking method, or even the scoring functions under investigation. In fact, some commercial molecular modeling software, such as SYBYL,¹⁶ has included consensus scoring as part of the drug design package.

Consensus scoring thus appears to have a clear advantage in structure-based virtual library screening approaches. All the consensus scoring approaches reported so far focus on testing a number of scoring functions on some specific biological targets. This kind of approach is valuable if one wants to explore the most efficient combination of scoring

* Corresponding author phone: (202)687-2028; fax: (202)687-4032; e-mail: wangs@georgetown.edu.

functions in a particular drug design project. However, since there are many scoring functions in existence and their performance actually varies from case to case, it is not clear whether the conclusions drawn from one project are transferable to another project. In addition, although consensus scoring is repeatedly shown to work more robust than any single scoring, its mechanism has not been adequately addressed.

In this paper we present an idealized computer experiment designed to investigate the theoretical basis of consensus scoring and explore the best strategy of combining multiple scoring functions in virtual library screening. A hypothetical set of 5000 compounds is used to represent a chemical library under screening. The binding affinities of all its member compounds to a certain biological target are assigned by mimicking a real situation. Based on the assumption that the error given by a scoring function in binding affinity estimation is a random number in a normal distribution, the calculated binding affinities of these compounds are also generated by computer. Then, with all these simulated binding affinities, the performance of the consensus scoring procedure is explored.

METHODS

Basic Assumptions. The central idea of our approach is to design an idealized procedure to simulate a virtual library screening, in which no specific biological target, chemical library, scoring function, or docking program is involved. Some basic assumptions therefore must be applied here. (i) All the compounds under screening are perfectly docked to the target. The error occurred in binding affinity estimation is solely determined by the accuracy of the scoring function. (ii) The error given by any scoring function in binding affinity estimation is a random number in a normal distribution. The normal distribution is centered at zero, which means there is no systematic error. For the convenience of computation, the accuracy of all the scoring functions is assumed to be at the same level. (iii) All the scoring functions are independent to each other. The error from one scoring function has no correlation with the error from another.

Data Preparation. A hypothetical chemical library that contained 5000 compounds was constructed first. Each individual candidate was assigned a floating random number between 0.00 and 10.00, representing its experimentally determined binding affinity to a certain biological target (in $-\log K_i$ units, i.e., negative logarithm of the dissociation constant). This set of random numbers, $X(i)$ ($i = 1, 2, \dots, 5000$), will be referred as the "experimental data set" in this paper. To reflect the common sense that most compounds in a chemical library are inactive to the target, these random numbers were generated from a normal distribution $N(0.00, 4.00^2)$. Therefore, only a small portion of them shows high binding affinity (see Figure 1).

Another set of data, $Y(i)$, was generated based on the experimental data set. Each number in this data set was generated by adding a random number, $E(i)$, to the corresponding one in the experimental data set, i.e., $Y(i) = X(i) + E(i)$. The number $E(i)$ was generated from a normal distribution $N(0.00, 2.00^2)$. This set of data, $Y(i)$, represented the predicted binding affinities for the 5000 candidates given by a certain scoring function. Note that the mean value of

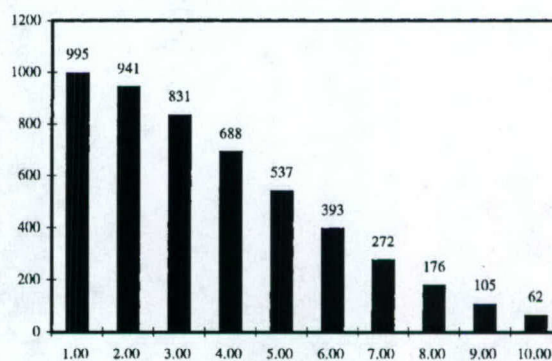


Figure 1. Distribution histogram of the experimental data set (X axis: binding affinity; Y axis: population).

$E(i)$ is 0.00 because the scoring function is supposed to have no systematic error. The variance of 2.00 log units reflects the average accuracy level that existing scoring functions can reach nowadays. Such a data set will be referred as "predicted data set" in this paper. In our experiment, 10 predicted data sets were independently generated in this way, i.e., $Y_1(i)$, $Y_2(i)$, ..., $Y_{10}(i)$. They were considered as the predicted results given by 10 individual scoring functions.

Data Analysis. A predicted data set will, of course, deviate from the experimental data set. Therefore, objective criteria for evaluating the overall quality of a given predicted data set are needed. Our first method is to count the total number of "misranks". To count this number, first we ranked all the candidates according to the predicted values, and then we checked every each pair of candidates to see whether it was ranked correctly. For example, suppose candidate i ranks higher than candidate j in the experimental data set. While if candidate i ranks lower than candidate j in the predicted data set, it will be considered as a "misrank". For all 5000 candidates, there are $5000 \times 4999 / 2 = 12\,497\,500$ pairs in total. We checked them all and counted the number of misranks. Obviously, the fewer misranks are observed, the better is the prediction. In the case that multiple scoring functions were combined to make prediction (consensus scoring), we simply ranked the candidates according to the average predicted results given by all the scoring functions and counted misranks in the same way.

Another method to evaluate the overall quality of a predicted data set is to count the hit-rates, which relates more directly to "real" library screening approaches. We defined arbitrarily that the top 2% candidates in the experimental data set were truly active compounds (hits). Since the size of the data set is 5000, there are exactly 100 of them. By checking the candidates appearing on the top of a predicted data set, e.g. top 2%, the number of true hits can be counted. In this way, the higher is the hit-rate, the better is the prediction. For consensus scoring, there is a special problem in how to rank candidates according to the predicted results since more than one scoring function is involved in this process. In our experiments, we have tested three ranking strategies. (1) All the candidates are ranked according to the average predicted values given by all the scoring functions. This is a straightforward way to combine multiple scoring functions in prediction. We will refer this as the "rank-by-number" strategy in this paper. (2) All the candidates are ranked by the average ranks predicted by all the involved scoring functions. For example, if a candidate ranks no. 10

according to scoring function A and ranks no. 20 according to scoring function B, then its average rank will be $(10+20)/2 = 15$. This strategy uses relative ranks rather than absolute binding affinities for ranking. We will refer this as the "rank-by-rank" strategy in this paper. (3) If a candidate is predicted to be on the top, e.g. 2%, by a certain scoring function, then it gets a "vote" from that scoring function. The final score of a candidate compound is the number of votes gathered from all the scoring functions, which may range from 0 to the total number of scoring functions. All the candidates will be ranked according to their final scores. We will refer to this as the "rank-by-vote" strategy in this paper.

All the possible scoring procedures, i.e., from single scoring to decadal scoring, have been tested. All the methods described above were used for data analysis. Another point should be addressed here: since we have used random numbers to generate the experimental data set and the predicted data sets, each experiment (experimental data set generation + 10 predicted data sets generation + data analysis) was repeated for 100 times to flatten the fluctuations in the statistical results. If not specified, all the data reported in this paper are the average results out of 100 individual runs.

RESULTS AND DISCUSSION

Rationale in an Idealized Computer Experiment. Before we proceed to present and analyze the results, we must explain the rationale in our idealized computer experiment: how closely does it resemble the reality? Let us go through the basic assumptions underlying our simulation one by one.

First, we assume that the docking procedure is perfect and the errors in binding affinity estimation are raised all by scoring functions. As mentioned in the Introduction section, in practice consensus scoring is performed after the docking procedure is completed. The orientation/conformation of the docked compound will certainly affect the result in binding affinity calculation. However, exploring how the docking procedure affects the performance of a virtual library screening approach is another issue. To concentrate on studying the consensus scoring itself, this assumption is essential.

Second, we assume that the error of each scoring function in binding affinity estimation is a random number in a normal distribution that is centered at zero. This is a reasonable assumption since an ideal scoring function should be so. A real scoring function is close to this ideality, too. Existing scoring functions are usually validated by a variety of receptor-ligand complexes. In a statistical sense, they are able to reproduce the known binding affinities with an acceptable accuracy. Furthermore, in practice one can test all his scoring functions in advance to see which ones work well for the given biological target and only apply to the good ones. By doing so, scoring functions that exhibit significant systematic errors will not enter the consensus scoring procedure.

Third, we assume that all the scoring functions involved in consensus scoring are independent to each other. This will not be a problem if the scoring functions have different origins: for example, one is an empirical scoring function, while the other is a potential of mean force approach. For the scoring functions falling in the same category, they are

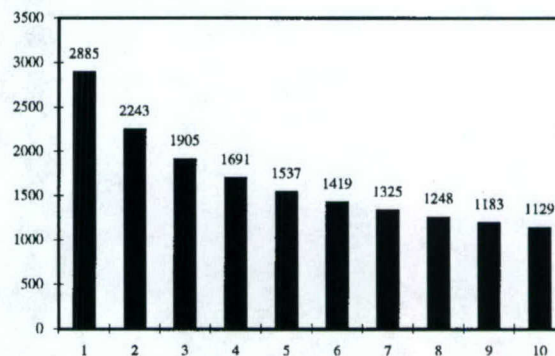


Figure 2. Relationship between the number of scoring functions used in consensus scoring (X axis) and the total number of mis-ranks (in thousand) observed in the predicted data set (Y axis).

not necessarily correlated either. For example, the empirical scoring functions may use different master equations to describe the binding free energy. Even for the same term in the master equation, such as hydrogen bonding and hydrophobic effect, the algorithms vary. For the potential of mean force approaches, they may differentiate each other in many aspects, such as choosing atom types, setting preference state, deriving potentials, and so on. In both cases, it is not unusual that the difference is more than trivial. Therefore it is reasonable to believe that the internal independence of all the involved scoring functions is not a demanding request. For our idealized computer experiment, it is not a problem at all. However, in a consensus scoring practice, special attention should be paid to the selection of scoring functions: if one scoring function is simply an enhanced or simplified version of another, one would better to avoid including them both.

Given these assumptions, the consensus scoring procedure can then be simulated with an idealized computer experiment. The beauty of such an experiment is that it is based purely on numbers. Not a single specific object, such as the biological target molecule, the chemical library, the docking program, or the scoring function, needs to be involved. As a result, the conclusions derived from this experiment will not be biased to any of them.

How Does Consensus Scoring Work? We have counted the numbers of mis-ranks observed in the predicted data sets from single scoring to decadal scoring. The results are shown in Figure 2. There is a clear trend that the overall errors in prediction decrease with the increase in the number of scoring functions. Compared to the results given by single scoring, double scoring drops the number of errors by 23%, triple scoring by 34%, and quadruple scoring by 41%. The number of errors continues to drop when even more scoring functions are employed in prediction. However, the dropping speed will slow significantly after three or four scoring functions are applied. We have performed the same kind of experiment with data sets sizing from 1000 to 10 000. It was found that the above observations are independent to the size of the data set.

If one accepts the basic assumptions underlying our simulation, then a simple explanation for the performance of consensus scoring exists: the mean value of repeated samplings tends to be closer to the true value than any single sampling. Let random variables E_1, E_2, \dots, E_n denote, respectively, the errors of n scoring functions in binding

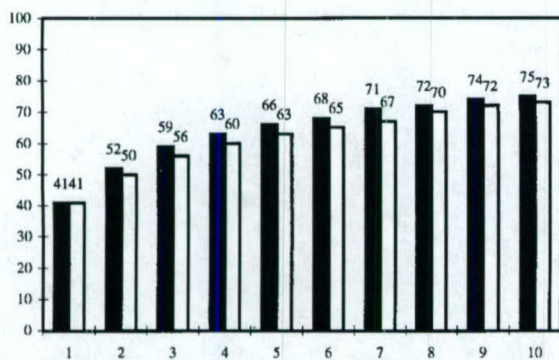


Figure 3. Relationship between the number of scoring functions used in consensus scoring (X axis) and the hit-rates observed among top 100 candidates (Y axis). (The solid bars denote for the "rank-by-number" strategy, while the opened bars denote for the "rank-by-rank" strategy.)

affinity prediction. According to the mathematical statistics theory,¹⁷ the larger n is, the closer the maximum likelihood estimator (\bar{E}) will be to the expectation value (μ). Since \bar{E} is also under a normal distribution, e.g. $N(\mu, \sigma^2/n)$, if we define $(\bar{E} - \mu \leq \sigma)$ is a successful prediction and ask the question how many samplings are required to achieve a successful prediction with the confidence interval of 95%, we need to solve the following equation:

$$\Pr\left(-\delta < \frac{\bar{E} - \mu}{\sigma/\sqrt{n}} < \delta\right) = 0.95 \quad (1)$$

By looking up the normal distribution integration table,¹⁷ the value of δ that fits the above equation is 1.96. Therefore, we can get $n \geq 4$ from this equation. Note that this conclusion is independent of the variance (σ). If the confidence interval changes to 90%, then the minimal n drops to 3. For consensus scoring the above conclusion can be interpreted as that, if the prediction is required to be accurate enough (close to the true value within the range of variance), then three or four scoring functions are required. As illustrated in Figures 2 and 3, introducing more scoring functions into a consensus scoring procedure becomes less effective. As indicated by eq 1, the efficiency is scaled with \sqrt{n} .

The above discussion will not be restricted to virtual library screening approaches. We would like to point out that, for any computational approach in which a method is employed to evaluate a certain feature of the system under investigation, if there is more than one method available and they are simply complementary to each other, then combining them in application will generally lead to improved results. But in other areas, it is not always referred as consensus scoring.

Which Ranking Strategy Is the Best? As mentioned in the Methods section, we have tested three different ranking strategies of consensus scoring, which are possible in virtual library screening approaches. The hit-rates observed among the top 2% of the predicted data set by adopting the "rank-by-number" strategy and the "rank-by-rank" strategy are shown together in Figure 3. As implied in this figure, (1) hit-rates can be increased steadily by using more scoring functions; (2) once again three or four scoring functions seem to be sufficient for improving the accuracy in prediction; and (3) the "rank-by-number" strategy slightly outperforms the "rank-by-rank" strategy. As having been described above,

Table 1. Hit-Rates Observed in the "Rank-by-Vote" Experiments (Voting for Top 2%)^a

votes	number of scoring functions				
	1	2	3	4	5
0	59(4900) ^b	36(4825)	22(4767)	13(4720)	8(4681)
1	41(100)	46(150)	41(174)	33(190)	25(197)
2		18(25)	30(50)	34(66)	34(79)
3			7(9)	17(21)	23(32)
4				3(3)	9(10)
5					1(1)

^a If a compound is predicted to be on the top 2% among all the 5000 candidates by a certain scoring function, it will get the vote from that scoring function. ^b The first number denotes for the true hits, while the number in brackets denotes for the population. For example, this cell should be read as "by single scoring, among the 4900 candidates with zero vote, there are 59 true hits".

the "rank-by-number" strategy is simply ranking all the candidates according to the mean values of all the scoring functions. Unfortunately this strategy cannot be applied if not all the scoring functions give results in a compatible unit. For example, empirical scoring functions give, as claimed, absolute binding free energies; force field based scoring functions give force field energies; while some other scoring functions give potentials of mean force. Thus, if the scoring functions employed in consensus scoring come from different categories, it is not proper to mix up their results. Nevertheless, the "rank-by-rank" strategy will work perfectly in such cases since it uses the relative ranks for instead. This strategy also has another potential advantage in practice: for a given compound, if the prediction of one scoring function deviates from all the others too much, using the rank as score will help to narrow the difference.

Another choice is the "rank-by-vote" strategy, which has been adopted, for example, by the consensus scoring module in the SYBYL software.¹⁶ Since the score of a given candidate could range only from 0 to the number of scoring functions, the idea of this strategy is to rank all the candidates in a semiquantitative manner. It is more complicated than the other two strategies since there are two adjustable variables embedded in its procedure: the voting criterion and the minimal votes needed to qualify a good candidate. We have tested different voting criteria with this ranking strategy in our experiment: (1) a candidate will get a vote if it is enlisted on the top 2%; (2) a candidate will get a vote if it is enlisted on the top 5%; and (3) a candidate will get a vote if it is enlisted on the top 10%. The results given by these three voting criteria are listed in Tables 1–3, respectively. From these tables, it is clear that the hit-rates are very high among the compounds with full votes. But the drawback is that such compounds become so rare when the number of scoring functions exceeds three or four. If one lowers the threshold to consider all the compounds with at least one vote, the false negatives can be eliminated efficiently. However, by doing so more compounds need to be tested in bioassay. As indicated in Tables 1–3, variation of voting criteria also shows the same tendency: by using "tighter" voting criterion (e.g. voting for top 2%), fewer false positives are found among the tested compounds, while by using "looser" voting criterion (e.g. voting for top 10%), fewer false negatives are found among the untested compounds. There is always a tradeoff between the number of false positives and the number of false negatives. Therefore, if

Table 2. Hit-Rates Observed in the "Rank-by-Vote" Experiments (Voting for Top 5%)^a

votes	number of scoring functions				
	1	2	3	4	5
0	33(4750) ^b	12(4594)	4(4482)	2(4397)	0(4326)
1	67(250)	43(313)	23(335)	11(343)	6(350)
2		45(93)	42(134)	28(152)	17(162)
3			31(49)	38(79)	31(93)
4				21(29)	31(51)
5					15(18)

^a If a compound is predicted to be on the top 5% among all the 5000 candidates by a certain scoring function, it will get the vote from that scoring function. ^b The first number denotes for the true hit, while the number in brackets denotes for the population. For example, this cell should be read as "by single scoring, among the 4750 candidates with zero vote, there are 33 true hits".

Table 3. Hit-Rates Observed in the "Rank-by-Vote" Experiments (Voting for Top 10%)^a

votes	number of scoring functions				
	1	2	3	4	5
0	14(4500) ^b	3(4234)	0(4054)	0(3920)	0(3813)
1	86(500)	24(532)	6(537)	1(537)	0(536)
2		73(234)	30(264)	10(269)	3(272)
3			64(145)	35(172)	13(177)
4				54(102)	37(126)
5					47(76)

^a If a compound is predicted to be on the top 10% among all the 5000 candidates by a certain scoring function, it will get the vote of that scoring function. ^b The first number denotes for the true hits, while the number in brackets denotes for the population. For example, this cell should be read as "by single scoring, among the 4500 candidates with zero vote, there are 14 true hits".

the "rank-by-vote" strategy is applied to a consensus scoring approach anyway, how to set these voting criteria properly should depend on the primary concern of the researcher.

By comparing the data in Figure 3 and Tables 1–3, we can see that the "rank-by-vote" strategy is basically inferior to the "rank-by-number" or the "rank-by-rank" strategy as far as the hit-rates are concerned. For example, by using four scoring functions and voting for top 10%, the hit-rate given by the "rank-by-vote" strategy is 54 among the top 102 candidates. While by the "rank-by-number" and the "rank-by-rank" strategy, the hit-rates are 63 and 60 among the top 100 candidates, respectively. The relatively poor performance of the "rank-by-vote" strategy is due to its semiquantitative nature: suppose n scoring functions are employed in the consensus scoring procedure, all the candidate compounds will be simply divided into $n+1$ classes. Such a classification is probably too rough when only three or four scoring functions are actually applied. Some quantitative information will be lost during this conversion.

CONCLUSIONS

We have demonstrated through an idealized computer experiment that consensus scoring improves the hit-rates in virtual library screening because of a simple reason: the mean value of repeated samplings tends to be closer to the true value. Therefore, in a statistical sense, consensus scoring is more robust and accurate than any single scoring procedure.

Our results also suggest that a moderate number of scoring functions, three or four, are sufficient for improving the results significantly. The idea of consensus scoring will be applicable not only to virtual library screening approaches but also to other similar approaches in which certain methods are needed to make predictions. As for the strategies of combining multiple scoring functions, the "rank-by-number" strategy works reliably. The "rank-by-rank" strategy can be used as an alternative when it is not practical to apply the "rank-by-number" strategy. The "rank-by-vote" strategy is generally not recommended.

ACKNOWLEDGMENT

This research is financially supported by the Department of Defense (Grant No. DOD DAMP17-93-V-3018). The authors are also grateful to the reviewers' comments, which make this paper more informative than its original form.

REFERENCES AND NOTES

- Walters, W. P.; Stahl, M. T.; Murcko, M. A. Virtual Screening: An Overview. *Drug Discovery Today* **1998**, *3*, 160–178.
- Drews, J. Drug Discovery: A Historical Perspective. *Science* **2000**, *287*, 1960–1964.
- Kuntz, I. D.; Blaney, J. M.; Oatley, S. J.; Langridge, R.; Ferrin, T. E. A geometric approach to macromolecule-ligand interactions. *J. Mol. Biol.* **1982**, *161*, 269–288.
- Morris, G. M.; Goodsell, D. S.; Halliday, R.; Huey, R.; Hart, W. E.; Belew, R. K.; Olson, A. J. Automated docking using a Lamarckian genetic algorithm and an empirical binding free energy function. *J. Comput. Chem.* **1998**, *19*, 1639–1662.
- Jones, G.; Willett, P.; Glen, R. C.; Leach, A. R.; Taylor, R. Development and validation of a genetic algorithm for flexible docking. *J. Mol. Biol.* **1997**, *267*, 727–748.
- Rarey, M.; Kramer, B.; Lengauer, T.; Klebe, G. A fast flexible docking method using an incremental construction algorithm. *J. Mol. Biol.* **1996**, *261*, 470–489.
- Eldridge, M. D.; Murray, C. W.; Auton, T. R.; Paolini, G. V. Mee, R. P. Empirical scoring functions: I. The development of a fast empirical scoring function to estimate the binding affinity of ligands in receptor complexes. *J. Comput.-Aided Mol. Des.* **1997**, *11*, 425–445.
- Bohm, H.-J. Prediction of binding constants of protein ligands: A fast method for the prioritization of hits obtained from de novo design or 3D database search programs. *J. Comput.-Aided Mol. Des.* **1998**, *12*, 309–323.
- Wang, R.; Liu, L.; Lai, L.; Tang, Y. SCORE: A new empirical method for estimating the binding affinity of a protein–ligand complex. *J. Mol. Model.* **1998**, *4*, 379–394.
- Muegge, I.; Martin, Y. C. A general and fast scoring function for protein–ligand interactions: A simplified potential approach. *J. Med. Chem.* **1999**, *42*, 791–804.
- Mitchell, J. B. O.; Laskowski, R. A.; Alex, A.; Thornton, J. M. BLEEP–Potential of mean force describing protein–ligand interactions: I. Generating potential. *J. Comput. Chem.* **1999**, *20*, 1165–1176.
- Gohlke, H.; Hendlich, M.; Klebe, G. Knowledge-based scoring function to predict protein–ligand interactions. *J. Mol. Biol.* **2000**, *295*, 337–356.
- Charifson, P. S.; Corkery, J. J.; Murcko, M. A.; Walters, W. P. Consensus scoring: A method for obtaining improved hit-rates from docking databases of three-dimensional structures into proteins. *J. Med. Chem.* **1999**, *42*, 5100–5109.
- Bissantz, C.; Folkers, G.; Rognan, D. Protein-based virtual screening of chemical databases. 1. Evaluation of different docking/scoring combinations. *J. Med. Chem.* **2000**, *43*, 4759–4767.
- Stahl, M.; Rarey, M. Detailed analysis of scoring functions for virtual screening. *J. Med. Chem.* **2001**, *44*, 1035–1042.
- The SYBYL software; Tripos Associates: St. Louis, MO. <http://www.tripos.com/>.
- Hogg, R. V.; Craig, A. T. In *Introduction to Mathematical Statistics*, 5th ed.; Pirtle, R. W., Ed.; Prentice Hall: NJ, 1995.

CI010025X

Optimizing signal/noise ratios in expression profiling: Project-specific algorithm selection and detection p value weighting in Affymetrix microarrays.

Jinwook Seo^{1,2}, Marina Bakay¹, Yi-Wen Chen¹, Sara Hilmer¹,
Ben Shneiderman², Eric P Hoffman^{1,*}
4/16/2004

¹Research Center for Genetic Medicine, Children's National Medical Center

²Human-Computer Interaction Lab and Department of Computer Science, University of Maryland

Abstract

Motivation: The most commonly utilized microarrays for mRNA profiling (Affymetrix) include "probe sets" of a series of perfect match and mismatch probes (typically 22 oligonucleotides per probe set). There are an increasing number of reported "probe set algorithms" that differ in their interpretation of a probe set to derive a single normalized "signal" representative of expression of each mRNA. These algorithms are known to differ in accuracy and sensitivity, and optimization has been done using a small set of standardized control microarray data. We hypothesized that different mRNA profiling projects have varying sources and degrees of confounding noise, and that these should alter choice of a specific probe set algorithm. Also, we hypothesized that use of the Microarray Suite (MAS) 5.0 probe set detection p value as a weighting function would improve the performance of all probe set algorithms.

Results: We built an interactive visual analysis software tool (HCE2W) to test and define parameters in Affymetrix analyses that optimize the ratio of signal (desired biological variable) versus noise (confounding uncontrolled variables). Five probe set algorithms were studied with and without statistical weighting of probe sets using the Microarray Suite (MAS) 5.0 probe set detection p values. The signal/noise optimization method was tested in two large novel microarray datasets with different levels of confounding noise; a 105 sample U133A human muscle biopsy data set (11 groups; mutation-defined; extensive noise), and a 40 sample U74A inbred mouse lung data set (8 groups; little noise). Performance was measured by the ability of the specific probe set algorithm, with and without detection p value weighting, to cluster samples into the appropriate biological groups (unsupervised agglomerative clustering with F-measure values). 50% random sampling analyses showed a highly statistically significant difference between probe set algorithms by ANOVA ($F(4,10) > 14$, $p < 0.0001$), with weighting by MAS 5.0 detection p value showing significance in the mouse data by ANOVA ($F(1,10) > 9$, $p < 0.013$) and paired t-test ($t(9) = -3.675$, $p = 0.005$). Probe set detection p-value weighting had the greatest positive effect on performance of dChip difference model, ProbeProfiler, and RMA algorithms. Importantly, probe set algorithms did indeed perform differently depending on the specific project, likely due to degree of confounding noise. Our data indicates that significantly improved data analysis of mRNA profile projects can be achieved by optimizing the choice of probe set algorithm with the noise levels intrinsic to a project, with dChip difference model with MAS 5.0 detection p value continuous weighting showing the best overall performance in both projects. Furthermore, both existing and newly developed probe set algorithms should incorporate a detection p value weighting to improve performance.

* To whom correspondence should be addressed, ehoffman@cnmcresearch.org

Availability: The Hierarchical Clustering Explorer 2.0 is available at <http://www.cs.umd.edu/hcil/hce/>. Murine arrays (40 samples) are publicly available at the PEPR resource (<http://microarray.cnmcresearch.org/pgadatatable.asp>) (Chen *et al.*, 2004).

Introduction

Simultaneous analysis of many thousands of genes on the microarray leads to an “expression profile” of the original cell or tissue. This profile represents the subset of the 40,000 genes that are being employed by that cell or tissue, at that particular point in time. High density oligonucleotide arrays containing up to 500,000 features are widely used for many projects in biological and medical research. The most popular Affymetrix GeneChip uses about 1 million oligonucleotide probes to query most (~40,000) human mRNAs in two small (1.28 cm²) glass arrays. Importantly, Affymetrix arrays have intrinsic redundancy of measurements for each gene, with 11-16 “perfect match” probes for different regions of each gene sequence, with each perfect match paired with a similar “mismatch” probe with a single destabilizing nucleotide change in the center of the 25 nucleotide sequence (Liu *et al.* 2002; Hubbel *et al.* 2002). The complete set of 16 probe pairs is called the “probe set” for any single gene. The mismatch is meant to serve as a “noise filter”; labeled mRNA binding to the “mismatch” is considered to represent a measure of non-specific binding, and thus a measure of “noise” for the corresponding perfect match (see The Tumor Analysis Best Practices Working Group 2004).

There are many confounding uncontrolled variables intrinsic to most microarray projects. For example in human patient samples, the outbred nature of humans leads to extensive genetic heterogeneity between individuals, even if sharing the same pathological condition or exposed to the same environmental or drug challenge. It is often difficult to precisely match age, sex, and ethnic background of human subjects in microarray projects, leading to considerable inter-individual variability in the analyses. Furthermore, human tissue samples typically show extensive tissue heterogeneity, with small size leading to sampling error, and variability in histological severity and cell content (e.g. variable amounts of fibrosis, fatty infiltration, inflammation, regeneration). Many of these variables are not a concern in studies of inbred mouse strains. Inbred mice show very little inter-individual variability, and the experimental manipulation of groups of mice leads to homogeneous treatment groups often with relatively high numbers of replicates. Moreover, the use of whole lungs or other tissues leads to a normalization of tissue heterogeneity.

There are also technical variables that could confound interpretation; quality and preservation of the biopsy material; quality of RNA, cDNA, and cRNA; hybridization and chip image variation; probe set signal algorithms, and statistical analysis methods. QC (Quality Control) and SOP (Standard Operating Procedure) can mitigate many confounding technical variables with factory-produced Affymetrix arrays, and these have been found to be a relatively minor source of confounding variation if QC parameters are employed (Bakay *et al.*, 2002a; Di Giovanni *et al.*, 2003).

“Probe set algorithms” refer to the method of interpreting the 11-16 probe pairs (22-32 oligonucleotide probes) in a probe set on an Affymetrix microarray that query a particular mRNA transcript. Key variables in different probe set algorithms include the penalty weight given to the mismatch probe of each probe pair, the weighting of specific probes in a probe set based on empirical “performance”, the manner by which a single “signal value” is derived from the interpretation of the probe set, and how this is normalized relative to other probe sets on the microarray or in the entire project. Most reports of new probe set algorithms, and comparison of existing algorithms, have been done using one or a few “test data sets” in the public domain; specifically “spike in” control data sets from Affymetrix (http://www.affymetrix.com/analysis/download_center2.affx) and GeneLogic

(<http://qolotus02.genelogic.com/datasets.nsf/>) (Li and Wong 2001b; Irizarry *et al.*, 2003b; Bolstad *et al.*, 2003). These data have shown that using only the perfect match probe, and ignoring the mismatch probe of each probe pair can considerably increase the sensitivity of the study, particularly at low signal levels (Irizarry *et al.*, 2003a). The performance of different probe set algorithms and normalization methods is typically done using ROC (Receiver Operating Characteristic) curves, providing an assessment of signal/noise for the spike-in control mRNAs.

As discussed above, different projects are known to have different levels of confounding noise. We hypothesized that the increased sensitivity of probe set algorithms that ignore the mismatch signal, such as RMA (Robust Multi-array Average) (Irizarry *et al.*, 2003b), would be expected to come at an increased cost of noise, where the quality of low level signals defined by RMA in “noisy” projects would lead to data interpretations of poor integrity. Specifically, detection of spike-in controls would be expected to be independent of confounding noise within arrays and projects. However, the increased sensitivity of some probe set algorithms would be expected to lead to a high proportion of false positives in projects where there was relatively high level of unwanted noise. We hypothesized that different probe set algorithms would show a “project-specific” performance, based upon the extent of confounding noise in a particular project.

The optimization of signal/noise is a critical issue in microarray experiments, where tens of thousands of transcripts are analyzed simultaneously. If a highly sensitive probe set algorithm is used in a noisy project, then the resulting data will have very poor quality and specificity, with many thousands of “false positives”. This would lead to both misclassification of samples, and very noisy results that could absorb large amounts of experimental time to parse through. Even though such noises and noise filtering methods strongly influence data analysis, signal/noise ratios are rarely optimized, or even considered in microarray data analyses. This is partly because of the lack of analysis tools that allow researchers to interactively test and verify various combinations of parameters for noise analysis.

Another aspect of microarray data interpretation that could alter results is the “weighting” of specific probe sets. Typically, once a particular probe set algorithm is employed on a microarray project, each probe set signal is considered as equal weight with any other probe set signal. However, probe sets that detect transcripts expressed at a very high level would be expected to show a “more robust” signal with greater quality, compared to probe sets that are performing poorly or detecting very low level transcripts (near background). A measure of the confidence of the performance of the probe set is a continuous “detection p value” assignment, which is a function of the signal difference between the PM (perfect match) and MM (mismatch) probes in a probe set and the signal intensity. In Affymetrix MAS 5.0, the Discrimination score, $R = (PM - MM) / (PM + MM)$, is calculated for each probe pair, and the One-Sided Wilcoxon’s Signed Rank test against a small positive number (default=0.015) is performed to generate the detection p-value (Affymetrix, 2001a, 2001b, 2001c). Two threshold values α_1 and α_2 are assigned where poor detection p values (less than α_1) are assigned an “absent” call, while more robust detection p values (greater than α_2) are assigned a “present” call (default $\alpha_1 = 0.04$ and $\alpha_2 = 0.06$). It is now standard practice in many publications using Affymetrix arrays to use the “present/absent” calls as a form of noise filters. For example, a “10% present call” noise filter requires any specific probe set to show a “present” call in at least 1 in 10 microarrays in that project, otherwise it is excluded from all further analyses (DiGiovanni *et al.*, 2003; DiGiovanni *et al.*, in press; Zhao *et al.*, 2002, 2003). Use of a threshold is not as statistically valid as a continuous weighting method, and here we tested the effect of weighting of all probe set algorithms by MAS 5.0 detection p values.

We hypothesized that it would be possible to identify the most appropriate probe set analysis and noise filtering methods by conducting permutational analysis of the probe set “signal” algorithm, and

noise filters using continuous MAS 5.0 probe set detection p-values. The goal was to use unsupervised hierarchical clustering to find the signal algorithm that maximized the separation of the “known” biological variable, while minimizing confounding “noise.” We enhanced our interactive visual analysis tool, the Hierarchical Clustering Explorer to enable researchers to perform the permutational study and to help them interactively evaluate the result. We report the analysis results of such permutational studies with very noisy human muscle biopsies samples and much cleaner inbred mouse lung biopsies samples.

In our previous work (Seo *et al.*, 2003), we performed a pilot permutational study with a small subset (25 samples of 3 groups) of our 105 human muscle biopsies. We varied probe set signal algorithms (MAS 5.0, RMA), “present call” filter thresholds, and clustering linkage methods, and “visually” investigated the results in HCE2 (the Hierarchical Clustering Explorer 2.0). For the dataset, the strength of the biological variable was maximized, and noise minimized, using MAS 5.0, 10% present call filter, and average linkage (or average group linkage). In this paper, we extend the pilot study to the extent that (1) we test not only the human muscle data with extensive noise but also the inbred mouse lung data expected to show considerably less biological noise (varying genetic background [polymorphisms], tissue heterogeneity), (2) compare 3 more signal algorithms (dChip, dChip difference model, Probe Profiler), (3) use a novel continuous noise filtering method instead of the binary 10 % “present call” filtering used previously, and (4) evaluate the unsupervised clustering results not only using visual inspection but also using a general external evaluation measure (F-measure).

We first explain our permutation study design and data sets in detail. Then, our novel noise filtering method incorporated into the unsupervised hierarchical clustering algorithm is presented. An external clustering evaluation measure – F-measure is explained and application of the measure to a hierarchical clustering result is explained in the following section. Then, we talk about how those two methods are implemented in *HCE2W* (the improved version of the Hierarchical Clustering Explorer 2.0 with p-value weighting and F-measure). After presenting results with discussions, we conclude our paper.

Methods and Systems

We selected two large Affymetrix data sets that were expected to differ in amount of mitigating, uncontrolled biological noise. Data generation for both data sets was subjected to standardized quality control and standard operating procedure. The first data set was a mouse experimental asthma project, of 40 individual mouse lungs studied in 8 biological groups (5 mice as independent replicates within each group) (see <http://microarray.cnmcresearch.org/pgadatatable.asp> ; U74A microarrays utilized). The studied biological variables were exposure to dust mite allergen and time points after exposure. This data set was expected to be relatively low in confounding biological noise; entire lungs were used that effectively removed tissue heterogeneity as an uncontrolled variable, and the inbred nature of the mouse lines used effectively removed uncontrolled genetic heterogeneity between individuals.

The second data set was a human muscle biopsy project, with 105 muscle biopsies used individually on U133A microarrays, in 11 biological (diagnostic) groups. Clinical heterogeneity, where different human patients may or may not share the same exact underlying initiating biochemical problem, is a major confounding variable in most human mRNA profiling studies. It is important to point out that clinical heterogeneity was not a confounding variable in the human samples studied here, as patients within a diagnostic group were mutation-positive for the same gene (e.g. shared the same “ground truth” in primary biochemical disorder) (Duchenne muscular dystrophy, Becker muscular dystrophy, spastic paraplegia, dysferlin deficiency, Fukutin related protein deficiency, Calpain III deficiency,

Fascioscapulohumeral muscular dystrophy, Emery Dreifuss muscular dystrophy). In two groups, there is no known single known gene causative of the disorder, but all patients in these groups were clearly affected by the condition as diagnosed by an acknowledged leader in that specific disorder (Acute Quadriplegic, Juvenile dermatomyositis). The 11 diagnostic groups were normal skeletal muscle from volunteers in exercise studies (n=19) (Chen *et al.*, 2003), Duchenne muscular dystrophy (n=9) (dystrophin mutations; Chen *et al.*, 2000; Bakay *et al.*, 2002a; Bakay *et al.*, 2002b), Acute Quadriplegic Myopathy (n=5) (TGFbeta/MAPK activation; DiGiovanni *et al.*, *in press*), spastic paraplegia (n=4) (spastin mutations; Molon *et al.*, *in press*), dysferlin deficiency (n=9) (dysferlin gene mutations; unpublished), Juvenile Dermatomyositis (n=18) (autoimmune disease; Tezak *et al.*, 2002), Fukutin related protein hypomorph (n=7) (homozygous missense for glycosylation enzyme; unpublished), Becker muscular dystrophy (n=5) (hypomorph for dystrophin; see Hoffman *et al.*, 1988, Hoffman *et al.*, 1989; microarray data unpublished), Calpain III deficiency (n=11) (Calpain III gene mutations; see Chou *et al.*, 1999; microarray data unpublished), Fascioscapulohumeral muscular dystrophy (n=13) (deletion of chromosome 4q; Winokur *et al.*, 2003), and Emery Dreifuss muscular dystrophy (n=4) (lamin A/C missense mutations; microarray data unpublished). This data set was expected to have considerably greater confounding biological noise. The age and sex of subjects varied, tissue heterogeneity is known to be significant, and genetic heterogeneity between subjects is substantial. Moreover, the differences between groups were expected to be relatively minor for some groups. For example, Duchenne muscular dystrophy and Becker muscular dystrophy are both caused by mutations of the same dystrophin gene, however Duchenne affects children and is caused by nonsense mutations, while Becker muscular dystrophy affects adults and is caused by partial-loss-of-function mutations. Thus, any attempt to distinguish some groups using unsupervised methods is expected to be considerably more challenging than for the murine lung data set. Note that all data was subjected to the same QC/SOP protocols, as described on our web site (<http://microarray.cnmcresearch.org>), and was generated in the same laboratory (Center for Genetic Medicine, Children's National Medical Center, Washington DC).

For the two data sets, we processed CEL files using five different probe set signal algorithms; MAS 5.0, dChip perfect match only, dChip difference, Probe Profiler and RMA. MAS 5.0 results were obtained using Affymetrix LIMS (Laboratory Information Management Systems) software, dChip results were generated using the official software release (Li and Wong, 2001a), Probe Profiler results were obtained using the Probe Profiler software by Corimbia Inc. (www.corimbia.com), and the RMA results were obtained using the affycomp package of the Bioconductor Project (<http://www.bioconductor.org>).

Previous comparison studies using well-known benchmark data sets such as spike-in and dilution experiments have evaluated probe set signal algorithms in terms of the known expected features (Baugh *et al.*, 2001; Hill *et al.*, 2001). Cope *et al.* have developed a graphical tool to evaluate probe set signal algorithms using statistical plots and summaries. They also utilized the benchmark data sets to identify the statistical features of the data for which the expected outcome is known in advance (Cope *et al.*, 2003). These studies can provide a general guideline of which method is suitable for a specific investigation. While one method is better than others in general, according to the studies using the benchmark data, the "ideal" method of probe set analysis could be different for different projects. What we suggest in this paper is a permutation study framework (see Figure 1) to help researchers choose a probe set signal algorithm that optimizes the signal/noise balance for their projects.

<< Fig. 1 will be shown around here >>

Samples (or columns in the input file) were clustered using the unsupervised hierarchical agglomerative clustering algorithm in *HCE2W* (the improved version of the Hierarchical Clustering Explorer 2.0), and the “unsupervised” clustering results are compared to the grouping by our target biological variable. In this way, we can evaluate the probe set signal algorithms by comparing the groupings naturally derived from the input data set to the groupings formed by our target biological variable.

Hierarchical agglomerative clustering has been the most commonly used method for microarray data clustering (Moreau et al., 2002) since Eisen *et al.* (1998) first applied it to microarray data analysis. In hierarchical agglomerative clustering, when we want to cluster m data items, each data item initially occupies a cluster by itself. The most similar two clusters are then merged to construct a new cluster. The similarity/distance values between the new cluster and the remaining clusters are then updated using a specific linkage algorithm. We ran *HCE2W* using the average linkage method (aka UPGMA: Unweighted Pair Group Method with Arithmetic Mean) in this current study. We have previously studied the effect of different linkage algorithms in agglomerative clustering, and found that the UPGMA linkage method provided the best sample distinction by visual output (Seo *et al.*, 2003). Typically for microarray data, the average linkage method gives acceptable results (Quackenbush, 2001). It is at least included or used as default measures in many standard microarray analysis tools (GeneSpring, Spotfire DecisionSite, S-plus ArrayAnalyzer, R, and so on).

Average linkage is summarized as follows. Let C_n be a new cluster, a merger of C_i and C_j at a stage of the hierarchical agglomerative clustering process. Let C_k be one of the remaining clusters. Then the distance between C_n and C_k can be calculated using the following equation where $\text{Dist}(C_a, C_b)$ is the distance (or dissimilarity) between C_a and C_b , $|C_a|$ is the number of items in a cluster C_a :

$$\text{Dist}(C_n, C_k) = \text{Dist}(C_i, C_k) * |C_i| / (|C_i| + |C_j|) + \text{Dist}(C_j, C_k) * |C_j| / (|C_i| + |C_j|)$$

The merge and update are repeated until there remains only one cluster of size m .

We also developed a novel probe set weighting scheme for data analysis. Newer Affymetrix MAS 5.0 software generates a probe set detection p value; this provides an assessment of the assuredness of the distinction between perfect match and mismatch probes across the entire 22 feature probe set, and thus a measure of the “performance” of the probe set. It would be expected that probe sets that performed well (e.g. highly significant detection p value) would provide “better” data than poorly performing probe sets. A corollary to this hypothesis is that weighting of probe sets so that clustering is driven more strongly by well-performing probe sets would provide a novel noise filter that would improve clustering results. Towards this end, we used each probe set algorithm tested with and without a continuous weighting of all probe sets based upon MAS 5.0 probe set detection p value. For each input signal data set, we ran HCE twice to obtain 20 comparison results in total (2 experiments x 5 signal algorithms x 2). First, we ran HCE without weighting with the Affymetrix MAS 5.0 detection p-values. Second, we ran HCE with weighting each signal value in the input data set with the detection p-values as explained in the following section. By comparing the two results, the effect of noise filtering methods can be verified across the five probe set signal algorithms and two data sets of different noise-level.

Incorporating probe set detection p-value to similarity calculation

Affymetrix noise calculations give us two outputs; one is the continuous detection p value assignment, and the other is a simple detection call (“present/absent”). Each signal intensity value has a confidence factor – detection p-value, which contributes to determining the detection call for the corresponding probe set. When the probe set detection p-value reaches a certain level of significance,

then the probe set is assigned a “present” call, while all those probe sets with less robust signal/noise ratios are assigned an “absent” call. This enables the use of a “present call” threshold noise filter that has been used in many published studies (Chen *et al.*, 2000, 2002; DiGiovanni *et al.*, 2003; DiGiovanni *et al.*, *in press*; Hittel, 2003). In our previous study (Seo *et al.*, 2003), we reported that a “10% present call” noise filter did improve the performance of probe set signal algorithms. While such “present call” based filtering improves performance, it is clearly an arbitrary threshold method, and thus it is highly possible that potentially important signals that might be conveyed by the probe sets are filtered out.

Affymetrix MAS 5.0 uses a two-step procedure to determine the detection p-value for a probe set. It calculates the discrimination score, $R=(PM-MM)/(PM+MM)$ for each probe pair, and then tests R against a small positive threshold value. It assigns a rank to each probe pair according to the distance from R and the given threshold, and then the one-sided Wilcoxon signed rank test is used to generate the detection p-value for the probe set. The discrimination score R describes the ability of a probe pair to detect its intended target, so the detection p-values are a reliable continuous indicator of how well the measured transcript is detected. Even though these detection p-values are given by Affymetrix MAS 5.0, they can be used with other signal algorithms since (1) all signal algorithms used the CEL files as their inputs and detection p-values are directly calculated from CEL files, and (2) the signal algorithm and detection algorithm are independent of each other in MAS 5.0. We used the detection p-values from MAS 5.0 as a continuous weighting for probe sets for all five tested signal algorithms in this study. By involving this confidence factor in the clustering process, we believe it would give greater potential sensitivity by considering all probe sets in an analysis without the cost of poor signal-noise ratio.

There are many possible similarity measures for unsupervised clustering methods, and it is also possible to develop weighted versions of most similarity measures. For example, we can derive a weighted Pearson correlation coefficient as follows from the Pearson correlation coefficient that has been widely used in the microarray analysis. Let $x = (x_1, \dots, x_n)$ and $y = (y_1, \dots, y_n)$ be the vectors representing two arrays to be compared, and let $p(y) = (p(y_1), \dots, p(y_n))$ and $p(x) = (p(x_1), \dots, p(x_n))$ be the vectors representing p-values for x and y respectively. Then the weighted Pearson correlation coefficient is given by

$$r_{xy} = \frac{\sum w_i (x_i - \bar{x}_w)(y_i - \bar{y}_w)}{\sqrt{\sum w_i (x_i - \bar{x}_w)^2 \sum w_i (y_i - \bar{y}_w)^2}} \quad (1)$$

, where $w_i = \frac{(1 - p(x_i)) + (1 - p(y_i))}{2}$, $\bar{y}_w = \sum w_i y_i / \sum w_i$, $\bar{x}_w = \sum w_i x_i / \sum w_i$

A similar weighting method is used in Eisen’s Cluster software and should be cited (see page 12 of <http://rana.lbl.gov/manuals/ClusterTreeView.pdf>). Our extension is that we use the complement of detection p-value to calculate the weight for each term since the smaller the p-value is, the more significant the signal is. Other similarity measures such as Euclidean distance, Manhattan distance, and cosine coefficient can be extended to their weighted version in a similar way to the weighted Pearson correlation coefficient.

Using External Measure for Evaluation of Unsupervised Clustering Results

In our previous pilot study (Seo *et al.*, 2003), we visually inspected the unsupervised clustering results to see how well the clustering result fit to the known biological variable. Visual inspection was the right choice for the study since we only have 25 arrays of 3 different groups of samples. But since we now

have 105 arrays of 11 different groups of samples, visual inspection is not realistic. Therefore, we decided to use reasonable clustering evaluation measures in addition to visual inspection in this study.

There are two kinds of clustering result evaluation measures, internal and external. The former is for the case where one is not certain what the correct clustering is. It compares the clusters using internal measures such as distance matrix without any external knowledge. The latter is for the case where we already know the correct classes of our samples. In this study, we already know the correct class labels of samples, and thus use external measures. Possible external measures include purity, entropy, and F-measures. Among them, F-measures (Rijsbergen, 1979) have been used as an external clustering result evaluation measure in many studies across many fields including information retrieval and text-mining (Lewis, 1994; Bjornar, 1999; Cohen, 2002). Furthermore F-measure has been successfully applied to hierarchical clustering results (Bjornar, 1999).

We applied F-measure to the entire hierarchical structure of clustering results and also to the set of clusters determined by the minimum similarity threshold in HCE2W. Let $C_1, \dots, C_i, \dots, C_n$ be the right clusters according to the target biological variable. Let $HC_1, \dots, HC_j, \dots, HC_m$ be the clusters from the hierarchical clustering results. In F-measure, each cluster is considered a query and each class (or each correct cluster) is considered the correct answer of the query. The F-measure of a correct cluster (or a class) C_i and an actual cluster HC_j is defined as follows:

$$F(i, j) = \frac{2P(i, j) \cdot R(i, j)}{P(i, j) + R(i, j)}, \text{ where } P(i, j) = \frac{|C_i \cap HC_j|}{|HC_j|}, R(i, j) = \frac{|C_i \cap HC_j|}{|C_i|}. \quad (2)$$

The precision values $P(i, j)$ and recall values $R(i, j)$ are defined by the information retrieval concepts. The F-measure of a class C_i is given by

$$F(i) = \max_{j=1}^m F(i, j). \quad (3)$$

Finally, the F-measure of the entire clustering result is given by

$$\sum_{i=1}^n \frac{|C_i|}{N} \cdot F(i), \text{ where } N \text{ is the total number of arrays in the experiment.} \quad (4)$$

The F-measure score is between 0 and 1. The higher the F-measure score is, the better the clustering result is. When we calculate the F-measure for the entire cluster hierarchy, for each external class we traverse the hierarchy recursively and consider each subtree as a cluster. Then the F-measure for an external class is the maximum of F-measures for all subtrees. The pseudo code for the overall F-measure calculation is shown in Figure 2.

<< Fig. 2 will be shown around here >>

Interactive Visual Analysis of Hierarchical Clustering Results

HCE2 (the Hierarchical Clustering Explorer 2.0) is an interactive visualization tool for hierarchical clustering results (Seo and Shneiderman, 2002; <http://www.cs.umd.edu/hcil/hce/>). HCE2 users load a microarray experiment data set from a tab-delimited file, and apply their desired hierarchical clustering methods to generate a dendrogram and a color mosaic. Users can immediately observe the entire clustering result in a single screen that enables identification of high-level patterns, major clusters, and distinct outliers. They can adjust the color mapping to highlight the separation of groups in the data set. Then they start their exploration of the groupings. Instead of using fingers and pencils on a static

clustering results, HCE2 users can use a dynamic query device called “minimum similarity bar” to find meaningful groups. The Y-coordinate of the bar determines the minimum similarity threshold. A cluster (a subtree of the dendrogram) will be shown only if any two items in the cluster are more similar than the minimum similarity threshold specified by the minimum similarity bar. Thus, users see tighter clusters as they pull the bar lower to increase the minimum similarity threshold. HCE2 is provided as a public domain software tool.

A troublesome problem related to clustering analysis is that there is no perfect clustering algorithm. Clustering results highly depend on the distance calculation method and linkage method used in the clustering process. Therefore, molecular biologists and other researchers need some mechanism to examine and compare two clustering results. HCE2 users can select two different clustering methods and compare the two clustering results in a single screen. When users double click on a cluster in one clustering result, HCE2 shows the mapping to the other clustering result by connecting the same items with a line (see <http://www.cs.umd.edu/hcil/hce/> for detail). Through this comparison, users can determine clustering parameters that most faithfully assemble items into the appropriate biological groups according to their known biological function.

Since sample clustering is the main task of this study, we implemented an improved version of HCE2, *HCE2W*, to enable users to better understand sample (or chip) clustering results. With *HCE2W*, users can focus on either sample clustering or gene clustering by switching the main dendrogram view between sample and gene. When the sample clustering result is on the main dendrogram view, each sample name is color-coded according to its biological class so that users can assess the quality of clustering from the visual representation. To facilitate signal/noise analyses for microarray experiments, we incorporated a weighting method for distance/similarity function and an external clustering evaluation method into *HCE2W* as described in the previous sections. *HCE2W* users can choose the option of using p-values as weights in the clustering dialogue box (Figure 3a) and get an instantaneous graphical feedback of F-measure for each minimum similarity threshold value (Figure 3b).

<< Fig. 3 will be shown around here >>

As users drag the minimum similarity bar, a line graph of F-measure score is overlaid on the main dendrogram view so that they can easily see the overall distribution of F-measure values right on the clustering result. Since the maximum F-measure value is highlighted with red dot on the F-measure distribution curve, users can easily know when to stop dragging the minimum similarity bar to get the best clustering results in terms of F-measure. This F-measure is calculated based on the current grouping determined by the current value of minimum similarity threshold. While this F-measure helps users find natural groupings in the data set, we need another measure that evaluates the clustering structure as a whole to compare many clustering results reasonably. We used the overall F-measure described in the previous section for this purpose. The overall F-measure evaluates the entire cluster hierarchy instead of considering only the groups by the current minimum similarity threshold. *HCE2W* shows the overall F-measure value at the top center of the main dendrogram view that is calculated by the pseudo code in the previous section (Figure 2).

Results and Discussion

We felt that the “ideal” method of probe set analysis was likely different for different projects. Application of any noise filter can be appropriate in one context, and inappropriate in another, depending

on the sensitivity desired, and the relative cost of noise that generally accompanies increased sensitivity. For example, the RMA method performs very well with known "spike in" RNAs, providing greater sensitivity and more stable "signals" from probe sets. However, the greater sensitivity of the RMA method would be expected to come at a cost to specificity; the less weight given to the mismatch "noise" filter by RMA would be expected to lead to greater signal/noise problems in complex solutions. The testing of two cell samples that vary only due to a single highly controlled variable would be best analyzed by RMA. On the other hand, comparison of human muscle biopsy profiles (as below) are complicated by many uncontrolled variables, such as inter-individual variation, and the biopsy content of different constituent cell types (myofiber, connective tissue, vasculature). In the latter experiment, the greater sensitivity of RMA would be offset by the high cost of specificity and noise resulting from non-specific hybridization and uncontrolled variables.

We investigated the systematic alteration of signal/noise ratios by iteratively altering the probe set analysis algorithm (five methods), and weighting of genes using MAS 5.0 probe set detection p value. The latter is, to our knowledge, a novel method of continuous weighting based upon the observed performance of each probe set, with better performing probes given greater weight in the resulting clustering. We also developed a new implementation, *HCE2W*, of our public domain HCE2 software, to effectively interrogate optimal signal/noise ratios by visualizing F-measures in unsupervised clustering analyses. To test the effectiveness of these methods, we utilized two large data sets that were expected to differ considerably in the amount of confounding and uncontrolled biological noise intrinsic to the projects; a "noisy" 105 human muscle biopsy U133A data set, and a "less noisy" 40 microarray U74A inbred mouse lung data set (see Methods and Description for description of the data sets). All microarrays were processed in the same laboratory, following the same quality control and standard operating procedures, thus minimizing non-biological technical noise in both projects.

All arrays were analyzed using five different signal algorithms including Affymetrix MAS 5.0, dChip perfect match only model, dChip difference model, Probe Profiler, and RMA method. We used the continuous probe set detection p value as a "weighting" function. Spreadsheets corresponding to each profile were then loaded into *HCE2W*. Unsupervised clustering of the profiles was done using permutations of signal algorithms, with and without a noise filter (continuous probe set detection p value weighting). For each signal algorithm, we prepared two data files; a signal value file and a detection p-value file where each column is a sample and each row is a probe set. Our *HCE2W* program supports 5 different linkage methods: average, average group, complete, single, and one-by-one linkage (Seo *et al.*, 2002). In this study, we choose average linkage since it is the most widely used linkage method and it was one of the most desirable linkage methods in our previous study (Seo *et al.*, 2003).

For each signal algorithm, we first ran *HCE2W* without applying any noise filter. Then, *HCE2W* was run again applying the noise filter (using the detection p-values as a continuous weighting function) to the data set. We visualized the unsupervised clustering of the data set to determine the method that provided the best clustering according to our "known" biological variable (specific biochemical defect; patient diagnosis), and thus was most effective in reducing undesirable noise. In the following bar graphs (Figure 4), we have determined the "performance" for each probe set algorithm using F-measure, either weighted by Affymetrix MAS 5.0 probe set detection p value (the "wt" bars), or un-weighted (the "no-wt" bars).

<< Fig. 4 will be shown around here >>

As expected, the two projects showed different results, with the inbred mouse lung data (low noise) showing greater success of unsupervised clustering into appropriate biological variables by all probe set algorithms and weighting methods. This reflects the much more highly controlled nature of the mouse data, with less confounding biological noise, as described above.

Using probe set p-value as a weight improved the performance of dChip difference model, Probe Profiler, and RMA probe set algorithms in both data sets (Figure 4). There was no detectable change in performance of MAS 5.0 and dChip PM only algorithms using unsupervised clustering and F measure (Figure 4). This suggests that utilizing a continuous weighting with MAS 5.0 detection p value would improve data analysis with three of the most commonly used probe set algorithms and clustering methods.

We then compared the relative performance of the different probe set algorithms. Most obvious was the differences in performance of RMA in the two data sets. RMA, a probe set algorithm that is thought to be among the most sensitive with low signal intensities, performed very well in the mouse data set, if used with MAS 5.0 detection p value weighting (Figure 4b). However, this same RMA algorithm showed the poorest performance of all algorithms in the human data (Figure 4a). We can conclude that the greater sensitivity of the RMA algorithm with low signal strengths is an advantage in projects with low confounding noise (e.g. inbred mouse data), but this same advantage becomes a liability driving poor performance in the human data with high levels of confounding noise. It is important to point out that the large majority of human subjects studied had a "known" primary genetic defect (e.g. gene mutation positive), as described in the Methods. Thus, underlying clinical heterogeneity could be ruled out in this specific project.

We performed paired t-tests with the two results to see if there is a statistically significant difference between the results with or without continuous detection p-value weighting. There was no statistically significant difference in the human muscle data. This is because the performance of MAS 5.0 and dChip PM only model was unchanged or slightly worse with the p-value weighting while those of others get better. Excluding the two cases, the difference was statistically significant. There was a statistically significant difference in the mouse lung data ($t(4)=-3.687$, $p=0.021$). We conclude that use of MAS 5.0 detection p value weighting is recommended for dChip difference model, ProbeProfiler and RMA.

We then used a random-sampling permutation study to determine the statistical significance of differences in performance found between the different probe set algorithms and to verify the previous t-test result on the effect of continuous detection p-value weighting with more samples (Figure 5). We random-sampled 50% of probe sets to partition our original data sets into two small data sets with only half the number of probe sets. For each randomly sampled partition of input data, we repeated the previously mentioned permutation study to get two-times larger external evaluation result.

We then conducted 5x2 two-way ANOVA on the effect of 5 probe set signal algorithms and our novel detection p-value weighting. The analysis showed that the probe set signal algorithms did have a statistically significant effect on the external evaluation measure for both the mouse and human experiments ($F(4,10)>14$, $p<0.0001$). The effect of the detection p-value weighting was statistically significant only for the inbred mouse lung data ($F(1,10)>9$, $p<0.013$). We also re-ran paired t-tests to verify the significance of the detection p-value weighting with more samples. The t-test results showed that the continuous detection p-value weighting made a more statistically significant difference for the inbred mouse lung data ($t(9)=-3.675$, $p=0.005$) than the previous result, but this again did not reach significance for the human muscle data.

<<Fig. 5 will be shown around here>>

Our data provides guidance of how researchers might optimize probe set algorithms and signal weights for individual projects. Our permutation study of noise level (two data sets), probe set analysis (five methods) and noise filtering (two methods – with or without detection p-value weighting) with *HCE2W* found that:

- **Performances of all probe set signal methods were better with a less-noisy data set (inbred mouse lung data set) than with noisy data set (human muscle biopsy).**
- **Noise filter using continuous probe set detection p-value improved the performances for *dChip difference model*, *Probe Profiler*, and *RMA*.**
- ***dChip difference model* with MAS 5.0 probe set detection p values as weights was the most consistent at maximizing the effect of the target biological variables on data interpretation of the two data sets.**

While our current implementation only uses hierarchical agglomerative clustering in our permutation study framework, it is also possible to employ other unsupervised clustering algorithms, such as K-Means clustering or SOM clustering. The novel F-measure and p-value weighting described here can also be used for those algorithms with minor modifications.

There are additional microarray experimental platforms available for mRNA profiling, including mechanically spotted cDNA and oligonucleotide arrays (see The Tumor Analysis Best Practices Workshop 2004 for review). Spotted arrays typically have a single ratio per gene, or, in some cases, replicate spots per array. The single measurement possible with spotted arrays does not permit the development of algorithms to determine “signal” across a larger “probe set” as with Affymetrix arrays. Thus, the methods described here are not easily applicable to spotted microarrays.

Conclusion

Our data suggests that large microarray projects should undergo a systematic “signal/noise” analysis, as we have presented here. By using permutations of probe set signal algorithms, and noise reduction filters (continuous variable probe set detection p values), with unsupervised clustering, the analysis method that most faithfully assembles profiles into the appropriate biological groups should maximize the signal from the biological variable, while minimizing the confounding noise intrinsic to the project. This results in a balanced signal/noise assay that should provide the best balance between sensitivity and specificity. Our future plans are to implement a more extensive and automated project analysis, where these and other variables are systemically varied to achieve the best clustering into the desired biological variable groupings.

Acknowledgements: This work was supported by N01 NS-1-2339 from the NIH.

References

- Affymetrix (2001a) Microarray Suite User Guide, Version 5.0. Affymetrix, Santa Clara, CA
<http://www.affymetrix.com/products/software/specific/mas.affx>
- Affymetrix (2001b) Data Analysis Fundamentals,
https://www.affymetrix.com/support/downloads/manuals/data_analysis_fundamentals_manual.pdf

- Affymetrix (2001c) Statistical Algorithm Reference Guide. Affymetrix, Santa Clara, CA, version 5 edition.
- Bakay, M., Chen, Y.W., Borup, R., Zhao, P., Nagaraju, K. and Hoffman, E.P. (2002a) Sources of variability and effect of experimental approach on expression profiling data interpretation, *BMC Bioinformatics*, 3, 4-15.
- Bakay, M., P. Zhao, Chen, J. and Hoffman, E. P. (2002b) A web-accessible complete transcriptome of normal human and DMD muscle, *Neuromuscular Disorders*, 12, S125-S141.
- Baugh, L.R., Hill, A.A., Brown, E.L. and Hunter, C.P. (2001) Quantitative analysis of mRNA amplification by in vitro transcription, *Nucleic Acids Res.*, 29, E29.
- Bjornar, L. and Aone, C. (1999) Fast and effective text mining using linear-time document clustering, *Proceedings of the fifth ACM SIGKDD International Conference on Knowledge Discovery and Data Mining*, 16 - 22.
- Bolstad, B.M., Irizarry, R.A., Astrand, M. and Speed, T.P. (2003) A comparison of normalization methods for high density oligonucleotide array data based on variance and bias, *Bioinformatics*, 19, 185-193.
- Chen, J., Zhao, P., Massaro, D., Clerch, L.B., Almon, R.R., DuBois, D.C., Jusko, W.J. and Hoffman, E.P. (2004) The PEPR GeneChip data warehouse and implementation of a dynamic time series query tool (SGQT) with graphical interface, *Nucleic Acids Res.*, 32, *in press*.
- Chen, Y.W., Hubal, M.J., Hoffman, E.P., Thompson, P.D. and Clarkson, P.M. (2003) Molecular responses of human muscle to eccentric exercise, *J. Appl. Physiol.*, 95, 2485-2494.
- Chen, Y.W., Nader, G., Baar, K.R., Hoffman, E.P. and Esser, K.A. (2002) Response of rat muscle to acute resistance exercise defined by transcriptional and translational profiling, *J. Physiol.*, 545, 27-41.
- Chen, Y.W., Zhao, P., Borup, R. and Hoffman, E.P. (2000) Expression profiling in the muscular dystrophies: Identification of novel aspects of molecular pathophysiology, *J. Cell Biol.*, 151, 1321-1336.
- Chou, F.L., Angelini, C., Daentl, D., Garcia, C., Greco, C. Hausmanowa-Petrusewicz, I., Fidzianska, A., Wessel, H. and Hoffman, E.P. (1999) Calpain III mutation analysis of a heterogeneous limb-girdle muscular dystrophy population, *Neurology*, 52, 1015-20.
- Cohen, W. W. and Richman, J. (2002) Learning to match and cluster large high-dimensional data sets for data integration, *Proceedings of the Eighth ACM SIGKDD International Conference on Knowledge Discovery and Data Mining*, 475-480.
- Cope, L.M., Irizarry, R.A., Jaffee, H., Wu, Z. and Speed, T.P. (2003) A Benchmark for Affymetrix GeneChip Expression Measures, *Bioinformatics*, 1, 1-10.
- DiGiovanni, S., Knoblach, S.M., Brandoli, C., Aden, S.A., Hoffman, E.P., and Faden, A.I. (2003) Gene profiling in spinal cord injury shows role of cell cycle in neuronal death. *Ann. Neurol.* 53, 454-68.
- DiGiovanni, S., Molon, A., Broccolini, A., Melcon, G., Mirabella, M., Hoffman, E.P. and Servidei, S. Myogenic atrophy in acute quadriplegic myopathy is specifically associated with activation of pro-apoptotic TGF beta-MAPK cascade, *Ann. Neurol.*, *in press*.
- Eisen, M.B., Spellman, P.T., Brown, P.O. and Botstein, D. (1998). Cluster Analysis and Display of Genome-Wide Expression Patterns. *Proc Natl Acad Sci USA*, Vol. 95, 14863-14868.
- Hill, A.A., Brown, E.L., Whitley, M.Z., Tucker-Kellogg, G., Hunter, C.P. and Slonim, D.K. (2001) Evaluation of normalization procedures for oligonucleotide array data based on spiked cRNA controls, *Proc. Natl. Acad. Sci. U S A.*, 98, 31-6.

- Hittel, D.S., Kraus, W.E. and Hoffman, E.P. (2003) Skeletal muscle dictates the fibrinolytic state after exercise training in overweight men with characteristics of metabolic syndrome, *J. Physiol.*, 548.2, 401-410.
- Hoffman, E.P., Fischbeck, K.H., Brown, R.H., Johnson, M., Medori, R., Loike, J.D., Harris, J.B., Waterston, R., Brooke, M., Specht, L., Kupsky, W., Chamberlain, J., Caskey, C.T., Shapiro, F. and Kunkel, L.M. (1988) Dystrophin characterization in muscle biopsies from Duchenne and Becker muscular dystrophy patients, *New Eng. J. Med.*, 318, 1363-1368.
- Hoffman, E.P., Kunkel, L.M., Angelini, C., Clarke, A., Johnson, M. and Harris JB. (1989) Improved diagnosis of Becker muscular dystrophy by dystrophin testing, *Neurology*, 39, 1011-1017.
- Hubbell, E., Liu, W.M., and Mei, R. (2002). Robust estimators for expression analysis. *Bioinformatics*, 18, 1585-92.
- Irizarry, R.A., Bolstad, B.M., Collin, F., Cope, L.M., Hobbs, B. and Speed, T.P. (2003a) Summaries of Affymetrix GeneChip probe level data, *Nucleic Acids Res.*, 31, e15.
- Irizarry, R.A., Hobbs, B., Collin, F., Beazer-Barclay, Y.D., Antonellis, K.J., Scherf, U. and Speed, T.P. (2003b) Exploration, normalization, and summaries of high density oligonucleotide array probe level data, *Biostatistics*, 4, 249-264.
- Lewis, D. D. and W. A. Gale (1994) A Sequential Algorithm for Training Text Classifiers, *Proceedings of the 17th Annual International ACM SIGIR Conference on Research and Development in Information Retrieval*, 3-12.
- Li, C. and Wong, W. (2001a) Model-based analysis of oligonucleotide arrays: Expression index computation and outlier detection. *Proc. Natl. Acad. Sci. U S A.*, 98, 31-36.
- Li, C. and Wong, W. (2001b) Model-based analysis of oligonucleotide arrays: model validation, design issues and standard error application, *Genome Biol.*, 2, research0032.1-research0032.11
- Liu, W.M., Mei, R., Di, X., Ryder, T.B., Hubbell, E., Dee, S., Webster, T.A., Harrington, C.A., Ho, M.H., Baid, J., Smeekens, S.P. (2002). Analysis of high density expression microarrays with signed-rank call algorithms. *Bioinformatics*, 18, 1593-9.
- Molon, A. DiGiovanni, S., Chen, Y.W., Clarkson, P.M., Angelini, C., Pegoraro, E. and Hoffman, E.P. Large-scale disruption of microtubule pathways in morphologically normal human spastin-haploinsufficient muscle, *Neurology*, in press.
- Moreau, Y., De Smet, F., Thijs, G., Marchal, K. and De Moor, B. (2002) Functional bioinformatics of microarray data: from expression to regulation, *Proceedings of the IEEE*, Volume: 90 Issue: 11, 1722-1743.
- Quackenbush, J. (2001) Computational analysis of microarray data. *Nat Rev Genet.* Jun;2(6):418-427.
- Rijsbergen, C. J. Van (1979) *Information Retrieval*, 2nd ed. Butterworth, London.
(<http://www.dcs.gla.ac.uk/Keith/Preface.html>)
- Seo, J. and Shneiderman, B. (2002) Interactively exploring hierarchical clustering results, *IEEE Computer*, 35, 80-86.
- Seo, J., Bakay, M., Zhao, P., Chen, Y., Clarkson, P., Shneiderman, B. and Hoffman, E. P. (2003) Interactive Color Mosaic and Dendrogram Displays for Signal/Noise Optimization in Microarray Data Analysis, *Proceedings of the IEEE International Conference on Multimedia and Expo*, III-461~III-464.
- Tezak, Z., Hoffman, E.P., Lutz, J., Fedczyna, T., Stephan, D., Bremer, E.G., Krasnoselska-Riz, I., Kumar, A. and Pachman L.M. (2002) Gene expression profiling in DQA1*0501⁺ children with untreated dermatomyositis: A novel model of pathogenesis, *J. Virol.*, 168, 4154-63.

- The Tumor Analysis Best Practices Working Group. (2004). Guidelines: Expression profiling - best practices for data generation and interpretation in clinical trials. *Nat Rev Genet.* 5, 229-237.
- Winokur, S.T., Chen, Y.W., Masny, P.S., Martin, J.H., Ehmsen, J.T., Tapscott, S.J., Van Der Maarel, S.M., Hayashi, Y. and Flanigan, K.M. (2003) Expression profiling of FHSD muscle supports a defect in specific stages of myogenic differentiation, *Hum. Mol. Genet.*, in press.
- Zhao, P., Iezzi, S., Sartorelli, V., Dressman, D. and Hoffman, E.P. (2002) Slug is downstream of myoD: Identification of novel pathway members via temporal expression profiling, *J. Biol. Chem.*, 277, 30091-30101.
- Zhao, P., Seo, J., Wang, Z., Wang, Y., Shneiderman, B. and Hoffman, E.P. (2003) In vivo filtering of in vitro MyoD target data: An approach for identification of biologically relevant novel downstream targets of transcription factors, *Comptes Rendus Biologies*, 326, 1049-1065.

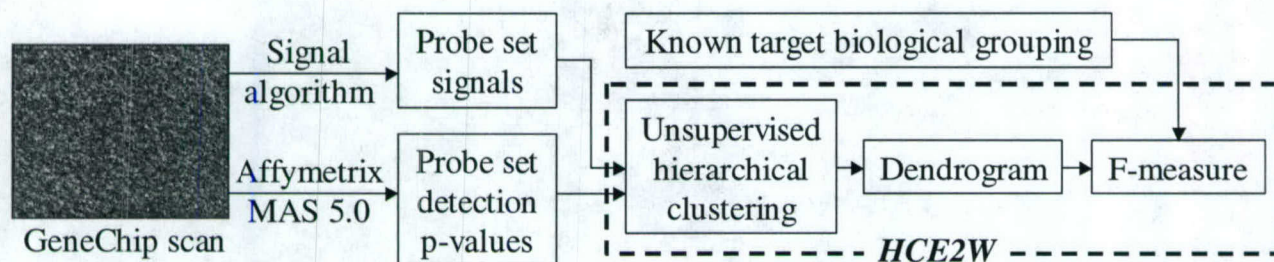
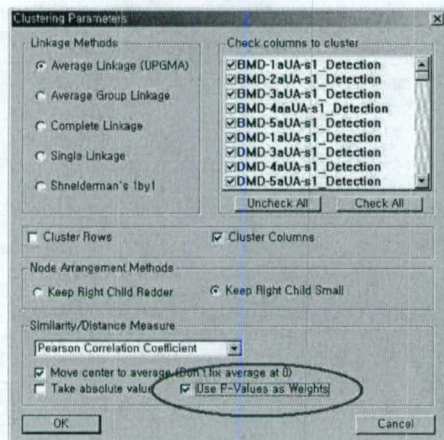


Fig. 1. Permutation Study Framework using Unsupervised Clustering in *HCE2W* (the improved version of the Hierarchical Clustering Explorer 2.0 with p-value weighting and F-measure). Inputs to the Hierarchical Clustering Explorer are two files, signal data file and p-value file. Each column of the two input files has values for a sample (or a chip), and the known target biological group index is assigned to each column of the signal data file. Success is measured using F-measure of a dendrogram and the known biological grouping.

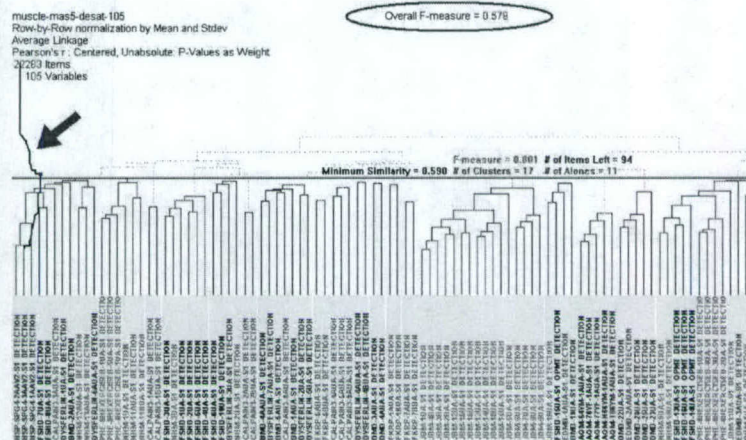
```

Overall_F-measure=0
FOR EACH class i
BEGIN
   $F(i)=0$  // the current maximum f-measure  $F(i)$  for class  $i$ 
  FOR EACH subtree j
  BEGIN
    calculate  $F(i,j)$  using [equation 2]
    IF  $F(i,j)$  is greater than  $F(i)$  THEN  $F(i)=F(i,j)$ 
  END
  Overall_F-measure = Overall_F-measure
    + (the number of samples of class  $i$ )* $F(i)$ /(the total number of samples)
END
  
```

Fig. 2. The pseudo code for the overall F-measure calculation



(a) Clustering DialogBox



(b) Visualization of a clustering result of human muscle samples

Fig. 3. Software development of HCE2W for probe set selection and detection p value weighting. (a) Researchers can check the option checkbox (highlighted with a red oval) to use the MAS 5.0 detection p-values as weights for distance/similarity measures. (b) Each sample name is color-coded by its biological class. Overall F-measure is highlighted with a green oval. The F-measure distribution is shown, as the distance from the left side, over the dendrogram display as indicated by an arrow mark.

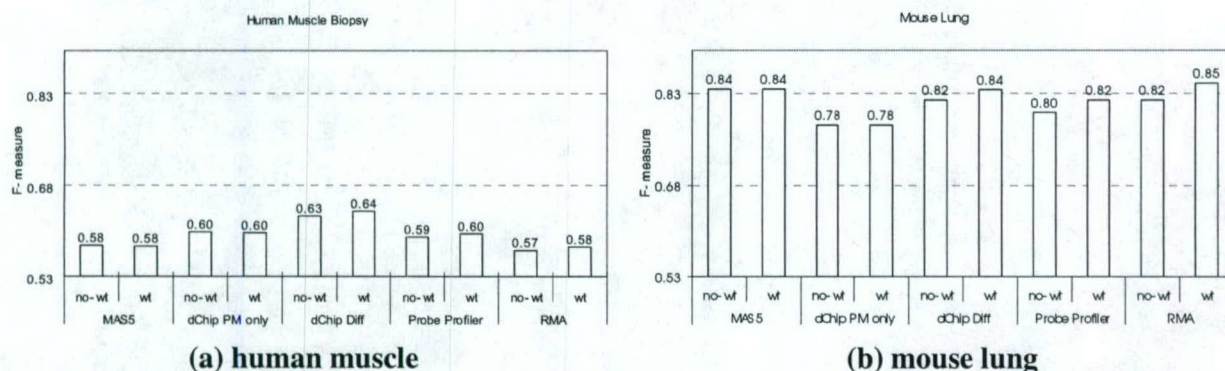


Fig. 4. External evaluation results using F-measure of unsupervised clustering. for the human muscular dystrophy data and the mouse lung biopsy data. “no-wt” bar represents the result without MAS 5.0 detection p-value weighting, and “wt” bar represents the result with p-value weighting.

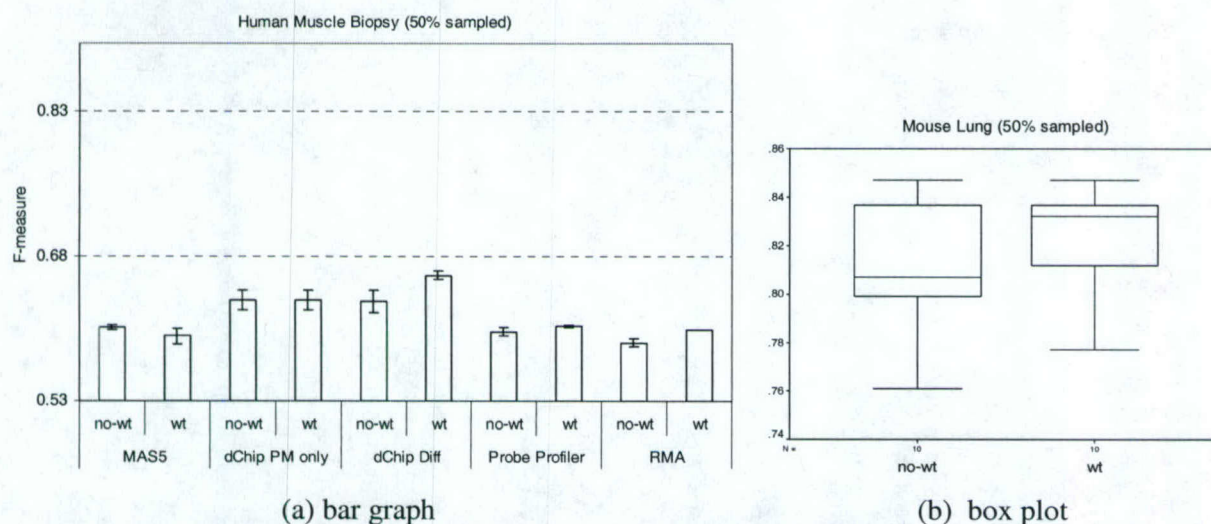


Fig. 5. Experiment results with 50% random sampled data sets. (a) dChip difference model with detection p-value weighting outperformed other probe set signal algorithms in human muscle data ($F(4,10) > 14$, $p < 0.0001$). (b) The result with p-value weighting (“wt”) was statistically significantly better than that without weighting (“no-wt”) for mouse lung data ($t(9) = -3.675$, $p = 0.005$).

Structural Basis of RasGRP Binding to High-Affinity PKC Ligands

Suo-Bao Rong,[†] Istvan J. Enyedy,[†] Lixin Qiao,^{†,‡} Lianyun Zhao,[†] Dawei Ma,[§] Larry L. Pearce,^{||} Patricia S. Lorenzo,^{||} James C. Stone,[‡] Peter M. Blumberg,^{||} Shaomeng Wang,^{*,†} and Alan P. Kozikowski^{*,†}

Drug Discovery Program, Department of Neurology, Georgetown University Medical Center, 3970 Reservoir Road, Washington, D.C. 20007, Molecular Mechanisms of Tumor Promotion Section, National Cancer Institute, Bethesda, Maryland 20892, 123, State Key Laboratory of Bio-organic and Natural Chemistry, Shanghai Institute of Organic Chemistry, Chinese Academy of Sciences, 354 Fenglin Lu, Shanghai 200032, China, and Department of Biochemistry, University of Alberta, Edmonton, Alberta T6G 2H7, Canada

Received September 7, 2001

The Ras guanyl releasing protein RasGRP belongs to the CDC25 class of guanyl nucleotide exchange factors that regulate Ras-related GTPases. These GTPases serve as switches for the propagation and divergence of signaling pathways. One interesting feature of RasGRP is the presence of a C-terminal C1 domain, which has high homology to the PKC C1 domain and binds to diacylglycerol (DAG) and phorbol esters. RasGRP thus represents a novel, non-kinase phorbol ester receptor. In this paper, we investigate the binding of indolactam(V) (ILV), 7-(*n*-octyl)-ILV, 8-(1-decynyl)benzolactam(V) (benzolactam), and 7-methoxy-8-(1-decynyl)benzolactam(V) (methoxylated benzolactam) to RasGRP through both experimental binding assays and molecular modeling studies. The binding affinities of these lactams to RasGRP are within the nanomolar range. Homology modeling was used to model the structure of the RasGRP C1 domain (C1-RasGRP), which was subsequently used to model the structures of C1-RasGRP in complex with these ligands and phorbol 13-acetate using a computational docking method. The structural model of C1-RasGRP exhibits a folding pattern that is nearly identical to that of C1b-PKC δ and is comprised of three antiparallel-strand β -sheets capped against a C-terminal α -helix. Two loops A and B comprising residues 8–12 and 21–27 form a binding pocket that has some positive charge character. The ligands phorbol 13-acetate, benzolactam, and ILV are recognized by C1-RasGRP through a number of hydrogen bonds with loops A and B. In the models of C1-RasGRP in complex with phorbol 13-acetate, benzolactam, and ILV, common hydrogen bonds are formed with two residues Thr12 and Leu21, whereas other hydrogen bond interactions are unique for each ligand. Furthermore, our modeling results suggest that the shallower insertion of ligands into the binding pocket of C1-RasGRP compared to C1b-PKC δ may be due to the presence of Phe rather than Leu at position 20 in C1-RasGRP. Taken together, our experimental and modeling studies provide us with a better understanding of the structural basis of the binding of PKC ligands to the novel phorbol ester receptor RasGRP.

Introduction

The Ras guanyl releasing protein (RasGRP) is expressed in the thymus, brain, spleen, and several lymphoid cell lines.¹ It modulates the Ras family of small GTPases that are essential elements in the signal transduction pathways in the cells and plays a crucial role in the regulation of cell growth and cytoskeletal rearrangements.² RasGRP functions as an upstream Ras activator through rapid conversion of the inactive GDP-bound Ras to the active GTP-bound form on the inner surface of the plasma membrane.³ The GTP bound state of Ras is able to bind and activate multiple downstream effectors such as Raf kinase and phosphatidylinositol 3-kinase that then initiate subsequent signaling cascades.⁴ The GTPases thus serve as switches for the propagation and divergence of signaling pathways.⁵

One interesting feature of RasGRP is the presence of a C-terminal cysteine-rich domain (also known as the C1 domain),^{1,6} which possesses high homology to the C1 domain of protein kinase C (PKC).⁷ The deletion of the RasGRP C1 domain (C1-RasGRP) and the reattachment of the PKC δ C1b domain (C1b-PKC δ) or C1-RasGRP to the C1-domain-deleted mutant revealed that the transforming activity of RasGRP is dependent on the presence of the C1 domain.¹

The C1 domain is a compact zinc-containing motif of ~50 amino acid residues, which was formerly identified as a conserved region responsible for the activation of PKCs by binding of diacylglycerol (DAG) and phorbol esters.⁸ For many years, signaling in response to the second messenger DAG was believed to proceed solely through the activation of one or more PKC isozymes. However, with the identification of RasGRP and other "non-kinase" phorbol ester receptors such as α - β -chimaerins⁹ and *Caenorhabditis elegans* Unc-13,¹⁰ it is now recognized that PKC constitutes only one of five families of receptors for DAG and the phorbol esters. Numerous experiments have shown that the phorbol esters may influence Ras signaling pathways by PKC-dependent pathways.^{11,12} A new and direct pathway

* To whom correspondence should be addressed. For A.P.K.: phone, 202-687-0686; fax, 202-687-5065; e-mail, kozikowa@georgetown.edu. For S.W.: phone, 202-687-2028; fax, 202-687-4032; e-mail, wangsm@gicc.georgetown.edu.

[†] Georgetown University Medical Center.

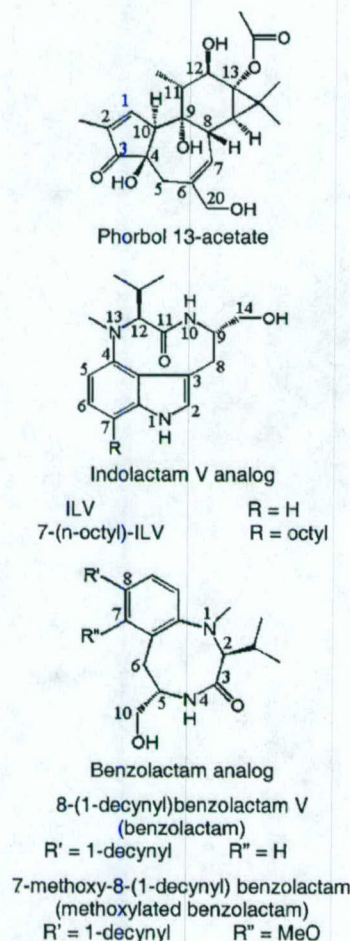
[‡] Current address: NeuroLogic Incorporation, 9700 Great Seneca Highway, Rockville, MD 20850.

[§] Shanghai Institute of Organic Chemistry.

^{||} National Cancer Institute.

[‡] University of Alberta.

Chart 1



from DAG to Ras signaling has been revealed by the recruitment of RasGRP to the plasma membrane in response to the binding of DAG and phorbol ester.¹

RasGRP binds to phorbol 12,13-dibutyrate (PDBu) with nanomolar affinity through its C1 domain.¹³ Structure-activity analysis of several phorbol esters revealed that the ligand selectivity of C1-RasGRP is somewhat different from that of C1b-PKC¹³ and that the binding of C1-RasGRP to phorbol esters is dependent on the presence of phospholipids.

The binding mode of phorbol 13-acetate to C1b-PKC δ has been determined by X-ray crystallography.¹⁴ NMR spectroscopy, molecular modeling, and site-directed mutagenesis have also been used to investigate the interaction of other PKC ligands with the C1 domains of PKC α , PKC δ , and β_2 -chimaerin.¹⁵ Here, we report our experimental and molecular modeling analysis of RasGRP binding to several high-affinity PKC ligands (see Chart 1).

Materials and Methods

Expression and Purification of RasGRP and PKC δ . The C1 domain of rat RasGRP (C1-RasGRP) and the second C1 domain of mouse PKC δ (C1b-PKC δ) were subcloned into a pGEX vector to produce GST fusion proteins in *E. coli*. The proteins were then purified using glutathione Sepharose 4B beads as described elsewhere.¹⁶ Note that the sequence of C1-RasGRP in the present study corresponds to that from SWISS-PROT (O88469), whereas we previously characterized¹³ the

RasGRP variant rbc7 in which Gly is replaced by Glu in position 35.¹

Binding Experiments. Binding assays were performed by the poly(ethylene glycol) precipitation method.¹⁷ The binding mixture contained 50 mM Tris-HCl, pH 7.4, 1 mg/mL bovine immunoglobulin G, 0.1 mM CaCl₂, 100 μ g/mL of sonicated phosphatidylserine, the protein to be assayed, and [³H]PDBu (2 nM) in the absence or presence of different concentrations of the compound being assayed. Incubations were carried out for 5 min at 18 °C for C1-RasGRP or 37 °C for C1b-PKC δ . Non-specific binding was measured using an excess of nonradioactive PDBu (30 μ M). Binding inhibition curves were determined with six to seven concentrations of the inhibitor, with triplicate values at each concentration in each experiment. Mean *K_i* values were calculated from a minimum of three separate experiments. Indolactam(V) (ILV) and *n*-octyl-ILV were from LC Laboratories (Woburn, MA). 8-(1-Decynyl)benzolactam(V) (benzolactam) and 7-methoxy-8-(1-decynyl)benzolactam(V) (methoxylated benzolactam) were synthesized as described previously.¹⁸

Sequence Alignment and Homology Modeling. The necessary sequence alignment data were retrieved from two different sources, one of these being a FASTA search of the Protein Data Bank (PDB)¹⁹ while the other made use of the protein family (Pfam) database.²⁰ From the sequence alignment, a 3D structural model of C1-RasGRP was constructed employing the Homology module implemented in InsightII (Molecular Simulation, Inc., San Diego, CA) and the crystal structure of C1b-PKC δ (PDB 1PTR) as template. Two Zn²⁺ ions extracted from the template protein were merged into the structural model of C1-RasGRP.

The initial model was refined in a stepwise manner by energy minimization with a stand-alone version of the CHARMM program²¹ (version c27b2) and the all-atom version 22 force field.²² First, the model was solvated by a 20 Å sphere of TIP3P water molecules²³ and energetically minimized for 2500 steps, with a fixed backbone, using the adopted-basis Newton-Raphson (ABNR) method to remove the unfavorable contacts. Then, the model was minimized for 2500 steps using harmonic constraints with a force constant of 10.0 kcal mol⁻¹ Å⁻² on the backbone, followed by another 2500 steps of minimization with a force constant of 5.0 kcal mol⁻¹ Å⁻² on the α -carbons. Finally, the whole model was minimized for 2500 steps or until an energy gradient of less than 0.05 kcal mol⁻¹ Å⁻¹ was achieved. The final model of C1-RasGRP was examined using the 3D profile approach²⁴ and checked by the program PROCHECK²⁵ to verify its folding and stereochemical quality.

Docking and Complex Modeling. The structure of phorbol 13-acetate was directly retrieved from the crystal structure of its complex with C1b-PKC δ (PDB 1PTR).¹⁴ The other molecules, including ILV and benzolactam, were modeled using the InsightII/Discover molecular modeling package.

Computational docking was performed using an automated docking method Autodock.²⁶ First, the crystal structure of C1b-PKC δ in complex with phorbol 13-acetate taken from PDB¹⁴ was used to validate the docking quality achieved by the Autodock program. Next, the three ligands phorbol 13-acetate, ILV and benzolactam were docked sequentially into the binding pocket of the model of C1-RasGRP formed by two loops comprising residues 8–12 and 21–27 (using consensus numbering for the C1 domains). In each case, 50 genetic algorithm dockings and energy evaluations were performed, followed by the cluster analysis based on a root-mean-square deviation tolerance of 0.5 Å. The lowest energy docked structure was selected as the starting complex model. The complex model soaked by a 20 Å sphere of water molecules was optimized by energy minimization for 10 000 steps or until an energy gradient of less than 0.05 kcal mol⁻¹ Å⁻¹ was reached.

MD Simulation and Analysis. The minimized complex models, together with a 20 Å sphere of water molecules, were used as the starting structures in the molecular dynamics (MD) simulations. The MD simulations were performed with a 10 ps heating period and a 40 ps equilibration, followed by

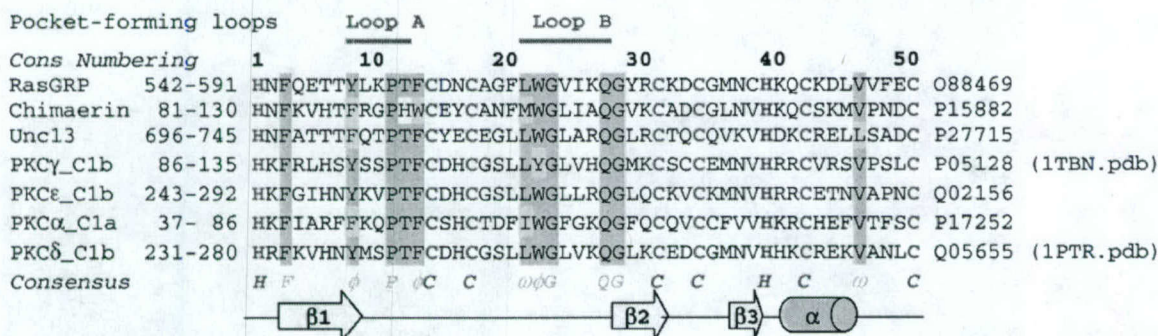


Figure 1. Sequence alignment of C1 domains. The SWISS-PROT accession numbers and PDB entries are indicated at the end of sequences. Consensus sequence numbering and amino acids are shown above and below the sequence alignment, respectively. ϕ and ω represent aromatic and aliphatic hydrophobic amino acids, respectively. Two clusters of the residues coordinating two Zn^{2+} ions are red and blue, respectively. The two binding pocket-forming loops A and B are indicated for the template protein by two orange bars at the top. Secondary structure elements of the template protein, C1b-PKC δ , are shown at the bottom. The green arrows and pink cylinder represent β -strands and α -helix, respectively.

a 100 ps constant temperature simulation at 300 K with a step size of 0.001 ps. The nonbonded energies and forces were smoothly shifted to zero at 12.0 Å,²⁷ and a dielectric constant was set to 1 for electrostatic interactions. The nonbonded list, including neighboring atoms within a 14.0 Å distance, was updated every 0.5 ps. All bonds to hydrogens were constrained with the SHAKE algorithm.²⁸ Trajectories were recorded every 0.5 ps of simulation for analysis. All MD simulations were performed on a Beowulf cluster with 450 MHz Pentium III CPU processors.

To examine the conformational changes upon ligand binding, the root-mean-square deviations (rmsd's) of the binding pocket were calculated from the trajectory at 0.5 ps intervals, with the initial structure as the reference.

Since hydrogen bonds are crucial for the interactions between PKC ligands and C1 domains,^{14,15} we examined the hydrogen bonding interactions based on the trajectories of the MD simulations. For the analysis of hydrogen bond interactions, a hydrogen bond (D-H...A) was defined by a distance between the donor and acceptor atoms of less than 3.0 Å and an angle $\theta_{\text{D-H-A}}$ of more than 120°. The percent occupancy and lifetime as well as the energy of the hydrogen bonds were calculated to evaluate the stability and the strength of the hydrogen bonds.

Results and Discussion

Experimental Determination of Ligand Binding Affinities.

The compounds ILV, *n*-octyl-ILV, benzolactam, and methoxylated benzolactam were tested for their ability to displace [³H]PDBu binding from C1-RasGRP and C1b-PKC δ . The binding affinity data are presented in Table 1 along with the binding affinities to C1b-PKC δ as determined previously.¹⁵ As can be seen in Table 1, the compounds fall into two categories based on their binding affinities for C1-RasGRP. The first group, including ILV and *n*-octyl-ILV, shows binding affinities around 1 nM for C1-RasGRP, with ILV being 3 times weaker than *n*-octyl-ILV. The second group comprises the two benzolactams. These two ligands are slightly less potent than ILV and *n*-octyl-ILV but still show binding affinities around 10 nM. The methoxylated benzolactam is about 2-fold less potent than benzolactam. Relative to C1b-PKC δ , C1-RasGRP binds the ligands with affinities ranging from 3-fold stronger to 8-fold weaker.

Homology Modeling. (a) Sequence Alignment.

The sequence alignments either obtained from the PDB FASTA search or taken directly from the Pfam database are identical and show 50% sequence identity and 70%

Table 1. Binding Affinities to C1-RasGRP and C1b-PKC δ ^a

compd	K_i , RasGRP (nM)	K_i , PKC δ (nM)
ILV	2.54 ± 0.16	2.01 ± 0.17 ^b
<i>n</i> -octyl-ILV	0.85 ± 0.01	0.10 ± 0.01 ^d
benzolactam	6.15 ± 0.41	10.7 ± 0.8 ^c
methoxylated benzolactam	13.92 ± 0.78	35.1 ± 2.3

^a K_i values were determined from binding inhibition curves using [³H]PDBu as the labeled ligand. Values represent the mean ± SEM of three or more experiments per compound. ^b Reference 15c. ^c Reference 15d. ^d Reference 10b.

similarity to the template protein (PDB 1PTR).¹⁴ Since a sequence identity above 50% generally guarantees that the modeled protein structure is correct at a level comparable to that of an X-ray crystal structure,²⁹ the sequence alignment (Figure 1) obtained from these two sources was used to model C1-RasGRP without any further modification.

The sequence alignment shows that the Zn^{2+} coordinating residues are conserved in all aligned sequences. In fact, these residues are completely conserved in all members of the C1 domain family.²⁰ On the basis of this conservation, two Zn^{2+} ions taken from the template protein were directly merged into the structural model of C1-RasGRP. In addition, the sequence alignment also contains 11 conserved amino acid residues, including four aromatic and two aliphatic hydrophobic residues, as well as two glycines, two glutamines, and one proline. It is noted that the two most conserved regions are distributed between the $\beta 1$ and $\beta 2$ strands, which correspond to loops A and B of the template protein that form the binding pocket (Figure 1).

(b) Structural Model of C1-RasGRP. The 3D profiles verification²⁴ method shows that the 3D/1D scores of our model are always positive and are similar to those of the template protein (Figure 2), which are within the range of scores for X-ray structure determinations. Additionally, PROCHECK²⁵ confirms that our model of C1-RasGRP not only has the correct folding but also possesses reasonable geometric structural parameters. Thus, it is expected that the structural model of C1-RasGRP is of sufficiently high quality to be used to investigate the ligand-protein interactions.

Identical to that of C1b-PKC δ , the modeled 3D structure of C1-RasGRP is made up of an antiparallel β -sheet, comprising three strands $\beta 1$, $\beta 2$, and $\beta 3$, and

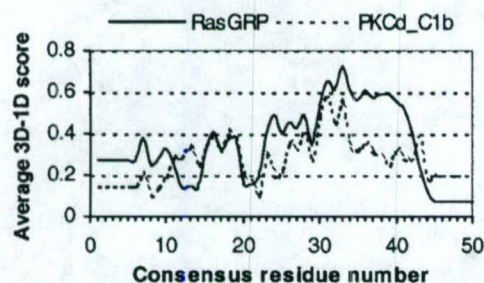


Figure 2. Plots obtained by the Verify3D program with a window of 10 residues using the coordinates of C1-RasGRP and the template protein (C1b-PKC δ , PDB 1PTR), respectively.

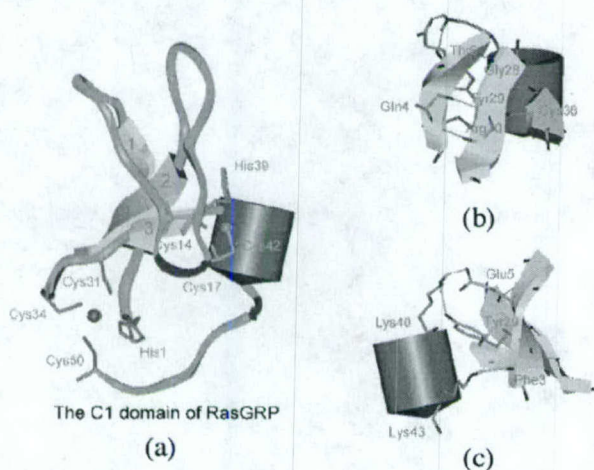


Figure 3. Structural model of C1-RasGRP. (a) Schematic drawing of the model. The β -strands, α -helix, turn, and coils are shown as the yellow arrow, red cylinder, blue ribbon, and green ribbon, respectively. Two Zn^{2+} ions and their coordinating residues are displayed as ball-and-stick models, respectively. (b) View is rotated 270° along the Y axis of panel a. Five hydrogen bonds are formed within the β -sheet. (c) View is rotated 180° along the Y axis of panel a and then -25° along the X axis. Three hydrogen bonds are formed between the α -helix and the β -sheet.

of a C-terminal α -helix proximate to the β -sheet. The domain scaffold is maintained by these three β -strands packed against the α -helix together with two independent zinc ions coordinated by two pairs of 3Cys–1His Zn^{2+} coordinating clusters (Figure 3).

Docking Studies. The docking test showed that the Autodock program could reproduce the binding of phorbol 13-acetate to C1b-PKC δ because the rms value is only 0.77 Å when the lowest energy docked structure was superimposed with the crystal structure. The hydrogen bond network predicted by the Autodock program is virtually identical to that found in the crystal structure. This docking test provides validation for using this program to perform docking studies of ligands to C1-RasGRP.

ILV exists in solution in two different conformations.³⁰ Both experimental evidence and molecular modeling studies have revealed that ILV adopts the *cis*-twist conformation when it binds to C1b-PKC δ .^{15,30,31} Similarly, the benzolactam, whose eight-membered ring forces the amide bond to be in the *cis* configuration, adopts a *cis*-twist conformation in order to bind to C1b-

PKC δ .¹⁵ Therefore, the *cis*-twist conformation was used for docking of these ligands to C1-RasGRP.

In the current modeling studies, we focused on the interaction between the ligands and C1-RasGRP and did not take into account the lipid interactions. For this reason, the hydrophobic side chains of both 7-*n*-octyl-ILV and benzolactam were truncated to four carbon atoms to expedite the docking studies.

Analysis of the Complex Models. (a) Ligand-Binding Pocket. The two loops A and B comprising residues 8–12 and 21–27 make up the ligand-binding pocket (Figures 1, 4, and 6). This binding pocket has some positive charge character. In the complex models, the three ligands phorbol 13-acetate, ILV, and benzolactam interact with loops A and B of RasGRP through complementary hydrogen bonds. All three ligands form hydrogen bonds with residues Thr12 and Leu21.

(b) Conformational Changes of the Binding Pocket upon Ligand Binding. To investigate the effect of ligand binding on the binding pocket conformation, the rmsd's have been calculated from the trajectories of a 100 ps MD production run for loops A and B (Table 2). Table 2 shows that upon ligand binding the rmsd values of loops A and B are reduced 3 and 4 times, respectively. This suggests that the binding pocket formed between loops A and B becomes less flexible upon ligand binding.

The distances between the α -carbons were also calculated for five pairs of residues on loops A and B (Table 3). Table 3 shows that the middle portion of the binding pocket opens up by ~ 0.5 Å upon ligand binding (C α ,Lys10–C α ,Val24 and C α ,Pro11–C α ,Gly23). This induced conformational change in the binding pocket upon ligand binding is consistent with the reported X-ray crystallography study, which showed that the binding of phorbol 13-acetate leads to an opening of 0.4 Å between the main chains of Pro11 and Gly23 in C1b-PKC δ .¹⁴

(c) Hydrogen Bonds Maintaining the Binding Pocket Conformation. We found that the conformation of the binding pocket is maintained by the presence of six hydrogen bonds formed between loops A and B (Figure 5 and Table 4). For uncomplexed C1-RasGRP, only two of these hydrogen bonds between loops A and B exhibit more than 90% occupancy over a 30 ps average lifetime; one is formed by the amide H atom of Leu21 and the carbonyl O atom of Thr12, and the other occurs between the side chain's carbonyl O atom of Gln27 and the amide H atom of Tyr8. Upon ligand binding, in addition to these two stable hydrogen bonds, another stable hydrogen bond appears between the side chain's amide H atom of Gln27 and the carbonyl O atom of Tyr8 (occupancy, 100%; average lifetime, 50 ps; energy, -2.93 ± 0.26 kcal/mol). These more stable hydrogen bonds are located at the two ends of the binding pocket. In contrast, the hydrogen bonds existing at the middle of the binding pocket become less stable, or disappear, upon ligand binding (occupancy, less than 10%; average lifetime, less than 1 ps), thus resulting in the ~ 0.5 Å opening in the middle portion of the binding pocket upon ligand binding.

Hydrogen Bonding Interactions between Ligands and C1-RasGRP. All hydrogen bonding interactions between C1-RasGRP and the ligands were

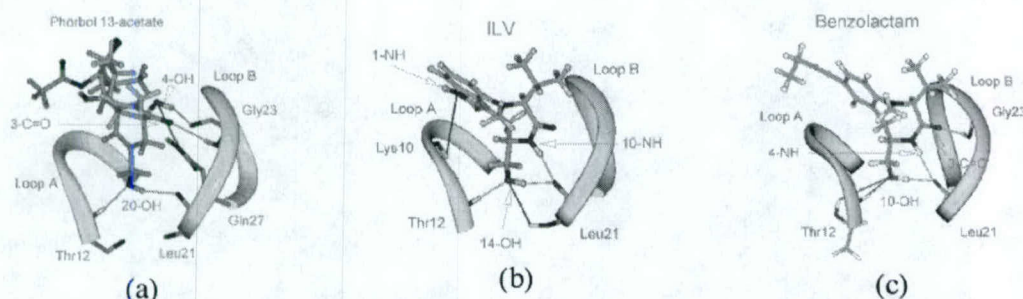


Figure 4. Hydrogen bond interactions between the ligands and C1-RasGRP. (a) The phorbol 13-acetate–C1-RasGRP complex. View is rotated 30° along the *X* axis of Figure 3a. (b) The ILV–C1-RasGRP complex. View is rotated –10° along the *Y* axis of panel a. (c) The benzolactam–C1-RasGRP complex. View is rotated –15° along the *Y* axis of panel a. During the MD simulations, the O atom of benzolactam's 4-OH group forms a hydrogen bond, alternatively, with the amide H atom (light blue) and the side chain's hydroxyl O atom (orange) of Thr12.

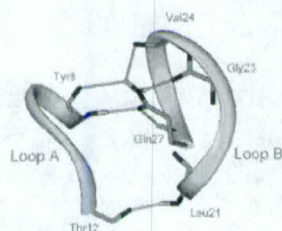


Figure 5. Hydrogen bonds formed between two binding pocket-forming loops A and B. View is rotated –15° along the *X* axis of Figure 3a.

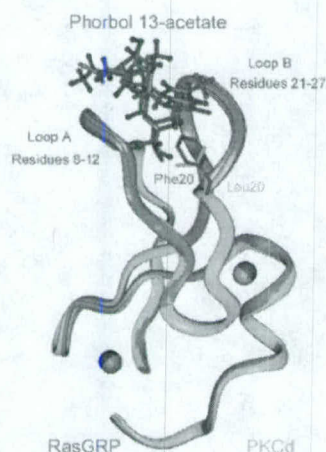


Figure 6. Structural model of C1-RasGRP in complex with phorbol 13-acetate superimposed with C1b-PKCδ in complex with phorbol 13-acetate (PDB 1PTR). The view is the same as the view in Figure 3a. The binding pocket-forming loops A and B are pink and blue, respectively, for the C1-RasGRP and C1b-PKCδ. The ligand's location within C1-RasGRP is different from that within C1b-PKCδ.

analyzed on the basis of the MD trajectories of the complex models (Figure 4, Table 5).

(a) ILV–RasGRP Complex. Three residues in C1-RasGRP form five hydrogen bonds with ILV. Leu21 forms three hydrogen bonds with ILV: the first between its amide group and the hydroxyl group at position 14 in ILV, the second between its carbonyl group and the amide group in ILV, and the third hydrogen bond between its carbonyl group and the hydroxyl group at position 14. Lys10 forms one hydrogen bond through its backbone with the amino group at position 1 in ILV. Thr12 also forms one hydrogen bond through its backbone amide with the hydroxyl group at position 14 in

Table 2. Root-Mean-Square Deviation (Å) of Two Binding Pocket-Forming Loops

	loop A (residues 8–12)		loop B (residues 21–27)	
	RasGRP	complex ^a	RasGRP	complex ^a
amino acids	0.5577	0.2267	0.8874	0.2216
backbone	0.3191	0.1356	0.5998	0.1443
side chain	0.5848	0.2003	0.9010	0.2116

^a In complex with phorbol 13-acetate.

Table 3. Distance (Å) between Two Binding Pocket-Forming Loops of C1-RasGRP

	RasGRP	complex ^a
Ca,Tyr8–Ca,Lys26	7.07 ± 0.16	6.97 ± 0.11
Ca,Leu9–Ca,Ile25	9.16 ± 0.16	9.02 ± 0.11
Ca,Lys10–Ca,Val24	9.52 ± 0.14	10.12 ± 0.13
Ca,Pro11–Ca,Gly23	10.26 ± 0.12	10.73 ± 0.12
Ca,Thr12–Ca,Trp22	9.11 ± 0.10	9.04 ± 0.13

^a In complex with phorbol 13-acetate.

ILV. On the basis of the occupancy, average lifetime, and hydrogen bond energy estimated for each of these five hydrogen bonds (Table 5), two hydrogen bonds are very stable and have the strongest hydrogen bond energies (O₁₄–OH...HN_{Thr12} and H₁₄–OH...O_{Leu21}).

(b) Benzolactam–RasGRP Complex. Thr12, Leu21, and Gly23 in C1-RasGRP form hydrogen bonds with the benzolactam (Figure 4, Table 5). Thr12 forms two hydrogen bonds through its backbone amide and its side chain hydroxyl groups with the hydroxyl O atom at position 10 in benzolactam. Leu21 forms two hydrogen bonds through its backbone carbonyl group with the hydroxyl H atom at position 10 and the amide H atom at position 4 in the ligand. Gly23 forms one hydrogen bond through its amide group with the carbonyl group at position 3. The two hydrogen bonds formed between Leu21 and the ligand (H₁₀–OH...O_{Leu21} and H₄–NH...O_{Leu21}) were found to be the most stable and have the highest hydrogen bond energies (Table 5).

Comparison of Ligand–Hydrogen Bond Interactions to C1-RasGRP and C1b-PKCδ. To gain further insight into ligands binding to C1-RasGRP, we compared the predicted binding model of phorbol 13-acetate in complex with C1-RasGRP and the X-ray structure of the same ligand with C1b-PKCδ. It was found that these two protein structures are virtually superimposed with an rmsd value of 0.16 Å for the backbone α-carbon atoms. The major difference is residue 20. C1b-PKCδ has a Leu residue at this position,

Table 4. Hydrogen Bonds Maintaining the Binding Pocket Conformation

hydrogen bond	occupancy (%)		average lifetime (ps)		HB parameter and energy			
	a	b	a	b	r_{DA} (Å)	θ_{D-H-A} (deg)	θ_{H-A-AA} (deg)	E_{HB} (kcal/mol)
RasGRP								
HN _{Leu21} ...O _{Thr12}	100	100	100.00	100.00	2.84 ± 0.07	157.7 ± 10.2	146.9 ± 9.4	-3.45 ± 0.07
HE22 _{Gln27} ...O _{Gly23}	23	23	2.67	2.30	2.83 ± 0.14	108.3 ± 13.9	129.6 ± 7.4	-3.33 ± 0.27
OE1 _{Gln27} ...HN _{Gln27}	72	70	2.50	3.50	3.00 ± 0.14	124.8 ± 8.1	120.5 ± 5.3	-3.39 ± 0.14
OE1 _{Gln27} ...HN _{Tyr8}	99.5	100	49.75	100.00	2.98 ± 0.15	149.0 ± 11.3	128.9 ± 9.2	-3.40 ± 0.15
HE21 _{Gln27} ...O _{Val24}	14	17	1.17	1.42	3.89 ± 0.24	40.5 ± 11.6	77.4 ± 6.0	-2.03 ± 0.42
HE21 _{Gln27} ...O _{Tyr8}	35	36	1.50	1.56	3.85 ± 0.21	39.0 ± 7.6	107.7 ± 5.8	-2.10 ± 0.36
Complex^c								
HN _{Leu21} ...O _{Thr12}	98.5	98	32.83	32.67	2.98 ± 0.10	152.2 ± 14.4	150.2 ± 10.6	-3.44 ± 0.08
HE22 _{Gln27} ...O _{Gly23}	11	9	1.00	1.12	3.51 ± 0.18	111.4 ± 7.8	117.4 ± 5.3	-2.68 ± 0.31
OE1 _{Gln27} ...HN _{Gln27}	85	85	4.39	6.07	2.82 ± 0.11	133.0 ± 12.7	111.7 ± 5.5	-3.37 ± 0.18
OE1 _{Gln27} ...HN _{Tyr8}	100	100	100.00	100.00	3.30 ± 0.16	154.3 ± 8.4	92.8 ± 6.1	-3.02 ± 0.25
HE21 _{Gln27} ...O _{Val24}	0.0	2	0.00	1.00	3.39 ± 0.24	45.2 ± 5.97	82.8 ± 4.5	-2.88 ± 0.32
HE21 _{Gln27} ...O _{Tyr8}	99.5	100	49.75	100.00	3.35 ± 0.16	49.5 ± 6.3	124.7 ± 6.6	-2.93 ± 0.26

^a Time cutoff 0.5 ps, resolution 0.5 ps. ^b Time cutoff 0.5 ps, resolution 1.0 ps. ^c In complex with phorbol 13-acetate.

Table 5. Hydrogen Bond Interactions between C1-RasGRP and the Ligands

hydrogen bond atom _{ligand} ...atom _{residue}	occupancy (%)		average lifetime (ps)		hydrogen bond parameter and energy			
	a	b	a	b	r_{DA} (Å)	θ_{D-H-A} (deg)	θ_{H-A-AA} (deg)	E_{HB} (kcal/mol)
ILV								
H _{10-NH} ...O _{Leu21}	9.50	11.00	1.00	1.00	3.88 ± 0.26	123.7 ± 9.3	139.1 ± 7.6	-2.06 ± 0.26
N _{1-NH} ...HN _{Lys10}	50.00	52.00	1.73	2.60	3.04 ± 0.12	119.1 ± 10.6	94.4 ± 5.5	-2.94 ± 0.08
O _{14-OH} ...HN _{Thr12}	99.00	98.00	49.25	49.00	2.97 ± 0.13	149.1 ± 12.5	116.2 ± 11.0	-3.42 ± 0.11
O _{14-OH} ...HN _{Leu21}	28.00	28.00	1.35	1.56	3.76 ± 0.14	127.6 ± 9.6	147.9 ± 5.7	-2.25 ± 0.22
H _{14-OH} ...O _{Leu21}	98.00	98.00	19.60	32.67	2.84 ± 0.12	141.4 ± 9.9	121.0 ± 6.9	-4.13 ± 0.14
							total	-14.8
Benzolactam								
O _{3-C=O} ...HN _{Gly23}	52.00	55.00	2.25	2.62	2.78 ± 0.11	120.8 ± 11.7	123.9 ± 8.3	-3.32 ± 0.20
O _{10-OH} ...HN _{Thr12}	59.50	61.00	1.88	2.54	2.77 ± 0.10	124.2 ± 13.3	145.6 ± 6.9	-3.32 ± 0.21
O _{10-OH} ...HG _{1Thr12}	67.50	71.00	2.40	4.18	3.66 ± 0.13	132.8 ± 6.7	88.1 ± 4.7	-2.54 ± 0.24
H _{10-OH} ...O _{Leu21}	100.00	100.00	100.00	100.00	2.84 ± 0.12	141.4 ± 9.9	121.0 ± 6.9	-4.13 ± 0.14
H _{4-NH} ...O _{Leu21}	99.50	100.00	49.75	100.00	2.96 ± 0.11	154.6 ± 11.3	150.9 ± 9.4	-3.44 ± 0.08
							total	-16.75

^a Time cutoff 0.5 ps, resolution 0.5 ps. ^b Time cutoff 0.5 ps, resolution 1.0 ps.

while C1-RasGRP has a Phe residue. For the ligand, its position is shifted up by 0.7 Å from the bottom of the binding pocket in the complex with C1-RasGRP versus PKC δ because of the residue difference at position 20 (Figure 6).

For phorbol 13-acetate,¹⁴ four common, strong hydrogen bonds are formed with C1b-PKC δ and C1-RasGRP (in light blue in Figure 4a). One difference in the hydrogen bonding network is that there is a weak hydrogen bond formed between the hydroxyl group at position 20 and the carbonyl group of Thr12 in the X-ray structure, while this hydrogen bond is replaced by another weak hydrogen bond between the hydroxyl group at position 4 in the ligand and the side chain's amide of Gln27 in the predicted RasGRP-phorbol 13 acetate complex (in orange in Figure 4a).

For ILV,¹⁵ three common hydrogen bonds are found with C1-RasGRP and C1b-PKC δ (light blue in Figure 4b). Interestingly, the hydrogen bond between the carbonyl group at position 11 and the amide group of Gly23 in the ILV/PKC δ complex was replaced by two hydrogen bonds in the predicted ILV-RasGRP complex; one occurs between the hydroxyl group at position 14 of the ligand and the amide group of Leu21, and the other is formed by the amino group at position 1 and the amide group of Lys10 (in orange in Figure 4b).

For benzolactam, four common hydrogen bonds are found with both C1b-PKC δ and C1-RasGRP residues Thr12, Leu21, and Gly23.¹⁵ However, a minor difference

is observed in the hydrogen bonding interactions with Thr12. In the C1b-PKC δ complex, the hydroxyl group at position 10 of the ligand forms only one hydrogen bond with the backbone amide of Thr12. In the RasGRP complex this hydroxyl group forms two alternating hydrogen bonds during the MD simulations, one with the amide H atom of Thr12 and the other with side chain's hydroxyl H atom of Thr12 (in orange in Figure 4c).

The differences in the ligand-hydrogen bond interactions with C1b-PKC δ and C1-RasGRP may stem from differences in the residue at position 20, since this specific residue is located at the edge of the binding pocket while all the other dissimilar residues at positions 8, 9, 24, 25, and 26 are directed outside the binding pocket. Since Phe is slightly larger than Leu in their side chains, Phe20 in C1-RasGRP may cause the ligand to shift upward slightly in order to avoid steric contacts, thus leading to a weakening of hydrogen bonding interactions at the Thr12/Leu21 end of the binding pocket. It should be noted, however, that the mutation of C1b-PKC δ at position 20 from Leu to Phe had little effect on the binding affinity of PDBu.¹⁵

Summary

Binding assays were performed to assess the affinities of several PKC activators for C1-RasGRP. The two benzolactam analogues studied were found to bind to C1-RasGRP in the nanomolar range. ILV and its *n*-octyl

derivative show the best affinities. All four ligands show generally similar affinities for C1-RasGRP and for C1b-PKC δ , although some selectivity is apparent.

Our molecular modeling studies reveal that the interactions of C1-RasGRP with phorbol 13-acetate, benzolactam, and ILV share a common structural feature; i.e., their hydroxymethyl-bearing rings are all inserted in a complementary fashion into the binding pocket formed by loops A and B comprising residues 8–12 and 21–27. In particular, the hydroxymethyl group of phorbol 13-acetate, benzolactam, and ILV plays a pivotal role in C1-RasGRP binding. This group contacts the bottom of the binding pocket, forming hydrogen bonds with Thr12 and Leu21. Some differences do, however, exist among the interactions of these ligands with C1-RasGRP.

The molecular modeling studies also show that the similar 3D structures of C1-RasGRP and C1b-PKC δ result in their common mode of interaction with various ligands, but the difference at residue 20 between these two domains is likely responsible for the lesser depth of penetration of ligands into the binding pocket of C1-RasGRP in comparison to C1b-PKC δ .

Taken together, our ligand binding experiments and molecular modeling studies further our understanding of the structural basis of the binding of PKC activators to the C1 domain of RasGRP. The studies provide a basis for exploring how other types of PKC ligands bind to C1-RasGRP, and such information may be useful for the design of RasGRP-selective ligands. The recent demonstration that RasGRP plays an early and obligatory role in T cell activation highlights the potential utility of such ligands.³²

Acknowledgment. This work was supported by NIH Grant CA79601 and the Department of Defense Grant DMAD 17-93-V-3018.

References

- (1) (a) Ebinu, J. O.; Bottorff, D. A.; Chan, E. Y.; Stang, S. L.; Dunn, R. J.; Stone, J. C. RasGRP, a Ras guanyl nucleotide-releasing protein with calcium- and diacylglycerol-binding motifs. *Science* **1998**, *280*, 1082–1086. (b) Tognon, C. E.; Kirk, H. E.; Passmore, L. A.; Whitehead, I. P.; Der, C. J.; Kay, R. J. Regulation of RasGRP via a phorbol ester-responsive C1 domain. *Mol. Cell Biol.* **1998**, *18*, 6995–7008.
- (2) Macara, I. G.; Lounsbury, K. M.; Richards, S. A.; McKiernan, C.; Bar-Sagi, D. The Ras superfamily of GTPases. *FASEB J.* **1996**, *10*, 625–630.
- (3) Downward, J. Control of Ras activation. *Cancer Surv.* **1996**, *27*, 87–100.
- (4) (a) Morrison, D. K.; Cutler, R. E. The complexity of Raf-1 regulation. *Curr. Opin. Cell Biol.* **1997**, *9*, 174–179. (b) Robinson, M. J.; Cobb, M. H. Mitogen-activated protein kinase pathways. *Curr. Opin. Cell Biol.* **1997**, *9*, 180–186. (c) Treisman, R. Regulation of transcription by MAP kinase cascades. *Curr. Opin. Cell Biol.* **1996**, *8*, 205–215. (d) Rodriguez-Viciana, P.; Warne, P. H.; Khwaja, A.; Marte, B. M.; Pappin, D.; Das, P.; Waterfield, M. D.; Ridley, A.; Downward, J. Role of phosphatidylinositol 3-OH kinase in cell transformation and control of the actin cytoskeleton by Ras. *Cell* **1997**, *89*, 457–467. (e) Feig, L. A.; Urano, T.; Cantor, S. Evidence for a Ras/Ral signaling cascade. *Trends Biochem. Sci.* **1996**, *21*, 438–441.
- (5) (a) Bokoch, G. M.; Der, C. J. Emerging concepts in the Ras superfamily of GTP-binding proteins. *FASEB J.* **1993**, *7*, 750–759. (b) Graham, S. M.; Vojtek, A. B.; Huff, S. Y.; Cox, A. D.; Clark, G. J.; Cooper, J. A.; Der, C. J. TC21 causes transformation by Raf-independent signaling pathways. *Mol. Cell Biol.* **1996**, *16*, 6132–6140.
- (6) Ron, D.; Kazanietz, M. G. New insights into the regulation of protein kinase C and novel phorbol ester receptors. *FASEB J.* **1999**, *13*, 1658–1676.
- (7) Hurley, J. H.; Newton, A. C.; Parker, P. J.; Blumberg, P. M.; Nishizuka, Y. Taxonomy and function of C1 protein kinase C homology domains. *Protein Sci.* **1997**, *6*, 477–480.
- (8) (a) Nishizuka, Y. Intracellular signaling by hydrolysis of phospholipids and activation of protein kinase C. *Science* **1992**, *258*, 607–614. (b) Newton, A. C. Regulation of protein kinase C. *Curr. Opin. Cell Biol.* **1997**, *9*, 161–167.
- (9) (a) Hall, C.; Monfries, C.; Smith, P. Lim, H. H.; Kozma, R.; Ahmed, S.; Vanniasingham, V.; Leung, T.; Lim, L. Novel human brain cDNA encoding a 34,000 Mr protein n-chimaerin, related to both the regulatory domain of protein kinase C and BCR, the product of the breakpoint cluster region gene. *J. Mol. Biol.* **1990**, *211*, 11–16. (b) Hall, C.; Sin, W. C.; Teo, M.; Michael, G. J.; Smith, P.; Dong, J. M.; Lim, H. H.; Manser, E.; Spurr, N. K.; Jones, T. A. Alpha 2-chimerin, an SH2-containing GTPase-activating protein for the ras-related protein p21rac derived by alternate splicing of the human n-chimerin gene, is selectively expressed in brain regions and testes. *Mol. Cell Biol.* **1993**, *13*, 4986–4998. (c) Leung, T.; How, B.-E.; Manser, E.; Lim, L. Germ cell beta-chimaerin, a new GTPase-activating protein for p21rac, is specifically expressed during the acrosomal assembly stage in rat testis. *J. Biol. Chem.* **1993**, *268*, 3813–3816. (d) Leung, T.; How, B.-E.; Manser, E.; Lim, L. Cerebellar beta 2-chimaerin, a GTPase-activating protein for p21 ras-related rac is specifically expressed in granule cells and has a unique N-terminal SH2 domain. *J. Biol. Chem.* **1994**, *269*, 12888–12892. (e) Areces, L. B.; Kazanietz, M. G.; Blumberg, P. M. Close similarity of baculovirus-expressed n-chimaerin and protein kinase C alpha as phorbol ester receptors. *J. Biol. Chem.* **1994**, *269*, 19553–19558. (f) Caloca, M. J.; Fernandez, N.; Lewin, N. E.; Ching, D.; Modali, R.; Blumberg, P. M.; Kazanietz, M. G. 2-Chimaerin Is a High Affinity Receptor for the Phorbol Ester Tumor Promoters. *J. Biol. Chem.* **1997**, *272*, 26488–26496.
- (10) (a) Maruyama, I. N.; Brenner, S. A phorbol ester/diacylglycerol-binding protein encoded by the unc-13 gene of *Caenorhabditis elegans*. *Proc. Natl. Acad. Sci. U.S.A.* **1991**, *88*, 5729–5733. (b) Kazanietz, M. G.; Lewin, N. E.; Bruns, J. D.; Blumberg, P. M. Characterization of the Cysteine-Rich Region of the *Caenorhabditis elegans* Protein Unc-13 as a High Affinity Phorbol Ester Receptor. *J. Biol. Chem.* **1995**, *270*, 10777–10783.
- (11) (a) Cai, H.; Smola, U.; Wixler, V.; Eisenmann-Tappe, I.; Diaz-Meco, M. T.; Moscat, J.; Rapp, U.; Cooper, G. M. Role of diacylglycerol-regulated protein kinase C isotypes in growth factor activation of the Raf-1 protein kinase. *Mol. Cell Biol.* **1997**, *17*, 732–741. (b) Marquardt, B.; Frith, D.; Stabel, S. Signaling from TPA to MAP kinase requires protein-kinase-C, RAF and MEK-reconstitution of the signaling pathway in vitro. *Oncogene* **1994**, *9*, 3213–3218. (c) Schönwasser, D. C.; Marais, R. M.; Marshall, C. J.; Parker, P. J. Activation of the mitogen-activated protein kinase/extracellular signal-regulated kinase pathway by conventional, novel, and atypical protein kinase C isotypes. *Mol. Cell Biol.* **1998**, *18*, 790–798. (d) El-Shermely, M. Y.; Besser, D.; Nagasawa, M.; Nagamine, Y. 12-*O*-Tetradecanoylphorbol-13-acetate activates the Ras/extracellular signal-regulated kinase (ERK) signaling pathway upstream of SOS involving serine phosphorylation of Shc in NIH3T3 cells. *J. Biol. Chem.* **1997**, *272*, 30599–30602. (e) Lorenzo, P. S.; Kung, J. W.; Bottorff, D. A.; Garfield, S. H.; Stone, J. C.; Blumberg, P. M. Phorbol esters modulate the Ras exchange factor RasGRP3. *Cancer Res.* **2001**, *61*, 943–949.
- (12) Marais, R.; Light, Y.; Maison, C.; Paterson, H.; Olson, M. F.; Marshall, C. J. Requirements of Ras-GTP-Raf complexes for activation of Raf-1 by protein kinase C. *Science* **1998**, *280*, 109–112.
- (13) Lorenzo, P. S.; Beheshti, M.; Pettit, G. R.; Stone, J. C.; Blumberg, P. M. The Guanine Nucleotide Exchange Factor RasGRP Is a High-Affinity Target for Diacylglycerol and Phorbol Esters. *Mol. Pharmacol.* **2000**, *57*, 840–846.
- (14) Zhang, G.; Kazanietz, M. G.; Blumberg, P. M.; Hurley, J. H. Crystal structure of the cys2 activator-binding domain of protein kinase C in complex with phorbol ester. *Cell* **1995**, *81*, 917–924.
- (15) (a) Hommel, U.; Zurini, M. Solution Structure of a Cysteine Rich Domain of Rat Protein Kinase C. *Nature Struct. Biol.* **1994**, *1*, 383–387. (b) Ichikawa, S.; Hatanaka, H.; Takeuchi, Y.; Ohno, S.; Inagaki, F. Solution Structure of Cysteine-Rich Domain of Protein Kinase C. *J. Biochem.* **1995**, *117*, 566–574. (c) Wang, S.; Liu, M.; Lewin, N. E.; Lorenzo, P. S.; Bhattacharya, D.; Qiao, L.; Kozikowski, A. P.; Blumberg, P. M. Probing the binding of indolactam-V to protein kinase C through site-directed mutagenesis and computational docking simulations. *J. Med. Chem.* **1999**, *42*, 3436–3446. (d) Kozikowski, A. P.; Wang, S.; Ma, D.; Yao, J.; Ahmad, S.; Glazer, R. I.; Bogi, K.; Acs, P.; Modarres, S.; Lewin, N. E.; Blumberg, P. M. Modeling, chemistry, and biology of the benzolactam analogues of indolactam V (ILV). 2. Identification of the binding site of the benzolactams in the CRD2 activator-binding domain of PKC δ and discovery of an ILV analogue of improved isozyme selectivity. *J. Med. Chem.* **1997**, *40*, 1316–1326. (e) Caloca, M. J.; Garcia-Bermejo, M. L.; Blumberg, P. M.; Lewin, N. E.; Kremmer, E.; Mischak, H.; Wang, S.; Nacro, K.; Bienfait, B.; Marquez, V. E.; Kazanietz, M. G. Beta2-chimaerin is a novel target for diacylglycerol: binding properties

- and changes in subcellular localization mediated by ligand binding to its C1 domain. *Proc. Natl. Acad. Sci. U.S.A.* **1999**, *96*, 11854–11859. (f) Wang, S.; Kazanietz, M. G.; Blumberg, P. M.; Marquez, V. E.; Milne, G. W. Molecular modeling and site-directed mutagenesis studies of a phorbol ester-binding site in protein kinase C. *J. Med. Chem.* **1996**, *39*, 2541–2553. (g) Wang, Q. J.; Fang, T. W.; Nacro, K.; Marquez, V. E.; Wang, S.; Blumberg, P. M. Role of hydrophobic residues in the C1b domain of protein kinase C delta on ligand and phospholipid interactions. *J. Biol. Chem.* **2001**, *276*, 19580–19587.
- (16) Kazanietz, M. G.; Wang, S.; Milne, G. W.; Lewin, N. E.; Liu, H. L.; Blumberg, P. M. Residues in the second cysteine-rich region of protein kinase C delta relevant to phorbol ester binding as revealed by site-directed mutagenesis. *J. Biol. Chem.* **1995**, *270*, 21852–21859.
- (17) Sharkey, N. E.; Blumberg, P. M. Highly lipophilic phorbol esters as inhibitors of specific [³H]phorbol 12,13-dibutyrate binding. *Cancer Res.* **1985**, *45*, 19–24.
- (18) Ma, D.; Zhang, T.; Wang, G.; Kozikowski, A. P.; Lewin, N. E.; Blumberg, P. M. Synthesis of 7,8-disubstituted benzolactam-V8 and its binding to protein kinase C. *Bioorg. Med. Chem. Lett.* **2001**, *11*, 99–101.
- (19) Berman, H. M.; Westbrook, J.; Feng, Z.; Gilliland, G.; Bhat, T. N.; Weissig, H.; Shindyalov, I. N.; Bourne, P. E. The Protein Data Bank. *Nucleic Acids Res.* **2000**, *28*, 235–242.
- (20) (a) Sonnhammer, E. L.; Eddy, S. R.; Durbin, R. Pfam: a comprehensive database of protein domain families based on seed alignments. *Proteins* **1997**, *28*, 405–420. (b) Bateman, A.; Birney, E.; Durbin, R.; Eddy, S. R.; Howe, K. L.; Sonnhammer, E. L. The Pfam Protein Families Database. *Nucleic Acids Res.* **2000**, *28*, 263–266.
- (21) Brooks, B. R.; Brucoleri, R. E.; Olafson, B. D.; States, D. J.; Swaminathan, S.; Karplus, M. CHARMM: A program for macromolecular energy, minimization, and dynamics calculations. *J. Comput. Chem.* **1983**, *4*, 187–217.
- (22) (a) MacKerell, A. D.; Wiorkiewicz-Kuczera, J. J.; Karplus, M. An all-atom empirical energy function for the simulation of nucleic acids. *J. Am. Chem. Soc.* **1995**, *117*, 11946–11975. (b) MacKerell, A. D.; Bashford, J. D.; Bellott, M.; Dunbrack, R. L., Jr.; Evanseck, J. D.; Field, M. J.; Fischer, S.; Gao, J.; Guo, H.; Ha, S.; Joseph-McCarthy, D.; Kuchnir, L.; Kuczera, K.; Lau, F. T. K.; Mattos, C.; Michnick, S.; Ngo, T.; Nguyen, D. T.; Prodhom, B.; Reiher, W. E.; Roux, B.; Schlenkrich, M.; Smith, J. C.; Stote, R.; Straub, J.; Watanabe, M.; Wiorkiewicz-Kuczera, J.; Yin, D.; Karplus, M. All-atom empirical potential for molecular modeling and dynamics studies of proteins. *J. Phys. Chem.* **1998**, *102*, 3586–3616.
- (23) Jorgensen, W. L.; Chandrasekhar, J.; Madura, J. D.; Impey, R. W.; Klein, M. L. Comparison of simple potential functions for simulating liquid water. *J. Chem. Phys.* **1983**, *79*, 926–935.
- (24) Luthy, R.; Bowie, J. U.; Eisenberg, D. Assessment of protein models with three-dimensional profiles. *Nature* **1992**, *356*, 83–85.
- (25) Rodriguez, R.; Chinea, G.; Lopez, N.; Pons, T.; Vriend, G. Homology modeling, model and software evaluation: three related resources. *Bioinformatics* **1998**, *14*, 523–528.
- (26) Morris, G. M.; Goodsell, D. S.; Halliday, R. S.; Huey, R.; Hart, W. E.; Belew, R. K.; Olson, A. J. Automated Docking Using a Lamarckian Genetic Algorithm and Empirical Binding Free Energy Function. *J. Comput. Chem.* **1998**, *19*, 1639–1662.
- (27) Steinbach, P. J.; Brooks, B. R. New spherical-cutoff methods for long-range forces in macromolecular simulation. *J. Comput. Chem.* **1994**, *15*, 667–683.
- (28) Ryckaert, J. P.; Ciccotti, G.; Berendsen, H. J. C. Numerical integration of the Cartesian equations of motion of a system with constraints: MD of *n*-alkanes. *J. Comput. Phys.* **1977**, *23*, 327–341.
- (29) (a) Chothia, C.; Lesk, A. M. The relation between the divergence of sequence and structure in proteins. *EMBO J.* **1986**, *5*, 823–826. (b) Sánchez, R.; Sali, A. Advances in comparative protein-structure modeling. *Curr. Opin. Struct. Biol.* **1997**, *7*, 206–214. (c) Tramontano, A. Homology modeling with low sequence identity. *Methods* **1998**, *14*, 293–300.
- (30) Endo, Y.; Hasegawa, M.; Itai, A.; Shudo, K.; Tori, M.; Asakawa, Y.; Sakai, S. Tumor promoters in two conformational states in solution. Stereochemistry of (±)-Indolactam-V. *Tetrahedron Lett.* **1985**, *26*, 1069–1072.
- (31) Kozikowski, A. P.; Ma, D.; Pang, Y.-P.; Shum, P.; Likic, V.; Mishra, P. K.; Macura, S.; Basu, A.; Lazo, J. S.; Ball, R. G. Synthesis, molecular modeling, 2-D-NMR, and biological evaluation of ILV mimics as potential modulators of protein kinase C. *J. Am. Chem. Soc.* **1993**, *115*, 3957–3965.
- (32) (a) Ebinu, J. O.; Stang, S. L.; Teixeira, C.; Bittorff, D. A.; Hooton, J.; Blumberg, P. M.; Barry, M.; Bleakley, R. C.; Ostergaard, H. L.; Stone, J. C. RasGRP links T-cell receptor signaling to Ras. *Blood* **2000**, *95*, 3199–3203. (b) Dower, N. A.; Stang, S. L.; Bittorff, D. A.; Ebinu, J. O.; Dickie, P.; Ostergaard, H. L.; Stone, J. C. RasGRP is essential for mouse thymocyte differentiation and TCR signaling. *Nat. Immunol.* **2000**, *1*, 317–321.

JM010422Z

- female relatives in successive generations. *Neurology* 1988;38:207-212.
44. van Duijn CM, Farrer LA, Cupples LA, Hofman A. Genetic transmission of Alzheimer's disease among families in a Dutch population based study. *J Med Genet* 1993;30:640-646.
45. Korten AE, Jorm AF, Henderson AS, Broe GA, Creasey H, McCusker E. Assessing the risk of Alzheimer's disease in first-degree relatives of Alzheimer's disease cases. *Psychol Med* 1993;23:915-923.
46. Lautenschlager NT, Cupples LA, Rao VS, et al. Risk of dementia among relatives of Alzheimer's disease patients in the MIRAGE study: what's in store for the "oldest old"? *Neurology* 1996;46:641-650.
47. Payami H, Zarepari S, Montee KR, et al. Gender difference in apolipoprotein E-associated risk for familial Alzheimer's disease: a possible clue to the higher incidence of Alzheimer's disease in women. *Am J Hum Genet* 1996;58:803-811.
48. Duara R, Barker WW, Lopez-Alberola R, et al. Alzheimer's disease: interaction of apolipoprotein E genotype, family history of dementia, gender, education, ethnicity and age of onset. *Neurology* 1996;46:1575-1579.
49. Henderson VW, Paganini-Hill A, Emanuel CK, et al. Estrogen replacement therapy in older women: comparisons between Alzheimer's disease cases and nondemented control subjects. *Arch Neurol* 1994;51:896-900.
50. Tang MX, Jacobs D, Stern Y, et al. Effect of estrogen during menopause on risk and age at onset of Alzheimer's disease. *Lancet* 1996;348:429-432.
51. Brenner DE, Kukull WA, Stergachis A, et al. Postmenopausal estrogen replacement therapy and the risk of Alzheimer's disease: a population-based case-control study. *Am J Epidemiol* 1994;140:262-267.
52. Kawas C, Resnick S, Morrison A, et al. A prospective study of estrogen replacement therapy and the risk of developing Alzheimer's disease: the Baltimore Longitudinal Study of Aging. *Neurology* 1997;48:1517-1521.
53. Jarvik GP, Wijsman EM, Kukull WA, Schellenberg GD, Yu C, Larson EB. Interactions of apolipoprotein E genotype, total cholesterol level, age, and sex in prediction of Alzheimer's disease: a case control study. *Neurology* 1995;45:1092-1096.
54. Reilly SL, Ferrell RE, Sing CF. The gender-specific apolipoprotein E genotype influence on the distribution of plasma lipids and apolipoproteins in the population of Rochester, MN. III. Correlations and covariances. *Am J Hum Genet* 1994;55:1001-1018.

Randomized pilot study of nimesulide treatment in Alzheimer's disease

P.S. Aisen, MD; J. Schmeidler, PhD; and G.M. Pasinetti, MD, PhD

Abstract—Background: Nonsteroidal anti-inflammatory drugs (NSAID) may be useful in the treatment of AD. Clinical and laboratory experience with nimesulide, an NSAID with preferential cyclooxygenase-2 inhibition, suggests that it may be a good candidate for AD therapy. **Methods:** This pilot study investigated the clinical feasibility of nimesulide treatment in AD. Forty persons with probable AD, most of whom were taking cholinesterase inhibitors, were enrolled in a randomized, controlled, parallel-group trial designed to assess tolerability and short-term cognitive/behavioral effects of nimesulide. In the initial 12-week double-blind phase, participants were treated with nimesulide 100 mg by mouth twice daily or matching placebo; during the second 12-week phase all participants received active drug. Participants who tolerated the drug well and perceived benefit were invited to continue open-label nimesulide treatment. **Results:** Short-term therapy with nimesulide, compared with placebo, had no significant effect on total assessment scores of measures of cognition, clinical status, activities of daily living, affect, and behavior. Long-term therapy was well tolerated for periods exceeding 2 years. **Conclusion:** These findings support the feasibility of nimesulide therapy in AD; assessment of efficacy will require a larger, long-term treatment study.

NEUROLOGY 2002;58:1050-1054

Results of epidemiologic studies suggest that use of nonsteroidal anti-inflammatory drugs (NSAID) confers some protection against AD and may slow the rate of cognitive decline in patients with the disease.^{1,2} This apparent therapeutic benefit may be explained by suppression of inflammatory activity in the AD brain³; many studies indicate that destructive inflammation contributes to the neurodegenerative process.⁴ More specifically, cyclooxygenase (COX), the inflammatory

enzyme targeted by NSAID, may be involved in the pathophysiology of AD.⁵

COX catalyzes the conversion of membrane-derived arachidonate to prostaglandin H₂, which is subsequently converted to prostaglandins with wide-ranging activity. Prostaglandins are important in inflammatory processes but are also involved in vascular regulation, platelet function, renal function, and protection of gastrointestinal mucosa. As a result, COX inhibitors are

From the Department of Neurology (Dr. Aisen), Georgetown University Medical Center, Washington, DC; and the Department of Psychiatry (Drs. Aisen, Schmeidler, and Pasinetti) and the Neuroinflammation Research Laboratories (Dr. Pasinetti), Department of Psychiatry, Mount Sinai Medical Center, New York, NY.

Supported by a grant from Helsinn Healthcare SA.

Received August 13, 2001. Accepted in final form December 13, 2001.

Address correspondence and reprint requests to Dr. Paul S. Aisen, Department of Neurology, Georgetown University Medical Center, 1 Bles Building, 3800 Reservoir Road, NW, Washington, DC 20007; e-mail: psa@georgetown.edu

anti-inflammatory drugs but commonly cause toxic effects such as gastrointestinal bleeding and azotemia.

The identification of two isoforms of COX, called COX-1 and COX-2, with distinct physiologic roles has been tremendously important to the pharmaceutical industry.⁶ Because COX-2 is an inducible form responsible for inflammatory activity, whereas COX-1 is important to maintenance of gastrointestinal mucosal integrity, the development of selective COX-2 inhibitors allows delivery of anti-inflammatory activity with reduced gastrointestinal toxicity. A growing body of evidence suggests that COX-2 may be involved in cellular processes unrelated to inflammation; for example, COX-2 upregulation may play a role in neoplasia.

Patients with AD may be particularly susceptible to adverse effects of traditional NSAID as a result of age and frailty. Thus, COX-2 preferential or selective inhibitors may be advantageous in AD trials. Evidence that COX-2 (but not COX-1) is upregulated in AD and may contribute to neuronal damage further supports the use of COX-2 inhibitors.^{5,7-9} Conversely, epidemiologic studies support the use of nonselective NSAID, and the presence of COX-1 in brain raises the possibility that some COX-1 inhibition may be useful. Retrospective human postmortem studies suggest that classic, nonselective NSAID such as ibuprofen reduce amyloid-associated microglial activation in brain,¹⁰ and prospective studies in transgenic mice indicate that ibuprofen reduces both inflammation and amyloid plaque load,¹¹ but it is unclear whether this effect is mediated by inhibition of COX-2, COX-1, or both.

Nimesulide is a COX-2 preferential NSAID¹² inhibiting primarily COX-2 but to a limited extent COX-1 as well.^{13,14} Nimesulide is widely used outside the United States, with more than 35 million individuals treated in each of the past 2 years (Helsinn Healthcare SA, unpublished data, 2001). It has a favorable safety/tolerability profile compared with nonselective NSAID,^{12,15-17} presumably related to limited COX-1 inhibition but perhaps also to its very weak acidity.¹⁸ Studies in rodents indicate nimesulide inhibition of brain COX-2 activity,^{19,20} attenuation of brain inflammation associated with excitotoxic damage,²¹ and inhibition of microglial activation and white matter lesions in a model of ischemia.²² Nimesulide also has antioxidant properties²³ that may be beneficial in the treatment of AD.

The current pilot study was conducted to test the feasibility of nimesulide in the treatment of AD.

Methods. Study design. The study was conducted at the Mount Sinai Medical Center in New York with approval of the Institutional Review Board. Participants with probable AD²⁴ were eligible if they were in stable medical condition; had serum creatinine less than 2 mg/dL; had no significant liver, neoplastic, inflammatory, or infectious disease; did not use NSAID (apart from low-dose aspirin prophylaxis); had a modified Hachinski Ischemic score²⁵ greater than or equal to 4; had no current evidence or history in the past 10 years of peptic ulcer disease, epi-

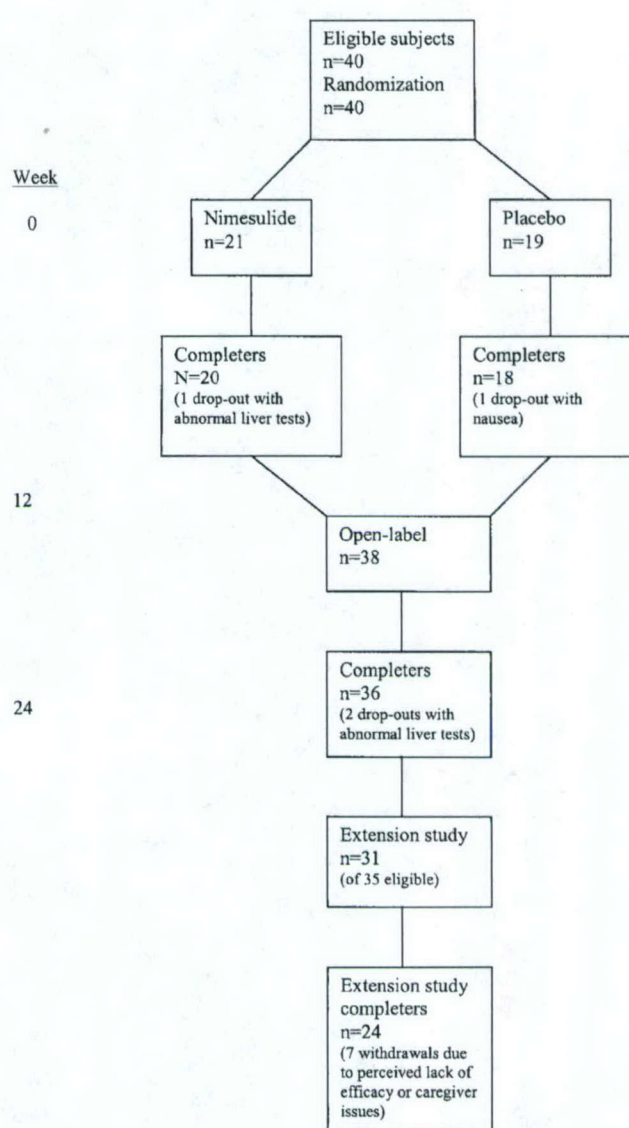


Figure. Patient flow through the study.

lepsy, stroke, focal brain lesion, or head injury with loss of consciousness and/or immediate confusion after the injury; and met no *Diagnostic and Statistical Manual, 3rd revision* criteria for any major psychiatric disorder. Stable use of cholinesterase inhibitors and vitamin E was allowed.

After informed consent was obtained from participants and responsible family members, 40 subjects were randomized to two treatment groups of similar size. The randomization schedule was generated in the research pharmacy; all investigators and study personnel remained blind to group assignment of participants until completion of data collection. The flow of subjects through the protocol is shown in the figure. In the initial 12-week double-blind phase, participants were treated twice daily with nimesulide 100 mg or identical placebo tablets; during the second 12-week phase all participants received active drug. Throughout the study, dosage adjustments (i.e., temporary discontinuation, dose reduction to 100 mg daily) were allowed as indicated by tolerability.

Outcome measures for the study included the cognitive

Table 1 Demographics and assessment scores at baseline

Characteristic/test	Placebo, n = 19	Nimesulide, n = 21	p Value
Age, y	74 ± 2	73 ± 2	0.60
Female sex, n	9	8	0.75
Education, y	14.8 ± 0.8	13.1 ± 11.2	0.27
Duration, y	2.5 ± 0.4	2.0 ± 0.5	0.43
MMSE score	22.7 ± 1.0	21.8 ± 1.1	0.54
ADAScog score	21.4 ± 2.6	19.8 ± 1.5	0.59
CDR sum of boxes score	4.6 ± 0.5	4.7 ± 0.7	0.91
ADL score	3.8 ± 0.5	3.3 ± 0.3	0.34
Ham-D score	3.8 ± 0.8	4.6 ± 0.8	0.52
BPRS score	29.6 ± 1.4	28.5 ± 1.4	0.59

Values are expressed as means ± SE unless indicated otherwise.

MMSE = Mini-Mental State Examination; ADAScog = AD Assessment Scale; CDR = Clinical Dementia Rating; ADL = Activities of Daily Living; Ham-D = Hamilton Depression Scale; BPRS = Brief Psychiatric Rating Scale.

subscale of the AD Assessment Scale (ADAScog),²⁶ the Mini-Mental State Examination,²⁷ the Clinical Dementia Rating Scale,²⁸ the Brief Psychiatric Rating Scale,²⁹ the Hamilton Depression Scale,³⁰ and the Blessed Activities of Daily Living Scale.³¹ Blood counts and chemistries were obtained at each visit.

At the conclusion of the 24-week study visit, participants who tolerated the drug well and perceived benefit were invited to continue nimesulide treatment. Those continuing treatment were followed at 2-month intervals with clinical assessments, routine laboratory monitoring, and ADAScog testing.

Sample size rationale and statistical analysis. The trial was designed as a pilot investigation of the feasibility of nimesulide treatment in AD. No significant difference between active treatment and placebo on any outcome measures during the 12-week double-blind phase was anticipated; sample size was chosen based on feasibility for a single-site study.

Continuous variables, including cognitive and behavioral assessment scores, were analyzed as change from baseline with between-group differences compared by analysis of variance. Side effects were analyzed with descriptive statistics and nonparametric tests.

Results. Baseline characteristics. Forty participants enrolled in the study, with 21 randomized to receive nimesulide and 19 to receive placebo. The majority of participants (88%) were taking donepezil for treatment of AD. As shown in table 1, baseline characteristics of the two groups were similar. There were no statistically significant differences between groups in sex, age, or baseline tests of cognition, clinical status, activities of daily living, mood, or behavior.

Analysis of outcome measures at 12 weeks. An intent-to-treat analysis of covariance, with baseline ADAScog score as a covariate, was used to assess change in ADAScog during treatment in the nimesulide group compared with the placebo group. The last observation carried forward method was used to impute missing scores. This

Table 2 Intent-to-treat analysis of change in outcomes at 12 weeks (double-blind phase)

Test	Placebo, n = 19	Nimesulide, n = 21	p Value
ADAScog score	-0.5 ± 1.0	0.9 ± 1.0	0.49
CDR sum of boxes score	0.2 ± 0.3	0.7 ± 0.3	0.70
ADL score	-0.3 ± 0.2	-0.2 ± 0.3	0.73
Ham-D score	1.0 ± 0.6	-0.2 ± 0.9	0.30
BPRS score	0.4 ± 0.9	0.4 ± 1.4	0.99

Negative change in scores indicates improvement.

ADAScog = AD Assessment Scale; CDR = Clinical Dementia Rating; ADL = Activities of Daily Living; Ham-D = Hamilton Depression Scale; BPRS = Brief Psychiatric Rating Scale.

analysis revealed no difference in cognitive decline between groups (table 2). The decline in cognition during the 12-week period was quite small (less than 1 point on the ADAScog), as expected, in both the active drug and the placebo groups.

In addition, as shown in table 2, there was no difference between groups in change in clinical stage (Clinical Dementia Rating Scale), activities of daily living, mood (Hamilton Depression Scale), or behavior (Brief Psychiatric Rating Scale).

Analysis of compliers at 12 weeks. As a secondary analysis, we assessed the impact of nimesulide treatment on the assessment scales among those who completed the 12-week phase on full-dose therapy without interruption. As with the intent-to-treat analyses, there was no significant difference between groups on any of the total outcome measures. Individual items on each scale were analyzed in this matter, and none of the differences retained significance after correction for multiple comparisons.

Analysis of week 24 data. There were no significant differences in outcome measures (ADAScog, Clinical Dementia Rating Scale, Activities of Daily Living Scale, Hamilton Depression Scale, Brief Psychiatric Rating Scale) between the two treatment groups at 24 weeks after completion of both the double-blind and the open-label study phases.

Safety evaluation. Short-term tolerability. Early discontinuation. Two participants, one in each treatment arm, discontinued medication early during the 12-week double-blind phase. One participant in the nimesulide group stopped medication after week 4 because of elevated liver chemistries and gastrointestinal discomfort; another in the placebo group discontinued medication after week 2 because of nausea and dizziness. Two participants discontinued study medication during the open-label phase as a result of elevated liver chemistries. Thus, 36 of 40 participants completed the 24-week protocol on study medication.

Abnormal liver chemistries. Six participants developed abnormal liver chemistries during the course of this study; of these, five seemed to be related to nimesulide treatment, whereas in one case the abnormalities appeared while the participant was on placebo. Thus, five of 39 participants (13%) developed liver chemistry abnormalities during exposure to nimesulide. In these cases, transaminase elevations occurred 2 to 8 weeks after starting nimesulide, with peak levels between 2 and 8 times the upper limit of nor-

Table 3 Adverse events reported more frequently by subjects in the nimesulide group

Symptom	Placebo group, %	Nimesulide group, %	p Value
Constipation	16	47	0.05
Elevated mood	32	67	0.06
Abdominal discomfort	11	47	0.02
Rash	11	47	0.02

mal; liver chemistries returned to normal within 4 weeks with interruption of therapy in all participants. Nimesulide was restarted in two of these participants after a 2- to 4-week hiatus, without further abnormality of liver chemistries.

Adverse symptoms. All participants were questioned specifically regarding 32 symptoms at each study visit. During the 12-week double-blind phase, the two treatment groups were compared in terms of number of participants with any report of each symptom and total number of reports of each symptom. Symptoms were generally mild; as noted above, only one participant in each treatment arm discontinued medication early during the double-blind phase, although several participants in the nimesulide group temporarily suspended medication because of adverse symptoms (rash, nausea, behavioral disturbance). As shown in table 3, four symptoms were more common in the nimesulide group compared with the placebo group—constipation, elevated mood, abdominal discomfort, and rash.

Long-term tolerability. Combining the double-blind, open-label, and long-term continuation phases, a total of 39 participants were exposed to nimesulide treatment (one participant in the placebo group dropped out after 2 weeks). Thirty-six of 39 participants (92%) completed 24 weeks on study medication; three participants discontinued study medication because of increased results of liver chemistry tests. An additional eight participants had some temporary adjustment of dose (elevated liver chemistries in two subjects, gastrointestinal symptoms in two, mild azotemia in one, mild anemia in one, rash in one, behavioral symptoms in one), whereas 28 of 39 (72%) tolerated full-dose nimesulide for at least 24 weeks.

Of the 35 eligible participants who completed the 24-week study on nimesulide, 31 (88%) continued treatment beyond the 24-week study period. (The final participant was not offered the option of continuing nimesulide treatment.) Among these 31 participants, seven (23%) later discontinued medication because of perceived lack of efficacy or caregiver issues. Twenty-four participants completed one year of treatment before the continuation phase ended, and eight completed 2 years of treatment.

Discussion. Results of this pilot study demonstrate the feasibility of nimesulide therapy in patients with mild to moderate AD. Although there were no serious adverse events related to treatment, transient elevations of liver chemistries occurred in some patients. The proportion of patients able to tolerate nimesulide therapy compares favorably with

published experience with other NSAID in this population.

There were no significant differences in cognitive, clinical, behavioral, and functional assessments between nimesulide and placebo groups in the 12-week double-blind phase of the study. This indicates that nimesulide has no short-term cognitive or behavioral toxicity, nor any clear symptomatic benefit on the manifestations of AD. The hypothesized benefit of nimesulide in AD involves inhibition of destructive cyclooxygenase-mediated inflammatory activity, resulting in slowing of the rate of cognitive decline; thus, no short-term benefit was anticipated. If nimesulide has a disease-modifying effect, a longer treatment period and a larger number of participants would be required to demonstrate the effect. The decline in cognition during the 12-week period was quite small (less than 1 point on the ADASCog), as expected, in both the active drug and the placebo groups.

The study was designed to assess adverse medical effects of nimesulide in patients with AD. Adverse symptoms, physical findings, and laboratory studies were monitored on a biweekly basis. This close monitoring revealed unexpected, asymptomatic elevation of liver chemistries in 13% of participants treated with the drug. Although this effect on laboratory studies is well known with NSAID, the relatively high frequency was unexpected, perhaps attributable to the close monitoring and perhaps the frailty of this population. It is not clear whether these abnormalities are clinically significant. We took a cautious approach, interrupting therapy in each case; abnormalities were reversible in each instance. In two participants, nimesulide was restarted within a few weeks without recurrence of the abnormalities. A recent review concluded that liver toxicity is not more common with nimesulide than with other NSAID.³² There have been sporadic reports of hepatic injury with nimesulide therapy, with most cases resolving spontaneously³³⁻³⁷; cases of hepatic failure, sometimes fatal, have also been reported.^{36,38-40} Therefore, it is appropriate that liver chemistries be monitored during additional clinical studies of nimesulide in this population.

The majority of participants in this study continued open-label nimesulide treatment for extended periods up to and exceeding 2 years. This experience suggests that nimesulide is well tolerated with long-term treatment: 92% tolerated the treatment; 72% remained at full dose without interruption for at least 24 weeks. This compares favorably with published tolerability of indomethacin (58% remained in the study at 26 weeks⁴¹) and diclofenac/misoprostol (50% remained in the study at 25 weeks).⁴² If benefits of nimesulide therapy on the course of AD are established in future trials, chronic, neuroprotective therapy with this drug appears to be feasible.

Interest in NSAID therapy for the treatment or the prevention of AD remains strong, although there are many unresolved issues, including the relative

importance of COX-2 vs COX-1 inhibition.⁴ A recent study demonstrating the efficacy of NSAID therapy in reducing both inflammatory activity and amyloid deposition in a transgenic model of AD-type amyloid pathology supports this therapeutic approach.¹¹ Large-scale trials of several agents are in progress. Tolerability, particularly with full anti-inflammatory doses of NSAID, remains a major concern. Nimesulide appears to be an attractive candidate for therapeutic trials in AD based on preclinical studies demonstrating suppression of brain inflammation that may contribute to AD neurodegeneration,²¹ and on demonstration of short- and long-term tolerability in the current study.

Acknowledgment

The authors thank Maureen Fusco, Annu Dimatteo, Stephanie Cosentino, Jennifer Nothrup, Jennifer Hoblyn, Elizabeth Fine, Carolyn Ward, and Deborah Marin.

References

- McGeer PL, Schulzer M, McGeer EG. Arthritis and anti-inflammatory agents as possible protective factors for Alzheimer's disease: a review of 17 epidemiologic studies. *Neurology* 1996;47:425-432.
- Stewart WF, Kawas C, Corrada M, Metter EJ. Risk of Alzheimer's disease and duration of NSAID use. *Neurology* 1997;48:626-632.
- Aisen PS. Inflammation and Alzheimer's disease: mechanisms and therapeutic strategies. *Gerontology* 1997;43:143-149.
- Akiyama H, Barger S, Barnum S, et al. Inflammation and Alzheimer's disease. *Neurobiol Aging* 2000;21:383-421.
- Pasinetti GM, Aisen PS. Cyclooxygenase-2 expression is increased in frontal cortex of Alzheimer's disease brain. *Neuroscience* 1998;87:319-324.
- Vane JR, Botting RM. Anti-inflammatory drugs and their mechanism of action. *Inflamm Res* 1998;47(suppl 2):S78-S87.
- Ho L, Osaka H, Aisen PS, Pasinetti GM. Induction of cyclooxygenase (COX)-2 but not COX-1 gene expression in apoptotic cell death. *J Neuroimmunol* 1998;89:142-149.
- Ho L, Pieroni C, Winger D, Purohit DP, Aisen PS, Pasinetti GM. Regional distribution of cyclooxygenase-2 in the hippocampal formation in Alzheimer's disease. *J Neurosci Res* 1999;57:295-303.
- Ho L, Purohit D, Haroutunian V, et al. Neuronal cyclooxygenase-2 expression in the hippocampal formation as a function of the clinical progression of Alzheimer disease. *Arch Neurol* 2001;58:487-492.
- Mackenzie IR. Anti-inflammatory drugs and Alzheimer-type pathology in aging. *Neurology* 2000;54:732-734.
- Lim GP, Yang F, Chu T, et al. Ibuprofen suppresses plaque pathology and inflammation in a mouse model for Alzheimer's Disease. *J Neurosci* 2000;20:5709-5714.
- Davis R, Brogren RN. Nimesulide. An update of its pharmacodynamic and pharmacokinetic properties, and therapeutic efficacy. *Drugs* 1994;48:431-454.
- Famaey JP. In vitro and in vivo pharmacological evidence of selective cyclooxygenase-2 inhibition by nimesulide: an overview. *Inflamm Res* 1997;46:437-446.
- Panara MR, Padovano R, Sculli MG, et al. Effects of nimesulide on constitutive and inducible prostanoid biosynthesis in human beings. *Clin Pharmacol Ther* 1998;63:672-681.
- Fossaluzza V, Montagnani G. Efficacy and tolerability of nimesulide in elderly patients with osteoarthritis: double-blind trial versus naproxen. *J Int Med Res* 1989;17:295-303.
- Calligaris A, Scaricabarozzi I, Vecchiet L. A multicentre double-blind investigation comparing nimesulide and naproxen in the treatment of minor sport injuries. *Drugs* 1993;46:187-190.
- Fusetti G, Magni E, Armandola MC. Tolerability of nimesulide. *Epidemiological data. Drugs* 1993;46:277-280.
- Bjarnason I, Thjodleifsson B. Gastrointestinal toxicity of non-steroidal anti-inflammatory drugs: the effect of nimesulide compared with naproxen on the human gastrointestinal tract. *Rheumatology (Oxford)* 1999;38(suppl 1):24-32.
- Taniguchi Y, Yokoyama K, Inui K, Deguchi Y, Furukawa K, Noda K. Inhibition of brain cyclooxygenase-2 activity and the antipyretic action of nimesulide. *Eur J Pharmacol* 1997;330:221-229.
- Koyfman L, Kaplanski J, Artru AA, Talmor D, Rubin M, Shapira Y. Inhibition of cyclooxygenase 2 by nimesulide decreases prostaglandin E2 formation but does not alter brain edema or clinical recovery after closed head injury in rats. *J Neurosurg Anesthesiol* 2000;12:44-50.
- Scali C, Prosperi C, Vannucchi MG, Pepeu G, Casamenti F. Brain inflammatory reaction in an animal model of neuronal degeneration and its modulation by an anti-inflammatory drug: implication in Alzheimer's disease. *Eur J Neurosci* 2000;12:1900-1912.
- Wakita H, Tomimoto H, Akiyama I, Lin JX, Miyamoto K, Oka N. A cyclooxygenase-2 inhibitor attenuates white matter damage in chronic cerebral ischemia. *Neuroreport* 1999;10:1461-1465.
- Facino RM, Carini M, Aldini G. Antioxidant activity of nimesulide and its main metabolites. *Drugs* 1993;46:15-21.
- McKhann G, Drachman D, Folstein M, Katzman R, Price D, Stadlan EM. Clinical diagnosis of Alzheimer's disease: report of the NINCDS-ADRDA Work Group. *Neurology* 1984;34:939-944.
- Hachinski VC, Iliff LD, Zilhka E, et al. Cerebral blood flow in dementia. *Arch Neurol* 1975;32:632-637.
- Rosen WG, Mohs RC, Davis KL. A new rating scale for Alzheimer's disease. *Am J Psychiatry* 1984;141:1356-1364.
- Folstein M, Folstein S, McHugh P. The Mini-Mental State Examination. *J Psychiatr Res* 1975;12:189-198.
- Morris JC. The Clinical Dementia Rating (CDR): current version and scoring rules. *Neurology* 1993;43:2412-2414.
- Overall JE, Gorham DR. Brief Psychiatric Rating Scale. *Psychology Reports* 1962;10:799-812.
- Hamilton M. A rating scale for depression. *J Neurol Neurosurg Psychiatry* 1960;23:56-62.
- Blessed G, Tomlinson BE, Roth M. The association between quantitative measures of dementia and of senile change in the cerebral grey matter of elderly subjects. *Br J Psychiatry* 1968;114:797-811.
- Rainsford KD. Relationship of nimesulide safety to its pharmacokinetics: assessment of adverse reactions. *Rheumatology (Oxford)* 1999;38(suppl 1):4-10.
- Van Steenberghe W, Peeters P, De Bondt J, et al. Nimesulide-induced acute hepatitis: evidence from six cases. *J Hepatol* 1998;29:135-141.
- Romero-Gomez M, Nevado Santos M, Otero Fernandez MA, Fovelo MJ, Suarez-Garcia E, Castro Fernandez M. Acute cholestatic hepatitis induced by nimesulide. *Liver* 1999;19:164-165.
- Ferreiro C, Vivas S, Jorquera F, et al. Toxic hepatitis caused by nimesulide, presentation of a new case and review of the literature. *Gastroenterol Hepatol* 2000;23:428-430.
- Weiss P, Mouallem M, Bruck R, et al. Nimesulide-induced hepatitis and acute liver failure. *Isr Med Assoc J* 1999;1:89-91.
- Tejos S, Torrejon N, Reyes H, Meneses M. Bleeding gastric ulcers and acute hepatitis: 2 simultaneous adverse reactions due to nimesulide in a case. *Rev Med Chil* 2000;128:1349-1353.
- McCormick PA, Kennedy F, Curry M, Traynor O. COX 2 inhibitor and fulminant hepatic failure. *Lancet* 1999;353:40-41.
- Schattner A, Sokolovskaya N, Cohen J. Fatal hepatitis and renal failure during treatment with nimesulide. *J Intern Med* 2000;247:153-155.
- Andrade RJ, Lucena MI, Fernandez MC, Gonzalez M. Fatal hepatitis associated with nimesulide. *J Hepatol* 2000;32:174. Letter.
- Rogers J, Kirby LC, Hempelman SR, et al. Clinical trial of indomethacin in Alzheimer's disease. *Neurology* 1993;43:1609-1611.
- Scharf S, Mander A, Ugoni A, Vajda F, Christophidis N. A double-blind, placebo-controlled trial of diclofenac/misoprostol in Alzheimer's disease. *Neurology* 1999;53:197-201.

The Past-Tense Debate

The past and future of the past tense

Steven Pinker and Michael T. Ullman

What is the interaction between storage and computation in language processing? What is the psychological status of grammatical rules? What are the relative strengths of connectionist and symbolic models of cognition? How are the components of language implemented in the brain? The English past tense has served as an arena for debates on these issues. We defend the theory that irregular past-tense forms are stored in the lexicon, a division of declarative memory, whereas regular forms can be computed by a concatenation rule, which requires the procedural system. Irregulars have the psychological, linguistic and neuropsychological signatures of lexical memory, whereas regulars often have the signatures of grammatical processing. Furthermore, because regular inflection is rule-driven, speakers can apply it whenever memory fails.

For fifteen years, the English past tense has been the subject of a debate on the nature of language processing. The debate began with the report of a connectionist model by Rumelhart and McClelland [1] and a critique by Pinker and Prince [2], and has since been the subject of many papers, conferences and simulation models [3–7] (see also McClelland and Patterson in this issue [8]).

The past tense is of theoretical interest because it embraces two strikingly different phenomena. Regular inflection, as in *walk-walked* and *play-played*, applies predictably to thousands of verbs and is productively generalized to neologisms such as *spam-spammed* and *mosh-moshed*, even by preschool children [9]. Irregular inflection, as in *come-came* and *feel-felt*, applies in unpredictable ways to some 180 verbs, and is seldom generalized; rather, the regular suffix is often overgeneralized by children to these irregular forms, as in *holded* and *breaked* [10,11]. A simple explanation is that irregular forms must be stored in memory, whereas regular forms can be generated by a rule that suffixes *-ed* to the stem [12,13]. Rumelhart and McClelland challenged that explanation with a pattern-associator model (RMM) that learned to associate phonological features of the stem with phonological features of the past-tense form. It thereby acquired several hundred regular and irregular forms and overgeneralized *-ed* to some of the irregulars.

The past tense has served as one of the main empirical phenomena used to contrast the strengths

and weaknesses of connectionist and rule-based models of language and cognition [8]. More generally, because inflections like the past tense are simple, frequent, and prevalent across languages, and because the regular and irregular variants can be equated for complexity and meaning, they have served as a test case for issues such as the neurocognitive reality of rules and other symbol-manipulating operations and the interaction between storage and computation in cognitive processing [5–7].

In this article we defend the side of this debate that maintains that rules are indispensable for explaining the past tense, and by extension, language and cognitive processes [3–5,14]. We review what the theory does and doesn't claim, the relevant evidence, the connectionist challenges, and our hopes for the future of the debate.

The Words-and-Rules theory

The Words and Rules (WR) theory claims that the regular-irregular distinction is an epiphenomenon of the design of the human language faculty, in particular, the distinction between lexicon and grammar made in most traditional theories of language. The lexicon is a subdivision of memory containing (among other things) the thousands of arbitrary sound-meaning pairings that underlie the morphemes and simple words of a language. The grammar is a system of productive, combinatorial operations that assemble morphemes and simple words into complex words, phrases and sentences. Irregular forms are just words, acquired and stored like other words, but with a grammatical feature like 'past tense' incorporated into their lexical entries. Regular forms, by contrast, can be productively generated by a rule, just like phrases and sentences. A stored inflected form of a verb blocks the application of the rule to that verb (e.g. *brought* pre-empts *bringed*). Elsewhere (by default) the rule applies: it concatenates *-ed* with the symbol 'V', and thus can inflect any word categorized as a verb (see Fig. 1).

Irregular forms, then, do not require an 'exception module'. They arise because the two subsystems overlap in their expressive power: a given combination of features can be expressed by words or rules. Thus either a word (irregular) or a rule-product (regular) can satisfy the demand of a syntactic or semantic representation that a feature such as past tense be overtly expressed. Diachronically, an irregular is born when (for various reasons) learners memorize a complex word outright, rather than parsing it into a stem and an affix that codes the feature autonomously [3].

Steven Pinker*

Dept of Brain and
Cognitive Sciences,
NE20-413, Massachusetts
Institute of Technology,
Cambridge, MA 02139,
USA.

*e-mail:
steve@psyche.mit.edu

Michael Ullman

Dept of Neuroscience,
Research Building EP-04,
Georgetown University,
3900 Reservoir Rd, NW,
Washington DC 20007,
USA.

e-mail: michael@
georgetown.edu

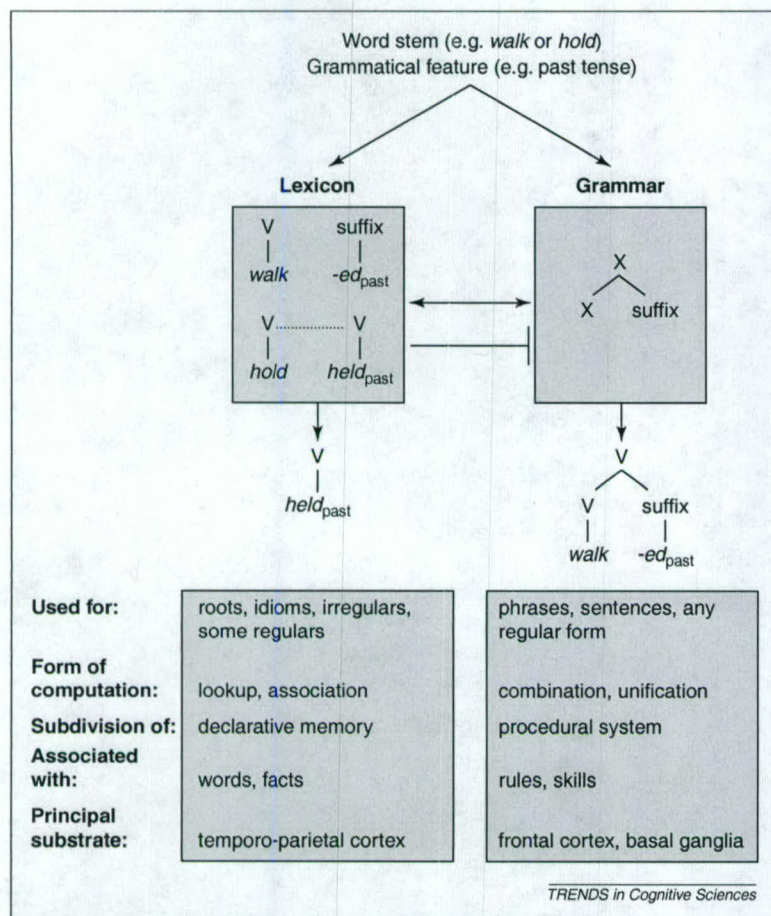


Fig. 1. Simplified illustration of the Words-and-Rules (WR) theory and the Declarative/Procedural (DP) hypothesis. When a word must be inflected, the lexicon and grammar are accessed in parallel. If an inflected form for a verb (V) exists in memory, as with irregulars (e.g. *held*), it will be retrieved; a signal indicating a match blocks the operation of the grammatical suffixation process via an inhibitory link from lexicon to grammar, preventing the generation of *holded*. If no inflected form is matched, the grammatical processor concatenates the appropriate suffix with the stem, generating a regular form.

The WR theory contrasts with classical theories of generative phonology and their descendents, such as those of Chomsky and Halle [15–17], which generate irregular forms by affixing an abstract morpheme to the stem and applying rules that alter the stem's phonological composition. Such theories are designed to account for the fact that most irregular forms are not completely arbitrary but fall into families displaying patterns, as in *ring-rang*, *sink-sank*, *sit-sat*, and *feel-felt*, *sleep-slept*, *bleed-bled*. A problem for this view is that irregular families admit numerous positive and negative counterexamples and borderline cases, so any set of rules will be complex and laden with exceptions, unless it posits implausibly abstract underlying representations (e.g. *rin* for *run*, which allows the verb to undergo the same rules as *sing-sang-sung*).

The theory also contrasts with the Rumelhart–McClelland model (RMM) and other connectionist models that posit a single pattern associator, with neither lexical entries nor a

combinatorial apparatus [1,18,19]. The key to these pattern associators is that rather than linking a word to a word stored in memory, they link sounds to sounds. Because similar words share sounds, their representations are partly superimposed, and any association formed to one is automatically generalized to the others. This allows such models to acquire families of similar forms more easily than arbitrary sets, and to generalize the patterns to new similar words. Having been trained on *fling-flung* and *cling-clung*, they may generalize to *spling-splung* (as children and adults occasionally do [20,21]); and having been trained on *flip-flipped* and *clip-clipped*, they generalize to *plip plipped*.

WR is descended from a third approach: the lexicalist theories of Jackendoff, Lieber, and others, who recognized that many morphological phenomena are neither arbitrary lists nor fully systematic and productive [22–25]. They posited 'lexical redundancy rules', which do not freely generate new forms but merely capture patterns of redundancy in the lexicon, and allow sporadic generalization by analogy. Pinker and Prince proposed that lexical redundancy rules are not rules at all, but consequences of the superpositional nature of memory: similar items are easier to learn than arbitrary sets, and new items resembling old ones tend to inherit their properties. They argued that RMM's successes came from implementing this feature of memory, and proposed the WR theory as a lexicalist compromise between the generative and connectionist extremes. Irregulars are stored in a lexicon with the superpositional property of pattern associators; regulars can be generated or parsed by rules.

Ullman and colleagues have recently extended the WR theory to a hypothesis about the neurocognitive substrate of lexicon and grammar. According to the Declarative/Procedural (DP) hypothesis [5,26], lexical memory is a subdivision of declarative memory, which stores facts, events and arbitrary relations [27,28]. The consolidation of new declarative memories requires medial-temporal lobe structures, in particular the hippocampus. Long-term retention depends largely on neocortex, especially temporal and temporo-parietal regions; other structures are important for actively retrieving and searching for these memories. Grammatical processing, by contrast, depends on the procedural system, which underlies the learning and control of motor and cognitive skills, particularly those involving sequences [27,28]. It is subserved by the basal ganglia, and by the frontal cortex to which they project – in the case of language, particularly Broca's area and neighboring anterior cortical regions. Irregular forms must be stored in the lexical portion of declarative memory; regular past-tense forms can be computed in the grammatical portion of the procedural system.

What the words-and-rules theory does not say

The WR theory does not literally posit the discrete rule 'to form the past tense, add *-ed* to the verb'. All it posits is the past-tense morpheme *-ed*, a variable 'V' (included both in the attachment conditions for *-ed* and the lexical entry of every verb), and a general operation of merging or unifying constituents. The 'regular rule' or 'past-tense rule' is shorthand for the unification operation applied to the past-tense morpheme. WR is thus compatible with constraint- and construction-based theories of language, as long as they allow for variables and combinatorial operations [29].

WR does not posit that regular forms are *never* stored, only that they do not *have to be* [3,30–32]. It would be difficult to prohibit regular forms from ever being stored, given that human memory can acquire many kinds of verbal material (e.g. idioms, clichés, poems). WR posits a parallel-race model, like those defended for inflection by Baayen and Caramazza and by many psycholinguists for visual word recognition [33–39]. Whether a regular form is stored, and whether stored regular forms are accessed, depends on word-, task-, and speaker-specific factors [5,40–43]. For example, regular forms that constitute doublets with irregulars, such as *dived/dove* and *dreamed/dreamt*, must be stored to escape blocking by the irregular. As predicted, judgments of the naturalness of regular doublet forms show strong effects of frequency but other regular forms do not [30]. The same is true for regular forms of verbs that resemble irregulars (such as *blinked* and *glided*), because the forms must overcome a partial blocking effect exerted by the similar irregulars [30,32]. Tasks that require people to be sensitive to the physical form of words (such as progressive demasking) or to the prior existence of words (such as lexical decision), as opposed to tasks that ask people to judge possible forms, are likely to tap stored representations for medium- and high-frequency regular forms [3,35,44].

Finally, WR is not a chimera of a connectionist pattern associator glued onto a rule system. The lexicon has superpositional properties similar to a pattern associator, but lexical entries have structured semantic, morphological, phonological and syntactic representations of a kind not currently implemented in pattern associators.

Empirical tests

The key predictions of WR are: (1) that irregulars should have the psychological, linguistic and neuropsychological signatures of lexical memory, whereas regulars will often have the signatures of grammatical processing; and (2) that speakers should apply regular inflection whenever memory fails to supply a form for that category. A stored form may be unavailable for many reasons: low or zero frequency, lack of a similar form that could inspire an analogy, inaccessibility because of a word's exocentric structure (see below), novelty of the form in childhood,

and various kinds of damage to the neurological substrate of lexical memory. The heterogeneity of these regular-eliciting circumstances offers converging evidence for distinguishable subsystems, including a productive default that does not critically depend on the statistics of patterns in memory. Here we discuss three types of evidence for a distinction between lookup and concatenation, and connectionists' attempts to provide alternative accounts (for reviews, see [3,4,14,31]).

Generalization to unusual novel words

The RMM model produced odd blends (*mail-membled*, *trilb-treelilt*), or no output, for novel words unlike those in its training set [2,20]. People, by contrast, readily apply regular inflections to novel unusual words [20]. According to WR, this is because *-ed* can attach to any word classified as a verb, even if dissimilar to existing stored regulars.

One connectionist explanation of the difficulties of the model is that they are specific to RMM, which is an early modeling exercise lacking a proper phonological representation, a hidden layer, and a proper output decoder. However, a pattern associator remedying all three deficiencies also had trouble generalizing to unusual words [45]. More recent models that are claimed to solve the problem do so, tellingly, by implementing or presupposing a rule. For example, Hare, Elman and Daugherty installed a 'clean-up network' in which the units for *-ed* strengthen the units for an unchanged stem vowel and inhibit the units for a changed vowel [46] – in effect, an innate mechanism dedicated to the English past tense. Many recent models have given up on generating past-tense forms; their output layer contains one unit for every past-tense change, turning inflection into a multiple-choice test among a few innate possibilities [47–49]. To convert the choice into an actual form, some other mechanism would have to copy the stem and apply the pattern corresponding to the selected unit. Such a mechanism is simply a rule. Marcus has argued that pattern associators' difficulty in generalizing to dissimilar forms is rooted in their design [4].

Another response is to claim that people's success at generalization depends on certain statistical patterns that also foster generalization in pattern associators. Many connectionists claimed that robust generalization depends on regular forms constituting the majority of forms in the child's input [50]. However, the onset and rate of over-regularization errors in children do not correlate with changes in the number or proportion of regular verbs used by parents [11,51,52]. Moreover, there are regular inflections in other languages, such as the German *-s* plural, that apply to a minority of nouns (~7%), but are generalized like English regular inflection, namely, to unusual nouns, exocentric nouns, and in childhood [50].

Several modelers now argue that it is not the number or proportion of regular words that is crucial but their distribution in phonological

Box 1. Systematic regularization

An intriguing aspect of inflection is that irregular forms can sometimes turn up in regular form. Some of these regularizations are unsystematic – for example, doublets such as *dived/dove* and *dreamt/dreamed*, in which the regular form is used sporadically because the irregular form is low in frequency and hence poorly remembered. But many are systematic: in particular contexts, the regular form is consistently used, such as *ringed the city* and *low-lives*.

The Words-and-Rules theory explains this phenomenon using an independently motivated theory of compositionality in word-formation [a,b] (see also Fig. 2 in main article). Irregular-sounding words are regularized if they lack a root in head position that can be marked for the inflectional feature (tense or number). The regular suffix applies as the default, as it does in other cases where memory access is disabled. This neatly explains a diverse set of systematic regularizations found in actual usages, laboratory experiments with adults and children, and many languages [c–f]:

The word lacks a noun or a verb root

- **onomatopoeia:** *dinged, pinged, zinged, peeped, beeped*
- **quotations:** 'I found three man's on page 1'; 'We to be'd and not to be'd in this room'
- **names:** the Julia Childs, the Thomas Manns, the Shelby Footes
- **truncations:** *synched, sysmans*
- **unassimilated borrowings:** *talismans, mongooses*

The root cannot be marked for the feature

- **verbs with noun or adjective roots:** *ringed the city, steeled myself, spitted the pig, bared his soul, righted the boat, stringed the peas*
- **nouns with verb roots:** *a few loafs* (episodes of loafing), *a couple of wolfs* (wolfing down food)

The word's structure is exocentric

- **verbs based on nouns based on verbs:** *grandstanded, flied out, costed out the grant, encasted his leg*
- **nouns based on names based on nouns:** *Mickey Mouses* (simpletons), *Renault Elfs*, *Top Shelves* (frozen food), *Seawolfs* (aircraft), *Toronto Maple Leafs*
- **nouns whose referents are distinct from those of their roots:** *low-lives, still lifes, sabre-tooths, Walkmans, tenderfoots*
- **nouns based on phrases:** *Bag-A-Leafs, Shear-A-Sheeps*

Although the meaning of the regularized forms differs from that of their irregular counterparts, regularization is rarely triggered by differences in

semantic features alone, as connectionists sometimes suggest [g,h]. If an irregular-sounding word changes in meaning, but retains a root in head position, it stays irregular, no matter how radical the change or opaque the metaphor:

- **compositional prefixing:** *overate, overshot, undid, preshrank, remade, outsold*
 - **non-compositional prefixing:** *overcame, understood, withdrew, beheld, withstood, undertook*
 - **compounding:** *bogeymen, superwomen, muskoxen, stepchildren, milkteeth*
 - **metaphors:** *straw men, chessmen, snowmen, sawteeth, metrical feet, six feet tall, brainchildren, children of a lesser god, beewolves, wolves in sheep's clothing*
 - **idioms:** *went out with* (dated), *went nuts* (demented), *went in for* (chose), *went off* (exploded), *went off* (spoiled); *took in* (swindled), *took off* (launched), *took in* (welcomed), *took over* (usurped), *took up* (commenced), *took a leak* (urinated), *took a bath* (lost money), *took a bath* (bathed), *took a walk* (walked); *blew over* (ended), *blew away* (assassinated), *blew away* (impressed), *blew up* (exploded), *blew up* (inflated), *blew off* (dismissed), *blew in* (arrived)
- [scores of other examples with *come, do, have, get, set, put, stand, throw*, etc.]

References

- Williams, E. (1981) On the notions of 'lexically related' and 'head of a word'. *Linguist. Inq.* 12, 245–274
- Selkirk, E.O. (1982) *The Syntax of Words*, MIT Press
- Pinker, S. (1999) *Words and Rules: The Ingredients of Language*, HarperCollins
- Kim, J.J. et al. (1994) Sensitivity of children's inflection to morphological structure. *J. Child Lang.* 21, 173–209
- Marcus, G.F. et al. (1995) German inflection: the exception that proves the rule. *Cogn. Psychol.* 29, 189–256
- Berent, I. et al. (1999) Default nominal inflection in Hebrew: evidence for mental variables. *Cognition* 72, 1–44
- Daugherty, K.G. et al. (1993) Why no mere mortal has ever flown out to center field but people often say they do. In *15th Annu. Conf. Cogn. Sci. Soc.*, Erlbaum
- Harris, C.L. (1992) Understanding English past-tense formation: the shared meaning hypothesis. In *Proc. 14th Annu. Conf. Cogn. Sci. Soc.*, Erlbaum

space [46,48,53,54]. If irregulars fall into clusters of similar forms (*sing, ring, spring, grow, throw, blow*, etc.), but regulars are sprinkled through no-man's-land, (*rhumba'd, oinked*, etc.), one can design pattern associators that devote some of their units and connections to the no-man's-land, and they will generalize to new unusual words. Putting aside the problem that most of these models have their inflections innately wired in, the models cannot deal with languages such as Hebrew, where regular and irregular nouns are intermingled in the same phonological neighborhoods. Nonetheless, Hebrew regular plural suffixes behave like -s in English and German: speakers apply them to unusual-sounding and exocentric nouns [55,56].

Systematic regularization

Some irregulars show up in regular form in certain contexts, such as *ringed the city* (not *rang*), *grandstanded* and *low-lives* [2,57] (see Box 1 for further examples). This shows that sound alone cannot be the input to the inflection system: a given

input, like *ring*, can be inflected either as *rang* or *ringed*, depending on some other factor.

The phenomenon falls out of the grammatical mechanism governing how complex words are formed [24,50,58,59]. Generally a complex English word inherits its features from its rightmost morpheme, its 'head'. For example, the head of *overeate* is *eat*; therefore, *overeate* is a verb (it inherits the 'V' category of *eat*), it refers to a kind of eating (because it inherits the semantic features of *eat*), and it has the irregular past-tense *overate* (because it inherits the stored past-tense form of *eat*) (see Fig. 2).

But there is a small family of exceptions: headless (exocentric) words, which for various reasons cannot get their features from their rightmost morpheme. For example, unlike endocentric verbs such as *overeate-overate* and *outdo-outdid*, which are verbs based on verbs, *to ring* and *to grandstand* are verbs based on nouns (*a ring, a grandstand*). In forming or parsing the word, the head-inheritance mechanism must be circumvented. With that data pathway plugged, there is no way for the irregular forms *rang*

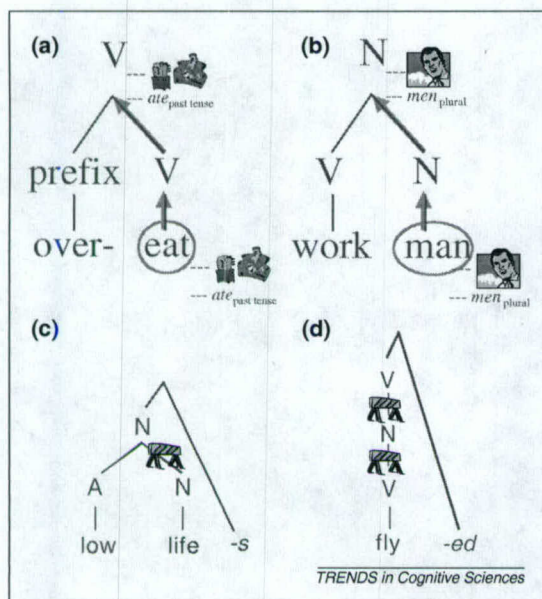


Fig. 2. Systematic regularization. Complex words are assembled out of simple morphemes according to a 'righthand-head' rule: the rightmost morpheme, the head, contributes its syntactic, semantic and morphological properties to the word as a whole. Thus in (a), the combination of *over-* and *eat* is a verb, because its head (circled), *eat*, is a verb (V); its meaning is a kind of eating (eating too much), because that is the meaning of *eat*, and its past-tense form is *overate*, because the irregular past-tense of *eat* is *ate*. All three kinds of information percolate up from the lexical entry for the head in memory along the rightmost edge of the word's tree structure (thick arrows). Similarly in (b), the combination of *work* and *man* is a noun (N), it refers to a kind of man, and its plural is *workmen*, the result of its inheriting all three properties from its head, *man*. However, a handful of derived words in English (headless or exocentric words) have to disable this inheritance mechanism. A *low-life* (c) is not a kind of life (in the way a *workman* is a kind of man) but a person who has a low life; for the word to work this way the usual data pipeline has to be blocked (depicted by the no entry sign). This leaves the irregular plural form (*lives*), trapped in memory, and the regular suffix *-s* applies as the default. The baseball term *fly out* (d) comes from the noun *a fly* (as in *an infield fly*), which itself came from the simple verb root to *fly* (at the bottom of the tree). The word's structure requires the inheritance mechanism to be blocked twice: to allow the verb root *fly* to be converted to the noun (because verbs ordinarily beget verbs, not nouns) and again to allow the noun to be converted back into a verb (because nouns ordinarily beget nouns). The irregular past-tense forms *flew* and *flown* are sealed in memory, and *-ed* is suffixed as the default, generating *flied out*.

or *stood* to percolate up from the entries for *ring* or *stand*. With the irregular form sealed in memory, the suffixation rule steps in as the default, yielding *ringed* and *grandstanded*. Many examples, involving diverse constructions from several language families, have been documented from naturalistic sources and experimentally elicited from children and adults [3,50,60,61]. Apparent counterexamples exist, but virtually all can independently be shown to be cases where people do not assign an exocentric structure to the word [3,60].

There have been three connectionist explanations. One is that if a pattern associator had semantic as well as phonological input units, a complex word with an altered meaning would dilute the associations to irregular forms, favoring the competing regular [62,63]. However, in almost every case in which an irregular

word's meaning changes, the irregular form is in fact retained, such as metaphors (*straw men*/**mans*, *sawteeth*, *God's children*) and idioms (*cut*/**cutted a deal*, *took a leak*, *hit the fan*, *put them down*) [2,3,50]. Accordingly, experiments have shown that just changing the meaning of an irregular verb does not cause people to switch to the regular [60,61]. Although all complex and derived words are semantically different from their bases, when semantic similarity and exocentric structure are unconfounded in a regression, exocentric structure accounts for a significant proportion of the variance in choice of inflectional form, and semantic similarity does not [60].

Equally unpromising is the suggestion that people regularize words to avoid ambiguity [63–65]. Many idioms are ambiguous between literal and idiomatic senses, such as *bought the farm* and *threw it up*, or among different idiomatic senses as well, such as *blew away* (impressed, assassinated), but this does not lead people to switch to a regular to disambiguate one of them (*buyed the farm*, *throwed up*). Conversely, *grandstood* and *low-lives* are unambiguous, but people still find them ungrammatical.

One connectionist model added nodes representing the semantic similarity of the verb to the homophonous noun (e.g. *to ring* and *a ring*) [64]. The network can then be trained to have these nodes turn off irregular patterns and turn on the regular one. But these unusual nodes are not part of the semantic representation of a verb itself; they are an explicit encoding of the verb's relation to the noun that heads it—that is, a crude implementation of morphological structure. In addition, the modelers had to train the network on regular past tenses of denominal verbs homophonous with irregulars. But such homophones are virtually absent from speech addressed to children, who nonetheless tend to regularize exocentric forms [61].

Neuropsychological dissociations

According to WR and DP, damage to the neural substrate for lexical memory should cause a greater impairment of irregular forms (and any regular forms that are dependent on memory storage), and a diminution of the tendency to analogize novel irregular-sounding forms according to stored patterns (as in *spling-splung*). In comparison, damage to the substrate for grammatical combination should cause a greater impairment of the use of the rule in regular forms, and of its generalization to novel forms.

Anomia is an impairment in word finding often associated with damage to left temporal/temporoparietal regions (see Fig. 3a). Patients often produce fluent and largely grammatical speech, suggesting that the lexicon is more impaired than grammatical combination [66]. In elicited past-tense production tasks, patients (compared with controls) do worse with irregular than with regular verbs (Fig. 3b), produce regularization errors like *swimmed* (which occur when no memorized form comes to mind and the rule applies

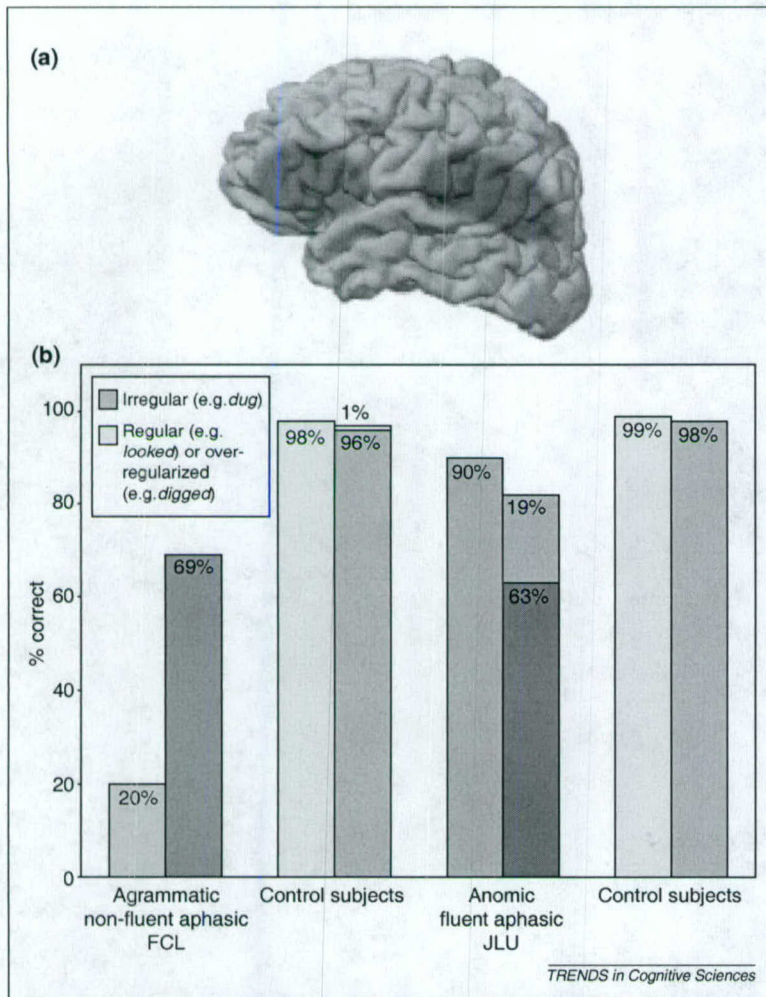


Fig. 3. Dissociating regular and irregular processing in aphasia. (a) The approximate lesion sites of patient FCL (red area, left anterior perisylvian regions), who had symptoms of agrammatism, and patient JLU (green area, left temporo-parietal region), who had symptoms of anomia. (b) Results of verb-inflection tests showed that the agrammatic patient had more trouble inflecting regular verbs (lighter bars) than irregular verbs (darker bars), whereas the anomic patient had more trouble inflecting irregular verbs – and overapplied the regular suffix to many of the irregulars (light green bar on top of dark green bar). The performance of age- and education-matched control subjects is shown in the grey bars.

as the default), rarely analogize irregular patterns to novel words (e.g. *spling-splung*), and are relatively unimpaired at generating novel regular forms like *plammed* [26,67,68]. Agrammatism, by contrast, is an impairment in producing fluent grammatical sequences, and is associated with damage to anterior perisylvian regions of the left hemisphere [69,70]. As predicted, agrammatic patients show the opposite pattern: more trouble inflecting regular than irregular verbs, a lack of errors like *swimmed*, and great difficulty suffixing novel words [26,67]. Similar effects have been documented in reading aloud, writing to dictation, repeating and judging words (even when controlling for frequency and length) [67], and in a regular/irregular contrast with Japanese-speaking patients [71].

The predicted double dissociation patterns are also seen in a comparison of neurodegenerative diseases. Alzheimer's disease (AD) is marked by greater

degeneration of medial and neocortical temporal lobe structures than of frontal cortex (particularly Broca's area) and the basal ganglia, and greater impairment of lexical and conceptual knowledge than of motor and cognitive skills, including aspects of grammatical processing [72]. Parkinson's disease (PD), associated with basal ganglia degeneration, is marked by greater impairment of motor and cognitive skills (including grammatical processing) than use of words and facts [72,73]. As predicted, AD patients have more trouble inflecting irregular than regular verbs, are relatively unimpaired at suffixing novel words, generate few irregular analogies for novel words, and produce over-regularization errors; PD patients show the contrasting patterns [26,32]. Moreover, the performance patterns correlate with the severity of the associated processing impairments in the two populations: anomia in AD, and right-side hypokinesia (an index of left-hemisphere basal ganglia degeneration) in PD [26,32].

Intriguingly, Huntington's Disease (HD), caused by degeneration of different basal ganglia structures, results in disinhibition of the projected frontal areas, leading to unsuppressible movements [73]. When HD patients inflect verbs, they show a third pattern: producing extra suffixes for regular and novel words like *walkeded*, *plaggged* and *dugged*, but not analogous errors on irregulars like *dugugor* or *keptet* – suggesting that these errors are instances of unsuppressed regular suffixation [26,32].

Converging findings come from other methodologies. In normal subjects, both regular and irregular inflected forms can prime their stems. By hypothesis, a regular form is parsed into affix and stem (which primes itself); an irregular form is associated with its stem, somewhat like semantic priming. Patients with left inferior frontal damage do not show regular priming (*walked-walk*), although they retain irregular priming (*found-find*) and semantic priming (*swan-geese*). A patient with temporal-lobe damage showed the opposite pattern [68,74,75]. In studies that have recorded event-related potentials (ERPs) to printed words, when a regular suffix is placed on an irregular word (e.g. the German *Muskels*) or omitted where it is obligatory (e.g. 'Yesterday I walk'), the electrophysiological response is similar to the Left Anterior Negativity (LAN) commonly seen with syntactic violations. When irregular inflection is illicitly applied (e.g. the German *Karusellen*) or omitted (e.g. 'Yesterday I dig'), the response is a central negativity similar to the N400 elicited by lexical anomalies, including pronounceable non-words [40,76–79]. This suggests that the brain processes regular forms like syntactic combinations and irregular forms like words.

Double dissociations are difficult to explain in pattern associators, because except for artificially small networks, 'lesioning' the networks hurts irregular forms more than regular ones [80]. A recent interesting model by Joanisse and Seidenberg

conceded that distinct subsystems have to be lesioned to produce double dissociations [81]. Although they called these modules 'phonological' and 'semantic,' the semantic module was in fact a lexicon: it had one unit dedicated to each word, with no representation of meaning. The finding that lesioning a lexicon differentially impairs irregular inflection is exactly what WR predicts. Moreover, the model failed to duplicate the finding that agrammatic patients have more trouble with regular than irregular verbs [26,67]. Lesioning the phonology module caused a consistent selective deficit only with novel verbs; regulars were no harder than irregulars. The report also claims that because a novel form has no meaning, 'the only way to generate its past tense is by analogy to known phonological forms' [81]. This predicts that patient groups should have parallel tendencies to generalize regular and irregular inflection to novel words (*planned* and *splung*, respectively), whereas in fact these tendencies dissociate [32,67]. Finally, the model predicts that selective difficulty with irregular forms should depend on semantic deficits. Miozzo reports an amonic patient who had difficulty accessing word forms but not word meanings; nonetheless, he had trouble with irregulars but not with regulars [82].

The future of the past-tense debate

The Rumelhart–McClelland model was deservedly influential, we believe, because it captured a real phenomenon. The persistence of families of irregular verbs with overlapping partial similarities, and people's use and occasional generalization of these family patterns according to similarity and frequency, can be simply explained by the assumption that human memory is partly superpositional and associative. Theories that try to explain every instance of redundancy among words using the same combinatorial mechanism used for productive syntax and regular morphology require needless complexity and esoteric representations, and fail to capture the many linguistic, psychological and neuropsychological phenomena in which irregular forms behave like words.

At the same time, the post-RMM connectionist models have revealed the problems in trying to explain *all* linguistic phenomena with a single pattern-associator architecture. Each model has been tailored to account for one phenomenon explained by the WR theory; unlike RMM, few models account for more than one phenomenon or predict new ones. And modelers repeatedly build in or presuppose surrogates for the linguistic phenomena they claim to eschew, such as lexical items, morphological structure and concatenation operations. We predict that the need for structured representations and combinatorial operations would assert itself even more strongly if modelers included phenomena that are currently ignored in current simulations, such as syntax and its interaction with inflection, the massively productive combinatorial inflection of polysynthetic languages, and the psychological events concealed by providing the models with correct past-tense forms during training (i.e. children's ability to recognize an input as a past-tense form, retrieve its stem from memory, compute their own form, and compare the two).

As an increasing number of linguistic and neuropsychological phenomena are addressed, especially the complex data from neuroimaging, inadequacies will no doubt be revealed in both kinds of models. Nothing in linguistics prevents theories from appealing to richer conceptions of memory than simple rote storage. Neither does neural network modeling prohibit structured or abstract representations, combinatorial operations, and subsystems for different kinds of computation. The adversarial nature of scientific debate might sometimes have prevented both sides from acknowledging that features of one model may correspond to constructs of the other, described at a different level of analysis. We suspect that allowing a full range of data to tell us which processes are most naturally explained by which kinds of mechanisms, rather than shoe-horning all phenomena into a single mechanism favored by one or another camp, holds the best hope for an eventual resolution of the past-tense debate.

Acknowledgements

We dedicate this paper to David Rumelhart and Jay McClelland, in acknowledgement of the stimulating effect of their model on psycholinguistic and neurolinguistic research. S.P. was supported by NIH grant HD-18381. M.T.U. was supported by a McDonnell-Pew grant in Cognitive Neuroscience, NSF SBR-9905273, NIH MH58189, and Army DAMD-17-93-V-3018/3019/3020 and DAMD-17-99-2-9007.

References

- 1 Rumelhart, D.E. and McClelland, J.L. (1986) On learning the past tenses of English verbs. In *Parallel Distributed Processing: Explorations in the Microstructures of Cognition* (Vol. 2) (McClelland, J.L. et al., eds), pp. 216–271, MIT Press
- 2 Pinker, S. and Prince, A. (1988) On language and connectionism: analysis of a parallel distributed processing model of language acquisition. *Cognition* 28, 73–193
- 3 Pinker, S. (1999) *Words and Rules: The Ingredients of Language*, HarperCollins
- 4 Marcus, G.F. (2001) *The Algebraic Mind: Integrating Connectionism and Cognitive Science*, MIT Press
- 5 Ullman, M.T. (2001) A neurocognitive perspective on language: the declarative/procedural model. *Nat. Rev. Neurosci.* 2, 717–726
- 6 Lima, S.D. et al. (eds) (1994) *The Reality of Linguistic Rules*, John Benjamins
- 7 Nootboom, S. et al. (eds) (2002) *Storage and Computation in the Language Faculty*, Kluwer
- 8 McClelland, J.L. and Patterson, K. (2002) Rules or connections in past-tense inflections: what does the evidence rule out? *Trends Cog. Sci.* 6, 465–472
- 9 Berko, J. (1958) The child's learning of English morphology. *Word* 14, 150–177
- 10 Chamberlain, A.F. (1906) Preterite forms, etc., in the language of English-speaking children. *Mod. Lang. Notes* 21, 42–44
- 11 Marcus, G.F. et al. (1992) Overregularization in language acquisition. *Monogr. Soc. Res. Child Dev.* 57, 1–165
- 12 Chomsky, N. (1959) A review of B.F. Skinner's *Verbal Behavior*. *Language* 35, 26–58
- 13 Pinker, S. (1984) *Language Learnability and Language Development*, Harvard University Press
- 14 Clahsen, H. (1999) Lexical entries and rules of language: a multidisciplinary study of German inflection. *Behav. Brain Sci.* 22, 991–1060
- 15 Chomsky, N. and Halle, M. (1968/1991) *The Sound Pattern of English*, MIT Press
- 16 Halle, M. and Mohanan, K.P. (1985) Segmental phonology of modern English. *Linguistic Inquiry* 16, 57–116
- 17 Halle, M. and Marantz, A. (1993) Distributed morphology and the pieces of inflection. In *The View from Building 20* (Hale, K. and Keyser, S.J., eds), MIT Press
- 18 Plunkett, K. and Marchman, V. (1993) From rote learning to system building: acquiring verb morphology in children and connectionist nets. *Cognition* 48, 21–69
- 19 Elman, J. et al. (1996) *Rethinking Innateness: A Connectionist Perspective on Development*, MIT Press

- 20 Prasada, S. and Pinker, S. (1993) Generalization of regular and irregular morphological patterns. *Lang. Cogn. Proc.* 8, 1–56
- 21 Xu, F. and Pinker, S. (1995) Weird past tense forms. *J. Child Lang.* 22, 531–556
- 22 Jackendoff, R.S. (1975) Morphological and semantic regularities in the lexicon. *Language* 51, 639–671
- 23 Aronoff, M. (1976) *Word Formation in Generative Grammar*, MIT Press
- 24 Lieber, R. (1980) On the organization of the lexicon. In *Linguistics and Philosophy*, MIT
- 25 Bresnan, J. (1978) A realistic transformational grammar. In *Linguistic Theory and Psychological Reality* (Halle, J.B. and Miller, G., eds), MIT Press
- 26 Ullman, M.T. et al. (1997) A neural dissociation within language: evidence that the mental dictionary is part of declarative memory, and that grammatical rules are processed by the procedural system. *J. Cogn. Neurosci.* 9, 266–276
- 27 Mishkin, M. et al. (1984) Memories and habits: Two neural systems. In *Neurobiology of Learning and Memory* (Lynch, G. et al., eds), pp. 65–77, Guilford Press
- 28 Squire, L.R. and Knowlton, B.J. (2000) The medial temporal lobe, the hippocampus, and the memory systems of the brain. In *The New Cognitive Neurosciences* (Gazzaniga, M.S., ed.), pp. 765–780, MIT Press
- 29 Jackendoff, R. (2002) *Foundations of Language: Brain, Meaning, Grammar, Evolution*, Oxford University Press
- 30 Ullman, M.T. (1993) The computation of inflectional morphology. In *Department of Brain and Cognitive Sciences*, pp. 263, Massachusetts Institute of Technology
- 31 Ullman, M.T. (2001) The declarative/procedural model of lexicon and grammar. *J. Psycholinguist. Res.* 30, 37–69
- 32 Ullman, M.T. Evidence that lexical memory is part of the temporal lobe declarative memory, and that grammatical rules are processed by the frontal/basal-ganglia procedural system. *Brain Lang.* (in press)
- 33 Badecker, W. and Caramazza, A. (1991) Morphological composition in the lexical output system. *Cogn. Neuropsychol.* 8, 335–367
- 34 Burani, C. et al. (1984) Morphological structure and lexical access. *Vis. Lang.* 18, 348–358
- 35 Baayen, R.H. et al. (1997) Singulars and plurals in Dutch: evidence for a parallel dual-route model. *J. Mem. Lang.* 37, 94–117
- 36 Balota, D.A. and Ferraro, R. (1993) A dissociation of frequency and regularity effects in pronunciation performance across young adults, older adults, and individuals with senile dementia of the Alzheimer types. *J. Mem. Lang.* 32, 573–592
- 37 Balota, D.A. and Spieler, D.H. (1997) The utility of item-level analyses in model evaluation: a reply to Seidenberg and Plaut. *Psychol. Sci.* 9, 238–240
- 38 Besner, D. et al. (1990) On the connection between connectionism and data: are a few words necessary? *Psychol. Rev.* 97, 432–446
- 39 Coltheart, M. et al. (1993) Models of reading aloud: dual-route and parallel-distributed-processing approaches. *Psychol. Rev.* 100, 589–608
- 40 Ullman, M.T. et al. Sex differences in the neurocognition of language. *Brain Lang.* (in press)
- 41 Ullman, M.T. and Gopnik, M. (1999) Inflectional morphology in a family with inherited specific language impairment. *Appl. Psycholinguist.* 20, 51–117
- 42 van der Lely, H.K.J. and Ullman, M.T. (2001) Past tense morphology in specifically language impaired and normally developing children. *Lang. Cogn. Proc.* 16, 177–217
- 43 Ullman, M.T. (2001) The neural basis of lexicon and grammar in first and second language: the declarative/procedural model. *Bilingual. Lang. Cogn.* 4, 105–122
- 44 Alegre, M. and Gordon, P. (1999) Frequency effects and the representational status of regular inflections. *J. Mem. Lang.* 40, 41–61
- 45 Sproat, R. (1992) *Morphology and Computation*, MIT Press
- 46 Hare, M. et al. (1995) Default generalization in connectionist networks. *Lang. Cogn. Proc.* 10, 601–630
- 47 Hare, M. and Elman, J. (1992) A connectionist account of English inflectional morphology: evidence from language change. In *14th Annu. Conf. Cogn. Sci. Soc.*, pp. 265–270, Erlbaum
- 48 Nakisa, R.C. and Hahn, U. (1996) Where defaults don't help: the case of the German plural system. In *Proc. 18th Annu. Conf. Cogn. Sci. Soc.* (Cottrell, G.W., ed.), pp. 177–182, Erlbaum
- 49 Hahn, U. and Nakisa, R.C. (2000) German inflection: single route or dual route? *Cogn. Psychol.* 41, 313–360
- 50 Marcus, G.F. et al. (1995) German inflection: the exception that proves the rule. *Cogn. Psychol.* 29, 189–256
- 51 Marcus, G.F. (1995) The acquisition of inflection in children and multilayered connectionist networks. *Cognition* 56, 271–279
- 52 Marcus, G.F. (1995) Children's overregularization of English plurals: a quantitative analysis. *J. Child Lang.* 22, 447–459
- 53 Forrester, N. and Plunkett, K. (1994) Learning the Arabic plural: the case for minority default mappings in connectionist networks. In *16th Annu. Conf. Cogn. Sci. Soc.*, Erlbaum
- 54 Plunkett, K. and Nakisa, R. (1997) A connectionist model of the Arab plural system. *Lang. Cogn. Proc.* 12, 807–836
- 55 Berent, I. et al. The nature of regularity and irregularity: evidence from Hebrew nominal inflection. *J. Psycholinguist. Res.* (in press)
- 56 Berent, I. et al. (1999) Default nominal inflection in Hebrew: evidence for mental variables. *Cognition* 72, 1–44
- 57 Kiparsky, P. (1982) Lexical phonology and morphology. In *Linguistics in the Morning Calm* (Yang, I.S., ed.), pp. 3–91, Hansin, Seoul.
- 58 Williams, E. (1981) On the notions of 'lexically related' and 'head of a word'. *Linguist. Inq.* 12, 245–274
- 59 Selkirk, E.O. (1982) *The Syntax of Words*, MIT Press
- 60 Kim, J.J. et al. (1991) Why no mere mortal has ever flown out to center field. *Cogn. Sci.* 15, 173–218
- 61 Kim, J.J. et al. (1994) Sensitivity of children's inflection to morphological structure. *J. Child Lang.* 21, 173–209
- 62 MacWhinney, B. and Leinbach, J. (1991) Implementations are not conceptualizations: revising the verb learning model. *Cognition* 40, 121–157
- 63 Harris, C.L. (1992) Understanding English past-tense formation: the shared meaning hypothesis. In *Proc. 14th Annu. Conf. Cogn. Sci. Soc.*, Erlbaum
- 64 Daugherty, K.G. et al. (1993) Why no mere mortal has ever flown out to center field but people often say they do. In *15th Annu. Conf. Cogn. Sci. Soc.*, Erlbaum
- 65 Shirai, Y. (1997) Is regularization determined by semantics, or grammar, or both? Comments on Kim, Marcus, Pinker, Hollander & Coppola. *J. Child Lang.* 24, 495–501
- 66 Goodglass, H. (1993) *Understanding Aphasia*, Academic Press
- 67 Ullman, M.T. et al. Neural correlates of lexicon and grammar: evidence from the production, reading, and judgment of inflection in aphasia. *Brain Lang.* (in press)
- 68 Tyler, L.K. et al. (2002) Dissociations in processing past tense morphology: neuropathology and behavioral studies. *J. Cogn. Neurosci.* 14, 79–94
- 69 Alexander, M.P. (1997) Aphasia: clinical and anatomic aspects. In *Behavioral Neurology and Neuropsychology* (Feinberg, T.E. and Farah, M.J., eds), pp. 133–150, McGraw-Hill
- 70 Damasio, A.R. (1992) Aphasia. *N. Engl. J. Med.* 326, 531–539
- 71 Hagiwara, H. et al. (1999) Neurolinguistic evidence for rule-based nominal suffixation. *Language* 75, 739–763
- 72 Feinberg, T.E. and Farah, M.J. (eds) (1997) *Behavioral Neurology and Neuropsychology*, McGraw-Hill
- 73 Jankovic, J. and Tolosa, E.E. (1993) *Parkinson's Disease and Movement Disorders*, Williams & Wilkins
- 74 Marslen-Wilson, W.D. and Tyler, L.K. (1997) Dissociating types of mental computation. *Nature* 387, 592–594
- 75 Marslen-Wilson, W.D. and Tyler, L.K. (1998) Rules, representations, and the English past tense. *Trends Cogn. Sci.* 2, 428–435
- 76 Weyerts, H. et al. (1997) Brain potentials indicate differences between regular and irregular German plurals. *Neuroreport* 8, 957–962
- 77 Penke, M. et al. (1997) How the brain processes complex words: an event-related potential study of German verb inflections. *Cogn. Brain Res.* 6, 37–52
- 78 Gross, M. et al. (1998) Human brain potentials to violations in morphologically complex Italian words. *Neurosci. Lett.* 241, 83–86
- 79 Rodriguez-Fornells, A. et al. (2001) Event-related brain responses to morphological violations in Catalan. *Cogn. Brain Res.* 11, 47–58
- 80 Bullinaria, J.A. and Chater, N. (1995) Connectionist modeling: implications for cognitive neuropsychology. *Lang. Cogn. Proc.* 10, 227–264
- 81 Joanisse, M.F. and Seidenberg, M.S. (1999) Impairments in verb morphology after brain injury: a connectionist model. *Proc. Natl. Acad. Sci. U. S. A.* 96, 7592–7597
- 82 Miozzo, M. On the processing of regular and irregular forms of verbs and nouns: evidence from neuropsychology. *Cognition* (in press)

Research article

Sources of variability and effect of experimental approach on expression profiling data interpretation

Marina Bakay¹, Yi-Wen Chen¹, Rehannah Borup¹, Po Zhao¹,
Kanneboyina Nagaraju² and Eric P Hoffman^{*1}

Address: ¹Research Center for Genetic Medicine, Children's National Medical Center, 111 Michigan Avenue, N.W., Washington, DC 20010 USA and ²Division of Rheumatology, Johns Hopkins School of Medicine, Ross 1042, Baltimore MD, USA

E-mail: Marina Bakay - mbakay@cnmc.org; Yi-Wen Chen - ychen@cnmc.org; Rehannah Borup - rborup@cnmc.org; Po Zhao - pzhao@cnmcresearch.org; Kanneboyina Nagaraju - knagaraj@mail.jhmi.edu; Eric P Hoffman^{*} - ehoffman@cnmcresearch.org

^{*}Corresponding author

Published: 31 January 2002

BMC Bioinformatics 2002, 3:4

Received: 27 November 2001

Accepted: 31 January 2002

This article is available from: <http://www.biomedcentral.com/1471-2105/3/4>

© 2002 Bakay et al; licensee BioMed Central Ltd. Verbatim copying and redistribution of this article are permitted in any medium for any purpose, provided this notice is preserved along with the article's original URL.

Abstract

Background: We provide a systematic study of the sources of variability in expression profiling data using 56 RNAs isolated from human muscle biopsies (34 Affymetrix MuscleChip arrays), and 36 murine cell culture and tissue RNAs (42 Affymetrix U74Av2 arrays).

Results: We studied muscle biopsies from 28 human subjects as well as murine myogenic cell cultures, muscle, and spleens. Human MuscleChip arrays (4,601 probe sets) and murine U74Av2 Affymetrix microarrays were used for expression profiling. RNAs were profiled both singly, and as mixed groups. Variables studied included tissue heterogeneity, cRNA probe production, patient diagnosis, and GeneChip hybridizations. We found that the greatest source of variability was often different regions of the same patient muscle biopsy, reflecting variation in cell type content even in a relatively homogeneous tissue such as muscle. Inter-patient variation was also very high (SNP noise). Experimental variation (RNA, cDNA, cRNA, or GeneChip) was minor. Pre-profile mixing of patient cRNA samples effectively normalized both intra- and inter-patient sources of variation, while retaining a high degree of specificity of the individual profiles (86% of statistically significant differences detected by absolute analysis; and 85% by a 4-pairwise comparison survival method).

Conclusions: Using unsupervised cluster analysis and correlation coefficients of 92 RNA samples on 76 oligonucleotide microarrays, we found that experimental error was not a significant source of unwanted variability in expression profiling experiments. Major sources of variability were from use of small tissue biopsies, particularly in humans where there is substantial inter-patient variability (SNP noise).

Background

Expression profiling is an emerging experimental method whereby RNA accumulation in cells and tissues can be assayed for many thousands of genes simultaneously in a single experiment. There are two common experimental

platforms for expression profiling: redundant oligonucleotide arrays (Affymetrix GeneChips) [1], and spotted cDNA microarrays [2-4]. The Affymetrix GeneChips have the inherent advantages of redundancy, specificity, and transportability; there are typically 30-40 oligonucleotide

probes (features) designed against each gene tested by the array, with paired perfect-match and mismatch probes, with standardized factory synthesis of arrays [5,6]. The uniform nature of the arrays permits databasing of individual profiles, which facilitates comparison of data generated by different laboratories.

Expression profiling has led to dramatic advances in understanding of yeast biology, where homogeneous cultures can be grown and exposed to timed environmental variables [7–12]. Such studies have led to the rapid assignment of function to a large number of anonymous gene sequences. Large-scale expression profiling studies of tissues from higher vertebrates are more challenging, due to the higher complexity of the genome, larger related gene families, and incomplete genomic resources. Nevertheless, DNA microarrays have been successfully applied in the analysis of aging and caloric restriction [13] and pulmonary fibrosis [14]. And many publications, particularly on cancer, have appeared [14–19]. Affymetrix has recently announced the availability of the U133 GeneChip series with 33,000 well-characterized human genes mined from genomic sequence. The nearly complete ascertainment of genes in the human genome should make expression-profiling studies of human tissues particularly powerful. However, identification of the sources of experimental variability, and knowledge of the relative contribution of variation from each source, is critical for appropriate experimental design in expression profiling experiments.

Mills and Gordon recently studied the relative contribution of experimental variability of probe production on the reproducibility of microarray results using mixed murine tissue RNA on Affymetrix Mu11K GeneChips [20]. In their study, the same RNA preparation was used as a template for distinct cDNA/cRNA amplifications and hybridizations. An additional variable studied was the effect of different laboratories processing the same RNAs. The authors found relatively poor concordance between duplicate arrays, with an average of 12% increase/decrease calls between the same RNA processed in parallel and hybridized to two Mu11K-A microarrays. The authors concluded that there was substantial experimental variability in the experimental procedure, necessitating extensive filtering and large numbers of arrays to detect accurate gene expression changes (LUT: look-up tables) [20]. In our laboratory, we have processed over 1,200 Affymetrix arrays, and have found significantly higher experimental reproducibility ($R^2 = 0.979$ for new generation U74A version 2 murine arrays or human U95 series, see Result and Discussion). In addition, a recent publication of a single human patient, where RNA was prepared from two distinct breast tumors, and placed on duplicate U95A GeneChips (four chips total) found a very low degree of experimental variability between microarrays ($R^2 = 0.995$), and be-

tween the two tumors ($R^2 = 0.987$) [21]. The marked differences in experimental variability between laboratories could be due to different quality control protocols (see [<http://microarray.cnmcresearch.org>]), newer more robust Affymetrix arrays now available (murine Mu11K versus U74A version 2 and new generation human U95 series), use of more recent algorithms for data interpretation, or due to more consistent processing of RNA, cDNA, and cRNA in the same laboratory.

The previous studies did not systematically address the reproducibility of GeneChip hybridization (e.g. the same biotinylated cRNA on two different microarrays). In addition to lingering questions concerning variability due to specific experimental procedures, there are other possible sources of variability that have not yet been investigated, specifically tissue heterogeneity and inter-individual variation. The latter two sources of variability are particularly important in human expression profiling studies. The study of human tissues often involves the use of tissue biopsies, where a relatively limited region of an organ is sampled. Tissue heterogeneity and sampling error might be expected to introduce significant variability in expression profiles. Second, tissues may derive from individuals from different ethnic backgrounds; humans are highly outbred, leading to the potential of significant polymorphic noise (herein called "SNP noise") between individuals unrelated to the disease or variable under study. SNP noise also exists between different inbred mouse strains, and some experiments have normalized this effect by breeding the same mutation on different strains, and profiling each individually [22]. Knowledge of the relative effect of each experimental, tissue, and patient variable on expression profiling results in humans is important, so that appropriate experimental designs can be employed.

We recently reported the design and production of a highly redundant oligonucleotide microarray for analysis of human muscle biopsies (Borup et al. *submitted*). This MuscleChip contains 4,601 probe sets corresponding to 3,369 distinct genes and ESTs expressed in human muscle. Each probe set contains between 16 to 40 oligonucleotides, such that the number of specific oligonucleotide probes on the array was 138,000.

Here, we utilize this MuscleChip to investigate the relative significance of variables affecting expression profiling data and interpretation. Specifically, we studied the correlation coefficients of profiles considering the following variables: 1. variation due to probe production (same RNA); 2. variation due to the microarray itself (same cRNA on different GeneChips); 3. tissue heterogeneity (different regions of the same muscle biopsy); 4. inter-patient variability (SNP noise); 5. diagnosis (underlying pathological variable); and 6. patient age.

Table 1: Patient data and characteristics of 34 MuscleChip expression profiles.

Patients/ Arrays	Individual or Mixed	Age (years)	Stage of histopathology	Scaling Factor	% Present Calls	% Diff Calls Paired samples	Four comparisons > 2-fold changes relative to controls 1a, 1b
1a 1b	Ind	5.5	mid	1.08 0.9	51 50	5.6	302
2a 2b	Ind	4.5	early stage	1.93 3.28	38 36	3	427
3a 3b	Ind	5	early/mid stage	0.53 0.97	49 44	8.6	312
3a-dup 3b-dup	Ind	5	early/mid stage	0.46 0.82	50 46	0.8 2.1	N/A
4a 4b	Ind	6	mid	0.78 1.02	51 50	18	324
5a 5b	Ind	5	early	1.26 2.13	51 40	6.2	453
6a 6b	Ind	12	mid	2.72 2.46	35 38	1.5	305
7a 7b	Ind	11	mid/moderate	0.79 0.9	51 49	2.6	356
8a 8b	Ind	10	mid	1.24 1.74	49 50	1.5	463
9a 9b	Ind	11	variable	1.04 1.37	50 46	8.5	266
10a 10b	Ind	10	mid/late	0.48 0.75	52 48	1.5	250
6-9mix-1a 6-9mix-1b	mix mix	6 to 9	5 patients biopsies, cRNAs mixed	0.82 1.16	49 55	3.2	289
5-6mix-1a 5-6mix-1b	mix mix	5 to 6	5 patients biopsies, cRNAs mixed	0.67 1.03	60 58	0.5	486

Table 1: Patient data and characteristics of 34 MuscleChip expression profiles. (Continued)

10-12mix-1a	mix	10 to 12	5 patients biopsies, cRNAs mixed	0.82	49	0.4	388
10-12mix-1b	mix			1.16	55		
control 1a	mix	6 to 9	5 normal biopsies, cRNAs mixed	0.71	53	1.5	N/A
control 1b	mix			0.48	54		
control 2a	mix	5 to 12	3 normal biopsies, cRNAs mixed	0.86	54	0.8	N/A
control 2b	mix			0.78	53		
control 3a	mix	4 to 13	3 normal biopsies, cRNAs mixed	0.95	51	1.1	N/A
control 3b	mix			0.78	55		

We have recently reported generation of expression profiling results using mixed patient samples [23]. Our hypothesis was that mixing of RNA samples from multiple regions of muscle biopsies, and from multiple patients matched for most variables (disease, age, sex), would effectively normalize both intra-patient variability (tissue heterogeneity), and inter-patient variability (SNP noise; e.g. normal human polymorphic variation unrelated to the primary defect). Here, we test this hypothesis directly, and show that sample mixing does indeed result in relatively high sensitivity and specificity for gene expression changes that would be detected by many individual expression profiles. Thus, sample mixing appears to be an appropriate first-pass method to obtain the most significant expression changes, while using small numbers of arrays.

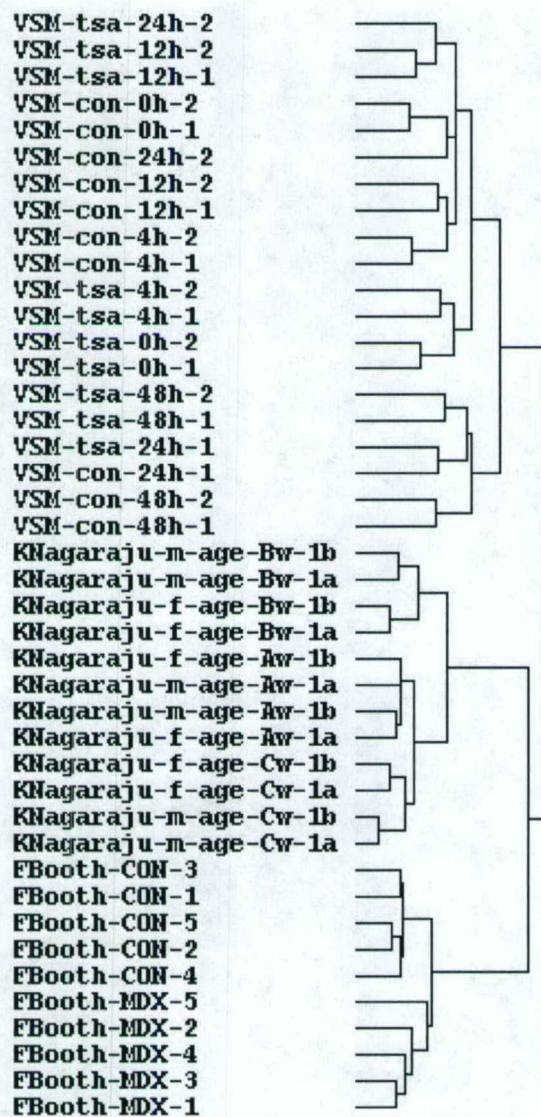
Results and discussion

Fifty six (56) different RNA samples were prepared from different regions of muscle biopsies from 28 individuals (15 Duchenne muscular dystrophy (DMD) patients, 13 normal controls). The profiles of five of the DMD patients and the five controls have been previously reported using the Affymetrix HuFL microarray [23]; however, we re-tested these same samples on the custom MuscleChip (Borup et al. *submitted*) for comparison to the other patients here. All RNAs were converted to double-stranded cDNA, and then to biotinylated cRNA. The cRNAs were then hybridized to the MuscleChip either singly, in mixed groups, or both, as described below. In total, 34 hybridizations were performed, scanned, and the data statistically analyzed using Affymetrix Microarray Suite and Excel. Quality control criteria were as described on our web site (<http://microarray.cnmcresearch.org>), link to "programs in genomic

applications"), and included sufficient cRNA amplification, and adequate post-hybridization scaling factors. Scaling factors (normalization needed to reach a common target intensity) ranged from 0.46 to 3.28 (Table 1). All raw image files, processed image files, and difference analyses are posted on a web-queried SQL database interface to our Affymetrix LIMS Oracle warehouse (see <http://microarray.cnmcresearch.org>) : link to "programs in genomic applications", "data", "human").

Among the 4,601 probe sets on the Affymetrix custom muscle microarray, we found a consistent percentage of "present" calls for each of the 34 cRNA samples tested (Duchenne dystrophy, 28 arrays, $48.2\% \pm 6.1\%$; controls 6 arrays, $53.3\% \pm 1.4\%$). To test for inter-array variability, two different hybridization solutions were applied to duplicate arrays, and correlation coefficients determined. A high correlation coefficient was found in this analysis, suggesting that inter-array variability of the MuscleChip used was a relatively minor variable (Patient 3 a and 3a-duplicate $R^2 = 0.96$ and percent shared [No Change (NC)] calls by Microarray Suite software was 99%; Patient 3b and 3b-duplicate $R^2 = 0.98$ and percent NC was 98%; Table 1). The high reproducibility of Affymetrix array results is consistent with other data in our laboratory, and from previously published data [6,21,23,24], and shows that experimental variability associated with hybridization and scanning of highly redundant oligonucleotide GeneChips is not a major source of experimental variability.

Given the previous report suggesting that the conversion of RNA to biotinylated cRNA probe was a major source of variability in murine array experiments [20], we tested a series of murine RNA from different sources, using the

**Figure 1**

Unsupervised hierarchical clustering of 42 murine U74Av2 Affymetrix arrays. Unsupervised hierarchical clustering of 42 murine U74Av2 Affymetrix arrays shows that probe synthesis and hybridization is not a major source of experimental variability. Expression profiles shown were from three different experimental groups; one using cultured murine myogenic cells (VSM samples), one using mouse spleens (KNagaraju samples), and one group from mouse skeletal muscle from normal and mdx mouse strains (FBooth samples). For the KNagaraju samples, the same spleen RNA was split prior to cDNA synthesis to create duplicate cDNA-cRNA-profile results; these duplicates show a very high correlation coefficient, and close relationship by Unsupervised clustering (low branches on dendrogram). The VSM cultured samples were each derived from different culture plates, and the FBooth samples from different murine muscles. The duplicate murine muscle samples are more closely related (high correlation coefficient) than the parallel cultures (VSM). Additional variables, such as male versus female (KNagaraju samples), and time after TSA treatment (VSM samples) are indicated, but are not relevant for this manuscript, and will be discussed in more detail elsewhere.

newer generation U74Av2 GeneChips. One series of samples was from murine spleens, where spleens from multiple animals for each variable under study were mixed, RNA isolated, RNA samples split, and duplicate cDNA, cRNA, and hybridizations processed in parallel for each RNA (Fig. 1, "KNagaraju" samples). We also compared RNAs processed from parallel murine myogenic cell cultures (Fig. 1, "VSM" samples), where each profile was from a different cell culture. Finally, we used a series of murine muscle tissues from normal and dystrophin-deficient mice, where each profile was from a different series of complete gastrocnemius muscles (Fig. 1, "FBooth" samples). The data from these 42 murine U74Av2 profiles were then analyzed by unsupervised clustering [25] to determine which profiles were most closely related to each other (Fig. 1). This analysis shows that the different sources of RNA cluster together, as expected. Importantly, the same RNA used as a template for two distinct cDNA/cRNA preparations and hybridizations showed a high correlation coefficient ($R^2 = 0.99$ for five of the six samples, with average $R^2 = 0.978$) (Fig. 1). The large muscle group profiles (FBooth samples) showed excellent correlation, both with respect to diagnosis; however here there was no sampling error as the entire muscle group was used rather than isolated biopsies. Finally, the parallel tissue culture experiments (VSM samples) showed greater variability between duplicates, suggesting that tissue culture conditions may be more subject to variability than *in vivo* tissues (Fig. 1). This murine data shows that variability from different cDNA-cRNA reactions is very low ($R^2 = 0.978$).

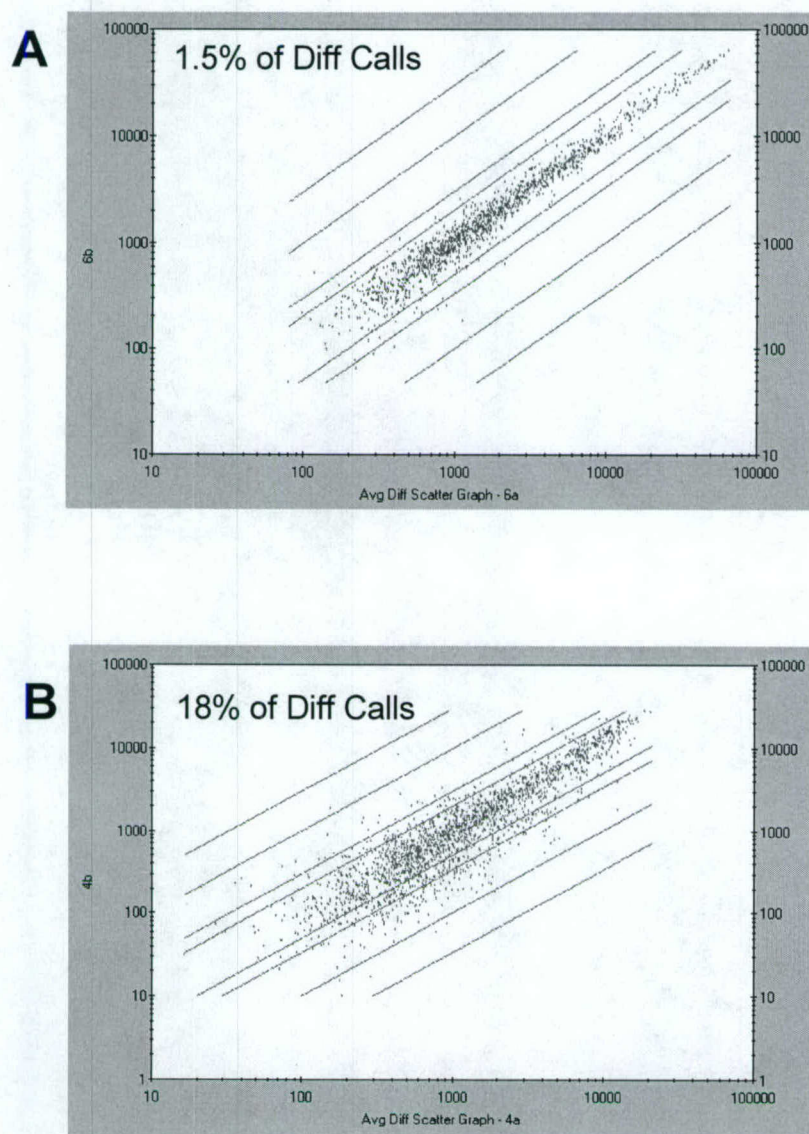
To analyze the impact of intra-patient variability (tissue heterogeneity), inter-patient variability (polymorphic noise in outbred populations), and the effect of sample mixing on the sensitivity of detection of gene expression differences between patient groups, we conducted a series of individual and mixed profiling (Table 1). Muscle biopsies from five 4–6 yr old DMD patients, and five 10–12 yr old patients were selected, each biopsy split into two parts, and RNA isolated independently from each of the 20 biopsy fragments. For these ten DMD patients, the two different regions of the same biopsy were expression profiled both individually (20 profiles), and also mixed into four pools where each pool originated from distinct RNA samples (Table 1). The resulting profiles were also compared to previously reported mixed 6–9 yr old DMD patient cRNAs, and mixed 6–9 yr old control cRNAs [23], as mentioned above.

As an initial statistical analysis, we used Affymetrix software to define genes that showed expression changes (Increased, Decreased or Marginal) in expression levels between pairs of profiles (difference analyses). This method of data interpretation showed that some muscle biopsies showed very little variance between different regions

of the same biopsy, while other patient biopsies showed considerable variability (see Fig. 2 for representative scatter graphs). Expressing this variance as a percentage of "Diff Calls" between the two regions of the same biopsy, as determined by Affymetrix default algorithms, we found considerable variability in the similarity of profiles, with values ranging from 1.5% to 18% of the 4,601 probe sets studied ($4.99\% \pm 4.94\%$). This data suggests that tissue heterogeneity (intra-patient variability) can be a major source of variation in expression profiling experiments, even when using relatively large pieces (50 mg) of relatively homogeneous tissues (such as muscle).

The most common strategy for interpreting Affymetrix microarray data is to use two profile comparisons, with an arbitrary threshold for "significant fold-change" in expression levels. Typically, multiple arrays are compared, with those gene expression changes showing the most consistent fold changes prioritized, although other methods have been reported [13,22,26,27]. To study inter-patient variability, we defined the gene expression changes surviving four pairwise comparisons with mixed control samples, as we have previously described [23]. Briefly, four comparisons were done by Affymetrix software (eg. DMD 1a versus control 1a; DMD 1a versus control 1b; DMD1b versus control 1a; DMD1b versus control 1b). The four data sets were then compared, with only those gene expression changes that showed >2-fold change in all four comparisons (four comparison survival method). The number of surviving diff calls by this method ranged from 250 to 463 (355 ± 80) (Table 1). Interestingly, those patients showing considerable variation between different regions of the same biopsy did not show a corresponding decrease in the number of gene expression changes surviving the iterative comparisons to controls (Table 1). This suggests (but does not prove) the most significant changes might be shared, independent of tissue variability (see below).

A different statistical method to determine the effect of the different variables under study is to perform hierarchical cluster analysis using nearest neighbor statistical methods [25]. Here, we subjected all profiles to unsupervised cluster analysis, as a means of determining which variables had the greatest effect (e.g. intra-patient variability [different regions of biopsy], versus diagnosis [DMD vs control], versus inter-patient variability [DMD patients in same age group], versus age of patient). For this analysis, we used the fluorescence intensity of each probe set (Average difference), after data scrubbing to remove genes that showed expression levels near background ("Absent" Calls) for all profiles (Fig. 3). This analysis shows that duplicate profiles of the same cRNA hybridization solution are the most highly related (Patient 3 a and duplicate (3a-d); 3b and duplicate (3b-d)), consistent with the high correlation found by the comparisons using Affymetrix

**Figure 2**

Different regions of the same tissue specimen can give highly similar or highly discordant expression profiles. Shown are scatter plots of the expression profiles of two different regions of the same muscle biopsy from patient 6 (Panel A), and patient 4 (Panel B). Only "present" calls are shown (~2,000 of the 4,600 probe sets studied). An example of one patient showing very high concordance between two different biopsy regions is shown (panel A), and an example of a second patient showing very poor correlation between the two biopsy fragments (panel B). The solid lines indicate two-, three-, ten- and thirty-fold difference thresholds.

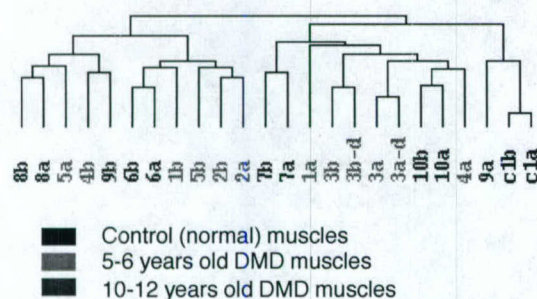


Figure 3
Unsupervised hierarchical clustering of 24 human MuscleChip Affymetrix arrays. A dendrogram of nearest neighbor analysis of 24 MuscleChip expression profiles shows that intra-patient tissue heterogeneity can be a greater source of experimental variability than inter-patient or age-dependent variation. The height of the branch-point of each tree reflects the extent of relatedness of the different profiles. The two profiles for each patient or mixed controls are from different regions of the same muscle biopsies.

Microarray Suite software described above. Again, this reflects the low amount of combined experimental variability intrinsic to the laboratory processing of RNA, cDNA, cRNA and hybridization.

When comparing two different regions of the same biopsy [intra-patient variability], we found widely varying results, depending on the patient studied (Fig. 3). For example, some individual patients showed very closely related profiles that approached the similarity of duplicate arrays on the same cRNA (Fig. 2; profiles 6a, 6b; 10a, 10b). On the other hand, some patients showed very distantly related profiles for two regions of the same biopsy (Fig. 3; profiles 1a, 1b; 4a, 4b; 9a, 9b). Importantly, the variation caused by intra-patient tissue variation often overshadowed all other variables. For example, a profile from DMD patient 9 (9a) clustered with the normal controls, rather than with the other DMD patients (Fig. 3). The histopathology of this patient was noted as being unusually variable in severity prior to expression profiling. Also, unsupervised clustering was unable to group patients of similar ages, despite DMD showing a progressive clinical course. We conclude that intra-patient tissue heterogeneity is a major source of experimental variability in expression profiling, and must be considered in experimental design.

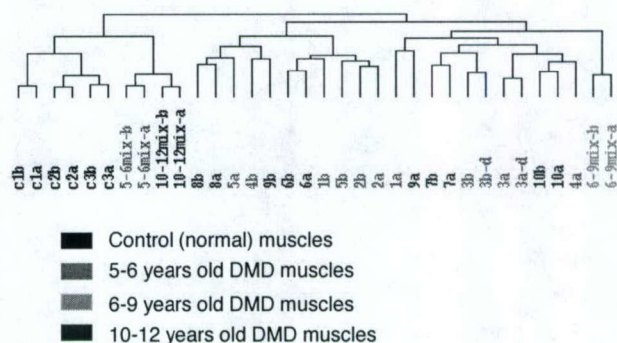


Figure 4
Unsupervised hierarchical clustering of mixed and individual profiles. Shown is a dendrogram of nearest neighbor analysis of 34 MuscleChip expression profiles including both individual and mixed samples. Mixed samples cluster as very highly related samples, even though different regions of the component biopsies were used to generate the duplicates. Importantly, the mixed DMD profiles cluster more closely with mixed normal controls than with individual DMD patient profiles. This data suggests that intra-patient (tissue heterogeneity) and inter-patient (SNP noise) can be significant sources of experimental variability.

The above findings suggested that both intra-patient variability (tissue heterogeneity) and inter-patient variability (polymorphic noise) had major effects on the expression profiles. One method to control for these sources of noise is to analyze large numbers of profiles, both on multiple patients, and on multiple regions of tissue from each patient. This would allow determinations of p values and statistical significance for a single controlled variable under study (e.g. DMD vs controls). An alternative method is to experimentally normalize these variables through mixing of samples from patient groups; such mixing would be expected to average out both intra- and inter-patient variation. The expectation is that the most significant and dramatic gene expression changes would still be identified, while using many less profiles (and thus a substantial reduction in cost of the analyses).

To test for the relative sensitivity of interpretation of sample mixing versus individual profiles, we mixed together the 10 cRNAs for the two different age groups of DMD patients (samples 1a - 5b; samples 6a - 10b). For this analysis, we also generated expression profiles for two additional groups of control individuals. One was a second set of five normal male biopsies ages 5-12 yrs (controls 2a, 2b), and the third control set was three normal

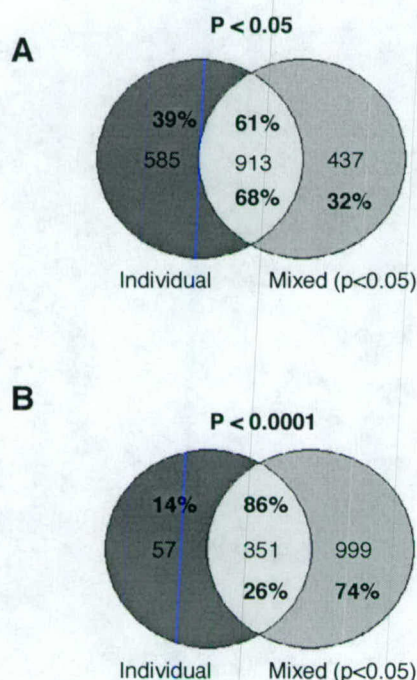


Figure 5
Comparison of individual profiles to mixed profiles by t-test statistics. Shown in green are differentially expressed genes for 2 mixed DMD 5–6 y profiles versus 6 mixed controls. Shown in red are differentially expressed genes for 10 individual DMD 5–6 y profiles and 6 mixed controls. P-value thresholds used to generate gene lists are indicated. The p-value for mixed profiles is held at $p < 0.05$, as the low sample number (2 versus 2) precludes obtaining more significant values. This analysis suggests that the use of t-test statistics for small number of mixed samples is relatively sensitive, but not highly specific.

age-matched female biopsies ages 4–13 yrs (controls 3a, 3b) (Fig. 4). As with the original male control group (control 1a, 1b), two different regions of each biopsy were processed independently through the biotinylated cRNA step, and then equimolar amounts of cRNA mixed for hybridization to the MuscleChip.

All 34 profiles (both individual and mixed samples) were again analyzed by unsupervised hierarchical clustering (Fig. 4) [25]. As described above, we scrubbed the profiles to eliminate all genes showing expression levels consistently at or below background hybridization intensities by requiring each gene to show a "Present Call" in one or more of the 34 profiles.

As above, duplicate profiles using the same cRNA hybridization solution on different arrays, whether mixed or individual samples, showed very highly correlated results (very low branch on dendrogram) (Fig. 4; mix 5–6 yrs, mix 10–12 yrs; patient 3a/3a-d; patient 3b/3b-d). As above, this indicates that experimental variability from laboratory procedures or different arrays is a relatively minor factor in interpretation of results. Mixed samples from different regions of the same biopsies showed the same, or only slightly more variation (mixed controls c1, c2, and c3, mixed DMD 6–9 yrs). This showed that sample mixing does indeed average out tissue heterogeneity (intra-patient variability), as well as inter-patient variability. We noted that all of the controls (both male and female) clustered in the same branch of the dendrogram, while the four of the six mixed DMD profiles clustered just one level away from the controls, separately from the other DMD profiles. This analysis suggests that there is considerable variability in the progressive tissue pathology induced by dystrophin deficiency, both within a patient, and between patients.

To test the sensitivity and specificity of sample mixing versus individual profiling, we defined differentially expressed genes using a two group t-test (GeneSpring [28,29]), comparing all 6 mixed control profiles and the 10 individual 5–6 yr old DMD profiles. Genes were retained that met specific p value thresholds between the two sets of profiles. In parallel, we compared the two corresponding mixed 5–6 yr old DMD profiles to the same 6 mixed control profiles.

Comparison of 10 individual 5–6 yr Duchenne dystrophy profiles to 6 mixed controls revealed 1,498 genes showing differential expression with $p < 0.05$ (Fig. 5). Comparison of the two mixed Duchenne dystrophy profiles to the 6 mixed controls showed 1,350 genes with $p < 0.05$ (Fig. 5A). Comparison of the two gene lists showed that 61% of differentially regulated genes detected by the 10 individual profiles were also detected by the two mixed profiles. This suggests that the sensitivity and specificity of using mixed samples is approximately half that of individual profiles. However, there was a rapid shift in specificity and sensitivity as stringency of the analysis was increased. Raising the statistical threshold to $p < 0.0001$ for individual profiles, while keeping the threshold for mixed profiles at $p < 0.05$ as required by the small number of data points (Fig. 5B), resulted in a sensitivity of 86% for mixed samples (351 of 408 genes $p < 0.0001$ detected). In conclusion, mixing detected about two thirds of statistically significant changes ($p < 0.05$). Mixing was a relatively sensitive method of detecting the most highly significant changes ($p < 0.0001$) (86% of changes detected), however it was not very specific; as many as one third of gene ex-

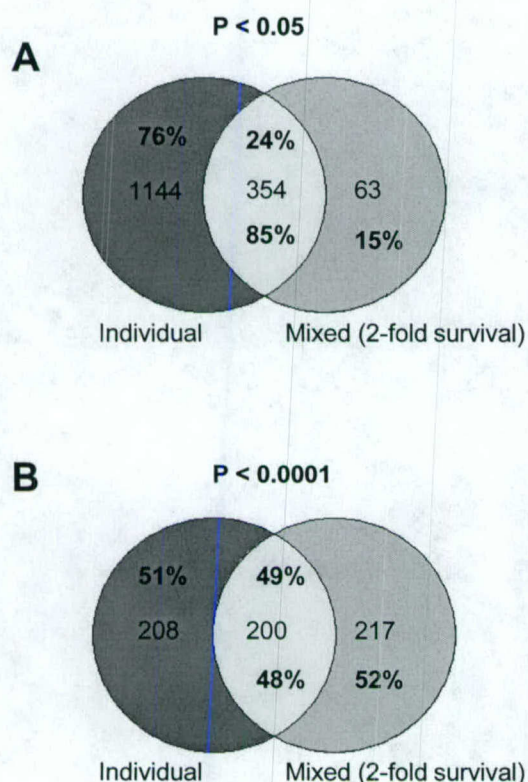


Figure 6
Use of >2-fold survival method provides relatively specific, but insensitive detection of significant gene changes. Shown in green is a representation of number of genes surviving four pair-wise comparisons to two mixed control profiles, with retention of only those genes showing fold changes > 2-fold in the four pair-wise comparisons. Shown in red are differentially expressed genes for 10 individual DMD 5–6 y profiles versus 6 mixed controls at the indicated p-value thresholds. This fold-change survival method shows good specificity at $p < 0.05$ for individual profiles (85%), however it is relatively insensitive.

pression changes showing $p < 0.05$ in mixed samples were not confirmed by individual profiles.

Use of t-test measurements is expected to contain significant amounts of noise, due to the very large number of comparisons involved in array studies; a value of $p = 0.05$ means that as many as 5% of gene expression changes are expected to be identified by "chance", and thereby not reflect true differences between samples. We have previously reported a very simple, yet potentially more stringent method for data analysis of small numbers of expression profiles, using duplicate profiles for control and experimental samples, and then identifying those genes that show consistent changes >2-fold in the four possible pair-

wise data comparisons (four comparison survival method) [23]. A similar pair-wise comparison method, using a less stringent average fold-change analysis, was recently reported for muscle from aging and calorie-restricted mouse muscle [13].

To investigate the validity of this approach we compared the sensitivity and specificity of t-test detection of expression changes versus the four-pairwise survival method. Two sample t-test of the 10 individual Duchenne dystrophy profiles compared to the 6 mixed control profiles revealed 1,498 genes showing $p < 0.05$ as above. In parallel, the mixed DMD duplicate profiles were compared to a single pair of mixed control sample profiles (c1a, c1b), using the pairwise comparison survival method [23]. Briefly, four comparisons were done (DMD 1a versus control 1a; DMD1b versus control 1a; DMD 1a versus control 1b; DMD1b versus control 1b), and only those genes retained which showed >2-fold change in all four comparisons. This method was indeed considerably more specific in identifying significant ($p < 0.05$) gene expression changes (Fig. 6A) with 85% of gene expression changes in the mixed profiles verified by individual profiles ($p < 0.05$). The sensitivity of this method depended on the p-value threshold for the individual profiles, but only reached a maximum of 49% sensitivity at $p < 0.0001$ (Fig. 6B).

The results above suggested that analysis of mixed samples using t-test methods was relatively sensitive but non-specific, while analysis of the same mixed profiles by 2-fold survival method was relatively specific but insensitive. To confirm this conclusion, we directly compared the sensitivity and specificity of the four pairwise comparison method to more standard t-test methods (Fig. 7A). We found that the pairwise survival method was indeed highly specific, with 97% of changes identified by this method also detected by t-test. However, as predicted, it was not very sensitive, with only 30% of the expression changes with $p < 0.05$ identified by t-test being detected by the pairwise survival method. Comparison of all three analysis methods showed that many (349) genes expression changes were detected by all three methods (Fig. 7B).

Conclusions

Microarray data analyses have been criticized as being "quite elusive about measurement reproducibility" [30]. This is largely the consequence of the large number of uncontrolled or unknown variables, and the prohibitive cost of isolating and investigating each variable. Here, we report the systematic isolation and study of most variables in microarray experiments using Affymetrix oligonucleotide arrays and human tissue biopsies. We found that all sources of experimental variability were quite minor (microarray $R^2 = 0.98$ – 0.99 ; probe synthesis + microarray $R^2 = 0.98$ – 0.99). On the other hand, tissue heterogeneity

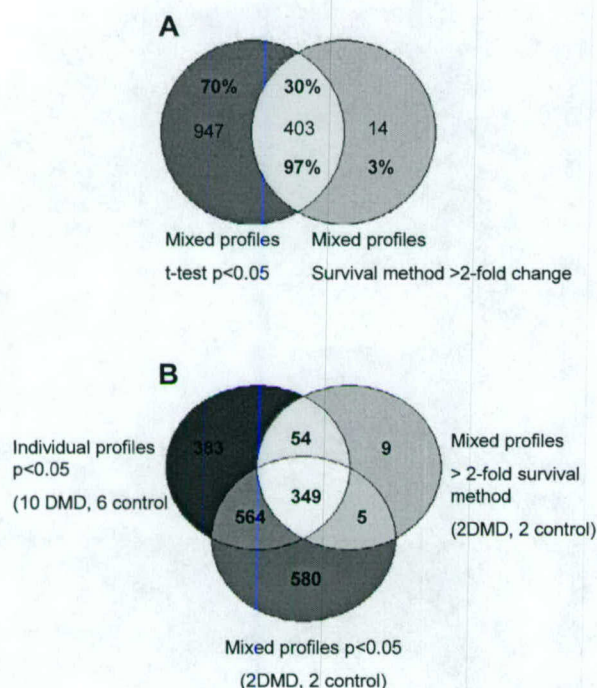


Figure 7
Direct comparison of t-test and four pairwise survival methods. Shown in green is list of 417 differentially expressed genes surviving four pair-wise comparisons to mixed control. Shown in red are differentially expressed genes for 2 mixed DMD 5–6 y profiles versus 6 mixed controls showing $p < 0.05$ by t-test. (Panel A) This analysis shows the survival method to be considerably more stringent than t-test. Most gene expression changes detected by the mixed sample survival method are included in changes from t-test analysis (both mixed and individual profiles). Panel B is the compilation of previous figures, showing that > 2 -fold survival method using only four mixed profiles (two DMD, two control) is highly specific but likely insensitive compared to t-test methods

(intra-patient variation; Average R^2 for 10 patients = 0.92 [0.85 to 0.98]), and differences between individual patients (SNP noise; Average R^2 = 0.76 [0.42 to 0.93]) were major sources of variability in expression profiling. Thus, tissue heterogeneity and SNP noise have a high potential to obscure sought after condition-specific gene expression changes, particularly in humans, where tissue samples can be limiting (sampling error), and inter-individual variation often is very large. We have shown that mixing of patient samples effectively normalizes much of the intra- and inter-patient noise, while still identifying the majority of the most significant gene expression changes that

would have been detected by larger numbers of individual patient profiles. Our results suggest that stringent yet robust data can be generated by mixing a small number of individuals with a defined condition ($n = 5$), preferably using different regions of tissue for duplicate arrays. Controls should be similarly processed. The resulting four arrays (2 controls, 2 experimental datasets) should then be subjected to the > 2 -fold survival method, as previously described [23]. This will yield a stringent set of expression changes that are likely to be verified by larger studies with individual arrays, but at low cost as only four arrays are employed. The preliminary data from just four mixed profiles (two experimental and two control) can then be used to generate functional clusters and pathophysiological models. These preliminary models can then direct more hypothesis-driven experiments, or more extensive expression profiling studies.

Materials and methods

Expression profiling

Human muscle biopsy samples were diagnostic specimens flash-frozen immediately after surgery in isopentane cooled in liquid nitrogen, with storage in small, airtight, humidified tubes at -80°C until RNA isolation. Duchenne muscular dystrophy patient samples were all shown to have complete lack of dystrophin by immunostaining and/or immunoblot analysis, and were shown to have excellent morphology and preservation of tissue. Controls included groups of males and female (age described in text) that showed no histopathological abnormality, normal dystrophy proteins, and normal serum creatine kinase levels. Biopsy sizes ranged from 50 mg to 2 grams, with approximately 20–30 mg used for RNA isolation (~ 10 – 15 micrograms of total RNA). As described in the text, all biopsies had two different regions of the same biopsy expression profiled separately.

Details concerning the murine profiles will be published elsewhere. In this report, we used the murine profiles simply to test the sources of variation during sample preparation prior to hybridization to oligonucleotides.

RNA isolation (Trizol, Gibco BRL), RNA purification (RNAeasy, Qiagen), cDNA synthesis and biotinylated cRNA were all done as per standard protocols provided by Affymetrix Inc. Quality control methods are described on our web site (<http://microarray.cnmcresearch.org/pga.htm>), with cRNA amplifications of between 5- and 13-fold for each of the samples. Ten micrograms of gel-verified fragmented biotinylated cRNA were hybridized to each MuscleChip or U74A v2 array, and scanning done after biotin/avidin/phycoerythrin amplification. Details on the specific patients studied, and details for each GeneChip (scaling factors, number of present calls, percentage difference calls between each duplicate sample, number

of difference calls surviving four pair-wise comparisons of duplicate chips) is provided (Table 1). All profiling data presented here is available on our web site ([http://microarray.CNMCRsearch.org]; data link), as image (.dat), absolute analysis (.chp), and ASCII text conversions of .chp (.txt) for each individual profile (see [http://microarray.cnmcresearch.org/pgs.htm] for file descriptions and use).

Bio-informatic methods

Absolute analysis (average difference determinations for each probe set) was done using Affymetrix default parameters. As described in the text, data was analyzed using a variety of methods, including unsupervised nearest-neighbor hierarchical clustering analyses (GeneSpring [28,29] [Silicon Genetics], and Cluster [25] [Stanford University]), t-test (GeneSpring) and four-comparison survival method [23]. The Cluster and Tree View software were download from [http://rana.lbl.gov] and installed on an NT workstation.

Acknowledgements

We would like to thank Brian S. Tseng and Frank W. Booth (Department of Physiology University of Missouri, Columbia, MO) and Simona Iezzi and Vittorio Sartorelli (Muscle Biophysics Section, Laboratory of Physical Biology NIAMS/NIH Bethesda, MD) for allowing to use their data in our analysis.

Drs. Bakay and Chen were supported by post-doctoral fellowships from the Stichting-Porticus Foundation. Supported in part by grants from the National Institutes of Health (5RO1 NS29525-10; and a "Programs in Genomic Applications" from NHLBI [UO1 HL66614-01]) to EPH.

References

- Lipshutz RJ, Fodor SP, Gingeras TR, Lockhart DJ: **High density synthetic oligonucleotide arrays.** *Nature Genetics* 1999, **21**:20-24
- Duggan DJ, Bittner M, Chen Y, Meltzer P, Trent JM: **Expression profiling using cDNA microarrays.** *Nature Genetics* 1999, **21**:10-14
- Brown PO, Botstein D: **Exploring the new world of the genome with DNA microarrays.** *Nature Genetics* 1999, **21**:33-37
- Cheung VG, Morley M, Aguilar F, Massimi A, Kucherlapati R, Childs G: **Making and reading microarrays.** *Nature Genetics* 1999, **21**:15-19
- McGall G, Labadie J, Brock P, Wallraff G, Nguyen T, Hinsberg W: **Light-directed synthesis of high-density oligonucleotide arrays using semiconducting photoresists.** *Proc. Natl. Acad. Sci. USA* 1996, **93**:13555-13560
- Lockhart DJ, Dong H, Byrne MC, Follett MT, Gallo MV, Chee MS, Mittmann M, Wang C, Kobayashi M, Horton H, Brown EL: **Expression monitoring by hybridization to high-density oligonucleotide arrays.** *Nat. Biotechnol.* 1996, **14**:1675-1680
- Winzler EA, Richards DR, Conway AR, Goldstein AL, Kalman S, McCullough MJ, McCusker JH, Stevens DA, Wodicka L, Lockhart DJ, Davis RW: **Direct allelic variation scanning of the yeast genome.** *Science* 1998, **281**:1194-1197
- Spellman PT, Sherlock G, Zhang MQ, Iyer VR, Anders K, Eisen MB, Brown PO, Botstein D, Futcher B: **Comprehensive identification of cell cycle-regulated genes of the yeast *Saccharomyces cerevisiae* by microarray hybridization.** *Mol Biol Cell* 1998, **9**:3273-3297
- Gasch AP, Spellman PT, Kao CM, Carmel-Harel O, Eisen MB, Storz G, Botstein D, Brown PO: **Genomic expression programs in the response of yeast cells to environmental changes.** *Mol Biol Cell* 2000, **11**:4241-4257
- Sudarsanam P, Iyer VR, Brown PO, Winston F: **Whole-genome expression analysis of *snf/swi* mutants of *Saccharomyces cerevisiae*.** *Proc. Natl. Acad. Sci. USA* 2000, **97**:12369-12374
- Cavaliere D, Townsend JP, Hartl DL: **Manifold anomalies in gene expression in a vineyard isolate of *Saccharomyces cerevisiae* revealed by DNA microarray analysis.** *Proc. Natl. Acad. Sci. USA* 2000, **97**:12369-12374
- Ogawa N, DeRisi J, Brown PO: **New components of a system for phosphate accumulation and polyphosphate metabolism in *Saccharomyces cerevisiae* revealed by genomic expression analysis.** *Mol Biol Cell* 2000, **11**:4309-4321
- Lee CK, Klopp RG, Weindrich R, Prolla TA: **Gene expression profile of aging and its retardation by caloric restriction.** *Science* 1999, **285**:1390-1393
- Kaminski N, Allard JD, Pittet JF, Zuo F, Griffiths MJ, Morris D, Huang X, Sheppard D, Heller RA: **Global analysis of gene expression in pulmonary fibrosis reveals distinct programs regulating lung inflammation and fibrosis.** *Proc. Natl. Acad. Sci. USA* 2000, **97**:1778-1783
- Golub TR, Slonim DK, Tamayo P, Huard C, Gaasenbeek M, Mesirov JP, Coller H, Loh ML, Downing JR, Caligiuri MA, Bloomfield CD, Lander ES: **Molecular classification of cancer: class discovery and class prediction by gene expression monitoring.** *Science* 1999, **286**:531-537
- Perou CM, Jeffrey SS, van de Rijn M, Rees CA, Eisen MB, Ross DT, Pergamenschikov A, Williams CF, Zhu SX, Lee JC, Lashkari D, Shalon D, Brown PO, Botstein D: **Distinctive gene expression patterns in human mammary epithelial cells and breast cancers.** *Proc. Natl. Acad. Sci. USA* 1999, **96**:9212-9217
- Sorlie T, Perou CM, Tibshirani R, Aas T, Geisler S, Johnsen H, Hastie T, Eisen MB, van de Rijn M, Jeffrey SS, Thorsen T, Quist H, Matese JC, Brown PO, Botstein D, Eystein Lonning P, Borresen-Dale AL: **Gene expression patterns of breast carcinomas distinguish tumor subclasses with clinical implications.** *Proc. Natl. Acad. Sci. USA* 2001, **98**:10869-74
- Bittner M, Meltzer P, Chen Y, Jiang Y, Sefter E, Hendrix M, Radmacher M, Simon R, Yakhini Z, Ben-Dor A, Sampas N, Dougherty E, Wang E, Marincola F, Gooden C, Lueders J, Glatfelter A, Pollock P, Carpten J, Gillanders E, Leja D, Dietrich K, Beaudry C, Berens M, Alberts D, Sondak V: **Molecular classification of cutaneous malignant melanoma by gene expression profiling.** *Nature* 2000, **406**:536-540
- Alon U, Barkai N, Notterman DA, Gish K, Ybarra S, Mack D, Levine AJ: **Broad patterns of gene expression revealed by clustering analysis of tumor and normal colon tissues probed by oligonucleotide arrays.** *Proc. Natl. Acad. Sci. USA* 1999, **96**:6745-6750
- Mills JC, Gordon JL: **A New approach for filtering noise from high-density oligonucleotide microarray datasets** *Nucleic Acids Res* 2001, **29**:E72-2
- Unger MA, Rishi M, Clemmer VB, Hartman JL, Keiper EA, Greshock JD, Chodosh LA, Liebman MN, Weber BL: **Characterization of adjacent breast tumors using oligonucleotide microarrays.** *Breast Cancer Res* 2001, **3**:336-341
- Nadler ST, Stoehr JP, Schueler KL, Tanimoto G, Yandell BS, Attie AD: **The expression of adipogenic genes is decreased in obesity and diabetes mellitus.** *Proc. Natl. Acad. Sci. USA* 2000, **97**:11371-11376
- Chen Y, Zhao P, Borup R, Hoffman EP: **Expression profiling in the muscular dystrophies: identification of novel aspects of molecular pathophysiology.** *J. Cell Biol.* 2000, **151**:1321-1336
- Kamb A, Ramaswami M: **A simple method for statistical analysis of intensity differences in microarray-derived gene expression data.** *BMC Biotechnol* 2001, **1**:8
- Eisen MB, Spellman PT, Brown PO, Botstein D: **Cluster analysis and display of genome-wide expression patterns.** *Proc. Natl. Acad. Sci. USA* 1998, **95**:14863-14868
- Der SD, Zhou A, Williams BR, Silverman RH: **Identification of genes differentially regulated by interferon alpha, beta, or gamma using oligonucleotide arrays.** *Proc. Natl. Acad. Sci. USA* 1998, **95**:15623-15628
- Hooper LV, Wong MH, Thelin A, Hansson L, Falk PG, Gordon JL: **Molecular analysis of commensal host-microbial relationships in the intestine.** *Science* 2001, **291**:881-884
- GeneSpring User Manual, version 4.0, March Silicon Genetics 2001
- GeneSpring Advanced Analysis Techniques, version 4.0, March Silicon Genetics 2001
- Claverie JM: **Computational methods for the identification of differential and coordinated gene expression.** *Hum Mol Genet* 1999, **8**:1821-1832

Gene Profiling in Spinal Cord Injury Shows Role of Cell Cycle in Neuronal Death

Simone Di Giovanni, MD,^{1,2} Susan M. Knoblach, PhD,¹ Cinzia Brandoli, PhD,² Sadia A. Aden, BS,¹ Eric P. Hoffman, PhD,² and Alan I. Faden, MD¹

Spinal cord injury causes secondary biochemical changes leading to neuronal cell death. To clarify the molecular basis of this delayed injury, we subjected rats to spinal cord injury and identified gene expression patterns by high-density oligonucleotide arrays (8,800 genes studied) at 30 minutes, 4 hours, 24 hours, or 7 days after injury (total of 26 U34A profiles). Detailed analyses were limited to 4,300 genes consistently expressed above background. Temporal clustering showed rapid expression of immediate early genes (30 minutes), followed by genes associated with inflammation, oxidative stress, DNA damage, and cell cycle (4 and 24 hours). Functional clustering showed a novel pattern of cell cycle mRNAs at 4 and 24 hours after trauma. Quantitative reverse transcription polymerase chain reaction verified mRNA changes in this group, which included *gadd45a*, *c-myc*, *cyclin D1* and *cdk4*, *pcna*, *cyclin G*, *Rb*, and *E2F5*. Changes in their protein products were quantified by Western blot, and cell-specific expression was determined by immunocytochemistry. Cell cycle proteins showed an increased expression 24 hours after injury and were, in part, colocalized in neurons showing morphological evidence of apoptosis. These findings suggest that cell cycle-related genes, induced after spinal cord injury, are involved in neuronal damage and subsequent cell death.

Ann Neurol 2003;53:454–468

Spinal cord injury (SCI) induces a sequence of endogenous autodestructive changes known as secondary injury, as well as reactive biochemical changes that are neuroprotective and/or promote recovery. The balance between such neuroprotective and autodestructive changes is believed to determine the extent of ultimate damage and recovery (see Dumont and colleagues¹ for review). Candidate gene studies have demonstrated several changes in certain mRNAs and proteins after SCI (see Yakovlev and Faden² and Dutcher and Michael³ for review), but technological limitations have narrowed the scope of such studies and generally precluded definition of the evolution of coordinated changes in gene regulation or (deleted) interactions.

Methodological advances now permit more extensive parallel studies of gene expression: microarrays have been developed using oligonucleotide or cDNA-based chips, thus permitting the concurrent analysis of hundreds or thousands of gene expression changes. Recently, two groups reported changes in gene regulation after experimental SCI using 1,200 gene oligonucleotide-based arrays^{4,5}; each used pooled spinal cord tissues and only examined a limited number of early time points. Both studies showed increased expression of specific transcription factors, inflammatory genes, and

heat shock proteins at 3 and 6 hours after trauma, followed at 24 hours by induction of mRNAs implicated in regenerative or neuroprotective processes. These studies provide an important first step in defining changes in gene expression after SCI.

In this study, we have assessed gene changes after SCI in a somewhat different and more comprehensive fashion. First, a lower level of injury was examined to elucidate changes more likely to be associated with apoptotic cell death, which is most often an active process requiring gene transcription/translation. Second, we studied individual rat samples, rather than pooled samples, to determine the inherent variability across subjects. Third, we evaluated both earlier and later time points (30 minutes, 4 and 24 hours, and 7 days) to better define the temporal pattern of changes. Fourth, we used a larger Affymetrix (Santa Clara, CA) chip with 8,800 probe sets to assess many potential gene changes. Fifth, we compared both sham-injured (operated) and naive controls, to eliminate changes potentially related to anesthesia or surgical stress. Finally, we used verification procedures, including quantitative reverse transcription polymerase chain reaction (RT-PCR), protein quantitation using immunoblotting, and localization of cell-specific protein expression by im-

From the ¹Department of Neuroscience, Georgetown University Medical Center; and ²Research Center for Genetic Medicine, Children's National Medical Center and Genetics Program, Washington, DC.

Received Aug 30, 2002, and in revised form Nov 8. Accepted for publication Nov 9, 2002.

Published online Mar 6, 2003, in Wiley InterScience (www.interscience.wiley.com). DOI: 10.1002/ana.10472

Address correspondence to Dr Faden, Department of Neuroscience, Research Building, Room EP-12, Georgetown University Medical Center, 3970 Reservoir Road NW, Washington, DC 20057. E-mail: fadena@georgetown.edu

munocytochemistry. Moreover, we addressed several important methodological considerations regarding quality control and analytical methods (standard deviations, reproducibility, multiple measurements, *p* values vs fold changes).

Materials and Methods

Experimental Spinal Cord Injury

Male Sprague-Dawley rats (275–325gm) were anesthetized with sodium pentobarbital (65mg/Kg, IP). Laminectomy was performed at T8–9. The spinal column was stabilized above and below the injury with clamps, and the animal was positioned so that the cord was parallel to the table surface. Injury was induced using a weight drop method (10gm dropped from 17.5mm), as previously detailed.⁶ Animals with this injury level show mild motor impairment; on the Basso, Beattie, Bresnahan scale, they averaged 17 ± 1 at 28 days after injury. After injury, the animal was removed from the clamps, and the wound was sutured in layers. Rat core temperature was maintained at 37°C throughout surgery, and for 2 hours during recovery via heating pads and feedback controlled heating lamps. Animals were fully anesthetized during the operative procedures, and experiments complied fully with the principles set forth in the "Guide for the Care and Use of Laboratory Animals" prepared by the Committee on Care and Use of Laboratory Animals of the Institute of Laboratory Resources, National Research Council (DHEW Pub. No. [NIH] 85-23, 2985).

Animals were killed by decapitation after anesthesia with sodium pentobarbital (67mg/kg). A 1cm section of the spinal cord, including 0.5cm above and below the injury site centered around T-9, was dissected and immediately fresh-frozen in liquid nitrogen. Spinal cords were collected from four injured and two sham-operated rats for each time point (30 minutes, 4 hours, 24 hours, and 7 days) and two naive controls (rats that did not undergo any surgical procedure) for a total of 26 animals. Seven milligrams of total RNA were used for cDNA and biotinylated cRNA synthesis. We processed and performed our expression profiling analysis using the Affymetrix rat U34A array. Each Genechip hybridization was obtained from one spinal cord tissue from each animal.

Expression Profiling

RNA was extracted from each cord sample individually using TRIzol reagent (GIBCO BRL, Gaithersburg, MD). Seven milligrams of total RNA from each tissue sample (26 samples total) were converted into double-stranded cDNA by using SuperScript choice system (GIBCO BRL) with an oligo-dT primer containing T7 RNA polymerase promoter (Genset, La Jolla, CA). The double-stranded cDNA was purified by phenol/chloroform extraction and then used for *in vitro* transcription using ENZO BioArray RNA transcript labeling kit. Biotin-labeled cRNA was purified by RNeasy kit (Qiagen, Chatsworth, CA) and fragmented randomly to approximately 200bp (200mM Tris-acetate, pH 8.2, 500mM KOAc, 150mM MgOAc). Each fragmented cRNA sample was hybridized to Affymetrix rat U34A microarray for 16 hours at 60rpm at 45°C. The microarray then was washed

and stained on the Affymetrix Fluidics Station 400 using instructions and reagents provided by Affymetrix. This involves removal of nonhybridized material and then incubation with phycoerythrin-streptavidin to detect bound cRNA (scan 1). The signal intensity was amplified by second staining with biotin-labeled antistreptavidin antibody followed by phycoerythrin-streptavidin staining (scan 2). Fluorescent images were read using the Hewlett-Packard G2500A Gene Array Scanner.

Microarray (Genechip) Quality Control and Normalizations

Each gene chip of our series underwent a stringent quality control regime. The following parameters were considered: cRNA fold changes (amount of cRNA obtained from starting RNA); scaling factor; percentage of "present" calls; average difference; housekeeping genes and internal probe set controls; comparison of hybridization intensity between scan 1 and 2 and comparison of distribution of hybridization intensity between gene chips from animals of the same experimental group (R^2). Values for these parameters are reported in results (expression profiling data generation section).

We needed two normalization processes: one for chip-chip comparisons (scaling factors) and one for temporal analysis (normalization to the average of the naive average difference values for each gene). The scaling factors determinations were conducted using default Affymetrix algorithms with a target intensity of chip sector fluorescence to 800. Both pre-amplification (s1) and poststreptavidin/phycoerythrin amplification (s2) scans were performed, and the scans were compared by scatterplots and correlation coefficients (see Fig 1A). Those probe sets showing evidence of saturation of the PMT in s2 were flagged.

Data Scrubbing and Statistical Analysis

We relied on the interpretation of probe sets hybridization performance (pairs of 20 perfect match and mismatch 25mer oligonucleotides per probe sets) as a measure of whether signal intensities were significantly above background and were specific to the gene of interest. We based all further analysis only on those probe sets that we deemed "present" (P "calls") in 40% or more of the 26 gene chip profiles in our complete data set. This value corresponds to the low percentage P calls threshold for each array. Although this is a stringent threshold, we found that this included most probe sets with reliable and consistent performance, showing average difference values for each probe set with tight standard deviations among members of the same experimental group.

Experiment normalization was performed normalizing gene chips from injured and sham controls to the mean of the two chips from naive animals considered as the baseline gene expression level. Normalized data then were compared for differential gene expression analysis across time points between sham and injured groups. Genes that showed at least a twofold change in one or more time points and a Welch ANOVA *t* test *p* value less than 0.05 between sham and injured groups for at least one time point were considered "significant." Although a *p* value of less than 0.05 alone would give many false-positives, the combination of fold change

threshold and *p* values would be expected to eliminate most of these false-positives.⁷

Expression Profiling Data Analysis

Four statistical analyses were used. First, we used default Affymetrix interpretations of probe set hybridization patterns (20 perfect match and 20 mismatch oligonucleotides for each gene) to provide an assessment of signal/noise ratios ("absent" or "present" calls). We then eliminated those probe sets where hybridization patterns were below or near background by retaining only those probe sets (genes/ESTs) showing 40% or more of "present" calls across all 26 profiles. This "data scrubbing" retained genes showing lower standard deviations between multiple measurements among arrays of the same experimental group and maintained approximately 50% of probe sets on the chips (4,300 probe sets from the 8,800 genes and ESTs represented on the rat u34A chip).

The third level of data analysis was definition of averaged, subtracted, and normalized hybridization intensities for the 40 oligonucleotides in each probe set (average difference values) for each array. Temporal clustering analyses with GeneSpring software used these average difference values for each gene. Temporal clustering included determination of "increased" and "decreased" expression levels and *p* value determinations of changes as a function of time (normalized to naive controls). All average difference values for the 4,300 genes surviving filtering for both injured and sham animals were normalized to the mean of the two profiles from naive animals; this mean was set as the "baseline" gene expression level for each of the 4,300 genes. Normalized data then were compared for differential gene expression analysis across time points between sham and injured groups. Genes that showed both greater than twofold changes and a *t* test *p* value less than 0.05 between sham and injured groups for at least one time point were considered "significant."

Quantitative Multiple Fluorescent Reverse Transcription Polymerase Chain Reaction

We chose three experimental genes, belonging to a functional and temporal gene cluster, for validation through quantitative multiple fluorescent (QMF) RT-PCR. These genes were *c-myc*, *gadd45a*, and *pcna*. They were significant at 4 and 24 hours after injury and belonged to the cell cycle gene cluster.

For each gene, we selected one time point corresponding to the best *p* value for each gene in the injured group and processed the same total RNAs used for microarray and synthesized sscDNA (according to Affymetrix protocol) from each injured (four samples) and sham (two samples) operated animal. The time points selected were the following: 4 hours for *c-myc*, 24 hours for *gadd45a* and *pcna*. Each experimental gene was compared with two control genes chosen upon their flat gene expression profiling (similar absolute intensity values) across time points in both injured and sham rats: *rat liver s1-1* and *2,4 dienoyl-CoA reductase precursor* were used as controls for *gadd45a* and *pcna*; *troponin I* and *steroid sulfatase* for *c-myc*. Each pair of control genes had an average difference in between two- and fourfold changes less than the corresponding experimental gene. The sequence of the primers we designed for the experimental and control genes were the following:

c-myc, 1511F: 5'-GAGAAACGAGCTGAAGCGTAGC -3'; 1652R: 5'-GAGTTTGTGCTCATCTGCTTGAAC-3'; *gadd45a*, 317F: 5'-GAGCTGTTGCTACTGGAGAAC-3'; 452R: 5'-CAAATAAGTTGACTTAAGGCAGG-3'; *pcna*, 528F: 5'-ATGCTGTGGTGATCTCCTG-3'; 679R: 5'-GTTAGCTGAAGTGGCTGATTC-3'; *S1-1*, 2751F: 5'-CATTGTGACACCCATTGAAGC-3'; 2875R: 5'-TCACTGGGCTTCATTGAAGCG-3'; *2,4 dienoyl-CoA reductase*, 873F: 5'-CAGTGATTATGCCTCTTGGATC-3'; 1113R: 5'-GTCTTTCTGATGAGGCCTTCG-3'; *steroid sulfatase*, 2075F: 5'-GAAACAGAGCCGCGCCATGG-3'; 2221R: 5'-CTTGGAAGGCAGGCAGAGCTG-3'; *troponin I*, 541F: 5'-CGGGCCAAGGAATCCTTGGAC-3'; 673R: 5'-CTTTCGGCCTTCCATTCCACTTA-3'.

We performed a multiplex PCR with the three pairs of fluorescein labeled primers (one from the experimental and two from the control genes) mixed in the same PCR for a total 15 cycles. One milliliter of each multiplex PCR was loaded on a Licor sequencer gel. PCR products ranged between 130 and 150bp, and they differed only in 5 to 15bp. The Licor sequencer scanner allowed detecting the intensity of the fluorescent signal for each product. The Geneanalytics software provided a nanogram intensity value for each band corresponding to the quantitative measure of the relative levels of mRNAs. The quantity of the expression level for each experimental gene versus each control gene was calculated based on the ratio between the intensity value of the experimental gene versus control 1 and versus control 2 for each sample for a total of eight comparisons for the injured group and four for the sham (see Fig 5). An ANOVA *t* test was performed to generate *p* values between injured and sham for each experimental gene.

Immunoblotting

Samples from 4- and 24-hour sham and injured spinal cords were prepared by rapid lysis of tissue collected by cutting 8mm sections (18–20 sections) for each spinal cord both 0.5cm below and above the injury site (9–10 sections each). The tissue sections were lysed in Laemmli sample buffer supplemented with protease inhibitors (10mg aprotinin/ml, 1mg leupeptin/ml, 1mM phenylmethyl sulfonyl fluoride) and subjected to immunoblotting analysis using standard methods.⁷

Equivalent loading of lanes was carefully determined by running pilot gels loaded with the same number of tissue sections (18–20) and analyzing images of Coomassie-stained gels using a digital documentation system and a software package for bands quantitation (UN-SCAN-IT Silk Scientific Co., Orem, UT). Adjustments in sample volumes were made based on this analysis, and the process was repeated until all the lanes were equivalently loaded. This method can reliably establish equivalent loading within a 10 to 20% error value for all lanes. Nevertheless, the intensity of the bands of our experimental proteins was always normalized to the amount of protein loaded for each lane (Coomassie gels). For immunoblotting, we used the following antibodies: rabbit polyclonal anti-rat Rb and ser795 *pRb* (diluted 1:100; BD, Beverly, MA); mouse monoclonal anti-rat *pcna* (diluted 1:300; Oncogene, Boston, MA); mouse monoclonal anti-rat *cyclin D* (diluted 1:100; Chemicon, Temecula, CA); and rabbit polyclonal anti-rat *E2F5* and rabbit polyclonal anti-rat

c-myc (diluted 1:200; Santa Cruz, La Jolla, CA). Signals were visualized with ECL chemiluminescence (Amersham, Arlington Heights, IL).

Immunocytochemistry

Immunocytochemistry from three injured and two sham animals was performed at 4 and 24 hours. The injured spinal cord was studied at three different levels from the injury site: at the injury site, 0.5 cm above and below the injury. Frozen 15 μ m spinal cord sections from three injured and two sham animals were incubated under the same coverslip and processed for immunocytochemistry as follows: sections were dried at room temperature, fixed in paraformaldehyde 4%, rinsed in phosphate-buffered saline (PBS), and incubated with 10% normal serum and Triton X-100 (Sigma, St. Louis, MO) 0.2% in PBS (goat or rabbit depending on the secondary antibodies used) for 60 minutes to mask nonspecific adsorption sites. Sections then were incubated overnight at 4° C with one or more of the following antibodies: rabbit polyclonal anti-rat *cmyc* (diluted 1:200; Santa Cruz), goat polyclonal anti-rat *c-myc*, rabbit polyclonal anti-rat *gadd45a*, rabbit polyclonal anti-rat *E2F5*, rabbit polyclonal anti-rat *cdk4*, rabbit polyclonal anti-rat *cyclin G* (diluted 1:100; Santa Cruz); mouse monoclonal anti-rat *cdk4* (diluted 2 mg/ml; Chemicon); rabbit polyclonal anti-rat *cyclin D* (diluted 1:300; Santa Cruz); mouse monoclonal anti-rat *cyclin D* (diluted 1:100; Chemicon); goat polyclonal anti-rat activated *caspase-3* (diluted 1:200; Santa Cruz); rabbit polyclonal anti-rat activated *caspase-3* (diluted 1,100; Chemicon); rabbit polyclonal anti-rat *pRb* (ser795, ser807, ser780; diluted 1:100; BD); mouse monoclonal anti-rat *pcna* (diluted 1:300; Oncogene); or mouse monoclonal anti-rat *pcna* (diluted 1:200; Chemicon).

Blocking peptides, omission of the primary antibodies, and/or their replacement by preimmune sera were used as controls. These peptides and negatives controls include: cyclin G1 rabbit polyclonal sc-320 and blocking peptide sc-320 P, *c-myc* rabbit polyclonal sc-788 and blocking peptide sc-788 P, *gadd45a* rabbit polyclonal sc-792 and blocking peptide sc-792 P, *E2F5* rabbit polyclonal sc-999 and blocking peptide sc-999 P, *cdk4* rabbit polyclonal sc-260 and blocking peptide sc-260 P, *caspase-3* p-20 goat polyclonal sc-1226 and blocking peptide sc-1226 P, all from Santa Cruz; *pcna* mouse monoclonal NA03-negative control and normal mouse IgG NI03 from Oncogene; and pRB no. 9300 and control proteins for phosph and nonphosphor RB from Cell Signaling (Beverly, MA).

After several rinses in PBS, the sections were incubated with the appropriate rhodamine, Texas red, fluorescein isothiocyanate, or AMCA-coupled secondary antibodies (goat anti-mouse or goat anti-rabbit), for 1 hour at room temperature and washed in PBS before mounting the slides with aqueous medium. Double and triple labeling also have been performed, combining mouse monoclonal anti-rat neuN (diluted 1:100; Chemicon) with each of the above antibodies in various combinations, to verify their colocalization in neurons.

TUNEL and Hoescht

The terminal deoxynucleotidyl transferase-mediated dUTP nick end labeling (TUNEL) technique was applied for detec-

tion of nuclear DNA fragmentation in situ. Fifteen-micrometer frozen spinal cord sections, derived from the same samples used for immunocytochemistry, were incubated with TUNEL reaction mixture with incorporated fluorescein-dUTP according to the manufacturer's instructions (in situ cell death detection kit; Boehringer, Indianapolis, IN). Negative experimental controls were incubated with label solution without terminal transferase instead of TUNEL reaction mixture. As a positive control, spinal cord sections were preincubated with DNase I for 10 minutes before the TUNEL procedure. TUNEL also was performed on the same spinal cord sections after immunocytochemistry for all the above antibodies to evaluate the colocalization of TUNEL-positive nuclei with individual antibodies. Alternatively, and after TUNEL, we also performed Hoescht 33258 staining (10 mg/ml) to visualize nuclear morphology and chromatin condensation.

Results

Expression Profiling Data Generation

We employed stringent quality control methods as previously published⁸ (see Materials and Methods) and detailed on our Web site: (<http://microarray.cnmcresearch.org>, link to "programs in genomic applications"). Expression profiles fulfilled the following quality control measures (see Materials and Methods for description): cRNA fold changes between 5 to 10, scaling factor from 0.3 to 1.5, percentage of "present" (P) calls from 40 to 55%, average difference levels between 900 and 1,100, housekeeping genes and internal probe set controls showed greater than 80% present calls, consistent values and 5' to 3' ratios greater than 0.8. We used a high setting for the scanner photomultiplier tube (PMT) to maximize sensitivity (1,800 V); however, this meant that the most highly expressed genes could saturate the PMT. To detect saturated probe sets, we conducted scans both after initial streptavidin/phycoerythrin binding (scan 1) and after biotin/streptavidin/phycoerythrin amplification signal (scan 2). Comparison of hybridization intensity defined by a scatterplot between scan 1 and 2 showed less than 3% saturated probe sets (Fig 1A). Saturated probes were flagged, and values for scan 1 used to detect differential gene expression. Comparison of average difference values defined by a scatterplot between gene chips from animals of the same experimental group and time point showed a correlation coefficient (R^2) from 0.75 to 0.98 (see Fig 1B and C). Eight profiles (approximately 30%) did not reach quality control standards; in these cases, expression profiling experiments were repeated to meet standards.

Expression Profiling Data Interpretation

We used three complementary clustering methods to define temporal relationships between expression responses of genes whose products have known functions (Fig 2). First, a gene (*c-fos*) whose expression is known to be upregulated in spinal cord injury was used to

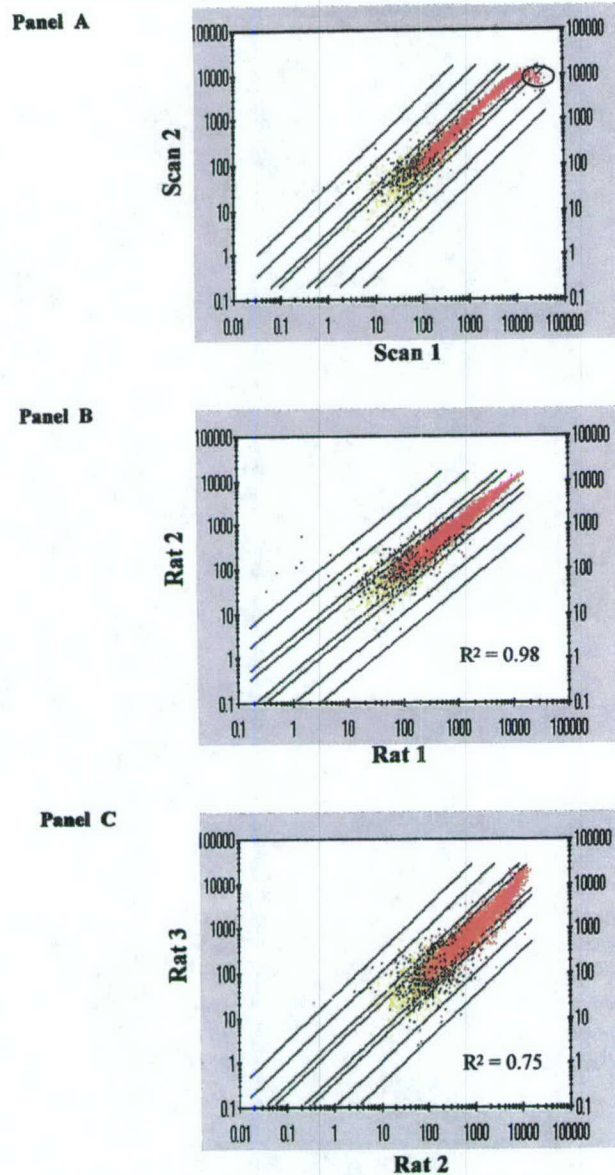


Fig 1. Representative scatterplot analyses of U34A spinal cord expression profiles and quality control. (A) Shown is a comparison of probe set hybridization intensities (average difference values) before (scan 1) and after streptavidin-phycoerythrin amplification (scan 2). All 8,700 probe sets are plotted, with "present" calls marked in red, "absent" in yellow, and "marginal" in blue. The circled probe sets show the 3% of probe sets showing evidence of PMT saturation; these are flagged and only scan 1 values are used for gene expression analysis. This method enhances sensitivity, while avoiding false expression changes caused by saturation. (B and C) Examples of scatterplots of two arrays from two different animals (4 hours). These represent the highest ($R^2 = 0.98$) (B) and the lowest correlation coefficients ($R^2 = 0.75$) (C) from our series.

nucleate coordinately expressed gene clusters (Fig 3). Second, we used previously defined functional groups of genes (eg, inflammation-related genes, cell cycle

genes; Figs 3 and 4) to determine the temporal regulation of specific cluster members. These members were coordinately overexpressed, respectively, at 24 hours to 7 days and 4 to 24 hours. Finally, we defined artificial temporal patterns (eg, increased expression at 4 and 24 hours; see Fig 4) and clustered patterns based on our self-defined patterns. In each of the three clustering approaches, we used standard and Pearson correlation coefficients ranging from 0.95 to 0.99. Visual output of clustering included graphs that showed small subsets of individual genes sharing temporal characteristics, or dendrograms (gene trees) to visualize larger groups of genes and/or their relationship to each other as a function of time after injury (see Figs 3 and 4). In addition, self-organizing maps were used to further group coordinated profiles in specific subclusters. In this way, we focused on a more defined temporal profiling relationship between members of a known cluster. *c-Myc*, *cyclin D1*, and *gadd45a* were in fact subclustered together and were significantly overexpressed at both 4 and 24 hours in the cell cycle cluster (see Fig 4B).

These clustering methods also allowed us to highlight those genes sharing a high correlation coefficient (a similar expression profile in the injured vs the sham group), with significant genes related to a specific function or to a specific temporal profile (see Figs 3 and 4). Genes that were not significant (in terms of p values and fold changes) but were tightly functionally- and temporally-related to a significant gene ($R^2 = 0.95$ – 0.99) were included for analysis (see Fig 4, cell cycle genes).

Of the 4,300 probe sets analyzed, we found 346 (8%) that showed a significant change in expression levels at one or more time points using our stringent criteria for significance (greater than twofold change and $p < 0.05$). Of these 346 changes, increased expression was found in 262 genes and decreased in only 84. Furthermore, the mean level of fold changes for significantly upregulated genes was nearly 3.5-fold vs 2-fold for downregulated genes. Only 94 genes showed significantly increased expression at two or more time points.

Expression Profiling Confirms Previous Candidate Gene Studies and Identifies New Members

To validate our data set, we queried our profiles for genes previously shown to be dysregulated after spinal cord injury.^{6,9–12} We also used these candidate genes to nucleate temporal clusters and identify novel coordinately expressed and functionally-related genes.

IMMEDIATE EARLY RESPONSE GENES. *c-fos*, *Krox24* (*Egr-1*, *NGFI-A*), and *NGFI-B*—each showed a peak of expression at 30 minutes after trauma (see Figs 2 and 3). Increased expression of these genes is consistent

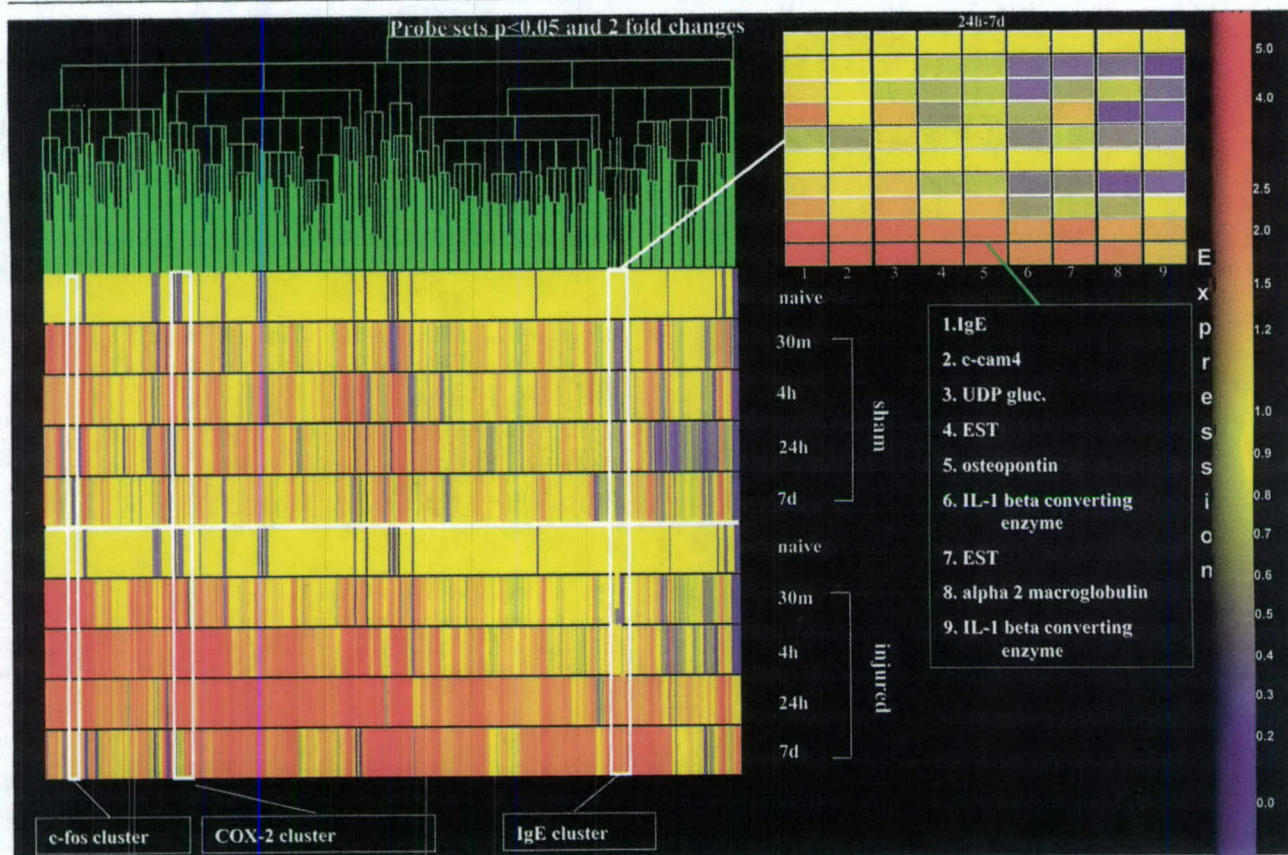


Fig 2. Temporal clustering shows all coordinately expressed gene clusters. Hierarchical clustering of data based on standard correlation (Genespring default distance and separation ratio parameters). Shown are only those genes surviving 40% "present" call data scrubbing and exhibiting $p < 0.05$ differences as well as twofold changes relative to sham controls (4,600 probe sets of the 8,800 assayed). The color reflects the relative expression level, and statistical significance of expression changes, with red indicating increased expression and blue decreased expression (right). Three nucleated temporal gene clusters are shown (c-fos, COX-2, and IgE, inset) with cluster members typically showing related function. The c-fos gene cluster is highly upregulated at 30 minutes (m) and 4 hours (h), COX-2 cluster at 4 hours and 24 hours, and Ig E cluster at 24 hours and 7 days (red). The IgE cluster is expanded to show individual branch members, as numbered in the insets.

with previous studies. Other immediate early response genes in the *c-fos* temporal cluster ($R^2 = 0.95$) previously unreported after SCI included *PTPase*, *Tis 11*, *ZFP36*, *PC3*, *FSH*-regulated protein, *FBR*, and *BTG-2* (see Fig 3). Certain of these transcription factors (eg, *TIS11*) remained overexpressed at later time intervals (7 days). Other members of the functional class of immediate response genes did not map to the *c-fos* cluster. For example, the JE immediate serum early responsive gene showed its most significant p value ($p < 0.05$) and increased fold change at 4 and 24 hours after injury, and *gro-1* showed its maximum fold increase at 4 and 24 hours (see gene list at <http://microarray.cnmcresearch.org/pgadatatable.asp> for complete list).

INFLAMMATORY AND OXIDATIVE STRESS GENES. *Cox-2*, *NOS*, *HO1*, *MnSOD*, *HSP70*, *IL-1* receptor, *IL-1 β* all had been shown previously to be induced by SCI

(inflammation-related genes and COX-2 similarity cluster). They showed a peak of expression at 4 hours after injury, but some remained highly expressed at 24 hours and 7 days. Some genes belonging to these clusters have not been previously associated with SCI, such as, *osteopontin* (see Fig 2).

As a result of the many probe sets studied, the robust experimental design and the statistical power of our study, many hundreds of mRNAs were shown to be significantly dysregulated by SCI. Here, we focus on cell cycle control gene expression in neurons. However, we have made publicly available all data presented here, including image files (.dat), processed image files (.cel), and interpretation files (.txt). We have also posted a list of significantly differentially regulated genes for each time point relative to sham controls and clustered them in temporal and functional groups, and have included a gene-based query tool on this site (see above).

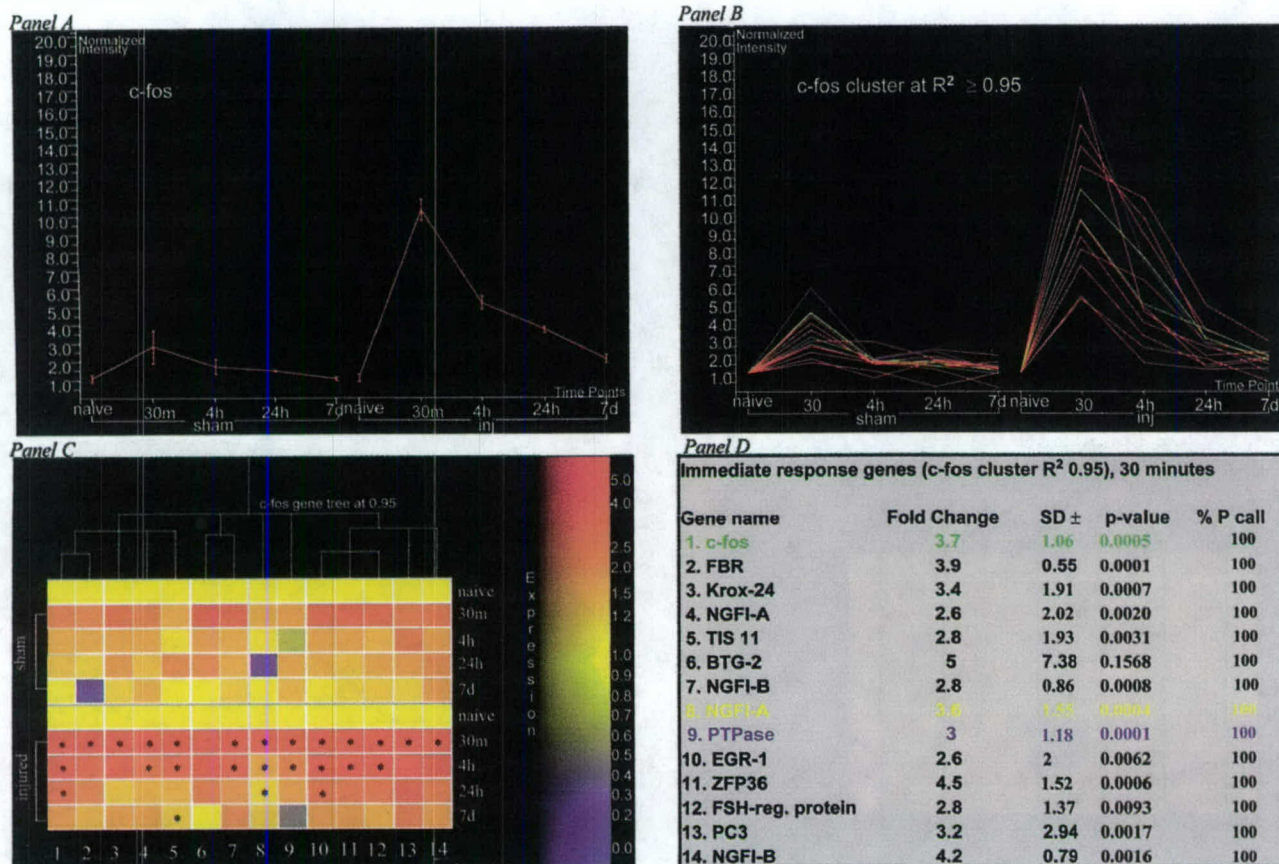


Fig 3. Analysis of the c-fos nucleated temporal cluster. (A) Temporal pattern of c-fos expression in both sham and injured samples (mean \pm standard deviation). B, C, and D show the c-fos temporal cluster with individual members annotated. In B, c-fos is the green line, PTPase in blue, NGFI-A in yellow, and all others in red. All genes showed significant differences between injured and sham time points (asterisks in panel C, p values for 30 minutes, panel D), with the exception of BTG-2, which showed the highest standard deviation (D). Two genes had two and four distinct probe sets each, with similar results obtained (NGFI-B, nos. 7 and 14) and (NGFI-A or Krox-24 or EGR-1, nos. 3, 4, 8, 10, different name for the same gene).

Cell Cycle Genes and Proteins Are Upregulated at 4 and 24 Hours after Injury and Are Localized in Neurons

Expression Profiling

We focused on genes involved in cell cycle regulation with particular relevance to DNA damage response and transition from G1 to S phase. This functionally related group of genes has been implicated in cell cycle control and is reported to play a role in neuronal apoptosis, but has not been linked previously in this regard.^{13,14} mRNAs from these were coordinated and upregulated at 4 and 24 hours in the injured spinal cord (see Fig 4). *c-myc*, *gadd45a*, and *cyclin D1* were upregulated at 4 and 24 hours (see Fig 4B and D); *c-myc* and *gadd45* showed a maximum expression increase at 4 hours, whereas this occurred for *cyclin D1* at 24 hours. *Pcna*, *cyclin G*, and *Rb* were upregulated at 24 hours (see Fig 4C and D). *gadd45a* showed temporal clustering with *c-myc* ($R^2 = 0.99$), whereas *pcna*, *cyclin D1*, *cyclin G*, *Rb*, and *E2F5* belonged to the same

temporal cluster ($R^2 = 0.99$). Additional genes showed temporal clustering to the 24-hour peak but did not fulfill our stringent criteria of both a twofold increase and significant p value relative to the corresponding sham profiles: *CDK4*, *E2F5*, and *caspase-3* ($R^2 = 0.95$; see Fig 4C and D). *Cyclin E* and *p38 mapk* profiles showed a peak expression level in the injured group at 24 hours and were included in our further analysis based on their close functional relationship with other cluster members.

Quantitative Multiple Fluorescent Reverse Transcription Polymerase Chain Reaction

To validate our microarray findings, we focused on some members of cell cycle-related genes *c-myc*, *gadd45a*, and *pcna*. We used QMF-RT-MPCR,¹⁵ using infrared primers in low cycle multiplex PCRs to quantitatively compare the experimental gene with control genes. The control genes were selected based on a highly statistically significant association with a

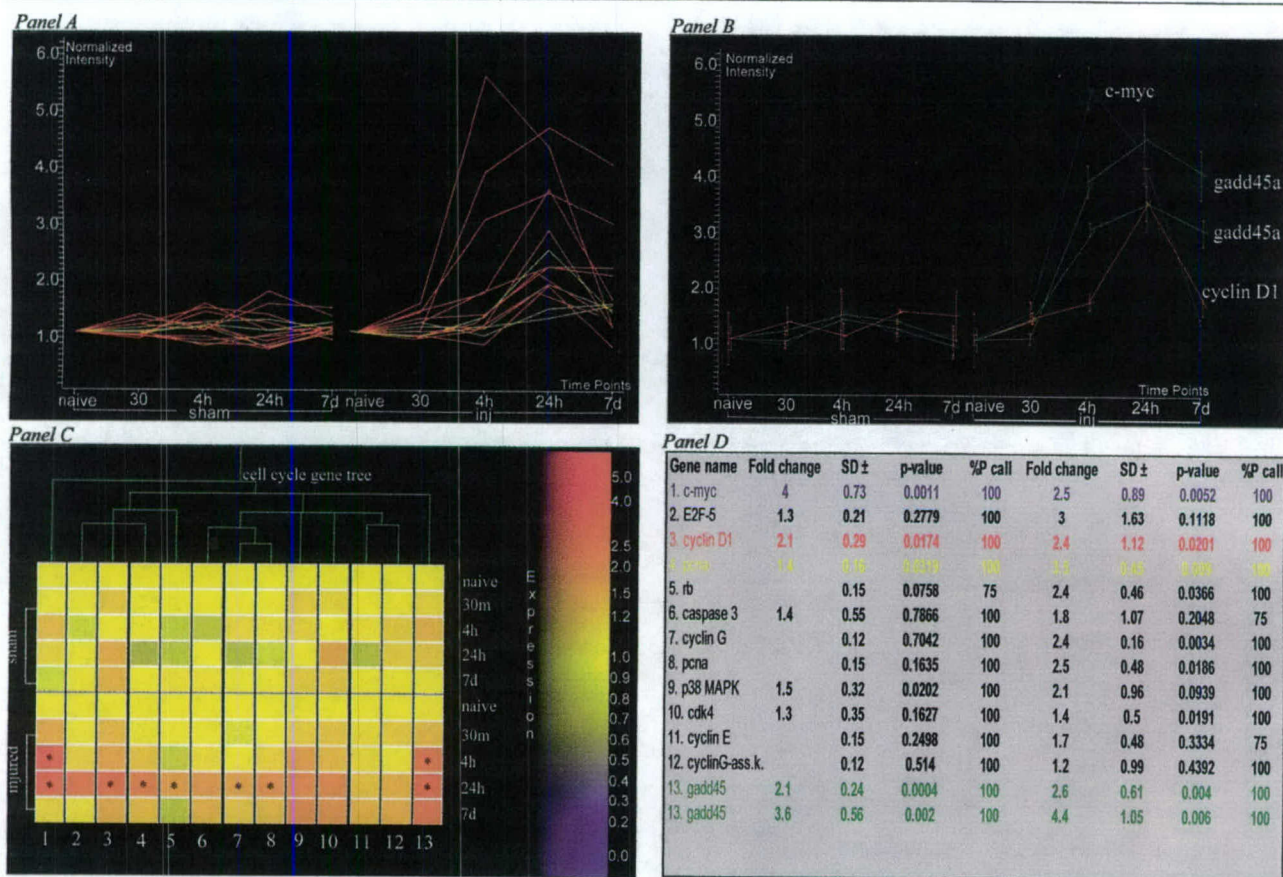


Fig 4. Functional clustering of cell cycle genes shows high expression 4 to 24 hours after injury. Functional clustering of genes based on involvement in cell cycle progression and apoptosis. Genes of this functional cluster also belong to smaller temporal clusters (gadd45a showed temporal clustering with c-myc, $R^2 = 0.99$), whereas pcna, cyclin D1, cyclin G, Rb, and E2F5 belonged to the same temporal cluster, $R^2 = 0.99$). Data for all cluster members are shown in panels A, C, and D, whereas data with standard deviations for multiple animals are shown in B. B shows a self-organizing map graph subcluster applied to the cell cycle gene cluster shown in A. Those genes showing significant p values (<0.05) and fold changes (twofold) between sham and injured time points are indicated with an asterisk in C.

user-defined flat profile ($R^2 = 0.99$) across all 26 profiles. Each experimental gene (*c-myc*, *gadd45a*, and *pcna*) was paired with two control genes showing similar expression levels (average difference hybridization intensities) and primers designed to amplify products differing by only a few base pairs. The three genes studied showed significant differences between injured and sham groups; moreover, fold changes were similar at the same time point as for expression profiling data (Fig 5 and Table).

Immunoblotting

Cell cycle proteins involved in the progression of the cell cycle (*c-myc*, *pcna*, *cyclin D1*, *cdk4*, *Rb*, *Rb* phosphorylated at ser795 and *E2F5*) were studied by duplicate Western blots comparing sham and injured spinal cords at the 4- and 24-hour time points (Fig 6). Each cell cycle-related gene showing increased mRNA expression also showed increased protein expression.

Moreover, the extent of mRNA changes was very similar to the protein expression changes. All proteins were studied at 24 hours, with the exception of *c-myc* and *cyclin D1*, which were examined at both 4 and 24 hours (the rest of the sentence deleted). Several proteins that appear to be related through cell cycle pathways, *c-myc*, *cyclinD1/cdk4*, *ser795 phosphorylated retinoblastoma (pRb)*, and *E2F5*, were increased at 24 hours after injury.

Immunocytochemistry and TUNEL/Hoescht

The cellular expression of *c-myc*, *gadd45a*, *pcna*, *cyclinD1*, *cdk4*, *cyclin G*, *E2F5*, *p38 MAPK*, *pRb* (at the three phosphorylation sites: ser807/811, ser780, and ser795), and *active caspase-3* was evaluated by immunocytochemistry at the injury site (± 0.5 cm). We focused on neuronal localization as indicated by colabeling with NeuN antibody, as the hypothesis was

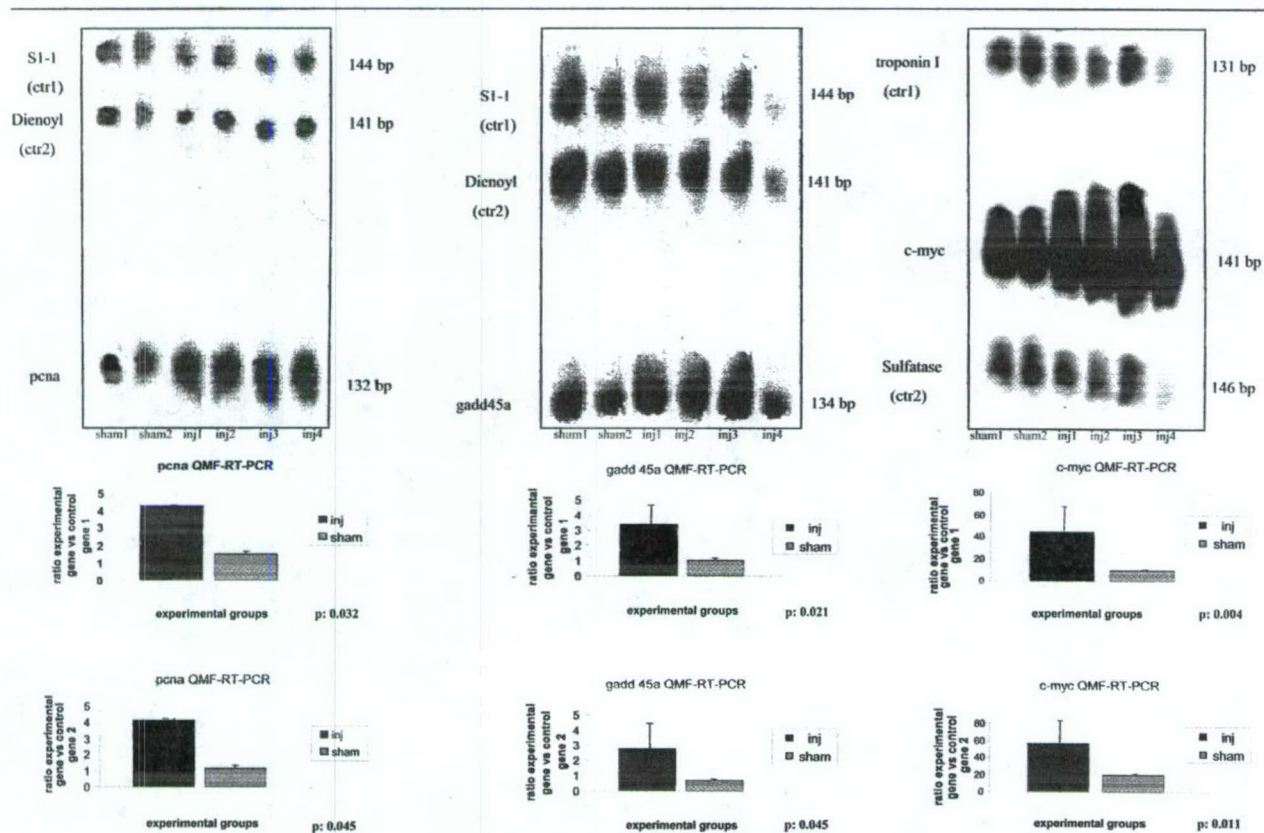


Fig 5. Quantitative multiple fluorescent (QMF) reverse transcription polymerase chain reaction (RT-PCR) verification shows significant transcriptional induction of *gadd45a*, *pcna*, and *c-myc* in the injured animals. QMF-RT-PCR using infrared labeled primers and low-cycle (15 cycles) RT-PCR. The expression of each experimental gene (*gadd45a*, *pcna*, and *c-myc*) was quantified relative to two control genes (S1-1, dyenoyl, troponin I, or sulfatase). Each lane corresponds to a sample from a different animal (two shams and four injured for each reaction). See Materials and Methods under "Quantitative Multiple Fluorescent Reverse Transcription Polymerase Chain Reaction" for more details. Quantitation of RT-PCR products are shown below the gel figures, with standard deviations, and p values versus two control genes. Data shown include the 24-hour time point for *gadd45a* and *pcna*, and the 4-hour time point for *c-myc*.

Table. Comparison between Affymetrix and QMF-RT-PCR Data

	Affymetrix Genechip		QMF-RT-PCR		Time Point (hr)
	Fold Change \pm SD	p	Fold Change \pm SD	p	
<i>c-myc</i>	4.0 \pm 0.73	0.001	3.8 \pm 2.3	0.035	4
<i>gadd45</i>	3.5 \pm 1.05	0.003	3.8 \pm 1.45	0.03	24
<i>pcna</i>	3.0 \pm 1.06	0.01	3.2 \pm 1.3	0.007	24

QMF-RT-PCR = quantitative multiple fluorescent reverse transcription polymerase chain reaction.

that these proteins may be important for neuronal cell death and/or DNA repair. In certain cases, sections were triple-labeled with NeuN, one antibody or a combination of two antibodies, or Hoechst or caspase-3.

All proteins were expressed in neurons, particularly in motor neurons, 0.5cm below the trauma site (Figs 7, 8, and 9). Minimal or no immunostaining was detected for *c-myc*, *cyclin D*, *cdk4*, *E2F5*, and *pRb* in the sham-injured tissue sections used as controls (Fig 10).

In contrast, *c-myc* and *gadd45a* showed substantial positive immunostaining at both 4 and 24 hours after trauma (see Figs 7 and 9). Some *c-myc*, *cyclin G*, *E2F5*, *gadd45a*, *cyclin D*, and *pRb*-positive shrunken neurons were also positive for TUNEL and *caspase-3* at 24 hours (see Fig 8 and 9). We also found some TUNEL-positive glial cells, a few of which were also positive for *c-myc* and *cyclin G*. In many neurons, TUNEL-positive nuclei appeared condensed and/or fragmented by Hoechst staining.

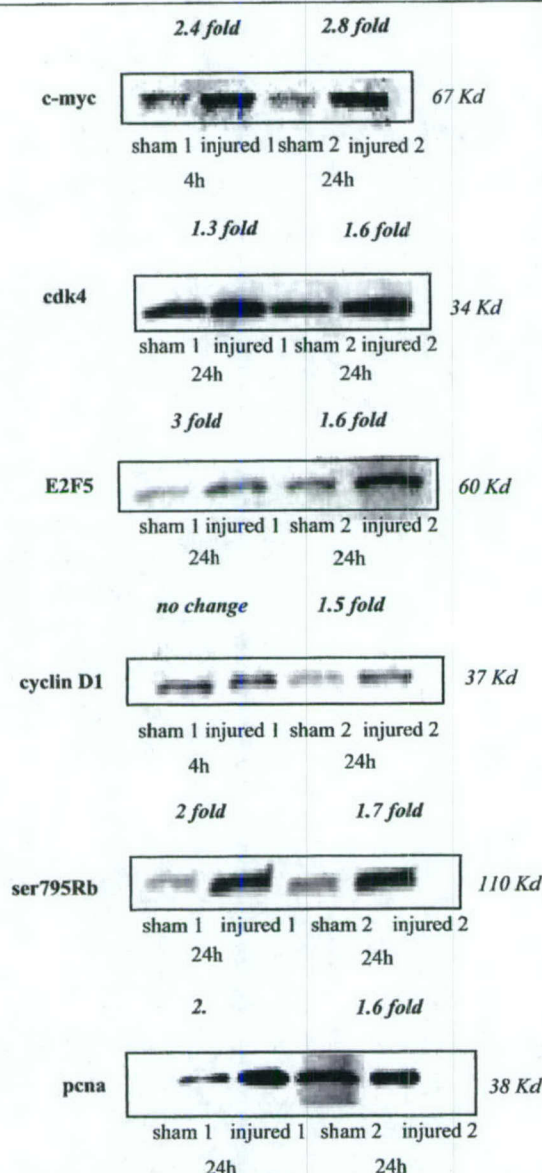


Fig 6. Immunoblot shows increased levels of cell cycle proteins. Western blots of sham and injured spinal cord, at either 4 or 24 hours after injury. Immunoblots show increased cell cycle proteins in the injured spinal cord at 24 hours after injury. c-myc and cyclin D1 also were investigated at the 4-hour time point. Fold changes between sham and injured cords are reported for each protein normalized to Coomassie blue-stained posttransfer proteins from the same lanes.

Discussion

Global Gene Expression Profiles

Spinal cord trauma induces a complex cellular response through the activation and/or suppression of a large number of transcriptional pathways in an environment populated by multiple cell types. Traditional analysis of mRNA expression for single genes using RT-PCR or in situ hybridization has demonstrated

selective changes in relatively few genes after spinal cord injury.^{2,9-12,16,17} In contrast, using the Affymetrix U34A high-density oligonucleotides, we were able to examine changes in 8,800 genes and ESTs induced by trauma.

We found a time-dependent increase in expression of immediate early genes showing highest values at 30 minutes (see Fig 3) followed by changes in expression of mRNAs related to cell cycle, oxidative stress, or inflammation (see Fig 2 and 4). Upregulated mRNAs outnumbered downregulated ones at 30 minutes and 4 hours. This may reflect, in part, the activation of immediate early genes that may function as positive transcription factors. Importantly, they may activate the transcription of other genes that appear to be upregulated at later time points after injury. One example may be *cyclin D1*, whose promoter can be activated by *c-fos* family members.¹⁸ mRNA levels for certain genes related to neuronal survival or glial proliferation also showed increases as early as 4 hours. Also identified were many novel genes whose mRNA expression showed temporal or functional clustering with previously reported changes related to immediate early genes, inflammation, or oxidative stress.^{2,4,5,9,11} All profiles of this experiment were clustered based on function and time point after injury and are accessible via a public Web site (<http://microarray.cnmcresearch.org/pgadatatable.asp>) that includes gene-based queries to investigate the expression level of any gene in the 26 gene chips presented here.

Cell Cycle Genes Are Associated with Neuronal Damage and Apoptotic Features

Cluster analysis identified a temporally defined group of mRNAs related to the cell cycle whose expression was significantly increased at 4 and 24 hours after injury (see Fig 4). The increased expression of some of these cluster members (*gadd45a*, *c-myc*, and *pcna*) was validated by QMF-RT-PCR; nearly identical expression changes were shown by the two methods (see Fig 5 and Table). Increased protein expression was also found 24 hours after injury for members closely related to cell cycle progression (*c-myc*, *cyclinD1*, *cdk4*, *pRb*, *E2F5*, and *pcna*). Several of these cell cycle proteins were coexpressed in neurons and were found in neurons that were TUNEL-positive or expressed *caspase-3*, a protein associated with apoptosis. Certain of these neurons expressing cell cycle proteins also showed morphological features of apoptosis by Hoechst staining.

Consistent with other studies, our data support the hypothesis that the genes belonging to the cell cycle

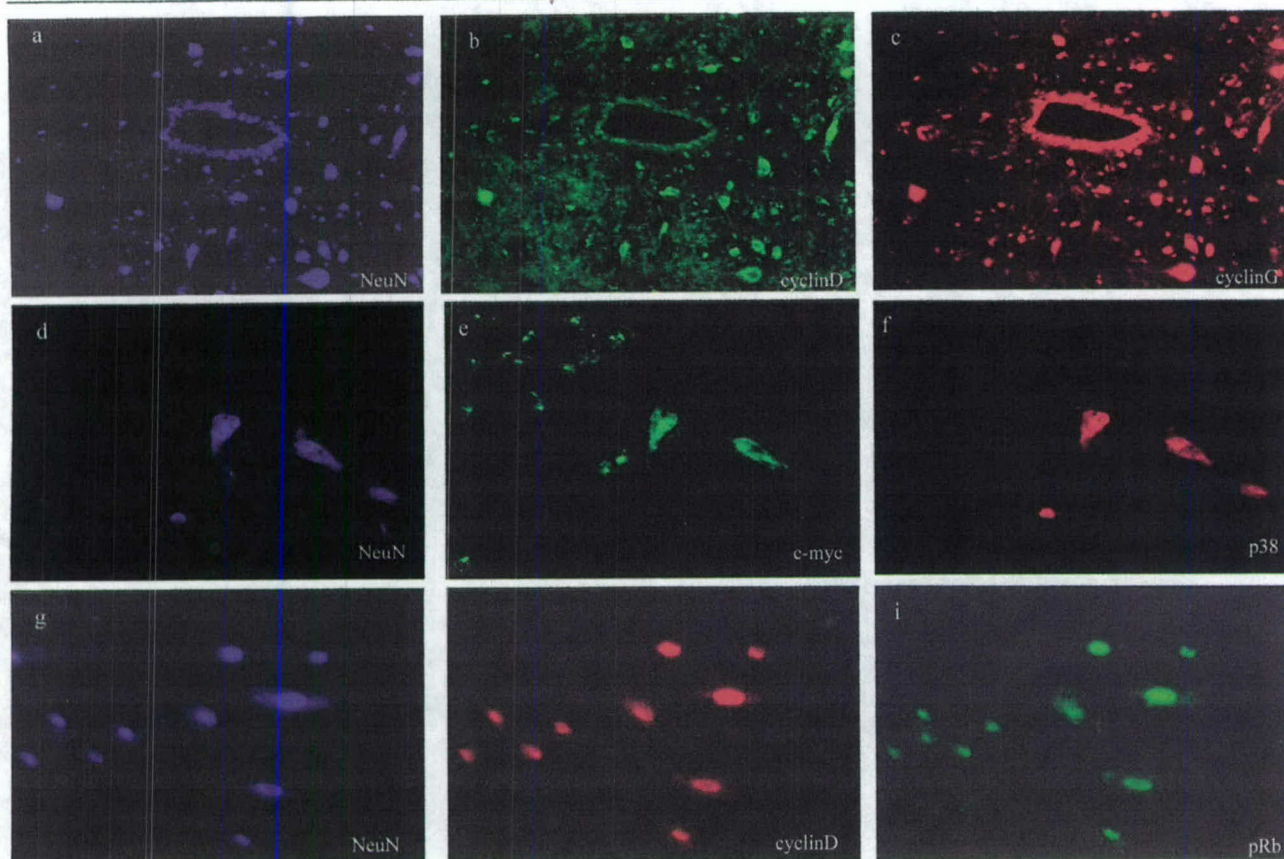


Fig 7. Triple immunofluorescence shows co-labeling of neurons with cell cycle genes 24 hours after mild spinal cord injury. Co-localization of neuronal specific antibody NeuN (a, d, g) with cyclin D (b) and cyclin G (c), c-myc (e), and p38 (f), cyclin D (h) and pRb (i) in the injured ventral horn 0.5 cm below (d-i) or above (a-c) the injury site. The majority of neurons are cyclin D and G positive (a-c), and cyclin D and G are co-localized (b, c). A sub-set of c-myc-positive neurons are immunolabeled with p38 in the ventral horn (d-f). c-myc is also localized in a sub-set of non-neuronal cells (e). Neurons (g) are also positive for both cyclin D and ser795pRb, with both proteins showing predominantly nuclear staining (h, i). Original magnification: $\times 125$ (a-c); $\times 250$ (d-i).

progression pathway are involved in neuronal responses to DNA damage and/or cell stress after SCI. Emerging consensus is that progression through the cell cycle has different and sometimes opposite effects in mitotic versus postmitotic cells.^{13,14} In postmitotic cells, such as neurons, cell cycle reentry may induce apoptotic cell death. Apoptotic neuronal cell death occurs after spinal cord injury and may contribute to the subsequent neurological dysfunction.^{19,20} On the other hand, astrocytic proliferation is known to induce posttraumatic tissue scar formation that can impede functional regeneration (see Fawcett and Asher²¹ McDonald and Sadowsky²² for review). Thus, genes favoring cell cycle progression may be involved in both neuronal apoptosis and astrocytic proliferation.

c-myc and *gadd45a* mRNAs were increased after injury and such increases preceded those for *pcna* and *cyclin D1*, as well as for genes sharing a similar profile ($R^2 = 0.99$ and 0.95), such as *cdk4*, *cyclin G*, *cyclin G*

associated kinase, *Rb*, *E2F5*, and *caspase-3*, or sharing a similar function, such as *cyclin E* and *p38 mapk* (see Fig 4D). Importantly, the cyclin-dependent kinase inhibitor *p21(waf1)*, present in our U34A genome, did not show mRNA expression changes between sham and injured animals at any time point. This suggests that the observed mRNA changes in cyclin members after injury was specific.

A body of evidence supports the concept that these cell cycle members participate in a common pathway involved in neuronal damage and cell death. Both c-myc and *gadd45a* can be activated by diverse conditions that serve to damage cells, and both act as DNA damage-responsive transcription factors.²³⁻²⁸ When induced, c-myc can serve as a proapoptotic factor through mechanisms related to activation of caspases or cell cycle progression to the G2 phase.^{23,24} c-myc-associated apoptosis can be induced by a variety of stimuli, including DNA damage, infection, serum or growth fac-

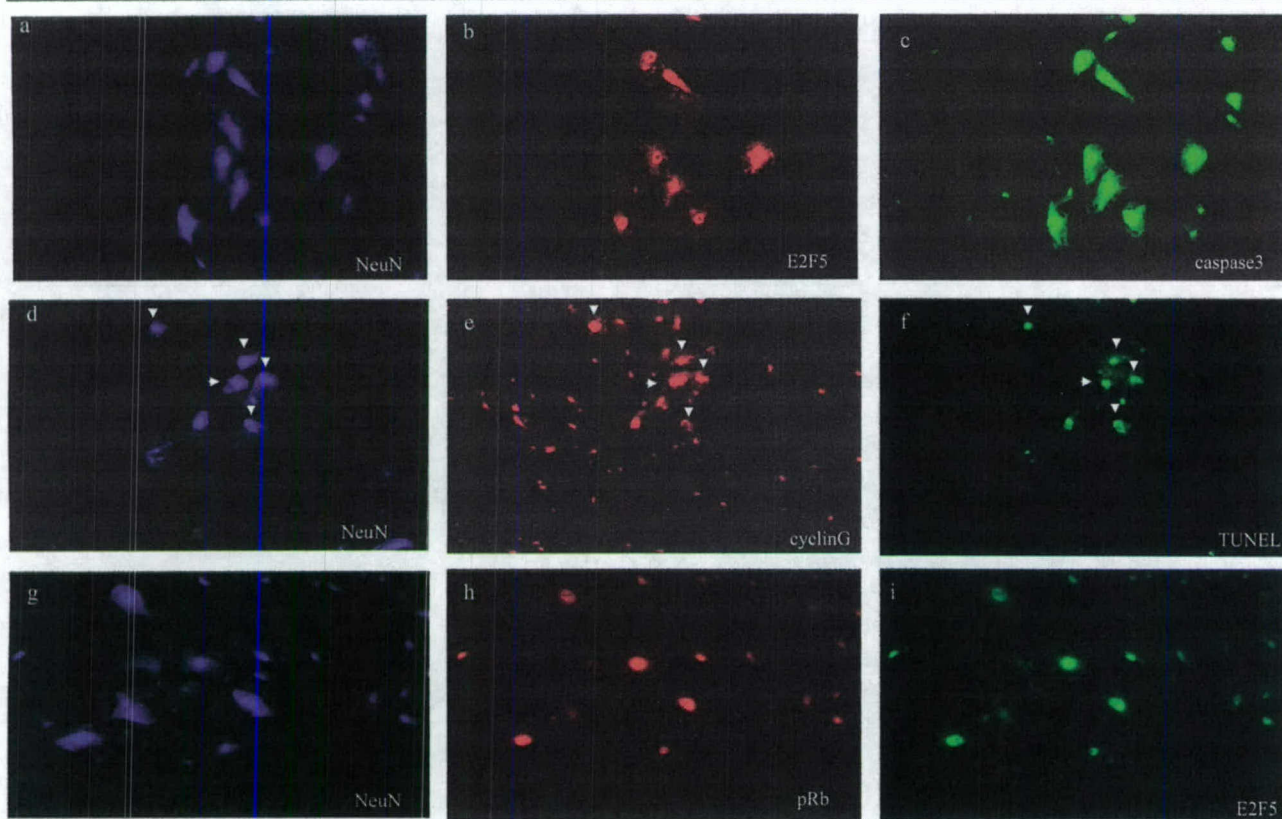


Fig 8. A sub-set of neurons showing co-immunostaining for cell cycle genes also expresses apoptotic features (TUNEL and caspase-3 positive). Triple immunostaining of ventral horn neurons (a-c) shows diffuse nuclear and cytoplasmic staining in the same neurons (a) that express E2F5(b) and caspase-3 (c). Immunocytochemistry for NeuN and cyclin G, with TUNEL on the same section (d-f) shows TUNEL positive neurons that are also positive for cyclin G (arrowheads, e, f). A sub-set of non-neuronal cells are cyclin G positive (e). Neuronal co-localization of ser795pRb and E2F5 show nuclear staining in the ventral horn in most neuN positive cells (g-i). Original magnification: $\times 250$.

tor deprivation, and TNF α or Fas signaling.^{29,30} *c-myc*-dependent apoptosis also can be induced by downstream activation of *p38 MAPK* and caspases.^{23,31} *p38 MAPK* may directly phosphorylate the Rb protein and release its inhibition of E2F family members.³² *c-myc* also can influence transcription of *cyclinD1-cdk4* and *cyclin D2*, and in quiescent cells can activate the expression of *cyclinE-cdk2*.^{33,34}

Both *c-myc* and *E2F* members have the ability to induce cell cycle reentry in quiescent cells and induce apoptosis.³⁵⁻⁴⁰ Phosphorylation and consequent inactivation of *Rb* (mainly at serine residue 95) by cyclin/cdks results in release and activation of the transcription factor family *E2F*, which in turn promotes S-phase transition and cycle progression.^{40,41} Importantly, *Rb* null mice, mimicking phosphorylation of *Rb*, exhibit neurological deficits and neuronal apoptosis.⁴²

gadd45a plays a role at the G1-S and G2-M checkpoints, regulating cell cycle progression: it mediates DNA repair together with *pcna*,⁴³ is a sensor of DNA

damage, and also may be involved in apoptosis regulation and genomic stability.²⁵⁻²⁷ *gadd45a* has been associated with cell death after stimulation by genes belonging to the inducible NGF family (significantly increased between 30 minutes and 4 hours in our profiles) by activating the proapoptotic downstream target *p38 MAPK* (see Fig 9).^{44,45} However, *gadd45a* mRNA and protein expression also have been localized in less vulnerable focal periischemic areas in rat brain, suggesting that it may exert a protective role against cell death under certain conditions.⁴⁶

In vitro experiments have shown that *c-fos*, *cyclin D/cdk4*, *cyclin G*, and *Rb/E2F* members play a role in apoptotic cell death of postmitotic neurons after trophic factor withdrawal, DNA damage, or KCL deprivation.^{42,47-50} In vivo studies of both cortical and spinal cord neurons after ischemia or excitotoxic-mediated DNA damage have shown the occurrence of apoptotic cell death associated with *cyclin D-cdk4*, *cyclin G*, *pcna*, or *Rb/E2F* protein and mRNA overexpression.⁵¹⁻⁵⁴ In addition, the expression of *cyclin D1*, *cyclin A*, *cdk4*,

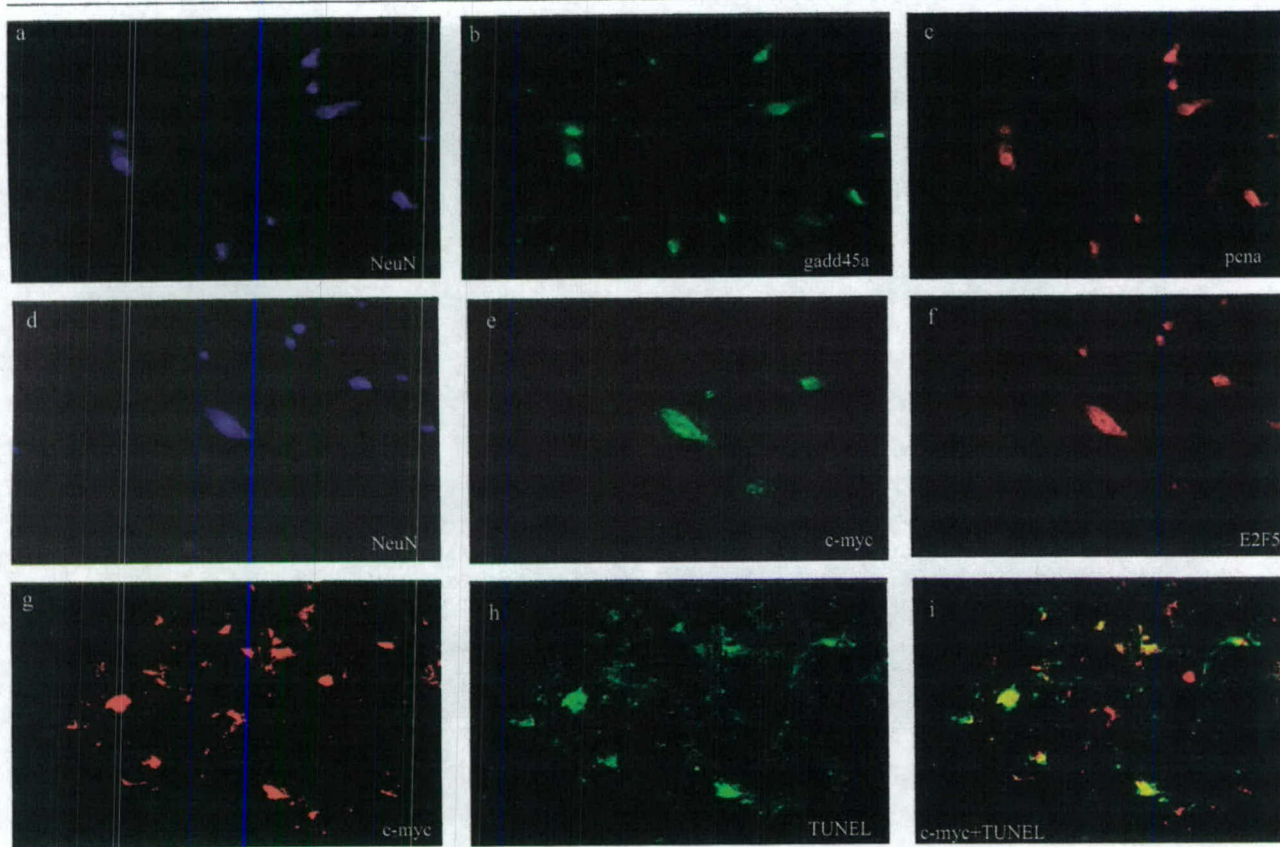


Fig 9. Neurons both above and below the injury site show co-labeling with gadd45a and pcna, c-myc and E2F5, in the ventral horns. c-myc positive neurons are also TUNEL-positive. Co-localization of neuronal specific antibody NeuN (a, d) with gadd45a (b) and pcna (c), c-myc (e) and E2F5 (f) in the injured ventral horn 0.5 cm below the injury site. Both gadd45a and pcna show nuclear localization. Pcna-positive cells are neurons and correspond to the same gadd45a positive-neurons (b, c). gadd45a also showed positive staining in some non-neuronal cells (neuN-negative) (b). c-myc shows both nuclear and cytoplasmic immunolabeling in neurons (e), and all c-myc positive cells also stained for E2F5 (e, f). Not all neurons are c-myc positive (e), whereas most of them express E2F5 in nucleus and cytoplasm (f). TUNEL-positive ventral horn neurons are also c-myc positive (g, h), as evident in the merged image (yellow cells, i). Original magnification: $\times 125$ (a-c); $\times 250$ (d-i).

and pcna have been documented in apoptotic cerebellar granule cells from Weaver mice.⁵⁵ This further suggests that reexpression of cell cycle proteins may be connected to DNA damage, repair, and apoptosis in injured neurons.

Our temporal data are consistent with the hypothesis that SCI causes early induction of c-myc and gadd45a, followed by downstream upregulation of E2F-5 family members either directly or through the activation of cyclinD/cdk4; in turn, these may promote Rb phosphorylation and the release of active E2F transcription factor (see Bartek and Lukas⁵⁶ for review). SCI caused increased ser795 phosphorylated RB, temporally associated with overexpression of cyclinD1/cdk4, p38MAPK, and E2F-5 at the mRNA and protein levels (see Figs 4 and 6). Increased protein expression in neurons at 24 hours (see Fig 6) was found for many of the cell cycle proteins that showed increases by expression profiling (see Figs 7-9). Subsets of these neurons also

demonstrated apoptotic features, as shown by TUNEL, caspase-3 (see Fig 8, 9) and Hoechst staining (not shown).

In conclusion, our data demonstrate that SCI causes diverse changes in mRNA expression for immediate early genes, followed by genes associated with inflammation, oxidative stress, DNA damage, and the cell cycle. Expression of cell cycle-related proteins after injury is colocalized in neurons showing apoptotic features or expression of caspase-3, thus implicating these proteins in posttraumatic cell death.

This work was supported by a grant from the National Institutes of Health (NO1-NS-1-2339, A.L.F., E.P.H.) and NIH Programs in Genomic Applications grant (U01 HL66614 HOPGENE, E.P.H.).

We thank A. Molon for her excellent technical support and thoughtful suggestions.

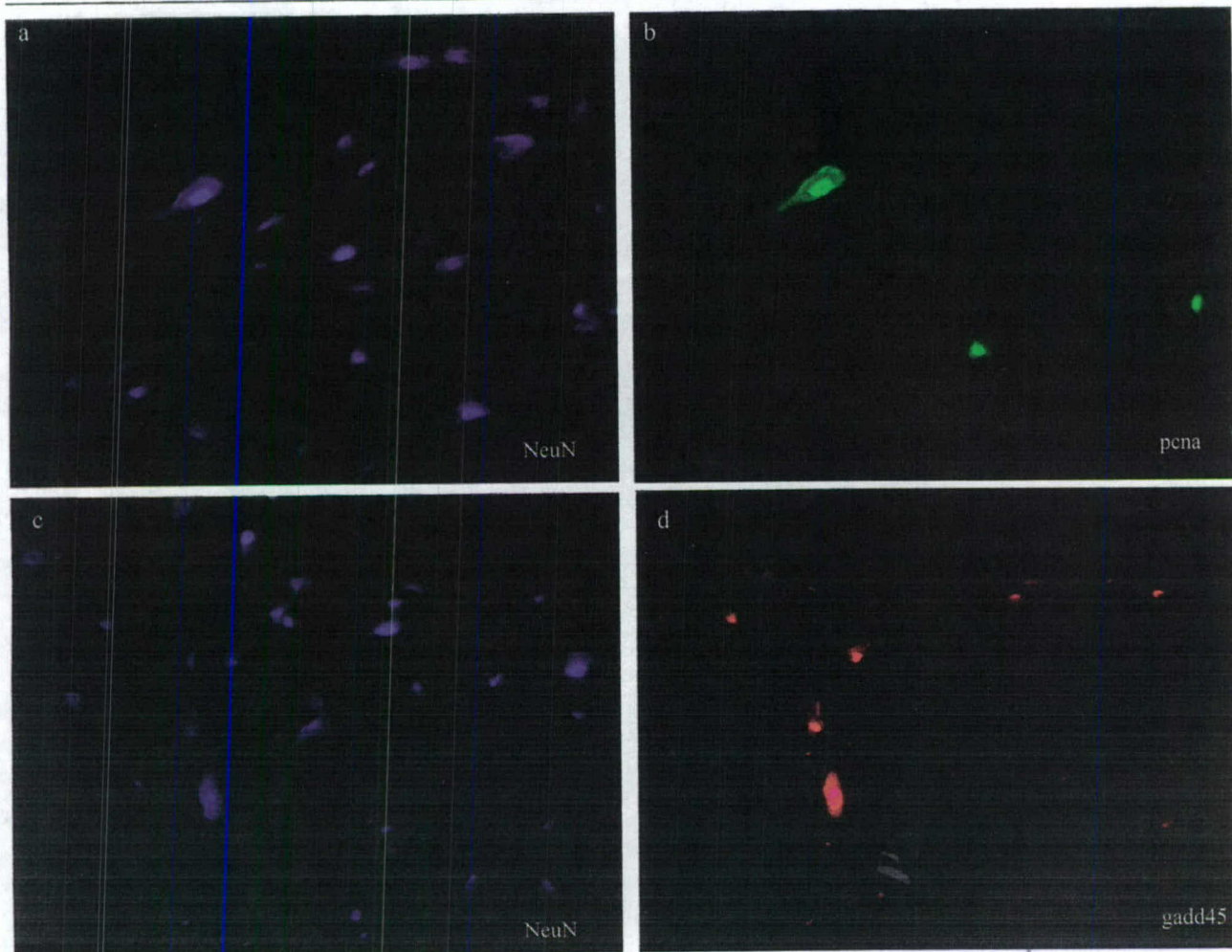


Fig 10. Double-label immunofluorescence for *gadd45* and *pcna* in sham-injured spinal cords at the 24-hour time point. Colocalization of neuronal-specific antibody NeuN (a, c), with *pcna* (b) and *gadd45a* (d) in sham-injured tissue. In contrast with injured tissue, relatively few neurons show positive immunostaining for either *pcna* (b) or *gadd45a* (d). Original magnification $\times 250$.

References

- Dumont RJ, Okonkwo DO, Verma S, et al. Acute spinal cord injury. Part I. pathophysiologic mechanisms. *Clin Neuropharmacol* 2001;24:254–264.
- Yakovlev AG, Faden AI. Molecular biology of CNS injury. *J Neurotrauma* 1995;12:767–777.
- Dutcher SA, Michael DB. Gene expression in neurotrauma. *Neurol Res* 2001;23:203–206.
- Carmel JB, Galante A, Soteropoulos P, et al. Gene expression profiling of acute spinal cord injury reveals spreading inflammatory signals and neuron loss. *Physiol Genomics* 2001;7:201–213.
- Song G, Cechvala C, Resnick DK, et al. GeneChip analysis after acute spinal cord injury in rat. *J Neurochem* 2001;79:804–815.
- Yakovlev AG, Faden AI. Sequential expression of *c-fos* protooncogene, *TNF-alpha*, and *dynorphin* genes in spinal cord following experimental traumatic injury. *Mol Chem Neuropathol* 1994;23:179–190.
- Bakay M, Chen YW, Borup R, et al. Sources of variability and effect of experimental approach on expression profiling data interpretation. *BMC Bioinformatics* 2002;3:4.
- Chen YW, Zhao P, Borup R, Hoffman EP. Expression profiling in the muscular dystrophies: identification of novel aspects of molecular pathophysiology. *J Cell Biol* 2000;151:1321–1336.
- Tonai T, Taketani Y, Ueda N, et al. Possible involvement of interleukin-1 in cyclooxygenase-2 induction after spinal cord injury in rats. *J Neurochem* 1999;72:302–309.
- Citron BA, Arnold PM, Sebastian C, et al. Rapid upregulation of caspase-3 in rat spinal cord after injury: mRNA, protein, and cellular localization correlates with apoptotic cell death. *Exp Neurol* 2000;166:213–226.
- Hayashi M, Ueyama T, Nemoto K, et al. Sequential mRNA expression for immediate early genes, cytokines, and neurotrophins in spinal cord injury. *J Neurotrauma* 2000;17:203–218.
- Mautes AE, Noble LJ. Co-induction of HSP70 and heme oxygenase-1 in macrophages and glia after spinal cord contusion in the rat. *Brain Res* 2000;883:233–237.
- Copani A, Uberti D, Sortino MA, et al. Activation of cell-cycle-associated proteins in neuronal death: a mandatory or dispensable path? *Trends Neurosci* 2001;24:25–31.

14. Liu DX, Greene LA. Neuronal apoptosis at the G1/S cell cycle checkpoint. *Cell Tissue Res* 2001;305:217-228.
15. Zhou J, Hoffman EP. Pathophysiology of sodium channelopathies. Studies of sodium channel expression by quantitative multiplex fluorescence polymerase chain reaction. *J Biol Chem* 1994;269:18563-18571.
16. Springer JE, Azbill RD, Knapp PE. Activation of the caspase-3 apoptotic cascade in traumatic spinal cord injury. *Nat Med* 1999;5:943-946.
17. Keane RW, Kraydieh S, Lotocki G, et al. Apoptotic and anti-apoptotic mechanisms following spinal cord injury. *J Neuro-pathol Exp Neurol* 2001;60:422-429.
18. Brown JR, Nigh E, Lee RJ, et al. Fos family members induce cell cycle entry by activating cyclin D1. *Mol Cell Biol* 1998;18:5609-5619.
19. Liu XZ, Xu XM, Hu R, et al. Neuronal and glial apoptosis after traumatic spinal cord injury. *J Neurosci* 1997;17:5395-5406.
20. Beattie MS, Farooqui AA, Bresnahan JC. Review of current evidence for apoptosis after spinal cord injury. *J Neurotrauma* 2000;17:915-925.
21. Fawcett JW, Asher RA. The glial scar and central nervous system repair. *Brain Res Bull* 1999;49:377-391.
22. McDonald JW, Sadowsky C. Spinal-cord injury. *Lancet* 2002;359:417-425.
23. Kangas A, Nicholson DW, Holttä E. Involvement of CPP32/caspase-3 in c-Myc-induced apoptosis. *Oncogene* 1998;16:387-398.
24. Adachi S, Obaya AJ, Han Z, et al. c-Myc is necessary for DNA damage-induced apoptosis in the G(2) phase of the cell cycle. *Mol Cell Biol* 2001;21:4929-4937.
25. Hollander MC, Sheikh MS, Bulavin DV, et al. Genomic instability in Gadd45a-deficient mice. *Nat Genet* 1999;23:176-184.
26. Sheikh MS, Hollander MC, Fornace AJ Jr. Role of Gadd45 in apoptosis. *Biochem Pharmacol* 2000;59:43-45.
27. Smith ML, Ford JM, Hollander MC, et al. p53-mediated DNA repair responses to UV radiation: studies of mouse cells lacking p53, p21, and/or gadd45 genes. *Mol Cell Biol* 2000;20:3705-3714.
28. Tang Y, Lu A, Arnov BJ, et al. Genomic response of the brain to ischemic stroke, intracerebral haemorrhage, kainate seizures, hypoglycemia, and hypoxia. *Eur J Neurosci* 15:1937-1952.
29. Evan GI, Wyllie AH, Gilbert CS, et al. Induction of apoptosis in fibroblasts by c-myc protein. *Cell* 1992;69:119-128.
30. Prendergast GC. Mechanisms of apoptosis by c-Myc. *Oncogene* 1999;18:2967-2987.
31. Deschesnes RG, Huot J, Valerie K, Landry J. Involvement of p38 in apoptosis-associated membrane blebbing and nuclear condensation. *Mol Biol Cell* 2001;12:1569-1582.
32. Wang S, Nath N, Minden A, Chellappan S. Regulation of Rb and E2F by signal transduction cascades: divergent effects of JNK1 and p38 kinases. *EMBO J* 1999;18:1559-1570.
33. Mateyak MK, Obaya AJ, Sedivy JM. c-Myc regulates cyclin D-Cdk4 and -Cdk6 activity but affects cell cycle progression at multiple independent points. *Mol Cell Biol* 1999;19:4672-4683.
34. Santoni-Rugiu E, Falck J, Mailand N, et al. Involvement of Myc activity in a G(1)/S-promoting mechanism parallel to the pRb/E2F pathway. *Mol Cell Biol* 2000;20:3497-3509.
35. Johnson DG, Schwarz JK, Cress WD, Nevins JR. Expression of transcription factor E2F1 induces quiescent cells to enter S phase. *Nature* 1993;365:349-352.
36. Shan B, Lee WH. Deregulated expression of E2F-1 induces S-phase entry and leads to apoptosis. *Mol Cell Biol* 1994;14:8166-8173.
37. Henriksson M, Lüscher B. Proteins of the Myc network: essential regulators of cell growth and differentiation. *Adv Cancer Res* 1996;68:109-182.
38. Amati B, Alevizopoulos K, Vlach J. Myc and the cell cycle. *Front Biosci* 1998;3:D250-D268.
39. Leone G, Sears R, Huang E, et al. Myc requires distinct E2F activities to induce S phase and apoptosis. *Mol Cell* 2001;8:105-113.
40. Connell-Crowley L, Harper JW, Goodrich DW. Cyclin D1/Cdk4 regulates retinoblastoma protein-mediated cell cycle arrest by site-specific phosphorylation. *Mol Biol Cell* 1997;8:287-301.
41. Ezhevsky SA, Nagahara H, Vocero-Akbani AM, et al. Hypophosphorylation of the retinoblastoma protein (pRb) by cyclin D:Cdk4/6 complexes results in active pRb. *Proc Natl Acad Sci USA* 1997;94:10699-10704.
42. Giovanni A, Keramaris E, Morris EJ, et al. E2F1 mediates death of B-amyloid-treated cortical neurons in a manner independent of p53 and dependent on Bax and caspase 3. *J Biol Chem* 2000;275:11553-11560.
43. Shivji KK, Kenny MK, Wood RD. Proliferating cell nuclear antigen is required for DNA excision repair. *Cell* 1992;69:367-374.
44. Takekawa M, Saito H. A family of stress-inducible GADD45-like proteins mediate activation of the stress-responsive MTK1/MEKK4 MAPKKK. *Cell* 1998;95:521-530.
45. Harkin DP, Bean JM, Miklos D, et al. Induction of GADD45 and JNK/SAPK-dependent apoptosis following inducible expression of BRCA1. *Cell* 1999;97:575-586.
46. Chen J, Uchimura K, Stetler RA, et al. Transient global ischemia triggers expression of the DNA damage-inducible gene GADD45 in the rat brain. *J Cereb Blood Flow Metab* 1998;18:646-657.
47. Freeman RS, Estus S, Johnson EM Jr. Analysis of cell cycle-related gene expression in postmitotic neurons: selective induction of Cyclin D1 during programmed cell death. *Neuron* 1994;12:343-355.
48. Kranenburg O, van der Eb AJ, Zantema A. Cyclin D1 is an essential mediator of apoptotic neuronal cell death. *EMBO J* 1996;15:46-54.
49. Boutillier AL, Trinh E, Loeffler JP. Caspase-dependent cleavage of the retinoblastoma protein is an early step in neuronal apoptosis. *Oncogene* 2000;19:2171-2178.
50. Park DS, Morris EJ, Bremner R, et al. Involvement of retinoblastoma family members and E2F/DP complexes in the death of neurons evoked by DNA damage. *J Neurosci* 2000;20:3104-3114.
51. van Lookeren Campagne M, Gill R. Cell cycle-related gene expression in the adult rat brain: selective induction of cyclin G1 and p21WAF1/CIP1 in neurons following focal cerebral ischemia. *Neuroscience* 1998;84:1097-1112.
52. Sakurai M, Hayashi T, Abe K, et al. Cyclin D1 and Cdk4 protein induction in motor neurons after transient spinal cord ischemia in rabbits. *Stroke* 2000;31:200-207.
53. Padmanabhan J, Park DS, Greene LA, Shelanski ML. Role of cell cycle regulatory proteins in cerebellar granule neuron apoptosis. *J Neurosci* 1999;19:8747-8756.
54. Ino H, Chiba T. Cyclin-dependent kinase 4 and cyclin D1 are required for excitotoxin-induced neuronal cell death in vivo. *J Neurosci* 2001;21:6086-6094.
55. Migheli A, Piva R, Casolino S, et al. A cell cycle alteration precedes apoptosis of granule cell precursors in the weaver mouse cerebellum. *Am J Pathol* 1999;155:365-373.
56. Bartek J, Lukas J. Pathways governing G1/S transition and their response to DNA damage. *FEBS Lett* 2001;490:117-122.